

Women in parasite and host 2021

Edited by

Tania F. De Koning-Ward, Maria Carolina Touz and Shailja Singh

Published in

Frontiers in Cellular and Infection Microbiology



FRONTIERS EBOOK COPYRIGHT STATEMENT

The copyright in the text of individual articles in this ebook is the property of their respective authors or their respective institutions or funders. The copyright in graphics and images within each article may be subject to copyright of other parties. In both cases this is subject to a license granted to Frontiers.

The compilation of articles constituting this ebook is the property of Frontiers.

Each article within this ebook, and the ebook itself, are published under the most recent version of the Creative Commons CC-BY licence. The version current at the date of publication of this ebook is CC-BY 4.0. If the CC-BY licence is updated, the licence granted by Frontiers is automatically updated to the new version.

When exercising any right under the CC-BY licence, Frontiers must be attributed as the original publisher of the article or ebook, as applicable.

Authors have the responsibility of ensuring that any graphics or other materials which are the property of others may be included in the CC-BY licence, but this should be checked before relying on the CC-BY licence to reproduce those materials. Any copyright notices relating to those materials must be complied with.

Copyright and source acknowledgement notices may not be removed and must be displayed in any copy, derivative work or partial copy which includes the elements in question.

All copyright, and all rights therein, are protected by national and international copyright laws. The above represents a summary only. For further information please read Frontiers' Conditions for Website Use and Copyright Statement, and the applicable CC-BY licence.

ISSN 1664-8714
ISBN 978-2-83252-079-6
DOI 10.3389/978-2-83252-079-6

About Frontiers

Frontiers is more than just an open access publisher of scholarly articles: it is a pioneering approach to the world of academia, radically improving the way scholarly research is managed. The grand vision of Frontiers is a world where all people have an equal opportunity to seek, share and generate knowledge. Frontiers provides immediate and permanent online open access to all its publications, but this alone is not enough to realize our grand goals.

Frontiers journal series

The Frontiers journal series is a multi-tier and interdisciplinary set of open-access, online journals, promising a paradigm shift from the current review, selection and dissemination processes in academic publishing. All Frontiers journals are driven by researchers for researchers; therefore, they constitute a service to the scholarly community. At the same time, the *Frontiers journal series* operates on a revolutionary invention, the tiered publishing system, initially addressing specific communities of scholars, and gradually climbing up to broader public understanding, thus serving the interests of the lay society, too.

Dedication to quality

Each Frontiers article is a landmark of the highest quality, thanks to genuinely collaborative interactions between authors and review editors, who include some of the world's best academicians. Research must be certified by peers before entering a stream of knowledge that may eventually reach the public - and shape society; therefore, Frontiers only applies the most rigorous and unbiased reviews. Frontiers revolutionizes research publishing by freely delivering the most outstanding research, evaluated with no bias from both the academic and social point of view. By applying the most advanced information technologies, Frontiers is catapulting scholarly publishing into a new generation.

What are Frontiers Research Topics?

Frontiers Research Topics are very popular trademarks of the *Frontiers journals series*: they are collections of at least ten articles, all centered on a particular subject. With their unique mix of varied contributions from Original Research to Review Articles, Frontiers Research Topics unify the most influential researchers, the latest key findings and historical advances in a hot research area.

Find out more on how to host your own Frontiers Research Topic or contribute to one as an author by contacting the Frontiers editorial office: frontiersin.org/about/contact

Women in parasite and host 2021

Topic editors

Tania F. De Koning-Ward — Deakin University, Australia

Maria Carolina Touz — Medical Research Institute Mercedes and Martin Ferreyra (INIMEC), Argentina

Shailja Singh — Jawaharlal Nehru University, India

Citation

De Koning-Ward, T. F., Touz, M. C., Singh, S., eds. (2023). *Women in parasite and host 2021*. Lausanne: Frontiers Media SA. doi: 10.3389/978-2-83252-079-6

Table of contents

- 06 **Maria M. Mota: Bringing *Plasmodium* Liver Infection to the Centre Stage of Malaria Research**
Sílvia Portugal, Ana Rodriguez and Miguel Prudêncio
- 12 ***Plasmodium falciparum* GBP2 Is a Telomere-Associated Protein That Binds to G-Quadruplex DNA and RNA**
James Edwards-Smallbone, Anders L. Jensen, Lydia E. Roberts, Francis Isidore G. Totañes, Sarah R. Hart and Catherine J. Merrick
- 26 **Metalloprotease Gp63-Targeting Novel Glycoside Exhibits Potential Antileishmanial Activity**
Amrita Chakrabarti, Chintam Narayana, Nishant Joshi, Swati Garg, Lalit C. Garg, Anand Ranganathan, Ram Sagar, Soumya Pati and Shailja Singh
- 43 **The Phosphodiesterase Inhibitor Tadalafil Promotes Splenic Retention of *Plasmodium falciparum* Gametocytes in Humanized Mice**
Daniela Barbieri, Lina Gomez, Ludivine Royer, Florian Dupuy, Jean-François Franetich, Maurel Tefit, Marie-Esther N'Dri, Dominique Mazier, Olivier Silvie, Alicia Moreno-Sabater and Catherine Lavazec
- 54 **Dominique Soldati-Favre: Bringing *Toxoplasma gondii* to the Molecular World**
Joana M. Santos and Karine Frénal
- 60 **Paving the Way: Contributions of Big Data to Apicomplexan and Kinetoplastid Research**
Robyn S. Kent, Emma M. Briggs, Beatrice L. Colon, Catalina Alvarez, Sara Silva Pereira and Mariana De Niz
- 99 **Adapt or Die: Targeting Unique Transmission-Stage Biology for Malaria Elimination**
Mariëtte E. van der Watt, Janette Reader and Lyn-Marié Birkholtz
- 118 **First Evidence of *Entamoeba* Parasites in Australian Wild Deer and Assessment of Transmission to Cattle**
Jose L. Huaman, Carlo Pacioni, Lily Kenchington-Evans, Mark Doyle, Karla J. Helbig and Teresa G. Carvalho
- 127 **Characterization of the B-Cell Epitopes of *Echinococcus granulosus* Histones H4 and H2A Recognized by Sera From Patients With Liver Cysts**
Andrea Maglioco, Facundo A. Agüero, María Pía Valacco, Alejandra Juárez Valdez, Margot Paulino and Alicia G. Fuchs
- 140 **Expanding the Malaria Antibody Toolkit: Development and Characterisation of *Plasmodium falciparum* RH5, CyRPA, and CSP Recombinant Human Monoclonal Antibodies**
Adéla Nacer, Gaily Kivi, Raini Pert, Erkki Juronen, Pavlo Holenya, Eduardo Aliprandini, Rogerio Amino, Olivier Silvie, Doris Quinkert, Yann Le Duff, Matthew Hurley, Ulf Reimer, Andres Tover, Simon J. Draper, Sarah Gilbert, Mei Mei Ho and Paul W. Bowyer

- 154 **Updated List of Transport Proteins in *Plasmodium falciparum***
Juliane Wunderlich
- 167 **Streamlined and Robust Stage-Specific Profiling of Gametocytocidal Compounds Against *Plasmodium falciparum***
Janette Reader, Mariette E. van der Watt and Lyn-Marié Birkholtz
- 178 **The Kinetoplastid-Specific Protein TcCAL1 Plays Different Roles During *In Vitro* Differentiation and Host-Cell Invasion in *Trypanosoma cruzi***
Jessica Rodríguez-Durán, Juan Pablo Gallardo, Catalina Dirney Alba Soto, Karina Andrea Gómez and Mariana Potenza
- 192 **Induction of Autophagy by Ursolic Acid Promotes the Elimination of *Trypanosoma cruzi* Amastigotes From Macrophages and Cardiac Cells**
María Cristina Vanrell, Santiago José Martínez, Lucila Ibel Muñoz, Betiana Nebaí Salassa, Julián Gambarte Tudela and Patricia Silvia Romano
- 204 ***Plasmodium vivax* Duffy Binding Protein-Based Vaccine: a Distant Dream**
Sonalika Kar and Abhinav Sinha
- 216 **Assessment of IgG3 as a serological exposure marker for *Plasmodium vivax* in areas with moderate–high malaria transmission intensity**
Yanie Tayipto, Jason Rosado, Dionicia Gamboa, Michael T. White, Benson Kiniboro, Julie Healer, D. Herbert Opi, James G. Beeson, Eizo Takashima, Takafumi Tsuboi, Matthias Harbers, Leanne Robinson, Ivo Mueller and Rhea J. Longley
- 230 **Rapid diagnosis of *Plasmodium falciparum* malaria using a point-of-care loop-mediated isothermal amplification device**
Madhu Puri, Harsimran Kaur Brar, Evanka Madan, Rajesh Srinivasan, Kapil Rawat, Sai Siva Gorthi, Geeta Kumari, Raj Sah, Sashi Bhusan Ojha, Subhendu Panigrahi, Gunanidhi Dhangadamajhi, Rohini Muthuswami, Shailja Singh and Rentala Madhubala
- 240 ***Giardia duodenalis* enolase is secreted as monomer during trophozoite-epithelial cell interactions, activates plasminogen and induces necroptotic damage**
Elisa Barroeta-Echegaray, Rocío Fonseca-Liñán, Raúl Argüello-García, Rafael Rodríguez-Muñoz, Rosa María Bermúdez-Cruz, Porfirio Nava and M. Guadalupe Ortega-Pierres
- 260 **Complementary crosstalk between palmitoylation and phosphorylation events in MTIP regulates its role during *Plasmodium falciparum* invasion**
Zille Anam, Geeta Kumari, Soumyadeep Mukherjee, Devasahayam Arokia Balaya Rex, Shreeja Biswas, Preeti Maurya, Susendaran Ravikumar, Nutan Gupta, Akhilesh Kumar Kushawaha, Raj Kumar Sah, Ayushi Chaurasiya, Jhalak Singhal, Niharika Singh, Shikha Kaushik, T. S. Keshava Prasad, Soumya Pati, Anand Ranganathan and Shailja Singh

- 277 **Identification and characterization of extracellular vesicles from red cells infected with *Babesia divergens* and *Babesia microti***
Divya Beri, Marilis Rodriguez, Manpreet Singh, Yunfeng Liu, Giselle Rasquinha, Xiuli An, Karina Yazdanbakhsh and Cheryl A. Lobo
- 295 **Extracellular vesicles from *Trypanosoma cruzi*-dendritic cell interaction show modulatory properties and confer resistance to lethal infection as a cell-free based therapy strategy**
Brenda Celeste Gutierrez, Maria Eugenia Ancarola, Izadora Volpato-Rossi, Antonio Marcilla, Marcel Ivan Ramirez, Mara Cecilia Rosenzvit, Marcela Cucher and Carolina Verónica Poncini
- 309 **Microwaves can kill malaria parasites non-thermally**
Lorena M. Coronado, José A. Stoute, Christopher T. Nadovich, Jiping Cheng, Ricardo Correa, Kevin Chaw, Guadalupe González, Maytee Zambrano, Rolando A. Gittens, Dinesh K. Agrawal, William D. Jemison, Carlos A. Donado Morcillo and Carmenza Spadafora



Maria M. Mota: Bringing *Plasmodium* Liver Infection to the Centre Stage of Malaria Research

Sílvia Portugal¹, Ana Rodriguez² and Miguel Prudêncio^{3*}

¹ Max Planck Institute for Infection Biology, Berlin, Germany, ² Department of Microbiology, New York University School of Medicine, New York City, NY, United States, ³ Instituto de Medicina Molecular, Faculdade de Medicina, Universidade de Lisboa, Lisboa, Portugal

Keywords: malaria, liver stage, sporozoites, *Plasmodium*, hepatocyte

OPEN ACCESS

Edited by:

Tania F. De Koning-Ward,
Deakin University, Australia

Reviewed by:

Volker Theo Heussler,
University of Bern, Switzerland
Purnima Bhanot,
Rutgers Biomedical and Health
Sciences, United States

*Correspondence:

Miguel Prudêncio
mprudencio@medicina.ulisboa.pt

Specialty section:

This article was submitted to
Parasite and Host,
a section of the journal
Frontiers in Cellular and
Infection Microbiology

Received: 09 January 2022

Accepted: 24 January 2022

Published: 08 February 2022

Citation:

Portugal S, Rodriguez A and
Prudêncio M (2022) Maria M. Mota:
Bringing *Plasmodium* Liver Infection to
the Centre Stage of Malaria Research.
Front. Cell. Infect. Microbiol. 12:851484.
doi: 10.3389/fcimb.2022.851484

INTRODUCTION

Mammalian infection by malaria parasites is initiated by the injection of *Plasmodium* sporozoites into the host's skin in preparation for a blood meal by an infected female *Anopheles* mosquito. Sporozoites then travel to the liver, where they invade hepatocytes and initiate an asymptomatic phase of asexual replication, known as the liver stage of infection. This process culminates in the release of thousands of newly-formed red blood cell-infective merozoites, which are responsible for malaria-associated pathology (Prudencio et al., 2006). Although the liver stage of the *Plasmodium* life cycle constitutes the initial and obligatory step of mammalian infection by malaria parasites, it remained as a biological black box for decades since its discovery by Shortt, Garnham and their team in 1948 (Shortt et al., 1948). Its clinically silent nature, coupled with the inherent limitations of its experimental address, meant that liver infection by *Plasmodium* remained largely unknown by researchers for decades. However, it is now known that this pivotal phase of the malaria parasite's life cycle plays critical roles in the establishment of mammalian infection by *Plasmodium*, in the host's response to the parasite, and in the outcome of disease. The *Plasmodium*-host hepatic interface is now commonly regarded not only as an ideal target for malaria prophylaxis and vaccination, but also as the site where a unique and extremely rich array of molecular interactions take place. And few people have contributed as much as Maria M. Mota to unveiling key features of the liver stage of the malaria parasite's life cycle. By engaging the most advanced *in vitro* and rodent models of *Plasmodium* infection (Langhorne et al., 2011; Prudencio et al., 2011; Zuzarte-Luis et al., 2014), Maria decisively helped to bring this once-relatively obscure phase of the parasite's life cycle to the limelight of malaria research.

Maria Manuel Mota obtained her BSc in Biology and her MSc in Immunology in 1992 and 1994, respectively, at the University of Porto, Portugal, followed by a PhD in Molecular Parasitology by the University College London in 1998. She then carried out her post-doctoral studies on host-parasite interactions in Victor Nussenzweig's lab at the New York University Medical School from 1999 to 2002. On this year, she returned to her home country of Portugal to become a group leader, initially at Instituto Gulbenkian de Ciência (IGC), and subsequently at Instituto de Medicina Molecular (iMM), where she became the Executive Director in 2014.

The authors of this article have been fortunate enough to interact closely with Maria M. Mota at different stages of her career. Maria spent part of her time at the laboratory of AR during her postdoctoral studies at the New York University; MP joined Maria's group as a postdoctoral researcher

soon after she became an independent scientist, and was a staff scientist in her laboratory before becoming an independent group leader at Lisbon's iMM; and SP was Maria's PhD student at a time when her position as a key player in malaria research was well solidified and internationally recognized. Each one of us has had the unique opportunity to perceive Maria's unique scientific drive, her contagious enthusiasm, and her unabashed commitment to research. We are all indebted to Maria for her continued support of our own scientific careers but, above all, we feel very fortunate to have witnessed some of the most remarkable discoveries made in the field of liver stage *Plasmodium* infection. As Maria's career as an independent scientist reaches its 20th anniversary, this is our account of some of her most relevant scientific achievements of the last two decades.

RE-DESIGNING THE LIFE CYCLE OF MALARIA PARASITES

In 2001, Maria M. Mota, working in the laboratory of AR, demonstrated for the first time that *Plasmodium* sporozoites traverse several hepatocytes before productively invading a final cell (Mota et al., 2001), and suggested that this migration might activate sporozoites for productive invasion of hepatocytes (Mota et al., 2002). Maria's work subsequently showed that hepatocyte growth factor (HGF), a molecule released by host cells upon wounding by traversing sporozoites, interacts with its receptor MET to promote the parasites' intrahepatic development (Carrolo et al., 2003) and to protect *Plasmodium*-infected cells from apoptosis (Leiriao et al., 2005). While the exact reasons for, and the implications of the parasite's migratory behavior remain incompletely elucidated, in the words of Victor Nussenzweig, Maria M. Mota's supervisor and mentor at the New York University, "Maria's finding literally changed the textbook representation of the life cycle of *Plasmodium* parasites".

HOST GENES AND DRUG TARGETS

As Maria initiated her independent research career in Portugal, her focus on the study of the liver stage of *Plasmodium* infection intensified and expanded, and she soon reported the first transcriptome profile of the hepatic host cell throughout infection by malaria parasites (Albuquerque et al., 2009). Soon thereafter, Maria's lab pioneered the use of RNA interference (RNAi) to identify host factors at play during hepatic *Plasmodium* infection. An RNAi screen of the entire human kinome implicated five host kinases in this process, further establishing a role for PKC ζ on hepatocyte invasion by sporozoites (Prudencio et al., 2008). A parallel RNAi screen additionally unveiled the hepatic host's scavenger receptor SR-BI as playing a critical role in both the sporozoite's ability to invade liver cells and to develop intracellularly (Rodrigues et al., 2008). During this period, the work of Maria's team also led to the identification of genistein as a potential drug for malaria prophylaxis (Cunha-Rodrigues et al., 2008), to the demonstration that *Plasmodium* liver infection can

be inhibited by a small molecule inhibitor of signal peptide peptidase, with an impact on malaria severity (Parvanova et al., 2009), and that CpG phosphothioate oligodeoxynucleotides can act directly on *Plasmodium* sporozoites to inhibit their gliding motility, cell traversal ability and capacity to invade hepatic cells (Liehl et al., 2010). In 2012, she was deeply involved in pioneering drug screens targeting the liver stage of the parasite's life cycle, which identified decoquinate as a potent multi-stage antiparasitic drug (da Cruz et al., 2012), and revealed that hepatic malaria parasites are vulnerable to diverse chemical scaffolds (Derbyshire et al., 2012). One year later, her lab identified torins as fast-acting anti-plasmodial compounds that efficiently target the parasite's liver and blood stages in a manner that is independent of those drug's canonical target, the mammalian target of rapamycin (mTOR) kinase (Hanson et al., 2013). Collectively, these and other achievements helped to define Maria's position at the forefront of liver stage *Plasmodium* infection research, a status that never ceased to solidify.

THE PATHOGENESIS OF SEVERE MALARIA

Always acutely aware of the pathology that ensues during the erythrocytic phase of the malaria parasite's life cycle, Maria's lab helped unveil heme oxygenase-1 (HO-1) as a host factor that not only promotes liver infection by *Plasmodium* parasites (Epiphany et al., 2008), but that also plays a crucial role in the development of experimental cerebral malaria (Pamplona et al., 2007). A few years later, the team established a DBA/2 mouse model for the study of *Plasmodium*-induced experimental acute lung injury, showing that this life-threatening condition is promoted by the host's vascular endothelial growth factor (VEGF), and can be inhibited by carbon monoxide's anti-inflammatory action (Epiphany et al., 2010). These achievements furthered our knowledge of malaria pathogenesis, and remain as a testimony of Maria's ability to think beyond the liver stage of infection and seeking solutions to combat the most grievous forms of malaria disease.

HEPATOCYTE INVASION BY *PLASMODIUM* SPOROZOITES

One of the questions that had puzzled the community for decades was how *Plasmodium* sporozoites could engage into a phase of intra-hepatic differentiation and multiplication so promptly after transitioning from the mosquito salivary glands to hepatocytes. Maria's lab contributed pivotally to our current knowledge of the molecular determinants of this process, by unveiling a Pumilio-2 (Puf2)-dependent post-translational repression mechanism that controls that transition (Gomes-Santos et al., 2011). Very recently, her team challenged the dogma that hepatocytes are passive players during the process of their invasion by sporozoites. This work showed that the pore-forming activity of the parasite's exported protein 2 (EXP2) triggers a response from the hepatic host cell, which leads to the production of acid sphingomyelinase. This enzyme then plays a

critical role in the repair of the host cell membrane, which is key for sporozoite invasion and establishment in hepatocytes (Mello-Vieira et al., 2020). This finding is a perfect illustration of Maria's ability to push the boundaries of knowledge beyond the *status quo*, by unveiling an active role for the hepatic host cell in a process long thought to depend solely on the parasite.

NEW TOOLS TO STUDY LIVER INFECTION BY *PLASMODIUM*

Throughout her career, Maria contributed several new instruments to the fight against malaria, thorough the establishment of new tools and platforms for the investigation of *Plasmodium* liver infection. Among other achievements, she and her team demonstrated the usefulness of transgenic malaria parasites expressing fluorescent or luminescent reporter genes as invaluable tools to identify and quantify *Plasmodium* infection, not only in the liver (Prudencio et al., 2008; Ploemen et al., 2009), but also in the blood (Zuzarte-Luis et al., 2014). During a sabbatical in Sangeeta Bhatia's laboratory at the Massachusetts Institute of Technology (MIT), Maria contributed to the generation of a human liver *in vitro* platform that is able to sustain the development of human malaria parasites (March et al., 2013), and showed that human induced pluripotent stem cell-derived hepatocyte-like cells support infection by multiple *Plasmodium* sporozoite species (Ng et al., 2015). These achievements, alongside the more recent establishment of a humanized mouse model bearing an ectopic artificial liver that can be infected by human malaria parasites (Ng et al., 2017), provided the community with invaluable new tools for the investigation of *Plasmodium* liver infection and the assessment of anti-plasmodial compounds.

IMMUNE RESPONSES TO *PLASMODIUM* LIVER INFECTION

The asymptomatic nature of the liver stage of *Plasmodium* infection contributed to the long-held assumption that this phase of the parasite's life cycle was also immunologically silent. Maria's work effectively challenged this view and showed that, quite the contrary, this a phase when a rich array of immune responses take place, with a clear impact on infection and pathology. Her early work on HO-1 had already shown that liver infection elicits a potent inflammatory response in the host (Epiphany et al., 2008). A few years later, work from Maria's lab showed that *Plasmodium* liver stages induce a potent type I interferon (IFN) response that prompts host cell sensors to activate an immune cell-mediated response (Liehl et al., 2014), the magnitude of which effectively inhibit re-infection in an IFN- γ -dependent way (Liehl et al., 2015). On the other hand, the lab also showed that IFN- γ produced by $\gamma\delta$ -T cells upon liver-stage infection can have a deleterious effect on the host and promote experimental cerebral malaria (ECM) pathogenesis (Ribot et al., 2019). The enormous potential of the liver stage of infection for immunization against malaria is now firmly established, and Maria has made important contributions to the whole-sporozoite-based vaccination approaches. In 2007, her team

showed that P36p-deficient *P. berghei* sporozoites can induce protection against a subsequent challenge with fully infectious parasites (Douradinha et al., 2007), contributing to the exploitation of genetically-attenuated parasites (GAP) as vaccination agents against malaria. More than 10 years later, she was involved in a pioneering study by MP that established the proof-of-concept of employing genetically modified rodent malaria parasites, expressing antigens of their human-infective counterparts, as a platform for vaccination against human malaria (Mendes et al., 2018). Collectively, these achievements helped redefine the liver stage of *Plasmodium* infection as an immunologically rich phase of the parasite's life cycle, once again challenging the prevailing dogma of its immune passiveness.

CROSS-TALK BETWEEN MAMMALIAN INFECTION STAGES

One of Maria's characteristics is her view of *Plasmodium* as a complex organism, whose different life cycle stages in the mammalian host should not be viewed independently of each other, as a bidirectional cross-talk exists, in which one stage of mammalian infection may impact the establishment and progression of the other. The identification of HO-1 as a host factor that operates both during the liver (Epiphany et al., 2008) and the blood (Pamplona et al., 2007) stages of infection by Maria's team nicely illustrates her holistic view of mammalian infection by *Plasmodium*. This is perhaps even better exemplified by Maria's investigation of the direct impact of blood stage *Plasmodium* on a subsequent hepatic infection by the same parasite. This work, carried out during SP's PhD, revealed for the first time that an ongoing *Plasmodium* blood stage infection potently inhibits a subsequent infection by *Plasmodium* sporozoites. An in depth look at the mechanisms behind this inhibition showed that this process depends at least partly on the iron regulatory hormone hepcidin. This finding unveiled a host-mediated quorum-sensing-like mechanism that regulates superinfection by malaria parasites in regions of high disease endemicity (Portugal et al., 2011).

EXPLOITATION OF HOST RESOURCES BY *PLASMODIUM* AND HOST RESPONSES TO INFECTION

Among the most pervasive questions throughout Maria M. Mota's scientific career are "how does the parasite exploit the host for its own benefit?" and "how does the host respond to the invading parasite?" Maria's curiosity about the role of host cell factors and host-mediated processes during liver infection by *Plasmodium* prompted an array of major achievements that significantly furthered our understanding of the biology of the malaria parasite's sporozoite and liver stages. Looking closely into the infected liver cell, Maria's lab described for the first time a highly dynamic set of hepatocyte actin reorganization events that occur around developing *Plasmodium* parasites inside hepatic cells, which may contribute to their elimination during development

in the liver (Gomes-Santos et al., 2012). Soon afterwards, the lab demonstrated that hepatic *Plasmodium* parasites take up phosphatidylcholine from the host to support their replication (Itoe et al., 2014), and that *Plasmodium*'s vacuolar iron-transporter (VIT) homologue plays an important role in iron detoxification, contributing to the parasite's normal development in the liver (Slavic et al., 2016). Maria's team further showed that liver infection by malaria parasites is facilitated by the host's hepatic endoplasmic reticulum (ER)-resident unfolded protein response (UPR) (Inacio et al., 2015), whereas signaling by the host's AMP-activated protein kinase (AMPK) exerts a suppressive effect on hepatic infection (Ruivo et al., 2016). Having contributed to the demonstration that the host's autophagy machinery contributes to the *Plasmodium*'s hepatic development (Thieleke-Matos et al., 2016), Maria's lab later showed that *Plasmodium* relies on its own upregulated in sporozoites 3 (UIS3) protein to outcompete the autophagy marker microtubule-associated protein 1 light chain 3 (LC3), decreasing its binding to the parasitophorous vacuole membrane (PVM), and thereby avoiding elimination (Real et al., 2018). Maria and her team then showed that this interaction between the parasite's UIS3 and the host's LC3 molecules can be chemically disrupted, inhibiting the parasite's ability to evade the host autophagy response and leading to its elimination (Setua et al., 2020). This array of discoveries has brought us closer to understanding why *Plasmodium* sporozoites "choose" the hepatocyte as their initial site of replication in the mammalian host, a key question in this field of research.

HOST-MEDIATED MODULATION OF INFECTION

Maria's conviction that *Plasmodium* infection can be modulated by the host prompted her and her team to investigate whether the host's nutritional status influences the course of infection and pathology. This study unveiled a novel mechanism whereby the *Plasmodium* kinase KIN acts as a sensor that enables the parasite to modulate its replication rate in accordance with the host's nutritional status (Mancio-Silva et al., 2017). This discovery was reported close to another one, addressing the modulation of *Plasmodium* liver infection by the host's dietary intake. This study showed that the oxidative stress induced by a high-fat diet causes the death of intra-hepatic parasites, leading to a major decrease in the overall *Plasmodium* liver load, and significantly decreasing the severity of the ensuing disease (Zuzarte-Luis et al., 2017). These discoveries have contributed decisively to enhancing the notion that the mammalian host plays a critical role in the development of malaria disease, and that the latter can be influenced through the modulation of the parasite's environment inside the former.

FINAL REMARKS

Maria's achievements as a malaria researcher have earned her worldwide recognition in the community. Her appointments as a Howard Hughes Medical Institute (HHMI) International Research Scholar from 2005 to 2010, and as a European Molecular Biology

Organization (EMBO) Member in 2016 constitute significant recognitions of both her accomplishments and her potential. Besides her scientific excellence, Maria has a captivating personality and is an engaging communicator, who has brought malaria research to the spotlight in Portugal and beyond, through her multiple public appearances in the media and her ability to entice her audiences. A staunch advocate for women's rights and equal education opportunities, she commonly features in the list of the most influential women in Portugal and has earned numerous national and international awards that further enhanced her standing in the malaria research community. She has helped foster iMM's reputation and recognition at both the national and international levels, and her actions have had an enormous impact on science policies in Portugal as a whole. She has inspired and guided more than one generation of scientists, many of whom have grown to lead their independent research labs.

Maria M. Mota's scientific career is an inspiring example of commitment to science, enthusiasm and excellence. She was able to carve a research niche that earned her international reputation and contributed greatly to Portugal's prominence in malaria research over the last couple of decades (Prudencio, 2021). Naturally, her achievements owe immensely to the efforts and dedication of her research team. Over the years, her laboratory has hosted numerous postdoctoral researchers, PhD and Master's students, laboratory technicians and managers, and visiting scientists, all of whom have been inspired by Maria, and all of whom have contributed enormously to the success of her research. Equally relevant, the respect earned by Maria in the scientific community has enabled her to establish an extended network of outstanding collaborators, to whom she also owes much of her success. As Maria likes to say, ideas appear when people come together and talk to each other about their science. Maria's ability to foster discussion, both within and beyond her own lab, has always been one of the distinctive features of her scientific drive. As Executive Director of iMM, Maria created the institute's motto "chasing questions", because she deeply believes that the formulation of the most creative questions is the key to all major scientific advances.

Maria's brain is constantly teeming with new interrogations that drive her creativity and fuel her passion for science. While it may not be easy to predict exactly what scientific achievements Maria's future will bring, it is certainly not hard to forecast that she will continue challenging the borders of our knowledge of the liver stage of *Plasmodium* infection. As such, we can be pretty confident that many fascinating discoveries still lie ahead in her path through science. Stay tuned!

AUTHOR CONTRIBUTIONS

All authors contributed to the article and approved the submitted version.

ACKNOWLEDGMENTS

Inês Domingues and Joana Costa are gratefully acknowledged for various discussions and for their critical review of the manuscript.

REFERENCES

- Albuquerque, S. S., Carret, C., Grosso, A. R., Tarun, A. S., Peng, X., Kappe, S. H., et al. (2009). Host Cell Transcriptional Profiling During Malaria Liver Stage Infection Reveals a Coordinated and Sequential Set of Biological Events. *BMC Genomics* 10, 270. doi: 10.1186/1471-2164-10-270
- Carrolo, M., Giordano, S., Cabrita-Santos, L., Corso, S., Vigario, A. M., Silva, S., et al. (2003). Hepatocyte Growth Factor and Its Receptor Are Required for Malaria Infection. *Nat. Med.* 9, 1363–1369. doi: 10.1038/nm947
- Cunha-Rodrigues, M., Portugal, S., Prudencio, M., Goncalves, L. A., Casalou, C., Bugar, D., et al. (2008). Genistein-Supplemented Diet Decreases Malaria Liver Infection in Mice and Constitutes a Potential Prophylactic Strategy. *PLoS One* 3, e2732. doi: 10.1371/journal.pone.0002732
- da Cruz, F. P., Martin, C., Buchholz, K., Lafuente-Monasterio, M. J., Rodrigues, T., Sonnichsen, B., et al. (2012). Drug Screen Targeted at Plasmodium Liver Stages Identifies a Potent Multistage Antimalarial Drug. *J. Infect. Dis.* 205, 1278–1286. doi: 10.1093/infdis/jis184
- Derbyshire, E. R., Prudencio, M., Mota, M. M., and Clardy, J. (2012). Liver-Stage Malaria Parasites Vulnerable to Diverse Chemical Scaffolds. *Proc. Natl. Acad. Sci. U. S. A.* 109, 8511–8516. doi: 10.1073/pnas.1118370109
- Douradinha, B., van Dijk, M. R., Ataide, R., van Gemert, G. J., Thompson, J., Franetich, J. F., et al. (2007). Genetically Attenuated P36p-Deficient Plasmodium Berghei Sporozoites Confer Long-Lasting and Partial Cross-Species Protection. *Int. J. Parasitol.* 37, 1511–1519. doi: 10.1016/j.ijpara.2007.05.005
- Epiphany, S., Campos, M. G., Pamplona, A., Carapau, D., Pena, A. C., Ataide, R., et al. (2010). VEGF Promotes Malaria-Associated Acute Lung Injury in Mice. *PLoS Pathog.* 6, e1000916. doi: 10.1371/journal.ppat.1000916
- Epiphany, S., Mikolajczak, S. A., Goncalves, L. A., Pamplona, A., Portugal, S., Albuquerque, S., et al. (2008). Heme Oxygenase-1 Is an Anti-Inflammatory Host Factor That Promotes Murine Plasmodium Liver Infection. *Cell Host Microbe* 3, 331–338. doi: 10.1016/j.chom.2008.04.003
- Gomes-Santos, C. S., Braks, J., Prudencio, M., Carret, C., Gomes, A. R., Pain, A., et al. (2011). Transition of Plasmodium Sporozoites Into Liver Stage-Like Forms Is Regulated by the RNA Binding Protein Pumilio. *PLoS Pathog.* 7, e1002046. doi: 10.1371/journal.ppat.1002046
- Gomes-Santos, C. S., Itoe, M. A., Afonso, C., Henriques, R., Gardner, R., Sepulveda, N., et al. (2012). Highly Dynamic Host Actin Reorganization Around Developing Plasmodium Inside Hepatocytes. *PLoS One* 7, e29408. doi: 10.1371/journal.pone.0029408
- Hanson, K. K., Ressurreicao, A. S., Buchholz, K., Prudencio, M., Herman-Ornelas, J. D., Rebelo, M., et al. (2013). Torins Are Potent Antimalarials That Block Replenishment of Plasmodium Liver Stage Parasitophorous Vacuole Membrane Proteins. *Proc. Natl. Acad. Sci. U. S. A.* 110, E2838–E2847. doi: 10.1073/pnas.1306097110
- Inacio, P., Zuzarte-Luis, V., Ruivo, M. T., Falkard, B., Nagaraj, N., Rooijers, K., et al. (2015). Parasite-Induced ER Stress Response in Hepatocytes Facilitates Plasmodium Liver Stage Infection. *EMBO Rep.* 16, 955–964. doi: 10.15252/embr.201439979
- Itoe, M. A., Sampaio, J. L., Cabal, G. G., Real, E., Zuzarte-Luis, V., March, S., et al. (2014). Host Cell Phosphatidylcholine Is a Key Mediator of Malaria Parasite Survival During Liver Stage Infection. *Cell Host Microbe* 16, 778–786. doi: 10.1016/j.chom.2014.11.006
- Langhorne, J., Buffet, P., Galinski, M., Good, M., Harty, J., Leroy, D., et al. (2011). The Relevance of Non-Human Primate and Rodent Malaria Models for Humans. *Malar. J.* 10, 23. doi: 10.1186/1475-2875-10-23
- Leiriao, P., Albuquerque, S. S., Corso, S., van Gemert, G. J., Sauerwein, R. W., Rodriguez, A., et al. (2005). HGF/MET Signalling Protects Plasmodium-Infected Host Cells From Apoptosis. *Cell Microbiol.* 7, 603–609. doi: 10.1111/j.1462-5822.2004.00490.x
- Liehl, P., Franca, A. R., Prudencio, M., Latz, E., Zaidman-Remy, A., and Mota, M. M. (2010). Phosphothioate Oligodeoxynucleotides Inhibit Plasmodium Sporozoite Gliding Motility. *Cell Microbiol.* 12, 506–515. doi: 10.1111/j.1462-5822.2009.01411.x
- Liehl, P., Meireles, P., Albuquerque, I. S., Pinkevych, M., Baptista, F., Mota, M. M., et al. (2015). Innate Immunity Induced by Plasmodium Liver Infection Inhibits Malaria Reinfections. *Infect. Immun.* 83, 1172–1180. doi: 10.1128/IAI.02796-14
- Liehl, P., Zuzarte-Luis, V., Chan, J., Zillinger, T., Baptista, F., Carapau, D., et al. (2014). Host-Cell Sensors for Plasmodium Activate Innate Immunity Against Liver-Stage Infection. *Nat. Med.* 20, 47–53. doi: 10.1038/nm3424
- Mancio-Silva, L., Slavic, K., Grilo Ruivo, M. T., Grosso, A. R., Modrzynska, K. K., Vera, I. M., et al. (2017). Nutrient Sensing Modulates Malaria Parasite Virulence. *Nature* 547, 213–216. doi: 10.1038/nature23009
- March, S., Ng, S., Velmurugan, S., Galstian, A., Shan, J., Logan, D. J., et al. (2013). A Microscale Human Liver Platform That Supports the Hepatic Stages of Plasmodium Falciparum and Vivax. *Cell Host Microbe* 14, 104–115. doi: 10.1016/j.chom.2013.06.005
- Mello-Vieira, J., Enguita, F. J., de Koning-Ward, T. F., Zuzarte-Luis, V., and Mota, M. M. (2020). Plasmodium Translocon Component EXP2 Facilitates Hepatocyte Invasion. *Nat. Commun.* 11, 5654. doi: 10.1038/s41467-020-19492-4
- Mendes, A. M., Machado, M., Goncalves-Rosa, N., Reuling, I. J., Foquet, L., Marques, C., et al. (2018). A Plasmodium Berghei Sporozoite-Based Vaccination Platform Against Human Malaria. *NPJ Vaccines* 3, 33. doi: 10.1038/s41541-018-0068-2
- Mota, M. M., Hafalla, J. C., and Rodriguez, A. (2002). Migration Through Host Cells Activates Plasmodium Sporozoites for Infection. *Nat. Med.* 8, 1318–1322. doi: 10.1038/nm785
- Mota, M. M., Pradel, G., Vanderberg, J. P., Hafalla, J. C., Frevet, U., Nussenzweig, R. S., et al. (2001). Migration of Plasmodium Sporozoites Through Cells Before Infection. *Science* 291, 141–144. doi: 10.1126/science.291.5501.141
- Ng, S., March, S., Galstian, A., Gural, N., Stevens, K. R., Mota, M. M., et al. (2017). Towards a Humanized Mouse Model of Liver Stage Malaria Using Ectopic Artificial Livers. *Sci. Rep.* 7, 45424. doi: 10.1038/srep45424
- Ng, S., Schwartz, R. E., March, S., Galstian, A., Gural, N., Shan, J., et al. (2015). Human iPSC-Derived Hepatocyte-Like Cells Support Plasmodium Liver-Stage Infection In Vitro. *Stem Cell Rep.* 4, 348–359. doi: 10.1016/j.stemcr.2015.01.002
- Pamplona, A., Ferreira, A., Balla, J., Jeney, V., Balla, G., Epiphany, S., et al. (2007). Heme Oxygenase-1 and Carbon Monoxide Suppress the Pathogenesis of Experimental Cerebral Malaria. *Nat. Med.* 13, 703–710. doi: 10.1038/nm1586
- Parvanova, I., Epiphany, S., Fauq, A., Golde, T. E., Prudencio, M., and Mota, M. M. (2009). A Small Molecule Inhibitor of Signal Peptide Peptidase Inhibits Plasmodium Development in the Liver and Decreases Malaria Severity. *PLoS One* 4, e5078. doi: 10.1371/journal.pone.0005078
- Ploemen, I. H., Prudencio, M., Douradinha, B. G., Ramesar, J., Fonager, J., van Gemert, G. J., et al. (2009). Visualisation and Quantitative Analysis of the Rodent Malaria Liver Stage by Real Time Imaging. *PLoS One* 4, e7881. doi: 10.1371/journal.pone.0007881
- Portugal, S., Carret, C., Recker, M., Armitage, A. E., Goncalves, L. A., Epiphany, S., et al. (2011). Host-Mediated Regulation of Superinfection in Malaria. *Nat. Med.* 17, 732–737. doi: 10.1038/nm.2368
- Prudencio, M. (2021). Portugal's Prominence in Malaria Research: How a Small Country Became a Key Player in European Research on One of the World's Deadliest Diseases. *EMBO Rep.* 22, e51692. doi: 10.15252/embr.202051692
- Prudencio, M., Mota, M. M., and Mendes, A. M. (2011). A Toolbox to Study Liver Stage Malaria. *Trends Parasitol.* 27, 565–574. doi: 10.1016/j.pt.2011.09.004
- Prudencio, M., Rodrigues, C. D., Ataide, R., and Mota, M. M. (2008). Dissecting In Vitro Host Cell Infection by Plasmodium Sporozoites Using Flow Cytometry. *Cell Microbiol.* 10, 218–224. doi: 10.1111/j.1462-5822.2007.01032.x
- Prudencio, M., Rodrigues, C. D., Hannus, M., Martin, C., Real, E., Goncalves, L. A., et al. (2008). Kinome-Wide RNAi Screen Implicates at Least 5 Host Hepatocyte Kinases in Plasmodium Sporozoite Infection. *PLoS Pathog.* 4, e1000201. doi: 10.1371/journal.ppat.1000201
- Prudencio, M., Rodriguez, A., and Mota, M. M. (2006). The Silent Path to Thousands of Merozoites: The Plasmodium Liver Stage. *Nat. Rev. Microbiol.* 4, 849–856. doi: 10.1038/nrmicro1529
- Real, E., Rodrigues, L., Cabal, G. G., Enguita, F. J., Mancio-Silva, L., Mello-Vieira, J., et al. (2018). Plasmodium UIS3 Sequesters Host LC3 to Avoid Elimination by Autophagy in Hepatocytes. *Nat. Microbiol.* 3, 17–25. doi: 10.1038/s41564-017-0054-x
- Ribot, J. C., Neres, R., Zuzarte-Luis, V., Gomes, A. Q., Mancio-Silva, L., Mensurado, S., et al. (2019). Gammadelta-T Cells Promote IFN-Gamma-Dependent Plasmodium Pathogenesis Upon Liver-Stage Infection. *Proc. Natl. Acad. Sci. U. S. A.* 116, 9979–9988. doi: 10.1073/pnas.1814440116

- Rodrigues, C. D., Hannus, M., Prudencio, M., Martin, C., Goncalves, L. A., Portugal, S., et al. (2008). Host Scavenger Receptor SR-BI Plays a Dual Role in the Establishment of Malaria Parasite Liver Infection. *Cell Host Microbe* 4, 271–282. doi: 10.1016/j.chom.2008.07.012
- Ruivo, M. T. G., Vera, I. M., Sales-Dias, J., Meireles, P., Gural, N., Bhatia, S. N., et al. (2016). Host AMPK Is a Modulator of Plasmodium Liver Infection. *Cell Rep.* 16, 2539–2545. doi: 10.1016/j.celrep.2016.08.001
- Setua, S., Enguita, F. J., Chora, A. F., Ranga-Prasad, H., Lahree, A., Marques, S., et al. (2020). Disrupting Plasmodium UIS3-Host LC3 Interaction With a Small Molecule Causes Parasite Elimination From Host Cells. *Commun. Biol.* 3, 688. doi: 10.1038/s42003-020-01422-1
- Shortt, H. E., Garnham, P. C., and Malamos, B. (1948). The Pre-Erythrocytic Stage of Mammalian Malaria. *Br. Med. J.* 1, 192–194. doi: 10.1136/bmj.1.4543.192
- Slavic, K., Krishna, S., Lahree, A., Bouyer, G., Hanson, K. K., Vera, I., et al. (2016). A Vacuolar Iron-Transporter Homologue Acts as a Detoxifier in Plasmodium. *Nat. Commun.* 7, 10403. doi: 10.1038/ncomms10403
- Thieleke-Matos, C., Lopes da Silva, M., Cabrita-Santos, L., Portal, M. D., Rodrigues, I. P., Zuzarte-Luis, V., et al. (2016). Host Cell Autophagy Contributes to Plasmodium Liver Development. *Cell Microbiol.* 18, 437–450. doi: 10.1111/cmi.12524
- Zuzarte-Luis, V., Mello-Vieira, J., Marreiros, I. M., Liehl, P., Chora, A. F., Carret, C. K., et al. (2017). Dietary Alterations Modulate Susceptibility to Plasmodium Infection. *Nat. Microbiol.* 2, 1600–1607. doi: 10.1038/s41564-017-0025-2
- Zuzarte-Luis, V., Mota, M. M., and Vigario, A. M. (2014). Malaria Infections: What and How can Mice Teach Us. *J. Immunol. Methods* 410, 113–122. doi: 10.1016/j.jim.2014.05.001
- Zuzarte-Luis, V., Sales-Dias, J., and Mota, M. M. (2014). Simple, Sensitive and Quantitative Bioluminescence Assay for Determination of Malaria Pre-Patent Period. *Malar. J.* 13, 15. doi: 10.1186/1475-2875-13-15

Conflict of Interest: The authors declare that the research was conducted in the absence of any commercial or financial relationships that could be construed as a potential conflict of interest.

Publisher's Note: All claims expressed in this article are solely those of the authors and do not necessarily represent those of their affiliated organizations, or those of the publisher, the editors and the reviewers. Any product that may be evaluated in this article, or claim that may be made by its manufacturer, is not guaranteed or endorsed by the publisher.

Copyright © 2022 Portugal, Rodriguez and Prudêncio. This is an open-access article distributed under the terms of the Creative Commons Attribution License (CC BY). The use, distribution or reproduction in other forums is permitted, provided the original author(s) and the copyright owner(s) are credited and that the original publication in this journal is cited, in accordance with accepted academic practice. No use, distribution or reproduction is permitted which does not comply with these terms.



***Plasmodium falciparum* GBP2 Is a Telomere-Associated Protein That Binds to G-Quadruplex DNA and RNA**

James Edwards-Smallbone^{1†}, Anders L. Jensen^{2†}, Lydia E. Roberts², Francis Isidore G. Totañes², Sarah R. Hart³ and Catherine J. Merrick^{2*}

¹ Centre for Applied Entomology and Parasitology, Faculty of Natural Sciences, Keele University, Staffordshire, United Kingdom,

² Department of Pathology, Cambridge University, Cambridge, United Kingdom, ³ School of Medicine, Faculty of Medicine and Health Sciences, Keele University, Staffordshire, United Kingdom

OPEN ACCESS

Edited by:

Maria Carolina Touz,
Medical Research Institute Mercedes
and Martin Ferreyra (INIMEC),
Argentina

Reviewed by:

Galadriel Hovel-Miner,
George Washington University,
United States
Victoria Jeffers,
University of New Hampshire,
United States

*Correspondence:

Catherine J. Merrick
cjm48@cam.ac.uk

[†]These authors have contributed
equally to this work and share
first authorship

Specialty section:

This article was submitted to
Parasite and Host,
a section of the journal
Frontiers in Cellular and
Infection Microbiology

Received: 24 September 2021

Accepted: 24 January 2022

Published: 22 February 2022

Citation:

Edwards-Smallbone J, Jensen AL,
Roberts LE, Totañes FIG, Hart SR and
Merrick CJ (2022) *Plasmodium*
falciparum GBP2 Is a Telomere-
Associated Protein That Binds to
G-Quadruplex DNA and RNA.
Front. Cell. Infect. Microbiol. 12:782537.
doi: 10.3389/fcimb.2022.782537

In the early-diverging protozoan parasite *Plasmodium*, few telomere-binding proteins have been identified and several are unique. *Plasmodium* telomeres, like those of most eukaryotes, contain guanine-rich repeats that can form G-quadruplex structures. In model systems, quadruplex-binding drugs can disrupt telomere maintenance and some quadruplex-binding drugs are potent anti-plasmodial agents. Therefore, telomere-interacting and quadruplex-interacting proteins may offer new targets for anti-malarial therapy. Here, we report that *P. falciparum* GBP2 is such a protein. It was identified via 'Proteomics of Isolated Chromatin fragments', applied here for the first time in *Plasmodium*. *In vitro*, PfGBP2 binds specifically to G-rich telomere repeats in quadruplex form and it can also bind to G-rich RNA. *In vivo*, PfGBP2 partially colocalises with the known telomeric protein HP1 but is also found in the cytoplasm, probably due to its affinity for RNA. Consistently, its interactome includes numerous RNA-associated proteins. PfGBP2 is evidently a multifunctional DNA/RNA-binding factor in *Plasmodium*.

Keywords: *Plasmodium*, malaria, G-quadruplex, telomere, proteomics of isolated chromatin fragments, GBP2

INTRODUCTION

Human malaria, caused by protozoan *Plasmodium* parasites, is responsible for widespread morbidity and around half a million deaths each year (WHO, 2020). *Plasmodium* lies in an early-diverging lineage which differs greatly from model eukaryotic organisms: it is an obligate intracellular parasite that lives inside host cells for much of its lifecycle, and divides primarily by schizogony rather than conventional binary fission.

Plasmodium maintains its genome in conventional linear chromosomes, capped by telomeres that consist of a simple guanine-rich repeat (Figueiredo et al., 2000). These telomeres must be constantly maintained to prevent their degradation during the many replicative rounds of the parasite's lifecycle. However, *Plasmodium* lacks discernible homologues of almost all of the telomere-binding factors previously identified in model organisms (Zakian, 2012), which control telomere maintenance, recruit or suppress telomerase, enforce transcriptional silencing of adjacent genes via the 'telomere position effect' (Gottschling et al., 1990) and suppress the recombination or fusion of DNA ends. In *Plasmodium* the telomere repeat sequence differs slightly from that of the human host (GGGTT(T/C)A instead of GGGTTA), but it is nevertheless likely that specific proteins exist to cap telomeres, monitor their length, regulate their maintenance and mediate their nuclear clustering and tethering, since all these

canonical features of telomere biology appear in *Plasmodium* (Bottius et al., 1998; Freitas-Junior et al., 2000).

The first telomeric protein characterized in *Plasmodium* was telomerase itself (Bottius et al., 1998; Figueiredo et al., 2005) and two new proteins were discovered more recently: a zinc-finger protein *PfTRZ* (Bertschi et al., 2017) and an *ApiAP2* transcription factor *PfAP2Tel* (Sierra-Miranda et al., 2017). Both are particular to *Plasmodium* telomeres, emphasizing the unusual nature of the *Plasmodium* telosome. Identifying additional telomere-binding factors in *Plasmodium* could improve our understanding of telomere biology beyond model organisms.

Importantly, studying *Plasmodium* telomeres could also reveal potential new drug targets, since all single-celled eukaryotes must maintain their telomeres in order to survive. Accordingly, various telomere-targeting drugs that were designed as anti-cancer agents have also been tested against *Plasmodium* (De Cian et al., 2008; Harris et al., 2018). These drugs are frequently designed to target a particular DNA structure called the guanine-quadruplex (G4), which can form in single-stranded guanine-rich sequences such as telomere repeats. G4s occur at eukaryotic telomeres and play important roles in telomere maintenance – hence their potential as anti-cancer targets (Murat and Balasubramanian, 2014). We have already reported that a G4-binding drug called quarfloxin kills *Plasmodium* parasites rapidly and potently *in vitro* (Harris et al., 2018), raising the possibility of repurposing it and/or other such drugs as anti-malarials.

Here, we aimed to identify and characterize novel telomere-binding proteins in *Plasmodium falciparum*, using the agnostic approach of pulling down fragments of telomeric chromatin and identifying the associated proteins by mass spectrometry. This method, called Proteomics of Isolated Chromatin fragments, or ‘PICh’, previously identified more than 80 telomere-binding components in human cells (Dejardin and Kingston, 2009). It was adapted to *P. falciparum* – a method that may prove useful in future for identifying other chromatin-domain-specific proteins – and it identified the protein *PfGBP2* (PF3D7_1006800). *PfGBP2* is an RRM-domain protein whose yeast homolog, ‘G-strand Binding Protein 2’, is known to bind to single-stranded telomeric DNA in *S. cerevisiae* (Lin and Zakian, 1994), as well as binding to mRNAs for nuclear/cytoplasmic shuttling (Windgassen and Krebber, 2003). It was recently identified in parallel studies in both *P. falciparum* (Gurung et al., 2021) and *P. berghei* (Niikura et al., 2020). We confirmed the interaction of *PfGBP2* with *Plasmodium* telomere repeats and also found that it interacts with G-rich RNAs *in vitro*. Consistent with this, tagged *PfGBP2* was found *in vivo* in the nucleus as well as the cytoplasm of blood-stage *P. falciparum* parasites. It interacted with numerous RNA-associated proteins, as well as some DNA-associated proteins. Thus, it seems likely that *PfGBP2* plays a role in telomere maintenance, *via* its binding to telomeric G4s, and also in RNA dynamics.

MATERIALS AND METHODS

Parasite Culture and Transfection

Laboratory strains of *P. falciparum*, 3D7, HB3, Dd2, K1, 7G8 and D10 were obtained from the MR4 repository (www.beiresources.org). 3D7 was used for all experiments except the telomere Southern

blots, which used genomic DNA from other strains. Parasites were maintained *in vitro* in human O+ erythrocytes at 4% haematocrit in RPMI 1640 medium supplemented with 25mM HEPES (Sigma-Aldrich), 0.25% sodium bicarbonate, 50 mg/L hypoxanthine (Sigma-Aldrich), 0.25% Albumax (Invitrogen) and 5% heat-inactivated pooled human serum, using standard procedures (Trager and Jensen, 1976).

Transfections were carried out after synchronization with 5% sorbitol and then maturation to highly synchronous late-stage trophozoites/schizonts. Transgenic parasites were generated by allowing these cultures to invade erythrocytes pre-loaded with 50 – 100 µg plasmid DNA as previously described (Deitsch et al., 2001). Parasites were allowed to grow for 48 hours before being exposed to drug selection, and then maintained with 5nM WR99210 (Jacobus Pharmaceuticals). For pSLI-mediated gene tagging, transfectants were subsequently selected with neomycin, as previously described (Birnbbaum et al., 2017), to select parasites carrying the genome-integrated construct. 2µg/ml blasticidin (Invitrogen) was also used to select for simultaneous expression of HP1-3HA in the HP1-3HA +GBP2-2Ty line.

Telomere Restriction Fragment Southern Blotting

Genomic DNA was extracted from parasites using the QIAamp DNA Blood Mini Kit (Qiagen), digested with restriction enzymes *AluI*, *DdeI*, *MboII* and *RsaI*, then blotted with a probe specific for telomeres as described previously (Bottius et al., 1998; Figueiredo et al., 2002).

Proteomics of Isolated Chromatin Segments

PICh assays were carried out essentially as described by Dejardin and Kingston (2009), with *Plasmodium*-specific modifications. A full step-by-step PICh method can be obtained from <https://www.epigenesys.eu/images/stories/protocols>. Briefly, parasite cultures were expanded and synchronized with two rounds of sorbitol treatment to yield 1L of synchronous late-stage trophozoites at 9% parasitaemia. Parasitized cells were collected by centrifugation and washed in PBS-PMSF, prior to erythrocyte lysis by addition of saponin to 0.1%. Free parasites were then collected by centrifugation and washed four times in PBS-PMSF, before being crosslinked for 30 mins in 3.7% formaldehyde/PBS-PMSF. Thereafter samples were treated as previously described (Dejardin and Kingston, 2009) with the following critical parameters: RNase incubation: 2 h at room temperature. Sonication: Total “on” time of 15 mins (4 x 7.5min), 30s on, 30s off. Chromatin preparations were split in two (1x target, 1x control) and hybridized with 30µl of probe per sample (a 50-fold molar excess). Probe sequences are provided in **Table S2**. Probe-chromatin complexes were captured magnetically, washed, eluted and then isolated by TCA precipitation. Protein pellets were de-crosslinked by boiling in 2% SDS, 0.5M 2-mercaptoethanol, 250mM Tris buffer for 30 mins.

PICh Protein Digestion *via* Filter/Gel-Aided Sample Preparation and Mass Spectrometry

De-crosslinked proteins were subjected to either filter-aided sample preparation (FASP) according to the methods of Mann and

coworkers (Wisniewski et al., 2009), or gel-aided sample preparation (GASP) following the methods of Fischer and Kessler (2015). In the FASP method, samples were processed using a FASP Protein Digestion Kit (Expedeon, Cambridgeshire), following the manufacturer's procedure. GASP was performed by adding acrylamide 40% (w/v) (Sigma-Aldrich) 1:1 v/v to the sample, enabling formation of protein-containing polyacrylamide plugs upon polymerization using ammonium persulphate and TEMED (Sigma-Aldrich). Gel plugs were then diced by spinning at 14,000 xg through plastic mesh, before being washed using two successive washes with 6 M urea and 100 mM ammonium bicarbonate in 50% acetonitrile, and subjected to in-gel digestion. Peptides extracted from gel pieces were dried under vacuum, dissolved in 0.1% formic acid and run using a Q-Exactive hybrid mass spectrometer (Thermo Fisher Scientific), coupled online to nanoflow HPLC. For both FASP and GASP-derived peptides, the mass spectrometer was operated in a 'top10' mode, whereby the ten most abundant new precursors observed per survey scan are subjected to product ion analysis by collisional dissociation (Michalski et al., 2011). Product ion spectra were then subjected to parsing by Mascot Distiller using standard settings for high resolution product ion spectra as recommended by the manufacturer, and database searching using an in-house Mascot server (Matrix Sciences, London), against a hybrid database comprised of sequences derived from *P. falciparum* (download date 20th July 2015), alongside common contaminant proteins from artefactual sources frequently seen in pulldown proteomics experiments (Mellacheruvu et al., 2013). Data were compared using Scaffold Q+ (v. 4.3.3, Proteome Software, Portland IR).

Protein Modelling

Structural modelling of *Pf*GBP2 was conducted using I-TASSER (Iterative Threading ASSEmblY Refinement) (Yang et al., 2015). Queries were submitted via the online server (<http://zhanglab.ccmb.med.umich.edu/I-TASSER/>) and modelling was conducted *ab initio* without optional guide templates or specification of secondary structure. Queries were submitted in October 2018.

Plasmid Construction

To clone the *Pf*GBP2 (*PF3D7_1006800*) gene for recombinant protein production, the full-length transcript minus the stop codon was amplified by PCR from *P. falciparum* cDNA and cloned into the pET-28a+ expression vector between the *Bam*HI and *Xho*I sites, resulting in a construct with dual 6xHis tags at the N and C termini. To clone plasmids for 3' HA or Ty tagging of the endogenous *Pf*GBP2 gene via the pSLI system, the latter half of the gene was cloned into a pSLI 3' HA tagging vector (Birnbaum et al., 2017) between the *Not*I and *Kpn*I sites. Subsequently, the 3' half of the gene downstream of an endogenous *Bgl*II site, together with the HA tag, were excised and replaced by the same gene portion with a 2xTy tag (this fusion having been previously generated in an episomal overexpression vector which was not tolerated by 3D7 parasites). All primer sequences are provided in Table S2.

Recombinant Protein Production

The pET-28a+ expression construct was transferred into BL21 (DE3)/pLys strain (Stratagene) and protein production was

induced at 37°C with 1 mM IPTG (isopropyl- β -D-thiogalactopyranoside) for 3h. Bacteria were lysed with Bugbuster reagent (Merck Millipore) plus complete protease inhibitors (Roche), and purification was conducted using gravity flow over nickel affinity resin (Thermo-Fisher Scientific) as previously described (North et al., 2005). Purified protein was further concentrated using Amicon Ultra Centrifugal Filter Units (Merck Millipore).

Western Blotting

Parasite fractions for western blotting were prepared as previously described (Voss et al., 2002). Samples were loaded onto 4-12% polyacrylamide gels and electrophoresed at 100V for 60 mins. Electrophoretic transfer to nitrocellulose membrane was carried out at 100V for 60 mins. Membranes were blocked in TBST with 5% milk protein and probed with the following antibodies: 1:2000 anti-Ty1 (Invitrogen), then 1:1500 goat anti-mouse IgG-HRP (Dako); 1:1000 anti-HA (Roche), then 1:1500 goat anti-rat IgG-HRP (Biolegend); anti-histone H4 (Abcam), then 1:1000 goat anti-rabbit IgG-HRP (Abcam); or 1:1000 13.3 anti-GAPDH (European Malaria Reagent Repository), then 1:1500 goat anti-mouse IgG-HRP (Dako). Membranes were washed for 3 x 5 mins in TBST after each antibody step. Clarity Western ECL substrate (Bio-Rad) was added for 3 mins and blots were imaged using a FluorChemM chemiluminescent detection camera (ProteinSimple).

Recombinant protein was blotted with anti-His antibody using the same method: 1:2000 mouse anti-tetra-His IgG (Qiagen); 1:1500 goat anti-mouse IgG-HRP (Dako). Coomassie staining of recombinant protein after gel electrophoresis was performed by addition of 0.1% Brilliant blue R-250 for 20 mins (Fisher), then destaining in 40% methanol 10% glacial acetic acid.

Electrophoretic Mobility Shift Assay

EMSA were optimized and performed using a LightShift optimization and control system (Thermo Scientific). Protein extracts containing *Pf*GBP2, and control extracts lacking the recombinant protein, were made as above. Crude extracts in Bugbuster reagent were purified using HisPur Ni-NTA resin (Thermo Scientific) and run through a Poly-Prep Chromatography Column (BioRad) by gravity. Purified GBP2 protein was used in western blotting and bacterial extracts +/- *Pf*GBP2 were used for all EMSAs.

Single-stranded oligonucleotides were labelled using a 3' biotin end-labelling kit (Thermo Scientific). Binding reactions were carried out at room temperature with 1 μ g of GBP2 in the presence of 50ng dIdC. Reactions were pre-incubated for 5 mins prior to the addition of 20 fmol of labelled probe, then incubated for a further 20 mins at room temperature. Unlabelled competitor oligonucleotides of the same sequence were added in 200-fold excess relative to probe. Reactions were then run at 100V on a cooled 0.5x TBE-acrylamide gel (4-12% gradient) for 100 mins. Samples were blotted onto nylon membrane (Perkin Elmer) at 380 mA for 60 mins, crosslinked under UV (125mJ) and then blocked, washed and developed using a LightShift chemiluminescent detection kit (Thermo Scientific). EMSA supershift assays were performed similarly, with prior 1h incubation of the biotinylated oligonucleotide with the anti-G4 antibody BG4 (Merck Millipore).

Dot Blotting

To allow G4 folding, DNA oligonucleotides were heated to 90°C for 5 mins before the addition of 100μM Tris buffer pH 7.8 and 100μM KCl, then cooled from 90°C to room temperature at a rate of 5°C/5 min. Alternatively, oligonucleotides were folded in increasing concentrations of LiCl instead of KCl, up to 1M. 5μl of oligonucleotides (1μM) were then spotted on to nitrocellulose membrane (Perkin Elmer) and crosslinked under UV (125mJ) for 5 mins. Membranes were washed and blocked as per western blotting protocol and probed with 1:1500 BG4 (Merck Millipore), 1:1500 DYKDDDK tag (anti-flag, Cell Signalling), and 1:1500 Goat anti-rabbit IgG-HRP (Abcam).

Thioflavin T Fluorescence Assay

Oligonucleotides at 20μM were treated with KCl or LiCl as above for dot blotting, then mixed with Thioflavin T (Sigma Aldrich) at a final concentration of 80μM and incubated at room temperature for 5 mins. 40μl of each oligonucleotide mixture was transferred in triplicate to the wells of a 96 well black, Uclear plate (Greiner), and analyzed using a FLUOstar Omega plate reader (BMG Labtech) at Ex. 420nm, Em. 480nm. *Pf*GBP2 competition assays were performed in the same way, with the addition of increasing concentrations of purified *Pf*GBP2, or BSA as a control, prior to the addition of ThT.

Immunofluorescence

Parasitized erythrocytes were smeared onto microscope slides and fixed in 4% formaldehyde/PBS for 10 mins, rinsed twice in PBS, treated with 0.03% triton/PBS for 10 mins, blocked with 1% BSA/PBS for 30 mins, then incubated with the following antibodies: 1:500 anti-Ty1 (Invitrogen), then 1:1000 Alexa Fluor 546-conjugated anti-rat IgG (Thermo Fisher Scientific); and/or 1:500 anti-HA (Roche), then 1:1000 Alexa Fluor 488-conjugated anti-rat IgG (Thermo Fisher Scientific). Slides were washed for 3 x 5 mins in PBS after each antibody step and in the penultimate wash 2μg/ml 4',6-diamidino-2-phenylindole (DAPI) (Molecular Probes) was added. Slides were mounted with ProLong Diamond antifade mountant (Thermo Fisher Scientific) and imaged with a Zeiss LSM700 Confocal Microscope.

ChIP-seq

Chromatin Preparation

Cultures of $1.6\text{--}3.6 \times 10^9$ sorbitol-synchronized parasites at 30–36 hpi were used for ChIP. Chromatin was crosslinked with 1% formaldehyde in culture media for 10 minutes at 37°C, then quenched with glycine at a final concentration of 0.125 M. Parasites were extracted by lysis with 0.05% saponin in PBS. Nuclei were extracted by gentle homogenisation in cell lysis buffer [10mM Tris pH 8.0, 3mM MgCl₂, 0.2% NP-40, 1x Pierce protease inhibitor (Thermo Fisher)] and centrifugation at 2000 rpm for 10 minutes in 0.25 M sucrose cushion in cell lysis buffer. Harvested nuclei were snap-frozen in 20% glycerol in cell lysis buffer. Thawed nuclei were resuspended in sonication buffer (50mM Tris-HCl, 1% SDS, 10mM EDTA, 1x protease inhibitor (Sigma-Aldrich), pH 8.0) and sonicated for 20–24 cycles of 30s ON, 30s OFF (setting high, Bioruptor™ Next Gen, Diagenode) (Fraschka et al., 2018).

Chromatin Immunoprecipitation

Each ChIP reaction was set up with 500 ng sonicated chromatin incubated in incubation buffer (0.15% SDS, 1% Triton-X100, 150mM NaCl, 1mM EDTA, 0.5mM EGTA, 1x protease inhibitor (Sigma-Aldrich), 20 mM HEPES, pH 7.4) with either 400 ng of α-HA (Roche 12158167001) or 1μl α-Ty (BB2, in-house hybridoma supernatant), together with 10 μl protA and 10 μl protG Dynabeads suspension (Thermo Fisher Scientific). For each sample, eight ChIP reactions were prepared and incubated overnight rotating at 4°C. Beads were washed twice with wash buffer 1 (0.1% SDS, 0.1% DOC, 1% Triton-X100, 150 mM NaCl, 1 mM EDTA, 0.5 mM EGTA, 20 mM HEPES, pH 7.4), once with wash buffer 2 (0.1% SDS, 0.1% DOC, 1% Triton-X100, 500 mM NaCl, 1 mM EDTA, 0.5 mM EGTA, 20 mM HEPES, pH 7.4), once with wash buffer 3 (250 mM LiCl, 0.5% DOC, 0.5% NP-40, 1 mM EDTA, 0.5 mM EGTA, 20 mM HEPES, pH 7.4) and twice with wash buffer 4 (1 mM EDTA, 0.5 mM EGTA, 20 mM HEPES, pH 7.4). Each wash step was performed for 5 min at 4°C while rotating. Immunoprecipitated chromatin was eluted in elution buffer (1% SDS, 0.1M NaHCO₃) at room temperature for 20 min. The eluted chromatin samples and the corresponding input samples (sonicated input chromatin containing 500 ng DNA) were de-crosslinked in 1% SDS/0.1M NaHCO₃/1M NaCl at 65°C for at least 4h while shaking, followed by column purification (PCR Purification Kit, Qiagen) and elution in 200ul EB buffer.

Quantitative PCR

qPCRs were performed with 5μL ChIP-ed DNA against a 10x dilution series of input DNA using iQ™ SYBR Green Supermix (Biorad) together with primers (Table S2) mixed according to manufacturers' instructions on a C1000 Touch CFX96 Real-Time System (Biorad).

Co-Immunoprecipitation and Mass Spectrometry

800ml of 3D7 WT and 3D7 GBP2-3HA cultures were saponin-treated to release the parasites ($1\text{--}2 \times 10^{10}$ parasites per sample, conducted in biological duplicate for GBP2). Parasites were re-suspended in lysis buffer (1% Triton, 50mM HEPES, 150mM NaCl, 1mM EDTA) and subjected to a freeze-thaw cycle three times, before treating with 1 unit of DNaseI for 10mins at 37°C (Thermo Fisher Scientific). Samples were then centrifuged for 30 mins at 4°C at 14500 rcf. Supernatant was added to Protein G magnetic beads (Pierce) pre-washed three times in wash buffer (0.1% Triton, 50mM HEPES, 150mM NaCl) and incubated for 1 h at 4°C. Magnetic beads were removed by magnet and 1mg/ml of anti-HA antibody (Roche) was added to the proteins for incubation overnight at 4°C. Following incubation, a new aliquot of Protein G magnetic beads was washed, added to the samples and incubated for 1 h at 4°C. Beads were again removed by magnet. Proteins were eluted by incubating in 30μl of 0.5mg/ml Influenza Hemagglutinin (HA) Peptide (Strattech Scientific) dissolved in elution buffer (0.1M Tris pH 7.4, 150mM NaCl, 0.1% SDS, 0.5% NP40) and 1μl of 0.1M DTT (Invitrogen) was added to samples. Eluted protein samples were boiled in 4x

sample loading buffer (Invitrogen) for 10 mins at 90°C. Samples were loaded onto a 4-12% polyacrylamide gel (BioRad) and electrophoresed at 150V for 10 mins, until the sample had run through the stacking wells.

Protein-containing gel was excised and cut into 1mm² pieces, destained, reduced using DTT, alkylated using iodoacetamide and subjected to enzymatic digestion with sequencing grade trypsin (Promega, Madison, WI, USA) overnight at 37°C. After digestion, the supernatant was pipetted into a sample vial and loaded onto an autosampler for automated LC-MS/MS analysis.

LC-MS/MS experiments were performed using a Dionex Ultimate 3000 RSLC nanoUPLC system (Thermo Fisher Scientific) and a Q Exactive Orbitrap mass spectrometer (Thermo Fisher Scientific). Separation of peptides was performed by reverse-phase chromatography at a flow rate of 300 nl/min and a Thermo Scientific reverse-phase nano Easy-spray column (Thermo Scientific PepMap C18, 2µm particle size, 100A pore size, 75 µm i.d. x 50 cm length). Peptides were loaded onto a pre-column (Thermo Scientific PepMap 100 C18, 5µm particle size, 100A pore size, 300µm i.d. x 5mm length) from the Ultimate 3000 autosampler with 0.1% formic acid for 3 mins at a flow rate of 15µl/min. After this period, the column valve was switched to allow elution of peptides from the pre-column onto the analytical column. Solvent A was water + 0.1% formic acid and solvent B was 80% acetonitrile, 20% water + 0.1% formic acid. The linear gradient employed was 2-40% B in 90 mins (the total run time including column washing and re-equilibration was 120 mins).

The LC eluant was sprayed into the mass spectrometer by means of an Easy-spray source (Thermo Fisher Scientific Inc.). All *m/z* values of eluting ions were measured in an Orbitrap mass analyzer, set at a resolution of 35000 and scanned between *m/z* 380-1500. Data dependent scans (Top 20) were employed to automatically isolate and generate fragment ions by higher energy collisional dissociation (HCD, Normalised collision energy (NCE):25%) in the HCD collision cell and measurement of the resulting fragment ions was performed in the Orbitrap analyser, set at a resolution of 17500. Singly charged ions and ions with unassigned charge states were excluded from being selected for MS/MS and a dynamic exclusion of 60 seconds was employed.

Post-run, all MS/MS data were converted to mgf files and the files were then submitted to the Mascot search algorithm (Matrix Science, London UK, version 2.6.0) and searched against a common contaminants database (125 sequences; 41129 residues); and the CCP_Plasmodium_falciparum Plasmodium_falciparum_20190315 (5449 sequences; 4173922 residues) database. Variable modifications of oxidation (M) and deamidation (NQ) were applied as well a fixed modification of carbamidomethyl (C). The peptide and fragment mass tolerances were set to 20ppm and 0.1 Da, respectively. A significance threshold value of *p*<0.05 and a peptide cut-off score of 20 were also applied.

Data were then analysed using MaxQuant software version 1.6.17.0 (Elias and Gygi, 2007). Files were searched against Plasmodium falciparum 3D7 PlasmoDB-50 annotated proteins database (downloaded February 2021). Protein N-terminal acetyl and methionine oxidation were set as variable modifications, whilst cysteine carbidomethylation was a fixed modifier. C-

terminal arginine was set as the enzyme specificity and trypsin as the protease. Minimum peptide length was 7 amino acids and maximum for peptide recognition was 4600 Da.

GO Enrichment Analysis

The analysis tool in PlasmoDB (Aurrecochea et al., 2009) was used to obtain GO terms for all gene IDs encoding proteins found by co-immunoprecipitation. Enrichment of GO terms versus their representation in the whole genome was calculated within PlasmoDB, with a cutoff of *p*=0.05 for statistically significant enrichment. Correction for multiple comparisons was conducted by both Benjamini-Hochberg FDR and the more stringent Bonferroni method, and GO terms with *p*-values remaining below 0.05 were considered to be enriched.

RESULTS

A PICh Protocol for Plasmodium Parasites

Telomere length in Plasmodium appears to be a complex trait. **Figure 1A** shows that there is striking variation in the average length at which telomeres are maintained in different strains of *P. falciparum*, yet their length is relatively stable per strain during *in vitro* culture [**Figure 1A**, (Merrick et al., 2012)]. To investigate the proteins involved in this phenomenon, we set out to identify new telosome components in the *P. falciparum* parasite.

The published protocol for PICh in HeLa cells was adapted for *P. falciparum* (**Figure 1B**), using DNA probes adapted to the Plasmodium telomere sequence (GGGTT(T/C)A with 67% T, 33% C at the variable position), and crosslinking the chromatin after releasing parasites from host erythrocytes and washing them thoroughly to reduce contamination from host haemoglobin. Parasite chromatin extracts were probed in parallel with either a telomere-repeat probe or a scrambled probe and the proteins thus purified were identified by mass spectrometry. Yields were initially very limited (a first experiment produced only five *P. falciparum* proteins, including histones and other highly-abundant proteins like elongation factor 1 alpha, which were largely similar in the telomere-probe and control-probe conditions). However, a second experiment using the alternative method of gel-aided rather than filter-aided sample preparation for mass spectrometry gave a much greater yield of over 30 *P. falciparum* proteins. There remained a high representation of histones and other abundant proteins (**Table S1**), and indeed similar issues were reported when PfTRZ and PfAP2Tel were previously identified *via* a different methodology (pull-down from nuclear extract onto telomeric versus scrambled DNA probes). In these studies only 12 out of 109 (Bertschi et al., 2017) or 7 out of 100 (Sierra-Miranda et al., 2017) of the proteins identified were telomere-probe-specific, but *bona fide* telomere proteins could nevertheless be selected. Similarly, one interesting candidate protein emerged from the PICh dataset.

PICh Identifies PfGBP2 as a Putative Telomere-Binding Protein

The most promising candidate protein found by PICh was encoded by the gene PF3D7_1006800: a putative homologue of *S. cerevisiae*

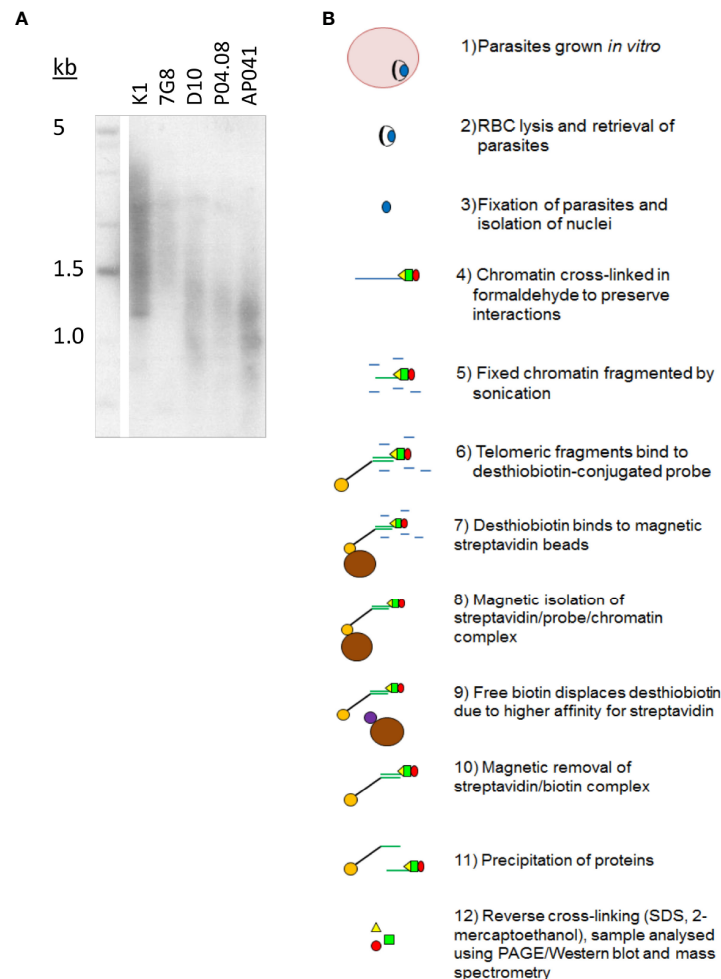


FIGURE 1 | *Plasmodium* telomeres vary in their set-point lengths. **(A)** Telomere Restriction Fragment Southern blot showing variation in telomere lengths in geographically diverse strains of *P. falciparum* (K1, Thailand; 7G8, Brazil; D10, Papua New Guinea; P04.08, Senegal; AP041, Nigeria). **(B)** Schematic showing the process of PICCh in *P. falciparum*.

GBP2. *Pf*GBP2 is a protein of 246 amino acids encoding two RNA Recognition Motif (RRM) domains. These domains are well-characterized to occur in proteins that bind to single-stranded nucleic acids, either DNA or RNA (Query et al., 1989). The RRM structure consists of two helices and four strands in an alpha/beta sandwich which can bind to a strand of nucleic acid, and indeed *Pf*GBP2 was modelled with two RRM domains, joined by a less structured linker region (Figure 2A). In contrast, *Sc*GBP2 is a larger protein with three RRM domains, the third of which is divergent and acts instead as a protein-protein interaction domain (Martinez-Lumbreras et al., 2016) (Figure 2B). This third domain is lacking in the *P. falciparum* homolog and both RRM domains in *Pf*GBP2 are actually most similar to RRM2 in *Sc*GBP2, which is the principal nucleic-acid-binding domain (Martinez-Lumbreras et al., 2016) (Figure 2C).

Several transcriptomic datasets collated in PlasmoDB (Aurrecochea et al., 2009) show that *Pf*GBP2 is expressed at all lifecycle stages, while polysomal RNA studies report that the

gene transcript is maximally translated in trophozoites (Painter et al., 2018). In proteomic studies, *Pf*GBP2 is in the nuclear proteome, as expected (Oehring et al., 2012). Overall, data from multiple sources including protein modelling, transcriptomics and proteomics all supported the probability that *Pf*GBP2, being nuclear, nucleic-acid-binding and maximally expressed at replicative stages, could be a *bona fide* telomere protein.

Recombinant *Pf*GBP2 Binds to G-Rich Telomere Sequences

To confirm that *Pf*GBP2 can actually bind to telomeric DNA, we produced a recombinant version of the protein (Figure 3A). Histidine-tagged *Pf*GBP2, expressed in *E. coli*, could be purified primarily as a full-length protein of ~35 kDa (predicted MW of 34 kDa including tags; some breakdown products were also co-purified, probably as single RRM domains after degradation at the flexible region). Extracts containing *Pf*GBP2 were then used in electrophoretic mobility shift assays (EMSAs) on a DNA

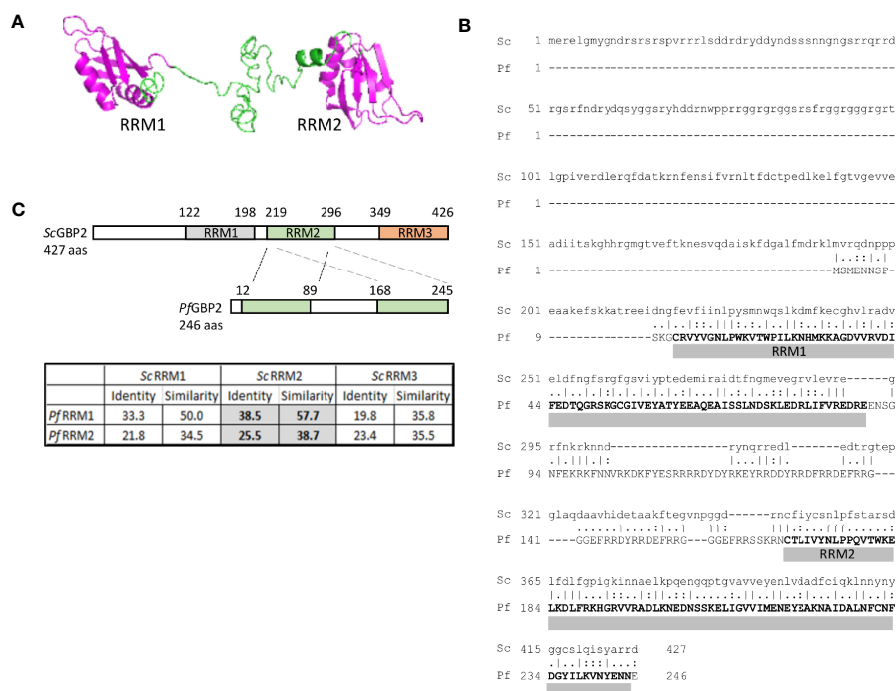


FIGURE 2 | PICh identifies *PfGBP2*, a RRM-motif protein. **(A)** Protein structure model for *PfGBP2*, modelled using iTASSER (C-score -2.44). **(B)** Amino acid alignment of *PfGBP2* with ScGBP2. Grey bars denotes the regions containing Prosite RRM motifs. **(C)** Schematic showing the domain structure of ScGBP2 and *PfGBP2*. Table shows amino acid identity and similarity scores from pairwise alignments of the individual RRM domains: grey highlighted boxes show that both RRM domains from *PfGBP2* score most highly against ScGBP2 RRM2.

oligonucleotide consisting of a series of G-rich telomere repeats. This DNA was clearly retarded due to protein binding, which was not the case with either a scrambled oligonucleotide or a sequence comprised of A and T bases only (**Figure 3B**). Thus, *PfGBP2* evidently has a tropism for G-rich DNA, and furthermore for G-triad motifs (e.g. GGGTTTA), since scrambling this sequence abrogated binding.

RRM-domain proteins commonly bind RNA as well as DNA, so we investigated whether *PfGBP2* might also bind to RNA: EMSAs performed with G-rich telomere repeat RNA oligos showed that this was indeed the case (**Figure 3C**). Unlike the behavior seen in the DNA EMSA, *PfGBP2* was not efficiently competed off by unlabeled RNA, and was only partially competed off by unlabeled DNA.

Recombinant *PfGBP2* Binds to G-Quadruplex DNA

Next, we sought to determine whether the G-rich telomere repeat sequence was actually folded into a G4 when bound to *PfGBP2*, since it was theoretically possible that the DNA would be bound either as a G4 or as a linear strand. Two independent assays showed that the *Plasmodium* telomere repeat sequences used here can indeed fold into G4s in the presence of K^+ ions, which are required to stabilize quadruplex structures. **Figure 4A** shows a dot-blot with the G4-structure-specific antibody BG4 (Biffi et al., 2013), while **Figure 4B** shows fluorescent emission from a G4-specific dye, thioflavin T, which induces G4 folding and

fluoresces strongly only when bound to a G4 (Mohanty et al., 2013; Renaud de la Faverie et al., 2014). In both these assays, two variants on the *Plasmodium* telomere repeat (GGGTT(T/C)A) were tested, with different representations at the variable T/C position ('G-rich 1' and 'G-rich 2', all oligonucleotides are listed in **Table S2**). Both variants behaved identically: when folded in the presence of K^+ they showed strong binding to the G4-specific antibody and strong emission from thioflavin T. By contrast, the equivalent treatment in the presence of Li^+ ions, which destabilize G4s, yielded lower signals in both assays, similar to those of a control A/T-only sequence. We also confirmed that four G-triads were required to form a G4, because the same sequence truncated to just three repeats did not give a strong G4 signal in either assay.

Having confirmed the specificities of these two assays for G4s, the BG4 antibody was then added to the DNA EMSA, where it exerted an additional shift upon the oligo-*PfGBP2* complex, showing that the complex indeed contained G4 DNA (**Figure 4C**). Finally, *PfGBP2* was also able to interfere with thioflavin T emission when added to a mixture of thioflavin T and DNA (**Figure 4D**), whereas an irrelevant protein (bovine serum albumin) could not. This interference could potentially occur *via* *PfGBP2* binding to the DNA and dampening the emission from the dye in its G4-bound form; alternatively, it could occur because *PfGBP2* actually competes the dye off the G4 motif. In summary, multiple independent assays showed that *PfGBP2* is a *bona fide* G4-binding protein.

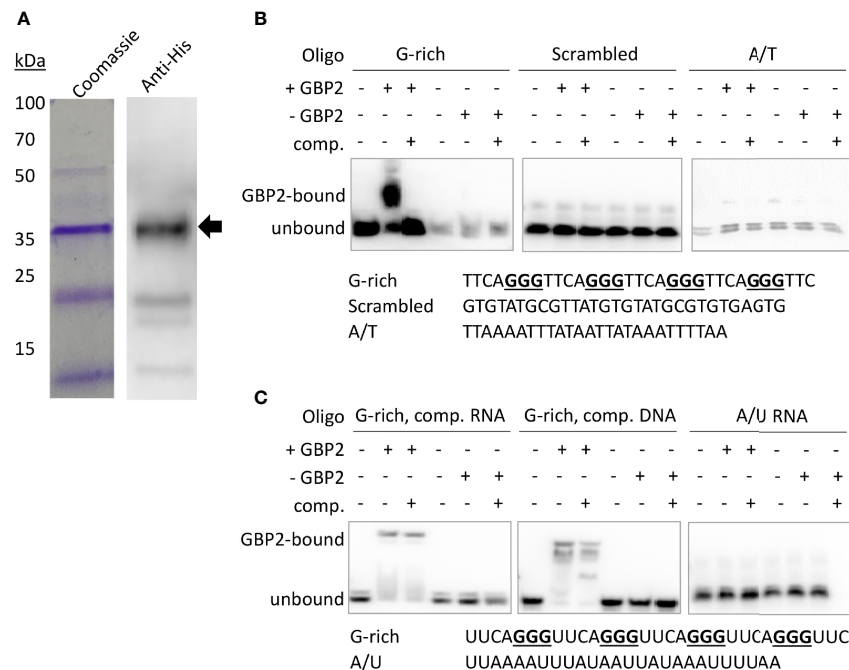


FIGURE 3 | *P*GBP2 binds to telomeric DNA and RNA sequences. **(A)** Recombinant 6x His-tagged *P*GBP2 (full-length protein marked with arrow), expressed in *E. coli* and purified via nickel resin. Coomassie-blue-stained gel and western blot against the 6x His-tag. Images are representative of several independent preparations. **(B)** EMSA assays with the indicated oligonucleotides and bacterial extract containing *P*GBP2 (+GBP2), or equivalent extract containing no recombinant protein (-GBP2) in the control condition. 'Comp', unlabeled competitor DNA of the same sequence. Images are representative of several independent experiments. (In all experiments, equal quantities of the A/T control oligo appeared less brightly: this was due to relatively inefficient biotinylation of the A/T oligo compared to the G-rich oligos.) **(C)** EMSA assay as in **(B)**, using RNA instead of DNA. Competition was attempted with an excess of either unlabeled RNA or unlabeled DNA.

***Pf*GBP2 Is Found in Both the Nucleus and Cytoplasm in Erythrocytic Parasites**

Having characterized *PfGBP2* *in silico* and *in vitro*, we proceeded to investigate its properties *in vivo*. A gene knockout of *PfGBP2* was not attempted because this was found to be very deleterious in a recent forward-genetics screen for essential genes in *P. falciparum* (Zhang et al., 2018): *PfGBP2* mutants had a fitness score of -2.5, only slightly higher than -3 in telomerase reverse transcriptase (TERT) knockouts. Instead, overexpression of the *PfGBP2* gene was attempted in 3D7 parasites, *via* a tagged version of the gene transfected in episomally in addition to the endogenous copy. No transgenic parasites were obtained after three separate transfections with two different plasmids, carrying *PfGBP2* with two different C-terminal tags (HA and Ty) and two different selectable markers: this strongly suggested that overexpression of tagged *PfGBP2* protein was also deleterious. Ultimately, in order to localize the *PfGBP2* protein in blood-stage parasites, the endogenous gene was C-terminally tagged with a triple HA tag using the selection-linked integration system (Birnbaum et al., 2017). Correct tagging was confirmed by PCR and the tagged protein was detected in parasites by both western blot and immunofluorescence (**Figure 5**).

Western blotting revealed PfGBP2-3HA in the nucleoplasm and chromatin-bound fractions of all erythrocytic parasite stages (**Figure 5A**), as would be expected for a telomere-binding protein, but it was also found in the cytoplasm at all stages,

most prominently in trophozoites. Consistently, *Pf*GBP2-3HA was detected by immunofluorescence in individual parasites as peri-nuclear foci which are characteristic of telomeric factors (**Figure 5B**): these appeared at all stages but *Pf*GBP2-3HA was always present in the parasite cytoplasm as well.

To further confirm that the peri-nuclear foci of *Pf*GBP2-3HA did represent telomeres, the *Pf*GBP2 gene was Ty-tagged in a line already expressing the well-characterised telomeric factor heterochromatin protein 1 (HP1) with an HA tag (Flueck et al., 2009) (**Figure 5C**). The two tags, HP1-HA and *Pf*GBP2-Ty, partially colocalised, particularly in late schizonts, with each merozoite bearing a perinuclear focus of both GBP2 and HP1. At earlier stages, however, HP1 foci were discrete, whereas *Pf*GBP2 was dispersed throughout the parasite (**Figure 5D**). This was consistent with the fractionation of these parasites showing that HP1 was entirely restricted to the nucleus whereas *Pf*GBP2 was not (**Figure 5C**). The tropism of GBP2 for RNA as well as DNA may explain the widespread localization of this protein. (When tagged with Ty versus HA, GBP2 was not always identically distributed, for example in trophozoites the Ty-tagged version appeared to be more chromatin-bound whereas the HA-tagged version was more nucleoplasmic. This may be because the two different tags – although they do not functionally compromise the protein – could influence how strongly it binds to DNA, and therefore how readily salt-extractable it is during biochemical fractionation.)

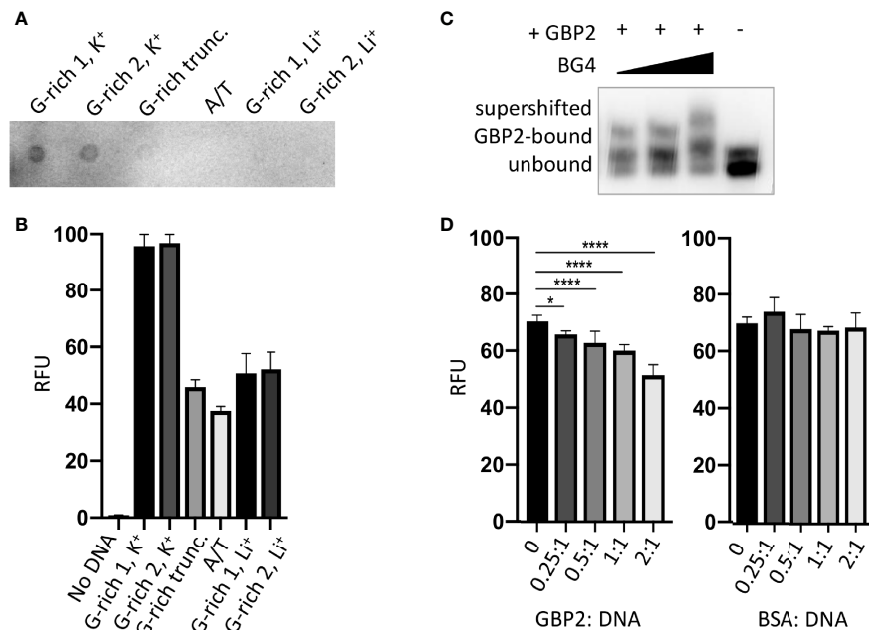


FIGURE 4 | *Pf*GBP2 binds to G4-folded DNA. **(A)** Dot-blot of the indicated oligonucleotides (Table S2) probed with the G4-specific antibody BG4. Image is representative of triplicate experiments. **(B)** Fluorescence emission from the indicated oligonucleotides in the presence of the G4-specific dye thioflavin T (ThT). Error bars represent SD from technical triplicates. **(C)** EMSA assay as in Figure 3B, with BG4 antibody added to the DNA/*Pf*GBP2 complex at 0.5:1, 1:1 and 2:1 molar ratio of antibody to purified *Pf*GBP2. **(D)** Fluorescence emission from G-rich oligonucleotide 1 bound to thioflavin T, as in (B), with the addition of increasing quantities of purified *Pf*GBP2 or the control protein BSA. Protein : DNA molar ratios between 0.25:1 and 2:1 were tested. * $P < 0.05$, **** $P < 0.0001$.

Finally, to define the binding sites of *Pf*GBP2 throughout the genome, chromatin immunoprecipitation (ChIP) was attempted. A ChIP/dot-blot suggested that *Pf*GBP2-3HA was modestly enriched on telomeric DNA (Figure S1A), but ChIP-seq for either *Pf*GBP2-3HA or *Pf*GBP2-Ty failed to give signals significantly above background at any locus. This compared with strong signals from the established sub-telomeric protein HP1 (Flueck et al., 2009) that was co-expressed in the *Pf*GBP2-Ty line. In a series of gene-directed ChIP experiments (Figure S1B), HP1 was enriched by over 50-fold at all sub-telomeric loci compared to chromosome-internal loci, whereas *Pf*GBP2 was enriched by only ~2-fold at sub-telomeric and G4-encoding loci compared to chromosome-internal loci. This demonstrated that the ChIP experiment was conducted correctly but that *Pf*GBP2 did not, in our hands, give a strong enough signal for a meaningful ChIP-seq experiment.

The Interactome of *Pf*GBP2 Suggests Roles in Both DNA and RNA Metabolism

To learn more about the potential biological roles of *Pf*GBP2, the HA-tagged protein was immunoprecipitated (IP) and its interactome was obtained *via* mass spectrometry. Duplicate IP experiments were conducted, yielding a total of 29 reproducible hits specific to *Pf*GBP2 (i.e. absent from an identical control experiment using wildtype parasites) (Figure 6A and Table S3). A larger group of 187 proteins appeared uniquely in just one of the two *Pf*GBP2 IP experiments (Figure 6B and Table S3).

Amongst the reproducible hits there was a clear preponderance of RNA-associated proteins. Gene ontology terms including ‘cytosolic ribosome’, ‘ribonucleoprotein complex’, and various terms concerning mRNA editing and base modification were enriched in the interactome (Figure 6A and Table S4). A few DNA-binding proteins were also represented, including a zinc-finger protein (PF3D7_1317400), but DNA-related GO terms were not strongly enriched overall, and the known telomeric proteins *Pf*TRZ or *Pf*AP2Tel did not appear. A broader analysis of all 187 putative *Pf*GBP2-interacting proteins yielded similar results, i.e. a clear enrichment of RNA-associated proteins (Table S4), as well as a few DNA-associated proteins.

These results were compared with those of a recent study that used machine learning to infer a proteome-wide interactome for *P. falciparum* (Hillier et al., 2019). This reported that at least 17 of the top 50 interactors for *Pf*GBP2 were RNA-associated proteins, including several initiation factors and snRNP-associated proteins, while 5 out of 50 were DNA-associated proteins, including a DNA helicase, a DNA repair protein, a transcription factor and the High Mobility Group protein HMGB1. Only 5 out of these 50 top interactors appeared as *Pf*GBP2 interactors in one of our two datasets, including the transcription factor (PF3D7_1426100) and *Pf*HMGB1 (PF3D7_1202900). The latter protein is particularly interesting because in human cells, it was recently reported to interact with telomeric G4 DNA (Amato et al., 2019), raising the possibility

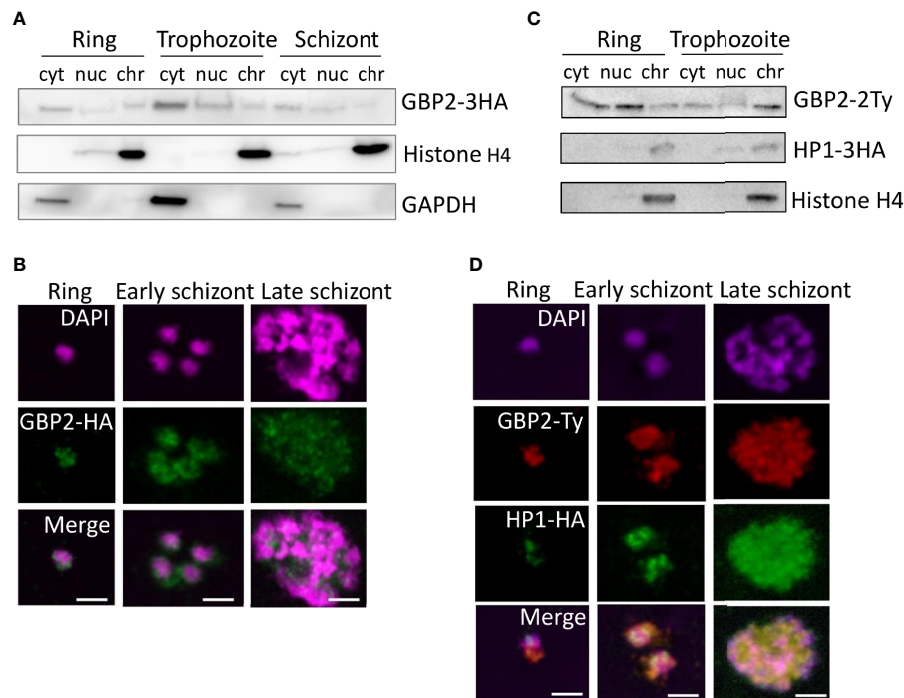


FIGURE 5 | *PfGBP2* is found in both the nucleus and cytoplasm in erythrocytic parasites. **(A)** Western blot of protein fractions (cyt, cytoplasm; nuc, nucleoplasm; chr, chromatin-bound) from ring, trophozoite and schizont 3D7 parasites expressing *PfGBP2*-3HA. Parallel control blots show histone H4 (nuclear) and glyceraldehyde 3-phosphate dehydrogenase (GAPDH, cytoplasmic). Images are representative of several independent fractionation experiments. **(B)** Representative immunofluorescence images of ring, trophozoite and schizont 3D7 parasites expressing *PfGBP2*-3HA, stained with an antibody against the HA tag and DAPI to identify parasite nuclei. Scale bar, 2µm. **(C)** Western blots as in **(A)** 3D7 parasites expressing *PfGBP2*-2Ty and HP1-3HA. **(D)** Representative immunofluorescence images as in **(B)**, parasites expressing *PfGBP2*-2Ty and HP1-3HA.

that *PfGBP2* and *PfHMGB1* might cooperate at telomeric G4s. Overall, the interactome strongly suggests that *PfGBP2* is present in RNA-binding as well as DNA-binding complexes.

DISCUSSION

This work set out to identify novel *Plasmodium* telosome components, and subsequently to characterise the GBP2 protein in *P. falciparum*. This involved the development of a ‘PICH’ method to pull down sequence-specific chromatin fragments from *P. falciparum*: a method that may have applications in future studies. PICH did identify a new telosome component, but it did not identify telomerase or other *Plasmodium*-specific telosome proteins, *PfTRZ* (Bertschi et al., 2017) or *PfAP2Tel* (Sierra-Miranda et al., 2017), which were both discovered *via* DNA-mediated pulldowns from parasite extracts. Those two reports did not identify one another’s proteins either, suggesting that no method is entirely comprehensive and that more proteins may be undiscovered. In PICH, however, the proteins are identified directly from native chromatin rather than from protein extracts that were subsequently re-bound to DNA probes, so there is potential to identify different sets of proteins. In particular, *PfGBP2* evidently targets the G-rich telomeric overhang, whereas *PfTRZ* and

PfAP2Tel (Myb- and AP2-domain proteins) bind to double-stranded DNA. The PICH technique may thus be better-placed to detect components of native telomeric chromatin that are not dsDNA-binders and are not pulled down by conventional DNA probes. Of note, however, a second study published during the preparation of this manuscript did identify *PfGBP2* *via* pulldown from parasite extracts, using a G-quadruplex-forming DNA sequence as the probe (Gurung et al., 2021).

Unlike *PfTRZ* and *PfAP2Tel*, *PfGBP2* is not unique to *Plasmodium*: homologues exist in eukaryotes including plants, yeast and humans, as well as other apicomplexans. In apicomplexans, GBP2 takes a short form with just two DNA-binding RRM domains. This is also the form found in plants, whereas in *S. cerevisiae* there is a third, divergent RRM domain which mediates protein-protein interaction with the THO/TREX mRNA export complex (Martinez-Lumbreras et al., 2016), and *ScGBP2* accordingly has dual functions in telomere binding and mRNA metabolism. Dual roles for such proteins are not unusual: some hnRNPs also bind to both G-rich RNA and telomeric ssDNA, and play roles in both RNA metabolism and telomere stabilisation (Tanaka et al., 2007). Indeed, we present here the first evidence that *PfGBP2* binds to G-rich RNA as well as DNA, and we also suggest that *PfGBP2* overexpression may be lethal, as *ScGBP2* overexpression is also lethal, owing to deregulated mRNA export (Windgassen and Krebber, 2003). Nevertheless,

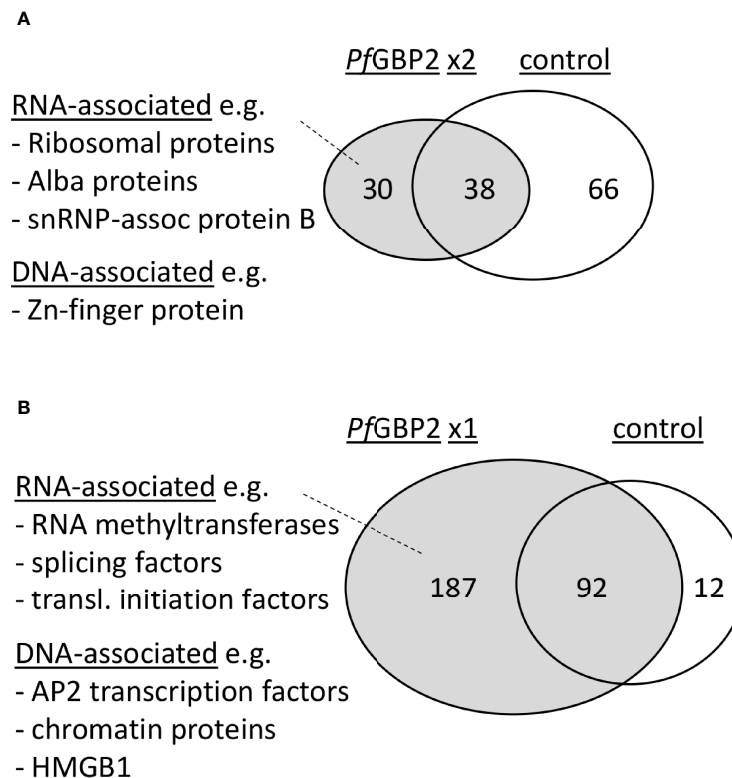


FIGURE 6 | *PfGBP2* interacts primarily with RNA-associated proteins. **(A)** Venn diagram showing the proportion of *PfGBP2*-interacting proteins found reproducibly in duplicate experiments but absent from the control experiment, with examples of representative proteins. **(B)** Venn diagram showing the larger number of *PfGBP2*-interacting proteins found in only one duplicate experiment, with examples of representative proteins.

the mRNA shuttling role played by *ScGBP2* is probably not directly conserved in *P. falciparum*, since *ScGBP2* requires its third domain for recruitment to nascent mRNA *via* TREX (Hurt et al., 2004), and not all components of the THO/TREX complex have even been identified in *Plasmodium* (Tuteja and Mehta, 2010). Therefore, any interaction with RNA may be mediated differently in parasites.

By contrast, it is clear that the role in telomeric DNA binding is conserved among yeasts, plants and apicomplexans. In *S. cerevisiae*, GBP2 lacks an essential telomeric function: it does protect telomeric ssDNA (Pang et al., 2003) but telomeres can still be maintained in its absence, albeit with mislocalisation of the Rap1 protein (Konkel et al., 1995). On the contrary, in plants, the telomere-binding role of GBP2 is essential. In *Nicotiana tabacum*, its loss causes severe developmental and chromosomal abnormalities with defective telomeres (Lee and Kim, 2010). *PfGBP2* has greater sequence similarity to the plant version than the yeast version, sharing 46% similarity with *NtGBP2*, and the *PfGBP2* gene was essential or near-essential in a *P. falciparum* genome-wide screen (Zhang et al., 2018). However, in their recent report on *PfGBP2*, Gurung and co-workers were able to achieve a knockout which surprisingly had no growth defect, nor was telomere maintenance affected (Gurung et al., 2021). A viable *P. berghei* GBP2 knockout has also been reported and

although its telomeres were not assessed, this parasite line did grow slowly (Niikura et al., 2020).

All these data call into question the expectation that GBP2 might be essential in *Plasmodium* and might play a role in telomere maintenance. It is possible that the genome-wide knockout screen was inaccurate for this particular gene, or that the previously reported knockouts may have been non-homogenous, particularly in *P. berghei*, since the genetic status of the knockout populations was not confirmed after long-term growth. A salient example in the literature reports the knockout of another essential telomeric protein, telomerase, *via* disruption of the *TERT* gene in *P. berghei*. Knockouts were briefly detected in bulk culture, but could never be cloned out before they were outgrown by healthier non-knockout parasites (Religa et al., 2014). This was probably because the telomeres in the knockout parasites quickly became critically degraded, so the authors concluded that *PbTERT* was essential. It would be interesting to establish whether outgrowth of non-knockout parasites could also occur if *GBP2* knockout parasites are debilitated by telomere loss.

Whether or not the telomere-binding role of *PfGBP2* is essential, the role clearly exists. On this point our work is consistent with that of Gurung et al., and also with a 2015 study (published in Spanish and not indexed *via* PubMed) which

previously identified *Pf*GBP2 *in silico* as a putative telosome component and confirmed that it binds specifically to G-rich telomere-repeat oligos *in vitro* (Calvo and Wasserman, 2015). The same property has been tested in other apicomplexans as well: *Eimeria* GBP2 was found at telomeres [via semi-quantitative ChIP-PCR (Zhao et al., 2014)], while *Cryptosporidium* GBP2 bound to telomeric DNA *in vitro* and specifically required its first RRM domain to do so (Liu et al., 2009). Our work goes further in examining the quadruplex-binding capacity of *Pf*GBP2: we conducted two independent assays to detect folded G4s in *Pf*GBP2-DNA complexes. The exact G4 binding mode of the protein is unknown, but if *Pf*GBP2 can directly compete with ThT to bind G4s (which is one explanation for the data in **Figure 4D**), then this would suggest an end-stacking mode, because thioflavin T is thought to end-stack onto the terminal G-quartet of a G4 (Mohanty et al., 2013). Further biophysical studies would be needed to confirm this. Finally, our work also goes further in exploring the binding of *Pf*GBP2 to RNA as well as DNA G4s. An affinity for RNA explains the broad cellular location of this protein, and is consistent with the presence of many RNA-binding proteins in the *Pf*GBP2 interactome,

The biological implications of *Pf*GBP2's clear affinity for DNA/RNA G4s still warrant further study. Gurung et al. reported that the G4 affinity is not restricted to telomeres: the protein was initially identified *via* pulldown on a non-telomeric G4, and it was then found throughout the genome *via* ChIP-seq (Gurung et al., 2021), although surprisingly the original G4 sequence used in the pulldown did not appear in the ChIP results. These authors reported that *Pf*GBP2 bound very broadly throughout the genome with an extreme enrichment of 500–2000 fold over input: this is an order of magnitude greater than that seen with the *bona fide* sub-telomeric protein HP1 (Flueck et al., 2009), and indeed than the enrichment seen in most other comparable ChIP experiments. By stark contrast, we were unable to obtain a meaningful ChIP signal, even when *Pf*GBP2 was identically C-terminally tagged in a chromatin preparation from which HP1 could be ChIPed with over 50-fold enrichment. Since Gurung *et al.* did not perform a similar ChIP control, the disparity between these two very similar experiments remains unexplained. Nevertheless, if *Pf*GBP2 does indeed bind very broadly to G-rich sequences throughout the *P. falciparum* genome, the protein could play interesting roles in G4 metabolism beyond telomeres.

Overall, the data presented here, together with the literature on GBP2 proteins across eukaryotes, indicate a triple role for *Pf*GBP2 – in telomeric G4 binding, in pan-genomic G4 binding, and in G4-RNA binding. *Pf*GBP2 is the first G4-binding protein to be identified in *Plasmodium*, and only the third protein, beside telomerase, to be identified as part of the divergent telosome in *Plasmodium*.

REFERENCES

- Amato, J., Cerofolini, L., Brancaccio, D., Giuntini, S., Iaccarino, N., Zizza, P., et al. (2019). Insights Into Telomeric G-Quadruplex DNA Recognition by HMGB1 Protein. *Nucleic Acids Res.* 47 (18), 9950–9966. doi: 10.1093/nar/gkz727
- Aurrecochea, C., Brestelli, J., Brunk, B. P., Dommer, J., Fischer, S., Gajria, B., et al. (2009). PlasmoDB: A Functional Genomic Database for Malaria Parasites. *Nucleic Acids Res.* 37 (Database issue), D539–D543. doi: 10.1093/nar/gkn814

DATA AVAILABILITY STATEMENT

The original contributions presented in the study are publicly available. This data can be found in the ProteomeXchange Consortium via the PRIDE partner repository with the dataset identifier PXD028903..

AUTHOR CONTRIBUTIONS

JE-S – Designed, optimized and conducted PICCh experiments. AJ – Conducted recombinant protein production, EMSA, ThT fluorescence, dot-blotting, western blotting and co-immunoprecipitation experiments. LR – Cloned the expression vector and conducted recombinant protein production. FT – Designed, optimized and conducted ChIP. SH – Coordinated and analysed data from mass spectrometry on PICCh samples. CM – Designed the study, conducted experiments (including Southern blotting, cloning, transfection and immunofluorescence assays), analysed data, made figures and wrote the manuscript. All authors contributed to the article and approved the submitted version.

FUNDING

The work was supported by the UK Medical Research Council (grant MR/L008823/1 to CM) and UK Biotechnology and Biological Sciences Research Council (grant BB/K009206/1 to CM).

ACKNOWLEDGMENTS

We acknowledge the Cambridge Centre for Proteomics and the Liverpool Centre for Proteome Research, particularly Philip Brownridge for expert assistance with PICCh mass spectrometry; Jerome Dejardin for helpful comments and advice regarding PICCh; Till Voss (Swiss TPH) for the HP1-HA parasite line; Richard Bartfai and Jonas Gockel (Radboud University) for help with ChIP-seq; Christian Happi (Redeemers' University) and the group of Dyann Wirth (Harvard University) for supplying parasite genomic DNAs from Nigeria and Senegal.

SUPPLEMENTARY MATERIAL

The Supplementary Material for this article can be found online at: <https://www.frontiersin.org/articles/10.3389/fcimb.2022.782537/full#supplementary-material>

- Bertschi, N. L., Toenhake, C. G., Zou, A., Niederwieser, I., Henderson, R., Moes, S., et al. (2017). Malaria Parasites Possess a Telomere Repeat-Binding Protein That Shares Ancestry With Transcription Factor IIIA. *Nat. Microbiol.* 2, 17033. doi: 10.1038/nmicrobiol.2017.33
- Biffi, G., Tannahill, D., McCafferty, J., and Balasubramanian, S. (2013). Quantitative Visualization of DNA G-Quadruplex Structures in Human Cells. *Nat. Chem.* 5 (3), 182–186. doi: 10.1038/nchem.1548
- Birnbaum, J., Flemming, S., Reichard, N., Soares, A. B., Mesen-Ramirez, P., Jonscher, E., et al. (2017). A Genetic System to Study Plasmodium

- Falciuparum Protein Function. *Nat. Methods* 14 (4), 450–456. doi: 10.1038/nmeth.4223
- Bottius, E., Bakhsis, N., and Scherf, A. (1998). Plasmodium Falciuparum Telomerase: *De Novo* Telomere Addition to Telomeric and Nontelomeric Sequences and Role in Chromosome Healing. *Mol. Cell. Biol.* 18 (2), 919–925. doi: 10.1128/MCB.18.2.919
- Calvo, E. T., and Wasserman, M. L. (2015). PfGBP: Una Proteína De Unión Al Telómero De Plasmodium Falciuparum. *Rev. Colomb. Quim.* 44 (1), 5–10. doi: 10.15446/rev.colomb.quim.v44n1.53977
- De Cian, A., Grellier, P., Mouray, E., Depoix, D., Bertrand, H., Monchaud, D., et al. (2008). Plasmodium Telomeric Sequences: Structure, Stability and Quadruplex Targeting by Small Compounds. *Chembiochem* 9 (16), 2730–2739. doi: 10.1002/cbic.200800330
- Deitsch, K., Driskill, C., and Welles, T. (2001). Transformation of Malaria Parasites by the Spontaneous Uptake and Expression of DNA From Human Erythrocytes. *Nucleic Acids Res.* 29 (3), 850–853. doi: 10.1093/nar/29.3.850
- Dejardin, J., and Kingston, R. E. (2009). Purification of Proteins Associated With Specific Genomic Loci. *Cell* 136 (1), 175–186. doi: 10.1016/j.cell.2008.11.045
- Elias, J. E., and Gygi, S. P. (2007). Target-Decoy Search Strategy for Increased Confidence in Large-Scale Protein Identifications by Mass Spectrometry. *Nat. Methods* 4 (3), 207–214. doi: 10.1038/nmeth1019
- Figueiredo, L. M., Freitas-Junior, L. H., Bottius, E., Olivo-Marin, J. C., and Scherf, A. (2002). A Central Role for Plasmodium Falciuparum Subtelomeric Regions in Spatial Positioning and Telomere Length Regulation. *EMBO J.* 21 (4), 815–824. doi: 10.1093/emboj/21.4.815
- Figueiredo, L. M., Pirrit, L. A., and Scherf, A. (2000). Genomic Organisation and Chromatin Structure of Plasmodium Falciuparum Chromosome Ends. *Mol. Biochem. Parasitol.* 106 (1), 169–174. doi: 10.1016/S0166-6851(99)00199-1
- Figueiredo, L. M., Rocha, E. P., Mancio-Silva, L., Prevost, C., Hernandez-Verdun, D., and Scherf, A. (2005). The Unusually Large Plasmodium Telomerase Reverse-Transcriptase Localizes in a Discrete Compartment Associated With the Nucleolus. *Nucleic Acids Res.* 33 (3), 1111–1122. doi: 10.1093/nar/gki260
- Fischer, R., and Kessler, B. M. (2015). Gel-Aided Sample Preparation (GASP)—a Simplified Method for Gel-Assisted Proteomic Sample Generation From Protein Extracts and Intact Cells. *Proteomics* 15 (7), 1224–1229. doi: 10.1002/pmic.201400436
- Flueck, C., Bartfai, R., Volz, J., Niederwieser, I., Salcedo-Amaya, A. M., Alako, B. T., et al. (2009). Plasmodium Falciuparum Heterochromatin Protein 1 Marks Genomic Loci Linked to Phenotypic Variation of Exported Virulence Factors. *PLoS Pathog.* 5 (9), e1000569. doi: 10.1371/journal.ppat.1000569
- Fraschka, S. A., Filarsky, M., Hoo, R., Niederwieser, I., Yam, X. Y., Brancucci, N. M. B., et al. (2018). Comparative Heterochromatin Profiling Reveals Conserved and Unique Epigenome Signatures Linked to Adaptation and Development of Malaria Parasites. *Cell Host Microbe* 23 (3), 407–420.e8. doi: 10.1016/j.chom.2018.01.008
- Freitas-Junior, L. H., Bottius, E., Pirrit, L. A., Deitsch, K. W., Scheidig, C., Guinet, F., et al. (2000). Frequent Ectopic Recombination of Virulence Factor Genes in Telomeric Chromosome Clusters of P. Falciuparum. *Nature* 407 (6807), 1018–1022. doi: 10.1038/35039531
- Gottschling, D. E., Aparicio, O. M., Billington, B. L., and Zakian, V. A. (1990). Position Effect at S. Cerevisiae Telomeres: Reversible Repression of Pol II Transcription. *Cell* 63 (4), 751–762. doi: 10.1016/0092-8674(90)90141-z
- Gurung, P., Gomes, A. R., Martins, R. M., Juranek, S. A., Alberti, P., Mbanga-Benet, D. E., et al. (2021). PfGBP2 Is a Novel G-Quadruplex Binding Protein in Plasmodium Falciuparum. *Cell. Microbiol.* 23 (4), e13303. doi: 10.1111/cmi.13303
- Harris, L. M., Monsell, K. R., Noulon, F., Famodimu, M. T., Smargiasso, N., Dambon, C., et al. (2018). G-Quadruplex DNA Motifs in the Malaria Parasite Plasmodium Falciuparum and Their Potential as Novel Antimalarial Drug Targets. *Antimicrobial Agents Chemother.* 62 (3), e01828-17. doi: 10.1128/AAC.01828-17
- Hillier, C., Pardo, M., Yu, L., Bushell, E., Sanderson, T., Metcalf, T., et al. (2019). Landscape of the Plasmodium Interactome Reveals Both Conserved and Species-Specific Functionality. *Cell Rep.* 28 (6), 1635–1647.e5. doi: 10.1016/j.celrep.2019.07.019
- Hurt, E., Luo, M. J., Rother, S., Reed, R., and Strasser, K. (2004). Cotranscriptional Recruitment of the Serine-Arginine-Rich (SR)-Like Proteins Gbp2 and Hrb1 to Nascent mRNA via the TREX Complex. *Proc. Natl. Acad. Sci. U. S. A.* 101 (7), 1858–1862. doi: 10.1073/pnas.0308663100
- Konkel, L. M., Enomoto, S., Chamberlain, E. M., McCune-Zierath, P., Iyadurai, S. J., and Berman, J. (1995). A Class of Single-Stranded Telomeric DNA-Binding Proteins Required for Rap1p Localization in Yeast Nuclei. *Proc. Natl. Acad. Sci. U. S. A.* 92 (12), 5558–5562. doi: 10.1073/pnas.92.12.5558
- Lee, Y. W., and Kim, W. T. (2010). Tobacco GTBP1, a Homolog of Human Heterogeneous Nuclear Ribonucleoprotein, Protects Telomeres From Aberrant Homologous Recombination. *Plant Cell* 22 (8), 2781–2795. doi: 10.1105/tpc.110.076778
- Lin, J. J., and Zakian, V. A. (1994). Isolation and Characterization of Two Saccharomyces Cerevisiae Genes That Encode Proteins That Bind to (TG1-3)N Single Strand Telomeric DNA *In Vitro*. *Nucleic Acids Res.* 22 (23), 4906–4913. doi: 10.1093/nar/22.23.4906
- Liu, C., Wang, L., Lancto, C. A., and Abrahamsen, M. S. (2009). Characterization of a Cryptosporidium Parvum Protein That Binds Single-Stranded G-Strand Telomeric DNA. *Mol. Biochem. Parasitol.* 165 (2), 132–141. doi: 10.1016/j.molbiopara.2009.01.013
- Martinez-Lumbreras, S., Taverniti, V., Zorrilla, S., Seraphin, B., and Perez-Canadillas, J. M. (2016). Gbp2 Interacts With THO/TREX Through a Novel Type of RRM Domain. *Nucleic Acids Res.* 44 (1), 437–448. doi: 10.1093/nar/gkv1303
- Mellacheruvu, D., Wright, Z., Couzens, A. L., Lambert, J. P., St-Denis, N. A., Li, T., et al. (2013). The CRAPome: A Contaminant Repository for Affinity Purification-Mass Spectrometry Data. *Nat. Methods* 10 (8), 730–736. doi: 10.1038/nmeth.2557
- Merrick, C. J., Huttenhower, C., Buckee, C., Amambua-Ngwa, A., Gomez-Escobar, N., Walther, M., et al. (2012). Epigenetic Dysregulation of Virulence Gene Expression in Severe Plasmodium Falciuparum Malaria. *J. Infect. Dis.* 205 (10), 1593–1600. doi: 10.1093/infdis/jis239
- Michalski, A., Damoc, E., Hauschild, J. P., Lange, O., Wieghaus, A., Makarov, A., et al. (2011). Mass Spectrometry-Based Proteomics Using Q Exactive, a High-Performance Benchtop Quadrupole Orbitrap Mass Spectrometer. *Mol. Cell. Proteomics* 10 (9), M111 011015. doi: 10.1074/mcp.M111.011015
- Mohanty, J., Barooah, N., Dhamodharan, V., Harikrishna, S., Pradeepkumar, P. I., and Bhasikuttan, A. C. (2013). Thioflavin T as an Efficient Inducer and Selective Fluorescent Sensor for the Human Telomeric G-Quadruplex DNA. *J. Am. Chem. Soc.* 135 (1), 367–376. doi: 10.1021/ja309588h
- Murat, P., and Balasubramanian, S. (2014). Existence and Consequences of G-Quadruplex Structures in DNA. *Curr. Opin. Genet. Dev.* 25, 22–29. doi: 10.1016/j.gde.2013.10.012
- Niikura, M., Fukutomi, T., Fukui, K., Inoue, S. I., Asahi, H., and Kobayashi, F. (2020). G-Strand Binding Protein 2 Is Involved in Asexual and Sexual Development of Plasmodium Berghiei. *Parasitol. Int.* 76, 102059. doi: 10.1016/j.parint.2020.102059
- North, B. J., Schwer, B., Ahuja, N., Marshall, B., and Verdin, E. (2005). Preparation of Enzymatically Active Recombinant Class III Protein Deacetylases. *Methods* 36 (4), 338–345. doi: 10.1016/j.jymeth.2005.03.004
- Oehring, S. C., Woodcroft, B. J., Moes, S., Wetzel, J., Dietz, O., Pulfer, A., et al. (2012). Organellar Proteomics Reveals Hundreds of Novel Nuclear Proteins in the Malaria Parasite Plasmodium Falciuparum. *Genome Biol.* 13 (11), R108. doi: 10.1186/gb-2012-13-11-r108
- Painter, H. J., Chung, N. C., Sebastian, A., Albert, I., Storey, J. D., and Llinas, M. (2018). Genome-Wide Real-Time *In Vivo* Transcriptional Dynamics During Plasmodium Falciuparum Blood-Stage Development. *Nat. Commun.* 9 (1), 2656. doi: 10.1038/s41467-018-04966-3
- Pang, T. L., Wang, C. Y., Hsu, C. L., Chen, M. Y., and Lin, J. J. (2003). Exposure of Single-Stranded Telomeric DNA Causes G2/M Cell Cycle Arrest in Saccharomyces Cerevisiae. *J. Biol. Chem.* 278 (11), 9318–9321. doi: 10.1074/jbc.M208347200
- Query, C. C., Bentley, R. C., and Keene, J. D. (1989). A Common RNA Recognition Motif Identified Within a Defined U1 RNA Binding Domain of the 70K U1 snRNP Protein. *Cell* 57 (1), 89–101. doi: 10.1016/0092-8674(89)90175-X
- Religa, A. A., Ramesar, J., Janse, C. J., Scherf, A., and Waters, A. P. P. (2014). Berghei Telomerase Subunit TERT Is Essential for Parasite Survival. *PLoS One* 9 (9), e108930. doi: 10.1371/journal.pone.0108930
- Renaud de la Faverie, A., Guedin, A., Bedrat, A., Yatsunyk, L. A., and Mergny, J. L. (2014). Thioflavin T as a Fluorescence Light-Up Probe for G4 Formation. *Nucleic Acids Res.* 42 (8), e65. doi: 10.1093/nar/gku111

- Sierra-Miranda, M., Vembar, S. S., Delgadillo, D. M., Avila-Lopez, P. A., Herrera-Solorio, A. M., Lozano Amado, D., et al. (2017). PfAP2Tel, Harboring a Non-Canonical DNA-Binding AP2 Domain, Binds to Plasmodium Falciparum Telomeres. *Cell. Microbiol.* 19 (9), e12742. doi: 10.1111/cmi.12742
- Tanaka, E., Fukuda, H., Nakashima, K., Tsuchiya, N., Seimiya, H., and Nakagama, H. (2007). HnRNP A3 Binds to and Protects Mammalian Telomeric Repeats *In Vitro*. *Biochem. Biophys. Res. Commun.* 358 (2), 608–614. doi: 10.1016/j.bbrc.2007.04.177
- Trager, W., and Jensen, J. B. (1976). Human Malaria Parasites in Continuous Culture. *Sci. (New York N.Y.)* 193 (4254), 673–675. doi: 10.1645/0022-3395(2005)091
- Tuteja, R., and Mehta, J. (2010). A Genomic Glance at the Components of the mRNA Export Machinery in Plasmodium Falciparum. *Commun. Integr. Biol.* 3 (4), 318–326. doi: 10.4161/cib.3.4.11886
- Voss, T. S., Mini, T., Jenoe, P., and Beck, H. P. (2002). Plasmodium Falciparum Possesses a Cell Cycle-Regulated Short Type Replication Protein A Large Subunit Encoded by an Unusual Transcript. *J. Biol. Chem.* 277 (20), 17493–17501. doi: 10.1074/jbc.M200100200
- WHO. (2020). *World Malaria Report 2020*. Available at: <https://scholar.google.co.uk/scholar?q=WHO+world+malaria+report+citation>.
- Windgassen, M., and Krebber, H. (2003). Identification of Gbp2 as a Novel Poly (A)+ RNA-Binding Protein Involved in the Cytoplasmic Delivery of Messenger RNAs in Yeast. *EMBO Rep.* 4 (3), 278–283. doi: 10.1038/sj.embor.embor763
- Wisniewski, J. R., Zougman, A., Nagaraj, N., and Mann, M. (2009). Universal Sample Preparation Method for Proteome Analysis. *Nat. Methods* 6 (5), 359–362. doi: 10.1038/nmeth.1322
- Yang, J., Yan, R., Roy, A., Xu, D., Poisson, J., and Zhang, Y. (2015). The I-TASSER Suite: Protein Structure and Function Prediction. *Nat. Methods* 12 (1), 7–8. doi: 10.1038/nmeth.3213
- Zakian, V. A. (2012). Telomeres: The Beginnings and Ends of Eukaryotic Chromosomes. *Exp. Cell Res.* 318 (12), 1456–1460. doi: 10.1016/j.yexcr.2012.02.015
- Zhang, M., Wang, C., Otto, T. D., Oberstaller, J., Liao, X., Adapa, S. R., et al. (2018). Uncovering the Essential Genes of the Human Malaria Parasite Plasmodium Falciparum by Saturation Mutagenesis. *Sci. (New York N.Y.)* 360 (6388), eaap7847. doi: 10.1126/science.aap7847
- Zhao, N., Gong, P., Li, Z., Cheng, B., Li, J., Yang, Z., et al. (2014). Identification of a Telomeric DNA-Binding Protein in Eimeria Tenella. *Biochem. Biophys. Res. Commun.* 451 (4), 599–602. doi: 10.1016/j.bbrc.2014.08.030

Conflict of Interest: The authors declare that the research was conducted in the absence of any commercial or financial relationships that could be construed as a potential conflict of interest.

Publisher's Note: All claims expressed in this article are solely those of the authors and do not necessarily represent those of their affiliated organizations, or those of the publisher, the editors and the reviewers. Any product that may be evaluated in this article, or claim that may be made by its manufacturer, is not guaranteed or endorsed by the publisher.

Copyright © 2022 Edwards-Smallbone, Jensen, Roberts, Totañes, Hart and Merrick. This is an open-access article distributed under the terms of the Creative Commons Attribution License (CC BY). The use, distribution or reproduction in other forums is permitted, provided the original author(s) and the copyright owner(s) are credited and that the original publication in this journal is cited, in accordance with accepted academic practice. No use, distribution or reproduction is permitted which does not comply with these terms.



Metalloprotease Gp63-Targeting Novel Glycoside Exhibits Potential Antileishmanial Activity

OPEN ACCESS

Edited by:

Jeroen P. J. Saeij,
University of California, Davis,
United States

Reviewed by:

Farhat Afrin,
JIS Institute of Advanced Studies and
Research, India
Sara M. Robledo,
University of Antioquia, Colombia

*Correspondence:

Shailja Singh
shailja.jnu@gmail.com
Soumya Pati
soumya.pati@snu.edu.in
Ram Sagar
ram.sagar@mail.jnu.ac.in

†Present Address:

Ram Sagar,
School of Physical Sciences,
Jawaharlal Nehru University (JNU),
New Delhi, India

†These authors have contributed
equally to this work

Specialty section:

This article was submitted to
Parasite and Host,
a section of the journal
Frontiers in Cellular and
Infection Microbiology

Received: 27 October 2021

Accepted: 14 March 2022

Published: 04 May 2022

Citation:

Chakrabarti A, Narayana C, Joshi N,
Garg S, Garg LC, Ranganathan A,
Sagar R, Pati S and Singh S (2022)
Metalloprotease Gp63-Targeting
Novel Glycoside Exhibits Potential
Antileishmanial Activity.
Front. Cell. Infect. Microbiol. 12:803048.
doi: 10.3389/fcimb.2022.803048

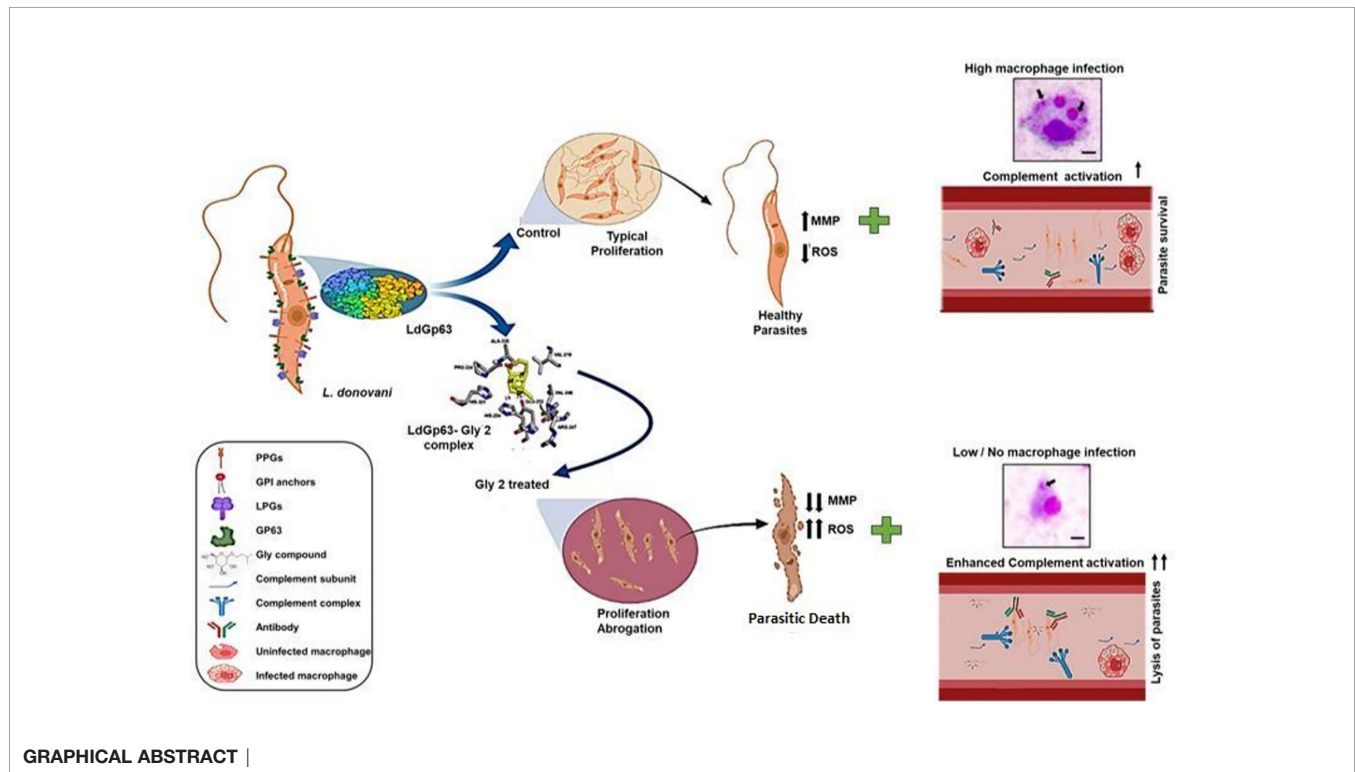
Amrita Chakrabarti^{1‡}, Chintam Narayana^{2‡}, Nishant Joshi¹, Swati Garg^{1,3}, Lalit C. Garg⁴,
Anand Ranganathan³, Ram Sagar^{2,5*†}, Soumya Pati^{1*†} and Shailja Singh^{1,3*}

¹ Department of Life Sciences, School of Natural Sciences, Shiv Nadar University, Greater Noida, India, ² Department of Chemistry, School of Natural Sciences, Shiv Nadar University, Greater Noida, India, ³ Special Centre for Molecular Medicine, Jawaharlal Nehru University (JNU), New Delhi, India, ⁴ Gene Regulation Laboratory, National Institute of Immunology, New Delhi, India, ⁵ Department of Chemistry, Institute of Science, Banaras Hindu University, Varanasi, India

Visceral leishmaniasis (VL) and post kala-azar dermal leishmaniasis (PKDL) affect most of the poor populations worldwide. The current treatment modalities include liposomal formulation or deoxycholate salt of amphotericin B, which has been associated with various complications and severe side effects. Encouraged from the recent marked antimalarial effects from plant-derived glycosides, in this study, we have exploited a green chemistry-based approach to chemically synthesize a library of diverse glycoside derivatives (Gly1–12) and evaluated their inhibitory efficacy against the AG83 strain of *Leishmania donovani*. Among the synthesized glycosides, the *in vitro* inhibitory activity of Glycoside-2 (Gly2) (1.13 μ M IC₅₀ value) on *L. donovani* promastigote demonstrated maximum cytotoxicity with ~94% promastigote death as compared to amphotericin B that was taken as a positive control. The antiproliferative effect of Gly2 on promastigote encouraged us to analyze the structure–activity relationship of Gly2 with Gp63, a zinc metalloprotease that majorly localizes at the surface of the promastigote and has a role in its development and multiplication. The result demonstrated the exceptional binding affinity of Gly2 toward the catalytic domain of Gp63. These data were thereafter validated through cellular thermal shift assay in a physiologically relevant cellular environment. Mechanistically, reduced multiplication of promastigotes on treatment with Gly2 induces the destabilization of redox homeostasis in promastigotes by enhancing reactive oxygen species (ROS), coupled with depolarization of the mitochondrial membrane. Additionally, Gly2 displayed strong lethal effects on infectivity and multiplication of amastigote inside the macrophage in the amastigote–macrophage infection model *in vitro* as compared to amphotericin B treatment. Gp63 is also known to bestow protection against complement-mediated lysis of parasites. Interestingly, Gly2 treatment enhances the complement-mediated lysis of *L. donovani* promastigotes in serum physiological conditions. In addition, Gly2 was found to be equally effective against the clinical promastigote forms of PKDL strain (IC₅₀ value of 1.97 μ M); hence, it could target both VL and PKDL simultaneously. Taken together, this study reports the serendipitous discovery of Gly2 with potent

antileishmanial activity and proves to be a novel chemotherapeutic prototype against VL and PKDL.

Keywords: *Leishmania*, Glycoside 2, LdGp63, post kala-azar dermal leishmaniasis (PKDL), cellular thermal shift assay (CETSA)



INTRODUCTION

Leishmaniasis is a globally neglected vector-borne disease transmitted by the bite of a female sand fly infected with the protozoan parasite of the genus *Leishmania*. It has many clinical manifestations ranging from a mild cutaneous variant to the life-threatening visceral form (Arenas et al., 2017). Patients cured of visceral leishmaniasis (VL) are prone to post kala-azar dermal leishmaniasis (PKDL), an aggressive clinical manifestation of VL (Zijlstra, 2016). Leishmaniasis, caused by *L. donovani*, is endemic in several parts of the tropics, subtropics, and southern Europe. The disease is a severe threat to 350 million people, with a prevalence of 12 million people worldwide (Oryan and Akbari, 2016). Nearly 0.7–1 million newly reported cases of leishmaniasis span about 100 endemic countries (Burza et al., 2018). An estimated 50,000–90,000 new cases of VL arise annually, majorly in parts of Brazil, East Africa, and India, only 25%–45% of which get reported to WHO (Bi et al., 2018). In Brazil, the average annual age-adjusted mortality rate stands at 0.15 deaths per 100,000 individuals, and the case fatality rate is 8.1% (Martins-Melo et al., 2014). Thus, to target this fatal disease, WHO has already declared the development of new treatments of utmost priority.

Over several years, the available diagnosis and treatment modalities for VL relied on pentavalent antimonials, but unfortunately, these drugs are found to be unsatisfactory in combating the disease, as evidenced by increasing disease burden due to high toxicity, delayed drug release and response, and inimical side effects (Croft et al., 2006; Ponte-Sucre et al., 2017). In the conquest of identifying better leishmanicidal compounds, plant-derived and mimicking products are gaining the attention of researchers. Products from aloe vera, luteolin, quassin, berberine chloride, and artemisinin are very prominent. These derivatives have a similar mode of action and induce oxidative stress leading to parasite death. Despite being plant derivatives, these drugs also depicted low efficacy with certain side effects (Sen and Chatterjee, 2011; Singh et al., 2016). This limited efficacy of currently available drugs demands efficient drug development strategies involving both target identification and validation in the pathogenesis of VL. Previous studies elucidated the role of various *Leishmania* spp. proteases involved in parasite life cycle and pathogenesis. Notably, leishmanolysin of *Leishmania* spp., the known zinc metalloprotease, Gp63 has been identified as an important multifunctional virulence factor, found in abundance on the surface of promastigotes and in limited quantities inside the

parasite (Etges et al., 1985; Yao et al., 2003; Sunter and Gull, 2017). It is the key enzyme responsible for parasite propagation, promastigote binding and internalization in macrophages, and attenuation of reactive oxygen intermediate formation that favors amastigote proliferation (Kamhawi, 2006). The myriad diversity as well as the high catalytic activity at the body's physiological temperature of this virulence factor favors the dissemination of the parasite in the host (Chaudhuri and Chang, 1988; Yao et al., 2002; McGwire et al., 2003; Yao et al., 2003). Recent reports from certain parasitic models demonstrated the protective nature of Gp63 against complement fixation and processing that shields *Leishmania* promastigotes during its transience into mammalian hosts (Brittingham et al., 1995; Joshi et al., 1998; Joshi et al., 2002). Emerging studies have shown that plant-derived glycoside formulations from Asteraceae extracts can inhibit protozoan parasites such as *Leishmania*, *Plasmodium*, *Trypanosoma*, and intestinal worms. Recently, oral administration of plant-derived beta-glycosides, such as esculin and amygdalin, to sand fly *Lutzomyia longipalpis*, the main vector of American VL, has shown to drastically affect the sand fly physiology and *Leishmania* development, thus proposed as promising transmission-blocking sugar baits. Additional study has identified promising antibacterial and antiparasitic activity of oleanolic acid and its glycosides isolated from marigold (*Calendula officinalis*) (Szakiel et al., 2008).

Based on this evidence, we strategized to develop a purely non-toxic and non-hazardous form of glycoside with no effect on human health or environment. Considering the green chemistry approach, we have designed and synthesized a library of novel glycoside derivatives with D-glucose and N-acetyl-D-glucosamine as the primary backbone template. Among these, **Gly2** showed promising results against both *L. donovani* promastigote and intra-macrophagic amastigote forms. **Gly2** treatment led to abrogation of parasite multiplication, induction of reactive oxygen species (ROS) generation, and disruption of mitochondrial membrane potential leading to promastigote death, suggesting its therapeutic implication against VL. Besides its inhibitory role in cultured parasites *in vitro*, **Gly2** demonstrated efficacy in the prevention of parasite evasion from complement-mediated lysis in an *in vitro* model mimicking the body's physiological condition. The structure-activity relationship (SAR) analysis of novel glycosides, along with cellular thermal shift assay (CETSA) and *in silico* studies, revealed efficient binding of **Gly2** molecule with Gp63 catalytic domain. Additionally, **Gly2** demonstrated excellent antileishmanial activity against the clinical isolate of PKDL. Overall, our work has discovered a purely non-toxic glycoside derivative with strong antileishmanial potential.

MATERIALS AND METHODS

Parasite Growth and Maintenance

Promastigote forms of *L. donovani* (MHOM/IN/1983/AG83) were cultured at 26°C in M199 (GIBCO, India), pH 7.4,

supplemented with 10% (v/v) inactivated fetal bovine serum (FBS, GIBCO, India) and 0.02 mg/ml gentamycin (Life Technologies, USA). The clinical isolate of PKDL, BS12, was obtained as a gift from Prof. Mitali Chatterjee [Department of Pharmacology, Institute of Postgraduate Medical Education and Research (IPGMER), Kolkata, India]. BS12 was routinely cultured at 22°C in M199 (GIBCO, India) with 100 U/ml penicillin-streptomycin (Gibco, Invitrogen, Thermo Fisher Scientific, NY, USA), 8 µM hemin (4 mM stock made in 50% triethanolamine) (Sigma, USA), 25 mM 4-(2-hydroxyethyl)-1-piperazineethanesulfonic acid (HEPES), supplemented with 10% heat-inactivated FBS (GIBCO, India). Cultures were maintained between 10⁶ and 10⁷ cells/ml for continuous exponential growth. In addition, 1 × 10⁶ cells/ml parasite count was constantly maintained for all the experiments (Ramu et al., 2017).

Cell Culture

The J774.A1 murine macrophage cells were grown in Roswell Park Memorial Institute (RPMI) 1640 medium in the presence of 10% (v/v) FBS and 100 U/ml penicillin–100 µg/ml streptomycin (Gibco, Invitrogen, Thermo Fisher Scientific, NY, USA) at 37°C (humidified) and 5% CO₂. Primary Madin–Darby canine kidney (MDCK) cells were obtained from the National Centre for Cell Science, Pune, India. MDCK cells were derived from the kidney tissue of an adult female Cocker Spaniel. These were grown in Dulbecco's modified Eagle's minimal essential medium (DMEM) in the presence of 10% (v/v) FBS and 100 U/ml penicillin–100 µg/ml streptomycin (Gibco, Invitrogen, Thermo Fisher Scientific, NY, USA) at 37°C (humidified) and 5% CO₂ (Ayana et al., 2018; Shivappagowdar et al., 2021).

Synthesis of Glycoside Derivatives

Pre-stirred solution of glucose (200 mg, 1.11 mmol) or glucosamine (200 mg, 1.11 mmol) was prepared in neat alcohol (5–10 ml), and Amberlite IR 120-H⁺ resin (400 mg) was added to it. The resulting mixture was stirred at 100°C for 24 h. After completion of the reaction, the mixture was cooled down to room temperature and filtered to remove the resin. The filtrate was evaporated under reduced pressure to obtain compounds 1–3 as a white solid in acceptable to good yield. Compounds 4–6 were prepared in good yield adopting a similar reaction protocol using the corresponding alcohol and glucose or glucosamine followed by acetylation using acetic anhydride in pyridine at room temperature. All the final compounds 1–6 were purified using flash column chromatography before using them for biological activity. The final compounds were formed as semisolid or solid and were characterized by ¹H-NMR and ¹³C-NMR. ¹H-NMR and ¹³C-NMR spectra in CD₃OD and D₂O were recorded on Bruker 400 MHz spectrometer at ambient temperature. Here, ¹H was recorded by 400 MHz and ¹³C was recorded by 100 MHz. Proton chemical shifts are given in ppm relative to the internal standard (tetramethylsilane) or referenced relative to the solvent residual peaks (CD₃OD: δ 3.31). Multiplicity was denoted as follows: s (singlet), d (doublet), t (triplet), q (quartet), m (multiplet), dd (doublet of doublet), dt (doublet of triplet), td (triplet of doublet), ddd (doublet of doublet of doublet), etc. Coupling constants (J) were reported in Hz. Column chromatography was performed by

using silica gel 100–200 and 230–400 mesh. High Resolution Mass Spectrometry (HRMS) spectra were determined from quadrupole/Q-TOF mass spectrometer with an ESI source (**Supplementary Material**) (Yu et al., 2004).

Treatment Procedure With Synthesized Glycosides

All the compounds were dissolved in dimethyl sulfoxide (DMSO) (Sigma-Aldrich) for 1 mM stock solution and were screened against promastigotes at a concentration of 5 μ M. For Glycosides (Gly) 2, 6, and 8, a range of concentrations starting from 100 nM to 100 μ M were screened against promastigote forms of parasite and mammalian cells. Parasites (AG83 and PKDL strain) treated with amphotericin B (3 μ g/ml) (Sigma-Aldrich) were maintained as the positive control.

Anti-Parasite Drug Susceptibility Assay

AG83 strain of *L. donovani* were exposed to various Gly compound concentrations (100 nM–100 μ M) in a 96-well microtiter plate (100 μ l/well volume) and were incubated for 72 h at 26°C. Finally, lactate dehydrogenase (LDH) cytotoxic assay was performed as per standard protocol (CytoTox 96 Non-Radioactive Cytotoxicity Assay-Promega, USA). The percent cytotoxicity of test compounds was calculated by normalizing with amphotericin B as 100%. Further percentage growth inhibition was calculated using the formula:

$$\% \text{ Growth Inhibition} = \frac{\text{Gly treated LDH activity} - \text{Spontaneous LDH activity}}{\text{Maximum LDH activity} - \text{Spontaneous LDH activity}} \times 100$$

As per the formula, the spontaneous LDH Activity = activity of the untreated cells and the maximum LDH activity = activity of the amphotericin B-treated cells. IC₅₀ value for Gly2, 6, and 8 treated was generated for AG83 and PKDL strain of *L. donovani* using sigmoidal dose–response model with nonlinear regression tool (Ramu et al., 2017).

Qualitative Estimation of Live/Dead Parasites

The toxic effect of the three compounds, Gly2, 6, and 8 on promastigotes at 5 μ M >IC₅₀ concentration was measured by Hoechst and propidium iodide (PI) double staining. After treatment with the compounds for 24 h, parasites were harvested, washed in 0.01 M PBS (pH = 7.4), and stained with Hoechst 33258 (1 μ g/ml) (Life Technologies, USA) and PI (5 μ g/ml) (Life Technologies, USA) followed by incubation for a period of 20 min at 37°C. Subsequently, cells were washed for excessive stain removal and visualized using fluorescence microscope with 510–560-nm filter block for PI red fluorescence and excitation/emission spectra at 361/497 for Hoechst (López-Arencibia et al., 2015).

In Silico Studies

The physicochemical properties of compounds were calculated using SwissADME (Daina et al., 2017) module provided in SIB (Swiss Institute of Bioinformatics) web server (<https://www.sib.swiss>). The designed Gly compounds were evaluated for their

ADME profile, including drug-likeness, partition coefficient, solubility, and oral bioavailability parameters according to Lipinski's "rule-of-five" (Daina et al., 2017).

Antibody Generation

Synthetic oligonucleotides encoding the catalytic motif of LdGp63 with PstI and HindIII overhangs were synthesized and ligated to PstI and HindIII-digested pQELTB plasmid and transformed into *Escherichia coli* DH5 α cells for propagation and into *E. coli* M15 cells for recombinant fusion protein expression. *E. coli* M15 cells containing the recombinant plasmid were induced with 1 mM Isopropyl β -D-1-thiogalactopyranoside (IPTG). The recombinant fusion protein was purified to near homogeneity from solubilized inclusion bodies using metal affinity chromatography, taking advantage of the histidine tag present at the N-terminal of the fusion protein. Female BALB/c mice were immunized with the purified fusion protein followed by a single booster on day 15 post immunization. Blood was obtained a week post booster administration through the retro-orbital plexus. Anti-fusion protein antiserum was obtained after incubating the blood at Room Temperature (RT) for 1 h followed by centrifugation at (1,957 g, 10 min) at 4°C. Antiserum thus prepared was stored at -80°C until further use (Nejad-Moghaddam and Abolhassani, 2009).

Western Blot Analysis

Immunoblotting assay was performed using generated mouse polyclonal anti-LdGp63 catalytic domain, which were used at 1:500 dilution. The whole-parasite lysates were washed twice with Phosphate Buffer Saline (PBS), lysed in lysis buffer (50 mM HEPES, 150 mM NaCl, 1% Triton X-100 and 1% IGEPAL, 1 mM phenylmethyl sulfonyl fluoride), and denatured at 70°C. The samples were then homogenized with a 1-ml syringe and a 22G needle before Sodium dodecyl-sulfate polyacrylamide gel electrophoresis (SDA-PAGE) and blotting onto nitrocellulose membranes with 0.2- μ m pore size. The membranes were blocked with 5% skimmed milk powder dissolved in PBS containing 0.1% Tween-20. After incubation for 2 h at room temperature, the blot was subsequently washed with PBS and later was probed with primary generated mouse polyclonal anti-LdGp63 antibody and rabbit IgG conjugated to horseradish peroxidase as secondary antibody. After incubation, the membrane was washed thrice with PBS, and the signals were observed under Enhanced Chemiluminescence (ECL)-exposed X-ray film at room temperature in a dark room having safe red light (Jost et al., 2011).

Confocal Imaging of Gp63 Localization in Promastigotes

Immunofluorescence assay was performed with anti-LdGp63 catalytic domain antibody that was used at 1:500 dilution. The smears of the parasites were stained with indicated primary antibodies and using secondary antibodies labeled with Alexa Fluor 488 (Invitrogen). Coverslips were mounted with ProLong Gold Anti fade DAPI (Invitrogen), and images were collected with an Olympus 1000 microscope (Cuevas et al., 2003).

Promastigote Proliferation Assay

AG83 parasite growth and multiplication were assessed by fluorescence-activated cell sorting and fluorescence microscopy with 6-carboxyfluorescein diacetate succinimidyl ester (CFDA-SE, Life Technologies, USA) as a probe. Promastigotes were washed thrice with PBS. The cells were labeled with CFDA-SE dye and were then incubated at 37°C for 10 min. These cells were then resuspended in ice-cold M199 medium. Furthermore, they were centrifuged at 1,200 g for 10 min (4°C) and resuspended in fresh medium. Cells were treated with the **Gly2** and were analyzed through BD FACS DIVA for 3 consecutive replicates after 0, 24, 48, and 72 h, respectively (Messaritakis et al., 2010).

Estimation of Reactive Oxygen Species Levels

The redox homeostasis of promastigotes was monitored both qualitatively and quantitatively by 2',7'-dichlorodihydrofluorescein diacetate (DCFDA) (Life Technologies, USA) staining. The untreated and **Gly2**-treated promastigotes (1×10^6 cells/ml) were cultured for 72 h. Following incubation, the parasites were harvested, washed with PBS, and stained with H₂DCFDA (20 μ M) for 20 min at 37°C. Excess stain was removed by washing with PBS, and samples were resuspended in PBS (50 μ l) followed by imaging. Fluorescence intensity was determined using an excitation filter at 485 nm and an emission filter at 535 nm using confocal microscope (Nikon Ti eclipse, USA). The samples were also analyzed through BD FACS diva (Shivappagowdar et al., 2019).

Quantification of Mitochondrial Membrane Potential

Mitochondrial membrane ($\Delta\psi_m$) potential was examined using 5,6-dichloro-2-[3-(5,6-dichloro-1,3-diethyl-1,3-dihydro-2H-benzimidazol-2-ylidene)-1-propenyl]-1,3-diethyl-iodide (JC-1 dye) (Life Technologies, USA) as a probe. Treated and untreated groups were incubated for 24 h. Cells were washed with PBS and JC-1 labeled, and samples were analyzed through FACS diva (Beckton-Dickinson, Pharmingen). The approximate fluorescence excitation/emission maxima of 514/529 nm for monomeric form and 585/590 nm for J-aggregate form were used. The labeled cells were also allowed to adhere to glass slides for visualization under fluorescence microscope (Nikon Ti eclipse, USA) (Shivappagowdar et al., 2019).

Detection of Complement-Mediated Cytolysis of Promastigotes by Uptake of Propidium Iodide

Parasites with an optimum 10% non-heat-inactivated normal human serum (NHS) were incubated with **Gly2** at 5- μ M concentration for 15 min. Promastigote lysis was detected by uptake of PI, by use of a FACS Diva flow cytometer (Beckton-Dickinson, Pharmingen), in accordance with the manufacturer's protocol. Promastigotes were washed for excessive stain removal and filter block for PI red fluorescence, 510–560 nm was used (Moreno et al., 2010).

In Silico Membrane Binding Studies and Docking Studies

Using PerMM web server for theoretical assessment of passive permeability of molecules across the lipid bilayer, we checked the membrane binding studies with synthesized glucoside compounds (Lomize et al., 2019). The three-dimensional (3D) protein structure of *L. major* GP63 (PDB ID- 1lml) was taken as template, and BLASTp with LdGp63 was performed to achieve sequence identity, followed by homology modeling. PROCHECK server was utilized to obtain Ramachandran plot (Laskowski et al., 1993). The chemical structures of compounds were synthesized through the ChemSketch (Spessard, 1998). Protein and ligand structures were optimized using Swiss PDBviewer and ChemBioDraw ultra version 12.0, respectively (Kaplan and Littlejohn, 2001; Cousins, 2011). Autodock version 4.2 and Cygwin terminal were utilized to execute the docking commands (Racine, 2000; Morris and Lim-Wilby, 2008). Binding site for the ligand was chosen around its catalytic domain residues. Chimera version 1.13.1, Ligplot version 2.2, Discovery Studio version 19.1.0, and Pymol version 2.3.2 (De Lano, 2002) software were used for further analysis of docking results [Accelrys Software Inc. (2009), Discovery Studio Modeling Environment, Release 2.5.1, San Diego, CA; crystallography and 2002; Pettersen et al., 2004; Laskowski and Swindells, 2011; Studio, 2015].

Cellular Thermal Shift Assay

For the CETSA in promastigotes, parasites were seeded in 6-well cell culture plates (1.0×10^6 cells/well) and exposed to Gly2 at the 5 μ M >IC₅₀ for 24 h in the incubator. Control cells were incubated with an equal volume of a vehicle. Following incubation, the parasites were washed with PBS to remove excess drug and harvested in 200 μ l of a lysis solution (50 mM HEPES, 150 mM NaCl, 1% Triton X-100 and 1% IGEPAL, 1 mM phenylmethyl sulfonyl fluoride). The lysates were centrifuged at 14,000 g for 20 min at 4°C, and supernatants were transferred to new tubes. Furthermore, the protein concentration was measured using the Pierce BCA protein assay kit. After preparation of lysates, 30 μ l (0.8 mg/ml) aliquots of the supernatants were heated individually on a Thermomixer compact (Eppendorf) at different temperatures for 7 min and then cooled at room temperature for 3 min. CETSA samples were separated by SDS-PAGE, and immunoblotting was performed as described previously using a mouse polyclonal anti-LdGp63 catalytic domain antibody (1:500) (Chakrabarti et al., 2021).

Inhibitory Activity of Compounds Against Intracellular Amastigotes

For evaluating the efficacy of compounds against intramacrophage amastigotes, Giemsa staining (Sigma-Aldrich) was performed. J774.A1 murine macrophage cells were plated at a cell density of 5×10^5 cell/well in a 6-well flat bottom plate. The cells were infected with late-stage *L. donovani*, rich in promastigotes at a ratio of 10:1. After 6 h, uninfected promastigotes were washed off with PBS. Infected macrophages were treated with compounds at their respective IC₅₀

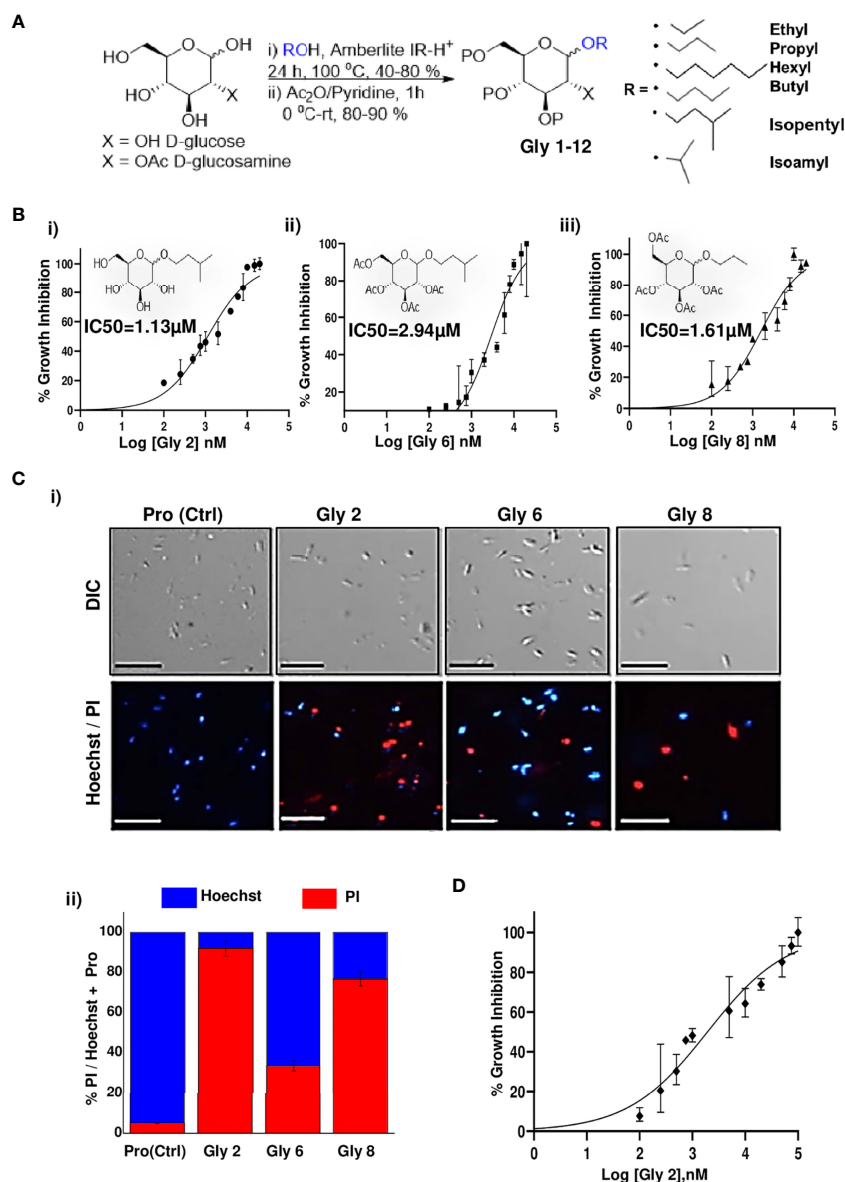


FIGURE 1 | Synthesis scheme of glycoside derivatives and concentration-dependent effects of potent novel glycosides on promastigotes of *Leishmania donovani* AG83 strain with variable membrane binding affinities. **(A)** Synthesis of designed glycosides was carried out with commercially available D-glucose and D-glucosamine coupling with various short- to long-chain alcohols under acidic conditions. **(B)** Percentage inhibition of promastigotes treated with Gly2, 6, and 8 was evaluated using LDH assay for 72 h and plotted as sigmoidal curve. Data normalization was done by taking into consideration the cytotoxicity induced by positive control (amphotericin B 3 $\mu\text{g}/\text{ml}$) as 100%. IC₅₀ values for promastigotes of the AG83 strain were analyzed using GraphPad Prism, represented as the mean \pm SD where $n = 3$, independent experiments. **(C)** (i) The representative screenshots of propidium iodide (PI)- and Hoechst-stained promastigotes at 72 h as assessed by fluorescence microscopy depicting parasite death on glycoside treatment. (ii) Percentage PI positivity vs. percentage Hoechst positivity represents death vs. viability of promastigotes at 72 h against treatment by novel glycosides. **(D)** Cytotoxic effect of **Gly2** on clinical PKDL isolate BS12 in a concentration-dependent manner.

concentrations and incubated for 24 h for visualization and counting of intracellular parasite load (Ayana et al., 2018).

Ethics Statement

NHS was obtained from Rotary Blood Bank, Tughlakabad, New Delhi. All methods were carried out in accordance with relevant guidelines and regulations. Ethics committees of Shiv Nadar

University approved all of the experiments carried out with NHS. The Animal Ethics Committee (IAEC Code #288/11) of the Jawaharlal Nehru University approved animal usage and procedures for the generation of antibody. The clinical isolate of PKDL, BS12, has been obtained as a kind gift from Prof. Mitali Chatterjee's Laboratory [Department of Pharmacology, Institute of Postgraduate Medical Education and Research (IPGMR),

Kolkata, West Bengal, India]. This strain was cultured in BSL2 lab facility under guidelines of the institutional biosafety committee, Shiv Nadar University.

Statistical Analysis

Student's t-test was performed to evaluate significant differences between treatment and control samples in all of the experiments performed using ANOVA test. P-values <0.05 and <0.01 were considered to be significant, indicated as * and **, respectively. Results represent the mean \pm SD of minimum three independent experiments. Calculated IC₅₀ value and all statistical analyses were performed using GraphPad Prism version 8.01. Intensity profiles for Western blots were calculated using ImageJ software (Schneider et al., 2012).

RESULTS

Synthesis of Glycoside-Based Compounds Using a Green Synthetic Route

Glycoside derivatives are highly abundant in nature and have relatively simpler conformations due to which they are gaining current momentum as bioactive molecules in pharmaceutical industries (Prassas and Diamandis, 2008). Herein, the commercially available D-glucose 1 and N-Acetyl-D-glucosamine 2 molecules were coupled along with various short- to long-chain alcohols under acidic conditions to design and synthesize glycoside-derived compounds. The synthesis of ethyl glycoside N-Acetyl-D-glucosamine (Glycoside-1) was prepared by refluxing 1 in ethanol for 24 h in the presence of amberlite-H+ IR-120, which gave us the desired product Glycoside-1 as an anomeric mixture in good yield as described (Figure 1A). The process does not involve any further purification, and amberlite resin can be reused by activating it with 1 N HCl in MeOH. In parallel, other compounds in this series, Glycoside-2 to Glycoside-6, were also prepared, adopting similar reaction protocols (methods), which resulted in good yields. Furthermore, the alkyl glycosides of N-Acetyl-D-Glucosamine Glycoside-7 to Glycoside-12 were prepared by refluxing N-Acetyl-D-Glucosamine with corresponding alkyl alcohols for 24 h in the presence of amberlite-H+ 100 IR-120 resin, which gave the desired products as an anomeric mixture in good yield as shown

(Supplementary Table S1). Further characterizations of all 12 compounds were done using NMR and quadrupole/Q-TOF mass spectrometer with an ESI source determined using HRMS spectra (Supplementary Material).

Absorption, Distribution, Metabolism, and Excretion (ADMET) and Drug-Likeness Evaluation

SwissADME provides detailed and extensive physicochemical profiles and medicinal chemistry properties of any compound using five different algorithms (Daina et al., 2017). The partition coefficient and solubility are the two parameters that play important roles in the physicochemical aspect. So, based on predicted LogP value for the compounds that represents partition coefficient, it is concluded that all 12 compounds lie within the range value of 1.6–3.6, depicting the drug-likeness (Waring, 2010).

In Vitro Metabolic Viability Assay-Based Screening Unraveled the Lead Glycoside Derivatives and Their Toxic Impact on *L. donovani* Promastigotes

To evaluate the cytotoxic effects of 12 compounds on *L. donovani* promastigotes, LDH assay was performed. This assay involves the reduction of tetrazolium salts to formazan during LDH-mediated catalysis of lactate to pyruvate, which can be detected at 490 nM. Rate of formazan formation is proportional to the release of LDH through damaged cell membranes. For the preliminary screening, the promastigotes were incubated with 12 compounds at a single concentration of 5 μ M for a period of 72 h, and the released LDH was estimated (Supplementary Figure S1A). Amphotericin B-treated promastigotes were taken as the positive control. A significant amount of formazan formation was observed in Glycoside (Gly) 2-, 6-, and 8-treated samples, suggesting that these glycosides have a toxic effect on parasites. It was observed that Gly2 (IC₅₀ = 1.13 μ M) demonstrated the lowest IC₅₀ value as compared to Gly6 (IC₅₀ = 2.94 μ M) and Gly8 (IC₅₀ = 1.61 μ M), and hence, it has the most prominent lethal effect (Figures 1Bi–iii). Having observed the antileishmanial effect of Gly2 on growth and proliferation of promastigotes, we next investigated the cytotoxicity of Gly2 on mammalian cells (MDCK, J774.1A) through MTT (3-(4, 5-dimethylthiazolyl-2)-2, 5-diphenyltetrazolium bromide) cell

TABLE 1 | IC₅₀/CC₅₀/SI values of glycoside derivatives.

	IC ₅₀ (μ M)	CC ₅₀ (μ M) Macrophages	SI Macrophages
Gly1	65	247.9	3.813
Gly2	1.13	2,900	2,566.371
Gly3	12.7	1,677.6	132.090
Gly4	4.6	167	36.304
Gly5	5.97	159.2	26.666
Gly6	3.4	1,033	303.823
Gly7	77	299	3.883
Gly8	1.6	959	599.375
Gly9	36	256	7.111
Gly10	25.22	239	9.476
Gly11	43	179	4.162
Gly12	95	279	2.936

viability assay (**Supplementary Figures S1B, C**). A minimum level of cytotoxicity could be detected for the compound in MDCK cells and macrophage cells. The CC50 values of **Gly2** analog was in the micromolar range. The selectivity index (SI) for the compound was calculated as the ratio between cytotoxicity (CC50) and activity (IC50) against promastigotes (**Table 1**). The SI value for **Gly2** were more than 1,000, suggesting that the analogs are at least 1,000 times more specific to parasites than host cells. The above result suggests that **Gly2** imposed profound cytotoxic effects in *Leishmania* with no lethal effect in mammalian macrophages and canine epithelial MDCK, ensuring their specificity toward *L. donovani* promastigotes and not on the host.

Promastigote death was further confirmed against **Gly2**, **6**, and **8** treatment for a period of 72 h using live/dead dual staining of treated parasites with Hoechst/PI staining, respectively, and analyzed through fluorescent microscopy. The results revealed that untreated promastigotes showed viability (Hoechst⁺/PI⁻), whereas the treated parasites showed cellular death (Hoechst⁺/PI⁺) (**Figure 1Ci**). Precisely, we found ~94.15% dead parasites in Gly2-treated samples as compared to ~33.72% and 75.47% in Gly6- and Gly8-treated promastigotes, respectively (**Figures 1Ci, ii**).

We further evaluated the effect the **Gly2** on the clinical isolate of PKDL strain, BS12 of *L. donovani* (Sengupta et al., 2019). The results showed a pronounced toxic effect of **Gly2** on the Indian origin *Leishmania* isolate of PKDL. As mentioned previously, LDH assay was carried out on promastigotes treated with different concentrations of **Gly2** for 72 h, while amphotericin B was used a positive control. The promastigotes showed IC50 value at 1.97 μ M with 50% parasitic death (**Figure 1D**). Along with **Gly2**, we also evaluated the cytotoxic effects of 12 compounds on *L. donovani* promastigotes derived from clinical isolates of PKDL strain at 5 μ M (**Supplementary Figure S2**). The data strongly suggest that **Gly2** could adversely affect the metabolic cell viability of the lab strain of *L. donovani* along with the clinical strain of PKDL.

Gly2 Inhibitor Has High Binding Affinity for *L. donovani* Gp63, A Promastigote Surface Molecule

Among the various molecules of *Leishmania* that are considered potential targets for drug development, Gp63 protein is the most potent surface target, as it is widely distributed over the entire surface of the promastigote. Gp63 has various functions in both the promastigote form and the amastigote form in mammalian hosts (Medina-Acosta et al., 1993). Since Gly2 enforced strong cytotoxic effects on both promastigotes of lab and clinical strain, leading to parasitic death, we hypothesized that the antileishmanial effect of Gly2 might be the result of Gly2–Gp63 interaction. As a proof of concept, we generated the structure of LdGp63 through homology modeling with *L. major* leishmanolysin in complex Zinc ion (1LML) as template that showed significant structural identity (**Supplementary Figure S3**). The generated model of LdGp63 was further refined and analyzed for interaction with **Gly2**, **Gly6**, and **Gly8** through *in silico* docking. The best conformations of the docked compounds were selected based on their lowest free binding energy to the catalytic domain. Analysis of this pocket unraveled

three residues (**His251**, **Glu252**, and **Pro334**) that are involved in binding to the compounds (**Figure 2Ai**). **Gly2** showed lower free binding energy as compared to others, suggesting efficient docking (**Supplementary Table S2**). In the docked complex, the O3, O4, and O5 residues of Gly2 formed a strong H-bond interaction with **His251**, **Glu252**, and **Pro334** residues of LdGp63 (2.83 Å, 2.71 Å, and 2.90 Å), respectively (**Figure 2Ai**).

Since Gp63 is the surface molecule, we next investigated the passive permeability of **Gly2**, **Gly6**, and **Gly8** inhibitors across the lipid bilayer *in silico*. We found that **Gly2** was impermeable to the plasma membrane with log of permeability coefficient of -9.3 at temperature 310K and neutral pH of 7. On the other hand, **Gly6** was permeable to plasma membrane with log of permeability coefficient of -1.3. In comparison of **Gly2**, **Gly8** was impermeable to membrane with log of permeability coefficient of -6.9. Further using GLMol, the interactive 3D images of a compound moving across the membrane have been visualized (**Figure 2Aii**). This strengthened our hypothesis regarding probable interaction of **Gly2** with membrane protein of parasite, leading to suitable target identification. Based on the docking result (interaction of **Gly2** with Gp63 catalytic domain), we have raised the antibody against the catalytic domain of Gp63 (LdGp63). The immunofluorescence assay with the LdGp63 antibody validated the maximum expression of Gp63 on the surface of the promastigote, whereas the rest remained localized to the intracellular level (**Figure 2B**).

Due to surface abundance Gp63 in promastigotes and considering the functional diversity of Gp63, we speculated that masking the promastigote surface with catalytic domain-specific anti-LdGp63 antibody should affect the proliferation of promastigotes as well. To test this possibility, we stained the LdGp63 antibody-treated promastigotes with CFDA-SE, a cell-permeable dye. The decrease in fluorescence intensity is proportional to multiplication of the promastigote daughter cells (Messaritakis et al., 2010). The findings indicated subsequent changes in the percentage of CFDA-positive cells in LdGp63 antibody-treated parasites for 24 (88.9%) and 48 h (74.8%) as compared to untreated cells at 24 (78.9%) and 48 h (69.6%), respectively (**Figure 2C**).

Furthermore, to verify the *in vitro* binding efficacy of **Gly2** inhibitor with gp63 in a physiologically relevant cellular environment, i.e., promastigote lysates, we performed CETSA. For this, first, the number of promastigotes (10^4 – 10^7 cells) was titrated and immunoblotted with LdGp63 antibody (**Figure 2Di**). We then focused on **Gly2**-treated and untreated promastigote lysates (10^7 cells), which were incubated for 24 h and subsequently exposed to different temperatures before immunoblotting. The results of the immunoblot demonstrated that, at higher temperature (80°C), the Gp63 molecule in the untreated cell lysate is destabilized, while in lysates treated with **Gly2**, Gp63 is found to be stable at higher temperature (**Figure 2Dii**). Here, the binding of **Gly2** to Gp63 caused protein stabilization event under physiologic conditions even at a remarkably high temperature of 80°C, without any sign of denaturation. This clearly suggested ligand-dependent stabilization of Gp63 by **Gly2** even at a much higher temperature than the normal physiological temperature, strongly corroborating *in silico* and *in vitro* analyses that represented **Gly2** as the potent inhibitor of Gp63.

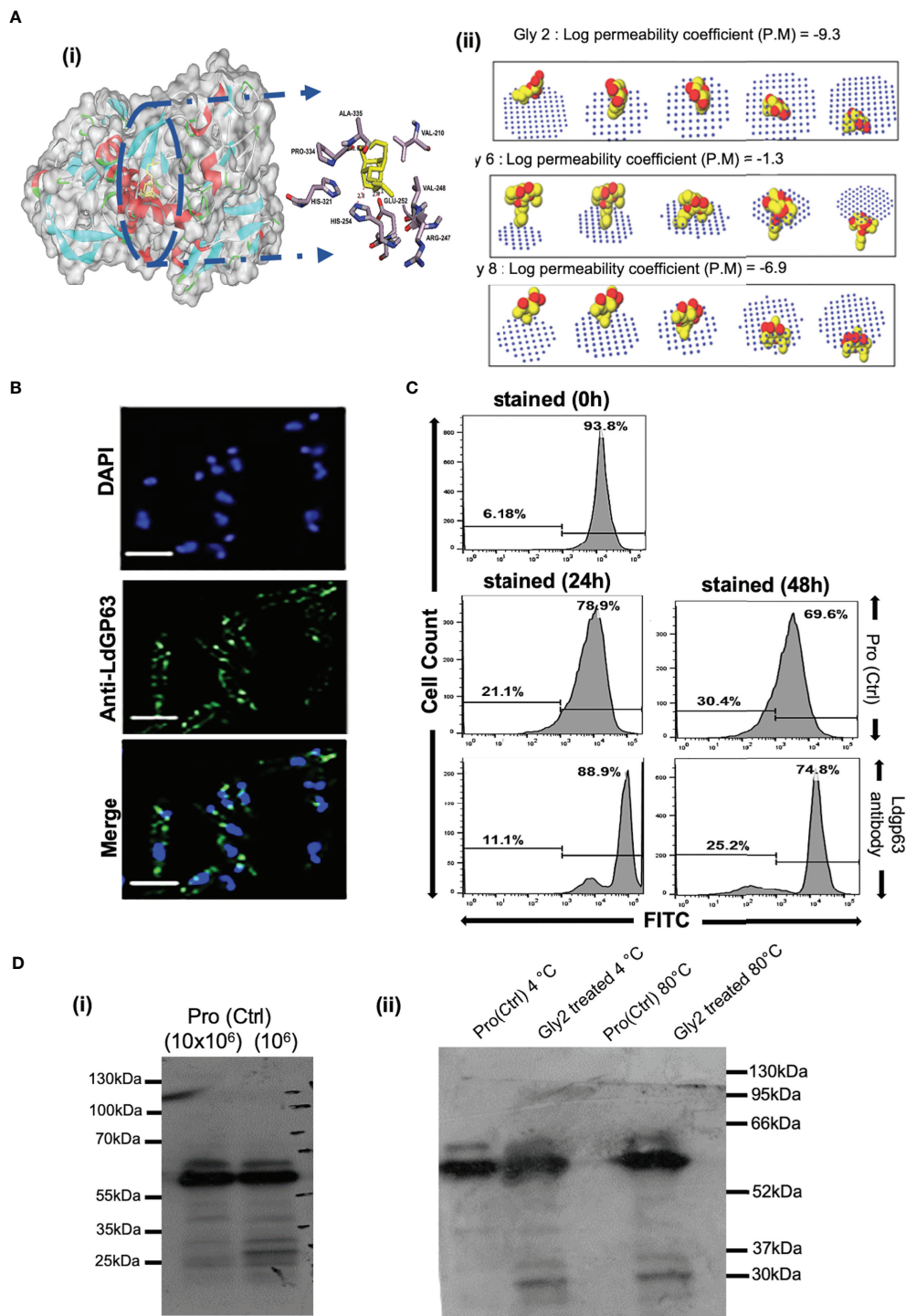


FIGURE 2 | Gp63, a surface molecule, is the target of **Gly2** and is involved in promastigote proliferation. **(A)** (i) Three-dimensional (3D) surface model of Gly2–LdGp63 complex denoted by the degree of hydrophobicity and surface accessible for ligand binding using a gray scheme. The defined region shows interacting residues of Gly2–LdGp63 complex. Ligplot version 2.2, Discovery Studio version 19.1.0, and Pymol version 2.3.2 have been used to generate these figures. (ii) Membrane binding affinity of Glycosides 2, 6, and 8 using PerMM server. **(B)** Immunofluorescence assay of *Leishmania donovani* promastigotes using anti-LdGp63 antibody. **(C)** Proliferation of promastigotes determined by FACS masked with anti-LdGp63 antibody using CFDA-SE dye for a consecutive period of 24, 48, and 72 h. **(D)** (i) LdGp63 was detected in variable numbers of promastigote lysate with generated polyclonal anti-LdGp63 antibody. (ii) The thermostability of LdGp63 was analyzed by immunoblotting in untreated or **Gly2** (5 μ M)-treated promastigotes at 4°C and 80°C.

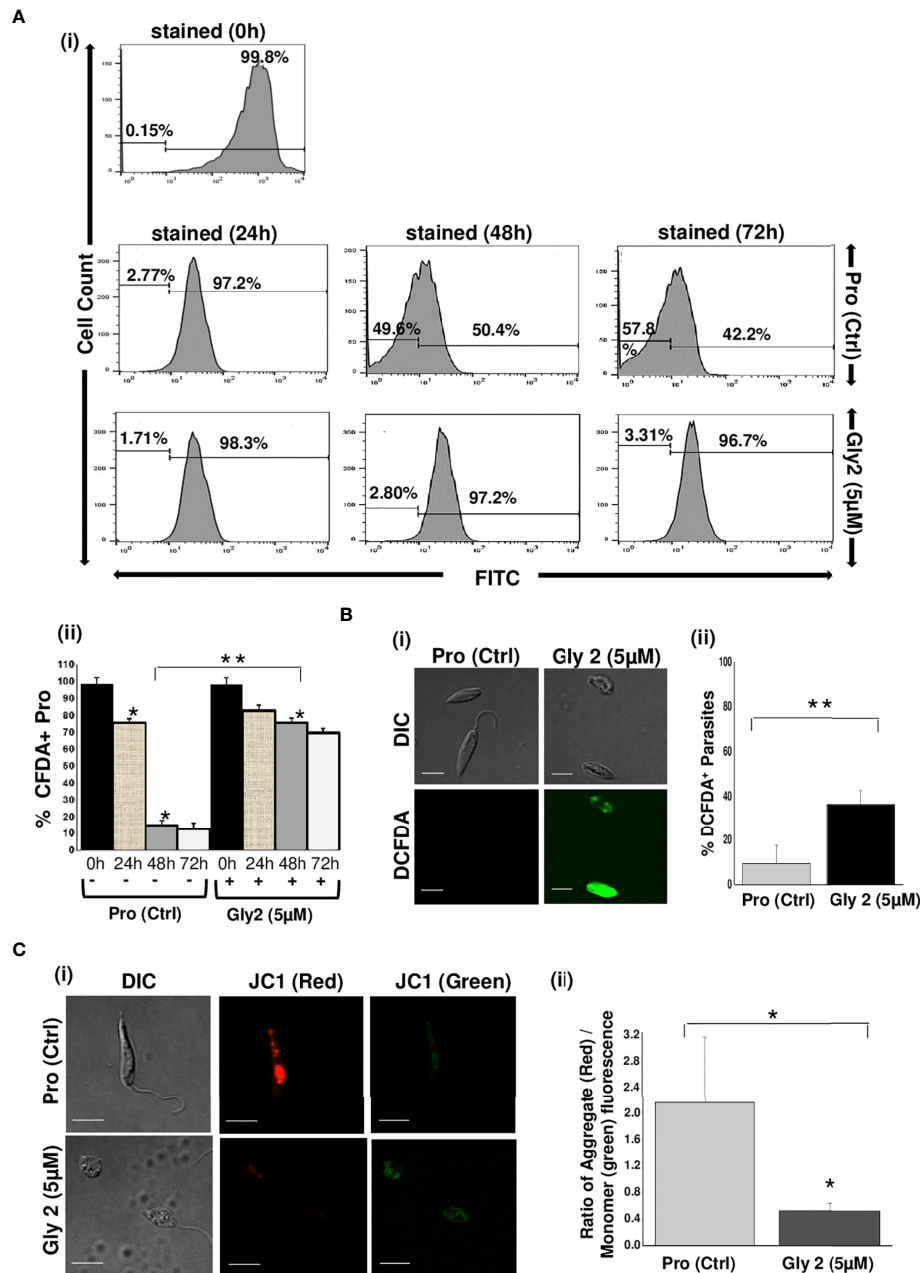


FIGURE 3 | Gly2 efficiently reduced promastigote proliferation, leading to elevated ROS levels and disruption of mitochondrial membrane potential. **(A)** (i) Rate of proliferation of promastigotes was determined by the change in CFDA-SE staining as represented by flow cytometry histograms, depicting huge cellular multiplication arrest upon treatment with Gly2 at 24, 48, and 72 h, respectively. Pro refers to untreated promastigotes. (ii) Nominal decrement observed in the percentage of CFDA-SE-positive promastigotes when treated by the compound for 24, 48, and 72 h. The asterisks (**) indicate statistical significance ($p < 0.01$, $n = 3$) between the indicated groups. **(B)** (i) Confocal imaging of DCFDA staining showed strong green fluorescence in Gly2-treated cells indicative of increased ROS levels. (ii) Bar graph representing significantly higher percentage of DCFDA+ promastigotes in Gly 2 treatment as compared to control. **(C)** (i) Effect of Gly2 on $\Delta\Psi_m$ of promastigotes was indicated by the conversion of monomer (green) to oligomer (red) forms of JC-1 using confocal micrographs. The shift in intensity of red fluorescence (JC1 aggregates/PE) to green fluorescence (JC1 monomers/FITC) implies destabilized $\Delta\Psi_m$ in promastigotes following the treatment. (ii) Bar graph showing the reduction in the ratio of JC-1 Red (aggregate)/Green (monomer) in Gly2-treated parasites. The asterisks (* and **) indicate statistical significance ($p < 0.05$ and $p < 0.01$, respectively, $n = 3$) between the indicated groups.

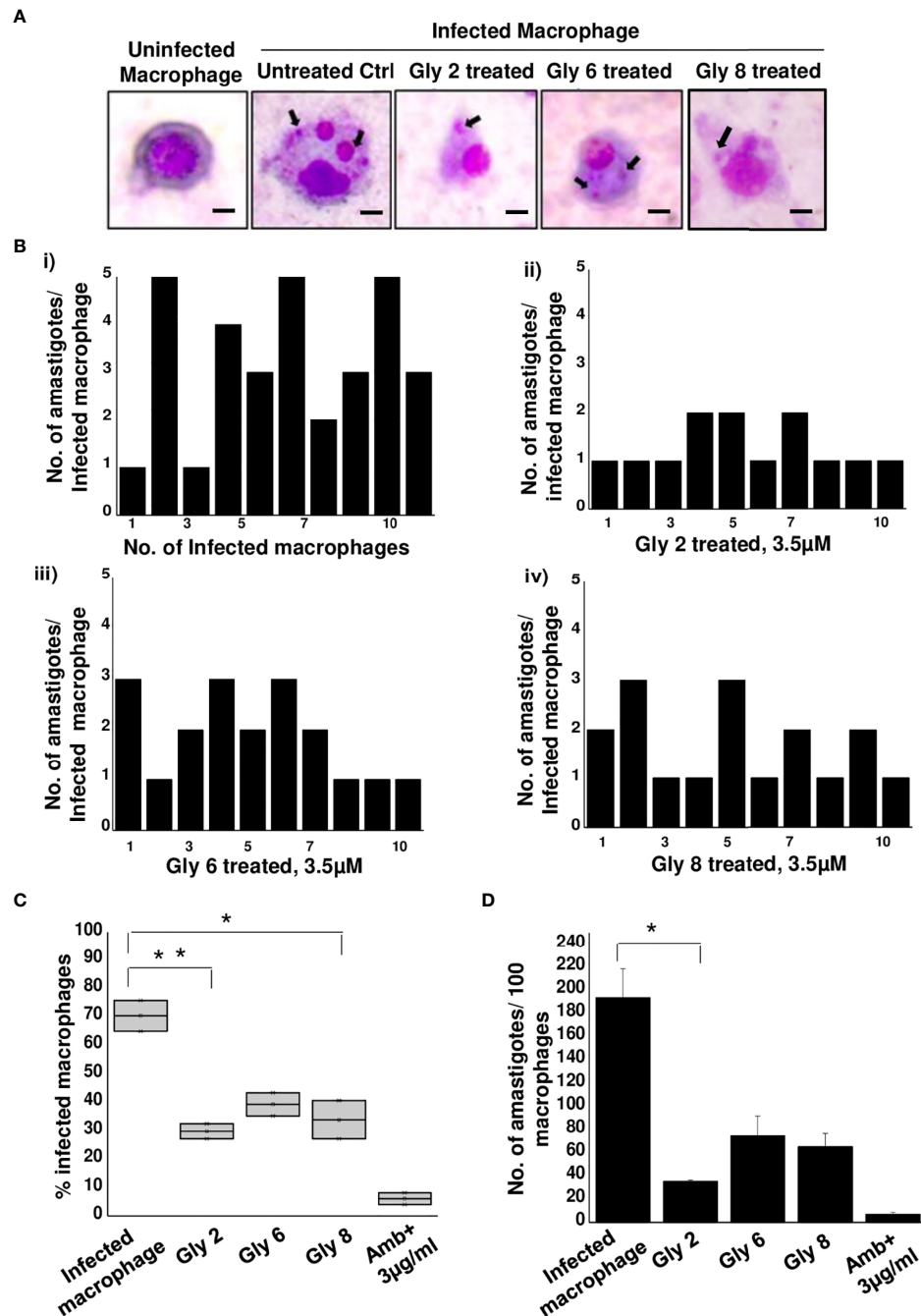


FIGURE 4 | Antileishmanial activity of Gly2 against intramacrophage amastigotes. **(A)** Glycoside-treated and untreated Geimsa-stained mouse macrophages infected with *L. donovani* amastigotes. **(B)** Number of amastigotes per infected macrophage in untreated (i) and glycoside (ii–iv)-treated cells that were counted individually for 10 distinct cells. **(C)** Percentage of infected macrophages in the presence and absence of glycoside treatment. **(D)** Number of amastigotes per 100 macrophages in both untreated and glycoside-treated cells. P-values * <0.05 and ** <0.01 were considered as values denoting significance.

Anti-Proliferative Effect of Gly2 Is Due to Disruption of Mitochondrial Membrane and Destabilization of Redox Potential

It has been reported that downregulation of Gp63 protein results in the loss of promastigote development and multiplication

(Hajmová et al., 2004; Pandey et al., 2004). Based on this information, we hypothesized that the binding of Gly2 to Gp63 protein might have an anti-proliferative effect on promastigotes. Therefore, we assessed the proliferation of promastigotes by quantifying the release of CFDA-SE, a cell-

permeable dye, during cell division. It was observed that, when the promastigotes were treated with 5 μM of **Gly2**, the percentage of CFDA-positive cells remained unchanged at 24 (81.59%), 48 (74.68%), and 72 h (68.48%) that implied the absence of cell division in the parental cell. However, the untreated promastigotes showed proliferation in a time-dependent manner as the CFDA-positive cells reduced gradually from 24 to 72 h (**Figure 3A**). From the above results, we deduced that there is a significant reduction in promastigotes' growth and multiplication upon treatment with **Gly2**. Previous studies, including the study from our own lab, have shown that the cellular mechanism of antileishmanial drugs might involve destabilization of $\Delta\Psi\text{m}$ -coupled ROS elevation leading to cellular death patterns in *Leishmania* spp. (Corral et al., 2016; Ramu et al., 2017). Therefore, we then asked whether **Gly2**-based inhibition of LdGp63 has any similar impact. To address the same, we have used DCFDA-based detection of ROS levels in promastigote forms of *L. donovani* (Corral et al., 2016; Ramu et al., 2017). The data represented an increased intensity of green fluorescence in **Gly2**-treated promastigotes, indicating enhancement in intracellular ROS levels, whereas control parasites showed balanced redox homeostasis (**Figure 3B**). The representative bar graph showed $\sim 50\%$ parasite population with DCFDA staining (% DCFDA⁺ parasites) suggestive of elevated ROS levels (**Figure 3B**). Elevation of intracellular ROS is usually coupled with the depolarization of mitochondrial membrane. Hence, to explore the effect of **Gly2** on $\Delta\Psi\text{m}$ of promastigotes, we have used a lipophilic cationic dye (JC-1) exhibiting green fluorescence in its monomeric form. Enhanced level of red fluorescence denotes more J aggregate formation due to higher $\Delta\Psi\text{m}$, whereas a shift toward lower red and/or accumulation of higher green fluorescence implies a strong indication of destabilized $\Delta\Psi\text{m}$ (Sivandzade et al., 2019). Upon treatment of promastigotes with **Gly2**, we found that the mitochondrial uptake of JC-1 dye was significantly decreased, as manifested by stronger green fluorescence as compared to the control healthy promastigotes displaying intense red fluorescence, depicting stable $\Delta\Psi\text{m}$ (**Figure 3C**). These data clearly inferred that in addition to its anti-proliferative effect, **Gly2** elevated the intracellular levels of ROS, leading to loss of $\Delta\Psi\text{m}$.

Gly2 Treatment Demonstrated a Significant Reduction in Infected Macrophages and Intramacrophagic Form of Amastigotes

With promising antileishmanial effect of **Gly2** on promastigote forms of *Leishmania* spp., we then studied its impact on intramacrophagic amastigote forms of *Leishmania*. The findings revealed that the parasite infection is severely reduced following glycoside treatment (**Figure 4A**). Furthermore, we asked whether these treatments could also affect the number of amastigotes per infected macrophage. As expected, the number of amastigotes was found to be predominantly reduced in **Gly2**-treated samples (~ 1 amastigotes/macrophages), wherein **Gly6** and **Gly8** treatments depicted ~ 3 or 2 amastigotes/macrophages, respectively (**Figures 4Bi–iv**). The control untreated macrophages had ~ 5 numbers of amastigotes/macrophages.

In addition, the percentage of macrophages infected was found to be very less following glycoside treatment as compared to untreated control (**Figure 4C**). The total amastigote load was also calculated per 100 macrophages, and the results have shown severe depletion in total amastigote load against glycoside treatments as compared to control (**Figure 4D**). Plausibly, **Gly2** has a pronounced effect on intracellular amastigotes in exceptionally low micromolar range, suggesting its potential antileishmanial activity in both stages.

Gly2 Induced Enhancement of Complement-Mediated Lysis of Promastigotes in Serum Physiological Conditions

Mimicking the physiological condition of the body, axenic promastigote cultures in late log phase were exposed to complement-mediated lysis using human serum, which was determined by measuring PI-stained cells (Dominguez et al., 2002; Bandyopadhyay et al., 2004). Histogram plots illustrate 55.40% population of promastigote death in 10% NHS within 30 min as compared to control that showed 0.06% parasite death and 99.00% intact promastigotes in 10% FBS (heat inactivated). The **Gly2**-treated promastigotes however showed 80.05% parasite death in the presence of 10% NHS. There was 24.65% increment in PI uptake that is directly proportional to promastigote killing. Majority of **Gly2**-treated promastigotes were non-motile when observed under the microscope. The precise size of this population was difficult to calculate, as in the presence of NHS, promastigote cell volume and refractile properties were altered, blurring the distinction between promastigotes, cell debris, and NHS background signal. These results indicate that the presence of **Gly2** and 10% NHS causes rapid lysis of *Leishmania* promastigotes (**Figure 5, Supplementary Figure S4**).

DISCUSSION

The major blockades involved in therapeutic interventions against leishmaniasis include inefficacious pharmacokinetics and pharmacodynamics of drugs, toxicity, drug resistance, and lack of vaccines (Sundar and Singh, 2018). These factors create an urgent requirement for discovering novel drug candidates and developing target-specific molecules for better preventive measures and treatment modalities. Earlier reports have elucidated the important role of flavonoid glycosides from biologically active aqueous plant extracts against VL (Shah et al., 2014). Notably, plant-based beta-glycosides and their aglycones have been detected as potent transmission-blocking sugar baits that alter the physiology of the vector *L. longipalpis* and the development of *Leishmania* spp. inside the same (Ferreira et al., 2018). Based on these facts, we have synthesized simple glucose and glucosamine backbone conferring natural product-inspired library of compounds using green synthetic chemistry with strong compliance to Lipinski's "rule-of-five." To evaluate the cytotoxic effect of

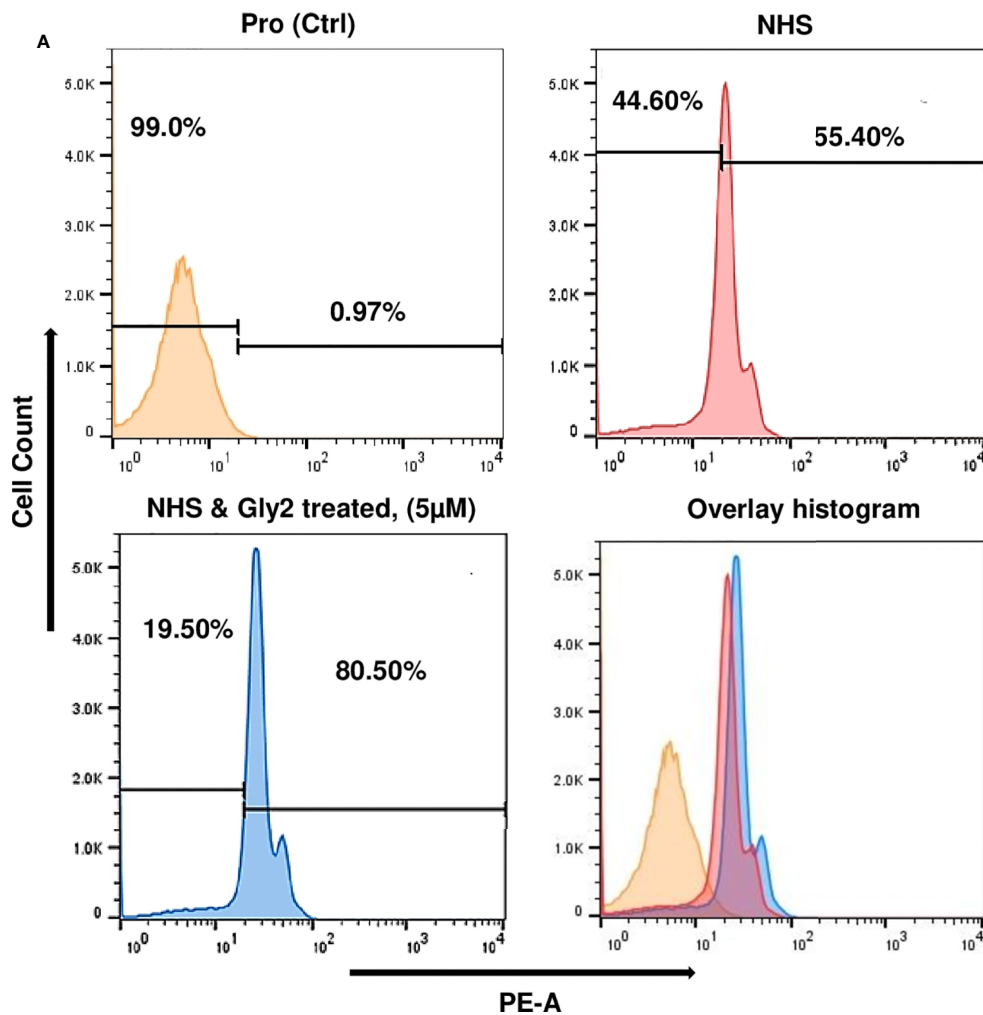


FIGURE 5 | Gly2-treated promastigotes enhance the complement-mediated lysis in serum physiological condition and the concentration-dependent cytotoxic effect of Gly2 on PKDL strain. (A) Promastigote lysis, triggered by 10% normal human serum, was analyzed by uptake of PI using flow cytometry.

these glycoside derivatives, on both parasites and host, we performed *in vitro* screening of the same on *L. donovani* promastigotes and in mammalian cells such as macrophages and MDCK. The findings represented profound cytotoxicity conferred by **Gly2**, **6**, and **8** on promastigotes, leading to significant parasitic death, with no lethal impact on mammalian cells. These data suggested strong selectivity of compounds toward parasites, also clearly depicted by their representative higher SI. However, among these compounds, Gly2 demonstrated the highest SI value (>1,000) and enhanced toxicity in both lab strain of *L. donovani* and in BS12, a clinical strain of PKDL, suggesting its potent antileishmanial ability.

Considering the profound cytotoxic effects enforced by **Gly2** on both lab and clinical forms of promastigotes, we assumed that Gly2 might possibly interact with membrane-associated proteins. It is noteworthy that Gp63/Leishmanolysin, a metalloproteinase containing a conserved zinc-binding/catalytic motif (HEXXH), is abundantly expressed on the surface of promastigotes and

known to play significant roles in multiple steps of the infection comprising their entry into macrophages until their intralysosomal survival (Liu and Chang, 1992; Brittingham et al., 1999; Cerdà-Costa and Gomis-Rüth, 2014). Since LdGp63 is widely expressed on the surface of promastigotes, it is hypothesized that the antileishmanial effect of Gly2 might be the result of Gly2–Gp63 interaction. Further *in silico* docking analysis of the 3D surface model of Gly2–LdGp63 complex revealed efficient binding of Gly2 with a unique pocket in the catalytic domain of LdGp63, strengthening this hypothesis. Next, using an *in silico* tool, the membrane permeability aspect of **Gly2**, **Gly6**, and **Gly8** was assessed that clearly depicted Gly2 to be the only non-permeant glycoside derivative with a strong membrane binding affinity, suggestive of its strong interaction with the catalytic pocket of LdGp63 expressed on the promastigote surface. This finding further enabled us to have a deeper look at the chemical structures of lead compounds, which revealed that **Gly2**, the most active compound derived from D-glucose,

has isopentyl as branched alkyl group with native free hydroxyl (OH) group that makes this molecule hydrophilic (clogP 0.26) and less cell penetrable. **Gly6**, having isopentyl as branched alkyl chain along with OH group, is being masked with acetyl (OAc) group, which makes the molecule more hydrophobic (clogP 2.4) that is suitable for cell permeability. **Gly8**, on the other hand, has a shorter straight or linear alkyl chain (propyl) along with masked OH group, representing a potent amphiphile (clogP 1.47) that might perform dual roles including surface binding and cell penetration. Plausibly, **Gly2**-mediated abrogation of promastigote multiplication further strengthened the possibility of Gly2–LdGp63 interaction on the promastigote surface. In addition, masking of promastigote surface with in-house-generated catalytic domain-specific mouse polyclonal anti-LdGp63 antibody represented partial abrogation of promastigote proliferation, substantiating the role of LdGp63 in proliferation of promastigotes. Furthermore, to assess interactions between **Gly2** and LdGp63 in a physiologically relevant cellular environment, we performed CETSA that has emerged as an efficient tool to validate drug–target engagement and target validation both in complex protein samples and in live cells. Precisely, CETSA solely works upon the principle of ligand binding-induced thermal stabilization of proteins. This assay induces heat-induced denaturation and precipitation of unbound proteins when subjected to higher temperatures, leaving the ligand-bound proteins in the solution that can be detected by Western blot (Langebäck et al., 2019). An accumulating number of studies suggest that CETSA has been widely used as a primary validation of drug–target engagement in case of apicomplexan parasites such as *Plasmodium falciparum* and *Toxoplasma gondii* (Herneisen et al., 2020).

In this study, CETSA revealed that Gly2 upon binding with Gp63 displayed protein complex stabilization even at a remarkably high temperature of 80°C under physiologic conditions. This phenomenon could be visualized prominently when the membrane was immunoblotted with anti-LdGp63 catalytic domain antibody, which represented an abundance of Gp63 in treated samples, confirming the possibility of high affinity binding of **Gly2** to LdGp63. Previous studies, including one from our group, have shown that drug treatment has a core impact toward parasite death through loss of $\Delta\Psi_m$ and ROS elevation, a coupled event associated with cellular death patterns in *Leishmania* spp. (Ramu et al., 2017). In line with such information, we checked if **Gly2** has any such impact on *L. donovani* promastigotes. As assumed, the results confirmed increased ROS generation followed by $\Delta\Psi_m$ loss, leading to almost ~90% of parasitic death against **Gly2** treatment. With such profound impact on promastigotes, next, we asked whether **Gly2** could impose any changes to intramacrophagic amastigote forms of *L. donovani*. To highlight, **Gly2** treatment indeed demonstrated significant depletion in infected macrophages and led to a substantial reduction in load of intracellular amastigotes as compared to the other glycoside hybrids. It is noteworthy that *Leishmania* modulates the complement system for its survival in the host, and the resistance to such innate immune component is associated with its two major GPI-

anchored surface glycoconjugates, namely, lipophosphoglycan (LPG) and GP63 (Cecílio et al., 2014; Verma et al., 2018; Elmahallawy et al., 2021). Interestingly, *L. major*, being deficient with these two surface determinants, has shown high sensitivity toward the complement system (Joshi et al., 2002; Späth et al., 2003). Thus, based on such information, we have determined the impact of Gly2 treatment on susceptibility of promastigotes toward complement-mediated lysis in NHS-enriched promastigote culture that mimicked similar pathophysiological conditions in the body. The observations suggested prominent increment in parasitic death contributing to ~80% of cytolysis. Overall, our study has discovered Gly2 as a novel glycoside hybrid with promising antileishmanial activity.

CONCLUSIONS

In the current scenario of drug-resistant *Leishmania* parasites, there is a requirement to develop new potent antileishmanials that are less prone to resistance development. Conclusively, we have introduced a novel glycoside derivative, **Gly2**, as a potential antileishmanial and suggested a prospective first-in-class therapeutic measure for both VL and PKDL to ascertain its clinical utility.

DATA AVAILABILITY STATEMENT

The original contributions presented in the study are included in the article/**Supplementary Material**, further inquiries can be directed to the corresponding authors.

AUTHOR CONTRIBUTIONS

AC has contributed to performing all the biological experiments. RS & CN designed the molecules and CN synthesized the molecules. AC and NJ have done preliminary analyses and *in silico* membrane binding studies and prepared the initial draft. SS and SP have conceived the study and planned the work plan. SG and SP have executed, troubleshooted, and analyzed the data. AR and LG have performed data analyses. AC and SP have written the final draft. SS, SP, and RS have corrected and edited the final version of the article.

FUNDING

This work was supported by funding from DBT builder program, DST, and JNU UPE II program. Dr. Shailja Singh and Dr. Anand Ranganathan are thankful for the funding support from the Science and Engineering Research Board (SERB, File no. IPA/2020/000007) and Drug and Pharmaceuticals Research Programme (DPRP, Project No. P/569/2016-1/TDT). Dr. Soumya Pati is grateful for the funding support from the Cognitive Science

Research Initiative (CSRI) program of the Department of Science and Technology (DST/CSRI/2018/247).

ACKNOWLEDGMENTS

AC and NJ are supported by Shiv Nadar Foundation fellowships. The Center for Informatics located within Shiv Nadar University is also duly acknowledged. SG is thankful for the funding support from DST INSPIRE grant. SP is grateful for the funding support from Shiv Nadar foundation. CN acknowledges the fellowship

supported by CSIR-NET. We sincerely acknowledge help from Prof. Madhubala Rentala, JNU, for gifting the J774.A1 murine macrophage cell line.

SUPPLEMENTARY MATERIAL

The Supplementary Material for this article can be found online at: <https://www.frontiersin.org/articles/10.3389/fcimb.2022.803048/full#supplementary-material>

REFERENCES

- Accelrys Software Inc (2009). *Discovery Studio Modeling Environment, Release 2.5.1* (San Diego, CA Accelrys Software Inc., 2012).
- Arenas, R., Torres-Guerrero, E., Quintanilla-Cedillo, M. R., and Ruiz-Esmenjaud, J. (2017). Leishmaniasis: A Review. *F1000Research* 6, 750–65. doi: 10.12688/F1000RESEARCH.11120.1
- Ayana, R., Yadav, P., Kumari, R., Ramu, D., Garg, S., Pati, S., et al. (2018). Identification and Characterization of a Novel Palmitoyl Acyltransferase as a Druggable Rheostat of Dynamic Palmitoylome in *L. Donovanii*. *Front. Cell. Infect. Microbiol.* 8. doi: 10.3389/FCIMB.2018.00186
- Bandyopadhyay, S., Chatterjee, M., Das, T., Bandyopadhyay, S., Sundar, S., and Mandal, C. (2004). Antibodies Directed Against O-Acetylated Sialoglycoconjugates Accelerate Complement Activation in *Leishmania* Donovanii Promastigotes. *J. Infect. Dis.* 190, 2010–2019. doi: 10.1086/425519/2/190-11-2010-FIG007.GIF
- Bi, K., Chen, Y., Zhao, S., Kuang, Y., and John Wu, C. H. (2018). Current Visceral Leishmaniasis Research: A Research Review to Inspire Future Study. *BioMed. Res. Int.* 2018, 1–13. doi: 10.1155/2018/9872095
- Brittingham, A., Chen, G., McGwire, B. S., Chang, K. P., and Mosser, D. M. (1999). Interaction of *Leishmania* Gp63 With Cellular Receptors for Fibronectin. *Infect. Immun.* 67, 4477–4484. doi: 10.1128/IAI.67.9.4477-4484.1999/ASSET/7A022910-C9C6-4EB3-83AA-0AE293423476/ASSETS/GRAPHIC/II0991512006.JPEG
- Brittingham, A., Morrison, C. J., McMaster, W. R., McGwire, B. S., Chang, K.-P., and Mosser, D. M. (1995). Role of the *Leishmania* Surface Protease Gp63 in Complement Fixation, Cell Adhesion, and Resistance to Complement-Mediated Lysis. *Parasitol. Today* 11, 445–446. doi: 10.1016/0169-4758(95)80054-9
- Burza, S., Croft, S. L., and Boelaert, M. (2018). Leishmaniasis. *Lancet* 392, 951–970. doi: 10.1016/S0140-6736(18)31204-2
- Cecílio, P., Pérez-Cabezas, B., Santarém, N., Maciel, J., Rodrigues, V., and da Silva, A. C. (2014). Deception and Manipulation: The Arms of *Leishmania*, a Successful Parasite. *Front. Immunol.* 5. doi: 10.3389/FIMMU.2014.00480
- Cerdà-Costa, N., and Gomis-Rüth, F. X. (2014). Architecture and Function of Metalloprotease Catalytic Domains. *Protein Sci.* 23, 123–144. doi: 10.1002/PRO.2400
- Chakrabarti, M., Joshi, N., Kumari, G., Singh, P., Shoaib, R., Munjal, A., et al. (2021). Interaction of *Plasmodium falciparum* Apicortin With α - and β -Tubulin Is Critical for Parasite Growth and Survival. *Sci. Rep.* 11, 1–16. doi: 10.1038/s41598-021-83513-5
- Chaudhuri, G., and Chang, K. P. (1988). Acid Protease Activity of a Major Surface Membrane Glycoprotein (Gp63) From *Leishmania mexicana* Promastigotes. *Mol. Biochem. Parasitol.* 27, 43–52. doi: 10.1016/0166-6851(88)90023-0
- Corral, M. J., Benito-Peña, E., Jiménez-Antón, M. D., Cuevas, L., Moreno-Bondí, M. C., and Alunda, J. M. (2016). Allicin Induces Calcium and Mitochondrial Dysregulation Causing Necrotic Death in *Leishmania*. *PLoS Negl. Trop. Dis.* 10, e0004525–35. doi: 10.1371/JOURNAL.PNTD.0004525
- Cousins, K. R. (2011). Computer Review of ChemDraw Ultra 12.0. *J. Am. Chem. Soc.* 133, 8388. doi: 10.1021/JA204075S
- Croft, S. L., Sundar, S., and Fairlamb, A. H. (2006). Drug Resistance in Leishmaniasis. *Clin. Microbiol. Rev.* 19, 111–126. doi: 10.1128/CMR.19.1.111-126.2006
- Cuevas, I. C., Cazzulo, J. J., and Sánchez, D. O. (2003). Gp63 Homologues in *Trypanosoma cruzi*: Surface Antigens With Metalloprotease Activity and a Possible Role in Host Cell Infection. *Infect. Immun.* 71, 5739–5749. doi: 10.1128/IAI.71.10.5739-5749.2003
- Daina, A., Michielin, O., and Zoete, V. (2017a). SwissADME: A Free Web Tool to Evaluate Pharmacokinetics, Drug-Likeness and Medicinal Chemistry Friendliness of Small Molecules. *Sci. Rep.* 7, 42717. doi: 10.1038/srep42717
- DeLano, W. L. (2002). Pymol: An Open-Source Molecular Graphics Tool. *CCP4 News/Protein Crystallogr.* 40, 82–92. Available at: http://www.ccp4.ac.uk/newsletters/newsletter40/11_pymol.pdf
- Dominguez, M., Moreno, I., López-Trascasa, M., and Toraño, A. (2002). Complement Interaction With Trypanosomatid Promastigotes in Normal Human Serum. *J. Exp. Med.* 195, 451–459. doi: 10.1084/JEM.20011319
- Elmahallawy, E. K., Alkhaldi, A. A. M., and Saleh, A. A. (2021). Host Immune Response Against Leishmaniasis and Parasite Persistence Strategies: A Review and Assessment of Recent Research. *Biomed. Pharmacother.* 139, 111671. doi: 10.1016/J.BIOPHA.2021.111671
- Etges, R. J., Bouvier, J., Hoffman, R., and Bordier, C. (1985). Evidence That the Major Surface Proteins of Three *Leishmania* Species are Structurally Related. *Mol. Biochem. Parasitol.* 14, 141–149. doi: 10.1016/0166-6851(85)90033-7
- Ferreira, T. N., Pita-Pereira, D., Costa, S. G., Brazil, R. P., Moraes, C. S., Díaz-Albiter, H. M., et al. (2018). Transmission Blocking Sugar Baits for the Control of *Leishmania* Development Inside Sand Flies Using Environmentally Friendly Beta-Glycosides and Their Aglycones. *Parasites Vectors* 11, 1–20. doi: 10.1186/S13071-018-3122-Z/TABLES/13
- Hajmová, M., Chang, K. P., Kolli, B., and Volf, P. (2004). Down-Regulation of Gp63 in *Leishmania Amazonensis* Reduces its Early Development in *Lutzomyia longipalpis*. *Microbes Infect.* 6, 646–649. doi: 10.1016/J.MICINF.2004.03.003
- Herneisen, A. L., Sidik, S. M., Markus, B. M., Drewry, D. H., Zuercher, W. J., and Lourido, S. (2020). Identifying the Target of an Antiparasitic Compound in Toxoplasma Using Thermal Proteome Profiling. *ACS Chem. Biol.* 15, 1801–1807. doi: 10.1021/ACSCHEMBIO.0C00369/SUPPL_FILE/CB0C00369_SI_006.PDF
- Joshi, P. B., Kelly, B. L., Kamhawi, S., Sacks, D. L., and McMaster, W. R. (2002). Targeted Gene Deletion in *Leishmania* Major Identifies Leishmanolysin (GP63) as a Virulence Factor. *Mol. Biochem. Parasitol.* 120, 33–40. doi: 10.1016/S0166-6851(01)00432-7
- Joshi, P. B., Sacks, D. L., Modi, G., and McMaster, W. R. (1998). Targeted Gene Deletion of *Leishmania* Major Genes Encoding Developmental Stage-Specific Leishmanolysin (GP63). *Mol. Microbiol.* 27, 519–530. doi: 10.1046/J.1365-2958.1998.00689.X
- Jost, K. L., Rottach, A., Milden, M., Bertulat, B., Becker, A., Wolf, P., et al. (2011). Generation and Characterization of Rat and Mouse Monoclonal Antibodies Specific for McCP2 and Their Use in X-Inactivation Studies. *PLoS One* 6, e26499–510. doi: 10.1371/JOURNAL.PONE.0026499
- Kamhawi, S. (2006). Phlebotomine Sand Flies and *Leishmania* Parasites: Friends or Foes? *Trends Parasitol.* 22, 439–445. doi: 10.1016/J.PT.2006.06.012
- Kaplan, W., and Littlejohn, T. G. (2001). Swiss-PDB Viewer (Deep View). *Brief Bioinform.* 2, 195–197. doi: 10.1093/BIB/2.2.195
- Langebäck, A., Bacanu, S., Laursen, H., Mout, L., Seki, T., Erkens-Schulze, S., et al. (2019). CETSA-Based Target Engagement of Taxanes as Biomarkers for Efficacy and Resistance. *Sci. Rep.* 9, 1–17. doi: 10.1038/s41598-019-55526-8
- Laskowski, R. A., MacArthur, M. W., Moss, D. S., and Thornton, J. M. (1993). PROCHECK: A Program to Check the Stereochemical Quality of Protein Structures. *J. Appl. Crystallogr.* 26, 283–291. doi: 10.1107/S002188892009944/FULL

- Laskowski, R. A., and Swindells, M. B. (2011). LigPlot+: Multiple Ligand–Protein Interaction Diagrams for Drug Discovery. *J. Chem. Inf. Model.* 51, 2778–2786. doi: 10.1021/C1200227U
- Liu, X., and Chang, K. P. (1992). Extrachromosomal Genetic Complementation of Surface Metalloproteinase (Gp63)-Deficient *Leishmania* Increases Their Binding to Macrophages. *Proc. Natl. Acad. Sci.* 89, 4991–4995. doi: 10.1073/PNAS.89.11.4991
- Lomize, A. L., Hage, J. M., Schnitzer, K., Golobokov, K., Lafaive, M. B., Forsyth, A. C., et al. (2019). PerMM: A Web Tool and Database for Analysis of Passive Membrane Permeability and Translocation Pathways of Bioactive Molecules. *J. Chem. Inf. Model.* 59, 3094–3099. doi: 10.1021/ACS.JCIM.9B00225/SUPPL_FILE/C19B00225_SI_001.PDF
- López-Arencibia, A., García-Velázquez, D., Martín-Navarro, C. M., Sifaoui, I., Reyes-Batlle, M., Lorenzo-Morales, J., et al. (2015). *In Vitro* Activities of Hexaazatrinaphthylenes Against *Leishmania* Spp. *Antimicrob. Agents Chemother.* 59, 2867–2874. doi: 10.1128/AAC.00226-15
- Martins-Melo, F. R., Lima, M. D. S., Ramos, A. N., Alencar, C. H., and Heukelbach, J. (2014). Mortality and Case Fatality Due to Visceral Leishmaniasis in Brazil: A Nationwide Analysis of Epidemiology, Trends and Spatial Patterns. *PloS One* 9, e93770–812. doi: 10.1371/JOURNAL.PONE.0093770
- McGwire, B. S., Chang, K. P., and Engman, D. M. (2003). Migration Through the Extracellular Matrix by the Parasitic Protozoan *Leishmania* Is Enhanced by Surface Metalloprotease Gp63. *Infect. Immun.* 71, 1008–1010. doi: 10.1128/IAI.71.2.1008-1010.2003
- Medina-Acosta, E., Karess, R. E., and Russell, D. G. (1993). Structurally Distinct Genes for the Surface Protease of *Leishmania Mexicana* are Developmentally Regulated. *Mol. Biochem. Parasitol.* 57, 31–45. doi: 10.1016/0166-6851(93)90241-O
- Messaritakis, I., Mazeris, A., Koutala, E., and Antoniou, M. (2010). *Leishmania* Donovanii s.L.: Evaluation of the Proliferation Potential of Promastigotes Using CFSE Staining and Flow Cytometry. *Exp. Parasitol.* 125, 384–388. doi: 10.1016/J.EXPPARA.2010.03.006
- Moreno, I., Domínguez, M., Cabañes, D., Aizpurua, C., and Toraño, A. (2010). Kinetic Analysis of *Ex Vivo* Human Blood Infection by *Leishmania*. *PloS Negl. Trop. Dis.* 4, e743. doi: 10.1371/JOURNAL.PNTD.0000743
- Morris, G. M., and Lim-Wilby, M. (2008). Molecular Docking. *Methods Mol. Biol.* 443, 365–382. doi: 10.1007/978-1-59745-177-2_19
- Nejad-Moghaddam, A., and Abolhassani, M. (2009). Production and Characterization of Monoclonal Antibodies Recognizing a Common 57-kDa Antigen of *Leishmania* Species. *Iran Biomed. J.* 13, 245–251.
- Oryan, A., and Akbari, M. (2016). Worldwide Risk Factors in Leishmaniasis. *Asian Pac J. Trop. Med.* 9, 925–932. doi: 10.1016/J.APJTM.2016.06.021 Available at: <http://www.ncbi.nlm.nih.gov/pubmed/19946351>.
- Pandey, S., Chakraborti, P., Sharma, R., Bandyopadhyay, S., Sarkar, D., and Adhya, S. (2004). Involvement of *Leishmania* Donovanii Major Surface Glycoprotein Gp63 in Promastigote Multiplication. *J. Biosci.* 29, 15–22. doi: 10.1007/BF02702557
- Pettersen, E. F., Goddard, T. D., Huang, C. C., Couch, G. S., Greenblatt, D. M., Meng, E. C., et al. (2004). UCSF Chimera—A Visualization System for Exploratory Research and Analysis. *J. Comput. Chem.* 25, 1605–1612. doi: 10.1002/JCC.20084
- Ponte-Sucre, A., Gamarro, F., Dujardin, J. C., Barrett, M. P., López-Vélez, R., García-Hernández, R., et al. (2017). Drug Resistance and Treatment Failure in Leishmaniasis: A 21st Century Challenge. *PloS Negl. Trop. Dis.* 11, e0006052–67. doi: 10.1371/JOURNAL.PNTD.0006052
- Prassas, I., and Diamandis, E. P. (2008). Novel Therapeutic Applications of Cardiac Glycosides. *Nat. Rev. Drug Discovery* 2008 711 7, 926–935. doi: 10.1038/nrd2682
- Racine, J. (2000). The Cygwin Tools: A GNU Toolkit for Windows. *J. Appl. Econom.* 15, 331–341. doi: 10.1002/1099-1255(200005/06)15:3<331::AID-JAE558>3.0.CO;2-G
- Ramu, D., Garg, S., Ayana, R., Keerthana, A. K., Sharma, V., Saini, C. P., et al. (2017). Novel β -Carboline-Quinazolinone Hybrids Disrupt *Leishmania* Donovanii Redox Homeostasis and Show Promising Antileishmanial Activity. *Biochem. Pharmacol.* 129, 26–42. doi: 10.1016/j.bcp.2016.12.012
- Schneider, C. A., Rasband, W. S., and Eliceiri, K. W. (2012). NIH Image to ImageJ: 25 Years of Image Analysis. *Nat. Methods* 9, 671–675. doi: 10.1038/NMETH.2089
- Sen, R., and Chatterjee, M. (2011). Plant Derived Therapeutics for the Treatment of Leishmaniasis. *Phytomedicine* 18, 1056–1069. doi: 10.1016/J.PHYMED.2011.03.004
- Sengupta, R., Chaudhuri, S. J., Moulik, S., Ghosh, M. K., Saha, B., Das, N. K., et al. (2019). Active Surveillance Identified a Neglected Burden of Macular Cases of Post Kala-Azar Dermal Leishmaniasis in West Bengal. *PloS Negl. Trop. Dis.* 13, e0007249–55. doi: 10.1371/JOURNAL.PNTD.0007249
- Shah, N. A., Khan, M. R., and Nadhman, A. (2014). Antileishmanial, Toxicity, and Phytochemical Evaluation of Medicinal Plants Collected From Pakistan. *BioMed. Res. Int.* 2014, 1–7. doi: 10.1155/2014/384204
- Shivappagowdar, A., Garg, S., Srivastava, A., Hada, R. S., Kalia, I., Singh, A. P., et al. (2021). Pathogenic Pore Forming Proteins of *Plasmodium* Triggers the Necrosis of Endothelial Cells Attributed to Malaria Severity. *Toxins (Basel)* 13, 62. doi: 10.3390/TOXINS13010062
- Shivappagowdar, A., Pati, S., Narayana, C., Ayana, R., Kaushik, H., Sah, R., et al. (2019). A Small Bioactive Glycoside Inhibits Epsilon Toxin and Prevents Cell Death. *DMM Dis. Model. Mech.* 12, 415. doi: 10.1242/DMM.040410/VIDEO-2
- Singh, O. P., Singh, B., Chakravarty, J., and Sundar, S. (2016). Current Challenges in Treatment Options for Visceral Leishmaniasis in India: A Public Health Perspective. *Infect. Dis. Poverty* 5, 19. doi: 10.1186/S40249-016-0112-2
- Sivandzade, F., Bhalerao, A., and Cucullo, L. (2019). Analysis of the Mitochondrial Membrane Potential Using the Cationic JC-1 Dye as a Sensitive Fluorescent Probe. *Bio-protocol* 9, 271. doi: 10.21769/BioProtoc.3128
- Späth, G. F., Lye, L. F., Segawa, H., Sacks, D. L., Turco, S. J., and Beverley, S. M. (2003). Persistence Without Pathology in Phosphoglycan-Deficient *Leishmania* Major. *Science* 301, 1241–1243. doi: 10.1126/SCIENCE.1087499
- Spessard, G. O. (1998). ACD Labs/LogP dB 3.5 and ChemSketch 3.5. *J. Chem. Inf. Comput. Sci.* 38, 1250–1253. doi: 10.1021/C1980264T
- Studio, D. (2015). Dassault Systemes BIOVIA, *Discovery Studio Modelling Environment, Release 4.5*. (Accelrys Softw. Inc.).
- Sundar, S., and Singh, B. (2018). Emerging Therapeutic Targets for Treatment of Leishmaniasis. *Expert Opin. Ther. Targets* 22, 467–486. doi: 10.1080/14728222.2018.1472241
- Sunter, J., and Gull, K. (2017). Shape, Form, Function and *Leishmania* Pathogenicity: From Textbook Descriptions to Biological Understanding. *Open Biol.* 7, 170165. doi: 10.1098/RSOB.170165
- Szakiel, A., Ruszkowski, D., Grudniak, A., Kurek, A., Wolska, K. I., Doligalska, M., et al. (2008). Antibacterial and Antiparasitic Activity of Oleanolic Acid and its Glycosides Isolated From Marigold (*Calendula Officinalis*). *Planta Med.* 74, 1709–1715. doi: 10.1055/S-0028-1088315
- Verma, S., Mandal, A., Ansari, M. Y., Kumar, A., Abhishek, K., Ghosh, A. K., et al. (2018). *Leishmania* Donovanii Inhibitor of Serine Peptidases 2 Mediated Inhibition of Lectin Pathway and Upregulation of C5aR Signaling Promote Parasite Survival Inside Host. *Front. Immunol.* 9. doi: 10.3389/FIMMU.2018.00063
- Waring, M. J. (2010). Lipophilicity in Drug Discovery. *Expert Opin. Drug Discov.* 5, 235–248. doi: 10.1517/17460441003605098
- Yao, C., Donelson, J. E., and Wilson, M. E. (2003). The Major Surface Protease (MSP or GP63) of *Leishmania* Sp. Biosynthesis, Regulation of Expression, and Function. *Mol. Biochem. Parasitol.* 132, 1–16. doi: 10.1016/S0166-6851(03)00211-1
- Yao, C., Leidal, K. G., Brittingham, A., Tarr, D. E., Donelson, J. E., and Wilson, M. E. (2002). Biosynthesis of the Major Surface Protease GP63 of *Leishmania* Chagasi. *Mol. Biochem. Parasitol.* 121, 119–128. doi: 10.1016/S0166-6851(02)00030-0
- Yu, Y., Ko, K. S., Zea, C. J., and Pohl, N. L. (2004). Discovery of the Chemical Function of Glycosidases: Design, Synthesis, and Evaluation of Mass-Differentiated Carbohydrate Libraries. *Org. Lett.* 6, 2031–2033. doi: 10.1021/OL049389B/SUPPL_FILE/OL049389BSI20040429_023501.PDF
- Zijlstra, E. E. (2016). The Immunology of Post-Kala-Azar Dermal Leishmaniasis (PKDL). *Parasites Vectors* 9, 1–9. doi: 10.1186/S13071-016-1721-0/FIGURES/3

Conflict of Interest: The authors declare that the research was conducted in the absence of any commercial or financial relationships that could be construed as a potential conflict of interest.

Publisher's Note: All claims expressed in this article are solely those of the authors and do not necessarily represent those of their affiliated organizations, or those of the publisher, the editors and the reviewers. Any product that may be evaluated in

this article, or claim that may be made by its manufacturer, is not guaranteed or endorsed by the publisher.

Copyright © 2022 Chakrabarti, Narayana, Joshi, Garg, Garg, Ranganathan, Sagar, Pati and Singh. This is an open-access article distributed under the terms of the

Creative Commons Attribution License (CC BY). The use, distribution or reproduction in other forums is permitted, provided the original author(s) and the copyright owner(s) are credited and that the original publication in this journal is cited, in accordance with accepted academic practice. No use, distribution or reproduction is permitted which does not comply with these terms.



The Phosphodiesterase Inhibitor Tadalafil Promotes Splenic Retention of *Plasmodium falciparum* Gametocytes in Humanized Mice

Daniela Barbieri¹, Lina Gomez¹, Ludivine Royer¹, Florian Dupuy¹, Jean-François Franetich², Maurel Tefit², Marie-Esther N'Dri¹, Dominique Mazier², Olivier Silvie², Alicia Moreno-Sabater^{2,3} and Catherine Lavazec^{1*}

¹ INSERM U1016, CNRS UMR8104, Université Paris Cité, Institut Cochin, Paris, France, ² Sorbonne Université, INSERM, CNRS, Centre d'Immunologie et des Maladies Infectieuses, Paris, France, ³ Service de Parasitologie-Mycologie Assistance Publique-Hôpitaux de Paris (AP-HP), Hôpital Saint-Antoine, Paris, France

OPEN ACCESS

Edited by:

Maria Carolina Touz,
Medical Research Institute Mercedes
and Martín Ferreyra (INIMEC),
Argentina

Reviewed by:

Mariana De Niz,
Universidade de Lisboa, Portugal
Daniel Youssef Bargieri,
University of São Paulo, Brazil

*Correspondence:

Catherine Lavazec
catherine.lavazec@inserm.fr

Specialty section:

This article was submitted to
Parasite and Host,
a section of the journal
Frontiers in Cellular and
Infection Microbiology

Received: 25 February 2022

Accepted: 26 April 2022

Published: 25 May 2022

Citation:

Barbieri D, Gomez L, Royer L, Dupuy F, Franetich J-F, Tefit M, N'Dri M-E, Mazier D, Silvie O, Moreno-Sabater A and Lavazec C (2022) The Phosphodiesterase Inhibitor Tadalafil Promotes Splenic Retention of *Plasmodium falciparum* Gametocytes in Humanized Mice. *Front. Cell. Infect. Microbiol.* 12:883759. doi: 10.3389/fcimb.2022.883759

The persistence of erythrocytes infected with *Plasmodium falciparum* gametocytes in the bloodstream is closely related to the modulation of their mechanical properties. New drugs that increase the stiffness of infected erythrocytes may thus represent a novel approach to block malaria parasite transmission. The phosphodiesterase inhibitor tadalafil has been shown to impair the ability of infected erythrocytes to circulate in an *in vitro* model for splenic retention. Here, we used a humanized mouse model to address *in vivo* the effect of tadalafil on the circulation kinetics of mature gametocyte-infected erythrocytes. We show that stiff immature gametocyte-infected erythrocytes are retained in the spleen of humanized mice at rates comparable to that of the *in vitro* model. Accordingly, tadalafil-induced stiffening of mature gametocyte-infected erythrocytes impairs their circulation in the bloodstream and triggers their retention by the spleen. These *in vivo* results validate that tadalafil is a novel drug lead potentially capable of blocking malaria parasite transmission by targeting GIE mechanical properties.

Keywords: *Plasmodium falciparum*, transmission, gametocytes, tadalafil, phosphodiesterase, humanized mice

INTRODUCTION

Malaria is a major public health problem that still causes more than half a million deaths per year (WHO, 2021). Clinical symptoms of malaria are ascribed to the asexual stages of the *Plasmodium* parasite, while gametocytes, the specialized sexual cells, are responsible for parasite transmission from humans to Anopheles mosquitoes. Most antimalarials target the asexual stages, and are less efficient in killing sexual stages (Birkholtz et al., 2016; Plouffe et al., 2016). This poses a significant challenge to malaria elimination strategies because infected individuals could still transmit the sexual parasites even several weeks after successful treatment of the asexual forms (Bousema et al., 2006). Thus, the development of novel compounds is urgently needed in order to target gametocytes. *Plasmodium falciparum* gametocytes require 8–10 days for maturation into five morphologically distinct phases (stages I–V) (Hawking et al., 1971). Stages I–IV are absent from blood circulation and are instead sequestered in the bone marrow where they develop into mature

stage V gametocytes (Farfour et al., 2012; Aguilar et al., 2014; Joice et al., 2014). Mature gametocyte-infected erythrocytes (GIE) are then released in the blood, infective for mosquitoes. The lifespan of circulating mature gametocytes has been estimated at several weeks during which stage V GIE are able to avoid splenic retention (Bousema et al., 2010; Cao et al., 2019). GIE persistence in the blood circulation is crucial for parasite transmission to mosquitoes; therefore, interfering with this process is an innovative approach to block malaria parasites transmission (Tiburcio et al., 2012; Duez et al., 2015). The filterability of mature GIE is closely related to the modulation of their mechanical properties. During their development, gametocytes decrease both the stiffness and the permeability of their host erythrocyte, thus increasing its filterability across the spleen and its osmotic stability (Aingaran et al., 2012; Dearnley et al., 2012; Tiburcio et al., 2012; Bouyer et al., 2020). These modifications of GIE mechanical properties are tightly regulated by cyclic AMP (cAMP) signaling pathway and phosphodiesterase (PDE) activity (Ramdani et al., 2015; Bouyer et al., 2020). *PfPDE δ* , the main PDE expressed by mature gametocyte stages, plays a key role in this process and appears to be the master regulator of mature GIE deformability (Ramdani et al., 2015). Importantly, studies using an *in vitro* model for splenic retention reported that the marketed PDE inhibitors sildenafil and tadalafil increase the stiffness of mature GIE (Ramdani et al., 2015; N'dri et al., 2021). These observations suggest that drugs targeting PDE are expected to promote the mechanical retention of mature GIE by the spleen and their clearance from the bloodstream in gametocyte carriers. PDE inhibitors therefore represent potential novel drug leads capable of blocking malaria parasite transmission. To reinforce this drug development effort, these promising observations should be validated *in vivo*. The effect of PDE inhibitors on the circulation of *Plasmodium* gametocytes was investigated using the rodent model *Plasmodium berghei* in a study showing that treatment of infected mice with sildenafil citrate results in gametocyte accumulation in bone marrow and spleen (De Niz et al., 2018). However, since *P. falciparum* parasites are highly specific for human red blood cells (hRBC) and exhibit a sexual development drastically different from that of rodent malaria parasites, the use of a humanized mouse model is the most relevant approach to validate the effect of PDE inhibitors *in vivo* (Moreno-Sabater et al., 2018). To this end, we used mice from the severe immunodeficient mouse strain NOD SCID gamma c (NSG) in which we induced a chemical depletion of macrophages and neutrophils. In these mice, the immunomodulation protocol allows the graft of hRBC and prevents the elimination of GIE by the immune system, thus making this humanized mouse model suitable for testing drugs against *P. falciparum* transmission stages (Duffier et al., 2016).

In this study, we used flow cytometry, bioluminescence imaging and RT-qPCR analyses to follow the kinetics of *P. falciparum* GIE in the blood circulation of this humanized mouse model over a short or a long period of time in order to quantify the effect of tadalafil on GIE persistence in the bloodstream and retention in the spleen.

MATERIAL AND METHODS

Parasites and Mice

The *P. falciparum* NF54 strain, the transgenic lines NF54-cg6-pfs16-CBG99 (Cevenini et al., 2014), NF54-pfs47-hsp70-GFP (Neveu et al., 2020) and NF54-hsp70-TurboFP635 (described in **Supplemental Methods**) have been used for our experiments. Parasites were cultured *in vitro* under standard conditions using RPMI-1640 medium supplemented with 10% heat-inactivated human serum and human erythrocytes at a 5% hematocrit. Synchronous production of specific gametocytes stages was achieved by treating synchronized cultures at the ring stage (10–15% parasitemia) with 50 mM N-acetylglucosamine (NAG) for 5 days to eliminate asexual parasites. Gametocytes were purified by magnetic isolation using a MACS depletion column (Miltenyi Biotec) in conjunction with a magnetic separator.

NSG mice were purchased from Charles River. All animal experiments were carried out in strict accordance with the guide for the care and use of laboratory animals from the Centre d'Expérimentation Fonctionnelle (CEF, La Pitié-Salpêtrière, Paris) and with the French and European regulations (2010/63/EU). The experimental protocols were approved by the Ministère de l'Éducation Nationale, de l'Enseignement Supérieur et de la Recherche (Authorization Number 01736.02). For all tests, 9–12 weeks-old mice were used. Infection experiments were performed using 10–15 animals per experiment, while GIE injections were performed using 1–6 animals per experiment.

Immunomodulation Treatment and hRBC Engraftment in Mice

NSG mice aged 9–12 weeks were bred at the CEF under strict pathogen-free conditions. hRBC were obtained from donors (Etablissement Français du Sang Ile-de-France, Rungis). Before peritoneal injection into mice, hRBC were washed twice with RPMI-1640 medium at 2500 rpm, 5 min at 4°C. Immunomodulation treatment was performed as described in (Duffier et al., 2016). The depletion of tissue macrophages was induced by clodronate encapsulated in liposomes (Liposoma). Neutrophils were depleted using the monoclonal antibody (mAb) NIMP-R14 produced by a hybridoma kindly provided by Dr M. Strath (National Institute for Medical Research, London, U.K.) (Tacchini-Cottier et al., 2000). To obtain the graft of hRBC and subsequent *P. falciparum* infection, each mouse received by intraperitoneal injection a dose of 1 mg/kg of mAb NIMP-R14 at day 0 and 6.25 mg/kg of lip-clod at day 1. At day 5 and day 7 each mouse received 1.5 mL of hRBC at 50% hematocrit in RPMI mixed with 1 mg/kg of mAb NIMP-R14 and 6.25 mg/kg of lip-clod. At day 9, mice were subjected to either infection with asexual parasites or injection of purified GIE. Hematological parameters (hematocrit, leucocytes, platelets, percentage of hRBC in peripheral blood) were followed up during the assay in blood samples taken from mouse tails and analyzed with an automatic hematology analyzer. Mice with incomplete hRBC engraftment at day 9 were excluded from subsequent analyses.

Mouse Infection Using Asexual Parasites

At day 9 after the beginning of immunomodulation treatment, each mouse received the same doses of immunomodulators in 1.5 mL of hRBC at 50% hematocrit containing 0.1% of NF54-pfs47-hsp70-GFP *P. falciparum* asexual parasites. Parasites used for infection were obtained from an *in vitro* culture maintained below 1.5% parasitemia to avoid *in vitro* induction of gametocytogenesis. After *P. falciparum* infection, mice were grafted with 1 to 1.5 mL of hRBC at 50% hematocrit containing 1 mg/kg of mAb NIMP-R14 and 6.25 mg/kg of lip-clod every 2–3 days. Mice with hematocrit above 60% and percentage of hRBC above 70% received the graft of hRBC only when hematocrit decreased to 50%.

Mouse Injection Using GIE

At day 9 after the beginning of immunomodulation treatment, each mouse received 6×10^7 *P. falciparum* GIE by retro-orbital injection. GIE preparations were enriched in different experiments by magnetic isolation. Stage III GIE were collected at day 4 and stage V GIE at day 9 after initiating NAG treatment. Parasites were kept at 37°C until injection to avoid activation of gametogenesis.

Tadalafil Treatment

The effect of tadalafil was assessed either upon incubation of purified GIE or upon mice treatment. In the first instance, MACS-purified stage V GIE preparations were pre-incubated 30 minutes at 37°C in RPMI-1640 medium supplemented with 100 μ M tadalafil (Euromedex) before retro-orbital injection of 100 μ L of RPMI/tadalafil 100 μ M in each mouse. Treatment of mice with tadalafil was administered either to uninfected mice before GIE injection or to infected mice when gametocytes were circulating in peripheral blood for more than 1 day. Uninfected mice were orally treated with a dose of 200 μ g Cialis® (Lilly) diluted in 0.9% NaCl, which corresponds to a tadalafil dose of 8 mg/kg, 30 minutes before retro-orbital injection with MACS-purified stage V GIE. This dose was chosen based on the interspecies dose extrapolation scaling to result in plasma concentrations of tadalafil equivalent to a human dose of 40 mg/day. In mouse infection experiments, 200 μ g of Cialis® (Lilly) diluted in 0.9% NaCl was administered by oral feeding daily during 4 days. For each mouse, gametocytemia was monitored on Giemsa-stained thin tail-blood smears collected daily until animal sacrifice at day 6 post drug treatment and by RT-qPCR analysis on blood collected at sacrifice.

Quantification of Parasitemia by Flow Cytometry

After GIE injection, the quantification of parasitemia in mouse peripheral blood was performed using flow cytometry. To increase the fluorescent signal, GIE NF54-pfs47-hsp70-GFP and NF54-hsp70-TurboFP635 were pre-incubated for 15 minutes at 37°C with WGA-GFP or WGA-PE Texas red (5 μ g/mL), respectively. Five minutes before the end of incubation, GIE were stained with Hoechst 33342 (1/10,000). Cells were then washed and resuspended in 100 μ L RPMI-1640 before retro-orbital injection in mice.

Parasitemia was followed up during the assay in blood samples taken from mouse tails at 10 minutes, 1 hour, 2 hours, 3 hours and 7 hours post GIE injection. The collected samples (100 μ L of peripheral blood) at each time point were washed with PBS 1 X and fixed for 10 min at room temperature with PBS, 1% PFA and 0.025% Glutaraldehyde. Parasitemia was quantified using Fortessa (BD Biosciences) cytometer.

Quantification of Parasitemia by RT-qPCR Analysis

Peripheral blood samples were added to Trizol (Life technologies) and vortexed, while spleen samples were grinded in Trizol. RNA was prepared using the PureLink RNA Mini kit (Life technologies) and treated using on-column DNase-Treatment with Pure Link DNase (Life technologies). Quantity and purity of RNA were assessed with Nanodrop 8000 (Thermo Scientific). cDNA synthesis was performed using the SuperScript III First-Strand Synthesis System (Life technologies). Different sets of primers were used to quantify parasites: when two transgenic parasite lines were co-injected in mice, primers designed for *gfp* (*sense* 5'-TTCTTCAAGTCCGCCATGCC, *antisense* 5'-TTGTACTCCAGCTTGTCGCC) or *turbofp635* (*sense* 5'-CAAAACCTTTATCAACCACACC, *antisense* 5'-CCGAGTGTTCCTTCTGCATC) were used to discriminate between the two subpopulations of co-injected gametocytes (stage III vs stage V or tadalafil-treated vs untreated), while primers for the ubiquitin-conjugating enzyme (*HK*, PF3D7_0812600, *sense* 5'-GGTGTTAGTGGCTCACC AATAGGA, *antisense* 5'-GTACCACCTTCCCATGGAGTATCA) were used to quantify the whole population of gametocytes. When only one transgenic parasite line was injected in mice, parasitemia was quantified using the absolute quantification method by determining a standard curve after amplification of the *gfp* sequence from serial dilutions of the pBLD588-hsp70-GFP plasmid (Neveu et al., 2020). qPCRs were performed in Light Cycler 480 (Roche), each sample was analyzed in duplicates.

Assessment of GIE Localization In Vivo

GIE distribution in mouse tissue was determined by bioluminescence imaging. Mice were retro-orbitally injected with 6×10^7 NF54-cg6-pfs16-CBG99 GIE. Seven hours post-injection, mice were injected intraperitoneally with D-luciferin (potassium salt, Perkin Elmer) at 100 mg/kg, sacrificed 3 minutes after injection, dissected and then organs (brain, heart, lung, liver, spleen and bone) were imaged within 10–15 min post-injection. IVIS Spectrum (Caliper Life Science, Hanover, MD, USA) was used to measure luciferase activity. Images were analyzed using the living Image 3.0 software (Caliper Life Science, Hanover, MD, USA). The luminescence signal was measured in photons $s^{-1} cm^{-2} sr^{-1}$.

Microspherification

Calibrated metal microspheres (96.50% tin, 3.00% silver, and 0.50% copper; Industrie des Poudres Sphériques) with 2 different size distributions (5- to 15- μ m-diameter and 15- to 25- μ m-diameter) composed a matrix used to assay infected erythrocyte

deformability under flow, as described (Lavazec et al., 2013). Suspensions of cultures containing 1.5% of stage III or stage V GIEs were perfused through the microsphere matrix at a flow rate of 60 mL/h using an electric pump (Syramed_sp6000, Arcomed_Ag), followed by a wash with 5 mL of complete medium. The upstream and downstream samples were collected and smeared onto glass slides for staining with Giemsa reagent, and parasitemia was assayed by counting 2000 erythrocytes to determine parasite retention versus flow-through.

Generation of the NF54-Pfs47-hsp70-TurboFP635 Transgenic Line

To generate the NF54-pfs47-hsp70-TurboFP635 line that expresses the far-red reporter TurboFP635 under the control of the constitutive promoter *hsp70*, cultures of the NF54 clone B10 were co-transfected with 70 µg of plasmid pDC2-Cas9-hDHFRyFCU and 70 µg of plasmid pBLD588-hsp70-TurboFP635 and selected with 2.5 nM WR99210 as previously described (Ghorbal et al., 2014). The plasmid pDC2-Cas9-hDHFRyFCU (Knuepfer et al., 2017) encodes a single guide RNA that recognizes a sequence located in the *pfs47* locus. Generation of pBLD588-hsp70-TurboFP635 plasmid was performed by a double digestion of the pBLD588-hsp70-GFP plasmid previously described (Neveu et al., 2020) with HindIII and XhoI restriction enzymes. The *turbofp635* was amplified from a gBlocks Gene Fragments (IDT) using the P2 (TTAAGAAAAAAGCTTATGGTGGGTGAGGATAGCGTGC) and P4 (CGTTATGTTACTCGAGTTAGCTGTGCCCCAGTTTGCTAGG) primers. The *turbofp635* fragment was then cloned in frame using the In-Fusion system (Ozyme). Following transfection and drug selection, clones were obtained by limiting dilution. Plasmid integration into the *pfs47* locus was confirmed by PCR using the primers P3 (GCGATATGTAATTCCATTACTGC) and P1 (CCTAACACATTATGTGTATAACATTTTATGC).

Statistical Analysis

Statistical significance was determined using a Mann Whitney test or a two-way ANOVA test with Sidak correction for multiple comparisons. Analyses were performed using GraphPad Prism Version 9.3.1 for Windows.

RESULTS

Stiff GIE Are Cleared Faster From the Peripheral Circulation Than Deformable GIE

To analyze the kinetics of *P. falciparum* GIE circulation *in vivo*, we used chemically immunomodulated NSG mice grafted with hRBC (Duffier et al., 2016). After successful hRBC engraftment, MACS-purified fluorescent GIE were retro-orbitally injected into mice and percentage of GIE was then monitored by flow cytometry in blood collected from the tail of the mice at several time points from 10 minutes post-injection until sacrifice. Preliminary results showed that almost all mature GIE injected in mice were cleared from the peripheral blood at 24 hours post injection (hpi), whereas approximately half of the GIE population remained in circulation

at 7 hpi (**Supplemental Figure 1**). Therefore, in the following experiments all mice were sacrificed at 7 hpi. To address the impact of GIE deformability on their circulation kinetics, stiff immature GIE and deformable mature GIE from two different fluorescent transgenic strains, which constitutively express either a green fluorescent reporter [NF54-Pfs47-hsp70-GFP (Neveu et al., 2020)] or a far red fluorescent reporter [NF54-Pfs47-hsp70-TurboFP635 (**Supplemental Figure 2**)], were simultaneously injected into each mouse (**Figure 1A**). This protocol allows to follow two populations of parasites in the same mouse by flow cytometry or by RT-qPCR using primers designed on the fluorescent reporter sequences. To avoid parasite strain effect, three mice were co-injected with 6×10^7 immature GFP-expressing GIE and 6×10^7 mature TurboFP635-expressing GIE, whereas three other mice were co-injected with 6×10^7 immature TurboFP635-expressing GIE and 6×10^7 mature GFP-expressing GIE. Flow cytometry analysis showed that about 50% of the mature GIE population disappeared from the peripheral blood in 6 hours whereas 3 hours were sufficient to observe the clearance of half of the immature GIE population. At 7 hpi, only 22% of immature GIE persisted in the peripheral blood compared to 47% of mature GIE, indicating that stiff GIE are cleared faster from the circulation than deformable GIE (**Figure 1B**). Interestingly, these proportions were comparable to the retention rates observed with the same parasites in an *in vitro* model for splenic retention (**Figure 1C**). These observations led to the hypothesis that clearance of GIE from the peripheral blood may result from retention in the mouse spleen. To address this hypothesis, we performed RT-qPCR on blood and spleen samples collected from mice sacrificed at 7 hpi, using primers designed on the fluorescent reporter sequences to discriminate between immature and mature GIE within the same sample. The RT-qPCR analysis showed that the ratio spleen-to-blood was 25-fold higher for stage III GIE than for stage V GIE (**Figure 1D**). These results indicate that immature GIE, which are stiff, persist less long in the peripheral blood and are retained more in the spleen of humanized mice than mature GIE, which are deformable.

Stiff GIE Are Retained in the Spleen of Humanized Mice

To analyze further the retention of GIE in different mouse organs, mice were injected with luciferase-expressing GIE from the NF54-cg6-pfs16-CBG99 strain (Cevenini et al., 2014). Immature and mature GIE localization was assessed at 7 hpi by quantifying bioluminescence in dissected organs (**Figure 2A**). Upon injection of immature GIE, measurement of luminescence signals in isolated organs revealed GIE accumulation in the lungs and the spleen (**Figure 2B**). In contrast, injection of mature GIE resulted in a much lower luminescence signal in the spleen (**Figures 2C, D**). The signal in the lungs was comparable after injection of both stages (**Figure 2E**), suggesting that accumulation of parasites in the lungs is not dependent of GIE deformability. These results confirm that stiff GIE are retained more in the spleen of humanized mice than deformable GIE. Taken together, these findings indicate that this mouse model can be used to test drugs that interfere with the mechanical properties of GIE.

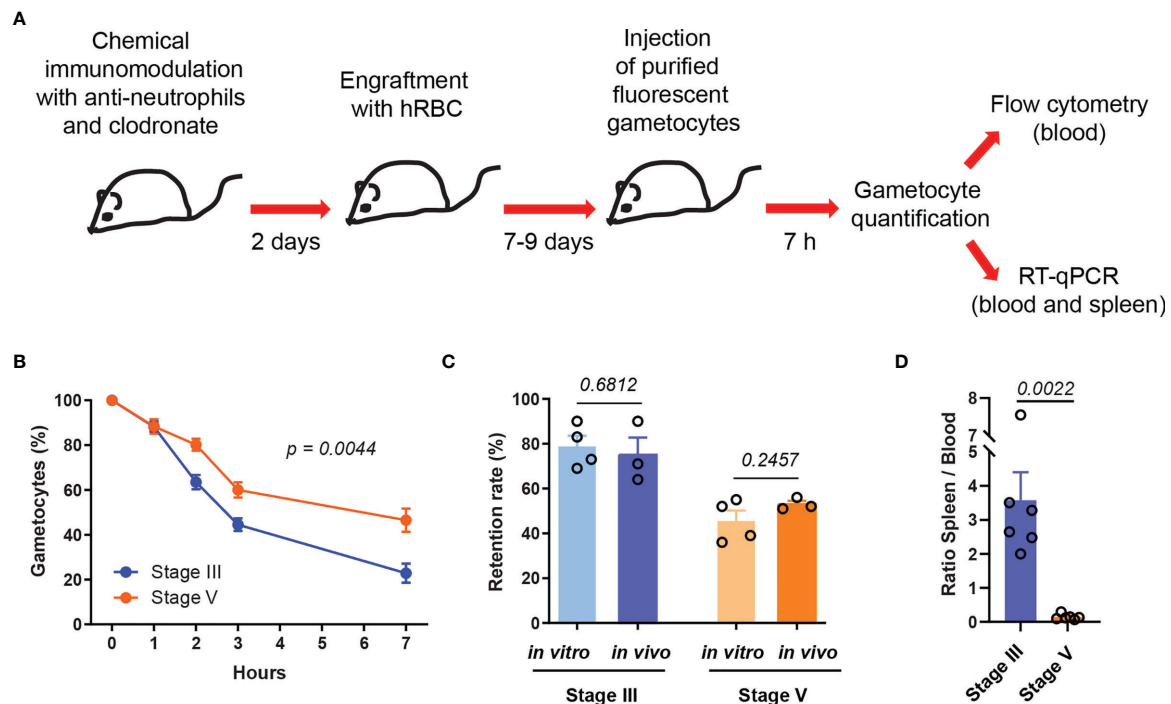


FIGURE 1 | Stiff immature GIE are cleared faster from the peripheral circulation than deformable mature GIE. **(A)** Schematic of experimental procedure for immunomodulation treatment and hRBC engraftment of NSG mice before injection with *P. falciparum* immature (stage III) and mature (stage V) fluorescent gametocytes. **(B)** Quantification of GIE clearance in peripheral blood, comparing stage III GIE (blue) and stage V GIE (orange) by flow cytometry ($n = 6$ mice from 2 independent experiments). The percentage of gametocytes is normalized to the gametocytemia at 10 minutes after injection. p indicates the statistical significance determined using a two-way ANOVA test. **(C)** Retention rate of stage III and stage V GIE determined *in vitro* by microsphere filtration ($n = 4$ filtration columns) and *in vivo* at 7hpi by flow cytometry ($n = 3$ mice). To determine GIE retention *in vitro* the upstream and downstream samples were smeared, stained with Giemsa and parasitemia was assayed by counting at least 2000 erythrocytes. **(D)** Quantitative analysis by real time RT-qPCR of GIE distribution in peripheral blood and spleen. Results were calculated as relative copy number of *gfp* or *turbofp635* gene transcripts to the control housekeeping *HK* gene transcripts in spleen and blood samples. The graph represents the ratio spleen-to-blood for 6 mice from 2 independent experiments. In C and D, p indicates the statistical significance determined using a Mann Whitney test. Error bars show the standard error of the mean (SEM).

Pre-Incubation of Mature GIE With Tadalafil Induces Their Retention in the Spleen

To address the effect of tadalafil treatment on GIE circulation *in vivo*, mature GIE were first pretreated *in vitro* before their injection in humanized mice. 6×10^7 GFP-expressing and 6×10^7 TurboFP635-expressing mature GIE were MACS-purified and one of these two transgenic lines was pre-incubated 30 min *in vitro* with 100 μ M tadalafil. The persistence of treated and untreated GIE in the peripheral blood was then analyzed by flow cytometry during 7 hours (**Figure 3A**). As observed for immature stages, tadalafil-treated mature GIE were cleared faster from the peripheral blood than control GIE, with half of treated GIE disappearing in less than 3 hours versus 6 hours for untreated GIE. At 7hpi, 71% of the initial tadalafil-treated GIE population was cleared from the peripheral blood of mice (**Figure 3B**). RT-qPCR analysis was performed to further quantify the distribution of control and treated GIE in the spleen and in the peripheral blood at 7 hpi. The ratio spleen-to-blood was 8-fold higher for treated GIE than for control GIE,

confirming that tadalafil-treated GIE persist less in blood circulation than untreated GIE and are retained more in the spleen (**Figure 3C**). These conclusions were strengthened by quantification of luminescence signals in the spleen after injection of luminescent GIE. Seven hours after injection of 6×10^7 untreated mature GIE expressing luciferase, the luminescence signal in the spleen was very weak, however the signal was much higher when mice were injected with mature GIE pre-incubated with 100 μ M tadalafil (**Figures 3D, E**). These results show that chemically-induced stiffening of mature GIE induces their retention in the spleen *in vivo* and therefore validate our previous results observed in an *in vitro* model for splenic retention (Ramdani et al., 2015; N'dri et al., 2021).

Circulation of Mature GIE Is Impaired in Humanized Mice Orally Treated With Tadalafil

To further address the effect of tadalafil on mature GIE circulation *in vivo*, we applied a protocol taking into account

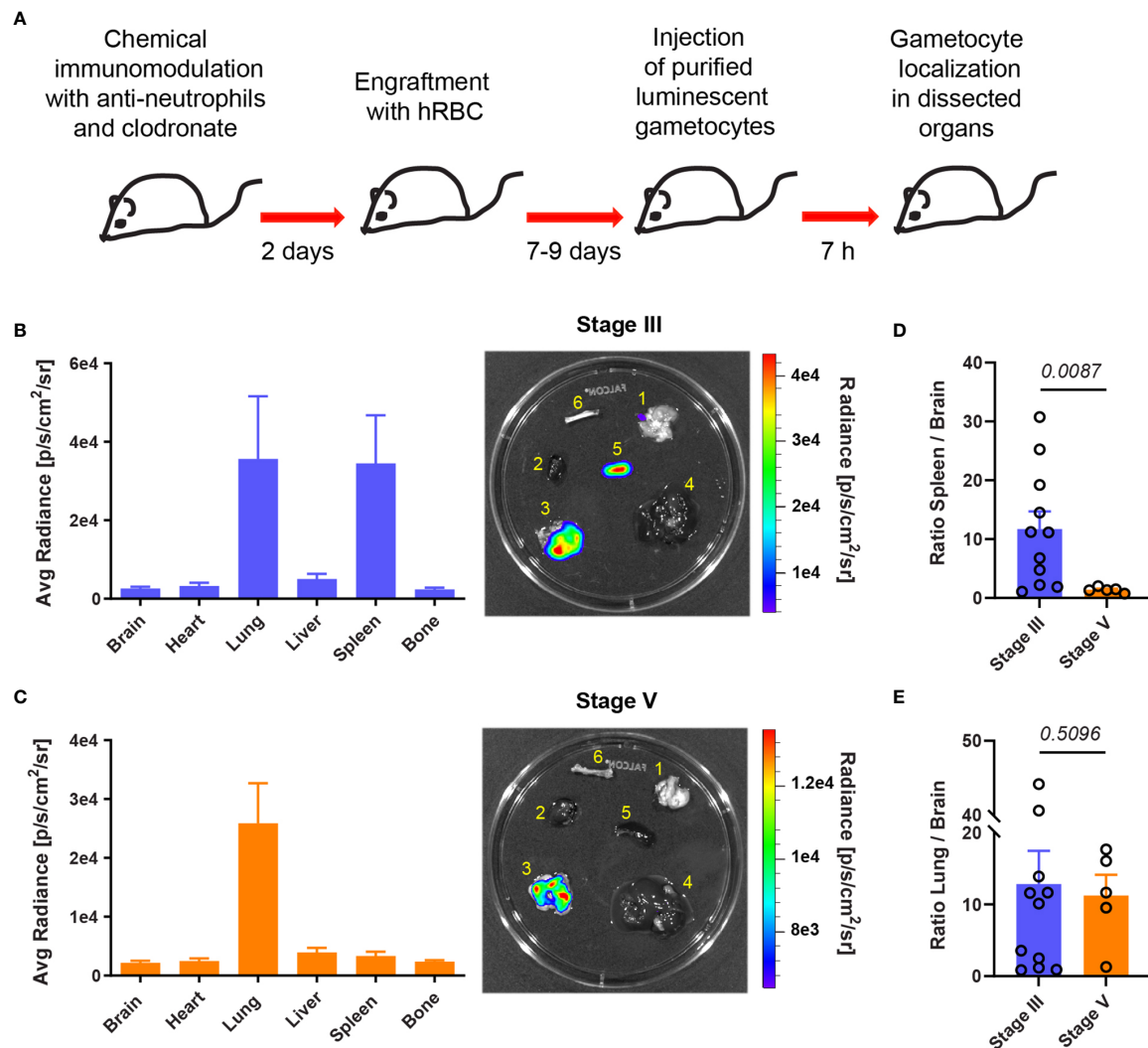


FIGURE 2 | Stiff immature GIE are retained in the spleen. **(A)** Schematic of experimental procedure for immunomodulation treatment and hRBC engraftment of NSG mice before injection with luciferase-expressing immature (stage III) and mature (stage V) gametocytes. GIE distribution was quantified 7 hpi by measuring luciferase activity in dissected organs. **(B, C)** Left: Quantification of GIE distribution visualized by measuring average radiance (p/s/cm²/sr) in dissected organs (B: stage III n=11 mice from 4 independent experiments; C: stage V n=5 mice from 2 independent experiments). Right: Representative images of luminescent signals in dissected organs (1, brain; 2, heart; 3, lungs; 4, liver; 5, spleen; and 6, bone) and heat map of radiance (p/s/cm²/sr). Rainbow shows the relative level of luciferase activity. Note that the scale of radiance can be different within separate illustration. **(D, E)** Quantification of luciferase activity calculated as the ratio of radiance in spleen and brain **(D)** or in lung and brain **(E)**. Circles indicate the number of mice from four independent experiments for stage III GIE and two independent experiments for stage V GIE. *p* indicates the statistical significance determined using a Mann Whitney test. Error bars show the SEM.

the pharmacokinetics of tadalafil. Mice were orally treated with the Cialis[®] drug, which is the pharmaceutical form of tadalafil. A group of 5 humanized NSG mice were orally treated with 200 µg of Cialis[®] 30 min before injection of 6x10⁷ purified GFP-expressing mature GIE (**Figure 4A**). At 7 hpi, the clearance of mature GIE in tadalafil-treated mice was significantly increased compared to untreated mice. Flow cytometry analysis revealed that an average of 57% gametocytes persisted in the peripheral blood of untreated mice compared to only 26% in the group of tadalafil-treated mice (**Figure 4B**). Quantification of GIE was then performed by RT-qPCR with primers designed on the *gfp*

sequence on blood and spleen samples collected from mice sacrificed at 7 hpi. The RT-qPCR analysis showed that the ratio spleen-to-blood was 13-fold higher in Cialis-treated mice than in untreated mice (**Figure 4C**). Together, these results show that mice treatment with tadalafil leads to a decrease of GIE presence in the circulation and their accumulation in the spleen. To further address the effect of tadalafil over a longer period of time, we used an infection protocol suitable for testing drugs against *P. falciparum* transmission stages (Duffier et al., 2016). In this protocol, NSG mice are humanized before being infected with asexual parasites, and then mature gametocytes are detected in the

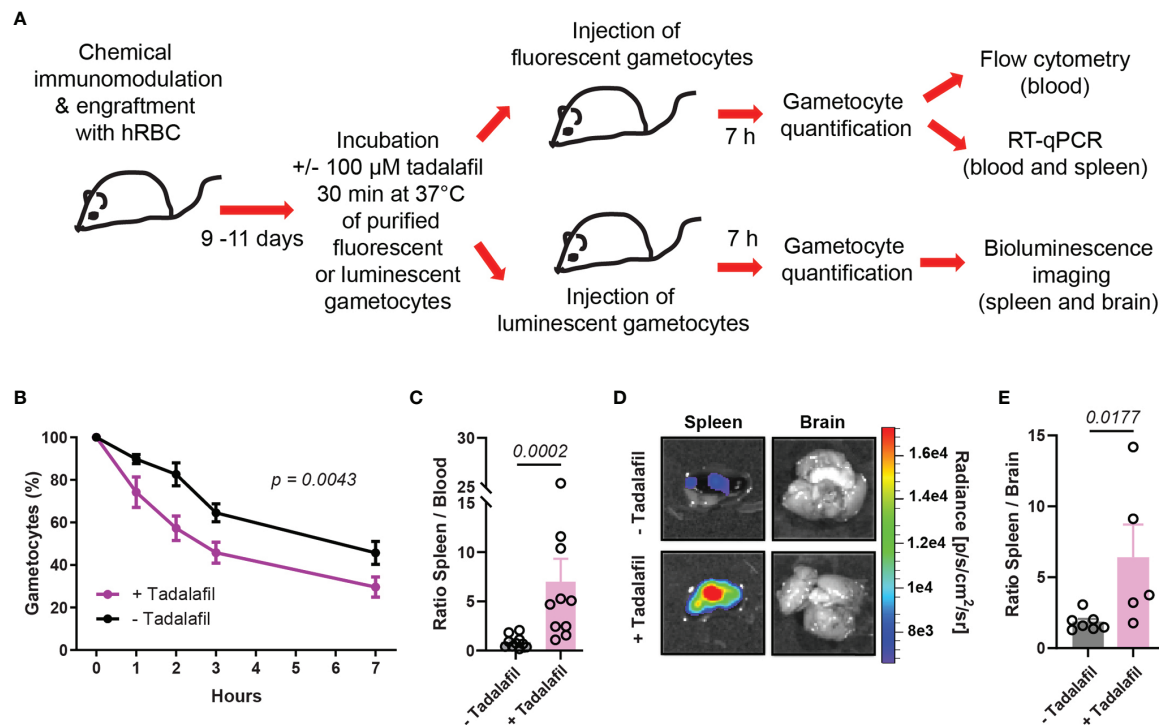


FIGURE 3 | Pre-incubation of mature GIE with tadalafil induces their retention in the spleen. **(A)** Schematic of experimental procedure for immunomodulation treatment and hRBC engraftment of NSG mice before injection with tadalafil-treated or untreated GIE. Stage V GIE were pre-incubated or not 30 min at 37°C with 100 μ M tadalafil before injection in mice. At 7 hpi, quantification of fluorescent GIE was performed by flow cytometry and RT-qPCR while quantification of luciferase-expressing GIE in spleen was performed by measuring the bioluminescence signal. **(B)** Quantification of GIE clearance in peripheral blood by flow cytometry ($n = 10$ mice from 5 independent experiments). The percentage of gametocytes is normalized to the gametocytemia at 10 minutes after injection. p indicates the statistical significance determined using a two-way ANOVA test. **(C)** Quantitative analysis by real time RT-qPCR of GIE distribution in peripheral blood and spleen. Results were calculated as relative copy number of *gfp* or *turbofp635* gene transcripts to the *HK* gene transcripts in spleen and blood samples. The graph represents the ratio spleen-to-blood for 10 mice from 5 independent experiments. **(D)** Representative image of luminescence signal in dissected spleen and brain from mice injected with tadalafil-treated and untreated GIE. The brain was used as negative control. **(E)** Quantification of luciferase activity calculated as the ratio of radiance in spleen and brain from mice injected with tadalafil-treated and untreated GIE. Circles indicate the number of mice from 5 independent experiments for untreated GIE and from 4 independent experiments for tadalafil-treated GIE. In C and E, p indicates the statistical significance determined using a Mann Whitney test. Error bars show the standard error of the mean (SEM).

peripheral circulation after an average of 10 days (Figure 4D). After the appearance of stage V gametocytes in peripheral blood, a group of 6 mice were daily treated with 200 μ g of Cialis® *per os* for 4 days (from day 0 to day 3). A group of 6 untreated mice was used as a control. For each mouse, gametocytemia was monitored in thin tail-blood Giemsa-stained smears collected daily until sacrifice at day 6 after initiating the drug treatment. Between day 0 and day 3, stage V gametocytemia increased approximately 2-fold in control mice, as a result of the increase of asexual parasitemia that occurred in these mice several days earlier (Figure 4E). In contrast, this increase was not observed in Cialis-treated mice in which the gametocytemia slightly decreased. The effect of tadalafil treatment was even more pronounced three days after the end of the treatment (at day 6) when stage V gametocytemia in control mice increased about 3-fold compared to day 0 whereas it decreased 2-fold in treated mice. These results indicate that tadalafil treatment impedes the increase in gametocytemia and promote gametocyte clearance from peripheral circulation.

DISCUSSION

Targeting the mechanical properties of mature GIE to interfere with their circulation across the spleen has been proposed as a promising strategy to block malaria parasite transmission (Tiburcio et al., 2012; Duez et al., 2015; Russell and Cooke, 2017; Henry et al., 2020). In this context, the PDE inhibitors sildenafil and tadalafil have previously shown their ability to block the filtration of mature GIE in an *in vitro* model of splenic retention (Ramdani et al., 2015; N'dri et al., 2021). In this study, we used a humanized mouse model to address *in vivo* the effect of tadalafil on the circulation of mature GIE. Our results indicate that the retention rates in the humanized mouse spleen are comparable to that observed *in vitro* by microspiltration, the physiological relevance of which has been validated with *ex vivo* perfused human spleens (Deplaine et al., 2011). Importantly, stiff GIE were retained in the mouse spleen, resulting in faster clearance from the peripheral blood than deformable GIE. Accordingly, upon pretreatment of GIE before injection or

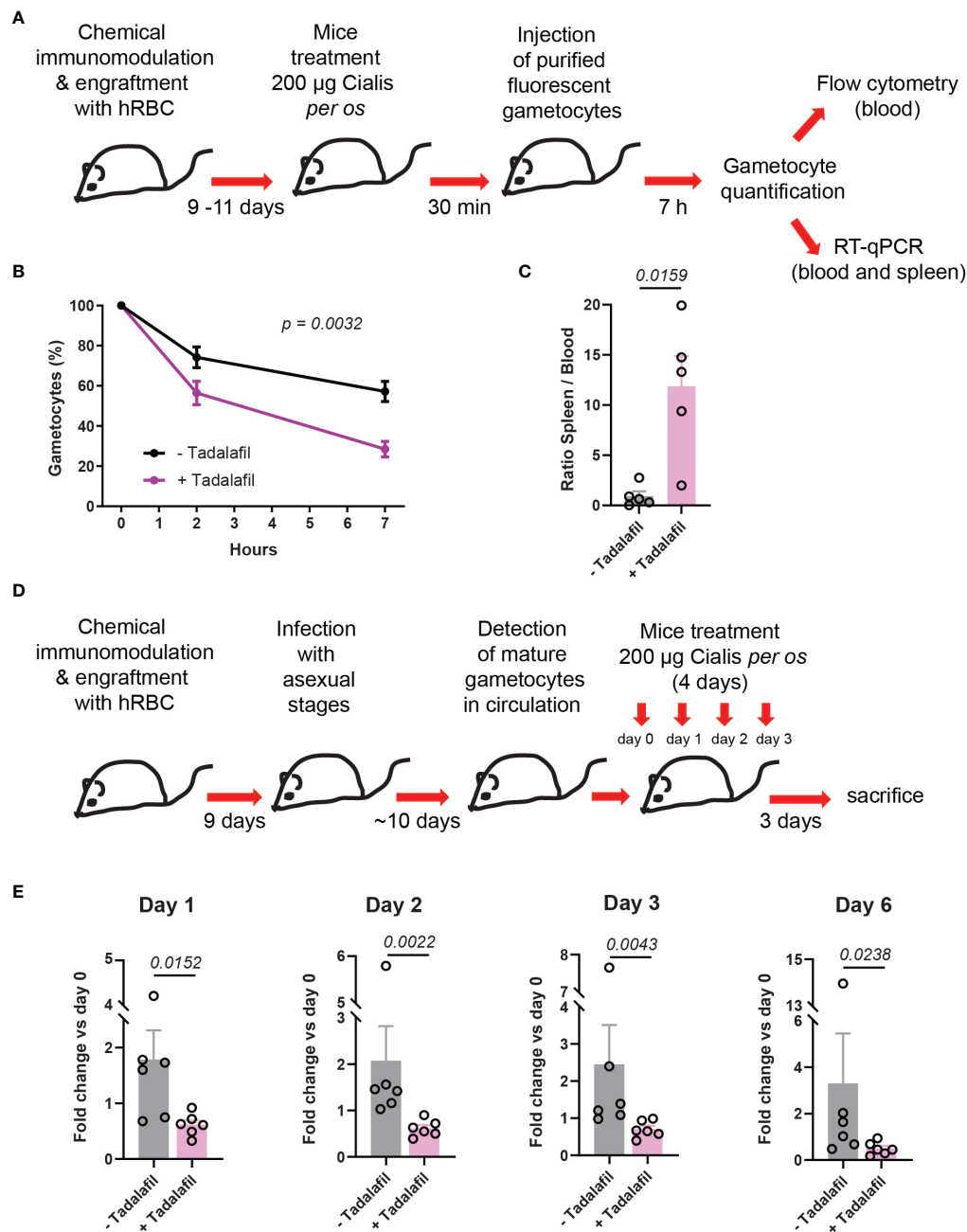


FIGURE 4 | Circulation of mature GIE is decreased in humanized mice treated orally with tadalafil. **(A)** Schematic of experimental procedure for immunomodulation treatment and hRBC engraftment of NSG mice before injection with NF54-pfs47-hsp70-GFP stage V GIE. Mice were orally treated with Cialis 30 min before stage V GIE injection. GIE quantification was performed at 7 hpi by flow cytometry and RT-qPCR. **(B)** Quantification of stage V GIE clearance in peripheral blood, comparing tadalafil-treated (violet) and untreated mice (black) by flow cytometry ($n = 5$ mice from 3 independent experiments). The percentage of gametocytes is normalized to the gametocytemia at 10 minutes after injection. p indicates the statistical significance determined using a two-way ANOVA test. **(C)** Quantitative analysis by real time RT-qPCR of GIE distribution in peripheral blood and spleen. Results were calculated as *gfp* transcript copy number using the absolute quantification method. Circles indicate the number of mice from 3 independent experiments. p indicates the statistical significance determined using a Mann Whitney test. **(D)** Experimental procedure for immunomodulation treatment and hRBC engraftment of NSG mice before infection with *P. falciparum* asexual parasites. Mice were treated orally with Cialis during 4 days and gametocytemia was monitored in thin tail-blood smears collected daily until sacrifice at day 6 after initiating drug treatment ($n = 6$ mice from 2 independent experiments). **(E)** Quantification stage V GIE in circulation at day 1, day 2, day 3 and day 6 after initiating the treatment. Gametocytemia was determined by counting 2000 to 4000 erythrocytes on thin tail-blood smears. p indicates the statistical significance determined using a Mann Whitney test. Circles indicate the number of mice from 2 independent experiments. Error bars show the SEM.

upon oral treatment of mice, tadalafil-induced stiffening of mature GIE also impaired their circulation and triggered their retention by the spleen. These results confirm that tadalafil represents a novel drug lead potentially capable of blocking malaria parasite transmission by impacting on GIE circulation. Although this humanized mouse model has previously been used to test the gametocytidal drug primaquine (Duffier et al., 2016), our results indicate that it is also suitable for testing drugs that impact the mechanical properties of infected erythrocytes. Another study reported that calyculin, a phosphatase inhibitor known to stiffen mature GIE (Ramdani et al., 2015), induces rapid elimination of pretreated GIE from the peripheral blood after injection in macrophage-depleted mice (Duez et al., 2015). However, the localization of GIE in mouse organs was not addressed in this study, and in the absence of hRBC graft, it is likely that GIE were sequestered in the liver rather than the spleen, as we observed in ungrafted mice (**Supplemental Figure 3**). In contrast, bioluminescent imaging analyses performed in our study confirmed that the main retention of stiff GIE occurs in the spleen, since every other day injection of hRBC may saturate the liver, which is the major site of hRBC sequestration (Song et al., 2021). Significant accumulation of GIE was also observed in the lungs, although this retention was not dependent on GIE deformability since the bioluminescent signal in the lungs was comparable after injection of either immature or mature GIE. Sequestration of *Plasmodium* parasites in the lungs has previously been observed in mice infected with asexual forms of the murine malaria parasite *P. berghei* (Franke-Fayard et al., 2005; Franke-Fayard et al., 2010; Fonager et al., 2012; De Niz et al., 2016). The class II scavenger-receptor CD36 was identified as the major receptor for *P. berghei* sequestration in this organ, however the parasite ligand(s) is not identified yet (Franke-Fayard et al., 2005). CD36 is a receptor widely distributed on endothelial cells and is a major binding receptor for several *Plasmodium* species, including *P. falciparum* (Ho and White, 1999). Thus, we can speculate that CD36 is involved in the accumulation of GIE observed in the lungs in this study. Our bioluminescent imaging analyses also reveal that injected stiff GIE are not detected in bones, whereas in previous study immature GIE accumulated in the bone marrow of *P. falciparum* infected mice (Duffier et al., 2016). A possible explanation is that immature gametocytes observed in the bone marrow upon infection originated from sexually-committed rings that entered the bone parenchyma and were sequestered there because of their high rigidity, whereas upon injection, the stiffness of infused immature GIE may prevent their entry into the bone marrow parenchyma.

Our results show that splenic retention of GIE upon tadalafil treatment is accompanied by a faster clearance from the peripheral blood, confirming that tadalafil represents a novel drug lead potentially capable of blocking malaria parasite transmission by impacting on GIE circulation. However, even after 4 days of tadalafil treatment, GIE were not completely eliminated from the bloodstream in this mouse model. It should be noted that these mice are depleted in macrophages due to clodronate treatment, therefore the low number of resident

splenic macrophages and the reversible effect of tadalafil (Seftel, 2004) may explain why some GIE are not destroyed in the spleen and are released into the bloodstream. It might be of interest to test the effect of tadalafil in a recent humanized mouse model which allows resident tissue macrophages to populate host tissues combined with enhanced reconstitution of human erythropoiesis and mature circulating hRBC (Song et al., 2021). This mouse model would allow to study not only the role of splenic macrophages on stiff GIE destruction but also the effect of drugs on gametocytes that develop in erythroblasts and reticulocytes (Neveu et al., 2020). None the way, we can speculate that in humans, resident splenic macrophages would be able to eliminate mature GIE retained in this organ upon stiffening treatment. As tadalafil is an FDA-approved drug, we may consider testing its effect on the circulation kinetics of *P. falciparum* mature GIE in a controlled model of human malaria infection (Collins et al., 2018; Reuling et al., 2018). In addition, the structure of tadalafil can be easily modified to suppress its effect on human targets and therefore generate *Plasmodium*-specific PDE inhibitors (Beghyn et al., 2011; Beghyn et al., 2012). Further optimization of these compounds through structural modifications could lead to more effective and irreversible inhibitors capable of completely removing gametocytes from the bloodstream.

DATA AVAILABILITY STATEMENT

The raw data supporting the conclusions of this article will be made available by the authors, without undue reservation.

ETHICS STATEMENT

The animal study was reviewed and approved by Ministère de l'Éducation Nationale, de l'Enseignement Supérieur et de la Recherche (Authorization Number 01736.02).

AUTHOR CONTRIBUTIONS

CL and DB conceived the project. DB, LG, LR, and FD performed the experiments. CL and DB designed and interpreted the experiments. J-FF, MT, M-EN, DM, OS, and AM-S contributed resources or data. CL and DB wrote the article. All authors contributed to the article and approved the submitted version.

FUNDING

This study was supported by grants from the Fondation pour la Recherche Médicale ("Equipe FRM" grant EQ20170336722 and "Ingenieur FRM" grant ING20160435478). We are grateful to François Lacoste for fruitful discussions and the Fonds Inkermann for financial support of the study. The authors also

acknowledge the financial support from the Cnrs, Inserm, the Laboratoire d'Excellence GR-Ex (ANR-11-LABX-0051) and the Laboratoire d'Excellence ParaFrap (ANR-11-LABX-0024).

ACKNOWLEDGMENTS

Authors thank Christelle Enond and Doriane Foret at "Phénotypage du petit animal" (UMS28) for technical support in *in vivo* experiments. We acknowledge the Flow Cytometry core facility CYBIO and the genomics core facility GENOM'IC of

the Institut Cochin for technical help. We thank Pietro Alano for providing the NF54-cg6-pfs16-CBG99 line. We thank Frederique Verdier, Tatyana Tavella and Ioanna Deni for critical reading of the manuscript.

SUPPLEMENTARY MATERIAL

The Supplementary Material for this article can be found online at: <https://www.frontiersin.org/articles/10.3389/fcimb.2022.883759/full#supplementary-material>

REFERENCES

- Aguilar, R., Magallon-Tejada, A., Achtman, A. H., Moraleda, C., Joice, R., Cistero, P., et al. (2014). Molecular Evidence for the Localization of *Plasmodium Falciparum* Immature Gametocytes in Bone Marrow. *Blood* 123, 959–966. doi: 10.1182/blood-2013-08-520767
- Aingaran, M., Zhang, R., Law, S. K., Peng, Z., Undisz, A., Meyer, E., et al. (2012). Host Cell Deformability is Linked to Transmission in the Human Malaria Parasite *Plasmodium Falciparum*. *Cell Microbiol.* 14 (7), 983–993. doi: 10.1111/j.1462-5822.2012.01786.x
- Beghyn, T. B., Charton, J., Leroux, F., Henninot, A., Reboule, I., Cos, P., et al. (2012). Drug-To-Genome-to-Drug, Step 2: Reversing Selectivity in a Series of Antiplasmodial Compounds. *J. Med. Chem.* 55, 1274–1286. doi: 10.1021/jm201422e
- Beghyn, T. B., Charton, J., Leroux, F., Laconde, G., Bourin, A., Cos, P., et al. (2011). Drug to Genome to Drug: Discovery of New Antiplasmodial Compounds. *J. Med. Chem.* 54, 3222–3240. doi: 10.1021/jm1014617
- Birkholtz, L. M., Coetzer, T. L., Mancama, D., Leroy, D., and Alano, P. (2016). Discovering New Transmission-Blocking Antimalarial Compounds: Challenges and Opportunities. *Trends Parasitol.* 32, 669–681. doi: 10.1016/j.pt.2016.04.017
- Bousema, T., Okell, L., Shekalaghe, S., Griffin, J. T., Omar, S., Sawa, P., et al. (2010). Revisiting the Circulation Time of *Plasmodium Falciparum* Gametocytes: Molecular Detection Methods to Estimate the Duration of Gametocyte Carriage and the Effect of Gametocytocidal Drugs. *Malar. J.* 9, 136. doi: 10.1186/1475-2875-9-136
- Bousema, J. T., Schneider, P., Gouagna, L. C., Drakeley, C. J., Tostmann, A., Houben, R., et al. (2006). Moderate Effect of Artemisinin-Based Combination Therapy on Transmission of *Plasmodium Falciparum*. *J. Infect. Dis.* 193, 1151–1159. doi: 10.1086/503051
- Bouyer, G., Barbieri, D., Dupuy, F., Marteau, A., Sissoko, A., N'dri, M. E., et al. (2020). *Plasmodium Falciparum* Sexual Parasites Regulate Infected Erythrocyte Permeability. *Commun. Biol.* 3, 726. doi: 10.1038/s42003-020-01454-7
- Cao, P., Collins, K. A., Zaloumis, S., Wattanakul, T., Tarning, J., Simpson, J. A., et al. (2019). Modeling the Dynamics of *Plasmodium Falciparum* Gametocytes in Humans During Malaria Infection. *Elife* 8, e49058. doi: 10.7554/eLife.49058.033
- Cevenini, L., Camarda, G., Michelini, E., Siciliano, G., Calabretta, M. M., Bona, R., et al. (2014). Multicolor Bioluminescence Boosts Malaria Research: Quantitative Dual-Color Assay and Single-Cell Imaging in *Plasmodium Falciparum* Parasites. *Anal. Chem.* 86, 8814–8821. doi: 10.1021/ac502098w
- Collins, K. A., Wang, C. Y., Adams, M., Mitchell, H., Rampton, M., Elliott, S., et al. (2018). A Controlled Human Malaria Infection Model Enabling Evaluation of Transmission-Blocking Interventions. *J. Clin. Invest.* 128, 1551–1562. doi: 10.1172/JCI98012
- Dearnley, M. K., Yeoman, J. A., Hanssen, E., Kenny, S., Turnbull, L., Whitchurch, C. B., et al. (2012). Origin, Composition, Organization and Function of the Inner Membrane Complex of *Plasmodium Falciparum* Gametocytes. *J. Cell Sci.* 125, 2053–2063. doi: 10.1242/jcs.099002
- De Niz, M., Meibalan, E., Mejia, P., Ma, S., Brancucci, N. M. B., Agop-Nersesian, C., et al. (2018). *Plasmodium* Gametocytes Display Homing and Vascular Transmigration in the Host Bone Marrow. *Sci. Adv.* 4, eaat3775. doi: 10.1126/sciadv.aat3775
- De Niz, M., Ullrich, A. K., Heiber, A., Blancke Soares, A., Pick, C., Lyck, R., et al. (2016). The Machinery Underlying Malaria Parasite Virulence is Conserved Between Rodent and Human Malaria Parasites. *Nat. Commun.* 7, 11659. doi: 10.1038/ncomms11659
- Deplaine, G., Safeukui, I., Jeddi, F., Lacoste, F., Brousse, V., Perrot, S., et al. (2011). The Sensing of Poorly Deformable Red Blood Cells by the Human Spleen can be Mimicked *In Vitro*. *Blood* 117, e88–e95. doi: 10.1182/blood-2010-10-312801
- Duez, J., Holleran, J. P., Ndour, P. A., Loganathan, S., Amireault, P., Francais, O., et al. (2015). Splenic Retention of *Plasmodium Falciparum* Gametocytes to Block the Transmission of Malaria. *Antimicrob. Agents Chemother.* 59, 4206–4214. doi: 10.1128/AAC.05030-14
- Duffier, Y., Lorthiois, A., Cistero, P., Dupuy, F., Jouvion, G., Fiette, L., et al. (2016). A Humanized Mouse Model for Sequestration of *Plasmodium Falciparum* Sexual Stages and *In Vivo* Evaluation of Gametocytidal Drugs. *Sci. Rep.* 6, 35025. doi: 10.1038/srep35025
- Farfour, E., Charlotte, F., Settegrana, C., Miyara, M., and Buffet, P. (2012). The Extravascular Compartment of the Bone Marrow: A Niche for *Plasmodium Falciparum* Gametocyte Maturation? *Malar. J.* 11, 285. doi: 10.1186/1475-2875-11-285
- Fonager, J., Pasini, E. M., Braks, J. A., Klop, O., Ramesar, J., Remarque, E. J., et al. (2012). Reduced CD36-Dependent Tissue Sequestration of *Plasmodium*-Infected Erythrocytes is Detrimental to Malaria Parasite Growth *In Vivo*. *J. Exp. Med.* 209, 93–107. doi: 10.1084/jem.20110762
- Franke-Fayard, B., Fonager, J., Braks, A., Khan, S. M., and Janse, C. J. (2010). Sequestration and Tissue Accumulation of Human Malaria Parasites: Can We Learn Anything From Rodent Models of Malaria? *PLoS Pathog.* 6, e1001032. doi: 10.1371/journal.ppat.1001032
- Franke-Fayard, B., Janse, C. J., Cunha-Rodrigues, M., Ramesar, J., Buscher, P., Que, L., et al. (2005). Murine Malaria Parasite Sequestration: CD36 is the Major Receptor, But Cerebral Pathology is Unlinked to Sequestration. *Proc. Natl. Acad. Sci. U.S.A.* 102, 11468–11473. doi: 10.1073/pnas.0503386102
- Ghorbal, M., Gorman, M., Macpherson, C. R., Martins, R. M., Scherf, A., and Lopez-Rubio, J. J. (2014). Genome Editing in the Human Malaria Parasite *Plasmodium Falciparum* Using the CRISPR-Cas9 System. *Nat. Biotechnol.* 32, 819–821. doi: 10.1038/nbt.2925
- Hawking, F., Wilson, M. E., and Gammage, K. (1971). Evidence for Cyclic Development and Short-Lived Maturity in the Gametocytes of *Plasmodium Falciparum*. *Trans. R Soc. Trop. Med. Hyg.* 65, 549–559. doi: 10.1016/0035-9203(71)90036-8
- Henry, B., Roussel, C., Carucci, M., Brousse, V., Ndour, P. A., and Buffet, P. (2020). The Human Spleen in Malaria: Filter or Shelter? *Trends Parasitol.* 36, 435–446. doi: 10.1016/j.pt.2020.03.001
- Ho, M., and White, N. J. (1999). Molecular Mechanisms of Cytoadherence in Malaria. *Am. J. Physiol.* 276, C1231–C1242. doi: 10.1152/ajpcell.1999.276.6.C1231
- Joice, R., Nilsson, S. K., Montgomery, J., Dankwa, S., Egan, E., Morahan, B., et al. (2014). *Plasmodium Falciparum* Transmission Stages Accumulate in the Human Bone Marrow. *Sci. Transl. Med.* 6, 244re5. doi: 10.1126/scitranslmed.3008882
- Knuepfer, E., Napiorkowska, M., Van Ooij, C., and Holder, A. A. (2017). Generating Conditional Gene Knockouts in *Plasmodium* - A Toolkit to

- Produce Stable DiCre Recombinase-Expressing Parasite Lines Using CRISPR/Cas9. *Sci. Rep.* 7, 3881. doi: 10.1038/s41598-017-03984-3
- Lavazec, C., Deplaine, G., Safeukui, I., Perrot, S., Milon, G., Mercereau-Puijalon, O., et al. (2013). Microsphere Filtration: A Microsphere Matrix to Explore Erythrocyte Deformability. *Methods Mol. Biol.* 923, 291–297. doi: 10.1007/978-1-62703-026-7_20
- Moreno-Sabater, A., Perignon, J. L., Mazier, D., Lavazec, C., and Soulard, V. (2018). Humanized Mouse Models Infected With Human Plasmodium Species for Antimalarial Drug Discovery. *Expert Opin. Drug Discov* 13, 131–140. doi: 10.1080/17460441.2018.1410136
- N'dri, M. E., Royer, L., and Lavazec, C. (2021). Tadalafil Impacts the Mechanical Properties of Plasmodium Falciparum Gametocyte-Infected Erythrocytes. *Mol. Biochem. Parasitol.* 244, 111392. doi: 10.1016/j.molbiopara.2021.111392
- Neveu, G., Richard, C., Dupuy, F., Behera, P., Volpe, F., Subramani, P. A., et al. (2020). Plasmodium Falciparum Sexual Parasites Develop in Human Erythroblasts and Affect Erythropoiesis. *Blood* 136, 1381–1393. doi: 10.1182/blood.2019004746
- Plouffe, D. M., Wree, M., Du, A. Y., Meister, S., Li, F., Patra, K., et al. (2016). High-Throughput Assay and Discovery of Small Molecules That Interrupt Malaria Transmission. *Cell Host Microbe* 19, 114–126. doi: 10.1016/j.chom.2015.12.001
- Ramdani, G., Naissant, B., Thompson, E., Breil, F., Lorthiois, A., Dupuy, F., et al. (2015). cAMP-Signalling Regulates Gametocyte-Infected Erythrocyte Deformability Required for Malaria Parasite Transmission. *PloS Pathog.* 11, e1004815. doi: 10.1371/journal.ppat.1004815
- Reuling, I. J., Van De Schans, L. A., Coffeng, L. E., Lanke, K., Meerstein-Kessel, L., Graumans, W., et al. (2018). A Randomized Feasibility Trial Comparing Four Antimalarial Drug Regimens to Induce Plasmodium Falciparum Gametocytemia in the Controlled Human Malaria Infection Model. *Elife* 7, e31549. doi: 10.7554/eLife.31549
- Russell, B. M., and Cooke, B. M. (2017). The Rheopathobiology of Plasmodium Vivax and Other Important Primate Malaria Parasites. *Trends Parasitol.* 33, 321–334. doi: 10.1016/j.pt.2016.11.009
- Seftel, A. D. (2004). Phosphodiesterase Type 5 Inhibitor Differentiation Based on Selectivity, Pharmacokinetic, and Efficacy Profiles. *Clin. Cardiol.* 27, 114–119. doi: 10.1002/clc.4960271305
- Song, Y., Shan, L., Gbyli, R., Liu, W., Strowig, T., Patel, A., et al. (2021). Combined Liver-Cytokine Humanization Comes to the Rescue of Circulating Human Red Blood Cells. *Science* 371, 1019–1025. doi: 10.1126/science.abe2485
- Tacchini-Cottier, F., Zweifel, C., Belkaid, Y., Mukankundiye, C., Vasei, M., Launois, P., et al. (2000). An Immunomodulatory Function for Neutrophils During the Induction of a CD4+ Th2 Response in BALB/c Mice Infected With Leishmania Major. *J. Immunol.* 165, 2628–2636. doi: 10.4049/jimmunol.165.5.2628
- Tiburcio, M., Niang, M., Deplaine, G., Perrot, S., Bischoff, E., Ndour, P. A., et al. (2012). A Switch in Infected Erythrocyte Deformability at the Maturation and Blood Circulation of Plasmodium Falciparum Transmission Stages. *Blood* 119, e172–e180. doi: 10.1182/blood-2012-03-414557
- World Malaria Report (2020). World Health Organization. *World Malaria Report 2018*.

Conflict of Interest: The authors declare that the research was conducted in the absence of any commercial or financial relationships that could be construed as a potential conflict of interest.

Publisher's Note: All claims expressed in this article are solely those of the authors and do not necessarily represent those of their affiliated organizations, or those of the publisher, the editors and the reviewers. Any product that may be evaluated in this article, or claim that may be made by its manufacturer, is not guaranteed or endorsed by the publisher.

Copyright © 2022 Barbieri, Gomez, Royer, Dupuy, Franetich, Tefit, N'Dri, Mazier, Silvie, Moreno-Sabater and Lavazec. This is an open-access article distributed under the terms of the Creative Commons Attribution License (CC BY). The use, distribution or reproduction in other forums is permitted, provided the original author(s) and the copyright owner(s) are credited and that the original publication in this journal is cited, in accordance with accepted academic practice. No use, distribution or reproduction is permitted which does not comply with these terms.



Dominique Soldati-Favre: Bringing *Toxoplasma gondii* to the Molecular World

Joana M. Santos^{1*} and Karine Frénal^{2*}

¹ Université Paris-Saclay, CEA, CNRS, Institute for Integrative Biology of the Cell (I2BC), Gif-sur-Yvette, France,

² Université Bordeaux, CNRS, Microbiologie Fondamentale et Pathogénicité, UMR 5234, Bordeaux, France

Keywords: apicomplexa parasite, *Toxoplasma*, pioneer, parasitology, breakthrough, molecular parasitology

OPEN ACCESS

Edited by:

Tania F. De Koning-Ward,
Deakin University, Australia

Reviewed by:

Hayley Bullen,
Burnet Institute, Australia

*Correspondence:

Joana M. Santos
joana.santos@i2bc.paris-saclay.fr
Karine Frénal
karine.frenal@u-bordeaux.fr

Specialty section:

This article was submitted to
Parasite and Host,
a section of the journal
Frontiers in Cellular and
Infection Microbiology

Received: 01 April 2022

Accepted: 29 April 2022

Published: 27 May 2022

Citation:

Santos JM and Frénal K (2022)
Dominique Soldati-Favre:
Bringing *Toxoplasma gondii*
to the Molecular World.
Front. Cell. Infect. Microbiol. 12:910611.
doi: 10.3389/fcimb.2022.910611

FROM RNA PROCESSING TO PARASITE BIOLOGY

Anyone that knows Dominique, knows that she has a real passion for science and discovery. This passion includes parasitology so it might come as a surprise that she moved to the parasitology field almost by accident.

After doing a brilliant PhD in Zurich, Switzerland, in the Schümperli team, working on RNA processing, Dominique, with the support of a Swiss National Foundation postdoctoral grant and an EMBO fellowship, decided to join a lab in the US East Coast, but life decided otherwise and, in 1991, she joined John Boothroyd's team at Stanford University, in California. This was an outstanding team, with access to exceptional facilities, but it was transitioning from working on Trypanosomes to studying *Toxoplasma gondii*. Although *Toxoplasma* was easily cultured in the lab, it had yet to be genetically modified. At a time when the genome had yet to be sequenced and molecular biology was done without kits, Dominique, with her high energy level and swiss organization, showed that *Toxoplasma* could be transfected, a first for an intracellular parasite (Soldati and Boothroyd, 1993). She also showed, with other team members, that the transfected parasites could be drug selected and used for transgene expression, gene knockout and complementation (Kim et al., 1993; Soldati and Boothroyd, 1995; Black et al., 1995; Soldati et al., 1995). Her work did an enormous amount for the field and things became easier afterwards.

In 1995, Dominique finished her postdoctoral studies and moved to Germany to become an independent group leader. She was appointed Assistant Professor at the Center for Molecular Biology at the University of Heidelberg. There, she adapted the Cre-loxP system to *Toxoplasma* (Brecht et al., 1999) and revolutionized the field yet again by establishing the first inducible knockdown system for an Apicomplexa (Meissner et al., 2001; Meissner et al., 2002b). In 2001, Dominique moved her team to the Imperial College London, in the UK, where she held a position as a Senior Lecturer and Reader. In 2004, she became a Visiting Professor in parasitology at Imperial College and was appointed Associate Professor at the Faculty of Medicine of the University of Geneva, where her team is still based at, and where she became a Full Professor in 2010.

UNDERSTANDING *TOXOPLASMA* AT THE MOLECULAR AND STRUCTURAL LEVEL

Dominique's lab is one of the most celebrated teams in the Apicomplexa and parasitology field, known for combining technology with biology to answer specific questions, to be highly productive and for focusing on many different aspects of *Toxoplasma* biology with endless curiosity. Dominique never "fears to enter new territory and/or to challenge old dogma that might not be right". The Soldati team has contributed immensely to our understanding of parasite motility, host cell invasion and egress, protein trafficking, energy metabolism and even mice behavior. Two long-term research topics of the lab have been investigation of the actomyosin machinery powering gliding; and microneme composition, secretion and biogenesis. In the last decade, the Soldati lab has also explored the metabolism of both *Toxoplasma* and *Plasmodium*, as well as other molecular aspects of the malaria parasite.

Gliding motility and invasion of Apicomplexans were known to be active processes powered by a parasite actomyosin system (Dobrowolski and Sibley, 1996; Dobrowolski et al., 1997) but Dominique's lab was the first to identify its molecular components. In an impressive endeavor, her team characterized the kinetic and mechanical properties of the myosin heavy chain protein A (TgMyoA) with protein directly purified from tachyzoites (Herm-Götz et al., 2002), a first for a myosin. Simultaneously, they demonstrated that TgMyoA is critical for parasite motility and host cell invasion (Meissner et al., 2002b). Finally, the name "glideosome" was proposed by Dominique's lab to describe this new and unique actomyosin system (Opitz and Soldati, 2002). Together with other labs, the team then identified and functionally characterized the glideosome components (Gaskins et al., 2004; Frénal et al., 2010; Nebl et al., 2011; Williams et al., 2015; Jacot et al., 2016), as well as regulators of actin dynamics (Plattner et al., 2008; Mehta and Sibley, 2010; Daher et al., 2010; Yadav et al., 2011; Salamun et al., 2014; Jacot et al., 2016). Later, identification of Myosin H (TgMyoH), actin nucleator Formin 1 (TgFRM1) and the glideosome-associated connector (TgGAC) at the tachyzoites conoid showed how gliding motility is initiated at the parasite's apical tip (Graindorge et al., 2016; Jacot et al., 2016). Finally, very recently, the lab used expansion microscopy to explore the apical complex structure and function, including that of the enigmatic conoid (Dos Santos Pacheco et al., 2021).

In parallel, Dominique's lab has had a continued interest on micronemes, specialized parasite apical secretory organelles, storing adhesins and other effector molecules implicated in gliding motility, host cell attachment, invasion and egress. The lab has identified several of its components and protein complexes, and investigated their trafficking, structure and function during the parasite lytic cycle (Di Cristina et al., 2000; Ferguson et al., 2000; Reiss et al., 2001; Brecht et al., 2001; Meissner et al., 2002a; Huynh et al., 2003; Mital et al., 2005; Blumenschein et al., 2007; Kessler et al., 2008; Friedrich et al., 2010; Sheiner et al., 2010; Marchant et al., 2012; Sardinha-Silva et al., 2019). In recent years, the team ventured into discovering

the mechanisms behind microneme biogenesis and exocytosis. In 2018, they identified Transporter Facilitator Protein 1 (TgTFP1) (Hammoudi et al., 2018), an essential protein for parasite survival due to its crucial role in microneme biogenesis and maturation. In 2016, the identification of the protein acylated pleckstrin homology domain-containing protein (TgAPH) as a phosphatidic acid sensor anchored at the surface of the micronemes (Bullen et al., 2016) prompted the lab to investigate the signaling cascade leading to microneme secretion and parasite egress (Bullen et al., 2016; Jia et al., 2017; Darvill et al., 2018; Bisio et al., 2019; Bisio et al., 2022) and, with other labs, to draw the picture we know today (Farrell et al., 2012; Brown and Sibley, 2018; Bisio and Soldati-Favre, 2019; Bullen et al., 2019; Yang et al., 2019).

Another topic frequently addressed by Dominique throughout the years has been parasite metabolism. She was one of the first in the field to propose that energy metabolism could be exploited therapeutically (Polonais and Soldati-Favre, 2010). Ever since, her team has defined the parasite metabolic needs and capabilities by using both *in silico* and *in vivo* approaches to investigate specific metabolic pathways (Limenitakis et al., 2013; Oppenheim et al., 2014; Kloehn et al., 2020; Kloehn et al., 2021) but also build metabolic models for *T. gondii* tachyzoite and bradyzoite stages (Tymoshenko et al., 2015; Krishnan et al., 2020).

The Soldati team has also ventured into studying *Plasmodium*, in collaboration with other teams but also solo, with as much success as with *Toxoplasma* (Pino et al., 2012; Chiappino-Pepe et al., 2017; Stanway et al., 2019; Bisio et al., 2020; Bertiaux et al., 2021). They have, for instance, identified a new multistage antimalarial inhibitor blocking both parasite invasion and egress (Pino et al., 2017) and investigated specific metabolic pathways of *P. berghei* intra-erythrocytic and liver stages (Oppenheim et al., 2014; Stanway et al., 2019).

RECOGNIZED BY HER PEERS

Parasitology is a small and relatively neglected field compared to others so even those who are exceptional are rarely praised. Even so, Dominique has been the recipient of multiple accolades, namely the Kar Asmund Rudolphi-Medal of the German Society for Parasitology in 2001, the Prize of the Gertrude von Meissner Foundation in 2009 and twice the Pfizer Prize for Basic Research in Infection, awarding specific lab publications, and the Cloëtta Foundation Prize in 2015 and the Alice and C. C. Wang Award in Molecular Parasitology in 2019, acknowledging Dominique's scientific career. She is a member of prestigious academies, including the Swiss Academy of Medical Sciences, the European Academy of Microbiology and EMBO, was an HHMI International Scholar and Senior Scholar in Infectious Diseases, and she has received a number of prominent grants, including a European Research Council (ERC) Advanced Grant, unarguably one of the most competitive European grants. She has also organized numerous parasitology meetings, including the Molecular Parasitology Meeting or the Gordon Research Conference on Host-Parasite Interactions, she is the Academic Editor of selected

publications for various journals (eLife, PLoS Pathogens, Traffic, Cell Host & Microbe, and others), she has been a contributor to the F1000 since 2006, and she has been a grant reviewer for national and international grant schemes and an expert for the ERC or the Wellcome Trust's Peer Review College.

Despite all the praises Dominique has received, and all the high impact papers she has published, many of the people we interviewed mentioned that they didn't actually know who Dominique was when they interviewed - it was "after talking to her in her little office that it became immediately clear to me that I absolutely wanted to join her lab - her personality and how she talked about science and her research inspired me from the minute I met her", it was "only after spending a few months in her lab that I realized how lucky I was!". This is a testament of Dominique's ability to never wanting to be the bigger person in the room and for always caring for the person in front of her - "she took a huge interest in my future career and supported me wherever she could", "I had always the freedom to make my own decisions and she would respect them".

“Dominique is firm when people want women to be nice”, someone said. Indeed, Dominique is straightforward and says exactly what she thinks. Despite what some called a steep learning curve, everyone was unanimous in saying that Dominique masters the art of getting everyone to push themselves and be motivated. From the very beginning of her career as a mentor, Dominique was certainly demanding but never pressured people to work harder or gave the impression that she thought that way (even if she might...).

Dominique always let people do side projects, think for themselves. Her enthusiasm and energy are an unlimited source of motivation that pushed us all to work more and be better. Some of us even remember presenting to her results of experiments done behind her back and having Dominique being very encouraging and open for new, even crazy ideas. This is certainly a result of the lab good atmosphere, which has lasted, even though the team has moved internationally twice. As a postdoc, Dominique was known to have fun and even played some unforgettable jokes on the lab head. We can say this trait has continued. The lab beer o'clocks and the department dress up Christmas parties were always memorable.

REPRESENTATION AND EMPOWERMENT

This essay is written in the context of a special issue of *Women in Parasitology*. Dominique would be the first to say that she is not a woman scientist but a scientist that is also a woman. When she became a group leader, there were not many women in that position and Dominique herself has said that the low number of women in the field was one of the obstacles she found in her career. While the number of women in the field has increased, men still dominate, especially at high positions. Women we interviewed said that working with Dominique was empowering as a woman not because of something she said or did in particular but because just seeing another woman doing well in your field is empowering.

Throughout her career, Dominique underwent changes family-wise, going from being a mother of 2 during her postdoc, to having 3 and then 4 children as a lab head. To her, family was at the center of her choices without being a barrier and that showed us that it doesn't have to be one or another but we can do both and do it well. It was always motivating to observe her living for science even if we all knew she had a family life outside the lab.

Dominique has been an example not only to the people that worked/work with her but to anyone that has interacted with her at workshops, training courses or conferences. At the University of Geneva, she has been vice-dean for research at the Faculty of Medicine for 10 years, she is the head of the department of Microbiology and Molecular Medicine since 2020 and, since 2008, she is the director of the Graduate School Biomedical Sciences. She has also taught numerous workshops, including a Cell biology workshop in Mali in 2012 and the Biology of Parasitism (BoP) and Middle-Eastern BOP courses. During these courses, Dominique always took the time to discuss with every student and was keen to learn about their culture, career, and ambitions. Dominique is also a mentor for women outside science, as part of the Swiss-French network for mentoring women careers.

FINAL THOUGHTS

The words used by her supervisor, colleagues, former students and postdocs to describe Dominique's career, personality and research are shown on **Figure 1** but we think that more than anything we can write, some of what was shared with us better exemplify the impact she has had on all of us: "I looked for a good supervisor and



mentor. Dominique was both from the very beginning”, “I am proud to have been in her lab”, “Dominique represents the person combining all the capacities to direct and lead research projects and above all the capacity to transmit these values”, “Dominique has undoubtedly shaped my way of doing science”, “Dominique has been the only PI who I felt really cared about her people in the lab and would ensure everyone was on the right track”, “Dominique’s work pushes us to do better science”, “Dominique is an inspirational colleague, rigorous in her science”.

We hope this essay highlights the pioneer and breakthrough work Dominique has done and continues to do but also what a role model she has been for all of us who have had the privilege to work with her. Both men and women see Dominique as a mentor and as an inspiration in the way she does science, shares her knowledge, runs the lab and is available even though she also has a family, travels frequently and has to attend to other professional obligations.

REFERENCES

- Bertiaux, E., Balestra, A. C., Bournonville, L., Louvel, V., Maco, B., Soldati-Favre, D., et al. (2021). Expansion Microscopy Provides New Insights Into the Cytoskeleton of Malaria Parasites Including the Conservation of a Conoid. *PLoS Biol.* 19, e3001020. doi: 10.1371/journal.pbio.3001020
- Bisio, H., Chaabene, R. B., Sabitzki, R., Maco, B., Marq, J. B., Gilberger, T.-W., et al. (2020). The ZIP Code of Vesicle Trafficking in Apicomplexa: SEC1/ Munc18 and SNARE Proteins. *mBio* 11, e02092-20. doi: 10.1128/ mBio.02092-20
- Bisio, H., Krishnan, A., Marq, J.-B., and Soldati-Favre, D. (2022). *Toxoplasma Gondii* Phosphatidylserine Flippase Complex ATP2B-CDC50.4 Critically Participates in Microneme Exocytosis. *PLoS Pathog.* 18, e1010438. doi: 10.1371/journal.ppat.1010438
- Bisio, H., Lunghi, M., Brochet, M., and Soldati-Favre, D. (2019). Phosphatidic Acid Governs Natural Egress in *Toxoplasma Gondii* via a Guanylate Cyclase Receptor Platform. *Nat. Microbiol.* 4, 420–428. doi: 10.1038/s41564-018-0339-8
- Bisio, H., and Soldati-Favre, D. (2019). Signaling Cascades Governing Entry Into and Exit From Host Cells by *Toxoplasma Gondii*. *Annu. Rev. Microbiol.* 73, 579–599. doi: 10.1146/annurev-micro-020518-120235
- Black, M., Seeber, F., Soldati, D., Kim, K., and Boothroyd, J. C. (1995). Restriction Enzyme-Mediated Integration Elevates Transformation Frequency and Enables Co-Transfection of *Toxoplasma Gondii*. *Mol. Biochem. Parasitol* 74, 55–63. doi: 10.1016/0166-6851(95)02483-2
- Blumenschein, T. M. A., Friedrich, N., Childs, R. A., Saouros, S., Carpenter, E. P., Campanero-Rhodes, M. A., et al. (2007). Atomic Resolution Insight Into Host Cell Recognition by *Toxoplasma Gondii*. *EMBO J.* 26, 2808–2820. doi: 10.1038/ sj.emboj.7601704
- Brecht, S., Carruthers, V. B., Ferguson, D. J., Giddings, O. K., Wang, G., Jakle, U., et al. (2001). The *Toxoplasma* Micronemal Protein MIC4 is an Adhesin Composed of Six Conserved Apple Domains. *J. Biol. Chem.* 276, 4119–4127. doi: 10.1074/jbc.M008294200
- Brecht, S., Erdhart, H., Soete, M., and Soldati, D. (1999). Genome Engineering of *Toxoplasma Gondii* Using the Site-Specific Recombinase Cre. *Gene* 234, 239–247. doi: 10.1016/S0378-1119(99)00202-4
- Brown, K. M., and Sibley, L. D. (2018). Essential cGMP Signaling in *Toxoplasma* Is Initiated by a Hybrid P-Type ATPase-Guanylate Cyclase. *Cell Host Microbe* 24, 804–816.e6. doi: 10.1016/j.chom.2018.10.015
- Bullen, H. E., Bisio, H., and Soldati-Favre, D. (2019). The Triumvirate of Signaling Molecules Controlling *Toxoplasma* Microneme Exocytosis: Cyclic GMP, Calcium, and Phosphatidic Acid. *PLoS Pathog.* 15, e1007670. doi: 10.1371/ journal.ppat.1007670
- Bullen, H. E., Jia, Y., Yamaryo-Botté, Y., Bisio, H., Zhang, O., Jemelin, N. K., et al. (2016). Phosphatidic Acid-Mediated Signaling Regulates Microneme Secretion

AUTHOR CONTRIBUTIONS

Both authors prepared, wrote and edited the manuscript and jointly made the figure.

ACKNOWLEDGMENTS

We thank John Boothroyd, Kami Kim, David Sibley and David Roos for taking the time to talk with us and former PhD students and post-docs, Arnault Graindorge, Pierre-Mehdi Hammoudi, Markus Meissner, Christina Mueller, Dinkorma Ouologuem, Fabienne Plattner, Valérie Polonais, Lilach Sheiner and Oscar Vardas, who answered our questionnaire. Dominique’s opinions were collected from her portrait for the “100 femmes” campaign (<https://100femmes.ch/portraits/dominique-soldati-favre/>).

- in *Toxoplasma*. *Cell Host Microbe* 19, 349–360. doi: 10.1016/j.chom.2016.02.006
- Chiappino-Pepe, A., Tymoshenko, S., Ataman, M., Soldati-Favre, D., and Hatzimanikatis, V. (2017). Bioenergetics-Based Modeling of *Plasmodium Falciparum* Metabolism Reveals Its Essential Genes, Nutritional Requirements, and Thermodynamic Bottlenecks. *PLoS Comput. Biol.* 13, e1005397. doi: 10.1371/journal.pcbi.1005397
- Daher, W., Plattner, F., Carlier, M.-F., and Soldati-Favre, D. (2010). Concerted Action of Two Formins in Gliding Motility and Host Cell Invasion by *Toxoplasma Gondii*. *PLoS Pathog.* 6, e1001132. doi: 10.1371/journal.ppat.1001132
- Darvill, N., Dubois, D. J., Rouse, S. L., Hammoudi, P.-M., Blake, T., Benjamin, S., et al. (2018). Structural Basis of Phosphatidic Acid Sensing by APH in Apicomplexan Parasites. *Structure* 26, 1059–1071.e6. doi: 10.1016/ j.str.2018.05.001
- Di Cristina, M., Spaccapelo, R., Soldati, D., Bistoni, F., and Crisanti, A. (2000). Two Conserved Amino Acid Motifs Mediate Protein Targeting to the Micronemes of the Apicomplexan Parasite *Toxoplasma Gondii*. *Mol. Cell Biol.* 20, 7332–7341. doi: 10.1128/MCB.20.19.7332-7341.2000
- Dobrowolski, J. M., Carruthers, V. B., and Sibley, L. D. (1997). Participation of Myosin in Gliding Motility and Host Cell Invasion by *Toxoplasma Gondii*. *Mol. Microbiol.* 26, 163–173. doi: 10.1046/j.1365-2958.1997.5671913.x
- Dobrowolski, J. M., and Sibley, L. D. (1996). *Toxoplasma* Invasion of Mammalian Cells is Powered by the Actin Cytoskeleton of the Parasite. *Cell* 84, 933–939. doi: 10.1016/S0092-8674(00)81071-5
- Dos Santos Pacheco, N., Tosetti, N., Krishnan, A., Haase, R., Maco, B., Suarez, C., et al. (2021). Revisiting the Role of *Toxoplasma Gondii* ERK7 in the Maintenance and Stability of the Apical Complex. *mBio* 12, e0205721. doi: 10.1128/mBio.02057-21
- Farrell, A., Thirugnanam, S., Lorestani, A., Dvorin, J. D., Eidell, K. P., Ferguson, D. J., et al. (2012). A DOC2 Protein Identified by Mutational Profiling is Essential for Apicomplexan Parasite Exocytosis. *Science* 335, 218–221. doi: 10.1126/ science.1210829
- Ferguson, D. J., Brecht, S., and Soldati, D. (2000). The Microneme Protein MIC4, or an MIC4-Like Protein, Is Expressed Within the Macrogamete and Associated With Oocyst Wall Formation in *Toxoplasma Gondii*. *Int. J. Parasitol* 30, 1203–1209. doi: 10.1016/S0020-7519(00)00096-5
- Frénal, K., Polonais, V., Marq, J.-B., Stratmann, R., Limenitakis, J., and Soldati-Favre, D. (2010). Functional Dissection of the Apicomplexan Glideosome Molecular Architecture. *Cell Host Microbe* 8, 343–357. doi: 10.1016/ j.chom.2010.09.002
- Friedrich, N., Santos, J. M., Liu, Y., Palma, A. S., Leon, E., Saouros, S., et al. (2010). Members of a Novel Protein Family Containing Microneme Adhesive Repeat Domains Act as Sialic Acid-Binding Lectins During Host Cell Invasion by Apicomplexan Parasites. *J. Biol. Chem.* 285, 2064–2076. doi: 10.1074/ jbc.M109.060988

- Gaskins, E., Gilk, S., DeVore, N., Mann, T., Ward, G., and Beckers, C. (2004). Identification of the Membrane Receptor of a Class XIV Myosin in *Toxoplasma Gondii*. *J. Cell Biol.* 165, 383–393. doi: 10.1083/jcb.200311137
- Graindorge, A., Frénal, K., Jacot, D., Salamun, J., Marq, J. B., and Soldati-Favre, D. (2016). The Conoid Associated Motor MyoH Is Indispensable for *Toxoplasma Gondii* Entry and Exit From Host Cells. *PLoS Pathog.* 12, e1005388. doi: 10.1371/journal.ppat.1005388
- Hammoudi, P.-M., Maco, B., Dogga, S. K., Frénal, K., and Soldati-Favre, D. (2018). *Toxoplasma Gondii* TFP1 Is an Essential Transporter Family Protein Critical for Microneme Maturation and Exocytosis. *Mol. Microbiol.* 109, 225–244. doi: 10.1111/mmi.13981
- Herm-Götz, A., Weiss, S., Stratmann, R., Fujita-Becker, S., Ruff, C., Meyhöfer, E., et al. (2002). *Toxoplasma Gondii* Myosin A and Its Light Chain: A Fast, Single-Headed, Plus-End-Directed Motor. *EMBO J.* 21, 2149–2158. doi: 10.1093/emboj/21.9.2149
- Huynh, M.-H., Rabenau, K. E., Harper, J. M., Beatty, W. L., Sibley, L. D., and Carruthers, V. B. (2003). Rapid Invasion of Host Cells by *Toxoplasma* Requires Secretion of the MIC2-M2AP Adhesive Protein Complex. *EMBO J.* 22, 2082–2090. doi: 10.1093/emboj/cdg217
- Jacot, D., Tosetti, N., Pires, I., Stock, J., Graindorge, A., Hung, Y. F., et al. (2016). An Apicomplexan Actin-Binding Protein Serves as a Connector and Lipid Sensor to Coordinate Motility and Invasion. *Cell Host Microbe* 20, 731–743. doi: 10.1016/j.chom.2016.10.020
- Jia, Y., Marq, J.-B., Bisio, H., Jacot, D., Mueller, C., Yu, L., et al. (2017). Crosstalk Between PKA and PKG Controls pH-Dependent Host Cell Egress of *Toxoplasma Gondii*. *EMBO J.* 36, 3250–3267. doi: 10.15252/embj.201796794
- Kessler, H., Herm-Götz, A., Hegge, S., Rauch, M., Soldati-Favre, D., Frischknecht, F., et al. (2008). Microneme Protein 8—a New Essential Invasion Factor in *Toxoplasma Gondii*. *J. Cell Sci.* 121, 947–956. doi: 10.1242/jcs.022350
- Kim, K., Soldati, D., and Boothroyd, J. C. (1993). Gene Replacement in *Toxoplasma Gondii* With Chloramphenicol Acetyltransferase as Selectable Marker. *Science* 262, 911–914. doi: 10.1126/science.8235614
- Kloehn, J., Lunghi, M., Varesio, E., Dubois, D., and Soldati-Favre, D. (2021). Untargeted Metabolomics Uncovers the Essential Lysine Transporter in *Toxoplasma Gondii*. *Metabolites* 11, 476. doi: 10.3390/metabo11080476
- Kloehn, J., Oppenheim, R. D., Siddiqui, G., De Bock, P.-J., Kumar Dogga, S., Coute, Y., et al. (2020). Multi-Omics Analysis Delineates the Distinct Functions of Sub-Cellular Acetyl-CoA Pools in *Toxoplasma Gondii*. *BMC Biol.* 18, 67. doi: 10.1186/s12915-020-00791-7
- Krishnan, A., Kloehn, J., Lunghi, M., Chiappino-Pepe, A., Waldman, B. S., Nicolas, D., et al. (2020). Functional and Computational Genomics Reveal Unprecedented Flexibility in Stage-Specific *Toxoplasma* Metabolism. *Cell Host Microbe* 27, 290–306.e11. doi: 10.1016/j.chom.2020.01.002
- Limenitakis, J., Oppenheim, R. D., Creek, D. J., Foth, B. J., Barrett, M. P., and Soldati-Favre, D. (2013). The 2-Methylcitrate Cycle Is Implicated in the Detoxification of Propionate in *Toxoplasma Gondii*. *Mol. Microbiol.* 87, 894–908. doi: 10.1111/mmi.12139
- Marchant, J., Cowper, B., Liu, Y., Lai, L., Pinzan, C., Marq, J. B., et al. (2012). Galactose Recognition by the Apicomplexan Parasite *Toxoplasma Gondii*. *J. Biol. Chem.* 287, 16720–16733. doi: 10.1074/jbc.M111.325928
- Mehta, S., and Sibley, L. D. (2010). *Toxoplasma Gondii* Actin Depolymerizing Factor Acts Primarily to Sequester G-Actin. *J. Biol. Chem.* 285, 6835–6847. doi: 10.1074/jbc.M109.068155
- Meissner, M., Brecht, S., Bujard, H., and Soldati, D. (2001). Modulation of Myosin A Expression by a Newly Established Tetracycline Repressor-Based Inducible System in *Toxoplasma Gondii*. *Nucleic Acids Res.* 29, E115. doi: 10.1093/nar/29.22.e115
- Meissner, M., Reiss, M., Viebig, N., Carruthers, V. B., Toursel, C., Tomavo, S., et al. (2002a). A Family of Transmembrane Microneme Proteins of *Toxoplasma Gondii* Contain EGF-Like Domains and Function as Escorts. *J. Cell Sci.* 115, 563–574. doi: 10.1242/jcs.115.3.563
- Meissner, M., Schlüter, D., and Soldati, D. (2002b). Role of *Toxoplasma Gondii* Myosin A in Powering Parasite Gliding and Host Cell Invasion. *Science* 298, 837–840. doi: 10.1126/science.1074553
- Mital, J., Meissner, M., Soldati, D., and Ward, G. E. (2005). Conditional Expression of *Toxoplasma Gondii* Apical Membrane Antigen-1 (TgAMA1) Demonstrates That TgAMA1 Plays a Critical Role in Host Cell Invasion. *Mol. Biol. Cell* 16, 4341–4349. doi: 10.1091/mbc.e05-04-0281
- Nebi, T., Prieto, J. H., Kapp, E., Smith, B. J., Williams, M. J., Yates, J. R., et al. (2011). Quantitative *In Vivo* Analyses Reveal Calcium-Dependent Phosphorylation Sites and Identifies a Novel Component of the *Toxoplasma* Invasion Motor Complex. *PLoS Pathog.* 7, e1002222. doi: 10.1371/journal.ppat.1002222
- Opitz, C., and Soldati, D. (2002). “The Glideosome”: A Dynamic Complex Powering Gliding Motion and Host Cell Invasion by *Toxoplasma Gondii*. *Mol. Microbiol.* 45, 597–604. doi: 10.1046/j.1365-2958.2002.03056.x
- Oppenheim, R. D., Creek, D. J., Macrae, J. I., Modrzynska, K. K., Pino, P., Limenitakis, J., et al. (2014). BCKDH: The Missing Link in Apicomplexan Mitochondrial Metabolism Is Required for Full Virulence of *Toxoplasma Gondii* and *Plasmodium Berghei*. *PLoS Pathog.* 10, e1004263. doi: 10.1371/journal.ppat.1004263
- Pino, P., Caldelari, R., Mukherjee, B., Vahokoski, J., Klages, N., Maco, B., et al. (2017). A Multistage Antimalarial Targets the Plasmeppins IX and X Essential for Invasion and Egress. *Science* 358, 522–528. doi: 10.1126/science.aaf8675
- Pino, P., Sebastian, S., Kim, E. A., Bush, E., Brochet, M., Volkmann, K., et al. (2012). A Tetracycline-Repressible Transactivator System to Study Essential Genes in Malaria Parasites. *Cell Host Microbe* 12, 824–834. doi: 10.1016/j.chom.2012.10.016
- Plattner, F., Yarovsky, F., Romero, S., Didry, D., Carlier, M.-F., Sher, A., et al. (2008). *Toxoplasma* Profilin Is Essential for Host Cell Invasion and TLR11-Dependent Induction of an Interleukin-12 Response. *Cell Host Microbe* 3, 77–87. doi: 10.1016/j.chom.2008.01.001
- Polonais, V., and Soldati-Favre, D. (2010). Versatility in the Acquisition of Energy and Carbon Sources by the Apicomplexa. *Biol. Cell* 102, 435–445. doi: 10.1042/BC20100005
- Reiss, M., Viebig, N., Brecht, S., Fourmaux, M. N., Soete, M., Di Cristina, M., et al. (2001). Identification and Characterization of an Escorter for Two Secretory Adhesins in *Toxoplasma Gondii*. *J. Cell Biol.* 152, 563–578. doi: 10.1083/jcb.152.3.563
- Salamun, J., Kallio, J. P., Daher, W., Soldati-Favre, D., and Kursula, I. (2014). Structure of *Toxoplasma Gondii* Coronin, an Actin-Binding Protein That Relocalizes to the Posterior Pole of Invasive Parasites and Contributes to Invasion and Egress. *FASEB J.* 28, 4729–4747. doi: 10.1096/fj.14-252569
- Sardinha-Silva, A., Mendonça-Natividade, F. C., Pinzan, C. F., Lopes, C. D., Costa, D. L., Jacot, D., et al. (2019). The Lectin-Specific Activity of *Toxoplasma Gondii* Microneme Proteins 1 and 4 Binds Toll-Like Receptor 2 and 4 N-Glycans to Regulate Innate Immune Priming. *PLoS Pathog.* 15, e1007871. doi: 10.1371/journal.ppat.1007871
- Sheiner, L., Santos, J. M., Klages, N., Parussini, F., Jemmely, N., Friedrich, N., et al. (2010). *Toxoplasma Gondii* Transmembrane Microneme Proteins and Their Modular Design. *Mol. Microbiol.* 77, 912–929. doi: 10.1111/j.1365-2958.2010.07255.x
- Soldati, D., and Boothroyd, J. C. (1993). Transient Transfection and Expression in the Obligate Intracellular Parasite *Toxoplasma Gondii*. *Science* 260, 349–352. doi: 10.1126/science.8469986
- Soldati, D., and Boothroyd, J. C. (1995). A Selector of Transcription Initiation in the Protozoan Parasite *Toxoplasma Gondii*. *Mol. Cell Biol.* 15, 87–93. doi: 10.1128/MCB.15.1.87
- Soldati, D., Kim, K., Kampmeier, J., Dubremetz, J.-F., and Boothroyd, J. C. (1995). Complementation of a *Toxoplasma Gondii* ROP1 Knock-Out Mutant Using Phleomycin Selection. *Mol. Biochem. Parasitology* 74, 87–97. doi: 10.1016/0166-6851(95)02487-5
- Stanway, R. R., Bushell, E., Chiappino-Pepe, A., Roques, M., Sanderson, T., Franke-Fayard, B., et al. (2019). Genome-Scale Identification of Essential Metabolic Processes for Targeting the *Plasmodium* Liver Stage. *Cell* 179, 1112–1128.e26. doi: 10.1016/j.cell.2019.10.030
- Tymoshenko, S., Oppenheim, R. D., Agren, R., Nielsen, J., Soldati-Favre, D., and Hatzimanikatis, V. (2015). Metabolic Needs and Capabilities of *Toxoplasma Gondii* Through Combined Computational and Experimental Analysis. *PLoS Comput. Biol.* 11, e1004261. doi: 10.1371/journal.pcbi.1004261
- Williams, M. J., Alonso, H., Enciso, M., Egarter, S., Sheiner, L., Meissner, M., et al. (2015). Two Essential Light Chains Regulate the MyoA Lever Arm to Promote *Toxoplasma* Gliding Motility. *MBio* 6, e00845-00815. doi: 10.1128/mBio.00845-15
- Yadav, R., Pathak, P. P., Shukla, V. K., Jain, A., Srivastava, S., Tripathi, S., et al. (2011). Solution Structure and Dynamics of ADF From *Toxoplasma Gondii*. *J. Struct. Biol.* 176, 97–111. doi: 10.1016/j.jsb.2011.07.011
- Yang, L., Uboldi, A. D., Seizova, S., Wilde, M.-L., Coffey, M. J., Katris, N. J., et al. (2019). An Apically Located Hybrid Guanylate Cyclase-ATPase Is Critical for

the Initiation of Ca²⁺ Signaling and Motility in *Toxoplasma Gondii*. *J. Biol. Chem.* 294, 8959–8972. doi: 10.1074/jbc.RA118.005491

Conflict of Interest: The authors declare that the research was conducted in the absence of any commercial or financial relationships that could be construed as a potential conflict of interest.

Publisher's Note: All claims expressed in this article are solely those of the authors and do not necessarily represent those of their affiliated organizations, or those of

the publisher, the editors and the reviewers. Any product that may be evaluated in this article, or claim that may be made by its manufacturer, is not guaranteed or endorsed by the publisher.

Copyright © 2022 Santos and Frénal. This is an open-access article distributed under the terms of the Creative Commons Attribution License (CC BY). The use, distribution or reproduction in other forums is permitted, provided the original author(s) and the copyright owner(s) are credited and that the original publication in this journal is cited, in accordance with accepted academic practice. No use, distribution or reproduction is permitted which does not comply with these terms.



Paving the Way: Contributions of Big Data to Apicomplexan and Kinetoplastid Research

Robyn S. Kent^{1†}, Emma M. Briggs^{2,3†}, Beatrice L. Colon^{4†}, Catalina Alvarez^{5†}, Sara Silva Pereira^{6†} and Mariana De Niz^{6,7*†}

¹ Department of Microbiology and Molecular Genetics, University of Vermont, Burlington, VT, United States, ² Institute for Immunology and Infection Research, School of Biological Sciences, University Edinburgh, Edinburgh, United Kingdom, ³ Wellcome Centre for Integrative Parasitology, Institute of Infection, Immunity and Inflammation, University of Glasgow, Glasgow, United Kingdom, ⁴ Wellcome Centre for Anti-Infectives Research, Division of Biological Chemistry and Drug Discovery, School of Life Sciences, University of Dundee, Dundee, United Kingdom, ⁵ de Duve Institute, Université Catholique de Louvain, Brussels, Belgium, ⁶ Instituto de Medicina Molecular João Lobo Antunes, Faculdade de Medicina da Universidade de Lisboa, Lisboa, Portugal, ⁷ Institut Pasteur, Paris, France

OPEN ACCESS

Edited by:

Tania F. De Koning-Ward,
Deakin University, Australia

Reviewed by:

Adam Sateriale,
Francis Crick Institute,
United Kingdom
Nathaniel Gadsby Jones,
University of York, United Kingdom

*Correspondence:

Mariana De Niz
mariana.deniz@medicina.ulisboa.pt

[†]These authors have contributed
equally to this work

Specialty section:

This article was submitted to
Parasite and Host,
a section of the journal
Frontiers in Cellular and
Infection Microbiology

Received: 21 March 2022

Accepted: 06 May 2022

Published: 06 June 2022

Citation:

Kent RS, Briggs EM, Colon BL,
Alvarez C, Silva Pereira S and De Niz M
(2022) Paving the Way: Contributions
of Big Data to Apicomplexan and
Kinetoplastid Research.
Front. Cell. Infect. Microbiol. 12:900878.
doi: 10.3389/fcimb.2022.900878

In the age of big data an important question is how to ensure we make the most out of the resources we generate. In this review, we discuss the major methods used in Apicomplexan and Kinetoplastid research to produce big datasets and advance our understanding of *Plasmodium*, *Toxoplasma*, *Cryptosporidium*, *Trypanosoma* and *Leishmania* biology. We debate the benefits and limitations of the current technologies, and propose future advancements that may be key to improving our use of these techniques. Finally, we consider the difficulties the field faces when trying to make the most of the abundance of data that has already been, and will continue to be, generated.

Keywords: genomics, transcriptomics, proteomics, functional screens, microscopy, apicomplexa, kinetoplastid

INTRODUCTION

The global disease burden caused by Apicomplexan and Kinetoplastid infections is devastating world-wide. Among the Apicomplexans (**Figure 1**), *Plasmodium* spp. are responsible for a yearly estimate of 241 million malaria cases (WHO, 2021a); *Toxoplasma gondii* infects 30% of the human population (Milne et al., 2020); and *Cryptosporidium parvum* causes a yearly estimate of 44.8 million infections in children under 5 (Khalil et al., 2018). Among the Kinetoplastids (**Figure 2**), *Trypanosoma cruzi* affects 6-7 million people, mostly within the Latin American sub-continent where Chagas disease is most prevalent (WHO, 2021c); and *Leishmania* spp. cause an estimate of 700,000 to 1 million new leishmaniasis cases annually (WHO, 2021d). Additionally, *Trypanosoma brucei*, now responsible for less than a thousand yearly cases of Human African trypanosomiasis (WHO, 2021b) due to highly efficient vector control, and monitoring and surveillance programs, remains a current public health threat, as well as being a relevant model organism; These parasites continue to pose a major global threat, urging scientists to create and utilize novel molecular, cellular, pharmaceutical, bioinformatic, and imaging-based toolkits, to further our understanding of

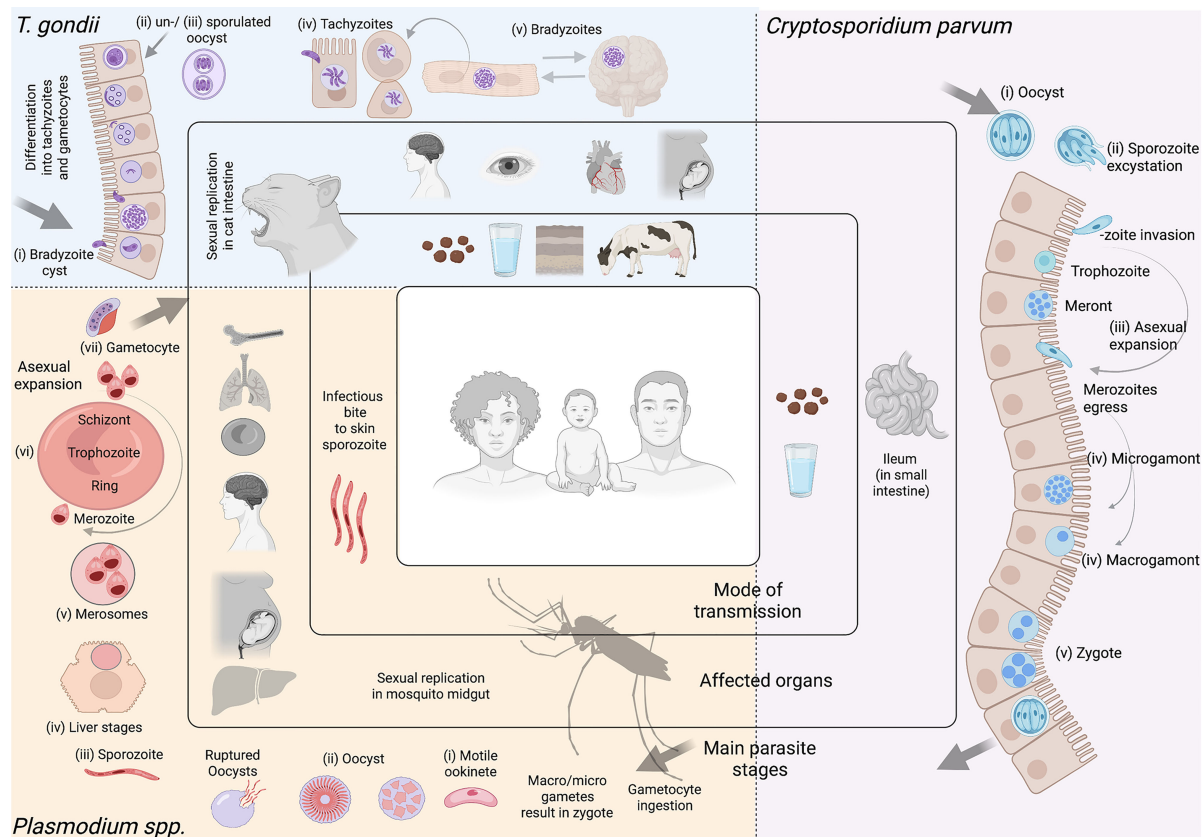


FIGURE 1 | Apicomplexan parasites. Most apicomplexan parasites have complex life cycles with several developmental stages that occur in different hosts and in different organs or tissues within the host. While advances have been made to culture many stages of these organisms *in vitro*, some are restricted to short-term culture. For others, only a limited number of stages can be sustained. Equally, not all stages are amenable to genetic modification. In this figure we summarize main features of *Toxoplasma gondii*, *Cryptosporidium parvum*, and *Plasmodium* spp. ***Toxoplasma gondii***. (i) After ingesting bradyzoite cysts from an intermediate host, the sexual developmental cycle of *T. gondii* occurs in the gut of felines culminating in the shedding of large numbers of (ii) unsporulated oocysts in their faeces. Within a few days, oocysts sporulate in the environment and become infective. (iii) Intermediate hosts can become infected by consuming contaminated soil, water or plants. Once consumed, oocysts transform into (iv) tachyzoites in the host's gut. Dissemination of a tachyzoite infection and repeated rounds of cell infection, replication and egress (lytic cycle) leads to a systemic infection. Immune pressure triggers some tachyzoites to form tissue cysts that contain (v) bradyzoites. In humans, tissue cysts most commonly found in skeletal muscle, the heart, the eyes and the brain. *T. gondii* tachyzoites are able to cross the placenta from mother to fetus. Reactivation of an encysted infection can occur upon immune suppression and ingestion of bradyzoite cysts by another intermediate host can transmit the infection (v to iii). Among these *T. gondii* stages, tachyzoites and bradyzoites can be cultured *in vitro* in large amounts. Tachyzoites are amenable to genetic modification. ***Cryptosporidium parvum***. (i) Sporulated oocysts are excreted by infected hosts through faeces and transmission to humans usually occurs via contaminated water. Following ingestion, the parasite undergoes excystation, whereby (ii) sporozoites are released, and invade the epithelial cells of the ileum. Here, *C. parvum* undergo (iii) 3 cycles of asexual expansion, followed by (iv) sexual commitment to either micro- or macrogametes. Fertilization occurs and results in the generation of a (v) zygote, which continues onto a sporulated oocyst. Some oocysts continue to reinfect the host while others are excreted. *Cryptosporidium* does not complete its lifecycle *in vitro* without the use of complex organoid systems. Even so, generating large amounts is limited. The sporozoite is the only stage used for transfections; to generate transgenic oocysts, transfected sporozoites must immediately infect an animal model or organoid. ***Plasmodium* spp.** Female *Anopheles* mosquitoes are responsible for transmitting *Plasmodium* spp. Mosquitoes are the definitive host, where *Plasmodium* undergoes sexual replication. This occurs in the mosquito's midgut, where micro/macro-gametes generate zygotes which become motile (i) (ookinetes) and invade the midgut wall. Here they develop into (ii) oocysts. As oocysts mature, they rupture, releasing (iii) sporozoites which migrate to various locations in the mosquito, including its salivary glands. Following an infectious bite, sporozoites migrate from the dermis to the blood vasculature in humans. This allows them to reach the host liver, where they invade hepatocytes, and undergo a single round of (iv) asexual replication (by schizogony) resulting in the release of (v) merozoites filled with merozoites. Merozoites rupture in the blood circulation and release thousands of merozoites, which then infect red blood cells (RBCs) and give rise to the erythrocytic stage of infection. Within RBCs, parasites develop into (vi) rings, trophozoites and schizonts. Mature schizonts rupture, releasing merozoites which invade other RBCs exponentially increasing the parasite mass. Some of these parasites will develop into sexual stages (called (vii) gametocytes). Mature asexual stages cause iRBC sequestration in organs including the brain, lungs, placenta, pancreas and adipose tissues, while sexual stages display preferential tropism to the bone marrow and other hematopoietic organs. Among these *Plasmodium* spp. stages, ookinetes, liver, asexual RBC, and sexual RBC stages can all be cultured *in vitro* in large amounts. Merozoites, rings, and schizonts are amenable to genetic modification. Note Large arrows in diagram refer to the completion of the cycle. Figure created with BioRender.com.

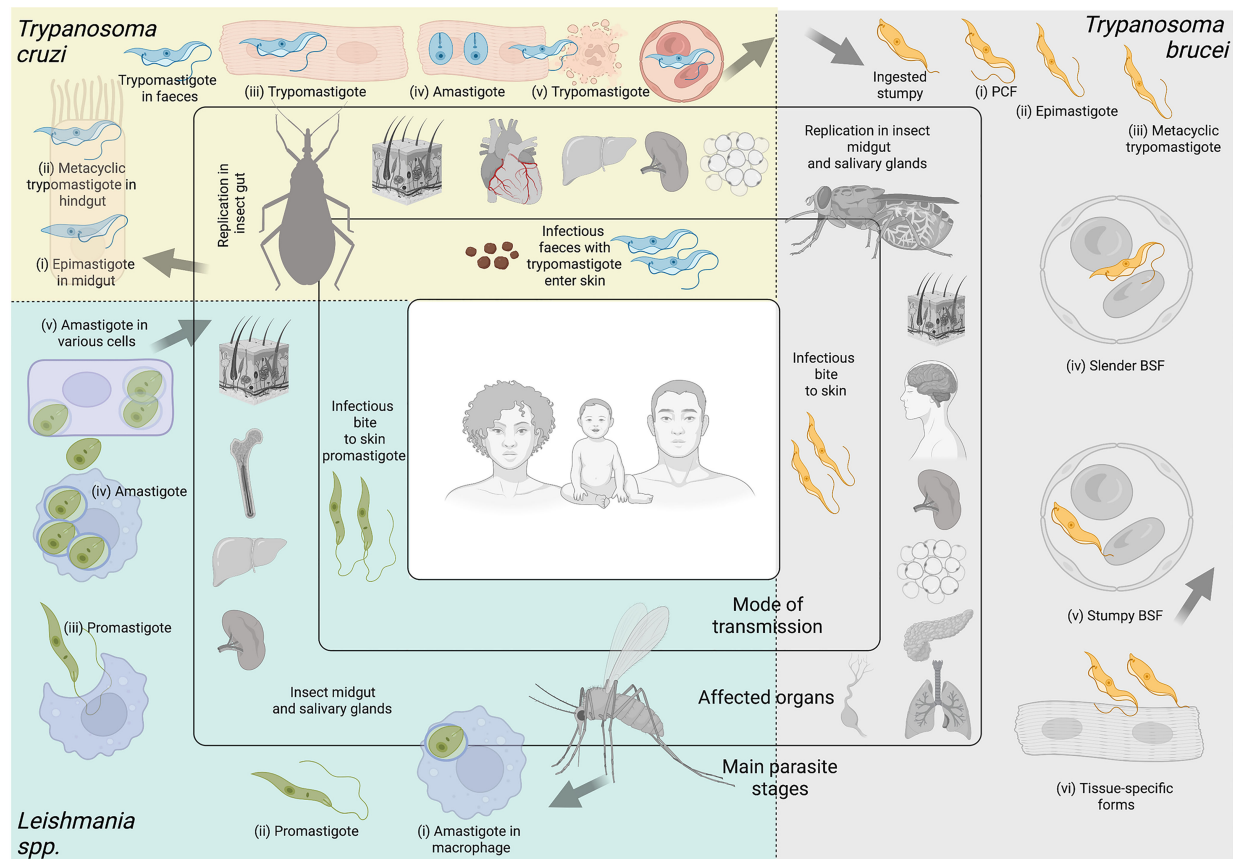


FIGURE 2 | Kinetoplastid parasites. Kinetoplastid parasites have complex life cycles with various stages occurring in insect vector and mammalian hosts, and in different organs or tissues within their hosts. While advances have been made to culture several stages of these organisms *in vitro*, many are restricted to short-term culture. For others, only a limited number of stages can be sustained. Equally, not all stages are amenable to genetic modification. In this figure we summarize main features of *Trypanosoma cruzi*, *Trypanosoma brucei*, and *Leishmania* spp. ***Trypanosoma cruzi***. Triatomine insect vectors of the genera *Triatoma*, *Rhodnius* and *Panstrongylus* become infected by feeding on infected blood (from humans or other animals). Ingested trypomastigote metacyclics transform into (i) epimastigotes in the insect's midgut. These multiply and differentiate into (ii) metacyclic trypomastigotes in the hindgut. Infected vectors release trypomastigotes through their faeces on the host skin. Parasites enter the skin via wounds or mucosal membranes (such as through the eyes). Inside the host, (iii) trypomastigotes invade cells of a plethora of tissues, and transform into (iv) amastigotes which multiply and differentiate again into trypomastigotes, which are released from lysed cells. Some of these travel in the (v) bloodstream, and can be ingested by triatomine vectors upon a bite for blood feeding. The most commonly affected organ is the heart, but others, including the liver, spleen, and adipose tissues are invaded too, some of them becoming important parasite reservoirs. Among these *T. cruzi* stages, epimastigotes, trypomastigotes and amastigotes can be cultured *in vitro* in large amounts, and the whole life cycle can be modeled *in vitro*. Epimastigotes, trypomastigotes and amastigotes are amenable to genetic modification. ***Trypanosoma brucei***. Tsetse flies (from the genus *Glossina*) become infected by feeding on infected blood (from humans and other animals). Within the fly's midgut, *T. brucei* stumpy forms transform into (i) procyclic trypomastigotes (PCF). These multiply, egress from the midgut, and transform into (ii) epimastigotes, which can reach the fly's salivary glands and continue to multiply. (iii) Metacyclic trypomastigotes are injected into the host skin during a bloodmeal. Inside the host, they transform into bloodstream form (BSF) trypomastigotes that can be (iv) slender or (v) stumpy forms, the latter of which rapidly transforms into procyclic forms in the tsetse midgut upon a blood meal. While slender BSFs multiply and thrive in the bloodstream, *T. brucei* is an extracellular parasite capable of invading multiple organs including the brain, spleen, adipose tissue, pancreas, lungs and lymphatic vasculature. These (iv) tissue-specific forms are relatively poorly understood. Among these *Trypanosoma brucei* stages, procyclics and BSFs can be cultured *in vitro* in large amounts, and the same stages are amenable to genetic modification. ***Leishmania* spp.** Phlebotomine sandflies become infected by ingesting infected cells during a bloodmeal. Within the sandfly, (i) amastigote forms of *Leishmania* spp. transform into (ii) promastigotes, which develop in the vector's gut, and migrate to the proboscis. Infected sandflies transmit (iii) promastigotes during a bloodmeal. After entry into the skin, promastigotes are ingested by phagocytic cells (eg. macrophages and neutrophils). Within these cells, promastigotes transform into (iv) amastigotes, which multiply and (v) infect other cells. Depending on parasite and host factors, cutaneous or visceral leishmaniasis can result. For the former, the skin and soft tissues like the nose and mouth can be affected. For the latter, affected organs commonly include the spleen, liver and bone marrow. Among these *Leishmania* spp. stages, promastigotes, axenic amastigotes and intracellular amastigotes can be cultured *in vitro* in large amounts. Promastigotes and amastigotes are amenable to genetic modification. Note Large arrows refer to the completion of the cycle. Figure created with BioRender.com.

parasite biology, and develop new interventions to combat the diseases associated with these organisms.

Together, ‘omics’ technologies have shed light on vital aspects of parasite biology. Current high-throughput bulk ‘omics’ technologies have allowed us to characterise parasite genomes, transcriptomes, and proteomes at specific timepoints, to take a snapshot of the parasite population. Conversely, single cell technologies, including microscopy and single cell ‘omics’, allow us to probe variation within the population and describe asynchronous or rare events. Genomics and advances in genetic manipulation now allow high-throughput phenotypic screens to investigate gene function. Equally, while imaging has historically been a powerful tool for parasitology, increasing the throughput of microscopy methods holds great potential in the context of integrative ‘systems biology’. Another important aspect is the vast amount of data generated, and the capacity to analyse and effectively use this data. In parasitology, we have made significant strides in creating data sharing platforms (eg. VEuPathDB (Aurrecoechea et al., 2010; Amos et al., 2022)). But as the complexity of these data increases, so do the challenges of data processing, integration, analysis, visualisation, interpretation and equitable sharing.

Here, we review seminal findings achieved in Apicomplexan and Kinetoplastid research by genomics, transcriptomics, proteomics, high-throughput functional screens, and imaging studies. We discuss the challenges, advances, and future directions of these technologies in the context of a key goal: how can we gain the most from the abundance of data that has already been, and will continue to be, generated?

GENOMICS

The early 2000’s were the advent of genome sequencing for Apicomplexan and Kinetoplastid research, as the genome sequences of *P. falciparum* (Gardner et al., 2002), *T. gondii* (Kissinger et al., 2003), *T. brucei* (Berriman et al., 2005), *T. cruzi* (El-Sayed et al., 2005), *L. major* (Ivens et al., 2005), *C. parvum* and *C. hominis* (Bankier et al., 2003; Abrahamsen et al., 2004; Puiu et al., 2004; Xu et al., 2004) were published. These laid the foundations for the high-throughput developments made since. Within less than two decades, the field has moved from Sanger and clone-by-clone sequencing to varied whole-genome shotgun sequencing technologies (Figure 3).

Sanger Sequencing

For a long time, genome sequencing relied on the Sanger method (also called first-generation sequencing), which involves the random incorporation of chain-terminating fluorescently labelled dideoxynucleotide triphosphates (ddNTPs) during DNA replication and capillary electrophoresis to detect sequencing products (Gomes and Korf, 2018; Hu et al., 2021). Sanger sequencing is still widely used due to its cost-effectiveness ratio for gene-specific analysis or a small subset of genes, but it is impractical for analysing larger regions and has a low discovery power.

Next Generation Sequencing

In the mid-1990s, sequencing by synthesis technology (SBS) was invented and provided the basis for next-generation sequencing (NGS) (also second-generation sequencing). The SBS approach relies on the incorporation of single fluorescently labelled dNTPs during DNA chain amplification. Illumina performs this in a parallel, high-throughput fashion, through cluster generation of DNA libraries by bridge amplification PCR (Hu et al., 2021). Together, all clusters in a flow cell could result in tens of millions of reads. Data generated by Illumina sequencing is highly accurate even for repetitive sequence regions and homopolymers. Compared to Sanger sequencing, NGS is high-throughput and provides higher sensitivity and coverage. However, because it generates short reads, it limits the analysis of structural variants, repetitive elements, and regions with a high GC content (Xiao and Zhou, 2020).

Third Generation Sequencing

In the late 2000s, third-generation sequencing (3rd Gen Seq, also known as long-read sequencing) was invented (Figure 3). The main 3rd Gen Seq platforms are the Single-molecule real-time (SMRT) sequencing from Pacific Biosciences (PacBio) and the Oxford Nanopore technology (ONT). SMRT sequencing relies on the fixation of a single DNA polymerase to zero-mode waveguides (ZMW) with a single DNA template molecule. Through the ZMW, the SMRT cell can detect which single fluorescently-labelled DNA nucleotide is incorporated by the DNA polymerase and make the corresponding base call (Rhoads and Au, 2015; Hu et al., 2021). Instead of DNA polymerases, ONT uses the pore-forming protein α -hemolysin embedded in a membrane. This protein has the inner diameter of the size of a single strand of DNA. So, when current is applied to the membrane, the DNA strand moves through the nanopores, which alters the electric current and allows base-calling (Clarke et al., 2009; Brinkerhoff et al., 2021; Hu et al., 2021). 3rd Gen Seq provides longer reads, allows detection of epigenetic markers, and can be portable, although error rates are still higher than NGS. Hybrid sequencing strategies have been implemented to improve sequence contiguity, error rates and affordability (Rhoads and Au, 2015).

Apicomplexans

Comparative genomics studies in Apicomplexan parasites have been done particularly amongst *Plasmodium*, *Toxoplasma*, and *Cryptosporidium* genera (Carlton et al., 2002; Coulson et al., 2004; Carlton et al., 2008; Mazurie et al., 2013; Miotto et al., 2013). They have helped our understanding of population structure, evolutionary dynamics, epidemiology, and drug resistance mechanisms. Apicomplexan genomes are typically small (~8.5 to 130 Mb) (DeBarry and Kissinger, 2011; Blazejewski et al., 2015) and quite different from the typical eukaryotic genome. Their nuclear genomes are compact, shaped by substantial gene loss, have few transposable elements, and almost no synteny outside of their genus (DeBarry and Kissinger, 2011).

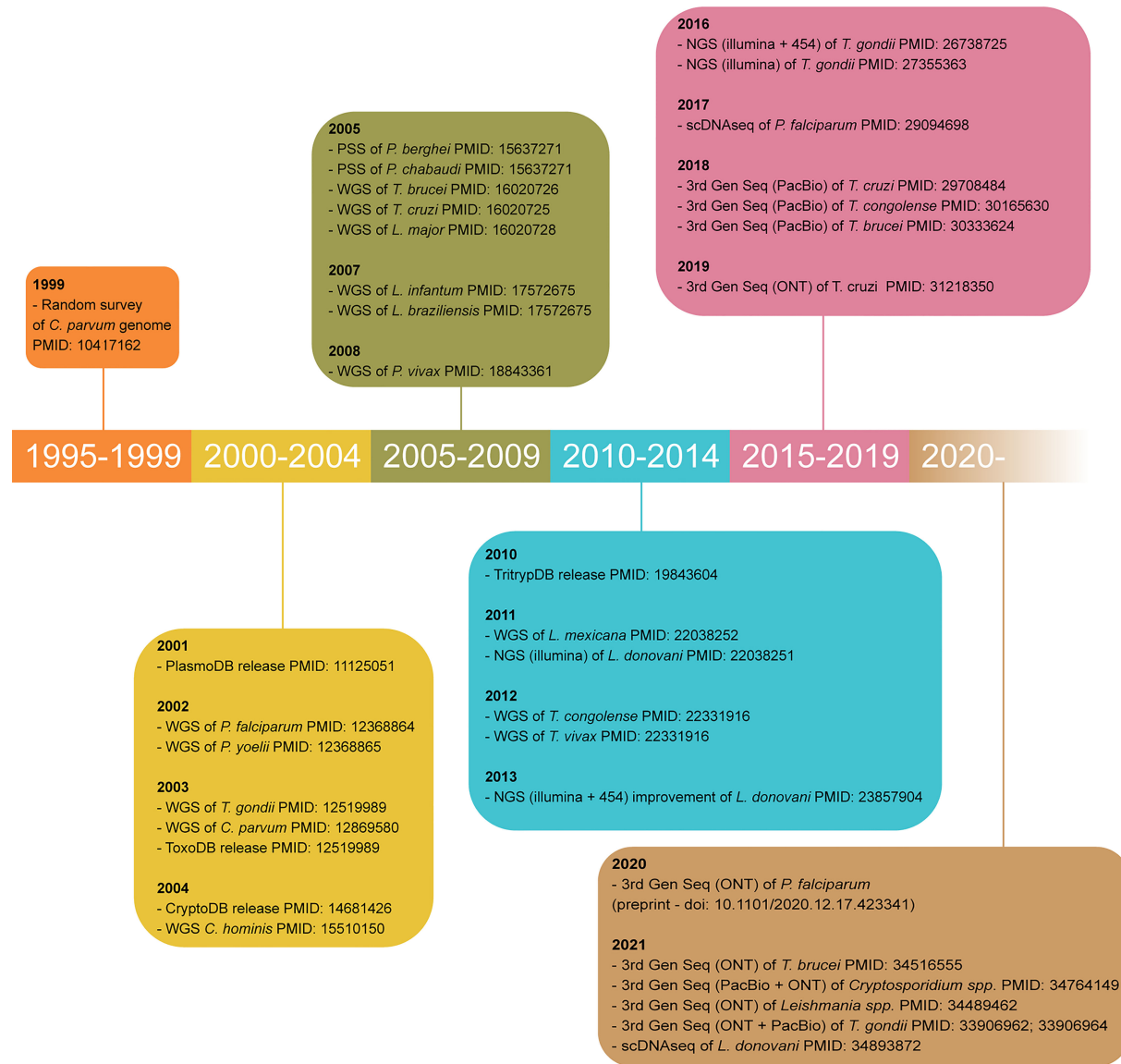


FIGURE 3 | Timeline of major achievements in parasite genome sequencing. Only the oldest article using each technology for each parasite is cited. WGS, whole genome shotgun sequencing; PSS, partial shotgun sequencing; 3rd Gen Seq, third generation sequencing or long-read sequencing; ONT, Oxford Nanopore technology; PacBio, Pacific Biosciences; PMID, PubMed identification number.

***Plasmodium* spp.**

The genomes of *Plasmodium* spp. are haploid, both in cell culture and in the vertebrate host, with approximately 23 Mb in size and encode for ~5500 genes throughout 14 well-defined chromosomes (Pegoraro and Weedall, 2021). The biggest challenge for *Plasmodium* genome sequencing has been their extremely low GC content [21–23% compared to 56% in the mouse genome (Videvall, 2018)], although modern technologies have become less sensitive to this difference. The genomes of multiple species of human and non-human malaria parasites are readily available (Carlton et al., 2002; Hall et al., 2005; Carlton et al., 2008; Ansari et al., 2016; Auburn et al., 2016; Böhme et al., 2018). Interestingly, more than 60% of the genes predicted from the *P. falciparum* genome do not have homologs in non-*Plasmodium* organisms and they encode putative proteins of unknown function (Gardner et al., 2002; Neafsey et al., 2021). Their subtelomeric regions are rich in contingency gene families, many of which are large (>200 genes), hypervariable due to high recombination pressure, and involved in immune evasion (Barry et al., 2003) (the major variant surface antigens (e.g. *var*, *vir*, *pir* genes) (Singh et al., 2014; Ansari et al., 2016); the STEVOR genes, which are necessary for erythrocyte invasion of merozoites (Cheng et al., 1998; Niang et al., 2014); and the *rif* gene family, which are putative virulence factors (Fernandez et al., 1999; Araujo et al., 2018).

Toxoplasma gondii

T. gondii is the only species of the *Toxoplasma* genus (Tenter et al., 2000; Dubey, 2010). *T. gondii*'s genome is 65 Mb, encoding ~8,000 genes throughout 13 chromosomes [previously annotated chromosomes VIIb and VIII are now a single chromosome (Lorenzi et al., 2016; Berná et al., 2021)]. The *T. gondii* genome contains multiple repetitive and low-complex regions evenly distributed across chromosomes (Berná et al., 2021).

Classical genetic studies of the population structure of *T. gondii* revealed three clonal lineages (types I–III) in North America and Europe (Darde et al., 1988; Dardé et al., 1992; Sibley and Boothroyd, 1992). These share a common ancestor (Su et al., 2003), despite distinct pathogenicity in rodent models (Shwab et al., 2018). Genomics revealed a fourth clonal lineage mostly found in wild animals in North America (Khan et al., 2011). South American *T. gondii* strains display the highest genetic diversity of the species with recent genetic bottlenecks and lack of clonal structure (Sibley and Ajioka, 2008; Lorenzi et al., 2016). Genome-wide SNP analyses have shown recent genomic admixture among *T. gondii* clades, where large chromosomal haploblocks are inherited. Genomics has been crucial to elucidate mechanisms of transmission, host range and pathogenesis, particularly amongst *T. gondii* strains that have inherited conserved haplotype groups (Lorenzi et al., 2016). Genomics has also shed light on *T. gondii* virulence factors, such as the ROP proteins, which are major determinants of pathogenicity in mice (El Hajj et al., 2006). Some of these ROP genes have undergone local tandem duplication, locus expansion events and are under strong selection pressure by the host's immune response (e.g. mouse Immunity Related GTPases) (Peixoto et al., 2010; Steinfeldt et al., 2010).

***Cryptosporidium* spp.**

There are currently 38 *Cryptosporidium* species reported that infect several host species (Feng et al., 2018). *Cryptosporidium* spp. genomes are ~9.1Mb in size, distributed across 8 chromosomes, and encoding ~4,000 proteins. Despite their much smaller size, *Cryptosporidium* spp. genomes have a gene density 1.8x higher than *Plasmodium* spp., a result of intron loss and reduction, intergenic regions shortening, and decrease of mean gene length (Keeling, 2004; DeBarry and Kissinger, 2011). Comparative genomics have shown that the most divergent regions of *C. parvum* and *C. hominis*, the most important human-infective species (Feng et al., 2018), are located near the telomeres. They are rich in transporters and surface-expressed genes, like other Apicomplexan and Kinetoplastid parasites (Bouzid et al., 2010; Widmer et al., 2012). These studies have also been key in identifying two new subtelomeric gene families that encode secreted glycoproteins [i.e. *C. parvum* specific proteins (Cops) and the *C. hominis* specific proteins (Chos)] (Bouzid et al., 2010), and are thought to play a role in the host-parasite interaction. Despite their name, advances in sequencing have shown that Cops is not species-specific, but rather conserved in *C. hominis* (Bouzid et al., 2013).

Most of the work done in this field has been based on SNPs found in the gp60 gene and revealed a very complex genetic structure (Tichkule et al., 2022). “Omics” analyses in *Cryptosporidium* have been delayed compared to remaining apicomplexans because the parasite is *quasi*-intracellular (i.e. intracellular but extra-cytoplasmic) throughout most of its life cycle; has a very small genome compared to the host cell, which reduces the power of direct sequencing; and long-term *in vitro* culture systems are technically challenging (Baptista et al., 2022). To date, the genomes of 15 species have been sequenced, 8 of which are annotated (Baptista et al., 2022).

Kinetoplastids

***Trypanosoma* spp.**

The genome sequencing of *T. brucei brucei* (Berriman et al., 2005) was followed by remaining *T. brucei* subspecies, *T. b. gambiense* (Jackson et al., 2010), *T. b. rhodesiense* (Sistrom et al., 2016), *T. b. evansi* (Carnes et al., 2015), and *T. b. equiperdum* (Hébert et al., 2017; Davaasuren et al., 2019). These genomes are ~32Mb in size and comparisons of these datasets have shown high synteny, large sequence homology and rare segmental duplications. However, these sequences, together with additional laboratory-adapted strains (Cross et al., 2014) and population isolates (Sistrom et al., 2014), have highlighted quite considerable diversity within the subtelomeres. The subtelomeres harbor multiple multi-copy gene families, of which the variant surface glycoproteins (VSG) are the most prominent. Comparative analyses of the genome sequences of *T. brucei*, *T. congolense* and *T. vivax*, have shown that each species has distinct mechanisms of generating antigenic diversity (Jackson et al., 2012; Silva Pereira et al., 2020) and thus have different strategies for establishing chronic infections. These genome sequencing projects have also allowed the determination of the cell surface phylome, a database of genes encoding cell-surface

genes and their evolutionary relationships within the main African trypanosome species (Jackson et al., 2013). Moreover, whole genome sequencing of clinical isolates from Human Sleeping Sickness patients has shown that disease relapse results from ineffective parasite clearance by melarsoprol (Richardson et al., 2016). On a larger scale, studies of population genomics have shown the importance of sexual replication in African trypanosome evolution. It is now clear that, although certain African trypanosomes, like *T. b. gambiense* type 1 (Weir et al., 2016) and at least particular lineages of *T. vivax* (Duffy et al., 2009) evolve clonally, others such as *T. congolense* (Morrison et al., 2009; Tihon et al., 2017) and *T. b. brucei* (Peacock et al., 2011; Peacock et al., 2014), undergo hybridization. Likewise, genomic analyses of *T. cruzi* have highlighted how the rapid evolution of immune evasion-related gene families accounts for intraspecific variation (Wang et al., 2021). Population genomics and genetics have also been key to understand the population structure of *Salivaria* and *Stercoraria* trypanosomes (Franzén et al., 2011; Reis-Cunha et al., 2015; Jackson, 2016; Tihon et al., 2017; Callejas-Hernández et al., 2018; Silva Pereira and Jackson, 2018; Silva Pereira et al., 2018; Silva Pereira et al., 2020) and the identification of new trypanosome species and strains (e.g. *T. vivax*-like (Rodrigues et al., 2008; Rodrigues et al., 2017; Rodrigues et al., 2020), *T. suis* (Hutchinson and Gibson, 2015), *T. suis*-like (Rodrigues et al., 2020).

***Leishmania* spp.**

Within the *Leishmania* field, research has focused on the *Leishmania* subgenus (i.e. *L. major*, *L. donovani*, *L. infantum*, *L. mexicana*). However, more recently, the subgenus *Viannia* has been attracting more attention, due to the growing recognition of the epidemiological importance of *Leishmania* (*V.*) *braziliensis*. With the exception of *L. amazonensis* (20Mb), *Leishmania* genomes contain 33Mb. Whilst genomics analyses of the *Leishmania* genus have revealed great chromosomal conservation (Ivens et al., 2005; Peacock et al., 2007; Rogers et al., 2011), studies of *L. braziliensis* and other *Viannia* species showed larger sequence diversity, differences in gene content, pseudogene number and chromosome copies, as well as novel mobile elements (Llanes et al., 2015; Valdivia et al., 2015; Ruy et al., 2019). The conservation of *Leishmania* genomes within different species contrasts with the extreme disparity in disease phenotype, tissue tropism, and clinical outcome. As in the trypanosome field, comparative genomics revealed a small number of highly-dynamic species-specific genes, as well as conserved gene families like the UDP-glycosyltransferases, that, despite their ancient origin, have diverged independently (Silva Pereira and Jackson, 2018). These examples of species-specific innovations are most frequent amongst the genes necessary for the coating and/or decoration of the parasite's cell surface, and are likely to determine key pathways for parasite survival and adaptation in different hosts and environments. Recently, the field has used whole genome amplification of single cells and single-cell sequencing as means to detect aneuploidy mosaicism and reveal the specifics of its generation and evolution (Imamura et al., 2020; Negreira et al., 2022).

Where Is the Genomics Field Going and What Remains to be Done?

A clear need in genome research is the improvement of reference genomes, both in terms of sequence contiguity and information. Long-read sequencing can help this because it resolves complex and repetitive regions and structural variants, and provides scaffolding evidence for already available genome sequences. Variations of these methods can also add information about epigenetic modifications, and genome architecture. It also facilitates sequencing of the minichromosomes and mitochondrial genomes. Furthermore, there is an urgent need for accurate and thorough annotation of reference genomes that support the increasingly sensitive transcriptomics and proteomics studies. Besides these points, genomics in the post-genomic era can answer key biological questions. Below we discuss two major examples.

Parasite Genomics Offer a Magnifying Glass Into the Evolution of Parasitism

The origin of Apicomplexans and Kinetoplastids is ancient, for instance, *Plasmodium*, *T. cruzi* and *T. brucei* diverged ~100 million years ago (Escalante et al., 1995; Stevens et al., 1998). Their genomes reflect that, by showcasing the expansions of contingency gene families and genome streamlining. This results from contractions in intergenic regions (Keeling, 2004; Panunzi and Agüero, 2014), loss of redundancy (Mendonça et al., 2011), and even some functional reduction (Bushell et al., 2017). *Cryptosporidium* spp. is an extreme example of genome compaction and reduction (Keeling, 2004), but this phenotype extends to remaining Apicomplexan and Kinetoplastid parasites, especially when compared to their free-living relatives. Genome sequencing of overlooked organisms can offer important insights into the development of pathogenicity and survival strategies, through the identification of parasite-specific innovations and/or loss of gene redundancy.

Comparative and Longitudinal Genomics Reveal the Microevolution of Parasite Lineages

Comparative genomics has been key to understanding the microevolution of parasite lineages, as a high-throughput method of population genetics. As the field progresses to single-cell genomics (Poran et al., 2017; Negreira et al., 2022) (Figure 3), long-read sequencing, and “post-genomic” tools (e.g. SNP barcoding panels (Daniels et al., 2008; Preston et al., 2014; Baniecki et al., 2015)), we will gain greater resolution into the dynamics of gene gain and loss, chromosomal reassortment, haplotype diversity and *de novo* mutations that may affect parasite fitness. Furthermore, these technologies allow a better understanding of parasite population history, geographical distribution, and the complex relationships between parasite and host co-evolution. They may also bring consensus to current debates in evolutionary biology, like the origin of *P. vivax* (Rougeron et al., 2020; Sharp et al., 2020). Finally, re-sequencing projects based on longitudinal sampling can offer a real-time overview of genome evolution dynamics, perhaps offering precious insights into how parasites respond to

environmental pressures, including the everlasting pressure of host coevolution. Systematic, longitudinal field isolate sequencing can uncover complex genetic and evolutionary links that are not detectable at current resolution, whilst improving our understanding of genetic diversity, namely within contingency gene families.

Challenges and Accessibility

A large bottleneck in the field of genomics has been the lack of analytical power to deconvolute complex data in a high-throughput manner. However, we have gathered a considerable set of computational tools that have streamlined the analysis of big data from parasite genomes. One of the most valuable platforms in parasitology is the VEuPathDB (<https://veupathdb.org/>), which integrates big data repositories across all ‘omics’ and multiple analytical and visualization tools. VEuPathDB has made an enormous impact on how parasitologists and vector biologists perform data mining. The specific impact and importance of VEuPathDB will be discussed in detail in the last section of this work. Nevertheless, there are other, more specialized tools include Companion, a web-based annotation tool (Steinbiss et al., 2016); VAPPER, a variant antigen profiler for trypanosomes based on diagnostic amino acid motifs and cluster of orthologs (Silva Pereira et al., 2019a), a *var* gene profiler based on DBLa domain sequence diversity (Barry et al., 2007), and CryptoGenotyper, which detects *Cryptosporidium* species from 18S/SSU rRNA sequences in mixed populations (Yanta et al., 2021). There have also been efforts to build biological sample repositories, where biological specimens or genomes from field isolates are archived, maintained, and made available to other researchers. Examples of these include the HAT Biobank (Franco et al., 2012), the TrypanoGEN biobank (Ilboudo et al., 2017), VAPPER (Silva Pereira et al., 2019a), and the Malaria Genomic Epidemiology Network (MalariaGEN) (Ahoudi et al., 2021). These are valuable sources of materials for future genome-wide projects. We take the view that future research will increasingly add to these tools, making genomic information readily available to all.

TRANSCRIPTOMICS

Transcriptomics has rapidly expanded over the past four decades, with each new technology generating a wave of increasingly large data (Chambers et al., 2019), enabling the discovery of novel transcripts and splicing variants, UTR annotation, and the quantification of transcriptome-wide changes in gene expression in populations and, most recently, single cells.

Technology/Methods

Key to the advancement of transcriptomics were complementary DNA (cDNA) libraries. Poly-adenylated mRNA is converted to cDNA *via* reverse transcription (RT) and cloned into bacterial plasmid vectors. Expressed sequence tag (EST) studies sequenced random library fragments and assembled them into partial

transcriptomes (Sim et al., 1979), even without an available reference genome (Marra et al., 1998). The first use of the term “transcriptome” came when ambitions moved from identifying and sequencing transcripts to their quantification with SAGE (Serial Analysis of Gene Expression) (Velculescu et al., 1997). SAGE fragmented cDNA libraries and ligated short tags together before sequencing to improve throughput and qualification (Velculescu et al., 1995). The assembly of transcriptomes with these methods (and genomics) led to the use of microarrays, where a set of short oligomer probes are arrayed onto a solid surface and fluorescently labelled transcripts are hybridized. Microarrays require much lower input of mRNA compared to SAGE and can be used at higher throughput and lower cost, popularising their use in parasitology (Figure 4), but prior knowledge of the transcriptome is required.

Later, high-throughput RNA sequencing (RNA-seq) emerged (Figure 4). RNA is extracted and converted to a library of cDNA *via* RT and PCR amplification. During the process, adaptor sequences are ligated to facilitate sequencing with NGS (see *Genomics*). RNA-seq allows the boundaries of transcripts to be found at single-nucleotide resolution, has a higher throughput, higher upper detection limit, lower expense, lower requirements for starting RNA and more accurate quantification (Hrdlickova et al., 2017). Most recently, single cell transcriptomics (scRNA-seq) has come to the forefront. As RNA-seq requires RNA to be extracted from a population of cells, differences between individual cells are lost. scRNA-seq allows dissection of diverse and related cell types from a mixed pool. All approaches aim to add a unique cell barcode to transcripts from each cell during the RT steps (Hwang et al., 2018; Choi and Kim, 2019). The barcoded cDNA from multiple cells is then combined for the remainder of the library preparation. After sequencing, each read has the cellular barcode information allowing the transcripts to be grouped by cell of origin. Methods vary in how they isolate individual cells for the initial barcoding steps and are thoroughly reviewed elsewhere (Aldridge and Teichmann, 2020; Adil et al., 2021; Nayak and Hasija, 2021).

Transcriptomics is now frequently applied in parasitology (Figure 4), often for comparisons of perturbed and non-perturbed samples. In this section we focus on large studies of unperturbed parasites and offer perspectives of how transcriptomes can further benefit the field.

Apicomplexans

Plasmodium spp.

EST and SAGE studies generated first transcriptomes of multiple *Plasmodium* spp. and their life cycle stages, uncovering novel genes and the prevalence of antisense transcription (Patankar et al., 2001). Microarrays and RNA-seq have since been used extensively to document the *Plasmodium* life cycle. Together these studies revealed the transcriptomic signatures of multiple aspects of the parasite’s biology, including the replicative stages, invasive stages and sexual stages. In particular, the developmental regulation of AP2 domain containing proteins has been uncovered, relating these key transcription factors to specific life cycle forms [reviewed in (Painter et al., 2011)].

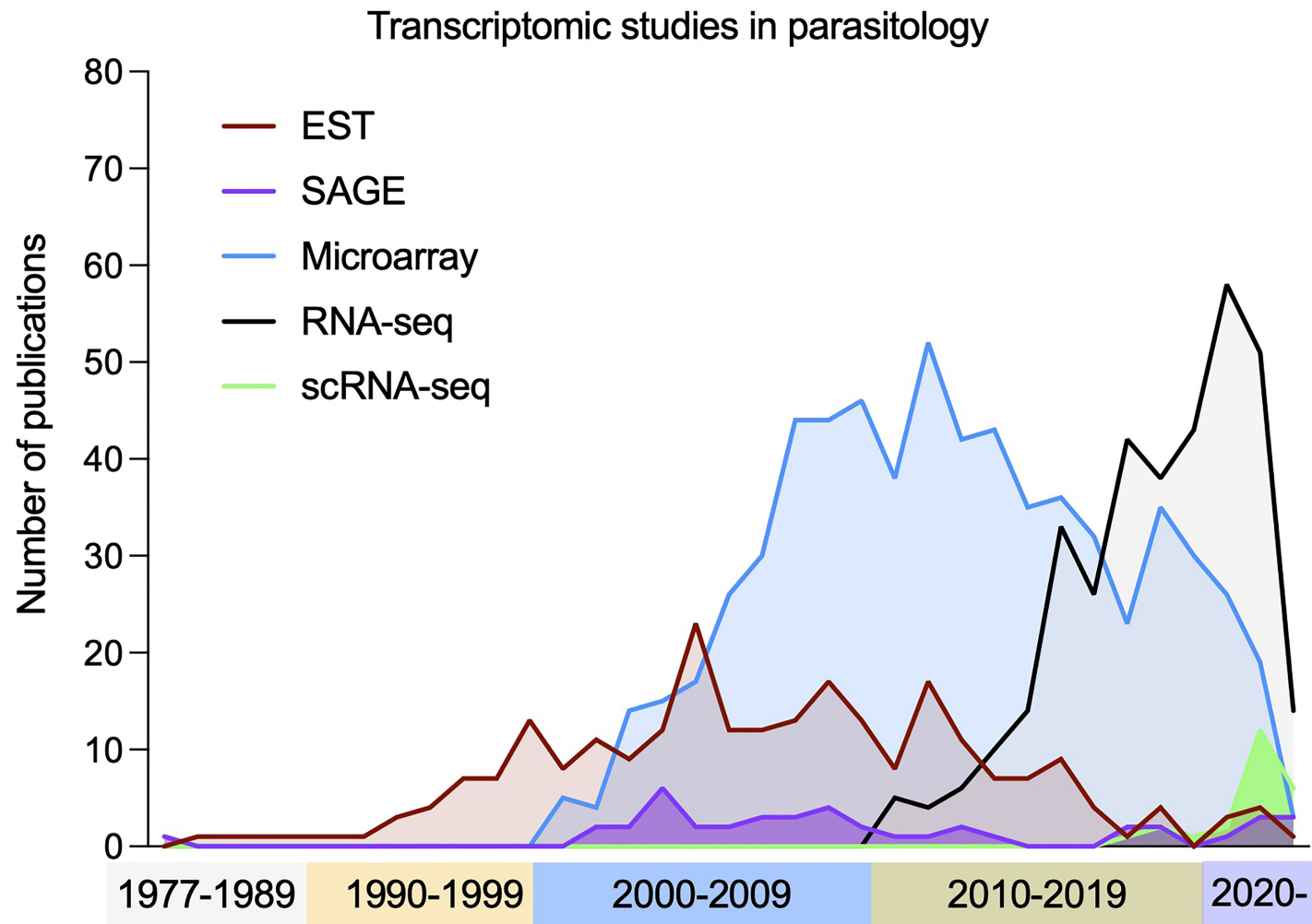


FIGURE 4 | Publication of transcriptomic studies in parasitology. The use of transcriptomics has had a rapid increased over time, with early techniques (ESTs, SAGE and microarrays) becoming less frequently used in favour of bulk RNA-seq. Most recently the number of studies using scRNA-seq methods has increased to deconvolve mixed populations. Note: *Each term was searched for in publication titles and/or abstracts, along with at least one species of unicellular parasites included in the VEuPathDB database (Amos et al., 2022).

The “Malaria Cell Atlas” (Sanger, 2020) consists of individual parasite transcriptomes assembled into a map of the complete life cycles of *P. berghei* and *P. falciparum* and a partial atlas containing asexual blood stages of *P. knowlesi* (Poran et al., 2017; Reid et al., 2018; Howick et al., 2019; Real et al., 2021). scRNA-seq-generated cell atlases can be mined for dynamic gene expression patterns, to identify stage specific marker genes, and used as a high-quality reference onto which query transcriptomes can be mapped (Figure 5), as demonstrated in by mapping isolated *P. knowlesi*, *P. malariae*, and *P. falciparum* parasites to the *P. berghei* cell atlas (Howick et al., 2019). Beyond life cycle assembly, analyzing gene expression patterns using scRNA-seq has uncovered the transcriptional signature of the sexual committed schizont subpopulation (Poran et al., 2017; Brancucci et al., 2018; Ngara et al., 2018); insights into gametocyte formation without the need of schizont pre-commitment (Kent et al., 2018; Bancells et al., 2019); genes key for *P. falciparum* sporozoite infectivity to humans (Real et al., 2021); markers for *P. vivax* and *P. falciparum* gametocytes; and *P. vivax* specific genes expressed in late schizont species mirroring the differences in RBC invasion between species (Sà et al., 2020).

Dual RNA-seq involves high depth sequencing of transcripts from infected host cells to analyse the host and parasite expression levels simultaneously. Although its application to *Plasmodium* research has enabled expression analysis of the host during infection, it remains difficult to assess parasite transcript changes due to the difference in host and parasite RNA levels in the sample (Lee et al., 2018). Dual scRNA-seq can now profile the transcriptomes of host cells and infecting parasites simultaneously, as performed with iRBC containing a single *P. falciparum* parasite (Poran et al., 2017). By identifying the subset of AP2-G expressing, sexually committed schizonts, the genes regulated by this master transcription factor could also be defined. Additionally, analysis of *var* genes expression challenged the previous dogma that *var* are mutually exclusive, as 3/17 individual cells expressed two *var* genes in parallel (Ngara et al., 2018).

Toxoplasma gondii

One of the most well studied *T. gondii* life cycle stages is the tachyzoite-to-bradyzoite differentiation step. As well as confirming the expression patterns of many genes identified with earlier technologies (such as bradyzoite specific secretory organelle proteins (Cleary et al., 2002)), the increased resolution of RNA-seq highlighted alternative splicing as a means of regulating expression, identified novel transcripts *via de novo* assembly and detected low expressed transcripts during this transition (Hassan et al., 2012; Chen et al., 2018; Garfoot et al., 2019). Oocyst maturation and subsequent reinfection of host cells by the sporozoites has been profiled using microarrays (Fritz et al., 2012) and SAGE (Radke et al., 2005), respectively. These provide the only profiles of transcript changes during these critical life cycle transitions to reveal stage-specific genes crucial for oocyst development and environmental survival. Dual RNA-seq of *T. gondii*-infected mouse forebrains

uncovered differences between acute and chronic parasite metabolisms, with chronic stage parasites downregulating TCA cycle components but upregulating glycolysis (Pittman et al., 2014).

Around a third of detected *T. gondii* mRNA genes show upregulation in one of two “transcription waves”, peaking in the G1 phase or the S and M phases of the tachyzoite cell cycle (Behnke et al., 2010). The latter group of genes largely relates to apicomplexan-specific processes, mirroring the functional links between mitosis, generation of daughter parasites, and invasion organelles. scRNA-seq also revealed two distinct transcription waves, which were dissected into G1, S, mitosis and cytokinesis-associated genes (Waldman et al., 2020; Xue et al., 2020). The greater resolution revealed over 500 additional cell cycle-regulated genes, and those associated with phase-specific organelle development (Xue et al., 2020).

scRNA-seq has also highlighted unexpected heterogeneity during asexual tachyzoites-to-bradyzoites development (Waldman et al., 2020; Xue et al., 2020), including a subpopulation expressing a novel AP2 domain-containing gene and an intermediate transcriptome between tachyzoites and bradyzoites (Xue et al., 2020). SAG1-related sequence (SRS) proteins are expressed on the cell surface and are suggested to constitute an antigenic repertoire. Yet, only a small subset of parasites expressed SRS transcripts and did so with unexplained sporadic variation, the biological implications of which are yet to be uncovered (Xue et al., 2020). Notably, while these findings correspond to *in vitro*-derived cultures, comparative studies between culture-derived bradyzoites and bradyzoites isolated from mice has shown important differences (Pittman et al., 2014).

Cryptosporidium spp.

Efforts were first put into profiling the transcriptome with real-time-PCR targeting 3,302 *C. parvum* genes during *in vitro* infection of epithelial cells, revealing the differential expression of AP2 domain-containing genes in this Apicomplexan organism (Mauzy et al., 2012). RNA-seq has since been used to profile the *C. parvum* life cycle, revealing transcriptome signatures specific to the oocysts (specialized to survival and sporozoite delivery) and the asexual replicative intracellular stages (indicating high transcription and translation levels) (Lippuner et al., 2018; Matos et al., 2019; Tandel et al., 2019) and the sexual stages (highlighting genes involved in meiosis) (Tandel et al., 2019). Several AP2 domain-containing transcripts varied in expression, yet none were found to be exclusive to any one stage, suggesting redundancy (Lippuner et al., 2018). RNA-seq was also employed to improve the annotations of the *C. parvum* and *C. hominis* reference genomes (Isaza et al., 2015; Baptista et al., 2022). Analysis has yet to be performed of these data to compare the transcriptomes of the oocyst stages from each species, to the best of our knowledge. Examining the use of older datasets, recently *C. parvum* ESTs (Wakaguri et al., 2009; Warrenfeltz and Kissinger, 2020) were mined to reveal extensive microRNAs (Ahsan et al., 2021) and RNA-seq to locate lncRNAs (Li et al., 2020).

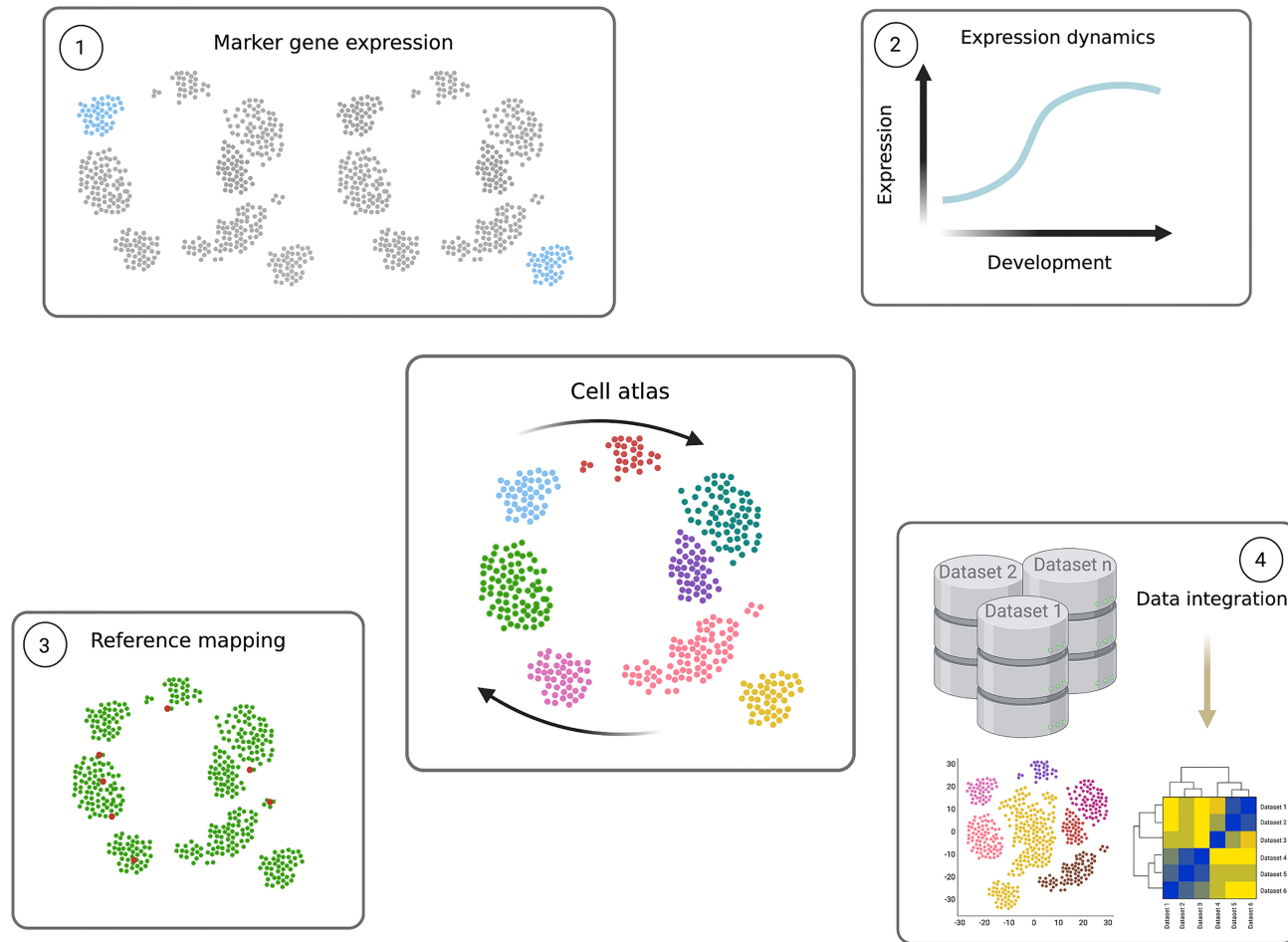


FIGURE 5 | Power of single cell transcriptomics. Cell atlases (central figure) contain the transcriptomes of individual cells, organised according to transcript signature similarities and differences in low dimensional space. The result is a transcriptomic map descriptive of the system in question, which in parasitology can reflect the parasite's complete life cycle (expressed as arrows). Individual parasite transcriptomes of the same life cycle form (single points) are positioned close together and, if captured, cells undergoing differentiation between different forms are positioned between the cell type clusters. These data can be mined and used as highly valuable resources in several ways. 1) Clustering analyses can be used to group similar cells in increasing resolution, often to identify life cycle forms. Differential expression analysis between clusters reveals novel marker genes, specifically expression in a particular cluster. 2) Pseudotime analysis can be performed to identify dynamic gene expression patterns across the life cycle. A path, or trajectory, is drawn through the cell atlas map connecting neighbouring cells and differential expression analysis is performed as a function of the trajectory. This reveals transcripts which change in level during the life cycle, and the exact expression pattern. Genes which peak in transitioning cells can reveal novel regulators. 3) The cell atlas can further be used as a reference to which query single cell transcriptomes can be mapped. For example, when only a few transcriptomes are available, or only those containing fewer transcripts per cell, mapping them to a high quality reference can identify their detailed position in the life cycle. 4) Transcriptomes of different genetically perturbed parasites, varied strains and even different species can also be mapped to the reference cell atlas through data integration methods. This allows detailed comparisons between datasets and across several cell types. Figure created with BioRender.com.

Kinetoplastids

Transcriptomics and genomics have revealed the unusual structure of Kinetoplastid genomes whereby one promoter precedes several genes that are transcribed as a polycistronic array and nearly all lack an intron-exon structure (Campbell et al., 2003; Haile and Papadopoulou, 2007). Transcripts are polyadenylated and a 5' splice leader (SL) cap is trans-spliced. By specifically targeting the SL sequencing during library preparation, RNA-seq variations have been used to enrich *Leishmania* transcripts from host material (Haydock et al., 2015; Cuyper et al., 2017) and efficiently capture the 5' ends of *T. brucei* transcripts (Kolev et al., 2015). This method has shown most genes have multiple SL and polyadenylation sites, and that these alternative sites can be used differentially between life cycle stages (Kolev et al., 2010; Nilsson et al., 2010; Siegel et al., 2010; Greif et al., 2013; Rastrojo et al., 2013; Jensen et al., 2014; Fiebig et al., 2015).

Trypanosoma spp.

Transcriptomics studies have revealed clear metabolism differences between life cycle forms of extracellular African trypanosomes. *T. b. brucei*, *T. vivax* and *T. b. gambiense* all show upregulation of glycolysis in BSFs in contrast to the tsetse stages which upregulate oxidative phosphorylation and the TCA cycle. Although *T. congolense* upregulates oxidative phosphorylation in procyclic and epimastigote stages, significant changes in glycolysis were not observed (Helm et al., 2009; Silvester et al., 2018). Analysis of tissue-specific *T. brucei* revealed further metabolic changes, as adipose resident forms further upregulate processes including glycolysis and purine salvage, and appear to uniquely express genes involved in fatty acid β -oxidation (Trindade et al., 2016). The intracellular parasite *T. cruzi* also exhibits strong metabolism switching between the mammal and triatomine vector (Minning et al., 2009). Interestingly, members of gene paralog clusters showed unexpected expression patterns during the life cycle, including amastins that were previously thought to be mainly exclusive to the amastigote stage appearing in insect stages (Minning et al., 2009).

During *Trypanosome* life cycles different cellular forms are often found in heterogeneous populations. scRNA-seq has been used to dissect mixed *T. b. brucei* populations and identify novel marker genes. These include slender and stumpy bloodstream forms generated *in vitro* (Briggs et al., 2021) and epimastigotes, gametes and metacyclics found in the tsetse fly salivary glands (Vigneron et al., 2020; Hutchinson et al., 2021; Howick et al., 2022). Additionally, midgut derived procyclic and proventricular forms have recently been profiled with scRNA-seq (Howick et al., 2022). If parasites transitioning between broad life cycle forms are also captured, trajectory analysis can be used to order individual parasites according to the gradual change in their transcriptome (Figure 5). Differential expression analysis is then used to find dynamic transcript changes during differentiation between life cycle forms. This approach uncovered genes peaking in expression during the slender to stumpy transition, including critical regulator ZC3H20 (Briggs et al., 2021), and highlighted

upregulation of transcripts associated with translation and the ribosome during development of both stumpy (Briggs et al., 2021) and metacyclic forms (Howick et al., 2022). Interestingly, scRNA-seq profiling of parasites extracted from tsetse salivary glands highlighted that pre-metacyclics express up to 6 mVSG before selecting just one for monoallelic expression in mature metacyclics (Hutchinson et al., 2021; Howick et al., 2022).

RNA-seq (Archer et al., 2011) and scRNA-seq (Briggs et al., 2021) have profiled phasic expression during the cell cycle of *T. b. brucei* pinpointing the peak expression time of several genes including cdc2-related kinases and cyclins, pairs of which most likely control transition between cell cycle checkpoints.

Leishmania spp.

Transcriptomics has been applied to multiple *Leishmania* spp. to reveal gene expression signatures associated with specific life cycle stages. Gene ontology (GO) term analysis of these signatures from RNA-seq found several similarities between species, such as upregulation of cellular motility and ATP synthesis in promastigotes compared to amastigotes, and phosphorylation upregulation in mammalian infective metacyclic and amastigote forms (Cruz and Freitas-Castro, 2019). Despite these similarities, only 12-35% of the differentially expressed genes have orthologs between *L. major*, *L. mexicana* and *L. braziliensis* (Cruz and Freitas-Castro, 2019), indicating clear differences in the life cycles of these species yet to be fully explored. RNA-seq revealed further molecular differences between morphology-defined forms, including the subtypes of the promastigotes (Inbar et al., 2017; Coutinho-Abreu et al., 2020). The transition from procyclic through nectomonad to metacyclic *L. major* was associated with downregulation of the cell cycle, consistent with reduced histone transcripts during *L. infantum* differentiation from procyclic to metacyclic. scRNA-seq has also been used to find transcripts unique to procyclic and metacyclic promastigote *L. tropica* in culture, and revealed differences in metacyclic formation between different strains in log-phase growth (Louradour et al., 2022).

Dual RNA-seq has also revealed that *L. major* and *L. amazonensis* both alter transcriptomes very early in macrophage infection, with little change observed in either parasite or host once parasites are in the intracellular niche, and uncovering genes involved in survival (Fernandes et al., 2016). Comparison of *L. donovani* dual RNA-seq additionally revealed putatively key virulence genes, including adenylate cyclase which is known to inhibit innate immune response in *T. brucei* infection (Shadab et al., 2019).

Perspectives and Future Directions

Completing the Life Cycles

Cell atlases of the *Plasmodium* life cycle are a highly valuable resource providing the transcriptomic signatures of each life cycle form as well as cells differentiating between forms. scRNA-seq was critical for gaining this level of resolution, as multiple transition steps occur asynchronously across the population and some life cycle forms are rare and only found as a sub-population which are difficult to isolate without marker genes. scRNAseq

datasets (current and future) can provide a wealth of information including: identification of novel marker genes; dynamic gene expression patterns identifying transcripts peaking in specific cell types; and variation between cell types to identify developmental regulators (summarized in **Figure 5**). High quality cell atlases can also be used as a reference for other query single cell transcriptomes, for example, of a genetically altered parasite line, clinical samples or alternative species or strains. The lower number of cells needed, and the ability to analyse mixed populations also means many life cycle forms are now accessible for the first time. However, challenges still remain, namely, to obtain highly-viable cells and detect lowly-expressed transcripts. Hence, bulk RNA-seq is still a valuable tool because it provides greater depth when populations can be isolated, and remains significantly more affordable. To overcome these challenges, integrated analyses of scRNA-seq and bulk RNA-seq has been explored in other fields (eg. cancer and vascular biology), and is a possibility that remains to be explored in parasitology.

Here we have focused on parasite-derived data, yet transcriptomics can clearly be leveraged to understanding host-pathogen interactions in detail. As well as dual RNA-seq and scRNA-seq, spatial transcriptomics at near single cell resolution can now be used to profile parasite and host cell transcriptomes within a tissue, and retain the spatial information (Rao et al., 2021). One such technology, Visium Spatial Gene Expression from 10x Genomics (<https://www.10xgenomics.com/products/spatial-gene-expression>), uses slides tiled with spots of adaptor oligos for RNA capture, where each spot has a specific barcode similar to scRNA-seq. When a tissue sample is laid over the slide it is imaged with microscopy and then the extracted RNA is barcoded according to its' position within the tissue. Thus, each transcriptome can be spatially organised. Although the size of each barcoded spot (currently 55 μm) is larger than Kinetoplastids and Apicomplexans, this level of resolution will likely have a huge impact on our understanding of parasitic life cycles within tissue niches and host responses.

Transcriptomics datasets could answer many key questions in the field, such as: how flexible is the African Trypanosome life cycle (Guegan and Figueiredo, 2021; Lisack et al., 2022; Matthews and Larcombe, 2022); how “persister-like” protozoa contribute to the life cycle and drug resistance (Barrett et al., 2019); and how intra- and extra-cellular parasites adapt to different microenvironments within their hosts (Silva Pereira et al., 2019b).

Improving Annotation

As discussed above, there is a clear need to invest in higher quality references with accurate annotations. This is important in transcriptomics as correct transcript (including UTR sequences) annotations are needed to generate accurate quantitative data. Transcriptomics can also aid genome annotation. Applying methods like SL primer RNA-seq in the Kinetoplastids to a greater variety of species, strains, and life cycle forms will allow researchers to select references much closer to the parasites investigated. Mining available RNA-seq data could also be highly valuable for defining missed transcripts, variable UTR boundaries and splicing variants not present in current

references. The use of long-read transcriptomics/genomics can also begin to resolve multigene families which are prevalent among parasites.

Data Integration and Comparison

Integration of multiple datasets would be highly impactful. For example, several scRNA-seq studies have analyzed different stages of the *T. brucei* life cycle. Despite these all using a variety of methods, the raw data could be integrated as bioinformatic methods improve (Argelaguet et al., 2021) to provide at least a particle life cycle atlas, as demonstrated in the Malaria field. Population-based transcriptomics constitute a highly significant bank of data which, with upgraded analysis methods, could be combined, analysed and compared to gain significant insight into these pathogens' biology. Here, we discuss only unperturbed parasite data, but these comparisons can clearly be extended to compare experimentally manipulated parasites. Lastly, “multi-omic” data integration would be hugely valuable to link transcript levels to protein levels and genomic features (Subramanian et al., 2020).

QUANTITATIVE PROTEOMICS

While mass spectrometry was being used in the 1990s for protein identification in parasitology, it was not until the early 2000s, once the respective genomes were published, that proteome datasets were derived. Quantitative proteomics remains an active field, as the advancement of mass analyzers has given rise to more sensitive mass spectrometers allowing for identification and quantification of low abundant ions in complex samples. These studies can generate large quantitative datasets where one can identify post-translational modifications, drug targets, life cycle differences, organellar compositions, among other applications.

Quantitative proteomics can be split into relative quantitation or absolute quantitation. In the Kinetoplastid and Apicomplexan fields, relative quantitation proteomics is more commonly used as seen by the number of publications (**Figure 6**). Here, we briefly describe some methods, consider their benefits and limitations, and discuss specific parasite-related examples and available datasets.

Relative Quantitation

There are three commonly used methods in the Apicomplexan and Kinetoplastid fields to identify the relative abundance of proteins in a sample: Stable Isotope Labeling of Amino Acids in Cell Culture (SILAC), Tandem Mass Tag (TMT) or Isobaric Tags for Relative and Absolute Quantitation (iTRAQ), and Label-Free Quantitation (LFQ).

SILAC works by introducing a stable isotope variant of an amino acid, commonly lysine or arginine, that becomes incorporated during protein synthesis. Once cells take up the ‘heavy’ or ‘light’ isotopes, the cell lysates can be combined and proceed through to protein digestion, liquid chromatography and tandem mass spectrometry (LC-MS/MS). Some benefits of

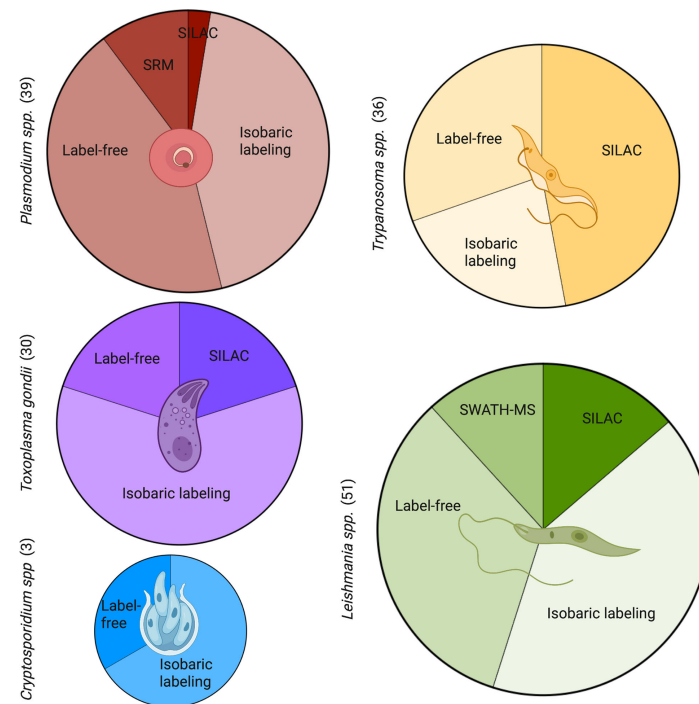


FIGURE 6 | Commonly used quantitative methods to study proteomics in Apicomplexans and Kinetoplastids. A PubMed search was carried out for each genus with key terms for the proteomic methods. The number of publications by term and by parasite are shown in brackets. *Leishmania* had the most quantitative proteomic publications, followed closely by *Plasmodium*, *Trypanosoma*, and *Toxoplasma*. Both *Leishmania* and *Plasmodium* showed a larger diversity of methods with the inclusion of SWATH-MS and SRM, respectively. *Cryptosporidium* had the least amount of publications in quantitative proteomics and least diversity of methods. SRM, selected reaction monitoring; SILAC, stable isotope labelling by amino acids in cell culture; SWATH-MS, sequential window acquisition of all theoretical mass spectra. Figure created with BioRender.com.

SILAC are the high and uniform labeling efficiency, minimizing sample loss by omitting peptide labeling, and labels are unaffected by protein purification steps (Ong et al., 2002). This technique is not ideal for life cycle stages where protein synthesis is inactive or bulk cell culture is difficult.

TMT and iTRAQ are two examples of isobaric labeling for mass spectrometry. They work similarly in that the labels used are of the same mass and are added after protein digestion to tag the peptides. Similar to SILAC, the individual samples are combined and run through LC-MS/MS, which allows for higher throughput in machine time and analysis with less run-to-run variability. TMT and iTRAQ currently have the ability to multiplex up to 18 and 8 samples, respectively. However, due to co-isolation and co-fragmentation there is a quantification distortion for low-abundant peptides. Additional statistical analysis or MS3 can be done to minimize this limitation.

LFQ differs from the previous techniques in that there is no label incorporation or tagging step. This can be beneficial as it allows for an unlimited number of samples to be compared, given that there is no limitation due to the number of available tags. However, this is at the expense of variation, technical variability, and throughput, as each sample is processed separately. Another benefit of LFQ, specifically compared with iTRAQ, is that the lower amount of protein loaded per run results in an average of 243 more identified proteins (with more than 1 peptide), with 34% increased sequence

coverage (Patel et al., 2009). This is especially beneficial for organisms where it is difficult to acquire a large amount of material, as previously described.

Apicomplexans

Plasmodium spp.

Although *Plasmodium* undergoes a complex life cycle in multiple hosts, most life stages are accessible enough to obtain sufficient material for proteomics, as seen with the hundreds of 'protein expression' datasets available on PlasmoDB (Aurrecochea et al., 2009). There are 5300 predicted proteins in *P. falciparum* (Hall et al., 2005). Using SILAC, Nirmalan et al. (Nirmalan et al., 2004) effectively used isoleucine as their heavy isotype to quantify protein levels across the blood stages of *P. falciparum*. Isoleucine was the amino acid of choice because it was not made *de novo* from parasites or scavenged from the host, but efficiently taken up. Additionally, it is an abundant amino acid in *P. falciparum*, which allows for labeling to be present in most of the tryptic peptides (Nirmalan et al., 2004). Quantitative proteomics of the liver stages were done using *P. berghei* infected HepG2 cells. Over 100,000 merozoites were used per replicate with LFQ to identify 1188 proteins (with minimum 2 peptides) as the merozoite proteome (Shears et al., 2019). Merozoites play a pivotal role as a 'bridge' between the liver and blood stages in the *Plasmodium* life cycle. Comparison with liver and blood *Plasmodium* proteomes showed both, significant similarities with

both stages, and a subset of proteins unique to merosomes which warrants further investigation. In addition to merosomes, sporozoites at different maturation stages have been isolated from mosquitos to produce a surface proteome using LFQ in both *P. yoelli* and *P. falciparum* (Lindner et al., 2019). This allowed the identification of two distinct translational repression programs active during sporozoite maturation, that temporally regulate protein expression. This in turn governs major sporozoite life events in both, mosquito and mammalian hosts.

Additionally there are studies using host blood plasma samples to study host-pathogen interactions in patients with *P. falciparum* and *P. vivax*. Kumar et al. (2020) identified biomarkers for malaria severity using TMT labeling with LC-MS/MS. They found an up-regulation of cell-to cell adhesion-related host proteins in *P. falciparum* infections and not in *P. vivax*. This study generated a large dataset of infected host blood plasma data that has been deposited to the ProteomeXchange Consortium via the PRIDE partner repository.

Toxoplasma gondii

There have been over 20 proteomic studies with available datasets on ToxoDB (Kissinger et al., 2003). Some examples include using LFQ to develop a bradyzoite proteomic profile (Garfoot et al., 2019), SILAC to create the phosphoproteome (Treeck et al., 2014; Beraki et al., 2019), and using LC-ESI-HDMS (liquid chromatography, electrospray ionization, high definition mass spectrometry) for absolute quantification of the secretome of tachyzoites (Ramírez-Flores et al., 2019). To identify differences across tachyzoites, bradyzoite-containing cysts, and sporulated oocysts, Wang et al. used iTRAQ with LC-MS/MS and found 6285 proteins across the 3 stages, with hundreds being differentially expressed (Wang et al., 2017).

Most recently, a study using hyperLOPIT, a method that uses ultracentrifugation to separate subcellular structures prior to TMT labeling, created a comprehensive proteomic dataset of subcellular compartments in the extracellular tachyzoite. In this study, Barylyuk et al. (2020) were able to match 1916 proteins to known compartments within the tachyzoite. Less than 20% of the matched proteins had a clear, defined function, stressing the significance of this dataset in providing compartment composition for *T. gondii* as well as all Apicomplexans.

***Cryptosporidium* spp.**

Since standard proteomic methods demand a highly concentrated protein sample, most of the stage-specific proteomes for *Cryptosporidium* are lacking. While there are not as many datasets available for *Cryptosporidium* as the other parasites, there are a few data sets available for the mammalian pathogen *C. parvum* on CryptoDB (Puiu et al., 2004) from the early 2000s identifying proteins in the intact oocyst, excysted oocyst and sporozoites (Truong and Ferrari, 2006; Snelling et al., 2007; Sanderson et al., 2008). These are currently the only life cycle stages where it has been feasible to collect enough material, as they are shed from large animal models, to perform proteomic analyses. Complementing the original proteomic data, there has been a quantitative study using iTRAQ with LC-MS/MS to compare sporozoites, intact oocysts, and

excysted oocysts finding 302 proteins total (Snelling et al., 2007). Comparing the same *C. parvum* stages, Sanderson et al. (Sanderson et al., 2008) used 3 approaches (MudPIT, gel LC-MS/MS, and 2-DE) to maximize coverage. In doing so, they identified 1237 unique proteins that map to 32% of the predicted proteome. *C. parvum* IOWA II has 3894 protein coding genes (Puiu et al., 2004).

Recently, using the bovine parasite, *C. andersoni*, with TMT labeling, 1786 proteins were identified in the oocysts and sporozoites, of which 17 were differentially expressed between excysted and intact oocysts (Li et al., 2021a). *C. andersoni* oocysts are able to excyst solely with temperature change, unlike oocysts of *C. parvum* which require a combination of multiple stimuli (temperature, pH, cholates, proteases) (Smith et al., 2005), so comparisons of differentially expressed proteins between these species may be limited. Another recent study using label-free proteomics identified 231 proteins that correspond to intracellular stages of *C. parvum* at 36 hours post infection of HCT8s, an adenocarcinoma cell line (Li et al., 2021b). This study also identified 121 host proteins that were changed during infection. However, as *C. parvum* cannot complete its life cycle in HCT8s, there is a limitation in the conclusions we can draw from these host-pathogen expression differences.

Kinetoplastids

***Trypanosoma* spp.**

Reference genomes for *T. cruzi* and *T. b. brucei* show 9039 and 9660 protein coding genes, respectively (Jackson et al., 2012). A non-quantitative proteomic lifecycle of *T. cruzi* has been carried out and identified 2784 proteins, 30% of which overlapped across each life-cycle stage (Atwood et al., 2005). Early proteomic studies have had difficulty identifying all present proteins in samples and quantifying the identified proteins. However, later studies have used quantitative methods to quantify proteins in different life cycle stages. Using LFQ to study early metacyclogenesis identified 2720 proteins (with 2 unique peptides) in stationary phase epimastigotes and exponential phase epimastigotes (Avila et al., 2018). Ribosomal proteins were identified as some of the most upregulated proteins in the exponential phase, while metabolic enzymes were upregulated in the stationary phase (Avila et al., 2018). Also using LFQ, 114 proteins were identified to be differentially expressed in metacyclic trypomastigotes when compared to epimastigotes *in vitro* (de Godoy et al., 2012).

Various quantitative proteomic methods have also been used with *T. b. brucei*. TMT labeling of procyclic *T. b. brucei* identified 5325 proteins, of which 384 proteins were associated with cell cycle regulation (Crozier et al., 2018). Additionally using SILAC, Tinti et al. (Tinti et al., 2019) developed another interactive platform to compare protein turnover between blood stage forms and procyclic forms [platform access: <https://tbrucei-iba927.pages.dev/> and <https://tbrucei-iba427.pages.dev/>]. To study proteomic changes during the differentiation between slender and stumpy forms, stumpy forms were treated with citrate/cis-aconitate and samples were collected at 7 time points up to 48 hours post-treatment. LFQ analysis from these samples quantified 4270 'protein groups', which were defined as groups

of proteins that are indistinguishable by mass spectrometry from the identified peptides. Of these 1308 protein groups were found to be upregulated during differentiation and 157 protein groups were downregulated (Dejung et al., 2016).

***Leishmania* spp.**

As both the amastigotes and promastigotes of *Leishmania* can be cultured *in vitro*, large amounts of material can be prepared for proteomic studies. Various datasets identifying proteins in the promastigote and amastigote forms have already been created (Brotherton et al., 2010; Nirujogi et al., 2014) and are available on tritrypdb.org (Aslett et al., 2010). Of the discussed protozoa, only in *Leishmania* was SWATH-MS used to identify differentially expressed proteins. Unlike the previously mentioned techniques, SWATH-MS is a data independent acquisition method. An example of this method is its use in identifying protein changes between 24 and 48 hours after *L. donovani* promastigote to amastigote differentiation. Routaray et al. identified 814 differentially expressed genes in the first 24 hours and 921 differentially expressed proteins at 48 hours post-differentiation (Routaray et al., 2022).

Another application of quantitative proteomics is thermal proteome profiling (TPP), which is an unbiased approach using TMT-labelling with mass spectrometry to identify drug targets. TPP studies generate quantitative datasets of bound proteins across a temperature gradient for all the soluble peptides in a sample. In this study Corpas-Lopez et al. used TPP to validate N-Myristoyltransferase (NMT) as a pharmacologically relevant target in *Leishmania* (Corpas-Lopez et al., 2019).

Future Advancements

As single-cell sequencing and transcriptomics become more common, the interest in single-cell proteomics rises. However, even with the increased sensitivity of mass analyzers in recent years, the ability to accurately quantify peptide ions from a single cell remains difficult. Recent studies have tested a creative solution to circumvent this issue by adding a carrier proteome in addition to isobaric labelling (Cheung et al., 2021; Ye et al., 2022). However, carrier proteomes can bias which peptide ions are being identified and there is still a lower quality of MS data in terms of background signal (Ye et al., 2022). There is still a need for more sensitive instruments and greater multiplexing capacity in order to perfect performance of single cell quantitative proteomic studies. However, the development and utilization of single-cell proteomics within protozoans will be a way to reach the life-cycle stages that are not easily bulked up for standard MS, providing great insight into these yet understudied stages.

ONT has also been recently adapted for quantitative proteomics (Huang et al., 2019; Lucas et al., 2021). There are many benefits of using ONT for proteomics including lower cost, higher throughput potential, less maintenance, and higher portability compared to mass spectrometers. Together, these characteristics make proteomic studies more accessible. Lower resolution is still a limitation, but one that is being addressed as the method and technology continue to be optimized. ONT for proteomics can be an accessible method

for drug discovery in Apicomplexans and Kinetoplastids as well as identifying vaccine targets (Aebischer, 2014).

While both of these technologies are providing large advancements for the proteomics field, there is still work to be done in optimizing quantitative accuracy, resolution, and accessibility. These methods are being tested with large cells, such as HeLa or K562, as well as synthetic peptides (Cheung et al., 2021), but remain to be implemented in Apicomplexan and Kinetoplastid research.

FUNCTIONAL SCREENING

Functional screens generally rely on the generation of mutant parasites *en masse* followed by specific screening assays to identify subpopulations that meet pre-defined criteria, before matching genotype to phenotype. The repertoire of tools for direct and conditional gene, mRNA and protein regulation developed and optimised for Apicomplexans (Briquet et al., 2021) and Kinetoplastids (Lander and Chiurillo, 2019; Horn, 2022) is extensive. Many of these technologies have also been scaled to enable functional screens (Figure 7).

Genome Mutagenesis

Early screens used whole genome mutagenesis by chemicals, like N-ethyl-N-nitrosourea (ENU) and Ethyl methanesulfonate (EMS), or untargeted genome insertional mutagenesis, using transposons like PiggyBac, to generate mutants across the genome. Although key discoveries were made using these techniques (Radke et al., 2000; Morrisette and Sibley, 2002; Mordue et al., 2007; Farrell et al., 2014), which are a key resource, they are limited by difficulties in identifying and confirming specificity of mutations and the possibilities of multiple insertions. Signature tagged mutagenesis (STM) strategies have been used with some success to track mutants when combined with transposons (Mazurkiewicz et al., 2006) or chemical mutagenesis (Knoll et al., 2001).

There are several gene disruption approaches that target all/much of the genome (Gomes et al., 2015; Sidik et al., 2018; Baker et al., 2021; Horn, 2022). Additional methods have been developed to study the mutants within a population by: quantifying relative fitness of mutants (Gomes et al., 2015; Sidik et al., 2018), studying their localisation, and classification with high-content imaging (Li et al., 2022; Smith et al., 2022), and isolating subpopulations with specific phenotypes (Stanway et al., 2019; Harding et al., 2020). The generation of mass knockouts has been achieved using traditional recombination methods (Gomes et al., 2015; Bushell et al., 2017) and CRISPR Cas9-mediated mutagenesis (Long et al., 2016; Sidik et al., 2016; Baker et al., 2021).

While many of these screens have been completed and have allowed us to parse out essential and non-essential genes in a variety of conditions, they have significant limitations, particularly in parasitic infections which have complex life cycles with only certain stages amenable to transfection and culture (Figure 8).

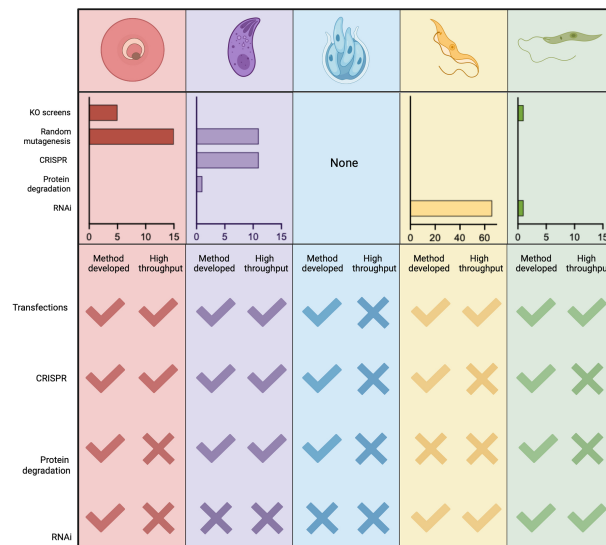


FIGURE 7 | Publications using functional screens in Apicomplexans and Kinetoplastids. The number of functional screens completed in various Apicomplexans and Kinetoplastids is summarised. PubMed searches were carried out for each genus and screening method (y-axis) manual curation confirmed whether the method was used for screening rather than follow-up studies. In *Plasmodium* spp. random insertional mutagenesis (*pf*) and KO screens (*pb*) have been used extensively. In *T. gondii* chemical mutagenesis and, more recently, mutagenesis using CrispR libraries dominate. Functional screens in *Trypanosoma* spp. have been exclusively and extensively completed using RNAi. Few screens have been completed in *Leishmania* spp. and these are recent. Due to the lack of high throughput technologies in *Cryptosporidium* spp. no screens have been carried out on the parasites, only host screens. A summary of currently available technologies and their adaptation to high throughput, required for screening, is also shown. Figure created with BioRender.com.

To combat this, several conditional systems have been developed; conditional gene excision or promoter inactivation can be achieved with conditional expression of site-specific recombinases [flp/FRT and Cre/loxP, (Combe et al., 2009; Andenmatten et al., 2013)] or by splitting the protein into nonfunctional subunits that regain functionality when fused together [DiCre, (Andenmatten et al., 2013) and splitCas [Li et al., 2022]].

RNA Regulation

As some kinetoplastids, like *T. brucei*, have functional, inducible RNA interference (RNAi) machinery, knockdown generation using short hairpin RNA (shRNA) is a widely used method for controlling expression. Other kinetoplastids with non-canonical RNAi mechanisms have been adapted for RNAi knockdowns (Horn, 2022) and even Apicomplexans, like *P. berghei*, can be adapted to express a minimal, non-canonical RNAi pathway (Hentzschel et al., 2020) enabling the use of RNAi to knockdown expression.

Protein Regulation

Several methods have been used to regulate protein expression including the shield regulated destabilisation domain (DD), the trimethoprim regulated DHFR destabilisation domain (DDD) and the auxin inducible degron (AID) (Briquet et al., 2021). In these systems the protein of interest is often tagged and the degradation sequence added allowing localisation and confirmation of depletion. When combined with high-content

imaging the localisation of tagged protein before and after induction of knockdowns can be used as a non-reducing screening method (see *Imaging* section). These degradation methods are limited to proteins accessible to the proteasome and those that can be tagged without interfering with function.

Apicomplexans

Plasmodium spp.

The development of the PlasmoGem vector community resource provided a publicly accessible library to disrupt or endogenously tag genes across the *P. berghei* genome without having to generate vectors in house (Pfander et al., 2011; Gomes et al., 2015; Bushell et al., 2017).

The first screen completed using recombineering vectors determined the relative growth rate (RGR) for each gene knockout from pooled transfections. In this screen, 44.9% of all genes were defined as essential and 18% resulted in slow growth. Therefore, 63% of all genes were considered important for asexual growth *in vivo* (Bushell et al., 2017). Screening of function at subsequent stages of the life cycle is impossible once a gene confers a severe fitness defect (**Figure 8**). However, screening of non-essential genes, including slow-growers, has been completed using recombineering vectors during gametocyte development (Russell et al., 2021 (preprint)) and in the mosquito and liver stages (Stanway et al., 2019).

Although not yet adapted for high-throughput assays, several conditional systems have been developed in *P. berghei* and *P. yoelii* that may permit functional screening at all life cycle stages

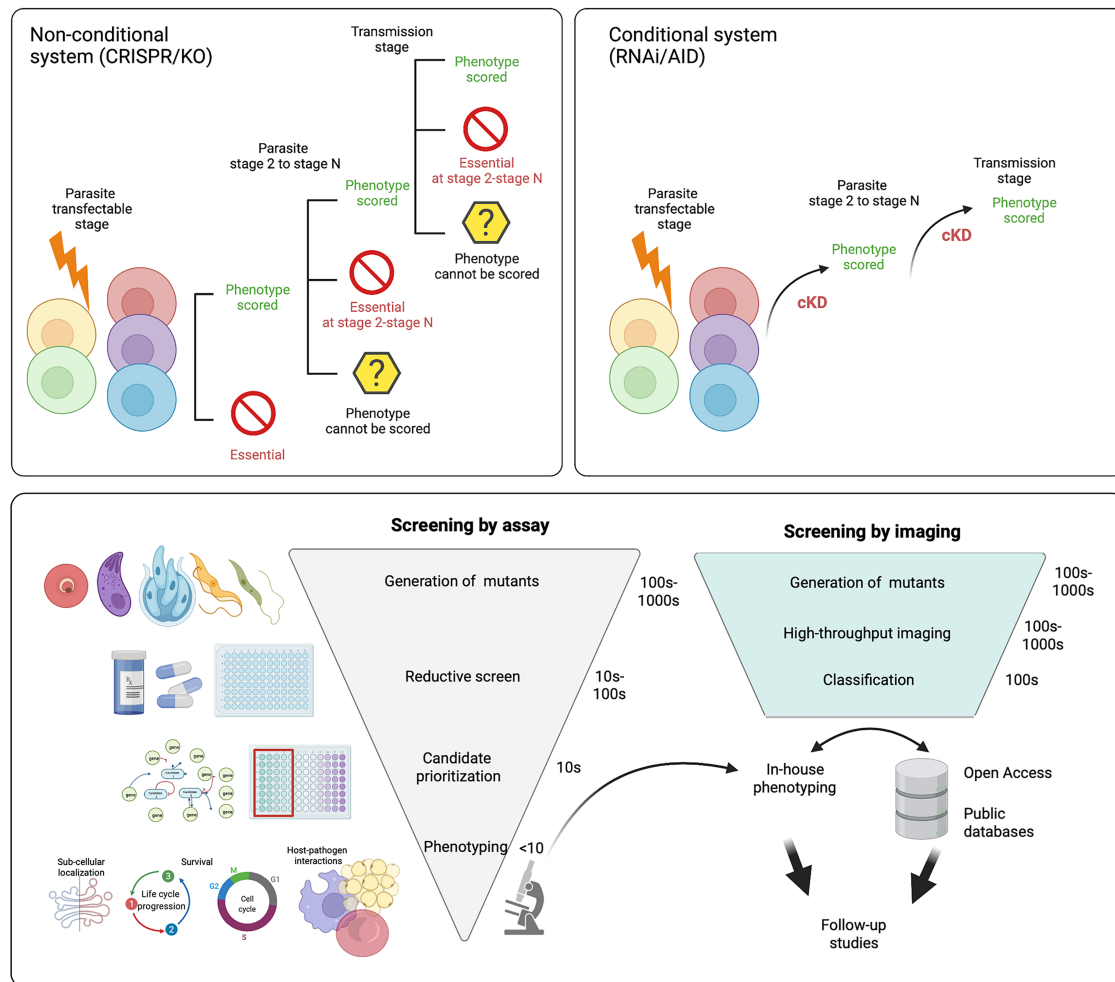


FIGURE 8 | Future directions for functional screens. Most functional screens in Apicomplexa rely on non-conditional gene depletion methods to phenotype mutants. **Top left panel** After the gene(s) of interest has been disrupted only those that are dispensable for growth during the transfected stage can be phenotyped. With life cycle progression (through stages 2 - N) more mutants within the pool will be lost as they become critical for survival. This means even without reducing the population with selective pressure (eg. drug) the number of mutants within the pool that can be characterised is not complete across the life cycle. **Top right panel** In conditional regulation systems the means of downregulation are integrated (eg. the auxin tag for the AID system) following transfection. Of note it is likely a few candidates will not tolerate the tag and will be lost from the population. As downregulation can be induced across the life cycle, all mutants within the population can be characterised and none are lost due to prior stage essentiality. **Bottom panel** After generation of mutants, many functional screens rely on reductive assays to select mutants with a specific phenotype (eg. drug resistance). This is followed by further candidate prioritisation before in-house phenotyping of a small number of mutants, often re-derived as conditionally regulatable knockdowns to allow characterisation throughout the life cycle. If pools of mutants are instead characterised by high-throughput imaging, they can be classified based on tagged protein localisation or, mutant phenotype. Classification of mutants allows for in house phenotyping and open access data sharing distributes follow up studies throughout the field and improves equitability. Figure created with BioRender.com.

regardless of essentiality. The AID-system for protein degradation (Philip and Waters, 2015; Liu et al., 2021) could be integrated into the endogenous tagging pipeline of the recombineering platform (Pfander et al., 2011) to enable simultaneous localisation and control of protein levels by addition of IAA. While knockdown of AID tagged proteins has been achieved in the peritoneum of mice (Brown and Sibley, 2018), more biologically relevant knockdowns have yet to be demonstrated, possibly due to the high dose of IAA required to induce a knockdown and its toxicity for rodents in *in vivo* studies (Yesbolatova et al., 2020). The AID2 system uses ph-IAA to

induce the knockdown and has been shown to function in mice with little toxicity (Saito and Kanemaki, 2021).

Although it was shown that the canonical RNAi machinery is not functional in *Plasmodium* spp. (Baum et al., 2009), recent work has supplemented the *P. berghei* genome with minimal RNAi machinery to allow control of expression at the mRNA level both constitutively and by using a stage specific promoter for temporal control of RNAi (Hentzschel et al., 2020).

Large scale functional genomic screens in *P. falciparum* have been hampered by difficulties with parasite genetic manipulation. However, transposon-mediated screens determined 50% of the

genome is essential for *in vitro* growth of *P. falciparum* (Zhang et al., 2018), identified roles for post-translational modifications during blood stream growth (Balu et al., 2005; Balu et al., 2009; Balu et al., 2010), identified key responses to heat shock (Bronner et al., 2016), and uncovered novel insights into drug mechanisms of action (Pradhan et al., 2015). Although only tested in low throughput, CRISPR-Cas9 mediated genome editing has been adapted to *P. falciparum* and proof of integration has been successfully demonstrated for site-directed mutagenesis (Ghorbal et al., 2014; Nishi et al., 2021), epitope tagging (Kuang et al., 2017; Nishi et al., 2021), and gene replacements (Ghorbal et al., 2014). The major limitation for this as a high throughput technology comes from the length of homology arms required to ensure homologous repair (Aravind et al., 2003; Bryant et al., 2019).

As 50% of the *P. falciparum* genome has been identified as important for *in vitro* culture, conditional systems of regulation will be essential to elucidate the role of many genes during the blood stage and to uncover their roles at other life cycle stages. Several conditional technologies, including; DiCre, at the genome level; glmS and tetR, at the mRNA level; and DD-system, knocksideways (KS) (Birnbaum et al., 2017; Kudyba et al., 2021) and AID system (Kreidenweiss et al., 2013) at the protein level, have been shown to function in *P. falciparum* and may be able to expand the tools available for high-throughput functional analysis.

Toxoplasma gondii

Early genetic screens in *T. gondii* utilised chemical mutagenesis where pools of mutagenised parasites were cultured under different conditions to identify subpopulations that contained a specific phenotype, or the ability to survive in a set condition. While phenotype-specific screens have been informative, identifying protein mediators of egress (Black et al., 2000; Garrison et al., 2012; McCoy et al., 2017), signaling (Coleman and Gubbels, 2012), and structure (Morrisette et al., 2004), they are time-consuming requiring both sequencing and post-screen assays to identify the cause of the phenotype. Signature tagged mutagenesis (STM), which barcodes the population of mutants, has enabled more ready identification post phenotyping (Knoll et al., 2001; Mazurkiewicz et al., 2006).

The first CRISPR screen carried out in *T. gondii* targeted all predicted genes and quantified the *in vitro* fitness score for tachyzoites (Sidik et al., 2016). Since this primary genome-wide screen, subsequent screens have used the same library to identify genes important for other biological functions including growth in naive and interferon- γ (IFN γ) stimulated murine bone-marrow-derived macrophages (BMDMs) (Wang et al., 2020); resistance to dihydroartemisinin (Harding et al., 2020); and tolerance of oxidative stress (Chen et al., 2021). The library has also been adapted to target genes in a type II strain, which efficiently forms bradyzoites *in vitro* and *in vivo*. In this strain, fitness scores were calculated for *in vitro* growth and this was compared to the mutant's ability to survive for 5 days *in vivo* (Young et al., 2019).

To enable the discovery of the role of genes that show a fitness deficiency or essentiality (at the tachyzoite stage) conditional

systems have begun to be employed in functional screens, thereby allowing assays that probe function at other stages to be employed. A split Cas9 (sCas9) genome editing method, combined with a high-content imaging approach, was recently used to functionally group mutants based on actin dynamics and apicoplast segregation (Li et al., 2022). Another conditionally-regulated imaging-based screen used CRISPR-Cas9-mediated genome editing to introduce mNeonGreen and a minimal auxin-inducible degron (mAID) to an array of proteins (Smith et al., 2022). In these studies, using imaging to classify mutants led to the identification of several interesting phenotypes and genes of interest rather than continually reducing the mutants of interest to a suitable set of candidates as reductive assays have previously done.

***Cryptosporidium* spp.**

Due to the lack of a robust *in vitro* model system, dependency on murine models for parasite passage, and lack of multiple selectable markers, *Cryptosporidium* is lagging behind the other apicomplexans and kinetoplastids in terms of high-throughput functional screens. However, there have been recent advancements such as the development of an accessible rodent model (Griffiths et al., 1998), air-liquid interface organoid culture system (Wilke et al., 2019), genetic tools (Vinayak et al., 2015) and validation of conditional gene regulation (Tandel et al., 2019) and protein degradation systems (Choudhary et al., 2020) that can advance the field. These could be used in conjunction with chemically mutagenised host cell lines to show different susceptibility to *Cryptosporidium* infection (Yu et al., 2017).

Kinetoplastids

***Trypanosoma* spp.**

The seminal RNAi screen in *T. brucei* procyclic stages was carried out in 2002 (Morris et al., 2002) to identify clones that were unable to bind the lectin concanavalin A (conA) including hexokinase 1. This study targeted the tsetse fly midgut stage, which was screened for *in vitro* fitness (Alsford et al., 2011), altered mitochondrial membrane potential (Verner et al., 2010) and tubercidin resistance mechanisms (Drew et al., 2003). This method paved the way for future screens improving on the laborious method for identification of mutants with the desired phenotype. To overcome slow mutant identification, RNA interference targeting sequencing (RITseq) is now used to quantify mutants within the population allowing fitness scoring (Alsford et al., 2011).

Improvements to the transfection protocols used on the cultured bloodstage form of *T. brucei* (Burkard et al., 2007) and the introduction of double stranded breaks (Glover and Horn, 2009) to further enhance efficiency has also enabled screens to be performed on this, more disease relevant, stage. To date, more than 60 screens have been performed on trypanosomes [reviewed in (Horn, 2022)] ranging from looking broadly at fitness (Alsford et al., 2011), to identifying mechanisms of drug resistance (Baker et al., 2011; Schumann Burkard et al., 2011) and biological processes like DNA repair

(Burkard et al., 2007) and cell cycle progression (Schumann Burkard et al., 2013).

While high throughput screening for function using RNAi is established in multiple African *Trypanosoma* spp., *T. cruzi* lacks the machinery to use this system (DaRocha et al., 2004). Genetic tools for this organism are also lacking, with downregulation of genes being inefficient and plagued with issues of additional integrations due to gene amplifications (Burle-Caldas et al., 2015). While recent developments have generated *T. cruzi* reporter parasites that will enable imaging based screening (Costa et al., 2018) and have shown some success with CRISPR/Cas9 mediated gene editing targeting flagellar proteins (Lander et al., 2015), there have also been reports of Cas9 toxicity with continued expression (Peng et al., 2014). Although, transient Cas9 expression or targeting Cas9 itself alongside the gene(s) of interest could eliminate this issue (Peng et al., 2014; Lander et al., 2015). New techniques for the generation of repair constructs *en masse* (Xu et al., 2009) coupled with advances in axenic amastigote culture methods (Akutsu et al., 2019) could provide the opportunity to carry out high throughput screens in *T. cruzi*, an organism that has been so intractable to previous editing.

***Leishmania* spp.**

Until 2015, double homologous recombination of laboriously generated vectors was the only way to screen for function in *Leishmania* parasites. However, supplementation of the genome with endogenous (*L. major*, *L. mexicana* (Beneke et al., 2017) and *L. braziliensis* (Espada et al., 2021)) or episomal (*L. mexicana*, *L. major* (Beneke et al., 2017), *L. tarentolae* (Turra et al., 2021), *L. donovani* (Martel et al., 2017) and *L. braziliensis* (Adaui et al., 2020) polymerase expression enabled the use of Cas9 mediated genome editing. Targeting a library of kinases in *L. mexicana* promastigotes, and using BarSeq to track mutants, showed that 79% of the kinome is dispensable for promastigote growth in culture, while 21% were refractory to gene knockout (Baker et al., 2021). Additionally, the requirement of these kinases was also evaluated *in vivo* and in the sandfly vector and the kinases were fluorescently tagged though this data has yet to be made publicly available (Baker et al., 2021). Recent developments to generate guide RNAs and homologous repair constructs in high throughput (Beneke and Gluenz, 2019), adapt barSeq technology (Beneke and Gluenz, 2020), and target both copies of a gene in a single transfection will all enable future high throughput screens in *Leishmania* spp.

In *L. tarentolae*, attempts have also been made to combine high-efficiency CRISPR-Cas9 mediated genome editing with the glmS conditional mRNA depletion system. However, only episomally expressed genes have been successfully knocked down (Turra et al., 2021). While this combination was unsuccessful, a conditional regulation system would prove valuable for studying the entire *Leishmania* spp. life cycle.

What's Next for Functional Screening?

Due to the complexity of parasite life cycles and the multistage requirement for many proteins, the use of conditional

techniques to determine the function of genes and proteins seems imperative, and many conditional technologies are being developed for low- and high-throughput analysis (Figure 7). As some life stages cannot yet be cultured *in vitro*, characterisation of all life cycle stages requires screening systems to be functional *in vivo* (Figure 8). The development of AID2 makes this system an appropriate choice as previous work has shown efficient protein degradation *in vitro* and *in vivo* (Saito and Kanemaki, 2021). Until now, most functional screens have used reducing assays, characterised growth rate in specific conditions, or identified a few candidates involved in a specific process or that confer resistance to a drug. These methods take an enormous number of mutants and filter them until the number of candidates is manageable for subsequent phenotyping analysis. The latter often relies on conditional regulation strategies to characterise function (Figure 8). Less reducing screening methods, such as coupling tagging and conditional mutant generation with high-content fluorescent imaging Li et al., 2022; Smith et al., 2022, or ultrastructure expansion microscopy (U-ExM) (Dos Santos Pacheco and Soldati-Favre, 2021) would allow testing a greater number of candidates and increase the descriptive detail of each, thus making the best use of screening outputs (see *Imaging* and Figure 8). Using unrestricted screens to classify mutants based on observations from high-content imaging would reduce the waste and/or duplication associated with reducing screening methods. Publication of these initial screens would also enable the sharing of preliminary phenotypes and allow a broader cohort of scientists, with different expertise, to follow-up on phenotypes of interest increasing equitable resource sharing.

When considering the classification of mutants following a functional screen, it is also worth noting that all techniques have limitations and interpretation of the data generated must be done cautiously. Descriptions of genes as essential must be treated with an awareness that this is only true for the life cycle stage being assayed and the growth conditions used. Furthermore, when transfecting pools of mutants, the loss of a mutant from the population may be more indicative of a severe growth defect and overgrowth, rather than an inability of the parasites to survive without this gene which may be uncovered with future phenotyping. Besides being a method of judicious gene selection, functional screens provide a wealth of data that should be utilised to its fullest.

IMAGING

Microscopy has been pivotal for, and specifically for Apicomplexan and Kinetoplastid parasitology research (Figure 9A), including in the identification of most parasites. The microscopy toolkit in parasitology currently includes electron-microscopy, optical microscopy, force nanoscopy, and bioluminescence imaging among others (Figure 10). In this section, we will discuss i) the current role of imaging in the functional characterization of candidates arising from large screens using 'omics' technologies; ii) imaging methods

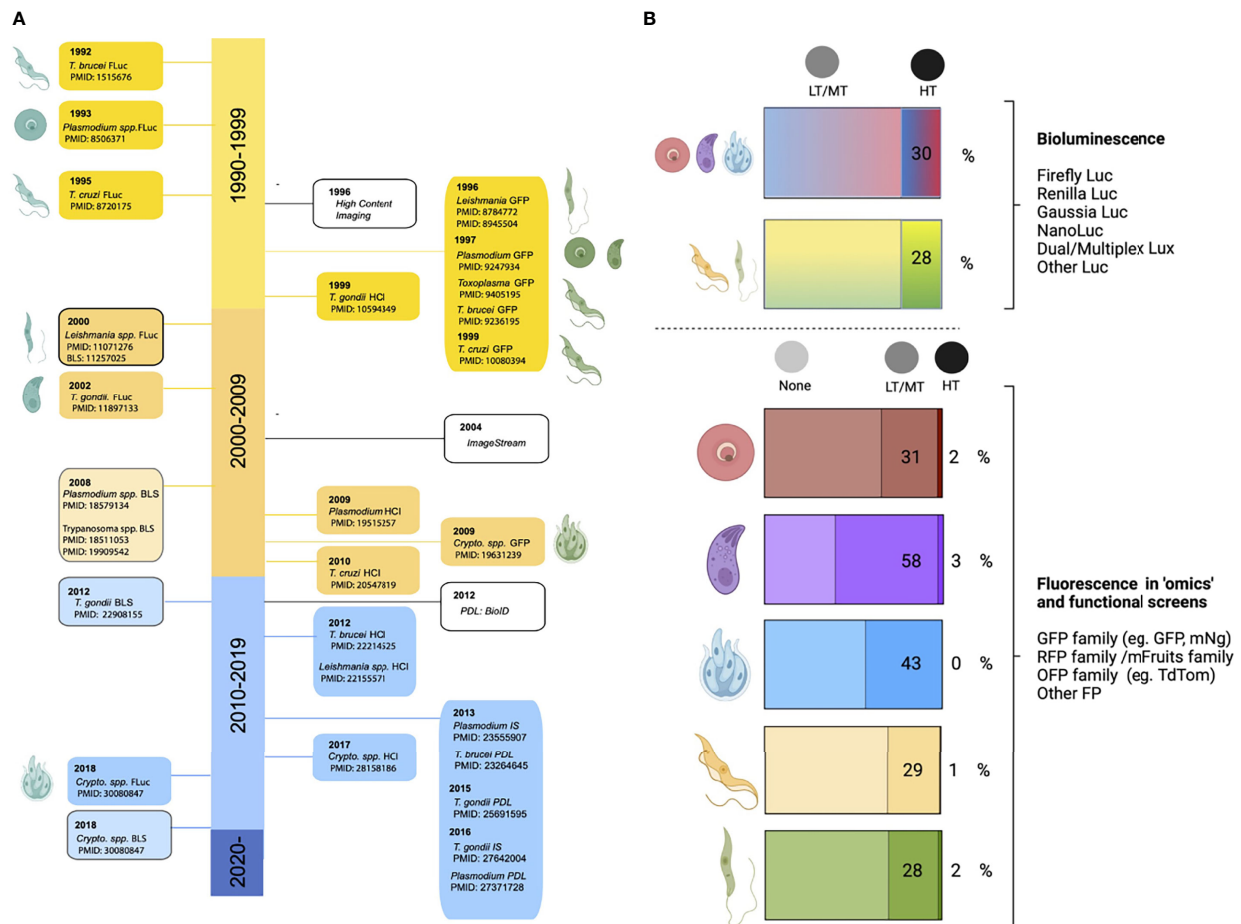


FIGURE 9 | Microscopy usage in parasitology. **(A)** Timeline of key developments allowing high-throughput bioluminescent and fluorescent studies. The left side of the timeline shows the first transgenic bioluminescent lines created for each parasite (*Plasmodium* spp., *Toxoplasma gondii*, *Cryptosporidium* spp., *Trypanosoma* spp., and *Leishmania* spp.), as well as the first luminescence-based high-throughput screen (BLS) performed for each parasite. The right side shows the first generation of fluorescent reporter lines for each parasite, and the first use of high-throughput fluorescence imaging, including the use of high content imaging (HCI), ImageStream, and proximity-dependent labelling (PDL). **(B)** Top section shows studies using bioluminescent reporter parasite lines, specifying the percentage used in high-throughput screens (HTS) for Apicomplexans (*Plasmodium* spp., *Toxoplasma gondii* and *Cryptosporidium* spp., Kinetoplastids (*Leishmania* spp., and *Trypanosoma* spp.). Bottom section shows the proportion of 'omics' and high-throughput screens using no imaging, low/medium throughput imaging (LT/MT), or high throughput imaging (HT). A PubMed search was performed for each genus, for all 'omics' methods, and each was explored to determine usage and throughput of microscopy. Figure created with BioRender.com.

currently used in parasitology as low-throughput and how they are being adapted to high-throughput; and iii) the advances in image analysis by the implementation of artificial intelligence.

The Current Role of Imaging as a High Throughput Technology in Parasitology

The two main platforms used for high-throughput analysis in parasitology are bioluminescence imaging and high-content fluorescence imaging (Figure 9). Genetic modification of *Plasmodium* spp., *Toxoplasma* spp., *Cryptosporidium* spp., *Leishmania* spp., *T. cruzi*, and *T. brucei* to generate fluorescent/bioluminescent reporter lines (Figure 9A) has been key for high-throughput screens, both in the context of 'omics' and drug discovery (Figure 9B). Reporter lines have been vital to gain insight into phenomena such as parasite invasion, development,

transmission, virulence and host-pathogen interactions, among others.

High Content Imaging

High content imaging maximizes data capture, and can be adapted to multiple imaging systems, samples, cameras, and fluorophores. When coupled with robotics, high-content imaging allows monitoring of specimens over extended amounts of time, as well as imaging of a large number of samples with relatively little need for user input (Adams and Sjaastad, 2009). Although high-content imaging began as a method best-applicable to microplates, two relatively recent technologies, Opera PhenixTM - a high content screening device compatible with spheroid visualization and 3D printing, and ImageStream (George et al., 2004) have expanded this important toolkit. ImageStream combines the strengths of standard

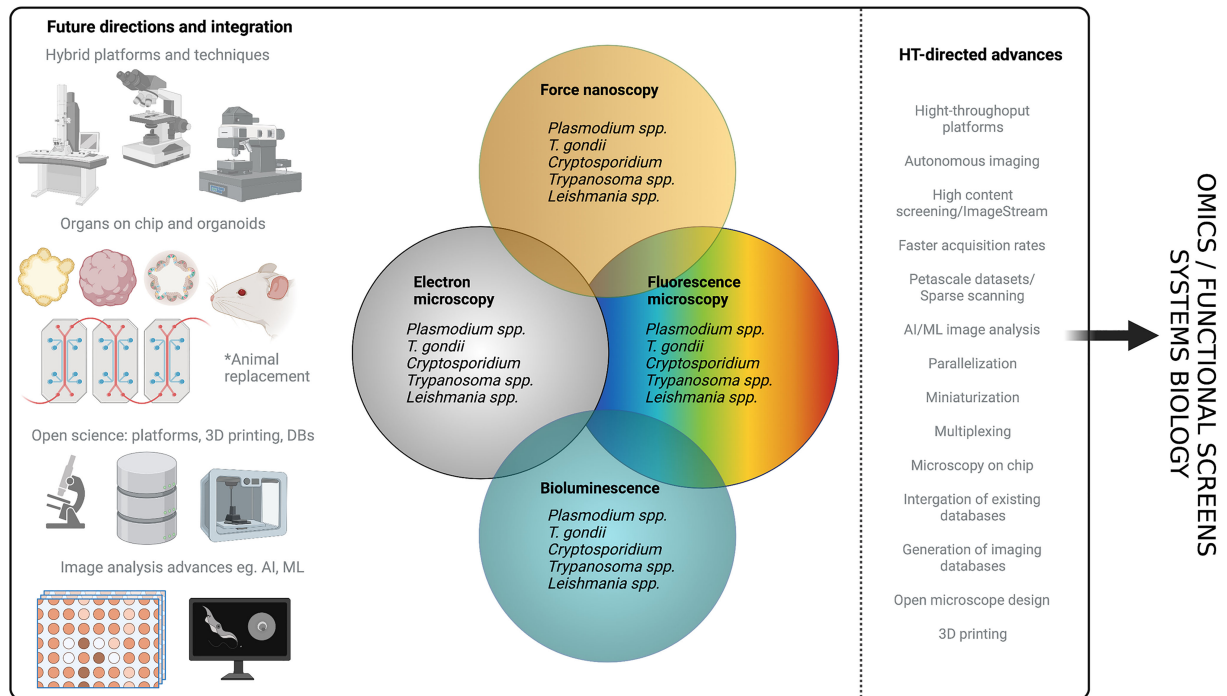


FIGURE 10 | Microscopy current contributions and future directions. Multiple imaging modalities, including electron microscopy, fluorescence microscopy, bioluminescence, and force nanoscopy, have been extensively used in Apicomplexan and Kinetoplastid research. Efforts on technology development have led to the generation of hybrid imaging platforms (eg. combining electron and fluorescence microscopy in CLEM); the integration of cell culture, microfluidics, and bioengineering advances (eg. organoids and organs-on-chip, consistent with animal replacement and reduction) with imaging methods; the integration of 3D printing and robotics for the generation of versatile imaging platforms, including high-content imaging; and the integration of artificial intelligence for image analysis. Many of these improvements are consistent with a philosophy of open science, and have facilitated data-sharing and the creation of low-cost complex imaging equipment. Most of these have already been incorporated into parasitology research, but not in high-throughput modalities. Efforts towards increasing the throughput of conventionally low-throughput techniques are shown on the left column, and include autonomous imaging (whereby user input is not required, reducing human resource demands), miniaturization and parallelization, multiplexing, and faster acquisition methods. Equally, a bottleneck for microscopy-based research is image analysis. Incorporation of artificial intelligence and machine learning, and integration with open databases and open code are promising fields for parasitology. Together, these various elements will likely play a major role on the integration of imaging into 'omics' studies to understand parasite biology. Figure created with BioRender.com.

optical microscopy (at single cell level), and the sample sizes/statistical significance afforded by standard flow cytometry. Notably, high-content imaging can be used in parallel with assays such as RNA fluorescence *in situ* hybridization (RNA-FISH), and proximity labeling techniques [reviewed in (Kimmel et al., 2021)] such as BioID (Roux et al., 2012; Kim et al., 2016), APEX (Rhee et al., 2013; Lam et al., 2015) and TurboID (Branon et al., 2018). Adaptations in this respect include proximity ligation imaging cytometry (PLIC) (Avin et al., 2017) and Flow-FISH (Luiza-Batista et al., 2021). Proximity labeling techniques have been particularly useful for the study of the interactome and network mapping (protein-centric, RNA-, and DNA-centric interactomes) (Roux et al., 2018; Trinkle-Mulcahy, 2019).

Bioluminescence Imaging

Bioluminescence imaging relies on the production of light by enzyme-catalysed reactions. In nature, bioluminescence is an evolutionary adaptation involving the natural production of light. Many bioluminescent substrates have been isolated, and the biochemical properties of their light defined (De Niz et al.,

2016; Syed and Anderson, 2021). Multiple luciferase-expressing parasites have been generated (Figure 9B). Upon exogenous addition of relevant substrates (eg. luciferin, coelenterazine, furimazine), luminescence occurs, thus being detectable and measurable by ultra-sensitive cameras. Altogether, bioluminescence is a high-throughput method that has a simple output, facilitating quantitative analysis. While bioluminescence has been a vital tool for parasitology (Siciliano and Alano, 2015; Avci et al., 2017; Novobilský and Höglund, 2020), especially in the context of drug screening, important limitations of this technique include a) that it lacks the resolution to give insight into sub-cellular phenomena, which is often a main interest for candidate validation in 'omics' studies, and b) that the half-life of some luciferases does not allow for specific event captures. Nevertheless, a major advantage of bioluminescence beyond the context of high-throughput screening, is its applicability to *in vivo* screening (eg. rodent models) in a non-invasive manner, allowing for longitudinal studies to be performed. This, however, is beyond the scope of this review.

Apicomplexans

Plasmodium spp.

Microscopy has allowed the investigation of *Plasmodium* invasion, development, deformability, pathogenesis, and genetic- and drug-screening (Gomes et al., 2015; Schwach et al., 2015; Brancucci et al., 2018; Duez et al., 2018; Kent et al., 2018; Tong et al., 2018; Stanway et al., 2019; Chia et al., 2021). A recent example of an ‘omics’ study directly incorporating high-throughput imaging to analyse *Plasmodium* liver stage development (Stanway et al., 2019) was based on a resource of individually barcoded gene knock out vectors (Pfander et al., 2011; Gomes et al., 2015; Bushell et al., 2017).

ImageStream has been used in high-throughput studies investigating anti-malarial drug effects against the *Plasmodium* digestive vacuole (Lee et al., 2014; Lee et al., 2016; Chia et al., 2017; Haridas et al., 2017), as well as to investigate the transcriptional signature and changes in parasite metabolism of *Plasmodium falciparum* sexually committed parasites (Brancucci et al., 2018). Furthermore, ImageStream and flow-FISH have been coupled to study gene expression in blood and liver stages of human malaria species (Luiza-Batista et al., 2021). Biotin-based proximity-labeling techniques have been successfully implemented to study various stages of *Plasmodium* (Kehrer et al., 2016; Khosh-Naucke et al., 2018; Schnider et al., 2018; Kimmel et al., 2021; Wichers et al., 2021) to investigate protein networks. The success of this implementation, and the potential for its coupling with large screen imaging methods (eg. ImageStream) holds great promise for the study of protein interactomes. Beyond fluorescence, several *Plasmodium* species have been engineered to express bioluminescent reporters across one or more of the parasite’s developmental life cycle stages. Main applications include the study of liver and blood stage development; *Plasmodium* strain-specific differences; stage-specificity of promoters and other regulatory elements; gametocyte development; functional studies of parasite proteins; parasite attenuation by genetic manipulation; anti-malarial activity of drugs (including extensive investigation of the Medicines for Malaria Venture (MMV) Malaria Box) (Khan et al., 2012; Cevenini et al., 2014; Vos et al., 2015; Ullah et al., 2017; Malebo et al., 2020); and investigating vaccine efficacy (Othman et al., 2017; Moita et al., 2021).

Toxoplasma gondii

Multiple *Toxoplasma gondii* fluorescent reporter lines have been invaluable for the phenotypic characterization of genetically modified parasites in terms of invasion capacity, growth, motility, survival/fitness, and host-parasite interactions (Bichet et al., 2016; Harding et al., 2016; Jacot et al., 2016; Sidik et al., 2016; Fréchal et al., 2017; Guérin et al., 2017; Periz et al., 2017; Brown et al., 2018; Lentini et al., 2021). Examples of studies that have incorporated high-content imaging include the development of CRISPR-mediated tagging to study the *T. gondii* kinome (Smith et al., 2022). Another genome-wide phenotypic screen using splitCas9 in combination with high-content imaging, used indicator parasites to visualize F-actin dynamics and apicoplast segregation, and identified two genes

critical for host cell egress (Li et al., 2022). Biotin-based proximity-labeling has also been extensively used in *T. gondii* research (Bradley et al., 2020; Kimmel et al., 2021). Examples include in investigation of components of the inner membrane complex (Chen et al., 2015a), calcium-dependent protein kinases and their function during parasite egress (Gaji et al., 2015), the apical annuli- a structure in the parasite cytoskeleton (Engelberg et al., 2020), and components of the tumour-suppressing Hippo pathway, mediating processes such as cytokinesis (Delgado et al., 2021). Bioluminescent *T. gondii* reporter strains have been equally useful for high-throughput drug screening (Key et al., 2020). To our knowledge, bioluminescent technology has not been widely integrated into ‘omics’ studies as a form of screening.

Cryptosporidium

Cryptosporidium research has incorporated high-content imaging into high-throughput phenotypic screens in the context of drug discovery (Sharling et al., 2010; Love and McNamara, 2020; Love and McNamara, 2021). Luciferase-expressing *Cryptosporidium* parasites (Vinayak et al., 2015; Hennessey et al., 2018) have been used in high throughput screens for parasite inhibitors; and for high-throughput developmental monitoring and genetic tractability (Wilke et al., 2019).

Kinetoplastids

Trypanosoma spp.

In the context of Chagas disease, high-content imaging has been used to study host-cell infection rates and drug screening (Alonso-Padilla and Rodríguez, 2014; Alonso-Padilla et al., 2015; Sykes and Avery, 2015; Franco et al., 2019; Fesser et al., 2020; Portella et al., 2021; Svensen et al., 2021). For *T. brucei*, high-content imaging has been used for the measurement of transcriptional activity (Hiraiwa et al., 2018). Proximity-dependent biotinylation approaches have been extremely useful for studying the protein interactome of *T. brucei* in various contexts. These include the identification of bilobe components (Morriswood et al., 2013); changes resulting from the ectopic expression of developmentally-regulated RNA-binding proteins (De Pablos et al., 2017); mapping the interactome of the *T. brucei* cytokinetic machinery (Hilton et al., 2018); identification of key proteins required for microtubule quartet anchorage to basal bodies (Dong et al., 2020); novel cytoskeleton-associated proteins essential for morphogenesis and cytokinesis (Schock et al., 2021); and flagellum tip-specific proteins (Vélez-Ramírez et al., 2021). Still within the umbrella of fluorescence, TrypTag has been an invaluable tool for the parasitology community. Large-scale endogenous tagging of *T. brucei* proteins was performed, and thousands of images generated and made publicly available (Dean et al., 2017). TrypTag aims to document the localization of every protein encoded in the *T. brucei* genome, generated with the aim of validating proteomics analyses, and is an example of the importance and potential of ‘imaging in systems biology’. Bioluminescence use in Kinetoplastid research has been extensive, both as an *in vivo* tool for studying parasite tropism and virulence, and as an *in vitro* high-throughput screening tool. Bioluminescent reporter lines of *T. cruzi* and multiple African

trypanosome species have been used to monitor parasite viability in the context of drug and vaccine screening (Hutchens and Luker, 2007; Lewis and Kelly, 2016; Ritchie et al., 2020), but to our knowledge, not within the context of ‘omics’ screens.

Leishmania spp.

For *Leishmania*, high-content imaging has been used to study anti-leishmanial compounds and their effects on parasites and hosts, comparative anti-parasitic activity against cutaneous and visceral leishmaniasis, or parasite development and infection capacity (Lakshmi et al., 2014; Dagley et al., 2015; Tegazzini et al., 2016; Lamotte et al., 2019; Alcántara et al., 2020; Rosazza et al., 2020; Tirado et al., 2020; Fehling et al., 2021). A recent example of successful integration of imaging in the context of systems biology, was the use of CRISPR-Cas9 genome editing to generate *Leishmania* mutants with altered flagellar function and motility. Dark field microscopy was used to track *Leishmania* swimming, and measure directionality and speed. Bar-seq technology was then used to test fitness mutants within the sandfly vector (Beneke et al., 2019). Another example is the integration of large-scale imaging to investigate morphometric parameters of *Leishmania* during its life cycle, or other cellular landmarks as a reference/basis for post-genomic analyses targeting the parasite’s cell biology (Wheeler et al., 2012; Halliday et al., 2019). These studies set precedence to the current value and future potential of the integration of imaging for high-throughput phenotypic screens. Bioluminescent reporter lines of *Leishmania* spp. have been used to monitor parasite viability in the context of drug and vaccine screening (Caridha et al., 2017; Álvarez-Velilla et al., 2019; Mendes Costa et al., 2019; Agostino et al., 2020; Cohen and Azas, 2021), but to our knowledge, not within the context of ‘omics’ screens.

Bottlenecks for High-Throughput in Optical and Electron Microscopy and Open Avenues for Future Implementations

The parasitology field has incorporated into its toolbox multiple ‘vanguard’ imaging technologies in optical, force, bioluminescence, and electron microscopy [reviewed in (De Niz et al., 2017)] (Figure 10). This includes improved resolution, imaging speed, and hybrid platforms that combine the strengths of more than one technology. So, why have many of these novel imaging methods not been used as high-throughput tools? Three main factors currently prevent several microscopy techniques from becoming high-throughput, and these factors are interrelated. High-throughput imaging relies on fast acquisition, relatively simple outputs, and/or high-throughput data processing. Fast acquisition comes at the expense of spatial and temporal resolution. Due to length restrictions, we focus the discussion below on optical and electron microscopy.

Fluorescence nanoscopy, or super-resolution microscopy, has been revolutionary for cell biology-related fields, including parasitology, and continues to extend its reach into structural biology (de Souza, 2018). Stimulated emission depletion (STED) (Willig et al., 2006), stochastic optical reconstruction microscopy (STORM) (Rust et al., 2006), and structured illumination

microscopy (SIM) (Vangindertael et al., 2018) have all been used in the context of Kinetoplastid and Apicomplexan research. Expansion microscopy (ExM) (Chen et al., 2015b) and ultrastructure expansion microscopy (U-ExM) (Gambaretto et al., 2021) have also been incorporated with great success (Amodeo et al., 2021; Bertiaux et al., 2021; Dos Santos Pacheco and Soldati-Favre, 2021; Gorlak et al., 2021; Kalichava and Ochsenreiter, 2021; Liffner and Absalon, 2021; Tomasina et al., 2021). Despite their value, important bottlenecks for using super-resolution in a high-throughput manner are the time required for image acquisition, and the volume of data produced for quantitation. Several adaptations have been designed to address these bottlenecks at the level of microscopy design and image acquisition and processing (Figure 10). The former include parallelized STED microscopy, (Bingen et al., 2011; Chmyrov et al., 2013); image scanning microscopy (Schulz et al., 2013); multifocal flat illumination for field-independent imaging (mfFIFI) (Mahecic et al., 2020); and analogue image processing, which increases data acquisition rates up to 100-fold over conventional SIM rates (York et al., 2013). Moreover, novel technologies also continue to advance in optics, imaging, and visualization, which hold important potential for parasitology, and can be incorporated into systems biology approaches at various scales. An example of this is vLUME, which uses virtual reality to enable visualization of single molecule localization (Spark et al., 2020). In addition to advances of the techniques themselves, tools from other fields such as cell biology and bioengineering, have successfully incorporated imaging to their workflow. Microfluidics, organs-on-chip, organoids, and/or tissue bioengineering combined with imaging (Figure 10), are important additions to the parasitology toolkit (Mellin and Boddey, 2020; Bernabeu et al., 2021; Sutrave and Richter, 2021). Coupled with advances in image analysis, organoids and spheroids could certainly become valuable tools for ‘omics’ high-throughput validation, and ‘systems biology’ in parasitology (Figure 10).

Electron microscopy has also been at the centre of parasitology for decades. Progress in electron microscopy methods over the last couple of decades has been invaluable for cell biology, introducing standalone and hybrid techniques such as focused ion beam scanning electron microscopy (FIB-SEM) (Heymann et al., 2006), scanning transmission electron microscopy (STEM) (von Ardenne, 1938; Kisielowski et al., 2008), cryogenic electron microscopy (cryo-TEM and cryo-EM) (Nakane et al., 2020; Yip et al., 2020), and correlative light and electron microscopy (CLEM) (de Boer et al., 2015). Electron microscopy is extremely labour intensive in terms of sample preparation, image acquisition, and image processing. While still unavailable in parasitology, several platforms have been generated to increase the throughput of electron microscopy (Eberle and Zeidler, 2018; Kornfeld and Denk, 2018; Bykov et al., 2019; Yin et al., 2020). Additional to high-throughput, some of these technologies are considered revolutionary for biology. Cryo-EM is an example, whereby several technical breakthroughs in both, software and hardware, have turned this tool into key for structural biology (Callaway, 2020). The value of this tool has been explored in the context of the *Plasmodium falciparum* proteome, already demonstrating its promising potential within the parasitology field (Beck and Ho, 2021; Chi-Min et al., 2021; Anton et al., 2022).

Bottleneck for High-Throughput: Progress and Development of Automated Image Analysis

It is important to consider the vast volume of data that the aforementioned methods generate and the importance of image analysis automation. Automated image analysis has been steadily incorporated into cell biology [reviewed in (von Chamier et al., 2019)] and clinical diagnosis in field settings. Beyond diagnosis, the field of parasitology has successfully generated multiple automated image analysis tools. This includes tools developed specifically for Apicomplexan (Kudella et al., 2016; Perez-Guaita et al., 2016; Touquet et al., 2018; Fisch et al., 2019; Bauman et al., 2020; Fisch et al., 2020; Hung et al., 2020; Dey et al., 2021; Shaw et al., 2021; Yoon et al., 2021) and Kinetoplastid research (Wheeler et al., 2012; Moon et al., 2014; Yazdanparast et al., 2014; Gomes-Alves et al., 2018; Moraes et al., 2019; Wheeler, 2020) and applied to a range of questions, from micrograph analysis, subcellular landmark investigation and parasite motility, to insect vector behavior. Many of these parameters are common outputs from ‘omics’ and large screen studies. HRMAN (Host Response to Microbe Analysis) is a high-throughput, high-content, single-cell image analysis platform which incorporates machine learning and deep convolutional neural networks (Fisch et al., 2019). Classification of features based on datasets has been used to distinguish phenotypic patterns of host-protein recruitment; detection and quantification of *T. gondii*-containing vacuoles; and analysis of host cell responses to *T. gondii* infection. More recent updates (HRMAN 2.0) offer the possibility to investigate 3D information, and applications to other pathogens beyond *T. gondii* (Fisch et al., 2021).

Despite the increased availability of image analysis tools, two ‘hurdles’ stand in the way of their widespread use among the parasitology community. The first is tool availability. Open source software has been pivotal for research, with ImageJ (Schneider et al., 2012), CellProfiler (Carpenter et al., 2006), Ilastik (Berg et al., 2019), OMERO (Allan et al., 2012; Li et al., 2016), ICY (Chaumont et al., 2011) being some examples of the most used tools for image analysis. A step, which remains to be more widely implemented in the parasitology imaging field is the existence of open repositories for code and image databases of both parasites and hosts, equivalent to VEuPathDB (Amos et al., 2022) resources, and under the lines of TrypTag (Dean et al., 2017). The second hurdle is tool accessibility: if the tools are available, can everyone in the parasitology community use them? We envisage that a step to achieve this is the development of user-friendly environments that allow users with little or no coding experience to use these resources. Recent successful examples include LOBSTER (Tosi et al., 2020), BIAFLOWS (Rubens et al., 2020), OpSeF (Rasse et al., 2020), and ZeroCostDL4Mic (von Chamier et al., 2021). Moreover, specialists are needed to bridge the two disciplines (artificial intelligence in imaging, and biology). A successful example in biology of such a training initiative is NEUBIAS (Martins et al., 2021).

Altogether, we envisage that advances in microscopy will allow its extensive integration into ‘omics’-based studies and functional screens, as a valuable tool to further our knowledge on parasite biology.

FURTHER INSIGHTS

Big Data in Context: How Big Is ‘Big Data’ in Parasitology, and What Can We Learn From Other Fields?

While we have addressed ‘big data’ in parasitology, it is worth asking how does such data compare to other research fields; what can we learn from other fields; and how will the growing scale of the data in parasitology be stored and handled computationally. Amongst the most striking example of big data generation is the European Council for Nuclear Research (CERN), with one of the most highly demanding computing environments in research, handling over 330 petabytes – and envisaging over the next decade, to require data storage capacities in the order of exabytes (10^{18} bytes). Its computing demands fostered the creation of vital resources such as the world wide web, which was initially conceived to facilitate data sharing amongst scientists worldwide. At the heart of CERN’s infrastructure are now the worldwide large hadron collider (LHC) computing grid, which gives physicists worldwide near-real-time access to LHC data (Geddes, 2012; Britton and Lloyd, 2014); the CERN Openlab, a public-private partnership through which CERN collaborates with information and communication technology (ICT) leading companies (such as Oracle, Micron, Intel, Siemens, Google, and IBM, among others); the data preservation in high energy physics (DPHEP) collaboration; and the CERN Internet eXchange Point (CIXP) among others. Other examples of large-scale research-focused collaborations include the 1,000 and 100,000 genomes projects. The 1000 genomes project aims at cataloguing common human genetic variation (Abecasis et al., 2010). For this project, several tools were developed and deployed to allow for widespread data access. This included the creation of a Data Coordination Centre (DCC), set up by the European Bioinformatics Institute (EBI) and the National Centre for Biotechnology (NCBI) to manage the data, and facilitate community access (Clarke et al., 2012). The 100,000 genomes project is an initiative to sequence genomes from thousands of patients affected by rare diseases, or cancer, and provide insights into the role of genomics in health/disease, and pave the way toward personalized medicine (Turnbull et al., 2018). What these major projects with ‘big’ data have in common is that they catalysed the generation of extraordinary tools at the level of hardware and software to ensure real-time open access by the scientific community as well as relevant data storage, maintenance and preservation capacities. Equally, these projects are based on international private and public partnerships from various sectors (including healthcare, governmental organizations, and information technology/computing developers). While generating such tools for parasitology alone might be a complex task, with these examples we aim to highlight the avenues that remain to be explored as well as the tools that already exist and could be capitalized on for our field and our understanding of both parasite and host.

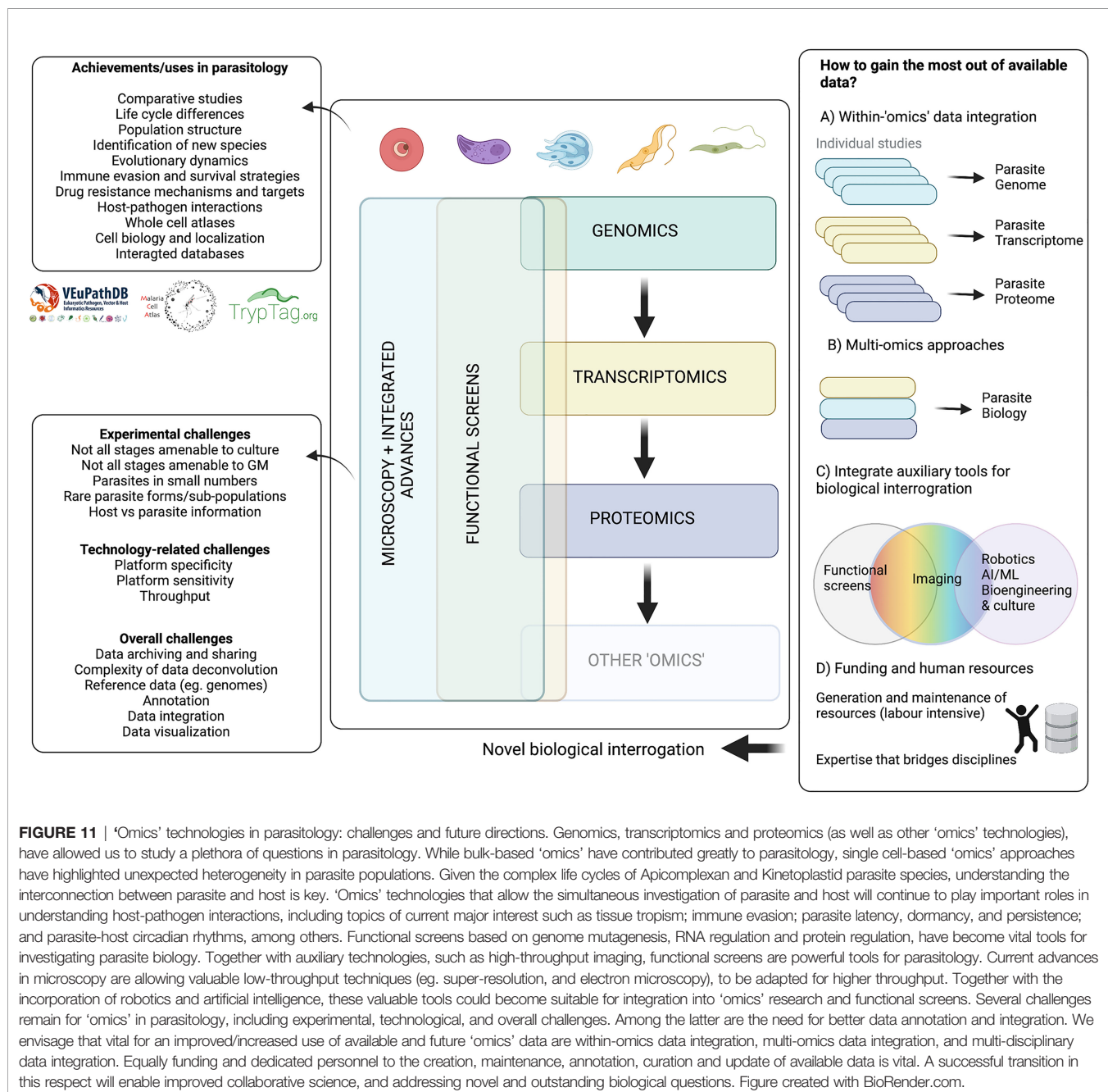
VEuPathDB and Its Role in Parasitology

A revolutionary resource in the parasitology field is VEuPathDB. This integrated database provides a repository of datasets across all “-omics” disciplines that can be accessed for free

(Warrenfeltz et al., 2018), ensuring equitable access to these resources. VEuPathDB is, however, not only a database, as the web-based service includes tools available for data searching, visualisation and comparisons. Moreover, the founding team is committed to democratizing science and frequently offer training world-wide to allowed hundreds of researchers across the global North and South, to access the full capacity of this tool. The online tutorials available through the resource also ensure that users with limited bioinformatics experience are able to mine the data deposited. Altogether, VEuPathDB has been committed to promoting equitable access to data generated across our field.

CONCLUDING REMARKS

In this review, we have explored 'omics'-based technologies and their major contributions to parasite biology (summarized in **Figure 11**). Addressing the fundamental question: how can we gain the most from the abundance of currently existing and future 'big data'? As 'omics' technologies progress and more studies incorporate them in their research questions, a risk that exists is the accumulation of data whose biological wealth is not fully explored or exploited. To avoid this, we require an advancement in data management/integration, and



potentially, a change in research practices towards ‘big data’. Improved annotation of reference genomes is key for ‘omics’ technologies, as is the need for constantly updated reference resources. This is a human resource-intensive task that should not be underestimated in its requirements for dedicated personnel and funding. Moreover, a research philosophy that envisages better data integration practices, at single ‘omics’ and ‘multi-omics’ levels, is vital. Improved accessibility is key for such integration. This comes in the form of improved data availability, improved data visualization tools, and a focus on training next generations of scientists to include expertise that bridges disciplines (eg. bioinformatics, artificial intelligence and biology). Together, ‘omics’ approaches and functional screens have pushed the boundaries of our knowledge on parasite biology, and we envisage that the aforementioned investments are some of many that will allow us to take the most advantage of current and future ‘big data’.

REFERENCES

- Abecasis, G. R., Altshuler, D., Auton, A., Brooks, L. D., Durbin, R. M., Gibbs, R. A., et al. (2010). A Map of Human Genome Variation From Population-Scale Sequencing. *Nature* 467, 1061–1073. doi: 10.1038/nature09534
- Abrahamsen, M. S., Templeton, T. J., Enomoto, S., Abrahante, J. E., Zhu, G., Lancto, C. A., et al. (2004). Complete Genome Sequence of the Apicomplexan, *Cryptosporidium Parvum*. *Science* 304, 441–445. doi: 10.1126/science.1094786
- Adams, C. L., and Sjaastad, M. D. (2009). Design and Implementation of High-Content Imaging Platforms: Lessons Learned From End User-Developer Collaboration. *Comb. Chem. High Throughput Screen.* 12, 877–887. doi: 10.2174/138620709789383240
- Adaui, V., Kröber-Boncardo, C., Brinker, C., Zirpel, H., Sellau, J., Arévalo, J., et al. (2020). Application of CRISPR/Cas9-Based Reverse Genetics in Leishmania (Brazilensis): Conserved Roles for HSP100 and HSP23. *Genes (Basel)* 11 (10), 1159. doi: 10.3390/genes11101159
- Adil, A., Kumar, V., Jan, A. T., and Asger, M. (2021). Single-Cell Transcriptomics: Current Methods and Challenges in Data Acquisition and Analysis. *Front. Neurosci.* 15. doi: 10.3389/fnins.2021.591122
- Aebischer, T. (2014). Leishmania Spp. Proteome Data Sets: A Comprehensive Resource for Vaccine Development to Target Visceral Leishmaniasis. *Front. Immunol.* 5. doi: 10.3389/fimmu.2014.00260
- Agostino, V. S., Trinconi, C. M., Galuppo, M. K., Price, H., and Uliana, S. R. B. (2020). Evaluation of NanoLuc, RedLuc and Luc2 as Bioluminescent Reporters in a Cutaneous Leishmaniasis Model. *Acta Trop.* 206, 105444. doi: 10.1016/j.actatropica.2020.105444
- Ahouldi, A., Ali, M., Almagro-Garcia, J., Amambua-Ngwa, A., Amaratunga, C., Amato, R., et al. (2021). An Open Dataset of Plasmodium Falciparum Genome Variation in 7,000 Worldwide Samples. *Wellcome Open Res.* 6, 42. doi: 10.12688/wellcomeopenres.16168.2
- Ahsan, M. I., Chowdhury, M. S. R., Das, M., Akter, S., Roy, S., Sharma, B., et al. (2021). In Silico Identification and Functional Characterization of Conserved miRNAs in the Genome of *Cryptosporidium Parvum*. *Bioinform. Biol. Insights* 15, 11779322211027664. doi: 10.1177/11779322211027665
- Akutsu, Y., Doi, M., Furukawa, K., and Takagi, Y. (2019). Introducing a Gene Knockout Directly Into the Amastigote Stage of *Trypanosoma Cruzi* Using the CRISPR/Cas9 System. *J. Vis. Exp.* 149. doi: 10.3791/59962
- Alcántara, L. M., Ferreira, T. C. S., Fontana, V., Chatelain, E., Moraes, C. B., and Freitas-Junior, L. H. (2020). A Multi-Species Phenotypic Screening Assay for Leishmaniasis Drug Discovery Shows That Active Compounds Display a High Degree of Species-Specificity. *Molecules* 25 (11), 2551. doi: 10.3390/molecules25112551
- Aldridge, S., and Teichmann, S. A. (2020). Single Cell Transcriptomics Comes of Age. *Nat. Commun.* 11(1), 4307. doi: 10.1038/s41467-020-18158-5

AUTHOR CONTRIBUTIONS

All authors listed have made a substantial, direct, and intellectual contribution to the work, and approved it for publication.

ACKNOWLEDGMENTS

We thank both reviewers whose comments improved our work. We thank also our various funders: RSK is funded by the American Heart Association Postdoctoral Fellowship (grant no. 20POST35220017) and U.S. Public Health Service (grant no. AI 139201). EMB is funded by the Wellcome Trust (grant no. 218648/Z/19/Z). SSP is funded by Marie Skłodowska-Curie Individual Standard European Fellowship (grant no. 839960) and Fundação Bial (Project 7/2021). MDN is funded by Human Frontier Science Individual Fellowship (grant LT000047/2019-L).

- Allan, C., Burel, J.-M., Moore, J., Blackburn, C., Linkert, M., Loynton, S., et al. (2012). OMERO: Flexible, Model-Driven Data Management for Experimental Biology. *Nat. Methods* 9, 245–253. doi: 10.1038/nmeth.1896
- Alonso-Padilla, J., Cutillo, I., Presa, J. L., Cantizani, J., Peña, I., Bardera, A. I., et al. (2015). Automated High-Content Assay for Compounds Selectively Toxic to *Trypanosoma Cruzi* in A Myoblastic Cell Line. *PLoS Negl. Trop. Dis.* 9, e0003493. doi: 10.1371/journal.pntd.0003493
- Alonso-Padilla, J., and Rodríguez, A. (2014). High Throughput Screening for Anti-*Trypanosoma Cruzi* Drug Discovery. *PLoS Negl. Trop. Dis.* 8, e3259. doi: 10.1371/journal.pntd.0003259
- Alsford, S., Turner, D. J., Obado, S. O., Sanchez-Flores, A., Glover, L., Berriman, M., et al. (2011). High-Throughput Phenotyping Using Parallel Sequencing of RNA Interference Targets in The African Trypanosome. *Genome Res.* 21, 915–924. doi: 10.1101/gr.115089.110
- Álvarez-Velilla, R., Gutiérrez-Corbo, M. D. C., Punzón, C., Pérez-Pertejo, M. Y., Balaña-Fouce, R., Fresno, M., et al. (2019). A Chronic Bioluminescent Model of Experimental Visceral Leishmaniasis for Accelerating Drug Discovery. *PLoS Negl. Trop. Dis.* 13, e0007133. doi: 10.1371/journal.pntd.0007133
- Amodeo, S., Kalichava, A., Fradera-Sola, A., Bertiaux-Lequoy, E., Guichard, P., Butter, F., et al. (2021). Characterization of the Novel Mitochondrial Genome Segregation Factor TAP110 in *Trypanosoma Brucei*. *J. Cell Sci.* 134 (5), jcs254300. doi: 10.1242/jcs.254300
- Amos, B., Aurrecoechea, C., Barba, M., Barreto, A., Basenko, E. Y., Bažant, W., et al. (2022). VEUPathDB: The Eukaryotic Pathogen, Vector and Host Bioinformatics Resource Center. *Nucleic Acids Res.* 50, D898–D911. doi: 10.1093/nar/gkab929
- Andenmatten, N., Egarter, S., Jackson, A. J., Jullien, N., Herman, J.-P., and Meissner, M. (2013). Conditional Genome Engineering in *Toxoplasma Gondii* Uncovers Alternative Invasion Mechanisms. *Nat. Methods* 10, 125–127. doi: 10.1038/nmeth.2301
- Ansari, H. R., Templeton, T. J., Subudhi, A. K., Ramaprasad, A., Tang, J., Lu, F., et al. (2016). Genome-Scale Comparison of Expanded Gene Families in *Plasmodium Ovale* Wallikeri and *Plasmodium Ovale* Curtisi With *Plasmodium Malariae* and With Other *Plasmodium* Species. *Int. J. Parasitol.* 46, 685–696. doi: 10.1016/j.ijpara.2016.05.009
- Anton, L., Cobb, D. W., and Ho, C.-M. (2022). Structural Parasitology of the Malaria Parasite *Plasmodium Falciparum*. *Trends Biochem. Sci.* 47, 149–159. doi: 10.1016/j.tibs.2021.10.006
- Araujo, R. B. D., Silva, T. M., Kaiser, C. S., Leite, G. F., Alonso, D., Ribolla, P. E. M., et al. (2018). Independent Regulation of *Plasmodium Falciparum* Rif Gene Promoters. *Sci. Rep.* 8, 9332. doi: 10.1038/s41598-018-27646-0
- Aravind, L., Iyer, L. M., Wellems, T. E., and Miller, L. H. (2003). *Plasmodium* Biology: Genomic Gleanings. *Cell* 115, 771–785. doi: 10.1016/s0092-8674(03)01023-7

- Archer, S. K., Inchaustegui, D., Queiroz, R., and Clayton, C. (2011). The Cell Cycle Regulated Transcriptome of *Trypanosoma Brucei*. *PLoS One* 6, e18425. doi: 10.1371/journal.pone.0018425
- Argelaguet, R., Cuomo, A. S. E., Stegle, O., and Marioni, J. C. (2021). Computational Principles and Challenges in Single-Cell Data Integration. *Nat. Biotechnol.* 39, 1202–1215. doi: 10.1038/s41587-021-00895-7
- Aslett, M., Aurrecochea, C., Berriman, M., Brestelli, J., Brunk, B. P., Carrington, M., et al. (2010). TriTrypDB: A Functional Genomic Resource for the Trypanosomatidae. *Nucleic Acids Res.* 38, D457–D462. doi: 10.1093/nar/gkp851
- Atwood, J. A. 3rd, Weatherly, D. B., Minning, T. A., Bundy, B., Cavola, C., Oppenheides, F. R., et al. (2005). The *Trypanosoma Cruzi* Proteome. *Science* 309, 473–476. doi: 10.1126/science.1110289
- Auburn, S., Böhme, U., Steinbiss, S., Trimarsanto, H., Hostetler, J., Sanders, M., et al. (2016). A New *Plasmodium Vivax* Reference Sequence With Improved Assembly of the Subtelomeres Reveals an Abundance of Pir Genes. *Wellcome Open Res.* 1, 4. doi: 10.12688/wellcomeopenres.9876.1
- Aurrecochea, C., Brestelli, J., Brunk, B. P., Dommer, J., Fischer, S., Gajria, B., et al. (2009). PlasmoDB: A Functional Genomic Database for Malaria Parasites. *Nucleic Acids Res.* 37, D539–D543. doi: 10.1093/nar/gkn814
- Aurrecochea, C., Brestelli, J., Brunk, B. P., Fischer, S., Gajria, B., Gao, X., et al. (2010). EuPathDB: A Portal to Eukaryotic Pathogen Databases. *Nucleic Acids Res.* 38, D415–D419. doi: 10.1093/nar/gkp941
- Avci, P., Karimi, M., Sadasivam, M., Antunes-Melo, W. C., Carrasco, E., and Hamblin, M. R. (2017). *In-Vivo* Monitoring of Infectious Diseases in Living Animals Using Bioluminescence Imaging. *Virulence* 9, 28–63. doi: 10.1080/21505594.2017.1371897
- Avila, C. C., Mule, S. N., Rosa-Fernandes, L., Viner, R., Barisón, M. J., Costa-Martins, A. G., et al. (2018). Proteome-Wide Analysis of *Trypanosoma Cruzi* Exponential and Stationary Growth Phases Reveals a Subcellular Compartment-Specific Regulation. *Genes (Basel)* 9 (8), 413. doi: 10.3390/genes9080413
- Avin, A., Levy, M., Porat, Z., and Abramson, J. (2017). Quantitative Analysis of Protein-Protein Interactions and Post-Translational Modifications in Rare Immune Populations. *Nat. Commun.* 8, 1524. doi: 10.1038/s41467-017-01808-6
- Baker, N., Alsford, S., and Horn, D. (2011). Genome-Wide RNAi Screens in African Trypanosomes Identify the Nifurtimox Activator NTR and the Eflornithine Transporter AAT6. *Mol. Biochem. Parasitol.* 176, 55–57. doi: 10.1016/j.molbiopara.2010.11.010
- Baker, N., Catta-Preta, C. M. C., Neish, R., Sadlova, J., Powell, B., Alves-Ferreira, E. V. C., et al. (2021). Systematic Functional Analysis of *Leishmania* Protein Kinases Identifies Regulators Of Differentiation or Survival. *Nat. Commun.* 12, 1244. doi: 10.1038/s41467-021-21360-8
- Balu, B., Chauhan, C., Maher, S. P., Shoue, D. A., Kissinger, J. C., Fraser, M. J. J., et al. (2009). Piggybac Is an Effective Tool for Functional Analysis of the *Plasmodium Falciparum* Genome. *BMC Microbiol.* 9, 83. doi: 10.1186/1471-2180-9-83
- Balu, B., Shoue, D. A., Fraser, M. J. J., and Adams, J. H. (2005). High-Efficiency Transformation of *Plasmodium Falciparum* by the Lepidopteran Transposable Element Piggybac. *Proc. Natl. Acad. Sci. U. S. A.* 102, 16391–16396. doi: 10.1073/pnas.0504679102
- Balu, B., Singh, N., Maher, S. P., and Adams, J. H. (2010). A Genetic Screen for Attenuated Growth Identifies Genes Crucial for Intraerythrocytic Development of *Plasmodium Falciparum*. *PLoS One* 5, e13282. doi: 10.1371/journal.pone.0013282
- Bancells, C., Llorà-Batlle, O., Poran, A., Nötzel, C., Rovira-Graells, N., Elemento, O., et al. (2019). Revisiting the Initial Steps of Sexual Development in the Malaria Parasite *Plasmodium Falciparum*. *Nat. Microbiol.* 4, 144–154. doi: 10.1038/s41564-018-0291-7
- Baniecki, M. L., Faust, A. L., Schaffner, S. F., Park, D. J., Galinsky, K., Daniels, R. F., et al. (2015). Development of a Single Nucleotide Polymorphism Barcode to Genotype *Plasmodium Vivax* Infections. *PLoS Negl. Trop. Dis.* 9, e0003539. doi: 10.1371/journal.pntd.0003539
- Bankier, A. T., Spriggs, H. F., Fartmann, B., Konfortov, B. A., Madera, M., Vogel, C., et al. (2003). Integrated Mapping, Chromosomal Sequencing and Sequence Analysis of *Cryptosporidium Parvum*. *Genome Res.* 13, 1787–1799. doi: 10.1101/gr.1555203
- Baptista, R. P., Li, Y., Sateriale, A., Sanders, M. J., Brooks, K. L., Tracey, A., et al. (2022). Long-Read Assembly and Comparative Evidence-Based Reanalysis of *Cryptosporidium* Genome Sequences Reveal Expanded Transporter Repertoire and Duplication of Entire Chromosome Ends Including Subtelomeric Regions. *Genome Res.* 32, 203–213. doi: 10.1101/gr.275325.121
- Barrett, M. P., Kyle, D. E., Sibley, L. D., Radke, J. B., and Tarleton, R. L. (2019). Protozoan Persister-Like Cells and Drug Treatment Failure. *Nat. Rev. Microbiol.* 17, 607–620. doi: 10.1038/s41579-019-0238-x
- Barry, J. D., Ginger, M. L., Burton, P., and McCulloch, R. (2003). Why are Parasite Contingency Genes Often Associated With Telomeres? *Int. J. Parasitol.* 33, 29–45. doi: 10.1016/s0020-7519(02)00247-3
- Barry, A. E., Leliwa-Sytek, A., Tavul, L., Imrie, H., Migot-Nabias, F., Brown, S. M., et al. (2007). Population Genomics of the Immune Evasion (Var) Genes of *Plasmodium Falciparum*. *PLoS Pathog.* 3, e34. doi: 10.1371/journal.ppat.0030034
- Barylyuk, K., Koreny, L., Ke, H., Butterworth, S., Crook, O. M., Lassadi, I., et al. (2020). A Comprehensive Subcellular Atlas of the *Toxoplasma* Proteome via hyperLOPIT Provides Spatial Context for Protein Functions. *Cell Host Microbe* 28, 752–766.e9. doi: 10.1016/j.chom.2020.09.011
- Bauman, N., Ilić, A., Lijeskić, O., Uzelac, A., Klun, I., Srbljanović, J., et al. (2020). Computational Image Analysis Reveals the Structural Complexity of *Toxoplasma Gondii* Tissue Cysts. *PLoS One* 15, e0234169. doi: 10.1371/journal.pone.0234169
- Baum, J., Papenfuss, A. T., Mair, G. R., Janse, C. J., Vlachou, D., Waters, A. P., et al. (2009). Molecular Genetics and Comparative Genomics Reveal RNAi is Not Functional in Malaria Parasites. *Nucleic Acids Res.* 37, 3788–3798. doi: 10.1093/nar/gkp239
- Beck, J. R., and Ho, C.-M. (2021). Transport Mechanisms at the Malaria Parasite-Host Cell Interface. *PLoS Pathog.* 17, e1009394. doi: 10.1371/journal.ppat.1009394
- Behnke, M. S., Wootton, J. C., Lehmann, M. M., Radke, J. B., Lucas, O., Nawas, J., et al. (2010). Coordinated Progression Through Two Subtranscriptomes Underlies the Tachyzoite Cycle of *Toxoplasma Gondii*. *PLoS One* 5, e12354. doi: 10.1371/journal.pone.0012354
- Beneke, T., Demay, F., Hookway, E., Ashman, N., Jeffery, H., Smith, J., et al. (2019). Genetic Dissection of a *Leishmania* Flagellar Proteome Demonstrates Requirement for Directional Motility in Sand Fly Infections. *PLoS Pathog.* 15, e1007828. doi: 10.1371/journal.ppat.1007828
- Beneke, T., and Gluenz, E. (2019). LeishGEdit: A Method for Rapid Gene Knockout and Tagging Using CRISPR-Cas9. *Methods Mol. Biol.* 1971, 189–210. doi: 10.1007/978-1-4939-9210-2_9
- Beneke, T., and Gluenz, E. (2020). Bar-Seq Strategies for the LeishGEdit Toolbox. *Mol. Biochem. Parasitol.* 239, 111295. doi: 10.1016/j.molbiopara.2020.111295
- Beneke, T., Madden, R., Makin, L., Valli, J., Sunter, J., and Gluenz, E. (2017). A CRISPR Cas9 High-Throughput Genome Editing Toolkit for Kinetoplastids. *R. Soc. Open Sci.* 4, 170095. doi: 10.1098/rsos.170095
- Beraki, T., Hu, X., Broncel, M., Young, J. C., O'Shaughnessy, W. J., Borek, D., et al. (2019). Divergent Kinase Regulates Membrane Ultrastructure of the *Toxoplasma Parasitophorous* Vacuole. *Proc. Natl. Acad. Sci. U. S. A.* 116, 6361–6370. doi: 10.1073/pnas.1816161116
- Berg, S., Kutra, D., Kroeger, T., Straehle, C. N., Kausler, B. X., Haubold, C., et al. (2019). Ilastik: Interactive Machine Learning for (Bio)Image Analysis. *Nat. Methods* 16, 1226–1232. doi: 10.1038/s41592-019-0582-9
- Bernabeu, M., Howard, C., Zheng, Y., and Smith, J. D. (2021). Bioengineered 3d Microvessels for Investigating *Plasmodium Falciparum* Pathogenesis. *Trends Parasitol.* 37, 401–413. doi: 10.1016/j.pt.2020.12.008
- Berná, L., Marquez, P., Cabrera, A., Greif, G., Francia, M. E., and Robello, C. (2021). Reevaluation of the *Toxoplasma Gondii* and *Neospora Caninum* Genomes Reveals Misassembly, Karyotype Differences, and Chromosomal Rearrangements. *Genome Res.* 31, 823–833. doi: 10.1101/gr.262832.120
- Berriman, M., Ghedin, E., Hertz-Fowler, C., Blandin, G., Renaud, H., Bartholomeu, D. C., et al. (2005). The Genome of the African Trypanosome *Trypanosoma Brucei*. *Science* 309, 416–422. doi: 10.1126/science.1112642
- Bertiaux, E., Balestra, A. C., Bournonville, L., Louvel, V., Maco, B., Soldati-Favre, D., et al. (2021). Expansion Microscopy Provides New Insights Into the Cytoskeleton of Malaria Parasites Including the Conservation of a Conoid. *PLoS Biol.* 19, e3001020. doi: 10.1371/journal.pbio.3001020

- Bichet, M., Touquet, B., Gonzalez, V., Florent, I., Meissner, M., and Tardieux, I. (2016). Genetic Impairment of Parasite Myosin Motors Uncovers the Contribution of Host Cell Membrane Dynamics to Toxoplasma Invasion Forces. *BMC Biol.* 14, 97. doi: 10.1186/s12915-016-0316-8
- Bingen, P., Reuss, M., Engelhardt, J., and Hell, S. W. (2011). Parallelized STED Fluorescence Nanoscopy. *Opt. Express* 19, 23716–23726. doi: 10.1364/OE.19.023716
- Birnbaum, J., Flemming, S., Reichard, N., Soares, A. B., Mesén-Ramírez, P., Jonscher, E., et al. (2017). A Genetic System to Study Plasmodium Falciparum Protein Function. *Nat. Methods* 14, 450–456. doi: 10.1038/nmeth.4223
- Black, M. W., Arrizabalaga, G., and Boothroyd, J. C. (2000). Ionophore-Resistant Mutants of Toxoplasma Gondii Reveal Host Cell Permeabilization as an Early Event in Egress. *Mol. Cell. Biol.* 20, 9399–9408. doi: 10.1128/MCB.20.24.9399-9408.2000
- Blazewski, T., Nursimulu, N., Pszeny, V., Dangoudoubiyam, S., Namasivayam, S., Chiasson, M. A., et al. (2015). Systems-Based Analysis of the Sarcocystis Neurona Genome Identifies Pathways That Contribute to a Heteroxenous Life Cycle. *MBio* 6 (1), e02445–14. doi: 10.1128/mBio.02445-14
- Böhme, U., Otto, T. D., Cotton, J. A., Steinbiss, S., Sanders, M., Oyola, S. O., et al. (2018). Complete Avian Malaria Parasite Genomes Reveal Features Associated With Lineage-Specific Evolution in Birds and Mammals. *Genome Res.* 28, 547–560. doi: 10.1101/gr.218123.116
- Bouzi, M., Hunter, P. R., McDonald, V., Elwin, K., Chalmers, R. M., and Tyler, K. M. (2013). A New Heterogeneous Family of Telomerically Encoded Cryptosporidium Proteins. *Evol. Appl.* 6, 207–217. doi: 10.1111/j.1752-4571.2012.00277.x
- Bouzi, M., Tyler, K. M., Christen, R., Chalmers, R. M., Elwin, K., and Hunter, P. R. (2010). Multi-Locus Analysis of Human Infective Cryptosporidium Species and Subtypes Using Ten Novel Genetic Loci. *BMC Microbiol.* 10, 213. doi: 10.1186/1471-2180-10-213
- Bradley, P. J., Rayatpisheh, S., Wohlschlegel, J. A., and Nadipuram, S. M. (2020). Using BioID for the Identification of Interacting and Proximal Proteins in Subcellular Compartments in Toxoplasma Gondii. *Methods Mol. Biol.* 2071, 323–346. doi: 10.1007/978-1-4939-9857-9_18
- Brancucci, N. M. B., De Niz, M., Straub, T. J., Ravel, D., Sollelis, L., Birren, B. W., et al. (2018). Probing Plasmodium Falciparum Sexual Commitment at the Single-Cell Level. *Wellcome Open Res.* 3, 70. doi: 10.12688/wellcomeopenres.14645.4
- Branon, T. C., Bosch, J. A., Sanchez, A. D., Udeshi, N. D., Svinkina, T., Carr, S. A., et al. (2018). Efficient Proximity Labeling in Living Cells and Organisms With TurboID. *Nat. Biotechnol.* 36, 880–887. doi: 10.1038/nbt.4201
- Briggs, E. M., Rojas, F., McCulloch, R., Matthews, K. R., and Otto, T. D. (2021). Single-Cell Transcriptomic Analysis of Bloodstream Trypanosoma Brucei Reconstructs Cell Cycle Progression and Developmental Quorum Sensing. *Nat. Commun.* 12, 5268. doi: 10.1038/s41467-021-25607-2
- Brinkerhoff, H., Kang, A. S. W., Liu, J., Aksimentiev, A., and Dekker, C. (2021). Multiple Rereads of Single Proteins at Single-Amino Acid Resolution Using Nanopores. *Science* 374, 1509–1513. doi: 10.1126/science.abl4381
- Briquet, S., Gissot, M., and Silvie, O. (2021). A Toolbox for Conditional Control of Gene Expression in Apicomplexan Parasites. *Mol. Microbiol.* 117 (3), 618–631. doi: 10.1111/mmi.14821
- Britton, D., and Lloyd, S. L. (2014). How to Deal With Petabytes of Data: The LHC Grid Project. *Rep. Prog. Phys.* 77, 65902. doi: 10.1088/0034-4885/77/6/065902
- Bronner, I. F., Otto, T. D., Zhang, M., Udenze, K., Wang, C., Quail, M. A., et al. (2016). Quantitative Insertion-Site Sequencing (QIsseq) for High Throughput Phenotyping of Transposon Mutants. *Genome Res.* 26, 980–989. doi: 10.1101/gr.200279.115
- Brotherton, M.-C., Racine, G., Foucher, A. L., Drummelsmith, J., Papadopolou, B., and Ouellette, M. (2010). Analysis of Stage-Specific Expression of Basic Proteins in Leishmania Infantum. *J. Proteome Res.* 9, 3842–3853. doi: 10.1021/pr100048m
- Brown, K. M., Long, S., and Sibley, L. D. (2018). Conditional Knockdown of Proteins Using Auxin-Inducible Degron (AID) Fusions in Toxoplasma Gondii. *Bio-protocol* 8 (4), e2728. doi: 10.21769/BioProtoc.2728
- Brown, K. M., and Sibley, L. D. (2018). Essential cGMP Signaling in Toxoplasma Is Initiated by a Hybrid P-Type ATPase-Guanylate Cyclase. *Cell Host Microbe* 24, 804–816.e6. doi: 10.1016/j.chom.2018.10.015
- Bryant, J. M., Baumgarten, S., Glover, L., Hutchinson, S., and Rachidi, N. (2019). CRISPR in Parasitology: Not Exactly Cut and Dried! *Trends Parasitol.* 35, 409–422. doi: 10.1016/j.pt.2019.03.004
- Burkard, G., Fragoso, C. M., and Roditi, I. (2007). Highly Efficient Stable Transformation of Bloodstream Forms of Trypanosoma Brucei. *Mol. Biochem. Parasitol.* 153, 220–223. doi: 10.1016/j.molbiopara.2007.02.008
- Burle-Caldas, G., de, A., Grazielle-Silva, V., Laibida, L. A., DaRocha, W. D., and Teixeira, S. M. R. (2015). Expanding the Tool Box for Genetic Manipulation of Trypanosoma Cruzi. *Mol. Biochem. Parasitol.* 203, 25–33. doi: 10.1016/j.molbiopara.2015.10.004
- Bushell, E., Gomes, A. R., Sanderson, T., Anar, B., Girling, G., Herd, C., et al. (2017). Functional Profiling of a Plasmodium Genome Reveals an Abundance of Essential Genes. *Cell* 170, 260–272.e8. doi: 10.1016/j.cell.2017.06.030
- Bykov, Y. S., Cohen, N., Gabrielli, N., Manenschi, H., Welsch, S., Chlanda, P., et al. (2019). High-Throughput Ultrastructure Screening Using Electron Microscopy and Fluorescent Barcoding. *J. Cell Biol.* 218, 2797–2811. doi: 10.1083/jcb.201812081
- Callaway, E. (2020). Revolutionary Cryo-EM is Taking Over Structural Biology. *Nature* 578, 201. doi: 10.1038/d41586-020-00341-9
- Callejas-Hernández, F., Rastrojo, A., Poveda, C., Gironès, N., and Fresno, M. (2018). Genomic Assemblies of Newly Sequenced Trypanosoma Cruzi Strains Reveal New Genomic Expansion and Greater Complexity. *Sci. Rep.* 8, 14631. doi: 10.1038/s41598-018-32877-2
- Campbell, D. A., Thomas, S., and Sturm, N. R. (2003). Transcription in Kinetoplastid Protozoa: Why be Normal? *Microbes Infect.* 5, 1231–1240. doi: 10.1016/j.micinf.2003.09.005
- Caridha, D., Parriot, S., Hudson, T. H., Lang, T., Ngundam, F., Leed, S., et al. (2017). Use of Optical Imaging Technology in the Validation of a New, Rapid, Cost-Effective Drug Screen as Part of a Tiered In Vivo Screening Paradigm for Development of Drugs To Treat Cutaneous Leishmaniasis. *Antimicrob. Agents Chemother.* 61 (4), e02048–16. doi: 10.1128/AAC.02048-16
- Carlton, J. M., Adams, J. H., Silva, J. C., Bidwell, S. L., Lorenzi, H., Caler, E., et al. (2008). Comparative Genomics of the Neglected Human Malaria Parasite Plasmodium Vivax. *Nature* 455, 757–763. doi: 10.1038/nature07327
- Carlton, J. M., Anguoli, S. V., Suh, B. B., Kooij, T. W., Perte, M., Silva, J. C., et al. (2002). Genome Sequence and Comparative Analysis of the Model Rodent Malaria Parasite Plasmodium Yoelii Yoelii. *Nature* 419, 512–519. doi: 10.1038/nature01099
- Carnes, J., Anupama, A., Balmer, O., Jackson, A., Lewis, M., Brown, R., et al. (2015). Genome and Phylogenetic Analyses of Trypanosoma Evansi Reveal Extensive Similarity To T. Brucei and Multiple Independent Origins for Dyskinetoplasty. *PLoS Negl. Trop. Dis.* 9, e3404. doi: 10.1371/journal.pntd.0003404
- Carpenter, A. E., Jones, T. R., Lamprecht, M. R., Clarke, C., Kang, I. H., Friman, O., et al. (2006). CellProfiler: Image Analysis Software for Identifying and Quantifying Cell Phenotypes. *Genome Biol.* 7, R100. doi: 10.1186/gb-2006-7-10-r100
- Cevenini, L., Camarda, G., Michelini, E., Siciliano, G., Calabretta, M. M., Bona, R., et al. (2014). Multicolor Bioluminescence Boosts Malaria Research: Quantitative Dual-Color Assay and Single-Cell Imaging in Plasmodium Falciparum Parasites. *Anal. Chem.* 86, 8814–8821. doi: 10.1021/ac502098w
- Chambers, D. C., Carew, A. M., Lukowski, S. W., and Powell, J. E. (2019). Transcriptomics and Single-Cell RNA-Sequencing. *Respirology* 24, 29–36. doi: 10.1111/resp.13412
- Chaumont, F., Dallongeville, S., and Olivo-Marin, J. (2011). “ICY: A New Open-Source Community Image Processing Software,” in *2011 IEEE International Symposium on Biomedical Imaging: From Nano to Macro*, Vol. 234–237. Chicago IL, USA: IEEE. doi: 10.1109/ISBI.2011.5872395
- Cheng, Q., Cloonan, N., Fischer, K., Thompson, J., Waine, G., Lanzer, M., et al. (1998). Stevor and Rif are Plasmodium Falciparum Multicopy Gene Families Which Potentially Encode Variant Antigens. *Mol. Biochem. Parasitol.* 97, 161–176. doi: 10.1016/s0166-6851(98)00144-3
- Chen, L.-F., Han, X.-L., Li, F.-X., Yao, Y.-Y., Fang, J.-P., Liu, X.-J., et al. (2018). Comparative Studies of Toxoplasma Gondii Transcriptomes: Insights Into Stage Conversion Based on Gene Expression Profiling and Alternative Splicing. *Parasitol. Vectors* 11, 402. doi: 10.1186/s13071-018-2983-5
- Chen, A. L., Kim, E. W., Toh, J. Y., Vashisht, A. A., Rashoff, A. Q., Van, C., et al. (2015a). Novel Components of the Toxoplasma Inner Membrane Complex Revealed by BioID. *MBio* 6, e02357–e02314. doi: 10.1128/mBio.02357-14

- Chen, Y., Liu, Q., Xue, J.-X., Zhang, M.-Y., Geng, X.-L., Wang, Q., et al. (2021). Genome-Wide CRISPR/Cas9 Screen Identifies New Genes Critical for Defense Against Oxidant Stress in *Toxoplasma Gondii*. *Front. Microbiol.* 12. doi: 10.3389/fmicb.2021.670705
- Chen, F., Tillberg, P. W., and Boyden, E. S. (2015b). Optical Imaging. Expansion Microscopy. *Science* 347, 543–548. doi: 10.1126/science.1260088
- Cheung, T. K., Lee, C.-Y., Bayer, F. P., McCoy, A., Kuster, B., and Rose, C. M. (2021). Defining the Carrier Proteome Limit for Single-Cell Proteomics. *Nat. Methods* 18, 76–83. doi: 10.1038/s41592-020-01002-5
- Chia, W., Gomez-Lorenzo, M. G., Castellote, I., Tong, J. X., Chandramohanadas, R., Thu Chu, T. T., et al. (2021). High-Content Phenotypic Screen of a Focused TCAMS Drug Library Identifies Novel Disruptors of the Malaria Parasite Calcium Dynamics. *ACS Chem. Biol.* 16, 2348–2372. doi: 10.1021/acscchembio.1c00512
- Chia, W. N., Lee, Y. Q., and Tan, K. S.-W. (2017). Imaging Flow Cytometry for the Screening of Compounds That Disrupt the *Plasmodium Falciparum* Digestive Vacuole. *Methods* 112, 211–220. doi: 10.1016/j.ymeth.2016.07.002
- Chi-Min, H., Jonathan, J., Mason, L., Xiaorun, L., E, G. D., R, B. J., et al. (2021). Native Structure of the RhoP Complex, a Key Determinant of Malaria Parasite Nutrient Acquisition. *Proc. Natl. Acad. Sci.* 118, e2100514118. doi: 10.1073/pnas.2100514118
- Chmyrov, A., Keller, J., Grotjohann, T., Ratz, M., d'Este, E., Jakobs, S., et al. (2013). Nanoscopy With More Than 100,000 'Doughnuts'. *Nat. Methods* 10, 737–740. doi: 10.1038/nmeth.2556
- Choi, Y. H., and Kim, J. K. (2019). Dissecting Cellular Heterogeneity Using Single-Cell RNA Sequencing. *Mol. Cells* 42, 189–199. doi: 10.14348/molcells.2019.2446
- Choudhary, H. H., Nava, M. G., Gartlan, B. E., Rose, S., and Vinayak, S. (2020). A Conditional Protein Degradation System To Study Essential Gene Function in *Cryptosporidium Parvum*. *MBio* 11 (4), e01231-20. doi: 10.1128/mBio.01231-20
- Clarke, J., Wu, H.-C., Jayasinghe, L., Patel, A., Reid, S., and Bayley, H. (2009). Continuous Base Identification for Single-Molecule Nanopore DNA Sequencing. *Nat. Nanotechnol.* 4, 265–270. doi: 10.1038/nano.2009.12
- Clarke, L., Zheng-Bradley, X., Smith, R., Kulesha, E., Xiao, C., Toneva, I., et al. (2012). The 1000 Genomes Project: Data Management and Community Access. *Nat. Methods* 9, 459–462. doi: 10.1038/nmeth.1974
- Cleary, M. D., Singh, U., Blader, I. J., Brewer, J. L., and Boothroyd, J. C. (2002). *Toxoplasma Gondii* Asexual Development: Identification of Developmentally Regulated Genes and Distinct Patterns of Gene Expression. *Eukaryot. Cell* 1, 329–340. doi: 10.1128/EC.1.3.329-340.2002
- Cohen, A., and Azas, N. (2021). Challenges and Tools for *In Vitro* Leishmania Exploratory Screening in the Drug Development Process: An Updated Review. *Pathog. (Basel Switzerland)* 10 (12), 1608. doi: 10.3390/pathogens10121608
- Coleman, B. I., and Gubbels, M.-J. (2012). A Genetic Screen to Isolate *Toxoplasma Gondii* Host-Cell Egress Mutants. *J. Vis. Exp.* 60, 3807. doi: 10.3791/3807
- Combe, A., Giovannini, D., Carvalho, T. G., Spath, S., Boisson, B., Loussert, C., et al. (2009). Clonal Conditional Mutagenesis in Malaria Parasites. *Cell Host Microbe* 5, 386–396. doi: 10.1016/j.chom.2009.03.008
- Corpas-Lopez, V., Moniz, S., Thomas, M., Wall, R. J., Torrie, L. S., Zander-Dinse, D., et al. (2019). Pharmacological Validation of N-Myristoyltransferase as a Drug Target in Leishmania Donovanii. *ACS Infect. Dis.* 5, 111–122. doi: 10.1021/acscinfecdis.8b00226
- Costa, F. C., Francisco, A. F., Jayawardhana, S., Calderano, S. G., Lewis, M. D., Olmo, F., et al. (2018). Expanding the Toolbox for *Trypanosoma Cruzi*: A Parasite Line Incorporating a Bioluminescence-Fluorescence Dual Reporter and Streamlined CRISPR/Cas9 Functionality for Rapid *In Vivo* Localisation and Phenotyping. *PLoS Negl. Trop. Dis.* 12, e0006388. doi: 10.1371/journal.pntd.0006388
- Coulson, R. M. R., Hall, N., and Ouzounis, C. A. (2004). Comparative Genomics of Transcriptional Control in the Human Malaria Parasite *Plasmodium Falciparum*. *Genome Res.* 14, 1548–1554. doi: 10.1101/gr.2218604
- Coutinho-Abreu, I. V., Serafim, T. D., Meneses, C., Kamhawi, S., Oliveira, F., and Valenzuela, J. G. (2020). Distinct Gene Expression Patterns in Vector-Residing Leishmania Infantum Identify Parasite Stage-Enriched Markers. *PLoS Negl. Trop. Dis.* 14, e0008014. doi: 10.1371/journal.pntd.0008014
- Cross, G. A. M., Kim, H.-S., and Wickstead, B. (2014). Capturing the Variant Surface Glycoprotein Repertoire (the VSGome) of *Trypanosoma Brucei* Lister 427. *Mol. Biochem. Parasitol.* 195, 59–73. doi: 10.1016/j.molbiopara.2014.06.004
- Crozier, T. W. M., Tinti, M., Wheeler, R. J., Ly, T., Ferguson, M. A. J., and Lamond, A. I. (2018). Proteomic Analysis of the Cell Cycle of Procyclic Form *Trypanosoma Brucei*. *Mol. Cell. Proteomics* 17, 1184–1195. doi: 10.1074/mcp.RA118.000650
- Cruz, A. K., and Freitas-Castro, F. (2019). Genome and Transcriptome Analyses of *Leishmania* Spp.: Opening Pandora's Box. *Curr. Opin. Microbiol.* 52, 64–69. doi: 10.1016/j.mib.2019.05.004
- Cuyppers, B., Domagalska, M. A., Meysman, P., Muylder, G., Vanaerschoot, M., Imamura, H., et al. (2017). Multiplexed Spliced-Leader Sequencing: A High-Throughput, Selective Method for RNA-Seq in Trypanosomatids. *Sci. Rep.* 7, 3725. doi: 10.1038/s41598-017-03987-0
- Dagley, M. J., Saunders, E. C., Simpson, K. J., and McConville, M. J. (2015). High-Content Assay for Measuring Intracellular Growth of Leishmania in Human Macrophages. *Assay Drug Dev. Technol.* 13, 389–401. doi: 10.1089/adt.2015.652
- Daniels, R., Volkman, S. K., Milner, D. A., Mahesh, N., Neafsey, D. E., Park, D. J., et al. (2008). A General SNP-Based Molecular Barcode for *Plasmodium Falciparum* Identification and Tracking. *Malar. J.* 7, 223. doi: 10.1186/1475-2875-7-223
- Darde, M. L., Bouteille, B., and Pestre-Alexandre, M. (1988). Isoenzymic Characterization of Seven Strains of *Toxoplasma Gondii* by Isoelectrofocusing in Polyacrylamide Gels. *Am. J. Trop. Med. Hyg.* 39, 551–558. doi: 10.4269/ajtmh.1988.39.551
- Dardé, M. L., Bouteille, B., and Pestre-Alexandre, M. (1992). Isoenzyme Analysis of 35 *Toxoplasma Gondii* Isolates and the Biological and Epidemiological Implications. *J. Parasitol.* 78, 786–794. doi: 10.2307/3283305
- DaRocha, W. D., Otsu, K., Teixeira, S. M. R., and Donelson, J. E. (2004). Tests of Cytoplasmic RNA Interference (RNAi) and Construction of a Tetracycline-Inducible T7 Promoter System in *Trypanosoma Cruzi*. *Mol. Biochem. Parasitol.* 133, 175–186. doi: 10.1016/j.molbiopara.2003.10.005
- Davaasuren, B., Yamagishi, J., Mizushima, D., Narantsatsral, S., Otgonsuren, D., Myagmarsuren, P., et al. (2019). Draft Genome Sequence of *Trypanosoma Equiperdum* Strain IVM-T1. *Microbiol. Resour. Announc.* 8 (9), e01119-18. doi: 10.1128/MRA.01119-18
- Dean, S., Sunter, J. D., and Wheeler, R. J. (2017). TrypTag.org: A Trypanosome Genome-Wide Protein Localisation Resource. *Trends Parasitol.* 33, 80–82. doi: 10.1016/j.pt.2016.10.009
- DeBarry, J. D., and Kissinger, J. C. (2011). Jumbled Genomes: Missing Apicomplexan Synteny. *Mol. Biol. Evol.* 28, 2855–2871. doi: 10.1093/molbev/msr103
- de Boer, P., Hoogenboom, J. P., and Giepmans, B. N. G. (2015). Correlated Light and Electron Microscopy: Ultrastructure Lights Up! *Nat. Methods* 12, 503–513. doi: 10.1038/nmeth.3400
- de Godoy, L. M. F., Marchini, F. K., Pavoni, D. P., Rampazzo, R., de, C. P., Probst, C. M., et al. (2012). Quantitative Proteomics of *Trypanosoma Cruzi* During Metacyclogenesis. *Proteomics* 12, 2694–2703. doi: 10.1002/pmic.201200078
- Dejung, M., Subota, I., Bucerius, F., Dindar, G., Freiwald, A., Engstler, M., et al. (2016). Quantitative Proteomics Uncovers Novel Factors Involved in Developmental Differentiation of *Trypanosoma Brucei*. *PLoS Pathog.* 12, e1005439. doi: 10.1371/journal.ppat.1005439
- Delgado, I. L. S., Tavares, A., Francisco, S., Santos, D., Coelho, J., Basto, A. P., et al. (2021). Characterization of a MOB1 Homolog in the Apicomplexan Parasite *Toxoplasma Gondii*. *Biol. (Basel)* 10 (12), 1233. doi: 10.3390/biology10121233
- De Niz, M., Burda, P. C., Kaiser, G., Del Portillo, H. A., Spielmann, T., Frischknecht, F., et al. (2017). Progress in Imaging Methods: Insights Gained Into Plasmodium Biology. *Nat. Rev. Microbiol.* 15, 37–54. doi: 10.1038/nrmicro.2016.158
- De Niz, M., Stanway, R. R., Wacker, R., Keller, D., and Heussler, V. T. (2016). An Ultrasensitive NanoLuc-Based Luminescence System for Monitoring *Plasmodium Berghei* Throughout its Life Cycle. *Malar. J.* 15, 1–24. doi: 10.1186/s12936-016-1291-9
- De Pablos, L. M., Kelly, S., de Freitas Nascimento, J., Sunter, J., and Carrington, M. (2017). Characterization of RBP9 and RBP10, Two Developmentally Regulated RNA-Binding Proteins in *Trypanosoma Brucei*. *Open Biol.* 7 (4), 160159. doi: 10.1098/rsob.160159
- de Souza, N. (2018). Structure via Super-Resolution. *Nat. Methods* 15, 30. doi: 10.1038/nmeth.4543

- Dey, S., Nath, P., Biswas, S., Nath, S., and Ganguly, A. (2021). Malaria Detection Through Digital Microscopic Imaging Using Deep Greedy Network With Transfer Learning. *J. Med. Imaging (Bellingham Wash.)* 8, 54502. doi: 10.1117/1.JMI.8.5.054502
- Dong, X., Lim, T. K., Lin, Q., and He, C. Y. (2020). Basal Body Protein TbSAF1 Is Required for Microtubule Quartet Anchorage to the Basal Bodies in *Trypanosoma Brucei*. *MBio* 11 (3), e00668–20. doi: 10.1128/mBio.00668-20
- Dos Santos Pacheco, N., and Soldati-Favre, D. (2021). Coupling Auxin-Inducible Degron System With Ultrastructure Expansion Microscopy to Accelerate the Discovery of Gene Function in *Toxoplasma Gondii*. *Methods Mol. Biol.* 2369, 121–137. doi: 10.1007/978-1-0716-1681-9_8
- Drew, M. E., Morris, J. C., Wang, Z., Wells, L., Sanchez, M., Landfear, S. M., et al. (2003). The Adenosine Analog Tubercidin Inhibits Glycolysis in *Trypanosoma Brucei* as Revealed by an RNA Interference Library. *J. Biol. Chem.* 278, 46596–46600. doi: 10.1074/jbc.M309320200
- Dubey, J. P. (2010). *Toxoplasmosis of Animals and Humans* (LLC: CRC Press - Taylor and Francis Group).
- Duez, J., Carucci, M., Garcia-Barbazan, I., Corral, M., Perez, O., Presa, J. L., et al. (2018). High-Throughput Microspherization to Assess Red Blood Cell Deformability and Screen for Malaria Transmission-Blocking Drugs. *Nat. Protoc.* 13, 1362–1376. doi: 10.1038/nprot.2018.035
- Duffy, C. W., Morrison, L. J., Black, A., Pinchbeck, G. L., Christley, R. M., Schoenefeld, A., et al. (2009). *Trypanosoma Vivax* Displays a Clonal Population Structure. *Int. J. Parasitol.* 39, 1475–1483. doi: 10.1016/j.ijpara.2009.05.012
- Eberle, A. L., and Zeidler, D. (2018). Multi-Beam Scanning Electron Microscopy for High-Throughput Imaging in Connectomics Research. *Front. Neuroanat.* 12. doi: 10.3389/fnana.2018.00112
- El Hajj, H., Demey, E., Poncet, J., Lebrun, M., Wu, B., Galéotti, N., et al. (2006). The ROP2 Family of *Toxoplasma Gondii* Rhoptry Proteins: Proteomic and Genomic Characterization and Molecular Modeling. *Proteomics* 6, 5773–5784. doi: 10.1002/pmic.200600187
- El-Sayed, N. M., Myler, P. J., Bartholomeu, D. C., Nilsson, D., Aggarwal, G., Tran, A.-N., et al. (2005). The Genome Sequence of *Trypanosoma Cruzi*, Etiologic Agent of Chagas Disease. *Science* 309, 409–415. doi: 10.1126/science.1112631
- Engelberg, K., Chen, C.-T., Bechtel, T., Sánchez Guzmán, V., Drozda, A. A., Chavan, S., et al. (2020). The Apical Annuli of *Toxoplasma Gondii* are Composed of Coiled-Coil and Signalling Proteins Embedded in the Inner Membrane Complex Sutures. *Cell. Microbiol.* 22, e13112. doi: 10.1111/cmi.13112
- Escalante, A. A., Barrio, E., and Ayala, F. J. (1995). Evolutionary Origin of Human and Primate Malaria: Evidence from the Circumsporozoite Protein Gene. *Mol. Biol. Evol.* 12, 616–626. doi: 10.1093/oxfordjournals.molbev.a040241
- Espada, C. R., Quilles, J. C. J., Albuquerque-Wendt, A., Cruz, M. C., Beneke, T., Lorenzon, L. B., et al. (2021). Effective Genome Editing in *Leishmania* (Viannia) *Braziliensis* Stably Expressing Cas9 and T7 RNA Polymerase. *Front. Cell. Infect. Microbiol.* 11. doi: 10.3389/fcimb.2021.772311
- Farrell, A., Coleman, B. I., Benenati, B., Brown, K. M., Blader, I. J., Marth, G. T., et al. (2014). Whole Genome Profiling of Spontaneous and Chemically Induced Mutations in *Toxoplasma Gondii*. *BMC Genomics* 15, 354. doi: 10.1186/1471-2164-15-354
- Fehling, H., Niss, H., Bea, A., Kottmayr, N., Brinker, C., Hoenow, S., et al. (2021). High Content Analysis of Macrophage-Targeting EhPib-Compounds Against Cutaneous and Visceral *Leishmania* Species. *Microorganisms* 9 (2), 422. doi: 10.3390/microorganisms9020422
- Feng, Y., Ryan, U. M., and Xiao, L. (2018). Genetic Diversity and Population Structure of *Cryptosporidium*. *Trends Parasitol.* 34, 997–1011. doi: 10.1016/j.pt.2018.07.009
- Fernandes, M. C., Dillon, L. A. L., Belew, A. T., Bravo, H. C., Mosser, D. M., and El-Sayed, N. M. (2016). Dual Transcriptome Profiling of *Leishmania*-Infected Human Macrophages Reveals Distinct Reprogramming Signatures. *MBio* 7(3): e00027–16. doi: 10.1128/mBio.00027-16
- Fernandez, V., Hommel, M., Chen, Q., Hagblom, P., and Wahlgren, M. (1999). Small, Clonally Variant Antigens Expressed on the Surface of the *Plasmodium Falciparum*-Infected Erythrocyte are Encoded by the Rif Gene Family and are the Target of Human Immune Responses. *J. Exp. Med.* 190, 1393–1404. doi: 10.1084/jem.190.10.1393
- Fesser, A. F., Braissant, O., Olmo, F., Kelly, J. M., Mäser, P., and Kaiser, M. (2020). Non-Invasive Monitoring of Drug Action: A New Live *In Vitro* Assay Design for Chagas' Disease Drug Discovery. *PLoS Negl. Trop. Dis.* 14, e0008487. doi: 10.1371/journal.pntd.0008487
- Fiebig, M., Kelly, S., and Gluenz, E. (2015). Comparative Life Cycle Transcriptomics Revises *Leishmania Mexicana* Genome Annotation and Links a Chromosome Duplication With Parasitism of Vertebrates. *PLoS Pathog.* 11, e1005186. doi: 10.1371/journal.ppat.1005186
- Fisch, D., Evans, R., Clough, B., Byrne, S. K., Channell, W. M., Dockterman, J., et al. (2021). HRMAN 2.0: Next-Generation Artificial Intelligence-Driven Analysis for Broad Host-Pathogen Interactions. *Cell. Microbiol.* 23, e13349. doi: 10.1111/cmi.13349
- Fisch, D., Yakimovich, A., Clough, B., Mercer, J., and Frickel, E.-M. (2020). Image-Based Quantitation of Host Cell-*Toxoplasma Gondii* Interplay Using HRMAN: A Host Response to Microbe Analysis Pipeline. *Methods Mol. Biol.* 2071, 411–433. doi: 10.1007/978-1-4939-9857-9_21
- Fisch, D., Yakimovich, A., Clough, B., Wright, J., Bunyan, M., Howell, M., et al. (2019). Defining Host-Pathogen Interactions Employing an Artificial Intelligence Workflow. *Elife* 8, e40560. doi: 10.7554/eLife.40560
- Franco, C. H., Alcántara, L. M., Chatelain, E., Freitas-Junior, L., and Moraes, C. B. (2019). Drug Discovery for Chagas Disease: Impact of Different Host Cell Lines on Assay Performance and Hit Compound Selection. *Trop. Med. Infect. Dis.* 4 (2):82. doi: 10.3390/tropicalmed4020082
- Franco, J. R., Simarro, P. P., Diarra, A., Ruiz-Postigo, J. A., and Jannin, J. G. (2012). The Human African Trypanosomiasis Specimen Biobank: A Necessary Tool to Support Research of New Diagnostics. *PLoS Negl. Trop. Dis.* 6, e1571. doi: 10.1371/journal.pntd.0001571
- Franzén, O., Ochaya, S., Sherwood, E., Lewis, M. D., Llewellyn, M. S., Miles, M. A., et al. (2011). Shotgun Sequencing Analysis of *Trypanosoma Cruzi* I Sylvio X10/1 and Comparison With T. *Cruzi* VI CL Brener. *PLoS Negl. Trop. Dis.* 5, e984. doi: 10.1371/journal.pntd.0000984
- Frénal, K., Jacot, D., Hammoudi, P.-M., Graindorge, A., Maco, B., and Soldati-Favre, D. (2017). Myosin-Dependent Cell-Cell Communication Controls Synchronicity of Division in Acute and Chronic Stages of *Toxoplasma Gondii*. *Nat. Commun.* 8, 15710. doi: 10.1038/ncomms15710
- Fritz, H. M., Buchholz, K. R., Chen, X., Durbin-Johnson, B., Rocke, D. M., Conrad, P. A., et al. (2012). Transcriptomic Analysis of *Toxoplasma* Development Reveals Many Novel Functions and Structures Specific to Sporozoites and Oocysts. *PLoS One* 7, e29998. doi: 10.1371/journal.pone.0029998
- Gaji, R. Y., Johnson, D. E., Treeck, M., Wang, M., Hudmon, A., and Arrizabalaga, G. (2015). Phosphorylation of a Myosin Motor by TgCDPK3 Facilitates Rapid Initiation of Motility During *Toxoplasma Gondii* Egress. *PLoS Pathog.* 11, e1005268. doi: 10.1371/journal.ppat.1005268
- Gambarotto, D., Hamel, V., and Guichard, P. (2021). Ultrastructure Expansion Microscopy (U-ExM). *Methods Cell Biol.* 161, 57–81. doi: 10.1016/bs.mcb.2020.05.006
- Gardner, M. J., Hall, N., Fung, E., White, O., Berriman, M., Hyman, R. W., et al. (2002). Genome Sequence of the Human Malaria Parasite *Plasmodium Falciparum*. *Nature* 419, 498–511. doi: 10.1038/nature01097
- Garfoot, A. L., Wilson, G. M., Coon, J. J., and Knoll, L. J. (2019). Proteomic and Transcriptomic Analyses of Early and Late-Chronic *Toxoplasma Gondii* Infection Shows Novel and Stage Specific Transcripts. *BMC Genomics* 20, 859. doi: 10.1186/s12864-019-6213-0
- Garrison, E., Treeck, M., Ehret, E., Butz, H., Garbuz, T., Oswald, B. P., et al. (2012). A Forward Genetic Screen Reveals That Calcium-Dependent Protein Kinase 3 Regulates Egress in *Toxoplasma*. *PLoS Pathog.* 8, e1003049. doi: 10.1371/journal.ppat.1003049
- Geddes, N. (2012). The Large Hadron Collider and Grid Computing. *Philos. Trans. Ser. A Math. Phys. Eng. Sci.* 370, 965–977. doi: 10.1098/rsta.2011.0465
- George, T. C., Basiji, D. A., Hall, B. E., Lynch, D. H., Ortyu, W. E., Perry, D. J., et al. (2004). Distinguishing Modes of Cell Death Using the ImageStream Multispectral Imaging Flow Cytometer. *Cytometry. A* 59, 237–245. doi: 10.1002/cyto.a.20048
- Ghorbal, M., Gorman, M., Macpherson, C. R., Martins, R. M., Scherf, A., and Lopez-Rubio, J.-J. (2014). Genome Editing in the Human Malaria Parasite *Plasmodium Falciparum* Using the CRISPR-Cas9 System. *Nat. Biotechnol.* 32, 819–821. doi: 10.1038/nbt.2925

- Glover, L., and Horn, D. (2009). Site-Specific DNA Double-Strand Breaks Greatly Increase Stable Transformation Efficiency in *Trypanosoma Brucei*. *Mol. Biochem. Parasitol.* 166, 194–197. doi: 10.1016/j.molbiopara.2009.03.010
- Gomes-Alves, A. G., Maia, A. F., Cruz, T., Castro, H., and Tomás, A. M. (2018). Development of an Automated Image Analysis Protocol for Quantification of Intracellular Forms of *Leishmania* Spp. *PLoS One* 13, e0201747. doi: 10.1371/journal.pone.0201747
- Gomes, A. R., Bushell, E., Schwach, F., Girling, G., Anar, B., Quail, M. A., et al. (2015). A Genome-Scale Vector Resource Enables High-Throughput Reverse Genetic Screening in a Malaria Parasite. *Cell Host Microbe* 17, 404–413. doi: 10.1016/j.chom.2015.01.014
- Gomes, A., and Korf, B. (2018). 'Chapter 5 - Genetic Testing Techniques' in *Farmer*. Eds. N. H. Robin and M. B. B. T.-P. C. G. (St Louis, Missouri, USA: Elsevier), 47–64. doi: 10.1016/B978-0-323-48555-5.00005-3
- Gorilak, P., Pružincová, M., Vachova, H., Olšinová, M., Schmidt Cernohorska, M., and Varga, V. (2021). Expansion Microscopy Facilitates Quantitative Super-Resolution Studies of Cytoskeletal Structures in Kinetoplastid Parasites. *Open Biol.* 11, 210131. doi: 10.1098/rsob.210131
- Greif, G., Ponce de Leon, M., Lamolle, G., Rodriguez, M., Piñeyro, D., Tavares-Marques, L. M., et al. (2013). Transcriptome Analysis of the Bloodstream Stage From the Parasite *Trypanosoma Vivax*. *BMC Genomics* 14, 149. doi: 10.1186/1471-2164-14-149
- Griffiths, J. K., Theodos, C., Paris, M., and Tzipori, S. (1998). The Gamma Interferon Gene Knockout Mouse: A Highly Sensitive Model for Evaluation of Therapeutic Agents Against *Cryptosporidium Parvum*. *J. Clin. Microbiol.* 36, 2503–2508. doi: 10.1128/JCM.36.9.2503-2508.1998
- Guegan, F., and Figueiredo, L. (2021). A Two-Stage Solution. *Elife* 10, e72980. doi: 10.7554/eLife.72980
- Guérin, A., Corrales, R. M., Parker, M. L., Lamarque, M. H., Jacot, D., El Hajj, H., et al. (2017). Efficient Invasion by *Toxoplasma* Depends on the Subversion of Host Protein Networks. *Nat. Microbiol.* 2, 1358–1366. doi: 10.1038/s41564-017-0018-1
- Haile, S., and Papadopolou, B. (2007). Developmental Regulation of Gene Expression in Trypanosomatid Parasitic Protozoa. *Curr. Opin. Microbiol.* 10, 569–577. doi: 10.1016/j.mib.2007.10.001
- Halliday, C., Billington, K., Wang, Z., Madden, R., Dean, S., Sunter, J. D., et al. (2019). Cellular Landmarks of *Trypanosoma Brucei* and *Leishmania Mexicana*. *Mol. Biochem. Parasitol.* 230, 24–36. doi: 10.1016/j.molbiopara.2018.12.003
- Hall, N., Karras, M., Raine, J. D., Carlton, J. M., Kooij, T. W. A., Berriman, M., et al. (2005). A Comprehensive Survey of the Plasmodium Life Cycle by Genomic, Transcriptomic, and Proteomic Analyses. *Science* 307, 82–86. doi: 10.1126/science.1103717
- Harding, C. R., Egarter, S., Gow, M., Jiménez-Ruiz, E., Ferguson, D. J. P., and Meissner, M. (2016). Gliding Associated Proteins Play Essential Roles During the Formation of the Inner Membrane Complex of *Toxoplasma Gondii*. *PLoS Pathog.* 12, e1005403. doi: 10.1371/journal.ppat.1005403
- Harding, C. R., Sidik, S. M., Petrova, B., Gnädig, N. F., Okombo, J., Herneisen, A. L., et al. (2020). Genetic Screens Reveal a Central Role for Heme Metabolism in Artemisinin Susceptibility. *Nat. Commun.* 11, 4813. doi: 10.1038/s41467-020-18624-0
- Haridas, V., Ranjbar, S., Vorobjev, I. A., Goldfeld, A. E., and Barteneva, N. S. (2017). Imaging Flow Cytometry Analysis of Intracellular Pathogens. *Methods* 112, 91–104. doi: 10.1016/j.mymeth.2016.09.007
- Hassan, M. A., Melo, M. B., Haas, B., Jensen, K. D. C., and Saeij, J. P. J. (2012). *De Novo* Reconstruction of the *Toxoplasma Gondii* Transcriptome Improves on the Current Genome Annotation and Reveals Alternatively Spliced Transcripts and Putative Long non-Coding RNAs. *BMC Genomics* 13, 696. doi: 10.1186/1471-2164-13-696
- Haydock, A., Terrao, M., Sekar, A., Ramasamy, G., Baugh, L., and Myler, P. J. (2015). RNA-Seq Approaches for Determining mRNA Abundance in *Leishmania*. *Methods Mol. Biol.* 1201, 207–219. doi: 10.1007/978-1-4939-1438-8_12
- Hébert, L., Moumen, B., Madeline, A., Steinbiss, S., Lakhdar, L., Van Reet, N., et al. (2017). First Draft Genome Sequence of the Dourine Causative Agent: *Trypanosoma Equiperdum* Strain OVI. *J. Genomics* 5, 1–3. doi: 10.7150/jgen.17904
- Helm, J. R., Hertz-Fowler, C., Aslett, M., Berriman, M., Sanders, M., Quail, M. A., et al. (2009). Analysis of Expressed Sequence Tags From the Four Main Developmental Stages of *Trypanosoma Congolense*. *Mol. Biochem. Parasitol.* 168, 34–42. doi: 10.1016/j.molbiopara.2009.06.004
- Hennessey, K. M., Rogiers, I. C., Shih, H.-W., Hulverson, M. A., Choi, R., McCloskey, M. C., et al. (2018). Screening of the Pathogen Box for Inhibitors With Dual Efficacy Against *Giardia Lamblia* and *Cryptosporidium Parvum*. *PLoS Negl. Trop. Dis.* 12, e0006673. doi: 10.1371/journal.pntd.0006673
- Hentzschel, F., Mitesser, V., Fraschka, S. A.-K., Krzikalla, D., Carrillo, E. H., Berkhout, B., et al. (2020). Gene Knockdown in Malaria Parasites via non-Canonical RNAi. *Nucleic Acids Res.* 48, e2. doi: 10.1093/nar/gkz927
- Heymann, J. A. W., Hayles, M., Gestmann, I., Giannuzzi, L. A., Lich, B., and Subramaniam, S. (2006). Site-Specific 3D Imaging of Cells and Tissues With a Dual Beam Microscope. *J. Struct. Biol.* 155, 63–73. doi: 10.1016/j.jsb.2006.03.006
- Hilton, N. A., Sladowski, T. E., Perry, J. A., Pataki, Z., Sinclair-Davis, A. N., Muniz, R. S., et al. (2018). Identification of TOEFAZI-Interacting Proteins Reveals Key Regulators of *Trypanosoma Brucei* Cytokinesis. *Mol. Microbiol.* 109, 306–326. doi: 10.1111/mmi.13986
- Hiraiwa, P. M., de Aguiar, A. M., and Ávila, A. R. (2018). Fluorescence-Based Assay for Accurate Measurement of Transcriptional Activity in Trypanosomatid Parasites. *Cytometry. A* 93, 727–736. doi: 10.1002/cyto.a.23387
- Horn, D. (2022). Genome-Scale RNAi Screens in African Trypanosomes. *Trends Parasitol.* 38, 160–173. doi: 10.1016/j.pt.2021.09.002
- Howick, V. M., Peacock, L., Kay, C., Collett, C., Gibson, W., and Lawniczak, M. K. N. (2022). Single-Cell Transcriptomics Reveals Expression Profiles of *Trypanosoma Brucei* Sexual Stages. *PLoS Pathog.* 18, e1010346. doi: 10.1371/journal.ppat.1010346
- Howick, V. M., Russell, A. J. C., Andrews, T., Heaton, H., Reid, A. J., Natarajan, K., et al. (2019). The Malaria Cell Atlas: Single Parasite Transcriptomes Across the Complete Plasmodium Life Cycle. *Science* 365. doi: 10.1126/science.aaw2619
- Hrdlickova, R., Toloue, M., and Tian, B. (2017). RNA-Seq Methods for Transcriptome Analysis. *Wiley Interdiscip. Rev. RNA* 8 (1), 10.1002/wrna.1364. doi: 10.1002/wrna.1364
- Huang, G., Voet, A., and Maglia, G. (2019). FraC Nanopores With Adjustable Diameter Identify the Mass of Opposite-Charge Peptides With 44 Dalton Resolution. *Nat. Commun.* 10, 835. doi: 10.1038/s41467-019-08761-6
- Hu, T., Chitnis, N., Monos, D., and Dinh, A. (2021). Next-Generation Sequencing Technologies: An Overview. *Hum. Immunol.* 82, 801–811. doi: 10.1016/j.humimm.2021.02.012
- Hung, J., Goodman, A., Ravel, D., Lopes, S. C. P., Rangel, G. W., Nery, O. A., et al. (2020). Keras R-CNN: Library for Cell Detection in Biological Images Using Deep Neural Networks. *BMC Bioinf.* 21, 300. doi: 10.1186/s12859-020-03635-x
- Hutchens, M., and Luker, G. D. (2007). Applications of Bioluminescence Imaging to the Study of Infectious Diseases. *Cell. Microbiol.* 9, 2315–2322. doi: 10.1111/j.1462-5822.2007.00995.x
- Hutchinson, S., Foulon, S., Crouzols, A., Menafra, R., Rotureau, B., Griffiths, A. D., et al. (2021). The Establishment of Variant Surface Glycoprotein Monoallelic Expression Revealed by Single-Cell RNA-Seq of *Trypanosoma Brucei* in the Tsetse Fly Salivary Glands. *PLoS Pathog.* 17, e1009904. doi: 10.1371/journal.ppat.1009904
- Hutchinson, R., and Gibson, W. (2015). Rediscovery of *Trypanosoma (Pycnomonas)* Suis, a Tsetse-Transmitted Trypanosome Closely Related to *T. Brucei*. *Infect. Genet. Evol. J. Mol. Epidemiol. Evol. Genet. Infect. Dis.* 36, 381–388. doi: 10.1016/j.meegid.2015.10.018
- Hwang, B., Lee, J. H., and Bang, D. (2018). Single-Cell RNA Sequencing Technologies and Bioinformatics Pipelines. *Exp. Mol. Med.* 50, 1–14. doi: 10.1038/s12276-018-0071-8
- Ilboudo, H., Noyes, H., Mulindwa, J., Kimuda, M. P., Koffi, M., Kaboré, J. W., et al. (2017). Introducing the TrypanoGEN Biobank: A Valuable Resource for the Elimination of Human African Trypanosomiasis. *PLoS Negl. Trop. Dis.* 11, e0005438. doi: 10.1371/journal.pntd.0005438
- Imamura, H., Monsieurs, P., Jara, M., Sanders, M., Maes, I., Vanaerschoot, M., et al. (2020). Evaluation of Whole Genome Amplification and Bioinformatic Methods for the Characterization of *Leishmania* Genomes at a Single Cell Level. *Sci. Rep.* 10, 15043. doi: 10.1038/s41598-020-71882-2
- Inbar, E., Hughitt, V. K., Dillon, L. A. L., Ghosh, K., El-Sayed, N. M., and Sacks, D. L. (2017). The Transcriptome of *Leishmania* Major Developmental Stages in

- Their Natural Sand Fly Vector. *MBio* 8 (2), e00029-17. doi: 10.1128/mBio.00029-17
- Isaza, J. P., Galván, A. L., Polanco, V., Huang, B., Matveyev, A. V., Serrano, M. G., et al. (2015). Revisiting the Reference Genomes of Human Pathogenic *Cryptosporidium* Species: Reannotation of *C. Parvum* Iowa and a New *C. Hominis* Reference. *Sci. Rep.* 5, 16324. doi: 10.1038/srep16324
- Ivens, A. C., Peacock, C. S., Worthey, E. A., Murphy, L., Aggarwal, G., Berriman, M., et al. (2005). The Genome of the Kinetoplastid Parasite, *Leishmania Major*. *Science* 309, 436–442. doi: 10.1126/science.1112680
- Jackson, A. P. (2016). Gene Family Phylogeny and the Evolution of Parasite Cell Surfaces. *Mol. Biochem. Parasitol.* 209, 64–75. doi: 10.1016/j.molbiopara.2016.03.007
- Jackson, A. P., Allison, H. C., Barry, J. D., Field, M. C., Hertz-Fowler, C., and Berriman, M. (2013). A Cell-Surface Phylome for African Trypanosomes. *PLoS Negl. Trop. Dis.* 7, e2121. doi: 10.1371/journal.pntd.0002121
- Jackson, A. P., Berry, A., Aslett, M., Allison, H. C., Burton, P., Vavrova-Anderson, J., et al. (2012). Antigenic Diversity is Generated by Distinct Evolutionary Mechanisms in African Trypanosome Species. *Proc. Natl. Acad. Sci. U. S. A.* 109, 3416–3421. doi: 10.1073/pnas.1117313109
- Jackson, A. P., Sanders, M., Berry, A., McQuillan, J., Aslett, M. A., Quail, M. A., et al. (2010). The Genome Sequence of *Trypanosoma Brucei* Gambiense, Causative Agent of Chronic Human African Trypanosomiasis. *PLoS Negl. Trop. Dis.* 4, e658. doi: 10.1371/journal.pntd.0000658
- Jacot, D., Tosetti, N., Pires, I., Stock, J., Graindorge, A., Hung, Y.-F., et al. (2016). An Apicomplexan Actin-Binding Protein Serves as a Connector and Lipid Sensor to Coordinate Motility and Invasion. *Cell Host Microbe* 20, 731–743. doi: 10.1016/j.chom.2016.10.020
- Jensen, B. C., Ramasamy, G., Vasconcelos, E. J. R., Ingolia, N. T., Myler, P. J., and Parsons, M. (2014). Extensive Stage-Regulation of Translation Revealed by Ribosome Profiling of *Trypanosoma Brucei*. *BMC Genomics* 15, 911. doi: 10.1186/1471-2164-15-911
- Kalichava, A., and Ochsenreiter, T. (2021). Ultrastructure Expansion Microscopy in *Trypanosoma Brucei*. *Open Biol.* 11, 210132. doi: 10.1098/rsob.210132
- Keeling, P. J. (2004). Reduction and Compaction in the Genome of the Apicomplexan Parasite *Cryptosporidium Parvum*. *Dev. Cell* 6, 614–616. doi: 10.1016/s1534-5807(04)00135-2
- Kehrer, J., Frischknecht, F., and Mair, G. R. (2016). Proteomic Analysis of the Plasmodium Berghei Gametocyte Egressome and Vesicular bioID of Osmiophilic Body Proteins Identifies Merozoite TRAP-Like Protein (MTRAP) as an Essential Factor for Parasite Transmission. *Mol. Cell. Proteomics* 15, 2852–2862. doi: 10.1074/mcp.M116.058263
- Kent, R. S., Modrzynska, K. K., Cameron, R., Philip, N., Billker, O., and Waters, A. P. (2018). Inducible Developmental Reprogramming Redefines Commitment to Sexual Development in The Malaria Parasite *Plasmodium Berghei*. *Nat. Microbiol.* 3, 1206–1213. doi: 10.1038/s41564-018-0223-6
- Key, M., Bergmann, A., Micchelli, C., Thornton, L. B., Millard, S., and Dou, Z. (2020). Determination of Chemical Inhibitor Efficiency Against Intracellular *Toxoplasma Gondii* Growth Using a Luciferase-Based Growth Assay. *J. Vis. Exp.* (158), 10.3791/60985. doi: 10.3791/60985
- Khalil, I. A., Troeger, C., Rao, P. C., Blacker, B. F., Brown, A., Brewer, T. G., et al. (2018). Morbidity, Mortality, and Long-Term Consequences Associated With Diarrhoea From *Cryptosporidium* Infection in Children Younger Than 5 Years: A Meta-Analyses Study. *Lancet Glob. Heal.* 6, e758–e768. doi: 10.1016/S2214-109X(18)30283-3
- Khan, A., Dubey, J. P., Su, C., Ajioka, J. W., Rosenthal, B. M., and Sibley, L. D. (2011). Genetic Analyses of Atypical *Toxoplasma Gondii* Strains Reveal a Fourth Clonal Lineage in North America. *Int. J. Parasitol.* 41, 645–655. doi: 10.1016/j.ijpara.2011.01.005
- Khan, T., van Brummelen, A. C., Parkinson, C. J., and Hoppe, H. C. (2012). ATP and Luciferase Assays to Determine the Rate of Drug Action in *In Vitro* Cultures of *Plasmodium Falciparum*. *Malar. J.* 11, 369. doi: 10.1186/1475-2875-11-369
- Khosh-Naucke, M., Becker, J., Mesén-Ramírez, P., Kiani, P., Birnbaum, J., Fröhle, U., et al. (2018). Identification of Novel Parasitophorous Vacuole Proteins in *P. Falciparum* Parasites Using BioID. *Int. J. Med. Microbiol.* 308, 13–24. doi: 10.1016/j.ijmm.2017.07.007
- Kim, D. I., Jensen, S. C., Noble, K. A., Kc, B., Roux, K. H., Motamedchaboki, K., et al. (2016). An Improved Smaller Biotin Ligase for BioID Proximity Labeling. *Mol. Biol. Cell* 27, 1188–1196. doi: 10.1091/mbc.E15-12-0844
- Kimmel, J., Kehrer, J., Frischknecht, F., and Spielmann, T. (2021). Proximity-Dependent Biotinylation Approaches to Study Apicomplexan Biology. *Mol. Microbiol.* 117 (3), 553–568. doi: 10.1111/mmi.14815
- Kisielowski, C., Freitag, B., Bischoff, M., van Lin, H., Lazar, S., Knippels, G., et al. (2008). Detection of Single Atoms and Buried Defects in Three Dimensions by Aberration-Corrected Electron Microscope With 0.5-Å Information Limit. *Microsc. Microanal.* 14, 469–477. doi: 10.1017/S1431927608080902
- Kissinger, J. C., Gajria, B., Li, L., Paulsen, I. T., and Roos, D. S. (2003). ToxoDB: Accessing the *Toxoplasma Gondii* Genome. *Nucleic Acids Res.* 31, 234–236. doi: 10.1093/nar/gkg072
- Knoll, L. J., Furie, G. L., and Boothroyd, J. C. (2001). Adaptation of Signature-Tagged Mutagenesis for *Toxoplasma Gondii*: A Negative Screening Strategy to Isolate Genes That are Essential in Restrictive Growth Conditions. *Mol. Biochem. Parasitol.* 116, 11–16. doi: 10.1016/s0166-6851(01)00295-x
- Kolev, N. G., Franklin, J. B., Carmi, S., Shi, H., Michaeli, S., and Tschudi, C. (2010). The Transcriptome of the Human Pathogen *Trypanosoma Brucei* at Single-Nucleotide Resolution. *PLoS Pathog.* 6, e1001090. doi: 10.1371/journal.ppat.1001090
- Kolev, N. G., Ullu, E., and Tschudi, C. (2015). Construction of *Trypanosoma Brucei* Illumina RNA-Seq Libraries Enriched for Transcript Ends. *Methods Mol. Biol.* 1201, 165–175. doi: 10.1007/978-1-4939-1438-8_9
- Kornfeld, J., and Denk, W. (2018). Progress and Remaining Challenges in High-Throughput Volume Electron Microscopy. *Curr. Opin. Neurobiol.* 50, 261–267. doi: 10.1016/j.conb.2018.04.030
- Kreidenweiss, A., Hopkins, A. V., and Mordmüller, B. (2013). 2A and the Auxin-Based Degron System Facilitate Control of Protein Levels in *Plasmodium Falciparum*. *PLoS One* 8, e78661. doi: 10.1371/journal.pone.0078661
- Kuang, D., Qiao, J., Li, Z., Wang, W., Xia, H., Jiang, L., et al. (2017). Tagging to Endogenous Genes of *Plasmodium Falciparum* Using CRISPR/Cas9. *Parasitol. Vectors* 10, 595. doi: 10.1186/s13071-017-2539-0
- Kudella, P. W., Moll, K., Wahlgren, M., Wixforth, A., and Westerhausen, C. (2016). ARAM: An Automated Image Analysis Software to Determine Rosetting Parameters and Parasitaemia in *Plasmodium* Samples. *Malar. J.* 15, 223. doi: 10.1186/s12936-016-1243-4
- Kudyba, H. M., Cobb, D. W., Vega-Rodriguez, J., and Muralidharan, V. (2021). Some Conditions Apply: Systems for Studying *Plasmodium Falciparum* Protein Function. *PLoS Pathog.* 17, e1009442. doi: 10.1371/journal.ppat.1009442
- Kumar, V., Ray, S., Aggarwal, S., Biswas, D., Jadhav, M., Yadav, R., et al. (2020). Multiplexed Quantitative Proteomics Provides Mechanistic Cues for Malaria Severity and Complexity. *Commun. Biol.* 3, 683. doi: 10.1038/s42003-020-01384-4
- Lakshmi, B. S., Wang, R., and Madhubala, R. (2014). *Leishmania* Genome Analysis and High-Throughput Immunological Screening Identifies Tuzin as a Novel Vaccine Candidate Against Visceral Leishmaniasis. *Vaccine* 32, 3816–3822. doi: 10.1016/j.vaccine.2014.04.088
- Lam, S. S., Martell, J. D., Kamer, K. J., Deerinck, T. J., Ellisman, M. H., Mootha, V. K., et al. (2015). Directed Evolution of APEX2 for Electron Microscopy and Proximity Labeling. *Nat. Methods* 12, 51–54. doi: 10.1038/nmeth.3179
- Lamotte, S., Aulner, N., Späth, G. F., and Prina, E. (2019). Discovery of Novel Hit Compounds With Broad Activity Against Visceral and Cutaneous *Leishmania* Species by Comparative Phenotypic Screening. *Sci. Rep.* 9, 438. doi: 10.1038/s41598-018-36944-6
- Lander, N., and Chiurillo, M. A. (2019). State-Of-the-Art CRISPR/Cas9 Technology for Genome Editing in *Trypanosomatids*. *J. Eukaryot. Microbiol.* 66, 981–991. doi: 10.1111/jeu.12747
- Lander, N., Li, Z.-H., Niyogi, S., and Docampo, R. (2015). CRISPR/Cas9-Induced Disruption of Paraflagellar Rod Protein 1 and 2 Genes in *Trypanosoma Cruzi* Reveals Their Role in Flagellar Attachment. *MBio* 6, e01012. doi: 10.1128/mBio.01012-15
- Lee, H. J., Georgiadou, A., Otto, T. D., Levin, M., Coin, L. J., Conway, D. J., et al. (2018). Transcriptomic Studies of Malaria: A Paradigm for Investigation of Systemic Host-Pathogen Interactions. *Microbiol. Mol. Biol. Rev.* 8 (2), e00071-17. doi: 10.1128/MMBR.00071-17
- Lee, Y. Q., Goh, A. S. P., Ch'ng, J. H., Nosten, F. H., Preiser, P. R., Pervaiz, S., et al. (2014). A High-Content Phenotypic Screen Reveals the Disruptive Potency of

- Quinacrine and 3',4'-Dichlorobenzamil on the Digestive Vacuole of *Plasmodium Falciparum*. *Antimicrob. Agents Chemother.* 58, 550–558. doi: 10.1128/AAC.01441-13
- Lee, Y. Q., Hall, B. E., and Tan, K. S. W. (2016). Screening for Drugs Against the *Plasmodium Falciparum* Digestive Vacuole by Imaging Flow Cytometry. *Methods Mol. Biol.* 1389, 195–205. doi: 10.1007/978-1-4939-3302-0_14
- Lentini, G., Ben Chaabene, R., Vadas, O., Ramakrishnan, C., Mukherjee, B., Mehta, V., et al. (2021). Structural Insights Into an Atypical Secretory Pathway Kinase Crucial for *Toxoplasma Gondii* Invasion. *Nat. Commun.* 12, 3788. doi: 10.1038/s41467-021-24083-y
- Lewis, M. D., and Kelly, J. M. (2016). Putting Infection Dynamics at the Heart of Chagas Disease. *Trends Parasitol.* 32, 899–911. doi: 10.1016/j.pt.2016.08.009
- Li, Y., Baptista, R. P., Sateriale, A., Striepen, B., and Kissinger, J. C. (2020). Analysis of Long Non-Coding RNA in *Cryptosporidium Parvum* Reveals Significant Stage-Specific Antisense Transcription. *Front. Cell. Infect. Microbiol.* 10. doi: 10.3389/fcimb.2020.608298
- Li, S., Besson, S., Blackburn, C., Carroll, M., Ferguson, R. K., Flynn, H., et al. (2016). Metadata Management for High Content Screening in OMERO. *Methods* 96, 27–32. doi: 10.1016/j.jmeth.2015.10.006
- Li, D.-F., Cui, Z.-H., Wang, L.-Y., Zhang, K.-H., Cao, L.-T., Zheng, S.-J., et al. (2021a). Tandem Mass Tag (TMT)-Based Proteomic Analysis of *Cryptosporidium Andersoni* Oocysts Before and After Excystation. *Parasitol. Vectors* 14, 608. doi: 10.1186/s13071-021-05113-6
- Liffner, B., and Absalon, S. (2021). Expansion Microscopy Reveals *Plasmodium Falciparum* Blood-Stage Parasites Undergo Anaphase With A Chromatin Bridge in the Absence of Mini-Chromosome Maintenance Complex Binding Protein. *Microorganisms* 9 (11), 2306. doi: 10.3390/microorganisms9112306
- Li, W., Grech, J., Stortz, J. F., Gow, M., Periz, J., Meissner, M., et al. (2022). A SplitCas9 Phenotypic Screen in *Toxoplasma Gondii* Identifies Proteins Involved in Host Cell Egress and Invasion. *Nat. Microb.* doi: 10.1038/s41564-01114-y
- Li, T., Liu, H., Jiang, N., Wang, Y., Wang, Y., Zhang, J., et al. (2021b). Comparative Proteomics Reveals *Cryptosporidium Parvum* Manipulation of the Host Cell Molecular Expression and Immune Response. *PLoS Negl. Trop. Dis.* 15, e0009949. doi: 10.1371/journal.pntd.0009949
- Lindner, S. E., Swearingen, K. E., Shears, M. J., Walker, M. P., Vrana, E. N., Hart, K. J., et al. (2019). Transcriptomics and Proteomics Reveal Two Waves of Translational Repression During the Maturation of Malaria Parasite Sporozoites. *Nat. Commun.* 10, 4964. doi: 10.1038/s41467-019-12936-6
- Lippuner, C., Ramakrishnan, C., Basso, W. U., Schmid, M. W., Okoniewski, M., Smith, N. C., et al. (2018). RNA-Seq Analysis During the Life Cycle of *Cryptosporidium Parvum* Reveals Significant Differential Gene Expression Between Proliferating Stages in the Intestine and Infectious Sporozoites. *Int. J. Parasitol.* 48, 413–422. doi: 10.1016/j.ijpara.2017.10.007
- Lisack, J., Morriswood, B., and Engstler, M. (2022). Response to Comment on 'Unexpected Plasticity in the Life Cycle of *Trypanosoma Brucei*'. *eLife* 11, e75922. doi: 10.7554/eLife.75922
- Liu, C., Yang, Z., Cai, M., Shi, Y., Cui, H., and Yuan, J. (2021). Generation of *Plasmodium Yoelii* Malaria Parasite for Conditional Degradation of Proteins. *Mol. Biochem. Parasitol.* 241, 111346. doi: 10.1016/j.molbiopara.2020.111346
- Llanes, A., Restrepo, C. M., Del Vecchio, G., Anguizola, F. J., and Leonart, R. (2015). The Genome of *Leishmania Panamensis*: Insights Into Genomics of the *L. (Viannia)* Subgenus. *Sci. Rep.* 5, 8550. doi: 10.1038/srep08550
- Long, S., Wang, Q., and Sibley, L. D. (2016). Analysis of Noncanonical Calcium-Dependent Protein Kinases in *Toxoplasma Gondii* by Targeted Gene Deletion Using CRISPR/Cas9. *Infect. Immun.* 84, 1262–1273. doi: 10.1128/IAI.01173-15
- Lorenzi, H., Khan, A., Behnke, M. S., Namasivayam, S., Swapna, L. S., Hadjithomas, M., et al. (2016). Local Admixture of Amplified and Diversified Secreted Pathogenesis Determinants Shapes Mosaic *Toxoplasma Gondii* Genomes. *Nat. Commun.* 7, 10147. doi: 10.1038/ncomms10147
- Louradour, I., Ferreira, T. R., Duge, E., Karunaweera, N., Paun, A., and Sacks, D. (2022). Stress Conditions Promote *Leishmania Hybridization In Vitro* Marked by Expression of the Ancestral Gamete Fusogen HAP2 as Revealed by Single-Cell RNA-Seq. *eLife* 11, e73488. doi: 10.7554/eLife.73488
- Love, M. S., and McNamara, C. W. (2020). High-Content Screening for *Cryptosporidium* Drug Discovery. *Methods Mol. Biol.* 2052, 303–317. doi: 10.1007/978-1-4939-9748-0_17
- Love, M. S., and McNamara, C. W. (2021). Phenotypic Screening Techniques for *Cryptosporidium* Drug Discovery. *Expert Opin. Drug Discov.* 16, 59–74. doi: 10.1080/17460441.2020.1812577
- Lucas, F. L. R., Versloot, R. C. A., Yakovlieva, L., Walvoort, M. T. C., and Maglia, G. (2021). Protein Identification by Nanopore Peptide Profiling. *Nat. Commun.* 12, 5795. doi: 10.1038/s41467-021-26046-9
- Luiza-Batista, C., Nardella, F., Thiberge, S., Serra-Hassoun, M., Ferreira, M. U., Scherf, A., et al. (2022). Flowcytometric and ImageStream RNA-FISH Gene Expression, Quantification and Phenotypic Characterization of Blood and Liver Stages From Human Malaria Species. *J. Infect. Dis.* 225 (9), 1621–1625. doi: 10.1093/infdis/jiab431
- Mahecic, D., Gambarotto, D., Douglass, K. M., Fortun, D., Banterle, N., Ibrahim, K. A., et al. (2020). Homogeneous Multifocal Excitation for High-Throughput Super-Resolution Imaging. *Nat. Methods* 17, 726–733. doi: 10.1038/s41592-020-0859-z
- Malebo, H. M., D'Alessandro, S., Ebstie, Y. A., Sorè, H., Tenoh Guedoung, A. R., Katani, S. J., et al. (2020). *In Vitro* Multistage Malaria Transmission Blocking Activity of Selected Malaria Box Compounds. *Drug Des. Devel. Ther.* 14, 1593–1607. doi: 10.2147/DDDT.S242883
- Marra, M. A., Hillier, L., and Waterston, R. H. (1998). Expressed Sequence Tags—Establishing Bridges Between Genomes. *Trends Genet.* 14, 4–7. doi: 10.1016/S0168-9525(97)01355-3
- Martel, D., Beneke, T., Gluenz, E., Späth, G. F., and Rachidi, N. (2017). Characterisation of Casein Kinase 1.1 in *Leishmania Donovanii* Using the CRISPR Cas9 Toolkit. *BioMed. Res. Int.* 2017, 4635605. doi: 10.1155/2017/4635605
- Martins, G. G., Cordelières, F. P., Colombelli, J., D'Antuono, R., Golani, O., Guet, R., et al. (2021). Highlights From the 2016–2020 NEUBIAS Training Schools for Bioimage Analysts: A Success Story and Key Asset for Analysts and Life Scientists. *F1000Research* 10, 334. doi: 10.12688/f1000research.25485.1
- Matos, L. V. S., McEvoy, J., Tzipori, S., Bresciani, K. D. S., and Widmer, G. (2019). The Transcriptome of *Cryptosporidium* Oocysts and Intracellular Stages. *Sci. Rep.* 9, 7856. doi: 10.1038/s41598-019-44289-x
- Matthews, K. R., and Larcombe, S. (2022). Comment on 'Unexpected Plasticity in the Life Cycle of *Trypanosoma Brucei*'. *eLife* 11, e74985. doi: 10.7554/eLife.74985
- Mauzy, M. J., Enomoto, S., Lancto, C. A., Abrahamsen, M. S., and Rutherford, M. S. (2012). The *Cryptosporidium Parvum* Transcriptome During *In Vitro* Development. *PLoS One* 7, e31715. doi: 10.1371/journal.pone.0031715
- Mazurie, A. J., Alves, J. M., Ozaki, L. S., Zhou, S., Schwartz, D. C., and Buck, G. A. (2013). Comparative Genomics of *Cryptosporidium*. *Int. J. Genomics* 2013, 832756. doi: 10.1155/2013/832756
- Mazurkiewicz, P., Tang, C. M., Boone, C., and Holden, D. W. (2006). Signature-Tagged Mutagenesis: Barcoding Mutants for Genome-Wide Screens. *Nat. Rev. Genet.* 7, 929–939. doi: 10.1038/nrg1984
- McCoy, J. M., Stewart, R. J., Uboldi, A. D., Li, D., Schröder, J., Scott, N. E., et al. (2017). A Forward Genetic Screen Identifies a Negative Regulator of Rapid Ca (2+)-Dependent Cell Egress (MS1) in the Intracellular Parasite *Toxoplasma Gondii*. *J. Biol. Chem.* 292, 7662–7674. doi: 10.1074/jbc.M117.775114
- Mellin, R., and Boddey, J. A. (2020). Organoids for Liver Stage Malaria Research. *Trends Parasitol.* 36, 158–169. doi: 10.1016/j.pt.2019.12.003
- Mendes Costa, D., Cecilio, P., Santarém, N., Cordeiro-da-Silva, A., and Tavares, J. (2019). Murine Infection With Bioluminescent *Leishmania Infantum* Axenic Amastigotes Applied To Drug Discovery. *Sci. Rep.* 9, 18989. doi: 10.1038/s41598-019-55474-3
- Mendonça, A. G., Alves, R. J., and Pereira-Leal, J. B. (2011). Loss of Genetic Redundancy in Reductive Genome Evolution. *PLoS Comput. Biol.* 7, e1001082. doi: 10.1371/journal.pcbi.1001082
- Milne, G., Webster, J. P., and Walker, M. (2020). *Toxoplasma Gondii*: An Underestimated Threat? *Trends Parasitol.* 36, 959–969. doi: 10.1016/j.pt.2020.08.005
- Minning, T. A., Weatherly, D. B., Atwood, J. 3rd, Orlando, R., and Tarleton, R. L. (2009). The Steady-State Transcriptome of the Four Major Life-Cycle Stages of *Trypanosoma Cruzi*. *BMC Genomics* 10, 370. doi: 10.1186/1471-2164-10-370
- Miotto, O., Almagro-Garcia, J., Manske, M., Macinnis, B., Campino, S., Rockett, K. A., et al. (2013). Multiple Populations of Artemisinin-Resistant *Plasmodium Falciparum* in Cambodia. *Nat. Genet.* 45, 648–655. doi: 10.1038/ng.2624

- Moita, D., Nunes-Cabaço, H., Mendes, A. M., and Prudêncio, M. (2021). A Guide to Investigating Immune Responses Elicited by Whole-Sporozoite Pre-Erythrocytic Vaccines Against Malaria. *FEBS J.* doi: 10.1111/febs.16016
- Moon, S., Siqueira-Neto, J. L., Moraes, C. B., Yang, G., Kang, M., Freitas-Junior, L. H., et al. (2014). An Image-Based Algorithm for Precise and Accurate High Throughput Assessment of Drug Activity Against the Human Parasite *Trypanosoma Cruzi*. *PLoS One* 9, e87188. doi: 10.1371/journal.pone.0087188
- Moraes, C. B., Witt, G., Kuzikov, M., Ellinger, B., Calogeropoulou, T., Prousis, K. C., et al. (2019). Accelerating Drug Discovery Efforts for Trypanosomatid Infections Using an Integrated Transnational Academic Drug Discovery Platform. *SLAS Discov. Adv. Life Sci. R D* 24, 346–361. doi: 10.1177/2472555218823171
- Mordue, D. G., Scott-Weathers, C. F., Tobin, C. M., and Knoll, L. J. (2007). A Patatin-Like Protein Protects *Toxoplasma Gondii* From Degradation in Activated Macrophages. *Mol. Microbiol.* 63, 482–496. doi: 10.1111/j.1365-2958.2006.05538.x
- Morrison, L. J., Tweedie, A., Black, A., Pinchbeck, G. L., Christley, R. M., Schoenefeld, A., et al. (2009). Discovery of Mating in the Major African Livestock Pathogen *Trypanosoma Congolense*. *PLoS One* 4, e5564. doi: 10.1371/journal.pone.0005564
- Morrisette, N. S., Mitra, A., Sept, D., and Sibley, L. D. (2004). Dinitroanilines Bind Alpha-Tubulin to Disrupt Microtubules. *Mol. Biol. Cell* 15, 1960–1968. doi: 10.1091/mbc.e03-07-0530
- Morrisette, N. S., and Sibley, L. D. (2002). Disruption of Microtubules Uncouples Budding and Nuclear Division in *Toxoplasma Gondii*. *J. Cell Sci.* 115, 1017–1025. doi: 10.1242/jcs.115.5.1017
- Morris, J. C., Wang, Z., Drew, M. E., and Englund, P. T. (2002). Glycolysis Modulates *Trypanosoma* Glycoprotein Expression as Revealed by an RNAi Library. *EMBO J.* 21, 4429–4438. doi: 10.1093/emboj/cdf474
- Morriswood, B., Havlicek, K., Demmel, L., Yavuz, S., Sealey-Cardona, M., Vidilaseris, K., et al. (2013). Novel Bilobe Components in *Trypanosoma Brucei* Identified Using Proximity-Dependent Biotinylation. *Eukaryot. Cell* 12, 356–367. doi: 10.1128/EC.00326-12
- Nakane, T., Kotecha, A., Sente, A., McMullan, G., Masiulis, S., Brown, P. M. G. E., et al. (2020). Single-Particle Cryo-EM at Atomic Resolution. *Nature* 587, 152–156. doi: 10.1038/s41586-020-2829-0
- Nayak, R., and Hasija, Y. (2021). A Hitchhiker's Guide to Single-Cell Transcriptomics and Data Analysis Pipelines. *Genomics* 113, 606–619. doi: 10.1016/j.ygeno.2021.01.007
- Neafsey, D. E., Taylor, A. R., and MacInnis, B. L. (2021). Advances and Opportunities in Malaria Population Genomics. *Nat. Rev. Genet.* 22, 502–517. doi: 10.1038/s41576-021-00349-5
- Negreira, G. H., Monsieus, P., Imamura, H., Maes, I., Kuk, N., Yagoubat, A., et al. (2022). High Throughput Single-Cell Genome Sequencing Gives Insights Into the Generation and Evolution of Mosaic Aneuploidy in *Leishmania Donovanii*. *Nucleic Acids Res.* 50, 293–305. doi: 10.1093/nar/gkab1203
- Ngara, M., Palmkvist, M., Sagasser, S., Hjelmqvist, D., Björklund, Å.K., Wahlgren, M., et al. (2018). Exploring Parasite Heterogeneity Using Single-Cell RNA-Seq Reveals a Gene Signature Among Sexual Stage *Plasmodium Falciparum* Parasites. *Exp. Cell Res.* 371, 130–138. doi: 10.1016/j.yexcr.2018.08.003
- Niang, M., Bei, A. K., Madnani, K. G., Pelly, S., Dankwa, S., Kanjee, U., et al. (2014). STEVOR Is a *Plasmodium Falciparum* Erythrocyte Binding Protein That Mediates Merozoite Invasion and Rosetting. *Cell Host Microbe* 16, 81–93. doi: 10.1016/j.chom.2014.06.004
- Nilsson, D., Gunasekera, K., Mani, J., Osteras, M., Farinelli, L., Baerlocher, L., et al. (2010). Spliced Leader Trapping Reveals Widespread Alternative Splicing Patterns in the Highly Dynamic Transcriptome of *Trypanosoma Brucei*. *PLoS Pathog.* 6, e1001037. doi: 10.1371/journal.ppat.1001037
- Nirmalan, N., Sims, P. F. G., and Hyde, J. E. (2004). Quantitative Proteomics of the Human Malaria Parasite *Plasmodium Falciparum* and Its Application to Studies of Development and Inhibition. *Mol. Microbiol.* 52, 1187–1199. doi: 10.1111/j.1365-2958.2004.04049.x
- Nirujogi, R. S., Pawar, H., Renuse, S., Kumar, P., Chavan, S., Sathe, G., et al. (2014). Moving From Unsequenced to Sequenced Genome: Reanalysis of the Proteome of *Leishmania Donovanii*. *J. Proteomics* 97, 48–61. doi: 10.1016/j.jprot.2013.04.021
- Nishi, T., Shinzawa, N., Yuda, M., and Iwanaga, S. (2021). Highly Efficient CRISPR/Cas9 System in *Plasmodium Falciparum* Using Cas9-Expressing Parasites and a Linear Donor Template. *Sci. Rep.* 11, 18501. doi: 10.1038/s41598-021-97984-z
- Novobilský, A., and Höglund, J. (2020). Small Animal *In Vivo* Imaging of Parasitic Infections: A Systematic Review. *Exp. Parasitol.* 214, 107905. doi: 10.1016/j.exppara.2020.107905
- Ong, S.-E., Blagoev, B., Kratchmarova, I., Kristensen, D. B., Steen, H., Pandey, A., et al. (2002). Stable Isotope Labeling by Amino Acids in Cell Culture, SILAC, as a Simple and Accurate Approach to Expression Proteomics. *Mol. Cell. Proteomics* 1, 376–386. doi: 10.1074/mcp.m200025-mcp200
- Othman, A. S., Marin-Mogollon, C., Salman, A. M., Franke-Fayard, B. M., Janse, C. J., and Khan, S. M. (2017). The Use of Transgenic Parasites in Malaria Vaccine Research. *Expert Rev. Vaccines* 16, 1–13. doi: 10.1080/14760584.2017.1333426
- Painter, H. J., Campbell, T. L., and Llinás, M. (2011). The Apicomplexan AP2 Family: Integral Factors Regulating *Plasmodium* Development. *Mol. Biochem. Parasitol.* 176, 1–7. doi: 10.1016/j.molbiopara.2010.11.014
- Panunzi, L. G., and Agüero, F. (2014). A Genome-Wide Analysis of Genetic Diversity in *Trypanosoma Cruzi* Intergenic Regions. *PLoS Negl. Trop. Dis.* 8, e2839. doi: 10.1371/journal.pntd.0002839
- Patankar, S., Munasinghe, A., Shoaibi, A., Cummings, L. M., and Wirth, D. F. (2001). Serial Analysis of Gene Expression in *Plasmodium Falciparum* Reveals the Global Expression Profile of Erythrocytic Stages and the Presence of Anti-Sense Transcripts in the Malarial Parasite. *Mol. Biol. Cell* 12, 3114–3125. doi: 10.1091/mbc.12.10.3114
- Patel, V. J., Thalassinou, K., Slade, S. E., Connolly, J. B., Crombie, A., Murrell, J. C., et al. (2009). A Comparison of Labeling and Label-Free Mass Spectrometry-Based Proteomics Approaches. *J. Proteome Res.* 8, 3752–3759. doi: 10.1021/pr900080y
- Peacock, L., Bailey, M., Carrington, M., and Gibson, W. (2014). Meiosis and Haploid Gametes in the Pathogen *Trypanosoma Brucei*. *Curr. Biol.* 24, 181–186. doi: 10.1016/j.cub.2013.11.044
- Peacock, L., Ferris, V., Sharma, R., Sunter, J., Bailey, M., Carrington, M., et al. (2011). Identification of the Meiotic Life Cycle Stage of *Trypanosoma Brucei* in the Tsetse Fly. *Proc. Natl. Acad. Sci. U. S. A.* 108, 3671–3676. doi: 10.1073/pnas.1019423108
- Peacock, C. S., Seeger, K., Harris, D., Murphy, L., Ruiz, J. C., Quail, M. A., et al. (2007). Comparative Genomic Analysis of Three *Leishmania* Species That Cause Diverse Human Disease. *Nat. Genet.* 39, 839–847. doi: 10.1038/ng2053
- Pegoraro, M., and Weedall, G. D. (2021). Malaria in the 'Omics Era'. *Genes (Basel)* 12 (6), 843. doi: 10.3390/genes12060843
- Peixoto, L., Chen, F., Harb, O. S., Davis, P. H., Beiting, D. P., Brownback, C. S., et al. (2010). Integrative Genomic Approaches Highlight a Family of Parasite-Specific Kinases That Regulate Host Responses. *Cell Host Microbe* 8, 208–218. doi: 10.1016/j.chom.2010.07.004
- Peng, D., Kurup, S. P., Yao, P. Y., Minning, T. A., and Tarleton, R. L. (2014). CRISPR-Cas9-Mediated Single-Gene and Gene Family Disruption in *Trypanosoma Cruzi*. *MBio* 6, e02097–e02014. doi: 10.1128/mBio.02097-14
- Perez-Guaita, D., Andrew, D., Heraud, P., Beeson, J., Anderson, D., Richards, J., et al. (2016). High Resolution FTIR Imaging Provides Automated Discrimination and Detection of Single Malaria Parasite Infected Erythrocytes on Glass. *Faraday Discuss.* 187, 341–352. doi: 10.1039/c5fd00181a
- Periz, J., Whitelaw, J., Harding, C., Gras, S., Del Rosario Minina, M. I., Latorre-Barragan, F., et al. (2017). *Toxoplasma Gondii* F-Actin Forms an Extensive Filamentous Network Required for Material Exchange and Parasite Maturation. *Elife* 6, e24119. doi: 10.7554/eLife.24119
- Pfander, C., Anar, B., Schwach, F., Otto, T. D., Brochet, M., Volkmann, K., et al. (2011). A Scalable Pipeline for Highly Effective Genetic Modification of a Malaria Parasite. *Nat. Methods* 8, 1078–1082. doi: 10.1038/nmeth.1742
- Philip, N., and Waters, A. P. (2015). Conditional Degradation of *Plasmodium Calcieneurin* Reveals Functions in Parasite Colonization of Both Host and Vector. *Cell Host Microbe* 18, 122–131. doi: 10.1016/j.chom.2015.05.018
- Pittman, K. J., Aliota, M. T., and Knoll, L. J. (2014). Dual Transcriptional Profiling of Mice and *Toxoplasma Gondii* During Acute and Chronic Infection. *BMC Genomics* 15, 806. doi: 10.1186/1471-2164-15-806
- Poran, A., Nötzel, C., Aly, O., Mencia-Trinchant, N., Harris, C. T., Guzman, M. L., et al. (2017). Single-Cell RNA Sequencing Reveals a Signature of Sexual Commitment in Malaria Parasites. *Nature* 551, 95–99. doi: 10.1038/nature24280

- Portella, D. C. N., Rossi, E. A., Paredes, B. D., Bastos, T. M., Meira, C. S., Nonaka, C. V. K., et al. (2021). A Novel High-Content Screening-Based Method for Anti-Trypanosoma Cruzi Drug Discovery Using Human-Induced Pluripotent Stem Cell-Derived Cardiomyocytes. *Stem Cells Int.* 2021, 2642807. doi: 10.1155/2021/2642807
- Pradhan, A., Siwo, G. H., Singh, N., Martens, B., Balu, B., Button-Simons, K. A., et al. (2015). Chemogenomic Profiling of Plasmodium Falciparum as a Tool to Aid Antimalarial Drug Discovery. *Sci. Rep.* 5, 15930. doi: 10.1038/srep15930
- Preston, M. D., Campino, S., Assefa, S. A., Echeverry, D. F., Ocholla, H., Amambua-Ngwa, A., et al. (2014). A Barcode of Organellar Genome Polymorphisms Identifies the Geographic Origin of Plasmodium Falciparum Strains. *Nat. Commun.* 5, 4052. doi: 10.1038/ncomms5052
- Puiu, D., Enomoto, S., Buck, G. A., Abrahamsen, M. S., and Kissinger, J. C. (2004). CryptoDB: The Cryptosporidium Genome Resource. *Nucleic Acids Res.* 32, D329–D331. doi: 10.1093/nar/gkh050
- Radke, J. R., Behnke, M. S., Mackey, A. J., Radke, J. B., Roos, D. S., and White, M. W. (2005). The Transcriptome of Toxoplasma Gondii. *BMC Biol.* 3, 26. doi: 10.1186/1741-7007-3-26
- Radke, J. R., Guerini, M. N., and White, M. W. (2000). Toxoplasma Gondii: Characterization of Temperature-Sensitive Tachyzoite Cell Cycle Mutants. *Exp. Parasitol.* 96, 168–177. doi: 10.1006/expr.2000.4568
- Ramírez-Flores, C. J., Cruz-Mirón, R., Mondragón-Castelán, M. E., González-Pozos, S., Ríos-Castro, E., and Mondragón-Flores, R. (2019). Proteomic and Structural Characterization of Self-Assembled Vesicles From Excretion/Secretion Products of Toxoplasma Gondii. *J. Proteomics* 208, 103490. doi: 10.1016/j.jprot.2019.103490
- Rao, A., Barkley, D., França, G. S., and Yanai, I. (2021). Exploring Tissue Architecture Using Spatial Transcriptomics. *Nature* 596, 211–220. doi: 10.1038/s41586-021-03634-9
- Rasse, T. M., Hollandi, R., and Horvath, P. (2020). OpSeF: Open Source Python Framework for Collaborative Instance Segmentation of Bioimages. *Front. Bioeng. Biotechnol.* 8. doi: 10.3389/fbioe.2020.558880
- Rastrojo, A., Carrasco-Ramiro, F., Martín, D., Crespillo, A., Reguera, R. M., Aguado, B., et al. (2013). The Transcriptome of Leishmania Major in the Axenic Promastigote Stage: Transcript Annotation and Relative Expression Levels by RNA-Seq. *BMC Genomics* 14, 223. doi: 10.1186/1471-2164-14-223
- Real, E., Howick, V. M., Dahalan, F. A., Witmer, K., Cudini, J., Andradi-Brown, C., et al. (2021). A Single-Cell Atlas of Plasmodium Falciparum Transmission Through the Mosquito. *Nat. Commun.* 12, 3196. doi: 10.1038/s41467-021-23434-z
- Reid, A. J., Talman, A. M., Bennett, H. M., Gomes, A. R., Sanders, M. J., Illingworth, C. J. R., et al. (2018). Single-Cell RNA-Seq Reveals Hidden Transcriptional Variation in Malaria Parasites. *Elife* 77, e33105. doi: 10.7554/eLife.33105
- Reis-Cunha, J. L., Rodrigues-Luiz, G. F., Valdivia, H. O., Baptista, R. P., Mendes, T. A. O., de Moraes, G. L., et al. (2015). Chromosomal Copy Number Variation Reveals Differential Levels of Genomic Plasticity In Distinct Trypanosoma Cruzi Strains. *BMC Genomics* 16, 499. doi: 10.1186/s12864-015-1680-4
- Rhee, H.-W., Zou, P., Udeshi, N. D., Martell, J. D., Mootha, V. K., Carr, S. A., et al. (2013). Proteomic Mapping of Mitochondria in Living Cells via Spatially Restricted Enzymatic Tagging. *Science* 339, 1328–1331. doi: 10.1126/science.1230593
- Rhoads, A., and Au, K. F. (2015). PacBio Sequencing and Its Applications. *Genomics Proteomics Bioinf.* 13, 278–289. doi: 10.1016/j.gpb.2015.08.002
- Richardson, J. B., Evans, B., Pyana, P. P., Van Reet, N., Siström, M., Büscher, P., et al. (2016). Whole Genome Sequencing Shows Sleeping Sickness Relapse is Due to Parasite Regrowth and Not Reinfection. *Evol. Appl.* 9, 381–393. doi: 10.1111/eva.12338
- Ritchie, R., Barrett, M. P., Mottram, J. C., and Myburgh, E. (2020). In Vivo Bioluminescence Imaging to Assess Compound Efficacy Against Trypanosoma Brucei. *Methods Mol. Biol.* 2116, 801–817. doi: 10.1007/978-1-0716-0294-2_48
- Rodrigues, C. M., Garcia, H. A., Rodrigues, A. C., Costa-Martins, A. G., Pereira, C. L., Pereira, D. L., et al. (2017). New Insights From Gorongosa National Park and Niassa National Reserve of Mozambique Increasing the Genetic Diversity of Trypanosoma Vivax and Trypanosoma Vivax-Like in Tsetse Flies, Wild Ungulates and Livestock From East Africa. *Parasitol. Vectors* 10, 337. doi: 10.1186/s13071-017-2241-2
- Rodrigues, C. M. F., Garcia, H. A., Rodrigues, A. C., Pereira, D. L., Pereira, C. L., Viola, L. B., et al. (2020). Expanding Our Knowledge on African Trypanosomes of the Subgenus Pycnomonas: A Novel Trypanosoma Suis-Like in Tsetse Flies, Livestock and Wild Ruminants Sympatric With Trypanosoma Suis in Mozambique. *Infect. Genet. Evol. J. Mol. Epidemiol. Evol. Genet. Infect. Dis.* 78, 104143. doi: 10.1016/j.meegid.2019.104143
- Rodrigues, A. C., Neves, L., Garcia, H. A., Viola, L. B., Marcili, A., Da Silva, F. M., et al. (2008). Phylogenetic Analysis of Trypanosoma Vivax Supports the Separation of South American/West African From East African Isolates and a New T. Vivax-Like Genotype Infecting a Nyala Antelope From Mozambique. *Parasitology* 135, 1317–1328. doi: 10.1017/S0031182008004848
- Rogers, M. B., Hilley, J. D., Dickens, N. J., Wilkes, J., Bates, P. A., Depledge, D. P., et al. (2011). Chromosome and Gene Copy Number Variation Allow Major Structural Change Between Species and Strains of Leishmania. *Genome Res.* 21, 2129–2142. doi: 10.1101/gr.122945.111
- Rosazza, T., Lecoeur, H., Blisnick, T., Moya-Nilges, M., Pescher, P., Bastin, P., et al. (2020). Dynamic Imaging Reveals Surface Exposure of Virulent Leishmania Amastigotes During Pyroptosis of Infected Macrophages. *J. Cell Sci.* 134 (5), jcs242776. doi: 10.1242/jcs.242776
- Rougeron, V., Elguero, E., Arnathau, C., Acuña Hidalgo, B., Durand, P., Houze, S., et al. (2020). Human Plasmodium Vivax Diversity, Population Structure and Evolutionary Origin. *PLoS Negl. Trop. Dis.* 14, e0008072. doi: 10.1371/journal.pntd.0008072
- Routeray, C. B., Choudhary, V., Prakash, D., Patil, R., Jagtap, S., Bai, S., et al. (2022). Quantitative Proteomic Analysis Reveals Differential Modulation of Crucial Stage Specific Proteins During Promastigote to Amastigote Differentiation in Leishmania Donovanii. *J. Proteins Proteomics* 13, 17–27. doi: 10.1007/s42485-021-00080-z
- Roux, K. J., Kim, D. I., Burke, B., and May, D. G. (2018). BioID: A Screen for Protein-Protein Interactions. *Curr. Protoc. Protein Sci.* 91, 19.23.1–19.23.15. doi: 10.1002/cpps.51
- Roux, K. J., Kim, D. I., Raida, M., and Burke, B. (2012). A Promiscuous Biotin Ligase Fusion Protein Identifies Proximal and Interacting Proteins in Mammalian Cells. *J. Cell Biol.* 196, 801–810. doi: 10.1083/jcb.201112098
- Rubens, U., Mormont, R., Paavola, L., Bäckér, V., Pavie, B., Scholz, L. A., et al. (2020). BIAFLOWS: A Collaborative Framework to Reproducibly Deploy and Benchmark Bioimage Analysis Workflows. *Patterns* 1, 100040. doi: 10.1016/j.patter.2020.100040
- Russell, A. J. C., Sanderson, T., Bushell, E., Talman, A. M., Anar, B., Girling, G., et al. (2021). Regulators of Male and Female Sexual Development Critical for Transmission of a Malaria Parasite. *bioRxiv* 2021. doi: 10.1101/2021.08.04.455056
- Rust, M. J., Bates, M., and Zhuang, X. (2006). Sub-Diffraction-Limit Imaging by Stochastic Optical Reconstruction Microscopy (STORM). *Nat. Methods* 3, 793–795. doi: 10.1038/nmeth929
- Ruy, P. D. C., Monteiro-Teles, N. M., Miserani Magalhães, R. D., Freitas-Castro, F., Dias, L., Aquino Defina, T. P., et al. (2019). Comparative Transcriptomics in Leishmania Braziliensis: Disclosing Differential Gene Expression of Coding and Putative Noncoding RNAs Across Developmental Stages. *RNA Biol.* 16, 639–660. doi: 10.1080/15476286.2019.1574161
- Sà, J. M., Cannon, M. V., Caleon, R. L., Welles, T. E., and Serre, D. (2020). Single-Cell Transcriptomic Analysis of Plasmodium Vivax Blood-Stage Parasites Identifies Stage- and Species-Specific Profiles of Expression. *PLoS Biol.* 18, e3000711. doi: 10.1371/journal.pbio.3000711
- Saito, Y., and Kanemaki, M. T. (2021). Targeted Protein Depletion Using the Auxin-Inducible Degron 2 (AID2) System. *Curr. Protoc.* 1, e219. doi: 10.1002/cpz1.219
- Sanderson, S. J., Xia, D., Prieto, H., Yates, J., Heiges, M., Kissinger, J. C., et al. (2008). Determining the Protein Repertoire of Cryptosporidium Parvum Sporozoites. *Proteomics* 8, 1398–1414. doi: 10.1002/pmic.200700804
- Sanger (2020). *Malaria Cell Atlas*. <https://www.sanger.ac.uk/tool/mca/>
- Schneider, C. A., Rasband, W. S., and Eliceiri, K. W. (2012). NIH Image to ImageJ: 25 Years of Image Analysis. *Nat. Methods* 9, 671–675. doi: 10.1038/nmeth.2089
- Schnider, C. B., Bausch-Fluck, D., Brühlmann, F., Heussler, V. T., and Burda, P.-C. (2018). BioID Reveals Novel Proteins of the Plasmodium Parasitophorous Vacuole Membrane. *mSphere* 3 (1), e00522-17. doi: 10.1128/mSphere.00522-17

- Schock, M., Schmidt, S., and Ersfeld, K. (2021). Novel Cytoskeleton-Associated Proteins in *Trypanosoma Brucei* Are Essential for Cell Morphogenesis and Cytokinesis. *Microorganisms* 9 (11), 2234. doi: 10.3390/microorganisms9112234
- Schulz, O., Pieper, C., Clever, M., Pfaff, J., Ruhlandt, A., Kehlenbach, R. H., et al. (2013). Resolution Doubling in Fluorescence Microscopy With Confocal Spinning-Disk Image Scanning Microscopy. *Proc. Natl. Acad. Sci. U. S. A.* 110, 21000–21005. doi: 10.1073/pnas.1315858110
- Schumann Burkard, G., Jutzi, P., and Roditi, I. (2011). Genome-Wide RNAi Screens in Bloodstream Form *Trypanosomes* Identify Drug Transporters. *Mol. Biochem. Parasitol.* 175, 91–94. doi: 10.1016/j.molbiopara.2010.09.002
- Schumann Burkard, G., Käser, S., de Araújo, P. R., Schimanski, B., Naguleswaran, A., Knüsel, S., et al. (2013). Nucleolar Proteins Regulate Stage-Specific Gene Expression and Ribosomal RNA Maturation in *Trypanosoma Brucei*. *Mol. Microbiol.* 88, 827–840. doi: 10.1111/mmi.12227
- Schwach, F., Bushell, E., Gomes, A. R., Anar, B., Girling, G., Herd, C., et al. (2015). PlasmoGEM, a Database Supporting a Community Resource for Large-Scale Experimental Genetics in Malaria Parasites. *Nucleic Acids Res.* 43, D1176–D1182. doi: 10.1093/nar/gku1143
- Shadab, M., Das, S., Banerjee, A., Sinha, R., Asad, M., Kamran, M., et al. (2019). RNA-Seq Revealed Expression of Many Novel Genes Associated With *Leishmania Donovani* Persistence and Clearance in the Host Macrophage. *Front. Cell. Infect. Microbiol.* 9. doi: 10.3389/fcimb.2019.00017
- Sharling, L., Liu, X., Gollapalli, D. R., Maurya, S. K., Hedstrom, L., and Striepen, B. (2010). A Screening Pipeline for Antiparasitic Agents Targeting *Cryptosporidium* Inosine Monophosphate Dehydrogenase. *PLoS Negl. Trop. Dis.* 4, e794. doi: 10.1371/journal.pntd.0000794
- Sharp, P. M., Plenderleith, L. J., and Hahn, B. H. (2020). Ape Origins of Human Malaria. *Annu. Rev. Microbiol.* 74, 39–63. doi: 10.1146/annurev-micro-020518-115628
- Shaw, M., Claveau, R., Manescu, P., Elmi, M., Brown, B. J., Scrimgeour, R., et al. (2021). Optical Mesoscopy, Machine Learning, and Computational Microscopy Enable High Information Content Diagnostic Imaging of Blood Films. *J. Pathol.* 255, 62–71. doi: 10.1002/path.5738
- Shears, M. J., Sekhar Nirujogi, R., Swearingen, K. E., Renuse, S., Mishra, S., Jaipal Reddy, P., et al. (2019). Proteomic Analysis of *Plasmodium* Merosomes: The Link Between Liver and Blood Stages in Malaria. *J. Proteome Res.* 18, 3404–3418. doi: 10.1021/acs.jproteome.9b00324
- Shwab, E. K., Saraf, P., Zhu, X.-Q., Zhou, D.-H., McFerrin, B. M., Ajzenberg, D., et al. (2018). Human Impact on the Diversity and Virulence of the Ubiquitous Zoonotic Parasite *Toxoplasma Gondii*. *Proc. Natl. Acad. Sci. U. S. A.* 115, E6956–E6963. doi: 10.1073/pnas.1722202115
- Sibley, L. D., and Ajioka, J. W. (2008). Population Structure of *Toxoplasma Gondii*: Clonal Expansion Driven by Infrequent Recombination and Selective Sweeps. *Annu. Rev. Microbiol.* 62, 329–351. doi: 10.1146/annurev-micro.62.081307.162925
- Sibley, L. D., and Boothroyd, J. C. (1992). Virulent Strains of *Toxoplasma Gondii* Comprise a Single Clonal Lineage. *Nature* 359, 82–85. doi: 10.1038/359082a0
- Siciliano, G., and Alano, P. (2015). Enlightening the Malaria Parasite Life Cycle: Bioluminescent *Plasmodium* in Fundamental and Applied Research. *Front. Microbiol.* 6. doi: 10.3389/fmicb.2015.00391
- Sidik, S. M., Huet, D., Ganesan, S. M., Huynh, M.-H., Wang, T., Nasamu, A. S., et al. (2016). A Genome-Wide CRISPR Screen in *Toxoplasma* Identifies Essential Apicomplexan Genes. *Cell* 166, 1423–1435.e12. doi: 10.1016/j.cell.2016.08.019
- Sidik, S. M., Huet, D., and Lourido, S. (2018). CRISPR-Cas9-Based Genome-Wide Screening of *Toxoplasma Gondii*. *Nat. Protoc.* 13, 307–323. doi: 10.1038/nprot.2017.131
- Siegel, T. N., Hekstra, D. R., Wang, X., Dewell, S., and Cross, G. A. M. (2010). Genome-Wide Analysis of mRNA Abundance in Two Life-Cycle Stages of *Trypanosoma Brucei* and Identification of Splicing and Polyadenylation Sites. *Nucleic Acids Res.* 38, 4946–4957. doi: 10.1093/nar/gkq237
- Silva Pereira, S., Casas-Sánchez, A., Haines, L. R., Ogugo, M., Absolomon, K., Sanders, M., et al. (2018). Variant Antigen Repertoires in *Trypanosoma Congolense* Populations and Experimental Infections can be Profiled From Deep Sequence Data Using Universal Protein Motifs. *Genome Res.* 28, 1383–1394. doi: 10.1101/gr.234146.118
- Silva Pereira, S., de Almeida Castilho Neto, K. J. G., Duffy, C. W., Richards, P., Noyes, H., Ogugo, M., et al. (2020). Variant Antigen Diversity in *Trypanosoma Vivax* is Not Driven by Recombination. *Nat. Commun.* 11, 844. doi: 10.1038/s41467-020-14575-8
- Silva Pereira, S., Heap, J., Jones, A. R., and Jackson, A. P. (2019a). VAPPER: High-Throughput Variant Antigen Profiling in African *Trypanosomes* of Livestock. *Gigascience* 8 (9), giz091. doi: 10.1093/gigascience/giz091
- Silva Pereira, S., and Jackson, A. P. (2018). UDP-Glycosyltransferase Genes in *Trypanosomatid* Genomes Have Diversified Independently to Meet the Distinct Developmental Needs of Parasite Adaptations. *BMC Evol. Biol.* 18, 31. doi: 10.1186/s12862-018-1149-6
- Silva Pereira, S., Trindade, S., De Niz, M., and Figueiredo, L. M. (2019b). Tissue Tropism in Parasitic Diseases. *Open Biol.* 9, 190036. doi: 10.1098/rsob.190036
- Silvester, E., Ivens, A., and Matthews, K. R. (2018). A Gene Expression Comparison of *Trypanosoma Brucei* and *Trypanosoma Congolense* in the Bloodstream of the Mammalian Host Reveals Species-Specific Adaptations to Density-Dependent Development. *PLoS Negl. Trop. Dis.* 12, e0006863–e0006863. doi: 10.1371/journal.pntd.0006863
- Sim, G. K., Kafatos, F. C., Jones, C. W., Koehler, M. D., Efstratiadis, A., and Maniatis, T. (1979). Use of a cDNA Library for Studies on Evolution and Developmental Expression of the Choriion Multigene Families. *Cell* 18, 1303–1316. doi: 10.1016/0092-8674(79)90241-1
- Singh, V., Gupta, P., and Pande, V. (2014). Revisiting the Multigene Families: Plasmodium Var and Vir Genes. *J. Vector Borne Dis.* 51, 75–81.
- Sistrom, M., Evans, B., Benoit, J., Balmer, O., Aksoy, S., and Caccione, A. (2016). *De Novo* Genome Assembly Shows Genome Wide Similarity Between *Trypanosoma Brucei* *Brucei* and *Trypanosoma Brucei* *Rhodesiense*. *PLoS One* 11, e0147660. doi: 10.1371/journal.pone.0147660
- Sistrom, M., Evans, B., Bjornson, R., Gibson, W., Balmer, O., Mäser, P., et al. (2014). Comparative Genomics Reveals Multiple Genetic Backgrounds of Human Pathogenicity in The *Trypanosoma Brucei* Complex. *Genome Biol. Evol.* 6, 2811–2819. doi: 10.1093/gbe/evu222
- Smith, T. A., Lopez-Perez, G. S., Shortt, E., and Lourido, S. (2022). Screening The *Toxoplasma* Kinome With High-throughput Tagging Identifies A Regulator Of Invasion and Egress. *Nat. Microb.* doi: 10.1038/s41564-022-01104-0
- Smith, H. V., Nichols, R. A. B., and Grimason, A. M. (2005). *Cryptosporidium* Excystation and Invasion: Getting to the Guts of the Matter. *Trends Parasitol.* 21, 133–142. doi: 10.1016/j.pt.2005.01.007
- Snelling, W. J., Lin, Q., Moore, J. E., Millar, B. C., Tosini, F., Pozio, E., et al. (2007). Proteomics Analysis and Protein Expression During Sporozoite Excystation of *Cryptosporidium Parvum* (Coccidia, Apicomplexa). *Mol. Cell. Proteomics* 6, 346–355. doi: 10.1074/mcp.M600372-MCP200
- Spark, A., Kitching, A., Esteban-Ferrer, D., Handa, A., Carr, A. R., Needham, L.-M., et al. (2020). vLUME: 3D Virtual Reality for Single-Molecule Localization Microscopy. *Nat. Methods* 17, 1097–1099. doi: 10.1038/s41592-020-0962-1
- Stanway, R. R., Bushell, E., Chiappino-Pepe, A., Roques, M., Sanderson, T., Franke-Fayard, B., et al. (2019). Genome-Scale Identification of Essential Metabolic Processes for Targeting the *Plasmodium* Liver Stage. *Cell* 179, 1112–1128.e26. doi: 10.1016/j.cell.2019.10.030
- Steinbiss, S., Silva-Franco, F., Brunk, B., Foth, B., Hertz-Fowler, C., Berriman, M., et al. (2016). Companion: A Web Server for Annotation and Analysis of Parasite Genomes. *Nucleic Acids Res.* 44, W29–W34. doi: 10.1093/nar/gkw292
- Steinfeldt, T., Könen-Waisman, S., Tong, L., Pawlowski, N., Lamkemeyer, T., Sibley, L. D., et al. (2010). Phosphorylation of Mouse Immunity-Related GTPase (IRG) Resistance Proteins is an Evasion Strategy for Virulent *Toxoplasma Gondii*. *PLoS Biol.* 8, e1000576. doi: 10.1371/journal.pbio.1000576
- Stevens, J., Noyes, H., and Gibson, W. (1998). The Evolution of *Trypanosomes* Infecting Humans and Primates. *Mem. Inst. Oswaldo Cruz* 93, 669–676. doi: 10.1590/s0074-02761998000500019
- Subramanian, I., Verma, S., Kumar, S., Jere, A., and Anamika, K. (2020). Multi-Omics Data Integration, Interpretation, and Its Application. *Bioinform. Biol. Insights* 14, 1177932219899051. doi: 10.1177/1177932219899051
- Su, C., Evans, D., Cole, R. H., Kissinger, J. C., Ajioka, J. W., and Sibley, L. D. (2003). Recent Expansion of *Toxoplasma* Through Enhanced Oral Transmission. *Science* 299, 414–416. doi: 10.1126/science.1078035
- Sutrave, S., and Richter, M. H. (2021). The Truman Show for Protozoan Parasites: A Review of *In Vitro* Cultivation Platforms. *PLoS Negl. Trop. Dis.* 15, e0009668. doi: 10.1371/journal.pntd.0009668

- Svensen, N., Wyllie, S., Gray, D. W., and De Rycker, M. (2021). Live-Imaging Rate-of-Kill Compound Profiling for Chagas Disease Drug Discovery With A New Automated High-Content Assay. *PLoS Negl. Trop. Dis.* 15, e0009870. doi: 10.1371/journal.pntd.0009870
- Syed, A. J., and Anderson, J. C. (2021). Applications of Bioluminescence in Biotechnology and Beyond. *Chem. Soc. Rev.* 50, 5668–5705. doi: 10.1039/d0cs01492c
- Sykes, M. L., and Avery, V. M. (2015). Development and Application of a Sensitive, Phenotypic, High-Throughput Image-Based Assay to Identify Compound Activity Against *Trypanosoma Cruzi* Amastigotes. *Int. J. Parasitol. Drugs Drug Resist.* 5, 215–228. doi: 10.1016/j.ijpddr.2015.10.001
- Tandel, J., English, E. D., Sateriale, A., Gullicksrud, J. A., Beiting, D. P., Sullivan, M. C., et al. (2019). Life Cycle Progression and Sexual Development of the Apicomplexan Parasite *Cryptosporidium Parvum*. *Nat. Microbiol.* 4, 2226–2236. doi: 10.1038/s41564-019-0539-x
- Tegazzini, D., Diaz, R., Aguilar, F., Peña, I., Presa, J. L., Yardley, V., et al. (2016). A Replicative *In Vitro* Assay for Drug Discovery Against *Leishmania Donovanii*. *Antimicrob. Agents Chemother.* 60, 3524–3532. doi: 10.1128/AAC.01781-15
- Tenter, A. M., Heckeroth, A. R., and Weiss, L. M. (2000). *Toxoplasma Gondii*: From Animals to Humans. *Int. J. Parasitol.* 30, 1217–1258. doi: 10.1016/S0020-7519(00)00124-7
- Tichkule, S., Cacciò, S. M., Robinson, G., Chalmers, R. M., Mueller, I., Emery-Corbin, S. J., et al. (2022). Global Population Genomics of Two Subspecies of *Cryptosporidium Hominis* During 500 Years of Evolution. *Mol. Biol. Evol.* 39, msac056. doi: 10.1093/molbev/msac056
- Tihon, E., Imamura, H., Dujardin, J.-C., Van Den Abbeele, J., and Van den Broeck, F. (2017). Discovery and Genomic Analyses of Hybridization Between Divergent Lineages of *Trypanosoma Congolense*, Causative Agent of Animal African Trypanosomiasis. *Mol. Ecol.* 26, 6524–6538. doi: 10.1111/mec.14271
- Tinti, M., Güther, M. L. S., Crozier, T. W. M., Lamond, A. I., and Ferguson, M. A. J. (2019). Proteome Turnover in the Bloodstream and Procytic Forms of *Trypanosoma Brucei* Measured by Quantitative Proteomics. *Wellcome Open Res.* 4, 152. doi: 10.12688/wellcomeopenres.15421.1
- Tirado, T. C., de Andrade, A. J., Ribeiro, M. C. V., da, C., and Figueiredo, F. B. (2020). Use of the high-content imaging system equipment to evaluate *in vitro* infection by *Leishmania braziliensis* in response to sand fly *Nyssomyia neivai* saliva. *Acta Trop.* 209, 105540. doi: 10.1016/j.actatropica.2020.105540
- Tomasina, R., González, F. C., and Francia, M. E. (2021). Structural and Functional Insights Into the Microtubule Organizing Centers of *Toxoplasma Gondii* and *Plasmodium Spp.* *Microorganisms* 9(12):2503. doi: 10.3390/microorganisms9122503
- Tong, J. X., Chandramohanadas, R., and Tan, K. S.-W. (2018). High-Content Screening of the Medicines for Malaria Venture Pathogen Box for *Plasmodium Falciparum* Digestive Vacuole-Disrupting Molecules Reveals Valuable Starting Points for Drug Discovery. *Antimicrob. Agents Chemother.* 62 (3), e02031-17. doi: 10.1128/AAC.02031-17
- Tosi, S., Bardia, L., Filgueira, M. J., Calon, A., and Colombelli, J. (2020). LOBSTER: An Environment to Design Bioimage Analysis Workflows for Large and Complex Fluorescence Microscopy Data. *Bioinformatics* 36, 2634–2635. doi: 10.1093/bioinformatics/btz945
- Touquet, B., Pelissier, L., Cavailles, P., Yi, W., Bellini, V., Mercier, C., et al. (2018). High-Content Imaging Assay to Evaluate *Toxoplasma Gondii* Infection and Proliferation: A Multiparametric Assay to Screen New Compounds. *PLoS One* 13, e0201678. doi: 10.1371/journal.pone.0201678
- Trecek, M., Sanders, J. L., Gaji, R. Y., LaFavers, K. A., Child, M. A., Arrizabalaga, G., et al. (2014). The Calcium-Dependent Protein Kinase 3 of *Toxoplasma* Influences Basal Calcium Levels and Functions Beyond Egress as Revealed by Quantitative Phosphoproteome Analysis. *PLoS Pathog.* 10, e1004197. doi: 10.1371/journal.ppat.1004197
- Trindade, S., Rijo-Ferreira, F., Carvalho, T., Pinto-Neves, D., Guegan, F., Aresta-Branco, F., et al. (2016). *Trypanosoma Brucei* Parasites Occupy and Functionally Adapt to the Adipose Tissue in Mice. *Cell Host Microbe* 19, 837–848. doi: 10.1016/j.chom.2016.05.002
- Trinkle-Mulcahy, L. (2019). Recent Advances in Proximity-Based Labeling Methods for Interactome Mapping. *F1000Research* 8, F1000 Faculty Rev-135. doi: 10.12688/f1000research.16903.1
- Truong, Q., and Ferrari, B. C. (2006). Quantitative and Qualitative Comparisons of *Cryptosporidium* Faecal Purification Procedures for the Isolation of Oocysts Suitable for Proteomic Analysis. *Int. J. Parasitol.* 36, 811–819. doi: 10.1016/j.ijpara.2006.02.023
- Turnbull, C., Scott, R. H., Thomas, E., Jones, L., Murugaesu, N., Pretty, F. B., et al. (2018). The 100 000 Genomes Project: Bringing Whole Genome Sequencing to the NHS. *BMJ* 361, k1687. doi: 10.1136/bmj.k1687
- Turra, G. L., Schneider, L., Liedgens, L., and Deponte, M. (2021). Testing the CRISPR-Cas9 and glmS Ribozyme Systems in *Leishmania Tarentolae*. *Mol. Biochem. Parasitol.* 241, 111336. doi: 10.1016/j.molbiopara.2020.111336
- Ullah, I., Sharma, R., Biagini, G. A., and Horrocks, P. (2017). A Validated Bioluminescence-Based Assay for the Rapid Determination of the Initial Rate of Kill for Discovery Antimalarials. *J. Antimicrob. Chemother.* 72, 717–726. doi: 10.1093/jac/dkw449
- Valdivia, H. O., Scholte, L. L. S., Oliveira, G., Gabaldón, T., and Bartholomeu, D. C. (2015). The *Leishmania* Metaphylogeny: A Comprehensive Survey of *Leishmania* Protein Phylogenetic Relationships. *BMC Genomics* 16, 887. doi: 10.1186/s12864-015-2091-2
- Vangindertael, J., Camacho, R., Sempels, W., Mizuno, H., Dedeker, P., and Janssen, K. P. F. (2018). An Introduction to Optical Super-Resolution Microscopy for the Adventurous Biologist. *Methods Appl. Fluoresc.* 6, 22003. doi: 10.1088/2050-6120/aae0c
- Velculescu, V. E., Zhang, L., Vogelstein, B., and Kinzler, K. W. (1995). Serial Analysis of Gene Expression. *Science* 270, 484–487. doi: 10.1126/science.270.5235.484
- Velculescu, V. E., Zhang, L., Zhou, W., Vogelstein, J., Basrai, M. A., Bassett, D. E. J., et al. (1997). Characterization of the Yeast Transcriptome. *Cell* 88, 243–251. doi: 10.1016/S0092-8674(00)81845-0
- Vélez-Ramírez, D. E., Shimogawa, M. M., Ray, S. S., Lopez, A., Rayatpisheh, S., Langousis, G., et al. (2021). APEX2 Proximity Proteomics Resolves Flagellum Subdomains and Identifies Flagellum Tip-Specific Proteins in *Trypanosoma Brucei*. *mSphere* 6(1):e01090-20. doi: 10.1128/mSphere.01090-20
- Verner, Z., Paris, Z., and Lukes, J. (2010). Mitochondrial Membrane Potential-Based Genome-Wide RNAi Screen of *Trypanosoma Brucei*. *Parasitol. Res.* 106, 1241–1244. doi: 10.1007/s00436-010-1754-9
- Videval, E. (2018). *Plasmodium* Parasites of Birds Have the Most AT-Rich Genes of Eukaryotes. *Microb. Genomics* 4 (2), e000150. doi: 10.1099/mgen.0.000150
- Vigneron, A., O'Neill, M. B., Weiss, B. L., Savage, A. F., Campbell, O. C., Kamhawi, S., et al. (2020). Single-Cell RNA Sequencing of *Trypanosoma Brucei* From Tsetse Salivary Glands Unveils Metacylogenesis and Identifies Potential Transmission Blocking Antigens. *Proc. Natl. Acad. Sci. U. S. A.* 117, 2613–2621. doi: 10.1073/pnas.1914423117
- Vinayak, S., Pawlowicz, M. C., Sateriale, A., Brooks, C. F., Studstill, C. J., Bar-Peled, Y., et al. (2015). Genetic Modification of the Diarrhoeal Pathogen *Cryptosporidium Parvum*. *Nature* 523, 477–480. doi: 10.1038/nature14651
- von Ardenne, M. (1938). Das Elektronen-Rastermikroskop. *Z. für Phys.* 109, 553–572. doi: 10.1007/BF01341584
- von Chamier, L., Laine, R. F., and Henriques, R. (2019). Artificial Intelligence for Microscopy: What You Should Know. *Biochem. Soc. Trans.* 47, 1029–1040. doi: 10.1042/BST20180391
- von Chamier, L., Laine, R. F., Jukkala, J., Spahn, C., Krentzel, D., Nehme, E., et al. (2021). Democratizing Deep Learning for Microscopy With ZeroCostDL4Mic. *Nat. Commun.* 12, 2276. doi: 10.1038/s41467-021-22518-0
- Vos, M. W., Stone, W. J. R., Koolen, K. M., van Gemert, G.-J., van Schaijk, B., Leroy, D., et al. (2015). A Semi-Automated Luminescence Based Standard Membrane Feeding Assay Identifies Novel Small Molecules That Inhibit Transmission of Malaria Parasites by Mosquitoes. *Sci. Rep.* 5, 18704. doi: 10.1038/srep18704
- Wakaguri, H., Suzuki, Y., Sasaki, M., Sugano, S., and Watanabe, J. (2009). Inconsistencies of Genome Annotations in Apicomplexan Parasites Revealed by 5'-End-One-Pass and Full-Length Sequences of Oligo-Capped cDNAs. *BMC Genomics* 10, 312. doi: 10.1186/1471-2164-10-312
- Waldman, B. S., Schwarz, D., Wadsworth, M. H.2nd, Saeji, J. P., Shalek, A. K., and Lourido, S. (2020). Identification of a Master Regulator of Differentiation in *Toxoplasma*. *Cell* 180, 359–372.e16. doi: 10.1016/j.cell.2019.12.013

- Wang, W., Peng, D., Baptista, R. P., Li, Y., Kissinger, J. C., and Tarleton, R. L. (2021). Strain-Specific Genome Evolution in *Trypanosoma Cruzi*, the Agent of Chagas Disease. *PLoS Pathog.* 17, e1009254. doi: 10.1371/journal.ppat.1009254
- Wang, Y., Sangaré, L. O., Paredes-Santos, T. C., Hassan, M. A., Krishnamurthy, S., Furuta, A. M., et al. (2020). Genome-Wide Screens Identify *Toxoplasma Gondii* Determinants of Parasite Fitness in IFN- γ -Activated Murine Macrophages. *Nat. Commun.* 11, 5258. doi: 10.1038/s41467-020-18991-8
- Wang, Z.-X., Zhou, C.-X., Elsheikha, H. M., He, S., Zhou, D.-H., and Zhu, X.-Q. (2017). Proteomic Differences Between Developmental Stages of *Toxoplasma Gondii* Revealed by iTRAQ-Based Quantitative Proteomics. *Front. Microbiol.* 8. doi: 10.3389/fmicb.2017.00985
- Warrenfeltz, S., Basenko, E. Y., Crouch, K., Harb, O. S., Kissinger, J. C., Roos, D. S., et al. (2018). EuPathDB: The Eukaryotic Pathogen Genomics Database Resource. *Methods Mol. Biol.* 1757, 69–113. doi: 10.1007/978-1-4939-7737-6_5
- Warrenfeltz, S., and Kissinger, J. C. (2020). Accessing *Cryptosporidium* Omic and Isolate Data via CryptoDB.Org. *Methods Mol. Biol.* 2052, 139–192. doi: 10.1007/978-1-4939-9748-0_10
- Weir, W., Capewell, P., Foth, B., Clucas, C., Pountain, A., Stekete, P., et al. (2016). Population Genomics Reveals the Origin and Asexual Evolution of Human Infective *Trypanosomes*. *Elife* 5, e11473. doi: 10.7554/eLife.11473
- Wheeler, R. J. (2020). ImageJ for Partially and Fully Automated Analysis of *Trypanosome* Micrographs. *Methods Mol. Biol.* 2116, 385–408. doi: 10.1007/978-1-0716-0294-2_24
- Wheeler, R. J., Gull, K., and Gluenz, E. (2012). Detailed Interrogation of *Trypanosome* Cell Biology via Differential Organelle Staining and Automated Image Analysis. *BMC Biol.* 10, 1. doi: 10.1186/1741-7007-10-1
- WHO (2021a). *Malaria*. Available at: https://www.who.int/health-topics/malaria#tab=tab_1.
- WHO (2021b). *Chagas Disease (American trypanosomiasis)*. Available at: <https://www.who.int/health-topics/chagas-disease>.
- WHO (2021c). *Leishmaniasis*. https://www.who.int/health-topics/leishmaniasis#tab=tab_1.
- WHO (2021d). *Human African Trypanosomiasis*. https://www.who.int/health-topics/human-african-trypanosomiasis#tab=tab_1
- Wichers, J. S., Wunderlich, J., Heincke, D., Pazicky, S., Strauss, J., Schmitt, M., et al. (2021). Identification of Novel Inner Membrane Complex and Apical Annuli Proteins of the Malaria Parasite *Plasmodium Falciparum*. *Cell. Microbiol.* 23, e13341. doi: 10.1111/cmi.13341
- Widmer, G., Lee, Y., Hunt, P., Martinelli, A., Tolkoff, M., and Bodi, K. (2012). Comparative Genome Analysis of Two *Cryptosporidium Parvum* Isolates With Different Host Range. *Infect. Genet. Evol. J. Mol. Epidemiol. Evol. Genet. Infect. Dis.* 12, 1213–1221. doi: 10.1016/j.meegid.2012.03.027
- Wilke, G., Funkhouser-Jones, L. J., Wang, Y., Ravindran, S., Wang, Q., Beatty, W. L., et al. (2019). A Stem-Cell-Derived Platform Enables Complete *Cryptosporidium* Development In Vitro and Genetic Tractability. *Cell Host Microbe* 26, 123–134.e8. doi: 10.1016/j.chom.2019.05.007
- Willig, K. I., Rizzoli, S. O., Westphal, V., Jahn, R., and Hell, S. W. (2006). STED Microscopy Reveals That Synaptotagmin Remains Clustered After Synaptic Vesicle Exocytosis. *Nature* 440, 935–939. doi: 10.1038/nature04592
- Xiao, T., and Zhou, W. (2020). The Third Generation Sequencing: The Advanced Approach to Genetic Diseases. *Transl. Pediatr.* 9, 163–173. doi: 10.21037/tp.2020.03.06
- Xu, D., Brandán, C. P., Basombrio, M. A., and Tarleton, R. L. (2009). Evaluation of High Efficiency Gene Knockout Strategies for *Trypanosoma Cruzi*. *BMC Microbiol.* 9, 90. doi: 10.1186/1471-2180-9-90
- Xue, Y., Theisen, T. C., Rastogi, S., Ferrel, A., Quake, S. R., and Boothroyd, J. C. (2020). A Single-Parasite Transcriptional Atlas of *Toxoplasma Gondii* Reveals Novel Control Of Antigen Expression. *Elife* 9, e54129. doi: 10.7554/eLife.54129
- Xu, P., Widmer, G., Wang, Y., Ozaki, L. S., Alves, J. M., Serrano, M. G., et al. (2004). The Genome of *Cryptosporidium Hominis*. *Nature* 431, 1107–1112. doi: 10.1038/nature02977
- Yanta, C. A., Bessonov, K., Robinson, G., Troell, K., and Guy, R. A. (2021). CryptoGenotyper: A New Bioinformatics Tool for Rapid *Cryptosporidium* Identification. *Food waterborne Parasitol.* 23, e00115. doi: 10.1016/j.fawpar.2021.e00115
- Yazdanparast, E., Dos Anjos, A., Garcia, D., Loeuillet, C., Shahbazkia, H. R., and Vergnes, B. (2014). INsPECT, an Open-Source and Versatile Software for Automated Quantification of (*Leishmania*) Intracellular Parasites. *PLoS Negl. Trop. Dis.* 8, e2850. doi: 10.1371/journal.pntd.0002850
- Ye, Z., Bath, T. S., Rüther, P., and Olsen, J. V. (2022). A Deeper Look at Carrier Proteome Effects for Single-Cell Proteomics. *Commun. Biol.* 5, 150. doi: 10.1038/s42003-022-03095-4
- Yesholatova, A., Saito, Y., Kitamoto, N., Makino-Itou, H., Ajima, R., Nakano, R., et al. (2020). The Auxin-Inducible Degron 2 Technology Provides Sharp Degradation Control in Yeast, Mammalian Cells, and Mice. *Nat. Commun.* 11, 5701. doi: 10.1038/s41467-020-19532-z
- Yin, W., Brittain, D., Borseth, J., Scott, M. E., Williams, D., Perkins, J., et al. (2020). A Petascale Automated Imaging Pipeline for Mapping Neuronal Circuits With High-Throughput Transmission Electron Microscopy. *Nat. Commun.* 11, 4949. doi: 10.1038/s41467-020-18659-3
- Yip, K. M., Fischer, N., Paknia, E., Chari, A., and Stark, H. (2020). Atomic-Resolution Protein Structure Determination by Cryo-EM. *Nature* 587, 157–161. doi: 10.1038/s41586-020-2833-4
- Yoon, J., Jang, W. S., Nam, J., Mihn, D.-C., and Lim, C. S. (2021). An Automated Microscopic Malaria Parasite Detection System Using Digital Image Analysis. *Diagnostics (Basel Switzerland)* 11 (3), 527. doi: 10.3390/diagnostics11030527
- York, A. G., Chandris, P., Nogare, D. D., Head, J., Wawrzusin, P., Fischer, R. S., et al. (2013). Instant Super-Resolution Imaging in Live Cells and Embryos via Analog Image Processing. *Nat. Methods* 10, 1122–1126. doi: 10.1038/nmeth.2687
- Young, J., Dominicus, C., Wagener, J., Butterworth, S., Ye, X., Kelly, G., et al. (2019). A CRISPR Platform for Targeted *In Vivo* Screens Identifies *Toxoplasma Gondii* Virulence Factors in Mice. *Nat. Commun.* 10, 3963. doi: 10.1038/s41467-019-11855-w
- Yu, X., Zhang, H., and Zhu, G. (2017). Characterization of Host Cell Mutants Significantly Resistant to *Cryptosporidium Parvum* Infection. *J. Eukaryot. Microbiol.* 64, 843–849. doi: 10.1111/jeu.12419
- Zhang, M., Wang, C., Otto, T. D., Oberstaller, J., Liao, X., Adapa, S. R., et al. (2018). Uncovering the Essential Genes of the Human Malaria Parasite *Plasmodium Falciparum* by Saturation Mutagenesis. *Science* 360 (6388), eaap7847. doi: 10.1126/science.aap7847

Conflict of Interest: The authors declare that the research was conducted in the absence of any commercial or financial relationships that could be construed as a potential conflict of interest.

Publisher's Note: All claims expressed in this article are solely those of the authors and do not necessarily represent those of their affiliated organizations, or those of the publisher, the editors and the reviewers. Any product that may be evaluated in this article, or claim that may be made by its manufacturer, is not guaranteed or endorsed by the publisher.

Copyright © 2022 Kent, Briggs, Colon, Alvarez, Silva Pereira and De Niz. This is an open-access article distributed under the terms of the Creative Commons Attribution License (CC BY). The use, distribution or reproduction in other forums is permitted, provided the original author(s) and the copyright owner(s) are credited and that the original publication in this journal is cited, in accordance with accepted academic practice. No use, distribution or reproduction is permitted which does not comply with these terms.



Adapt or Die: Targeting Unique Transmission-Stage Biology for Malaria Elimination

Mariëtte E. van der Watt¹, Janette Reader^{1,2} and Lyn-Marié Birkholtz^{1,2*}

¹ Institute for Sustainable Malaria Control, School of Health Systems and Public Health, University of Pretoria, Pretoria, South Africa, ² Department of Biochemistry, Genetics and Microbiology, University of Pretoria, Pretoria, South Africa

OPEN ACCESS

Edited by:

Tania F. De Koning-Ward,
Deakin University, Australia

Reviewed by:

Michael Delves,
University of London, United Kingdom
Mariana De Niz,
Universidade de Lisboa, Portugal

*Correspondence:

Lyn-Marié Birkholtz
lbirkholtz@up.ac.za

Specialty section:

This article was submitted to
Parasite and Host,
a section of the journal
Frontiers in Cellular and
Infection Microbiology

Received: 22 March 2022

Accepted: 06 May 2022

Published: 09 June 2022

Citation:

van der Watt ME, Reader J and
Birkholtz L-M (2022) Adapt or Die:
Targeting Unique Transmission-Stage
Biology for Malaria Elimination.
Front. Cell. Infect. Microbiol. 12:901971.
doi: 10.3389/fcimb.2022.901971

Plasmodium parasites have a complex life cycle that includes development in the human host as well as the *Anopheles* vector. Successful transmission of the parasite between its host and vector therefore requires the parasite to balance its investments in asexual replication and sexual reproduction, varying the frequency of sexual commitment to persist within the human host and generate future opportunities for transmission. The transmission window is extended further by the ability of stage V gametocytes to circulate in peripheral blood for weeks, whereas immature stage I to IV gametocytes sequester in the bone marrow and spleen until final maturation. Due to the low gametocyte numbers in blood circulation and with the ease of targeting such life cycle bottlenecks, transmission represents an efficient target for therapeutic intervention. The biological process of *Plasmodium* transmission is a multistage, multifaceted process and the past decade has seen a much deeper understanding of the molecular mechanisms and regulators involved. Clearly, specific and divergent processes are used during transmission compared to asexual proliferation, which both poses challenges but also opportunities for discovery of transmission-blocking antimalarials. This review therefore presents an update of our molecular understanding of gametocyte and gamete biology as well as the status of transmission-blocking activities of current antimalarials and lead development compounds. By defining the biological components associated with transmission, considerations for the development of new transmission-blocking drugs to target such untapped but unique biology is suggested as an important, main driver for transmission-blocking drug discovery.

Keywords: antimalarials, gamete, gametocyte, malaria, *Plasmodium*, sexual commitment, transmission blocking

Abbreviations: ABS, asexual blood stage; AP2-G, Apetala 2-G; CCp, complement control protein; CDPK1, calcium dependent protein kinase 1; EDC, exo-erythrocytic developmental cycle; EF2, Elongation factor 2; GDV-1, gametocyte development 1; HKMT, histone lysine methyltransferases; HP1, heterochromatin protein 1; IDC, intra-erythrocytic developmental cycle; IMC, inner membrane complex; GEXP, gametocyte exported proteins; MDV-1, male development protein 1; NPP, new permeation pathways; PEG3, protein of early gametocyte 3; PMT, phosphoethanolamine methyltransferase; STEVOR, subtelomeric variable open reading frame.

INTRODUCTION

Amongst infectious diseases, malaria has caused one of the most longstanding global health burdens ever. The impact of malaria on public health systems and socio-economic growth remains hard felt in several developing countries, with the World Health Organization (WHO) Africa region still carrying 94% of the global malaria burden. Concerted global efforts aimed towards malaria elimination did result in a 28% reduction in global malaria morbidity and 43% reduction in mortality, with countries such as Algeria, Argentina, China, and El Salvador now newly certified as malaria-free. Unfortunately, aside from these successes, global progress has stalled since 2015. In 2020 alone, there were approximately 241 million cases in 85 malaria-endemic countries with an estimated 627 000 deaths (WHO, 2021). Alarming increases in both incident rates (9%) and the number of fatalities (12%) were observed year-on-year due to compounding factors, not least of which were disruptions experienced in clinical services caused by the ongoing COVID-19 pandemic (WHO, 2021). Although most of the gains against this disease are the result of highly effective vector control strategies, the efficacy of these is also under threat and effective elimination of the disease must rely on multipronged approaches. These include using tools to target the parasite pool as causative agent for disease, with innovations including vaccines such as RTS,S recently approved by the WHO for use in children under five (Laurens, 2020), and using antimalarial agents for additional applications aside from their continued chemotherapeutical use. This importantly also includes transmission-blocking capabilities, although the majority of clinically used antimalarials do not have this ability mostly due to differences associated with the variant biology of the different life cycle forms of malaria parasites (Burrows et al., 2017; Birkholtz et al., 2022). This therefore motivates strategies towards the discovery of transmission-blocking antimalarial agents, focused on targeting unique transmission-associated biology; both as the focus of this review.

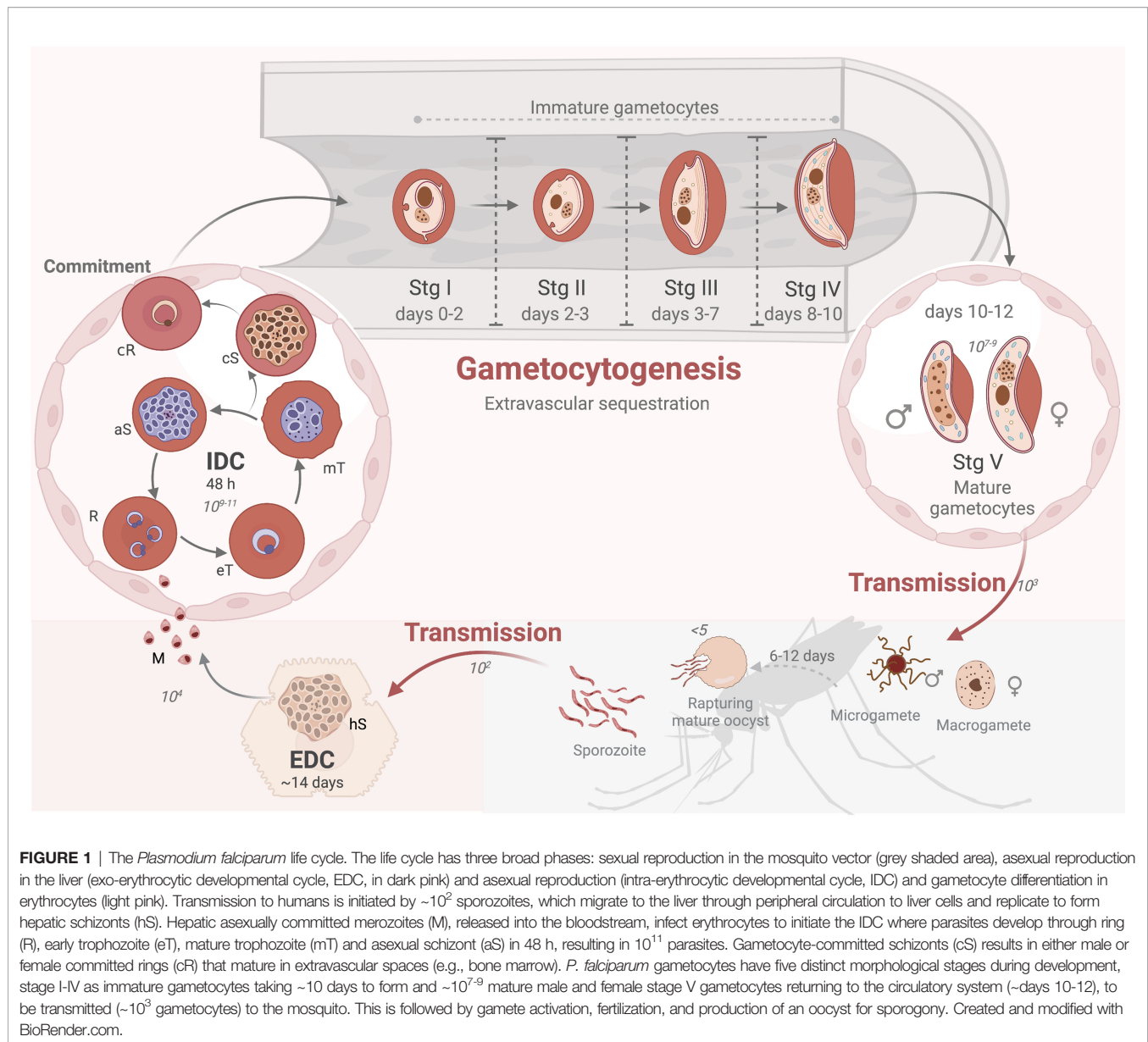
PLASMODIUM SPP. AND TRANSMISSION TO MOSQUITOES

Infectious diseases caused by parasites represent some of the most complex and complicated biological systems, the least of which is malaria. This disease requires intricate interplay of three entities – the human host (with all its genotypic and social complexities), ~40 dominant malaria transmission species of *Anopheles* mosquitoes and parasitic protists of the genus *Plasmodium*. Not only can six species of *Plasmodium* cause various severity of disease in humans [including *P. falciparum*, *P. vivax*, *P. malariae*, *P. ovale* (with subspecies *P. ovale curtisi* and *P. ovale wallikeri*), and zoonotic *P. knowlesi* and *P. cynomolgi*, (Ngotho et al., 2019)], but these parasites have some of the most complex life cycles yet characterized.

An infection in humans is initiated when as few as 100 sporozoites of the 10^3 available in the salivary gland of a

feeding female *Anopheles* mosquito are injected into the skin of a human as it takes a blood meal (Graumans et al., 2020). These sporozoites are the result of sporogony in a mature oocyst that formed in an infective mosquito after 6–12 days (Figure 1). Upon inoculation, sporozoites glide through the dermis into peripheral blood circulation within 30 min and migrate to the liver sinusoids to infect hepatocytes within 2 min, followed by the initiation of exo-erythrocytic schizogony (Prudencio et al., 2006). This characterizes the first obligate intracellular auxotroph stage as a true hallmark of parasitism. Succeeding ~14 rounds of replication in the liver during the asexual, exo-erythrocytic developmental cycle (EDC, Figure 1), mass cytokinesis occurs followed by the release of $\sim 10^4$ of hepatic merozoites from a single sporozoite into the bloodstream. Blood stage infection is established when these merozoites invade erythrocytes, thus initiating the asexual 48 h intra-erythrocytic developmental cycle (IDC, Figure 1). A single, haploid merozoite evolves into a ring-stage parasite within 6 h post-invasion (hpi) (Butler et al., 2014; Van Biljon et al., 2018), followed by development into metabolically active trophozoites (Teng et al., 2009). Schizogony commences when the single trophozoite nucleus begins to divide into two daughter nuclear bodies around 33–36 hpi and results in a polyploid, multi-nucleated syncytium (Gerald et al., 2011; Van Biljon et al., 2018; Simon et al., 2021). Erythrocyte rupture occurs at 42–48 hpi, releasing 8–24 merozoites per schizont (Bannister and Mitchell, 2003; Gerald et al., 2011) and each released merozoite proceeds to infect a new erythrocyte, allowing for persistent cycles of infection. This coordinated, rapid amplification results in a massive population expansion for the parasite, reaching up to 10^{11} parasites per infected, untreated, immune-naïve individual, and is enabled by the ability of the parasite to evade the immune system, efficiently use its intracellular microenvironment for cellular growth ('tropho' for nourishment) and asexual replication (schizogony). This highly coordinated replication cycle is associated with malaria pathology in humans.

Possibly the most extraordinary and important biological feat associated with the parasite's life cycle is its ability to differentiate to ensure transmission, and therefore continued spread of the disease and guaranteed survival of the organism (Figure 1). In a terminal differentiative process, only a small sub-population of asexual parasites (<10%) commit to sexual differentiation during an IDC, thereby ensuring the remaining proliferating parasites are available to seed subsequent differentiation and cause continuous transmission. This initiates gametocytogenesis to ensure transmission, a process requiring only 10^3 mature male and female gametocytes in an average 1–2 μL *Anopheles* blood meal. It is during this process that these gametocytes are activated, and male gametocytes respond to the changed environment to undergo an extraordinary 3 mitotic divisions, forming 8 axonemes in <20 min (in a process called exflagellation) as one of the best examples of the ability of eukaryotic cells to respond rapidly to signaling events (Figure 1). Although most *Plasmodium* spp. form gametocytes within ~24–48 h, in the most important human malaria parasite, *P. falciparum*, gametocytes uniquely develop through five



morphologically, biochemically and physiologically distinct stages in 10-12 days (**Figure 1**) (Sinden et al., 1977; Dixon and Tilley, 2021). This prolonged development is unique to the *Laverania* [*falciparum* and *reichenowi* (Ngotho et al., 2019)]. Additionally, gametocytogenesis in *P. falciparum* is associated with tissue sequestration of immature forms around erythroblastic islands in e.g. the bone marrow parenchyma (Venugopal et al., 2020), which is mechanistically different to asexual parasite infected erythrocyte sequestration to host cells in both *P. falciparum* and other rodent spp (Tiburcio et al., 2013). Lastly, prolonged survival of mature forms [mean lifespan ~ 5.5 days, *in vivo* circulation of up to 55 days (Bousema et al., 2010)] also conceptually contributes to the sustained transmission success that is achieved by *P. falciparum*.

P. falciparum stage I gametocytes resemble the rounded, asexual trophozoite but can be distinguished from these since

hemozoin crystals do not form punctate clusters in stage I gametocytes (Brancucci et al., 2018) and there are no knobs on the host cell (**Figure 1**). Stage II gametocytes mark the start of drastic morphological changes, and these adopt a lemon shape with mononuclear content. As stage II to stage III transition occurs, the gametocyte (including its nucleus and mitochondria) elongates to a length to width of ratio $\sim 2:1$, facilitated by extensive ultrastructural changes, with one side flattening while the opposite side curves forming an elongated D-shape (top hat shape) (Parkyn Schneider et al., 2017; Dixon and Tilley, 2021). The nuclear elongation (maximal in stage III, retracts in stage V) is clear from 3D analysis performed through serial block-face scanning electron microscopy (EM) (Parkyn Schneider et al., 2017) and reiterated in a study of gametocyte nuclear pore proteins, visualized by fluorescence microscopy (Boltryk et al., 2021).

Sexual dimorphism now also becomes more pronounced with small differences microscopically observable between the sexes, including the larger nucleus of the male and the cytoplasm of the female now containing more mitochondria (detectable through fluorescent probes) and extensive endoplasmic reticulum (ER), Golgi vesicles and dense spherules (the latter observed by electron microscopy) compared to the male. Stage IV gametocytes are maximally elongated with a crescent banana shape (length to width ratio of 4:1) with aciculate ends; this differentiates them from mature stage V male and female gametocytes (macro- and microgametocytes). These retain the characteristic falciform crescent shape from which the species *falciparum* derives its name ('falx' meaning sickle or curved shape and 'parere' to 'bring forth'). These mature stages have characteristic rounded ends and a length to width of ratio of 3:1; the host erythrocyte is reduced to a thin background layer referred to as a Laveran's bib. Female gametocytes are distinguished from males as they are slightly more curved and have concentrated nuclear material, well developed ER, mitochondria and apicoplast in preparation for development as zygote. Membrane-bound osmiophilic bodies are visible in both sexes as distinct vesicle-like structures and allow release of the gametocytes from the erythrocytes during gametogenesis.

TARGETING TRANSMISSION FOR MALARIA ELIMINATION

Interventions that will inhibit the formation of gametocytes, and thereby transmission, are required to contribute to malaria elimination strategies (Leroy et al., 2014; Birkholtz et al., 2016; Sinden, 2017; Delves et al., 2018a; Birkholtz et al., 2022). There are multiple reasons why human to mosquito transmission of *Plasmodium* is an attractive target for intervention. Gametocytes represent a targetable population bottleneck (Sinden, 2017); they are present in the pharmacologically accessible blood compartment; mature, stage V gametocytes can persist for days and mature sexual parasites are extracellular for ~24 h in the mosquito, creating a significant window during which to target the parasite for therapeutic/immune destruction. Transmission-blocking antimalarials would drastically reduce the parasite reservoir (even in high-transmission settings), could target the significant proportion of asymptomatic parasite carriers and, possibly the most enticing, could protect the lifespan of antimalarials that kill asexual blood stages (ABS) if used in combination, by preventing the spread of resistant parasites against the ABS active antimalarial (Delves et al., 2018a; Birkholtz et al., 2022).

Clear differentiation between *P. falciparum* gametocytes and ABS explains why most ABS antimalarials are inactive against mature gametocyte stages and therefore not useful to block transmission. Currently, whilst primaquine, methylene blue and atovaquone can target malaria transmission, each have concerns ranging from toxicity in certain populations (Howes et al., 2012; Gonçalves et al., 2016) to a very narrow target parasite population (e.g., atovaquone targeting ookinetes). The

search for new compounds targeting the transmissible stages have been skewed towards compounds targeting biology important to proliferation of the ABS and large screening campaigns have mostly prioritized hits based on ABS activity as primary filter – with transmission-blocking activity seen as advantageous additional activity for dual-active antimalarials. However, if the same molecular activity is targeted in both ABS and gametocytes/gametes, and resistance develops against such antimalarial hit, spread of resistance is a real threat (Witmer et al., 2021). Alternative strategies towards identifying antimalarial hits with transmission-blocking activity include *de novo* screening against either mature gametocytes or gametes (Miguel-Blanco et al., 2017; Delves et al., 2018b; Reader et al., 2021). This has revealed novel chemotypes associated with targetable biology in these stages. In principle, our broader understanding of the unique biology of gametocytes and gametes (Delves, 2012; Meibalan and Marti, 2017; Josling et al., 2018; Ngotho et al., 2019; Schneider and Reece, 2021; Usui and Williamson, 2021) therefore present a major, unexplored avenue to discover new antimalarials, and with the toolkit associated with transmission-blocking screens now well established (Delves et al., 2018a; Birkholtz et al., 2022), these should be exploited with renewed effort (Sinden et al., 2012; Leroy et al., 2014; Nilsson et al., 2015; Delves et al., 2018a). Open areas worth investigating include the commitment phase, early differentiation processes during immature gametocytogenesis, maturation of stage V gametocytes and gametogenesis itself, although the latter will rely on irreversibly compromising (sterilizing) mature stage V gametocytes, as these will be the target of intervention in humans.

COMMITMENT TO SEXUAL DIFFERENTIATION

Commitment to sexual differentiation marks the key decision point at which the parasite responds to signals to 'adapt or die' i.e., to transmit or not. This irreversible and binomial decision is variable and can take place within the same IDC cycle, whereby merozoites entering erythrocytes either directly initiate gametocytogenesis at low frequency (same cycle conversion), or complete another round of asexual replication after which daughter merozoites released from the committed schizont invade erythrocytes and only then initiate gametocytogenesis (next cycle conversion) (Bancells et al., 2019). This depends on the temporal expression of factors responsible for sexual differentiation. In either situation, the merozoite progeny of a single schizont will become either all male or all female gametocytes, resulting in the biased production of committed schizonts and the 4:1 (female:male) sex ratio of *P. falciparum* (Silvestrini et al., 2000; Smith et al., 2000).

Commitment is a clear example of eukaryotic processes employed by *Plasmodium* in response to external factors, the majority of which are related to host or environmental stressors that the parasite can sense and that forces it into sexual commitment in a classic mechanism of species survival (Paul et al., 2002; Talman et al., 2004; Sowunmi et al., 2008). These

signals include high parasitemia or increased pathology experienced in the host [anemia or hemolysis, high lymphocyte or reticulocyte densities (Gautret et al., 1996; Trager et al., 1999), and immune pressure (Ono et al., 1986)] or external factors including co-infections (Menezes et al., 2018). But nutrient sensing is one of the main external factors inducing commitment. LysoPC restriction (a phosphatidyl choline, PC, abundant in serum) induces gametocyte production *in vitro* (Brancucci et al., 2017) due to the complete reliance of ABS on PC for conversion into lipid membranes through the Kennedy pathway. When LysoPC is depleted, ABS parasites can only survive for a single asexual cycle by using phosphoethanolamine (PE) methyltransferase (*PfPMT*) to produce PC *via* the trimethylation of PE (Witola et al., 2008; Brancucci et al., 2018).

Molecular role players downstream of LysoPC sensing that regulate gametocytogenesis have been somewhat elucidated and include *P. falciparum* gametocyte development 1 (*PfGDV-1*) as the key role player in gametocytogenesis, specific to *P. falciparum* and divergent from rodent *Plasmodium* spp. (Brancucci et al., 2017). *PfGDV-1* regulates expression of the transcription factor *PfAP2-G* from the apicomplexan-specific Apetala2 transcription factor family (Eksi, 2012; Filarsky et al., 2018), by evicting heterochromatin protein 1 (*PfHP1*) from the histone post-translational modification (PTM) H3K9me3 site upstream of *ap2-g* (Filarsky et al., 2018), a mark that is maintained by histone deacetylase 2 (*PfHda2*). *PfGDV-1* is itself regulated by an antisense RNA mechanism (Broadbent et al., 2015), and *AP2-G* can regulate its own transcription through feedback inhibition (Kafsack et al., 2014; Sinha et al., 2014). A key outstanding question is how these metabolites link to the maintenance of heterochromatin that controls the frequency of *ap2-g* activation. One connection is the requirement of S-adenosylmethionine (SAM) for both histone methylation (H3K9me3) and PE methylation by *PfPMT*. With *PfPMT* likely consuming 3x the amount of SAM under PC restricting conditions, H3K9me3 may not be maintained (Neveu et al., 2020a), thereby lifting the heterochromatic restriction on the *ap2-g* locus.

Can Sexual Commitment be Targeted?

Commitment to gametocytogenesis can seemingly be increased *in vivo* due to drug treatment including the presence of steroid hormones (Lingnau et al., 1993), fansidar (Putz and Manyando, 1997), chloroquine, sulphadoxine-pyrimethamine (Talman et al., 2004) and other antimalarials (Peatey et al., 2009; Portugaliza et al., 2020). This has often raised a concern as to potential increased transmission of the parasite under sub-optimal treatment conditions. Indeed, quantitative data on sexual commitment rates after drug (including antimalarials) exposure indicated elevated sexual commitment as a general stress response at a narrow window around the IC₅₀ and in the case of mefloquine and pyrimethamine, resulted in a net increase in gametocyte production (Thommen et al., 2022). Whether this translates to therapeutic induction of gametocytes is unclear, but it would be a concern if antimalarials are not used at effective doses, as can often be the case in some endemic regions.

The question then remains if there are any druggable processes during commitment that would prevent the initiation

of the evolutionary escape process? With the involvement of *PfPMT*, the Kennedy pathway and epigenetic modulators, one could foresee potential for small molecule interventions. However, beyond the above evidence of drugs inducing gametocytogenesis when used on ABS parasites, no reports of drugs preventing gametocyte commitment by targeting the molecular role players are available, possibly due to the difficulty associated with detecting committed ring and schizont stages that precludes large scale investigations. The development of new *P. falciparum* reporter lines to detect commitment (Thommen et al., 2022) may open up investigations of new antimalarial leads blocking this process. Genetic manipulation have indeed resulted in several gametocyte deficient cell lines [e.g. *gdv1* (Tiburcio et al., 2021), *ap2-g* (Kafsack et al., 2014) and *pmt* (Bobenchik et al., 2011)], validating the importance of these regulators to gametocytogenesis and opening up potential avenues for intervention. Enzymes involved in *Plasmodium* spp. Kennedy pathway are of interest. *PfPMT* can be inhibited on a protein level by MMV019918 (Vallone et al., 2018), hexadecyltrimethylammonium, dodecyltrimethylammonium and amodiaquine (Bobenchik et al., 2010; Garg et al., 2015) although whole cell inhibition data is lacking. Choline kinase (CK) is essential to *P. berghei* blood stages (Aoyama et al., 2004; Witola et al., 2008; Dechamps et al., 2010) and structural mimics of choline cause selective inhibition of CK (Witola and Ben Mamoun, 2007; Alberge et al., 2009).

Based on the strong involvement of epigenetic regulation of *PfAP2-G* activation and the key H3K9me3/ac balance, it would be interesting to investigate if inhibitors of e.g. histone lysine methyltransferases (HKMTs) such as BIX01294 (that prevents ABS proliferation and gametocyte viability [Malmquist et al., 2015; Coetzee et al., 2020]), histone demethylases such as JIB-04 or ML324 [active against mature gametocytes (Matthews et al., 2020; Reader et al., 2021)], or hydroxamate-based HDACi (with potent antiplasmodial activity and limited cytotoxicity (Coetzee et al., 2020; Vanheer et al., 2020)), also prevent gametocyte conversion and commitment.

Whether targeting any of these processes will in any form translate to compounds with therapeutic advantage is questionable. Indeed, such a compound will not clear ABS parasites, and will not prevent gametocyte maturation and transmission, unless commitment can be entirely halted before same cycle conversion occurs. Sole inhibition of commitment is therefore not a justifiable profile, and commitment-blocking activity will likely only be considered as an additional advantage of compounds with ABS activity, although the contribution of such added activity to overall efficacy (either as ABS cure or transmission-blocking active) is difficult to quantify.

THE EARLY PHASE OF GAMETOCYTE DIFFERENTIATION AND DEVELOPMENT

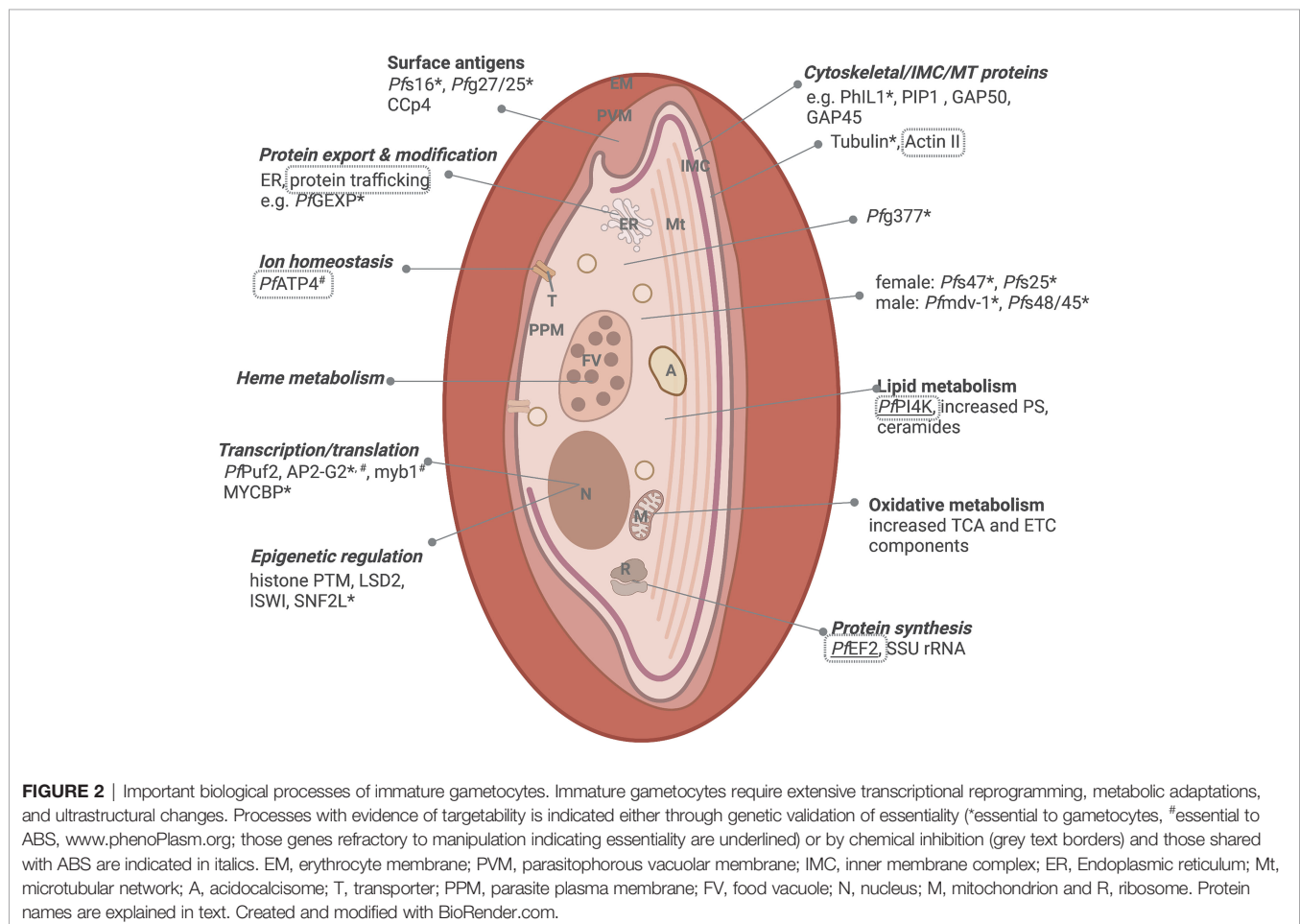
Once committed to gametocytogenesis, the early phase of gametocyte differentiation is marked by massive ultrastructural and functional adaptations in the associated immature (stage I-

IV) gametocytes. Importantly, to avoid splenic clearance and elude the host immune system, immature gametocytes sequester in the extravascular space (erythroblastic islands) of the bone marrow parenchyma and in the spleen (Neveu et al., 2020b). The bone marrow provides a nutrient-rich, anaerobic environment with the relative distribution of fatty acids, including LysoPC, in the bone marrow, that differs greatly from that in serum (Brancucci et al., 2017).

Morphologically, early stage I-III *P. falciparum* gametocytes are characterized by the increased presence of food vacuoles, extended polyribosomes, and the deposition of a network of sub-pellicular inner membranes (the inner membrane complex, IMC), to form the characteristic D-shape of stage III, subtended by a dense deposition of microtubules (MT), actin and formin-1 (Figure 2) (Dixon and Tilley, 2021). The IMC and MT network associates with glideosome components (GAP50, GAP45 and MTIP) and membrane trafficking proteins, PhIL1 and PIP (Parkyn Schneider et al., 2017). Immature *P. falciparum* gametocytes further actively remodel the host erythrocyte, thereby exposing antigens for cell-cell interactions (Messina et al., 2018), distinct from those used by ABS. Active protein export in *P. falciparum* immature gametocytes is exemplified by the upregulation of gametocyte exported proteins (GEXP)

(Silvestrini et al., 2010), a third of which belong to the *Plasmodium* helical interspersed subtelomeric (PHIST) protein family (Sargeant et al., 2006) with known roles in host cell remodeling and protein trafficking (Warncke et al., 2016). Immature gametocytes also export rhopty proteins to increase permeability and activate (reversibly) new permeation pathways (NPP) that mediate nutrient uptake in immature gametocytes (Bouyer et al., 2020). Taken together, these changes result in increased stiffness in the immature gametocyte to allow mechanical retention in the bone marrow and avoid splenic clearance.

On a molecular level, immature gametocytes are substantially distinguished from ABS by divergent sex- and stage-specific transcriptomes (Lopez-Barragan et al., 2011; Lasonder et al., 2016; Van Biljon et al., 2019). *PfGEXP5* is the earliest detected gametocyte marker expressed in an AP2-G independent manner (Tiburcio et al., 2015), but AP2-G dependent gametocyte-specific markers include *Pfs16*, *Pfg27/25*, *Pfg14.744*, *Pfg14.745*, *Pfg14.748* and *ETRAPM10.3/PEG4* (Kafsack et al., 2014), in addition to 308 other markers expressed in committed schizonts and early gametocytes (Pelle et al., 2015). The molecular role players associated with transcriptional reprogramming during immature gametocyte development have been somewhat



elucidated, and include transcription factors like AP2-G2 (essential to maturation in these immature (Singh et al., 2021b)), whilst increased expression implicates factors such as *PfMyb1* and MYCBP (a c-Myc binding protein) in sex-specific gene regulation. Post-commitment epigenetic regulators include unique histone methylation repressive marks associated with repression of ABS related genes (Coetzee et al., 2017; Connacher et al., 2021; Von Gruning et al., 2022), the upregulation of putative chromatin remodelers like ISWI and SNF2L (Poran et al., 2017) and expansion of HP1 occupancy (Fraschka et al., 2018) and use of repressive histone PTMs (e.g. H3K36me2/3) for a resultant heterochromatic nature (Connacher et al., 2022). The conversion to commitment is further evident in changes in mRNA dynamics with subsets of gametocyte-specific transcripts stabilized in these early stages, and ABS related mRNAs undergoing active decay (Painter et al., 2017).

The transcriptional reprogramming manifests on a metabolic level, firstly to adapt the gametocyte to aerobic energy production and secondly, to enable lipid biosynthesis towards eventual fertilization. This switch is most likely due to the gametocytes' move to the hypoxic hematopoietic bone marrow where host-derived glutamine is the main carbon source (Srivastava et al., 2017). Whilst ABS parasites rely mostly on glycolysis for energy production, during early gametocytogenesis, metabolism moves to become more fermentative and occurs partly through the tricarboxylic acid (TCA) cycle and aerobic energy production *via* the electron transport chain (ETC) (Macrae et al., 2013). This is exemplified by the upregulation of 15/16 transcripts involved in TCA metabolism (Lasonder et al., 2016; Van Biljon et al., 2019), the presence of a large, branched mitochondrion and a 7-fold increase in the activity of cytochrome b (Crofts, 2004). The gametocyte lipidome also differs significantly from other life cycle stages with a clear enrichment (>8-fold) in phosphatidylserine (PS), ceramides and dihydroceramides in gametocytes (Lamour et al., 2014; Gulati et al., 2015).

Male-specific proteins (those required for later genome replication in preparation for exflagellation) appear earlier at stage I/II development (Van Biljon et al., 2019). Sex-specific proteins include *Pfg377*, involved in osmiophilic body production produced from stage III and important to females (Alano et al., 1995; Severini et al., 1999; de Koning-Ward et al., 2008), *Pfs47* – a 6-cysteine domain protein expressed exclusively in females from stage II (Van Schaijk et al., 2006) and *Pfs25* and *CCp4* as female-specific surface protein (Schneider et al., 2015; Meerstein-Kessel et al., 2018). Although *PfMDV-1/PEG3* (male development protein 1 and protein of early gametocyte 3, respectively) is expressed in both sexes and its expression is regulated by *PfAP2-G2* (Xu et al., 2020), disruption of *pfmdv-1* results in a dramatic reduction in functionally mature male gametocytes and partially perturbed mosquito infectivity (Furuya et al., 2005). *Pfs48/45* is expressed from stage II (Lobo et al., 1999) and its ablation reduces male fertility (Van Schaijk et al., 2006) whereas *PfPuf2* is a regulatory protein whose deletion results in aberrant male gametocyte differentiation (Miao et al., 2010).

Targeting Immature Gametocytes

Targeting the process of early gametocyte sequestration and differentiation could have a dramatic impact on transmission and provides motivation for further investigation into the mechanisms parasites use to establish themselves in the bone marrow microenvironment. The majority of antimalarials with ABS activity will retain their activity on immature gametocytes if a similar biology/protein is targeted e.g., hemoglobin metabolism, which is only active until stage III development (Plouffe et al., 2016). This could therefore prevent any development beyond the immature stages. However, in some cases (e.g., the 4-aminoquinolines targeting heme metabolism, which is inactive by stage IV), there is a loss in activity and the effective concentration targeting immature gametocytes is higher than that required to kill the ABS; in some cases this is even more pronounced in stage IV gametocytes (**Table 1**) (Plouffe et al., 2016). In this scenario, if any immature gametocytes are formed, and cannot be effectively targeted, they will continue to seed mature gametocytes. Since only 20 parasites/ μ L can result in an infective mosquito (Usui and Williamson, 2021), this poses a high risk to transmission-blocking activity. Additionally, if the same biology is targeted between ABS and immature gametocytes, and resistance develops in the ABS stages to a particular antimalarial, this would be transferred to the immature stage, rendering the antimalarial completely ineffective as transmission-blocking active and resulting in spread of resistant parasites. Lastly, several ABS targeting antimalarials are completely ineffective against immature stages (e.g., pyrimethamine and atovaquone), and data on the activity of some frontrunner and development compounds like Ganaplacide [KAF156, an imidazolopiperazine targeting protein secretion (Kuhlen et al., 2014)], P218 (a pyrimidine targeting dihydrofolate reductase [(Posayapisit et al., 2021)] and MMV183 [a panthothenate targeting acetyl coA synthetase (Schalkwijk et al., 2019)], are lacking.

Several antimalarial frontrunners retain activity against immature gametocytes with inhibition of Na^{2+} homeostasis by targeting the cation transporting ATPase *PfATP4* (e.g., Cipargamin, KAF246), protein synthesis through inhibition of elongation factor *PfEF2* (e.g. M5717) and the phosphatidylinositol (PI)-4 kinase (PfPI4K) inhibitor MMV390048 (Paquet et al., 2017), resulting in some of the most potent compounds in development currently (**Table 1**). Their almost equipotent activity between ABS and immature gametocytes is imminently useful to block gametocytogenesis. This is also thought to be mediated by the NPP, still active in immature gametocytes (Bouyer et al., 2020).

As immature gametocytes are associated with transcriptional reprogramming, metabolic adaptations, and ultrastructural changes, any of these processes become appealing from an inhibitory perspective (**Figure 2**). However, aside from the compounds with additional ABS activity, for which targets have been elucidated, very few target-specific indicators have been described in these immature stages. But extrapolations from genetic validation of the essential nature of some of the processes involved in these early phases of gametocytogenesis could provide an avenue worth exploring to validate druggability of

TABLE 1 | Summary of historical antimalarials, current front-runner and development compounds and novel hits with sub-micromolar *in vitro* activity against *P. falciparum* immature (stage II/III) gametocytes.

Compound	IC ₅₀ (nM)		Target / MoA	Ref
	Stg II/III	Stg IV		
Artemether	5	19	Hemoglobin metabolism and hemozoin formation	(Plouffe et al., 2016)
Artemisinin	20	37		
Artemisone	2	4		
Artesunate	4	49		
DHA	3	21		
OZ277	4	8		
Artefenomel (OZ439)	5	2		
Amodiaquine	6	2456		
AQ-13	33	6471		
Chloroquine	98	6250		
Hydroxychloroquine	131	6250		
Naphthoquine	14	4167		
Piperaquine	14	4167		
Pyronaridine	10	2579		
Lumefantrine	13	599	Unknown	(Coertzen et al., 2018) (Klonis et al., 2011; Coertzen et al., 2018) (Giannangelo et al., 2020) (Giannangelo et al., 2020) (Plouffe et al., 2016)
Mefloquine (+RS)	39	579		
Halofantrine	1	1509		
Quinidine	208	12500		
Quinine	496	12500		
Cipargamin (KAE609)	100 ^{&}	–		
KAF246	2	2		
M5717 (DDD498)	5	2		
MMV390048	214	–		
KDU691	565	2327		
Methylene blue	15	12		
Pentamidine	591	813		
KAI407	636	329		
NSC158011	90*	–		
GNF179	64	9		
BIX01294	14	–		
Cycloheximide	640	477		

*Inhibition of gametocyte viability 5 μ M (%).[&]Inhibition of gametocyte viability 50 nM (%).

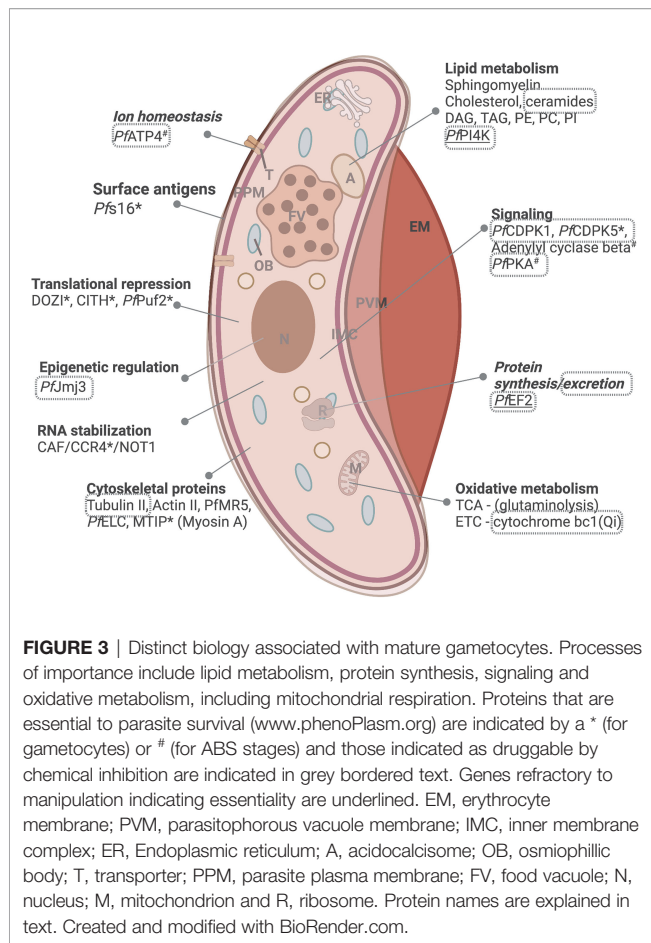
these processes. For instance, the genetic validation of the importance of PhIL1, PIP1 (and 3) and α -tubulin II to early gametocyte structural changes (Parkyn Schneider et al., 2017; Dixon and Tilley, 2021), mark these as potential drug targets, although no evidence of successful inhibition of homologues to these structural proteins is available. By contrast, the actin filaments that polarize to the opposite ends of the cell and co-localize with the actin nucleation factor, formin-1, are sensitive to cytochalasin-D, affecting bone marrow and spleen sequestration in *P. berghei* gametocytes, suggesting actin is required for tissue homing and the gametocytes' subsequent return to circulation (De Niz et al., 2018).

MATURATION OF GAMETOCYTES TO TRANSMISSIBLE FORMS

The ultimate step in gametocyte development and differentiation requires the parasite to mature to be transmissible. Stage V gametocytes therefore change in shape to become less rigid to allow the parasite to return to the blood circulatory system and secondly, they adapt metabolically to survive in the human host

for prolonged periods. The deformability switch leading to the release of stage V gametocytes from bone marrow or splenic retention is mediated by loosening of the IMC and disruption/partial disruption of associated proteins and with the loss of the MT network and STEVOR proteins (Dearnley et al., 2012; Tiburcio et al., 2013; Nilsson et al., 2015; Dixon and Tilley, 2021).

Metabolically, mature gametocytes do not metabolize hemoglobin and slow their flux through glycolysis. These parasites remain metabolically active but now, like typical eukaryotic cells, utilize glutaminolysis for oxidative metabolism through the TCA cycle for energy production (MacRae et al., 2013; Lamour et al., 2014) (**Figure 3**). This is underscored by distinct changes in the mature gametocyte transcriptome and metabolome. These shifts highlight the requirement of mature gametocytes to prepare for the challenging environment in the mosquito, where the energy demands are high, and efficiency is vital for transmission. Transcriptional reprogramming therefore results in ~20-25% of the *Plasmodium* genome expressed specifically in the sexual stages (Lasonder et al., 2016; van Biljon et al., 2019), creating an epigenetically-mediated transcriptionally poised state (Coetzee et al., 2017; von Gruning et al., 2022) including translational repression of



female-associated transcripts (Lasonder et al., 2016). Regulators of translation like DOZI and CITH mediate the storage of mRNA transcripts in the form of ribonucleoprotein complexes within female gametocytes for rapid translation during female gamete activation. mRNA targets are bound by *PfPuf2*, the disruption of which results in translation and the increased production of the associated protein (Miao et al., 2013). Those transcripts not stabilized are regulated by the CAF1/CCR4/NOT complex causing mRNA decay and thereby translational repression (Figure 3) (Hart et al., 2019; Hart et al., 2021).

Genes transcribed later in gametocytogenesis relate to the processes specific to maturation and include the switch from sequestration to peripheral circulation (deformability), as well as processes involved in readying the parasite for transmission to the mosquito (protein synthesis for locomotion, host cell entry and actin depolymerization) (van Biljon et al., 2019). The marked expansion of mitochondrial numbers and the exclusive presence of cristae observed in mature gametocytes (Evers et al., 2021) correlate with a 40-fold increase in ETC components (Evers et al., 2021) and upregulation of TCA associated genes (Figure 3) (Lasonder et al., 2016; van Biljon et al., 2019). Furthermore, vast changes in the lipid requirements in mature gametocytes ensure fluidity (Dearnley et al., 2012; Tibúrcio et al., 2012) and allow preparation for fertilization requiring membrane biogenesis, protein trafficking and cell signaling.

This is evident in upregulation of actin depolymerization factors 1 and 2, leading to increased cellular deformability, enrichment of cholesterol esters and dihydrosphingomyelin in female gametocytes; the latter crucial for both sexes' viability (Ridgway et al., 2022) and an up to 60-fold enrichment in diacylglycerol and triacylglycerol, associated with the presence of fatty acid-rich and osmiophilic bodies (including PE & PC) at the gametocyte periphery (Tran et al., 2016). These serve as energy storage to fuel the increases in protein and phospholipid biosynthesis during gametogenesis and subsequent fertilization (Besteiro et al., 2010). PI is essential for vesicle trafficking and as secondary messengers in gametocyte activation by mobilizing intracellular Ca^{2+} stores (Brochet et al., 2014). Other intracellular signaling role players include CDPK1, CDPK5, adenylyl cyclase beta and cAMP dependent protein kinase A (PKA-c and PKA-r) (van Biljon et al., 2019). Sex-specific transcripts upregulated in mature stages include cytoskeletal proteins α -tubulin II and actin II (Deligianni et al., 2011; van Biljon et al., 2019) and *PfMR5* (Eksi et al., 2006), both involved in the motility and viability of exflagellating gametes.

Targeting Mature Gametocytes

Transmission-blocking requires compounds to either kill or substantially compromise (sterilize) mature gametocytes, such that drugs delivered to affected humans will prevent transmission (Birkholtz et al., 2022). However, most ABS actives – which typically target proliferative processes – are inactive on mature gametocytes, simply because the underlying biology is so markedly different or alternatively, uptake into mature gametocytes may be compromised due to inactive NPPs (Bouyer et al., 2020). Indeed, as indicated above, mature gametocytes are not quiescent but rather metabolically more like normal eukaryotic cells than the ABS, which are more alike cancerous cells with high metabolic flux through glycolysis and induction of the Warburg effect, resulting in fermentative states (Salcedo-Sora et al., 2014).

Protein synthesis, protein secretion, ion homeostasis and lipid metabolism remain powerful processes to target with M5717, GNFI79, Cipargamin (KAE609) & KAF246, and MMV390048, respectively, displaying transmission-blocking activities at concentrations amenable to therapeutic indices (Table 2). However, if resistance develops against these compounds, it would likely be transmitted as the compounds would lose efficacy against mature gametocytes as well. This could be resolved by combination therapies where a compound targeting specific biology associated with gametocytes are combined with compounds targeting proliferative processes in ABS. Conceptually, this would protect the ABS component from resistance spread. However, with this strategy, it is essential to target unique biology in gametocytes. Such potential targets include the deformability of mature gametocytes, where the two light chains of the myosin motor *PfMyoA*, *PfELC* and MTIP were shown to be essential and could be starting points for the development of novel antimalarials targeting the glideosome (Moussaoui et al., 2020) (Figure 3). Additional targets around deformability include cAMP signaling and STEVOR dephosphorylation with inhibition of phosphodiesterase by sildenafil citrate or PKA inhibition by KT5720 and H89 changing the flexibility of gametocytes (Ramdani

TABLE 2 | Summary of key antimalarials, front-runner and development compounds as well as investigative hits with *in vitro* activity (< 5 μ M) against *P. falciparum* mature gametocytes.

Compound	IC ₅₀ (nM) Stg V	Target	Ref
Mefloquine (+RS)	158	80S ribosome	(Plouffe et al., 2016)
ELQ-300	72	Cytochrome bc1(Qi)	(Nilsen et al., 2013)
Cipargamin (KAE609)	100*	PfATP4 / Na ²⁺ homeostasis	(Van Pelt-Koops et al., 2012)
KAF246	2		(Rottmann et al., 2010; Plouffe et al., 2016)
M5717 (DDD498)	9	PfEF2 / protein synthesis	(Rottmann et al., 2010; Plouffe et al., 2016)
MMV390048	140	PfPI4K	(Paquet et al., 2017)
AZD-0156	236		(Reader et al., 2021)
KDU691	150		(Mcnamara et al., 2013)
ML324	77	Pfjfm3	(Reader et al., 2021)
JIB-04	3630		(Matthews et al., 2020)
Methylene blue	258	Glutathione reductase	(Buchholz et al., 2008; Plouffe et al., 2016)
GNF179	3	Protein secretory pathway	(Plouffe et al., 2016)
Birinapant	135	Unknown (caspase 3 inhibitor)	(Reader et al., 2021)
MMV1581558	130	Unknown (Adenosine A3 receptor)	
MMV1580843	108	Unknown	
SQ109	104	Unknown (MmpL3 in Mtb)	
Epoxomicin	6.6	β 2 and 5 proteasome subunits	(D'Alessandro et al., 2016)

*% inhibition of gametocyte viability 500 nM.

et al., 2015). Ceramides and complex sphingolipids regulate membrane fluidity and increase in abundance during maturation. Two compounds targeting dhCer (ceramide precursor) synthase and displaying gametocytocidal activity were recently identified (Gulati et al., 2015), suggesting that lipid synthesis might be a viable target in mature gametocytes.

Gametocyte-specific biology that is currently under investigation include a renewed focus on mitochondrial respiration, although the differentiation associated with TCA and the ETC in gametocytes have to be taken into account (Van Biljon et al., 2019; Evers et al., 2021), which explains the lack of activity of dihydroorotate inhibitors (e.g. DSM265). Targeting of cytochrome bc1 seems highly dependent on structural motifs of antimalarial compounds either bidding the oxidative (Qo) site and a reductive (Qi) site (Fisher et al., 2020). Atovaquone binds the Qo site but this does not change gametocyte viability and atovaquone activity only manifests in ookinete formation (Jeevaratnam et al., 1992). However, targeting of the Qi site by ELQ-300 shows potent activity against mature gametocytes (Table 2). This potency emphasizes the importance of the TCA cycle in mature gametocytes for primary energy metabolism (Macrae et al., 2013; Lamour et al., 2014) and marking this as a prime targetable process, currently being investigated by the Medicine for Malaria Venture (Stickles et al., 2015a; Stickles et al., 2015b). Several other hit compounds are being used to explore such transmission-specific biology including histone demethylase inhibitors ML324 and JIB-04 (Table 2) (Matthews et al., 2020; Reader et al., 2021), and compounds with polypharmacology in protists including the protonophore SQ109 (Reader et al., 2021).

GAMETOGENESIS TO FORM OOCYSTS IN THE MOSQUITO VECTOR

In an extraordinary feat of biology, gametogenesis in *Plasmodium* is a result of finetuned responses to environmental

signals associated with host to vector environmental changes, including a 5°C temperature drop, presence of xanthurenic acid and pH increase (7.2 to 8) (Arai et al., 2001). This results in rapid activation of DNA synthesis/replication, protein synthesis, axoneme assembly and egress within the male gametocyte, as well as protein synthesis and egress in the female gametocyte (Delves, 2012). Fertilization requires active motility, cell-to-cell recognition and membrane fusion, whereas ookinete development is dependent on vegetative growth, protein synthesis and motility (Delves, 2012).

The subsequent activation of guanylyl cyclase (GC α) and cyclic guanosine 3', 5'-monophosphate (cGMP) signaling is crucial to activation of protein kinase G (PKG) as key role player in gametogenesis and egress (Kuehn and Pradel, 2010; Balestra et al., 2021), the signal transduction of which occurs, in part, through the multipass membrane protein ICM1 (Balestra et al., 2021) (Figure 4). The PKG mediated cascade (including involvement of PfPI4K and phosphatidylinositol 4-phosphate 5-kinase, PIP5K) results ultimately in opening of IP₃-gated calcium channels on the ER and a resultant increase in intracellular Ca²⁺ (Bennink et al., 2016). Activation of several sex-specific CDPKs ensues (Brochet et al., 2021), including CDPK1-mediated release of DOZI, CITH and PfPuf2 for translation in female gametes and CDPK4 to activate cyclins and cyclin-dependent kinases for cell division in male gametes (Kumar et al., 2021) (Figure 4). The latter is mediated by successive S and M cell cycle phases (Raabe et al., 2009; Meibalan and Marti, 2017). The high energy demands of replicating, motile male gametes are satisfied through exclusive reliance on glycolysis (Talman et al., 2014; Srivastava et al., 2016).

Egress is mediated by the osmiophilic body proteins Pf377, PfMDV-1 and gamete egress and sporozoite survival (GEST) protein (De Koning-Ward et al., 2008; Bargieri et al., 2016), as well as the egress vesicle proteins, perforin-like protein (PPLP2) that mediates the formation of pores in the erythrocyte membrane (Sologub et al., 2011) (Figure 4). Cysteine and serine proteases

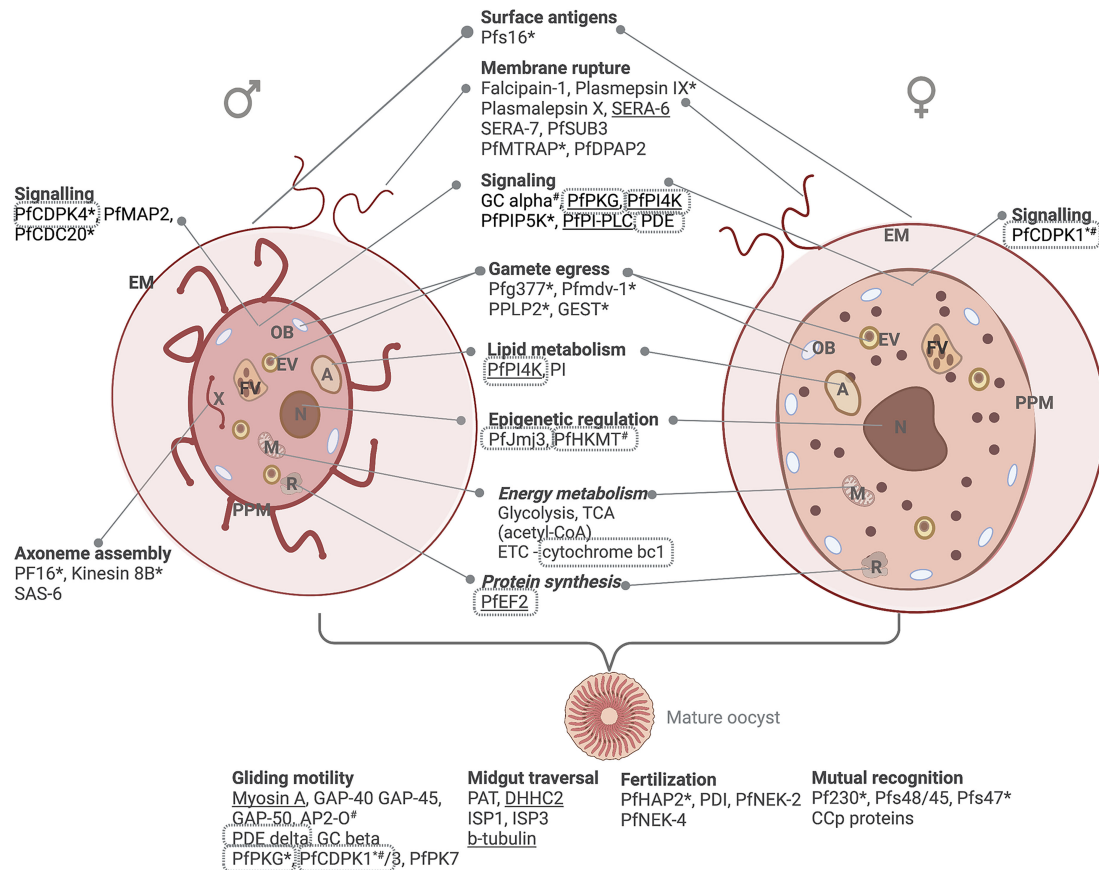


FIGURE 4 | Male and female gametes and their differentiative biological processes. Gametogenesis involves intracellular signaling, DNA synthesis, lipid metabolism and energy metabolism reminiscent of the asexual stages (glycolysis and TCA cycle). Protein essentiality (www.phenoPlasm.org) is indicated by a * (gametocytes) or # (asexual stages) or underlined where the gene is refractory to deletion. Proteins that are validated as potential target through chemical inhibition are indicated in grey borders. EM, erythrocyte membrane; ER, Endoplasmic reticulum; A, acidocalcisome; EV, egress vesicle; OB, osmiophilic body; PPM, parasite plasma membrane; FV, food vacuole; N, nucleus; M, mitochondrion and R, ribosome. Protein names are explained in text.

(falcipain-1, plasmepsin IX, plasmalepsin X, SERA-6, SERA-7, and PfSUB3), MTRAP and PfDPAP2 are involved in PVM and erythrocyte membrane rupture, and aspartic proteases in gamete round-up (Munsamy et al., 2018). Egress is followed by exflagellation, mediated by the male-specific axoneme assembly (flagellum formation) proteins (e.g., the armadillo repeat protein PF16, Kinesin 8B, SAS-6 (Straschil et al., 2010; Depoix et al., 2020); MAP2 and CDC20 (Kumar et al., 2021); cytoskeletal proteins α -tubulin II and actin II (Elena et al., 2011) and *PfMR5* (Eksi et al., 2006). Mutual recognition and male and female gamete attachment are mediated by P230, Pfs48/45, Pfs47 (Van Dijk et al., 2010), complement control CCP proteins (Baker, 2010) and Pb115 (Liu et al., 2019) (**Figure 4**).

After fertilization, the resultant zygote develops into an ookinete with pronounced energy requirements through oxidative phosphorylation and the glycolytic pathway (Delves et al., 2019). HAP2 (Kuehn and Pradel, 2010) and protein disulphide isomerase (PDI) (Angrisano et al., 2019) are responsible for nuclear fusion, and genome tetraploidy in the resulting zygote is mediated by NIMA-related kinases, NEK-2 and

NEK-4 (Pradel, 2007). The mature ookinete is motile and capable of cell invasion, which is mediated by glideosome machinery under the regulation of AP-O (Singh et al., 2021b) and involving cGMP mediated signaling (Gao et al., 2018) and kinases such as PKG, CDPK1, CDPK3, and PK7 (Singh et al., 2021a) (**Figure 4**).

Targeting Parasite Development in the Mosquito

Since gametogenesis involves re-activation of processes that were targetable during ABS development (such as DNA replication) as well as male and female specific events, targeting of gametogenesis and oocyst formation have been the topic of much discussion. Indeed, several screening cascades places gamete formation or downstream oocyst formation as primary endpoints to identify transmission-blocking antimalarials, with the potential broader hit detection capacities compared to gametocytocidal screens that will not be able to detect compounds that do not affect their viability but only compromise mature gametocytes, thereby sterilizing them for downstream fertilization (Delves et al., 2019). In fact, the

transmission-blocking activity of any compound active on mature gametocytes has to be validated on oocyst formation (Birkholtz et al., 2022). Importantly, this must consider natural oocyst densities, which then prioritizes development candidates M5717, MMV048 and KAE609 as the most effective for transmission-blocking (**Table 3**) (Dechering et al., 2017). Compounds with sole gametocidal or sporontocidal activity will be challenging to develop since they would need an extraordinarily long human serum half-life to still be effective once taken up into the mosquito vector. Strategies focused on direct delivery to mosquitoes is currently seen as only viable alternative (Paton et al., 2019).

As expected, signaling cascades associated with gametogenesis are inherently targetable, with PDE and PKG on the forefront, both being essential to gametogenesis and chemically targeted by Zaprinast, (McRobert et al., 2008) and imidazopyridines such as ML10 (McRobert et al., 2008; Taylor et al., 2010; Baker et al., 2017; Baker et al., 2020), respectively (**Table 3**). Ca^{2+} homeostasis is inherently targetable with several CDPKs having been investigated;

CDPK1 with imidazopyridazines (Lemercier et al., 2009; Chapman et al., 2013; Large et al., 2013; Ansell et al., 2014; Chapman et al., 2014); CDPK4 by bumped kinase inhibitors (Huang et al., 2016) and pyrazolopyrimidine derivatives (Vidadala et al., 2014). This extends to CDPK3 and PK7 during fertilization, with other activities such as PDI and PDE also potentially important (Angrisano et al., 2019). Targeting energy metabolism is important in the metabolically active ookinetes and oocysts, as evident by sporonticides atovaquone and ELQ-300 as potent inhibitors of cytochrome bc1 (**Table 3**) and recent evidence also points to the importance of targeting cytoskeletal proteins such as *Pfs16* (Yahiya et al., 2021) that plays a role during the immediate phase of microgametogenesis with DDD01035881 (Delves et al., 2018b).

CONCLUSION AND FUTURE DIRECTIONS

The vast expansion of our understanding of the processes mediating transmission and survival of malaria parasites over

TABLE 3 | Summary of key antimalarials, front-runner and development compounds as well as investigative hits with *in vitro* activity (>70% inhibition, or < 5 μM IC_{50}) against male and female gametes, as well as oocyst formation.

Compound	Gametes (%) ^a		TRA% ^b	Target	Ref
	Male	Female			
Chlorproguanil	–	–	100	DNA replication/ transcription	(Vos et al., 2015)
Cycloguanil	96	0			(Delves et al., 2013)
P218	4*	–	99		(Vos et al., 2015; Posayapisit et al., 2021)
Pyrimethamine	94	0	100		(Delves et al., 2013; Vos et al., 2015)
Atovaquone	12	12	100	Cytochrome bc1 (Qo)	(Delves et al., 2013; Vos et al., 2015)
ELQ-300			100	Cytochrome bc1 (Qi)	(Nielsen et al., 2013)
Cycloheximide	100 [#]	–	100	Unknown	(Vos et al., 2015)
KDU691	–	–	100	<i>Pf</i> PI4K	(McNamara et al., 2013)
MMV390048	90*	–	69		(Paquet et al., 2017)
AZD-0156	84 ^{&}	–	65 ^{&}		(Reader et al., 2021)
M5717 (DDD498)	–	–	1.8*	<i>Pf</i> EF2	(Baragana et al., 2015)
GNF179	–	–	100	Protein secretory pathway	(Plouffe et al., 2016)
Ganaplacide (KAF156)	–	–	90		(Kuhlen et al., 2014)
ML324	93 ^{&}	–	95 ^{&}	<i>Pf</i> Jmj3	(Reader et al., 2021)
JIB-04	10	80	–		(Matthews et al., 2020)
ML10	–	–	41*	<i>Pf</i> PKG	(Baker et al., 2017)
MMV030084	141*	0	–		(Vanaerschot et al., 2020)
Methylene blue	98	11	99	Glutathione reductase	(Delves et al., 2013; Vos et al., 2015)
Epoxomicin	–	–	100	β 2 and 5 subunits of the proteasome	(Czesny et al., 2009)
BIX01294	120*	727*	–	HKMT	(Malmquist et al., 2015)
SJ733			5mg/kg [@]	<i>Pf</i> ATP4	(Dechering et al., 2017)
KAE609 (NITD609)			100		(Van Pelt-Koops et al., 2012)
Birinapant	75 ^{&}		78 ^{&}	Caspase 3	(Reader et al., 2021)
MMV1581558	79 ^{&}		80 ^{&}	Unknown (Adenosine A3 receptor)	
MMV1580843	70 ^{&}		84 ^{&}	Unknown	
SQ109	53 ^{&}		80 ^{&}	Unknown (MmpL3 in Mtb)	
TCMDC-137173	76	21	25*	Unknown	(Delves et al., 2019)
TCMDC-134114	99	0	56*		
DDD01035881	540*	>10*		<i>Pfs16</i>	(Delves et al., 2018b; Yahiya et al., 2021)
DDD01028074	220*	>10*		Unknown	(Delves et al., 2018b)

^a% inhibition at 1 μM .

^bTRA: transmission-reducing activity at 5 μM .

* IC_{50} (nM).

% inhibition at 10 μM .

[&] Inhibition of gamete formation at 2 μM .

[@] ED_{50} in *P. berghei*.

the past decade has provided a deep insight into the possibilities and challenges associated with the identification and development of transmission-blocking interventions. ‘Omics data clearly indicates the importance of transcriptional reprogramming that manifests as metabolic adaptations and is initiated during commitment but evidently established in immature gametocytes and progressing during maturation to result in differentiated sexual parasites. Although such ‘blueprints’ are inherently informative, we are far from understanding the regulatory mechanisms involved but we do understand the involvement of epigenetic, transcriptional, and post-transcriptional mechanisms. New developments in inducible gene manipulation systems will allow a deeper investigation of the importance of gametocyte-specific regulators (Tiburcio et al., 2019), and this information could be translated to identify druggable candidates for guided, target-based discovery of novel transmission-blocking chemotypes. Additionally, the use of proteomics to identify and validate drug targets in gametocytes have been developed (Dziekan et al., 2019; Yahiya et al., 2021), yet, we are far from a streamlined drug target identification and mode-of-action platform for gametocytes similar to the extensive pipeline used to characterize ABS actives (Yang et al., 2021). Indeed, if any of the new transmission-selective hits are to be further developed, this area needs investment and development. Knowledge of a transmission-blocking compound’s target is particularly needed to allow combinations with ABS actives with a different target to have any success in preventing spread of resistance. If we are successful in identifying unique transmission-blocking antimalarials, it is envisaged that they could be used as add-on to current therapeutic strategies in combination with ABS actives or can be used as stand-alone treatments to clear gametocyte carriers of parasites. Innovations such as alternative culture

conditions for gametocytogenesis to more closely reflect the *in vivo* environment associated with *P. falciparum* gametocyte development; humanized mouse models of *P. falciparum* transmission to evaluate efficacy of transmission-blocking actives; adipo formulations for long-lasting release of gametocytocidal drugs, or compounds targeting the parasite when delivered directly to the mosquito vector, may indeed be promising to prevent the spread of malaria parasites and hence this disease.

AUTHOR CONTRIBUTIONS

L-MB conceived the work and MvdW, JR, and L-MB wrote and edited the paper. All authors contributed to the article and approved the submitted version.

ACKNOWLEDGMENTS

L-MB acknowledges the South African Medical Research Council Strategic Health Innovation Partnership and the Department of Science and Innovation South African Research Chairs Initiative, administered through the South African National Research Foundation (UID 84627). Research is supported by a BMGF Grand Challenges Africa grant (GCA/DD2/Round10/021/001) and by the Medicines for Malaria Venture as Global Test Centre for stage-specific gametocytocidal assays to L-MB. The UP ISMC acknowledges the South African Medical Research Council (SA MRC) as Collaborating Centre for Malaria Research. Figures were generated in BioRender.com under a standard academic license.

REFERENCES

- Alano, P., Read, D., Bruce, M., Aikawa, M., Kaido, T., Tegoshi, T., et al. (1995). COS Cell Expression Cloning of Pfg377, a *Plasmodium Falciparum* Gametocyte Antigen Associated With Osmiophilic Bodies. *Mol. Biochem. Parasitol.* 74, 143–156. doi: 10.1016/0166-6851(95)02491-3
- Alberge, B., Gannoun-Zaki, L., Bascunana, C., Tran Van Ba, C., Vial, H., and Cerdan, R. (2009). Comparison of the Cellular and Biochemical Properties of *Plasmodium Falciparum* Choline and Ethanolamine Kinases. *Biochem. J.* 425, 149–158. doi: 10.1042/BJ20091119
- Angrisano, F., Sala, K. A., Tapanelli, S., Christophides, G. K., and Blagborough, A. M. (2019). Male-Specific Protein Disulphide Isomerase Function is Essential for *Plasmodium* Transmission and a Vulnerable Target for Intervention. *Sci. Rep.* 9, 18300. doi: 10.1038/s41598-019-54613-0
- Ansell, K. H., Jones, H. M., Whalley, D., Hearn, A., Taylor, D. L., Patin, E. C., et al. (2014). Biochemical and Antiparasitic Properties of Inhibitors of the *Plasmodium Falciparum* Calcium-Dependent Protein Kinase Pfcdpk1. *Antimicrob. Agents Chemother.* 58, 6032–6043. doi: 10.1128/AAC.02959-14
- Aoyama, C., Liao, H., and Ishidate, K. (2004). Structure and Function of Choline Kinase Isoforms in Mammalian Cells. *Prog. Lipid Res.* 43, 266–281. doi: 10.1016/j.plipres.2003.12.001
- Arai, M., Billker, O., Morris, H. R., Panico, M., Delcroix, M., Dixon, D., et al. (2001). Both Mosquito-Derived Xanthurenic Acid and a Host Blood-Derived Factor Regulate Gametogenesis of *Plasmodium* in the Midgut of the Mosquito. *Mol. Biochem. Parasitol.* 116, 17–24. doi: 10.1016/S0166-6851(01)00299-7
- Baker, D. A. (2010). Malaria Gametocytogenesis. *Mol. Biochem. Parasitol.* 17257–, 65. doi: 10.1016/j.molbiopara.2010.03.019
- Baker, D. A., Matralis, A. N., Osborne, S. A., Large, J. M., and Penzo, M. (2020). Targeting the Malaria Parasite cGMP-Dependent Protein Kinase to Develop New Drugs. *Front. Microbiol.* 11, 602803. doi: 10.3389/fmicb.2020.602803
- Baker, D. A., Stewart, L. B., Large, J. M., Bowyer, P. W., Ansell, K. H., Jimenez-Diaz, M. B., et al. (2017). A Potent Series Targeting the Malarial cGMP-Dependent Protein Kinase Clears Infection and Blocks Transmission. *Nat. Commun.* 8, 430. doi: 10.1038/s41467-017-00572-x
- Balestra, A. C., Koussis, K., Klages, N., Howell, S. A., Flynn, H. R., Bantscheff, M., et al. (2021). Ca(2+) Signals Critical for Egress and Gametogenesis in Malaria Parasites Depend on a Multipass Membrane Protein That Interacts With PKG. *Sci. Adv.* 7, 1–17. doi: 10.1126/sciadv.abe5396
- Bancells, C., Llorca-Battle, O., Poran, A., Notzel, C., Rovira-Graells, N., Elemento, O., et al. (2019). Revisiting the Initial Steps of Sexual Development in the Malaria Parasite *Plasmodium Falciparum*. *Nat. Microbiol.* 4, 144–154. doi: 10.1038/s41564-018-0291-7
- Bannister, L., and Mitchell, G. (2003). The Ins, Outs and Roundabouts of Malaria. *Trends Parasitol.* 19, 209–213. doi: 10.1016/S1471-4922(03)00086-2
- Baragana, B., Hallyburton, I., Lee, M. C., Norcross, N. R., Grimaldi, R., Otto, T. D., et al. (2015). A Novel Multiple-Stage Antimalarial Agent That Inhibits Protein Synthesis. *Nature* 522, 315–320. doi: 10.1038/nature14451
- Bargieri, D. Y., Thiberge, S., Tay, C. L., Carey, A. F., Rantz, A., Hischen, F., et al. (2016). *Plasmodium* Merozoite TRAP Family Protein Is Essential for Vacuole

- Membrane Disruption and Gamete Egress From Erythrocytes. *Cell Host Microbe* 20, 618–630. doi: 10.1016/j.chom.2016.10.015
- Bennink, S., Kiesow, M. J., and Pradel, G. (2016). The Development of Malaria Parasites in the Mosquito Midgut. *Cell Microbiol.* 18, 905–918. doi: 10.1111/cmi.12604
- Besteiro, S., Vo Duy, S., Perigaud, C., Lefebvre-Tournier, I., and Vial, H. J. (2010). Exploring Metabolomic Approaches to Analyse Phospholipid Biosynthetic Pathways in Plasmodium. *Parasitology* 137, 1343–1356. doi: 10.1017/S0031182009991934
- Birkholtz, L. M., Alano, P., and Leroy, D. (2022). Transmission-Blocking Drugs for Malaria Elimination. *Trends Parasitol.* 38, 390–403. doi: 10.1016/j.pt.2022.01.011
- Birkholtz, L. M., Coetzer, T. L., Mancama, D., Leroy, D., and Alano, P. (2016). Discovering New Transmission-Blocking Antimalarial Compounds: Challenges and Opportunities. *Trends Parasitol.* 32, 669–681. doi: 10.1016/j.pt.2016.04.017
- Bobenchik, A. M., Augagneur, Y., Hao, B., Hoch, J. C., and Ben Mamoun, C. (2011). Phosphoethanolamine Methyltransferases in Phosphocholine Biosynthesis: Functions and Potential for Antiparasite Therapy. *FEMS Microbiol. Rev.* 35, 609–619. doi: 10.1111/j.1574-6976.2011.00267.x
- Bobenchik, A. M., Choi, J. Y., Mishra, A., Rujan, I. N., Hao, B., Voelker, D. R., et al. (2010). Identification of Inhibitors of *Plasmodium Falciparum* Phosphoethanolamine Methyltransferase Using an Enzyme-Coupled Transmethylation Assay. *BMC Biochem.* 11, 4. doi: 10.1186/1471-2091-11-4
- Bobenchik, A. M., Witola, W. H., Augagneur, Y., Nic Lochlainn, L., Garg, A., Pachikara, N., et al. (2013). *Plasmodium Falciparum* Phosphoethanolamine Methyltransferase is Essential for Malaria Transmission. *Proc. Natl. Acad. Sci. U.S.A.* 110, 18262–18267. doi: 10.1073/pnas.1313965110
- Boltryk, S. D., Passecker, A., Alder, A., Carrington, E., Van De Vegte-Bolmer, M., Van Gemert, G. J., et al. (2021). CRISPR/Cas9-Engineered Inducible Gametocyte Producer Lines as a Valuable Tool for Plasmodium Falciparum Malaria Transmission Research. *Nat. Commun.* 12, 4806. doi: 10.1038/s41467-021-24954-4
- Bousema, T., Okell, L., Shekalaghe, S., Griffin, J. T., Omar, S., Sawa, P., et al. (2010). Revisiting the Circulation Time of *Plasmodium Falciparum* Gametocytes: Molecular Detection Methods to Estimate the Duration of Gametocyte Carriage and the Effect of Gametocytocidal Drugs. *Malar. J.* 9, 136. doi: 10.1186/1475-2875-9-136
- Bouyer, G., Barbieri, D., Dupuy, F., Marteau, A., Sissoko, A., N'dri, M. E., et al. (2020). *Plasmodium Falciparum* Sexual Parasites Regulate Infected Erythrocyte Permeability. *Commun. Biol.* 3, 726. doi: 10.1038/s42003-020-01454-7
- Brancucci, N. M. B., De Niz, M., Straub, T. J., Ravel, D., Sollelis, L., Birren, B. W., et al. (2018). Probing *Plasmodium Falciparum* Sexual Commitment at the Single-Cell Level. *Wellcome Open Res.* 3, 70. doi: 10.12688/wellcomeopenres.14645.4
- Brancucci, N. M. B., Gerdt, J. P., Wang, C., De Niz, M., Philip, N., Adapa, S. R., et al. (2017). Lysophosphatidylcholine Regulates Sexual Stage Differentiation in the Human Malaria Parasite *Plasmodium Falciparum*. *Cell* 171, 1–13. doi: 10.1016/j.cell.2017.10.020
- Broadbent, K. M., Broadbent, J. C., Ribacke, U., Wirth, D., Rinn, J. L., and Sabeti, P. C. (2015). Strand-Specific RNA Sequencing in *Plasmodium Falciparum* Malaria Identifies Developmentally Regulated Long non-Coding RNA and Circular RNA. *BMC Genomics* 16, 454. doi: 10.1186/s12864-015-1603-4
- Brochet, M., Balestra, A. C., and Brusini, L. (2021). cGMP Homeostasis in Malaria Parasites-The Key to Perceiving and Integrating Environmental Changes During Transmission to the Mosquito. *Mol. Microbiol.* 115, 829–838. doi: 10.1111/mmi.14633
- Brochet, M., Collins, M. O., Smith, T. K., Thompson, E., Sebastian, S., Volkman, K., et al. (2014). Phosphoinositide Metabolism Links cGMP-Dependent Protein Kinase G to Essential Ca(2+) Signals at Key Decision Points in the Life Cycle of Malaria Parasites. *PLoS Biol.* 12, e1001806. doi: 10.1371/journal.pbio.1001806
- Buchholz, K., Schirmer, R. H., Eubel, J. K., Akoachere, M. B., Dandekar, T., Becker, K., et al. (2008). Interactions of Methylene Blue With Human Disulfide Reductases and Their Orthologues From *Plasmodium Falciparum*. *Antimicrob. Agents Chemother.* 52, 183–191. doi: 10.1128/AAC.00773-07
- Burrows, J. N., Duparc, S., Gutteridge, W. E., Hooft Van Huijsdijnen, R., Kaszubska, W., Macintyre, F., et al. (2017). New Developments in Anti-Malarial Target Candidate and Product Profiles. *Malaria J.* 16, 26. doi: 10.1186/s12936-016-1675-x
- Butler, C. L., Lucas, O., Wuchty, S., Xue, B., Uversky, V. N., and White, M. (2014). Identifying Novel Cell Cycle Proteins in Apicomplexa Parasites Through Co-Expression Decision Analysis. *PLoS One* 9, e97625. doi: 10.1371/journal.pone.0097625
- Chapman, T. M., Osborne, S. A., Boulou, N., Large, J. M., Wallace, C., Birchall, K., et al. (2013). Substituted Imidazopyridazines are Potent and Selective Inhibitors of *Plasmodium Falciparum* Calcium-Dependent Protein Kinase 1 (Pfcdpk1). *Bioorg. Med. Chem. Lett.* 23, 3064–3069. doi: 10.1016/j.bmcl.2013.03.017
- Chapman, T. M., Osborne, S. A., Wallace, C., Birchall, K., Boulou, N., Jones, H. M., et al. (2014). Optimization of an Imidazopyridazine Series of Inhibitors of *Plasmodium Falciparum* Calcium-Dependent Protein Kinase 1 (Pfcdpk1). *J. Med. Chem.* 57, 3570–3587. doi: 10.1021/jm500342d
- Coertzen, D., Reader, J., van der Watt, M., Nondaba, S. H., Gibbard, L., Wiesner, L., et al. (2018). Artemisone and Artemiside Are Potent Panreactive Antimalarial Agents That Also Synergize Redox Imbalance in *Plasmodium Falciparum* Transmissible Gametocyte Stages. *Antimicrob. Agents Chemother.* 62, 1–17. doi: 10.1128/AAC.02214-17
- Coetzee, N., Sidoli, S., Van Biljon, R., Painter, H., Llinas, M., Garcia, B. A., et al. (2017). Quantitative Chromatin Proteomics Reveals a Dynamic Histone Post-Translational Modification Landscape That Defines Asexual and Sexual *Plasmodium Falciparum* Parasites. *Sci. Rep.* 7, 607. doi: 10.1038/s41598-017-00687-7
- Coetzee, N., Von Gruning, H., Opperman, D., van der Watt, M., Reader, J., and Birkholtz, L. M. (2020). Epigenetic Inhibitors Target Multiple Stages of *Plasmodium Falciparum* Parasites. *Sci. Rep.* 10, 2355. doi: 10.1038/s41598-020-59298-4
- Connacher, J., Josling, G. A., Orchard, L. M., Reader, J., Llinas, M., and Birkholtz, L. M. (2021). H3K36 Methylation Reprograms Gene Expression to Drive Early Gametocyte Development in *Plasmodium Falciparum*. *Epigenet. Chromatin.* 14, 19. doi: 10.1186/s13072-021-00393-9
- Connacher, J., Von Gruning, H., and Birkholtz, L. (2022). Histone Modification Landscapes as a Roadmap for Malaria Parasite Development. *Front. Cell Dev. Biol.* 10. doi: 10.3389/fcell.2022.848797
- Crofts, A. R. (2004). The Cytochrome bc1 Complex: Function in the Context of Structure. *Annu. Rev. Physiol.* 66, 689–733. doi: 10.1146/annurev.physiol.66.032102.150251
- Czesny, B., Goshu, S., Cook, J. L., and Williamson, K. C. (2009). The Proteasome Inhibitor Epoxomicin has Potent *Plasmodium Falciparum* Gametocytocidal Activity. *Antimicrob. Agents Chemother.* 53, 4080–4085. doi: 10.1128/AAC.00088-09
- D'alessandro, S., Camarda, G., Corbett, Y., Siciliano, G., Parapini, S., Cevenini, L., et al. (2016). A Chemical Susceptibility Profile of the *Plasmodium Falciparum* Transmission Stages by Complementary Cell-Based Gametocyte Assays. *J. Antimicrob. Chemother.* 71, 1148–1158. doi: 10.1093/jac/dkv493
- Dearnley, M. K., Yeoman, J. A., Hanssen, E., Kenny, S., Turnbull, L., Whitchurch, C. B., et al. (2012). Origin, Composition, Organization and Function of the Inner Membrane Complex of *Plasmodium Falciparum* Gametocytes. *J. Cell Sci.* 125, 2053–2063. doi: 10.1242/jcs.099002
- Dechamps, S., Wengelnik, K., Berry-Sterkers, L., Cerdan, R., Vial, H. J., and Gannoun-Zaki, L. (2010). The Kennedy Phospholipid Biosynthesis Pathways are Refractory to Genetic Disruption in *Plasmodium Berghei* and Therefore Appear Essential in Blood Stages. *Mol. Biochem. Parasitol.* 173, 69–80. doi: 10.1016/j.molbiopara.2010.05.006
- Decher, K. J., Duerr, H. P., Koelen, K. M. J., Gemert, G. V., Bousema, T., Burrows, J., et al. (2017). Modelling Mosquito Infection at Natural Parasite Densities Identifies Drugs Targeting EF2, PI4K or ATP4 as Key Candidates for Interrupting Malaria Transmission. *Sci. Rep.* 7, 17680. doi: 10.1038/s41598-017-16671-0
- De Koning-Ward, T. F., Olivieri, A., Bertuccini, L., Hood, A., Silvestrini, F., Charvalias, K., et al. (2008). The Role of Osmiophilic Bodies and Pf377 Expression in Female Gametocyte Emergence and Mosquito Infectivity in the Human Malaria Parasite *Plasmodium Falciparum*. *Mol. Microbiol.* 67, 278–290. doi: 10.1111/j.1365-2958.2007.06039.x
- Deligianni, E., Morgan, R. N., Bertuccini, L., Kooij, T. W., Laforge, A., Nahar, C., et al. (2011). Critical Role for a Stage-Specific Actin in Male Exflagellation of

- the Malaria Parasite. *Cell Microbiol.* 13, 1714–1730. doi: 10.1111/j.1462-5822.2011.01652.x
- Delves, M. J. (2012). Plasmodium Cell Biology Should Inform Strategies Used in the Development of Antimalarial Transmission-Blocking Drugs. *Future Med. Chem.* 4, 2251–2263. doi: 10.4155/fmc.12.182
- Delves, M. J., Angrisano, F., and Blagborough, A. M. (2018a). Antimalarial Transmission-Blocking Interventions: Past, Present, and Future. *Trends Parasitol.* 34, 735–746. doi: 10.1016/j.pt.2018.07.001
- Delves, M., Lafuente-Monasterio, M. J., Upton, L., Ruecker, A., Leroy, D., Gamo, F. J., et al. (2019). Fueling Open Innovation for Malaria Transmission-Blocking Drugs: Hundreds of Molecules Targeting Early Parasite Mosquito Stages. *Front. Microbiol.* 10, 2134. doi: 10.3389/fmicb.2019.02134
- Delves, M. J., Miguel-Blanco, C., Matthews, H., Molina, I., Ruecker, A., Yahya, S., et al. (2018b). A High Throughput Screen for Next-Generation Leads Targeting Malaria Parasite Transmission. *Nat. Commun.* 9, 3805. doi: 10.1038/s41467-018-05777-2
- Delves, M. J., Ruecker, A., Straschil, U., Lelièvre, J., Marques, S., López-Barragán, M. J., et al. (2013). Male and Female *Plasmodium Falciparum* Mature Gametocytes Show Different Responses to Antimalarial Drugs. *Antimicrobial Agents Chemother.* 57, 3268–3274. doi: 10.1128/AAC.00325-13
- De Niz, M., Meibalan, E., Mejia, P., Ma, S., Brancucci, N. M. B., Agop-Nersesian, C., et al. (2018). Plasmodium Gametocytes Display Homing and Vascular Transmigration in the Host Bone Marrow. *Sci. Adv.* 4, eaat3775. doi: 10.1126/sciadv.aat3775
- Depoix, D., Marques, S. R., Ferguson, D. J., Chaouch, S., Duguet, T., Sinden, R. E., et al. (2020). Vital Role for Plasmodium Berghei Kinesin8B in Axoneme Assembly During Male Gamete Formation and Mosquito Transmission. *Cell Microbiol.* 22, e13121. doi: 10.1111/cmi.13121
- Dixon, M. W. A., and Tilley, L. (2021). *Plasmodium Falciparum* Goes Bananas for Sex. *Mol. Biochem. Parasitol.* 244, 111385. doi: 10.1016/j.molbiopara.2021.111385
- Dzikan, J. M., Yu, H., Chen, D., Dai, L., Wirjanata, G., Larsson, A., et al. (2019). Identifying Purine Nucleoside Phosphorylase as the Target of Quinine Using Cellular Thermal Shift Assay. *Sci. Transl. Med.* 11, 1–12. doi: 10.1126/scitranslmed.aau3174
- Eksi, S. (2012). *Plasmodium Falciparum* Gametocyte Development 1 (Pfgdv1) and Gametocytogenesis Early Gene Identification and Commitment to Sexual Development. *PLoS Pathog.* 8, 1–14. doi: 10.1371/journal.ppat.1002964
- Eksi, S., Czesny, B., Van Gemert, G. J., Sauerwein, R. W., Eling, W., and Williamson, K. C. (2006). Malaria Transmission-Blocking Antigen, Pfs230, Mediates Human Red Blood Cell Binding to Exflagellating Male Parasites and Oocyst Production. *Mol. Microbiol.* 61, 991–998. doi: 10.1111/j.1365-2958.2006.05284.x
- Elena, D., N., M. R., Lucia, B., A., K. T. W., Alice, L., Carolin, N., et al. (2011). Critical Role for a Stage-Specific Actin in Male Exflagellation of the Malaria Parasite. *Cell. Microbiol.* 13, 1714–1730. doi: 10.1111/j.1462-5822.2011.01652.x
- Evers, F., Cabrera-Orefice, A., Elurbe, D. M., Kea-Te Lindert, M., Boltryk, S. D., Voss, T. S., et al. (2021). Composition and Stage Dynamics of Mitochondrial Complexes in *Plasmodium Falciparum*. *Nat. Commun.* 12, 3820. doi: 10.1038/s41467-021-23919-x
- Filarsky, M., Frashka, S. A., Niederwieser, I., Brancucci, N. M. B., Carrington, E., Carrio, E., et al. (2018). GDV1 Induces Sexual Commitment of Malaria Parasites by Antagonizing HP1-Dependent Gene Silencing. *Science* 359, 1259–1263. doi: 10.1126/science.aan6042
- Fisher, N., Meunier, B., and Biagini, G. A. (2020). The Cytochrome Bc1 Complex as an Antipathogenic Target. *FEBS Lett.* 594, 2935–2952. doi: 10.1002/1873-3468.13868
- Frashka, S. A., Filarsky, M., Hoo, R., Niederwieser, I., Yam, X. Y., Brancucci, N. M. B., et al. (2018). Comparative Heterochromatin Profiling Reveals Conserved and Unique Epigenome Signatures Linked to Adaptation and Development of Malaria Parasites. *Cell Host Microbe* 23, 407–420. doi: 10.1016/j.chom.2018.01.008
- Furuya, T., Mu, J., Hayton, K., Liu, A., Duan, J., Nkrumah, L., et al. (2005). Disruption of a *Plasmodium Falciparum* Gene Linked to Male Sexual Development Causes Early Arrest in Gametocytogenesis. *Proc. Natl. Acad. Sci. U.S.A.* 102, 16813–16818. doi: 10.1073/pnas.0501858102
- Gao, H., Yang, Z., Wang, X., Qian, P., Hong, R., Chen, X., et al. (2018). ISP1-Anchored Polarization of GCbeta/CDC50A Complex Initiates Malaria ookinete Gliding Motility. *Curr. Biol.* 28, 2763–2776, e2766. doi: 10.1016/j.cub.2018.06.069
- Garg, A., Lukt, T., Kumar, V., Choi, J. Y., Augagneur, Y., Voelker, D. R., et al. (2015). Structure, Function and Inhibition of the Phosphoethanolamine Methyltransferases of the Human Malaria Parasites *Plasmodium Vivax* and *Plasmodium Knowlesi*. *Sci. Rep.* 5, 9064. doi: 10.1038/srep09064
- Gautret, P., Miltgen, F., Gantier, J. C., Chabaud, A. G., and Landau, I. (1996). Enhanced Gametocyte Formation by *Plasmodium Chabaudi* in Immature Erythrocytes: Pattern of Production, Sequestration, and Infectivity to Mosquitoes. *J. Parasitol.* 82, 900–906. doi: 10.2307/3284196
- Gerald, N., Mahajan, B., and Kumar, S. (2011). Mitosis in the Human Malaria Parasite *Plasmodium Falciparum*. *Eukaryot. Cell* 10, 474–482. doi: 10.1128/EC.00314-10
- Giannangelo, C., Siddiqui, G., De Paoli, A., Anderson, B. M., Edgington-Mitchell, L. E., Charman, S. A., et al. (2020). System-Wide Biochemical Analysis Reveals Ozonide Antimalarials Initially Act by Disrupting *Plasmodium Falciparum* Haemoglobin Digestion. *PLoS Pathog.* 16, e1008485. doi: 10.1371/journal.ppat.1008485
- Goncalves, B. P., Tiono, A. B., Ouedraogo, A., Guelbeogo, W. M., Bradley, J., Nebie, I., et al. (2016). Single Low Dose Primaquine to Reduce Gametocyte Carriage and *Plasmodium Falciparum* Transmission After Artemether-Lumefantrine in Children With Asymptomatic Infection: A Randomised, Double-Blind, Placebo-Controlled Trial. *BMC Med.* 14, 40. doi: 10.1186/s12916-016-0581-y
- Graumans, W., Jacobs, E., Bousema, T., and Sinnis, P. (2020). When Is a Plasmodium-Infected Mosquito an Infectious Mosquito? *Trends Parasitol.* 36, 705–716. doi: 10.1016/j.pt.2020.05.011
- Gulati, S., Ekland, E. H., Ruggles, K. V., Chan, R. B., Jayabalasingham, B., Zhou, B., et al. (2015). Profiling the Essential Nature of Lipid Metabolism in Asexual Blood and Gametocyte Stages of *Plasmodium Falciparum*. *Cell Host Microbe* 18, 371–381. doi: 10.1016/j.chom.2015.08.003
- Hart, K. J., Oberstaller, J., Walker, M. P., Minns, A. M., Kennedy, M. F., Padykula, I., et al. (2019). Plasmodium Male Gametocyte Development and Transmission are Critically Regulated by the Two Putative Deadenylases of the CAF1/CCR4/NOT Complex. *PLoS Pathog.* 15, e1007164. doi: 10.1371/journal.ppat.1007164
- Hart, K. J., Power, B. J., Rios, K. T., Sebastian, A., and Lindner, S. E. (2021). The Plasmodium NOT1-G Paralogue is an Essential Regulator of Sexual Stage Maturation and Parasite Transmission. *PLoS Biol.* 19, e3001434. doi: 10.1371/journal.pbio.3001434
- Howes, R. E., Piel, F. B., Patil, A. P., Nyangiri, O. A., Gething, P. W., Dewi, M., et al. (2012). G6PD Deficiency Prevalence and Estimates of Affected Populations in Malaria Endemic Countries: A Geostatistical Model-Based Map. *PLoS Med.* 9, e1001339. doi: 10.1371/journal.pmed.1001339
- Huang, W., Hulverson, M. A., Zhang, Z., Choi, R., Hart, K. J., Kennedy, M., et al. (2016). 5-Aminopyrazole-4-Carboxamide Analogues are Selective Inhibitors of *Plasmodium Falciparum* Microgametocyte Exflagellation and Potential Malaria Transmission Blocking Agents. *Bioorg. Med. Chem. Lett.* 26, 5487–5491. doi: 10.1016/j.bmcl.2016.10.014
- Jeevaratnam, K., Vidya, S., and Vaidyanathan, C. S. (1992). *In Vitro* and *In Vivo* Effect of Methyl Isocyanate on Rat Liver Mitochondrial Respiration. *Toxicol. Appl. Pharmacol.* 117, 172–179. doi: 10.1016/0041-008X(92)90234-J
- Josling, G. A., Williamson, K. C., and Llinás, M. (2018). Regulation of Sexual Commitment and Gametocytogenesis in Malaria Parasites. *Annu. Rev. Microbiol.* 72, 501–519. doi: 10.1146/annurev-micro-090817-062712
- Kafsack, B. F. C., Rovira-Graells, N., Clark, T. G., Bancells, C., Crowley, V. M., Campino, S. G., et al. (2014). A Transcriptional Switch Underlies Commitment to Sexual Development in Malaria Parasites. *Nature* 507, 248–254. doi: 10.1038/nature12920
- Klonis, N., Crespo-Ortiz, M. P., Bottova, I., Abu-Bakar, N., Kenny, S., Rosenthal, P. J., et al. (2011). Artemisinin Activity Against *Plasmodium Falciparum* Requires Hemoglobin Uptake and Digestion. *Proc. Natl. Acad. Sci. U.S.A.* 108, 11405–11410. doi: 10.1073/pnas.1104063108
- Kuehn, A., and Pradel, G. (2010). The Coming-Out of Malaria Gametocytes. *J. Biomed. Biotechnol.* 2010, 1–11. doi: 10.1155/2010/976827
- Kuhen, K. L., Chatterjee, A. K., Rottmann, M., Gagaring, K., Borboa, R., Buenviaje, J., et al. (2014). KAF156 is an Antimalarial Clinical Candidate With Potential for Use in Prophylaxis, Treatment, and Prevention of Disease Transmission. *Antimicrob. Agents Chemother.* 58, 5060–5067. doi: 10.1128/AAC.02727-13

- Kumar, S., Haile, M. T., Hoopmann, M. R., Tran, L. T., Michaels, S. A., Morrone, S. R., et al. (2021). *Plasmodium Falciparum* Calcium-Dependent Protein Kinase 4 is Critical for Male Gametogenesis and Transmission to the Mosquito Vector. *mBio* 12, e0257521. doi: 10.1128/mBio.02575-21
- Lamour, S. D., Straschil, U., Saric, J., and Delves, M. J. (2014). Changes in Metabolic Phenotypes of *Plasmodium Falciparum* In Vitro Cultures During Gametocyte Development. *Malaria J.* 13, 468. doi: 10.1186/1475-2875-13-468
- Large, J. M., Osborne, S. A., Smiljanic-Hurley, E., Ansell, K. H., Jones, H. M., Taylor, D. L., et al. (2013). Imidazopyridazines as Potent Inhibitors of *Plasmodium Falciparum* Calcium-Dependent Protein Kinase 1 (PfCDPK1): Preparation and Evaluation of Pyrazole Linked Analogues. *Bioorg. Med. Chem. Lett.* 23, 6019–6024. doi: 10.1016/j.bmcl.2013.08.010
- Lasonder, E., Rijpmma, S. R., Van schaijk, B. C., Hoeijmakers, W. a., Kensch, P. R., Gresnigt, M. S., et al. (2016). Integrated Transcriptomic and Proteomic Analyses of *P. Falciparum* Gametocytes: Molecular Insight Into Sex-Specific Processes and Translational Repression. *Nucleic Acids Res.* 44, 6087–6101. doi: 10.1093/nar/gkw536
- Laurens, M. B. (2020). RTS/AS01 Vaccine (Mosquirix™): An Overview. *Hum. Vaccines Immunother.* 16, 480–489. doi: 10.1080/21645515.2019.1669415
- Lemercier, G., Fernandez-Montalvan, A., Shaw, J. P., Kugelstadt, D., Bomke, J., Domostoj, M., et al. (2009). Identification and Characterization of Novel Small Molecules as Potent Inhibitors of the Plasmodial Calcium-Dependent Protein Kinase 1. *Biochemistry* 48, 6379–6389. doi: 10.1021/bi9005122
- Leroy, D., Campo, B., Ding, X. C., Burrows, J. N., and Cherbuin, S. (2014). Defining the Biology Component of the Drug Discovery Strategy for Malaria Eradication. *Trends Parasitol.* 30, 478–490. doi: 10.1016/j.pt.2014.07.004
- Lingnau, A., Margos, G., Maier, W. A., and Seitz, H. M. (1993). The Effects of Hormones on the Gametocytogenesis of *Plasmodium Falciparum* In Vitro. *Appl. Parasitol.* 34, 153–160.
- Liu, F., Liu, Q., Yu, C., Zhao, Y., Wu, Y., Min, H., et al. (2019). An MFS-Domain Protein Pb115 Plays a Critical Role in Gamete Fertilization of the Malaria Parasite *Plasmodium Berghei*. *Front. Microbiol.* 10, 2193. doi: 10.3389/fmicb.2019.02193
- Lobo, C. A., Fujioka, H., Aikawa, M., and Kumar, N. (1999). Disruption of the Pfg27 Locus by Homologous Recombination Leads to Loss of the Sexual Phenotype in *P. Falciparum*. *Mol. Cell* 3, 793–798. doi: 10.1016/S1097-2765(01)80011-3
- Lopez-Barragan, M. J., Lemieux, J., Quinones, M., Williamson, K. C., Molina-Cruz, A., Cui, K., et al. (2011). Directional Gene Expression and Antisense Transcripts in Sexual and Asexual Stages of *Plasmodium Falciparum*. *BMC Genomics* 12, 587. doi: 10.1186/1471-2164-12-587
- Macrae, J. I., Dixon, M. W. A., Dearnley, M. K., Chua, H. H., Chambers, J. M., Kenny, S., et al. (2013). Mitochondrial Metabolism of Sexual and Asexual Blood Stages of the Malaria Parasite *Plasmodium Falciparum*. *BMC Biol.* 11, 1–10. doi: 10.1186/1741-7007-11-67
- Malmquist, N. A., Sundriyal, S., Caron, J., Chen, P., Witkowski, B., Menard, D., et al. (2015). Histone Methyltransferase Inhibitors are Orally Bioavailable, Fast-Acting Molecules With Activity Against Different Species Causing Malaria in Humans. *Antimicrob. Agents Chemother.* 59, 950–959. doi: 10.1128/AAC.04419-14
- Matthews, K. A., Senagbe, K. M., Notzel, C., Gonzales, C. A., Tong, X., Rijo-Ferreira, F., et al. (2020). Disruption of the *Plasmodium Falciparum* Life Cycle Through Transcriptional Reprogramming by Inhibitors of Jumonji Demethylases. *ACS Infect. Dis.* 6, 1058–1075. doi: 10.1021/acsinfecdis.9b00455
- Mcnamara, C. W., Lee, M. C., Lim, C. S., Lim, S. H., Roland, J., Simon, O., et al. (2013). Targeting Plasmodium Pi(4)K to Eliminate Malaria. *Nature* 504, 248–253. doi: 10.1038/nature12782
- McRobert, L., Taylor, C. J., Deng, W., Fivelman, Q. L., Cummings, R. M., Polley, S. D., et al. (2008). Gametogenesis in Malaria Parasites is Mediated by the cGMP-Dependent Protein Kinase. *PLoS Biol.* 6, e139. doi: 10.1371/journal.pbio.0060139
- Meerstein-Kessel, L., Andolina, C., Carrio, E., Mahamar, A., Sawa, P., Diawara, H., et al. (2018). A Multiplex Assay for the Sensitive Detection and Quantification of Male and Female *Plasmodium Falciparum* Gametocytes. *Malar. J.* 17, 441. doi: 10.1186/s12936-018-2584-y
- Meibalan, E., and Marti, M. (2017). Biology of Malaria Transmission. *Cold Spring Harb. Perspect. Med.* 7, 1–15. doi: 10.1101/cshperspect.a025452
- Menezes, R., Gomes, M. D. S. M., Mendes, A. M., Couto, A. A. R. A., Nacher, M., Pimenta, T. S., et al. (2018). Enteroparasite and Vivax Malaria Co-Infection on the Brazil-French Guiana Border: Epidemiological, Haematological and Immunological Aspects. *PLoS One* 13, e0189958. doi: 10.1371/journal.pone.0189958
- Messina, V., Valtieri, M., Rubio, M., Falchi, M., Mancini, F., Mayor, A., et al. (2018). Gametocytes of the Malaria Parasite *Plasmodium Falciparum* Interact With and Stimulate Bone Marrow Mesenchymal Cells to Secrete Angiogenic Factors. *Front. Cell Infect. Microbiol.* 8, 50. doi: 10.3389/fcimb.2018.00050
- Miao, J., Fan, Q., Parker, D., Li, X., Li, J., and Cui, L. (2013). Puf Mediates Translation Repression of Transmission-Blocking Vaccine Candidates in Malaria Parasites. *PLoS Pathog.* 9, e1003268. doi: 10.1371/journal.ppat.1003268
- Miao, J., Li, J., Fan, Q., Li, X., Li, X., and Cui, L. (2010). The Puf-Family RNA-Binding Protein PfPuf2 Regulates Sexual Development and Sex Differentiation in the Malaria Parasite *Plasmodium Falciparum*. *J. Cell Sci.* 123, 1039–1049. doi: 10.1242/jcs.059824
- Miguel-Blanco, C., Molina, I., Bardera, A. I., Diaz, B., De Las Heras, L., Lozano, S., et al. (2017). Hundreds of Dual-Stage Antimalarial Molecules Discovered by a Functional Gametocyte Screen. *Nat. Commun.* 8, 15160. doi: 10.1038/ncomms15160
- Moussaoui, D., Robblee, J. P., Auguin, D., Kremontsova, E. B., Haase, S., Blake, T. C. A., et al. (2020). Full-Length *Plasmodium Falciparum* Myosin A and Essential Light Chain PfELC Structures Provide New Anti-Malarial Targets. *Elife* 9, 1–24. doi: 10.7554/eLife.60581.sa2
- Munsamy, G., Agoni, C., and Soliman, M. E. S. (2018). A Dual Target of Plasmapsin IX and X: Unveiling the Atomistic Superiority of a Core Chemical Scaffold in Malaria Therapy. *J. Cell Biochem.* 120, 7876–7887. doi: 10.1002/jcb.28062
- Neveu, G., Beri, D., and Kafsack, B. F. (2020a). Metabolic Regulation of Sexual Commitment in *Plasmodium Falciparum*. *Curr. Opin. Microbiol.* 58, 93–98. doi: 10.1016/j.mib.2020.09.004
- Neveu, G., Richard, C., Dupuy, F., Behera, P., Volpe, F., Subramani, P. A., et al. (2020b). *Plasmodium Falciparum* Sexual Parasites Develop in Human Erythroblasts and Affect Erythropoiesis. *Blood* 136, 1381–1393. doi: 10.1182/blood.2019004746
- Ngotho, P., Soares, A. B., Hentzschel, F., Achcar, F., Bertuccini, L., and Marti, M. (2019). Revisiting Gametocyte Biology in Malaria Parasites. *FEMS Microbiol. Rev.* 43, 401–414. doi: 10.1093/femsre/fuz010
- Nilsen, A., Lacure, A. N., White, K. L., Forquer, I. P., Cross, R. M., Marfurt, J., et al. (2013). Quinolone-3-Diarylethers: A New Class of Antimalarial Drug. *Sci. Transl. Med.* 5, 177ra137. doi: 10.1126/scitranslmed.3005029
- Nilsson, S. K., Childs, L. M., Buckee, C., and Marti, M. (2015). Targeting Human Transmission Biology for Malaria Elimination. *PLoS Pathog.* 11, e1004871. doi: 10.1371/journal.ppat.1004871
- Ono, T., Nakai, T., and Nakabayashi, T. (1986). Induction of Gametocytogenesis in *Plasmodium Falciparum* by the Culture Supernatant of Hybridoma Cells Producing Anti-*P. Falciparum* Antibody. *Biken J.* 29, 77–81.
- Painter, H. J., Carrasquilla, M., and Llinas, M. (2017). Capturing In Vivo RNA Transcriptional Dynamics From the Malaria Parasite *Plasmodium Falciparum*. *Genome Res.* 27, 1074–1086. doi: 10.1101/gr.217356.116
- Paquet, T., Le Manach, C., Cabrera, D. G., Younis, Y., Henrich, P. P., Abraham, T. S., et al. (2017). Antimalarial Efficacy of MMV390048, an Inhibitor of Plasmodium Phosphatidylinositol 4-Kinase. *Sci. Transl. Med.* 9, 1–14. doi: 10.1126/scitranslmed.aad9735
- Parkyn Schneider, M., Liu, B., Glock, P., Suttie, A., Mchugh, E., Andrew, D., et al. (2017). Disrupting Assembly of the Inner Membrane Complex Blocks *Plasmodium Falciparum* Sexual Stage Development. *PLoS Pathog.* 13, e1006659. doi: 10.1371/journal.ppat.1006659
- Paton, D. G., Childs, L. M., Itoe, M. A., Holmdahl, I. E., Buckee, C. O., and Catteruccia, F. (2019). Exposing Anopheles Mosquitoes to Antimalarials Blocks Plasmodium Parasite Transmission. *Nature* 567, 239–243. doi: 10.1038/s41586-019-0973-1
- Paul, R. E. L., Brey, P. T., and Robert, V. (2002). *Plasmodium* Sex Determination and Transmission to Mosquitoes. *Trends Parasitol.* 18, 32–38. doi: 10.1016/S1471-4922(01)02122-5
- Peatey, C. L., Skinner-Adams, T. S., Dixon, M. W., McCarthy, J. S., Gardiner, D. L., and Trenholme, K. R. (2009). Effect of Antimalarial Drugs on *Plasmodium Falciparum* Gametocytes. *J. Infect. Dis.* 200, 1518–1521. doi: 10.1086/644645
- Pelle, K. G., Oh, K., Buchholz, K., Narasimhan, V., Joice, R., Milner, D. A., et al. (2015). Transcriptional Profiling Defines Dynamics of Parasite Tissue

- Sequestration During Malaria Infection. *Genome Med.* 7, 19. doi: 10.1186/s13073-015-0133-7
- Plouffe, D. M., Wree, M., Du, A. Y., Meister, S., Li, F., Patra, K., et al. (2016). High-Throughput Assay and Discovery of Small Molecules That Interrupt Malaria Transmission. *Cell Host Microbe* 19, 114–126. doi: 10.1016/j.chom.2015.12.001
- Poran, A., Notzel, C., Aly, O., Mencia-Trinchant, N., Harris, C. T., Guzman, M. L., et al. (2017). Single-Cell RNA Sequencing Reveals a Signature of Sexual Commitment in Malaria Parasites. *Nature* 551, 95–99. doi: 10.1038/nature24280
- Portugaliza, H. P., Miyazaki, S., Geurten, F. J., Pell, C., Rosanas-Urgell, A., Janse, C. J., et al. (2020). Artemisinin Exposure at the Ring or Trophozoite Stage Impacts *Plasmodium Falciparum* Sexual Conversion Differently. *Elife* 9, 1–22. doi: 10.7554/eLife.60058.sa2
- Posayapisit, N., Pengon, J., Prommana, P., Shoram, M., Yuthavong, Y., Uthapibull, C., et al. (2021). Transgenic Pyrimethamine-Resistant *Plasmodium Falciparum* Reveals Transmission-Blocking Potency of P218, a Novel Antifolate Candidate Drug. *Int. J. Parasitol.* 51, 635–642. doi: 10.1016/j.ijpara.2020.12.002
- Pradel, G. (2007). Proteins of the Malaria Parasite Sexual Stages: Expression, Function and Potential for Transmission Blocking Strategies. *Parasitology* 134, 1911–1929. doi: 10.1017/S0031182007003381
- Prudencio, M., Rodriguez, A., and Mota, M. M. (2006). The Silent Path to Thousands of Merozoites: The Plasmodium Liver Stage. *Nat. Rev. Microbiol.* 4, 849–856. doi: 10.1038/nrmicro1529
- Putz, C., and Manyando, C. (1997). Enhanced Gametocyte Production in Fansidar-Treated *Plasmodium Falciparum* Malaria Patients: Implications for Malaria Transmission Control Programmes. *Trop. Med. Int. Health* 2, 227–229. doi: 10.1046/j.1365-3156.1997.d01-267.x
- Raabe, A. C., Billker, O., Vial, H. J., and Wengelnik, K. (2009). Quantitative Assessment of DNA Replication to Monitor Microgametogenesis in *Plasmodium Berghiei*. *Mol. Biochem. Parasitol.* 168, 172–176. doi: 10.1016/j.molbiopara.2009.08.004
- Ramdani, G., Naissant, B., Thompson, E., Breil, F., Lorthiois, A., Dupuy, F., et al. (2015). cAMP-Signalling Regulates Gametocyte-Infected Erythrocyte Deformability Required for Malaria Parasite Transmission. *PLoS Pathog.* 11, e1004815. doi: 10.1371/journal.ppat.1004815
- Reader, J., van der Watt, M. E., Taylor, D., Le Manach, C., Mittal, N., Otilie, S., et al. (2021). Multistage and Transmission-Blocking Targeted Antimalarials Discovered From the Open-Source MMV Pandemic Response Box. *Nat. Commun.* 12, 269. doi: 10.1038/s41467-020-20629-8
- Ridgway, M. C., Cihlova, D., Brown, S. H. J., Tran, P., Mitchell, T. W., and Maier, A. G. (2022). Analysis of Sex-Specific Lipid Metabolism of Plasmodium Falciparum Points to the Importance of Sphingomyelin for Gametocytogenesis. *J. Cell Sci.* 135, 1–13. doi: 10.1242/jcs.259592
- Rottmann, M., McNamara, C., Yeung, B. K., Lee, M. C., Zou, B., Russell, B., et al. (2010). Spiroindolones, a Potent Compound Class for the Treatment of Malaria. *Science* 329, 1175–1180. doi: 10.1126/science.1193225
- Salcedo-Sora, J. E., Caamano-Gutierrez, E., Ward, S. A., and Biagini, G. A. (2014). The Proliferating Cell Hypothesis: A Metabolic Framework for Plasmodium Growth and Development. *Trends Parasitol.* 30, 170–175. doi: 10.1016/j.pt.2014.02.001
- Sargeant, T. J., Marti, M., Caler, E., Carlton, J. M., Simpson, K., Speed, T. P., et al. (2006). Lineage-Specific Expansion of Proteins Exported to Erythrocytes in Malaria Parasites. *Genome Biol.* 7, R12. doi: 10.1186/gb-2006-7-2-r12
- Schalkwijk, J., Allman, E. L., Jansen, P., De Vries, L. E., Verhoef, J. M. J., Jackowski, S., et al. (2019). Antimalarial Pantothenamide Metabolites Target Acetyl-Coenzyme A Biosynthesis in *Plasmodium Falciparum*. *Sci. Transl. Med.* 11, 1–12. doi: 10.1126/scitranslmed.aas9917
- Schneider, P., and Reece, S. E. (2021). The Private Life of Malaria Parasites: Strategies for Sexual Reproduction. *Mol. Biochem. Parasitol.* 244, 111375. doi: 10.1016/j.molbiopara.2021.111375
- Schneider, P., Reece, S. E., Van Schaijk, B. C., Bousema, T., Lanke, K. H., Meaden, C. S., et al. (2015). Quantification of Female and Male *Plasmodium Falciparum* Gametocytes by Reverse Transcriptase Quantitative PCR. *Mol. Biochem. Parasitol.* 199, 29–33. doi: 10.1016/j.molbiopara.2015.03.006
- Severini, C., Silvestrini, F., Sannella, A., Barca, S., Gradoni, L., and Alano, P. (1999). The Production of the Osmiophilic Body Protein Pfg377 is Associated With Stage of Maturation and Sex in *Plasmodium Falciparum* Gametocytes. *Mol. Biochem. Parasitol.* 100, 247–252. doi: 10.1016/S0166-6851(99)00050-X
- Silvestrini, F., Alano, P., and Williams, J. L. (2000). Commitment to the Production of Male and Female Gametocytes in the Human Malaria Parasite *Plasmodium Falciparum*. *Parasitology* 121, 465–471. doi: 10.1017/S0031182099006691
- Silvestrini, F., Lasonder, E., Olivieri, A., Camarda, G., Van Schaijk, B., Sanchez, M., et al. (2010). Protein Export Marks the Early Phase of Gametocytogenesis of the Human Malaria Parasite *Plasmodium Falciparum*. *Mol. Cell Proteomics* 9, 1437–1448. doi: 10.1074/mcp.M900479-MCP200
- Simon, C. S., Sturmer, V. S., and Guizetti, J. (2021). How Many Is Enough? - Challenges of Multinucleated Cell Division in Malaria Parasites. *Front. Cell Infect. Microbiol.* 11, 658616. doi: 10.3389/fcimb.2021.658616
- Sinden, R. E. (2017). Developing Transmission-Blocking Strategies for Malaria Control. *PLoS Pathog.* 13, e1006336. doi: 10.1371/journal.ppat.1006336
- Sinden, R. E., Canning, E. U., Bray, R. S., and Smalley, M. E. (1977). Gametocyte and Gamete Development in *Plasmodium Falciparum*. *Proc. R. Soc.* 201, 375–399. doi: 10.1098/rspb.1978.0051
- Sinden, R. E., Carter, R., Drakeley, C., and Leroy, D. (2012). The Biology of Sexual Development of Plasmodium: The Design and Implementation of Transmission-Blocking Strategies. *Malar. J.* 11, 70. doi: 10.1186/1475-2875-11-70
- Singh, S., Santos, J. M., Orchard, L. M., Yamada, N., Van Biljon, R., Painter, H. J., et al. (2021b). The PfAP2-G2 Transcription Factor is a Critical Regulator of Gametocyte Maturation. *Mol. Microbiol.* 115, 1005–1024. doi: 10.1111/mmi.14676
- Singh, M., Suryanshu, Kanika, Singh, G., Dubey, A., and Chaitanya, R. K. (2021a). Plasmodium's Journey Through the Anopheles Mosquito: A Comprehensive Review. *Biochimie* 181, 176–190. doi: 10.1016/j.biochi.2020.12.009
- Sinha, A., Hughes, K. R., Modrzynska, K. K., Otto, T. D., Pfander, C., Dickens, N. J., et al. (2014). A Cascade of DNA-Binding Proteins for Sexual Commitment and Development in *Plasmodium*. *Nature* 507, 253–257. doi: 10.1038/nature12970
- Smith, T. G., Lourenco, P., Carter, R., Walliker, D., and Ranford-Cartwright, L. C. (2000). Commitment to Sexual Differentiation in the Human Malaria Parasite, *Plasmodium Falciparum*. *Parasitology* 121 (Pt 2), 127–133. doi: 10.1017/S0031182099006265
- Sologub, L., Kuehn, A., Kern, S., Przyborski, J., Schillig, R., and Pradel, G. (2011). Malaria Proteases Mediate Inside-Out Egress of Gametocytes From Red Blood Cells Following Parasite Transmission to the Mosquito. *Cell Microbiol.* 13, 897–912. doi: 10.1111/j.1462-5822.2011.01588.x
- Sowunmi, A., Balogun, S. T., Gbotosho, G. O., and Happi, C. T. (2008). *Plasmodium Falciparum* Gametocyte Sex Ratios in Children With Acute, Symptomatic, Uncomplicated Infections Treated With Amodiaquine. *Malaria J.* 7, 1–13. doi: 10.1186/1475-2875-7-169
- Srivastava, A., Evans, K. J., Sexton, A. E., Schofield, L., and Creek, D. J. (2017). Metabolomics-Based Elucidation of Active Metabolic Pathways in Erythrocytes and HSC-Derived Reticulocytes. *J. Proteome Res.* 16, 1492–1505. doi: 10.1021/acs.jproteome.6b00902
- Srivastava, A., Philip, N., Hughes, K. R., Georgiou, K., Macrae, J. I., Barrett, M. P., et al. (2016). Stage-Specific Changes in Plasmodium Metabolism Required for Differentiation and Adaptation to Different Host and Vector Environments. *PLoS Pathog.* 12, e1006094. doi: 10.1371/journal.ppat.1006094
- Stickles, A. M., De Almeida, M. J., Morrissey, J. M., Sheridan, K. A., Forquer, I. P., Nilsen, A., et al. (2015a). Subtle Changes in Endochin-Like Quinolone Structure Alter the Site of Inhibition Within the Cytochrome bc1 Complex of *Plasmodium Falciparum*. *Antimicrob. Agents Chemother.* 59, 1977–1982. doi: 10.1128/AAC.04149-14
- Stickles, A. M., Ting, L. M., Morrissey, J. M., Li, Y., Mather, M. W., Meermeier, E., et al. (2015b). Inhibition of Cytochrome bc1 as a Strategy for Single-Dose, Multi-Stage Antimalarial Therapy. *Am. J. Trop. Med. Hyg.* 92, 1195–1201. doi: 10.4269/ajtmh.14-0553
- Straschil, U., Talman, A. M., Ferguson, D. J., Bunting, K. A., Xu, Z., Bailes, E., et al. (2010). The Armadillo Repeat Protein PF16 is Essential for Flagellar Structure and Function in Plasmodium Male Gametes. *PLoS One* 5, e12901. doi: 10.1371/journal.pone.0012901
- Talman, A. M., Paul, R. E., Sokhna, C. S., Domarle, O., Arie, F., Trape, J. F., et al. (2004). Influence of Chemotherapy on the *Plasmodium* Gametocyte Sex Ratio of Mice and Humans. *Am. J. Trop. Med. Hyg.* 71, 739–744. doi: 10.4269/ajtmh.2004.71.739

- Talman, A. M., Prieto, J. H., Marques, S., Ubaida-Mohien, C., Lawniczak, M., Wass, M. N., et al. (2014). Proteomic Analysis of the Plasmodium Male Gamete Reveals the Key Role for Glycolysis in Flagellar Motility. *Malar. J.* 13, 315. doi: 10.1186/1475-2875-13-315
- Taylor, H. M., McRobert, L., Grainger, M., Sicard, A., Dluzewski, A. R., Hopp, C. S., et al. (2010). The Malaria Parasite Cyclic GMP-Dependent Protein Kinase Plays a Central Role in Blood-Stage Schizogony. *Eukaryot. Cell* 9, 37–45. doi: 10.1128/EC.00186-09
- Teng, R., Junankar, P. R., Bubbs, W. A., Rae, C., Mercier, P., and Kirk, K. (2009). Metabolite Profiling of the Intraerythrocytic Malaria Parasite *Plasmodium Falciparum* by (1)H NMR Spectroscopy. *NMR BioMed.* 22, 292–302. doi: 10.1002/nbm.1323
- Thommen, B. T., Passecker, A., Buser, T., Hitz, E., Voss, T. S., and Brancucci, N. M. B. (2022). Revisiting the Effect of Pharmaceuticals on Transmission Stage Formation in the Malaria Parasite *Plasmodium Falciparum*. *Front. Cell Infect. Microbiol.* 12, 802341. doi: 10.3389/fcimb.2022.802341
- Tiburcio, M., Dixon, M. W., Looker, O., Younis, S. Y., Tilley, L., and Alano, P. (2015). Specific Expression and Export of the *Plasmodium Falciparum* Gametocyte Exported Protein-5 Marks the Gametocyte Ring Stage. *Malaria J.* 14, 334. doi: 10.1186/s12936-015-0853-6
- Tiburcio, M., Hitz, E., Niederwieser, I., Kelly, G., Davies, H., Doerig, C., et al. (2021). A 39-Amino-Acid C-Terminal Truncation of GDV1 Disrupts Sexual Commitment in *Plasmodium Falciparum*. *mSphere* 6, 1–13. doi: 10.1128/mSphere.01093-20
- Tibúrcio, M., Niang, M., Deplaine, G., Perrot, S., Bischoff, E., Ndour, P. A., et al. (2012). A Switch in Infected Erythrocyte Deformability at the Maturation and Blood Circulation of *Plasmodium Falciparum* Transmission Stages. *Blood* 119, 172–180. doi: 10.1182/blood-2012-03-414557
- Tiburcio, M., Silvestrini, F., Bertuccini, L., Sander, A. F., Turner, L., Lavtsen, T., et al. (2013). Early Gametocytes of the Malaria Parasite *Plasmodium Falciparum* Specifically Remodel the Adhesive Properties of Infected Erythrocyte Surface. *Cell. Microbiol.* 15, 647–659. doi: 10.1111/cmi.12062
- Tiburcio, M., Yang, A. S. P., Yahata, K., Suarez-Cortes, P., Belda, H., Baumgarten, S., et al. (2019). A Novel Tool for the Generation of Conditional Knockouts To Study Gene Function Across the *Plasmodium Falciparum* Life Cycle. *mBio* 10, 1–12. doi: 10.1128/mBio.01170-19
- Trager, W., Gill, G. S., Lawrence, C., and Nagel, R. L. (1999). *Plasmodium Falciparum*: Enhanced Gametocyte Formation In Vitro in Reticulocyte-Rich Blood. *Exp. Parasitol.* 91, 115–118. doi: 10.1006/expr.1998.4347
- Tran, P. N., Brown, S. H. J., Rug, M., Ridgway, M. C., Mitchell, T. W., and Maier, A. G. (2016). Changes in Lipid Composition During Sexual Development of the Malaria Parasite *Plasmodium Falciparum*. *Malaria J.* 15, 73. doi: 10.1186/s12936-016-1130-z
- Usui, M., and Williamson, K. C. (2021). Stressed Out About *Plasmodium Falciparum* Gametocytogenesis. *Front. Cell Infect. Microbiol.* 11, 790067. doi: 10.3389/fcimb.2021.790067
- Vallone, A., D'alessandro, S., Brogi, S., Brindisi, M., Chemi, G., Alfano, G., et al. (2018). Antimalarial Agents Against Both Sexual and Asexual Parasites Stages: Structure-Activity Relationships and Biological Studies of the Malaria Box Compound 1-[5-(4-Bromo-2-Chlorophenyl)Furan-2-Yl]-N-[(Piperidin-4-Yl)Methyl]Methanamine (MMV019918) and Analogues. *Eur. J. Med. Chem.* 150, 698–718. doi: 10.1016/j.ejmech.2018.03.024
- Vanaerschot, M., Muriithi, J. M., Pasaje, C. F. A., Ghidelli-Disse, S., Dwomoh, L., Bird, M., et al. (2020). Inhibition of Resistance-Refractory P. Falciparum Kinase PKG Delivers Prophylactic, Blood Stage, and Transmission-Blocking Antiplasmodial Activity. *Cell Chem. Biol.* 27, 806–816.e808. doi: 10.1016/j.chembiol.2020.04.001
- Van Biljon, R., Niemand, J., Van Wyk, R., Clark, K., Verlinden, B., Abrie, C., et al. (2018). Inducing Controlled Cell Cycle Arrest and Re-Entry During Asexual Proliferation of *Plasmodium Falciparum* Malaria Parasites. *Sci. Rep.* 8, 16581. doi: 10.1038/s41598-018-34964-w
- Van Biljon, R., Van Wyk, R., Painter, H. J., Orchard, L., Reader, J., Niemand, J., et al. (2019). Hierarchical Transcriptional Control Regulates *Plasmodium Falciparum* Sexual Differentiation. *BMC Genomics* 20, 920. doi: 10.1186/s12864-019-6322-9
- Van Dijk, M. R., Van Schaijk, B. C., Khan, S. M., Van Dooren, M. W., Ramesar, J., Kaczanowski, S., et al. (2010). Three Members of the 6-Cys Protein Family of Plasmodium Play a Role in Gamete Fertility. *PLoS Pathog.* 6, e1000853. doi: 10.1371/journal.ppat.1000853
- Vanheer, L. N., Zhang, H., Lin, G., and Kafsack, B. F. C. (2020). Activity of Epigenetic Inhibitors Against *Plasmodium Falciparum* Asexual and Sexual Blood Stages. *Antimicrob. Agents Chemother.* 64, 1–6. doi: 10.1128/AAC.02523-19
- Van Pelt-Koops, J. C., Pett, H. E., Graumans, W., van der Vegte-Bolmer, M., Van Gemert, G. J., Rottmann, M., et al. (2012). The Spiroindolone Drug Candidate NITD609 Potently Inhibits Gametocytogenesis and Blocks *Plasmodium Falciparum* Transmission to Anopheles Mosquito Vector. *Antimicrob. Agents Chemother.* 56, 3544–3548. doi: 10.1128/AAC.06377-11
- Van Schaijk, B. C., Van Dijk, M. R., Van De Vegte-Bolmer, M., Van Gemert, G. J., Van Dooren, M. W., Eksi, S., et al. (2006). Pfs47, Paralog of the Male Fertility Factor Pfs48/45, is a Female Specific Surface Protein in *Plasmodium Falciparum*. *Mol. Biochem. Parasitol.* 149, 216–222. doi: 10.1016/j.molbiopara.2006.05.015
- Venugopal, K., Hentzschel, F., Valkiunas, G., and Marti, M. (2020). Plasmodium Asexual Growth and Sexual Development in the Haematopoietic Niche of the Host. *Nat. Rev. Microbiol.* 18, 177–189. doi: 10.1038/s41579-019-0306-2
- Vidadala, R. S., Ojo, K. K., Johnson, S. M., Zhang, Z., Leonard, S. E., Mitra, A., et al. (2014). Development of Potent and Selective *Plasmodium Falciparum* Calcium-Dependent Protein Kinase 4 (PfCDPK4) Inhibitors That Block the Transmission of Malaria to Mosquitoes. *Eur. J. Med. Chem.* 74, 562–573. doi: 10.1016/j.ejmech.2013.12.048
- Von Gruning, H., Coradin, M., Mendoza, M. R., Reader, J., Sidoli, S., Garcia, B. A., et al. (2022). and Combinatorial Histone Code Drives Malaria Parasite Asexual and Sexual Development. *Mol. Cell Proteomics*, 100199.
- Vos, M. W., Stone, W. J., Koolen, K. M., Van Gemert, G. J., Van Schaijk, B., Leroy, D., et al. (2015). A Semi-Automated Luminescence Based Standard Membrane Feeding Assay Identifies Novel Small Molecules That Inhibit Transmission of Malaria Parasites by Mosquitoes. *Sci. Rep.* 5, 18704. doi: 10.1038/srep18704
- Warncke, J. D., Vakonakis, I., and Beck, H. P. (2016). Plasmodium Helical Interspersed Subtelomeric (PHIST) Proteins, at the Center of Host Cell Remodeling. *Microbiol. Mol. Biol. Rev.* 80, 905–927. doi: 10.1128/MMBR.00014-16
- WHO (2021). *World Malaria Report 2021* (Geneva).
- Witmer, K., Dahalan, F. A., Delves, M. J., Yahya, S., Watson, O. J., Straschil, U., et al. (2021). Transmission of Artemisinin-Resistant Malaria Parasites to Mosquitoes Under Antimalarial Drug Pressure. *Antimicrob. Agents Chemother.* 65, e00898–e00820. doi: 10.1128/AAC.00898-20
- Witola, W. H., and Ben Mamoun, C. (2007). Choline Induces Transcriptional Repression and Proteasomal Degradation of the Malarial Phosphoethanolamine Methyltransferase. *Eukaryot. Cell* 6, 1618–1624. doi: 10.1128/EC.00229-07
- Witola, W. H., El Bissati, K., Pessi, G., Xie, C., Roepe, P. D., and Mamoun, C. B. (2008). Disruption of the *Plasmodium Falciparum* PfPMT Gene Results in a Complete Loss of Phosphatidylcholine Biosynthesis via the Serine-Decarboxylase-Phosphoethanolamine-Methyltransferase Pathway and Severe Growth and Survival Defects. *J. Biol. Chem.* 283, 27636–27643. doi: 10.1074/jbc.M804360200
- Xu, Y., Qiao, D., Wen, Y., Bi, Y., Chen, Y., Huang, Z., et al. (2020). PfAP2-G2 Is Associated to Production and Maturation of Gametocytes in Plasmodium Falciparum via Regulating the Expression of PfMDV-1. *Front. Microbiol.* 11, 631444. doi: 10.3389/fmicb.2020.631444
- Yahiya, S., Saunders, C., Strachil, U., Fischer, O., Rueda-Zubiaurre, A., Vizcay-Barrena, G., et al. (2021). *Plasmodium Falciparum* Protein Pfs16 is a Target for Transmission-Blocking Antimalarial Drug Development. *BioRxiv*. doi: 10.1101/2021.06.14.448287
- Yang, T., Otilie, S., Istvan, E. S., Godinez-Macias, K. P., Lukens, A. K., Baragana, B., et al. (2021). MalDA, Accelerating Malaria Drug Discovery. *Trends Parasitol.* 37, 493–507. doi: 10.1016/j.pt.2021.01.009

Conflict of Interest: The authors declare that the research was conducted in the absence of any commercial or financial relationships that could be construed as a potential conflict of interest.

Publisher's Note: All claims expressed in this article are solely those of the authors and do not necessarily represent those of their affiliated organizations, or those of the publisher, the editors and the reviewers. Any product that may be evaluated in

this article, or claim that may be made by its manufacturer, is not guaranteed or endorsed by the publisher.

Copyright © 2022 van der Watt, Reader and Birkholtz. This is an open-access article distributed under the terms of the Creative Commons Attribution License (CC BY).

The use, distribution or reproduction in other forums is permitted, provided the original author(s) and the copyright owner(s) are credited and that the original publication in this journal is cited, in accordance with accepted academic practice. No use, distribution or reproduction is permitted which does not comply with these terms.



First Evidence of *Entamoeba* Parasites in Australian Wild Deer and Assessment of Transmission to Cattle

Jose L. Huaman¹, Carlo Pacioni^{2,3}, Lily Kenchington-Evans¹, Mark Doyle⁴, Karla J. Helbig¹ and Teresa G. Carvalho^{1*}

¹ Department of Microbiology, Anatomy, Physiology and Pharmacology, School of Agriculture, Biomedicine and Environment, La Trobe University, Melbourne, VIC, Australia, ² Department of Environment, Land, Water and Planning, Arthur Rylah Institute for Environmental Research, Melbourne, VIC, Australia, ³ Environmental and Conservation Sciences, Murdoch University, Perth, WA, Australia, ⁴ Far South Coast, South East Local Land Services, Bega, NSW, Australia

OPEN ACCESS

Edited by:

Maria Carolina Touz,
Medical Research Institute Mercedes
and Martín Ferreyra (INIMEC),
Argentina

Reviewed by:

Manigandan Lejeune,
Cornell University, United States
Karen Luisa Haag,
Federal University of Rio Grande do
Sul, Brazil

*Correspondence:

Teresa G. Carvalho
t.carvalho@latrobe.edu.au

Specialty section:

This article was submitted to
Parasite and Host,
a section of the journal
Frontiers in Cellular and
Infection Microbiology

Received: 24 February 2022

Accepted: 10 May 2022

Published: 10 June 2022

Citation:

Huaman JL, Pacioni C,
Kenchington-Evans L, Doyle M,
Helbig KJ and Carvalho TG (2022)
First Evidence of *Entamoeba*
Parasites in Australian Wild Deer and
Assessment of Transmission to Cattle.
Front. Cell. Infect. Microbiol. 12:883031.
doi: 10.3389/fcimb.2022.883031

Australian wild deer populations have significantly expanded in size and distribution in recent decades. Due to their role in pathogen transmission, these deer populations pose a biosecurity risk to the livestock industry. However, little is known about the infection status of wild deer in Australia. The intestinal parasite *Entamoeba bovis* has been previously detected in farm and wild ruminants worldwide, but its epidemiology and distribution in wild ruminants remain largely unexplored. To investigate this knowledge gap, faecal samples of wild deer and domestic cattle from south-eastern Australia were collected and analysed for the presence of *Entamoeba* spp. using PCR and phylogenetic analysis of the conserved 18S rRNA gene. *E. bovis* parasites were detected at high prevalence in cattle and wild deer hosts, and two distinct *Entamoeba* ribosomal lineages (RLs), RL1 and RL8, were identified in wild deer. Phylogenetic analysis further revealed the existence of a novel *Entamoeba* species in sambar deer and a novel *Entamoeba* RL in fallow deer. While we anticipated cross-species transmission of *E. bovis* between wild deer and cattle, the data generated in this study demonstrated transmission is yet to occur in Australia. Overall, this study has identified novel variants of *Entamoeba* and constitutes the first report of *Entamoeba* in fallow deer and sambar deer, expanding the host range of this parasite. Epidemiological investigations and continued surveillance of *Entamoeba* parasites in farm ruminants and wild animals will be required to evaluate pathogen emergence and transmission to livestock.

Keywords: *Entamoeba bovis*, wild deer, cattle, cross-species infection, Australia, ribosomal lineages, 18S rRNA

INTRODUCTION

Parasites of the genus *Entamoeba* comprise unicellular anaerobic organism that infect humans (Shirley et al., 2018; Cui et al., 2019), domestic animals (Noble and Noble, 1952; Stensvold et al., 2010; Cui et al., 2019; Ai et al., 2021) and wild animals (Stensvold et al., 2010; Shilton et al., 2018; Cui et al., 2019). *Entamoeba* parasites develop through a faecal-oral life cycle, and infections with

pathogenic species can cause intestinal disease and damage the liver and brain (Ngui et al., 2012). The initial classification of *Entamoeba* species was established based on the type of host in which the parasites were identified (Noble and Noble, 1952) and on parasite morphological features (Stensvold et al., 2011), such as cyst size and the number of nuclei. Using this approach, *Entamoeba* species have been classified into four distinct groups, including *E. gingivalis*-like group (species without cysts), *E. bovis*-like group (uni-nucleated cysts), *E. histolytica*-like group (quadri-nucleated cysts), and *E. coli*-like group (octo-nucleated cysts) (Clark et al., 2006; Stensvold et al., 2011). In recent years, the analysis of *Entamoeba* 18S ribosomal RNA (18S rRNA) sequences has significantly expanded the repertoire of genetically distinct *Entamoeba* organisms (Clark et al., 2006; Stensvold et al., 2011; Jacob et al., 2016). Although morphology-based analysis will be required to consolidate such findings, they provide unique insights into variation within species, evolutionary relationships, and host specificity (Clark et al., 2006; Stensvold et al., 2011; Jacob et al., 2016). Moreover, analysis of *Entamoeba* DNA sequences is an essential tool in endemic countries where microscopy does not allow for the distinction of pathogenic and non-pathogenic *Entamoeba* species (Nath et al., 2015). The genetic diversity of morphologically identical parasites, and the host promiscuity of *Entamoeba* organisms, highlights an ongoing need for further characterisation of genetic variants and host range, particularly in pathogenic species and emerging zoonotic species infections.

In animals, ruminants such as cattle and sheep appear to be common hosts of the uni-nucleated cyst *Entamoeba* species (Noble and Noble, 1952; Clark et al., 2006; Stensvold et al., 2010). Nevertheless, cyst morphology varies greatly within and between uni-nucleated cyst-producing species isolated from different ruminant hosts (Stensvold et al., 2010). The term “ribosomal lineage” (RL) was introduced to name newly discovered *Entamoeba* 18S rRNA sequences with greater than 5% divergence from known species. These RLs represent organisms not yet described morphologically and not referable to described species (Jacob et al., 2016). The analysis of *Entamoeba* 18S rRNA sequences detected in farmed and wild ruminants over the last decade revealed the presence of *E. bovis* and eight RLs. Of these, four RLs are closely related to *E. bovis* (*Entamoeba* RL 1-3 and 8) (Jacob et al., 2016). Besides being detected in cattle (*Bos taurus*) (Stensvold et al., 2010; Jacob et al., 2016; Nolan et al., 2017; Matsubayashi et al., 2018; Ai et al., 2021) and sheep (*Ovis aries*) (Stensvold et al., 2010; Jacob et al., 2016; Ai et al., 2021), *E. bovis* and *Entamoeba* RLs have also been detected in goats (*Capra hircus*) (Nolan et al., 2017; Al-Habsi et al., 2017; Ai et al., 2021), horses (*Equus ferus*) (Ai et al., 2021), camels (*Camelus ferus*) (Ai et al., 2021), and cervids. Among the studies conducted on cervids, white-tailed deer (*Odocoileus virginianus*) from the USA (Kingston and Stabler, 1978), fallow deer (*Dama dama*) from Mauritius (Jacob et al., 2016), and reindeer (*Rangifer tarandus*) from Iceland (Stensvold et al., 2010) tested positive for *E. bovis*, while *Entamoeba* RL 1 was detected in roe deer (*Capreolus capreolus*) from Sweden (Stensvold et al., 2010). Information about the pathogenicity of *E. bovis* and

Entamoeba RLs in ruminants remains limited; however, their detection in cattle in the absence of clinical symptoms such as diarrhoea, suggests low pathogenicity (Matsubayashi et al., 2018; Ai et al., 2021). *E. bovis* have a broad ruminant host range and can be transmitted by faecal excretion of cysts followed by oral ingestion of contaminated food or water (Noble and Noble, 1952; Clark et al., 2006; Stensvold et al., 2010). Based on the oral-faecal life cycle of *Entamoeba* parasites, the transmission of *E. bovis* between different host taxa that share common land is highly likely.

To date, *Entamoeba* parasites have only been identified twice in Australian wild animals. *E. ranarum* was detected and characterised in wild cane toads (*Rhinella marina*) (Shilton et al., 2018), and *E. bovis* was detected in feral goats in Western Australia rangeland with a 6.4% prevalence (Al-Habsi et al., 2017). The prevalence and distribution of *Entamoeba* species in Australian farmed and wild ruminants, such as wild deer, remains yet to be investigated. Wild deer and livestock commonly share grazing areas in agricultural landscapes and are equally susceptible to a wide range of pathogens of agricultural importance (Cripps et al., 2019). Wild deer represent a significant source of pathogen transmission; thus, we hypothesised wild deer to be involved in the transmission of *Entamoeba* parasites to livestock and *vice versa*. In recent years, our team has investigated the role of wild deer as carriers of livestock pathogens in Australia (Huaman et al., 2020; Huaman et al., 2021; Huaman et al., 2021a; Huaman et al., 2021b), and here, we report the first detection of *Entamoeba* parasites in wild deer sampled in Australia. Further, we assess the prevalence, distribution, and characterisation of *Entamoeba* species and RLs as well as the potential of cross-species transmission.

MATERIALS AND METHODS

Sample Collection

Faecal samples were collected from Australian wild deer to assess their infection status (Huaman et al., 2021a; Huaman et al., 2021b). Opportunistic sampling during field necropsies was carried out on deer culled with the assistance of recreational and professional hunters as part of control operations in New South Wales and Victoria (**Figure 1**) between August 2019 and October 2020. All samples were collected from the large intestine and placed in sterile plastic containers (Techno Plas, Australia).

Cattle faecal samples collected for clinical investigations independent from this study were analysed here for the presence of *Entamoeba* parasites. Cattle samples were collected from beef and dairy farms within a 20 kilometres radius of the deer sampling areas between September 2020 and April 2021. All samples were collected directly from the animals, placed in individual sterile plastic containers and immediately refrigerated. Samples were transported to the Laboratory of Molecular Parasitology within the Department of Microbiology, Anatomy, Physiology and Pharmacology at La Trobe University, and stored at -80°C until further use.



FIGURE 1 | Geographic locations of deer (1 to 4) and cattle (1, 2 and 4) sample collection in south-eastern Australia. (1) Kiah, (2) Outer Melbourne, (3) Yellingbo, (4) Bunyip. ©d-maps.com.

DNA Extraction and PCR Amplification

Frozen faecal samples were aliquoted into 0.25 g frozen portions. Genomic DNA was extracted using a DNeasy® PowerSoil® Kit (Qiagen, Valencia, CA, USA) following the manufacturer's instructions. PCR was performed with primers EntboF2 and EntboR3 (Matsubayashi et al., 2018; Ai et al., 2021) to amplify an internal fragment of 850 bp of the 18S rRNA *Entamoeba* gene. In addition, the methodology published by Ali et al. (2005) was employed to detect tRNA-linked short tandem repeats (STRs). Six previously published primer pairs (A-L5/A-L3, D-A5/D-A3, N-K5/N-K3, R-R5/R-R3, S^{TGA}-D5/S^{TGA}-D3, S-Q5/S-Q3) were selected and tested in all the deer and cattle samples. These primers were originally designed to amplify *E. histolytica* t-RNA STRs. PCR amplification was performed in a 25 µL reaction mixture containing 1x Green GoTaq Flexi buffer, 2 mM of MgCl₂, 10 mM of dNTPs, 0.2 µM of each primer, 0.625 units of GoTaq G2 DNA polymerase (Promega, Madison, WI, USA), and 1 µL of template DNA. Amplification was carried out in a T100 thermal cycler (BioRad, Hercules, CA, USA), and amplification products were visualised by gel electrophoresis, using a 2% agarose gel stained with RedSafe™ (iNtRON Biotechnology, Gyeonggi-do, Korea), and the high-resolution ChemiDoc™ MP Imaging System (Bio-Rad, Hercules, CA, USA).

DNA Sequencing and Phylogenetic Analysis

PCR products were sequenced by bi-directional Sanger sequencing at the Australian Genome Research Facility (Melbourne, Australia),

then analysed and edited using Geneious software 11.1.4 (Biomatters Ltd., Auckland, New Zealand, version 11.1.4). Multiple sequence alignments were performed using Clustal X (Thompson et al., 1997). A phylogenetic tree was built based on *Entamoeba* 18S rRNA sequences using the substitution model with the lowest BIC scores (Tamura 3-parameter model + G) and the maximum-likelihood method in MEGA 7 (Kumar et al., 2016). Thus, *Entamoeba* sequences obtained in the present study were aligned with 31 *Entamoeba* reference sequences deposited in GenBank (Table S1). These reference sequences represented 17 recognised species and 5 published ribosomal lineages. Statistical support for the trees was evaluated by bootstrapping based on 1,000 repetitions. Moreover, the number of nucleotide differences and the mean sequence divergence of *Entamoeba* clades identified in our sequences were calculated in MEGA 7. The nucleotide 18S rRNA sequences detected in this study were submitted to GenBank under accession number OM415364 - OM415424 (Table S2).

Bayesian Divergence Time Estimates

As deer were introduced in Australia only 200 years ago, estimating the most recent common ancestors (TMRCA) of *E. bovis* detected in wild deer and cattle can reveal whether parasite transmission occurred between the two hosts in Australia. Therefore, the reported split ages (Romero et al., 2016) between *E. nuttalli* and *E. histolytica* (5.93 ± 0.28 Mya), along with *E. histolytica* and *E. invadens* (68.18 ± 16.04 Mya), were used as calibrations for the Bayesian analysis using a lognormal distribution with a mean of 1.78 and 4.5, and a standard

deviation of 0.05 and 0.25, respectively. The phylogenetic trees were modelled using a birth-death tree prior, a lognormal relaxed clock in BEAST v2.6.3 (Bouckaert et al., 2019), and a gamma distribution (shape=1, rate=0.00001) for the substitution rate parameter. Two independent runs of 200 million steps were computed, sampling parameters every 10,000 steps and discarding the first 10% of each chain as burn-in. Tracer v1.7.1 (Rambaut et al., 2018) was used to ensure that the length of the burn-in phase was sufficient and guaranteed convergence of the two analyses. Results were obtained after combining the two chains with LogCombiner. The programs TreeAnnotator v2.6.2 (Bouckaert et al., 2019) and FigTree v1.4.4 (<http://tree.bio.ed.ac.uk/software/figtree/>) were used to summarise the posterior tree distribution and visualise the annotated Maximum Clade Credibility (MCC) tree.

RESULTS

High Prevalence of Entamoeba DNA Found in Wild Deer and Cattle Samples

A total of twenty-three cattle faecal samples were obtained from south-eastern Australia, as well as seventy-one wild deer faecal samples, including sixty samples from fallow deer (*Dama dama*) and eleven samples from sambar deer (*Rusa unicolor*) (Table 1). All samples were screened by PCR for the presence of the 18S rRNA *Entamoeba* gene using primers EntboF2 and EntboR3 (Matsubayashi et al., 2018). The overall prevalence of *Entamoeba* spp. in wild deer from south-eastern Australia was found to be 81.7% (58/71), ranging from 72.9% to 100% depending on the host species and the sample geographic location (Table 1). In the cattle faecal samples, the prevalence of *Entamoeba* spp. was 100% (Table 1). All the *Entamoeba* 18S rRNA PCR amplicons generated (seventy-one from wild deer samples and twenty-three from cattle samples) were analysed by Sanger sequencing. Subsequent analysis of the ninety-four 18S rRNA sequences revealed *E. bovis* as the dominant species detected with a total prevalence of 74.6% (53/71) in wild deer and 100% (23/23) in cattle.

Phylogenetic Analysis of Entamoeba Sequences Reveals the Existence of RL Variants in Wild Deer Samples

Out of the 850 bp *Entamoeba* 18S amplicons generated by PCR, a good quality DNA fragment of 778 bp was successfully

sequenced for each of the ninety-four deer and cattle samples. This 778 bp fragment covered nearly 50% of the *Entamoeba* 18S rRNA gene and was therefore used to investigate the phylogenetic relationship and the levels of divergence of the ninety-four *Entamoeba* sequences. A high proportion of the wild deer-derived sequences fell into the *E. bovis* clade, which includes isolates from rangeland goats, cattle, sheep, and reindeer (Figure 2). Further, the cattle-derived sequences clustered exclusively within the *E. bovis* clade. The genetic similarity among all *E. bovis* sequences obtained in this study (both derived from deer and cattle) ranged from 92.5% to 100%. Moreover, the mean divergence within the cattle-derived sequences is 5 to 7-fold smaller than the divergence observed within the deer-derived sequences (Table 2). Within the 778 bp 18S rRNA gene fragment, a mean of 21 nucleotide differences was found between the two host group sequences (Table 2).

Interestingly, five 18S rRNA sequences of deer origin (VIC89, NSW304, NSW332, VIC93 and VIC91) clustered with distinct *Entamoeba* RLs, while none of the sequences identified in this study clustered with *Entamoeba* RLs 2, 3 and 4, which were previously reported in ruminants (Figure 2). Sequence VIC89, sourced from sambar deer, clustered with *Entamoeba* RL1 (FN666253) detected in roe deer from Sweden and shared 98.6% of the nucleotide sequence. Sequence NSW304 sourced from fallow deer, clustered with *Entamoeba* RL8 (KR025406), detected in cattle from the United Kingdom, with a homology of 99.9%. Comparison of sequence NSW304 with two additional *Entamoeba* RL8 sequences detected in camel (MN749974) and goat (MN749989) from China revealed a nucleotide identity of 99.9% and 95.1%, respectively. The alignment of these four *Entamoeba* RL8 sequences (NSW304, FN666253, MN749974, and MN749989) revealed an identity of 100% between sequences NSW304, FN666253, and MN749974; while three insertions (at positions 715, 716 and 750) and one deletion (at position 677) were identified in the strain detected in the goat (MN749989) (Figure S1). Sequences VIC93 and NSW332 sourced from fallow deer fell into the same clade, displaying 99% sequence identity; however, these two sequences did not cluster with any *Entamoeba* RL reference sequence, therefore emerging as a divergent *Entamoeba* RL (Figure 2). Sequence VIC91 obtained from sambar deer was genetically distinct from the *Entamoeba* sequences identified in other deer and cattle samples with high sequence divergence (mean 26.2%) and nucleotide difference (mean 133.76) (Table 2). Nucleotide similarity between sequence VIC91 and the reference *Entamoeba* sequences ranged from 82% to 86%. Overall, these findings suggest sample VIC91 belongs to a novel *Entamoeba* species.

TABLE 1 | *Entamoeba* species and RLs identified in deer and cattle faecal samples collected across south-eastern Australia.

Host species	Geographic location	Total	PCR positive (%)	<i>Entamoeba</i> species (n)
Fallow deer	NSW	48	35 (72.9)	<i>E. bovis</i> (33), <i>Entamoeba</i> RL 8 (1), <i>Entamoeba</i> RL ^a (1)
	VIC	12	12 (100)	<i>E. bovis</i> (11), <i>Entamoeba</i> spp ^b (1)
Sambar deer	VIC	11	11 (100)	<i>E. bovis</i> (9), <i>Entamoeba</i> RL 1 (1), <i>Entamoeba</i> RL ^a (1)
Cattle	NSW	15	15 (100)	<i>E. bovis</i> (23)
	VIC	8	8 (100)	

NSW, New South Wales; VIC, Victoria; ^a novel *Entamoeba* RL, ^b novel *Entamoeba* species.

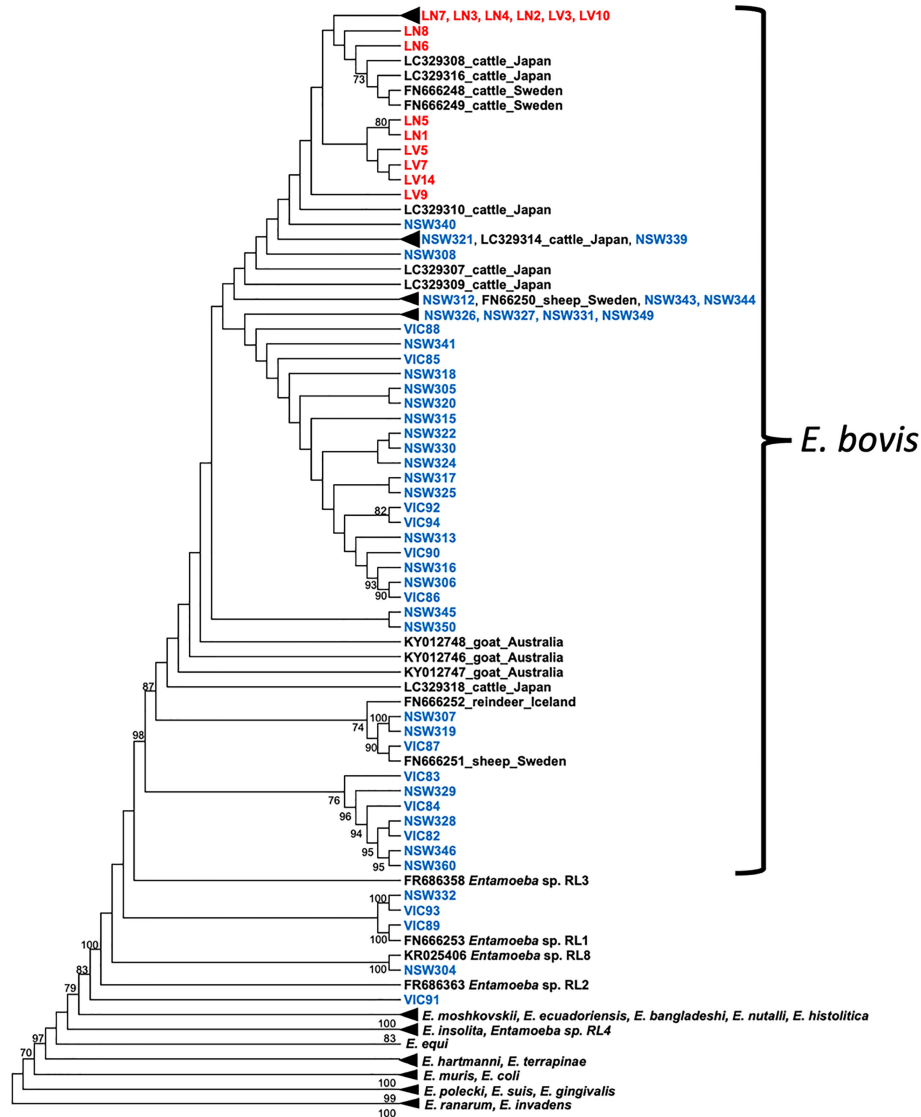


FIGURE 2 | Cladogram of *Entamoeba* partial 18S rRNA sequences. Deer sequences are indicated in blue and cattle sequences in red. Reference sequences are indicated in black. The tree was constructed using the maximum likelihood method and Tamura 3-parameter + G substitution model. Bootstrap values above 70% are shown at the nodes. Note: substitutions do not scale branches in this tree. The phylogenetic tree with scaled branches and alignment is shown in **Figures S2, S3**, respectively.

TABLE 2 | Mean sequence divergence and number of differences (nucleotides) between Australian deer and cattle sequences within clades.

Clades	Sequence divergence %	Number of differences
<i>E. bovis</i> deer vs <i>E. bovis</i> cattle	2.9 % ± 0.4 %	20.88 ± 2.8
Within <i>E. bovis</i> deer	3.5 % ± 0.4 %	24.32 ± 2.8
Within <i>E. bovis</i> cattle	0.7 % ± 0.2 %	5.06 ± 1.3
All deer vs all cattle	4.2 % ± 0.5 %	27.72 ± 3
within all deer	5.8 % ± 0.6 %	36.70 ± 3.1
within all cattle	0.7 % ± 0.2 %	5.06 ± 1.3
Non-VIC91 deer vs VIC91	26.2 % ± 2.9 %	133.76 ± 10

STRs Were Amplified in Deer and Cattle Samples But Not Successfully Sequenced

Amplicons were obtained for all the STRs tested except for D-A5/D-A3 (**Figure S4**), albeit a slight difference in size when compared to amplicons of *E. histolytica* (Ali et al., 2005). A total of ten samples, including 4 wild deer samples and 6 cattle samples (**Figures S4A, B**, respectively) were sequenced using primers S^{TGA}-D5 and S^{TGA}-D3 (Ali et al., 2005). However, DNA sequences of good quality could not be obtained, even when cloning the STR amplicons prior to sequencing.

Divergence Time Analysis Suggests Lack of *Entamoeba* Transmission Between Wild Deer and Cattle

To determine the transmission of *Entamoeba* parasites between wild deer and cattle in this study, a phylogenetic tree was constructed using a birth-death tree prior under a Bayesian framework and two calibration nodes (Figure 3). This approach aims to reconstruct the speciation process and, by using the time of divergence between two taxa as calibration, it converts the unit of the branches from substitutions to time (years in this case). The trees explored are then annotated in a maximum clade credibility (MCC) tree. The MCC tree revealed a clear species structure with the cattle-derived *Entamoeba* sequences well separated from the wild deer-derived *Entamoeba* sequences, like the previously generated maximum likelihood (ML) tree (Figure 2). Sequence NSW340 was, however, an exception to the species separation as it clustered with LV7 and LV14 (Figure 3). Overall, sequences sourced from wild deer clustered within four clades (Figure 3). There was little resolution within the deer group, as reflected in the low node posterior probabilities (< 0.7); however, deer clade 2 and 3 grouped with posterior probabilities > 0.8 , and similar strong support was found in the ML tree. The MCC tree confirmed that sequences VIC89 and NSW304 belong to *Entamoeba* RL1 and RL8, respectively, and corroborated that sequence VIC91 is genetically distinct from the other sequences analysed in this study. In the ML tree sequences, LN1 (cattle origin) and VIC92 (deer origin) clustered within the *E. bovis* clade, although they fell outside of any other cluster, which is in contrast with the output of the ML tree (Figure 2). The most recent node between sequences obtained from a deer and a cow in Australia was estimated to be 171 million years ago (Mya) (95% HPD: 31.5 – 377.9 Mya). While the most recent common ancestors (TMRCA) between Australian wild deer and cattle clades was estimated at 632 Mya, but with considerable uncertainty (95% HPD: 163 – 1308 Mya) (Figure 3).

DISCUSSION

In recent decades, Australian wild deer populations have significantly increased in abundance and distribution, leading to regular close interactions between deer and livestock, which increases the risk of pathogen transmission (Davis et al., 2016; Cripps et al., 2019). However, little is known about the epidemiology of pathogens that Australian deer may transmit to livestock, other domestic animals, or wildlife. The present study complements our initial work on investigating pathogens in wild deer across multiple geographic locations in Australia (Huaman et al., 2020; Huaman et al., 2021; Huaman et al., 2021a; Huaman et al., 2021b). Here we report the identification of *Entamoeba* sequences in wild deer and cattle faecal samples collected in south-eastern Australia, with subsequent phylogenetic analysis to evaluate the cross-species transmission of *Entamoeba* parasites. This baseline information is of value for

monitoring the status of parasitic infections in Australian deer and evaluating the risk of disease transmission between wild deer and livestock. Additionally, the data provided by this study increases our knowledge of the host range and distribution of *Entamoeba*, a group of parasites prevalent in ruminant livestock. Finally, this study represents the first molecular screening and characterisation of *Entamoeba* in Australian wild deer.

The predominant *Entamoeba* species identified in the wild deer and cattle samples collected and analysed in this study was *Entamoeba bovis*, a species recognised to infect ruminants, including livestock animals (Stensvold et al., 2010; Matsubayashi et al., 2018; Ai et al., 2021). The prevalence of *Entamoeba* infections previously reported in cattle are relatively low [2.5% in Costa Rica (Jimenez et al., 2007), 4.8% in Korea (Ismail et al., 2010)] when detected by microscopic analysis; while higher prevalences have been reported following PCR analysis [72% in Japan (Matsubayashi et al., 2018), 80% in Uganda (Nolan et al., 2017), 100% in China (Ai et al., 2021)]. Similar to these last reports, the present study detected a prevalence of 100% for *E. bovis* in cattle samples ($n=23$) using a PCR-based analysis.

E. bovis has also been previously detected in wild cervids, including in wild goats from Western Australia with a prevalence of 6.4% (Al-Habsi et al., 2017). This relatively low *E. bovis* prevalence contrasts with the much higher prevalence of 74.6% (53/71) reported here in fallow deer and sambar deer from eastern Australia. This difference could be attributed to methodology, as *E. bovis* was identified in wild goats from Western Australia (Nolan et al., 2017) by microscopy analysis. Indeed, microscopy and morphology-based detection methods are likely to underestimate parasite prevalence, as discussed above for the case of cattle samples, and are less sensitive methods when compared to the molecular detection tools employed in the present study. Although microscopy detection methods might underestimate the number of *E. bovis* infections, it is not excluded that lower parasite prevalence can exist, for example, due to climatic reasons. The sampling areas of this study are located in south-eastern Australia, where a Mediterranean-like climate prevails with significantly humid winters, which can facilitate the maintenance of parasites in the environment (Shirley et al., 2018). In contrast, the sampling area of Al-Habsi et al. (2017) was the semiarid rangeland area in Western Australia.

Wild deer and cattle-derived *Entamoeba* 18S rRNA sequences cluster within the *E. bovis* clade, although different species-specific clades are formed (Figure 3). Pairwise analysis revealed differences within sequences of wild deer origin, indicating high parasite diversity within this host. Polymorphic markers such as serine-rich protein genes and tRNA-linked short tandem repeats (STRs) have been used for the genotyping and correlation with the geographical distribution of other *Entamoeba* species such as *E. histolytica*, *E. dispar*, and *E. nuttalli* (Tawari et al., 2007; Weedall and Hall, 2011; Feng et al., 2014). However, this approach is yet to be used to identify *E. bovis*. We employed a methodology previously used in *E. histolytica* (Ali et al., 2005); however, the sequencing of ten

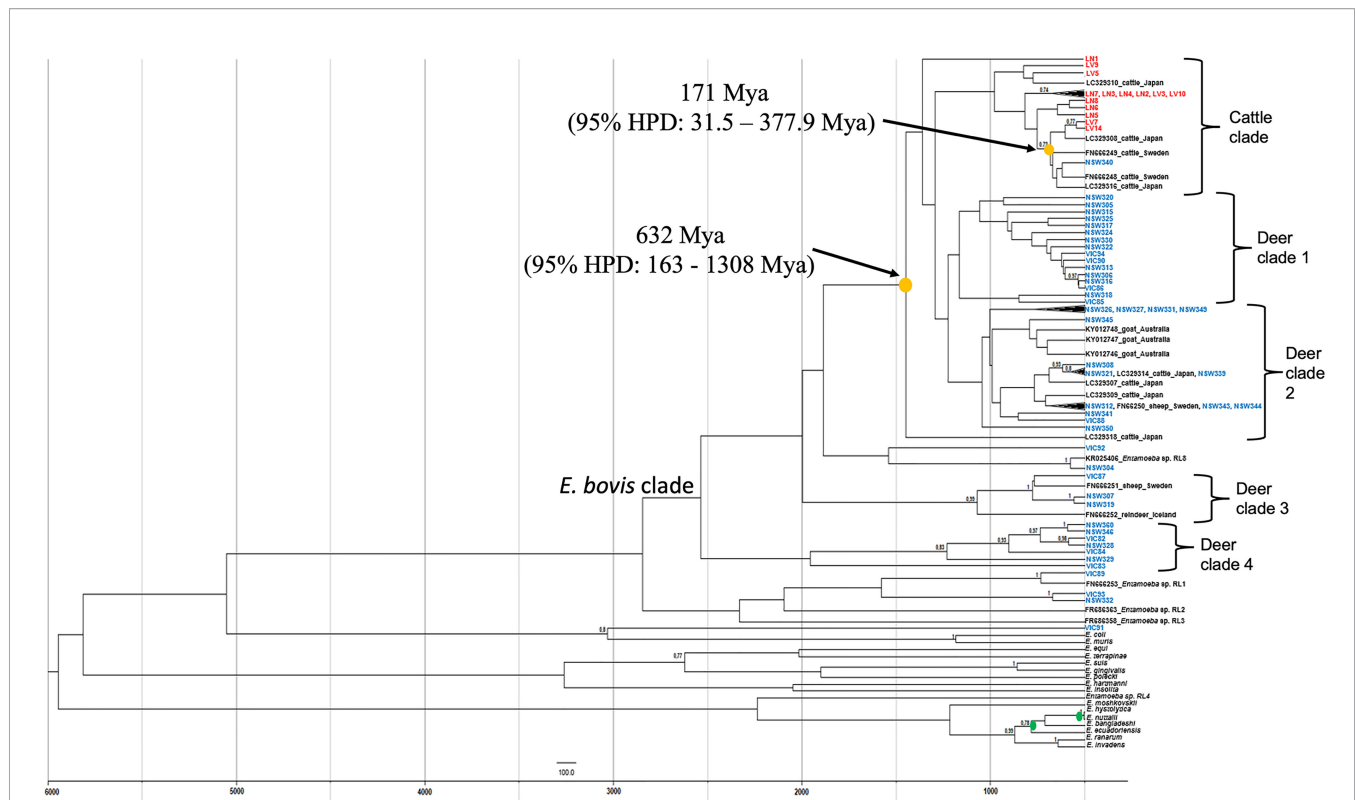


FIGURE 3 | Maximum clade credibility tree of *Entamoeba* obtained from Bayesian inference using split ages reported previously as calibrations (green dots). Yellow dots indicate the estimated mean ages for the most recent common ancestor (TMRCA) of *Entamoeba* detected in Australian wild deer and cattle. Deer sequences are indicated in blue and cattle sequences in red. Reference sequences are indicated in black. HPD, highest posterior density, Mya, Million years ago.

samples (4 wild deer and 6 cattle samples) using primers S^{TGA} -D5 and S^{TGA} -D3 did not generate good quality DNA sequences, even when STR amplicons were cloned prior to sequencing. The primers used here were originally designed to amplify *E. histolytica* t-RNA STRs (Ali et al., 2005). Therefore, the presence of polymorphisms in the t-RNA gene of *E. bovis* and/or the sensitivity of the primers could account for the low quality of the sequences generated.

In the absence of STR data and to determine whether a potential *E. bovis* cross-species transmission was possible, the time of the most common ancestor between *E. bovis* sequences of wild deer and cattle origin was estimated (Figure 3). The most common ancestor of *E. bovis* identified in wild deer and cattle hosts was estimated to have existed well before 200 years ago (before cattle and deer were introduced in Australia). Both ML and Bayesian phylogenetic analyses grouped the sequences according to their host species with moderate sequence divergence. Therefore, taken together, these results provide no evidence of *E. bovis* transmission between wild deer and cattle in Australia. This finding was somewhat unexpected, but it is possible that since wild deer populations have only recently increased in density, they did not play an important role in the transmission of these parasites thus far. However, this may change in the future due to deer density expansion, increasing contact rates (direct or indirect) and transmission events with livestock species.

Phylogenetic analysis of all *Entamoeba* sequences of deer origin identified that two sequences (VIC89 and NSW304) cluster with two distinct *Entamoeba* RL. The term “ribosomal lineage” (RL) was proposed to name *Entamoeba* strains with greater than 5% sequence divergence from known species (Jacob et al., 2016). Sequence VIC89 detected in a sambar deer from Victoria clustered with high genetic similarity with an *Entamoeba* RL1 sequence from a roe deer from Sweden (FN666253). This RL was also detected in one gazelle and one bighorn sheep in the USA; however, their sequences are not available for comparison (Jacob et al., 2016). Sequence NSW304, detected in a fallow deer from NSW, clustered with an *Entamoeba* RL8 sequence (KR025406). This ribosomal lineage has been previously identified in a variety of hosts, including cow (Jacob et al., 2016), camel (Ai et al., 2021) and goat (Ai et al., 2021). The sequence NSW304 presents high homology with an RL8 sequence of a cow (99.9%; KR025406) and camel (99.9%; MN749974) origin and lower homology with a sequence of goat origin (95.1%; MN749989). Here we present the first identification of *Entamoeba* RL1 and *Entamoeba* RL8 sequences in wild deer. These results broaden the host range of both RLs.

Interestingly, *Entamoeba* sequences (NSW332, VIC93 and VIC91) detected in three wild deer animals did not cluster with any 18S rRNA reference sequence. One sambar deer-sourced sequence (VIC91) was genetically distinct from other *Entamoeba*

species found in ruminants, suggesting a possible novel *Entamoeba* species. Sequences NSW332 and VIC93 of fallow deer origin displayed 100% identity with each other and clustered as a sister clade with the VIC89/*Entamoeba* RL1 clade. Jacob et al. (2016) proposed the classification for RL sequences based on two criteria: i) sequences with $\geq 80\%$ coverage of the 18S rRNA region, and ii) $\geq 5\%$ difference with previously known sequences. Our phylogenetic analysis has identified NSW332 and VIC93 as a putative novel RL; however, the sequences generated here are shorter than 80% (48%) of the full *Entamoeba* 18S rRNA gene. Therefore, future studies to determine the complete 18S rRNA gene sequence of NSW332 and VIC93 are needed to confirm this finding.

In conclusion, here we present evidence of three *Entamoeba* RLs in Australian ruminants: *E. bovis* in wild deer and cattle, *Entamoeba* RL1 in wild sambar deer, and *Entamoeba* RL8 in wild fallow deer. Our study represents the first identification of *Entamoeba* parasites in Australian deer, expanding the host range of *Entamoeba* parasites. Further, we present evidence of a potential novel *Entamoeba* species (VIC91) of wild deer origin, closely related to *Entamoeba* RL1. We detected a high prevalence of *E. bovis* (100%) in cattle in the absence of clinical signs, which aligns with the low pathogenicity of *E. bovis* and its alleged commensal relationship with its cattle host (Ai et al., 2021). Finally, our study suggests a lack of current *E. bovis* transmission between wild deer and cattle in Australia. However, considering the ongoing expansion of wild deer populations in Australia, both in size and distribution, this scenario is likely to change in the future.

DATA AVAILABILITY STATEMENT

The datasets presented in this study can be found in online repositories. The names of the repository/repositories and accession number(s) can be found in the article/**Supplementary Material**.

ETHICS STATEMENT

The work presented in this manuscript required no specific ethical approval. Deer culling was carried out as management operations and independently from this research. Similarly, cattle samples were collected as part of clinical investigations independently from this research. In both cases, we accessed the samples opportunistically.

AUTHOR CONTRIBUTIONS

Conceptualisation, CP and TC. Methodology, JH, CP, and TC. Formal analysis, LK-E and JH. Investigation, JH, CP, and TC. Funding: CP, KH, and TC. Resources, CP, MD and TC.

Data curation, JH. Writing—original draft preparation, JH and TC. Writing—review and editing, CP, MD, KH and TC. All authors have read and agreed to the published version of the manuscript.

FUNDING

This study was funded by the Centre for Invasive Species Solutions (Grant PO1-L-002).

ACKNOWLEDGMENTS

We thank Jake Haddad (VPAC), Andrew Bengsen, Troy Crittle and Quentin Hart (New South Wales Department of Primary Industries), and the staff from Parks Victoria for assisting with sample collection.

SUPPLEMENTARY MATERIAL

The Supplementary Material for this article can be found online at: <https://www.frontiersin.org/articles/10.3389/fcimb.2022.883031/full#supplementary-material>

Supplementary Figure 1 | Alignment of partial 18S rRNA DNA sequences obtained from sample NSW304 and three *Entamoeba* sp. RL8 reference strains (KR025406, MN749974, MN749989). Numbers indicate nucleotide positions. '*' denotes an identical nucleotide residue across all four sequences. '-' indicates the absence of a nucleotide residue. Gap positions are highlighted in green.

Supplementary Figure 2 | Phylogenetic analysis of *Entamoeba* partial 18S rRNA DNA sequences. Deer sequences are highlighted in blue and cattle sequences in red. Reference sequences are indicated in black. The tree was constructed using the maximum likelihood method and Tamura 3-parameter + G substitution model. Only bootstrap values $>70\%$ are shown at the nodes. The scale bar indicates nucleotide substitutions per site.

Supplementary Figure 3 | Alignment of 18S rRNA sequences included in our phylogenetic and bayesian analysis. Numbers indicate nucleotide positions. '*' denotes an identical nucleotide across the alignment. '-' indicates the absence of a nucleotide residue.

Supplementary Figure 4 | PCR amplification of the six STRs assessed in this study [based on (21)]. **(A)** Amplification of STRs D-A5/D-A3 (400/500 bp), STGA-D5/STGA-D3 (150/200 bp), A-L5/A-L3 (500/600 bp), R-R5/R-R3 (700 bp), N-K5/N-K3 (600/800 bp), and SQ5/SQ3 (400/500 bp) was attempted in four deer samples (N301, N304, N306, N308). **(B)** Amplification of STRs N-K5/N-K3 (600/800 bp), A-L5/A-L3 (500/600 bp), SQ5/SQ3 (400/500 bp), STGA-D5/STGA-D3 (150/200 bp) was attempted in six cattle samples (LN2, LN4, LN6, LV1, LV4, 300).

Supplementary Table 1 | List of 18S rRNA *Entamoeba* sequences included on the phylogenetic and divergence time analysis.

Supplementary Table 2 | List of accession number of the *Entamoeba* 18S rRNA DNA sequences obtained in the present study and submitted to GenBank.

REFERENCES

- Ai, S., Zhang, Z., Wang, X., Zhang, Q., Yin, W., and Duan, Z. (2021). The First Survey and Molecular Identification of *Entamoeba* Spp. In Farm Animals on Qinghai-Tibetan Plateau of China. *Comp. Immunol. Microbiol. Infect. Dis.* 75, 101607. doi: 10.1016/j.cimid.2020.101607
- Al-Habsi, K., Yang, R., Ryan, U., Jacobson, C., and Miller, D. W. (2017). Morphological and Molecular Characterization of an Uninucleated Cyst-Producing *Entamoeba* Spp. In Captured Rangeland Goats in Western Australia. *Vet. Parasitol.* 235, 41–46. doi: 10.1016/j.vetpar.2017.01.013
- Ali, I. K. M., Zaki, M., and Clark, C. G. (2005). Use of PCR Amplification of tRNA Gene-Linked Short Tandem Repeats for Genotyping *Entamoeba histolytica*. *J. Clin. Microbiol.* 43 (12), 5842–5847. doi: 10.1128/JCM.43.12.5842-5847.2005
- Bouckaert, R., Vaughan, T. G., Barido-Sottani, J., Duchene, S., Fourment, M., Gavryushkina, A., et al. (2019). BEAST 2.5: An Advanced Software Platform for Bayesian Evolutionary Analysis. *PLoS Comput. Biol.* 15 (4), e1006650. doi: 10.1371/journal.pcbi.1006650
- Clark, C. G., Kaffashian, F., Tawari, B., Windsor, J. J., Twigg-Flesner, A., Davies-Morel, M. C. G., et al. (2006). New Insights Into the Phylogeny of *Entamoeba* Species Provided by Analysis of Four New Small-Subunit rRNA Genes. *Int. J. Syst. Evol. Microbiol.* 56 (9), 2235–2239. doi: 10.1099/ijs.0.64208-0
- Cripps, J. K., Pacioni, C., Scroggie, M. P., Woolnough, A. P., and Ramsey, D. S. L. (2019). Introduced Deer and Their Potential Role in Disease Transmission to Livestock in Australia. *Mammal Rev.* 49 (1), 60–77. doi: 10.1111/mam.12142
- Cui, Z., Li, J., Chen, Y., and Zhang, L. (2019). Molecular Epidemiology, Evolution, and Phylogeny of *Entamoeba* Spp. *Infect. Genet. Evol.* 75, 104018. doi: 10.1016/j.meegid.2019.104018
- Davis, N. E., Bennett, A., Forsyth, D. M., Bowman, D. M. J. S., Lefroy, E. C., Wood, S. W., et al. (2016). A Systematic Review of the Impacts and Management of Introduced Deer (Family Cervidae) in Australia. *Wildl. Res.* 43 (6), 515–532. doi: 10.1071/WR16148
- Feng, M., Komiyama, T., Yanagi, T., Cheng, X., Sherchand, J. B., and Tachibana, H. (2014). Correlation Between Genotypes of tRNA-Linked Short Tandem Repeats in *Entamoeba Nuttalli* Isolates and the Geographical Distribution of Host Rhesus Macaques. *Parasitol. Res.* 113 (1), 367–374. doi: 10.1007/s00436-013-3664-0
- Huaman, J. L., Pacioni, C., Forsyth, D. M., Pople, A., Hampton, J. O., Carvalho, T. G., et al. (2020). Serosurveillance and Molecular Investigation of Wild Deer in Australia Reveals Seroprevalence of Pestivirus Infection. *Viruses* 12 (7), 752–767. doi: 10.3390/v12070752
- Huaman, J. L., Pacioni, C., Forsyth, D. M., Pople, A., Hampton, J. O., Helbig, K. J., et al. (2021). Evaluation of Haemoparasite and *Sarcocystis* Infections in Australian Wild Deer. *Int. J. Parasitol. Parasites. Wildl.* 15, 262–269. doi: 10.1016/j.ijppaw.2021.06.006
- Huaman, J. L., Pacioni, C., Sarker, S., Doyle, M., Forsyth, D. M., Pople, A., et al. (2021a). Molecular Epidemiology and Characterization of Picobirnavirus in Wild Deer and Cattle From Australia: Evidence of Genogroup I and II in the Upper Respiratory Tract. *Viruses* 13 (8), 1492. doi: 10.3390/v13081492
- Huaman, J. L., Pacioni, C., Sarker, S., Doyle, M., Forsyth, D. M., Pople, A., et al. (2021b). Novel Picornavirus Detected in Wild Deer: Identification, Genomic Characterisation, and Prevalence in Australia. *Viruses* 13 (12), 2412. doi: 10.3390/v13122412
- Ismail, H. A., Jeon, H. K., Yu, Y. M., Do, C., and Lee, Y. H. (2010). Intestinal Parasite Infections in Pigs and Beef Cattle in Rural Areas of Chungcheongnam-Do, Korea. *Korean J. Parasitol.* 48 (4), 347–349. doi: 10.3347/kjp.2010.48.4.347
- Jacob, A. S., Busby, E. J., Levy, A. D., Komm, N., and Clark, C. G. (2016). Expanding the *Entamoeba* Universe: New Hosts Yield Novel Ribosomal Lineages. *J. Eukaryot. Microbiol.* 63 (1), 69–78. doi: 10.1111/jeu.12249
- Jimenez, A. E., Montenegro, V. M., Hernandez, J., Dolz, G., Maranda, L., Galindo, J., et al. (2007). Dynamics of Infections With Gastrointestinal Parasites and *Dictyocaulus viviparus* in Dairy and Beef Cattle From Costa Rica. *Vet. Parasitol.* 148 (3–4), 262–271. doi: 10.1016/j.vetpar.2007.06.015
- Kingston, N., and Stabler, R. M. (1978). Two Species of *Entamoeba* From White-Tailed Deer, *Odocoileus virginianus*, From Georgia. *J. Parasitol.* 64 (1), 14–16. doi: 10.2307/3279600
- Kumar, S., Stecher, G., and Tamura, K. (2016). MEGA7: Molecular Evolutionary Genetics Analysis Version 7.0 for Bigger Datasets. *Mol. Biol. Evol.* 33 (7), 1870–1874. doi: 10.1093/molbev/msw054
- Matsubayashi, M., Matsuura, Y., Nukata, S., Daizi, Y., Shibahara, T., Teramoto, I., et al. (2018). First Detection and Molecular Identification of *Entamoeba Bovis* From Japanese Cattle. *Parasitol. Res.* 117 (1), 339–342. doi: 10.1007/s00436-017-5689-2
- Nath, J., Ghosh, S. K., Singha, B., and Paul, J. (2015). Molecular Epidemiology of Amoebiasis: A Cross-Sectional Study Among North East Indian Population. *PLoS Negl. Trop. Dis.* 9 (12), e0004225. doi: 10.1371/journal.pntd.0004225
- Ngui, R., Angal, L., Fakhrurrazi, S. A., Lian, Y. L., Ling, L. Y., Ibrahim, J., et al. (2012). Differentiating *Entamoeba histolytica*, *Entamoeba dispar* and *Entamoeba moshkovskii* Using Nested Polymerase Chain Reaction (PCR) in Rural Communities in Malaysia. *Parasit. Vectors* 5, 187. doi: 10.1186/1756-3305-5-187
- Noble, G. A., and Noble, E. R. (1952). *Entamoebae* in Farm Mammals. *J. Parasitol.* 38 (6), 571–595. doi: 10.2307/3273985
- Nolan, M. J., Unger, M., Yeap, Y. T., Rogers, E., Millet, I., Harman, K., et al. (2017). Molecular Characterisation of Protist Parasites in Human-Habituated Mountain Gorillas (*Gorilla beringei beringei*), Humans and Livestock, From Bwindi Impenetrable National Park, Uganda. *Parasit. Vectors* 10 (1), 340. doi: 10.1186/s13071-017-2283-5
- Rambaut, A., Drummond, A. J., Xie, D., Baele, G., and Suchard, M. A. (2018). Posterior Summarization in Bayesian Phylogenetics Using Tracer 1.7. *Syst. Biol.* 67 (5), 901–904. doi: 10.1093/sysbio/syy032
- Romero, M., Cerritos, R., and Ximenez, C. (2016). Horizontal Gene Transfers From Bacteria to *Entamoeba* Complex: A Strategy for Dating Events Along Species Divergence. *J. Parasitol. Res.* 2016, 3241027. doi: 10.1155/2016/3241027
- Shilton, C. M., Slapeta, J., Shine, R., and Brown, G. P. (2018). Invasive Colonic Entamoebiasis in Wild Cane Toads, Australia. *Emerg. Infect. Dis.* 24 (8), 1541–1543. doi: 10.3201/eid2408.180101
- Shirley, D. T., Farr, L., Watanabe, K., and Moonah, S. (2018). A Review of the Global Burden, New Diagnostics, and Current Therapeutics for Amebiasis. *Open Forum Infect. Dis.* 5 (7), 161. doi: 10.1093/ofid/ofy161
- Stensvold, C. R., Lebbad, M., and Clark, C. G. (2010). Genetic Characterisation of Uninucleated Cyst-Producing *Entamoeba* Spp. From Ruminants. *Int. J. Parasitol.* 40 (7), 775–778. doi: 10.1016/j.ijpara.2010.03.003
- Stensvold, C. R., Lebbad, M., Victory, E. L., Verweij, J. J., Tannich, E., Alfellani, M., et al. (2011). Increased Sampling Reveals Novel Lineages of *Entamoeba*: Consequences of Genetic Diversity and Host Specificity for Taxonomy and Molecular Detection. *Protist* 162 (3), 525–541. doi: 10.1016/j.protis.2010.11.002
- Tawari, B., Ali, I. K. M., Scott, C., Quail, M. A., Berriman, M., Hall, N., et al. (2007). Patterns of Evolution in the Unique tRNA Gene Arrays of the Genus *Entamoeba*. *Mol. Biol. Evol.* 25 (1), 187–198. doi: 10.1093/molbev/msm238
- Thompson, J. D., Gibson, T. J., Plewniak, F., Jeanmougin, F., and Higgins, D. G. (1997). The CLUSTAL_X Windows Interface: Flexible Strategies for Multiple Sequence Alignment Aided by Quality Analysis Tools. *Nucleic Acids Res.* 25 (24), 4876–4882. doi: 10.1093/nar/25.24.4876
- Weedall, G. D., and Hall, N. (2011). Evolutionary Genomics of *Entamoeba*. *Res. Microbiol.* 162 (6), 637–645. doi: 10.1016/j.resmic.2011.01.007

Conflict of Interest: The authors declare that the research was conducted in the absence of any commercial or financial relationships that could be construed as a potential conflict of interest.

Publisher's Note: All claims expressed in this article are solely those of the authors and do not necessarily represent those of their affiliated organizations, or those of the publisher, the editors and the reviewers. Any product that may be evaluated in this article, or claim that may be made by its manufacturer, is not guaranteed or endorsed by the publisher.

Copyright © 2022 Huaman, Pacioni, Kenchington-Evans, Doyle, Helbig and Carvalho. This is an open-access article distributed under the terms of the Creative Commons Attribution License (CC BY). The use, distribution or reproduction in other forums is permitted, provided the original author(s) and the copyright owner(s) are credited and that the original publication in this journal is cited, in accordance with accepted academic practice. No use, distribution or reproduction is permitted which does not comply with these terms.



Characterization of the B-Cell Epitopes of *Echinococcus granulosus* Histones H4 and H2A Recognized by Sera From Patients With Liver Cysts

Andrea Maglioco^{1,2}, Facundo A. Agüero^{1,2}, María Pía Valacco³, Alejandra Juárez Valdez¹, Margot Paulino^{4*} and Alicia G. Fuchs^{1,5*}

OPEN ACCESS

Edited by:

Piotr Bąska,
Warsaw University of Life
Sciences, Poland

Reviewed by:

Mohammad M. Pourseif,
Tabriz University of Medical
Sciences, Iran
Hamidreza Majidiani,
Neyshabur University of Medical
Sciences, Iran
Seyyed Ali Shariatzadeh,
Mazandaran University of Medical
Sciences, Iran

*Correspondence:

Margot Paulino
margot@fq.edu.uy
Alicia G. Fuchs
fuchsaliciagraciela@gmail.com

Specialty section:

This article was submitted to
Parasite and Host,
a section of the journal
Frontiers in Cellular and
Infection Microbiology

Received: 22 March 2022

Accepted: 02 May 2022

Published: 13 June 2022

Citation:

Maglioco A, Agüero FA, Valacco MP, Valdez AJ, Paulino M and Fuchs AG (2022) Characterization of the B-Cell Epitopes of *Echinococcus granulosus* Histones H4 and H2A Recognized by Sera From Patients With Liver Cysts. *Front. Cell. Infect. Microbiol.* 12:901994. doi: 10.3389/fcimb.2022.901994

¹ Universidad Abierta Interamericana (UAI), Centro de Altos Estudios en Ciencias Humanas y de la Salud (CAECIHS), Buenos Aires, Argentina, ² Consejo Nacional de Investigaciones Científicas y Técnicas (CONICET), Buenos Aires, Argentina, ³ Centro de Estudios Químicos y Biológicos por Espectrometría de Masas (CEQUIBIEM), Instituto de Química Biológica Ciencias Exactas y Naturales- Consejo Nacional de Investigaciones Científicas y Técnicas (IQUIBICEN-CONICET), Facultad de Ciencias Exactas y Naturales- Universidad de Buenos Aires (UBA), Buenos Aires, Argentina, ⁴ Departamento de Experimentación y Teoría de la Estructura de la Materia y sus Aplicaciones, Facultad de Química, Bioinformática DETEMA-Udelar, Universidad de la República, Montevideo, Uruguay, ⁵ Instituto Nacional de Parasitología "Dr Mario Fatala- Chaben", (Administración Nacional de Laboratorios e Institutos de Salud) ANLIS-Malbrán, Buenos Aires, Argentina

Cystic echinococcosis (CE) is a zoonotic disease worldwide distributed, caused by the cestode *Echinococcus granulosus* sensu lato (*E. granulosus*), with an incidence rate of 50/100,000 person/year and a high prevalence in humans of 5-10%. Serology has variable sensitivity and specificity and low predictive values. Antigens used are from the hydatid fluid and recombinant antigens have not demonstrated superiority over hydatid fluid. A cell line called EGPE was obtained from *E. granulosus* sensu lato G1 strain from bovine liver. Serum from CE patients recognizes protein extracts from EGPE cells with higher sensitivity than protein extracts from hydatid fluid. In the present study, EGPE cell protein extracts and supernatants from cell colonies were eluted from a protein G affinity column performed with sera from 11 CE patients. LC-MS/MS proteomic analysis of the eluted proteins identified four *E. granulosus* histones: one histone H4 in the cell extract and supernatant, one histone H2A only in the cell extract, and two histones H2A only in the supernatant. This differential distribution of histones could reflect different parasite viability stages regarding their role in gene transcription and silencing and could interact with host cells. Bioinformatics tools characterized the linear and conformational epitopes involved in antibody recognition. The three-dimensional structure of each histone was obtained by molecular modeling and validated by molecular dynamics simulation and PCR confirmed the presence of the epitopes in the parasite genome. The three histones H2A were very different and had a less conserved sequence than the histone H4. Comparison of the histones of *E. granulosus* with those of other organisms showed exclusive regions for *E. granulosus*. Since histones play a role in the host-parasite relationship they could be good candidates to improve the predictive value of serology in CE.

Keywords: Histones, *Echinococcus granulosus*, epitopes, cell extract, extracellular

1 INTRODUCTION

Cystic echinococcosis (CE) is a zoonotic disease worldwide distributed, caused by the cestode *Echinococcus granulosus* sensu lato, with an incidence rate of 50/100,000 person/year and a high prevalence in humans of 5-10%. In Latin American countries, it is an endemic disease with active transmission, with a proportion of infected young people that reaches 15% (Larrieu et al., 2019). In Argentina, 630 CE cases were confirmed in 2018-2019 (in a period of 48 weeks)¹ and 12.1% out of the 479 new cases confirmed in Buenos Aires province in 2014-2016 were younger than 18 years old (Álvarez et al., 2018). Based on the latest expert consensus on cystic echinococcosis four genotypes clusters have been demonstrated for *E. granulosus* s.l. including: sensu stricto (G1/3), *E. equinus* (G4), *E. ortleppi* (G5) and *E. canadensis* (G6-8/10) (Vuitton et al., 2020). In Argentina, *E. granulosus* sensu stricto (G1/3) has the highest prevalence in both patients and livestock (Cucher et al., 2016).

The parasite has a complex life cycle involving two hosts. The hermaphrodite worm is developed in the intestinal lumen of canids, which are the definitive hosts. Then, fertile proglottids containing oncospheres are shed into the soil by feces, and the intermediate hosts, ungulate animals, or aberrant hosts such as humans or cats (Avila et al., 2021), acquire the parasite *per os*. The cycle closes when canids become infected by eating visceral organs from infected ungulate animals. In the intermediate host, oncospheres come into the abdominal cavity through the intestinal wall after activation, and colonize visceral organs. In humans, the liver has the highest frequency (80%) of infection, followed by the lung (15%) and other organs. The parasitic infection causes high morbidity mainly when it is located in the bone or central nervous system (3-5%). The larva or metacestode, which develops in the intermediate host, has an asexual reproduction, forming protoscoleces from the germinal layer, which is the most internal layer in contact with the cyst cavity full of hydatid fluid. This fluid contains protoscoleces, cells, salts, proteins, and amino acids, and its composition changes according to metacestode viability (Ahn et al., 2015). The germinal layer is covered by the laminar layer, which is the parasite outer acellular layer that participates in the host-parasite interchange. The laminar layer could be damaged by trauma, cyst growth or complications, a fact that leads the protoscoleces to spill in the host body, colonizing other organs.

The clinical suspicion of CE is based mainly on epidemiological data and symptoms. The infection is then confirmed by typical images, which allow disease staging; serology helps to confirm the imaging diagnosis (Zait and Hamrioui, 2020) and analysis of parasite material constitutes the *gold standard* (Reinehr et al., 2020; Pena et al., 2021). The serology methods, standardized in each laboratory, have variable sensitivity and specificity due to cross-reactions or weak antigen recognition and thus, low predictive values. Serology for

differential CE diagnosis and infection follow-up is a research field in progress, with new laboratory methods such as Raman spectroscopy to evaluate serum samples (Yue et al., 2020) and the proposal of new recombinant antigens, initially examined in infected livestock (Liang et al., 2020). However, no recombinant antigen has demonstrated superiority over hydatid fluid extract for CE diagnosis, and serology is not a useful method for infection or treatment follow-up in humans (Sánchez-Ovejero et al., 2020).

In our laboratory, a cell line called EGPE was obtained from *E. granulosus* sensu lato G1 strain from bovine liver (Echeverría et al., 2010). By using this cell line in a paired case-control study, we have previously found that serum from CE patients recognizes protein extracts from EGPE cells at two growth stages with higher sensitivity than those extracted from hydatid fluid (Maglioco et al., 2019).

Histones are proteins associated with cell cycle regulation, protein synthesis and DNA repair. In *E. granulosus*, histones have been found in the nucleosome and other subcellular localizations of protoscoleces (Lorenzatto et al., 2015). Histones H2A, H2B, H3 and H4 are core histones assembled into an octamer around DNA, forming a nucleosome. They are basic proteins divided into two classes: lysine-rich (H1, H2A and H2B) and arginine-rich (H3 and H4) (DeLange and Smith, 1971), sharing a similar structure: three central α -helices connected by loops on C-terminal and N-terminal end. The N-terminus is the site where post-translational modifications, such as acetylation, methylation, citrullination, ubiquitination, phosphorylation and SUMOylation, occur. Histone epigenetic modification is triggered by autocrine factors and parasite-host interactions (Magalhães et al., 2020). Moreover, histone overexpression could be involved in the parasite response to injury (Singh et al., 2010). Histones are encoded by different multi-variable genes and variability contributes to chromatin regulation (Ferrand et al., 2020). Canonical histones are synthesized in the S phase of the cellular cycle, and histone variants substitute for H4, H3, H2A, H2B and H1 confer structural and functional features, and are synthesized independently of the cell cycle, having a single-copy gene (Singh et al., 2010).

In CE, detection of reactive antibodies against *E. granulosus* metacestode antigenic proteins varies depending on the parasite localization. Serological tests have revealed differences in sensitivity whether the parasite is localized in the liver or lungs². Serology specificity also varies because *E. granulosus* shares antigens with other parasites such as *Taenia solium*, *Fasciola hepatica* and *E. multilocularis* (Rassy et al., 2010).

To improve CE serology, we chose the histone family, among the antigenic proteins recognized by sera from CE patients only in the liver. Histones were chosen due to their intra- and extracellular localization and for their role in the naïve immune response. The histones identified were characterized and bioinformatics molecular studies of the epitopes were

¹Dirección Nacional de Epidemiología y Análisis de la Situación de Salud. Ministerio de Salud y Desarrollo Social de la Nación (Argentina, 2019). Boletín Integrado de Vigilancia N 459, <https://bancos.salud.gob.ar/sites/default/files/2020-01/boletin-integrado-vigilancia-n459.pdf>. View 12/15/2021.

²Retamozo, A.R., Agüero, F.A., Fuchs, A.G. and Maglioco, A. (2021). Serological diagnosis in hydatidosis: searching standardized antigenic support. Systematic review and the meta-analysis. Interamerican Journal of Health Sciences 1: e89-108. <https://ijhsc.com/journal/article/view/41/10>. View 02/01/2022.

performed. PCR and sequencing were used to confirm the epitope identification in the *E. granulosus* sensu stricto G1 strain.

2 MATERIALS AND METHODS

2.1 Ethics Statement and Serum Samples

Serum samples from CE patients were obtained by Dr. Jorge Gentile from Hospital Municipal Ramón Santamarina, Tandil, Argentina. Sera from patients with cysticercosis and fascioliasis were donated by Dr. Elizabeth Luz Sánchez Romani, Laboratorio de Zoonosis Parasitaria CNSP-INS-Perú. All protocols and procedures were approved by the Ethics Committee of the 'Universidad Abierta Interamericana', Buenos Aires, Argentina (number 01011). Patient serum samples were from an anonymized laboratory serum stock (Maglioco et al., 2019).

2.2 EGPE Cell Culture, Protein Extracts, and Supernatant

EGPE is a cell line obtained from bovine *E. granulosus* pe G1 maintained at our laboratory. Cells from passages 35 to 40 were used for all experiments. Briefly, EGPE cells were grown in medium 199 (Sigma), 1 mM sodium pyruvate (sodium salt, extra pure, Anhedra, Beijing, China) and 78 µg/mL β-mercaptoethanol (Merck, Darmstadt, Germany) at pH 7.9 (37°C; CO₂:air; 5/95%) and EGPE cell colonies were performed in 2% agarose (20,000 cells/well) (Echeverría et al., 2010). Cells were grown in a liquid medium for 20 days and protein extracts were obtained as previously (Maglioco et al., 2019). Briefly, cells were washed five times with DPBS and incubated in lysis buffer (8 mmol/L CHAPS, MP Biomedicals, 10 mmol/L Tris -HCl, pH 8, 2 mmol/L EDTA, 0.1% B-mercaptoethanol, MP Biomedicals, and 1/100 protease inhibitor cocktail, Sigma-Aldrich), at 4°C for 2 hours. Samples were then frozen-thawed three times and spun down at 10 000 g.

Cell colony supernatants were obtained after 5 days of incubation. Debris was removed by centrifuging the supernatants three times (3000 rpm). Then, samples were stored in aliquots at -20°C until use.

2.3 Protein Identification

2.3.1 Extraction of Protein Fraction

EGPE cell protein extracts were first passed through a gel filtration column (1.6 cm x 90 cm, Sephacryl S-200 HR GE Healthcare). Protein fractions were identified by absorbance (205-280 nm) in a spectrophotometer (Biowave II+, Biochrome Ltd., Cambridge, England). Every fraction with higher absorbance was concentrated through a 3K cut-off membrane concentrator (Pierce, Thermo Scientific). The reactivity of these fractions and that of the supernatant of EGPE colonies was analyzed by Western blot (Maglioco et al., 2019) by using a pool of sera from 11 patients with CE with only hepatic localization (**Supplementary Figure 1**). Then, reactive protein fractions were passed through an affinity column (Protein G HP SpinTrap - GE Healthcare) prepared with this pool of CE sera (cases) or through an affinity column performed with a pool of sera from two patients with cysticercosis and two patients with fascioliasis (controls). Eluted

proteins were concentrated through a 3K cut-off membrane concentrator (Pierce, Thermo Scientific). A 15% SDS-PAGE was performed to concentrate and clean-up protein extracts prior to in-gel digestion (data not shown).

2.3.2 Protein Digestion and Mass Spectrometry Analysis

Proteins were then digested and analyzed by Mass Spectrometry Analysis at the Proteomics Core Facility of the CEQUIBIEM, Faculty of Exact Sciences, University of Buenos Aires/IQUIBICEN CONICET, National Research Council, Argentina. Protein bands excised from Coomassie blue-stained SDS-PAGE gels were sequentially washed and destained with 50 mM ammonium bicarbonate, 25 mM ammonium bicarbonate, 50% acetonitrile, and 100% acetonitrile, and then reduced and alkylated with 10 mM dithiothreitol and 20 mM iodoacetamide and in-gel digested with 100 ng Trypsin (Promega V5111) in 25 mM ammonium bicarbonate overnight at 37°C. Peptides were recovered by elution with 50% acetonitrile-0.5% trifluoroacetic acid, including brief sonication, and further concentrated by speed-vacuum drying. Samples were resuspended in 15 µL of water containing 0.1% formic acid, desalted using C18 zip tips (Merck Millipore) and eluted in 10 µL of water: acetonitrile: formic acid 40:60:0.1%. The digests were analyzed by nanoLC-MS/MS in a Thermo Scientific QExactive Mass Spectrometer coupled with a nanoHPLC EASY-nLC 1000 (Thermo Scientific). For LC-MS/MS analysis, approximately 2 µg of peptides was loaded onto a reverse-phase column (C18, 2 µm, 100Å, 50 µm x 150 mm) Easy-Spray Column PepMap RSLC (P/N ES801) suitable to separate protein complexes with a high degree of resolution. The flow rate used for the nano-column was 300 nL min⁻¹ and the solvent range from 7% B (5 min) to 35% (120 min). Solvent A was 0.1% formic acid in water, whereas solvent B was 0.1% formic acid in acetonitrile. The injection volume was 2 µL. A voltage of 3.5 kV was used for Electro Spray Ionization (Thermo Scientific, EASY-SPRAY).

XCalibur 3.0.63 (Thermo Scientific) software was used for data acquisition. Full-scan mass spectra were acquired in an Orbitrap analyzer. The scanned mass range was 400-1800 m/z, at a resolution of 70000 at 400 m/z, and the twelve most intense ions in each cycle were sequentially isolated, fragmented by higher-energy collision dissociation, and measured in an Orbitrap analyzer. Peptides with a charge of +1 or with an unassigned charge state were excluded from fragmentation for MS2.

QExactive raw data were processed using the Proteome Discoverer software (version 2.1.1.21, Thermo Scientific) and searched against the *E. granulosus* sequence database with trypsin specificity and a maximum of one missed cleavage per peptide. Carbamidomethylation of cysteine residues was set as a fixed modification and oxidation of methionine was set as variable modification. Proteome Discoverer searches were performed with a precursor mass tolerance of 10 ppm and product ion tolerance of 0.05 Da. Protein hits were filtered for high-confidence peptide matches with a maximum protein and peptide false discovery rate of 1%, calculated by using a reverse database strategy.

2.4 Protein Analysis

2.4.1 Prediction of Physicochemical Parameters

The complete amino acid sequence of histones H4-W6ULY2, H2A-W6UJM4, H2A-W6U132, and H2A-W6U0N3 were obtained from UniProt. Online tools from ExPASy Prot Param (Wilkins et al., 1999) were used to analyze the histones identified.

2.4.2 Analysis of Histone Similarity

Similarities between histones from *E. granulosus* and other organisms were studied by BLAST-P³ with the complete sequence of each histone, non-redundant database, and the organism as inputs.

2.4.3 Prediction of the Secondary Structure, Domain, and Post-Translational Modification Site of the *E. granulosus* Histones Identified

Prediction analysis was performed using the following on-line analysis software: SOPMA⁴ for secondary structure, Pfam⁵, Conserved Domains tool from NCBI⁶ and Interpro⁷ for domains, and MusiteDeep⁸, DeepNitro (Xie, Y. 2018) and CKSAAP_CitrSite⁹ for post-translational modification site.

2.4.4 Prediction of the Tertiary Structure of Histones

The amino acid sequence of each protein was used to search structurally homologous sequences in the Protein Data Bank, using the Sequences Annotated by Structure (SAS) (Milburn et al., 1998). Since the best templates from SAS for the sequences of histones H4 and H2A did not cover a large part of each sequence, the *Ab initio* methodology was selected. Molecular modeling was performed using *ab initio* modeling from the Robetta¹⁰ platform. Histone H4 was modeled by the *Ab initio* method, in which the target starts as an extended chain and the *Ab initio* Rosetta fragment assembly method folds the chain. Histones H2A were modeled by the TrRosetta method, a deep learning-based modeling method (threading). The quality of the models was analyzed by the ERRAT platform, using the Ramachandran, ERRAT and VERIFY3D options. Then, each model was validated by molecular dynamics simulation by using the Nanoscale Molecular Dynamics software. Each protein was solvated with explicit solvent by using the TIP3 water model, in a water box with the following dimensions: 79.31, 71.26, 52.77; 59.50, 66.47, 134.07; 91.28, 98.08, 144.33 and 97.56, 66.92, 82.35 (x, y, z in Å) for H4-W6ULY2, H2A-W6UJM4, H2A-W6U132 and H2A-W6U0N3, respectively. The system was neutralized with NaCl at an ionic concentration of 0.15 M. Periodic boundary conditions were used. The CHARMM36 force field was used in all molecular dynamics simulations in a standard number of particles, pressure (1 atm) and temperature. The

simulation protocols involved: 2000 steps of minimization by the conjugate gradient method; 0.29 ns of heating from 60K to 300K; 1 ns equilibration maintained at 300K; and unrestrained production of 50 ns maintained at 300K, considering potential energy to confirm the thermodynamic equilibration of each molecule. The root mean-square deviation (RMSD) and root mean square fluctuation (RMSF) were calculated. Structures were analyzed and visualized with Visual Molecular Dynamics (version 1.9.3) and Molecular Operating Environment.

2.5 Histone Epitope Studies by Bioinformatics

The B-cell linear epitopes (Lep) of each protein were predicted using eight software programs. The results selected were those of ABCpred (score above 0.85) (Saha and Raghava, 2006), also identified in regions of at least five adjacent amino acids by BepiPred Linear Epitope Prediction 2.0 (threshold: 0.5) or by BepiPred Linear Epitope Prediction (threshold: 0.35) and by at least three of the following software programs: Chou & Fasman Beta-Turn Prediction (threshold indicated by the server for each protein sequence), Emini Surface Accessibility Prediction (threshold: 1.0), Karplus & Schulz Flexibility Prediction (threshold: 1.0), Kolaskar & Tongaonkar Antigenicity (threshold indicated by the server for each protein sequence), and Parker Hydrophilicity Prediction (threshold indicated by the server for each protein sequence) in IEDB (Immune epitope database and analysis resource)¹¹. The B-cell conformational epitopes (Cep) of each protein were predicted with DiscoTope¹² 2.0, using a threshold of -3.7 (sensitivity= 0.47 and specificity= 0.75) for the final structure (50 ns - unrestricted trajectory) of each histone. This software uses a combination of amino acid statistics, spatial information, and surface exposure. It is trained on a compiled data set of discontinuous epitopes from X-ray structures of antibody/antigen protein complexes.

2.6 Sequencing of Genomic DNA Encoding Histone Epitopes From the *E. granulosus* G1

E. granulosus DNA was extracted from an *E. granulosus* G1 metacestode obtained from a cow's liver, from a slaughterhouse located in Buenos Aires, Argentina (Dr. Tatiana Aronowicz, SENASA). DNA was isolated with a lysis solution of 2% cetyltrimethyl ammonium bromide (w/v) (Stanton, Buenos Aires, Argentina), 1.4 M NaCl₂, 20 mM EDTA (Merck Química Argentina, Buenos Aires, Argentina), 100 mM Tris-Cl (Plus one Tris, GE-Healthcare, Bio-sciences, Uppsala, Sweden), 0.175% β-mercaptoethanol (MP Illkirch- France) (v/v), pH 7.5 and then chloroform/isoamyl alcohol (24:1), precipitated with isopropyl alcohol and washed with 70% ethanol/10 mM ammonium acetate. The final DNA concentration was 730 ng/μL (260 nm, spectrophotometer, WPA BIOWAVE II+, Biochrom Ltd., Cambridge, England) and 18 ng was used for the integrity study in gel electrophoresis (1% agarose LE; PBL-Buenos Aires, Argentina) and for PCR. All primers were

³ <https://blast.ncbi.nlm.nih.gov/Blast.cgi?PAGE=Proteins>; viewed 12/27/2021

⁴ https://npsa-prabi.ibcp.fr/cgi-bin/npsa_automat.pl?page=/NPSA/npsa_sopma.html; viewed 03/12/2021

⁵ <http://pfam.xfam.org/>; viewed 12/09/21

⁶ <https://www.ncbi.nlm.nih.gov/Structure/cdd/wrpsb.cgi>; viewed 12/09/21

⁷ <http://www.ebi.ac.uk/interpro/>; viewed 2/10/22

⁸ <https://www.musite.net/>; viewed 12/09/21

⁹ 123.206.31.171/CKSAAP_CitrSite/; viewed 01/12/22

¹⁰ <https://robetta.bakerlab.org/>; 11/05/20

¹¹ IEDB; Viewed 04/24/2022

¹² DiscoTope; Viewed 09/01/2021

obtained from Gene Biotech SRL (Buenos Aires, Argentina). The genotype of the metacestode was determined by COX1C, using the primer F: 5'-CTGTTTTGGCTGCGGCTATT-3'; R: 5'-AGCCGTCTTCACATCCAACC-3'. Then, specific primers were designed to amplify an optimal fragment size between ≈250 bp-500 bp including the coding region for each predicted linear epitope with the Primer-Blast tool available in the NCBI website (Ye et al., 2012). The primer sequences are listed in **Table 1**. Each reaction tube contained: 1.5 mM MgCl₂ (5x, Colorless GoTaq[®] Reaction Buffer, Promega, Madison, WI, USA), 0.2 mM of dNTPs mix (dGTP, dCTP, dTTP and dATP, Promega, Madison, WI, USA), 1 μM forward primer, 1 μM reverse primer, 1.25 units of DNA polymerase (GoTaq[®] polymerase, Promega, Madison, WI, USA), 18 ng of DNA template and nuclease-free water up to 50 μL (ultrapure, PB-L, Productos Bio-lógicos). The PCR protocols consisted of an initial denaturation of the template (95° C for 2 min) followed by 35 cycles of template denaturation (95° C for 1 min), annealing of primers (appropriate temperature according to pair of primers for 1 min), and DNA extension (72° C for the corresponding time according to product size); and a final extension of 72° C for 5 min, using a Mastercycler personal (Eppendorf, Hamburg, Germany). Then, 17.5 μL of product was observed by agarose electrophoresis (LE molecular biology grade, PB-L, Productos Bio-Lógicos, Buenos Aires, Argentina) using the 100-1000-bp ladder (Dongsheng Biotech Co., Ltd., Guangzhou, China). Bands were purified using the Wizard[®] SV Gel and PCR Clean-Up System (Promega Co., USA) and sequenced in the CEDIE "Dr César Bergadá (CONICET- Hospital de Niños 'Ricardo Gutiérrez', Buenos Aires, Argentina). The sequences obtained were studied by BLAST and manual alignment.

3 RESULTS

3.1 Characterization of *E. granulosus* Antigenic Histones

Several proteins from EGPE cells were recognized by the CE sera after performing the affinity column. Histones H4-W6UJY2, H2A-W6UJM4 and H2A-W6U132 were identified in the

supernatant of EGPE colonies. The same histone H4 and histone H2A-W6U0N3 were recognized in the cellular extracts. The sequence of the histones' peptides obtained by MS/MS are shown in **Table 2** and, the histones complete sequences are shown in **Figure 1**. Some histone sequences of *F. hepatica* are similar to those of *E. granulosus* (**Table 3**). Despite this, control sera only recognized histone H2A-W6U0N3. No protein sequences were described for histones H4 or H2A in *Taenia solium*.

For all the histones analyzed, the estimated half-life was 30 h in *in vitro* mammalian reticulocytes, more than 20 h in yeast and more than 10 h in *Escherichia coli*. Histones H4-W6UJY2 and H2A-W6U132 had an instability index above 40, which allows classifying the proteins as unstable, whereas histones H2A-W6UJM4 and H2A-W6U0N3 were classified as stable. The aliphatic index, the Grand average of hydropathicity (GRAVY) and the predicted secondary structure of histones are shown in **Table 4**. The predicted secondary structure of histones H2A was different: H2A-W6U0N3 had the highest content of α-helices, H2A-W6UJM4 showed the lowest number of β-turns and H2A-W6U0N3 showed the lowest proportion of random coil and highest number of extended strands. H2A-W6U132 had the same proportion of β-turns as H2A-W6U0N3 and the same proportion of random coils as H2A-W6UJM4.

A high-quality tridimensional model was obtained for each histone according to Ramachandran plot analysis (89.9 - 97.1% of the residues in the most favored region); ERRAT (94.94 - 100% of the protein with an error value below the rejection limit) and VERIFY3D (71.24 - 84.57% of the residues with an average score 3D/1D ≥ 0.2). A molecular dynamics simulation was performed for each model. The analysis of total potential energy showed that all models reached the thermodynamic equilibrium during the equilibration step of the molecular dynamics simulation, reaching average values of -92488 ± 153, -165501 ± 192, -404888 ± 321 and -168200 ± 193 Kcal/mol over all trajectories for histones H4-W6UJY2, H2A-W6UJM4, H2A-W6U132, and H2A-W6U0N3, respectively. The analysis of the RMSD showed that the global mobility is generally associated with high RMSD rates, even when average structure is taken as reference (**Table 5** and **Supplementary Figure 2**). In addition, a

TABLE 1 | Primer sequences used for amplifying epitope sequences by PCR.

Epitope	Primer sequences	Product size (bp)	Tm (°C)	Extension time (seconds)
H4-W6UJY2 ₁₁₋₂₆	F: 5'-ATGTCTGGTCGCGGTAAGG-3' R: 5'-ACGACCCTGGCGTTTAAGAG-3'	288	54	18
H4-W6UJY2 _{134-149;158-173}	F: 5'-TGGGTGCAAGTCAGTGATACC-3' R: 5'-CGCCTCACCAGTAACCTACA-3'	227	54	14
H2A-W6UJM4 ₂₇₋₄₂	F: 5'-TCCGTCAGTGGCAACATTCA-3' R: 5'-GGGCGGCCTAGATGGACTTA-3'	324	56	20
H2A-W6UJM4 ₉₂₋₁₀₇	F: 5'-ACACCAAGAGGTTTGGACGG-3' R: 5'-TCATGCGTGTTTTAGGCTGG-3'	470	54	28
H2A-W6U132 ₁₇₅₋₁₉₀	F: 5'-AGCCACCGTAAAGCTGACA-3' R: 5'-AATGGGCGGTAAGAAGTCCA-3'	281	52	17
H2A-W6U132 ₂₆₂₋₂₇₇	F: 5'-GATGTGGAATGCTACCGGA-3' R: 5'-GCCGTGGAGAGTAGTTGGTC-3'	294	56	18
H2A-W6U0N3 _{123-138,138-153,170-185}	F: 5'-TGCCTAATACCACGTACGGC-3' R: 5'-CGCTGACCAACAGTTCAAGC-3'	342	54	21

TABLE 2 | Histone identified by proteomic analysis: MS/MS-Data.

Protein Source	Description(UniProt Accesion)	Coverage [%]	Peptides/sequence	PSMs/TheoreticalMH + [Da]	Unique Peptides	Theoretical MW [kDa]	Calculated pI	SequestScore Value
Colonies supernatant	Histone H4 OS=Echinococcus granulosus OX=6210 GN=EGR_10657 PE=3 SV=1 (W6ULY2)	16	3 / DAVTYTEHAK ISGLIYEETR VFLENVIR	3 / 1134.54258 1180.62083 989.57784	3	19.3	10.48	7.72
Colonies supernatant	Histone H2A OS=Echinococcus granulosus OX=6210 GN=EGR_06849 PE=3 SV=1 (W6UJM4)	8	2 / AGLQFPVGR HLQLAIR	3 / 944.53123 850.52575	2	20.2	10.08	4.51
Colonies supernatant	Histone H2A OS=Echinococcus granulosus OX=6210 GN=EGR_10393 PE=3 SV=1 (W6U132)	2	1 / AGLEFPVGR	1 / 945.51524	1	56.6	9.45	1.76
Cell extract	Histone H4 OS=Echinococcus granulosus OX=6210 GN=EGR_10657 PE=3 SV=1 (W6ULY2)	10	2 / ISGLIYEETR VFLENVIR	2 / 1180.62083 989.57784	2	19.3	10.48	4.79
Cell extract	Histone H2A OS=Echinococcus granulosus OX=6210 GN=EGR_11152 PE=3 SV=1 (W6U0N3)	5	1 / AGLQFPVGR	1 / 944.53123	1	21.1	10.27	1.75

graphical revision of the dynamic trajectories showed that some regions are clearly very stable in the space and have relative movements between them. This observation is confirmed by the lowered rates in the RMSD values as it is shown in the **Supplementary Figure 2** for each sequence range.

However, a graphical revision of the dynamic trajectories showed that some regions are clearly very stable in the space and have relative movements between them. These histones have a tridimensional structure domain under canonical histone folding, which would function like histones, and other domains that could have other properties.

Histone H4 showed a region with more mobility, involving 64.3% of non-polar amino acids, particularly glycine among the first fourteen amino acids, and β -turns in the C-terminus. The three histones H2A had different tertiary structures. Histone H2A-W6UJM4 showed a more mobile region, a 160-189 amino acid sequence, with a high content of non-polar amino acids (66.6%), particularly glycine and proline. Histone H2A-W6U0N3 had a histone fold with a tail in the N-terminal region with high content of non-polar amino acids (50.0%), particularly glycine. Histone H2A-W6U132 showed a typical histone domain in the N-terminus, linked to a mobile region with high content of non-polar amino acids (57.1%), particularly proline. Its amino acid composition was found to be similar to the C-terminus of histone H2A (pfam16211 and IPR032454, amino acids 117-149); a second folded domain involves two domains: WGR (pfam05406 and IPR008893, amino acids 334-397 and 350-397, respectively) and PARP (pfam00644 and IPR012317, amino acids 466-516 and 410-518, respectively). **Figure 1** (insert in C) shows the different structures acquired during the molecular dynamics simulation of histone H2A-W6U132. The distance between amino acids 1-130 and 150-518 decreases by 45% between the minimized structure and the 50 ns structure.

3.2 Epitope Prediction

The epitopes were localized mainly in the mobile regions of the histones (**Figure 1** and the RMSF in **Supplementary Figure 3**). In the epitopes, the ubiquitination and only-methylation sites were found to be localized only in the Cep. Those for ubiquitination were found only in H2A-Cep from the supernatant in W6UJM4 (K74 and K180) and W6U132 (K42 and K145), whereas those for methylation were found in H2A-W6U132 (R2 and R33) and in H2A-W6U0N3 and H4-W6ULY2 (R4). Two putative sites for citrullination were shared with those for methylation: R4 in the Cep of H4-W6ULY2 and H2A-W6U0N3, and R33 in the Cep of H2A-W6U132. In H2A-W6U132, the only-citrullination sites were Cep sites (R343 and R350), whereas those in H2A-W6U0N3 were Cep R11 and Lep (R136, R139, R176 and R179); those in H2A-W6UJM4 were Lep R93 and Lep-Cep R104, and those in H4-W6ULY2 were Lep (R18 and R170). The putative site for phosphorylation in the intracellular H2A-W6U0N3 was only in Cep (S2), whereas those in H4-W6ULY2 were in Cep (S2) and Lep (S138) and those in H2A-W6U132 were in Lep (S184 and S272) and Cep (S348). The acetylation or methylation putative sites were shared for Lep and Cep in the same amino acid, K21 for H4-W6ULY2 and K66 for H2A-W6UJM4. The putative site for acetylation was absent in epitopes of H2A-W6U132, whereas that in the intracellular histone H2A-W6U0N3 was only in Cep (K6 and K9) and that in the supernatant of H2A-W6UJM4 was in Cep (K72) and shared K63 and K70 in Cep-Lep. H4-W6ULY2 presented more putative sites for acetylation in epitopes, in Lep K17, in Cep K6, K9 and K80 and in Lep-Cep K13. No nitration sites were found in the epitopes of these histones.

E. granulosus and *F. hepatica* were found to share Lep 11-26 from histone H4-W6ULY2 and Lep 92-107 from H2A-W6UJM4 but, these histones were not eluted by the control affinity column.

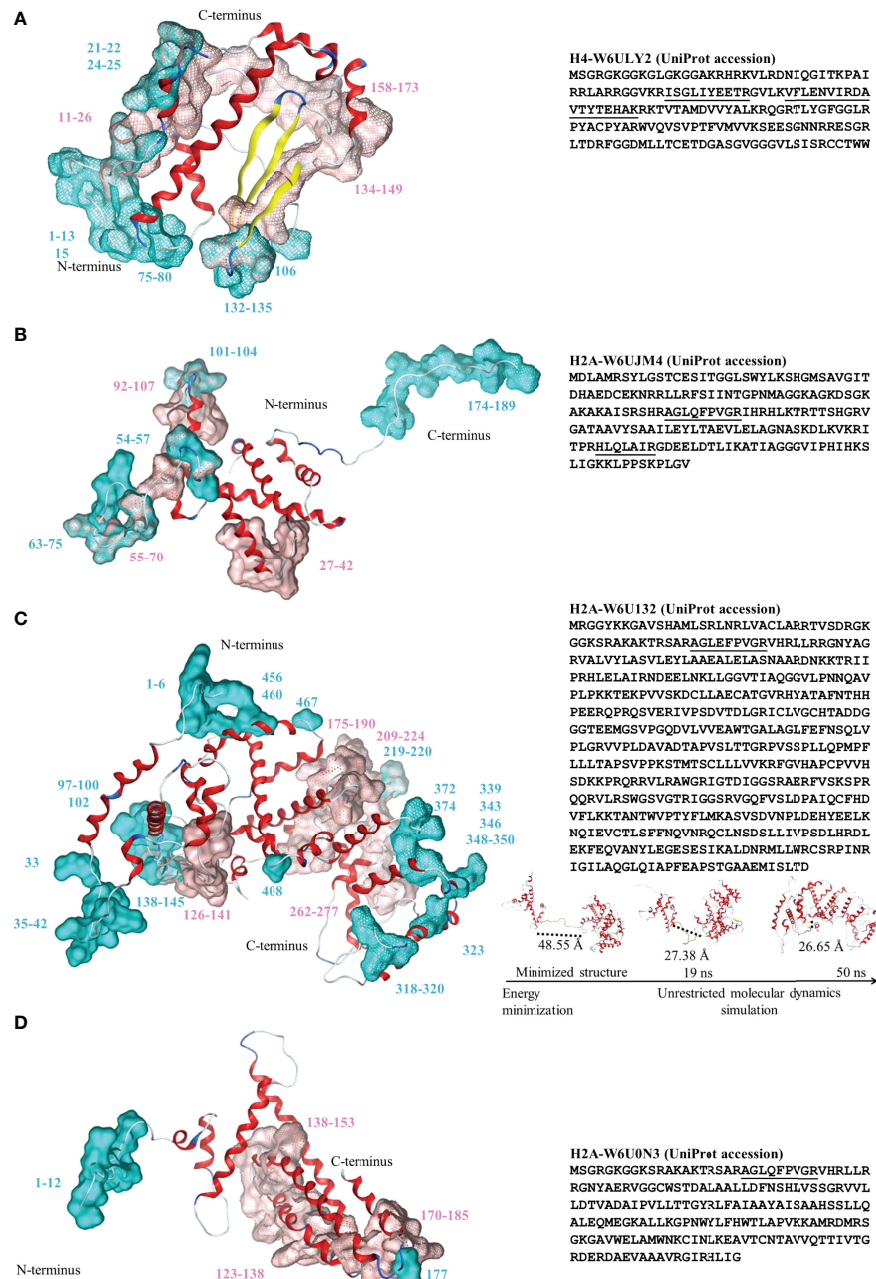


FIGURE 1 | Left: Three-dimensional structure for the histones identified by proteomic analysis. **(A)** Histone H4-W6U1Y2, **(B)** Histone H2A-W6UJM4, **(C)** Histone H2A-W6U132, and **(D)** Histone H2A-W6U0N3. Conformational and linear epitopes are annotated over the three-dimensional structure by cyan and pink van der Waals surfaces, respectively. The backbone 3D structure is shown in ribbons: alpha-helices (red), beta-sheet (yellow), turns (blue) and loops (light-blue). Right: the corresponding sequences in one-letter code for the four studied histones. The peptides identified by MS/MS are underlined. For the special case of H2A-W6U132 **(C, right, bottom)**, snapshots of the structural conformation after the energy minimization/molecular dynamics steps are shown and dotted lines shown the loop distances between the histone and the WGR-PARP domains.

3.3 DNA Sequencing of Histone Epitope in the *E. granulosus* G1 Genome

The *E. granulosus* genotype was identified by COX1 analysis (**Figure 2A**). The predictive histone epitopes were amplified by

PCR in DNA from a metacestode localized in a bovine liver (**Figure 2B**). The epitopes sequenced bands obtained showed 90.06 to 100% identity to the corresponding coding gene by Clustal Omega. The double band < 200 bp found in H2A-W6U132₁₇₅₋₁₉₀ could not be sequenced.

TABLE 3 | Amino acid sequence similarity with *Fasciola hepatica*.

Histone	Identity (%)	Accession (NCBI)
H4-W6ULY2 (amino acids 1-103)	100	THD21169.1
H2A-W6UJM4 (amino acids 59-189)	97.71	THD 18298.1
H2A-W6U132 (amino acids 30-149)	86.18	THD21592.1
H2A-W6U0N3 (amino acids 1-58)	81.03	THD21592.1

TABLE 4 | Physicochemical parameters and secondary structure of the histones identified.

Histone	Instability index	Aliphatic index	Hydropathicity (GRAVY)	Structure			
				α -helices	B-turns	Random coils	Extended strands
H4-W6ULY2	52.68	78.46	-0.371	36.00	10.86	35.43	17.71
H2A-W6UJM4	35.07	93.02	-0.225	42.86	6.88	38.62	11.64
H2A-W6U132	47.10	93.53	-0.174	38.03	10.04	37.84	14.09
H2A-W6U0N3	24.36	96.15	0.009	51.28	11.79	20.51	16.41

4 DISCUSSION

Serological diagnosis in CE lacks inter-laboratory standard, although many recombinant or synthetic proteins have been proposed to be useful. However, the recombinant or synthetic antigenic proteins assayed have less sensitivity and specificity than *ex vivo* parasite antigens and/or predictive values have not been conclusive. These are the cases of AgB (Hernández-González et al., 2008; Savardashtaki et al., 2017; Han et al., 2019; Salah et al., 2021), Ag5 (Barbieri et al., 1998), EPC1-calcium binding protein from *E. granulosus* protoscoleces (Fathi et al., 2016), and recombinant tubulins obtained, but not clinical studies with these antigens have been performed (Liu et al., 2018).

In this work, we studied several histones identified by proteomic analysis of antisera affinity of human host CE sera. Histones are proteins localized mainly in cellular nucleosomes and less frequently in the cytoplasm and extracellular space. Histone concentration in human serum is a marker of tissue damage (normal values: 0.8 ng/mL). In severe trauma, sepsis, cancer and autoimmune disease, high histone concentration and other markers predict multi-organic failure and death (Chen et al., 2014; Silk et al., 2017; Lu et al., 2020). Histones H4, H3, H2A and H2B stabilize the chromatin in

the nucleosome (147 bp) and H1 and H5 are the linkers between nucleosomes. Although histones are conserved among evolution, protists have more diversity than intermediate eukaryotes. Galindo et al. (2004) described H1 genetic divergences between the Platyhelminth phyla Cestode and Trematode and, showed that *E. granulosus* has two different H1 codified by different genes, one of them like that of *Trypanosoma cruzi*. Every histone has specific physiological functions and complex regulation. Histone function regulation includes chaperones, co-chaperones, and post-translational modifications (Strahl and Allis, 2000; Hammond et al., 2017), which regulate DNA and tRNA-histone associations, causing different physiological effects.

One of the findings of the present study is that, except the reactive histone H4 found intracellularly and in the supernatant of cell colonies, H2A-W6U0N3 was localized only intracellularly and the other two H2A only in the supernatant. These findings could be attributed to the histone representativeness between the two spaces, intra- and extracellular, or to the characteristics of EGPE cells (Echeverría et al., 2010). The four histones were recognized by CE sera and the sequences of the epitopes were found in DNA from the *E. granulosus* G1 metacestode with high identity. No reactivity to H1, H3 or H2B histones was found.

TABLE 5 | Histones RMSD for the total protein and the regions.

Protein	RMSD \pm SD (Minimized structure) Å	RMSD \pm SD (Average structure) Å
H4 - W6ULY2 (175 aa)	5.57 \pm 1.44	3.90 \pm 0.85
1-14	5.18 \pm 1.57	3.53 \pm 0.65
14-175	4.00 \pm 0.95	1.85 \pm 0.69
H2A - W6UJM4 (189 aa)	8.64 \pm 2.34	5.88 \pm 1.57
1-160	4.74 \pm 1.24	2.75 \pm 0.65
160-189	5.54 \pm 1.43	4.60 \pm 1.04
H2A - W6U132 (518 aa)	12.86 \pm 4.96	7.78 \pm 1.50
1-130	6.79 \pm 1.51	4.11 \pm 0.83
130-150	8.68 \pm 2.89	5.27 \pm 1.43
150-518	5.27 \pm 1.15	2.23 \pm 0.73
H2A - W6U0N3 (195 aa)	5.41 \pm 1.20	3.72 \pm 0.74
1-14	4.13 \pm 1.53	3.30 \pm 1.12
14-195	4.25 \pm 1.00	2.17 \pm 0.61

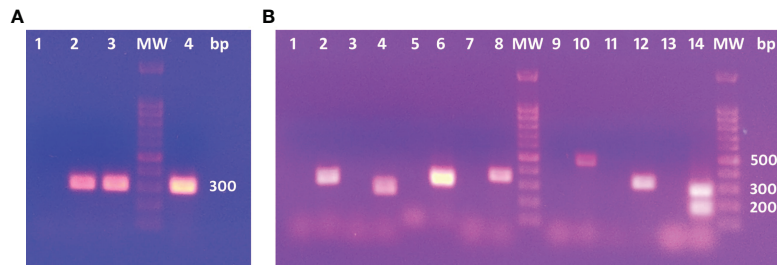


FIGURE 2 | (A) PCR products in electrophoresis agarose gel for COX1C primers. 1: No template. 2 and 3: Positive controls. 4: Cow's liver DNA template. **(B)** Agarose gel electrophoresis for PCR products. 1, 3, 5, 7, 9, 11 and 13: No template controls for each PCR assay. 2: H4-W6ULY2₁₁₋₂₆. 4: H4-W6ULY2₁₃₄₋₁₄₉; 158-173. 6: H2A-W6U0N3_{123-138,138-153,170-185}. 8: H2A-W6U0N3_{123-138,138-153,170-185}. 10: H2A-W6UJM4₉₂₋₁₀₇. 12: H2A-W6UJM4₂₇₋₄₂. 14: H2A-W6U132₁₇₅₋₁₉₀. H2A-W6U132₁₇₅₋₁₉₀ shows two bands: the expected product of 281 bp and an unspecific product with lower molecular weight.

Histones are released to the extracellular space by exocytosis of exosomes, or by NETosis, described in granulocytes, an ionic calcium- and PAD4 dependent mechanism with or without ROS or NADPH oxidase as initial pathway (Vorobjeva and Chernyak, 2020). Wu et al. (2019) demonstrated that a non-specific inflammatory response *via* NOD and RIP2, together with a MHC-related gene and histones, can lead to the production of antibacterial peptides. In addition, immunoglobulins with degradative capacity against histones, known as Abzymes, have been detected in HIV-infected patients and autoimmune disease (Baranova et al., 2018). In addition, Waga et al. (1987) described mouse IgG3 against histones H2A and H4 and IgG2b against H2B in DNA-histone complexes released in bovine milk. However, species-specific epitope studies have not yet been performed and the effectiveness of serological markers in the humoral response of *E. granulosus*-infected hosts has not yet been studied.

For B-cell epitope analysis we chose a software program based on recurrent neural network trained with B-cell epitopes as positive data and random peptides as negative data, with a 65.9% prediction accuracy of ABCPred for Lep epitopes (Saha and Raghava, 2006) and DiscoTope for Cep epitopes (Kringelum et al., 2012). Additionally, several software programs based on different antigen characteristics were used to select the linear sequences with a high probability to be antigenic determinants. In the literature, there are different algorithms to predict epitopes, as the recently work by Pourseif et al. (2021), who proposed to analyze the epitope prediction processing of the result by adding normalization and averaging steps. However, we chose to analyze the epitope prediction by all the above-mentioned platforms using the score of every program independently.

Among the 16 amino acids considered before, five consecutive amino acids must be included by other epitope prediction machine learning software, such as a program trained on epitopes from crystal structure or by a program combining a hidden Markov model and a propensity scale method and considering three of the following characteristics: the presence of B-turns, surface accessibility, chain flexibility, antigenicity and hydrophilicity (**Supplementary Table 1**). Conformational B-cell epitopes, which constitute approximately 90% of the B-cell

epitopes, were predicted with the three-dimensional structures of histones, considering solvent accessibility, amino acid statistic and spatial information with an area under the curve performance of 0.727 (Kringelum et al., 2012).

The root mean square fluctuation indicates the residue-specific flexibility of the protein system. Most of the epitopes predicted in the histones were in regions composed of loops or turns and with high RMSF values. The flexibility of the epitopes may facilitate the conformational adaptation upon antibody binding (Karplus and Schulz, 1985; Rubinstein et al., 2008). As the histones are molecules conserved among organisms, comparison between *E. granulosus* and *F. hepatica*, another relevant organism for differential serological diagnosis, highlighted Lep H4-W6ULY2₁₃₄₋₁₄₉, 158-173, H2A-W6UJM4₂₇₋₄₂, 55-70, H2A-W6U132₁₂₆₋₁₄₁, 175-190, 209-224, 262-277, and H2A-W6U0N3₁₂₃₋₁₃₈, 138-153, 170-185 as unshared epitopes.

The four histones from *E. granulosus* here described are different from those from other organisms. About 58% of the sequence of histone H4-W6ULY2 has 100% identity to that from humans (NCBI: NP_001029249.1), that from *E. multilocularis* (NCBI: CDI96644.1), that from *F. hepatica* (NCBI: THD21169.1), and that from *Hymenolepis microstoma* (NCBI: CDS25250.2). About 66% of the sequence of histone H2A-W6UJM4 has 96% identity to that from humans (NCBI: 3WAA_C). About 29% of the sequence of H2A-W6U0N3 presents 76.27% of identity to H2ATYPE1-H (NCBI: NP_542163.1), and only 22% of the sequence of histone H2A-W6U132 has 82.79% of identity to H2ATYPE2-B (NCBI: NP_778235.1). Similarities were also found in the sequences of the H2A histones of *E. granulosus*, *E. multilocularis*, *F. hepatica* and *H. microstoma*. About 29% of the sequence of H2A-W6U0N3 has 81.03-82.76% of identity to that from *E. multilocularis* (NCBI: CDS35646.1), that from *F. hepatica* (NCBI: THD21592.1) and that from *H. microstoma* (NCBI: CDS33856.1). About 23-27% of the sequence of H2A-W6U132 has 85.16-88.89% identity to that from *E. multilocularis* (NCBI: CDS36059.2), that from *F. hepatica* (NCBI: THD21592.1), and that from *H. microstoma* (NCBI: CDS33856.1). Finally, 59-69% of the sequence of H2A-W6UJM4 has 64.6-100% identity to that from *E. multilocularis* (NCBI: CDS41611.1), that from *F. hepatica* (NCBI: THD18298.1), and that from *H. microstoma* (NCBI: CDS33856.1). Similar proteins described as unnamed were

found in *Hydatigera taeniaeformis*, *Dibothriocephalus latus*, *Schistocephalus solidus*, *Taenia asiatica*, *Hymenolepis diminuta*, *Rodentolepis nana*, *Mesocostoides corti*, and *Spirometra erinaceieuropaei*, and as putative histones in *Schistosoma mansoni*.

The metacestode development, from oncosphere or protoscoleces, constitutes a parasite complex biological transition involved cell proliferation, differentiation and death (Kozioł and Brehm, 2015) releasing cell molecules by shedding or exosomes. Moreover, inflammatory host response increases the laminar layer micro-injury producing hydatid liquid and particulate release (Casaravilla et al., 2020) favoring the interchange between host and parasite molecules (Spotin et al., 2012), Wang et al. (2019) found histone H4 from *E. granulosus* in exosomes from CE human sera, together with α -1C and β -tubulin, whereas Fratini et al. (2020) found tubulin but not histones among parasite proteins contained in the exosomes of CE patients. Increased biosynthesis of histones H3 and H4 has been related to autophagy and increased *Drosophila* life span (Lu et al., 2021). Genotoxicity insults decrease H4 biosynthesis and stimulate degradation, decreasing DNA homologous recombination and DNA repair but, in pathogenic species such as *Candida glabrata*, a high rate of non-homologous end-joining recombination and reduction in H4 levels have been described (Kumar et al., 2020). Extracellular histones H4 and H3 could interact with endothelial cells and lymphocytes, inducing lymphocyte endothelial adhesion by a complex mechanism (Yoo et al., 2016). In the present study, histone H4-W6UJY2, found intracellularly and in the supernatant of colonies, was recognized by IgG CE sera. Among H4-W6UJY2 epitopes, Lep 11-26 was found in H4 from *E. multilocularis* by bioinformatics studies.

Histones H2A and H2B have been found to be physiologically expressed in early zebrafish embryos, decaying after 48 h post-fertilization (Wu et al., 2019), and to be involved in defense mechanisms against bacteria from diverse organisms, including mammals and shrimps (Hoeksema et al., 2016), as well as to be able to confer drug resistance (Singh et al., 2010). Regarding the three H2A here described, two were found in the supernatant (W6UJM4 and W6UJ132) and only one in an intracellular localization (W6U0N3).

Suspicion of CE is justified when a person from an endemic area begins to suffer allergic manifestation. Parasite or host circulating histones could be responsible for the allergic manifestations and the phosphorylation and citrullination of an epitope alter the autoantibody binding, as shown in R060 kDa, a member of the Ro/LaRNP ribonucleoprotein complex (Terzoglou et al., 2006). Histone H2A-W6UJ132 has three putative residues for phosphorylation in epitopes (S184 and S272, S348) and other three in non-epitope sites (S357, 360 and 515). This is the most phosphorylatable histone found by sera reactivity. It is the lengthiest one with the typical histone domain within a 1-130 amino-acid section, followed by a linker from amino acid 130 to 150 and a second folded domain from amino acid 150 to 518, which is similar to the PARP domain. The two folded domains have very different mobility, and the linker shows further evidence of bending between domains. The secondary structure of the

PARP is helicoidal and some authors consider PARP as the third nucleic acid (Dabin et al., 2016). The PARP macrodomain fold is found in numerous proteins and is able to bind different ADP ribose metabolites. Overall, ADP-ribosylation seems to act as a mediator of stress response upon DNA damage, converted in the nucleus to ADP-ATP-ribose repairing DNA damage. Also, PARP modulates metabolic requirements during differentiation and responds to changes in environmental signals and metabolic milieu, facilitating the adaptation of the cell to a new situation (Simonin et al., 1993; Marjanovic et al., 2017). Although the sequences of the macroH2A1.1 and this histone do not match, the tertiary protein structure is similar. The macroH2A1.1 binds ADPribose and PARP, sharing actions and interactions on chromatin, recruits PELP1 to promoters of macroH2A1-dependent genes, and cooperates to control gene expression. PARP activity regulates nuclear receptors and mediates the expression of ATP-binding cassette transporter A1 in macrophages (Marjanovic et al., 2017). This cassette is involved in drug resistance, excluding drugs from the intracellular space.

The extracellular histone H2A-W6UJM4, found in the supernatant, has a long mobile region with a high content of non-polar amino acids and 95.87% of identity with the human H2AZ in the 121 amino acids from 60 to 180. It shares the residue 38-T of H2AZ.2 corresponding to 97 of H2A-W6UJM4, according to the sequence of human H2AZ, described by Redon et al. (2002) and Horikoshi et al. (2013). This histone is not exactly as that described by Redon et al. (2002) because of the localization of a T instead of an S, described by Bönisch et al. (2012). It could be involved in a slower histone exchange in the nucleosome (Horikoshi et al., 2013), and plays a role in chromosome segregation, embryonic stem cell differentiation, asexual reproductive cell cycle (Hanson et al., 2013) and suppression of temperature-sensitive damage (Ahamed et al., 2007), necessary for host change (36 -39°C). This histone is dispersed in the nucleus and the nucleosomes containing this histone are unstable (Redon et al., 2002). This last characteristic could explain its extracellular localization, since it may be released with unstable nucleosomes. Finally, histone H2A-W6UJM4 shares the Lep 92-107 with *E. multilocularis*.

Sites for putative ubiquitination in epitopes were found in all the histones analyzed. Only histone H2A-W6U0N3 has two sites for ubiquitination (although not in an epitope region), involved in non-homologous DNA end-joining repairs (K13 and K15) (Mattioli et al., 2012). This histone is the H2A recognized only in intracellular protein homogenates and the ubiquitination sites are involved in DNA reparation and protein degradation (Weake and Workman, 2008), this histone would be the less representative in our experimental condition, cell colony supernatant, than intracellular localization but, it triggers humoral immune response *in vivo*. Its epitope has the putative site for phosphorylation (S2), while methylated H4 histone could join this complex (Fradet-Turcotte et al., 2013). Both histones have the putative site for methylation in the epitope (R4). EGPE cells have telomere-telomere association (Echeverría et al., 2010). When the cell cycle is accelerated, G1 and/or G0 decrease, which could generate telomere-telomere association, needing end-

joining repair for the parasite survival success. *E. granulosus* metacystode grows slowly and, probably, the cell cycle acceleration does not allow the protoscoleces to sprout and mature from the proliferative layer. However, this behavior could be responsible for the multiple sterile vesicles found in hosts, as described in Avila et al. (2021). Moreover, as here described, the release of intracellular or degraded histone H2A-W6U0N3 was enough to stimulate detectable reactivity of the human immune system.

Antibodies are the answer to parasite antigen presentation to the host and may represent an “old” photograph of parasite behavior. Besides, the lack of reactivity could also have a predictive meaning. The reactivity of CE sera to the parasite histones described and analyzed in this work needs further research. The histones-antigen-specific sequences are tools to investigate the correlation between host-parasite behavior and disease stage and open a new way to investigate the specific histones involved in the evolution of the infection. Every histone plays its own role: H2A-W6U132 could be involved in the expression of ATP binding cassette transporter A1 for drug resistance, H2A-W6U0N3 could be involved in cyst sterilization, H4-W6ULY2 could be involved in parasite life span, and H2A-W6UJM4 could be involved in embryonic proliferation. Among the described histones the H4-W6ULY2 is the most robust candidate because, it is canonical and it was found in both studied localization, intracellular and extracellular, in agreement with other authors (Wang et al., 2019), it is involved in the life span of the parasite and triggers the innate and adaptive immune response.

This work mainly contributed to identifying the parasite histones recognized by CE sera, providing information about the tertiary structure and putative sites for post-translational modifications, and identifying putative singular epitopes. The epitope study of histones, or any other antigenic protein, is useful to build, in the next future, multi-epitope recombinant proteins. Those which identify only one histone, could increase mainly specificity, and could be correlated with biological meaning, increasing the predictive value. Moreover, in the case of sensitivity, the next study could approach the utility of multi-epitope containing the best epitopes of each antigenic protein.

REFERENCES

- Ahamed, S., Dul, B., Qiu, X., and Walworth, N. C. (2007). Msc1 Acts Through Histone H2A.Z to Promote Chromosome Stability in *Schizosaccharomyces Pombe*. *Genetics* 177, 1487–1497. doi: 10.1534/genetics.107.078691
- Ahn, C.-S., Han, X., Bae, Y.-A., Ma, X., Kim, J.-T., Cai, H., et al. (2015). Alteration of Immunoproteome Profile of *Echinococcus Granulosus* Hydatid Fluid With Progression of Cystic Echinococcosis. *Parasitol. Vectors* 8, 8–10. doi: 10.1186/s13071-014-0610-7
- Álvarez, P., Castiglione, N., Moreno, S., and Bolpe, J. (2018). Hidatidosis En Niños De La Provincia De Buenos Aires. *Arch. Argent. Pediatr.* 116, e476–e481. doi: 10.5546/aap.2018.e476
- Avila, H. G., Magliocco, A., Getiser, M. L., Ferreyra, M. P., Ferrari, F., Klinger, E., et al. (2021). First Report of Cystic Echinococcosis Caused by *Echinococcus Granulosus* Sensus Stricto/G1 in Felix Catus From the Patagonian Region of Argentina. *Parasitol. Res.* 120, 747–750. doi: 10.1007/s00436-021-07048-4

DATA AVAILABILITY STATEMENT

The raw data supporting the conclusions of this article will be made available by the authors, without undue reservation.

ETHICS STATEMENT

The studies involving human participants were reviewed and approved by Comité de Ética para la Investigación Científica y Tecnológica de la Universidad Abierta Interamericana. The patients/participants provided their written informed consent to participate in this study.

AUTHOR CONTRIBUTIONS

AM performed protein purification, *in silico* and data analysis, and contribute to manuscript writing. FA performed cell culture, contributed *in silico* data analysis and obtained PCR results. MV performed proteomic protein identification and analysis. AJ contribute with cell culture and biochemical experiments. MP was a director of *in silico* experiments and data analysis and contribute to manuscript writing. AF was research and work director, conceived and designed the results analysis and wrote the manuscript. All authors contributed to the article and approved the submitted version.

FUNDING

This work was supported by the Fundación Iberoamericana de Estudios Superiores. Chacabuco 90, Buenos Aires, Argentina.

SUPPLEMENTARY MATERIAL

The Supplementary Material for this article can be found online at: <https://www.frontiersin.org/articles/10.3389/fcimb.2022.901994/full#supplementary-material>

- Baranova, S. V., Dmitrenok, P. S., Zubkova, A. D., Ivanisenko, N. V., Odintsova, E. S., Buneva, V. N., et al. (2018). Antibodies Against H3 and H4 Histones From the Sera of HIV-Infected Patients Catalyze Site-Specific Degradation of These Histones. *J. Mol. Recognit.* 31, e2703. doi: 10.1002/jmr.2703
- Barbieri, M., Fernández, V., González, G., Luaces, V. M., and Nieto, A. (1998). Diagnostic Evaluation of a Synthetic Peptide Derived From a Novel Antigen B Subunit as Related to Other Available Peptides and Native Antigens Used for Serology of Cystic Hydatidosis. *Parasite Immunol.* 20, 51–61. doi: 10.1046/j.1365-3024.1998.00117.x
- Bönisch, C., Schneider, K., Pünzeler, S., Wiedemann, S. M., Bielmeier, C., Bocola, M., et al. (2012). H2A.Z.2.2 Is an Alternatively Spliced Histone H2A.Z Variant That Causes Severe Nucleosome Destabilization. *Nucleic. Acids Res.* 40, 5951–5964. doi: 10.1093/nar/gks267
- Casavilla, C., Pittini, Á., Rückert, D., Allen, J. E., and Díaz, Á. (2020). Activation of the NLRP3 Inflammasome by Particles From the *Echinococcus Granulosus* Laminated Layer. *Infect. Immun.* 88, e00190–e00120. doi: 10.1128/IAI.00190-20

- Chen, R., Kang, R., Fan, X.-G., and Tang, D. (2014). Release and Activity of Histone in Diseases. *Cell Death Dis.* 5, e1370. doi: 10.1038/cddis.2014.337
- Cucher, M. A., Macchiaroli, N., Baldi, G., Camicia, F., Prada, L., Maldonado, L., et al. (2016). Cystic Echinococcosis in South America: Systematic Review of Species and Genotypes of *Echinococcus Granulosus* Sensus Lato in Humans and Natural Domestic Hosts. *Trop. Med. Int. Health* 21, 166–175. doi: 10.1111/tmi.12647
- Dabin, J., Fortuny, A., and Polo, S. E. (2016). Epigenome Maintenance in Response to DNA Damage. *Mol. Cell* 62, 712–727. doi: 10.1016/j.molcel.2016.04.006
- DeLange, R. J., and Smith, E. L. (1971). Histones: Structure and Function. *Annu. Rev. Biochem.* 40, 279–314. doi: 10.1146/annurev.bi.40.070171.001431
- Echeverría, C. I., Isolabella, D. M., Prieto Gonzalez, E. A., Leonardelli, A., Prada, L., Perrone, A., et al. (2010). Morphological and Biological Characterization of Cell Line Developed From Bovine *Echinococcus Granulosus*. *In Vitro Cell. Dev. Biol. Anim.* 46, 781–792. doi: 10.1007/s11626-010-9345-8
- Fathi, S., Jalousian, F., Hosseini, S. H., Parsa, H., and Kordafshari, S. (2016). A Study of Cross-Reactivity Between Recombinant EPC1 Antigen of *Echinococcus Granulosus* in Serum From Patients With Confirmed Cystic Echinococcosis Infection and Other Parasitic Infections. *Am. J. Trop. Med. Hyg.* 94, 1313–1317. doi: 10.4269/ajtmh.15-0680
- Ferrand, J., Rodinelli, B., and Polo, S. E. (2020). Histones Variants: Guardians of Genome Integrity. *Cells* 9, 2424. doi: 10.3390/cells9112424
- Fradet-Turcotte, A., Canny, M. D., Escribano-Diaz, C., Orthwein, A., Leung, C. C. Y., Huang, H., et al. (2013). 53BP1 Is a Reader of the DNA Damage-Induced H2A Lys15 Ubiquitin Mark. *Nature* 499, 50–54. doi: 10.1038/nature12318
- Fratini, F., Tamarozzi, F., Macchia, G., Bertuccini, L., Mariconti, M., Birago, C., et al. (2020). Proteomic Analysis of Plasma Exosomes From Cystic Echinococcosis Patients Provides *In Vivo* Support for Distinct Immune Response Profiles in Active vs Inactive Infection and Suggests Potential Biomarkers. *PLoS Negl. Trop. Dis.* 14, e0008586. doi: 10.1371/journal.pntd.0008586
- Galindo, M., Varela, N., Espinoza, I., Toro, G. C., Hellman, U., Wernstedt, C., et al. (2004). Chromatin From Two Classes of Platyhelminthes Display Both Protost H1 and Higher Eukaryote Core Histones. *FEBS Lett.* 567, 225–229. doi: 10.1016/j.febslet.2004.04.065
- Hammond, C. M., Stromme, C. B., Huang, H., Patel, D. J., and Groth, A. (2017). Histone Chaperone Networks Shaping Chromatin Function. *Nat. Rev. Mol. Cell Biol.* 18, 141–158. doi: 10.1038/nrm.2016.159
- Han, X., Kim, J.-G., Wang, H., Cai, H., Ma, X., Duong, D. H., et al. (2019). Survey of Echinococcoses in Southeastern Qinghai Province, China, and Serodiagnostic Insights of Recombinant *Echinococcus Granulosus* Antigen B Isoforms. *Parasitol. Vectors* 12, 323. doi: 10.1186/s13071-019-3569-6
- Hanson, S. J., Stelzer, C.-P., Welch, D. B. M., and Logsdon, J. J. M. (2013). Comparative Transcriptome Analysis of Obligately Asexual and Cyclically Sexual Rotifers Reveals Genes With Putative Functions in Sexual Reproduction, Dormancy, and Asexual Egg Production. *BMC Genomics* 14, 412. doi: 10.1186/1471-2164-14-412
- Hernández-González, A., Muro, A., Barrera, I., Ramos, G., Orduña, A., and Siles-Lucas, M. (2008). Usefulness of Four Different *Echinococcus Granulosus* Recombinant Antigens for Serodiagnosis of Unilocular Hydatid Disease (UHD) and Postsurgical Follow-Up of Patients Treated for UHD. *Clin. Vaccine Immunol.* 15, 147–153. doi: 10.1128/CVI.00363-07
- Hoeksema, M., van Eijk, M., Haagsman, H. P., and Hartshorn, K. L. (2016). Histones as Mediators of Host Defense, Inflammation, and Thrombosis (Review). *Future Microbiol.* 11, 441–453. doi: 10.2217/fmb.15.151
- Horikoshi, N., Sato, K., Shimada, K., Arimura, Y., Osakabe, A., Tachiwana, H., et al. (2013). Structural Polymorphism in the L1 Loop Regions of Human H2A.Z.1 and H2A.Z.2. *Acta Cryst. D* 69, 2431–2439. doi: 10.1107/S090744491302252x
- Karplus, P. A., and Schulz, G. E. (1985). Prediction of Chain Flexibility in Proteins. A Tool for the Selection of Peptide Antigens. *Naturwissenschaften* 72, 212–213. doi: 10.1007/BF01195768
- Kozioł, U., and Brehm, K. (2015). Recent Advances in Echinococcus Genomics and Stem Cell Research. *Vet. Parasitol.* 213, 92–102. doi: 10.1016/j.vetpar.2015.07.031
- Kringelum, J. V., Lundegaard, C., Lund, O., and Nielsen, M. (2012). Reliable B Cell Epitope Predictions: Impacts of Method Development and Improved Benchmarking. *PLoS Comput. Biol.* 8, e1002829. doi: 10.1371/journal.pcbi.1002829
- Kumar, K., Moirangthem, R., and Kaur, R. (2020). Genome Protection: Histone H4 and Beyond. *Curr. Genet.* 66, 945–950. doi: 10.1007/s00294-020-01088-6
- Larrieu, E., Gavidia, C. M., and Lightowers, M. W. (2019). Control of Cystic Echinococcosis: Background and Prospects. *Zoonoses Public Health* 66, 889–899. doi: 10.1111/zph.12649
- Liang, Y., Song, H., Wu, M., Xie, Y., Gu, X., He, R., et al. (2020). Preliminary Evaluation of Recombinant EPC1 and TPx for Serological Diagnosis of Animal Cystic Echinococcosis. *Front. Cell. Infect. Microbiol.* 10. doi: 10.3389/fcimb.2020.00177
- Liu, C., Yao, J., Yin, J., Xue, J., and Zhang, H. (2018). Recombinant α - and β -Tubulin From *Echinococcus Granulosus*: Expression, Purification, and Polymerization. *Parasite* 25, 62. doi: 10.1051/parasite/2018063
- Lorenzatto, K. R., Kim, K., Ntai, I., Paludo, G. P., Camargo de Lima, J., Thomas, P., et al. (2015). Top Down Proteomics Reveals Mature Proteoforms Expressed in Subcellular Fractions of the *Echinococcus Granulosus* Preadult Stage. *J. Proteome Res.* 14, 4805–4814. doi: 10.1021/acs.jproteome.5b00642
- Lu, N.-F., Jiang, L., Zhu, B., Yang, D.-G., Zheng, R.-Q., Saho, J., et al. (2020). Elevated Plasma Histone H4 Level Predicts Increased Risk of Mortality in Patients With Sepsis. *Ann. Palliat. Med.* 9, 1084–1091. doi: 10.21037/apm-20-1011
- Lu, Y.-X., Regan, J. C., Eßer, J., Drews, L. F., Weinseis, T., Stinn, J., et al. (2021). A TORC1-Histone Axis Regulates Chromatin Organization and Non-Canonical Induction of Autophagy to Ameliorate Ageing. *eLife* 10, e62233. doi: 10.7554/eLife.62233
- Magalhães, R. D. M., Mattos, E. C., Rozanski, A., Galante, P. A. F., Palmisano, G., Cruz, A. K., et al. (2020). Global Changes in Nitration Levels and DNA Binding Profile of *Trypanosoma Cruzi* Histones Induced by Incubation With Host Extracellular Matrix. *PLoS Negl. Trop. Dis.* 14, e0008262. doi: 10.1371/journal.pntd.0008262
- Maglioco, A., Gentile, J., Barbary Venturi, M. S., Jensen, O., Hernández, C., Gertiser, M. L., et al. (2019). Detection of *Echinococcus Granulosus* Sensus Lato Infection by Using Extracts Derived From a Protoscoleces G1 Cell Line. *Parasite Immunol.* 41, e12674. doi: 10.1111/pim.12674
- Marjanovic, M. P., Crawford, K., and Ahel, I. (2017). PARP, Transcription, and Chromatin Modeling (Review). *Semin. Cell. Dev. Biol.* 63, 102–113. doi: 10.1016/j.semcdb.2016.09.014
- Mattioli, F., Vissers, J. H. A., van Dijk, W. J., Ikpa, P., Citterio, E., Vermeulen, W., et al. (2012). RNF168 Ubiquitinates K13-15 on H2A/H2AX to Drive DNA Damage Signaling. *Cell* 150, 1182–1195. doi: 10.1016/j.cell.2012.08.005
- Milburn, D., Laskowski, R. A., and Thornton, J. M. (1998). Sequences Annotated by Structure: A Tool to Facilitate the Use of Structural Information in Sequence Analysis. *Protein Eng.* 11, 855–859. doi: 10.1093/protein/11.10.855
- Pena, G. P., Berenstein, C. K., Oliveira, S. B. E., Leite, R. F. G., and Ribeiro, C. A. (2021). Hooklets Are Important Clues in Echinococcosis Diagnosis. *Int. J. Surg. Pathol.* 29, 184–185. doi: 10.1177/1066896920918304
- Pourseif, M. M., Parvizpour, S., Jafari, B., Dehghani, J., Naghili, B., and Omid, Y. (2021). A Domain-Based Vaccine Construct Against SARS-CoV-2, the Causative Agent of COVID-19 Pandemic: Development of Self-Amplifying mRNA and Peptide Vaccines. *BioImpacts* 11, 65–84. doi: 10.34172/bi.2021.11
- Rassy, D., Bobes, R. J., Rosas, G., Anaya, V. H., Brehm, K., Hernández, B., et al. (2010). Characterization of S3Pvac Anti-Cysticercosis Vaccine Components: Implications for the Development of an Anti-Cestodiasis Vaccine. *PLoS One* 5, e11287. doi: 10.1371/journal.pone.0011287
- Redon, C., Pilch, D., Rogakou, E., Sedelnikova, O., Newrock, K., and Bonner, W. (2002). Histone H2A Variants H2AX and H2AZ. *Curr. Opin. Genet. Dev.* 12, 162–169. doi: 10.1016/S0959-437X(02)00282-4
- Reinehr, M., Micheloud, C., Grimm, F., Kronenberg, P. A., Grimm, J., Beck, A., et al. (2020). Pathology of Echinococcosis. *Am. J. Surg. Pathol.* 44, 43–54. doi: 10.1097/PAS.0000000000001374
- Rubinstein, N. D., Mayrose, I., Halperin, D., Yekutieli, D., Gershoni, J. M., and Pupko, T. (2008). Computational Characterization of B-Cell Epitopes. *Mol. Immunol.* 45, 3477–3489. doi: 10.1016/j.molimm.2007.10.016
- Saha, S., and Raghava, G. P. S. (2006). Prediction of Continuous B-Cell Epitopes in an Antigen Using Recurrent Neural Network. *Proteins* 65, 40–48. doi: 10.1002/prot.21078

- Salah, E. B., Barrera, C., Mosbahi, S., Gottstein, B., Siles-Lucas, M., Belhassen, S., et al. (2021). Promising Proteins Detected by Western Blot From *Echinococcus Granulosus* Protoscoleces for Predicting Early Post-Surgical Outcomes in CE-Affected Tunisian Children. *Parasitol. Vectors* 14, 180. doi: 10.1186/s13071-021-04679-5
- Sánchez-Ovejero, C., Akdur, E., Manzano-Román, R., Hernández-González, A., González-Sánchez, M., Becerro-Recio, D., et al. (2020). Evaluation of the Sensitivity and Specificity of GST-Tagged Recombinant Antigens 2b2t, Ag5t and DIPOL in ELISA for the Diagnosis and Follow Up of Patients With Cystic Echinococcosis. *PLoS Negl. Trop. Dis.* 14, e0008892. doi: 10.1371/journal.pntd.0008892
- Savardashtaki, A., Sarkari, B., Arianfar, F., and Mostafavi-Pour, Z. (2017). Immunodiagnostic Value of *Echinococcus Granulosus* Recombinant B8/1 Subunit of Antigen B. *Iran J. Immunol.* 14, 111–122.
- Silk, E., Zhao, H., Weng, H., and Ma, D. (2017). The Role of Extracellular Histone in Organ Injury. (Review). *Cell Death Dis.* 8, e2812. doi: 10.1038/cddis.2017.52
- Simonin, F., Höfferer, L., Panzeter, P. L., Muller, S., de Murcia, G., and Althaus, F. R. (1993). The Carboxyl-Terminal Domain of Human Poly(ADP-Ribose) Polymerase. *J. Biol. Chem.* 268, 13454–13461. doi: 10.1016/S0021-9258(19)38671-5
- Singh, R., Kumar, D., Duncan, R. C., Nakhasi, H. L., and Salotra, P. (2010). Overexpression of Histone H2A Modulates Drug Susceptibility in *Leishmania* Parasites. *Int. J. Antimicrob. Agents* 36, 50–57. doi: 10.1016/j.ijantimicag.2010.03.012
- Spotin, A., Majdi, M. M., Sankian, M., and Varasteh, A. (2012). The Study of Apoptotic Bifunctional Effects in Relationship Between Host and Parasite in Cystic Echinococcosis: A New Approach to Suppression and Survival of Hydatid Cyst. *Parasitol. Res.* 110, 1979–1984. doi: 10.1007/s00436-011-2726-4
- Strahl, B. D., and Allis, C. D. (2000). The Language of Covalent Histone Modifications. *Nature* 403, 41–45. doi: 10.1038/47412
- Terzoglou, A. G., Routsias, J. G., Moutsopoulos, H. M., and Tzioufas, A. G. (2006). Post-Translational Modifications of the Major Linear Epitope 169-190aa of Ro60 kDa Autoantigen Alter the Autoantibody Binding. *Clin. Exp. Immunol.* 146, 60–65. doi: 10.1111/j.1365-2249.2006.03192.x
- Vorobjeva, N. V., and Chernyak, B. V. (2020). NETosis: Molecular Mechanisms, Role in Physiology and Pathology. (Review). *Biochem. (Moscow)* 85, 1178–1190. doi: 10.1134/S0006297920100065
- Vuitton, D. A., McManus, D. P., Rogan, M. T., Romig, T., Gottstein, B., Naidich, A., et al. (2020). International Consensus on Terminology To Be Used in the Field of Echinococcoses. *Parasite* 27, 41. doi: 10.1051/parasite/2020024
- Waga, S., Tan, E. M., and Rubin, R. L. (1987). Identification and Isolation of Soluble Histones From Bovine Milk and Serum. *Biochem. J.* 244, 675–682. doi: 10.1042/bj2440675
- Wang, W., Zhou, X., Cui, F., Shi, C., Wang, Y., Men, Y., et al. (2019). Proteomic Analysis on Exosomes Derived From Patients' Sera Infected With *Echinococcus Granulosus*. *Korean J. Parasitol.* 57, 489–497. doi: 10.3347/kjp.2019.57.5.489
- Weake, V. M., and Workman, J. L. (2008). Histone Ubiquitination: Triggering Gene Activity. *Mol. Cell* 29, 653–663. doi: 10.1016/j.molcel.2008.02.014
- Wilkins, M. R., Gasteiger, E., Bairoch, A., Sanchez, J.-C., Williams, K. L., Appel, R. D., et al. (1999). Protein Identification and Analysis Tools in the ExPASy Server. *Meth. Mol. Biol.* 112, 531–552. doi: 10.1385/1-59259-584-7:531
- Wu, X. M., Cao, L., Nie, P., and Chang, M. X. (2019). Histone H2A Cooperates With RIP2 to Induce the Expression of Antibacterial Genes and MHC Related Genes. *Dev. Comp. Immunol.* 101, 103455. doi: 10.1016/j.dci.2019.103455
- Xie, Y., Luo, X., Li, Y., Chen, L., Ma, W., Huang, J., et al. (2018). DeepNitro: Prediction of Protein Nitration and Nitrosylation Sites by Deep Learning. *Genomics Proteomics Bioinf.* 16, 294–306. doi: 10.1016/j.gpb.2018.04.007
- Ye, J., Coulouris, G., Zaretskaya, I., Cutcutache, I., Rozen, S., and Madden, T. L. (2012). Primer-BLAST: A Tool to Design Target-Specific Primers for Polymerase Chain Reaction. *BMC Bioinf.* 13, 134. doi: 10.1186/1471-2105-13-134
- Yoo, H. J., Lee, J.-S., Kim, J.-E., Gu, J. Y., Koh, Y., Kim, I., et al. (2016). Extracellular Histone Released From Leukemic Cells Increases Their Adhesion to Endothelium and Protects Them From Spontaneous and Chemotherapy-Induced Leukemic Cell Death. *PLoS One* 11, e0163982. doi: 10.1371/journal.pone.0163982
- Yue, X., Li, H., Tang, J., Liu, J., and Jiao, J. (2020). Rapid and Label-Free Screening of Echinococcosis Serum Profiles Through Surface-Enhanced Raman Spectroscopy. *Anal. Bioanal. Chem.* 412, 279–288. doi: 10.1007/s00216-019-02234-x
- Zait, H., and Hamrioui, B. (2020). Human Cystic Echinococcosis: Serological Diagnosis by Indirect Hemagglutination Test, Enzyme-Linked Immunosorbent Assay, Immunoelectrophoresis, and Immunoblotting in Surgically Confirmed Patients Versus Cases Diagnosed by Imaging Techniques. *Med. Mal. Infect.* 50, 676–683. doi: 10.1016/j.medmal.2019.10.001

Conflict of Interest: The authors declare that the research was conducted in the absence of any commercial or financial relationships that could be construed as a potential conflict of interest.

Publisher's Note: All claims expressed in this article are solely those of the authors and do not necessarily represent those of their affiliated organizations, or those of the publisher, the editors and the reviewers. Any product that may be evaluated in this article, or claim that may be made by its manufacturer, is not guaranteed or endorsed by the publisher.

Copyright © 2022 Maglioco, Agüero, Valacco, Valdez, Paulino and Fuchs. This is an open-access article distributed under the terms of the Creative Commons Attribution License (CC BY). The use, distribution or reproduction in other forums is permitted, provided the original author(s) and the copyright owner(s) are credited and that the original publication in this journal is cited, in accordance with accepted academic practice. No use, distribution or reproduction is permitted which does not comply with these terms.



Expanding the Malaria Antibody Toolkit: Development and Characterisation of *Plasmodium falciparum* RH5, CyRPA, and CSP Recombinant Human Monoclonal Antibodies

Adéla Nacer^{1*}, Gaily Kivi², Raini Pert², Erkki Juronen², Pavlo Holenya³, Eduardo Aliprandini⁴, Rogerio Amino⁴, Olivier Silvie⁵, Doris Quinkert⁶, Yann Le Duff⁷, Matthew Hurley⁷, Ulf Reimer³, Andres Tover², Simon J. Draper⁶, Sarah Gilbert⁷, Mei Mei Ho¹ and Paul W. Bowyer^{1*}

OPEN ACCESS

Edited by:

Tania F. De Koning-Ward,
Deakin University, Australia

Reviewed by:

Miguel Prudêncio,
Universidade de Lisboa, Portugal
Gerhard Wunderlich,
University of São Paulo, Brazil

*Correspondence:

Adéla Nacer
dela.nacer@gmail.com
Paul W. Bowyer
Paul.Bowyer@nibsc.org

Specialty section:

This article was submitted to
Parasite and Host,
a section of the journal
Frontiers in Cellular and
Infection Microbiology

Received: 21 March 2022

Accepted: 20 May 2022

Published: 16 June 2022

Citation:

Nacer A, Kivi G, Pert R, Juronen E, Holenya P, Aliprandini E, Amino R, Silvie O, Quinkert D, Le Duff Y, Hurley M, Reimer U, Tover A, Draper SJ, Gilbert S, Ho MM and Bowyer PW (2022) Expanding the Malaria Antibody Toolkit: Development and Characterisation of *Plasmodium falciparum* RH5, CyRPA, and CSP Recombinant Human Monoclonal Antibodies. *Front. Cell. Infect. Microbiol.* 12:901253. doi: 10.3389/fcimb.2022.901253

¹ Division of Bacteriology, National Institute for Biological Standards and Control (NIBSC), Medicines and Healthcare products Regulatory Agency (MHRA), Potters Bar, United Kingdom, ² Icosagen Cell Factory OÜ, Tartumaa, Estonia, ³ Research and Development, JPT Peptide Technologies GmbH, Berlin, Germany, ⁴ Malaria Infection & Immunity Unit, Institut Pasteur, Paris, France, ⁵ Sorbonne Université, INSERM, CNRS, Centre d'Immunologie et des Maladies Infectieuses, CIMI-Paris, Paris, France, ⁶ Department of Biochemistry, University of Oxford, Oxford, United Kingdom, ⁷ Centre for Aids Reagents, National Institute for Biological Standards and Control (NIBSC), Medicines and Healthcare products Regulatory Agency (MHRA), Potters Bar, United Kingdom

Malaria, an infection caused by apicomplexan parasites of the genus *Plasmodium*, continues to exact a significant toll on public health with over 200 million cases worldwide, and annual deaths in excess of 600,000. Considerable progress has been made to reduce malaria burden in endemic countries in the last two decades. However, parasite and mosquito resistance to frontline chemotherapies and insecticides, respectively, highlights the continuing need for the development of safe and effective vaccines. Here we describe the development of recombinant human antibodies to three target proteins from *Plasmodium falciparum*: reticulocyte binding protein homologue 5 (PfRH5), cysteine-rich protective antigen (PfCyRPA), and circumsporozoite protein (PfCSP). All three proteins are key targets in the development of vaccines for blood-stage or pre-erythrocytic stage infections. We have developed potent anti-PfRH5, PfCyRPA and PfCSP monoclonal antibodies that will prove useful tools for the standardisation of assays in preclinical research and the assessment of these antigens in clinical trials. We have generated some very potent anti-PfRH5 and anti-PfCyRPA antibodies with some clones >200 times more potent than the polyclonal anti-AMA-1 antibodies used for the evaluation of blood stage antigens. While the monoclonal and polyclonal antibodies are not directly comparable, the data provide evidence that these new antibodies are very good at blocking invasion. These antibodies will therefore provide a valuable resource and have potential as biological standards to help harmonise pre-clinical malaria research.

Keywords: *Plasmodium falciparum*, monoclonal antibodies, standardisation, assay development, malaria, PfRH5, PfCyRPA, PfCSP

1 INTRODUCTION

Malaria is a vector-borne disease endemic to large parts of the world. It is estimated that nearly half of the global population is at risk with annual deaths of over 627,000 people, primarily African children under 5 years of age (WHO, 2021). The first malaria vaccine for children in areas of moderate to high transmission was recommended by the World Health Organisation (WHO) in October 2021. This recommendation is based on the results from an extended pilot programme of Mosquirix® (RTS,S/AS01) in Ghana, Malawi, and Kenya as part of routine childhood immunisations (Adepoju, 2019) and represents significant progress in the fight against malaria. In addition, a second generation subunit vaccine (R21/Matrix-M; Datto et al., 2021) received authorisation for a phase 3 clinical trial (NCT04704830). Additionally, phase I clinical trials in controlled human malaria infections with whole attenuated sporozoite vaccines have recently been published (NCT02511054, NCT03083847) with promising results (Mwakingwe-Omari et al., 2021). Finally, a blood-stage vaccine has undergone phase I/IIa clinical trials (Minassian et al., 2021), further adding to the vaccine portfolio.

Malaria is caused by parasites of the genus *Plasmodium* that have a complex life cycle with development in a mosquito vector and in a vertebrate host. In humans, the first step of infection occurs when parasites enter the human host *via* an infected mosquito bite and begin to replicate in the liver. Parasites released from the liver enter the circulation where they replicate within erythrocytes; the intra-erythrocytic cycle is associated with malaria pathology and is the primary target of anti-malarial chemotherapies (Maier et al., 2019). While anti-malarial drugs and control strategies are vital to malaria control efforts, parasite drug resistance and mosquito insecticide resistance are on the rise and pose risks to the gains obtained over the past two decades (WHO, 2021). Furthermore, disruptions in healthcare access caused by the COVID-19 pandemic have increased deaths resulting from malaria infection in 2020 with an estimated 241 million cases and 627,000 deaths (WHO, 2021).

Bearing in mind that eradicating malaria parasites following infection requires protracted treatment regimens with serious socioeconomic consequences, the need for malaria vaccines remains as urgent as ever. Malaria vaccines targeting parasite antigens across all key stages of the parasite life cycle are being developed. These include vaccines blocking transmission to the vector (Challenger et al., 2021) and those targeting liver infection (Mwakingwe-Omari et al., 2021), and blood stage parasites (Vijayan and Chitnis, 2019). In addition, vaccines to prevent placental malaria are also in phase Ia clinical trials (Sirima et al., 2020). The vaccines closest to regulatory approval and licensure, including Mosquirix® (RTS,S/AS01) and R21/Matrix-M, target parasite infection of the liver with other vaccine candidates targeting development of the parasites in red blood cells (Sato, 2021a; Sato, 2021b).

Many assays are available for malaria research, but they are not standardised, making inter-laboratory comparison of data very challenging. Furthermore, the high genetic variability of *P.*

falciparum presents an additional, and considerable, challenge for harmonisation of the field, especially in diagnosis and treatment of the disease. Additional challenges exist in the characterisation of immune responses, disease surveillance, and in the spectrum of assays used to understand the disease in terms of management and treatment. The first serological WHO Reference Reagent for *P. falciparum* (Bryan et al., 2017) and the first WHO International Standard for *P. falciparum* antigens (Harris et al., 2017) were major breakthroughs for standardising vaccine assays and diagnostics, respectively. However, reagents that enable standardisation throughout all aspects of preclinical development of malaria vaccine candidates are still needed for reliable quantification of malaria antigens. The evaluation of vaccine efficacy using *in vitro* and *in vivo* assays is not currently harmonised which in turn effects reproducibility, inhibits progress and squanders investment.

Preclinical evaluation of malaria vaccines prior to controlled human malaria infection studies and clinical trials (Chattopadhyay and Pratt, 2017; Good and Miller, 2018; Artaud et al., 2019; Matuschewski and Borrmann, 2019; Lyke et al., 2020) includes standard laboratory assays for malaria blood stages, such as *in vitro* growth inhibition activity (GIA) assay (Malkin et al., 2005) *in vivo* passive antibody transfer in mice as well as lesser used immunogenicity and efficacy studies in non-human primates (Douglas et al., 2015). Variability in these assays can be caused by the community using a number of different reagents, some being commercial or shared, some being used by one or few laboratories, and many being finite (e.g. the anti-AMA-1 polyclonal antibody BG98 (Faber et al., 2013), meaning again that results are not always or comparable across laboratories and over time. The lack of a defined standard makes meaningful comparisons difficult and impedes the development of novel invasion-blocking candidate antigens.

In addition to these problems for assays directed against blood stage malaria parasites, similar challenges exist for assays involved in targeting *P. falciparum* sporozoites, e.g. invasion, cell traversal, opsonic phagocytosis and cytotoxicity assays (Sinnis et al., 2013; Tavares et al., 2013a; Tavares et al., 2013b; Formaglio et al., 2014; Steel et al., 2017; Aliprandini et al., 2018). The 'gold standard' control antibody for these assays is a mouse monoclonal antibody named 2A10 that recognises NANP repeats of the *P. falciparum* circumsporozoite protein (PfCSP) (Zavala et al., 1983; Hollingdale et al., 1984; Anker et al., 1990; Zhang et al., 2017). However, the hybridoma cell line used for production of has 2A10 been widely shared and propagated in different laboratories likely leading to a drift in its biochemical and biophysical properties. Differences may arise due to the potential for genetic instability of the hybridomas - as such it is no longer suitable as a standard (Bradbury and Pluckthun, 2015). This potential drift is difficult to quantify in the absence of a primary standard. As such the generation of the recombinant monoclonal antibodies described here provides an opportunity for the development new standards that target PfCSP.

The European Research Infrastructures for Poverty Related Diseases (EURIPRED) was a collaborative research and infrastructure project that aimed to generate, coordinate and integrate resources to support international research on HIV/

AIDS, tuberculosis, malaria and Hepatitis B & C. As part of this project we generated recombinant human monoclonal antibodies that could be used to develop and standardise assays for *P. falciparum* malaria vaccine research and development. These materials, intended to support the research and development community, are available from the Centre for AIDS Reagents repository at NIBSC (www.nibsc.org).

We have generated recombinant human monoclonal antibodies directed against the *P. falciparum* blood stage invasion proteins Reticulocyte binding protein Homologue 5 (PfRH5), Cysteine-Rich Protective Antigen (PfCyRPA) and the dominant sporozoite antigen circumsporozoite protein (PfCSP). PfRH5 is a leading blood stage malaria vaccine target and forms a complex with PfCyRPA and PfRH5-interacting protein (PfRIPR) critical for red-cell invasion by merozoites (Healer et al., 2019; Knuepfer et al., 2019; Ragotte et al., 2020; Ndwiwa et al., 2021). Antibodies to both antigens are highly effective at inhibiting growth of *P. falciparum* (Dreyer et al., 2012; Douglas et al., 2014; Volz et al., 2016) and such antibodies may provide suitable reference reagents to standardise GIA assays and other erythrocyte invasion assays – by having a standard with defined neutralising activity, to which the neutralising activity of other materials can be compared. We also developed human monoclonal antibodies to PfCSP, the key antigen of the Mosquirix® (Wilby et al., 2012; Adepoju, 2019; Cotton, 2020) and R21 (Datoo et al., 2021) vaccines designed to prevent *P. falciparum* infection in the liver. PfCSP is expressed on the surface of sporozoites and is the main target of the immune response during the initial phase of infection (Zhang et al., 2017).

Here we describe the generation and characterisation of human monoclonal antibodies against key *P. falciparum* antigens and discuss how their use may support malaria vaccine development. We hope that these monoclonal antibodies will facilitate better cross-laboratory comparisons of novel blood and liver stage malaria vaccine candidates.

2 MATERIALS AND METHODS

2.1 Plasmodium falciparum Parasites

P. falciparum laboratory isolates FCR3 and NF54 were obtained from The European Malaria Reagent Repository (<http://www.malaria-research.eu/>). Parasites were maintained at 4% haematocrit in A+ erythrocytes (National Health Service Blood and Transplant, UK) at 5% CO₂ and atmospheric O₂ as previously described (Trager and Jensen, 1976).

2.2 Immunogens and Immunizations

Recombinant monoclonal antibodies were produced using HybriFree Technology (Icosagen) as previously described (Kivi et al., 2016). Two 4–8 month old chickens (1.7–2.1 kg) and three rabbits (4–5.5 kg) of >4 months old each were immunised with recombinant PfRH5 (Jin et al., 2018) and PfCyRPA (generated in house, Jenner Institute, University of Oxford) and recombinant PfCSP (kindly provided by D. Narum, NIAID, NIH, DHHS) as previously described (Kivi et al., 2016). Rabbits and chickens

were immunised in parallel as antigens elicit different responses in different species thereby increasing the likelihood of identifying antibodies of interest. Briefly, 0.2 mg of antigen per test animal per injection was used. Rabbits received four subscapular immunisations at approximately 3 week intervals. Chickens were immunised intramuscularly three times with at ~2 week intervals. The primary immunisation was performed in Freund's complete adjuvant, while all subsequent immunisations were with Freund's incomplete adjuvant (IFA). Booster doses were performed as two separate injections, where the first (0.1 mg) was administered by subscapular injection (rabbits) or intramuscularly (chickens) in Freund's incomplete adjuvant and the second (0.1 mg) was administered intravenously in phosphate buffered saline (PBS) – both injections were given in this way to all test animals and at the same time point (Kivi et al., 2016). Spleens were isolated 3 days after the final boost, homogenized in ice-cold PBS, and cryopreserved in heat inactivated foetal bovine serum with 10% DMSO prior to long-term storage in liquid nitrogen (Kivi et al., 2016). All procedures on animals were performed in compliance with European Union directive 86/609/EEC and approved by the Estonian National Board of Animal Experiments (No. 115, 07.09.2012; No. 87, 28.08.2007).

2.3 Production of Human Recombinant Monoclonal Antibodies

Recombinant monoclonal antibodies were generated as previously described (Kivi et al., 2016). Briefly, panning of 2 × 10⁴ splenic cells from immunised animals was performed on antigen-coated (5 µg/ml) immune modules (ThermoFisher Scientific) for 45 min after which unbound cells were removed by washing in PBS. RNA was extracted from the bound cells, reverse transcribed in cDNA using the Superscript IV First-Strand Synthesis System (Invitrogen), which was subsequently used as a template to amplify by PCR the variable light (VL) and heavy (VH) chains.

Amplified VL and VH chains were cloned into human immunoglobulin G1 (hIgG1) expression vectors by circular polymerase extension cloning (CPEC) (Quan and Tian, 2009). *Escherichia coli* DH5α were transformed with hIgG1 expression vector pools and grown in liquid medium on a shaker at 37°C overnight. Plasmid DNA was extracted, purified, and transfected into a transgenic Chinese hamster ovary (CHO) cell line named CHOEBNALT85-1E9 for hIgG1 pool production as previously described (Kivi et al., 2016). Single clones were selected on Luria Broth ampicillin agar medium. 48–72 hours after transfection, recombinant human IgG1 (rIgG1) pools were tested in enzyme linked immunosorbent assay (ELISA). Maxisorp Immuno modules (Thermo Fisher Scientific) were coated with the specific antigen at 1 µg/ml in PBS overnight. Plates were washed 4 times and blocked with PBS containing 2% bovine serum albumin (BSA) and 0.05% Tween-20. Colonies from ELISA positive pools were grown in liquid medium overnight in a shaker at 37°C and in a 96-well microtiter plate. Plasmid DNA was isolated and transfected into CHOEBNALT85-1E9 cells for transient antibody production and cell culture

supernatants were collected after 48 - 72 h and analysed by ELISA to confirm antigen specific binding. Positive clones were then sequenced for VH/VL sequence verification using the international ImmunoGeneTics (IMGT) information system (Lefranc et al., 1999; Giudicelli et al., 2005; Lefranc, 2014; Lefranc et al., 2015).

Plasmid clones were transfected into CHOEBNALT85-1E9 for transient production in 2 ml of media. Ten days after transfection, cells were removed by centrifugation (300g for 5 min) and 1.5 ml of each supernatant was aliquoted into microtubes. The concentration of the antibodies produced in crude cell supernatant was measured by biolayer interferometry (Octet® K2 System; ForteBio) using Protein A sensors and appropriate human IgG1 standards. The supernatants were stored at -80°C until further testing. Cell culture supernatants containing anti-*Pf*RH5 and anti-*Pf*CyRPA antibodies were individually screened using the red cell invasion assay to assess functional activity. Selected *Pf*RH5 and *Pf*CyRPA mAbs were then expressed and purified on a small scale to confirm inhibitory activity, followed by scale up to 400 ml cultures of CHOEBNALT85-1E9 cells and purified by HiTrap MabSelect SuRe affinity chromatography with buffer exchange using HiTrap Desalting Columns to PBS pH 7.4 (GE Healthcare). Purified antibodies were adjusted to a concentration of 1 mg/ml, analysed by ELISA and non-reduced gel electrophoresis, filtered, aliquoted and stored at -75°C; no additives or stabilising reagents were added to the purified antibodies to prevent interference in the functional assays. Culture supernatants containing anti-*Pf*CSP mAbs were used for initial screenings and concentrations determined as described above for the *Pf*Rh5 and *Pf*CyRPA antibodies. Further work to express and purify anti-*Pf*CSP mAbs is on-going. All mAbs described here are available from the Centre for AIDS Reagents repository at NIBSC (www.nibsc.org).

2.4 Blocking Activity of *Pf*RH5 and *Pf*CyRPA Recombinant IgGs

*Pf*RH5 and *Pf*CyRPA form a complex with *Pf*RIPR during merozoite invasion of erythrocytes (Healer et al., 2019; Knuepfer et al., 2019; Ndwigwa et al., 2021). The formation of the complex is required for erythrocyte invasion (Volz et al., 2016). Biolayer interferometry (Octet® K2 System, Pall ForteBio) (Li et al., 2017) was performed to determine the potential of the mAbs to block *Pf*CyRPA-*Pf*RH5 interactions. Monoclonal antibody cell culture supernatants were incubated with immobilised recombinant proteins to measure the dissociation of antigen-antibody and infer antibody blocking activity.

Recombinant *Pf*CyRPA molecules were conjugated to biotin with a ratio of 1:5 using Thermo Scientific™ EZ-Link™ NHS-PEG4-Biotin, No-Weigh™ Format (A39259). Two streptavidin (SA) sensors were incubated in kinetic buffer (PBS containing 0.1% BSA, 0.02% Tween-20, and 0.1% Proclin™ 300) for 11 min in plates with shaking at 1000 rpm to determine the baseline. The two sensors were then used to immobilise biotinylated *Pf*CyRPA by incubation in kinetic buffer containing *Pf*CyRPA-biotin (2 µg/ml) for 11 min at 1000 rpm. The sensors were incubated once

more in kinetic buffer alone for 11 min at 1000 rpm to reset to baseline and then incubated in cell culture supernatants diluted 1:2 with kinetic buffer for 22 min at 1000 rpm to saturate the immobilised *Pf*CyRPA-biotin molecules with anti-*Pf*CyRPA antibodies. The sensors were incubated again in kinetic buffer alone for 11 min at 1000 rpm. Finally, one sensor was incubated in kinetic buffer and the other in kinetic buffer containing 12 µg/ml (~0.08 nM) recombinant *Pf*RH5 for 33 min at 1000 rpm.

Blocking activity measurements of anti-*Pf*RH5 antibodies were performed with the following differences. Anti-*Pf*RH5 antibody cell culture supernatants were incubated with recombinant *Pf*RH5 (5 µg/ml) for ≥ 1h at room temperature (RT) to achieve a state of equilibrium. In addition, between sample measurements, used sensors were regenerated using glycine buffer (pH 1.7) and kinetic buffer. Finally, one sensor was incubated in negative cell culture supernatant diluted 1:2 with kinetic buffer containing recombinant *Pf*RH5 (5 µg/ml) and the other sensor was incubated in *Pf*RH5 antibody cell culture supernatant diluted 1:2 in kinetic buffer containing 5 µg/ml recombinant *Pf*RH5 for 33 min at 1000 rpm. The operating temperature for the Octet was at 30°C and all other processes performed at RT unless indicated otherwise.

2.5 Generation and Validation of *P. falciparum* Peptide Microarrays

We generated overlapping 15-mer peptides for 18 *P. falciparum* and 3 *P. vivax* antigens. We included key vaccine antigens for both species (e.g. *Pf*AMA-1, *Pf*CSP, and *Pf*s25 or *Pv*CSP, *Pvs*25, and *Pv*DBP). To ensure we captured sequence diversity for these highly polymorphic antigens we used sequence information available from MalariaGEN (MalariaGen et al., 2021). We included all mutations found in *P. vivax* and only those with a frequency of >0.5% for *P. falciparum* proteins. The peptides were synthesised and spotted onto microarray slides (RT-HD-Plas, JPT Technologies). Peptides were printed into three individual subarrays per slide and used to screen the polyclonal sera, culture supernatants containing the mAbs, and purified mAbs. Briefly, samples were diluted 1:2000 for cell culture supernatants or used at 50 µg/ml for purified recombinant mAbs in Superblock T20 buffer (Thermo/Pierce, #37516); 300 µl was added to the slides and they were incubated for 2 h at 30°C on each of the triplicate arrays. The primary analyte was washed 5 times for 3 min with 2-4 ml of wash buffer (1X Tris buffered saline (TBS) + 0.1% Tween20). The arrays were then incubated with a Cy5-conjugated anti-human IgG1, anti-rabbit IgG, or anti-chicken IgY secondary antibody, as appropriate, diluted to 1 µg/ml in blocking buffer for 45 min at 30°C. Slides were washed again in wash buffer and dried with a gentle stream of nitrogen and stored in the dark until fluorescence scanning on a GenePix 4330A scanner using a scanning resolution of 10 µm per pixel.

2.6 Screening by Invasion Assay of Antibodies From Cell Culture Supernatants

2.6.1 *Pf*RH5 and *Pf*CyRPA Recombinant IgGs

Crude cell culture supernatants containing anti-*Pf*RH5 and anti-*Pf*CyRPA antibodies were screened by invasion assay to

determine their capacity to inhibit invasion of *P. falciparum* FCR3 parasites *in vitro*. Briefly, *P. falciparum* FCR3 mature stage parasites (schizonts) were enriched by magnet purification, diluted into culture medium containing A+ red blood cells at 4% haematocrit and dispensed into 96-well plates. Three dilutions were tested in duplicate for each antibody; 1:5, 1:25, and 1:125. Antibodies were added to each well for a final volume of 125 µl/well. For each plate a serial dilution of BG98 antibodies (anti-*Pf*AMA-1; NIBSC #NR0014) starting at 6 mg/ml was included to provide a standard curve as well as a positive control for the inhibition of merozoite invasion. Cell culture supernatant from non-transfected cells was used as a negative control. Finally, a minimum of 8 wells containing no antibodies was included per plate as an additional control. A volume of 25 µl of culture was removed from each well, fixed with PBS containing 1% PFA and 0.05% GTA. Cells were stained with SYBR Green to determine parasitaemia by flow cytometry. A further 25 µl was removed 48 h later to measure parasitaemia and calculate invasion inhibition after one intra-erythrocytic cycle. For the selection of the recombinant mAb candidates, invasion assays were performed as described above with some modifications. Three concentrations were tested in duplicate for each antibody; 16.4 µg/ml [112.3 nM], 3.28 µg/ml [22.5 nM], and 0.656 µg/ml [4.5 nM]. These concentrations, based on the antibodies with the lowest concentrations within the crude cell supernatant, were selected to enable comparisons at set concentrations across all antibodies.

2.6.2 *Pf*CSP Recombinant IgGs

Sporozoite cell traversal assays were performed using Hepa1-6 cells (ATCC CRL-1830) and *P. falciparum* NF54 sporozoites (*Pf*NF54) isolated by hand dissection of infected *A. stephensi* mosquitoes (provided by the Department of Medical Microbiology, University Medical Centre, St Radboud, Nijmegen, the Netherlands). Hepa1-6 cells were seeded at 3×10^4 /well in 96 well plates and cultured at 37°C under 5% CO₂ in DMEM medium (41966029, Gibco) supplemented with 10% (v/v) foetal calf serum (10500064, Gibco), 2 mM L-glutamine (25030024, Thermo Scientific), and 1% (v/v) of a penicillin-streptomycin solution (15140122, Gibco). The following day 5×10^4 *Pf*NF54 sporozoites in complete culture medium were added to the cells in triplicate wells with 1 mg/ml rhodamine-conjugated Dextran (D1817, Molecular Probes) and either 2 or 20 µg/ml of the test antibodies with normal cell culture supernatant as a negative control. Cell cultures were incubated for 3 h at 37°C, then washed, trypsinised, fixed in 1% formaldehyde in PBS, and analysed on a Guava EasyCyte 6/2L bench cytometer equipped with a 532 nm laser (Millipore), for detection and quantification of dextran-positive cells.

Characterisation of antibody binding to sporozoites was performed using 2.5×10^4 *P. falciparum* NF54 sporozoites per sample fixed in 2% PFA in PBS and detected with 2 µg/ml of the rIgG1 diluted in 1% BSA-PBS. Sporozoites were labelled in 15 µl final solution for 1 h on ice before addition of 4 µg/ml AlexaFluor 488 goat anti-human IgG1 (H + L) (Invitrogen, A11013) + 0.5 µg/ml AlexaFluor 647-conjugated 2A10 in 1% BSA-PBS in a final volume of 30 µl. Samples were incubated for 30 min on ice and

analysed by flow cytometry on a CytoFLEX S flow cytometer (Beckman Coulter). A minimum of 3000 2A10-positive *Pf*NF54 sporozoites were acquired.

Antibody cytotoxicity was determined as previously described (Aliprandini et al., 2018) using *P. berghei* NK65 sporozoites expressing GFP and a hybrid CSP containing the central repeats region of *P. falciparum* CSP (*PbPf*-GFP). After incubation of 1.2×10^4 sporozoites for 45 min at 37°C with 80 µg/ml of *Pf*CSP antibodies (except for 2G12, which was tested at 60 µg/ml) in HybriMed supernatant and 10% FCS, and with 5 µg/ml of propidium iodide (PI), sporozoites were analysed by flow cytometry. Viable sporozoites were considered as GFP positive and PI negative, and viability was normalized to HybriMed medium without *Pf*CSP antibodies, set to 100% viability.

2.7 Characterisation of the Purified Recombinant *Pf*RH5 and *Pf*CyRPA IgGs

Invasion assays were performed as described above. Briefly, *P. falciparum* FCR3 or *Pf*NF54 mature stage parasites (schizonts) were enriched by magnet purification, diluted into culture medium containing A+ red blood cells at 4% haematocrit and dispensed into 96-well plates. Three concentrations were tested in duplicate for each antibody; 16.4 µg/ml [112.3 nM], 3.28 µg/ml [22.5 nM], and 0.656 µg/ml [4.5 nM]. Antibodies were added to each well for a final volume of 125 µl/well. For each plate a serial dilution of BG98 antibodies (anti-*Pf*AMA-1; NIBSC #NR0014) starting at 6 mg/ml was included to provide a standard curve as well as a positive control for the inhibition of merozoite invasion. Finally, a minimum of 2 wells without antibodies was included per plate as a negative control. A volume of 25 µl of culture was removed from each well, fixed with PBS containing 1% PFA and 0.05% GTA. Cells were stained with SYBR Green to determine parasitaemia by flow cytometry. A further 25 µl was removed 48 h later to measure parasitaemia and calculate invasion inhibition relative to the no antibody control after one intra-erythrocytic cycle. Statistical analyses were performed using a General Linear Model in Minitab® 21.1.1 after verifying assumptions for a parametric test were met (i.e. equality of variances and normal distribution).

3 RESULTS

3.1 Generation of *Pf*RH5 and *Pf*CYRPA Recombinant Human IgGs

A total of 64 and 32 panning reactions were performed for *Pf*RH5 from chicken and rabbit splenocytes, respectively (Table 1), from which 1034 clones were tested by ELISA and 256 were positive. A total of 194 *Pf*RH5 positive clones were sequenced and of those 33 unique sequences were identified; 26/33 unique sequences were obtained from chicken immunisations and 7/33 from rabbits. Cell culture supernatants from the 33 *Pf*RH5 antibody clones were tested for antigen binding using biolayer interferometry (BLI), which identified 18 *Pf*RH5 mAbs with blocking activity. To do this, biotinylated recombinant *rPf*RH5 was exposed to its recombinant binding partner

TABLE 1 | Summary of *P. falciparum* RH5 and CyRPA monoclonal antibody generation.

Antigen	Species	Panning Reactions	+ cloning reactions	+ clones (ELISA)	Unique clones (sequencing)	Clones with blocking activity
<i>Pf</i> CyRPA	Chicken	64	25	125	12	11
	Rabbit	16	11	14	5	2
<i>Pf</i> RH5	Chicken	64	23	240	26	17
	Rabbit	32	9	16	7	1

The table shows the number of independent clones that were generated through key steps in the development of the recombinant monoclonal antibodies. Isolated splenocytes were panned on the target antigen. + cloning reactions indicates the number of positive clones isolated following cloning into the hlgG1 expression vectors. RNA from bound cells was used for cloning into the expression vector. + clones (ELISA) indicates the number of those clones that bound to the antigen by ELISA. The number of unique clones as identified by sequencing is also shown. The number clones with blocking activities as measured by biolayer interferometry is shown in the last column.

*rPf*CyRPA in the presence or absence of the mAb. **Figure 1** shows examples of two different BLI profiles observed for *Pf*RH5 and *Pf*CyRPA recombinant IgG1 clones. The clones shown exhibit either a reduced *rPf*RH5-*rPf*CyRPA binding (5E6#36, 3A7#22) or not (1A4#27, 3G11#15). All but one of the *Pf*RH5 mAbs with blocking activity were isolated from chicken.

Similarly to *Pf*RH5, 64 panning reactions were performed for *Pf*CyRPA from chicken splenocytes and sixteen from rabbit splenocytes (**Table 1**). Of those, 55 cDNAs were synthesised and antibody expression of positive clones confirmed by ELISA. Of the 1040 clones tested, 139 were positive for *Pf*CyRPA of

which 91 were sequenced; 17 unique sequences were identified. Twelve of the unique *Pf*CyRPA sequences were obtained from the chicken immunisations and 5 from rabbits. Again, using the Octet K2 system to evaluate the blocking activity, cell culture supernatants from the 17 *Pf*CyRPA antibody clones were tested. 13 Thirteen had blocking activity (11 from chicken immunisations and 2 from rabbits). Biolayer interferometry traces for *Pf*RH5 and *Pf*CyRPA of rIgG1 monoclonal antibodies with and without blocking activity are shown in **Supplementary Figure 1**.

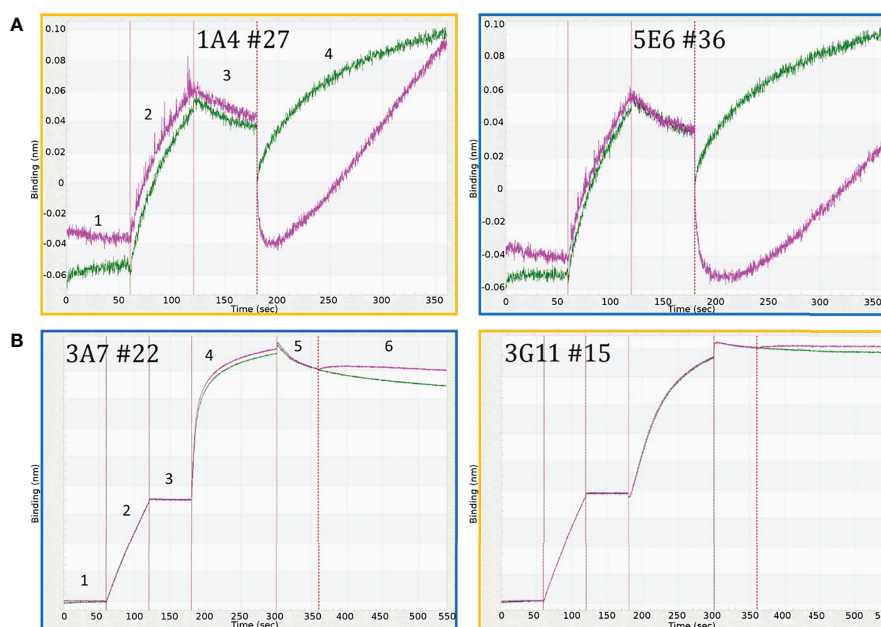


FIGURE 1 | Biolayer interferometry traces of crude hlgG1 clones showing different blocking profiles for **(A)** *Pf*RH5 clones 1A4#27 and 5E6#36; and **(B)** *Pf*CyRPA clones 3A7#22 and 3G11#15. For *Pf*RH5 **(A)** traces show cell culture supernatant containing only *Pf*RH5 recombinant hlgG1 antibodies (green) and cell culture supernatant containing both recombinant *Pf*RH5 (*rPf*RH5) and recombinant human IgG1 antibodies (pink). Antibody 1A4#27 does not block *Pf*RH5 binding to *Pf*CyRPA. Conversely, antibody 5E6#39 blocks binding of *Pf*RH5 to *Pf*CyRPA (step 4). The numbered steps show 1) baseline for both sensors incubated in kinetic buffer; 2) incubation of the sensors with recombinant *Pf*CyRPA-biotin conjugate (*rPf*CyRPA); 3) baseline with the immobilised *rPf*CyRPA-biotin in kinetic buffer; and 4) association of *rPf*RH5 to *Pf*CyRPA. For *Pf*CyRPA **(B)** traces show incubation of one sensor in kinetic buffer (green) and incubation of the other sensor (pink) with *rPf*RH5 in association step (step 6). The numbered steps show 1) baseline readings for both sensors in kinetic buffer; 2) incubation with biotin-conjugated recombinant *Pf*CyRPA in kinetic buffer; 3) baseline readings for sensors with immobilised *rPf*CyRPA in kinetic buffer; 4) saturation of the sensors with crude antibody cell culture supernatant containing specific anti-*Pf*CyRPA recombinant hlgG1s (pink); 5) baseline with immobilised *Pf*CyRPA-antibody complex in kinetic buffer; 6) One sensor incubated in kinetic buffer (green) and the second in kinetic buffer containing *Pf*RH5 (pink). Clone 3G11#15 shows blocking activity (orange outline) while antibody clone 3A7#22 does not block binding of *rPf*RH5 to *rPf*CyRPA (blue outline). The y-axis shows binding (nm) and x-axis time (sec).

3.2 Selection of *Pf*RH5 and *Pf*CyRPA Recombinant Human IgGs

The ability of the recombinant antibodies to block *P. falciparum* invasion was next tested by screening all 33 *Pf*RH5 clones and 17 *Pf*CyRPA clones with the *in vitro* invasion assay. Invasion assays using *Pf*FCR3 parasites revealed a range invasion inhibition activities for culture supernatant containing *Pf*RH5 and *Pf*CyRPA rIgG1 antibodies (**Figure 2**). Furthermore, invasion inhibition of antibodies during the initial screening of crude supernatants showed concentration-dependent effects for most antibodies (**Figure 2**). The potency of the antibodies was compared to the anti-AMA-1 polyclonal antibody BG98 by parallel line analysis (CombiStats 7.0). Relative potency estimates for each of the rIgG1 tested compared to anti-AMA-1 (BG98) ranged from 1 to 967 (median 20) for *Pf*RH5 and from 3 to 201 (median 27) for *Pf*CyRPA (**Supplementary Table 1**). All of the antibodies generated here were either as effective (relative potency of 1) or better at inhibiting invasion than BG98 (relative potency >1). Furthermore, the antibodies with the highest invasion blocking activity for *Pf*RH5 and *Pf*CyRPA compared to BG98, were 967-fold and 201-fold more potent than BG98, respectively (see **Supplementary Table 1** for the full list of antibodies). It should be noted that the potency of these rIgG1 clones is not directly comparable to BG98 as it is a polyclonal antibody mix and it is not possible to assess the potency of individual clones within the mixture to the mAbs generated here.

Interestingly, three anti-*Pf*RH5 clones (1D8#11, 14D5#250, 15D12#256) and one anti-*Pf*CyRPA clone (7B7#7) showed invasion inhibition activity in the invasion assays despite having no blocking activity by BLI (**Supplementary Figure 1**). Of those, 1D8#11 recognised a single overlapping peptide by peptide microarray (ISEEIDDKSEETDDETEEVDSI). Invasion inhibition data along with BLI traces (**Supplementary Figure 1**) and microarray data (see **Supplementary Figure 2** and **Supplementary Spreadsheet File**) were used to select clones for a more comparable assessment of mAb activity of the crude supernatants. Thirteen *Pf*RH5 mAbs and 10 *Pf*CyRPA mAbs displaying dilution effects in the initial screen were further evaluated, using the invasion assay, at defined antibody concentrations (16.4 µg/ml [112 nM], 3.28 µg/ml [22.5 nM], 0.656 µg/ml [4.5 nM]; data not shown) confirming concentration-dependent effects allowing further down selection.

Four anti-*Pf*RH5 clones and 4 anti-*Pf*CyRPA clones were selected for up-scaled production and purification. These purified mAbs retained invasion inhibition activity (**Figure 3**) and generally showed greater specificity by microarray with single or overlapping epitopes binding to the target antigen in the majority of cases (**Supplementary Figure 3**). Recombinant anti-*Pf*RH5 and anti-*Pf*CyRPA antibodies inhibited invasion in both *Pf*FCR3 and *Pf*NF54, but as can be seen in **Figure 3**, *Pf*FCR3 parasites were consistently more susceptible to rIgG1 invasion blocking activity. With the exception of clone 2A7#70 *Pf*RH5 rhIgG1 clones were significantly more inhibitory in *Pf*FCR3 compared to *Pf*NF54 ($GLM_{(1,3,2,2)}; P < 0.001$). All four purified *Pf*CyRPA rhIgG1 clones showed greater inhibition of invasion in *Pf*FCR3 ($GLM_{(1,3,2,2)}; P < 0.001$). Similarly, significant differences

in replication rate between *Pf*FCR3 and *Pf*NF54 were observed for *Pf*RH5 rhIgG1 clones 5E6#36 ($GLM_{(2,1,2)}; P = 0.001$) and 15E3#259 ($GLM_{(2,1,2)}; P = 0.001$). No significant differences in replication rate were observed for rhIgG1 clones 2A7#70 ($GLM_{(2,1,2)}; P = 0.242$) and 15D12#256 ($GLM_{(2,1,2)}; P = 0.068$). For *Pf*CyRPA all rIgG1 clones tested were significantly different between *Pf*FCR3 and *Pf*NF54; 3A7#22 ($GLM_{(2,1,2)}; P = 0.005$), 3B3#17 ($GLM_{(2,1,2)}; P < 0.001$), 4D12#30 ($GLM_{(2,1,2)}; P < 0.05$), 7B8#13 ($GLM_{(2,1,2)}; P = 0.004$), 5E6#36 ($GLM_{(2,1,2)}; P = 0.001$), 15D12#256 ($GLM_{(2,1,2)}; P = 0.068$), 15E3#259 ($GLM_{(2,1,2)}; P = 0.001$) (**Supplementary Figure 4**).

3.3 Generation and Characterisation of *Pf*CSP mAbs

The only available malaria vaccine, Mosquirix (RTS,S/AS01) includes the *Pf*CSP antigen, and new *Pf*CSP vaccines in development, so we next sought to produce anti-*Pf*CSP antibodies. For both chicken and rabbit immunisations a total of 128 panning reactions were performed resulting in 110 cloning reactions. Heavy and light chains were amplified and cloned into human IgG1 expression vectors, with a total of 50 panning reactions from chicken immunisations, and 76 from rabbit immunisations. Following transient expression, the presence of anti-*Pf*CSP antibodies in culture media was determined using ELISA. Eleven rIgG1 pools were positive; ~470 clones were selected of which 47 were bound to *Pf*CSP. From these, 19 clones were selected for sequencing and 7 unique sequence were identified; 3 were derived from chicken immunisations and 4 from rabbits.

Using immunofluorescence and flow cytometry, 4/7 clones were found to bind to the surface of parasites (2G12#8, 4E11#20, 4H1#15 [rabbit] and 6F1#25 [chicken]; **Figure 4A**) and 3/7 displayed cytotoxicity and cell traversal inhibition profiles at 20 and 2 µg/ml (2G12#8, 4H11, 4E11#20, and 6F1#25; **Figure 4B** and **Table 2**).

To determine the range of epitopes present from the immunisations in rabbits and chickens the sera from the final bleeds was tested by peptide microarray. We found the major target was the *Pf*CSP NANP repeats (**Supplementary Figure 4**), with some additional reactivity against two additional regions outside of the NANP repeats. Sera from two of the immunised rabbits bound strongly to a 15-mer peptide (QGHNMPNDPNRNVD). Sera from only one rabbit bound to an overlapping peptide (RNVDENANANSVKNNNNEEPPSKHI). However, no clones were recovered from that animal. For the chicken immunisations, only sera from one chicken bound outside the NANP repeats to peptide EPSDKHIKEYLNKIQ but with no reactivity to the polymorphic sequences (EPSDKHITEYLNKIQ and EPSDKHIEEYLNKIQ). Three clones were isolated from that immunization; 2C4#2, 6F1#25, 6F8#32).

4 DISCUSSION

Here we describe the generation and initial characterisation of novel reference reagents to support malaria vaccine development.

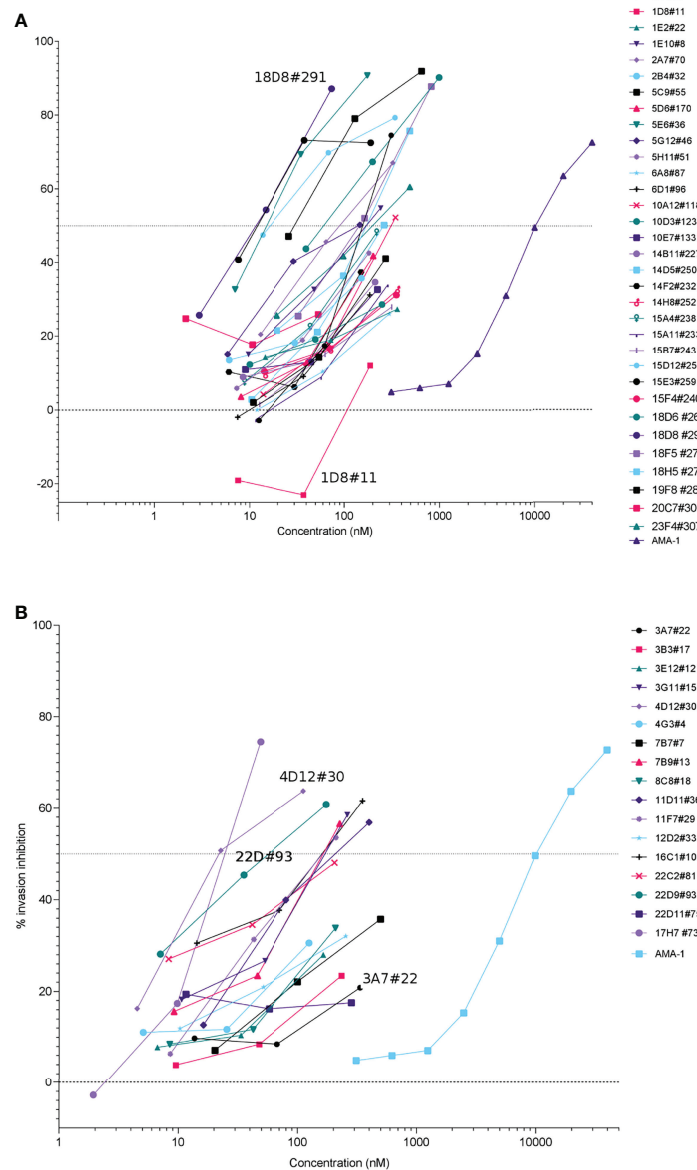


FIGURE 2 | Initial screen of crude cell culture supernatant of expressed anti-*PfRH5* (A) and anti-*PfCyRPA* (B) antibodies. Antibodies were tested on *P. falciparum* FCR3 during one intra-erythrocytic cycle. Invasion inhibition was determined by measuring parasitaemia by flow cytometry, percentage inhibition was calculated relative to the no antibody control wells. Invasion of parasite by AMA-1 polyclonal antibodies (BG98 standard) is shown for comparison. Many monoclonal antibodies show high potency at low nanomolar (nM) concentrations as compared to polyclonal anti-AMA-1 where the concentration of total IgG is used rather than the antigen-specific fraction.

Through the EURIPRED project, we have produced, characterised and made available recombinant human IgG1 for the wider malaria research community. The recombinantly produced *PfRH5* and *PfCyRPA* antibodies described provide a characterised and sequence defined material that can be used to standardise assays. Indeed, the antibodies produced inhibited invasion at similar concentrations (~16 µg/ml [~100 nM]) to some previously reported antibodies isolated from animals and humans (Douglas et al., 2011; Alanine et al., 2019; Knudsen et al., 2021). Furthermore, the activity of the some of the recombinant

human antibodies described here appears to be comparable to monoclonal antibodies isolated from humans (Alanine et al., 2019) suggesting they have potential for development as biological standards.

We evaluated the antibodies to blood stage antigens in terms of relative potency compared to an existing reference material (BG98). BG98 represents a large, but finite, supply of antibodies to *PfAMA-1* (Faber et al., 2013) and in this work also demonstrates the utility of a reference material. Indeed, the potency of the rhIgG1 clones described here at concentrations

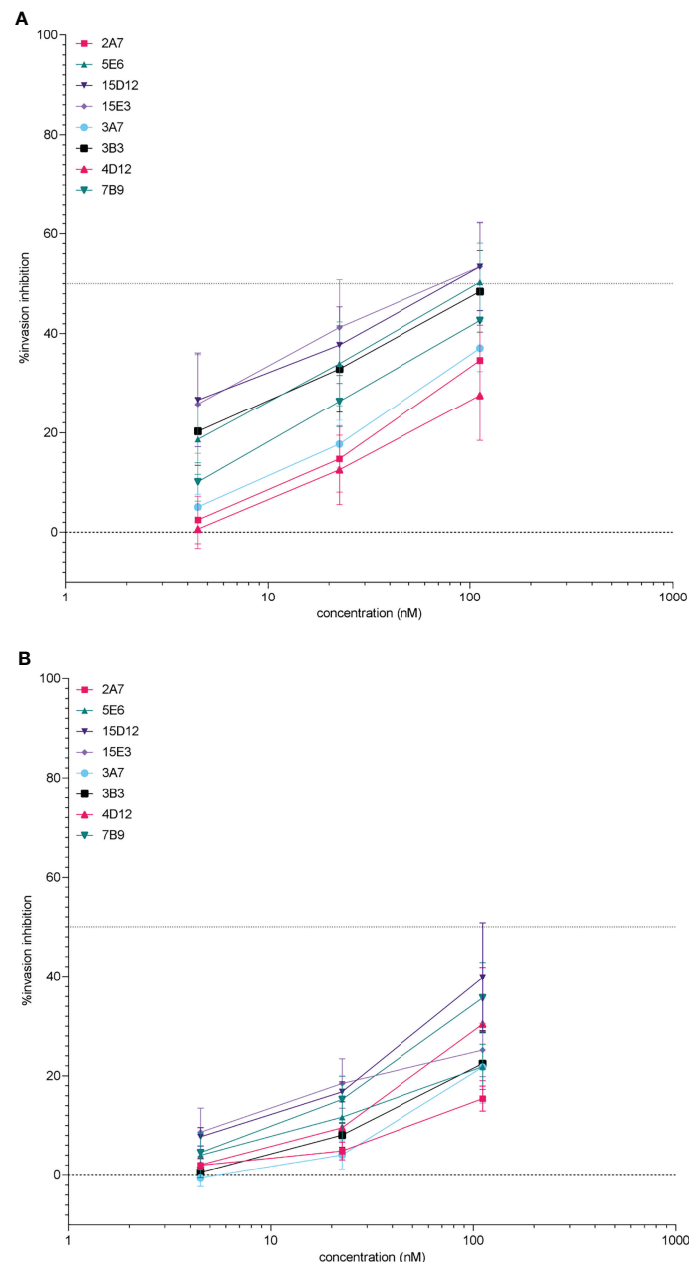


FIGURE 3 | Potency of purified anti-*PRH5* and -*PfCyRPA* monoclonal antibodies on *P. falciparum* FCR3 (A) and NF54 parasites (B) after incubation during one intra-erythrocytic cycle. Invasion inhibition was determined by measuring parasitaemia by flow cytometry, percentage inhibition was calculated relative to the no antibody control wells. The percentage inhibition and standard error of the mean (error bars) are shown for 3 replicate experiments. Assays were performed using antibodies diluted to 112.3, 22.5, and 4.5 nM (i.e. 16.4, 3.28, and 0.656 $\mu\text{g/ml}$ respectively) to facilitate comparisons with data using cell culture supernatants. Recombinant hIgG1 clones 2A7#70, 5E6#36, 15D12#256, and 15E3#259 are all directed against *PRH5*. Antibodies to *PfCyRPA* are 3A7#22, 3B3#17, 4D12#30, and 7B9#13.

similar to previously reported *PfCyRPA* and *PfRH5* antibodies (e.g. Douglas et al., 2011; Alanine et al., 2019; Knudsen et al., 2021) may make them more suitable as standards than BG98 which requires high concentrations to be used. In addition, independent testing to determine inter-laboratory variability of the antibodies was performed by GIA using *Pf3D7*. The relative

antibody activity was consistent across laboratories (data not shown) highlighting that these materials can be used to harmonise laboratory tests globally. Indeed, the rIgG1 revealed similar potency of the antibodies as determined by rank order for inhibition (data not shown). Interestingly we observed increased sensitivity of *PfFCR3* to blocking antibodies relative to *PfNF54*.

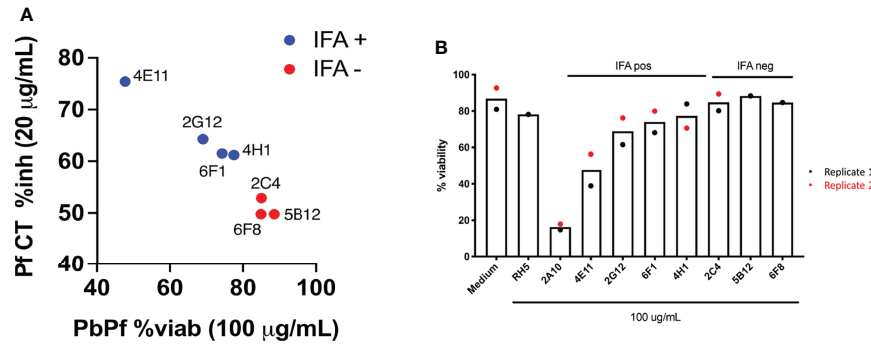


FIGURE 4 | (A) Inhibition and cytotoxicity of recombinant IgG1 (rIgG1) against *Pf*CSP from cell culture supernatants. Cell traversal (CT) inhibition (y-axis) of *Pf*NF54 sporozoites is shown against viability of *P. berghei* *Pf*CSP transgenic parasites following incubation with the various mAbs. To note, cytotoxic activity in *PbPf*CSP sporozoites correlates with inhibition of *Pf* CT. Antibodies that do not bind to the *Pf*CSP on the sporozoite surface (red) are non-cytotoxic. IFA, immunofluorescence assay. **(B)** Viability of transgenic *P. berghei* *Pf* CSP parasites following incubation with cell culture supernatant containing recombinant anti-*Pf*CSP rIgG1. Controls included in the assay were cell culture medium alone and a recombinant anti-*Pf*RH5 rIgG1. The recombinant antibodies generated had a limited effect on sporozoite viability with 4E11#20 showing a moderate reduction in viability.

The initial screening and selection steps were performed with only one laboratory isolate (*Pf*FCR3) which highlights, again, the value of standards as these differences can be identified and quantified. Strain differences in growth inhibition assays has previously been reported for both *Pf*RH5 (Douglas et al., 2011) and *Pf*CyRPA (Knudsen et al., 2021) despite low levels of polymorphisms in both antigens. Our data support these observations in additional laboratory isolates. Interestingly, we identified assay-dependent variability with the blocking antibodies, with *Pf*3D7 showing increased sensitivity to the rIgG1 in the invasion assay compared to GIA (data not shown); this has been found with other neutralising antibodies (Coxon et al., 2021) and is another reason why reference reagents are so valuable as they highlight that reliance on a single assay or strain can cause reproducibility issues and inconsistencies.

We observed few clones for the purified anti-*Pf*RH5 rIgG1 that recognised linear epitopes on the microarray. Conversely,

most anti-*Pf*CyRPA rIgG1 bound to multiple epitopes on their target antigen but also on the other antigens present on the array. It is likely that conformational epitopes are critical for the binding and blocking activities of the rIgG1 described here. Indeed, it has previously been reported that many *Pf*RH5 epitopes are conformational (Alanine et al., 2019). This may explain why some of the antibodies for which we could not clearly identify linear epitopes were potent in inhibiting invasion (e.g. 3A7#22, 3B3#17, 4D12#30). Furthermore, the epitopes recognized by the purified rhIgG1 clones did not contain polymorphic sequences, suggesting that differences in antibody activity in *Pf*FCR3 and *Pf*NF54 are likely due to conformational epitopes. It will be interesting that given we found differences in invasion inhibition between strains, to fine tune epitope mapping to determine if these can be used to predict or confirm likely differences in antibody potency.

TABLE 2 | Summary of anti-*Pf*CSP mAb activity in sporozoite cell traversal (CT) assays.

Clone	CT assay (%blocking)		Binding of antibodies to sporozoite surface			Cytotoxicity (% viability)*
			Imaging	Flow Cytometry		
	Concentration	NF54 Pf SPZ	NF54 Pf SPZ	PbPf-GFP SPZ	PbPf-GFP SPZ (80 µg/ml)	
	20 µg/ml	2 µg/ml				
2C4#2	52.9 (± 19.4)	40.4 (± 41.5)	-	-	-	98
2G12#8	64.3 (± 14.6)	50.5 (± 19.7)	+	+	+	79 [#]
4H1#15	61.2 (± 9.9)	37.7 (± 7.2)	+	+	+	89
4E11#20	75.4 (± 12.1)	42.8 (± 21.2)	+	+	+	54
5B12#21	49.8 (± 9.5)	22.2 (± 15.5)	-	-	-	100
6F1#25	61.5 (± 11.3)	35.5 (± 2.4)	+	+	+	85
6F8#32	49.8 (± 16.1)	37.8 (± 15.0)	-	-	-	100
2A10			+	+	+	19
HybriMed	-9.8 (± 35.9)	-	-	-	-	100

Cell culture supernatants of seven recombinant human IgG1 clones were tested in cell traversal and cell toxicity assays. The mAbs were also used to confirm binding to native CSP expressed on the surface of *P. falciparum* NF54 sporozoites as well as on *P. berghei* chimeric for *Pf*CSP. *Mean of two independent experiments for mAb recognizing non-permeabilised sporozoites. [#]cytotoxicity measured at 60 µg/ml. + denotes positive surface staining of sporozoites and - indicates no surface staining was observed.

The materials evaluated were developed and purified as part of this work were prepared in relatively small quantity, but importantly the sequence and therefore the capability to prepare more are available. As these antibodies are recombinant they theoretically constitute an infinite resource ensuring a supply for the future. However, as a note of caution the route of production may be important as it is known that glycosylation patterns of immunoglobulins are important for functional activity (Schroeder and Cavacini, 2010; Subedi and Barb, 2015; van de Bovenkamp et al., 2016). Indeed, if we are proposing that the community uses these antibodies to harmonise and standardise assays, it is important that we understand the effects of post-translational modifications on the material and ensure we are using a defined and optimised production process. Indeed, work by our group and others (Ragotte et al., 2022) has already shown that the choice of cell expression system used in the production of the antibodies affects antibody activity and we currently are investigating this in more detail at NIBSC. Furthermore, it is known that post-translational modifications are important for the activity of biological molecules including glycosylation in the context of immunoglobulins (Schroeder and Cavacini, 2010; Subedi and Barb, 2015; van de Bovenkamp et al., 2016). Glycosylation can be influenced by many factors including the cells used for the production of antibodies and the additives used in cell culture media (Kim et al., 2018; Ehret et al., 2019). It is therefore important to consider production of recombinant monoclonal antibodies. Indeed, variations in the biological activity of antibodies may result not from their sequences but their glycosylation patterns.

All the antibodies described were tested individually. It is probable that further screening of the purified rIgG1 would enable the identification of synergistic effects with different antibody combinations as has been previously reported for *Pf*CyRPA (Knudsen et al., 2021) and *Pf*RH5 (Alanine et al., 2019). As *Pf*RH5 and *Pf*CyRPA form a complex during invasion, the presence of antibodies to both antigens could further inhibit invasion. Combining antibodies to the same target with different binding profiles could allow for the identification of more inhibitory antibody cocktails which would also enable the formulation of more robust standards. This approach would enable the formulation of polyclonal rIgG1 materials that may be more commutable and therefore comparable to the breadth of responses seen in individuals exposed to *P. falciparum*. In addition, many antibodies with high potency were not purified and further characterised, and these may warrant further investigation such as anti-*Pf*RH5 clone 18D8 #291 with >900-fold increased potency compared to anti-AMA-1 (BG98), or anti-*Pf*CyRPA clone 17H7 #73 with a potency 80-fold higher than anti-AMA-1 (BG98).

The antibodies described here also offer significant opportunities to generate new reference materials and research reagents as recombinant antibodies can be cloned into different immunoglobulin backbones. Specific subclasses of IgG are associated with *P. falciparum* infection (Dobano et al., 2019), namely IgG1 and IgG3. The system described here for the expression of human recombinant IgGs allows for the

complementary determining regions (CDRs) to be cloned into other IgG subclasses (e.g., IgG3 framework) to determine how changing Fc functionality affects *in vitro* or *in vivo* activity at the two key stages of the parasite life-cycle (liver and blood). Altering the IgG subclass may enable the development of other reagents that more closely reflect the human immune response in assays and therefore, provide better indicators of candidate antigen performance during clinical development. These would also provide standardisation reagents more closely aligned to the biological targets of interest.

While the production of the *Pf*CSP antibodies was challenging we have successfully generated seven new monoclonal antibodies. The reasons for the difficulties in expression and isolation of the *Pf*CSP rIgG1 are not clear and further work is on-going with the clones generated. The microarray data showed that the polyclonal sera from one chicken and two rabbits bound to regions outside the NANP repeats. Three clones were isolated from the immunized chicken (2C4#2, 6F1#25, 6F8#32) and one clone from the rabbits (5B12#21). Determining what epitopes the purified rhIgG1 clones recognise by microarray will further allow characterisation of these mAbs. The antibodies generated did not show increased potency compared to 2A10 as crude cell supernatants. However, the data obtained from the crude supernatants is encouraging and all antibodies generated showed some activity in the various assays used (i.e. cell traversal inhibition, cell toxicity). For example, antibody 4E11#20 showed relatively high levels of activity in the cell traversal assay ($75.45 \pm 12.1\%$ inhibition) and cytotoxicity (54% viability). Further work will be required on the purified rIgG1 to better understand their activity and potential as reference reagents and/or research reagents.

The materials described here are a first step in the provision of quality standards for malaria research that can support robust assay development and material characterisation for vaccines.

5 REAGENTS

The recombinant human monoclonal antibodies described herein are available from CFAR-NIBSC.

NIBSC Catalogue #	Description
NR0025	Purified mAb anti- <i>Pf</i> CSP1 (4E11#20)
NR0026	Purified mAb anti- <i>Pf</i> CSP1 (5B12#21)
NR0027	Purified mAb anti- <i>Pf</i> CSP1 (6F1#25)
NR0028	Purified mAb anti- <i>Pf</i> CSP1 (2G12#8)
NR0029	Purified mAb anti- <i>Pf</i> CSP1 (4H1#15)
NR0030	Purified mAb anti- <i>Pf</i> CSP1 (2C4#2)
NR0031	Purified mAb anti- <i>Pf</i> CSP1 (6F8#32)
100851	Purified mAb anti- <i>Pf</i> RH5 (2A7#70)
100852	Purified mAb anti- <i>Pf</i> RH5 (5E6#36)
100853	Purified mAb anti- <i>Pf</i> RH5 (15D12#256)
100854	Purified mAb anti- <i>Pf</i> RH5 (15E3#259)
100855	Purified mAb anti- <i>Pf</i> CyRPA (3A7#22)
100856	Purified mAb anti- <i>Pf</i> CyRPA (3B3#17)
100857	Purified mAb anti- <i>Pf</i> CyRPA (4D12#30)
100858	Purified mAb anti- <i>Pf</i> CyRPA (7B9#13)

DATA AVAILABILITY STATEMENT

The VH/VL sequence were analysed and validated using the international ImmunoGeneTics (IMGT) information system <https://www.imgt.org/>.

ETHICS STATEMENT

The animal study was reviewed and approved by Estonian National Board of Animal Experiments (No. 115, 07.09.2012; No. 87, 28.08.2007).

AUTHOR CONTRIBUTIONS

AN performed the invasion assays, blood-stage antibody selection, data analysis, project management, coordinated with partners for assays, and wrote the manuscript. GK performed antibody isolation by HybriFree technology and project management. RP performed the immunisations, Octet blocking assay, and project management. EJ did the antibody purification and antibody screening by ELISA. PH performed the microarray experiments. EA and RA performed the sporozoite cytotoxicity, cell traversal and immunofluorescence assays and corresponding figures. OS performed the sporozoite cell traversal assays. DQ performed GIA with the purified mAbs. YLD and MH provided critical logistics for the shipment and storage of the antibodies, and project management. UR led the work at JPT Technologies, designed the microarray slides, provided data insights and analysis. AT generated the monoclonal antibodies, and

provided scientific insights. SJD provided reagents and input into the selection of the antigens. SG and MMH coordinated the EURIPRED grant. PWB conceived of the project, selected the antigens and provided project management. All authors reviewed the manuscript and agreed with the version submitted.

FUNDING

This work was the European Union's Seventh Framework Programme [FP7-INFRA-2012] under Grant Agreement No: 312661 - European Research Infrastructures for Poverty Related Diseases (EURIPRED). SD is a Jenner Investigator, a Lister Institute Research Prize Fellow, and held a Wellcome Trust Senior Fellowship (106917/Z/15/Z).

ACKNOWLEDGMENTS

BG98 was generously provided by Ed Remarque (BPRC, Netherlands) and is available from CFAR-NIBSC (cat# NR0014). The authors thank Carmen Coxon (NIBSC, UK) for critically reviewing the manuscript and providing valuable suggestions and feedback.

SUPPLEMENTARY MATERIAL

The Supplementary Material for this article can be found online at: <https://www.frontiersin.org/articles/10.3389/fcimb.2022.901253/full#supplementary-material>

REFERENCES

- Adepoju, P. (2019). RTS,S Malaria Vaccine Pilots in Three African Countries. *Lancet* 393 (10182), 1685. doi: 10.1016/S0140-6736(19)30937-7
- Alanine, D. G. W., Quinkert, D., Kumarasingha, R., Mehmood, S., Donnellan, F. R., Minkah, N. K., et al. (2019). Human Antibodies That Slow Erythrocyte Invasion Potentiate Malaria-Neutralizing Antibodies. *Cell* 178 (1), 216–228.e221. doi: 10.1016/j.cell.2019.05.025
- Aliprandini, E., Tavares, J., Panatieri, R. H., Thiberge, S., Yamamoto, M. M., Silvie, O., et al. (2018). Cytotoxic Anti-Circumsporozoite Antibodies Target Malaria Sporozoites in the Host Skin. *Nat. Microbiol.* 3 (11), 1224–1233. doi: 10.1038/s41564-018-0254-z
- Anker, R., Zavala, F., and Pollok, B. A. (1990). VH and VL Region Structure of Antibodies That Recognize the (NANP)₃ Dodecapeptide Sequence in the Circumsporozoite Protein of Plasmodium Falciparum. *Eur. J. Immunol.* 20 (12), 2757–2761. doi: 10.1002/eji.1830201233
- Artaud, C., Kara, L., and Launay, O. (2019). Vaccine Development: From Preclinical Studies to Phase 1/2 Clinical Trials. *Methods Mol. Biol.* 2013, 165–176. doi: 10.1007/978-1-4939-9550-9_12
- Bradbury, A., and Pluckthun, A. (2015). Reproducibility: Standardize Antibodies Used in Research. *Nature* 518 (7537), 27–29. doi: 10.1038/518027a
- Bryan, D., Silva, N., Rigsby, P., Dougall, T., Corran, P., Bowyer, P. W., et al. (2017). The Establishment of a WHO Reference Reagent for Anti-Malaria (Plasmodium Falciparum) Human Serum. *Malar. J.* 16 (1), 314. doi: 10.1186/s12936-017-1958-x
- Challenger, J. D., Olivera Mesa, D., Da, D. F., Yerbanga, R. S., Lefevre, T., Cohuet, A., et al. (2021). Predicting the Public Health Impact of a Malaria Transmission-Blocking Vaccine. *Nat. Commun.* 12 (1), 1494. doi: 10.1038/s41467-021-21775-3
- Chattopadhyay, R., and Pratt, D. (2017). Role of Controlled Human Malaria Infection (CHMI) in Malaria Vaccine Development: A U.S. Food & Drug Administration (FDA) Perspective. *Vaccine* 35 (21), 2767–2769. doi: 10.1016/j.vaccine.2017.03.072
- Cotton, M. (2020). The Mosquirix (RTS,S) Malaria Vaccine. *Trop. Doct.* 50 (2), 107. doi: 10.1177/0049475520916978
- Coxon, C. H., Yu, X., Beavis, J., Diaz-Saez, L., Riches-Duit, A., Ball, C., et al. (2021). Characterisation and Application of Recombinant FVIII-Neutralising Antibodies From Haemophilia A Inhibitor Patients. *Br. J. Haematol.* 193 (5), 976–987. doi: 10.1111/bjh.17227
- Dattoo, M. S., Natama, M. H., Some, A., Traore, O., Rouamba, T., Bellamy, D., et al. (2021). Efficacy of a Low-Dose Candidate Malaria Vaccine, R21 in Adjuvant Matrix-M, With Seasonal Administration to Children in Burkina Faso: A Randomised Controlled Trial. *Lancet* 397 (10287), 1809–1818. doi: 10.1016/S0140-6736(21)00943-0
- Dobano, C., Santano, R., Vidal, M., Jimenez, A., Jairoce, C., Ubillos, I., et al. (2019). Differential Patterns of IgG Subclass Responses to Plasmodium Falciparum Antigens in Relation to Malaria Protection and RTS,S Vaccination. *Front. Immunol.* 10. doi: 10.3389/fimmu.2019.00439
- Douglas, A. D., Baldeviano, G. C., Lucas, C. M., Lugo-Roman, L. A., Crosnier, C., Bartholdson, S. J., et al. (2015). A PfPR5-5-Based Vaccine is Efficacious Against Heterologous Strain Blood-Stage Plasmodium Falciparum Infection in Aotus Monkeys. *Cell Host Microbe* 17 (1), 130–139. doi: 10.1016/j.chom.2014.11.017
- Douglas, A. D., Williams, A. R., Illingworth, J. J., Kamuyu, G., Biswas, S., Goodman, A. L., et al. (2011). The Blood-Stage Malaria Antigen PfPRH5 is

- Susceptible to Vaccine-Inducible Cross-Strain Neutralizing Antibody. *Nat. Commun.* 2, 601. doi: 10.1038/ncomms1615
- Douglas, A. D., Williams, A. R., Knuepfer, E., Illingworth, J. J., Furze, J. M., Crosnier, C., et al. (2014). Neutralization of Plasmodium Falciparum Merozoites by Antibodies Against Pfrh5. *J. Immunol.* 192 (1), 245–258. doi: 10.4049/jimmunol.1302045
- Dreyer, A. M., Matile, H., Papastogiannidis, P., Kamber, J., Favuzza, P., Voss, T. S., et al. (2012). Passive Immunoprotection of Plasmodium Falciparum-Infected Mice Designates the CyRPA as Candidate Malaria Vaccine Antigen. *J. Immunol.* 188 (12), 6225–6237. doi: 10.4049/jimmunol.1103177
- Ehret, J., Zimmermann, M., Eichhorn, T., and Zimmer, A. (2019). Impact of Cell Culture Media Additives on IgG Glycosylation Produced in Chinese Hamster Ovary Cells. *Biotechnol. Bioeng.* 116 (4), 816–830. doi: 10.1002/bit.26904
- Faber, B. W., Younis, S., Remarque, E. J., Rodríguez García, R., Riasat, V., Walraven, V., et al. (2013). Diversity Covering AMA1-MSP119 Fusion Proteins as Malaria Vaccines. *Infect. Immun.* 81 (5), 1479–1490. doi: 10.1128/IAI.01267-12
- Formaglio, P., Tavares, J., Menard, R., and Amino, R. (2014). Loss of Host Cell Plasma Membrane Integrity Following Cell Traversal by Plasmodium Sporozoites in the Skin. *Parasitol. Int.* 63 (1), 237–244. doi: 10.1016/j.parint.2013.07.009
- Giudicelli, V., Chaume, D., Jabado-Michaloud, J., and Lefranc, M. P. (2005). Immunogenetics Sequence Annotation: The Strategy of IMGT Based on IMGT-ONTOLOGY. *Stud. Health Technol. Inform* 116, 3–8.
- Good, M. F., and Miller, L. H. (2018). Interpreting Challenge Data From Early Phase Malaria Blood Stage Vaccine Trials. *Expert Rev. Vaccines* 17 (3), 189–196. doi: 10.1080/14760584.2018.1435278
- Harris, L. M., Campillo, A., Rigsby, P., Atkinson, E., Poonawala, R., Aidoo, M., et al. (2017). *Collaborative Study to Evaluate the Proposed First World Health Organization International Standard for Plasmodium Falciparum Antigens* (Geneva: World Health Organization).
- Healer, J., Wong, W., Thompson, J. K., He, W., Birkinshaw, R. W., Miura, K., et al. (2019). Neutralising Antibodies Block the Function of Rh5/Ripr/CyRPA Complex During Invasion of Plasmodium Falciparum Into Human Erythrocytes. *Cell Microbiol.* 21 (7), e13030. doi: 10.1111/cmi.13030
- Hollingdale, M. R., Nardin, E. H., Tharavanij, S., Schwartz, A. L., and Nussenzweig, R. S. (1984). Inhibition of Entry of Plasmodium Falciparum and P. Vivax Sporozoites Into Cultured Cells; an *In Vitro* Assay of Protective Antibodies. *J. Immunol.* 132 (2), 909–913.
- Jin, J., Tarrant, R. D., Bolam, E. J., Angell-Manning, P., Soegaard, M., Pattinson, D. J., et al. (2018). Production, Quality Control, Stability, and Potency of cGMP-Produced Plasmodium Falciparum RH5.1 Protein Vaccine Expressed in Drosophila S2 Cells. *NPJ Vaccines* 3, 32. doi: 10.1038/s41541-018-0071-7
- Kim, S.-M., Chang, K.-H., and Oh, D. J. (2018). Effect of Environmental Parameters on Glycosylation of Recombinant Immunoglobulin G Produced From Recombinant CHO Cells. *Biotechnol. Bioprocess Eng.* 23 (4), 456–464. doi: 10.1007/s12257-018-0109-8
- Kivi, G., Teesalu, K., Parik, J., Kontkar, E., Ustav, M. Jr., Noodla, L., et al. (2016). HybriFree: A Robust and Rapid Method for the Development of Monoclonal Antibodies From Different Host Species. *BMC Biotechnol.* 16, 2. doi: 10.1186/s12896-016-0232-6
- Knudsen, A. S., Björnsson, K. H., Bassi, M. R., Walker, M. R., Kok, A., Cristinoi, B., et al. (2021). Strain-Dependent Inhibition of Erythrocyte Invasion by Monoclonal Antibodies Against Plasmodium Falciparum CyRPA. *Front. Immunol.* 12. doi: 10.3389/fimmu.2021.716305
- Knuepfer, E., Wright, K. E., Kumar Prajapati, S., Rawlinson, T. A., Mohring, F., Koch, M., et al. (2019). Divergent Roles for the RH5 Complex Components, CyRPA and RIPR in Human-Infective Malaria Parasites. *PLoS Pathog.* 15 (6), e1007809. doi: 10.1371/journal.ppat.1007809
- Lefranc, M. P. (2014). Antibody Informatics: IMGT, the International ImMunoGeneTics Information System. *Microbiol. Spectr.* 2 (2), 2.2.01. doi: 10.1128/microbiolspec.AID-0001-2012
- Lefranc, M. P., Giudicelli, V., Duroux, P., Jabado-Michaloud, J., Folch, G., Aouinti, S., et al. (2015). IMGT(R), the International ImMunoGeneTics Information System(R) 25 Years on. *Nucleic Acids Res.* 43 (Database issue), D413–D422. doi: 10.1093/nar/gku1056
- Lefranc, M. P., Giudicelli, V., Ginestoux, C., Bodmer, J., Muller, W., Bontrop, R., et al. (1999). IMGT, the International ImMunoGeneTics Database. *Nucleic Acids Res.* 27 (1), 209–212. doi: 10.1093/nar/27.1.209
- Li, C., Li, W., Lucio de Esarte, E., Guo, H., van den Elzen, P., Aarts, E., et al. (2017). Cell Attachment Domains of the Porcine Epidemic Diarrhea Virus Spike Protein Are Key Targets of Neutralizing Antibodies. *J. Virol.* 91 (12), e00273–17. doi: 10.1128/JVI.00273-17
- Lyke, K. E., Singer, A., Berry, A. A., Reyes, S., Chakravarty, S., James, E. R., et al. (2020). Multidose Priming and Delayed Boosting Improve PfSPZ Vaccine Efficacy Against Heterologous P. Falciparum Controlled Human Malaria Infection. *Clin. Infect. Dis.* 73 (7), e2424–e2435. doi: 10.1093/cid/ciaa1294
- Maier, A. G., Matuschewski, K., Zhang, M., and Rug, M. (2019). Plasmodium Falciparum. *Trends Parasitol.* 35 (6), 481–482. doi: 10.1016/j.pt.2018.11.010
- MalariaGen, Ahouidi, A., Ali, M., Almagro-Garcia, J., Amambua-Ngwa, A., Amaratunga, C., et al. (2021). An Open Dataset of Plasmodium Falciparum Genome Variation in 7,000 Worldwide Samples. *Wellcome Open Res.* 6, 42. doi: 10.12688/wellcomeopenres.16168.2
- Malkin, E. M., Diemert, D. J., McArthur, J. H., Perreault, J. R., Miles, A. P., Giersing, B. K., et al. (2005). Phase 1 Clinical Trial of Apical Membrane Antigen 1: An Asexual Blood-Stage Vaccine for Plasmodium Falciparum Malaria. *Infect. Immun.* 73 (6), 3677–3685. doi: 10.1128/IAI.73.6.3677-3685.2005
- Matuschewski, K., and Borrmann, S. (2019). Controlled Human Malaria Infection (CHMI) Studies: Over 100 Years of Experience With Parasite Injections. *Methods Mol. Biol.* 2013, 91–101. doi: 10.1007/978-1-4939-9550-9_7
- Minassian, A. M., Silk, S. E., Barrett, J. R., Nielsen, C. M., Miura, K., Diouf, A., et al. (2021). Reduced Blood-Stage Malaria Growth and Immune Correlates in Humans Following RH5 Vaccination. *Med. (N Y)* 2 (6), 701–719. doi: 10.1016/j.medj.2021.03.014
- Mwakingwe-Omari, A., Healy, S. A., Lane, J., Cook, D. M., Kalhori, S., Wyatt, C., et al. (2021). Two Chemoattenuated PfSPZ Malaria Vaccines Induce Sterile Hepatic Immunity. *Nature* 595 (7866), 289–294. doi: 10.1038/s41586-021-03684-z
- Ndwiga, L., Osoti, V., Ochwedo, K. O., Wamae, K., Bejon, P., Rayner, J. C., et al. (2021). The Plasmodium Falciparum Rh5 Invasion Protein Complex Reveals an Excess of Rare Variant Mutations. *Malar. J.* 20 (1), 278. doi: 10.1186/s12936-021-03815-x
- Quan, J., and Tian, J. (2009). Circular Polymerase Extension Cloning of Complex Gene Libraries and Pathways. *PLoS One* 4 (7), e6441. doi: 10.1371/journal.pone.0006441
- Ragotte, R. J., Higgins, M. K., and Draper, S. J. (2020). The RH5-CyRPA-Ripr Complex as a Malaria Vaccine Target. *Trends Parasitol.* 36 (6), 545–559. doi: 10.1016/j.pt.2020.04.003
- Ragotte, R. J., Pulido, D., Lias, A. M., Quinkert, D., Alanine, D. G. W., Jamwal, A., et al. (2022). Heterotypic Interactions Drive Antibody Synergy Against a Malaria Vaccine Candidate. *Nat. Commun.* 13 (1), 933. doi: 10.1038/s41467-022-28601-4
- Sato, S. (2021a). Correction to: Plasmodium-A Brief Introduction to the Parasites Causing Human Malaria and Their Basic Biology. *J. Physiol. Anthropol.* 40 (1), 3. doi: 10.1186/s40101-021-00254-0
- Sato, S. (2021b). Plasmodium-A Brief Introduction to the Parasites Causing Human Malaria and Their Basic Biology. *J. Physiol. Anthropol.* 40 (1), 1. doi: 10.1186/s40101-020-00251-9
- Schroeder, H. W. Jr., and Cavacini, L. (2010). Structure and Function of Immunoglobulins. *J. Allergy Clin. Immunol.* 125 (2 Suppl 2), S41–S52. doi: 10.1016/j.jaci.2009.09.046
- Sinnis, P., de la Vega, P., Coppi, A., Krzych, U., and Mota, M. M. (2013). Quantification of Sporozoite Invasion, Migration, and Development by Microscopy and Flow Cytometry. *Methods Mol. Biol.* 923, 385–400. doi: 10.1007/978-1-62703-026-7_27
- Sirima, S. B., Richert, L., Chene, A., Konate, A. T., Campion, C., Dechavanne, S., et al. (2020). PRIMVAC Vaccine Adjuvanted With Alhydrogel or GLA-SE to Prevent Placental Malaria: A First-in-Human, Randomised, Double-Blind, Placebo-Controlled Study. *Lancet Infect. Dis.* 20 (5), 585–597. doi: 10.1016/S1473-3099(19)30739-X
- Steel, R. W., Sack, B. K., Tsuji, M., Navarro, M. J., Betz, W., Fishbaugher, M. E., et al. (2017). An Opsonic Phagocytosis Assay for Plasmodium Falciparum Sporozoites. *Clin. Vaccine Immunol.* 24 (2), e00445–16. doi: 10.1128/CI.00445-16
- Subedi, G. P., and Barb, A. W. (2015). The Structural Role of Antibody N-Glycosylation in Receptor Interactions. *Structure* 23 (9), 1573–1583. doi: 10.1016/j.str.2015.06.015
- Tavares, J., Formaglio, P., Medvinsky, A., Menard, R., and Amino, R. (2013a). Imaging Sporozoite Cell Traversal in the Liver of Mice. *Methods Mol. Biol.* 923, 401–410. doi: 10.1007/978-1-62703-026-7_28
- Tavares, J., Formaglio, P., Thiberge, S., Mordelet, E., Van Rooijen, N., Medvinsky, A., et al. (2013b). Role of Host Cell Traversal by the Malaria Sporozoite During Liver Infection. *J. Exp. Med.* 210 (5), 905–915. doi: 10.1084/jem.20121130

- Trager, W., and Jensen, J. B. (1976). Human Malaria Parasites in Continuous Culture. *Science* 193 (4254), 673–675. doi: 10.1126/science.781840
- van de Bovenkamp, F. S., Hafkenscheid, L., Rispens, T., and Rombouts, Y. (2016). The Emerging Importance of IgG Fab Glycosylation in Immunity. *J. Immunol.* 196 (4), 1435–1441. doi: 10.4049/jimmunol.1502136
- Vijayan, A., and Chitnis, C. E. (2019). Development of Blood Stage Malaria Vaccines. *Methods Mol. Biol.* 2013, 199–218. doi: 10.1007/978-1-4939-9550-9_15
- Volz, J. C., Yap, A., Sisquella, X., Thompson, J. K., Lim, N. T., Whitehead, L. W., et al. (2016). Essential Role of the PfRh5/PfRipr/CyRPA Complex During Plasmodium Falciparum Invasion of Erythrocytes. *Cell Host Microbe* 20 (1), 60–71. doi: 10.1016/j.chom.2016.06.004
- WHO (2021). *World Malaria Report* (Geneva: World Health Organization).
- Wilby, K. J., Lau, T. T., Gilchrist, S. E., and Ensom, M. H. (2012). Mosquirix (RTS, S): A Novel Vaccine for the Prevention of Plasmodium Falciparum Malaria. *Ann. Pharmacother.* 46 (3), 384–393. doi: 10.1345/aph.1AQ634
- Zavala, F., Cochrane, A. H., Nardin, E. H., Nussenzweig, R. S., and Nussenzweig, V. (1983). Circumsporozoite Proteins of Malaria Parasites Contain a Single Immunodominant Region With Two or More Identical Epitopes. *J. Exp. Med.* 157 (6), 1947–1957. doi: 10.1084/jem.157.6.1947
- Zhang, M., Mandraju, R., Rai, U., Shiratsuchi, T., and Tsuji, M. (2017). Monoclonal Antibodies Against Plasmodium Falciparum Circumsporozoite Protein. *Antibodies (Basels)* 6 (3), 11. doi: 10.3390/antib6030011

Conflict of Interest: SJD is a named inventor on patent applications relating to PjRH5 and/or other malaria vaccines, mAbs, and immunisation regimes. UR and PH are employed by JPT Peptide Technologies GmbH. GK, RP, EJ, and AT are employed by Icosagen Cell Factory.

The remaining authors declare that the research was conducted in the absence of any commercial or financial relationships that could be construed as a potential conflict of interest.

Publisher's Note: All claims expressed in this article are solely those of the authors and do not necessarily represent those of their affiliated organizations, or those of the publisher, the editors and the reviewers. Any product that may be evaluated in this article, or claim that may be made by its manufacturer, is not guaranteed or endorsed by the publisher.

Copyright © 2022 Nacer, Kivi, Pert, Juronen, Holenya, Aliprandini, Amino, Silvie, Quinkert, Le Duff, Hurley, Reimer, Tover, Draper, Gilbert, Ho and Bowyer. This is an open-access article distributed under the terms of the Creative Commons Attribution License (CC BY). The use, distribution or reproduction in other forums is permitted, provided the original author(s) and the copyright owner(s) are credited and that the original publication in this journal is cited, in accordance with accepted academic practice. No use, distribution or reproduction is permitted which does not comply with these terms.



Updated List of Transport Proteins in *Plasmodium falciparum*

Juliane Wunderlich^{1,2,3*}

¹ Max Planck Institute for Infection Biology, Berlin, Germany, ² European Molecular Biology Laboratory, Hamburg Unit, Hamburg, Germany, ³ Centre for Structural Systems Biology, Hamburg, Germany

OPEN ACCESS

Edited by:

Tania F. De Koning-Ward,
Deakin University, Australia

Reviewed by:

Kevin Brown,
University of Oklahoma Health
Sciences Center, United States
Benjamin Liffner,
Indiana University, United States
Mikha Gabriela,
The University of Melbourne, Australia

*Correspondence:

Juliane Wunderlich
wunderlich@mpiib-berlin.mpg.de

Specialty section:

This article was submitted to
Parasite and Host,
a section of the journal
Frontiers in Cellular and
Infection Microbiology

Received: 22 April 2022

Accepted: 23 May 2022

Published: 24 June 2022

Citation:

Wunderlich J (2022) Updated
List of Transport Proteins in
Plasmodium falciparum.
Front. Cell. Infect. Microbiol. 12:926541.
doi: 10.3389/fcimb.2022.926541

Malaria remains a leading cause of death and disease in many tropical and subtropical regions of the world. Due to the alarming spread of resistance to almost all available antimalarial drugs, novel therapeutic strategies are urgently needed. As the intracellular human malaria parasite *Plasmodium falciparum* depends entirely on the host to meet its nutrient requirements and the majority of its transmembrane transporters are essential and lack human orthologs, these have often been suggested as potential targets of novel antimalarial drugs. However, membrane proteins are less amenable to proteomic tools compared to soluble parasite proteins, and have thus not been characterised as well. While it had been proposed that *P. falciparum* had a lower number of transporters (2.5% of its predicted proteome) in comparison to most reference genomes, manual curation of information from various sources led to the identification of 197 known and putative transporter genes, representing almost 4% of all parasite genes, a proportion that is comparable to well-studied metazoan species. This transporter list presented here was compiled by collating data from several databases along with extensive literature searches, and includes parasite-encoded membrane-resident/associated channels, carriers, and pumps that are located within the parasite or exported to the host cell. It provides updated information on the substrates, subcellular localisation, class, predicted essentiality, and the presence or absence of human orthologs of *P. falciparum* transporters to quickly identify essential proteins without human orthologs for further functional characterisation and potential exploitation as novel drug targets.

Keywords: *Plasmodium falciparum*, malaria, drug target, transport pathway, transporters and channels, systems biology, calcium homeostasis, nutrient uptake

INTRODUCTION

To sustain rapid growth within human red blood cells, *Plasmodium falciparum* requires sufficient nutrients and electrolytes for its active metabolism. Therefore, the parasite expresses a wide range of transport proteins to acquire substrates and efflux metabolites. As the majority of these carriers, channels, and pumps are predicted to be essential during intraerythrocytic stages (Martin, 2020) and have no identified human orthologs, these could be exploited as targets of novel drugs (Ludin et al., 2012). Due to the emergence of parasite resistance to most available antimalarials, new therapeutic strategies are urgently needed (Plowe, 2022). There are many reports on transporters associated with drug resistance (Cowell and Winzeler, 2019; Martin, 2020; Murithi et al., 2021;

Shafik et al., 2022), and advances in the development of drugs that target solute transporters were recently reviewed (Belete, 2020; Monteiro Júnior et al., 2022). Here, an extended list of *P. falciparum* transport proteins is presented with many new additions and updated information on transporter localisation and essentiality based on experimental evidence and orthology inference.

The last two transporter lists were published in 2020 and 2016 and contained 117 (Martin, 2020) and 139 (Weiner and Kooij, 2016) proteins, corresponding to 2.2% and 2.6% of the predicted *P. falciparum* proteome, respectively. The localisation within the parasite-infected host cell was not indicated for all of these, as microscopic examination after endogenous tagging with fluorescent proteins or staining using specific antibodies was not conducted for all transporters. However, precise knowledge of the location of a transport protein and its orientation in the membrane is paramount for understanding its function and the dynamics of solute transport processes between cellular compartments. Therefore, the list presented here contains new information on subcellular localisation and function based on results from recent microscopy experiments (Edaye and Georges, 2015; Haase et al., 2021; Murithi et al., 2021; Wichers et al., 2021; Ahiya et al., 2022; Wichers et al., 2022), solubility assays, immunoprecipitation, proximity-dependent biotinylation or subcellular fractionation followed by immunoblot or proteomic analyses (Boucher et al., 2018; Balestra et al., 2021; Bullen et al., 2022), functional and structural studies (Shafik et al., 2020; Beck and Ho, 2021), the presence of targeting signals (Sayers et al., 2018; van Esveld et al., 2021), and Gene Ontology (GO) annotations (Blake et al., 2015). In addition, data on essentiality of *P. falciparum* genes are usually based on a large piggyBac screen (Zhang et al., 2018) that is known to contain some false-positive and false-negative results (Martin, 2020), highlighting the need for verification by other studies. Thus, results from the latest publications (Jiang et al., 2020; Swift et al., 2020; Oberstaller et al., 2021; Wichers et al., 2022) were included in the list along with information on the presence or absence of human orthologs, as this is important for therapeutic development and was not systematically specified previously. Of note, this mini review focuses mainly on asexual blood-stage parasites and also contains recent data on other stages, as transporters are likely important throughout the life cycle.

Plasmodium gene annotations are still incomplete with a large proportion of genes completely lacking characterisation of their function and localisation or only having sparse functional annotation deduced by orthology (Böhme et al., 2019). The lower number of genes representing the malaria transportome reported in earlier studies may be due to the lack of conventional transmembrane domains in some *P. falciparum* transporters (Desai, 2012) and difficult analysis by mass spectrometry. The reduced number of detected peptides (Lu et al., 2021) stems both from the typically low protein amounts extracted from parasite culture that are subjected to subcellular fractionation or immunoprecipitation and from the fact that membrane proteins such as transporters are less amenable to proteomics

compared to soluble proteins. This has resulted in the conclusion that *P. falciparum* may have a reduced set of transporters compared to metazoan reference genomes (Weiner and Kooij, 2016; Martin, 2020).

Here, additional putative transporters were detected by compiling data from several databases (Aurrecochea et al., 2009; Blake et al., 2015; Saier et al., 2016; Elbourne et al., 2017) and the literature. This mini review also covers newly identified putative calcium transporters (Balestra et al., 2021; Gupta et al., 2022), as calcium homeostasis is thought to be critical for all parasite stages (Brochet and Billker, 2016) and likely a promising drug target (Gupta et al., 2022). However, the molecular identity of most of the transporters involved in calcium transport has remained unclear (Lourido and Moreno, 2015), with contrasting results and conclusions regarding their substrates and subcellular localisation as well as the cellular compartment used for calcium storage (Brochet and Billker, 2016). The manually curated list of 197 transporter genes presented here represents almost 4% of 5720 *P. falciparum* 3D7 genes, of which 5318 are protein-coding (Aurrecochea et al., 2009), a proportion that is comparable to the 3 – 5% reported for well-studied metazoan species (Elbourne et al., 2017). It includes the most recent published data and provides an updated overview on the substrates, localisation, function, classification, essentiality, and human orthologs of *P. falciparum* transporters and may serve as a basis for improved annotations of transporter genes and further functional characterisation of potential drug targets.

APPROACHES FOR TRANSPORT PROTEIN IDENTIFICATION AND COMPILATION OF A COMPREHENSIVE LIST

Whole-genome sequencing, genome-wide searches and comparative genomics enabled the detection and fast annotation of many *P. falciparum* transporter genes by assigning functions that are computationally inferred from orthology across hundreds of species, facilitating functional characterisation at a large scale. However, molecular pathways and mechanisms that occur in parasites can differ tremendously from model organisms (Woo et al., 2015), and some known *Plasmodium* transporters are genus-specific and/or lack conventional transmembrane domains (Desai, 2012). Thus, function predictions based on the presence of protein features and on orthology inference harbour the possibility of incomplete or incorrect annotations. For example, PF3D7_1368200 was annotated as “ABC transporter E family member 1, putative (ABCE1)” due to its ATP-binding cassette that similar to that of ABC transporters (Koenderink et al., 2010). However, it is unlikely to be a transporter because of its function in RNA processing (Mather et al., 2007; Sinha et al., 2021), demonstrating the need for manual curation of GO terms and gene annotations.

The existing transporter list published in 2020 (Martin, 2020) was extended by collating data from various sources. Therefore, a table of 123 transport proteins from the *P. falciparum* strain 3D7 (genome version 3.0) with information on substrates, transporter classes and families was downloaded from <http://www.membranetransport.org/transportDB2/index.html> (Elbourne et al., 2017). Additional transporters associated with the GO term “transmembrane transporter activity” (GO:0022857) (Blake et al., 2015), mentioned on Malaria Parasite Metabolic Pathways (<https://mpmp.huji.ac.il/maps/transporters.html>) (Ginsburg and Tilley, 2011) or in research articles were included. For example, *PfTMCO1* (transmembrane and coiled-coil domain-containing protein, PF3D7_1362300), identified based on orthology to proteins in other protozoan parasites (Gupta et al., 2022), was added. In contrast, glideosome-associated protein 40 (*PfGAP40*, PF3D7_0515700) and rhoptyr protein *PfROP14* (PF3D7_0613300) were removed, as new data on their function and localisation suggest that these are not transporters (Anantharaman et al., 2007; Zuccala et al., 2012; Ferreira et al., 2020).

As different names were sometimes used for the same protein (Weiner and Kooij, 2016; Staines et al., 2017; Martin, 2020), all alternative names found in the literature are mentioned in the table for clarification (Table 1). Transporter localisation, substrates and functions are indicated as in Martin, (2020) and predicted gene essentiality according to Zhang et al. (2018), unless stated otherwise. Transporter classes were assigned according to the Transport Classification Database (TCDB) (Saier et al., 2016) and if the transporter family was unknown, it was assigned according to the top TCDB blast hit (<http://www.tcd.org/progs/blast.php>) based on sequence similarity to known transport proteins (Altschul et al., 1997). Data on the presence of human orthologs was retrieved from https://mpmp.huji.ac.il/maps/orth_hsap.html (Ginsburg and Tilley, 2011), a list compiled using recent publications. The existence of human orthologs was further verified using the TCDB protein blast.

In total, 197 transport proteins were identified (Table 1), with some of these forming a complex, e.g. the *Plasmodium* Translocon of EXported proteins (PTEX), consisting of three core components (de Koning-Ward et al., 2009; Beck and Ho, 2021). Protein complex components residing in or associated with the respective membrane that are required for substrate translocation were included, whereas accessory and auxiliary subunits were excluded. For clarity, only the likely site of active transport is indicated for each protein, although it might be detectable in other subcellular compartments during trafficking.

CALCIUM TRANSPORT PROTEINS AS POTENTIAL DRUG TARGETS

Calcium homeostasis was chosen as an example for illustrating transport pathways in the *P. falciparum*-infected erythrocyte (Figure 1), as Ca^{2+} signalling is known to be critical throughout the parasite life cycle (Brochet and Billker, 2016)

and a link between Ca^{2+} uptake and virulence has been proposed in the related parasite *Toxoplasma gondii* (Pace et al., 2014). In fact, Ca^{2+} transporters such as *PfATP6* (PF3D7_0106300) are currently under investigation as novel antimalarial drug targets (Gupta et al., 2022; Monteiro Júnior et al., 2022). While the concentration of free Ca^{2+} is ~1.8 mM in the blood plasma, mature erythrocytes only contain 30 – 60 nM Ca^{2+} (Brochet and Billker, 2016) due to active ion extrusion by the P-type plasma membrane Ca^{2+} ATPases (PMCA) 1 and 4 and slow Ca^{2+} uptake via several channels such as Piezo1, the erythroid N-methyl D-aspartate (NMDA) receptor, and the voltage-dependent anion channel (VDAC) (Kaestner et al., 2020).

A malaria parasite that resides within an erythrocyte maintains a cytosolic calcium level of approximately 100 nM by permeabilising its host cell and using a regulatory Ca^{2+} pool (Garcia et al., 1996). Extracellular Ca^{2+} is thought to first pass through a parasite-encoded channel in the erythrocyte plasma membrane (EPM) that is independent of PSAC (plasmodial surface anion channel), thereby increasing the intracellular Ca^{2+} concentration of the infected red blood cell (Zipprer et al., 2014). One candidate for this channel is hemolysin III (*PfHlyIII*, PF3D7_1455400), which forms an ion-permeable pore of approximately 3.2 nm in EPMs after its release from the parasite digestive vacuole (DV) upon merozoite egress (Moonah et al., 2014). Another potential route of Ca^{2+} entry into the infected erythrocyte is via enhanced activity of a host channel induced by the parasite, as suggested for VDAC (Bouyer et al., 2011).

Passage through the parasitophorous vacuole membrane (PVM) likely occurs via a nutrient pore for solutes < 1.4 kDa formed by *PfEXP1* (PF3D7_1121600) and *PfEXP2* (PF3D7_1471100) (Garten et al., 2018; Mesén-Ramírez et al., 2019). The ion may then enter the parasite cytosol via a parasite-encoded channel, one candidate being the calcium-permeable stress-gated cation channel *PfCSC* (PF3D7_1250200) that is activated by high external calcium levels (Martin, 2020). The localisation of this transporter at the PPM was inferred from an ancestral gene (Gaudet et al., 2011) and although this remains to be confirmed experimentally, it seems plausible due to the identification of this protein as an immunoreactive antigen with high serodominance in exposed individuals (Doolan et al., 2008). As *PfCSC* is highly expressed in sporozoites (Le Roch et al., 2003), its exposure to the immune system may occur at this parasite stage.

Calcium can then be stored in the endoplasmic reticulum upon active import by the SERCA-type Ca^{2+} -ATPase *PfATP6* (Lourido and Moreno, 2015; Martin, 2020). In case of Ca^{2+} overload of the ER, the putative calcium load-activated calcium channel *PfTMCO1* (Gupta et al., 2022) may become active and release ions into the cytosol (Lourido and Moreno, 2015; Wang et al., 2016). Ca^{2+} efflux from the mitochondrion is likely mediated by the cation/ H^{+} antiporters *PfLETM1* (PF3D7_0417300) (Martin, 2020) and *PfCAX/PfCHA* (PF3D7_0603500) in exchange for protons that travel along the H^{+} gradient across the inner mitochondrial membrane (Rotmann et al., 2010).

TABLE 1 | Characteristics of known and putative *P. falciparum* transport proteins.

Gene ID	Product	Substrate and function	Family	Localisation	Essential	Human ortholog
PF3D7_1227200	K1, Kch1	voltage-gated potassium channel	1.A.1	e - EPM (Waller et al., 2008)	b - yes	yes
PF3D7_1465500	K2, Kch2	voltage-gated potassium channel	1.A.1	e - PPM (Waller et al., 2008)	b - no	yes
PF3D7_1436100	NIC	putative K ⁺ channel (Ginsburg and Tilley, 2011)	1.A.1	c - PPM	b - yes	no
PF3D7_1132800	AQP	channel for water, glycerol and polyols	1.A.8	e - PPM (Swearingen et al., 2016)	b - yes	yes
PF3D7_1438100	SEC62	protein import in complex with Sec61 (Marapana et al., 2018)	1.A.15	e - ER (Marapana et al., 2018)	b - yes	yes
PF3D7_1250200	CSC, CSC1	calcium-activated stress-gated channel for Ca ²⁺ , K ⁺ and Na ⁺	1.A.17	c - PPM (Blake et al., 2015)	b - yes	yes
PF3D7_1107900	MSCS	putative mechanosensitive anion channel	1.A.23	c - PPM? (Blake et al., 2015)	b - no	no
PF3D7_1120300	MIT1	magnesium/nickel/cobalt ion channel (Ginsburg and Tilley, 2011)	1.A.35	c - mitochondrion (van Esveld et al., 2021)	b - no	yes
PF3D7_1304200	MIT2	magnesium/nickel/cobalt ion channel (Ginsburg and Tilley, 2011)	1.A.35	c - mitochondrion (Blake et al., 2015)	b - yes	no
PF3D7_1427600	MIT3	magnesium/nickel/cobalt ion channel (Ginsburg and Tilley, 2011)	1.A.35	c - mitochondrion (Blake et al., 2015)	b - no	yes
PF3D7_1333800	ICln	anion channel	1.A.47	c - PPM	b - no	no
PF3D7_1439000	CTR1	copper channel	1.A.56	e - EPM, PPM	b - yes	no
PF3D7_1421900	CTR2	copper channel	1.A.56	c - apicoplast	b - yes	no
PF3D7_0306700	MMgT, EMC5	magnesium channel	1.A.67	c - ER	b - yes	no
PF3D7_0302500	CLAG3.1, RhopH1	PSAC/RhopH complex components for nutrient uptake (anions/organic cations)	1.A.91.1.1	e - EPM	b - no	no
PF3D7_0302200	CLAG3.2, RhopH1			e - EPM	b - no	no
PF3D7_0220800	CLAG2			c - EPM	b - no	no
PF3D7_0831600	CLAG8			c - EPM	b - no	no
PF3D7_0935800	CLAG9			c - EPM	b - no (Nacer et al., 2011)	no
PF3D7_0929400	RhopH2	Ca ²⁺ channel, prevents ER overfilling? (Wang et al., 2016)	1.A.106	e - EPM	b - yes	no
PF3D7_0905400	RhopH3			e - EPM	b - yes	no
PF3D7_1362300	TMCO1			c - ER? (Blake et al., 2015)	unknown	yes
PF3D7_1432100	OMPP, VDAC	solute channel	1.B.8.5.2	c - mitochondrion (Blake et al., 2015)	unknown	no
PF3D7_0823700	TOM7	components of TOM complex for protein import across outer membrane (Sheiner and Soldati-Favre, 2008; Schmidt et al., 2010)	1.B.8	c - mitochondrion (Schmidt et al., 2010)	b - yes	no
PF3D7_0524700	TOM22			e - mitochondrion (van Dooren et al., 2006)	b - yes	no
PF3D7_0617000	TOM40			e - mitochondrion (Das et al., 2017)	b - yes	no
PF3D7_0408700	PLP1, PPLP1	erythrocyte permeabilisation and rupture (Garg et al., 2013)	1.C.39	e - EPM (Garg et al., 2013)	b - no, s - yes (Yang et al., 2017)	no
PF3D7_1216700	PLP2, PPLP2	erythrocyte permeabilisation and rupture (Wirth et al., 2014)	1.C.39	e - EPM (Wirth et al., 2014)	b - no, g - yes (Wirth et al., 2014)	no
PF3D7_0923300	PLP3, PPLP3	host cell permeabilisation and rupture (Sassmannshausen et al., 2020)	1.C.39	c - host cell membrane (Sassmannshausen et al., 2020)	unknown	no
PF3D7_0819400	PLP4, PPLP4	rupture of mosquito midgut epithelial cells (Wirth et al., 2015)	1.C.39	e - host cell membrane (Sassmannshausen et al., 2020)	b - no, o - yes (Wirth et al., 2015)	no

(Continued)

TABLE 1 | Continued

Gene ID	Product	Substrate and function	Family	Localisation	Essential	Human ortholog
PF3D7_0819200	PLP5, PPLP5	host cell permeabilisation and rupture (Sassmannshausen et al., 2020)	1.C.39	c - host cell membrane (Sassmannshausen et al., 2020)	b - yes	no
PF3D7_1331500		putative calcium channel (Gupta et al., 2022)	1.C.105	c - PPM? (Blake et al., 2015)	unknown	yes
PF3D7_1234600	TOC75	protein import across 2 nd inner membrane (Agrawal and Striepen, 2010)	1.C.105	c - apicoplast (Boucher et al., 2018)	b - yes	no
PF3D7_0104100	E140, MPMP	unknown	1.C.105	c - PPM? (Blake et al., 2015)	b - yes	no
PF3D7_1455400	HlyIII	forms pore (~3.2 nm) for solutes and ions	1.C.113	e - EPM	b - yes	no
PF3D7_0204700	HT1	imports glucose and fructose	2.A.1.1	e - PPM	b - yes	yes
PF3D7_0516500	MFS1, MDT	putative metabolite/drug transporter	2.A.1.2	unknown	b - no	yes
PF3D7_0916000	MFS2	putative sugar transporter	2.A.1.1	unknown	b - no	yes
PF3D7_0919500	MFS3	putative sugar transporter	2.A.1.1	e - PPM? (Swearingen et al., 2016), c - mitochondrion (Blake et al., 2015)	b - no	yes
PF3D7_1203400	MFS4	putative transporter	2.A.1	unknown	b - no	no
PF3D7_1428200	MFS5	putative metabolite transporter	2.A.1	unknown	b - no	no
PF3D7_1440800	MFS6	H ⁺ import, metabolite/drug export	2.A.1	e - apicoplast	b - no	no
PF3D7_1117000	P115	unknown	2.A.1	c - PPM (Blake et al., 2015)	b - no	no
PF3D7_0614300	MFR1	putative organic anion transporter	2.A.1.2	unknown	b - no	no
PF3D7_0104700	MFR2, ApiAT9	putative amino acid transporter	2.A.1	e - PPM (Wichers et al., 2021)	b - no	no
PF3D7_0312500	MFR3, ApiAT10	putative amino acid transporter	2.A.1	e - PPM (Wichers et al., 2021)	b - no	no
PF3D7_0914700	MFR4, ApiAT2	putative amino acid transporter	2.A.1	e - PPM (Wichers et al., 2021)	b - no	no
PF3D7_1129900	MFR5, ApiAT4	putative amino acid transporter	2.A.1	e - PPM (Wichers et al., 2021)	b - no	no
PF3D7_0104800	NPT1, ApiAT8	putative amino acid transporter	2.A.1	e - PPM (Wichers et al., 2021)	b - no	no
PF3D7_0210300	MCT1, MCP1	exports monocarboxylate	2.A.1	c - PPM	b - yes	yes
PF3D7_0926400	MCT2, MCP2	exports organic solutes, imports H ⁺	2.A.1	e - apicoplast (Boucher et al., 2018)	b - no	no
PF3D7_1036800	ACT, AT, AT1	imports acetyl-CoA, exports CoA	2.A.1.25	e - ER	b - no	yes
PF3D7_1104800	UMF	pantothenate:H ⁺ import	2.A.1.63	c - PPM	b - yes	no
PF3D7_0206200	TFP1, PAT	pantothenate:H ⁺ import (Ginsburg and Tilley, 2011)	2.A.1.66	e - PPM	b - no	yes
PF3D7_0529200	GPH	putative sugar:cation symporter	2.A.2	unknown	b - no	no
PF3D7_0715900	CDF, ZIP3	Zn ²⁺ import? (Huang et al., 2014)	2.A.4	e - cytoplasmic vesicle (Wichers et al., 2022)	b - no	yes
PF3D7_0609100	ZIP1	Zn ²⁺ import? (Ginsburg and Tilley, 2011)	2.A.5	e - PPM (Wichers et al., 2022)	b - no	yes
PF3D7_1022300	ZIPCO, ZIP2	Zn ²⁺ /Fe ²⁺ import into cytosol	2.A.5	c - PPM? (Blake et al., 2015)	b - no	yes
PF3D7_0107500	NCR1, NPC1R	cholesterol/sterol/lipid export, H ⁺ import	2.A.6.6	e - PPM	b - yes	yes
PF3D7_0715800	DMT1	organic solute transport	2.A.7.3	c - apicoplast	b - no	yes
PF3D7_0716900	DMT2	IPP export	2.A.7	e - apicoplast	b - yes	no
PF3D7_0709000	CRT	drug/peptide:H ⁺ export	2.A.7.3	e - DV	b - yes	no
PF3D7_0508300	TPT, _o TPT, _o pPT	PEP/3GP import, P _i export	2.A.7.9	e - apicoplast	b - yes	yes
PF3D7_0530200	PPT, _i TPT, _i pPT	PEP/3GP import, P _i export	2.A.7.9	e - apicoplast	b - yes (Swift et al., 2020)	yes
PF3D7_1218400	TPT3	putative organic phosphate ester:P _i antiporter	2.A.7.9	unknown	b - no	yes

(Continued)

TABLE 1 | Continued

Gene ID	Product	Substrate and function	Family	Localisation	Essential	Human ortholog
PF3D7_0505300	NGT	UDP-N-acetylglucosamine import, UMP export	2.A.7.10	c - Golgi	b - no	yes
PF3D7_1113300	UGT	UDP-galactose/UDP-glucose import, UMP export	2.A.7.11	e - ER	b - yes	yes
PF3D7_0212000	GFT	GDP-fucose import, GMP export	2.A.7.16	c - Golgi	b - yes	yes
PF3D7_0522600	NIPA	Mg ²⁺ import	2.A.7.25	e - PPM	b - yes	yes
PF3D7_0629500	AAT1	transports Ile, Leu, Met	2.A.18	c - PPM, DV	b - yes	yes
PF3D7_1208400	AAT2	transports amino acids, GABA	2.A.18	c - PPM	b - no	yes
PF3D7_1231400	AAAP3, ICM1	transports Ile, Leu, Met or Ca ²⁺ (Balestra et al., 2021)	2.A.18	unknown	b - yes	no
PF3D7_0603500	CAX, CHA	imports H ⁺ , exports Ca ²⁺ /Mg ²⁺ /Mn ²⁺	2.A.19	e - mitochondrion (Rotmann et al., 2010)	b - no	no
PF3D7_1340900	PiT	imports phosphate and Na ²⁺ into cytosol	2.A.20	e - PPM	b - yes	yes
PF3D7_0209600	NSS1	putative amino acid transporter	2.A.22	c - PPM (Blake et al., 2015)	b - yes	yes
PF3D7_0515500	GEP1, NSS2	neurotransmitter:Na ²⁺ symport (Ginsburg and Tilley, 2011)	2.A.22	c - cytoplasmic vesicle (Jiang et al., 2020)	b - no	no
PF3D7_1132500	NSS3	amino acid/GABA transport	2.A.22	c - PPM	b - no	yes
PF3D7_0714100	MAATS1	export of H ⁺ and amino acids (Ginsburg and Tilley, 2011)	2.A.22	unknown	b - no	yes
PF3D7_1368700	TPC, DNC	thiamine pyrophosphate import, nucleotide export	2.A.29	c - mitochondrion	b - yes	yes
PF3D7_0905200	MRS3, MC5	putative Fe ²⁺ importer (Blake et al., 2015)	2.A.29	c - mitochondrion	b - yes	yes
PF3D7_0407500	MTM1, MC3	unknown	2.A.29	c - mitochondrion	b - yes	yes
PF3D7_1241600	SAMC, PET8	imports S-adenosylmethionine, exports S-adenosylhomocysteine	2.A.29	e - mitochondrion	b - yes	yes
PF3D7_0108400	MME1, MC1	unknown	2.A.29	c - mitochondrion	b - no	yes
PF3D7_0108800	AMC1, MC2	unknown	2.A.29	c - mitochondrion	b - yes	no
PF3D7_0811100	AMC2, MC4	unknown	2.A.29	c - mitochondrion	b - no	yes
PF3D7_0908800	AMC3, MC6	unknown	2.A.29	c - mitochondrion	b - yes	yes
PF3D7_1037300	AAC1, ADT	ADP/ATP antiporter (Blake et al., 2015)	2.A.29	e - mitochondrion (Hatin et al., 1992)	b - yes	yes
PF3D7_1004800	AAC2, PAAC	ADP/ATP antiporter (Blake et al., 2015)	2.A.29	c - mitochondrion (van Esveld et al., 2021)	b - yes	yes
PF3D7_1223800	COC, YHM2	imports oxoglutarate, exports citrate	2.A.29	c - mitochondrion	b - no	yes
PF3D7_0823900	DTC, OMT	imports dicarboxylate, exports tricarboxylate	2.A.29	e - mitochondrion	b - yes	yes
PF3D7_1202200	MPC, PIC, PIC2	P _i /H ⁺ import	2.A.29	c - mitochondrion	b - no	yes
PF3D7_1303500	NHE	H ⁺ import into cytosol in exchange for Na ⁺	2.A.36	c - PPM (Blake et al., 2015)	b - no	yes
PF3D7_0924500		putative Na ⁺ :H ⁺ exchanger (Saier et al., 2016)	2.A.36	unknown	b - yes	yes
PF3D7_0827700	MgT1	Mg ²⁺ :H ⁺ antiporter (Blake et al., 2015)	2.A.36	unknown	b - no	yes
PF3D7_1135000		unknown	2.A.43	c - apicoplast (Boucher et al., 2018)	unknown	no
PF3D7_0316600	FNT	lactate/formate and H ⁺ release from cytosol	2.A.44	e - PPM, DV	b - no	no
PF3D7_1471200	SulP	inorganic anion antiporter	2.A.53	e - PPM	b - yes	yes
PF3D7_0523800	NRAMP2, NRAMP, FVRT1	Fe ²⁺ /Mn ²⁺ :H ⁺ export	2.A.55	e - DV (Wichers et al., 2022)	b - yes	yes
PF3D7_1347200	NT1, ENT1	purine base import	2.A.57	e - PPM	b - yes	no
PF3D7_0824400	NT2, ENT2	nucleoside/nucleobase import	2.A.57	e - ER	b - no	no
PF3D7_1469400	NT3, ENT3	putative nucleoside transporter	2.A.57	unknown	b - no	no
PF3D7_0103200	NT4, ENT4	adenine/adenosine import	2.A.57	c - PPM	b - yes	no
PF3D7_0212800	MATE	putative organic solute:Na ⁺ /H ⁺ antiporter	2.A.66.1	unknown	b - no	yes
PF3D7_0828600	FT1	imports pABA and folates	2.A.71	e - PPM	b - no	no
PF3D7_1116500	FT2	imports pABA, folates, 5-methyltetrahydrofolate	2.A.71	e - PPM	b - no	no
PF3D7_1223700	VIT	imports Fe ²⁺ for detoxification, exports H ⁺	2.A.89	unknown	b - no	no
PF3D7_0417300	LETM1	imports H ⁺ , exports Ca ²⁺ /K ⁺	2.A.97	c - mitochondrion (van Esveld et al., 2021)	b - yes	yes
PF3D7_1340800	MPC1	pyruvate:H ⁺ importer	2.A.105	c - mitochondrion	b - yes	yes

(Continued)

TABLE 1 | Continued

Gene ID	Product	Substrate and function	Family	Localisation	Essential	Human ortholog
PF3D7_1470400	MPC2	pyruvate:H ⁺ importer	2.A.105	c - mitochondrion	unknown	yes
PF3D7_1033000	HPR1, AMC4	unknown	2.A.123	c - mitochondrion? (van Esveld et al., 2021)	b - yes	no
PF3D7_0216600	SWEET	putative glucose/galactose transporter	2.A.123	c - ER/Golgi	b - yes	yes
PF3D7_0305300		unknown	2.A.123	unknown	b - no	no
PF3D7_0523000	MDR1, ABCB1, Pgh1	active drug and solute import (Friedrich et al., 2014)	3.A.1.201	e - DV (Papalexis et al., 2001)	b - yes	yes
PF3D7_1447900	MDR2, ABCB2	active Cd ²⁺ extrusion from cytosol	3.A.1.210	e - PPM, DV	b - no (van der Velden et al., 2015)	yes
PF3D7_1145500	MDR3, ABCB3	active peptide efflux	3.A.1.209	e - apicoplast (Boucher et al., 2018)	b - no	yes
PF3D7_0302600	MDR4, ABCB4	active peptide/heavy metal cation transport	3.A.1.209	e - apicoplast	b - no	yes
PF3D7_1339900	MDR5, ABCB5	active solute export	3.A.1.201	e - PPM	b - no	yes
PF3D7_1352100	MDR6, ABCB6, Atm1	active glutathione trisulfide efflux	3.A.1.210	c - mitochondrion, apicoplast	b - yes	yes
PF3D7_1209900	MDR7, ABCB7	active peptide efflux	3.A.1.209	c - mitochondrion	b - no	yes
PF3D7_0112200	MRP1, ABCC1	active export of drugs and glutathione conjugates	3.A.1.208	e - PPM	b - no	yes
PF3D7_1229100	MRP2, ABCC2	active export of glutathione conjugates	3.A.1.208	e - PPM	b - no	yes
PF3D7_0813700	ABCF1	heme import? (Blake et al., 2015)	3.A.1	e - apicoplast (Boucher et al., 2018)	b - yes	yes
PF3D7_1426500	ABCG, ABCG1, ABCG2	putative cell metabolite exporter (Edaye and Georges, 2015)	3.A.1.204	e - PPM (Edaye and Georges, 2015)	b - no	yes
PF3D7_0319700	ABCI3	active solute transport (Murithi et al., 2021)	3.A.1	e - cytoplasmic vesicle (Murithi et al., 2021)	unknown	yes
PF3D7_0810200	ABCK1	active peptide efflux (Ginsburg and Tilley, 2011)	3.A.1	c - mitochondrion (van Esveld et al., 2021)	b - yes	yes
PF3D7_1004600		drug transport? (Park et al., 2012)	3.A.1	unknown	b - no	no
PF3D7_0812900		drug transport? (Park et al., 2012)	3.A.1	unknown	b - no	no
PF3D7_1434000	CAF16	putative ABC transporter (Blake et al., 2015)	3.A.1	unknown	b - yes	yes
PF3D7_0614900		unknown	3.A.1	c - PPM (Blake et al., 2015)	b - no	yes
PF3D7_1144700	TIC20	protein import across innermost membrane (Agrawal and Striepen, 2010)	3.A.1	c - apicoplast (Boucher et al., 2018)	b - yes	no
PF3D7_1121600	EXP1	pore for solutes < 1.4 kDa with EXP2 (Mesén-Ramírez et al., 2019)	3.A.1	e - PVM (Mesén-Ramírez et al., 2019)	b - yes (Maier et al., 2008)	no
PF3D7_0217100	ATP α , F ₁ α	H ⁺ -importing ATP synthase subunits	3.A.2	e - mitochondrion	b - yes	yes
PF3D7_1235700	ATP β , F ₁ β				b - no	yes
PF3D7_1311300	ATP γ , F ₁ γ				b - yes	yes
PF3D7_1147700	ATP δ , F ₁ δ				b - no	no
PF3D7_0715500	ATP ϵ , F ₁ ϵ				b - no	no
PF3D7_1310000	OSCP				b - yes	yes
PF3D7_0719100	F ₀ a				b - yes	no
PF3D7_1125100	F ₀ b				b - yes	no
PF3D7_0705900	F ₀ c				b - yes	yes
PF3D7_0311800	F ₀ d				b - yes	no

(Continued)

TABLE 1 | Continued

Gene ID	Product	Substrate and function	Family	Localisation	Essential	Human ortholog
PF3D7_1311900	vapA, V ₁ subunit A	V-ATPase subunits: active H ⁺ export from cytosol	3.A.2	e - PPM, DV, cytoplasmic vesicle (Hayashi et al., 2000)	b - yes	yes
PF3D7_0406100	vapB, V ₁ subunit B				b - yes	yes
PF3D7_0106100	vapC, V ₁ subunit C				b - yes	yes
PF3D7_1341900	vapD, V ₁ subunit D				b - yes	yes
PF3D7_0934500	vapE, V ₁ subunit E				b - yes	yes
PF3D7_1140100	vapF, V ₁ subunit F				b - no	yes
PF3D7_1323200	vapG, V ₁ subunit G				b - yes	no
PF3D7_1306600	vapH, V ₁ subunit H				b - yes	yes
PF3D7_0806800	V _o subunit a				b - yes	yes
PF3D7_0519200	V _o subunit c, 16-kDa proteolipid				b - no	yes
PF3D7_1354400	V _o subunit c*, 21-kDa proteolipid	extrusion of inorganic cations from cytosol	3.A.3	e - PPM, DV	b - yes	yes
PF3D7_1464700	V _o subunit d, C/AC39				b - yes	yes
PF3D7_0721900	V _o subunit e				b - yes	no
PF3D7_0516100	ATP1				b - no	yes
PF3D7_1219600	ATP2				b - yes	yes
PF3D7_0504000	ATP3				b - yes	yes
PF3D7_1211900	ATP4				b - yes	yes
PF3D7_0106300	ATP6				b - yes	yes
PF3D7_0319000	ATP7				b - no	yes
PF3D7_1223400	ATP8				b - yes	yes
PF3D7_1348800	ATP9	active Ca ²⁺ import?	3.A.3	c - DV?	b - no	yes
PF3D7_0727800	ATP10		3.A.3	c - apicoplast	b - yes	yes
PF3D7_1468600	ATP11		3.A.3	c - PPM (Blake et al., 2015)	b - no	yes
PF3D7_0904900	CuTP		3.A.3	e - EPM, PPM	b - no	yes
PF3D7_1138400	GCα	phospholipid flippase	3.A.3	c - cytoplasmic vesicle (Jiang et al., 2020)	b - yes (Taylor et al., 2008)	yes
PF3D7_1360500	GCβ	phospholipid flippase	3.A.3	c - PPM	b - no	yes
PF3D7_1346100	SEC61α	components of ER translocon for import of proteins destined for export, interact with SEC62 (Marapana et al., 2018)	3.A.5	e - ER (Marapana et al., 2018)	b - no	yes
PF3D7_0821800	SEC61β				b - no	yes
PF3D7_0210000	SEC61γ				b - yes	yes
PF3D7_1318800	SEC63	components of TIM23/PAM complex for protein import across inner membrane (Sheiner and Soldati-Favre, 2008; Schmidt et al., 2010)	3.A.8	c - mitochondrion (van Esveld et al., 2021)	b - yes	yes
PF3D7_0724400	TIM14, PAM18				b - yes	yes
PF3D7_0513500	TIM16, PAM16				unknown	no
PF3D7_1434700	TIM17				b - yes	yes
PF3D7_1356200	TIM23				b - yes	no
PF3D7_1125400	TIM44				b - yes	yes
PF3D7_0726900	TIM50				b - yes	yes
PF3D7_0627400	TIM22				b - yes	yes
PF3D7_1456800	VP1	active H ⁺ export	3.A.10	e - PPM (Ahiya et al., 2022)	b - yes	no
PF3D7_1235200	VP2	putative Ca ²⁺ -dependent H ⁺ export from cytosol	3.A.10	e - PPM, cytoplasmic	b - no	no

(Continued)

TABLE 1 | Continued

Gene ID	Product	Substrate and function	Family	Localisation	Essential	Human ortholog
PF3D7_0810400	AQP2	water channel (Blake et al., 2015)	3.A.16	vesicles (Marchesini et al., 2000) c - PPM (Blake et al., 2015)	b - no	no
PF3D7_0314300	Der1-1	protein import across periplastid membrane (Spork et al., 2009)	3.A.25.2.1	e - apicoplast (Spork et al., 2009)	b - yes	no
PF3D7_1452300	Der1-2	protein import across periplastid membrane (Spork et al., 2009)	3.A.25.2.1	e - apicoplast (Spork et al., 2009)	unknown	yes
PF3D7_0216800		unknown	3.A.25	unknown	b - yes	yes
PF3D7_0315700		unknown	3.A.25	unknown	b - no	no
PF3D7_1471100	EXP2	PTEX core components for protein export (Beck and Ho, 2021), EXP2 also functions as a pore for solutes < 1.4 kDa together with EXP1 (Garten et al., 2018; Mesén-Ramírez et al., 2019)	3.A.26.1.1	e - PVM (de Koning-Ward et al., 2009)	b - yes	no
PF3D7_1436300	PTEX150				b - yes (de Koning-Ward et al., 2009)	no
PF3D7_1116800	HSP101				b - yes	yes
PF3D7_1404600	AC α	putative K ⁺ channel	8.A.85	unknown	b - no	no
PF3D7_1022700	PLSCR	phospholipid scramblase (Haase et al., 2021)	9.A.36	e - parasite periphery (Haase et al., 2021)	b - no	no
PF3D7_1332100		putative transporter	9.B.14	unknown	b - no	no
PF3D7_0530500		putative transporter	9.B.14	unknown	b - no	no
PF3D7_0628400		unknown	9.B.14	unknown	b - no	no
PF3D7_1135300	PMRT1	unknown	9.B.14	e - PPM (Wichers et al., 2022)	b, g - yes (Wichers et al., 2022)	no
PF3D7_1022200	FBT	putative metabolite/vitamin transporter (Ginsburg and Tilley, 2011)	9.B.14	unknown	b - yes	no
PF3D7_0321900	CARL	unknown	9.B.314	e - cis-Golgi (LaMonte et al., 2016)	b - no	yes
PF3D7_0824700	LMF1	putative transporter	9.B.365.5.1	c - ER (Blake et al., 2015)	b - no	yes

Substrates, functions, and localisations are indicated as in Martin (2020), unless stated otherwise. Known or putative localisation refers to the site of active function of the transport protein regardless of its trafficking route, as evidenced either by experimental data (e) or computational analysis (c). DV: digestive vacuole, EPM, erythrocyte plasma membrane; PPM, parasite plasma membrane; PVM, parasitophorous vacuole membrane. Transporter families were assigned according to the Transport Classification Database (Saler et al., 2016). 1: channels and pores, 1.A: α -type channels, 1.B: β -barrel porins, 1.C: pore-forming toxins. 2: electrochemical potential-driven transporters, 2.A: porters (uniporters, symporters, antiporters), 3: primary active transporters, 3.A: P-P-bond-hydrolysis-driven transporters, 8: accessory factors involved in transport, 8.A: auxiliary transport proteins, 9: incompletely characterised transport systems, 9.A: recognised transporters of unknown biochemical mechanism, 9.B: putative transport proteins. Predicted gene essentiality refers to Zhang et al. (2018), unless another reference is given. The tested life cycle stages are indicated as b, asexual blood stage; g, gametocytes; o, ookinetes; s, sporozoites. Information on the presence of human orthologs is listed according to https://mpmp.huji.ac.il/maps/orth_hsap.html (Ginsburg and Tilley, 2011).

Another putative intracellular Ca²⁺ pool may consist of acidocalcisomes – small electron-dense vesicles that are conserved from bacteria to humans and contain high concentrations of Ca²⁺, pyrophosphate, polyphosphate, iron, and zinc (Huang et al., 2014). Accordingly, acidocalcisome membranes contain a variety of specific transporters for these substrates across the tree of life (Huang et al., 2014). While many transporters were shown to reside in the acidocalcisome membrane in *Trypanosoma brucei* through proteomic studies and microscopy (Huang et al., 2014), no protein has been definitely localised to these organelles in *P. falciparum* (Magowan et al., 1997; Ruiz et al., 2004). Their low internal pH is likely required for the secondary active import of various ions and thought to be established and maintained by the plant-like H⁺-pump V-ATPase (Wunderlich et al., 2012; de Oliveira et al., 2021). This has yet to be verified experimentally, and there may be differences between parasite species. For

example, *PfVFP1* (PF3D7_1456800), an ortholog of the acidocalcisome marker in *T. brucei* (Huang et al., 2014) and *T. gondii* (Rohloff et al., 2011), was previously suggested to localise to the parasite plasma membrane (PPM), DV and acidocalcisomes in *P. falciparum*, but could only be detected at the PPM by microscopy (Ahiya et al., 2022).

Other proteins that may translocate calcium and whose subcellular localisation has not yet been confirmed are *PfATP9* (PF3D7_1348800), the putative calcium channel PF3D7_1331500, and *PfICM1* (PF3D7_1231400). Elucidating their location and function is an important knowledge gap to be addressed (Kustatscher et al., 2022). Of the aforementioned putative Ca²⁺ transport proteins, *PfICM1* and *PfHlyIII* may be worth exploring as drug targets due to their predicted essentiality and the absence of human counterparts.

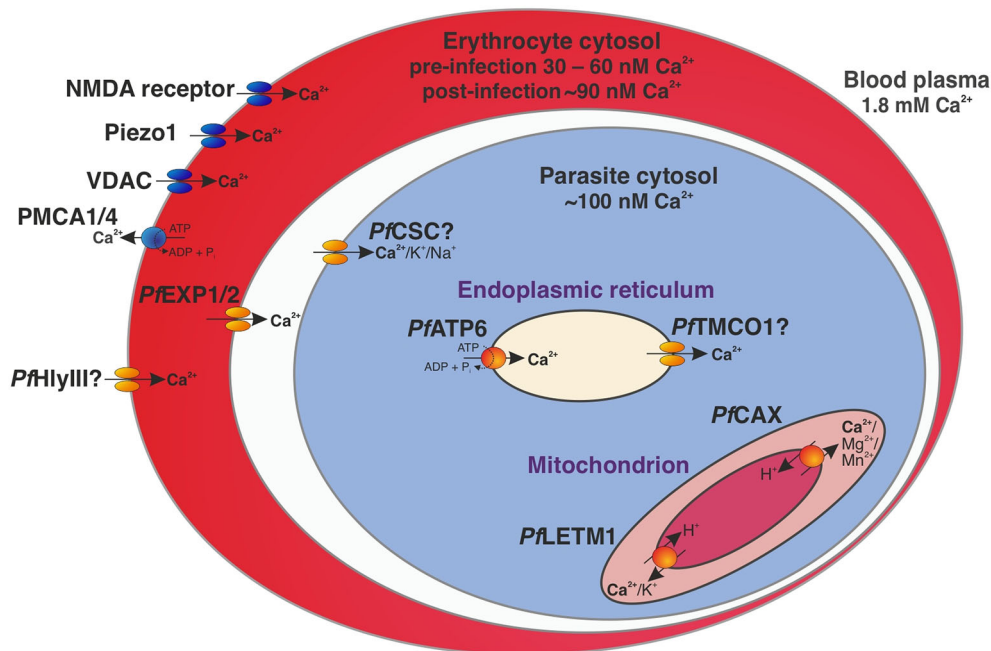


FIGURE 1 | Calcium homeostasis in a trophozoite-stage *P. falciparum*-infected erythrocyte. Under resting conditions, the concentration of free Ca^{2+} is ~1.8 mM in the blood plasma, 30 – 60 nM in cytosol of an uninfected erythrocyte (Brochet and Billker, 2016), ~90 nM in the cytosol of the infected erythrocyte (Rohrbach et al., 2005), and ~100 nM in the cytosol of *P. falciparum* (Garcia et al., 1996). Transport proteins affecting intracellular calcium concentrations in the parasite-infected erythrocyte include the human P-type plasma membrane Ca^{2+} -ATPases (PMCA) 1 and 4, human Piezo1, the erythroid N-methyl D-aspartate (NMDA) receptor, the voltage-dependent anion channel (VDAC) (Kaestner et al., 2020), and likely the parasite-encoded hemolysin III (*PfHlyIII*) (Moonah et al., 2014). A nutrient pore formed by *PfEXP1* and *PfEXP2* mediates passage through the parasitophorous vacuole membrane (Garten et al., 2018; Mesén-Ramírez et al., 2019) and the calcium-permeable stress-gated cation channel *PfCSC* may be responsible for Ca^{2+} entry into the parasite cytosol (Martin, 2020). The SERCA-type Ca^{2+} -ATPase *PfATP6* actively imports Ca^{2+} into the endoplasmic reticulum as an intracellular reservoir (Lourido and Moreno, 2015; Martin, 2020), while the putative calcium load-activated calcium channel *PfTMCO1* (Gupta et al., 2022) may release ions back into the cytosol to avoid overload (Lourido and Moreno, 2015; Wang et al., 2016). Ca^{2+} efflux from the mitochondrion is likely mediated by the cation/ H^+ antiporters *PfCAX* (Rotmann et al., 2010) and *PfLETM1* (Martin, 2020) via secondary active transport. Human-encoded transporters and channels are shown in blue and parasite-encoded proteins in orange.

CONCLUSIONS AND FUTURE PERSPECTIVES

This mini review consolidates data from various databases and provides an up-to-date overview of the subcellular localisation, function, predicted essentiality, and human orthologs of *P. falciparum* transporters for the fast identification of essential parasite transporters without human orthologs that may be promising novel targets for therapeutic development. Many of these candidates localise to the apicoplast, the mitochondrion, or the digestive vacuole, which are known to be “druggable” (Wunderlich et al., 2012; Oberstaller et al., 2021).

Moreover, the new transporter list will improve gene annotations and serve as a basis for further functional characterisation of the proteins. It will also be useful for systems biology approaches as it allows more reliable screening of e.g. genomic, transcriptomic, and proteomic data for *P. falciparum* transporters. The low coverage of the *P. falciparum* membrane proteome that complicates target profiling (Lu et al., 2021) may be overcome by large-scale culturing (Dalton et al., 2012) and more sensitive mass spectrometry techniques (McClure and Williams, 2018). Chemogenomic and transcriptional profiling of mutant-

parasite libraries with altered drug sensitivities will further guide the determination of the mechanisms of drug action (Adjalley et al., 2015; Pradhan et al., 2015).

AUTHOR CONTRIBUTIONS

The author confirms being the sole contributor of this work and has approved it for publication.

FUNDING

JW was supported by the Boehringer Ingelheim Foundation and the European Research Council under the European Union’s Horizon 2020 Research and Innovation Programme (grant agreement 759534).

ACKNOWLEDGMENTS

The author thanks Jan Strauss for providing many helpful tips and gratefully acknowledges Silvia Portugal and Eileen Devaney for critical reading of the manuscript.

REFERENCES

- Adjalley, S. H., Scanfeld, D., Kozlowski, E., Llinas, M., and Fidock, D. A. (2015). Genome-Wide Transcriptome Profiling Reveals Functional Networks Involving the *Plasmodium Falciparum* Drug Resistance Transporters PfCRT and Pfmdr1. *BMC Genomics* 16, 1090. doi: 10.1186/s12864-015-2320-8
- Agrawal, S., and Striepen, B. (2010). More Membranes, More Proteins: Complex Protein Import Mechanisms Into Secondary Plastids. *Protist* 161 (5), 672–687. doi: 10.1016/j.protis.2010.09.002
- Ahiya, A. I., Bhatnagar, S., Morrissey, J. M., Beck, J. R., and Vaidya, A. B. (2022). Dramatic Consequences of Reducing Erythrocyte Membrane Cholesterol on Plasmodium Falciparum. *Microbiol. Spectr.* 10 (1), e0015822. doi: 10.1128/spectrum.00158-22
- Altschul, S. F., Madden, T. L., Schäffer, A. A., Zhang, J., Zhang, Z., Miller, W., et al (1997). Gapped BLAST and PSI-BLAST: A New Generation of Protein Database Search Programs. *Nucleic Acids Res.* 25 (17), 3389–3402. doi: 10.1093/nar/25.17.3389
- Anantharaman, V., Iyer, L. M., Balaji, S., and Aravind, L. (2007). Adhesion Molecules and Other Secreted Host-Interaction Determinants in Apicomplexa: Insights From Comparative Genomics. *Int. Rev. Cytol.* 262, 1–74. doi: 10.1016/S0074-7696(07)62001-4
- Aurrecochea, C., Brestelli, J., Brunk, B. P., Dommer, J., Fischer, S., Gajria, B., et al. (2009). PlasmoDB: A Functional Genomic Database for Malaria Parasites. *Nucleic Acids Res.* 37 (Database issue), D539–D543. doi: 10.1093/nar/gkn814
- Balestra, A. C., Koussis, K., Klages, N., Howell, S. A., Flynn, H. R., Bantscheff, M., et al (2021). Ca²⁺ Signals Critical for Egress and Gametogenesis in Malaria Parasites Depend on a Multipass Membrane Protein That Interacts With PKG. *Sci. Adv.* 7 (13), eabe5396. doi: 10.1126/sciadv.abe5396
- Beck, J. R., and Ho, C. M. (2021). Transport Mechanisms at the Malaria Parasite-Host Cell Interface. *PLoS Pathog.* 17 (4), e1009394. doi: 10.1371/journal.ppat.1009394
- Belete, T. M. (2020). Recent Progress in the Development of New Antimalarial Drugs With Novel Targets. *Drug Des. Devel. Ther.* 14, 3875–3889. doi: 10.2147/DDDT.S265602
- Blake, J. A., Christie, K. R., Dolan, M. E., Drabkin, H. J., Hill, D. P., Ni, L., et al (2015). Gene Ontology Consortium: Going Forward. *Nucleic Acids Res.* 43 (D1), D1049–D1056. doi: 10.1093/nar/gku1179
- Böhme, U., Otto, T. D., Sanders, M., Newbold, C. I., and Berriman, M. (2019). Progression of the Canonical Reference Malaria Parasite Genome From 2002–2019. *Wellcome Open Res.* 4, 58. doi: 10.12688/wellcomeopenres.15194.1
- Boucher, M. J., Ghosh, S., Zhang, L., Lal, A., Jang, S. W., Ju, A., et al (2018). Integrative Proteomics and Bioinformatic Prediction Enable a High-Confidence Apicoplast Proteome in Malaria Parasites. *PLoS Biol.* 16 (9), e2005895. doi: 10.1371/journal.pbio.2005895
- Bouyer, G., Cuffe, A., Egée, S., Kmiecik, J., Maksimova, Y., Glogowska, E., et al (2011). Erythrocyte Peripheral Type Benzodiazepine Receptor/Voltage-Dependent Anion Channels are Upregulated by Plasmodium Falciparum. *Blood* 118 (8), 2305–2312. doi: 10.1182/blood-2011-01-329300
- Brochet, M., and Billker, O. (2016). Calcium Signalling in Malaria Parasites. *Mol. Microbiol.* 100 (3), 397–408. doi: 10.1111/mmi.13324
- Bullen, H. E., Sanders, P. R., Dans, M. G., Jonsdottir, T. K., Riglar, D. T., Looker, O., et al (2022). The Plasmodium Falciparum Parasitophorous Vacuole Protein P113 Interacts With the Parasite Protein Export Machinery and Maintains Normal Vacuole Architecture. *Mol. Microbiol.* 117 (5), 1245–1262. doi: 10.1111/mmi.14904
- Cowell, A. N., and Winzeler, E. A. (2019). Advances in Omics-Based Methods to Identify Novel Targets for Malaria and Other Parasitic Protozoan Infections. *Genome Med.* 11 (1), 63. doi: 10.1186/s13073-019-0673-3
- Dalton, J. P., Demanga, C. G., Reiling, S. J., Wunderlich, J., Eng, J. W., and Rohrbach, P. (2012). Large-Scale Growth of the Plasmodium Falciparum Malaria Parasite in a Wave Bioreactor. *Int. J. Parasitol.* 42 (3), 215–220. doi: 10.1016/j.ijpara.2012.01.001
- Das, S., Lemgruber, L., Tay, C. L., Baum, J., and Meissner, M. (2017). Multiple Essential Functions of Plasmodium Falciparum Actin-1 During Malaria Blood-Stage Development. *BMC Biol.* 15 (1), 70. doi: 10.1186/s12915-017-0406-2
- de Koning-Ward, T. F., Gilson, P. R., Boddey, J. A., Rug, M., Smith, B. J., Papenfuss, A. T., et al (2009). A Newly Discovered Protein Export Machine in Malaria Parasites. *Nature* 459 (7249), 945–949. doi: 10.1038/nature08104
- de Oliveira, L. S., Alborghetti, M. R., Carneiro, R. G., Bastos, I. M. D., Amino, R., Grellier, P., et al (2021). Calcium in the Backstage of Malaria Parasite Biology. *Front. Cell Infect. Microbiol.* 11, 708834. doi: 10.3389/fcimb.2021.708834
- Desai, S. A. (2012). Ion and Nutrient Uptake by Malaria Parasite-Infected Erythrocytes. *Cell Microbiol.* 14 (7), 1003–1009. doi: 10.1111/j.1462-5822.2012.01790.x
- Doolan, D. L., Mu, Y., Unal, B., Sundares, S., Hirst, S., Valdez, C., et al (2008). Profiling Humoral Immune Responses to P. Falciparum Infection With Protein Microarrays. *Proteomics* 8 (22), 4680–4694. doi: 10.1038/nature08104
- Edaye, S., and Georges, E. (2015). Characterization of Native PfABCG Protein in Plasmodium Falciparum. *Biochem. Pharmacol.* 97 (2), 137–146. doi: 10.1016/j.bcp.2015.06.035
- Elbourne, L. D., Tetu, S. G., Hassan, K. A., and Paulsen, I. T. (2017). TransportDB 2.0: A Database for Exploring Membrane Transporters in Sequenced Genomes From All Domains of Life. *Nucleic Acids Res.* 45 (D1), D320–D324. doi: 10.1093/nar/gkw1068
- Ferreira, J. L., Heinicke, D., Wichers, J. S., Liffner, B., Wilson, D. W., and Gilberger, T. W. (2020). The Dynamic Roles of the Inner Membrane Complex in the Multiple Stages of the Malaria Parasite. *Front. Cell Infect. Microbiol.* 10, 611801. doi: 10.3389/fcimb.2020.611801
- Friedrich, O., Reiling, S. J., Wunderlich, J., and Rohrbach, P. (2014). Assessment of Plasmodium Falciparum PfMDR1 Transport Rates Using Fluo-4. *J. Cell Mol. Med.* 18 (9), 1851–1862. doi: 10.1111/jcmm.12313
- Garcia, C., Dluzewski, A., Catalani, L., Burtin, R., Hoyland, J., and Mason, W. (1996). Calcium Homeostasis in Intraerythrocytic Malaria Parasites. *Eur. J. Cell Biol.* 71 (4), 409–413.
- Garg, S., Agarwal, S., Kumar, S., Yazdani, S. S., Chitnis, C. E., and Singh, S. (2013). Calcium-Dependent Permeabilization of Erythrocytes by a Perforin-Like Protein During Egress of Malaria Parasites. *Nat. Commun.* 4, 1736. doi: 10.1038/ncomms2725
- Garten, M., Nasamu, A. S., Niles, J. C., Zimmerberg, J., Goldberg, D. E., and Beck, J. R. (2018). EXP2 is a Nutrient-Permeable Channel in the Vacuolar Membrane of Plasmodium and is Essential for Protein Export via PTEX. *Nat. Microbiol.* 3 (10), 1090–1098. doi: 10.1038/s41564-018-0222-7
- Gaudet, P., Livstone, M. S., Lewis, S. E., and Thomas, P. D. (2011). Phylogenetic-Based Propagation of Functional Annotations Within the Gene Ontology Consortium. *Brief Bioinform.* 12 (5), 449–462. doi: 10.1093/bib/bbr042
- Ginsburg, H., and Tilley, L. (2011). Plasmodium Falciparum Metabolic Pathways (MPMP) Project Upgraded With a Database of Subcellular Locations of Gene Products. *Trends Parasitol.* 27 (7), 285–286. doi: 10.1016/j.pt.2011.03.001
- Gupta, Y., Goicoechea, S., Pearce, C. M., Mathur, R., Romero, J. G., Kwofie, S. K., et al (2022). The Emerging Paradigm of Calcium Homeostasis as a New Therapeutic Target for Protozoan Parasites. *Med. Res. Rev.* 42 (1), 56–82. doi: 10.1002/med.21804
- Haase, S., Condron, M., Miller, D., Cherkaoui, D., Jordan, S., Gulbis, J. M., et al (2021). Identification and Characterisation of a Phospholipid Scramblase in the Malaria Parasite Plasmodium Falciparum. *Mol. Biochem. Parasitol.* 243, 111374. doi: 10.1016/j.molbiopara.2021.111374
- Hatin, I., Jambou, R., Ginsburg, H., and Jaureguiberry, G. (1992). Single or Multiple Localization of ADP/ATP Transporter in Human Malarial Plasmodium Falciparum. *Biochem. Pharmacol.* 43 (1), 71–75. doi: 10.1016/0006-2952(92)90663-4
- Hayashi, M., Yamada, H., Mitamura, T., Horii, T., Yamamoto, A., and Moriyama, Y. (2000). Vacuolar H⁺-ATPase Localized in Plasma Membranes of Malaria Parasite Cells, Plasmodium Falciparum, is Involved in Regional Acidification of Parasitized Erythrocytes. *J. Biol. Chem.* 275 (44), 34353–34358. doi: 10.1074/jbc.M003323200
- Huang, G., Ulrich, P. N., Storey, M., Johnson, D., Tischer, J., Tovar, J. A., et al (2014). Proteomic Analysis of the Acidocalcisome, an Organelle Conserved From Bacteria to Human Cells. *PLoS Pathog.* 10 (12), e1004555. doi: 10.1371/journal.ppat.1004555
- Jiang, Y., Wei, J., Cui, H., Liu, C., Zhi, Y., Jiang, Z., et al (2020). An Intracellular Membrane Protein GEPI Regulates Xanthurenic Acid Induced Gametogenesis of Malaria Parasites. *Nat. Commun.* 11 (1), 1764. doi: 10.1038/s41467-020-15479-3

- Kaestner, L., Bogdanova, A., and Egee, S. (2020). Calcium Channels and Calcium-Regulated Channels in Human Red Blood Cells. *Adv. Exp. Med. Biol.* 1131, 625–648. doi: 10.1007/978-3-030-12457-1_25
- Koenderink, J. B., Kavishe, R. A., Rijpma, S. R., and Russel, F. G. (2010). The ABCs of Multidrug Resistance in Malaria. *Trends Parasitol.* 26 (9), 440–446. doi: 10.1016/j.pt.2010.05.002
- Kustatscher, G., Collins, T., Gingras, A. C., Guo, T., Hermjakob, H., Ideker, T., et al (2022). Understudied Proteins: Opportunities and Challenges for Functional Proteomics. *Nat. Methods.* doi: 10.1038/s41592-022-01454-x
- LaMonte, G., Lim, M. Y., Wree, M., Reimer, C., Nachon, M., Corey, V., et al (2016). Mutations in the *Plasmodium Falciparum* Cyclic Amine Resistance Locus (PfCARL) Confer Multidrug Resistance. *mBio* 7 (4), e00696–e00616. doi: 10.1128/mBio.00696-16
- Le Roch, K. G., Zhou, Y., Blair, P. L., Grainger, M., Moch, J. K., Haynes, J. D., et al (2003). Discovery of Gene Function by Expression Profiling of the Malaria Parasite Life Cycle. *Science* 301 (5639), 1503–1508. doi: 10.1126/science.1087025
- Lourido, S., and Moreno, S. N. (2015). The Calcium Signaling Toolkit of the Apicomplexan Parasites *Toxoplasma Gondii* and *Plasmodium* Spp. *Cell Calcium* 57 (3), 186–193. doi: 10.1016/j.ceca.2014.12.010
- Ludin, P., Woodcroft, B., Ralph, S. A., and Mäser, P. (2012). *In Silico* Prediction of Antimalarial Drug Target Candidates. *Int. J. Parasitol. Drugs Drug Resist.* 2, 191–199. doi: 10.1016/j.ijddr.2012.07.002
- Lu, K. Y., Mansfield, C. R., Fitzgerald, M. C., and Derbyshire, E. R. (2021). Chemoproteomics for *Plasmodium* Parasite Drug Target Discovery. *ChemBiochem* 22 (16), 2591–2599. doi: 10.1002/cbic.202100155
- Magowan, C., Brown, J. T., Liang, J., Heck, J., Coppel, R. L., Mohandas, N., et al (1997). Intracellular Structures of Normal and Aberrant *Plasmodium Falciparum* Malaria Parasites Imaged by Soft X-Ray Microscopy. *Proc. Natl. Acad. Sci. U.S.A.* 94 (12), 6222–6227. doi: 10.1073/pnas.94.12.6222
- Maier, A. G., Rug, M., O'Neill, M. T., Brown, M., Chakravorty, S., Szelestak, T., et al (2008). Exported Proteins Required for Virulence and Rigidity of *Plasmodium Falciparum*-Infected Human Erythrocytes. *Cell* 134 (1), 48–61. doi: 10.1016/j.cell.2008.04.051
- Marapana, D. S., Dagley, L. F., Sandow, J. J., Nebl, T., Triglia, T., Pasternak, M., et al (2018). Plasmepsin V Cleaves Malaria Effector Proteins in a Distinct Endoplasmic Reticulum Translocation Interactome for Export to the Erythrocyte. *Nat. Microbiol.* 3 (9), 1010–1022. doi: 10.1038/s41564-018-0219-2
- Marchesini, N., Luo, S., Rodrigues, C. O., Moreno, S. N., and Docampo, R. (2000). Acidocalcisomes and a Vacuolar H⁺-Pyrophosphatase in Malaria Parasites. *Biochem. J.* 347 (Pt 1), 243–253. doi: 10.1042/bj3470243
- Martin, R. E. (2020). The Transportome of the Malaria Parasite. *Biol. Rev. Camb. Philos. Soc.* 95 (2), 305–332. doi: 10.1111/brv.12565
- Mather, M. W., Henry, K. W., and Vaidya, A. B. (2007). Mitochondrial Drug Targets in Apicomplexan Parasites. *Curr. Drug Targets* 8 (1), 49–60. doi: 10.2174/138945007779315632
- McClure, R. A., and Williams, J. D. (2018). Impact of Mass Spectrometry-Based Technologies and Strategies on Chemoproteomics as a Tool for Drug Discovery. *ACS Med. Chem. Lett.* 9 (8), 785–791. doi: 10.1021/acsmchemlett.8b00181
- Mesén-Ramírez, P., Bergmann, B., Tran, T. T., Garten, M., Stäcker, J., Naranjo-Prado, I., et al (2019). EXP1 Is Critical for Nutrient Uptake Across the Parasitophorous Vacuole Membrane of Malaria Parasites. *PLoS Biol.* 17 (9), e3000473. doi: 10.1371/journal.pbio.3000473
- Monteiro Júnior, J. C., Krüger, A., Palmisano, G., and Wrenger, C. (2022). Transporter-Mediated Solutes Uptake as Drug Target in *Plasmodium Falciparum*. *Front. Pharmacol.* 13, 845841. doi: 10.3389/fphar.2022.845841
- Moonah, S., Sanders, N. G., Persichetti, J. K., and Sullivan, D. J. Jr. (2014). Erythrocyte Lysis and *Xenopus Laevis* Oocyte Rupture by Recombinant *Plasmodium Falciparum* Hemolysin III. *Eukaryot. Cell.* 13 (10), 1337–1345. doi: 10.1128/EC.00088-14
- Murithi, J. M., Deni, I., Pasaje, C. F. A., Okombo, J., Bridgford, J. L., Gnädig, N. F., et al (2021). The *Plasmodium Falciparum* ABC Transporter ABCI3 Confers Parasite Strain-Dependent Pleiotropic Antimalarial Drug Resistance. *Cell Chem. Biol.* 28, 1–16. doi: 10.1016/j.chembiol.2021.06.006
- Nacer, A., Roux, E., Pomel, S., Scheidig-Benatar, C., Sakamoto, H., Lafont, F., et al (2011). Clag9 Is Not Essential for PfEMP1 Surface Expression in non-Cytoadherent *Plasmodium Falciparum* Parasites With a Chromosome 9 Deletion. *PLoS One* 6 (12), e29039. doi: 10.1371/journal.pone.0029039
- Oberstaller, J., Otto, T. D., Rayner, J. C., and Adams, J. H. (2021). Essential Genes of the Parasitic Apicomplexa. *Trends Parasitol.* 37 (4), 304–316. doi: 10.1016/j.pt.2020.11.007
- Pace, D. A., McKnight, C. A., Liu, J., Jimenez, V., and Moreno, S. N. (2014). Calcium Entry in *Toxoplasma Gondii* and its Enhancing Effect of Invasion-Linked Traits. *J. Biol. Chem.* 289 (28), 19637–19647. doi: 10.1074/jbc.M114.565390
- Papalexis, V., Siomos, M. A., Campanale, N., Guo, X., Kocak, G., Foley, M., et al (2001). Histidine-Rich Protein 2 of the Malaria Parasite, *Plasmodium Falciparum*, is Involved in Detoxification of the by-Products of Haemoglobin Degradation. *Mol. Biochem. Parasitol.* 115 (1), 77–86. doi: 10.1016/S0166-6851(01)00271-7
- Park, D. J., Lukens, A. K., Neafsey, D. E., Schaffner, S. F., Chang, H. H., Valim, C., et al (2012). Sequence-Based Association and Selection Scans Identify Drug Resistance Loci in the *Plasmodium Falciparum* Malaria Parasite. *Proc. Natl. Acad. Sci. U.S.A.* 109 (32), 13052–13067. doi: 10.1073/pnas.1210585109
- Plowe, C. V. (2022). Malaria Chemoprevention and Drug Resistance: A Review of the Literature and Policy Implications. *Malar. J.* 21 (1), 104. doi: 10.1186/s12936-022-04115-8
- Pradhan, A., Siwo, G. H., Singh, N., Martens, B., Balu, B., Button-Simons, K. A., et al (2015). Chemogenomic Profiling of *Plasmodium Falciparum* as a Tool to Aid Antimalarial Drug Discovery. *Sci. Rep.* 5, 15930. doi: 10.1038/srep15930
- Rohloff, P., Miranda, K., Rodrigues, J. C., Fang, J., Galizzi, M., Plattner, H., et al (2011). Calcium Uptake and Proton Transport by Acidocalcisomes of *Toxoplasma Gondii*. *PLoS One* 6 (4), e18390. doi: 10.1371/journal.pone.0018390
- Rohrbach, P., Friedrich, O., Hentschel, J., Plattner, H., Fink, R. H., and Lanzer, M. (2005). Quantitative Calcium Measurements in Subcellular Compartments of *Plasmodium Falciparum*-Infected Erythrocytes. *J. Biol. Chem.* 280 (30), 27960–27969. doi: 10.1074/jbc.M500777200
- Rotmann, A., Sanchez, C., Guiguemde, A., Rohrbach, P., Dave, A., Bakouh, N., et al (2010). PfCHA is a Mitochondrial Divalent Cation/H⁺ Antiporter in *Plasmodium Falciparum*. *Mol. Microbiol.* 76 (6), 1591–1606. doi: 10.1111/j.1365-2958.2010.07187.x
- Ruiz, F. A., Luo, S., Moreno, S. N., and Docampo, R. (2004). Polyphosphate Content and Fine Structure of Acidocalcisomes of *Plasmodium Falciparum*. *Microsc. Microanal.* 10 (5), 563–567. doi: 10.1017/S1341927604040875
- Saier, M. H. Jr., Reddy, V. S., Tsu, B. V., Ahmed, M. S., Li, C., and Moreno-Hagelsieb, G. (2016). The Transporter Classification Database (TCDB): Recent Advances. *Nucleic Acids Res.* 44 (D1), D372–D379. doi: 10.1093/nar/gkv1103
- Sassmannshausen, J., Pradel, G., and Bannink, S. (2020). Perforin-Like Proteins of Apicomplexan Parasites. *Front. Cell Infect. Microbiol.* 10, 578883. doi: 10.3389/fcimb.2020.578883
- Sayers, C. P., Mollard, V., Buchanan, H. D., McFadden, G. I., and Goodman, C. D. (2018). A Genetic Screen in Rodent Malaria Parasites Identifies Five New Apicomplast Putative Membrane Transporters, One of Which is Essential in Human Malaria Parasites. *Cell Microbiol.* 20 (1), e12789. doi: 10.1111/cmi.12789
- Schmidt, O., Pfanner, N., and Meisinger, C. (2010). Mitochondrial Protein Import: From Proteomics to Functional Mechanisms. *Nat. Rev. Mol. Cell Biol.* 11 (9), 655–667. doi: 10.1038/nrm2959
- Shafik, S. H., Cobbold, S. A., Barkat, K., Richards, S. N., Lancaster, N. S., Llinás, M., et al (2020). The Natural Function of the Malaria Parasite's Chloroquine Resistance Transporter. *Nat. Commun.* 11 (1), 3922. doi: 10.1038/s41467-020-17781-6
- Shafik, S. H., Richards, S. N., Corry, B., and Martin, R. E. (2022). Mechanistic Basis for Multidrug Resistance and Collateral Drug Sensitivity Conferred to the Malaria Parasite by Polymorphisms in PfMDR1 and PfCRT. *PLoS Biol.* 20 (5), e3001616. doi: 10.1371/journal.pbio.3001616
- Sheiner, L., and Soldati-Favre, D. (2008). Protein Trafficking Inside *Toxoplasma Gondii*. *Traffic* 9 (5), 636–646. doi: 10.1111/j.1600-0854.2008.00713.x
- Sinha, A., Baumgarten, S., Distiller, A., McHugh, E., Chen, P., Singh, M., et al (2021). Functional Characterization of the M⁶a-Dependent Translational Modulator PLYTH2 in the Human Malaria Parasite. *mBio* 12 (2), e00661–e00621. doi: 10.1128/mBio.00661-21

- Spork, S., Hiss, J. A., Mandel, K., Sommer, M., Kooij, T. W., Chu, T., et al (2009). An Unusual ERAD-Like Complex is Targeted to the Apicoplast of Plasmodium Falciparum. *Eukaryot. Cell* 8 (8), 1134–1145. doi: 10.1128/EC.00083-09
- Staines, H. M., Moore, C. M., Slavic, K., and Krishna, S. (2017). Transmembrane Solute Transport in the Apicomplexan Parasite Plasmodium. *Emerg. Top. Life Sci.* 1 (6), 553–561. doi: 10.1042/etls20170097
- Swearingen, K. E., Lindner, S. E., Shi, L., Shears, M. J., Harupa, A., Hopp, C. S., et al (2016). Interrogating the Plasmodium Sporozoite Surface: Identification of Surface-Exposed Proteins and Demonstration of Glycosylation on CSP and TRAP by Mass Spectrometry-Based Proteomics. *PLoS Pathog.* 12 (4), e1005606. doi: 10.1371/journal.ppat.1005606
- Swift, R. P., Rajaram, K., Keutcha, C., Liu, H. B., Kwan, B., Dziedzic, A., et al (2020). The NTP Generating Activity of Pyruvate Kinase II is Critical for Apicoplast Maintenance in Plasmodium Falciparum. *eLife* 9, e50807. doi: 10.7554/eLife.50807.sa2
- Taylor, C. J., McRobert, L., and Baker, D. A. (2008). Disruption of a Plasmodium Falciparum Cyclic Nucleotide Phosphodiesterase Gene Causes Aberrant Gametogenesis. *Mol. Microbiol.* 69 (1), 110–118. doi: 10.1111/j.1365-2958.2008.06267.x
- van der Velden, M., Rijpmma, S. R., Russel, F. G., Sauerwein, R. W., and Koenderink, J. B. (2015). PfMDR2 and PfMDR5 are Dispensable for Plasmodium Falciparum Asexual Parasite Multiplication But Change In Vitro Susceptibility to Anti-Malarial Drugs. *Malar. J.* 14, 76. doi: 10.1186/s12936-015-0581-y
- van Dooren, G. G., Stimmer, L. M., and McFadden, G. I. (2006). Metabolic Maps and Functions of the Plasmodium Mitochondrion. *FEMS Microbiol. Rev.* 30 (4), 596–630. doi: 10.1111/j.1574-6976.2006.00027.x
- van Esvelde, S. L., Meerstein-Kessel, L., Boshoven, C., Baaij, J. F., Barylyuk, K., Coolen, J. P. M., et al (2021). A Prioritized and Validated Resource of Mitochondrial Proteins in Plasmodium Identifies Unique Biology. *mSphere* 6 (5), e0061421. doi: 10.1128/mSphere.00614-21
- Waller, K. L., McBride, S. M., Kim, K., and McDonald, T. V. (2008). Characterization of Two Putative Potassium Channels in Plasmodium Falciparum. *Malar. J.* 7, 19. doi: 10.1186/1475-2875-7-19
- Wang, Q. C., Zheng, Q., Tan, H., Zhang, B., Li, X., Yang, Y., et al (2016). TMCO1 Is an ER Ca²⁺ Load-Activated Ca²⁺ Channel. *Cell* 165 (6), 1454–1466. doi: 10.1016/j.cell.2016.04.051
- Weiner, J., and Kooij, T. W. (2016). Phylogenetic Profiles of All Membrane Transport Proteins of the Malaria Parasite Highlight New Drug Targets. *Microb. Cell* 3 (10), 511–521. doi: 10.15698/mic2016.10.534
- Wichers, J. S., Mesén-Ramírez, P., Fuchs, G., Yu-Strzelczyk, J., Stäcker, J., von Thien, H., et al (2022). PMRT1, a Plasmodium-Specific Parasite Plasma Membrane Transporter, is Essential for Asexual and Sexual Blood Stage Development. *mBio* 13 (2), e0062322. doi: 10.1128/mbio.00623-22
- Wichers, J. S., van Gelder, C., Fuchs, G., Ruge, J. M., Pietsch, E., Ferreira, J. L., et al (2021). Characterization of Apicomplexan Amino Acid Transporters (ApiATs) in the Malaria Parasite Plasmodium Falciparum. *mSphere* 6 (6), e0074321. doi: 10.1128/mSphere.00743-21
- Wirth, C. C., Bennink, S., Scheuermayer, M., Fischer, R., and Pradel, G. (2015). Perforin-Like Protein PPLP4 is Crucial for Mosquito Midgut Infection by Plasmodium Falciparum. *Mol. Biochem. Parasitol.* 201 (2), 90–99. doi: 10.1016/j.molbiopara.2015.06.005
- Wirth, C. C., Glushakova, S., Scheuermayer, M., Repnik, U., Garg, S., Schaack, D., et al (2014). Perforin-Like Protein PPLP2 Permeabilizes the Red Blood Cell Membrane During Egress of Plasmodium Falciparum Gametocytes. *Cell Microbiol.* 16 (5), 709–733. doi: 10.1111/cmi.12288
- Woo, Y. H., Ansari, H., Otto, T. D., Klinger, C. M., Kolisko, M., Michálek, J., et al (2015). Chromerid Genomes Reveal the Evolutionary Path From Photosynthetic Algae to Obligate Intracellular Parasites. *eLife* 4, e06974. doi: 10.7554/eLife.06974.033
- Wunderlich, J., Rohrbach, P., and Dalton, J. P. (2012). The Malaria Digestive Vacuole. *Front. Biosci. (Schol. Ed.)* 4, 1424–1448. doi: 10.2741/s344
- Yang, A. S. P., O'Neill, M. T., Jennison, C., Lopaticki, S., Allison, C. C., Armistead, J. S., et al (2017). Cell Traversal Activity is Important for Plasmodium Falciparum Liver Infection in Humanized Mice. *Cell Rep.* 18 (13), 3105–3116. doi: 10.1016/j.celrep.2017.03.017
- Zhang, M., Wang, C., Otto, T. D., Oberstaller, J., Liao, X., Adapa, S. R., et al (2018). Uncovering the Essential Genes of the Human Malaria Parasite Plasmodium Falciparum by Saturation Mutagenesis. *Science* 360 (6388), eaap7847. doi: 10.1126/science.aap7847
- Zipprer, E. M., Neggers, M., Kushwaha, A., Rayavara, K., and Desai, S. A. (2014). A Kinetic Fluorescence Assay Reveals Unusual Features of Ca⁺⁺ Uptake in Plasmodium Falciparum-Infected Erythrocytes. *Malar. J.* 13, 184. doi: 10.1186/1475-2875-13-184
- Zuccala, E. S., Gout, A. M., Dekiwadia, C., Marapana, D. S., Angrisano, F., Turnbull, L., et al (2012). Subcompartmentalisation of Proteins in the Rhoptries Correlates With Ordered Events of Erythrocyte Invasion by the Blood Stage Malaria Parasite. *PLoS One* 7 (9), e46160. doi: 10.1371/journal.pone.0046160

Author Disclaimer: The funders had no role in study design, data collection, decision to publish, or preparation of the manuscript.

Conflict of Interest: The author declares that the research was conducted in the absence of any commercial or financial relationships that could be construed as a potential conflict of interest.

Publisher's Note: All claims expressed in this article are solely those of the authors and do not necessarily represent those of their affiliated organizations, or those of the publisher, the editors and the reviewers. Any product that may be evaluated in this article, or claim that may be made by its manufacturer, is not guaranteed or endorsed by the publisher.

Copyright © 2022 Wunderlich. This is an open-access article distributed under the terms of the Creative Commons Attribution License (CC BY). The use, distribution or reproduction in other forums is permitted, provided the original author(s) and the copyright owner(s) are credited and that the original publication in this journal is cited, in accordance with accepted academic practice. No use, distribution or reproduction is permitted which does not comply with these terms.



Streamlined and Robust Stage-Specific Profiling of Gametocytocidal Compounds Against *Plasmodium falciparum*

Janette Reader¹, Mariette E. van der Watt^{1,2} and Lyn-Marié Birkholtz^{1*}

¹ Department of Biochemistry, Genetics and Microbiology, University of Pretoria, Pretoria, South Africa, ² Institute for Sustainable Malaria Control, School of Health Systems and Public Health, University of Pretoria, Pretoria, South Africa

OPEN ACCESS

Edited by:

Tania F. De Koning-Ward,
Deakin University, Australia

Reviewed by:

Rapatbhorn Patrapuvich,
Mahidol University, Thailand
Che Julius Ngwa,
RWTH Aachen University, Germany

*Correspondence:

Lyn-Marié Birkholtz
lbirkholtz@up.ac.za

Specialty section:

This article was submitted to
Parasite and Host,
a section of the journal
Frontiers in Cellular and
Infection Microbiology

Received: 22 April 2022

Accepted: 30 May 2022

Published: 30 June 2022

Citation:

Reader J, van der Watt ME and
Birkholtz L-M (2022) Streamlined and
Robust Stage-Specific Profiling of
Gametocytocidal Compounds Against
Plasmodium falciparum.
Front. Cell. Infect. Microbiol. 12:926460.
doi: 10.3389/fcimb.2022.926460

Malaria elimination is dependent on the ability to target both the pathogenic and transmissible stages of the human malaria parasite, *Plasmodium falciparum*. These forms of the parasite are differentiated by unique developmental stages, each with their own biological mechanisms and processes. These individual stages therefore also respond differently to inhibitory compounds, and this complicates the discovery of multistage active antimalarial agents. The search for compounds with transmission-blocking activity has focused on screening for activity on mature gametocytes, with only limited descriptions available for the activity of such compounds on immature stage gametocytes. This therefore poses a gap in the profiling of antimalarial agents for pan-reactive, multistage activity to antimalarial leads. Here, we optimized an effective and robust strategy for the simple and cost-effective description of the stage-specific action of gametocytocidal antimalarial compounds.

Keywords: gametocyte, luciferase, malaria, *Plasmodium*, transmission-blocking, drug discovery

INTRODUCTION

Increased resistance to currently available antimalarials continues to pose a threat to worldwide malaria elimination efforts and motivates the continued discovery of new antimalarial agents (World Health Organisation, 2020). Target profiling of candidate antimalarial agents now routinely requires evidenced killing of multiple life cycle stages of malaria parasites (Burrows et al., 2017). As such, antimalarial lead candidates are firstly profiled for activity against asexual blood stage (ABS) parasites, addressing the therapeutic necessity of killing parasite stages associated with morbidity and mortality. However, to be useful in and contribute to malaria elimination strategies, antimalarial candidates with such established ABS activity are typically profiled for additional abilities, including being able to block human-to-mosquito transmission of the parasite. This would thereby curb the spread of the disease, with various strategies proposed to exploit such transmission-blocking agents (Birkholtz et al., 2022).

In the human malaria parasite, *Plasmodium falciparum*, human-to-mosquito parasite transmission is dependent on the differentiation and development of mature gametocyte forms of the parasite. In this species, gametocyte development is a uniquely prolonged process (~12 days) characterized by five

morphologically distinct stages (I–V) (Young et al., 2005), each of which is associated with distinct biological processes (Sinden, 2015; Ngotho et al., 2019; Van der Watt et al., 2022). After the stochastic conversion of $\leq 10\%$ of *P. falciparum* ABS parasites to gametocytogenesis, immature gametocytes (stages I–IV) develop and sequester in extravascular environments including the bone marrow (Day et al., 1998; Aguilar et al., 2014). Terminally differentiated, mature falciform gametocytes (stage V) can re-enter the circulatory system and are the only gametocyte stage that can be transmitted back to the mosquito (Sinden, 2015; Meibalan and Marti, 2017; Ngotho et al., 2019). Mature gametocytes can be maintained in circulation for up to 55 days [mean life span, ~ 5.5 days (Bousema et al., 2010)] and are thereby continuously able to ensure transmission of the parasite in the human population, with only $\sim 10^3$ mature gametocytes required for transmission to occur. Therefore, blocking human-to-mosquito parasite transmission is conceptually associated with the ease of targeting such low numbers of long-lasting mature gametocytes. Additionally, as they are circulating in the blood compartment, they are accessible to pharmacological intervention (Birkholtz et al., 2022).

Profiling of antimalarial candidates with ABS activity for additional transmission-blocking activity is frequently only performed on mature stage V gametocytes (D'alessandro et al., 2016; Plouffe et al., 2016; Van Voorhis et al., 2016; Miguel-Blanco et al., 2017; Paquet et al., 2017; Van Der Watt et al., 2018) or male and female gametes (Miguel-Blanco et al., 2017; Delves et al., 2018; Delves et al., 2019). In both instances, a reduction of oocyst numbers (and by implication sporozoite formation) is used to validate transmission-blocking activity (Vos et al., 2015; Birkholtz et al., 2016). However, such a screening pipeline would be fragmented and would not consider the different gametocyte stages of *P. falciparum*, each stage of which is associated with differential biological activities (Delves, 2012; Meibalan and Marti, 2017; Ngotho et al., 2019; Schneider and Reece, 2021; Usui and Williamson, 2021). This translates to compounds having variant activity profiles against these different stages of *P. falciparum* gametocytes (Duffy and Avery, 2013; Miguel-Blanco et al., 2017; Delves et al., 2018; Delves et al., 2019; Abraham et al., 2020). Although the majority of ABS actives do retain activity against immature gametocytes, very few are active against mature gametocytes (Duffy and Avery, 2013). Importantly, not all ABS actives are able to target immature gametocytes. For example, atovaquone, which is potent against ABS parasites, has no activity against immature and mature gametocytes (Plouffe et al., 2016). In these instances, if the entire ABS population is not rapidly cleared, any gametocytes that are formed and not targeted in their immature stages will continuously seed formation of mature gametocytes that will then be transmitted. In such scenarios, transmission will not be blocked, and the parasite will continue to be spread. Moreover, this is of particular concern given the presence of same cycle sexual conversion, i.e., induction of gametocytogenesis within the first cycle of ABS proliferation (Bancells et al., 2019) and evidence that some ABS actives (chloroquine, antifolates, and mefloquine) can shift the parasite population into sexual

differentiation and increase the gametocytaemia of immature stages *in vivo* (Buckling et al., 1999; Price et al., 1999; Sowunmi and Fateye, 2003; Sowunmi et al., 2006; Fehintola et al., 2012; Thommen et al., 2022).

Evaluation of the stage-specific gametocytocidal activity of small molecules has been sparse (Duffy and Avery, 2013; Miguel-Blanco et al., 2017; Delves et al., 2018; Delves et al., 2019; Abraham et al., 2020) and, where these assays have been performed, they made use of extensive, complicated, and expensive manipulation of the gametocyte populations to enrich for specific stages (Adjalley et al., 2011; Lucantoni et al., 2013; Lucantoni et al., 2016; Plouffe et al., 2016). These processes run the risk of compromising gametocyte viability and negate the use of such assays in resource-constrained settings and for robust and reproducible high-throughput applications. Consequently, a more streamlined method is required to allow the stage-specific production of gametocytes with minimal manipulation, to accurately assess the activity of small molecules against immature and mature gametocyte populations. Additionally, the application of such an optimized, streamlined “whole-gametocytocidal” assay beyond proof of principle is required (Lucantoni et al., 2016). Here, we report an optimization of such whole-gametocytocidal assay to allow straightforward, robust, and routine investigation of stage-specific gametocytocidal activity of antimalarial candidates. We validate this strategy with key antimalarial lead candidates with known ABS activity and confirm the importance of characterising any new antimalarial lead compound for stage-specific action against various gametocyte stages including immature gametocytes. With this, we complete the gap in the current profiling of antimalarial candidates with potential transmission-blocking ability by including evaluation of stage-specific gametocytocidal activity.

MATERIALS AND METHODS

Ethics Statement

Parasitology work and volunteer human blood donation at the University of Pretoria are covered under ethical approval from the Health Sciences Ethics Committee (506/2018) and Natural and Agricultural Sciences Ethics Committee (180000094).

In Vitro Parasite Culturing

NF54-*Pfs16*-GFP-luc *P. falciparum* asexual parasites [kind gift from David Fidock, Columbia University, USA (Adjalley et al., 2011)] were maintained at 37°C in A⁺/O⁺ human erythrocytes at 5% hematocrit in complete culture medium under hypoxic conditions as previously described (Reader et al., 2015). Asexual parasites were synchronized at least twice at 12 h intervals with 5% (w/v) D-sorbitol. This staggered synchronization resulted in a parasite population containing >97% ring-stage parasites that were all detected and quantified morphologically to be within a tight developmental window of 5- to 10-h post-invasion. Such age binning and compartmentalization of these ring-stage parasites were performed as described before (Van Biljon et al., 2018; Van Biljon et al., 2019). All cultures were maintained with

daily medium changes and synchronicity evaluated with Giemsa-stained thin smear stage binning under 1,000× magnification.

Stage-Specific Gametocyte Production

Gametocytogenesis was induced on a tightly synchronised (>97% rings) asexual parasite culture (0.5% parasitemia and 6% hematocrit) with a combination of nutrient starvation and a decrease in hematocrit, as previously described (Reader et al., 2015). Gametocyte development was allowed to occur in culture medium prepared as for growth of asexual parasites but without additional glucose supplementation (day -3) under hypoxic conditions, stationary growth, with daily media replacement (from day -1) and parasites/gametocytes were morphologically monitored as per recent molecular descriptors (Brancucci et al., 2018; Dixon and Tilley, 2021). The hematocrit was reduced to 4% after 72 h (day 0), mimicking anemic conditions in the patient. For immature gametocytes (stage II/III), cultures were exposed to 50 mM *N*-acetyl glucosamine (NAG) on days 1–4 to eliminate residual asexual parasites and harvested at days 5–6 (Figure 1). For mature (stage V) gametocytes, NAG treatment only occurred from days 3–7 and harvested at day 13 (Figure 1).

Male Gamete Formation Assay

The male exflagellation inhibition assay (EIA) was performed as described previously (Coetzee et al., 2020; Reader et al., 2021) by capturing the temporal movement of exflagellation centers by

video microscopy. Mature *Pf*NF54 gametocytes (>95% stage V) were treated with 2 μM compound [with methylene blue (MB) as inhibition control at 10 μM] in complete culture media [final dimethyl sulfoxide (DMSO) concentration of <0.1% (v/v), 50% (v/v) A+ male human serum] for 48 h at 37°C under hypoxic conditions. Male gametogenesis was induced on these populations with 100 μM xanthurenic acid at room temperature for 16 min and exflagellation was measured in a Neubauer chamber. Movement was recorded by video microscopy (Carl Zeiss NT 6V/10 W Stab microscope, MicroCapture camera, 10× magnification) and quantified semiautomatically on 16 videos of 8–10 s each, captured between 16 and 24 min after incubation at 30 s intervals. The total exflagellating centers per treatment were quantified using ICY (open-source imaging software GPLv3) normalized to an untreated control.

Viability Determination With Hydroethidine or Determining Adenosine Triphosphate Levels

The viability of both immature and mature gametocytes was evaluated microscopically by staining treated (DHA, 1× IC₅₀ which equates to 20 nM and 5 μM on immature and mature gametocyte, respectively) and untreated gametocytes with 5 μM hydroethidine (HE) for 2 h at room temperature. After removal of excess dye with 1× PBS washes, parasites were fixed in 0.025% (v/v) paraformaldehyde onto a poly-L-lysine-coated cover slide,

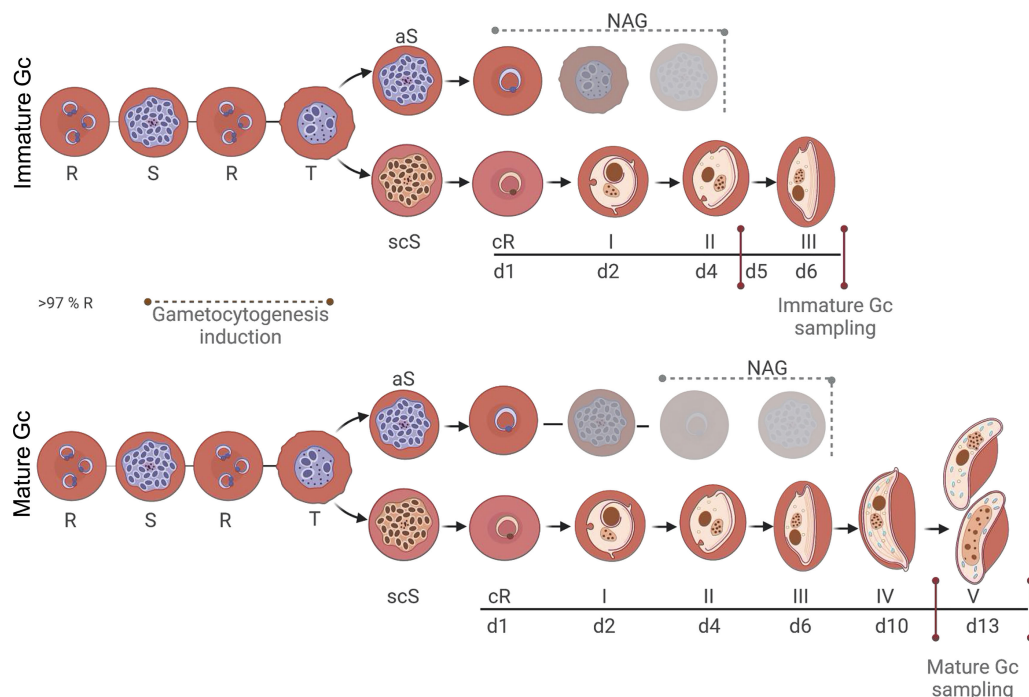


FIGURE 1 | *P. falciparum* stage-specific gametocyte production and development. Asexual parasites (0.5% parasitemia, 6% hematocrit) were D-sorbitol synchronized for two consecutive cycles to ensure a highly synchronized (>97%) ring population. Initiation of gametocytogenesis (same cycle conversion) was induced on day 0 by a decrease in hematocrit, mimicking anemic conditions. Asexual parasites were eliminated with *N*-acetyl glucosamine treatment from days 1 to 4 for immature gametocytes and days 3 to 7 for mature gametocytes. Assays were performed on days 5–6 or 13 for immature and mature gametocytes, respectively. R-ring, S-schizont, T-trophozoite, aS-asexual schizont, scS-sexual committed schizont, cR-committed ring, Gc-gametocyte. Created and modified with BioRender.com.

overnight at 4°C. Micrographs were generated with a Zeiss 510-Meta confocal laser scanning microscope and a HeNe laser with a 543 nm wavelength to excite HE.

Viability was also confirmed by determining ATP levels as a proxy for metabolic activity as previously described (Reader et al., 2015; Reader et al., 2021). Mature stage gametocytes (>90% stage V) were enriched using density gradient centrifugation in Nycoprep (Axis Shield) and magnetic separation using LS columns and a MidiMacs magnet. Approximately 62,000 gametocytes, in glucose-supplemented complete medium, were added to the well in a final volume of 100 µl. Plates were incubated for periods for 0, 12, 24, or 48 h in a humidified gas chamber (90% N₂, 5% O₂, and 5% CO₂) at 37°C. Subsequently, the BacTiter-Glo™ assay (Promega) was performed according to the manufacturer's instructions at room temperature in the dark, with assay substrate incubated for 10 min, to detect ATP levels. Bioluminescence was detected at an integration constant of 0.5 s with the GloMax®-Multi Detection System with Instinct® software. MB (20 µM) was included as control.

Stage-Specific Gametocytocidal Assay

Compounds [supplied by the Medicine for Malaria Venture (www.mmv.org), in DMSO] were evaluated after 48 h drug pressure on either immature (stage II/III) or mature (stage V) gametocytes (2% gametocytemia, 1.5% hematocrit) under hypoxic conditions at 37°C. Drug pressure of 48 h allowed standardization and comparison of activity of compounds if measured on additional transmission-blocking assays such as gamete and oocyst formation (Almela et al., 2015; Miguel-Blanco et al., 2017; Coetzee et al., 2020; Reader et al., 2021). Luciferase activity was determined in 30 µl of parasite lysate by adding 30 µl of luciferin substrate (Promega Luciferase Assay System) at room temperature and detection of bioluminescence at an integration constant of 10 s with a GloMax®-Multi Detection System with Instinct® software. All single point screens were performed at 5 µM of the compound. All dose-response analyses were performed for 9–18 concentrations of 2-fold dilutions to determine the inhibitory concentration at which 50% of the gametocyte population was no longer viable (IC₅₀). In both these assays, MB and the *P. falciparum* phosphatidylinositol-4-kinase inhibitor, MMV390048, were used as internal controls (at 5 µM each). Inhibition was enumerated as luciferase levels compared to control viable gametocytes and the IC₅₀ with non-linear curve fitting and four parametric equations (GraphPad Prism). All assays were performed on three independent biological repeats, each in technical triplicates.

Genotyping of the *Pf*NF54 Reporter Line

ABS parasites obtained from the NF54-*Pfs16*-GFP-luc reporter line expressing green fluorescent protein luciferase (Adjalley et al., 2011) were harvested and genomic DNA was isolated using Quick-DNA™ MiniPrep kit (ZYMO, Research, USA) according to the manufacturer's instructions. Correct integration of reporter construct into the *cg6* locus was analyzed by PCR amplification of the fragments on each side of the attB integration site. The PCR fragments were amplified using KAPA Taq Ready Mix (Roche).

RESULTS

Streamlined Production of Stage-Stratified, Viable Gametocytes

An essential requirement for the stage-specific evaluation of gametocytocidal activity of new antimalarial compounds is the compartmentalized production of immature (stage II/III) and mature (stage V) gametocytes (Figure 1). Our protocol relied on the use of highly synchronized ring-stage asexual parasites as a starting population ($97.1 \pm 0.6\%$ synchronicity, all with <6-h age window, $n = 50$), from which gametocytes were induced (Figure 1). This allowed manipulation of the asexual population, which is less prone to adverse effects due to this treatment, rather than manipulation of the gametocyte population. For instance, magnetic purification of gametocytes, as is typically used in other protocols (Lelievre et al., 2012; Lucantoni et al., 2013; Lucantoni et al., 2016; Plouffe et al., 2016), results in a significant >2-fold drop in viability ($P = 0.0004$, paired, two-tailed *t*-test, $n = 3$) as rapidly as 12-h post-enrichment on stage IV/V gametocytes but is more pronounced at 24 and 48 h ($P < 0.0001$, paired, two-tailed *t*-test, $n = 3$) (Figure S1). Importantly, to further ensure pure gametocyte populations, asexual parasites were continuously eliminated from the gametocyte population after induction at optimized exposure times for either immature or mature gametocyte populations (Figure 1), with <1 and 0.2% asexual parasites remaining in the immature (on days 5–6) or mature (day 13) gametocytes, respectively.

Immature gametocytes were harvested only when stringent morphological stage binning (Figure S2) indicated >80% enrichment to stage II/III gametocytes (Figure 2A; $16.5 \pm 1.7\%$ stage I, $62.3 \pm 3.6\%$ stage II, and $21.2 \pm 3.3\%$ stage III; 826 gametocytes evaluated), with routine gametocytaemias of $3.3 \pm 0.16\%$ obtained ($n = 81$ independent inductions). These stage distributions were highly comparative to those obtained previously but with additional purification steps required (Lucantoni et al., 2013; Plouffe et al., 2016). Immature gametocyte populations containing any stage IV gametocytes were not used in downstream assays to ensure that drug efficacy was evaluated only on stage II/III gametocytes, even after 48-h drug pressure where the typical stage distribution remained at ~82% stage II/III gametocytes. By comparison, a more homogeneous population of mature stage gametocytes was obtained ($2.7 \pm 0.16\%$ gametocytaemia, $n = 50$ independent inductions) consisting of >90% stage V gametocytes ($10 \pm 1.9\%$ stage IV and $90 \pm 2.3\%$ stage V; 270 gametocytes counted; Figure 2B) due to continued removal of asexual parasites from day 3 and the natural attainment of endpoint differentiation (Figure 1). This stage distribution in the mature gametocyte population again correlates well with that obtained for other protocols, but without needing the additional purification as used in other protocols, e.g., through magnetic separation (Lucantoni et al., 2013; Plouffe et al., 2016), exposing committed rings to sorbitol treatment (Plouffe et al., 2016) or gradient separations (Lelievre et al., 2012), both during the gametocytogenesis process or downstream during the actual use of these gametocytes in gametocytocidal assays.

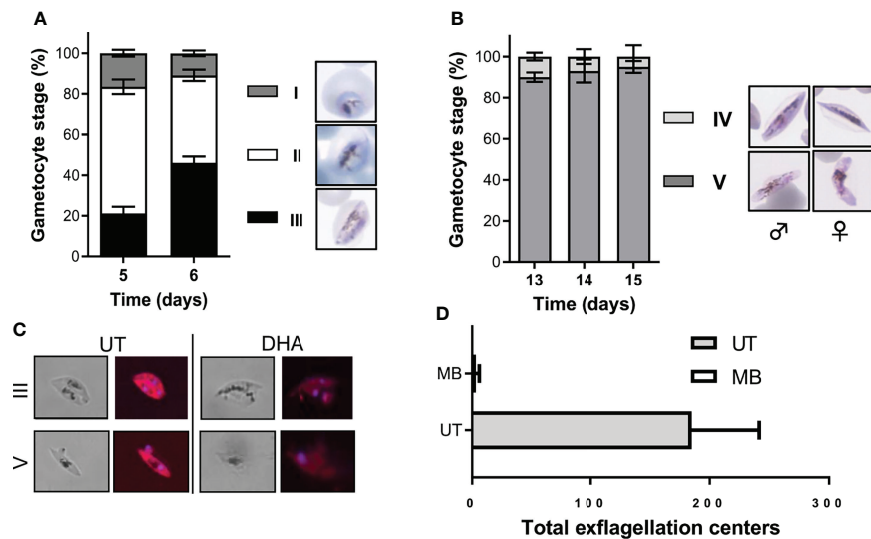


FIGURE 2 | Morphological stage distribution and viability confirmation of immature and mature gametocytes. Quantification of the stage distribution of **(A)** immature gametocytes indicated at >80% enrichment to stage II/III gametocytes and **(B)** >90% stage V mature gametocytes on the day of assay. $N > 30$ individual exp, ~ 500 red blood cell counted/exp \pm S.E. **(C)** Hydroethidine-stained confocal images confirmed the viability of untreated gametocytes and the “dead” phenotype observed following DHA treatment on both immature and mature gametocytes (at $1 \times \text{IC}_{50}$ of 20 nM and 5 μM , respectively). Magnification, $\times 1,000$. **(D)** Viability of mature gametocytes was further evaluated by confirming male exflagellation before initiating any assays ($N > 25$, \pm S.E.). MB, methylene blue (10 μM) treated gametocytes; UT, untreated gametocytes.

Stage-stratified gametocyte populations were produced here at low cost from a single parasite line and, in contrast to previous protocols, required minimal manipulation and no additional purification or enrichment steps. Our gametocyte populations were viable as measured with live-dead staining (**Figure 2C**) without any detectable morphological abnormalities. Additionally, mature gametocytes produced in this manner were fully functional and able to produce high numbers of exflagellating male gametes (15–20 exflagellation centers per field, 16 fields counted, average of 184.8 ± 56.7 total exflagellation centers per experiment; **Figure 2D**), comparable to previous work (13–50 exflagellation centers per field) (Delves et al., 2013).

Evaluating Gametocytocidal Action on Different Stages of Gametocytes

The immature and mature gametocyte populations produced above were subsequently used to evaluate gametocytocidal action of compounds by detecting differences in luciferase signal after a 48 h incubation period. This signal remained detectable in the NF54-*Pfs16*-GFP-luc line used to produce the different stages of gametocytes for more than 10 generations (**Figure S3**). Luciferase expression could be detected throughout gametocytogenesis (**Figure 3A**) but was expectedly higher in immature gametocytes compared to mature gametocytes, as this is associated with *Pfs16* promoter activity that is higher in the immature stages but still active in mature stages (Bruce et al., 1994; Van Biljon et al., 2019). For both the immature and mature gametocytes, a linear

relationship between gametocyte numbers and luciferase expression was present (R^2 [immature] = 0.9991 and R^2 [mature] = 0.9927; **Figures 3B, C**) with sensitive detection of signal in as little as $\sim 3,000$ gametocytes per well (in a 96-well format) for both immature and mature gametocytes. Saturation in the luciferase readout could not be observed at even the highest cell count tested (15×10^3 immature gametocytes and $\sim 50 \times 10^3$ mature gametocytes per well), similar to previous reports with luciferase expression (D'alessandro et al., 2016). Overall assay performance indicated high reproducibility with Z' -factors of 0.83 ± 0.02 (immature gametocyte assay; $n = 81$) and 0.84 ± 0.02 (mature gametocyte assay, $n = 50$) routinely obtained (**Figures 3D, E**).

To benchmark and validate the use of the stage-stratified gametocytes produced in gametocytocidal assays, a set of 12 known antimalarial compounds were evaluated against both immature and mature gametocytes and compared to published data (**Table S1**). The gametocytocidal activity of the compounds against our immature gametocyte population strongly correlated with that previously observed for both stage II (Pearson $R^2 = 0.98$) and stage III gametocytes (Pearson $R^2 = 0.82$; **Figure 4A**) (Plouffe et al., 2016) supporting the prevalence of stage II/III gametocytes in our immature gametocyte population and the absence of stage IV gametocytes (Pearson $R^2 = 0.48$ with stage IV gametocytocidal action as reported (Plouffe et al., 2016)). Moreover, the gametocytocidal action of the compounds against immature gametocytes correlated weakly (Pearson $R^2 = 0.55$; **Figure 4B**) with their activity against ABS parasites. Particularly, pyrimethamine and atovaquone that are potent ABS actives have no ($>5,000$ nM) activity against immature

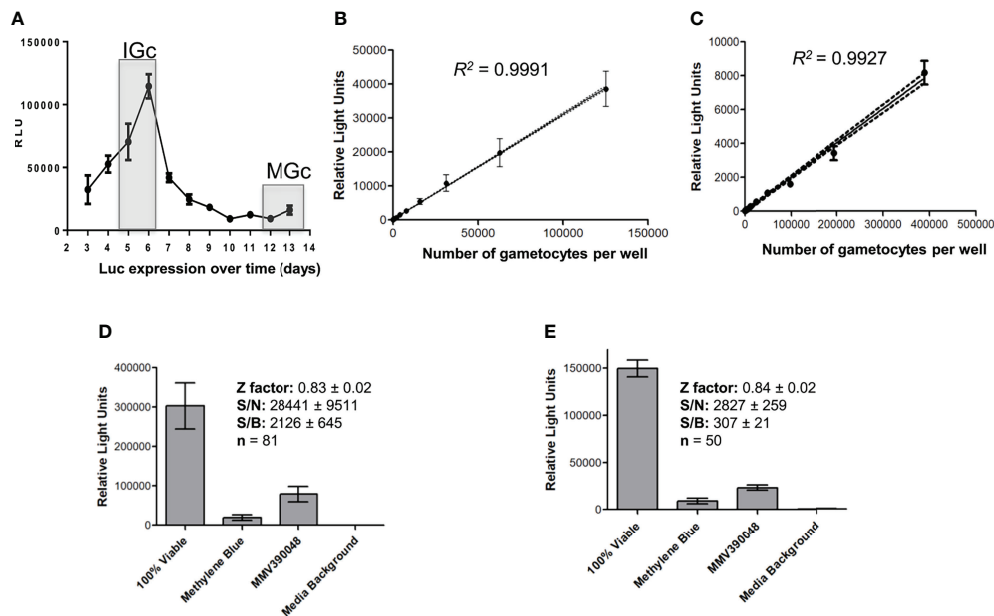


FIGURE 3 | Luciferase reporter assay metrics. **(A)** Assessment of luciferase expression (RLU) throughout gametocytogenesis for the transgenic line NF54-*pfs16*-GFP-Luc on immature gametocytes (IGc, days 5–6), and the mature gametocytes (days 12–14, MGc). The linearity of luminescence readout compared to number of gametocytes per well for both the **(B)** immature and the **(C)** mature gametocytes. Data are from three independent biological experiments each performed in technical triplicates, \pm SEM, 95% confidence intervals on each point indicated as ribbons. Assay metrics, including signal-to-noise (S/N), signal-to-background (S/B), and Z'-factor values for the luminescence readout (relative light units) on both the **(D)** immature and the **(E)** mature gametocyte assays, with 5 μ M of either MMV390048 or MB.

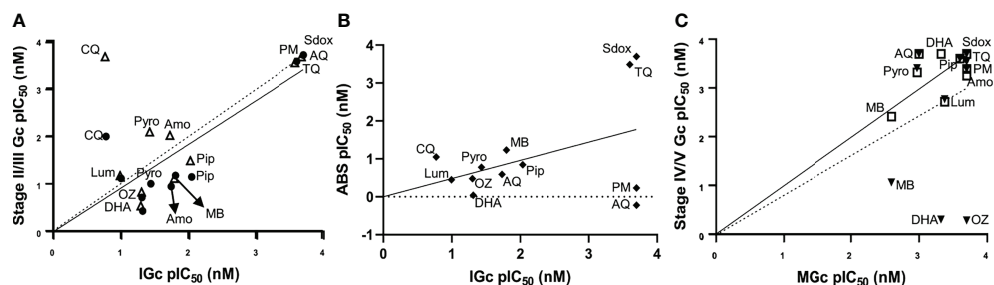


FIGURE 4 | Stage-specific gametocytocidal action evaluation with known antimalarials. Correlation of the gametocytocidal activities of known antimalarials between the luciferase assay on **(A)** immature gametocytes and data from stage II (filled black circle; solid line) and stage III gametocytes (open triangle; dashed line) from a previous report (Plouffe et al., 2016). **(B)** Comparison between activity on immature gametocytes and ABS parasites. **(C)** Mature gametocyte activity compared to stage V (squares; solid line) and stage IV gametocytes (filled black triangles; dashed line) from a previous report (Plouffe et al., 2016). Data are from three independent biological experiments (n = 3), each performed in technical triplicates. DHA, dihydroartemisinin; OZ, artefenomel (OZ439); CQ, chloroquine; Amo, amodiaquine; Pip, piperazine; Pyro, pyronaridine; Lum, lumefantrine; MB, methylene blue; AQ, atovaquone; PM, pyrimethamine; Sdox, sulfadoxine; TQ, tafenoquine.

gametocytes (D'alessandro et al., 2016; Plouffe et al., 2016). The gametocytocidal action of the compounds against the mature gametocyte population confirmed the enrichment of stage V gametocytes, with a stronger correlation (Pearson $R^2 = 0.82$) with the stage V population from the “Plouffe” data set (Plouffe et al., 2016), compared to the stage IV population (Pearson $R^2 = 0.48$; **Figure 4C**). Comparison of individual IC₅₀ values validated our data compared to previous reports [Table

S1, (Lucantoni et al., 2013; Lucantoni et al., 2016; Plouffe et al., 2016)] and included, for instance, comparable IC₅₀s of 20 and 0.9–7 nM for DHA on immature gametocytes (**Table S1**), while our mature assay accurately indicated the loss of activity of this compound on mature gametocytes (>2,000 nM), similar to data from Plouffe et al. (Plouffe et al. (2016)) and more accurate than those reported on late-stage gametocytes (Lucantoni et al., 2016; Coertzen et al., 2018).

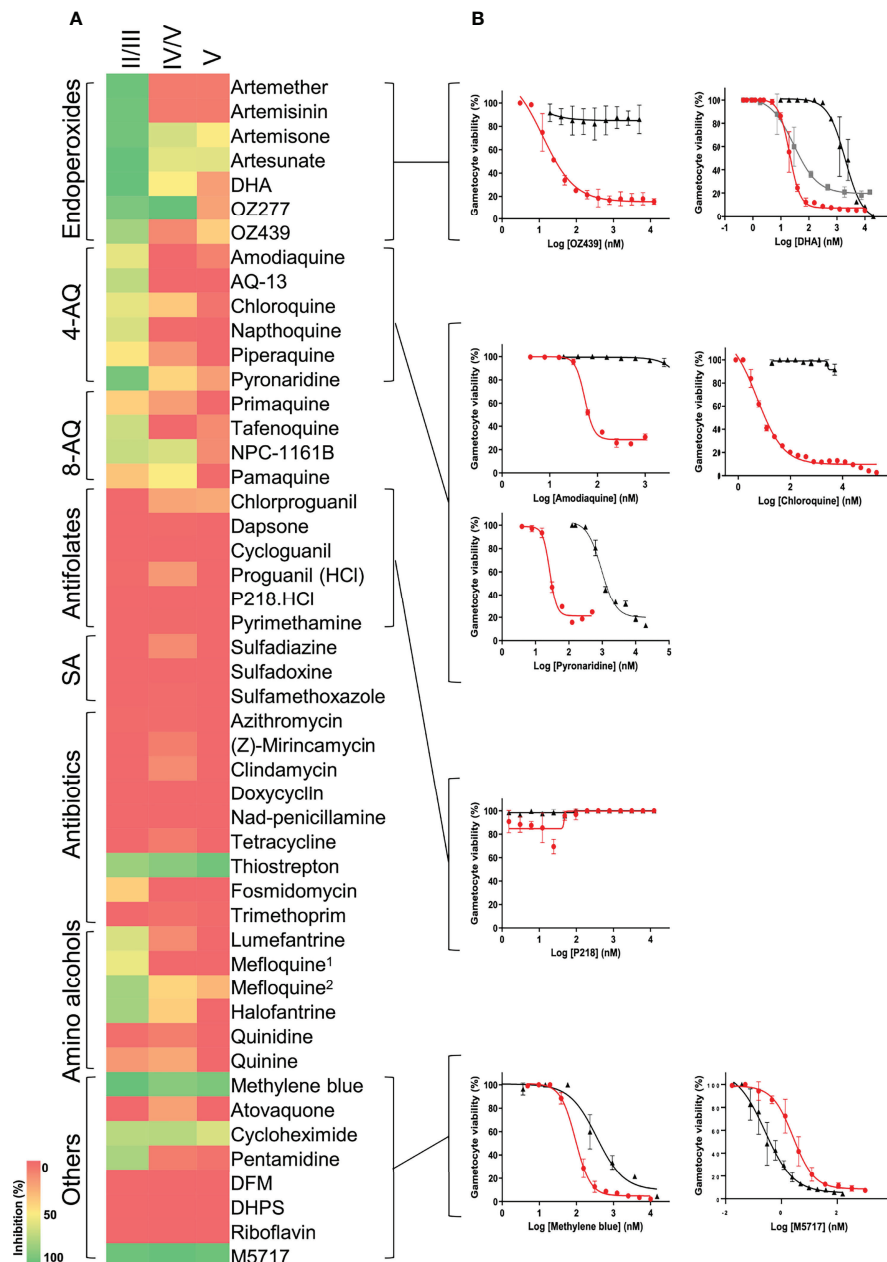


FIGURE 5 | Evaluation of gametocytocidal activity of key MMV compounds. **(A)** Gametocytocidal profiling of the compounds (5 μ M for 48 h) against immature (stage II/III), a mixture of stage IV and V and mature (stage V) gametocytes. **(B)** Dose-response curves of selected compounds indicating the IC_{50} shift between immature (red), mature (black), and mixed stage IV and V gametocyte populations (gray). ¹Racemic, ²(+RS); DFM, deferoxamine mesylate salt; DHPS, dehydroepiandrosterone sulphate. Data are from three independent biological repeats ($n = 3$), performed in technical triplicates, mean \pm S.E indicated.

When the stage-specific evaluation of gametocytocidal activity was extended to include additional investigative and frontrunner reference compounds from the Medicines for Malaria Venture (<https://www.mmv.org/>), we could confirm the presence of unique profiles associated with the susceptibility of different stages of gametocytes for different chemical classes (**Figure 5**). Amino alcohols (e.g., lumefantrine, halofantrine, and mefloquine), 4-aminoquinolines (such as amodiaquine, chloroquine,

piperaquine, and pyronaridine), and the endoperoxides, which are all active against ABS parasites in a nanomolar range (Duffy and Avery, 2013), retain comparative activity in immature gametocytes with an average loss in activity of only ~ 3 -fold observed for these classes. These compounds are inactive against mature stage V gametocytes ($IC_{50} > 5 \mu$ M). The 8-aminoquinolines such as NPC-1161B and pamaquine show little activity on ABS (Duffy and Avery, 2013), which is also observed

here (~60% inhibition for NPC-1161B and <50% inhibition for pamaquine at 5 μ M; **Figure 5**), but the inactivity of primaquine in these *in vitro* assays is associated with its requirement of metabolic activation *in vivo*, as primaquine has validated transmission-blocking activity (Goncalves et al., 2016). Some activity for the above compounds is only reported when stage IV gametocytes were present (e.g., DHA with an IC_{50} of 88 nM in a stage IV/V population, but not active against stage V gametocytes; **Figure 5**), due to their known ability of targeting haem detoxification in the food vacuole, a process only active until stages III–IV of development and not important in mature, differentiated gametocytes (Lucantoni et al., 2013; Lucantoni et al., 2016; Plouffe et al., 2016). Only derivatives such as artemisone, artesunate, and artefenomel (OZ439) have some activity against mature gametocytes, associated with general disruption of redox homeostasis, as these processes are known to be downregulated in the mature gametocytes, enhancing the effect of increased reactive oxygen species production (Coertzen et al., 2018). Pyronaridine displays submicromolar activity against mature gametocytes (IC_{50} = 938 nM), in contrast to earlier reports (Duffy and Avery, 2013; Plouffe et al., 2016). The sulfonamides and antifolates (e.g., P218) have no activity against any stage of gametocytes, although antifolates are potently active against ABS (Duffy and Avery, 2013; Pethrak et al., 2022). The antibiotic, thiostrepton, retains activity against all stages, possibly through targeting general processes such as protein degradation. Importantly, more specific protein targets include the protein synthesis inhibitor with M5717 that inhibits elongation factor P_{EF2} (Baragana et al., 2015), equipotently active (IC_{50} s of 3.57 ± 0.7 and 0.25 ± 0.09 nM), against immature and mature gametocytes, respectively ($P = 0.04$, unpaired *t*-test, $n = 3$). This confirms its importance as frontrunner antimalarial candidate with ABS and gametocytocidal activity and its potential use in transmission-blocking strategies.

DISCUSSION

The recent detailed descriptors of the differential biology associated with the different stages of gametocytogenesis in *P. falciparum* have provided biological support and clarification for the stage-specific action of antimalarial compounds. It has become clear that profiling of compounds on immature gametocytes, in addition to mature gametocytes, is therefore of importance to progress leads and frontrunner clinical candidates as multistage active compounds. Such activities will ensure that sexual stages are targeted from the onset of gametocytogenesis and this will decrease the chances of mature gametocytes forming. In addition, if used in combination with an ABS active, but where the compound with gametocytocidal activity targets a different biological process, it will prolong the life span of ABS active as ABS-resistant parasites will not be able to spread (Birkholtz et al., 2022).

For stage-specific gametocyte assays to be routinely included to profile antimalarial candidates, we optimized a platform to allow robust, sensitive, and cost-efficient assays for stage-specific gametocytocidal activity to address the current caveat in the

profiling of antimalarial candidates. This included the use of luciferase as viability indicator, produced from a single cell line and assayed in specific gametocyte stages, thereby proving previous proposals (Lucantoni et al., 2016) that such a whole-gametocytocidal assay is possible and can be widely applied to various antimalarial screening applications. Importantly, we prove that our platform allowed interrogation of the stage-specific gametocytocidal activity of frontrunner antimalarial candidates after 48 h drug pressure and therefore provide the first set of data to compare the activity of these compounds to data where they were evaluated on other life cycle stages after 48 h. Although longer incubation times (e.g., 72 h employed before) have improved compound activity against mature gametocytes (Lucantoni et al., 2017), this may indicate artificial potency as has been the case with DHA, where this compound could only be shown to be active on mature gametocytes upon longer incubation times (D'alessandro et al., 2016; Coertzen et al., 2018), inconsistent with the consensus that mature gametocytes are resistant to endoperoxides (Plouffe et al., 2016), as we confirm here. The reduced incubation period (compared to 72 h employed before) did not detrimentally affect assay performance, with high assay reproducibility still maintained (Z' -factors of 0.83 and 0.84 obtained on our platform with 48 h assay compared to previous reports of Z' -factors of 0.79–0.85 for a 72 h incubation on immature and mature gametocytes (Lucantoni et al., 2016). Additionally, using only a 48 h incubation on immature gametocytes ensures that stage-specific action is measured only on stage II/III gametocytes, while longer incubation periods run the risk of also measuring activity on developing stage IV gametocytes.

Additionally, our platform streamlined previous processes where either multiple *P. falciparum* luciferase expressing lines were required (Adjalley et al., 2011; Siciliano et al., 2017; Marin-Mogollon et al., 2019) or expensive instrumentation was needed, such as high-content imaging screening assays requiring expensive robotic imaging systems or monoclonal antibodies (Duffy and Avery, 2013; Lucantoni et al., 2015; Plouffe et al., 2016; Miguel-Blanco et al., 2017) rendering them impractical in developing countries or as routine profiling platforms. Similar to previous reports using the same cell line (Lucantoni et al., 2013; Lucantoni et al., 2016), the use of luciferase as viability indicator remains superior to other indicators including fluorescent signals (e.g., tdTomato), which may not be gametocyte-specific (McLean et al., 2019) and requires expensive flow cytometry approaches (Matthews et al., 2020). Furthermore, luciferase is not influenced by assay differences as experienced with metabolic readouts (Reader et al., 2015; Reader et al., 2021). Importantly, expression of luciferase under the *pfs16* promotor is gametocyte-specific and not influenced by the presence of asexual parasites (Lucantoni et al., 2013; Lucantoni et al., 2016). The latter is a major concern during drug screens particularly on immature gametocyte to distinguish activity of compounds from killing ABS parasites and therefore being seemingly active (Marin-Mogollon et al., 2019).

Previous stage-specific gametocyte assays made use of extensive, complicated manipulation of the gametocyte populations to enrich for specific stages (Adjalley et al., 2011; Lucantoni et al., 2013; Lucantoni et al., 2016; Plouffe et al., 2016),

which compromises gametocyte viability and negates the use of such assays in resource constrained settings and in reproducible high-throughput applications. Furthermore, none of these methods result in any improved enrichment of specific stages above what we report here. Currently, stage stratification of gametocytes remains a mostly subjective process, dependent on expertise in morphological analyses of gametocyte stages. However, recent reports have guided this process as more detailed mechanistic data, and stage-specific features have been revealed (Dixon and Tilley, 2021), associated with the individual gametocyte stages in *P. falciparum*. Moreover, with the description of gametocyte-specific transcripts present exclusively in certain stages of gametocyte development (Van Biljon et al., 2019), these could be explored to generate lines with stage-specific expression of multiple reporter genes.

One of the main outcomes of this work is the unique gametocyte stage-specific profiles observed for an investigative and frontrunner reference set of compounds. This highlights the importance to investigate the chemosensitivity of the immature gametocytes to compounds in the developmental pipeline. Compounds that are unable to target immature gametocytes could result in seeding of mature gametocytes and could compromise their efficacy against these mature stages. The streamlined and robust process of gametocyte production and stage-specific evaluation of gametocytocidal activity of antimalarial compounds described here therefore provides affordable and sustainable enabling technology, which is immediately useful to studies performed in developing countries.

DATA AVAILABILITY STATEMENT

The original contributions presented in the study are included in the article/**Supplementary Material**. Further inquiries can be directed to the corresponding author.

REFERENCES

- Abraham, M., Gagaring, K., Marino, M. L., Vanaerschot, M., Plouffe, D., Calla, J., et al. (2020). Probing the Open Global Health Chemical Diversity Library for Multistage-Active Starting Points for Next-Generation Antimalarials. *ACS Infect. Dis.* 6 (4), 613–628. doi: 10.1021/acscinfdis.9b00482
- Adjalley, S. H., Johnston, G. L., Li, T., Eastman, R. T., Ekland, E. H., Eappen, A. G., et al. (2011). Quantitative Assessment of *Plasmodium Falciparum* Sexual Development Reveals Potent Transmission-Blocking Activity by Methylene Blue. *Proc. Natl. Acad. Sci. U.S.A.* 108, E1214–E1223. doi: 10.1073/pnas.1112037108
- Aguliar, R., Magallon-Tejada, A., Achtman, A. H., Moraleda, C., Joice, R., Cisteró, P., et al. (2014). Molecular Evidence for the Localization of *Plasmodium Falciparum* Immature Gametocytes in Bone Marrow. *Blood J. Am. Soc. Hematol.* 123, 959–966. doi: 10.1182/blood-2013-08-520767
- Almela, M. J., Lozano, S., Lelievre, J., Colmenarejo, G., Coteron, J. M., Rodrigues, J., et al. (2015). A New Set of Chemical Starting Points With Plasmodium Falciparum Transmission-Blocking Potential for Antimalarial Drug Discovery. *PLoS One* 10, e0135139. doi: 10.1371/journal.pone.0135139
- Bancells, C., Llorca-Batlle, O., Poran, A., Notzel, C., Rovira-Graells, N., Elemento, O., et al. (2019). Revisiting the Initial Steps of Sexual Development in the Malaria Parasite *Plasmodium Falciparum*. *Nat. Microbiol.* 4, 144–154. doi: 10.1038/s41564-018-0291-7

AUTHOR CONTRIBUTIONS

L-MB conceived the study with JR and MvdW performing all assays and doing data analyses. JR and L-MB wrote the paper with input from MvdW. All authors contributed to the article and approved the submitted version.

FUNDING

L-MB acknowledges the South African Medical Research Council Strategic Health Innovation Partnership and the Department of Science and Innovation South African Research Chairs Initiative, administered through the South African National Research Foundation (UID 84627). Research is supported by a BMGF Grand Challenges Africa grant (GCA/DD2/Round10/021/001) and by the Medicines for Malaria Venture as Global Test center for stage-specific gametocytocidal assays to L-MB. The UP ISMC acknowledges the South African Medical Research Council (SA MRC) as Collaborating Centre for Malaria Research.

ACKNOWLEDGMENTS

We thank Seike Garny and Elisha Mugo for technical assistance. We furthermore thank the MMV for the compounds provided.

SUPPLEMENTARY MATERIAL

The Supplementary Material for this article can be found online at: <https://www.frontiersin.org/articles/10.3389/fcimb.2022.926460/full#supplementary-material>

- Baragana, B., Hallyburton, I., Lee, M. C., Norcross, N. R., Grimaldi, R., Otto, T. D., et al. (2015). A Novel Multiple-Stage Antimalarial Agent That Inhibits Protein Synthesis. *Nature* 522, 315–320. doi: 10.1038/nature14451
- Birkholtz, L. M., Alano, P., and Leroy, D. (2022). Transmission-Blocking Drugs for Malaria Elimination. *Trends Parasitol.* 38, 390–403. doi: 10.1016/j.pt.2022.01.011
- Birkholtz, L. M., Coetzer, T. L., Mancama, D., Leroy, D., and Alano, P. (2016). Discovering New Transmission-Blocking Antimalarial Compounds: Challenges and Opportunities. *Trends Parasitol.* 32, 669–681. doi: 10.1016/j.pt.2016.04.017
- Bousema, T., Okell, L., Shekalaghe, S., Griffin, J. T., Omar, S., Sawa, P., et al. (2010). Revisiting the Circulation Time of *Plasmodium Falciparum* Gametocytes: Molecular Detection Methods to Estimate the Duration of Gametocyte Carriage and the Effect of Gametocytocidal Drugs. *Malar. J.* 9, 136. doi: 10.1186/1475-2875-9-136
- Brancucci, N. M. B., De Niz, M., Straub, T. J., Ravel, D., Sollelis, L., Birren, B. W., et al. (2018). Probing *Plasmodium Falciparum* Sexual Commitment at the Single-Cell Level. *Wellcome Open Res.* 3, 70. doi: 10.12688/wellcomeopenres.14645.4
- Bruce, M. C., Carter, R. N., Nakamura, K., Aikawa, M., and Carter, R. (1994). Cellular Location and Temporal Expression of the *Plasmodium Falciparum* Sexual Stage Antigen Pfs16. *Mol. Biochem. Parasitol.* 65, 11–22. doi: 10.1016/0166-6851(94)90111-2
- Buckling, A., Ranford-Cartwright, L., Miles, A., and Read, A. (1999). Chloroquine Increases *Plasmodium Falciparum* Gametocytogenesis *In Vitro*. *Parasitology* 118, 339–346. doi: 10.1017/S0031182099003960

- Burrows, J. N., Duparc, S., Gutteridge, W. E., Hooft Van Huijsduijnen, R., Kaszubska, W., Macintyre, F., et al. (2017). New Developments in Anti-Malarial Target Candidate and Product Profiles. *Malar. J.* 16, 26. doi: 10.1186/s12936-016-1675-x
- Coertzen, D., Reader, J., van der Watt, M., Nondaba, S. H., Gibbard, L., Wiesner, L., et al. (2018). Artemisone and Artemiside Are Potent Panreactive Antimalarial Agents That Also Synergize Redox Imbalance in *Plasmodium Falciparum* Transmissible Gametocyte Stages. *Antimicrob. Agents Chemother.* 62, e02214-17. doi: 10.1128/AAC.02214-17
- Coetzee, N., Von Gruning, H., Opperman, D., van der Watt, M., Reader, J., and Birkholtz, L. M. (2020). Epigenetic Inhibitors Target Multiple Stages of *Plasmodium Falciparum* Parasites. *Sci. Rep.* 10, 2355. doi: 10.1038/s41598-020-59298-4
- D'alessandro, S., Camarda, G., Corbett, Y., Siciliano, G., Parapini, S., Cevenini, L., et al. (2016). A Chemical Susceptibility Profile of the *Plasmodium Falciparum* Transmission Stages by Complementary Cell-Based Gametocyte Assays. *J. Antimicrob. Chemother.* 71, 1148–1158. doi: 10.1093/jac/ckv493
- Day, K. P., Hayward, R. E., and Dyer, M. (1998). The Biology of *Plasmodium Falciparum* Transmission Stages. *Parasitology* 116, 95–109. doi: 10.1017/S0031182000084985
- Delves, M. J. (2012). *Plasmodium* Cell Biology Should Inform Strategies Used in the Development of Antimalarial Transmission-Blocking Drugs. *Future Med. Chem.* 4, 2251–2263. doi: 10.4155/fmc.12.182
- Delves, M., Lafuente-Monasterio, M. J., Upton, L., Ruecker, A., Leroy, D., Gamo, F. J., et al. (2019). Fueling Open Innovation for Malaria Transmission-Blocking Drugs: Hundreds of Molecules Targeting Early Parasite Mosquito Stages. *Front. Microbiol.* 10, 2134. doi: 10.3389/fmicb.2019.02134
- Delves, M. J., Miguel-Blanco, C., Matthews, H., Molina, I., Ruecker, A., Yahya, S., et al. (2018). A High Throughput Screen for Next-Generation Leads Targeting Malaria Parasite Transmission. *Nat. Commun.* 9, 3805. doi: 10.1038/s41467-018-05777-2
- Delves, M. J., Ruecker, A., Straschil, U., Lelievre, J., Marques, S., Lopez-Barragan, M. J., et al. (2013). Male and Female *Plasmodium Falciparum* Mature Gametocytes Show Different Responses to Antimalarial Drugs. *Antimicrob. Agents Chemother.* 57, 3268–3274. doi: 10.1128/AAC.00325-13
- Dixon, M. W. A., and Tilley, L. (2021). *Plasmodium Falciparum* Goes Bananas for Sex. *Mol. Biochem. Parasitol.* 244, 111385. doi: 10.1016/j.molbiopara.2021.111385
- Duffy, S., and Avery, V. M. (2013). Identification of Inhibitors of *Plasmodium Falciparum* Gametocyte Development. *Malar. J.* 12, 408. doi: 10.1186/1475-2875-12-408
- Fehintola, F., Balogun, S., and Adeoye, S. (2012). Intermittent Preventive Treatment During Pregnancy With Sulphadoxine-Pyrimethamine may Promote *Plasmodium Falciparum* Gametocytogenesis. *Med. Principles Pract.* 21, 63–67. doi: 10.1159/000332405
- Goncalves, B. P., Tiono, A. B., Ouedraogo, A., Guelbeogo, W. M., Bradley, J., Nebie, I., et al. (2016). Single Low Dose Primaquine to Reduce Gametocyte Carriage and *Plasmodium Falciparum* Transmission After Artemether-Lumefantrine in Children With Asymptomatic Infection: A Randomised, Double-Blind, Placebo-Controlled Trial. *BMC Med.* 14, 40. doi: 10.1186/s12916-016-0581-y
- Lelievre, J., Almela, M. J., Lozano, S., Miguel, C., Franco, V., Leroy, D., et al. (2012). Activity of Clinically Relevant Antimalarial Drugs on *Plasmodium Falciparum* Mature Gametocytes in an ATP Bioluminescence "Transmission Blocking" Assay. *PloS One* 7, e35019. doi: 10.1371/journal.pone.0035019
- Lucantoni, L., Duffy, S., Adjalley, S. H., Fidock, D. A., and Avery, V. M. (2013). Identification of MMV Malaria Box Inhibitors of *Plasmodium Falciparum* Early-Stage Gametocytes Using a Luciferase-Based High-Throughput Assay. *Antimicrob. Agents Chemother.* 57, 6050–6062. doi: 10.1128/AAC.00870-13
- Lucantoni, L., Fidock, D. A., and Avery, V. M. (2016). Luciferase-Based, High-Throughput Assay for Screening and Profiling Transmission-Blocking Compounds Against *Plasmodium Falciparum* Gametocytes. *Antimicrob. Agents Chemother.* 60, 2097–2107. doi: 10.1128/AAC.01949-15
- Lucantoni, L., Loganathan, S., and Avery, V. M. (2017). The Need to Compare: Assessing the Level of Agreement of Three High-Throughput Assays Against *Plasmodium Falciparum* Mature Gametocytes. *Sci. Rep.* 7, 45992. doi: 10.1038/srep45992
- Lucantoni, L., Silvestrini, F., Signore, M., Siciliano, G., Eldering, M., Decherling, K. J., et al. (2015). A Simple and Predictive Phenotypic High Content Imaging Assay for *Plasmodium Falciparum* Mature Gametocytes to Identify Malaria Transmission Blocking Compounds. *Sci. Rep.* 5, 16414. doi: 10.1038/srep16414
- Marin-Mogollon, C., Salman, A. M., Koolen, K. M. J., Bolscher, J. M., Van Pul, F. J. A., Miyazaki, S., et al. (2019). A *P. Falciparum* NF54 Reporter Line Expressing Mcherry-Luciferase in Gametocytes, Sporozoites, and Liver-Stages. *Front. Cell Infect. Microbiol.* 9, 96. doi: 10.3389/fcimb.2019.00096
- Matthews, K. A., Senagbe, K. M., Notzel, C., Gonzales, C. A., Tong, X., Rijo-Ferreira, F., et al. (2020). Disruption of the *Plasmodium Falciparum* Life Cycle Through Transcriptional Reprogramming by Inhibitors of Jumonji Demethylases. *ACS Infect. Dis.* 6, 1058–1075. doi: 10.1021/acscinfecdis.9b00455
- McLean, K. J., Straimer, J., Hopp, C. S., Vega-Rodriguez, J., Small-Saunders, J. L., Kanatani, S., et al. (2019). Generation of Transmission-Competent Human Malaria Parasites With Chromosomally-Integrated Fluorescent Reporters. *Sci. Rep.* 9, 13131. doi: 10.1038/s41598-019-49348-x
- Meibalan, E., and Marti, M. (2017). Biology of Malaria Transmission. *Cold Spring Harb. Perspect. Med.* 7. doi: 10.1101/cshperspect.a025452
- Miguel-Blanco, C., Molina, I., Bardera, A. I., Diaz, B., De Las Heras, L., Lozano, S., et al. (2017). Hundreds of Dual-Stage Antimalarial Molecules Discovered by a Functional Gametocyte Screen. *Nat. Commun.* 8, 15160. doi: 10.1038/ncomms15160
- Ngotho, P., Soares, A. B., Hentzschel, F., Achcar, F., Bertuccini, L., and Marti, M. (2019). Revisiting Gametocyte Biology in Malaria Parasites. *FEMS Microbiol. Rev.* 43, 401–414. doi: 10.1093/femsre/fuz010
- Paquet, T., Le Manach, C., Cabrera, D. G., Younis, Y., Henrich, P. P., Abraham, T. S., et al. (2017). Antimalarial Efficacy of MMV390048, an Inhibitor of *Plasmodium* Phosphatidylinositol 4-Kinase. *Sci. Transl. Med.* 9. doi: 10.1126/scitranslmed.aad9735
- Pethrak, C., Posayapisit, N., Pengon, J., Suwanakitti, N., Saeung, A., Shorum, M., et al. (2022). New Insights Into Antimalarial Chemopreventive Activity of Antifolates. *Antimicrob. Agents Chemother.* 66, e0153821. doi: 10.1128/aac.01538-21
- Plouffe, D. M., Wree, M., Du, A. Y., Meister, S., Li, F., Patra, K., et al. (2016). High-Throughput Assay and Discovery of Small Molecules That Interrupt Malaria Transmission. *Cell Host Microbe* 19, 114–126. doi: 10.1016/j.chom.2015.12.001
- Price, R., Nosten, F., Simpson, J. A., Luxemburger, C., Phaipun, L., Ter Kuile, F., et al. (1999). Risk Factors for Gametocyte Carriage in Uncomplicated *Falciparum* Malaria. *Am. J. Trop. Med. Hyg.* 60, 1019–1023. doi: 10.4269/ajtmh.1999.60.1019
- Reader, J., Botha, M., Theron, A., Lauterbach, S. B., Rossouw, C., Engelbrecht, D., et al. (2015). Nowhere to Hide: Interrogating Different Metabolic Parameters of *Plasmodium Falciparum* Gametocytes in a Transmission Blocking Drug Discovery Pipeline Towards Malaria Elimination. *Malar. J.* 14, 213. doi: 10.1186/s12936-015-0718-z
- Reader, J., van der Watt, M. E., Taylor, D., Le Manach, C., Mittal, N., Otilie, S., et al. (2021). Multistage and Transmission-Blocking Targeted Antimalarials Discovered From the Open-Source MMV Pandemic Response Box. *Nat. Commun.* 12, 269. doi: 10.1038/s41467-020-20629-8
- Schneider, P., and Reece, S. E. (2021). The Private Life of Malaria Parasites: Strategies for Sexual Reproduction. *Mol. Biochem. Parasitol.* 244, 111375. doi: 10.1016/j.molbiopara.2021.111375
- Siciliano, G., Santha Kumar, T. R., Bona, R., Camarda, G., Calabretta, M. M., Cevenini, L., et al. (2017). A High Susceptibility to Redox Imbalance of the Transmissible Stages of *Plasmodium Falciparum* Revealed With a Luciferase-Based Mature Gametocyte Assay. *Mol. Microbiol.* 104, 306–318. doi: 10.1111/mmi.13626
- Sinden, R. (2015). The Cell Biology of Malaria Infection of Mosquito: Advances and Opportunities. *Cell. Microbiol.* 17, 451–466. doi: 10.1111/cmi.12413
- Sowunmi, A., Adediji, A., Gbotosho, G., Fateye, B., and Happi, T. (2006). Effects of Pyrimethamine-Sulphadoxine, Chloroquine Plus Chlorpheniramine, and Amodiaquine Plus Pyrimethamine-Sulphadoxine on Gametocytes During and After Treatment of Acute, Uncomplicated Malaria in Children. *Memórias do Instituto Oswaldo Cruz* 101, 887–893. doi: 10.1590/S0074-02762006000800011
- Sowunmi, A., and Fateye, B. (2003). *Plasmodium Falciparum* Gametocytaemia in Nigerian Children: Before, During and After Treatment With Antimalarial

- Drugs. *Trop. Med. Int. Health* 8, 783–792. doi: 10.1046/j.1365-3156.2003.01093.x
- Thommen, B. T., Passecker, A., Buser, T., Hitz, E., Voss, T. S., and Brancucci, N. M. B. (2022). Revisiting the Effect of Pharmaceuticals on Transmission Stage Formation in the Malaria Parasite *Plasmodium Falciparum*. *Front. Cell Infect. Microbiol.* 12, 802341. doi: 10.3389/fcimb.2022.802341
- Usui, M., and Williamson, K. C. (2021). Stressed Out About *Plasmodium Falciparum* Gametocytogenesis. *Front. Cell Infect. Microbiol.* 11, 790067. doi: 10.3389/fcimb.2021.790067
- Van Biljon, R., Niemand, J., Van Wyk, R., Clark, K., Verlinden, B., Abrie, C., et al. (2018). Inducing Controlled Cell Cycle Arrest and Re-Entry During Asexual Proliferation of *Plasmodium Falciparum* Malaria Parasites. *Sci. Rep.* 8, 16581. doi: 10.1038/s41598-018-34964-w
- Van Biljon, R., Van Wyk, R., Painter, H. J., Orchard, L., Reader, J., Niemand, J., et al. (2019). Hierarchical Transcriptional Control Regulates *Plasmodium Falciparum* Sexual Differentiation. *BMC Genomics* 20, 920. doi: 10.1186/s12864-019-6322-9
- Van Der Watt, M. E., Reader, J., and Birkholtz, L. (2022). Adapt or Die: Targeting Unique Transmission-Stage Biology for Malaria Elimination. *Front. Cell Infect. Microbiol.* doi: 10.3389/fcimb.2022.901971
- Van Der Watt, M. E., Reader, J., Churchyard, A., Nondaba, S. H., Lauterbach, S. B., Niemand, J., et al. (2018). Potent *Plasmodium Falciparum* Gametocytocidal Compounds Identified by Exploring the Kinase Inhibitor Chemical Space for Dual Active Antimalarials. *J. Antimicrob. Chemother.* 73, 1279–1290. doi: 10.1093/jac/dky008
- Van Voorhis, W. C., Adams, J. H., Adelfio, R., Ah Yong, V., Akabas, M. H., Alano, P., et al. (2016). Open Source Drug Discovery With the Malaria Box Compound Collection for Neglected Diseases and Beyond. *PloS Pathog.* 12, e1005763. doi: 10.1371/journal.ppat.1005763
- Vos, M. W., Stone, W. J., Koolen, K. M., Van Gemert, G. J., Van Schaijk, B., Leroy, D., et al. (2015). A Semi-Automated Luminescence Based Standard Membrane Feeding Assay Identifies Novel Small Molecules That Inhibit Transmission of Malaria Parasites by Mosquitoes. *Sci. Rep.* 5, 18704. doi: 10.1038/srep18704
- World Health Organisation (2020). *World Malaria Report 2020* (Geneva: World Health Organisation).
- Young, J. A., Fivelman, Q. L., Blair, P. L., de la Vega, P., Le Roch, K. G., Zhou, Y., et al. (2005). The *Plasmodium Falciparum* Sexual Development Transcriptome: A Microarray Analysis Using Ontology-Based Pattern Identification. *Mol. Biochem. Parasitol.* 143, 67–79. doi: 10.1016/j.molbiopara.2005.05.007

Conflict of Interest: The authors declare that the research was conducted in the absence of any commercial or financial relationships that could be construed as a potential conflict of interest.

Publisher's Note: All claims expressed in this article are solely those of the authors and do not necessarily represent those of their affiliated organizations, or those of the publisher, the editors and the reviewers. Any product that may be evaluated in this article, or claim that may be made by its manufacturer, is not guaranteed or endorsed by the publisher.

Copyright © 2022 Reader, van der Watt and Birkholtz. This is an open-access article distributed under the terms of the Creative Commons Attribution License (CC BY). The use, distribution or reproduction in other forums is permitted, provided the original author(s) and the copyright owner(s) are credited and that the original publication in this journal is cited, in accordance with accepted academic practice. No use, distribution or reproduction is permitted which does not comply with these terms.



The Kinetoplastid-Specific Protein TcCAL1 Plays Different Roles During *In Vitro* Differentiation and Host-Cell Invasion in *Trypanosoma cruzi*

Jessica Rodríguez-Durán¹, Juan Pablo Gallardo¹, Catalina Dirney Alba Soto², Karina Andrea Gómez¹ and Mariana Potenza^{1*}

¹ Laboratorio de Biología e Inmunología de las Infecciones por Tripanosomátidos, Instituto de Investigaciones en Ingeniería Genética y Biología Molecular "Dr. Héctor Torres"—CONICET, Buenos Aires, Argentina, ² Instituto de Microbiología y Parasitología Médica, Departamento de Microbiología, Facultad de Medicina, Universidad de Buenos Aires, Buenos Aires, Argentina

OPEN ACCESS

Edited by:

Maria Carolina Touz,
Medical Research Institute Mercedes
and Martín Ferreyra (INIMEC),
Argentina

Reviewed by:

Noelia Lander,
University of Cincinnati, United States
Beatriz Simonsen Stolf,
University of São Paulo, Brazil

*Correspondence:

Mariana Potenza
marian.potenza@gmail.com;
potenza@dna.uba.ar

Specialty section:

This article was submitted to
Parasite and Host,
a section of the journal
Frontiers in Cellular and
Infection Microbiology

Received: 22 March 2022

Accepted: 27 May 2022

Published: 30 June 2022

Citation:

Rodríguez-Durán J, Gallardo JP,
Alba Soto CD, Gómez KA
and Potenza M (2022) The
Kinetoplastid-Specific Protein
TcCAL1 Plays Different Roles During
In Vitro Differentiation and Host-Cell
Invasion in *Trypanosoma cruzi*.
Front. Cell. Infect. Microbiol. 12:901880.
doi: 10.3389/fcimb.2022.901880

In the pathogen *Trypanosoma cruzi*, the calcium ion (Ca^{2+}) regulates key processes for parasite survival. However, the mechanisms decoding Ca^{2+} signals are not fully identified or understood. Here, we investigate the role of a hypothetical Ca^{2+} -binding protein named TcCAL1 in the *in vitro* life cycle of *T. cruzi*. Results showed that the overexpression of TcCAL1 fused to a 6X histidine tag (TcCAL1-6xHis) impaired the differentiation of epimastigotes into metacyclic trypomastigotes, significantly decreasing metacyclogenesis rates. When the virulence of transgenic metacyclic trypomastigotes was explored in mammalian cell invasion assays, we found that the percentage of infection was significantly higher in Vero cells incubated with TcCAL1-6xHis-overexpressing parasites than in controls, as well as the number of intracellular amastigotes. Additionally, the percentage of Vero cells with adhered metacyclic trypomastigotes significantly increased in samples incubated with TcCAL1-6xHis-overexpressing parasites compared with controls. In contrast, the differentiation rates from metacyclic trypomastigotes to axenic amastigotes or the epimastigote proliferation in the exponential phase of growth have not been affected by TcCAL1-6xHis overexpression. Based on our findings, we speculate that TcCAL1 exerts its function by sequestering intracellular Ca^{2+} by its EF-hand motifs (impairing metacyclogenesis) and/or due to an unknown activity which could be amplified by the ion binding (promoting cell invasion). This work underpins the importance of studying the kinetoplastid-specific proteins with unknown functions in pathogen parasites.

Keywords: *Trypanosoma cruzi*, EF-hand, hypothetical protein, differentiation, host-cell invasion

INTRODUCTION

Chagas disease, or American Trypanosomiasis, is caused by the parasite *Trypanosoma cruzi*, which is mainly transmitted by blood-sucking triatomine insects. Nearly seven million people are infected worldwide, mostly in Latin America, where this neglected disease is endemic but also in non-endemic countries due to migration movements (Lidani et al., 2019). Without treatment, Chagas disease progresses from an acute phase, characterized by high parasitemia, to chronicity. In the

latter, patients can stay asymptomatic for the rest of their lives or, in ~40% of the cases, develop severe digestive, cardiac, and/or neurological pathology (World Health Organization, 2022). However, there is still no vaccine and the current chemotherapy has frequent toxic side effects, being poorly effective in the chronic phase (Hasslocher-Moreno et al., 2020). Therefore, safer and more effective drugs in the chronic phase would improve the outcome of the disease. Research on *T. cruzi* biology can identify novel metabolic targets in the parasite, leading to the development of new chemotherapeutic agents.

The *T. cruzi* life cycle involves the passage from an insect vector to a mammalian host and vice versa, where the parasite survives and proliferates by adapting to different environments. At least four main developmental forms can be morphologically identified in this journey. In the hindgut of the insect, proliferating non-infective epimastigote forms differentiate into infective cell cycle-arrested metacyclic trypomastigotes, a process called metacyclogenesis. These parasite forms are eliminated by the triatomine feces and deposited near the bite during the blood meal. The parasite entrance commonly occurs through a wound in the skin or mucosal membrane of the mammalian host. Once in the bloodstream, metacyclic forms invade different host cell types and tissues and then differentiate intracellularly into amastigotes, which proliferate by binary fission. When the host cell harbors a high number of parasites, amastigotes turn into highly motile trypomastigotes, which promote cell lysis and invade neighboring cells or reach the bloodstream to disseminate the infection. These bloodstream trypomastigotes can also be taken up by triatomine bugs when feeding on the blood of the mammalian host (Teixeira et al., 2012).

Ca^{2+} signaling modulates diverse biological activities in eukaryotic cells. Cytosolic Ca^{2+} binds to a plethora of effectors responsible for regulating different cell type-dependent processes, establishing unique signaling pathways for each cell (Berridge et al., 2003). Ca^{2+} binding proteins (CBP) are some of these effectors, exerting functions ranging from the maintenance of intracellular homeostasis to the modulation of enzymatic activity. Most CBPs are characterized by the presence of EF-hand domains, a highly conserved structure of helix-loop-helix responsible for binding Ca^{2+} . Typically, these motifs occur in pairs, facilitating the cooperative binding of two ions per protein, although it is also possible to find CBP with an odd number of domains (Chazin, 2011).

Experimental evidence has pointed out the importance of Ca^{2+} signaling and homeostasis in regulating key processes of the *T. cruzi* life cycle, such as proliferation, differentiation, and parasite–host interplay (Yoshida, 2006; Caradonna and Burleigh, 2011; Hashimoto et al., 2016). It has been found that during metacyclogenesis, the cytosolic Ca^{2+} ($[\text{Ca}^{2+}]_c$) increases abruptly and temporarily regardless of the extracellular ion concentration, suggesting this signal is triggered by intracellular reservoirs (Lammel et al., 1996). Also, during the invasion of mammalian cells *in vitro*, measurements with fluorescent indicators showed that the $[\text{Ca}^{2+}]_c$ in trypomastigotes transiently increases as a consequence of parasite adhesion to the outer membrane of the host cell (Moreno et al., 1994; Yakubu

et al., 1994). Furthermore, the $[\text{Ca}^{2+}]_c$ increase observed in tissue culture-derived trypomastigotes is also triggered by interaction with mammalian extracellular matrix proteins (Manchola Varón et al., 2021). Regarding this, the main intracellular reservoirs studied to date for Ca^{2+} storage and mobilization are the acidocalcisomes, the endoplasmic reticulum and the mitochondria (Lu et al., 1998; Maeda et al., 2012; Chiurillo et al., 2020). Nearly a dozen Ca^{2+} transport channels have been identified and/or characterized in these organelles, as well as in plasma or flagellar membranes (Furuya et al., 2001; Hamed et al., 2015; Ramakrishnan and Docampo, 2018; Chiurillo et al., 2019; Dave et al., 2021), which handle the mobilization, flux, and extrusion of Ca^{2+} ions among the different compartments and the extracellular environment. The differences in structure, location, and regulation found in some of these channels in comparison to those present in mammalian cells, in addition to their relevance in parasite physiology, make these channels an attractive target for therapeutic treatment (Benaim et al., 2020). However, few CBP containing EF-hand domains have been characterized in *T. cruzi*. Among them, it has been shown that calmodulin modulates the activity of enzymes such as Ca^{2+} and Mg^{2+} dependent ATPases and cyclic AMP phosphodiesterase (Tellez-Iñón et al., 1985; Benaim et al., 1991). In addition, other CBPs have been characterized functionally to some extent. In this regard, the Ca^{2+} /calmodulin-dependent kinase CaMK II, the calcineurin regulatory subunit B and the flagellar Ca^{2+} -binding protein FCaBP have been implicated in epimastigote proliferation (Souza et al., 2009; Nogueira et al., 2011), mammalian host-cell invasion (Araya et al., 2008) and flagellum assembly (Wingard et al., 2008), respectively. Calreticulin, a CBP lacking EF-hand domains, was shown to play a role in *T. cruzi* infection (Sánchez-Valdez et al., 2014). In turn, Ca^{2+} modulates enzymatic activity in several proteins, such as the adenylyl cyclase, which is involved in parasite motility (D'Angelo et al., 2002). Overall, these studies demonstrated the presence of Ca^{2+} signaling in *T. cruzi* metabolism and physiology, although its actors and mechanisms are not fully identified or completely understood.

Since the annotation of *T. cruzi* genomes, several CBP and Ca^{2+} channels have been identified. These proteins probably generate the fluctuations in calcium concentration and decode its signals, although most of them remain uncharacterized (El-Sayed et al., 2005). Furthermore, many of these genes encode hypothetical proteins, which lack significant sequence homology in other eukaryotes. These trypanosomatid-exclusive novel proteins of unknown function represent ~39% of the protein-coding genes in the *T. cruzi* genome (Berná et al., 2018). Unraveling their role would lead to the identification of novel chemotherapeutic targets against these pathogens (Martins et al., 2011).

This study contributes to the knowledge of Ca^{2+} signaling in *T. cruzi*. For this purpose, we carried out a multi-step strategy search in the *T. cruzi* databases to identify the hypothetical Ca^{2+} -binding proteins with experimental evidence of their expression. We selected one of these proteins, named TcCAL1, to investigate its role in the *T. cruzi* life cycle. To achieve this, parasites expressing different levels of TcCAL1 were evaluated regarding their proliferation,

differentiation, and host cell invasion. Our results reinforce the importance of studying and revealing the function of hypothetical proteins, which may be relevant for parasite survival.

MATERIAL AND METHODS

Identification of Kinetoplastid-Specific Proteins and Phylogenetic Analysis

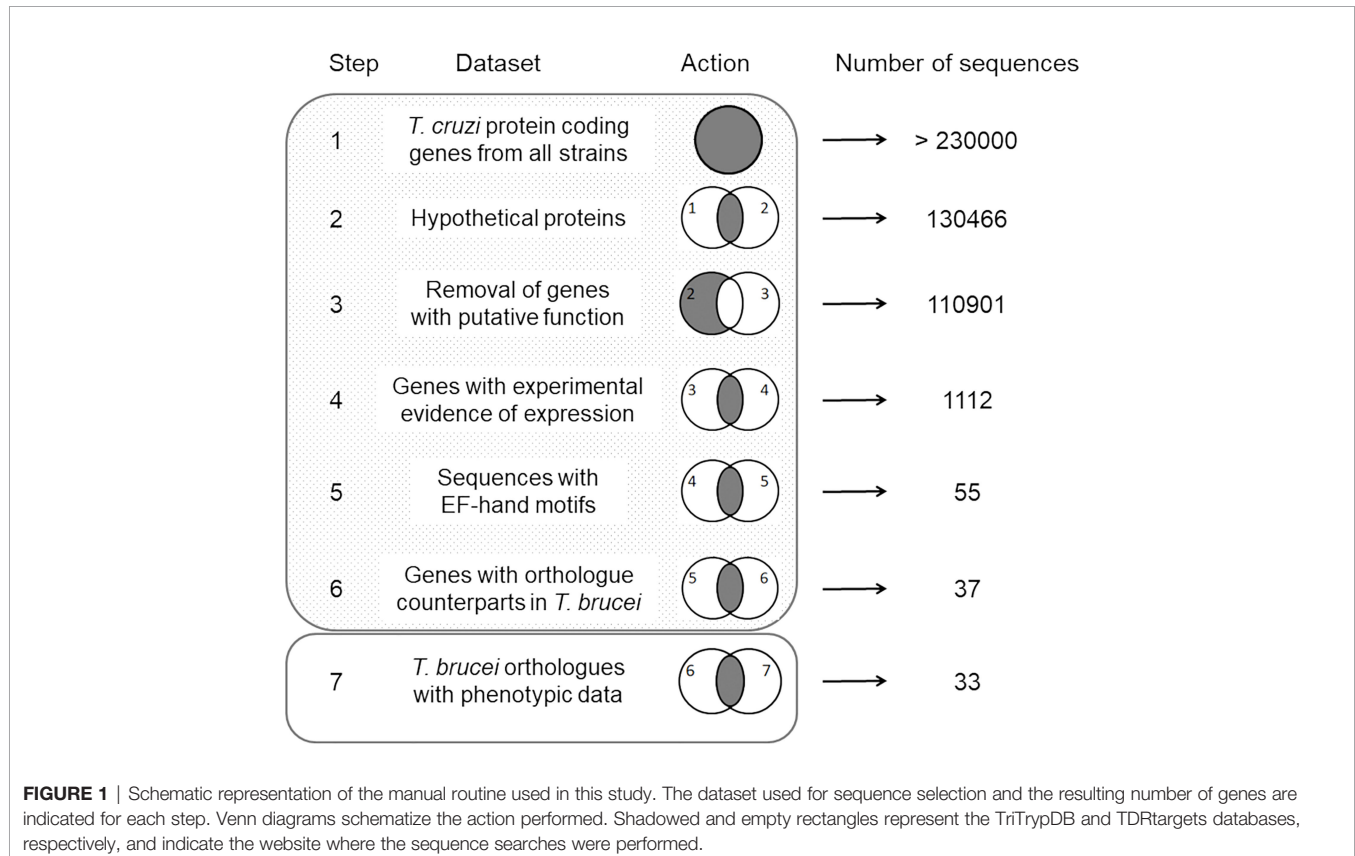
Searches for protein coding sequences were performed on the TriTrypDB and TDRtargets databases (Aslett et al., 2010; Alsford et al., 2011). Sequence processing was carried out following these user-defined steps: 1—selection of sequences annotated as hypothetical proteins in the *T. cruzi* genomes (last accessed March 1st, 2022), 2—removal of sequences with any putative function assigned, 3—selection of hypothetical proteins containing at least one EF-hand domain, 4—selection of proteins with experimental evidence of expression by proteome analysis, 5—selection of sequences having orthologues in *Trypanosoma brucei*, and 6—selection of sequences whose *T. brucei* orthologues revealed evidence of essentiality in parasite proliferation and differentiation. This strategy is schematized in **Figure 1**.

The evolutionary history of the TcCAL1 protein was constructed using the homologous protein sequences from parasites of the Kinetoplastid order retrieved from the TriTrypDB database. The homologous sequence of *Bodo saltans*

was used as the outgroup (Deschamps et al., 2011). Multiple sequence alignment of these sequences (MSA) was constructed using the MAFFT 7 server using BLOSUM 62 as the scoring matrix and visualized with the MEGA-X software (Katoh et al., 2019). The MSA was used to perform phylogenetic analysis using the Maximum Likelihood method in RAxML (Stamatakis, 2014). ProtTest 3.4 was used to calculate the phylogenetic parameters (Darriba et al., 2011). A 500-rapid bootstrap was selected to estimate the robustness of the phylogenetic inference. The transfer bootstrap expectations were calculated using BOOSTER (booster.pasteur.fr/) (Lemoine et al., 2018). FigTree (<https://tree.bio.ed.ac.uk/software/figtree>) was used to visualize and edit the trees. The protein structure prediction was performed using AlphaFold (Jumper et al., 2021) and visualized and edited using the molecular graphics system PyMOL (<https://www.schrodinger.com/products/pymol>). The ion binding sites were predicted using the COACH server (<https://zhanggroup.org/COACH/>).

Recombinant Protein Expression and Polyclonal Antiserum Production

The coding sequence of TcCAL1 was amplified from *T. cruzi* genomic DNA by PCR using the primers 5'-GCGCCATG GCTATGCAACGCAGTCTAAT-3' and 5'-GCGGTCTG ACTCGCTG AGCAAAATT-3'. The amplified fragment was cloned into the *NcoI-SalI* restriction sites of the pET22 expression vector, fused to a C-terminal six histidine tag



(6xHis), and transformed into BL21 pLysS *E. coli* cells. The recombinant protein TcCAL1-6xHis was purified from bacterial extracts by affinity chromatography using a nickel-charged agarose resin (Ni-NTA Agarose, Qiagen). Four adult male BALB/c mice were immunized with three boosts of 30–50 µg of TcCAL1-6xHis each. A pre-immune sample was taken from the mice prior to immunization. Fourteen days after the last boost, the mice were bled and the antisera were obtained. Procedures concerning animal treatments in this study were carried out in accordance with the bioethics guidelines of the National Research Council regarding the care and use of laboratory animals (Garber, 2011).

Parasite Culture and Samples

T. cruzi epimastigote forms from the Discrete Typing Units DTUI and DTUII (hereafter named CL and Y, respectively), were grown at 28°C in Liver Infusion Tryptose medium (LIT) supplemented with 10% Fetal Bovine Serum (FBS) (Natocor), 20 mM glucose, 20 µM hemin (Sigma-Aldrich), 10 U/ml Penicillin and 10 mg/ml Streptomycin (*In vivogen*). Samples of epimastigotes, cell culture-derived trypomastigotes, and Vero cells infected with intracellular amastigotes from the *T. cruzi* Brazil strain were kindly provided by Dr. Cecilia Albareda.

Overexpression of TcCAL1-6xHis in *T. cruzi*

To generate transgenic parasites, the sequence coding for TcCAL1-6xHis was isolated by PCR from the pET22 recombinant vector generated in *Recombinant Protein Expression and Polyclonal Antiserum Production* using the primers 5'-GCTCTAGAATGCAACGAGTCTAAT-3' and 5'-GCGCATCGATCTCAGTGGTGGTGGT-3', and sub-cloned into the *XbaI-XhoI* restriction sites of the pTREX expression vector (Vazquez and Levin, 1999). The recombinant plasmid pTREX/TcCAL1-6xHis was amplified in DH5α *E. coli* cells and purified using the PureYield™ Plasmid Midiprep System (Promega, USA). *T. cruzi* epimastigotes from CL or Y strains were transfected with pTREX/TcCAL1-6xHis following a standard electroporation protocol (Potenza et al., 2012). Early mid-log phase epimastigote cultures were washed twice with cold phosphate saline buffer (PBS; 39 mM Na₂HPO₄, 10 mM NaH₂PO₄, 137 mM NaCl, 22 mM KCl, pH 7.4) and resuspended in 350 µl of cold transfection buffer (0.1 Mm of CaCl₂, 0.5 of mM MgCl₂, and 272 of mM sucrose in PBS, pH 7.2) at a density of 1×10^8 parasites/ml. The cells were mixed with 40 µg of DNA, transferred to 0.2 mm electroporation cuvettes, and incubated on ice for 5 min. Parasites were electroporated with one pulse at 400 V and 500 µF using a Gene Pulser® II electroporator (Biorad, USA), recovered on ice 5 min and then incubated in 7 ml of LIT supplemented with 20% of FBS at 28°C overnight. The selection of recombinant parasites was performed for 4 weeks in the presence of increasing concentrations of Geneticin (G418, InvivoGen) up to 500 µg/µl. To perform the culture controls, the transfection and selection procedures were performed using the empty vector pTREX on epimastigotes from CL or Y strains.

Proliferation Assays

A total of 1×10^5 epimastigotes/ml from CL or Y *T. cruzi* cultures stably transfected with TcCAL1-6xHis or the empty vector pTREX (hereafter named CL-CAL1 and CL-C or Y-CAL1 and Y-C, respectively) were grown in LIT supplemented with G418. Cultures were incubated at 28°C over time and samples were taken at 24 or 48 h intervals. The number of parasites was counted in triplicate using a Neubauer chamber and an optical microscope. Growth curves were expressed in the number of parasites per ml.

Metacyclogenesis Assays

Epimastigote forms from CL-C and CL-CAL1 or Y-C and Y-CAL1 cultures were differentiated into metacyclic trypomastigotes using the protocol described by Rodríguez Durán et al. (2021). Briefly, $\sim 3 \times 10^7$ epimastigotes growing in 3 ml of LIT supplemented with G418 were added to 15 ml-conical tubes containing blood-agar slants (generating a biphasic medium), and incubated at 28°C for three weeks. Parasites transformed into metacyclic trypomastigotes as well as non-differentiated epimastigotes were counted in triplicate for each culture. Epimastigotes from the Y strain were also differentiated using the Triatomine Artificial Urine (TAU) method (Contreras et al., 1985). For this, a 7-day-old epimastigote culture was incubated in TAU medium (190 mM of NaCl, 17 mM of KCl, 2 mM of MgCl₂, 2 mM of CaCl₂, and 8 mM of sodium phosphate buffer, pH 6.0, all from Biopack) for 2 h at room temperature. Then, the parasites were pelleted by centrifugation, resuspended in TAU-3AAG medium (TAU supplemented with 50 mM sodium glutamate, 10 mM L-proline, 2 mM sodium aspartate, and 10 mM glucose, all from Sigma-Aldrich) and incubated for up to 72 h at 28°C. Every 24 h, metacyclic forms were counted in triplicate. For both protocols, the percentage of metacyclogenesis was calculated using the formula: (metacyclic trypomastigote number \times 100)/(metacyclic trypomastigote number + epimastigote number).

Metacyclic Trypomastigotes Isolation

Y-C or Y-CAL1 metacyclic trypomastigotes from the biphasic medium were isolated from the remaining non-differentiated epimastigote forms by complement-mediated parasite lysis, as previously described (Cestari et al., 2009). In brief, the liquid phase of the biphasic medium containing both the metacyclics and the non-differentiated epimastigote forms was centrifuged and resuspended in 800 µl of non-heat inactivated FBS diluted in 200 µl of RPMI medium. After incubation at 37°C for 1 h, the suspension was centrifuged again to pellet the metacyclic forms and the cellular debris generated by the epimastigote lysis. Then, the sample was resuspended in RPMI supplemented with 5% heat-inactivated FBS, incubated for 3 h at 37°C to allow the motile metacyclic trypomastigotes to swim back to the supernatant, and finally transferred to a new tube. Purified metacyclic trypomastigotes were washed thoroughly with RPMI supplemented with FBS prior to downstream applications. Centrifugations were performed at 3,000×g for 10 min.

Adhesion and Invasion Assays

Metacyclic trypomastigotes isolated as described in *Metacyclic Trypomastigotes Isolation* were used to infect Vero cells at a 300:1 parasite:host cell ratio. Due to the differences in multiplicity of infection among Y-C and Y-CAL1 parasites, the 300:1 ratio allowed us the comparison of the following parameters. For adhesion assays, 6×10^6 parasites were placed on 13 mm round glass coverslips coated with 2×10^4 Vero cells and incubated for 2 h at 37°C followed by five washings. Coverslips were stained with ColorPack panoptic dye kit (BioPack) following the instructions of the supplier. Stained cells were visualized and photographed using an optical microscope to calculate the percentages of cells containing adhered parasites and the number of parasites per host cell in randomly selected fields. A total of 200 host cells were counted in triplicate. For invasion assays, a similar experimental procedure was carried out by incubating parasites with Vero cells for 24 h. After 48 h post-infection, coverslips were stained with Giemsa and observed using a microscope to calculate the percentages of infected cells and the number of intracellular amastigotes per host cell in randomly selected fields. Here, 300 host cells were counted in triplicate. All incubations were made in RPMI plus 5% FBS. All washes were performed using PBS. The adhesion index was calculated by multiplying the percentage of Vero cells with attached parasites by the mean number of adhered parasites per cell. The invasion index was determined by multiplying the percentage of infected Vero cells by the mean number of amastigotes per infected cell. The index-fold change (FC) was calculated using the formula $FC = (I_{Y-CAL1} - I_{Y-C})/I_{Y-C}$, where I_{Y-CAL1} or I_{Y-C} refer to the adhesion or invasion indices for Vero cells incubated with Y-C or Y-CAL1 parasites, respectively.

Amastigogenesis Assay

In vitro amastigogenesis was performed following the protocol described elsewhere (Hernández-Osorio et al., 2010). For example, 1×10^7 metacyclic trypomastigotes were collected by centrifugation at $3,000 \times g$ for 10 min. Pellets were subsequently washed three times with MEM pH 7.4 and twice with MEM pH 5, in the absence of FBS. Parasites were then resuspended in 100 μ l of MEM pH 5 supplemented with 0.4% BSA and incubated at 37°C. Samples were taken at 0, 4, and 6 h and processed as described in *Immunofluorescence Microscopy* for microscopic analysis. The percentages of axenic amastigotes and intermediate or non-differentiated forms were determined by counting 300 parasites in randomly selected fields per sample.

Immunofluorescence Microscopy

T. cruzi-infected Vero cells grown on round glass coverslips or parasites adhered to poly-lysine coated microscope slides were fixed with 4% paraformaldehyde for 30 min, permeabilized with 0.1% Triton X-100 for 3 min, and washed twice. After blocking samples in 2% bovine serum albumin (BSA), slides were incubated with the anti-TcCAL1 or pre-immune antiserum, an anti-parafagellar rod mouse monoclonal antibody (anti-PFR, kindly provided by Dr. S. Schenkman) to reveal the flagellum or an anti-tubulin rat antibody, clone YL1/2 (anti-TUB, Chemicon)

to detect the parasite body by its affinity to tyrosinated tubulin (diluted 1:300, 1:2, or 1:500, respectively, in 1% BSA). The secondary antibodies were Alexa Fluor 488-conjugated goat anti-mouse (Invitrogen) or Cy3-conjugated goat anti-rat (Jackson), both diluted 1:1,000. All washes and compound dilutions were performed in PBS. All incubations lasted for 1 h each at room temperature. Slides were mounted on Vectashield® Antifade reagent (Vector Laboratories), containing 10 mg/ml of 4,6-diamino-2-phenylindole (DAPI). The Cells were observed using an Olympus BX-61 fluorescence microscope.

Protein Extracts and Western Blot

To obtain protein parasite extracts, epimastigotes or metacyclic forms were harvested by centrifugation at $1,000 \times g$, washed with PBS, resuspended in cold cell lysis buffer containing 50 mM Tris-HCl pH 7.5, 14 mM β -mercaptoethanol, protease inhibitor cocktail (Roche), and disrupted by six freezing-thawing cycles in liquid nitrogen. Protein-soluble fractions were separated from the cellular debris by centrifugation at $12,000 \times g$ for 10 min at 4°C and then quantified using Bradford's method (Bradford, 1976). Pellets containing cellular debris were solubilized by the addition of 5 \times SDS-PAGE sample buffer (0.25 M Tris-HCl pH 6.8, 0.5 M DTT, 10% SDS, 50% Glycerol, 0.5% bromophenol blue) up to an equal volume of soluble fraction. All samples were separated on 15% SDS-PAGE polyacrylamide gels and then transferred to nitrocellulose membranes (Amersham Biosciences). The membranes were blocked with 5% non-fat milk in PBS for 1 h and then incubated overnight at 4°C with anti-TcCAL1 or mouse monoclonal anti- α -tubulin (Sigma Aldrich) diluted 1:300 or 1:8,000, respectively. The membranes were then washed four times with PBS-0.1% Tween 20 and incubated with peroxidase-conjugated goat anti-mouse IgG secondary antibody (Kirkegaard & Perry Laboratories KPL), diluted 1:1,000 for 1 h. Incubations were performed at room temperature unless otherwise indicated. Protein bands were revealed using Western Lightning® Plus-ECL (Perkin Elmer) chemiluminescence reagent and visualized on a GeneGenome XRQ device (Syngene).

Statistics

All statistical analysis was performed using the tests indicated in figure legends and the GraphPad Prism 5.0 (GraphPad Software). All data were considered statistically significant at $p < 0.05$ and values are expressed as means \pm standard deviation (SD).

RESULTS

TcCAL1 is a Kinetoplastid-Specific Protein With Predicted Ca^{2+} Binding

To address the identification of novel proteins potentially involved in *T. cruzi* Ca^{2+} signaling, we performed user-defined sequence searches at the TriTrypDB web site, a database containing the annotation of several kinetoplastid genomes integrated into bioinformatics resources and experimental datasets. Therefore, we identified gene sequences from *T. cruzi*

that codify for proteins containing at least one EF-domain for Ca^{2+} binding and exhibited experimental evidence of their expression by proteome analysis. The proteins with any putative function were excluded from the dataset by removing the coding sequences containing the term “putative” in their annotation. Based on data from RNAi experiments (Alsford et al., 2011), we selected the *T. cruzi* proteins that had orthologue counterparts and experimental evidence of essentiality in *T. brucei*. As a result, 33 proteins were identified and one of them was selected for further study (TcCLB.507165.30). This protein, named TcCAL1, is 103 amino acid-long, with two predicted EF-hand motifs spanning the residues 31–97 and one phosphorylation site at serine 4 (Marchini et al., 2011) (Figure 2A). *Ab initio* protein structure prediction using AlphaFold allowed us to assign the putative tridimensional folding only in the EF-hand regions of the protein, since the first 31 amino acids did not match to any other structure with confidence enough to make a prediction

(Figure 2B). Other TcCAL1-orthologues were identified in other *Trypanosoma* species and *Leishmania* genera, as well as in the free-living *B. saltans*. The phylogenetic relationships inferred from the tree based on TcCAL1-orthologues fit well with the current taxonomy of kinetoplastids (Figure 2C). However, in BLAST searches at NCBI, no clear orthologues were found in organisms other than kinetoplastids.

TcCAL1 Localization in *T. cruzi*

To reveal the subcellular localization of TcCAL1 in the main *in vitro* developmental forms of *T. cruzi*, we used a polyclonal antiserum against the purified recombinant TcCAL1-6xHis produced in *E. coli* by immunofluorescence microscopy. Images showed that TcCAL1 was present along the entire body of the parasite cell but to a lesser extent in organelles containing the nuclear and mitochondrial DNA (Figure 3A). In accordance, western blot (WT) of protein extracts using the anti-TcCAL1-6xHis antibody also revealed that the signal corresponding to

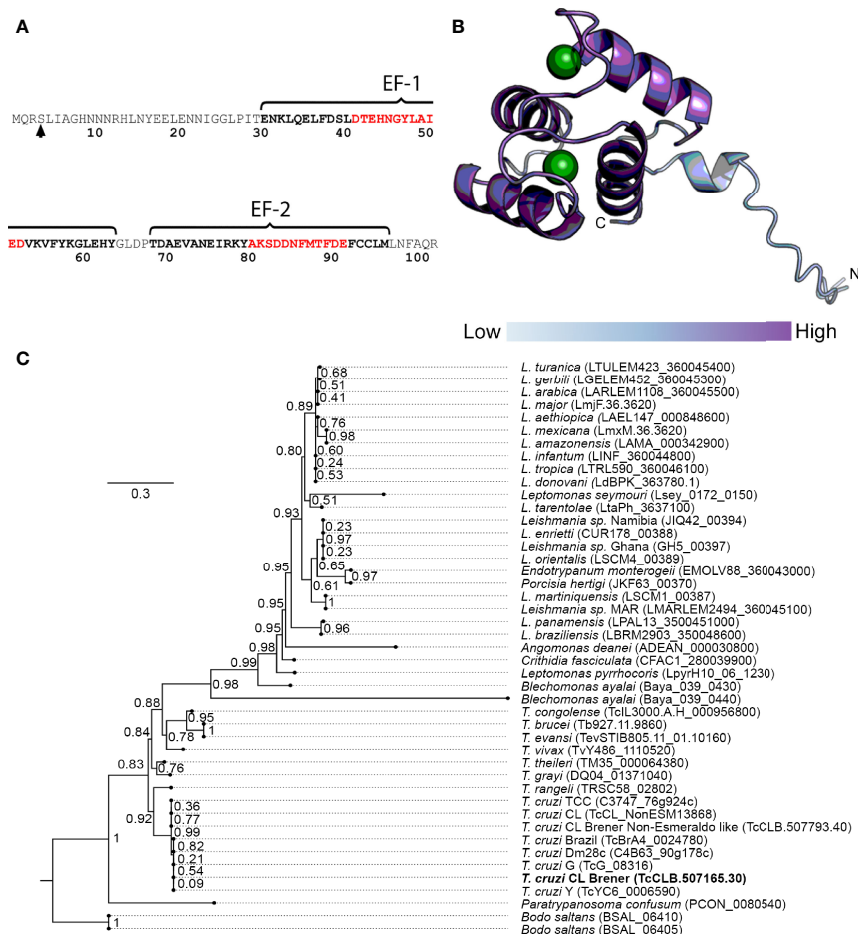


FIGURE 2 | Sequence features of TcCAL1 and a phylogenetic tree. **(A)** Amino acid sequence and position of the EF-hand motifs. Residues in black and red bold indicate the alpha helices and the Ca^{2+} binding cleft, respectively. The arrow indicates the phosphorylated serine. **(B)** Predicted tridimensional structure of TcCAL1. The circles represent Ca^{2+} ions. The different color intensity indicates the model confidence, being high at the C-terminus and lower at the N-terminus (dark and light blue, respectively). **(C)** TcCAL1 evolutionary relationship with different species of trypanosomatids. The scale-bar represents 0.3 substitutions per position in the amino acid sequence. The numbers at the branches indicate bootstrap values. TcCAL1 is highlighted in bold.

TcCAL1 was mainly present in the soluble fraction of epimastigote forms (**Figure 3B**).

Effect of TcCAL1-6xHis Overexpression on *T. cruzi* Proliferation and Differentiation

To address the functional characterization of TcCAL1, we first analyzed the effect of its over-expression on the proliferation and differentiation of *T. cruzi* epimastigotes. For this, we generated transgenic cultures overexpressing the fusion protein TcCAL1-6xHis or harboring the empty vector pTREX, used as a control. The effect of TcCAL1-6xHis overexpression on proliferation was determined by measuring the number of epimastigotes per ml of culture over time. Growth curves showed no significant differences in proliferation during the exponential phase in TcCAL1-6xHis overexpressing parasites compared to controls for both Y and CL strains (**Figure 4A**). However, significant differences were found in the stationary phase of growth in the CL strain. TcCAL1-6xHis overexpressing parasites stopped growing on day 9 of culture, while control parasites continued to divide. This pattern was observed until day 11, when the number of parasites in TcCAL1-6xHis-overexpressing and control cultures was 1.75×10^7 versus 2.5×10^7 epimastigotes/ml, respectively.

Then, we moved forward to study the effect of TcCAL1-6xHis overexpression on the metacyclogenesis process by performing differentiation assays in biphasic medium. The metacyclogenesis rates for parasites overexpressing TcCAL1-6xHis and controls were calculated after 19 days, when the number of metacyclics in both cultures had risen to the maximum. The better performance in differentiation for the CL strain was found on day 38. Therefore, metacyclogenesis rates were calculated after this period of incubation (**Figure 4B**). Results showed a significant decrease in metacyclogenesis percentages in TcCAL1-6xHis overexpressing parasites compared to controls for both strains (Y: 24.4 ± 2.5 vs 40.3 ± 3.9 ; CL: 9.0 ± 3.2 vs 18.1 ± 1.0). In parallel,

we also performed differentiation assays for the Y strain following the TAU protocol. Although the total number of metacyclics reached by this method was lower than that of the biphasic medium, we found that the metacyclogenesis was also impaired in TcCAL1-6xHis overexpressing parasites compared to controls (4.7 ± 0.6 vs 8.0 ± 1.0). WB analysis corroborated the expression of TcCAL1-6xHis in metacyclics obtained after differentiation in biphasic medium for the Y strain (tCAL1, **Figure 4B**). Here, a sample control (e-tC, **Figure 4B**) was performed to confirm that the signal detected in WB corresponding to either the endogenous TcCAL1 or the recombinant TcCAL1-6xHis came from metacyclic trypomastigotes and not from residual complement-lysed epimastigote debris. For this, epimastigotes overexpressing TcCAL1-6xHis were mixed with metacyclic trypomastigotes carrying the empty pTREX vector (controls) and complement-mediated lysed by the addition of non-heat inactivated FBS. Then, the sample was washed to remove the TcCAL1-6xHis from epimastigote forms and subjected to WB analysis. The absence of signal at the TcCAL1-6xHis expected size indicated that the proteins detected in all samples were derived exclusively from metacyclic trypomastigotes.

We further wondered whether TcCAL1-6xHis overexpression would alter the differentiation of metacyclic trypomastigotes into axenic amastigotes. Hence, we performed amastigogenesis assays in which we incubated parasites from the Y strain in a low pH medium without serum (**Figure 5A**). Samples were taken at different times and, to better visualize the parasite morphology, immunofluorescence microscopy was carried out to reveal the nuclear and kinetoplast DNA, as well as the presence or absence of the flagellum. Besides trypomastigotes and amastigotes, we also counted the intermediate forms, which are rounded parasites with a relative position of nuclear and kinetoplast DNA similar to trypomastigotes with or without a flagellum (IF/+FLG or IF/-FLG, respectively) (**Figure 5B**).

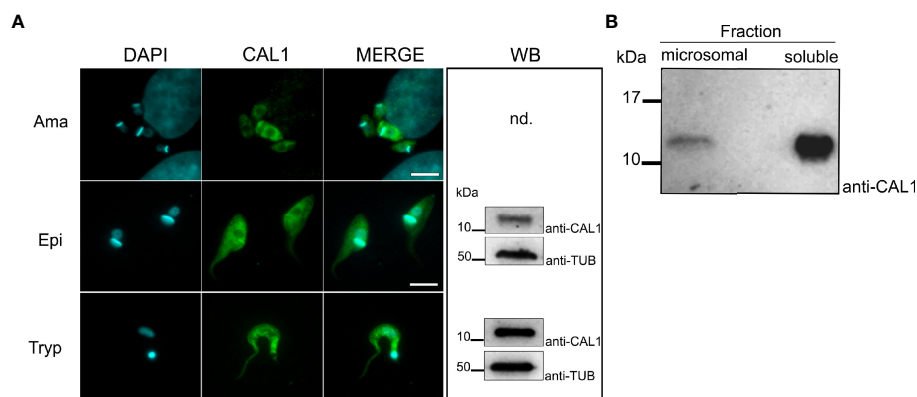


FIGURE 3 | Expression and localization of endogenous TcCAL1. **(A)** Immunofluorescence microscopy of different stages of *T. cruzi* from the Brazil strain. Ama, Epi, and Tryp denote amastigote, epimastigote, and trypomastigote forms, respectively. DAPI and anti-CAL1 indicate staining of the nuclei and kinetoplast, and the signal corresponding to the anti-TcCAL1-6xHis serum, respectively. Scale bar: 7 μ m. WB, Western blot analysis of whole-cell extract from the corresponding developmental form using the anti-TcCAL1-6xHis serum. Nd, not determined (due to limited sample size). **(B)** WB analysis of microsomal and soluble fractions from epimastigote protein lysates. In panels **(A, B)**, 30 μ g of total protein extract was loaded in each lane. Nitrocellulose membranes were incubated with the anti-TcCAL1-6xHis antiserum (anti-CAL1). In **(A)**, an anti-Tubulin antibody (Anti-TUB) was used as a loading control. Band signals appeared at the expected sizes. kDa, kiloDaltons.

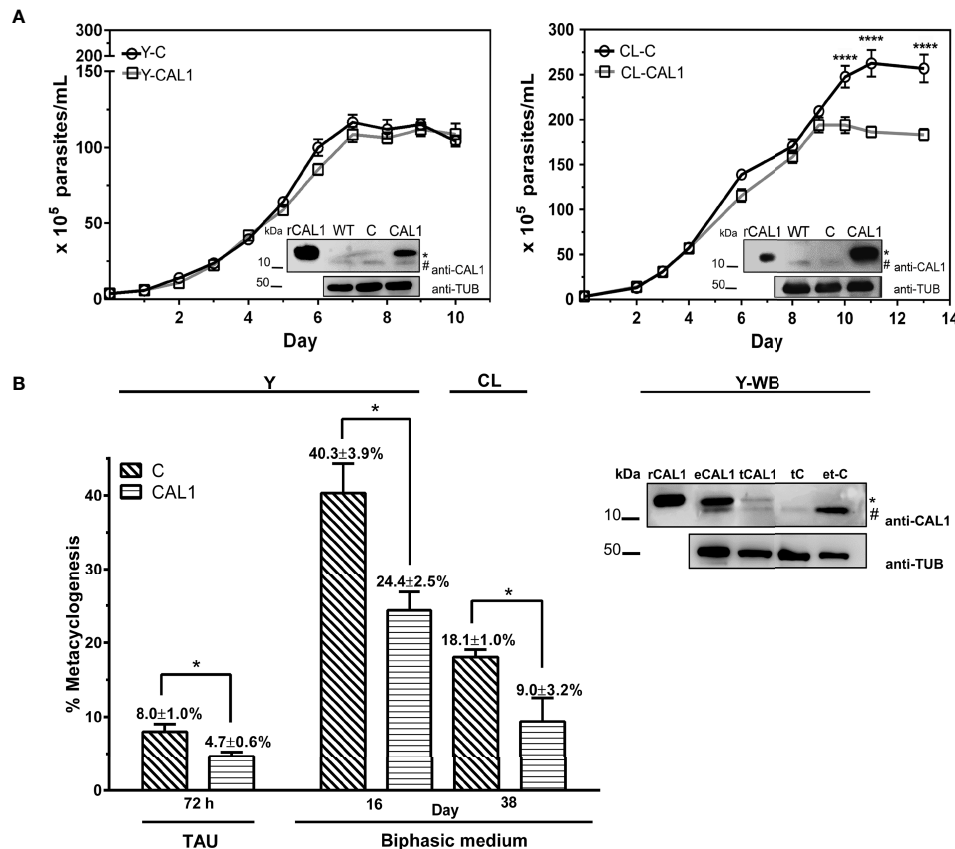


FIGURE 4 | Effect of TcCAL1-6xHis overexpression on epimastigote proliferation and differentiation. **(A)** Growth curves of TcCAL1-6xHis overexpressing parasites from Y and CL strains. Epimastigote cultures overexpressing TcCAL1-6xHis (CAL1) or transfected with the pTREC empty vector (C) were counted over time. Statistical analyses were performed using a one-way ANOVA test. **** $p < 0.0001$. At the inset of each curve, WB shows the overexpression of TcCAL1-6xHis in *E. coli* and WT, C rCAL1, recombinant CAL1 and CAL1, protein extracts from wild type, controls, and TcCAL1-6xHis-overexpressing parasites, respectively. A total of 20 μ g of total protein extracts were loaded into each well. **(B)** Metacyclogenesis rates for parasites from Y and CL strains overexpressing TcCAL1-6xHis and the respective controls. The method used to differentiate epimastigotes into metacyclic trypomastigotes is indicated (TAU or biphasic medium). Statistical analyses were performed using the Student's t-test. * $p < 0.05$. In the right panel, WB analysis of Y strain shows the expression of TcCAL1-6xHis in metacyclic trypomastigotes from biphasic medium. eCAL1 and tCAL1, epimastigotes and metacyclic trypomastigotes expressing TcCAL1-6xHis, respectively; tC, control metacyclics carrying the empty vector pTREC; e-tC, isolation sample control (prepared with trypomastigotes transfected with pTREC after incubation and subsequent washes of TcCAL1-6xHis-overexpressing epimastigote protein lysates). A total of 15 μ g of total protein extracts were loaded into each well. In panels **(A, B)**, graphs and WB show one representative result of four and three independent experiments, respectively. The anti-TcCAL1-6xHis antiserum (anti-CAL1) was used to detect the recombinant protein and the endogenous TcCAL1 (indicated with a dot and a numeral, respectively). An anti-Tubulin antibody (Anti-TUB) was used as a loading control. kDa, kiloDaltons.

Although the number of amastigotes increased over time, no significant differences were found in amastigogenesis rates for TcCAL1-6xHis overexpressing parasites compared with controls in the period analyzed.

Overexpression of TcCAL1-6xHis Enhances the Infectivity of *T. cruzi*

We next evaluated the effect of TcCAL1 on the interaction with the mammalian host *in vitro* by adhesion assays. To that end, TcCAL1-6xHis-expressing metacyclic trypomastigotes from the Y strain, obtained by differentiation in biphasic medium, were incubated with Vero cells for 2 h, washed, and then stained for analysis and counting. The results showed that the percentage of cells with adhered parasites was significantly higher in mammalian cultures incubated with transgenic

trypomastigotes than in controls (76.3 ± 14 vs 44.8 ± 3.5 , respectively). Consistently, the number of parasites adhered per Vero cell was significantly higher for cultures incubated with trypomastigotes expressing TcCAL1-6xHis compared to controls ($8,603 \pm 128$ vs 296 ± 60 , respectively) (Figure 6A). We then assessed the effect of TcCAL1-6xHis overexpression during the host cell invasion process. Thus, isolated metacyclic trypomastigotes overexpressing TcCAL1-6xHis or controls were loaded on coverslips coated with Vero cells for 24 h following subsequent washes. After 48 h post infection, cultured cells were analyzed to compare the invasion capacity of parasites. As shown in Figure 6B, the percentages of infected cells, as well as the number of internalized amastigotes, were significantly higher in Vero cells infected with TcCAL1-6xHis-expressing trypomastigotes than in controls (41.2 ± 6.23 vs 18.9

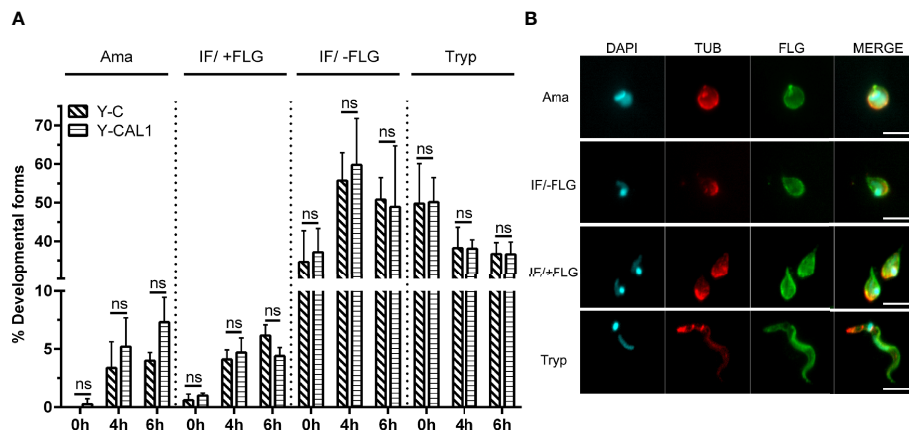


FIGURE 5 | Effect of TcCAL1-6xHis overexpression on *in vitro* amastigogenesis. **(A)** Metacyclic trypomastigotes from Y strain expressing TcCAL1-6xHis or carrying the empty vector (Y-CAL1 or Y-C, respectively) were incubated in low pH medium. Samples were taken at 0, 4, and 6 h for counting and examination of the different morphological forms. The graph shows the percentage of each parasite form at different times. Ama, Tryp, IF/+FLG and IF/-FLG indicate axenic amastigotes, metacyclic trypomastigotes, and intermediate forms with or without flagellum, respectively. Statistical analyses were performed using Student's t-test. ns, no significant. This graph shows one representative result of two independent experiments. **(B)** Immunofluorescence microscopy showing the morphology of each developmental form. DAPI staining reveals the kinetoplast and nuclear DNA. TUB and FLG indicate incubation with anti-Tubulin or anti-PFR antibody, respectively.

$\pm 5.34\%$ and $1,398 \pm 48$ vs 926 ± 124 parasites/100 host cells, respectively).

Overall, both the adhesion and invasion processes were promoted in Vero cultures incubated with TcCAL1-6xHis overexpressing parasites compared to controls. Nevertheless, the fold change comparing transgenic and control cultures was 3.96 for the adhesion index, whereas for the invasion index it was 2.21. This finding suggests a more pronounced beneficial effect of recombinant TcCAL1-6xHis during the attachment of parasites to the surface of Vero cells compared to the internalization process.

DISCUSSION

Herein, we explored the role of TcCAL1, a novel protein which renders both evidence of expression and putative Ca^{2+} binding domains, throughout the *in vitro* life cycle of *T. cruzi*. Our data showed that the overexpression of a tagged version of TcCAL1 impaired the metacyclogenesis of epimastigotes and enhanced the infectivity of metacyclic tripomastigotes to invade Vero cells. However, this overexpression had no substantial effects on the exponential proliferation of epimastigote forms or on the differentiation of metacyclic trypomastigotes into amastigotes. These findings reveal that TcCAL1 protein levels may exert a relevant role in *T. cruzi* metacyclogenesis and host-cell invasion.

The number of peptides found in datasets from proteomic studies (Atwood et al., 2005; Marchini et al., 2011; Queiroz et al., 2014; Jesus et al., 2017), and the presence of the endogenous TcCAL1 on our WB (Figure 3B), show evidence of its abundance in this organism. It could also be possible that TcCAL1 may not be tightly regulated during parasite

proliferation. Even more, TcCAL1-6xHis overexpression was non-detrimental for other organisms since we were able to produce this recombinant protein in *E. coli* and *Leishmania*. That said, the curve for the CL strain exhibited a faint but significant phenotypic difference after the exponential growth, in which parasites overexpressing TcCAL1-6xHis reached the stationary phase earlier in comparison to control cultures. Previously, it was shown that under starving conditions, epimastigote proliferation becomes more sensitive to Ca^{2+} availability for maintaining mitochondrial bioenergetics (Chiurillo et al., 2019). Here, independent or synergistic mechanisms would explain this slightly lower performance in the cell density achieved by TcCAL1-6xHis-overexpressing cultures. Among them, a reduced cytosolic Ca^{2+} availability due to ion-sequestering by TcCAL1-6xHis would lead to early parasite starvation. A dominant negative effect exerted by the tagged version of TcCAL1, which is evidenced only at high levels of expression and culture densities, would also impair the parasite growth. By contrast, no difference was observed at the stationary stage of growth between control and TcCAL1-6xHis-overexpressing epimastigotes from Y strain. In comparison to CL, parasites from Y strain rendered lower culture densities ($\sim 2.7 \times 10^7$ vs 1.2×10^7 , respectively) and recombinant TcCAL1-6xHis expression levels (see insets in Figure 4A). Both aforesaid evidences would explain the absence of measurable changes in the growth curves of transgenic and control parasites from Y strain, in addition to the intrinsic differences that cultures belonging to different DTU have in response to the same stimulus or condition (Ruiz et al., 1998; Majeau et al., 2021).

Along with a change in the morphology and the metabolic state, an abrupt but transitional increase in the cytosolic Ca^{2+} occurs during *T. cruzi* metacyclogenesis (Lammel et al., 1996;

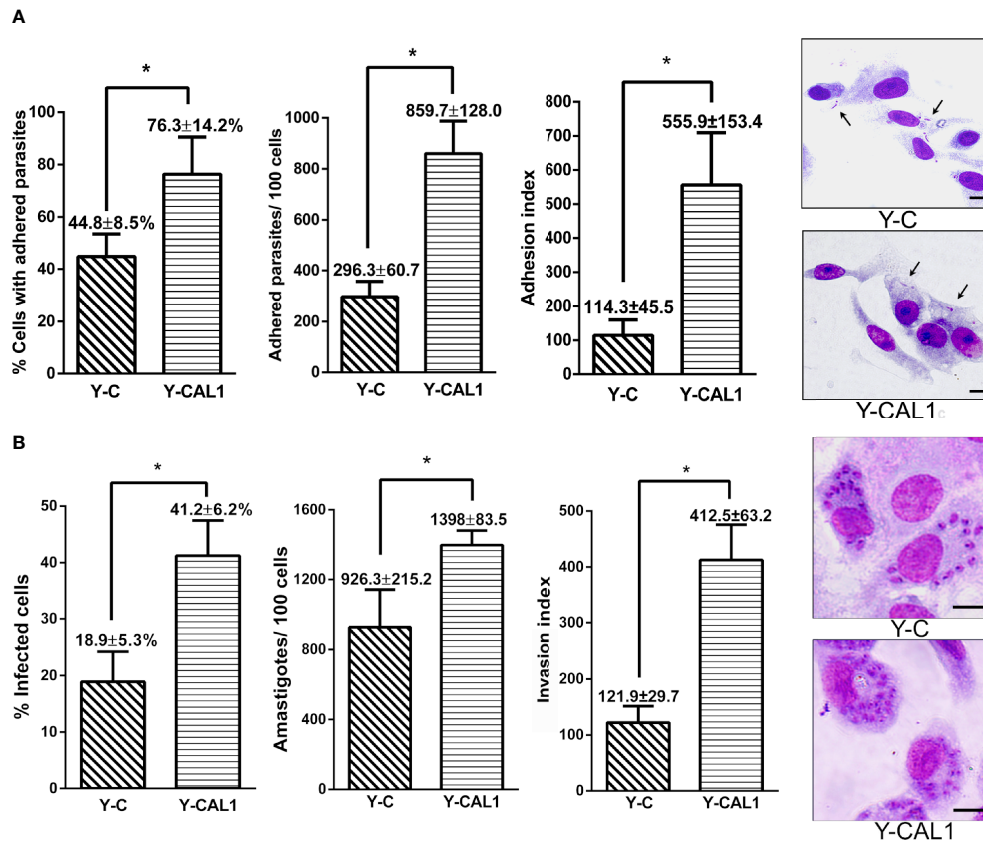


FIGURE 6 | Effect of TcCAL1-6xHis expression on the infectivity of *T. cruzi*. **(A)** *In vitro* adhesion assay. Metacyclic trypomastigotes from Y strain expressing TcCAL1-6xHis or carrying the empty vector (Y-CAL1 or Y-C, respectively) were incubated with Vero cells for 2 h to calculate the percentage of cells with adhered parasites, the number of parasites adhered per 100 cells, and the adhesion index. On the right panel, panoptic stained cultures for each condition. Black arrows indicate some adhered parasites. **(B)** *In vitro* invasion assays. Metacyclic trypomastigotes from Y strain expressing TcCAL1-6xHis or carrying the empty vector (Y-CAL1 or Y-C, respectively) were incubated with Vero cells to calculate the infection percentages, determined by counting the number of infected cells after 48 h post-infection. The total number of internalized amastigotes in 100 Vero cells, as well as the invasion indexes, are also shown. On the right panel, Giemsa staining of infected Vero cells. In panels **(A, B)**, statistical analyses were performed using Student's t-test. **p* < 0.05. Data from one representative experiment of three independent experiments is shown. Scale bar, 10 μ m.

Hashimoto et al., 2016; Gonçalves et al., 2018). Several Ca^{2+} - or Ca^{2+} -activated channels involved in metacyclogenesis and other processes have been identified in the parasite (Furuya et al., 2001; Ramakrishnan and Docampo, 2018; Chiurillo et al., 2019; Dave et al., 2021). Meanwhile, few Ca^{2+} -binding or -regulated proteins have been characterized so far (Belaunzarán et al., 2009; Hamedi et al., 2015; Lander et al., 2018), and three proteins involved in calcium homeostasis have been shown to play a role in metacyclogenesis: MICU1 and MICU2 (Bertolini et al., 2019) and Letm1 (Dos Santos et al., 2021). Here, we found that the metacyclogenesis rates were significantly lower in parasites overexpressing TcCAL1-6xHis for both CL and Y strains. One possible explanation may rely on an exacerbated Ca^{2+} chelating-like effect exerted by TcCAL1-6xHis, which in turn limits the availability of this ion in the cytosol. As a result, this limiting cytosolic Ca^{2+} level would downregulate the function of key enzymatic activities needed for parasite differentiation. On the other hand, TcCAL1 is a relatively small protein containing two

EF-hand motifs located at 31–97 amino acid positions. There is no other putative functional domain in its sequence, and the AlphaFold algorithm failed to predict the tridimensional structure in the region spanning the amino acids 1 to 30, probably due to a high sequence divergence. EF-hand-containing proteins are a huge family of sequences with a broad range of functions (Chazin, 2011). In nature, small proteins containing one pair of EF-hands can act not only as Ca^{2+} buffering systems, but also exhibit catalytic functions or binding proprieties, as in the case of calmoduline, S100 proteins, or parvalbumin (Haiech et al., 2019; Mohanta et al., 2019; Elies et al., 2020). If TcCAL1 has a catalytic or functional domain besides the EF-hand motifs, which in turn could be modulated upon Ca^{2+} binding, relevant for metacyclogenesis, is an important issue that needs further investigation. Certainly, the determination of Ca^{2+} -binding properties of TcCAL1 by circular dichroism, the measurement of Ca^{2+} -binding association/dissociation constants, and the analysis of conformational

changes upon Ca^{2+} binding by magnetic resonance would address some of the hypotheses raised here (Pinto et al., 2003; Shan et al., 2018). It is worth mentioning that the effect of TcCAL1-6xHis overexpression on metacyclogenesis has been observed in both strains analyzed using two different methods. In fact, the percentages of metacyclic trypomastigotes overexpressing TcCAL1-6xHis from CL or Y strains significantly decreased ~50 and 40%, respectively, compared to control cultures. In fact, Y cultures followed the same behavior when incubated in TAU medium, resulting in ~40% fewer metacyclics in TcCAL1-6xHis overexpressing parasites than controls. Unfortunately, it was not possible to differentiate CL parasites using the TAU medium, probably because years of culturing as epimastigote forms dampened their response to external stimulus.

The effect of TcCAL1-6xHis on the *in vitro* *T. cruzi* life cycle was further investigated in host-cell invasion assays. We showed that the overexpression of TcCAL1-6xHis enhanced metacyclic adhesion to Vero cells as well as the infectivity of *T. cruzi*. At this point, it is important to mention that we chose the hexa-histidine sequence as the fusion tag for TcCAL1 to properly differentiate the recombinant from the endogenous protein in transgenic parasites. Although it cannot be completely ruled out, it seems unlikely that the presence of this fusion tag has exerted both beneficial and harmful phenotypes for *T. cruzi*, on the basis of the different parameters analyzed in this work.

The key early events in the invasion of mammalian cells by *T. cruzi* involve the recognition and adhesion to the target-plasma membrane, the parasite internalization and maturation inside a recently-assembled parasitophorous vacuole, and the release from this organelle-like-structure to differentiate into replicative amastigotes in the host cytosol (Andrews and Colli, 1982; Maeda et al., 2012; Rodríguez-Bejarano et al., 2021). Prior to cell invasion, the interaction of membrane surface molecules in *T. cruzi* and their ligands expressed in the host extracellular matrix initiates bidirectional signaling cascades which include Ca^{2+} mobilization in the parasite (Manchola Varón et al., 2021). Then, *T. cruzi* harnesses several mechanisms for its internalization into the host cell, including lysosome-dependent exocytosis, endocytosis, or phagocytosis (Andrade and Andrews, 2004; Barrias et al., 2013; Batista et al., 2020). All these mechanisms depend on the developmental stage and/or the parasite strain and the host cell/tissue type. Some virulence factors have been identified for metacyclic trypomastigotes, such as the surface glycoprotein gp82, which mediates Ca^{2+} -dependent entrance into the host cell (Mortara et al., 2005; Yoshida and Cortez, 2008). In light of the above findings, we envisage a scenario in which *T. cruzi* virulence is fostered by some beneficial function induced by TcCAL1-6xHis instead of cytosolic Ca^{2+} sequestration. In fact, more virulent strains trigger higher Ca^{2+} concentrations during their infection process (Ruiz et al., 1998; Epting et al., 2010). Would it be possible that TcCAL1 binds and/or activates key players in the invasion process?

Could this protein be released outside the parasite, promoting the recognition, adhesion, or internalization, directly or indirectly into the host cell? Without doubt, the identification of the associated proteins or complexes, if any, and the localization of TcCAL1 during the invasion process could provide some clues to answer these questions. In this regard, Jesus et al. (2017) found TcCAL1 associated with parasite chromatin by proteomic tools. Although the authors pointed out that a mislocation due to contamination cannot be completely excluded, TcCAL1 was detected in two of the three extraction assays, being one of the most abundant proteins associated with chromatin. One interesting issue to be addressed is whether endogenous or recombinant TcCAL1 could regulate transcription, leading both to favor parasite virulence.

Finally, we observed a slight difference between the number of intracellular TcCAL1-6xHis-expressing amastigotes per Vero cell and their controls, which could correlate to some extent with the amastigote rates (Figure 5A). Although axenic and intracellular amastigotes exhibit differential features (Silva et al., 1998; Alcantara et al., 2021), the activity of phosphoinositide phospholipase C is Ca^{2+} -dependent, an enzyme that is upregulated during differentiation from trypomastigotes into amastigotes (Furuya et al., 2000). However, there are no studies measuring the Ca^{2+} levels during this process. The role of TcCAL1 and its interaction with Ca^{2+} during amastigogenesis, and parasite attachment and internalization into the host cell is a current matter of investigation in our laboratory. In summary, our work strengthens the relevance of characterization the functions of hypothetical proteins to unravel *T. cruzi* biology.

DATA AVAILABILITY STATEMENT

The datasets presented in this study can be found in online repositories. The names of the repository/repositories and accession number(s) can be found below: <https://tritypdb.org/tritypdb/app/workspace/strategies/import/6f350a00e98b079b>. All other data in the study are available on request from the corresponding author.

ETHICS STATEMENT

The animal study was reviewed and approved by the Institutional Commission for the Care and Use of Laboratory Animals (CICUAL) of University of Buenos Aires.

AUTHOR CONTRIBUTIONS

JRD and MP designed the study. JRD, JG, CAS, and MP performed the experiments and statistical analysis. MP supervised the study. KG and MP acquired funding. JRD and JG performed the artwork.

JRD and MP wrote the original manuscript. JRD, JG, CAS, KG, and MP revised and edited the manuscript. JRD, KG, and MP reviewed and edited the final manuscript. All authors listed have made a substantial, direct, and intellectual contribution to the work and approved it for publication.

FUNDING

This research was supported by grants from the Consejo Nacional de Investigaciones Científicas y Técnicas (CONICET; PIP No. 112-2015010-0937) and the Agencia Nacional de

Promoción Científica y Tecnológica, Argentina (ANPCyT; PICT No. 2016-1028).

ACKNOWLEDGMENTS

We thank Dr. Sergio Schenkman (Federal University of Sao Paulo, Brazil) for the anti-PFR antibody, Arturo Muñoz-Calderón for technical assistance and for typifying the *T. cruzi* strains, and Dr. Cecilia Albareda (from Instituto Nacional de Parasitología Dr. M. Fátala Chaben, Argentina) for *T. cruzi* samples.

REFERENCES

- Alcantara, C. L., de Souza, W., and Cunha E Silva, N. L. (2021). The Cytostome-Cytopharynx Complex of Intracellular and Extracellular Amastigotes of *Trypanosoma Cruzi* Exhibit Structural and Functional Differences. *Cell. Microbiol.* 23 (9), e13346. doi: 10.1111/cmi.13346
- Alsford, S., Turner, D. J., Obado, S. O., Sanchez-Flores, A., Glover, L., Berriman, M., et al. (2011). High-Throughput Phenotyping Using Parallel Sequencing of RNA Interference Targets in the African Trypanosome. *Genome Res.* 21 (6), 915–924. doi: 10.1101/gr.115089.110
- Andrade, L. O., and Andrews, N. W. (2004). Lysosomal Fusion Is Essential for the Retention of *Trypanosoma Cruzi* Inside Host Cells. *J. Exp. Med.* 200 (9), 1135–1143. doi: 10.1084/jem.20041408
- Andrews, N. W., and Colli, W. (1982). Adhesion and Interiorization of *Trypanosoma Cruzi* in Mammalian Cells. *J. Protozool.* 29, 264–269. doi: 10.1111/j.1550-7408.1982.tb04024.x
- Araya, J. E., Cornejo, A., Orrego, P. R., Cordero, E. M., Cortéz, M., Olivares, H., et al. (2008). Calcineurin B of the Human Protozoan Parasite *Trypanosoma Cruzi* Is Involved in Cell Invasion. *Microbes Infect.* 10 (8), 892–900. doi: 10.1016/j.micinf.2008.05.003
- Aslett, M., Aurrecochea, C., Berriman, M., Brestelli, J., Brunk, B. P., Carrington, M., et al. (2010). TriTrypDB: A Functional Genomic Resource for the Trypanosomatidae. *Nucleic Acids Res.* 38 (Database issue), D457–D462. doi: 10.1093/nar/gkp851
- Atwood, J. A., Weatherly, D. B., Minning, T. A., Bundy, B., Cavola, C., Oppendoes, F. R., et al. (2005). The *Trypanosoma Cruzi* Proteome. *Science* 309 (5733), 473–476. doi: 10.1126/science.1110289
- Barrias, E. S., de Carvalho, T. M., and De Souza, W. (2013). *Trypanosoma Cruzi*: Entry Into Mammalian Host Cells and Parasitophorous Vacuole Formation. *Front. Immunol.* 4. doi: 10.3389/fimmu.2013.00186
- Batista, M. F., Nájera, C. A., Meneghelli, I., and Bahia, D. (2020). The Parasitic Intracellular Lifestyle of Trypanosomatids: Parasitophorous Vacuole Development and Survival. *Front. Cell Dev. Biol.* 8. doi: 10.3389/fcell.2020.00396
- Belaunzarán, M. L., Lammel, E. M., Giménez, G., Wainszelbaum, M. J., and de Isola, E. L. (2009). Involvement of Protein Kinase C Isoenzymes in *Trypanosoma Cruzi* Metacyclogenesis Induced by Oleic Acid. *Parasitol. Res.* 105 (1), 47–55. doi: 10.1007/s00436-009-1359-3
- Benaïm, G., Losada, S., Gadelha, F. R., and Docampo, R. (1991). A Calmodulin-Activated (Ca²⁺-Mg²⁺)-ATPase Is Involved in Ca²⁺ Transport by Plasma Membrane Vesicles From *Trypanosoma Cruzi*. *Biochem. J.* 280 (Pt 3), 715–720. doi: 10.1042/bj2800715
- Benaïm, G., Paniz-Mondolfi, A. E., Sordillo, E. M., and Martinez-Sotillo, N. (2020). Disruption of Intracellular Calcium Homeostasis as a Therapeutic Target Against *Trypanosoma Cruzi*. *Front. Cell. Infect. Microbiol.* 10. doi: 10.3389/fcimb.2020.00046
- Berná, L., Rodríguez, M., Chiribao, M. L., Parodi-Talice, A., Pita, S., Rijo, G., et al. (2018). Expanding an Expanded Genome: Long-Read Sequencing of *Trypanosoma Cruzi*. *Microb. Genom.* 4 (5), e000177. doi: 10.1099/mgen.0.000177
- Berridge, M. J., Bootman, M. D., and Roderick, H. L. (2003). Calcium Signalling: Dynamics, Homeostasis and Remodelling. *Nat. Rev. Mol. Cell Biol.* 4 (7), 517–529. doi: 10.1038/nrm1155
- Bertolini, M. S., Chiurillo, M. A., Lander, N., Vercesi, A. E., and Docampo, R. (2019). MICU1 and MICU2 Play an Essential Role in Mitochondrial Ca²⁺ Uptake, Growth, and Infectivity of the Human Pathogen *Trypanosoma Cruzi*. *mBio* 10 (3), e00348–e00319. doi: 10.1128/mBio.00348-19
- Bradford, M. M. (1976). A Rapid and Sensitive Method for the Quantitation of Microgram Quantities of Protein Utilizing the Principle of Protein-Dye Binding. *Anal. Biochem.* 72, 248–254. doi: 10.1006/abio.1976.9999
- Caradonna, K. L., and Burleigh, B. A. (2011). Mechanisms of Host Cell Invasion by *Trypanosoma Cruzi*. *Adv. Parasitol.* 76, 33–61. doi: 10.1016/B978-0-12-385895-5.00002-5
- Cestari, L., Krarup, A., Sim, R. B., Inal, J. M., and Ramirez, M. I. (2009). Role of Early Lectin Pathway Activation in the Complement-Mediated Killing of *Trypanosoma Cruzi*. *Mol. Immunol.* 47 (2–3), 426–437. doi: 10.1016/j.molimm.2009.08.030
- Chazin, W. J. (2011). Relating Form and Function of EF-Hand Calcium Binding Proteins. *Acc. Chem. Res.* 44 (3), 171–179. doi: 10.1021/ar100110d
- Chiurillo, M. A., Lander, N., Bertolini, M. S., Vercesi, A. E., and Docampo, R. (2019). Functional Analysis and Importance for Host Cell Infection of the Ca²⁺-Conducting Subunits of the Mitochondrial Calcium Uniporter of *Trypanosoma Cruzi*. *J. Mol. Cell Biol.* 30 (14), 1676–1690. doi: 10.1091/mbc.E19-03-0152
- Chiurillo, M. A., Lander, N., Vercesi, A. E., and Docampo, R. (2020). IP₃ Receptor-Mediated Ca²⁺ Release From Acidocalcisomes Regulates Mitochondrial Bioenergetics and Prevents Autophagy in *Trypanosoma Cruzi*. *Cell Calcium* 92, 102284. doi: 10.1016/j.ceca.2020.102284
- Contreras, V. T., Salles, J. M., Thomas, N., Morel, C. M., and Goldenberg, S. (1985). *In Vitro* Differentiation of *Trypanosoma Cruzi* Under Chemically Defined Conditions. *Mol. Biochem. Parasitol.* 16 (3), 315–327. doi: 10.1016/0166-6851(85)90073-8
- D'Angelo, M. A., Montagna, A. E., Sanguinetti, S., Torres, H. N., and Flawiá, M. M. (2002). A Novel Calcium-Stimulated Adenylyl Cyclase From *Trypanosoma Cruzi*, Which Interacts With the Structural Flagellar Protein Paraflagellar Rod. *J. Biol. Chem.* 277 (38), 35025–35034. doi: 10.1074/jbc.M204696200
- Darriba, D., Taboada, G. L., Doallo, R., and Posada, D. (2011). ProtTest 3: Fast Selection of Best-Fit Models of Protein Evolution. *Bioinformatics* 27 (8), 1164–1165. doi: 10.1093/bioinformatics/btr088
- Dave, N., Cetiner, U., Arroyo, D., Fonbuena, J., Tiwari, M., Barrera, P., et al. (2021). A Novel Mechanosensitive Channel Controls Osmoregulation, Differentiation, and Infectivity in *Trypanosoma Cruzi*. *eLife* 10, e67449. doi: 10.7554/eLife.67449
- Deschamps, P., Lara, E., Marande, W., López-García, P., Ekelund, F., and Moreira, D. (2011). Phylogenomic Analysis of Kinetoplastids Supports That Trypanosomatids Arose From Within Bodonids. *Mol. Biol. Evol.* 28 (1), 53–58. doi: 10.1093/molbev/msq289
- Dos Santos, G., Rezende Leite, A. C., Lander, N., Chiurillo, M. A., Vercesi, A. E., and Docampo, R. (2021). *Trypanosoma Cruzi* Letm1 Is Involved in Mitochondrial Ca²⁺ Transport, and Is Essential for Replication, Differentiation, and Host Cell Invasion. *FASEB J.* 35 (7), e21685. doi: 10.1096/fj.202100120RR

- Elies, J., Yáñez, M., Pereira, T., Gil-Longo, J., MacDougall, D. A., and Campos-Toimil, M. (2020). An Update to Calcium Binding Proteins. *Adv. Exp. Med. Biol.* 1131, 183–213. doi: 10.1007/978-3-030-12457-1_8
- El-Sayed, N. M., Myler, P. J., Bartholomeu, D. C., Nilsson, D., Aggarwall, G., Tran, A., et al. (2005). The Genome Sequence of *Trypanosoma Cruzi*, Etiologic Agent of Chagas Disease. *Science* 309 (5733), 409–415. doi: 10.1126/science.1112631
- Epting, C. L., Coates, B. M., and Engman, D. M. (2010). Molecular Mechanisms of Host Cell Invasion by *Trypanosoma Cruzi*. *Exp. Parasitol.* 126 (3), 283–291. doi: 10.1016/j.exppara.2010.06.023
- Furuya, T., Kashuba, C., Docampo, R., and Moreno, S. N. (2000). A Novel Phosphatidylinositol-Phospholipase C of *Trypanosoma Cruzi* That Is Lipid Modified and Activated During Trypomastigote to Amastigote Differentiation. *J. Biol. Chem.* 275 (9), 6428–6438. doi: 10.1074/jbc.275.9.6428
- Furuya, T., Okura, M., Ruiz, F. A., Scott, D. A., and Docampo, R. (2001). TcSCA Complements Yeast Mutants Defective in Ca²⁺ Pumps and Encodes a Ca²⁺ +ATPase That Localizes to the Endoplasmic Reticulum of *Trypanosoma Cruzi*. *J. Biol. Chem.* 276 (35), 32437–32445. doi: 10.1074/jbc.M104000200
- Garber, J. C. National Research Council. (2011). *Guide for the Care and Use of Laboratory Animals. Eighth Edition* (Washington, DC: The National Academies). doi: 10.17226/12910
- Gonçalves, C. S., Rodrigues, A. A., de Souza, W., Motta, M. C., and Cavalcanti, D. P. (2018). Revisiting the *Trypanosoma Cruzi* Metacyclogenesis: Morphological and Ultrastructural Analyses During Cell Differentiation. *Parasit. Vectors* 11 (1), 83. doi: 10.1186/s13071-018-2664-4
- Haiech, J., Moreau, M., Leclerc, C., and Kilhoffer, M. C. (2019). Facts and Conjectures on Calmodulin and Its Cousin Proteins, Parvalbumin and Troponin C. *Biochim. Biophys. Acta Mol. Cell* 1866 (7), 1046–1053. doi: 10.1016/j.bbamcr.2019.01.014
- Hamed, A., Botelho, L., Britto, C., Frago, S. P., Umaki, A. C., Goldenberg, S., et al. (2015). *In Vitro* Metacyclogenesis of *Trypanosoma Cruzi* Induced by Starvation Correlates With a Transient Adenylyl Cyclase Stimulation as Well as With a Constitutive Upregulation of Adenylyl Cyclase Expression. *Mol. Biochem. Parasitol.* 200 (1–2), 9–18. doi: 10.1016/j.molbiopara.2015.04.002
- Hashimoto, M., Doi, M., Kurebayashi, N., Furukawa, K., Hirawake-Mogi, H., Ohmiya, Y., et al. (2016). Inositol 1,4,5-Trisphosphate Receptor Determines Intracellular Ca²⁺ Concentration in *Trypanosoma Cruzi* Throughout its Life Cycle. *FEBS J.* 6 (12), 1178–1185. doi: 10.1002/2211-5463.12126
- Hasslocher-Moreno, A. M., Saraiva, R. M., Sangenis, L., Xavier, S. S., de Sousa, A. S., Costa, A. R., et al. (2020). Benzimidazole Decreases the Risk of Chronic Chagas Disease Progression and Cardiovascular Events: A Long-Term Follow Up Study. *EclinicalMedicine* 31, 100694. doi: 10.1016/j.eclinm.2020.100694
- Hernández-Osorio, L. A., Márquez-Dueñas, C., Florencio-Martínez, L. E., Ballesteros-Rodea, G., Martínez-Calvillo, S., and Manning-Cela, R. G. (2010). Improved Method for *In Vitro* Secondary Amastigogenesis of *Trypanosoma Cruzi*: Morphometrical and Molecular Analysis of Intermediate Developmental Forms. *J. BioMed. Biotechnol.* 2010, 283842. doi: 10.1155/2010/283842
- Jesus, T. C., Calderano, S. G., Vitorino, F. N., Llanos, R. P., Lopes, M. C., de Araújo, C. B., et al. (2017). Quantitative Proteomic Analysis of Replicative and Nonreplicative Forms Reveals Important Insights Into Chromatin Biology of *Trypanosoma Cruzi*. *Mol. Cell. Proteom* 16 (1), 23–38. doi: 10.1074/mcp.M116.061200
- Jumper, J., Evans, R., Pritzel, A., Green, T., Figurnov, M., Ronneberger, O., et al. (2021). Highly Accurate Protein Structure Prediction With AlphaFold. *Nature* 596 (7873), 583–589. doi: 10.1038/s41586-021-03819-2
- Katoh, K., Rozewicki, J., and Yamada, K. D. (2019). MAFFT Online Service: Multiple Sequence Alignment, Interactive Sequence Choice and Visualization. *Brief. Bioinform.* 20 (4), 1160–1166. doi: 10.1093/bib/bbx108
- Lammel, E. M., Barbieri, M. A., Wilkowsky, S. E., Bertini, F., and Isola, E. L. (1996). *Trypanosoma Cruzi*: Involvement of Intracellular Calcium in Multiplication and Differentiation. *Exp. Parasitol.* 83 (2), 240–249. doi: 10.1006/expr.1996.0070
- Lander, N., Chiurillo, M. A., Bertolini, M. S., Storey, M., Vercesi, A. E., and Docampo, R. (2018). Calcium-Sensitive Pyruvate Dehydrogenase Phosphatase Is Required for Energy Metabolism, Growth, Differentiation, and Infectivity of *Trypanosoma Cruzi*. *J. Biol. Chem.* 293 (45), 17402–17417. doi: 10.1074/jbc.RA118.004498
- Lemoine, F., Domelevo Entfellner, J. B., Wilkinson, E., Correia, D., Dávila Felipe, M., De Oliveira, T., et al. (2018). Renewing Felsenstein's Phylogenetic Bootstrap in the Era of Big Data. *Nature* 556 (7702), 452–456. doi: 10.1038/s41586-018-0043-0
- Lidani, K., Andrade, F. A., Bavia, L., Damasceno, F. S., Beltrame, M. H., Messias-Reason, I. J., et al. (2019). Chagas Disease: From Discovery to a Worldwide Health Problem. *Front. Public Health* 7. doi: 10.3389/fpubh.2019.00166
- Lu, H. G., Zhong, L., de Souza, W., Benchimol, M., Moreno, S., and Docampo, R. (1998). Ca²⁺ Content and Expression of an Acidocalcisomal Calcium Pump Are Elevated in Intracellular Forms of *Trypanosoma Cruzi*. *Mol. Cell. Biol.* 18 (4), 2309–2323. doi: 10.1128/MCB.18.4.2309
- Maeda, F. Y., Cortez, C., and Yoshida, N. (2012). Cell Signaling During *Trypanosoma Cruzi* Invasion. *Front. Immunol.* 3. doi: 10.3389/fimmu.2012.00361
- Majeau, A., Murphy, L., Herrera, C., and Dumonteil, E. (2021). Assessing *Trypanosoma Cruzi* Parasite Diversity Through Comparative Genomics: Implications for Disease Epidemiology and Diagnostics. *Pathogens* 10 (2), 212. doi: 10.3390/pathogens10020212
- Manchola Varón, N. C., Dos Santos, G., Colli, W., and Alves, M. (2021). Interaction With the Extracellular Matrix Triggers Calcium Signaling in *Trypanosoma Cruzi* Prior to Cell Invasion. *Front. Cell. Infect. Microbiol.* 11. doi: 10.3389/fcimb.2021.731372
- Marchini, F. K., de Godoy, L. M., Rampazzo, R. C., Pavoni, D. P., Probst, C. M., Gnäd, F., et al. (2011). Profiling the *Trypanosoma Cruzi* Phosphoproteome. *PLoS One* 6 (9), e25381. doi: 10.1371/journal.pone.0025381
- Martins, C., Reis-Cunha, J. L., Silva, M. N., Pereira, E. G., Pappas, G. Jr, Bartholomeu, D. C., et al. (2011). Identification of Genes Encoding Hypothetical Proteins in Open-Reading Frame Expressed Sequence Tags From Mammalian Stages of *Trypanosoma Cruzi*. *Genet. Mol. Res.* 10 (3), 1589–1630. doi: 10.4238/vol10-3gmr1140
- Mohanta, T. K., Yadav, D., Khan, A. L., Hashem, A., Abd Allah, E. F., and Al-Harrasi, A. (2019). Molecular Players of EF-Hand Containing Calcium Signaling Event in Plants. *Int. J. Mol. Sci.* 20 (6), 1476. doi: 10.3390/ijms20061476
- Moreno, S. N., Silva, J., Vercesi, A. E., and Docampo, R. (1994). Cytosolic-Free Calcium Elevation in *Trypanosoma Cruzi* Is Required for Cell Invasion. *Exp. Med.* 180 (4), 1535–1540. doi: 10.1084/jem.180.4.1535
- Mortara, R. A., Andreoli, W. K., Taniwaki, N. N., Fernandes, A. B., Silva, C. V., Fernandes, M. C., et al. (2005). Mammalian Cell Invasion and Intracellular Trafficking by *Trypanosoma Cruzi* Infective Forms. *An. Acad. Bras. Cienc.* 77 (1), 77–94. doi: 10.1590/s0001-37652005000100006
- Nogueira, N. P., de Souza, C. F., Saraiva, F. M., Sultano, P. E., Dalmau, S. R., Bruno, R. E., et al. (2011). Heme-Induced ROS in *Trypanosoma Cruzi* Activates CaMKII-Like That Triggers Epimastigote Proliferation. One Helpful Effect of ROS. *PLoS One* 6 (10), e25935. doi: 10.1371/journal.pone.0025935
- Pinto, A. P., Campana, P. T., Beltrami, L. M., Silber, A. M., and Araújo, A. P. (2003). Structural Characterization of a Recombinant Flagellar Calcium-Binding Protein From *Trypanosoma Cruzi*. *Biochim. Biophys. Acta* 1652 (2), 107–114. doi: 10.1016/j.bbapap.2003.08.008
- Potenza, S., Laverrière, M., and Tellez-Inon, M. T. (2012). Functional Characterization of TcCYC2 Cyclin From *Trypanosoma Cruzi*. *Exp. Parasitol.* 132 (4), 537–545. doi: 10.1016/j.exppara.2012.09.002
- Queiroz, R. M., Charneau, S., Bastos, I. M., Santana, J. M., Sousa, M. V., Roepstorff, P., et al. (2014). Cell Surface Proteome Analysis of Human-Hosted *Trypanosoma Cruzi* Life Stages. *J. Proteome Res.* 13 (8), 3530–3541. doi: 10.1021/pr401120y
- Ramakrishnan, S., and Docampo, R. (2018). Membrane Proteins in *Trypanosomatids* Involved in Ca²⁺ Homeostasis and Signaling. *Genes* 9 (6), 304. doi: 10.3390/genes9060304
- Rodríguez-Bejarano, O. H., Avendaño, C., and Patarroyo, M. A. (2021). Mechanisms Associated With *Trypanosoma Cruzi* Host Target Cell Adhesion, Recognition and Internalization. *Life* 11 (6), 534. doi: 10.3390/life11060534
- Rodríguez Durán, J., Muñoz-Calderón, A., Gómez, K. A., and Potenza, M. (2021). *In Vitro* Differentiation of *Trypanosoma Cruzi* Epimastigotes Into Metacyclic Trypomastigotes Using a Biphasic Medium. *STAR Protoc.* 2 (3), 100703. doi: 10.1016/j.xpro.2021.100703

- Ruiz, R. C., Favoreto, S. J. R., Dorta, M. L., Oshiro, M. E., Ferreira, A. T., Manque, P. M., et al. (1998). Infectivity of *Trypanosoma Cruzi* Strains Is Associated With Differential Expression of Surface Glycoproteins With Differential Ca²⁺ Signalling Activity. *Biochem. J.* 330 (Pt 1), 505–511. doi: 10.1042/bj3300505
- Sánchez-Valdez, F. J., Pérez Brandán, C., Ramírez, G., Uncos, A. D., Zago, M. P., Cimino, R. O., et al. (2014). A Monoallelic Deletion of the TcCRT Gene Increases the Attenuation of a Cultured *Trypanosoma Cruzi* Strain, Protecting Against an *In Vivo* Virulent Challenge. *PLoS Negl. Trop. Dis.* 8 (2), e2696. doi: 10.1371/journal.pntd.0002696
- Shan, F., Ye, K., Zhang, J., Liao, S., Zhang, X., Xu, C., et al. (2018). Solution Structure of TbCentrin4 From *Trypanosoma Brucei* and Its Interactions With Ca²⁺ and Other Centrinins. *Biochem. J.* 475 (23), 3763–3778. doi: 10.1042/BCJ20180752
- Silva, E. O., Saraiva, E. M., De Souza, W., and Souto-Padrón, T. (1998). Cell Surface Characterization of Amastigotes of *Trypanosoma Cruzi* Obtained From Different Sources. *Parasitol. Res.* 84 (4), 257–263. doi: 10.1007/s004360050392
- Souza, C. F., Carneiro, A. B., Silveira, A. B., Laranja, G. A., Silva-Neto, M. A., Costa, S. C., et al. (2009). Heme-Induced *Trypanosoma Cruzi* Proliferation Is Mediated by CaM Kinase II. *Biochem. Biophys. Res. Commun.* 390 (3), 541–546. doi: 10.1016/j.bbrc.2009.09.135
- Stamatakis, A. (2014). RAxML Version 8: A Tool for Phylogenetic Analysis and Post-Analysis of Large Phylogenies. *Bioinformatics* 9), 1312–1313. doi: 10.1093/bioinformatics/btu033
- Teixeira, D. E., Benchimol, M., Crepaldi, P. H., and de Souza, W. (2012). Interactive Multimedia to Teach the Life Cycle of *Trypanosoma Cruzi*, the Causative Agent of Chagas Disease. *PLoS Negl. Trop. Dis.* 6 (8), e1749. doi: 10.1371/journal.pntd.0001749
- Tellez-Inón, M. T., Ulloa, R. M., Torruella, M., and Torres, H. N. (1985). Calmodulin and Ca²⁺-Dependent Cyclic AMP Phosphodiesterase Activity in *Trypanosoma Cruzi*. *Mol. Biochem. Parasitol.* 17 (2), 143–153. doi: 10.1016/0166-6851(85)90013-1
- Vazquez, M. P., and Levin, M. J. (1999). Functional Analysis of the Intergenic Regions of TcP2beta Gene Loci Allowed the Construction of an Improved *Trypanosoma Cruzi* Expression Vector. *Gene* 239 (2), 217–225. doi: 10.1016/s0378-1119(99)00386-8
- Wingard, J. N., Ladner, J., Vanarotti, M., Fisher, A. J., Robinson, H., Buchanan, K. T., et al. (2008). Structural Insights Into Membrane Targeting by the Flagellar Calcium-Binding Protein (FCaBP), a Myristoylated and Palmitoylated Calcium Sensor in *Trypanosoma Cruzi*. *J. Biol. Chem.* 283 (34), 23388–23396. doi: 10.1074/jbc.M803178200
- World Health Organization (2022) *Chagas Disease: Control and Elimination*. Available at: <https://www.who.int/chagas/resources>.
- Yakubu, M. A., Majumder, S., and Kierszenbaum, F. (1994). Changes in *Trypanosoma Cruzi* Infectivity by Treatments That Affect Calcium Ion Levels. *Mol. Biochem. Parasitol.* 66 (1), 119–125. doi: 10.1016/0166-6851(94)90042-6
- Yoshida, N. (2006). Molecular Basis of Mammalian Cell Invasion by *Trypanosoma Cruzi*. *An. Acad. Bras. Cienc.* 78 (1), 87–111. doi: 10.1590/s0001-37652006000100010
- Yoshida, N., and Cortez, M. (2008). *Trypanosoma Cruzi*: Parasite and Host Cell Signaling During the Invasion Process. *Subcell. Biochem.* 47, 82–91. doi: 10.1007/978-0-387-78267-6_6

Conflict of Interest: The authors declare that the research was conducted in the absence of any commercial or financial relationships that could be construed as a potential conflict of interest.

Publisher's Note: All claims expressed in this article are solely those of the authors and do not necessarily represent those of their affiliated organizations, or those of the publisher, the editors and the reviewers. Any product that may be evaluated in this article, or claim that may be made by its manufacturer, is not guaranteed or endorsed by the publisher.

Copyright © 2022 Rodríguez-Durán, Gallardo, Alba Soto, Gómez and Potenza. This is an open-access article distributed under the terms of the Creative Commons Attribution License (CC BY). The use, distribution or reproduction in other forums is permitted, provided the original author(s) and the copyright owner(s) are credited and that the original publication in this journal is cited, in accordance with accepted academic practice. No use, distribution or reproduction is permitted which does not comply with these terms.



Induction of Autophagy by Ursolic Acid Promotes the Elimination of *Trypanosoma cruzi* Amastigotes From Macrophages and Cardiac Cells

María Cristina Vanrell^{1,2*}, Santiago José Martínez¹, Lucila Ibel Muñoz³, Betiana Nebaí Salassa^{1,4}, Julián Gambarte Tudela² and Patricia Silvia Romano^{1,2*}

¹ Laboratorio de biología de *Trypanosoma cruzi* y la célula hospedadora, Instituto de Histología y Embriología de Mendoza, Instituto de Histología y Embriología de Mendoza-Consejo Nacional de Investigaciones Científicas y Técnicas (IHEM-CONICET)-Universidad Nacional de Cuyo, Mendoza, Argentina, ² Facultad de Ciencias Médicas, Universidad Nacional de Cuyo, Mendoza, Argentina, ³ Facultad de Farmacia y Bioquímica, Universidad Juan Agustín Maza, Mendoza, Argentina, ⁴ Facultad de Odontología, Universidad Nacional de Cuyo, Mendoza, Argentina

OPEN ACCESS

Edited by:

María Carolina Touz,
Medical Research Institute Mercedes
and Martín Ferreyra (INIMEC),
Argentina

Reviewed by:

Chiranjib Pal,
West Bengal State University, India
Nívea Pereira De Sa,
Stony Brook University, United States

*Correspondence:

María Cristina Vanrell
cristiv2002@hotmail.com
Patricia Silvia Romano
promano@fcm.uncu.edu.ar

Specialty section:

This article was submitted to
Parasite and Host,
a section of the journal
Frontiers in Cellular and
Infection Microbiology

Received: 13 April 2022

Accepted: 14 June 2022

Published: 08 July 2022

Citation:

Vanrell MC, Martínez SJ,
Muñoz LI, Salassa BN, Gambarte
Tudela J and Romano PS (2022)
Induction of Autophagy by Ursolic
Acid Promotes the Elimination of
Trypanosoma cruzi Amastigotes From
Macrophages and Cardiac Cells.
Front. Cell. Infect. Microbiol. 12:919096.
doi: 10.3389/fcimb.2022.919096

Chagas disease, caused by the parasite *Trypanosoma cruzi*, is an infectious illness endemic to Latin America and still lacks an effective treatment for the chronic stage. In a previous study in our laboratory, we established the protective role of host autophagy *in vivo* during *T. cruzi* infection in mice and proposed this process as one of the mechanisms involved in the innate immune response against this parasite. In the search for an autophagy inducer that increases the anti-*T. cruzi* response in the host, we found ursolic acid (UA), a natural pentacyclic triterpene with many biological actions including autophagy induction. The aim of this work was to study the effect of UA on *T. cruzi* infection *in vitro* in the late infection stage, when the nests of intracellular parasites are forming, in both macrophages and cardiac cells. To test this effect, the cells were infected with *T. cruzi* for 24 h and then treated with UA (5–10 μ M). The data showed that UA significantly decreased the number of amastigotes found in infected cells in comparison with non-treated cells. UA also induced the autophagy response in both macrophages and cardiac cells under the studied conditions, and the inhibition of this pathway during UA treatment restored the level of infection. Interestingly, LC3 protein, the main marker of autophagy, was recruited around amastigotes and the acidic probe LysoTracker localized with them, two key features of xenophagy. A direct cytotoxic effect of UA was also found on trypomastigotes of *T. cruzi*, whereas epimastigotes and amastigotes displayed more resistance to this drug at the studied concentrations. Taken together, these data showed that this natural compound reduces *T. cruzi* infection in the later stages by promoting parasite damage through the induction of autophagy. This action, in addition to the effect of this compound on trypomastigotes, points to UA as an interesting lead for Chagas disease treatment in the future.

Keywords: Chagas disease, *Trypanosoma cruzi*, amastigotes, autophagy, xenophagy, ursolic acid

INTRODUCTION

Chagas disease (CD) or American trypanosomiasis is caused by the protozoan parasite *Trypanosoma cruzi*. The WHO estimates that 8 to 10 million people are infected worldwide, mostly in Latin America, where the disease is endemic. CD is also one of the so-called neglected tropical diseases because of the low attention that governments and industries gave to these illnesses in the past. Benznidazole (BNZ) and nifurtimox are currently the only two drugs approved for the treatment of CD. Although several laboratories are working in the search for new therapies, the lack of effective drugs for the chronic stage is still unsolved.

T. cruzi has a biphasic biological cycle that develops in both the insect vector and the mammalian hosts. In the latter, *T. cruzi* behaves as an obligate intracellular parasite, interacting with compartments from the vesicular transport pathways to invade the host cell and establish its replicative niche (Nunes et al., 2013; Dias, 2017; Guarner, 2019). *T. cruzi* is capable of infecting several classes of host cells. Macrophages are the first line of defense during *T. cruzi* invasion. Macrophages may either suppress *T. cruzi* replication or provide a favorable environment where the parasite can reproduce and be distributed to other tissues within the body (Peluffo et al., 2004; Holzmüller et al., 2018). However, cardiac cells are one of the main targets of *T. cruzi*, in which the parasite establishes its replicative niche to form the amastigote nests that are present in the heart of the chronic patients (De Alba-Alvarado et al., 2020).

Ursolic acid (UA) is a naturally occurring pentacyclic triterpene with many biological properties. This compound is widely distributed in nature, in aromatic plants such as rosemary, basil, oregano, and eucalyptus, as well as medlar fruits, apple skin, and coffee seeds. It has been shown that UA displays anti-inflammatory, antioxidant, and anticancer activities (Chen et al., 2020; Khwaza et al., 2020). Moreover, UA exerts potent antiviral action (Tohmé et al., 2019) and has an antiprotozoal effect against species of *Leishmania* and *Plasmodium* (Bilbao-Ramos et al., 2020; Son and Lee, 2020). In *T. cruzi*, UA displayed trypanocidal activity on epimastigotes at a concentration of 100 μ M (Uchiyama et al., 2006). Oral administration of UA reduces the parasitemia peaks in mice infected with *T. cruzi* Y strain in an acute model of infection (da Silva Ferreira et al., 2013). Interestingly, UA has been described as an autophagy inducer in cancer cells (Deng et al., 2019; Lin et al., 2020). UA inhibited proliferation and induced autophagy and apoptosis in several cancer models, including breast carcinoma, melanoma, leukemia, hepatoma, and prostate cancer (Pathak et al., 2007; Shanmugam et al., 2011; Leng et al., 2013; Zhao et al., 2013). In a primary brain tumor model, UA activated autophagy by modulation of the calmodulin-dependent kinase protein kinase (CaMKK)/AMPK/mTOR through the induction of ER stresses and Ca^{2+} release (Shen et al., 2014). This mechanism was also observed in gemcitabine-resistant human pancreatic cancer cells treated with UA (Deng et al., 2019; Lin et al., 2020). Other works have also demonstrated the effects of different natural or synthetic compounds on the intracellular stages of protozoan parasites (Mallick et al., 2011; Yousuf et al., 2015; Sultana et al.,

2018; Mukherjee et al., 2020). These studies evaluated the effect of compounds against *Leishmania* spp. *in vitro* and *in vivo*, showing actions on both parasitic targets (mitochondrion, antioxidant enzymes, etc.) and increasing the innate immune response of the infected host.

In a previous study, we demonstrated that the deficiency of autophagy in the Beclin-1 heterozygous knockout mice exacerbates *T. cruzi* infection. This effect correlated with a higher parasite load observed in both peritoneal macrophages obtained from these mice and in macrophages obtained from wild-type (WT) animals treated with autophagy inhibitors (Casassa et al., 2019). In agreement with these data, there is evidence that *T. cruzi* is able to induce an increase in the expression of LC3-II, as well as the formation of autophagosomes and autolysosomes in macrophages, and that the pharmacological inhibition of the autophagy machinery impairs the ability of macrophages to control amastigote replication (Matteucci et al., 2019). Given that autophagy plays a protective role in *T. cruzi* infection *in vivo* and that UA induces autophagy in different cellular models, we proposed that UA treatment impairs *T. cruzi* infection due to its action on autophagy on infected cells. To test this hypothesis, we studied the effect of UA in the intracellular cycle of *T. cruzi* in both macrophages and cardiac cells, two main cells targeted by *T. cruzi* during the course of human infection. Moreover, considering that the chronic stage of infection is still difficult to cure because of the presence of intracellular parasites hidden in the tissues, these studies were conducted in the late stages of infection, when amastigotes are replicating in the cytosol of host cells.

METHODS

Reagents

Dulbecco's Modified Eagle Medium (DMEM), penicillin, and streptomycin were obtained from Gibco BRL/Life Technologies (Carlsbad, CA, USA). The polyclonal rabbit anti-LC3 antibody and UA were purchased from Sigma-Aldrich (St. Louis, MO, USA). The polyclonal mouse anti- β TUBULIN was obtained from Developmental Studies Hybridoma Bank. Serum from *T. cruzi*-infected C57 mouse was obtained and used for *T. cruzi* detection. The secondary antibody Cy3-conjugated anti-Goat IgG was purchased from Jackson ImmunoResearch Laboratories (West Grove, PA, USA). The secondary antibody Alexa 488 was obtained from Thermo Fisher (Waltham, MA, USA). The DNA marker Hoechst 33342 and LysoTracker Red were purchased from Life Technologies. The fetal bovine serum (FBS) was purchased from Natocor (Cordoba, Argentina). Red DQ-BSA was obtained from Invitrogen (Carlsbad, CA, USA). The nitrocellulose and chemiluminescence detection kit was from Amersham (Pittsburgh, PA, USA), and the *In Situ* Cell Death Detection Kit was purchased from Roche (Basel, Switzerland).

Cell Culture

RAW 264.7 (murine macrophages) and H9C2 (rat myoblast) cells were maintained in flasks in DMEM supplemented with 10% FBS and antibiotics in a 5% CO_2 atmosphere.

Preparation of Bone Marrow Macrophages

Bone marrow was obtained from the femur bones of C57BL/6J WT and KD (Beclin-1 heterozygous knockout mice, Beclin-1 \pm) mice and resuspended in cold DMEM, containing 40 μ g/ml of gentamicin, following standard procedures. These bone marrow progenitor cells were recovered in 100-mm plates, containing 10% FBS, 40 μ g/ml gentamicin, 2 mM of L-glutamine, and a conditioned medium derived from 30% L929 cell culture, for 4 days. Then, they were washed, and the same medium was added for an additional 6 days. Finally, the cells were typed by flow cytometry (BD FACSaria III, BD Biosciences, San Jose, CA, USA) using the markers F480 (PerCP) and CD11b (APC) to confirm the identity of macrophages (Supplementary Figure 1).

Quantification of *Trypanosoma cruzi* Infection

RAW macrophages, bone marrow macrophages (BMMs) from C57 WT and KD mice (Beclin-1 heterozygous knockout mice, deficient in the autophagic pathway), and H9C2 cells were infected with 10 trypomastigotes (multiplicity of infection (MOI) = 10) of Y strain (for Indirect Immunofluorescence analysis, IIF) or Y-GFP (for Western blotting study) per cell for 24 h. After being washed to eliminate the parasites that did not infect the cells, a fresh medium was added with or without 5 or 10 μ M of UA and incubated for 24, 48, or 72 h. Cells were then processed to detect *T. cruzi* amastigotes by Western blotting or indirect immunofluorescence.

For indirect immunofluorescence, the cells were fixed with 4% paraformaldehyde in phosphate-buffered saline (PBS) for 20 min at room temperature, then washed with PBS, blocked with 50 mM of NH_4Cl , and permeabilized with 1% saponin in PBS containing 1% bovine serum albumin (BSA). Samples were then incubated with an anti-*T. cruzi*-specific antibody followed by incubation with an anti-rabbit secondary antibody conjugated with Cy3 fluorophore or Alexa 488 and then mounted with Mowiol 4-88 reagent containing Hoechst 33342. Samples were then examined by confocal microscopy using an Olympus Confocal FV1000 microscope (Tokyo, Japan) and processed with the program FV10-ASW 1.7 for further analysis.

For Western blotting studies, infected cells were lysed with sample buffer, and protein samples were run on a 10% polyacrylamide gel and transferred to nitrocellulose membranes. The membranes were then blocked overnight (ON) in Blotto at 4°C (5% non-fat milk, 0.1% Tween 20, and PBS), washed twice with PBS, and incubated with a primary antibody anti-*T. cruzi* (1:800 dilution) followed by a peroxidase-conjugated secondary antibody (1:5,000 dilution). The primary anti-TUBULIN antibody (1:300 dilutions) was used to detect TUBULIN as a loading control. The bands were detected by using an enhanced chemiluminescence detection kit (Amersham, Piscataway, NJ, USA; RPN2109) followed by the detection of signals in a Fujifilm LAS-4000.

Detection of LC3 Protein

Autophagy was induced by amino acid starvation. RAW macrophages and H9C2 cells grown in 6- or 24-well plates were washed three times with PBS and incubated with a control medium or Earle's balanced salt solution (starvation

medium) at 37°C for 2 h in the presence or absence of drugs (100 nM of wortmannin or 10 μ M of UA).

For detection by immunofluorescence, the cells were fixed with 4% paraformaldehyde in PBS for 15 min at room temperature, washed with PBS, and blocked with 50 mM of NH_4Cl . Subsequently, cells were permeabilized with 1% saponin in PBS containing 1% BSA, followed by incubation with an anti-LC3-specific antibody. After incubation with a Cy3-conjugated anti-rabbit antibody, each sample was mounted with Mowiol 4-88 reagent and examined by confocal microscopy using an Olympus Confocal FV1000 microscope (Japan). Images were then processed with the program FV10-ASW 1.7. The percentage of cells was determined with more than 5 or 10 LC3 dots/cell. Confocal images of 10 random fields were quantified, representing around 100 cells per experiment. Data are presented as mean values, and error bars indicate the SEM from at least three independent experiments. Statistical calculations were made using Kyplot statistical software.

Western blotting analysis was performed as explained above. Samples were run on a 12.5% polyacrylamide gel, transferred to nitrocellulose membranes, and incubated with a primary antibody anti-LC3 (1:800 dilution) followed by a peroxidase-conjugated secondary antibody (1:10,000 dilution). Anti-TUBULIN (1:300 dilution) was used to detect TUBULIN as a loading control. The corresponding bands were detected using an enhanced chemiluminescence detection kit (Amersham, RPN2109) in a Fujifilm LAS-4000.

DQ-BSA Labeling

RAW macrophages overexpressing GFP-LC3 grown in 24-well plates were washed three times with PBS and incubated with a control medium at 37°C for 2 h in the presence or absence of 10 μ M of UA. Thirty minutes before the end of the reaction, 10 μ g/ml of DQ-BSA was added. This compound was used to identify degradative compartments by fluorescence microscopy. Cells were then fixed with 4% paraformaldehyde in PBS for 15 min at room temperature, washed with PBS, blocked with 50 mM of NH_4Cl in PBS, and mounted with Mowiol 4-88 reagent containing Hoechst 33342 to label DNA. Samples were examined by confocal microscopy, using an Olympus Confocal FV1000 microscope (Japan), and processed with the program FV10-ASW 1.7.

LysoTracker Labeling

RAW macrophages overexpressing GFP-LC3 grown in 24-well plates were washed three times with PBS and incubated with a control medium at 37°C for 2 h in the presence of LysoTracker Red and the presence or absence of 10 μ M of UA. The cells were then fixed with 3% paraformaldehyde in PBS for 15 min at room temperature, washed with PBS, and blocked with 50 mM of NH_4Cl in PBS. They were mounted with Mowiol 4-88 reagent containing Hoechst 33342, examined by confocal microscopy, using an Olympus Confocal FV1000 microscope (Japan), and processed with the program FV10-ASW 1.7.

In addition, RAW macrophages were infected with trypomastigotes of the Y strain with 10 parasites per cell (MOI 10), for 24 h. Then they were washed to eliminate the parasites

that did not cause infection, and a fresh medium was added with or without 10 μ M of UA for 24 additional hours. Two hours before the end of the reaction, LysoTracker Red was added. Then the cells were fixed with 3% paraformaldehyde in PBS for 15 min at room temperature, washed with PBS, and blocked with 50 mM of NH_4Cl in PBS. They were mounted with Mowiol 4-88 reagent containing Hoechst 33342 and examined by confocal microscopy, using an Olympus Confocal FV1000 microscope (Japan), and processed with the program FV10-ASW 1.7.

Epimastigote Viability

Epimastigotes of the Y strain were grown in Diamond medium alone or with the addition of 5, 10, 12.5, 25, 50, and 100 μ M of UA at 28°C for 24 h. A small sample was extracted, and live epimastigotes were counted in a Neubauer chamber. To calculate the inhibitory concentration 50 (IC50) and the graphs, the Microsoft Excel program was used. Some of these parasites were analyzed by transmission electron microscopy (TEM), as explained above.

Trypomastigote Viability

Trypomastigotes (1,000,000 for each condition) of the Y strain were incubated for 0, 1.5, 3.5, 6, and 24 h at 4°C in DMEM alone or more than 10 or 50 μ M of UA. At different times, a small sample was extracted, and live trypomastigotes were counted in a Neubauer chamber. To calculate the half maximal effective concentration (EC50) and the graphs, the Microsoft Excel program was used.

Amastigote Viability

RAW macrophages and H9C2 cells were infected with trypomastigotes of the Y strain with 10 parasites per cell (MOI 10) for 24 h. They were then washed to eliminate the parasites that did not cause infection, and a fresh medium was added without or with 10 μ M of UA for 24 additional hours. Subsequently, the instructions of the manufacturer of the *In Situ* Cell Death Detection Kit were followed.

Transmission Electron Microscopy

RAW macrophages and H9C2 cells were infected with trypomastigotes of the Y strain with 10 parasites per cell (MOI 10) for 24 h. They were then washed to eliminate the parasites that did not cause infection, and a fresh medium was added with or without 10 μ M of UA for 24 additional hours. After that, cells were fixed with 2.5% glutaraldehyde (Pelco International, Fresno, CA, USA) in PBS at 10°C and processed by the Servicio de Preparación de Muestras de Microscopía Electrónica, STAN 3371IHEM-CONICET.

Briefly, each sample was washed in the same buffer, post-fixed in 1% OsO₄ for 1 h at room temperature, dehydrated in a graded acetone solution series, and embedded in low viscosity epoxy resin (Pelco International). Then, ultrathin sections with interference color gray were cut by ultramicrotome Leica Ultracut R, mounted on grids, and stained with uranyl acetate and lead citrate (Reynolds 1963). Grids were examined under a Zeiss 900 electron microscope, with a Gatan digital camera (model Orius SC 1000).

RESULTS

Effect of Ursolic Acid on the Late Stages of *Trypanosoma cruzi* Infection *In Vitro*

To analyze the possible effect of UA on the infection of *T. cruzi*, we infected macrophages derived from BMM, RAW macrophages, and H9C2 cells (rat cardioblasts) with trypomastigotes of the *T. cruzi* Y or Y-GFP strain for 24 h and treated them with 5 or 10 μ M of UA for an additional time of 24, 48, or 72 h. Both cell types are important in CD since macrophages are the first line of defense and muscle-derived cells, such as H9C2 cells, are the main target cells with which *T. cruzi* displays a great affinity. Subsequently, we quantified the number of amastigotes present in the treated cells by either Western blotting or confocal microscopy in comparison with infected cells maintained in the control medium (**Figure 1**). The number of amastigotes in RAW cells was studied at different times of treatment by detection of the GFP protein present in the parasites with an anti-GFP-specific antibody by Western blotting. A marked reduction in the infection was observed in the conditions with UA (10 μ M) in comparison with the control conditions (**Figure 1A**). Because the effect of the UA on the number of amastigotes was observed from 24 h, further studies were carried out at this time.

Lower detection of *T. cruzi* amastigotes was also observed by confocal microscopy in RAW cells, as well as in BMM treated with 10 or 5 μ M of UA for 24 h. Quantitative data showed that UA significantly reduced the number of amastigotes/cells in both cell types (**Figures 1B, C**). A similar effect on the content of amastigotes was observed in H9C2 cells (**Figure 1D**).

Due to the known anticancer effect of UA, prior to these studies, we demonstrated that UA is not toxic in RAW macrophages or H9C2 cells at the concentrations studied. With the use of the AlamarBlue reagent, similar cell vitality was observed in cells treated with 10 μ M of UA in comparison with untreated controls for both macrophages and cardiac-derived cells (**Supplementary Figure 2**). Taken together, these data demonstrated that UA impairs the intracellular cycle of *T. cruzi*, resulting in a significant reduction in the number of amastigotes present in the host cell cytoplasm at late times of infection.

Ursolic Acid Induces Autophagy and Xenophagy of *Trypanosoma cruzi* Amastigotes

In a previous study, we demonstrated that autophagy plays a protective effect in a mouse model of *T. cruzi* infection. We observed that mice deficient in autophagy (heterozygous knockout for *Beclin-1* gene) (Qu et al., 2003; Haspel et al., 2011) developed a more aggressive infection characterized by higher parasitemia values and earlier death than did autophagy-competent mice. This study also showed that macrophages from deficient mice or WT macrophages treated with autophagy inhibitors displayed a lower capacity to clear amastigotes by the process of xenophagy (Casassa et al., 2019). Xenophagy, the process of capture and degradation of intracellular pathogens, is

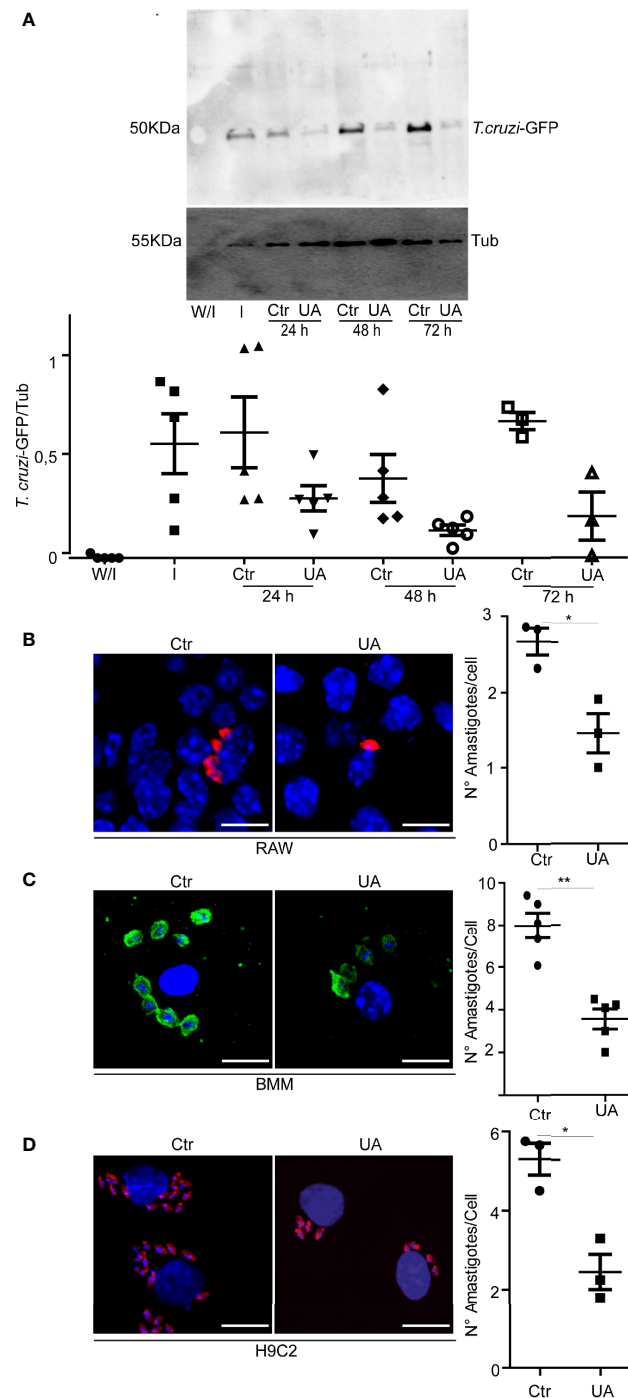


FIGURE 1 | Effect of UA on the number of intracellular amastigotes. RAW macrophages, BMM, or H9C2 cells infected with *Trypanosoma cruzi* Y or Y-GFP strain (MOI = 10) for 24 h and then treated for additional 24, 48, or 72 h under different conditions. **(A)** Representative immunoblots are depicted. Densitometry was performed using NIH ImageJ. We calculated the GFP/TUBULIN. Data represent the mean \pm SEM of five independent experiments. **(B)** Confocal images showing amastigotes of *T. cruzi* (red) in RAW macrophages under the indicated conditions. Scale bars, 10 μ m. Quantification of the number of amastigotes per cell. Data represent the mean \pm SEM of three independent experiments (number of counted cells \approx 100). *p < 0.05, Tukey's test. **(C)** Confocal images showing amastigotes of *T. cruzi* (Green) in BMM under the indicated conditions; here we used 5 μ M of UA. Scale bars, 10 μ m. Quantification of the number of amastigotes per cell. Data represent the mean \pm SEM of at least three independent experiments (number of counted cells in each experiment \approx 100). **p < 0.01, Tukey's test. **(D)** Confocal images showing amastigotes of *T. cruzi* (red) H9C2 under the indicated conditions at 48 h of treatment. Scale bars, 10 μ m. Quantification of the number of amastigotes per cell at 24 h of treatment. Data represent the mean \pm SEM of at least three independent experiments (number of counted cells \approx 100). UA, ursolic acid; BMM, bone marrow macrophage; MOI, multiplicity of infection.

a class of selective autophagy that belongs to the repertoire of the innate immune responses activated in phagocytic cells against intracellular microorganisms (Sharma et al., 2018). Since UA was previously shown to be an autophagy inducer (Leng et al., 2016), next, we asked whether the action of this compound in the reduction of amastigotes was produced by xenophagy.

To test this hypothesis, we first studied the possible effect of UA on the autophagy response of RAW and H9C2 cells. Cells were

treated with UA for 2 h, and the presence of autophagosomes was analyzed by detection of endogenous LC3 protein by IIF followed by confocal microscopy. Cells subjected to conditions of induction (starvation (Stv)) or inhibition (Stv+Wort) of autophagy were added as controls (see details in *Methods*). As shown in **Figure 2A**, a different number of autophagosomes formed in each condition and according to the class of cell assayed. We next quantified the percentage of cells with more than 5 (for RAW cells) or 10 (for

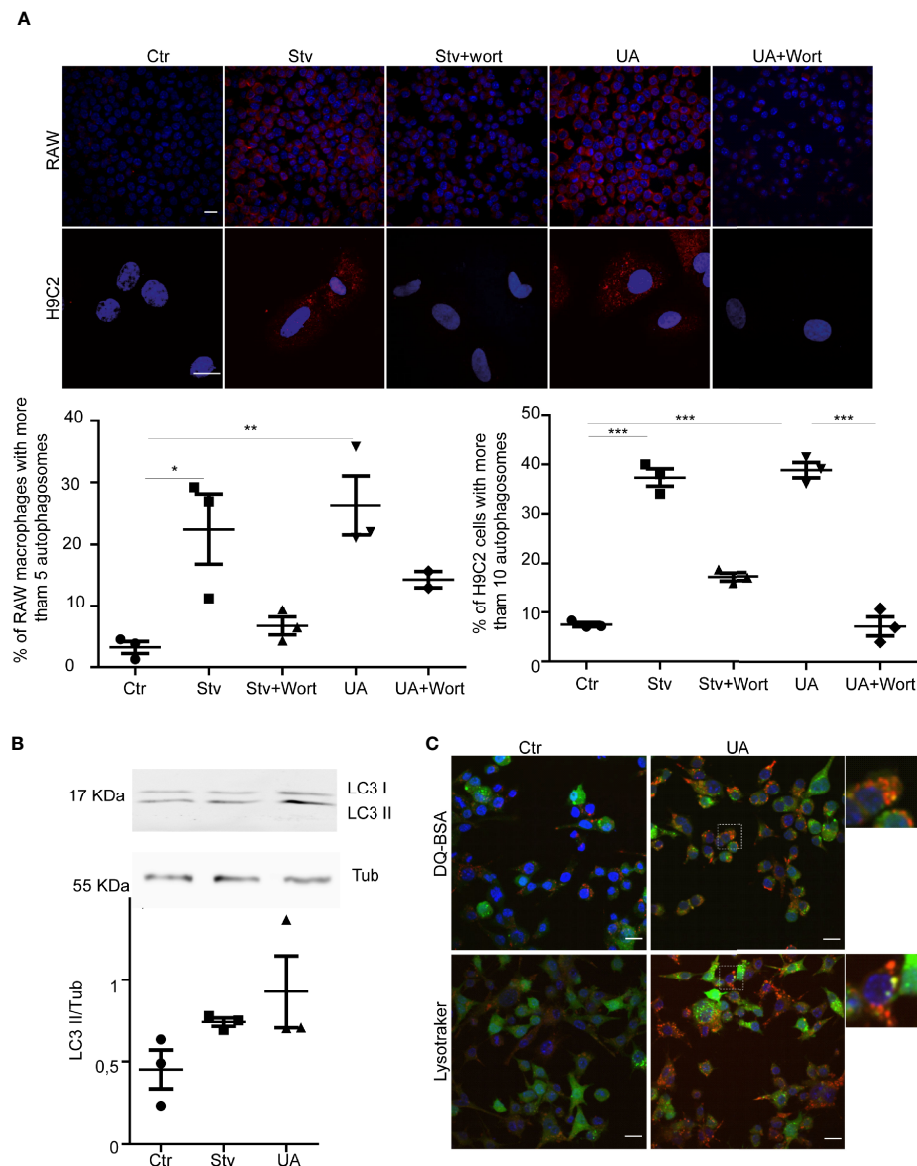


FIGURE 2 | Ursolic acid (UA) stimulates autophagy in RAW macrophages and H9C2 cells. RAW macrophages or H9C2 cells were incubated for 2 h in control or starvation medium (Stv) or in control medium supplemented with 10 μ M of UA alone (UA) or in the presence of 100 nM of wortmannin (UA+Wort) or starvation medium (Stv) in the presence of 100 nM of wortmannin (Stv+Wort) as indicated in *Methods*. **(A)** Images show the LC3 (red) distribution in the indicated conditions. Scale bars, 10 μ m. Graph represents the percentage of cells with more than 5 dots (RAW macrophages) or 10 dots per cell (H9C2 cells) in each condition. Data represent the mean \pm SEM of three independent experiments (number of counted cells in each experiment \approx 100). * p < 0.05, ** p < 0.01. Tukey's test. **(B)** Top panel: representative immunoblot of three experiments corresponding to LC3 detection is depicted. Bottom panel: quantification of the LC3II/Tub ratio. Data are representative of three independent experiments. **(C)** RAW macrophages overexpressing GFP-LC3 were grown in control medium in the presence or absence of 10 μ M of UA (UA) for 2 h. Confocal images depict GFP-LC3 and DQ-BSA or LysoTracker distribution under the indicated conditions. Scale bars, 10 μ m.

H9C2 cells) autophagosomes/cell, indicative of an active autophagy response, as previously shown (Vanrell et al., 2013). As expected, the values significantly increased in cells under starvation in comparison with control cells (Ctr) and decreased in the presence of wortmannin, a classic autophagy inhibitor. Interestingly, as with starvation, the treatment with UA increased the number of autophagosomes, which also diminished in the presence of wortmannin. To confirm these data, we next detected the endogenous LC3 by Western blotting and observed an increment in the level of LC3-II in the presence of UA (Figure 2B). Together, these data showed that UA treatment produced a significant increment in the number of autophagosomes in both RAW macrophages and H9C2 cells. Both inductions of autophagy and inhibition of autophagy degradation resulted in an increase in the number of autophagosomes. Therefore, to confirm the action of UA on autophagy, we next treated RAW cells overexpressing GFP-LC3 with UA and then incubated them with DQ-BSA and LysoTracker, markers of hydrolytic and acidic compartments, respectively, to study the nature of autophagosomes. As shown in Figure 2C, under UA treatment, many autophagosomes decorated with GFP-LC3 were also stained with DQ-BSA or LysoTracker, indicating their autolysosomal nature and confirming that treatment with UA induced a functional autophagy response.

Next, we studied the possible participation of autophagy in the elimination of amastigotes. RAW macrophages and H9C2 cells were infected with trypomastigotes of *T. cruzi* Y strain for 24 h and then treated with a control medium alone or with 10 μ M of UA for an additional 24 h. After fixation, cells were processed to detect the possible recruitment of LC3 protein to amastigotes and the presence of LysoTracker. Interestingly, both markers were found in amastigotes under control or UA-treated conditions. However, under UA conditions, the percentage of amastigotes with LC3 recruited was greater than in the control in both cell types. Similar differences were obtained when LysoTracker staining was quantified (Figure 3A). These data suggest that reduction in the number of amastigotes in UA-treated cells is mediated by an increment in amastigote xenophagy in these cells. To confirm that UA-induced autophagy was responsible for the clearance of amastigotes in the host cell cytoplasm, we performed similar experiments in the presence of the autophagy-specific PI3K inhibitor, Spautin-1 (Correa et al., 2014). RAW macrophages or H9C2 cells were infected with trypomastigotes of *T. cruzi* for 24 h and treated with 10 or 10 μ M of UA in the presence of 10 μ M of Spautin-1 for an additional 24 h. Cells were then fixed and processed to detect amastigotes by IIF by using an anti-*T. cruzi*-specific antibody. Notably, the inhibition of the autophagy pathway by Spautin-1 reversed the effect of UA on the number of amastigotes (Figure 3B). These data confirm that UA induces autophagy, and as a consequence, it promotes the elimination of amastigotes from the cytoplasm of host cells.

In another set of experiments, we performed primary cultures of BMM obtained from *Beclin-1* heterozygous

knockout mice (KD) and studied the level of infection in the presence of UA in comparison with cells obtained from WT animals. In agreement with our previous results (Casassa et al., 2019), the number of amastigotes in cells that displayed reduced autophagy was higher than that in the BMM WT. Treatment of control cells with UA reduced the number of amastigotes by $\approx 50\%$, as expected. In contrast, the same treatment in KD cells produced a partial effect due to the low autophagy response displayed by these cells (Supplementary Figure 3).

Exploring a Direct Action of Ursolic Acid Against *Trypanosoma cruzi*

To further study the possibility of a direct cytotoxic action of UA on *T. cruzi*, we analyzed the effect of this compound on the two replicative stages of this parasite, epimastigotes, and amastigotes, as well as in the infective trypomastigote stage.

First, we studied the cell viability of epimastigotes and trypomastigotes by treating the parasites with increased concentrations of UA for 24 h. As shown in Figures 4A, C, while the IC₅₀ for epimastigotes was $101.02 \pm 9.91 \mu\text{M}$, the EC₅₀ for trypomastigotes was 5.39 ± 0.02 . The cytotoxic effect on epimastigotes was confirmed by the observation of damaged parasitic cells by TEM at 100 μM without changes in the cellular morphology at lower concentrations (Figure 4B). These data indicate that UA showed high toxicity for *T. cruzi* trypomastigotes but not for epimastigotes.

Next, we studied the direct action of UA on amastigotes, the replicative stage of *T. cruzi* in mammalian cells. RAW macrophages and H9C2 cells were infected with *T. cruzi* trypomastigotes Y strain for 24 h and then incubated in a control medium alone or with the addition of 10 μM of UA or 50 nM of BNZ, which was used as a positive control of death. Using the TUNEL reagent for fluorescence microscopy, we evaluated the apoptosis of amastigotes by the green fluorescence emitted by the nucleus of dead parasites. As shown in Figure 4D, apoptotic parasites were produced under BNZ treatment in both RAW and H9C2 cells, while controls and UA-treated cells were negative for TUNEL staining, indicating the absence of apoptosis in these conditions. Note that the kinetoplasts of live amastigotes can be stained with this reagent, but the nuclei cannot, as these are stained when the amastigote dies by apoptosis (De Souza et al., 2010). However, in cells treated with BNZ, positive apoptotic nuclei were observed in amastigotes and the host cell, evidencing the cytotoxic action of this drug even in the mammalian cells (Figure 4D).

To confirm the low cytotoxic effect of UA on amastigotes, we further studied the ultrastructure of amastigotes developed in the host cells by TEM. No structural differences were observed in the amastigotes present in cells under a control medium or treated with UA (Figure 4E). These data showed that UA has a direct cytotoxic action on trypomastigotes of *T. cruzi* but not on the replicative stages, epimastigotes, and amastigotes and confirm that the host cell autophagy is required for the elimination of amastigotes from the host cell.

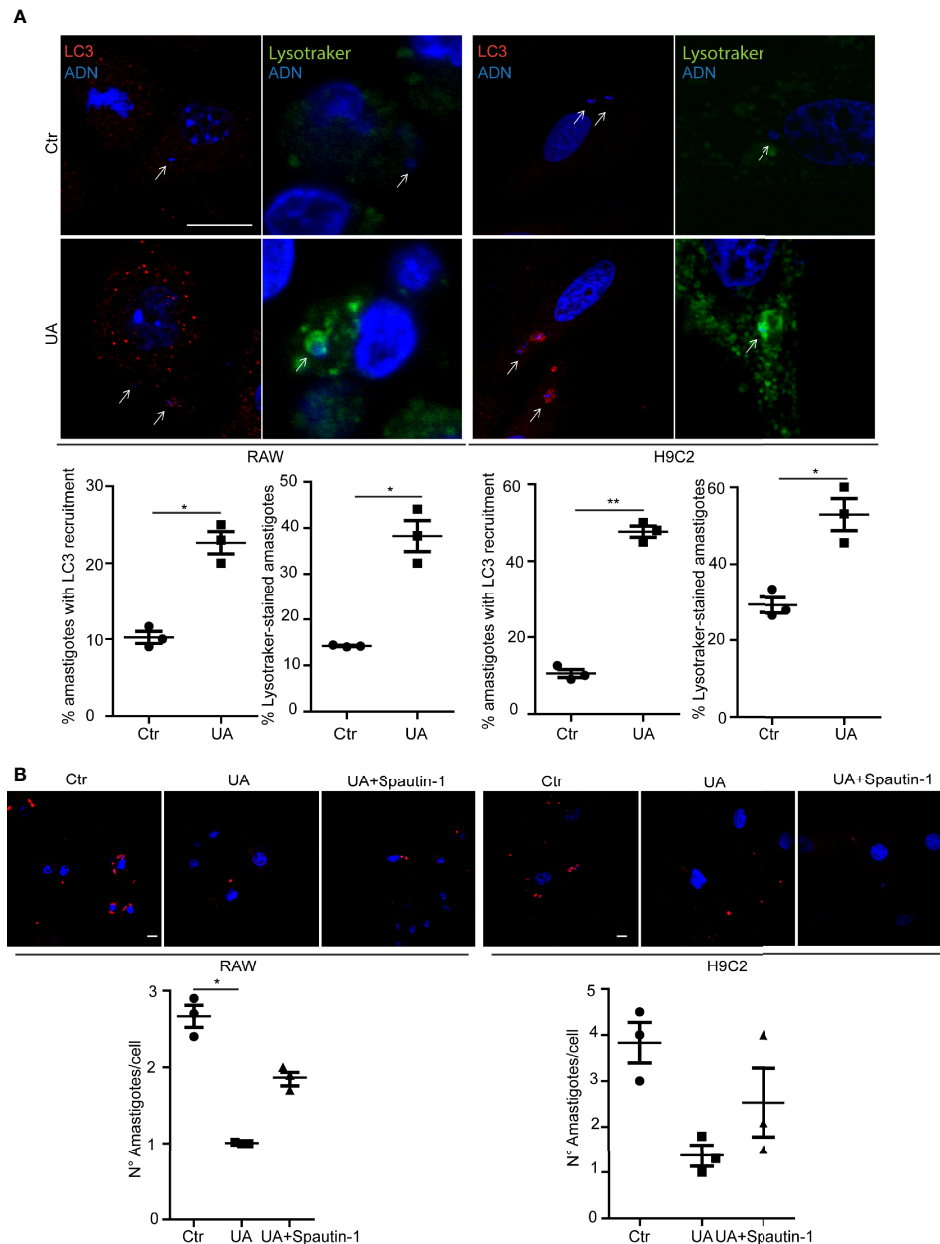


FIGURE 3 | Study of the *Trypanosoma cruzi* xenophagy. RAW macrophages or H9C2 cells infected with *T. cruzi* strain Y (MOI = 10) for 24 h and then treated for additional 2 or 24 h in different conditions. **(A)** RAW macrophages or H9C2 cells infected with *T. cruzi* Y strain for 24 h and then treated for an additional 2 h under different conditions. Confocal images depicting recruitment of LC3 (red) detected by indirect immunofluorescence or LysoTracker (Green) to *T. cruzi* amastigotes. Scale bars, 10 μ m. White arrows point to amastigotes. The graphs show the percentage of the mean \pm SD of three independent experiments on the recruitment of LC3 or LysoTracker in the different conditions. ** $p < 0.01$. Tukey's test. **(B)** RAW macrophages or H9C2 cells infected with *T. cruzi* Y strain (MOI = 10) for 24 h and then treated for an additional 24 h in different conditions, control, 10 μ M of UA, or 10 μ M of UA with Spautin-1. Confocal images show *T. cruzi* amastigotes (red) under different conditions. The graphs represent the mean \pm SEM of the number of amastigotes per cell under the different conditions. MOI, multiplicity of infection.

DISCUSSION

One of the main challenges in the search for new drugs for the treatment of CD is to find more effective compounds for the chronic stage than the current therapies. The persistence of

amastigote nests in the tissues of chronic patients induces an immune response that further produces the complications of this disease, evidencing the necessity of a trypanocidal action that clears the tissue parasitosis (Monteon-Padilla et al., 2001; Inst et al., 2011). Many strategies are being studied to reach this goal:

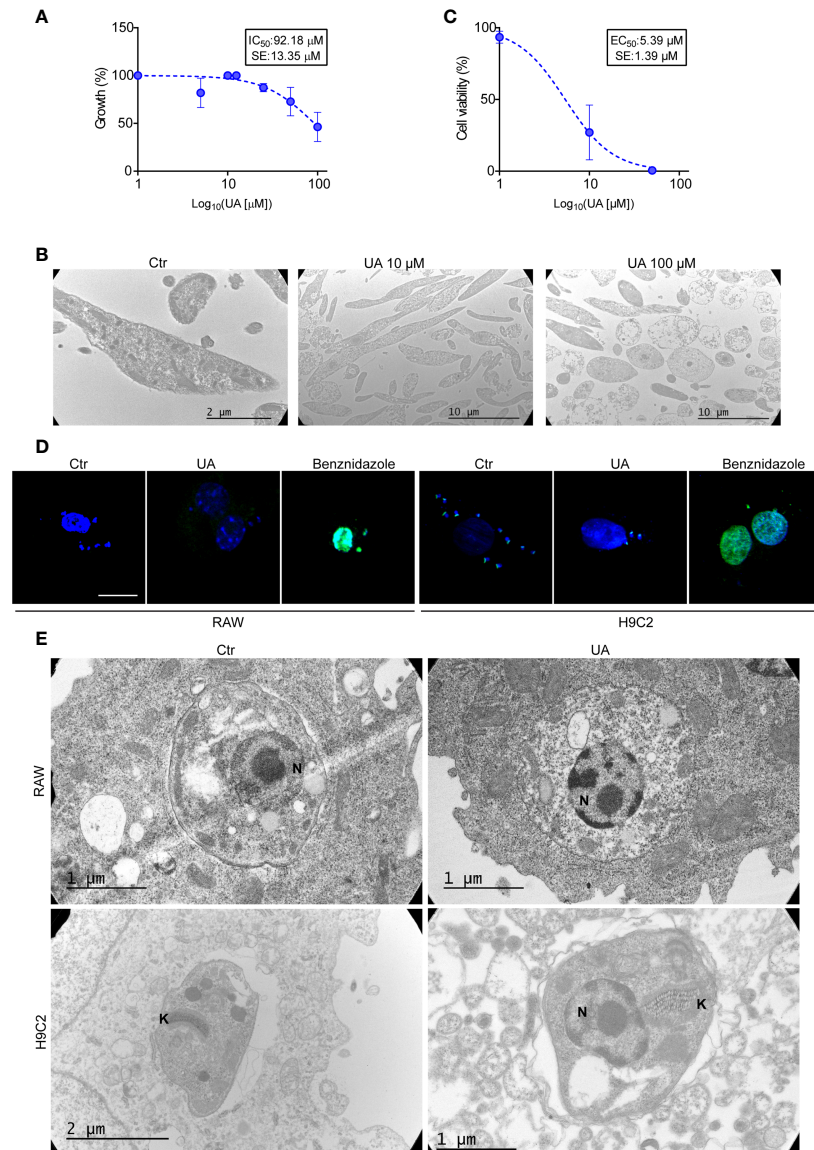


FIGURE 4 | Direct action of UA on different stages of *Trypanosoma cruzi*. **(A)** Epimastigotes were grown at different concentrations of UA for 24 h at 28°C. The graph shows the quantification of IC₅₀. **(B)** Transmission electron microscopy images of epimastigotes treated under different conditions for 24 h. **(C)** The trypomastigotes were treated at different concentrations of UA for 24 h at 4°C. The graph shows the quantification of the EC₅₀. **(D)** RAW macrophages and H9C2 cells were infected with *T. cruzi* trypomastigotes Y strain (MOI = 10) for 24 h and then treated for an additional 24 h under the different conditions. Subsequently, we evaluated apoptosis of the amastigotes and/or host cells using the TUNEL assay. White arrows point to amastigotes. **(E)** RAW macrophages and H9C2 cells were infected with *T. cruzi* trypomastigotes Y strain (MOI = 10) for 24 h and then treated for an additional 24 h under the different conditions. Transmission electron microscopy images show amastigotes inside the host cell. UA, ursolic acid; MOI, multiplicity of infection.

inhibition of ergosterol synthesis, impairment of the action of virulence factors such as cruzipain, inhibition of the parasite redox metabolism, and other strategies that target vital processes for *T. cruzi*. Other less explored strategies include the regulation of the host immune responses to enhance their antiparasitic activity. This study was focused on the latter paradigm. Based on evidence showing the key role of autophagy in the control of *T. cruzi* infection *in vitro* and *in vivo* (Márquez et al., 2018; Casassa et al., 2019; Matteucci et al., 2019), we decided to search for a

compound that increases the autophagy response of host cells and, consequently, interferes with the *T. cruzi* intracellular cycle. Since not all inducers of autophagy can be administered to patients due to their toxic action or because they display other unwanted effects, we selected UA. This natural compound has many biological actions including autophagy induction on different tumor-derived cells (Deng et al., 2019).

The first results of this work demonstrated that UA reduced the content of amastigotes in macrophages, as well as in cardiac

cells, without affecting host cell viability, as shown in the AlamarBlue assays. Interestingly, a direct cytotoxicity action of UA on amastigotes was also discarded in the TUNEL and TEM assays, indicating that the action of UA was executed by mechanisms other than apoptotic cell death. In contrast, UA was highly cytotoxic on the infective trypomastigote forms with an EC50 around half of the working concentration (10 μ M). In agreement with these data, Uchiyama and colleagues showed a significant reduction in the parasitemia peak in *T. cruzi*-infected mice treated with UA (da Silva Ferreira et al., 2013). Like the amastigotes, epimastigotes, the extracellular replicative form of *T. cruzi*, displayed high resistance to the UA treatment with an IC50 that is ten times higher than that of the working concentration. These data showed the importance of testing compounds at the distinct biological forms of a pathogen given the possible different susceptibilities of these forms to the compound studied, as in the case of *T. cruzi*. Similar results have been observed in the treatment of *Leishmania donovani* with a semi-purified fraction of the wild mushroom *Grifola frondosa* (Sultana et al., 2018).

In our system, we demonstrated that UA induces autophagy in both macrophages and cardiac cells and that this response was functional due to the localization of acidic and hydrolytic markers on autophagosomes formed in the presence of the drug. We also observed that LC3 is recruited to amastigotes at the same time as LysoTracker staining, evidencing the connection of parasites with autolysosomes in cells treated with UA. Moreover, inhibition of autophagy with Spautin-1, the specific inhibitor of the PI3K of autophagy, interferes with the action of UA on amastigotes. In agreement with this, UA is less active to clear amastigotes in the autophagy-deficient macrophages obtained from Beclin-1 heterozygous knockout mice. Altogether, these data demonstrate that enhanced autophagy response occurred in the presence of UA, the most important mechanism in the elimination of *T. cruzi* amastigotes by the process of xenophagy. Other intracellular pathogens, such as *Mycobacterium tuberculosis* (Chai et al., 2019) and *Salmonella* (Ammanathan et al., 2019), were also eliminated by xenophagy. We conclude that UA could be a good candidate for the treatment of CD alone or in combination with the current therapies.

DATA AVAILABILITY STATEMENT

The original contributions presented in the study are included in the article/Supplementary Material. Further inquiries can be directed to the corresponding authors.

REFERENCES

- Ammanathan, V., Mishra, P., Chavalmane, A. K., Muthusamy, S., Jadhav, V., Siddamadappa, C., et al. (2019). Restriction of Intracellular *Salmonella* Replication by Restoring TFEB-Mediated Xenophagy. *Autophagy*, 16 (9), 1584–1597. doi: 10.1080/15548627.2019.1689770
- Barbosa, MGE, de Albuquerque, D. M., Batista, A. M., Andrade, P. D., Guariento, M. E., Almeida, E. A., et al. (2011). Trypanosoma cruzi: parasite persistence in

AUTHOR CONTRIBUTIONS

MV has contributed with the design, execution and analysis of experiments. She also contributed in the writing of the manuscript. SM, LM, BS, and JG collaborated in the design, performance and analysis of experiments. PR has contributed to the design of experiments and analysis of results. Also in the writing of the manuscript. All authors contributed to the article and approved the submitted version.

FUNDING

This work has been partly supported by grants from Secretaría de Ciencia, Técnica y Posgrado (Sectyp, Universidad Nacional de Cuyo) and Agencia Nacional de Promoción Científica y Tecnológica (PICT# 2017 1456) to PR.

ACKNOWLEDGMENTS

We are grateful to Julieta Scelta, Luz Estefania Altamirano, Elisa Bocanegra, Alfonsina Morales, Jorge Ibañez, and Norberto Domizio for their technical assistance. The content of this manuscript has been partly presented at the “The 1st International Electronic Conference on Biomolecules: Natural and Bio-inspired Therapeutics for Human Diseases (IECBM 2020),” Proceedings 2020, DOI:10.3390/IECBM2020-08807.

SUPPLEMENTARY MATERIAL

The Supplementary Material for this article can be found online at: <https://www.frontiersin.org/articles/10.3389/fcimb.2022.919096/full#supplementary-material>

Supplementary Figure 1 | Flow cytometry of Bone Marrow-derived Macrophages typing. (A): Population of macrophages obtained. (B): Doublet Elimination. C and D: Histograms show relative fluorescence intensity of CD11b-APC and F480 PERCP CY5 staining respectively.

Supplementary Figure 2 | Alamar blue assay to assess UA toxicity in the cell models studied. RAW macrophages and H9C2 cells were treated for 24 h with 10 μ M of UA and then cell viability was evaluated with Alamar blue reagent. Quantification of fluorescence intensity at 540 nm. Data represent the mean \pm SEM of at least three independent experiments.

Supplementary Figure 3 | Number of amastigotes in bone marrow macrophages of WT and Beclina KD mice. Bone marrow macrophages obtained from C57 wt and Beclin-1 KD mice (deficient in the Beclin-1 protein that participates in the autophagic pathway) were infected with trypomastigotes Y strain of *T. cruzi* (MOI=10) for 24 h and then the cells were washed and incubated in control medium alone or with 10 μ M UA. The graph shows the quantification of the average number of amastigotes per cell \pm SEM of four experiments.

- tissues in chronic chagasic Brazilian patients. *Memórias do Instituto Oswaldo Cruz* 106, 85–91. doi: 10.1590/S0074-02762011000100014
- Bilbao-Ramos, P., Serrano, D. R., Ruiz Saldaña, H. K., Torrado, J. J., Bolás-Fernández, F., and Dea-Ayuela, M. A. (2020). Evaluating the Potential of Ursolic Acid as Bioproduct for Cutaneous and Visceral Leishmaniasis. *Molecules (Basel Switzerland)* 25 (6), 1394. doi: 10.3390/MOLECULES25061394
- Casassa, A. F., Vanrell, M. C., Colombo, M. I., Gottlieb, R. A., and Romano, P. S. (2019). Autophagy Plays a Protective Role Against Trypanosoma Cruzi

- Infection in Mice. *Virulence* 10, 151–165. doi: 10.1080/21505594.2019.1584027
- Chai, Q., Wang, X., Qiang, L., Zhang, Y., Ge, P., Lu, Z., et al. (2019). A Mycobacterium Tuberculosis Surface Protein Recruits Ubiquitin to Trigger Host Xenophagy. *Nat. Commun.* 10 (1), 1973. doi: 10.1038/S41467-019-09955-8
- Chen, Z., Liu, Q., Zhu, Z., Xiang, F., Zhang, M., Wu, R., et al. (2020). Ursolic Acid Protects Against Proliferation and Inflammatory Response in LPS-Treated Gastric Tumour Model and Cells by Inhibiting NLRP3 Inflammasome Activation. *Cancer Manage. Res.* 12, 8413–8424. doi: 10.2147/CMAR.S264070
- Correa, R. J. M., Valdes, Y. R., Peart, T. M., Fazio, E. N., Bertrand, M., McGee, J., et al. (2014). Combination of AKT Inhibition With Autophagy Blockade Effectively Reduces Ascites-Derived Ovarian Cancer Cell Viability. *Carcinogenesis* 35, 1951–1961. doi: 10.1093/CARCIN/BGU049
- da Silva Ferreira, D., Esperandim, V. R., Toldo, M. P. A., Kuehn, C. C., do Prado Júnior, J. C., Cunha, W. R., et al. (2013). *In Vivo* Activity of Ursolic and Oleonic Acids During the Acute Phase of Trypanosoma Cruzi Infection. *Exp. Parasitol.* 134, 455–459. doi: 10.1016/j.exppara.2013.04.005
- De Alba-Alvarado, M., Bucio-Torres, M. I., Zenteno, E., Sampedro-Carrillo, E., Hernández-Lopez, M., Reynoso-Ducoing, O., et al. (2020). Response to Infection by Trypanosoma Cruzi in a Murine Model. *Front. Veterinary Sci.* 7. doi: 10.3389/FVETS.2020.568745
- Deng, S., Shanmugam, M. K., Kumar, A. P., Yap, C. T., Sethi, G., and Bishayee, A. (2019). Targeting Autophagy Using Natural Compounds for Cancer Prevention and Therapy. *Cancer* 125, 1228–1246. doi: 10.1002/CNCR.31978
- De Souza, E. M., Nefertiti, A. S. G., Bailly, C., Lansiaux, A., and Soeiro, M. N. C. (2010). Differential Apoptosis-Like Cell Death in Amastigote and Trypomastigote Forms From Trypanosoma Cruzi-Infected Heart Cells *In Vitro*. *Cell Tissue Res.* 341, 173–180. doi: 10.1007/s00441-010-0985-5
- Dias, J. C. P. (2017). Facing Chagas Disease. *Rev. da Sociedade Bras. Medicina Trop.* 50, 285–286. doi: 10.1590/0037-8682-0254-2017
- Guarner, J. (2019). Chagas Disease as Example of a Reemerging Parasite. *Semin. Diagn. Pathol.* 36, 164–169. doi: 10.1053/J.SEMDP.2019.04.008
- Haspel, J., Shaik, R. S., Ifedigbo, E., Nakahira, K., Dolinay, T., Englert, J. A., et al. (2011). Characterization of Macroautophagic Flux *In Vivo* Using a Leupeptin-Based Assay. *Autophagy* 7, 629–642. doi: 10.4161/auto.7.6.15100
- Holzmueller, P., Geiger, A., Nzoumbou-Boko, R., Pissarra, J., Hamrouni, S., Rodrigues, V., et al. (2018). Trypanosomatid Infections: How Do Parasites and Their Excreted-Secreted Factors Modulate the Inducible Metabolism of L-Arginine in Macrophages? *Front. Immunol.* 9. doi: 10.3389/FIMMU.2018.00778
- Khwaza, V., Oyedeji, O. O., and Aderibigbe, B. A. (2020). Ursolic Acid-Based Derivatives as Potential Anti-Cancer Agents: An Update. *Int. J. Mol. Sci.* 21, 1–27. doi: 10.3390/IJMS21165920
- Leng, S., Hao, Y., Du, D., Xie, S., Hong, L., Gu, H., et al. (2013). Ursolic Acid Promotes Cancer Cell Death by Inducing Atg5-Dependent Autophagy. *Int. J. Cancer* 133, 2781–2790. doi: 10.1002/IJC.28301
- Leng, S., Iwanowycz, S., Saaoud, F., Wang, J., Wang, Y., Sergin, I., et al. (2016). Ursolic Acid Enhances Macrophage Autophagy and Attenuates Atherogenesis. *J. Lipid Res.* 57, 1006–1016. doi: 10.1194/jlr.M065888
- Lin, J. H., Chen, S. Y., Lu, C. C., Lin, J. A., and Yen, G. C. (2020). Ursolic Acid Promotes Apoptosis, Autophagy, and Chemosensitivity in Gemcitabine-Resistant Human Pancreatic Cancer Cells. *Phytother. Research : PTR* 34, 2053–2066. doi: 10.1002/PTR.6669
- Mallick, S., Dutta, A., Ghosh, J., Maiti, S., Mandal, A. K., Banerjee, R., et al. (2011). Protective Therapy With Novel Chromone Derivative Against Leishmania Donovanii Infection Induces Th1 Response *In Vivo*. *Chemotherapy* 57, 388–393. doi: 10.1159/000330856
- Márquez, J. D. R., Ana, Y., Baigorri, R. E., Stempi, C. C., and Cerban, F. M. (2018). Mammalian Target of Rapamycin Inhibition in Trypanosoma Cruzi-Infected Macrophages Leads to an Intracellular Profile That Is Detrimental for Infection. *Front. Immunol.* 9. doi: 10.3389/FIMMU.2018.00313
- Matteucci, K. C., Pereira, G. J. S., Weinlich, R., and Bortoluci, K. R. (2019). Frontline Science: Autophagy is a Cell Autonomous Effector Mechanism Mediated by NLRP3 to Control Trypanosoma Cruzi Infection. *J. Leukocyte Biol.* 106, 531–540. doi: 10.1002/JLB.HI1118-461R
- Monteon-Padilla, V., Hernandez-Becerril, N., Ballinas-Verdugo, M. A., Aranda-Fraustro, A., and Reyes, P. A. (2001). Persistence of Trypanosoma Cruzi in Chronic Chagasic Cardiopathy Patients. *Arch. Med. Res.* 32, 39–43. doi: 10.1016/S0188-4409(00)00261-7
- Mukherjee, D., Yousuf, M., Dey, S., Chakraborty, S., Chaudhuri, A., Kumar, V., et al. (2020). Targeting the Trypanothione Reductase of Tissue-Residing Leishmania in Hosts' Reticuloendothelial System: A Flexible Water-Soluble Ferrocenylquinoline-Based Preclinical Drug Candidate. *J. Medicinal Chem.* 63, 15621–15638. doi: 10.1021/ACS.JMEDCHEM.0C00690
- Nunes, M. C. P., Dones, W., Morillo, C. A., Encina, J. J., and Ribeiro, A. L. (2013). Chagas Disease: An Overview of Clinical and Epidemiological Aspects. *J. Am. Coll. Cardiol.* 62, 767–776. doi: 10.1016/J.JACC.2013.05.046
- Pathak, A. K., Bhutani, M., Nair, A. S., Kwang, S. A., Chakraborty, A., Kadara, H., et al. (2007). Ursolic Acid Inhibits STAT3 Activation Pathway Leading to Suppression of Proliferation and Chemosensitization of Human Multiple Myeloma Cells. *Mol. Cancer Research : MCR* 5, 943–955. doi: 10.1158/1541-7786.MCR-06-0348
- Peluffo, G., Piacenza, L., Irigoín, F., Alvarez, M. N., and Radi, R. (2004). L-Arginine Metabolism During Interaction of Trypanosoma Cruzi With Host Cells. *Trends Parasitol.* 20, 363–369. doi: 10.1016/J.PT.2004.05.010
- Qu, X., Yu, J., Bhagat, G., Furuya, N., Hibshoosh, H., Troxel, A., et al. (2003). Promotion of Tumorigenesis by Heterozygous Disruption of the Beclin 1 Autophagy Gene. *J. Clin. Invest.* 112, 1809–1820. doi: 10.1172/JCI20039
- Reynolds, E. S. (1963). The Use of Lead Citrate at High pH as an Electron-Opaque Stain in Electron Microscopy. *J. Cell Biol.* 17 (1), 208–12. doi: 10.1083/jcb.17.1.208
- Shanmugam, M. K., Rajendran, P., Li, F., Nema, T., Vali, S., Abbasi, T., et al. (2011). Ursolic Acid Inhibits Multiple Cell Survival Pathways Leading to Suppression of Growth of Prostate Cancer Xenograft in Nude Mice. *J. Mol. Med. (Berlin Germany)* 89, 713–727. doi: 10.1007/S00109-011-0746-2
- Sharma, V., Verma, S., Seranova, E., Sarkar, S., and Kumar, D. (2018). Selective Autophagy and Xenophagy in Infection and Disease. *Front. Cell Dev. Biol.* 6. doi: 10.3389/FCELL.2018.00147
- Shen, S., Zhang, Y., Zhang, R., Tu, X., and Gong, X. (2014). Ursolic Acid Induces Autophagy in U87MG Cells via ROS-Dependent Endoplasmic Reticulum Stress. *Chemico-Biological Interact.* 218, 28–41. doi: 10.1016/j.cbi.2014.04.017
- Son, J., and Lee, S. Y. (2020). Therapeutic Potential of Ursolic Acid: Comparison With Ursolic Acid. *Biomolecules* 10, 1–16. doi: 10.3390/B10111505
- Sultana, S. S., Ghosh, J., Chakraborty, S., Mukherjee, D., Dey, S., Mallick, S., et al. (2018). Selective *In Vitro* Inhibition of Leishmania Donovanii by a Semi-Purified Fraction of Wild Mushroom Grifola Frondosa. *Exp. Parasitol.* 192, 73–84. doi: 10.1016/J.EXPPARA.2018.07.006
- Tohmé, M. J., Giménez, M. C., Peralta, A., Colombo, M. I., and Delgui, L. R. (2019). Ursolic Acid: A Novel Antiviral Compound Inhibiting Rotavirus Infection *In Vitro*. *Int. J. Antimicrobial Agents* 54, 601–609. doi: 10.1016/J.IJANTIMICAG.2019.07.015
- Uchiyama, N., Kiuchi, F., Ito, M., Honda, G., Takeda, Y., Khodzimatov, O. K., et al. (2006). Trypanocidal Constituents of Dracocephalum Komarovii. *Tetrahedron* 62, 4355–4359. doi: 10.1016/J.TET.2006.02.067
- Vanrell, M. C., Cueto, J. A., Barclay, J. J., Carrillo, C., Colombo, M. I., Gottlieb, R. A., et al. (2013). Polyamine Depletion Inhibits the Autophagic Response Modulating Trypanosoma Cruzi Infectivity. *Autophagy* 9, 1080–1093. doi: 10.4161/auto.24709
- Yousuf, M., Mukherjee, D., Pal, A., Dey, S., Mandal, S., Pal, C., et al. (2015). Synthesis and Biological Evaluation of Ferrocenylquinoline as a Potential Antileishmanial Agent. *ChemMedChem* 10, 546–554. doi: 10.1002/CMDC.201402537
- Zhao, C., Yin, S., Dong, Y., Guo, X., Fan, L., Ye, M., et al. (2013). Autophagy-Dependent EIF2AK3 Activation Compromises Ursolic Acid-Induced Apoptosis Through Upregulation of MCL1 in MCF-7 Human Breast Cancer Cells. *Autophagy* 9, 196–207. doi: 10.4161/AUTO.22805

Conflict of Interest: The authors declare that the research was conducted in the absence of any commercial or financial relationships that could be construed as a potential conflict of interest.

Publisher's Note: All claims expressed in this article are solely those of the authors and do not necessarily represent those of their affiliated organizations, or those of the publisher, the editors and the reviewers. Any product that may be evaluated in

this article, or claim that may be made by its manufacturer, is not guaranteed or endorsed by the publisher.

Copyright © 2022 Vanrell, Martinez, Muñoz, Salassa, Tudela and Romano. This is an open-access article distributed under the terms of the Creative Commons Attribution

License (CC BY). The use, distribution or reproduction in other forums is permitted, provided the original author(s) and the copyright owner(s) are credited and that the original publication in this journal is cited, in accordance with accepted academic practice. No use, distribution or reproduction is permitted which does not comply with these terms.



Plasmodium vivax Duffy Binding Protein-Based Vaccine: a Distant Dream

Sonalika Kar and Abhinav Sinha*

Parasite Host Biology, Indian Council of Medical Research-National Institute of Malaria Research, New Delhi, India

OPEN ACCESS

Edited by:

Tania F. De Koning-Ward,
Deakin University, Australia

Reviewed by:

Mohammad Zeeshan,
University of London, United Kingdom
Dalma Maria Banic,
Oswaldo Cruz Foundation (Fiocruz),
Brazil

*Correspondence:

Abhinav Sinha
abhinavsinha@icmr.gov.in

Specialty section:

This article was submitted to
Parasite and Host,
a section of the journal
Frontiers in Cellular and
Infection Microbiology

Received: 09 April 2022

Accepted: 21 June 2022

Published: 13 July 2022

Citation:

Kar S and Sinha A (2022) *Plasmodium vivax* Duffy Binding Protein-Based Vaccine: a Distant Dream.
Front. Cell. Infect. Microbiol. 12:916702.
doi: 10.3389/fcimb.2022.916702

The neglected but highly prevalent *Plasmodium vivax* in South-east Asia and South America poses a great challenge, with regards to long-term in-vitro culturing and heavily limited functional assays. Such visible challenges as well as narrowed progress in development of experimental research tools hinders development of new drugs and vaccines. The leading vaccine candidate antigen *Plasmodium vivax* Duffy Binding Protein (PvDBP), is essential for reticulocyte invasion by binding to its cognate receptor, the Duffy Antigen Receptor for Chemokines (DARC), on the host's reticulocyte surface. Despite its highly polymorphic nature, the amino-terminal cysteine-rich region II of PvDBP (PvDBPII) has been considered as an attractive target for vaccine-mediated immunity and has successfully completed the clinical trial Phase 1. Although this molecule is an attractive vaccine candidate against vivax malaria, there is still a question on its viability due to recent findings, suggesting that there are still some aspects which needs to be looked into further. The highly polymorphic nature of PvDBPII and strain-specific immunity due to PvDBPII allelic variation in Bc epitopes may complicate vaccine efficacy. Emergence of various blood-stage antigens, such as PvRBP, PvEBP and supposedly many more might stand in the way of attaining full protection from PvDBPII. As a result, there is an urgent need to assess and re-assess various caveats connected to PvDBP, which might help in designing a long-term promising vaccine for *P. vivax* malaria. This review mainly deals with a bunch of rising concerns for validation of DBPII as a vaccine candidate antigen for *P. vivax* malaria.

Keywords: Malaria, *Plasmodium vivax*, vaccine, blood stage malaria antigen, PvDBP

PREFACE

Infectious diseases have played an important role in modeling human demography and genetics. Malaria is considered to be one of the most devastating infectious diseases affecting mankind and is believed to be one of the strongest selective pressures in recent human history (Haldane, 2004; Kwiatkowski, 2005). At least nine species of the unicellular eukaryotic parasite of genus *Plasmodium* are reported to cause infection in humans including *P. falciparum*, *P. vivax*, *P. malariae*, *P. ovale curtisi*, *P. ovale wallikeri* (Sutherland et al., 2010), *P. knowlesi*, *P. cynomolgi* (Ta et al., 2014), *P. simium* (Deane, 1992; Brasil et al., 2017), and *P. brasilianum* (Lalremruata et al., 2015). Out of these nine species, only *Plasmodium falciparum* and *Plasmodium vivax* emerge to be the major threats

escalating the malaria load globally. Though great progress has been made in the fight against malaria since 2000, an increase in the number of cases in the last few years has placed doubt on the objective of eliminating the illness. In 2020, an estimated 241 million malaria cases were reported in 85 malaria-endemic countries (World Health Organization, 2021). The WHO African Region accounted for around 95% of cases in 2020, with an anticipated 228 million cases (World Health Organization, 2021). There has been an increase in the proportion of malaria caused by *P. vivax* in co-endemic regions where intensive malaria-control measures have lowered the burden of *P. falciparum*. In co-endemic areas, there is an increased risk of *P. vivax* after *P. falciparum* therapy, suggesting that universal radical cure for both parasites might be beneficial in some situations.

P. vivax is by far the most predominant source of human malaria across Asia and the Asia-Pacific regions, which account for approximately 80% of the worldwide *P. vivax* burden due to large populations and a diminishing prevalence of *P. falciparum* infections (Howes et al., 2016). Its existence has also been reported in the horn of Africa, Madagascar, and parts of Central and South America (World Health Organization, 2020). The sensitivity of the present-generation RDTs employed for *P. vivax* diagnosis is comparable to that of microscopy (Chu and White, 2021). In malaria-endemic areas, it has been found that ultrasensitive PCR technologies detects parasite densities as low as 28/ml (Imwong et al., 2014). This indicates a substantially greater prevalence of asymptomatic *P. vivax* infection than previously thought. In areas where *P. falciparum* and *P. vivax* malaria coexist, the *P. vivax* burden has overtaken the *P. falciparum* burden (Battle et al., 2019). *P. falciparum*, which is well known to cause complicated and fatal malaria, has overshadowed the clinical and public health importance of *P. vivax* malaria (Baird, 2007; Conway, 2007). Contrary to the belief that *P. vivax* causes a relatively benign and self-limiting infection, evidence documenting severe and complicated *P. vivax* malaria are escalating gradually (Price et al., 2007; Herrera et al., 2007; Baird, 2013a; Baird, 2013b). Concomitant or chronic illness could result into a severe *P. vivax* infection.

It is increasingly becoming visible that efforts towards understanding *P. vivax* have been inadequate in comparison to those for *P. falciparum* (Price et al., 2009) and one of the main reasons behind the lag of *P. vivax* research is the inability of achieving a stable and long-term *in-vitro* culture for *P. vivax* leading to significantly restricted laboratory-based experimental studies. Advances in *in vitro* culture of *P. knowlesi* in human RBCs, have given critical support for more sophisticated laboratory investigations (Moon et al., 2013; Mohring et al., 2019), allowing some practical functional studies of *P. vivax* to be conducted. *Plasmodium* spp. other than *P. vivax* target almost all stages of RBCs, whereas *P. vivax* preferentially invades immature RBCs or reticulocytes (Kitchen, 1938), which normally account for 1–2% of the red blood cells in the peripheral blood circulation. Although advancement has been made in understanding the molecular basis underlying *P. vivax* reticulocyte preference for

invasion (Gruszczyk et al., 2018a), still a powerful tool lacks (Krotoski et al., 1982; Mueller et al., 2009) which will help us in overcoming the difficulties in maintaining *P. vivax* in long-term cultures as it is relatively more difficult to repeatedly obtain and supplement reticulocyte-rich human blood to *P. vivax* cultures.

Another unique challenge with *P. vivax* is its ability to produce a dormant liver-stage forms or hypnozoites (Krotoski et al., 1982; Markus, 2011) which are responsible for multiple clinical relapses after a primary infection (Imwong et al., 2007). Prevention of *P. vivax* relapses is a must for *P. vivax* malaria to be eliminated. The distinction between relapse, recrudescence, and reinfection, and thus identifying early resistance, is a fundamental difficulty in therapeutic assessment. Chloroquine and the ACT companion medications are very slowly removed, so suppressive blood concentrations can last for weeks post medication (White, 2021).

Clinical intervention of *P. vivax* malaria requires clinical suspicion, an accurate blood test, and access to an efficient schizonticidal and hypnozoiticidal medication regimens. Although *P. vivax* is known to be still sensitive to chloroquine combined with primaquine, cases of chloroquine and sulfadoxine-pyrimethamine drug resistant *P. vivax* have also been reported from many areas of the globe including Australia, Ethiopia, Pakistan, Indonesia, Papua New Guinea, S. Korea and India (Rieckmann et al., 1989; Schunk et al., 2006; Price et al., 2009; Khatoon, 2010; Price, 2014). In addition, the main problem in managing a *P. vivax* infection is the management of frequent relapses for which both primaquine and its new counterpart, tafenoquine, have problems related to treatment adherence and safety with respect to G6PD deficiency. Thus, the unique clinical biology of *P. vivax* and restricted progress in the advancement of research tools (Su, 2019), create an obstacle in the way of growth of efficacious drugs and vaccines for vivax malaria. Adding to the above reasons, lack of financing, a paucity of resources and a high cost to create new vaccines contributes to the slow progress in case of development of a successful *P. vivax* vaccine.

AN IDEAL *PLASMODIUM VIVAX* MALARIA VACCINE

Regardless of decades of continuous efforts, only one vaccine (pre-erythrocytic vaccine RTS, S/ASO1 also known as Mosquirix) for *P. falciparum*, has been licensed for human use (RTS,S Clinical Trials Partnership, 2014; Laurens, 2020), but no vaccine for *P. vivax* is available yet. *Plasmodium* spp. exhibits a unique set of antigens at each stage of its life which makes it difficult for a researcher to identify the best vaccine candidate. The complex biology of *P. vivax*, its extensive antigenic diversity and its pathway of immune evasion make vaccine development against *P. vivax* malaria challenging. *P. vivax* is reported to exhibit greater genetic diversity in comparison to *P. falciparum* (Neafsey et al., 2012; Winter et al., 2015). While selecting a vaccine candidate for *P. vivax*, it is highly crucial to focus on those playing a role in invasion and those with a conserved

epitope, which can be targeted by neutralizing the strain transcending antibodies. The discovery of broadly conserved inhibitory epitopes provides important new themes for the next generation of *P. vivax* malaria vaccines, as well as a foundation for rational structure-based vaccine design that will impart global strain-transcending protection (Chen et al., 2016). Multiple clinical isolates of *P. vivax* were used to investigate a panel of human monoclonal antibodies for their ability to inhibit PvDBP from binding to the DARC, as well as their ability to impede red blood cell invasion and reticulocyte invasion. This led to the discovery of a widely neutralizing human monoclonal antibody that prevented *P. vivax* invasion in all tested strains (Rawlinson et al., 2019).

CURRENT STATUS OF CANDIDATE *P. VIVAX* MALARIA VACCINES

The designing and distribution of a successful *P. vivax* vaccine tends to be a prime concern for speeding up malaria elimination in the Asia-Pacific and the Americas (Tanner et al., 2015). Only a few *P. vivax* vaccine candidates are close to or have reached different stages of clinical trials (Mueller et al., 2015; Draper et al., 2018). The delay in the development of a CSP-based vaccine for *P. falciparum*, RTS,S/AS01 (RTS,S) clearly indicates that much more work awaits for a comparable *P. vivax* vaccine. Although there is potential current research into *P. vivax* vaccine targets and immunisation tactics, the odds of a *P. vivax* vaccine becoming available in the near future are low. To date, human clinical trials have only been carried out for three *P. vivax* antigens namely, the PvCSP-based pre-erythrocytic vaccine, the PvDBP-based blood stage vaccine and the transmission-blocking candidate Pvs25 (Rainbow Tables, WHO). Several novel vaccine candidates are now being studied in a pre-clinical setting and there are excellent reviews discussing them (Galinski and Barnwell, 2008; Valencia et al., 2011).

The VMP001/AS01_B vaccine, which encompasses the N- and C- terminal regions of the CSP and a short repeat region comprising of repeat sequences from both the VK210 (type 1) and the VK247 (type 2) genotypes of *P. vivax* has been shown to clear the Phase I/IIa trial, increasing antibody and cell-mediated immune responses and subsequently resulting in a delay in the pre-patency period in 30 Duffy-positive vaccines (Bennett et al., 2016), but no sterile protection was achieved. However, a combination of PvCSP and PvTRAP provided sterile protection in mice using doses that individually conferred low or no protection (Atcheson et al., 2018). Phase II trials with another candidate, PvRAS (*Plasmodium vivax* Radiation-Attenuated Sporozoites), showed immunogenic and sterile immunity in only 42% of the Duffy +ve (Fy+) subjects (Arevalo-Herrera et al., 2016). Transmission Blocking Vaccines targeting either a) pre-fertilization antigens expressed by gametocytes (Pvs48/45 and Pvs47) and gametes (Pvs230) (Sauerwein and Bousema, 2015; Tachibana et al., 2015) and b) post-fertilization antigens expressed by zygotes/ookinets/oocysts (Pvs25 and Pvs28) (Hisaeda et al., 2000; Sauerwein and Bousema, 2015). To date,

the Pvs25 protein present on the surface of ookinets and oocysts (Tsuboi et al., 1998), is one of the best characterized Transmission Blocking Vaccine candidate Blagborough et al. (2016). Phase 1 trial using Pvs25 formulated with Montanide ISA 51 as an adjuvant has demonstrated significant antibody responses in volunteers, but trial was stopped due to frequent local reactogenicity such as erythema, induration, swelling, and tenderness at the site of injection (Wu et al., 2008). However, pre-clinical and clinical studies with P25 proteins shows that inclusion of a carrier protein could potentially boost its immunogenicity (Qian et al., 2007; Parzych et al., 2017; Radtke et al., 2017).

While evaluating a novel vaccine candidate antigen's eligibility, it should be checked whether the gene that encodes it is required for parasite growth, as targeting a non-essential gene would appear to favour parasites that do not rely on the gene product and hence are immune to the vaccine. Although progress has been observed in identification and antigenic characterization of different *P. vivax* antigens, this review mainly focuses on the blood stage vaccine candidates and that too on PvDBP, the only to-date blood stage vaccine candidate that has reached Phase 1 clinical trial (de Cassan et al., 2015; Bhardwaj et al., 2017; Payne et al., 2017; Singh et al., 2018). Antigens expressed on the merozoite surface are considered as blood stage vaccine targets. An effective vaccination against *P. vivax* blood stages would decrease symptoms and pathology associated with such repeated infections, and so potentially play a crucial role in controlling the species. In addition to provision of safety and efficacy, an ideal blood-stage vaccine candidate antigen should be capable of eliciting a strong immune response that inhibits *Plasmodium* from invading the target host cell. In comparison to 15 *P. falciparum*'s blood stage vaccine candidates that have been described in literature so far (Illingworth et al., 2019), only a few candidates have been studied in case of *P. vivax* (Table 1), including Duffy Binding Protein (PvDBP), Merozoite Surface Protein 1 (MSP1), Apical Membrane Antigen 1 (PvAMA1) and Reticulocyte Binding Protein (PvRBP2b), a distant homologue of Reticulocyte Binding Protein Homologue 5 (PfRh5). Utilizing *P. knowlesi* as a screening model, research on a panel of *P. vivax* proteins (PvMSP7.1, PvMSP3.10, Pv12, Pv41, PvGAMA, PvCyRPA and PvARP) hypothesized to act in erythrocyte invasion, found an additional erythrocytic stage vaccine candidates (Ndegwa et al., 2021). Taking into account all of the benefits and drawbacks of any model system, it can be concluded that *P. knowlesi* might serve as an accessible and efficient model to screen for new candidates until a robust and long-term *P. vivax* culture is produced.

To date, human trials in the erythrocytic stage have only been carried out for PvDBP-based vaccine. *P. vivax* invasion of human RBCs is restricted to interaction of PvDBP with human reticulocytes (via the Duffy Antigen Receptor for Chemokines, DARC) expressing the Iron Importer, Transferrin Receptor 1 (TfR1) or Cluster of Differentiation 71 (CD71) (Malleret et al., 2015). Till date, only two vaccines targeting the conserved cysteine-rich region II of PvDBP have reached clinical trials,

TABLE 1 | *Plasmodium vivax* blood stage vaccine candidates.

	Description/delivery system	Development phase	Antigen	Reference
PvDBPII/GLA-SE	Recombinant PvDBPII with Glucopyranosyl Lipid Adjuvant-Stable Emulsion	Phase I b	PvDBP	Bharadwaj et al., 2017; Singh et al., 2018
ChAd63-MVA PvDBP RII	Prime boost, viral vectors (Chimpanzee Adenovirus 63/Modified Vaccinia Ankara)	Phase I a	PvDBP	de Cassan et al., 2015; Payne et al., 2017
PvDBPII-DEK ^{null}	Recombinant protein	Pre-clinical	PvDBP	Ntumngia and Adams, 2012
PvMSP1 ₁₉	Recombinant protein-Montanide ISA720	Pre-clinical	PvMSP1	Fonseca et al., 2016
ChAd63-PvAMA1/MVA-PvAMA1	Chimpanzee Adenovirus 63/Modified Vaccinia Ankara	Pre-clinical	PvAMA1	Bouillet et al., 2011
PvAMA1	Recombinant protein-adjuvant	Pre-clinical	PvAMA1	Vicentin et al., 2014; Arévalo-Pinzón et al., 2017
PvRBP2b	Recombinant protein	Pre-clinical	PvRBP	Gruszczyk et al., 2018a, Gruszczyk et al., 2018b

ChAd63/MVA PvDBP RII (Payne et al., 2017) and PvDBPII/GLA-SE (Bhardwaj et al., 2017; Singh et al., 2018).

PvDBP, AN ESSENTIAL PARASITE LIGAND FOR HUMAN RETICULOCYTE INVASION

A number of distinct invasion pathways have been identified by *Plasmodium* spp. that exploit unique sets of human red blood cell (RBC) receptors for invasion. Two major protein families of *Plasmodium*, the **Erythrocyte-Binding-Like (EBL) family**, expressed from the *erythrocyte-binding-like (ebl)* genes (Fang et al., 1991) and the **Reticulocyte-Binding-Like (RBL) protein homologs (RBL or Rh)**, expressed from *reticulocyte binding protein* genes (Galinski et al., 1992) are responsible for parasite's tight interactions with different stages of host's RBCs. There exists a species-specific variation in the count of EBL proteins, *P. falciparum* having five members while *P. vivax* has only a single member (Adams et al., 1992; Adams et al., 2001). The EBL family further consists of the Duffy-Binding-Like (DBL-EBL) and Erythrocyte-Binding Protein sub-families (EBP) (Adams et al., 2001). The DBL-EBL proteins are characterized by presence of two cysteine-rich regions and a Duffy-binding domain in the N-terminal cysteine-rich region (Adams et al., 1992). On the other hand, the members of the RBL family solely target the reticulocytes as well as normocytes, producing parasite proteins which facilitate reticulocyte binding and/or invasion (Ntumngia et al., 2018). Reticulocyte-binding proteins (RBPs) were originally discovered in *P. vivax* (Galinski et al., 1992) and are the classic instances of reticulocyte binding-like/reticulocyte-binding homolog (RBL/RH) proteins, which have also been discovered in *P. cynomolgi* (Okenu et al., 2005) and *P. yoelii* (Ogun et al., 2011). In *P. vivax*, the RBL determine the reticulocyte restriction of this species. Out of the five PvRBPs, only one (PvRBP2b) is found to bind exclusively to reticulocytes (França et al., 2016).

DUFFY-BINDING-LIKE SUB-FAMILY OF ERYTHROCYTE-BINDING-LIKE FAMILY

A huge macromolecular cascade of proteins is likely involved in host cell selection and invasion activities. However, just a few will be crucial participants in allowing the parasite to retain a significant red blood cell invasion capacity in the face of physiological and immunological changes in the host. This adds to the latency of the infection and, as a result, enhance the possibilities of transmission. These proteins are most likely parasite ligands involved in the erythrocyte surface binding events that contribute to effective invasion. Sequestered in the micronemes of merozoites, the DBL-EBPs are type-I membrane proteins which are supposed to be released during the invasion process (Adams et al., 1990). The first DBL-EBL was identified in *P. knowlesi* and was called Duffy-Binding Protein (PkDBP) as it was shown to bind the Duffy Antigen Receptor for Chemokines (DARC) on RBCs (Chitnis and Miller, 1994). Subsequently, its orthologues in *P. vivax* and *P. falciparum* have also been identified (Haynes et al., 1988). Members of DBL-EBL family are characterized to have six extracellular regions (RI-RVI), subsequently followed by a type I trans-membrane domain, and a short cytoplasmic tail (Adams et al., 1992). Out of the six extracellular regions, the two hydrophobic cysteine-rich regions (N-terminal RII and C-terminal RVI) are functionally conserved in all erythrocyte binding proteins (EBLs) and separated by three low-homology regions (RIII-RV). The N-terminal cysteine-rich region (RII) carries the binding residues responsible for binding to the DARC (Chitnis and Miller, 1994), whereas the C-terminal cysteine-rich region (RVI) has no clear known function, although a high degree of amino acid conservation among the three *Plasmodium* species (*P. falciparum*, *P. vivax* and *P. knowlesi*) is observed which suggests that this domain might have some importance (Adams et al., 1992). *P. falciparum* and *P. knowlesi* exhibit a variety of proteins (PfEBL-1, PfEBA-140, PfEBA-175, PfEBA-181, PfEBA-165, PkDBP α and multiple DBP-like ligands) belonging to DBL-EBL family, creating alternative pathways of RBC invasion, whereas, *P. vivax* comprises of a single protein, PvDBP (Adams et al., 1992) of the DBL-EBL family. PvEBP, in addition to PvDBP, is a new member to this family (Roesch et al., 2018).

Plasmodium vivax Duffy Binding Protein (PvDBP) is a 140-kDa trans-membrane protein responsible for reticulocyte invasion of *P. vivax* and is dependent on the host's Duffy Antigen Receptor for Chemokines (DARC) (Horuk et al., 1993). The *Pvdbp* gene (PlasmoDB Gene ID = PVX_110810) is present in chromosome 6 of *P. vivax* spanning a length of 3,762 nucleotides Carlton et al. (2008) (**Figure 1A**) and comprising of five exons and four introns (Fang et al., 1991). Exon 1 (57 nucleotides) of *Pvdbp* encodes a signal sequence, exon 2 (2,959 nucleotides) encodes 986 amino acids and covers the six extracellular regions, RI-RVI of the translated protein, exon 3 spans 79 nucleotides and comprises a trans-membrane domain (18 amino acids), exons 4 and 5 spanning 74 and 44 nucleotides, respectively. Exons 4 and 5 and a portion of exon 3 translates into a cytoplasmic tail (45 amino acids) (Adams et al., 1990; Adams et al., 1992) (**Figure 1B**). The N-terminal cysteine rich region (RII) comprises of DBL domains (Chitnis and Miller, 1994) which contain binding residues responsible for formation of tight junction between PvDBP and DARC. The C-terminal cysteine-rich region (RVII), is separated from RII by three hydrophilic regions III, IV and V and is followed by the trans-membrane domain.

The N-terminal cysteine rich region (RII) of PvDBP starts and ends at H206 and Q530, respectively (VanBuskirk et al., 2004b) (**Figure 1C**). It has been found that RII spans 325 aa residues, and not 330 aa, as it was thought previously. This 325 aa region (RII) comprises of 12 conserved cysteine residues (C217, C230, C237, C246, C300, C377, C415, C427, C432, C436, C505, and C507) (Fang et al., 1991; Adams et al., 1992). The cysteines are reported to contribute to DBL's structural integrity (Singh et al., 2003; Singh et al., 2006), and so the parasite may not afford changes in these residues. The region deepest within the DBL domain, i.e. between cysteines 4 and 8, have been marked as the portion bearing the prime components for receptor recognition (Tsuboi et al., 1994; Ranjan and Chitnis, 1999; Xainli et al., 2000). The minimal binding region of PvDBPII to the human DARC is localized between cysteines 4 and 7 (Ranjan and Chitnis, 1999; Batchelor et al., 2011). Residues between cysteines 7 and 8 are supposed to be surface-exposed and are not significantly involved in receptor binding (Ranjan and Chitnis, 1999; VanBuskirk et al., 2004b).

Pka/Pv-DBL is a compact helical, monomeric module spread over three distinct subdomains (SD1, SD2 and SD3). *Pka/Pv-DBL*

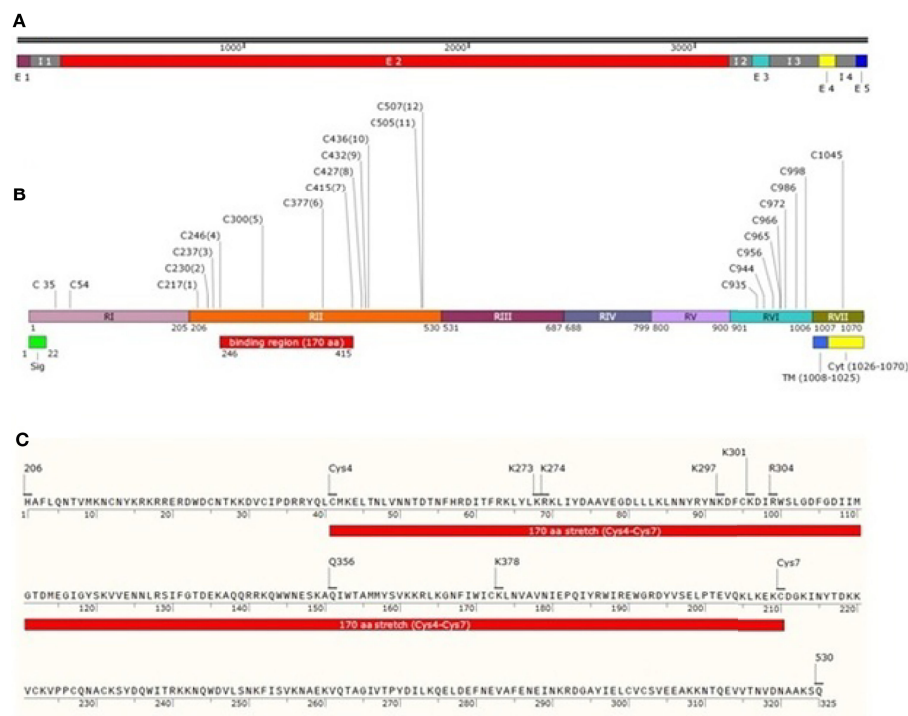


FIGURE 1 | Schematic drawing of PvDBP. **(A)** *Pvdbp* gene (3762 nucleotides) with 5 exons (1-57, 193-3151, 3257-3335, 3554-3627 and 3719-3762, respectively) and 4 introns (58-192, 3152-3256, 3336-3553 and 3628-3718, respectively). **(B)** PvDBP consisting of 1070 amino acid residues. The shared boundaries for regions I-VII (205, 530, 687, 799, 900, 1006 and 1070 amino acids, respectively) (Adams et al., 1992; Okenu et al., 2005). Labelled in it are the positions corresponding to seven regions (RI-RVII) of PvDBP, the cysteine-rich regions (RII and RVII), signal peptide shaded in green (1-22aa), transmembrane domain shaded in blue (1008-1025aa) and cytoplasmic domain shaded in yellow (1026-1070aa). PvDBP consists of 23 cysteines (two in RI, twelve in RII, eight in RVI and one in RVII). The cysteines are labelled along with their amino acid position. The binding residues map to a 170 aa stretch which starts from Cys4 and ends at Cys7 (C246-C415) **(C)** PvDBPII spans a length of 325 aa from 206-530aa (Adams et al., 1990). The PvDBPII binding residues at sub domain 2: Site 1 (K297, K301, R304 and K378 (VanBuskirk et al., 2004b)) and Site 2 (K273, K274 and Q356 (Hans et al., 2005)) are responsible for reticulocyte binding with respect to 1070 aa residues of PvDBP (NCBI protein id: XP_001608387.1).

consists of twelve cysteine residues which are stabilized by intra-domain disulfide bonds mostly conserved amongst the DBL family of EBPs (Singh et al., 2006). The indispensable and invariant residues required for DARC recognition (**Figure 1C**) were mapped within a region on SD2 (Singh et al., 2003; Hans et al., 2005; Singh et al., 2006; Yogavel et al., 2018), which lies between Cys4 (C246) - Cys7 (C415). Cys1 (C217) - Cys3 (C237) and Cys8 (C427) - Cys12 (C507) which flank SD2 (Cys4-Cys7) might play a structural role in the intact DBL domain (Ranjan and Chitnis, 1999; Singh et al., 2003; Singh et al., 2006) (**Table 2**). SD1 is not required for DBL-DARC interaction (Singh et al., 2003) whereas the functional significance of SD3 is still in question.

Although region II plays a significant role in receptor recognition, this region with respect to the rest of *Pvdbp* gene is hyper-variable with a high ratio of non-synonymous to synonymous mutations (Tsuboi et al., 1994; Xainli et al., 2000; Cole-Tobian and King, 2003), which might be one of the factors which help the parasite to escape host immunity (Tsuboi et al., 1994; Xainli et al., 2000). Exploration of *PvdbpII* genetic variation among *P. vivax* endemic regions showed that *PvDBPII* is highly polymorphic, however, no changes in the cysteine residues have been reported so far (Tsuboi et al., 1994; Ampudia et al., 1996; Xainli et al., 2000; Kho et al., 2001; Cole-Tobian and King, 2003; Sousa et al., 2006; Gosi et al., 2008; Babaeekhou et al., 2009; Batchelor et al., 2011; Premaratne et al., 2011; Chenet et al., 2012; Ju et al., 2012; Ju et al., 2013).

The polymorphic residues adjacent to the binding site are reported to escape the binding inhibitory antibodies thus keeping the binding site of the protein undisturbed. Site-directed mutagenesis of *PvDBPII* identified several residues which are vital for receptor recognition (VanBuskirk et al., 2004b). The conserved residues present in the binding region of *PvDBP* were found to be responsible for ligand receptor interaction. The variant residues are reported to flank the functionally important residues. So, changes occurring in the conserved amino acid residues (which are not exposed on the surface, as a result are not detected by hosts immunity) might be accountable for loss of binding activity. The reported polymorphic residues were not found to affect reticulocyte binding as they are found to be mapped in the face opposite to the residues critical for binding to DARC (Chitnis and Sharma, 2008).

Batchelor et al. elucidated the crystal structure of *PvDBPII* (PDB: 3RRC), which indicates a model for receptor recognition through *PvDBP* dimerization, facilitating the development of a complex composed of two *PvDBP* and two DARC molecules, which might pave way towards invasion (Batchelor et al., 2011). The critical binding residues required for reticulocyte binding were found to be structurally and functionally conserved, and are also targets of immune response (Batchelor et al., 2011). Protective

antibodies targeting the critical binding regions in *PvDBPII* were found to disturb dimerization and/or inhibit receptor binding. A step-wise binding model has also been proposed which involves receptor-induced *PvDBPII* dimerization facilitating the formation of a heterotrimer that eventually employs a second DARC molecule to form a heterotetramer (PDB: 4NUU and 4NUV) Batchelor et al. (2014). Although these structural and biophysical studies provide deep insight into *PvDBPII*-DARC engagement, further studies are required to assess these models as this region is prone to polymorphisms (Mittal et al., 2020) and as a result, the inherent variability in *PvDBL* might render the *PvDBP*-based vaccines inefficacious. Further, Yogavel et al. reported the existence of two binding sites in *PvDBPII*, a) Site 1 which includes residues K266, K270, R273 and K347 and, b) Site 2 including residues K242, R243 and H325 (from PDB: 3RRC, 4NUU and 4NUV) (Yogavel et al., 2018). The DARC peptide, by means of its sulfated Tyr41 and phosphorylated Tyr30, engages at sites 1 and 2, respectively on *Pv/Pk*-DBLs. This is a testable model depicting DARC's engagement with *Pv/Pk*-DBP and needs to be experimentally assessed for further confirmation.

Keeping allelic variation in mind, a successful and efficacious *DBPII*-based vaccine should aim at conserved epitopes which are supposed to be the prospective targets of strain-transcending neutralizing immunity. Naturally acquired binding-inhibitory antibodies to *PvDBPII* are associated with clinical immunity of the subject to *P. vivax* malaria and thus potentially neutralize the *P. vivax* invasion mechanism (Grimberg et al., 2007; Chootong et al., 2010; Nicolette et al., 2016).

For the first time, studies using ELISA and flow cytometry confirmed that both rabbit and human antibodies inhibited recombinant *PvDBPII*-DARC interactions and were found to reduce invasion efficiency of wild *P. vivax* by up to 64%, while a reduced *P. vivax* invasion by up to 54% was observed in a combined *PvDBPII* antisera from people exposed to *P. vivax* (Grimberg et al., 2007). Polymorphisms in *PvDBPII* and the presence of multiple strains in endemic regions present unique challenges in the path of vaccine design (VanBuskirk et al., 2004a; Cole-Tobian et al., 2009; Ntumngia et al., 2012). In spite of the variations that exists in *PvDBPII*, broadly conserved epitopes of three inhibitory murine monoclonal antibodies have been recognized in *PvDBPII* (subdomain 3) (Chen et al., 2016) which were not found to lie in close vicinity to the dimer interface as well as the DARC-binding site (Chen et al., 2016). Clinical trials in humans using *PvDBPII* produced antibodies that block *in vitro* binding of different allelic variants of *PvDBPII* to the DARC for more than 100 days following three immunization doses (Payne et al., 2017; Singh et al., 2018). Both the vaccine candidates of *PvDBP* which are in clinical trial (*PvDBPII*/GLA-SE, ChAd63-MVA *PvDBP* RII) were found

TABLE 2 | *PvDBPII* separated into 3 sub-domains.

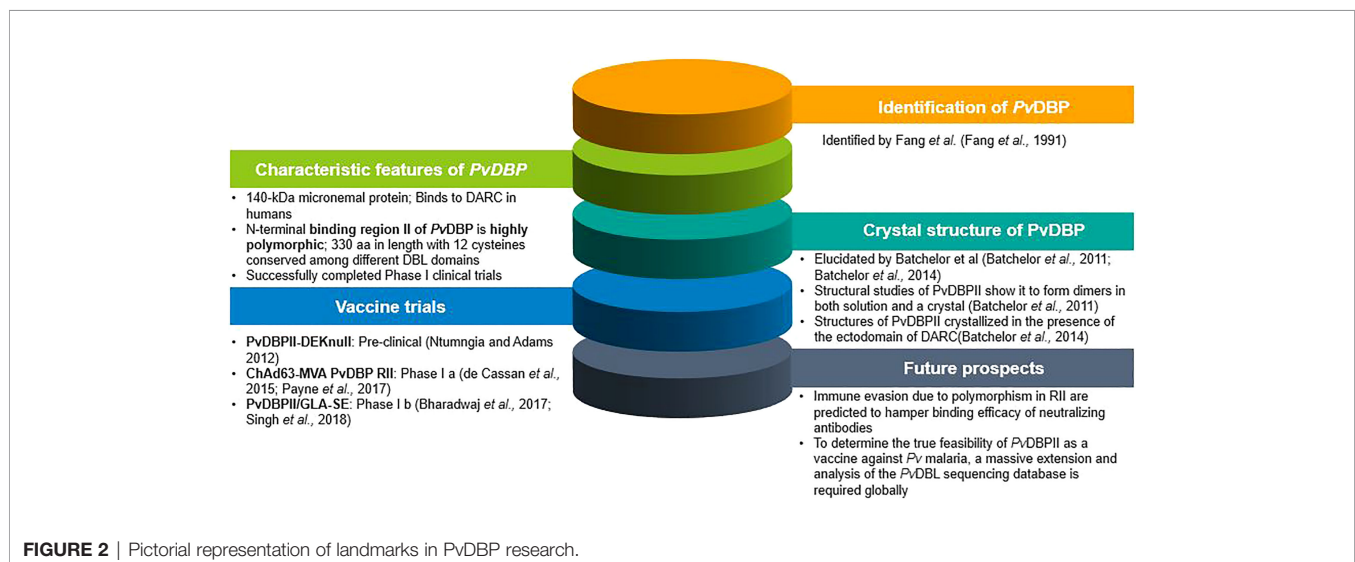
	Amino acid residues	No. of Intra sub-domain sulfides
Sub-domain 1	N211-L253	2 (C217-C246 and C230-C237)
Sub-domain 2	Y271-E386	1 (C300-C377)
Sub-domain 3	P387-S508	3 (C415-C432, C427-C507 and C436-C505)

to give rise to strain-transcending antibodies. By means of human mAbs produced in the course of vaccination or through natural *P. vivax* exposure, a broadly neutralizing human mAb have been identified which inhibited the invasion of all tested strains of *P. vivax*, thus indicating the molecular basis for inhibition. that will thus aid in the design of successful and efficient DBP-based vaccine for *P. vivax* malaria (Rawlinson et al., 2019; Urusova et al., 2019). The various landmarks achieved in PvDBP research are shown in **Figure 2**.

DUFFY NEGATIVITY AND OTHER CHALLENGES

The Duffy antigens act as receptors for a wide range of chemokines and are therefore called as Duffy Antigen Receptor for Chemokines (DARC). The same Duffy antigens also serve as receptors for *P. knowlesi*, *P. vivax* and *P. cynomolgi* (Kosaisavee et al., 2017). Absence of DARC on the reticulocyte surface is thought to confer protection against blood stage infections caused by *P. vivax* in Africa (Sanger et al., 1955; Miller et al., 1976). However, Duffy-negative individuals infected with *P. vivax* have been reported in sub-Saharan Africa (Ryan et al., 2006; Gosi et al., 2008; Ménard et al., 2010; Woldearegai et al., 2013; Djeunang Dongho et al., 2021), which points to the fact that there might be an alternative route of invading human reticulocytes lacking DARC. A recent study conducted in 952 individuals observed the absence of *P. vivax* infections in Ghana where a high frequency of the Duffy-negative genotype was reported (Brown et al., 2021). Human *P. vivax* strains have been reported in Madagascar and parts of Africa, which might be due to the re-establishment of this parasite (Culleton and Carter, 2012). However, it is still to be confirmed whether these cases have emerged due to the introduction of a new *P. vivax* strain which may use an alternative pathway which is independent of DARC. Of late, a novel *P. vivax* Erythrocyte Binding Protein (PvEBP, also known as DBP2) was reported

which may enable interactions with other membrane proteins on erythrocytes (Hester et al., 2013). *Pvebp* gene belongs to the DBL-EBP family, which harbours all the key features of EBPs, suggesting its ability to bind to human erythrocytes and facilitate RBC invasion (106). This gene was found to be expressed in the blood-stage of *P. vivax* and was found in all *P. vivax* strains examined, comprising an extensive geographical span (Hester et al., 2013). Both PvDBP and PvEBP were found to be antigenically distinct. The discovery of PvEBP promptly highlights an alternative invasion pathway and could perhaps illuminate the initial step towards decoding the principle underlying *P. vivax* infection of the Duffy-negatives. Further investigations on PvEBP revealed its preferential binding to young (CD71^{high}) Duffy positive reticulocytes and minimal binding capacity for Duffy-negative reticulocytes (Ntumngia et al., 2016). This study proposes that PvEBP might not serve as a ligand for Duffy-negative reticulocytes, but may act as an alternative pathway for invading Duffy-positive population. Whole genome sequencing studies show that *Pvdbp* gene is duplicated (at a higher rate) in Madagascar population, where both Duffy-negative and Duffy-positive individuals co-exist (Menard et al., 2013), and was supposed to be associated with infection in Duffy negatives possibly in response to constraints imposed by Duffy negativity in some human populations. In addition to this another study confirmed the presence of multiple copies of *Pvdbp* gene (3 and 8 copies) in two Duffy-negative Ethiopian isolates (Gunalan et al., 2016; Roesch et al., 2018). But this observation was contradicted by emergence of widespread *Pvdbp* gene duplication in malaria endemic areas of South-east Asia comprising Duffy-positive population (Hostetler et al., 2016). Although an excess of nonsynonymous mutations and no synonymous mutations was observed in *Pvebp* in comparison to *Pvdbp*, but in terms of allelic diversity, *Pvebp* was found to be less diverse than *Pvdbp* in Madagascar (both Duffy-negative and Duffy-positive) and Cambodian population (Duffy-positive). The absence of synonymous mutation in this case clearly marks that the *Pvebp* gene is under strong positive selection



and validates the importance of this protein in reticulocyte invasion as well as Duffy-independent invasion pathways used by *Plasmodium vivax* (Roesch et al., 2018).

CONCLUSION

P. vivax has evolved with a variety of mechanisms to overcome immune defense at every step of communication with its host species. Developing an effective vaccine that provides protection and prevents transmission is highly essential in eliminating *P. vivax* malaria. The Region II of PvDBP, the only blood-stage vaccine candidate, spans 325 aa residues, and not 330 aa, as was previously reported. PvDBPII is the lone vaccine candidate that has entered clinical trial Phase 1b and is crucially involved in *P. vivax* merozoite invasion of human reticulocytes.

In spite of the fact that PvDBP is crucial for blood-stage infection, its exercise for vaccine development constitutes of major obstacles as cited below.

- (i) Polymorphisms in PvDBP seem to be critical for the evasion of host immune response. A brief exposure of PvDBP to the host's immune system, due to its micronemal location and the rapid kinetics of parasite invasion, allows a short-term exposure of PvDBP to the host immune system. As a result of this phenomenon, the parasite might gain an advantage of escaping the host's immunity. Immune selection being a major driving force for allelic variation, as even a single amino acid substitution can change the antigenic nature of a pathogen. Also the evolutionary arms race between the parasite and human indicates that the parasite genome is evolving at a higher rate than the latter. The amount of polymorphic data available globally is insufficient for declaring PvDBP as a long-lasting and effective vaccine candidate. Therefore, a global (covering the *P. vivax* endemic regions) rigorous survey in terms of allelic diversity of PvDBL domain is required. All these points lead to the fact that we are in requirement of a candidate antigen that is less polymorphic.
- (ii) The surfacing of *P. vivax* infection in Duffy negative population is an alarming condition.
- (iii) Emergence of newly reported *P. vivax* ligands targeting RBCs questions the viability of PvDBPII as the lone vaccine candidate and (iv) presence of more than single copy (1-4 reported) of *Pvdbp* might create an obstacle in the way of attaining an efficacious vaccine.
- (iv) A strain transcending PvDBPII-based vaccine demands a globally conserved epitope. Mittal *et al.*, in their global Single Amino Acid Polymorphism (SAAP) data analysis reported that from the four PvDBL-mAb complex structures, 2 out of the 4 purported neutralizing mAbs do not bind near the supposed dimer interface (Mittal et al., 2020). Such discoveries points towards the fact that a vaccine against *P.*

vivax could have more impact if above challenges of PvDBPII (as the lone candidate) were considered.

- (v) Considering PvDBPII as a potential vaccine target, its immunodominant variant epitopes deflect immune responses, compromising the vaccine efficacy in triggering high titer neutralising antibodies against conserved strain-transcending functional epitopes (Chootong et al., 2010; Ntumngia and Adams, 2012).

Contributing to the formulation of preventative and/or therapeutic approaches which will assist in minimising the effects of malaria, there is a requirement of deciphering and combining functional and structural investigations (Patarroyo et al., 2020). While PvDBP may still be required for the invasion of Duffy negative erythrocytes (Gunalan et al., 2018; Lo et al., 2019), the only focus on PvDBP as a vaccine candidate certainly needs to be reconsidered, and alternative targets explored as potential substitutes for PvDBP or in conjunction with it. A vaccine targeting only a single-stage parasite antigen faces challenges in retaining similar antibody responses due to the genomic changes in parasite ligands which in turn might improve the fitness of *P. vivax* isolates. Most of the *P. vivax* vaccines in pipeline target individual stages and are based on single antigens. Combination allele vaccines in case of *PvdbpII* achieve greater specificity by targeting a majority of antibody to common epitopes among the constituent alleles that form the vaccine (De et al., 2021; Ntumngia et al., 2013). This suggested that a vaccine with multiple DBPII variant alleles is necessary for broader coverage. For finding new interaction hotspots to which malaria elimination approaches can be directed, a profound analysis is needed to correlate structural, functional (adhesion, invasion, and inhibition), and polymorphism data (Patarroyo et al., 2020). Moreover, a blood stage vaccine has to face a huge number of merozoites in comparison to a few as in case of pre-erythrocytic and transmission blocking stage. So, it is of high importance to combine antigens including multi-stages of parasite life cycle to attain the purpose of developing an effective vaccine for *P. vivax* malaria.

AUTHOR CONTRIBUTIONS

AS conceptualized the study, coordinated, drafted and critically revised the manuscript. SK aided in conception, literature search and drafting the whole manuscript. All authors gave final approval for publication and agree to be held accountable for the work performed therein.

ACKNOWLEDGMENTS

The authors thank and acknowledge ICMR-NIMR for its support and assistance towards providing a working environment.

REFERENCES

- Adams, J. H., Hudson, D. E., Torii, M., Ward, G. E., Welles, T. E., Aikawa, M., et al. (1990). The Duffy Receptor Family of Plasmodium Knowlesi Is Located Within the Micronemes of Invasive Malaria Merozoites. *Cell* 63 (1), 141–153. doi: 10.1016/0092-8674(90)90295-p
- Adams, J. H., Sim, B. K., Dolan, S. A., Fang, X., Kaslow, D. C., Miller, L. H., et al. (1992). A Family of Erythrocyte Binding Proteins of Malaria Parasites. *Proc. Natl. Acad. Sci. U.S.A.* 89 (15), 7085–7089. doi: 10.1073/pnas.89.15.7085
- Adams, J. H., Blair, P. L., Kaneko, O., and Peterson, D. S. (2001). An Expanding Ebl Family of Plasmodium Falciparum. *Trends Parasitol.* 17 (6), 297–299. doi: 10.1016/s1471-4922(01)01948-1
- Ampudia, E., Patarroyo, M. A., Patarroyo, M. E., and Murillo, L. A. (1996). Genetic Polymorphism of the Duffy Receptor Binding Domain of Plasmodium Vivax in Colombian Wild Isolates. *Mol. Biochem. Parasitol.* 78 (1–2), 269–272. doi: 10.1016/s0166-6851(96)02611-4
- Arévalo-Herrera, M., Vásquez-Jiménez, J. M., Lopez-Perez, M., Vallejo, A. F., Amado-Garavito, A. B., Céspedes, N., et al. (2016). Protective Efficacy of Plasmodium Vivax Radiation-Attenuated Sporozoites in Colombian Volunteers: A Randomized Controlled Trial. *PLoS Negl. Trop. Dis.* 10 (10), e0005070. doi: 10.1371/journal.pntd.0005070
- Arévalo-Pinzón, G., Bermúdez, M., Hernández, D., Curtidor, H., and Patarroyo, M. A. (2017). Plasmodium Vivax Ligand-Receptor Interaction: PvAMA-1 Domain I Contains the Minimal Regions for Specific Interaction With CD71 + Reticulocytes. *Sci. Rep.* 7 (1), 9616. doi: 10.1038/s41598-017-10025-6
- Atcheson, E., Bauza, K., Salaman, A. M., Alves, E., Blight, J., Viveros-Sandoval, M. E., et al. (2018). Tailoring a Plasmodium Vivax Vaccine To Enhance Efficacy Through a Combination of a CSP Virus-Like Particle and TRAP Viral Vectors. *Infect. Immun.* 86 (9), e00114–e00118. doi: 10.1128/IAI.00114-18
- Babaeekhou, L., Zakeri, S., and Djadid, N. D. (2009). Genetic Mapping of the Duffy Binding Protein (DBP) Ligand Domain of Plasmodium Vivax From Unstable Malaria Region in the Middle East. *Am. J. Trop. Med. Hyg.* 80 (1), 112–118. doi: 10.4269/ajtmh.08-0241err
- Baird, J. K. (2007). Neglect of Plasmodium Vivax Malaria. *Trends Parasitol.* 23 (11), 533–539. doi: 10.1016/j.pt.2007.08.011
- Baird, J. K. (2013a). Malaria Caused by Plasmodium Vivax: Recurrent, Difficult to Treat, Disabling, and Threatening to Life—the Infectious Bite Preempts These Hazards. *Pathog. Glob. Health* 107 (8), 475–479. doi: 10.1179/2047772413Z.000000000179
- Baird, J. K. (2013b). Evidence and Implications of Mortality Associated With Acute Plasmodium Vivax Malaria. *Clin. Microbiol. Rev.* 26 (1), 36–57. doi: 10.1128/CMR.00074-12
- Batchelor, J. D., Zahm, J. A., and Tolia, N. H. (2011). Dimerization of Plasmodium Vivax DBP Is Induced Upon Receptor Binding and Drives Recognition of DARC. *Nat. Struct. Mol. Biol.* 18 (8), 908–914. doi: 10.1038/nsmb.2088
- Batchelor, J. D., Malpede, B. M., Omattage, N. S., DeKoster, G. T., Henzler-Wildman, K. A., and Tolia, N. H. (2014). Red Blood Cell Invasion by Plasmodium Vivax: Structural Basis for DBP Engagement of DARC. *PLoS Pathog.* 10 (1), e1003869. doi: 10.1371/journal.ppat.1003869
- Battle, K. E., Lucas, T., Nguyen, M., Howes, R. E., Nandi, A. K., Twohig, K. A., et al. (2019). Mapping the Global Endemicity and Clinical Burden of Plasmodium Vivax 2000–17: A Spatial and Temporal Modelling Study. *Lancet (London England)* 394 (10195), 332–343. doi: 10.1016/S0140-6736(19)31096-7
- Bennett, J. W., Yadava, A., Tosh, D., Sattabongkot, J., Komisar, J., Ware, L. A., et al. (2016). Phase 1/2a Trial of Plasmodium Vivax Malaria Vaccine Candidate VMP001/AS01B in Malaria-Naive Adults: Safety, Immunogenicity, and Efficacy. *PLoS Negl. Trop. Dis.* 10 (2), e0004423. doi: 10.1371/journal.pntd.0004423
- Bhardwaj, R., Shakri, A. R., Hans, D., Gupta, P., Fernandez-Becerra, C., Del Portillo, H. A., et al. (2017). Production of Recombinant PvDBP-II, Receptor Binding Domain of Plasmodium Vivax Duffy Binding Protein, and Evaluation of Immunogenicity to Identify an Adjuvant Formulation for Vaccine Development. *Protein Expr. Purif.* 136, 52–57. doi: 10.1016/j.pep.2015.06.011
- Blagborough, A. M., Musychuk, K., Bi, H., Jones, R. M., Chichester, J. A., Streatfield, S., et al. (2016). Transmission Blocking Potency and Immunogenicity of a Plant-Produced Pvs25-Based Subunit Vaccine Against Plasmodium Vivax. *Vaccine* 34 (28), 3252–3259. doi: 10.1016/j.vaccine.2016.05.007
- Bouillet, L. É., Dias, M. O., Dorigo, N. A., Moura, A. D., Russell, B., Nosten, F., et al. (2011). Long-Term Humoral and Cellular Immune Responses Elicited by a Heterologous Plasmodium Vivax Apical Membrane Antigen 1 Protein Prime/Adenovirus Boost Immunization Protocol. *Infect. Immun.* 79 (9), 3642–3652. doi: 10.1128/IAI.05048-11
- Brasil, P., Zalis, M. G., de Pina-Costa, A., Siqueira, A. M., Júnior, C. B., Silva, S., et al. (2017). Outbreak of Human Malaria Caused by Plasmodium Simium in the Atlantic Forest in Rio De Janeiro: A Molecular Epidemiological Investigation. *Lancet Glob. Health Engl.* 5 (10), e1038–e1046. doi: 10.1016/S2214-109X(17)30333-9
- Brown, C. A., Pappoe-Ashong, P. J., Duah, N., Ghansah, A., Asmah, H., Afari, E., et al. (2021). High Frequency of the Duffy-Negative Genotype and Absence of Plasmodium Vivax Infections in Ghana. *Malar. J.* 20, 99. doi: 10.1186/s12936-021-03618-0
- Carlton, J. M., Adams, J. H., Silva, J. C., Bidwell, S. L., Lorenzi, H., Caler, E., et al. (2008). Comparative Genomics of the Neglected Human Malaria Parasite Plasmodium Vivax. *Nature* 455 (7214), 757–763. doi: 10.1038/nature07327
- Chen, E., Salinas, N. D., Huang, Y., Ntumngia, F., Plasencia, M. D., Gross, M. L., et al. (2016). Broadly Neutralizing Epitopes in the Plasmodium Vivax Vaccine Candidate Duffy Binding Protein. *Proc. Natl. Acad. Sci. U.S.A.* 113 (22), 6277–6282. doi: 10.1073/pnas.1600488113
- Chen, S. M., Tapia, L. L., Escalante, A. A., Durand, S., Lucas, C., and Bacon, D. J. (2012). Genetic Diversity and Population Structure of Genes Encoding Vaccine Candidate Antigens of Plasmodium Vivax. *Malaria J.* 11, 68. doi: 10.1186/1475-2875-11-68
- Chitnis, C. E., and Miller, L. H. (1994). Identification of the Erythrocyte Binding Domains of Plasmodium Vivax and Plasmodium Knowlesi Proteins Involved in Erythrocyte Invasion. *J. Exp. Med.* 180 (2), 497–506. doi: 10.1084/jem.180.2.497
- Chitnis, C. E., and Sharma, A. (2008). Targeting the Plasmodium Vivax Duffy-Binding Protein. *Trends Parasitol.* 24 (1), 29–34. doi: 10.1016/j.pt.2007.10.004
- Chootong, P., Ntumngia, F. B., VanBuskirk, K. M., Xainli, J., Cole-Tobian, J. L., Campbell, C. O., et al. (2010). Mapping Epitopes of the Plasmodium Vivax Duffy Binding Protein With Naturally Acquired Inhibitory Antibodies. *Infect. Immun.* 78 (3), 1089–1095. doi: 10.1128/IAI.01036-09
- Chu, C. S., and White, N. J. (2021). The Prevention and Treatment of Plasmodium Vivax Malaria. *PLoS Med.* 18 (4), e1003561. doi: 10.1371/journal.pmed.1003561
- Cole-Tobian, J. L., Michon, P., Biasor, M., Richards, J. S., Beeson, J. G., Mueller, I., et al. (2009). Strain-Specific Duffy Binding Protein Antibodies Correlate With Protection Against Infection With Homologous Compared to Heterologous Plasmodium Vivax Strains in Papua New Guinean Children. *Infect. Immun.* 77 (9), 4009–4017. doi: 10.1128/IAI.00158-09
- Cole-Tobian, J., and King, C. L. (2003). Diversity and Natural Selection in Plasmodium Vivax Duffy Binding Protein Gene. *Mol. Biochem. Parasitol.* 127 (2), 121–132. doi: 10.1016/s0166-6851(02)00327-4
- Conway, D. J. (2007). Molecular Epidemiology of Malaria. *Clin. Microbiol. Rev.* 20 (1), 188–204. doi: 10.1128/CMR.00021-06
- Culleton, R., and Carter, R. (2012). African Plasmodium Vivax: Distribution and Origins. *Int. J. Parasitol.* 42 (12), 1091–1097. doi: 10.1016/j.ijpara.2012.08.005
- Deane, L. M. (1992). Simian Malaria in Brazil. *Mem. Inst. Oswaldo Cruz Brazil* 87 Suppl 3, 1–20. doi: 10.1590/s0074-02761992000700001
- De, S. L., Ntumngia, F. B., Nicholas, J., and Adams, J. H. (2021). Progress Towards the Development of a P. Vivax Vaccine. *Expert Rev Vaccines* 20 (2), 97–112. doi: 10.1080/14760584.2021.1880898
- de Cassan, S. C., Shakri, A. R., Llewellyn, D., Elias, S. C., Cho, J. S., Goodman, A. L., et al. (2015). Preclinical Assessment of Viral Vectored and Protein Vaccines Targeting the Duffy-Binding Protein Region II of Plasmodium Vivax. *Front. Immunol.* 6. doi: 10.3389/fimmu.2015.00348
- Djeunang Dongho, G. B., Gunalan, K., L'Episcopia, M., Paganotti, G. M., Menegon, M., Efeutmecheh Sangong, R., et al. (2021). Plasmodium Vivax Infections Detected in a Large Number of Febrile Duffy-Negative Africans in Dschang, Cameroon. *Am. J. Trop. Med. Hyg.* 104 (3), 987–992. doi: 10.4269/ajtmh.20-1255
- Draper, S. J., Sack, B. K., King, C. R., Nielsen, C. M., Rayner, J. C., Higgins, M. K., et al. (2018). Malaria Vaccines: Recent Advances and New Horizons. *Cell Host Microbe* 24 (1), 43–56. doi: 10.1016/j.chom.2018.06.008
- Fang, X. D., Kaslow, D. C., Adams, J. H., and Miller, L. H. (1991). Cloning of the Plasmodium Vivax Duffy Receptor. *Mol. Biochem. Parasitol.* 44 (1), 125–132. doi: 10.1016/0166-6851(91)90228-x

- Fonseca, J. A., Cabrera-Mora, M., Singh, B., Oliveira-Ferreira, J., da Costa Lima-Junior, J., Calvo-Calle, J. M., et al. (2016). A Chimeric Protein-Based Malaria Vaccine Candidate Induces Robust T Cell Responses Against Plasmodium Vivax MSP119. *Sci. Rep.* 6, 34527. doi: 10.1038/srep34527
- França, C. T., He, W. Q., Gruszczyk, J., Lim, N. T., Lin, E., Kiniboro, B., et al. (2016). Plasmodium Vivax Reticulocyte Binding Proteins Are Key Targets of Naturally Acquired Immunity in Young Papua New Guinean Children. *PLoS Negl. Trop. Dis.* 10 (9), e0005014. doi: 10.1371/journal.pntd.0005014
- Galinski, M. R., and Barnwell, J. W. (2008). Plasmodium Vivax: Who Cares? *Malar. J.* 7, S9. doi: 10.1186/1475-2875-7-S1-S9
- Galinski, M. R., Medina, C. C., Ingravall, P., and Barnwell, J. W. (1992). A Reticulocyte-Binding Protein Complex of Plasmodium Vivax Merozoites. *Cell* 69 (7), 1213–1226. doi: 10.1016/0092-8674(92)90642-p
- Gosi, P., Khushmith, S., Khalambaheti, T., Lanar, D. E., Schaecher, K. E., Fukuda, M. M., et al. (2008). Polymorphism Patterns in Duffy-Binding Protein Among Thai Plasmodium Vivax Isolates. *Malaria J.* 7, 112. doi: 10.1186/1475-2875-7-112
- Grimberg, B. T., Udomsangpet, R., Xainli, J., McHenry, A., Panichakul, T., Sattabongkot, J., et al. (2007). Plasmodium Vivax Invasion of Human Erythrocytes Inhibited by Antibodies Directed Against the Duffy Binding Protein. *PLoS Med.* 4 (12), e337. doi: 10.1371/journal.pmed.0040337
- Gruszczyk, J., Kanjee, U., Chan, L. J., Menant, S., Malleret, B., Lim, N., et al. (2018a). Transferrin Receptor 1 Is a Reticulocyte-Specific Receptor for Plasmodium Vivax. *Science (New York N.Y.)* 359 (6371), 48–55. doi: 10.1126/science.aan1078
- Gruszczyk, J., Huang, R. K., Chan, L. J., Menant, S., Hong, C., Murphy, J. M., et al. (2018b). Cryo-EM Structure of an Essential Plasmodium Vivax Invasion Complex. *Nature* 559 (7712), 135–139. doi: 10.1038/s41586-018-0249-1
- Gunalan, K., Lo, E., Hostetler, J. B., Yewhalaw, D., Mu, J., Neafsey, D. E., et al. (2016). Role of Plasmodium Vivax Duffy-Binding Protein 1 in Invasion of Duffy-Null Africans. *Proc. Natl. Acad. Sci. U.S.A.* 113 (22), 6271–6276. doi: 10.1073/pnas.1606113113
- Gunalan, K., Niangaly, A., Thera, M. A., Doumbo, O. K., and Miller, L. H. (2018). Plasmodium Vivax Infections of Duffy-Negative Erythrocytes: Historically Undetected or a Recent Adaptation? *Trends Parasitol.* 34 (5), 420–429. doi: 10.1016/j.pt.2018.02.006
- Haldane, J. B. (2004). The Rate of Spontaneous Mutation of a Human Gene. 1935. *J. Genet.* 83 (3), 235–244. doi: 10.1007/BF02717892
- Hans, D., Pattnaik, P., Bhattacharyya, A., Shakri, A. R., Yazdani, S. S., Sharma, M., et al. (2005). Mapping Binding Residues in the Plasmodium Vivax Domain That Binds Duffy Antigen During Red Cell Invasion. *Mol. Microbiol.* 55 (5), 1423–1434. doi: 10.1111/j.1365-2958.2005.04484.x
- Haynes, J. D., Dalton, J. P., Klotz, F. W., McGinniss, M. H., Hadley, T. J., Hudson, D. E., et al. (1988). Receptor-Like Specificity of a Plasmodium Knowlesi Malarial Protein That Binds to Duffy Antigen Ligands on Erythrocytes. *J. Exp. Med.* 167 (6), 1873–1881. doi: 10.1084/jem.167.6.1873
- Herrera, S., Corradin, G., and Arévalo-Herrera, M. (2007). An Update on the Search for a Plasmodium Vivax Vaccine. *Trends Parasitol.* 23 (3), 122–128. doi: 10.1016/j.pt.2007.01.008
- Hester, J., Chan, E. R., Menard, D., Mercereau-Puijalon, O., Barnwell, J., Zimmerman, P. A., et al. (2013). De Novo Assembly of a Field Isolate Genome Reveals Novel Plasmodium Vivax Erythrocyte Invasion Genes. *PLoS Negl. Trop. Dis.* 7 (12), e2569. doi: 10.1371/journal.pntd.0002569
- Hisaeda, H., Stowers, A. W., Tsuboi, T., Collins, W. E., Sattabongkot, J. S., Suwanabun, N., et al. (2000). Antibodies to Malaria Vaccine Candidates Pvs25 and Pvs28 Completely Block the Ability of Plasmodium Vivax to Infect Mosquitoes. *Infect. Immun.* 68 (12), 6618–6623. doi: 10.1128/IAI.68.12.6618-6623.2000
- Horuk, R., Chitnis, C. E., Darbonne, W. C., Colby, T. J., Rybicki, A., Hadley, T. J., et al. (1993). A Receptor for the Malarial Parasite Plasmodium Vivax: The Erythrocyte Chemokine Receptor. *Science (New York N.Y.)* 261 (5125), 1182–1184. doi: 10.1126/science.7689250
- Hostetler, J. B., Lo, E., Kanjee, U., Amaratunga, C., Suon, S., Sreng, S., et al. (2016). Independent Origin and Global Distribution of Distinct Plasmodium Vivax Duffy Binding Protein Gene Duplications. *PLoS Negl. Trop. Dis.* 10 (10), e0005091. doi: 10.1371/journal.pntd.0005091
- Howes, R. E., Battle, K. E., Mendis, K. N., Smith, D. L., Cibulskis, R. E., Baird, J. K., et al. (2016). Global Epidemiology of Plasmodium Vivax. *Am. J. Trop. Med. Hyg.* 95 (6 Suppl), 15–34. doi: 10.4269/ajtmh.16-0141
- Illingworth, J. J., Alanine, D. G., Brown, R., Marshall, J. M., Bartlett, H. E., Silk, S. E., et al. (2019). Functional Comparison of Blood-Stage Plasmodium Falciparum Malaria Vaccine Candidate Antigens. *Front. Immunol.* 10. doi: 10.3389/fimmu.2019.01254
- Imwong, M., Snounou, G., Pukrittayakamee, S., Tanomsing, N., Kim, J. R., Nandy, A., et al. (2007). Relapses of Plasmodium Vivax Infection Usually Result From Activation of Heterologous Hypnozoites. *J. Infect. Dis.* 195 (7), 927–933. doi: 10.1086/512241
- Imwong, M., Hanchana, S., Malleret, B., Rénia, L., Day, N. P., Dondorp, A., et al. (2014). High-Throughput Ultrasensitive Molecular Techniques for Quantifying Low-Density Malaria Parasitemias. *J. Clin. Microbiol.* 52 (9), 3303–3309. doi: 10.1128/JCM.01057-14
- Ju, H. L., Kang, J. M., Moon, S. U., Kim, J. Y., Lee, H. W., Lin, K., et al. (2012). Genetic Polymorphism and Natural Selection of Duffy Binding Protein of Plasmodium Vivax Myanmar Isolates. *Malaria J.* 11, 60. doi: 10.1186/1475-2875-11-60
- Ju, H. L., Kang, J. M., Moon, S. U., Bahk, Y. Y., Cho, P. Y., Sohn, W. M., et al. (2013). Genetic Diversity and Natural Selection of Duffy Binding Protein of Plasmodium Vivax Korean Isolates. *Acta Trop.* 125 (1), 67–74. doi: 10.1016/j.actatropica.2012.09.016
- Khatoun, L. (2010). Genetic Structure of Plasmodium Vivax and Plasmodium Falciparum in the Bannu District of Pakistan. *Malaria J.* 9, 112. doi: 10.1186/1475-2875-9-112
- Kho, W. G., Chung, J. Y., Sim, E. J., Kim, D. W., and Chung, W. C. (2001). Analysis of Polymorphic Regions of Plasmodium Vivax Duffy Binding Protein of Korean Isolates. *Korean J. Parasitol.* 39 (2), 143–150. doi: 10.3347/kjp.2001.39.2.143
- Kitchen, S. F. (1938). The Infection of Reticulocytes by Plasmodium Vivax. *Am. J. Trop. Med.* s1-18 (4), 347–359. doi: 10.4269/ajtmh.1938.s1-18.347
- Kosaisavee, V., Suwanarusk, R., Chua, A., Kyle, D. E., Malleret, B., Zhang, R., et al. (2017). Strict Tropism for CD71+/CD234+ Human Reticulocytes Limits the Zoonotic Potential of Plasmodium Cynomolgi. *Blood* 130 (11), 1357–1363. doi: 10.1182/blood-2017-02-764787
- Krotoski, W. A., Collins, W. E., Bray, R. S., Garnham, P. C., Cogswell, F. B., Gwadz, R. W., et al. (1982). Demonstration of Hypnozoites in Sporozoite-Transmitted Plasmodium Vivax Infection. *Am. J. Trop. Med. Hyg.* 31 (6), 1291–1293. doi: 10.4269/ajtmh.1982.31.1291
- Kwiatkowski, D. P. (2005). How Malaria has Affected the Human Genome and What Human Genetics can Teach Us About Malaria. *Am. J. Hum. Genet.* 77 (2), 171–192. doi: 10.1086/432519
- Lalremruata, A., Magris, M., Vivas-Martinez, S., Koehler, M., Esen, M., Kempaiah, P., et al. (2015). Natural Infection of Plasmodium Brasiliense in Humans: Man and Monkey Share Quartan Malaria Parasites in the Venezuelan Amazon. *EBioMedicine* 2 (9), 1186–1192. doi: 10.1016/j.ebiom.2015.07.033
- Laurens, M. B. (2020). RTS,S/AS01 Vaccine (Mosquirix™): An Overview. *Hum. Vaccin. Immunother.* 16 (3), 480–489. doi: 10.1080/21645515.2019.1669415
- Lo, E., Hostetler, J. B., Yewhalaw, D., Pearson, R. D., Hamid, M., Gunalan, K., et al. (2019). Frequent Expansion of Plasmodium Vivax Duffy Binding Protein in Ethiopia and its Epidemiological Significance. *PLoS Negl. Trop. Dis.* 13 (9), e0007222. doi: 10.1371/journal.pntd.0007222
- Malleret, B., Li, A., Zhang, R., Tan, K. S., Suwanarusk, R., Claser, C., et al. (2015). Plasmodium Vivax: Restricted Tropism and Rapid Remodeling of CD71-Positive Reticulocytes. *Blood* 125 (8), 1314–1324. doi: 10.1182/blood-2014-08-596015
- Markus, M. B. (2011). Malaria: Origin of the Term “Hypnozoite”. *J. Hist. Biol.* 44 (4), 781–786. doi: 10.1007/s10739-010-9239-3
- Ménard, D., Barnadas, C., Bouchier, C., Henry-Hallidin, C., Gray, L. R., Ratsimbaoa, A., et al. (2010). Plasmodium Vivax Clinical Malaria is Commonly Observed in Duffy-Negative Malagasy People. *Proc. Natl. Acad. Sci. U.S.A.* 107 (13), 5967–5971. doi: 10.1073/pnas.0912496107
- Menard, D., Chan, E. R., Benedet, C., Ratsimbaoa, A., Kim, S., Chim, P., et al. (2013). Whole Genome Sequencing of Field Isolates Reveals a Common Duplication of the Duffy Binding Protein Gene in Malagasy Plasmodium Vivax Strains. *PLoS Negl. Trop. Dis.* 7 (11), e2489. doi: 10.1371/journal.pntd.0002489
- Miller, L. H., Mason, S. J., Clyde, D. F., and McGinniss, M. H. (1976). The Resistance Factor to Plasmodium Vivax in Blacks. The Duffy-Blood-Group Genotype, FyFy. *N. Engl. J. Med.* 295 (6), 302–304. doi: 10.1056/NEJM197608052950602

- Mittal, P., Mishra, S., Kar, S., Pande, V., Sinha, A., Sharma, A., et al. (2020). Global Distribution of Single Amino Acid Polymorphisms in Plasmodium Vivax Duffy-Binding-Like Domain and Implications for Vaccine Development Efforts. *Open Biol.* 10 (9), 200180. doi: 10.1098/rsob.200180
- Mohring, F., Hart, M. N., Rawlinson, T. A., Henrici, R., Charleston, J. A., Diez Benavente, E., et al. (2019). Rapid and Iterative Genome Editing in the Malaria Parasite *Plasmodium Knowlesi* Provides New Tools for *P. Vivax* Research. *eLife* 8, e45829. doi: 10.7554/eLife.45829
- Moon, R. W., Hall, J., Rangkuti, F., Ho, Y. S., Almond, N., Mitchell, G. H., et al. (2013). Adaptation of the Genetically Tractable Malaria Pathogen *Plasmodium Knowlesi* to Continuous Culture in Human Erythrocytes. *Proc. Natl. Acad. Sci. U.S.A.* 110 (2), 531–536. doi: 10.1073/pnas.1216457110
- Mueller, I., Galinski, M. R., Baird, J. K., Carlton, J. M., Kochar, D. K., Alonso, P. L., et al. (2009). Key Gaps in the Knowledge of Plasmodium Vivax, a Neglected Human Malaria Parasite. *Lancet Infect. Dis.* 9 (9), 555–566. doi: 10.1016/S1473-3099(09)70177-X
- Mueller, I., Shakri, A. R., and Chitnis, C.E.. (2015). Development of Vaccines for Plasmodium Vivax Malaria. *Vaccine* 33 (52), 7489–7495. doi: 10.1016/j.vaccine.2015.09.060
- Ndegwa, D. N., Kundu, P., Hostetler, J. B., Marin-Menendez, A., Sanderson, T., Mwikali, K., et al. (2021). Using Plasmodium Knowlesi as a Model for Screening Plasmodium Vivax Blood-Stage Malaria Vaccine Targets Reveals New Candidates. *PLoS Pathog.* 17 (7), e1008864. doi: 10.1371/journal.ppat.1008864
- Neafsey, D. E., Galinsky, K., Jiang, R. H., Young, L., Sykes, S. M., Saif, S., et al. (2012). The Malaria Parasite Plasmodium Vivax Exhibits Greater Genetic Diversity Than Plasmodium Falciparum. *Nat. Genet.* 44 (9), 1046–1050. doi: 10.1038/ng.2373
- Nicolette, V. C., Frischmann, S., Barbosa, S., King, C. L., and Ferreira, M. U.. (2016). Naturally Acquired Binding-Inhibitory Antibodies to Plasmodium Vivax Duffy Binding Protein and Clinical Immunity to Malaria in Rural Amazonians. *J. Infect. Dis.* 214 (10), 1539–1546. doi: 10.1093/infdis/jiw407
- Ntumngia, F. B., and Adams, J. H. (2012). Design and Immunogenicity of a Novel Synthetic Antigen Based on the Ligand Domain of the Plasmodium Vivax Duffy Binding Protein. *Clin. Vaccine Immunol.* 19 (1), 30–36. doi: 10.1128/CI.05466-11
- Ntumngia, F. B., Schloegel, J., Barnes, S. J., McHenry, A. M., Singh, S., King, C. L., et al. (2012). Conserved and Variant Epitopes of Plasmodium Vivax Duffy Binding Protein as Targets of Inhibitory Monoclonal Antibodies. *Infect. Immun.* 80 (3), 1203–1208. doi: 10.1128/IAI.05924-11
- Ntumngia, F. B., Schloegel, J., McHenry, A. M., Barnes, S. J., and George, M. T.. (2013). Immunogenicity of Single Versus Mixed Allele Vaccines of Plasmodium Vivax Duffy Binding Protein Region II. *Vaccine* 31 (40), 4382–4388. doi: 10.1016/j.vaccine.2013.07.002
- Ntumngia, F. B., Thomson-Luque, R., Torres, L., Gunalan, K., Carvalho, L. H., and Adams, J. H. (2016). A Novel Erythrocyte Binding Protein of Plasmodium Vivax Suggests an Alternate Invasion Pathway Into Duffy-Positive Reticulocytes. *mBio* 7 (4), e01261–e01261. doi: 10.1128/mBio.01261-16
- Ntumngia, F. B., Thomson-Luque, R., Galusic, S., Frato, G., Frischmann, S., Peabody, D. S., et al. (2018). Identification and Immunological Characterization of the Ligand Domain of Plasmodium Vivax Reticulocyte Binding Protein 1a. *J. Infect. Dis.* 218 (7), 1110–1118. doi: 10.1093/infdis/jiy273
- Ogun, S. A., Tewari, R., Otto, T. D., Howell, S. A., Knuepfer, E., Cunningham, D. A., et al. (2011). Targeted Disruption of Py235ebp-1: Invasion of Erythrocytes by Plasmodium Yoelii Using an Alternative Py235 Erythrocyte Binding Protein. *PLoS Pathog.* 7 (2), e1001288. doi: 10.1371/journal.ppat.1001288
- Okenu, D. M., Meyer, E. V., Puckett, T. C., Rosas-Acosta, G., Barnwell, J. W., Galinski, M. R., et al. (2005). The Reticulocyte Binding Proteins of Plasmodium Cynomolgi: A Model System for Studies of P. Vivax. *Mol. Biochem. Parasitol.* 143 (1), 116–120. doi: 10.1016/j.molbiopara.2005.04.010
- Parzych, E. M., Miura, K., Ramanathan, A., Long, C. A., and Burns, J. M.. (2017). Evaluation of a Plasmodium-Specific Carrier Protein To Enhance Production of Recombinant Pfs25, a Leading Transmission-Blocking Vaccine Candidate. *Infect. Immun.* 86 (1), e00486–e00417. doi: 10.1128/IAI.00486-17
- Patarroyo, M. A., Molina-Franky, J., Gómez, M., Arévalo-Pinzón, G., Patarroyo, M. E., et al. (2020). Hotspots in Plasmodium and RBC Receptor-Ligand Interactions: Key Pieces for Inhibiting Malarial Parasite Invasion. *Int. J. Mol. Sci.* 21 (13), 4729. doi: 10.3390/ijms21134729
- Payne, R. O., Silk, S. E., Elias, S. C., Milne, K. H., Rawlinson, T. A., Llewellyn, D., et al. (2017). Human Vaccination Against Plasmodium Vivax Duffy-Binding Protein Induces Strain-Transcending Antibodies. *JCI Insight* 2 (12), e93683. doi: 10.1172/jci.insight.93683
- Premaratne, P. H., Aravinda, B. R., Escalante, A. A., and Udagama, P.V.. (2011). Genetic Diversity of Plasmodium Vivax Duffy Binding Protein II (PvDBPII) Under Unstable Transmission and Low Intensity Malaria in Sri Lanka. *Infect. Genet. Evol.* 11 (6), 1327–1339. doi: 10.1016/j.meegid.2011.04.023
- Price, R. N. (2014). Global Extent of Chloroquine-Resistant Plasmodium Vivax: A Systematic Review and Meta-Analysis. *Lancet Infect. Dis.* 14 (10), 982–991. doi: 10.1016/S1473-3099(14)70855-2
- Price, R. N., Tjitra, E., Guerra, C. A., Yeung, S., White, N. J., and Anstey, N. M.. (2007). Vivax Malaria: Neglected and Not Benign. *Am. J. Trop. Med. Hyg.* 77 (6 Suppl), 79–87.
- Price, R. N., Douglas, N. M., and Anstey, N. M.. (2009). New Developments in Plasmodium Vivax Malaria: Severe Disease and the Rise of Chloroquine Resistance. *Curr. Opin. Infect. Dis.* 22 (5), 430–435. doi: 10.1097/QCO.0b013e32832f14c1
- Qian, F., Wu, Y., Muratova, O., Zhou, H., Dobrescu, G., Duggan, P., et al. (2007). Conjugating Recombinant Proteins to Pseudomonas Aeruginosa ExoProtein A: A Strategy for Enhancing Immunogenicity of Malaria Vaccine Candidates. *Vaccine* 25 (20), 3923–3933. doi: 10.1016/j.vaccine.2007.02.073
- Radtke, A. J., Anderson, C. F., Riteau, N., Rausch, K., Scaria, P., Kelnhofer, E. R., et al. (2017). Adjuvant and Carrier Protein-Dependent T-Cell Priming Promotes a Robust Antibody Response Against the Plasmodium Falciparum Pfs25 Vaccine Candidate. *Sci. Rep.* 7, 40312. doi: 10.1038/srep40312
- Ranjan, A., and Chitnis, C. E.. (1999). Mapping Regions Containing Binding Residues Within Functional Domains of Plasmodium Vivax and Plasmodium Knowlesi Erythrocyte-Binding Proteins. *Proc. Natl. Acad. Sci. U.S.A.* 96 (24), 14067–14072. doi: 10.1073/pnas.96.24.14067
- Rawlinson, T. A., Barber, N. M., Mohring, F., Cho, J. S., Kosaisavee, V., Gérard, S. F., et al. (2019). Structural Basis for Inhibition of Plasmodium Vivax Invasion by a Broadly Neutralizing Vaccine-Induced Human Antibody. *Nat. Microbiol.* 4 (9), 1497–1507. doi: 10.1038/s41564-019-0462-1
- Registration T. *Tables of Malaria Vaccine Projects Globally*. Available at: [http://www.who.int/immunization/research/development/Rainbow tables/en/](http://www.who.int/immunization/research/development/Rainbow%20tables/en/).
- Rieckmann, K. H., Davis, D. R., and Hutton, D. C.. (1989). Plasmodium Vivax Resistance to Chloroquine? *Lancet (Lond. Engl.)* 2 (8673), 1183–1184. doi: 10.1016/s0140-6736(89)91792-3
- Roesch, C., Popovici, J., Bin, S., Run, V., Kim, S., Ramboarina, S., et al. (2018). Genetic Diversity in Two Plasmodium Vivax Protein Ligands for Reticulocyte Invasion. *PLoS Negl. Trop. Dis.* 12 (10), e0006555. doi: 10.1371/journal.pntd.0006555
- RTS,S Clinical Trials Partnership. (2014). Efficacy and Safety of the RTS,S/AS01 Malaria Vaccine During 18 Months After Vaccination: A Phase 3 Randomized, Controlled Trial in Children and Young Infants at 11 African Sites. *PLoS Med.* 11 (7), e1001685. doi: 10.1371/journal.pmed.1001685
- Ryan, J. R., Stoute, J. A., Amon, J., Dunton, R. F., Mtalib, R., Koros, J., et al. (2006). Evidence for Transmission of Plasmodium Vivax Among a Duffy Antigen Negative Population in Western Kenya. *Am. J. Trop. Med. Hyg.* 75 (4), 575–581. doi: 10.4269/ajtmh.2006.75.575
- Sanger, R., Race, R. R., and Jack, J.. (1955). The Duffy Blood Groups of New York Negroes: The Phenotype Fy (a-B-). *Br. J. Haematol.* 1 (4), 370–374. doi: 10.1111/j.1365-2141.1955.tb05523.x
- Sauerwein, R. W., and Bousema, T.. (2015). Transmission Blocking Malaria Vaccines: Assays and Candidates in Clinical Development. *Vaccine* 33 (52), 7476–7482. doi: 10.1016/j.vaccine.2015.08.073
- Schunk, M., Kumma, W. P., Miranda, I. B., Osman, M. E., Roewer, S., Alano, A., et al. (2006). High Prevalence of Drug-Resistance Mutations in Plasmodium Falciparum and Plasmodium Vivax in Southern Ethiopia. *Malar. J.* 5, 54. doi: 10.1186/1475-2875-5-54
- Singh, S. K., Singh, A. P., Pandey, S., Yazdani, S. S., Chitnis, C. E., Sharma, A., et al. (2003). Definition of Structural Elements in Plasmodium Vivax and P. Knowlesi Duffy-Binding Domains Necessary for Erythrocyte Invasion. *Biochem. J.* 374 (Pt 1), 193–198. doi: 10.1042/BJ20030622
- Singh, S. K., Hora, R., Belrhali, H., Chitnis, C. E., and Sharma, A.. (2006). Structural Basis for Duffy Recognition by the Malaria Parasite Duffy-Binding-Like Domain. *Nature* 439 (7077), 741–744. doi: 10.1038/nature04443

- Singh, K., Mukherjee, P., Shakri, A. R., Singh, A., Pandey, G., Bakshi, M., et al. (2018). Malaria Vaccine Candidate Based on Duffy-Binding Protein Elicits Strain Transcending Functional Antibodies in a Phase I Trial. *NPJ Vaccines* 3, 48. doi: 10.1038/s41541-018-0083-3
- Sousa, T. N., Cerávolo, I. P., Fernandes Fontes, C. J., Couto, A., Carvalho, L. H., Brito, C. F., et al. (2006). The Pattern of Major Polymorphisms in the Duffy Binding Protein Ligand Domain Among Plasmodium Vivax Isolates From the Brazilian Amazon Area. *Mol. Biochem. Parasitol.* 146 (2), 251–254. doi: 10.1016/j.molbiopara.2005.11.006
- Su, X. Z. (2019). Plasmodium Genomics and Genetics: New Insights Into Malaria Pathogenesis, Drug Resistance, Epidemiology, and Evolution. *Clin. Microbiol. Rev.* 32 (4), e00019–e00019. doi: 10.1128/CMR.00019-19
- Sutherland, C. J., et al. (2010). Two Nonrecombining Sympatric Forms of the Human Malaria Parasite Plasmodium Ovale Occur Globally. *J. Infect. Dis. United States* 201 (10), 1544–1550. doi: 10.1086/652240
- Tachibana, M., Suwanabun, N., Kaneko, O., Iriko, H., Otsuki, H., Sattabongkot, J., et al. (2015). Plasmodium Vivax Gametocyte Proteins, Pvs48/45 and Pvs47, Induce Transmission-Reducing Antibodies by DNA Immunization. *Vaccine* 33 (16), 1901–1908. doi: 10.1016/j.vaccine.2015.03.008
- Ta, T. H., Hisam, S., Lanza, M., Jiram, A. I., Ismail, N., Rubio, J. M., et al. (2014). First Case of a Naturally Acquired Human Infection With Plasmodium Cynomolgi. *Malaria J.* 13 (1), 1–7. doi: 10.1186/1475-2875-13-68
- Tanner, M., Greenwood, B., Whitty, C. J., Ansah, E. K., Price, R. N., Dondorp, A. M., et al. (2015). Malaria Eradication and Elimination: Views on How to Translate a Vision Into Reality. *BMC Med.* 13, 167. doi: 10.1186/s12916-015-0384-6
- Tsuboi, T., Kappe, S. H., al-Yaman, F., Prickett, M. D., Alpers, M., Adams, J. H., et al. (1994). Natural Variation Within the Principal Adhesion Domain of the Plasmodium Vivax Duffy Binding Protein. *Infect. Immun.* 62 (12), 5581–5586. doi: 10.1128/iai.62.12.5581-5586.1994
- Tsuboi, T., Kaslow, D. C., Gozar, M. M., Tachibana, M., Cao, Y. M., Torii, M., et al. (1998). Sequence Polymorphism in Two Novel Plasmodium Vivax Ookinete Surface Proteins, Pvs25 and Pvs28, That are Malaria Transmission-Blocking Vaccine Candidates. *Mol. Med. (Cambridge Mass.)* 4 (12), 772–782. doi: 10.1007/BF03401770
- Urusova, D., Carias, L., Huang, Y., Nicolette, V. C., Popovici, J., Roesch, C., et al. (2019). Structural Basis for Neutralization of Plasmodium Vivax by Naturally Acquired Human Antibodies That Target DBP. *Nat. Microbiol.* 4 (9), 1486–1496. doi: 10.1038/s41564-019-0461-2
- Valencia, S. H., Rodríguez, D. C., Acero, D. L., Ocampo, V., and Arévalo-Herrera, M. (2011). Platform for Plasmodium Vivax Vaccine Discovery and Development. *Mem. Inst. Oswaldo Cruz* 106 Suppl 1 (Suppl 1), 179–192. doi: 10.1590/s0074-02762011000900023
- VanBuskirk, K. M., Cole-Tobian, J. L., Baisor, M., Sevova, E. S., Bockarie, M., King, C. L., et al. (2004a). Antigenic Drift in the Ligand Domain of Plasmodium Vivax Duffy Binding Protein Confers Resistance to Inhibitory Antibodies. *J. Infect. Dis.* 190 (9), 1556–1562. doi: 10.1086/424852
- VanBuskirk, K. M., Sevova, E., and Adams, J. H. (2004b). Conserved Residues in the Plasmodium Vivax Duffy-Binding Protein Ligand Domain are Critical for Erythrocyte Receptor Recognition. *Proc. Natl. Acad. Sci. U.S.A.* 101 (44), 15754–15759. doi: 10.1073/pnas.0405421101
- Vicentin, E. C., Françoso, K. S., Rocha, M. V., Iourtov, D., Dos Santos, F. L., Kubrusly, F. S., et al. (2014). Invasion-Inhibitory Antibodies Elicited by Immunization With Plasmodium Vivax Apical Membrane Antigen-1 Expressed in Pichia Pastoris Yeast. *Infect. Immun.* 82 (3), 1296–1307. doi: 10.1128/IAI.01169-13
- White, N. J. (2021). Anti-Malarial Drug Effects on Parasite Dynamics in Vivax Malaria. *Malaria J.* 20 (1), 161. doi: 10.1186/s12936-021-03700-7
- Winter, D. J., Pacheco, M. A., Vallejo, A. F., Schwartz, R. S., Arevalo-Herrera, M., Herrera, S., et al. (2015). Whole Genome Sequencing of Field Isolates Reveals Extensive Genetic Diversity in Plasmodium Vivax From Colombia. *PLoS Negl. Trop. Dis.* 9 (12), e0004252. doi: 10.1371/journal.pntd.0004252
- Woldearegai, T. G., Kremsner, P. G., Kun, J. F., and Mordmüller, B. (2013). Plasmodium Vivax Malaria in Duffy-Negative Individuals From Ethiopia. *Trans. R. Soc. Trop. Med. Hyg.* 107 (5), 328–331. doi: 10.1093/trstmh/trt016
- World Health Organisation. (2021). *World Malaria Report 2021* (Geneva, Switzerland: World Health Organization).
- World Health Organization. (2020). *World Malaria Report 2020* (Geneva, Switzerland: World Health Organization).
- Wu, Y., Ellis, R. D., Shaffer, D., Fontes, E., Malkin, E. M., Mahanty, S., et al. (2008). Phase I Trial of Malaria Transmission Blocking Vaccine Candidates Pfs25 and Pvs25 Formulated With Montanide ISA 51. *PLoS One* 3 (7), e2636. doi: 10.1371/journal.pone.0002636
- Xainli, J., Adams, J. H., and King, C. L. (2000). The Erythrocyte Binding Motif of Plasmodium Vivax Duffy Binding Protein is Highly Polymorphic and Functionally Conserved in Isolates From Papua New Guinea. *Mol. Biochem. Parasitol.* 111 (2), 253–260. doi: 10.1016/s0166-6851(00)00315-7
- Yogavel, M., Chhibber-Goel, J., Jamwal, A., Gupta, S., and Sharma, A. (2018). Engagement Rules That Underpin DBL-DARC Interactions for Ingress of Plasmodium Knowlesi and Plasmodium Vivax Into Human Erythrocytes. *Front. Mol. Biosci.* 5. doi: 10.3389/fmolb.2018.00078

Conflict of Interest: The authors declare that the research was conducted in the absence of any commercial or financial relationships that could be construed as a potential conflict of interest.

Publisher's Note: All claims expressed in this article are solely those of the authors and do not necessarily represent those of their affiliated organizations, or those of the publisher, the editors and the reviewers. Any product that may be evaluated in this article, or claim that may be made by its manufacturer, is not guaranteed or endorsed by the publisher.

Copyright © 2022 Kar and Sinha. This is an open-access article distributed under the terms of the Creative Commons Attribution License (CC BY). The use, distribution or reproduction in other forums is permitted, provided the original author(s) and the copyright owner(s) are credited and that the original publication in this journal is cited, in accordance with accepted academic practice. No use, distribution or reproduction is permitted which does not comply with these terms.



OPEN ACCESS

EDITED BY

Abhai K. Tripathi,
Bloomberg School of Public Health,
Johns Hopkins University,
United States

REVIEWED BY

Berlin L. Londono-Renteria,
Tulane University, United States
Maya Aleshnick,
Oregon Health and Science University,
United States

*CORRESPONDENCE

Rhea J. Longley
Longley.r@wehi.edu.au

SPECIALTY SECTION

This article was submitted to
Parasite and Host,
a section of the journal
Frontiers in Cellular and
Infection Microbiology

RECEIVED 23 May 2022

ACCEPTED 15 July 2022

PUBLISHED 09 August 2022

CITATION

Tayipto Y, Rosado J, Gamboa D,
White MT, Kiniboro B, Healer J,
Opi DH, Beeson JG, Takashima E,
Tsuboi T, Harbers M, Robinson L,
Mueller I and Longley RJ (2022)
Assessment of IgG3 as a serological
exposure marker for *Plasmodium vivax*
in areas with moderate–high malaria
transmission intensity.
Front. Cell. Infect. Microbiol. 12:950909.
doi: 10.3389/fcimb.2022.950909

COPYRIGHT

© 2022 Tayipto, Rosado, Gamboa,
White, Kiniboro, Healer, Opi, Beeson,
Takashima, Tsuboi, Harbers, Robinson,
Mueller and Longley. This is an open-
access article distributed under the
terms of the [Creative Commons
Attribution License \(CC BY\)](#). The use,
distribution or reproduction in other
forums is permitted, provided the
original author(s) and the copyright
owner(s) are credited and that the
original publication in this journal is
cited, in accordance with accepted
academic practice. No use,
distribution or reproduction is
permitted which does not comply with
these terms.

Assessment of IgG3 as a serological exposure marker for *Plasmodium vivax* in areas with moderate–high malaria transmission intensity

Yanie Tayipto^{1,2}, Jason Rosado³, Dionicia Gamboa⁴,
Michael T. White³, Benson Kiniboro⁵, Julie Healer¹,
D. Herbert Opi^{6,7,8}, James G. Beeson^{6,7,8,9}, Eizo Takashima¹⁰,
Takafumi Tsuboi¹⁰, Matthias Harbers^{11,12}, Leanne Robinson^{1,6},
Ivo Mueller^{1,2} and Rhea J. Longley^{1,2*}

¹Population Health and Immunity Division, Walter and Eliza Hall Institute of Medical Research, Melbourne, VIC, Australia, ²Department of Medical Biology, University of Melbourne, Melbourne, VIC, Australia, ³Unité Malaria: Parasites et Hôtes, Département Parasites et Insectes Vecteurs, Institut Pasteur, Paris, France, ⁴Laboratorio Internacional Centers of Excellence for Malaria Research (ICEMR)-Amazonia, Laboratorios de Investigación y Desarrollo, Facultad de Ciencias y Filosofía, Universidad Peruana Cayetano Heredia, Lima, Peru, ⁵Vector Borne Disease Unit, Papua New Guinea Institute of Medical Research, Goroka, Papua New Guinea, ⁶Life Sciences, Burnet Institute, Melbourne, VIC, Australia, ⁷Department of Immunology and Pathology, Monash University, Melbourne, VIC, Australia, ⁸Department of Medicine, The Doherty Institute, The University of Melbourne, Melbourne, VIC, Australia, ⁹Department of Microbiology and Central Clinical School, Monash University, Clayton, VIC, Australia, ¹⁰Proteo-Science Center, Ehime University, Matsuyama, Japan, ¹¹CellFree Sciences Co., Ltd., Yokohama, Japan, ¹²RIKEN Centre for Integrative Medical Sciences, Yokohama, Japan

A more sensitive surveillance tool is needed to identify *Plasmodium vivax* infections for treatment and to accelerate malaria elimination efforts. To address this challenge, our laboratory has developed an eight-antigen panel that detects total IgG as serological markers of *P. vivax* exposure within the prior 9 months. The value of these markers has been established for use in areas with low transmission. In moderate–high transmission areas, there is evidence that total IgG is more long-lived than in areas with low transmission, resulting in poorer performance of these markers in these settings. Antibodies that are shorter-lived may be better markers of recent infection for use in moderate–high transmission areas. Using a multiplex assay, the antibody temporal kinetics of total IgG, IgG1, IgG3, and IgM against 29 *P. vivax* antigens were measured over 36 weeks following asymptomatic *P. vivax* infection in Papua New Guinean children ($n = 31$), from an area with moderate–high transmission intensity. IgG3 declined faster to background than total IgG, IgG1, and IgM. Based on these kinetics, IgG3 performance was then assessed for classifying recent exposure in a cohort of Peruvian individuals ($n = 590$; age 3–85 years) from an area of moderate transmission intensity. Using antibody responses against individual antigens, the highest performance of IgG3 in classifying recent *P. vivax* infections in the prior 9 months was to one

of the Pv-fam-a proteins assessed (PVX_125728) (AUC = 0.764). Surprisingly, total IgG was overall a better marker of recent *P. vivax* infection, with the highest individual classification performance to RBP2b₁₉₈₆₋₂₆₅₃ (PVX_094255) (AUC = 0.838). To understand the acquisition of IgG3 in this Peruvian cohort, relevant epidemiological factors were explored using a regression model. IgG3 levels were positively associated with increasing age, living in an area with (relatively) higher transmission intensity, and having three or more PCR-detected blood-stage *P. vivax* infections within the prior 13 months. Overall, we found that IgG3 did not have high accuracy for detecting recent exposure to *P. vivax* in the Peruvian cohort, with our data suggesting that this is due to the high levels of prior exposure required to acquire high IgG3 antibody levels.

KEYWORDS

malaria, *Plasmodium vivax*, multiplex assay, surveillance, malaria elimination, antibody, IgG3

Introduction

Plasmodium vivax is a malaria-causing parasite that is mostly found outside sub-Saharan Africa. Like other *Plasmodium* species, *P. vivax* is transmitted by female *Anopheles* mosquitoes. Infected mosquitoes inject saliva containing sporozoites into the skin during feeding times. Sporozoites travel to the liver where some become arrested, a stage known as hypnozoites, and others develop into merozoites that are released into the bloodstream. Merozoites then infect red blood cells, while hypnozoites can later reactivate and develop into merozoites, resulting in a relapse of infection. This biological characteristic of *P. vivax* presents challenges for malaria control programs. Hypnozoites hidden in the liver are not detected by current diagnostic tests (including microscopy, rapid diagnostic tests, and PCR), as they can only detect parasites present in the blood. Current diagnostics tests also have low sensitivity, largely because the density of blood-stage *P. vivax* parasites is low due to the preference of *P. vivax* for young red blood cells that are more abundant in other organs, such as the spleen (Jiménez et al., 2007; Lacerda et al., 2012; Aggarwal et al., 2014) and bone marrow (O'Donnell et al., 1998; Imirzalioglu et al., 2006; Ru et al., 2009; Raghunandan et al., 2012).

To improve screening tools for malaria and to accelerate toward elimination, our laboratory has developed a serological tool that utilizes antibodies to infer recent exposure history to *P. vivax*. This tool can predict the likelihood of *P. vivax* infection within the prior 9 months in low transmission areas, such as Thailand, Brazil, and the Solomon Islands (Longley et al., 2020). People identified as exposed, but who have not received antimalarial treatment, could then be administered with radical cure (complete elimination of parasites) for *P. vivax*,

which by necessity includes primaquine or tafenoquine to clear liver-stage hypnozoites. This provides a unique opportunity for an alternative strategy to rapidly reduce *P. vivax* transmission within a selected area and accelerate elimination efforts. This approach, termed sero-testing and treatment (“seroTAT”), has potential advantages over other strategies for eliminating the hypnozoite reservoir, such as mass testing and treatment and mass drug administration (Greenhouse et al., 2019). Mass testing and treatment will not efficiently eliminate the infectious reservoir due to the low sensitivity of current commercial rapid diagnostic tests and their reliance on detecting parasites in the peripheral blood (i.e., not hypnozoites (Sutanto et al., 2018)). Even if sensitive molecular tools such as PCR were used, they only detect individuals with current blood-stage infections and not those with hidden hypnozoites. Mass drug administration, conversely, is effective at reducing *P. vivax* transmission (Hsiang et al., 2013) but results in substantial overtreatment in low transmission settings which is potentially challenging due to i) potential side effects of 8-aminoquinolines in individuals with glucose-6-phosphate-dehydrogenase deficiency (Ashley et al., 2014), ii) lack of hypnozoite-clearing antimalarials approved for use in people who are pregnant, and iii) community acceptability (Aung et al., 2021).

Further studies conducted by our laboratory, however, have indicated that the performance of our serological tool was poorer in a Peruvian cohort from an area with moderate transmission intensity (during the last 9 months of follow-up, 65.6% of individuals experienced at least one blood-stage *P. vivax* infection) (Rosado et al., 2021). IgG responses to the target antigens appear to be longer-lived in this population due to repeated exposures. This is supported by prior evidence demonstrating longer-lived antibodies in higher compared to lower transmission settings (Longley et al., 2017). Hence, we

aimed to adapt our tool for areas with moderate–high transmission intensity by using a different type of antibody as a marker of exposure. *P. vivax* infections typically induce cytophilic IgG1 and IgG3 subclass responses, with minimal IgG2 and IgG4 (Liu et al., 2022). We hypothesized that a shorter-lived serological response would be a better marker of exposure than total IgG (Tayipto et al., 2022). For example, a study in Uganda indicated that among IgG subclasses, IgG3 to most *Plasmodium falciparum* blood-stage antigens waned when transmission moved from high to low (Ssewanyana et al., 2021). Thus, in this study, we aimed to characterize the longevity of a panel of antibody isotypes and subclasses, including IgG3, following *P. vivax* infection, and then to test the response that was shorter-lived for its ability to act as a marker of recent *P. vivax* exposure in an area with moderate transmission intensity.

Materials and methods

Study populations

Papua New Guinea cohort: Antibody kinetics

The Papua New Guinea (PNG) cohort study was conducted in Maprik District, East Sepik Province, PNG, from August 2009 to May 2010, where *P. vivax* was hyperendemic (Robinson et al., 2015). Malaria transmission in the province is moderately seasonal, with a peak from December to March in line with the wet season. Five hundred and twenty-four children aged 5–10 years were enrolled in this study regardless of *Plasmodium* infection status at the time of enrolment

(subsequently, 47.4% were shown to be *P. vivax* positive at enrolment *via* PCR). Participants were randomized to receive the following antimalarial treatments to clear infections: chloroquine and artemether–lumefantrine for 3 days and either a placebo or primaquine for 20 days. For this project, samples from a subset of 31 children were selected as described previously (Longley et al., 2017). Briefly, these children had asymptomatic *P. vivax* infection at enrolment, had no *Plasmodium* reinfection during follow-up (with not more than one missed sample), and were randomized to receive primaquine (an anti-hypnozoite drug, all 31 children received primaquine treatment). Only the children that fulfilled these criteria were selected, leading to the final sample size of 31. Samples were collected up to 36 weeks: at enrolment, 1 month after enrolment (once drug treatment was completed), then every 2 weeks for 12 weeks, and every 4 weeks for the remaining weeks (Figure 1A). The number of samples available for each timepoint was as follows: week 0 ($n = 31$), week 4 ($n = 29$), week 6 ($n = 31$), week 8 ($n = 30$), week 10 ($n = 27$), week 12 ($n = 29$), week 14 ($n = 30$), week 16 ($n = 30$), week 20 ($n = 25$), week 24 ($n = 22$), week 28 ($n = 28$), week 32 ($n = 25$), and week 36 ($n = 31$).

Peruvian cohort: Classification performance

The Peruvian observational cohort study was conducted in Cahuide and San José de Lupuna, Loreto, Peru, from December 2012 to December 2015 (Rosas-Aguirre et al., 2017). Transmission at that time was stable in both Lupuna and Cahuide, with a peak season from November to May. There were 2,197 participants (from a possible 2,447 according to

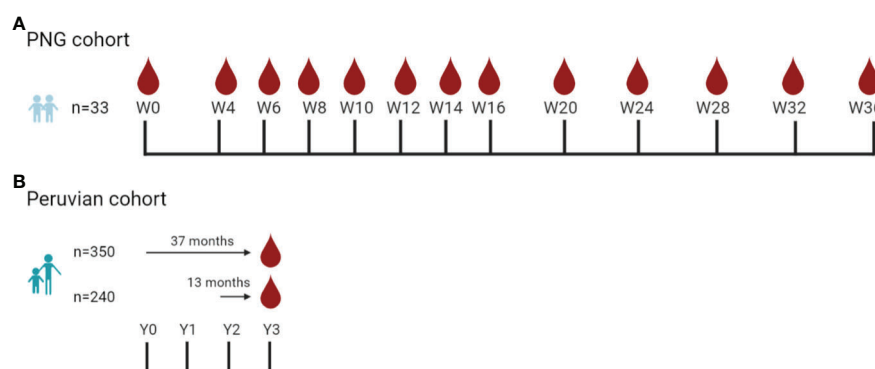


FIGURE 1

Sample collection timepoints used in the antibody kinetics study and the classification assessment study. (A) Asymptomatic children aged 5–10 years ($n = 31$) were enrolled in the Papua New Guinea (PNG) cohort study (Albinama), conducted in Maprik District, PNG, from August 2009 to May 2010 (Robinson et al., 2015). There were no reinfections during follow-up. Samples were collected at 13 timepoints for 36 weeks. (B) The Peruvian cohort study was conducted in Cahuide and San José de Lupuna, Loreto, Peru, from December 2012 to December 2015 (Rosas-Aguirre et al., 2017). Serum collected at the end of the study in the Peruvian cohort (Rosas-Aguirre et al., 2017) was used to assess the performance of IgG3 and total IgG antibody levels as markers for classifying recent *P. vivax* infection in the prior 9 months. In total, there were 590 individuals aged 3–85 years: 350 samples from individuals that were followed up for 37 months and 240 samples from individuals that were followed up for 13 months and qPCR data available in the last 13 months. Created in BioRender.com.

census data) scheduled for enrolment and follow-up in this cohort to enable estimates of population-based incidence rates of malaria in two different ecological settings (Cahuide: riverine; Lupuna: road-associated deforestation), with the goal of better understanding temporal and spatial dynamics of malaria transmission (Rosas-Aguirre et al., 2021). Initially, 1,029 participants were enrolled and followed with passive case detection monthly for 12 months, with a subsample of 456 individuals, then followed up monthly for another 24 months. Participants detected with microscopically confirmed *P. vivax* were treated with chloroquine for 3 days and primaquine for 7 days. The PCR prevalence at the beginning of the cohort was 16% for *P. vivax* and 2% for *P. falciparum* (Rosado et al., 2021). Serum samples analyzed in this project were collected at the end of the study period ($n = 590$, aged 3–85 years) and had qPCR data from at least the prior 13 months. This included 350 participants that were followed up for 37 months and another 240 participants that were followed up for 13 months (Rosado et al., 2021) (Figure 1B). In the final year of follow-up, December 2014 to December 2015, a total of 7,612 blood samples were collected with 14.2% (1,083/7,612) of these positive for *P. vivax* by PCR (Rosado et al., 2020). Of these *P. vivax* PCR-positive samples, only 11.8% (128/1,083) were positive by microscopy and only 2.8% were symptomatic (30/1,083) (Rosado et al., 2020).

Negative controls

Plasma samples for the negative control panel were collected from 102 volunteers from the Volunteer Blood Donor Registry in Melbourne (VBDR), Australia; 100 volunteers from the Australian Red Cross (ARC) in Melbourne, Australia; and 72 samples from the Thai Red Cross (TRC), Bangkok, Thailand. These volunteers were unlikely to have had prior malaria infections as they were sourced from non-malaria endemic areas or countries. The VBDR excludes individuals who had a travel history in malaria-endemic areas. The TRC excludes individuals who have had a malaria infection in the last 3 years or traveled to malaria-endemic areas in the last year.

Informed consent and ethical approvals

All individuals gave informed consent and/or assent to participate in the study. The PNG cohort was approved by the PNG Institute of Medical Research Institutional Review Board (0908), the PNG Medical Advisory Committee (09.11), the Ethics Committee of Basel (237/11), and the WEHI HREC (approval numbers 14/02 and 07/07). The Peruvian cohort was approved by the Ethics Review Board of Universidad Peruana Cayetano Heredia (SIDISI code # 57395), the University of California San Diego Human Subjects Protection Program (Project # 100765), and the WEHI HREC (approval numbers 14/02 and 07/07). The use of the negative controls was approved by the WEHI (#14/02).

Antigen coupling to magnetic beads

There were 32 *P. vivax* antigens used in this study (Supplementary Table S1). They were selected as potential markers of recent exposure to *P. vivax* based on data from previous studies (Longley et al., 2020). Twenty-eight proteins were made by CellFree Sciences Co., Ltd. (CFS) using the wheat germ cell-free (WGCF) expression system as previously described (Longley et al., 2020); three proteins [CSP210, CSP247 (PVX_119355), and AMA-1 (Palo Alto sequence)] were made at the Burnet Institute using the Expi293 expression system as previously described (Drew et al., 2017; Kurtovic et al., 2019); one antigen (PVX_090240 CyRPA) was made at the WEHI using a Baculovirus expression system as previously described (Longley et al., 2020); and one antigen (PVX_094255 RBP2b₁₆₁₋₁₀₀₉) was made at Ehime University using the WGCF system as previously described (Bourke et al., 2022). Not all antibody responses were measured for all cohorts for all proteins, due to the availability of protein at that time. IgG1 and IgG3 responses were not measured against PVX_082735 (TRAP/SSP2), PVX_090240 (CyRPA), and PVX_119355 (CSP247) in any cohort. Total IgG responses were not measured for any cohort against PVX_090240 (CyRPA) and PVX_094255 (RBP2b₁₆₁₋₁₀₀₉).

P. vivax antigens were coupled to magnetic BioPlex COOH beads [Bio-Rad South Granville, Australia, 171506(*xxx – unique for each region*)] following the manufacturer's instructions, with modifications as per previously published methods (Mazhari et al., 2020). Briefly, each antigen was coupled to a unique set of microspheres. Stock microspheres were sonicated in a water bath for 15 s then vortexed for 10 s. Two hundred microliters of microspheres were immobilized in a magnetic separator rack (Bio-Rad, 1614916) for 30–60 s. The supernatant was removed, and the microspheres were resuspended with 200 μ l of MQ-H₂O. The resuspension was vortexed for 20 s and placed in the magnetic separator again. The supernatant was then removed. The microspheres were resuspended with 100 mM of monobasic sodium phosphate, pH 6.2, and vortexed for 20 s. Twenty microliters of 50 mg/ml sulfo-N-hydroxysuccinimide (S-NHS) (Sigma, 56485) in MQ-H₂O was then added to the suspension and vortexed gently for 10 s, followed by 20 μ l of 50 mg/ml of N-ethyl-N'-(3-(dimethylamino)propyl)carbodiimide (EDC) (Sigma, 3449) in MQ-H₂O again with gentle vortexing for 10 s. The mixture was incubated for 20 min in the dark at room temperature on a tube rotator. The microcentrifuge tubes were then placed in a magnetic separator for 30–60 s and the supernatant was removed. The microspheres were resuspended with 500 μ l of 1 \times phosphate-buffered saline (PBS), pH 7.4, and vortexed for 20 s. This washing process was repeated one more time. The antigens in 1 \times PBS, pH 7.4, were then added, following the amounts stated in Supplementary Table S1. After the addition of the antigen, the mixture was incubated at room

temperature for 2 h or at 4°C overnight on a tube rotator. Then, the mixture was washed 3× using 500 µl of 1× PBS-TBN, pH 7.4 [made in-house, PBS, 0.1% bovine serum albumin (BSA) (Sigma, A7906), 0.02% Tween-20, 0.05% azide] before final resuspension in 500 µl of 1× PBS-TBN, pH 7.4. The coupled beads were stored at 4°C in the dark.

Multiplex antibody assays

Antibody responses were measured in plasma samples using the antigen-coupled microspheres prepared as previously described. Variations of the assay were used to measure total IgG (Mazhari et al., 2020), IgG1 and IgG3 subclasses (Liu et al., 2022), and IgM (Longley et al., 2021). Plasma or sera samples were diluted in PBT (made in-house, 1× PBS, 1% BSA, 0.05% Tween-20) with the following dilution: 1/200 for IgM assay, 1/100 for total IgG, and 1/50 for IgG1 and IgG3 assays. A two-fold serial dilution of the positive control pool (PNG hyperimmune plasma) diluted from 1/50 to 1/25,600 was included on each plate. Blanks (PBT and beads, no plasma) were included to measure the fluorescence background, prepared in triplicate. Fifty microliters of diluted plasma and 50 µl of bead mixture were added to each well of a 96-well Greiner Bio-One plate (Interpath, Heidelberg West, Australia, 655090). The antigen-coupled bead mixture was composed of 0.1 µl of each antigen-coupled bead per well. The mixture of plasma and antigen was incubated for 30 min in the dark on a plate shaker. After incubation, the plate was washed 3× with 100 µl of PBT using a plate washer. One hundred microliters of the relevant secondary antibody was then added per well, with the following dilutions: 1/400 in PBT for IgM (Jackson ImmunoResearch, 709-116-073), 1/100 in PBT for total IgG (Jackson ImmunoResearch, Pennsylvania, USA, 709-116-098), and 1/50 in PBT for the IgG subclasses (IgG1: SouthernBiotech, 9052-09, IgG3: SouthernBiotech, Alabama, USA, 9210-09). Plates were incubated for 15 min in the dark on a plate shaker and then washed 3× with 100 µl of PBT. Finally, for all assay variations, the mixture was resuspended with 80 µl of PBT and incubated for at least 5 min in the dark on a plate shaker. The plate was then read on a MAGPIX instrument (Luminex, Austin, USA). Data readout from the machines was in median fluorescence intensity (MFI). Results were then checked: quality control ensured bead number per well >15, blanks were <50 MFI, and standard curves for each antigen were consistent across plates.

Data analyses

For multiplexed assays (total IgG, IgG1, IgG3, IgM), MFI was converted to relative antibody units (RAU) to normalize the values of different plates using the positive control standard curve. This was performed using a five-parameter logistic

regression model in the R program established in a previous study (Franca et al., 2016). For visualization in the figures of antibody kinetics, the antigen-specific background (median of negative controls) was subtracted from the median antibody level at each timepoint, in an antigen-specific manner. Raw RAU data are shown in the [Supplementary Figures](#). A seropositivity cutoff was set at the average of negative controls plus two times the standard deviation. Where appropriate, antibody data were log-transformed prior to statistical analysis, as detailed in the *Results* section. Locally estimated scatterplot smoothing (LOESS) for antibody kinetic graphs was fitted using RStudio 1.4.1106 (Boston, USA). Antibody classification performance was analyzed using receiver operator characteristic (ROC) curves in R as previously described (Longley et al., 2020). The ROC curves plot sensitivity (true-positive rate) and 1-specificity (false-positive rate) at different classification thresholds or cutoffs. The area under the curve (AUC) is an aggregate of performance using all possible classification thresholds. Multiple linear regression models were performed in STATA/SE 16.1 (Texas, USA) to explore the effect of various epidemiological factors on the acquisition of IgG3 antibody levels. Correlation analysis was performed using Spearman in R. Correlations with r values <0.3 were considered weak, 0.3–0.7 moderate, and >0.7 strong correlations.

Results

Antigen-specific antibody kinetics following asymptomatic *P. vivax* infections in PNG children

P. vivax antigen-specific antibody kinetics ($n = \max 32$ antigens) over 36 weeks were first characterized following asymptomatic *P. vivax* infections in 31 PNG children (5–10 years) from Maprik, an area with moderate–high transmission intensity, with the goal of identifying antibody response pattern/s that would suggest suitability as markers of recent exposure to *P. vivax*. Antibody responses in a panel of 274 malaria-naïve individuals from non-malaria endemic areas were used as controls. Baseline refers to the median antigen-specific antibody response of the negative controls. A seropositivity cutoff was calculated as the median of negative controls plus two times the standard deviation.

Total IgG responses against 30 *P. vivax* antigens

Total IgG levels in the PNG cohort to most antigens were above baseline and maintained for at least 12 weeks following asymptomatic *P. vivax* infection, followed by a slight decrease ([Figure 2A](#)). For most antigens, median IgG levels were maintained above baseline throughout the entire 36-week follow-up, with only a few exceptions including AMA1, the

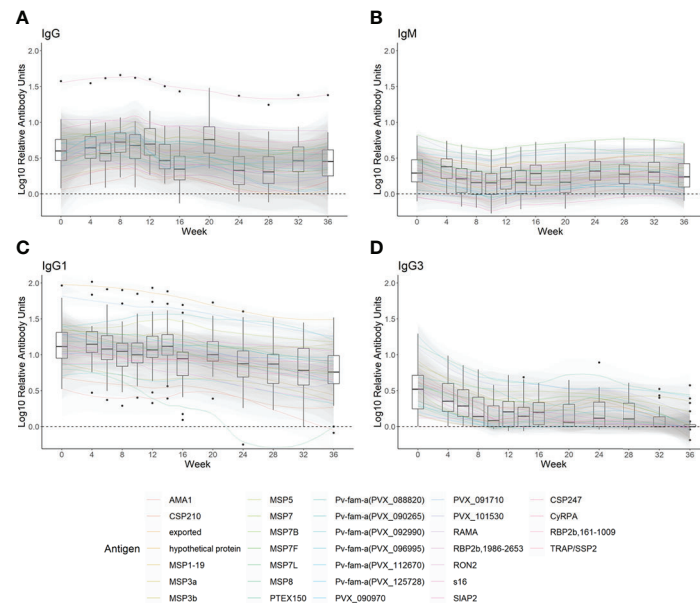


FIGURE 2

The kinetics of (A) total IgG, (B) IgM, (C) IgG1, and (D) IgG3 against 29–32 *Plasmodium vivax* antigens following asymptomatic *P. vivax* infections in PNG children. Antibody responses following asymptomatic *P. vivax* infections in PNG children ($n = 31$) over 36 weeks were measured using a multiplex assay. (A) Total IgG to 30 *P. vivax* antigens, (B) IgM to 32 *P. vivax* antigens, and (C) IgG1 and (D) IgG3 to 29 *P. vivax* antigens were measured. To standardize across antigens, the median of each antigen-specific antibody measured at each timepoint is shown after subtraction of the median antibody responses measured in negative controls (total IgG $n = 274$, IgM $n = 260$, IgG1 $n = 248$, and IgG3 $n = 256$). Box plots for each timepoint show the median of the adjusted medians of all antigen-specific antibodies, with black dots outside the whiskers indicating outlier protein responses. The kinetics of each type of antibody are presented in locally estimated scatterplot smoothing (LOESS) lines with 95% confidence intervals.

hypothetical protein (PVX_097715), and CSP210. RBP2b₁₉₈₆₋₂₆₅₃ was highly immunogenic and a notable outlier with total IgG levels well above baseline over 36 weeks (Figure 2A). Supplementary Figure S1 shows the total IgG antibody levels at a per-person level for each antigen separately and provides an indication of the antigen-specific seropositivity cutoff. Most individual IgG responses against RBP2b₁₉₈₆₋₂₆₅₃ were also above the seropositivity cutoff for 36 weeks (Supplementary Figure S1). Total IgG levels against the other *P. vivax* antigens in PNG children often fell within the seropositivity cutoff. At the time of *P. vivax* infection (week 0), 3.0%–84.9% of individuals in the PNG cohort had a seropositive total IgG response (Supplementary Table S2). There were 10 proteins in this cohort where the total IgG level of the children, using a local regression line (LOESS), trended above the seropositivity cutoff at week 0 and declined over the 36 weeks (Supplementary Figure S1, indicated by an *).

IgM responses against 32 *P. vivax* antigens

IgM levels tended to be high at week 0 for most proteins (i.e., above baseline), with a slight decline over 10 weeks before rising again to the IgM level as detected at enrolment (Figure 2B). The IgM seropositivity at week 0 was 0%–75.8% (Supplementary

Table S2). In contrast to the IgG responses in this cohort, there were fewer *P. vivax* antigens that elicited clear IgM responses following asymptomatic *P. vivax* infections in PNG children that were above the seropositivity cutoff (Supplementary Figure S2). Exceptions were for MSP7F and MSP7L where LOESS IgM levels were maintained slightly above the seropositivity cutoff for 36 weeks (Supplementary Figure S2). There were no antigens that induced the required IgM profile (for markers of recent exposure) of seropositive at week 0 followed by a decline in magnitude over 36 weeks.

IgG subclass responses against 29 *P. vivax* antigens

Median IgG1 levels to most *P. vivax* proteins were maintained, or declined slightly, over 36 weeks following asymptomatic *P. vivax* infection (Figure 2C). At the time of infection, IgG1 was detected in most *P. vivax* antigens (15.2%–97.0% seropositivity at week 0) (Supplementary Table S2). LOESS IgG1 levels to 14 *P. vivax* proteins were higher than the seropositivity cutoff at the time of infection, then declined to below the seropositivity cutoff within 36 weeks (Supplementary Figure S3, indicated by an *). This included 7/10 of the same antigens with this longevity pattern as per total IgG.

In comparison to IgG1, the decline in median IgG3 levels to most *P. vivax* antigens over time was more prominent, even reaching the baseline by 8 weeks post-infection to some antigens (Figure 2D). IgG3 was not induced as robustly as IgG1 at week 0 (seropositivity rates of 6.1%–69.7% per antigen) (Supplementary Table S2). LOESS IgG3 responses were elicited above the seropositivity cutoff at enrolment but then declined to below the seropositivity cutoff after 6–8 weeks to 18 out of 29 antigens (Supplementary Figure S4, indicated by an *). This included 6/10 of the same antigens with this longevity pattern as per total IgG, 10/14 as per IgG1, and 6 unique to IgG3. LOESS IgG3 levels to MSP3a were maintained above the seropositivity cutoff over 36 weeks (Supplementary Figure S4).

Performance of IgG3 in classifying recent *P. vivax* infections in an area with moderate transmission intensity

Given the sharp decline in IgG3 levels over time to most *P. vivax* antigens in PNG following asymptomatic *P. vivax* infection, IgG3 was selected for further assessment as a potential serological exposure marker. Both the IgG3 response and total IgG (for comparison) to 29 *P. vivax* proteins were measured in samples collected in Cahuide and San José de

Lupuna, Loreto, Peru (Rosas-Aguirre et al., 2017). The plasma samples used were collected at the end of a longitudinal cohort ($n = 590$) with qPCR data available from the previous 13 months (Figure 1B). A summary of the epidemiological characteristics of these samples is listed in Supplementary Table S3.

IgG3 responses to most *P. vivax* antigens were low (Figure 3). The seropositivity rate of IgG3 was less than 20% to 21 out of 29 *P. vivax* antigens in the panel (calculated on those infected within the last 9 months, Supplementary Table S4). Only one of the Pv-fam-a proteins (PVX_125728) had IgG3 seropositivity >50% in the overall cohort and among those infected in the last 9 months. In addition, there was a high level of individual variability in the IgG3 response generated as indicated by outlier data points, such as to Pvs16 (Figure 3). In comparison, total IgG levels to most *P. vivax* proteins were strongly induced in the Peruvian cohort (Supplementary Figure S5), with clear patterns of decreasing IgG with increasing time since prior infection to proteins such as MSP5 and AMA1. In total, 12 *P. vivax* proteins had significantly higher mean antibody levels in individuals with *P. vivax* infections in the prior 9 months compared to those with no infections or infections more than 9 months ago (Supplementary Figure S5). Notably, only three of these were antigens that also had a short-lived total IgG profile in the PNG children cohort (MSP7L, MSP3a, RBP2b₁₉₈₆₋₂₆₅₃). There were six antigens where total IgG

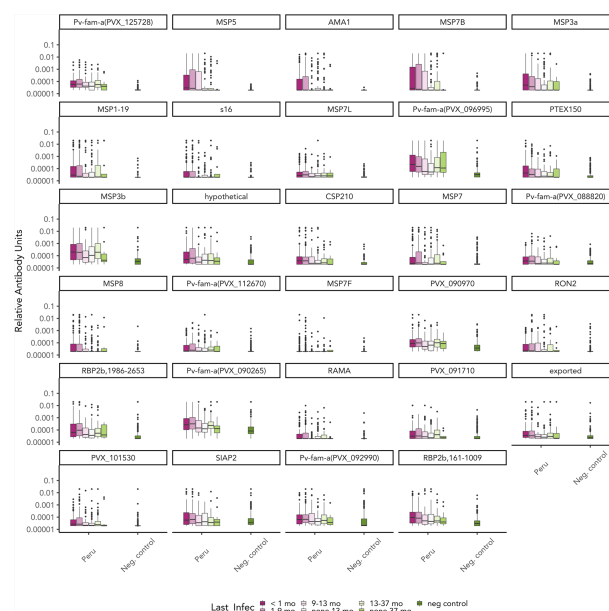


FIGURE 3

IgG3 responses to 29 *Plasmodium vivax* antigens of the Peruvian cohort based on time since prior *P. vivax* blood-stage infection. IgG3 responses to 29 *P. vivax* antigens were measured at the end of the Peruvian cohort ($n = 590$). IgG3 antibody responses are presented in relative antibody units (log) with box plots showing the median with interquartile range. The level of antibody was classified based on the prior *P. vivax* infection status as detected by qPCR: currently infected (<1 month) ($n = 160$), infected in the last 1–9 months ($n = 228$), infected in the last 9–13 months ($n = 56$), not infected within the last 13 months ($n = 75$), infected in the last 13–37 months ($n = 59$), and not infected in the last 37 months ($n = 12$). Antigens are ordered by the highest seropositivity rates (see Table S4).

responses were detected at similar levels regardless of the recency of *P. vivax* infection, suggesting a long-lived IgG response. Notably, this included three antigens that had a short-lived profile in PNG children (MSP1-19, the Pv-fam-a protein PVX_125728, and MSP7B). The remainder was poorly immunogenic in the Peruvian individuals with *P. vivax* infections in the prior 9 months (<40% seropositivity, [Supplementary Table S4](#)). The seropositivity of total IgG to most antigens was higher than that of IgG3 in the Peruvian individuals with *P. vivax* infection history ([Supplementary Table S4](#)).

The classification performance of each antibody was then assessed, with qPCR data as reference for time since previous *P. vivax* infection. The balance of sensitivity and specificity when using varying antibody levels as the cutoff for each *P. vivax* protein is depicted in receiver operator characteristic (ROC) curves. The area under the ROC curve (AUC) value was used to summarize these results (no predictive power AUC = 0.5, perfect predictor AUC = 1). IgG3 resulted in poor performance compared to total IgG in classifying recent *P. vivax* infection within the previous 9 months. Only 6 out of 29 antigen-specific IgG3 responses resulted in AUC >0.7 (range 0.571–0.764, [Table 1](#)). In contrast, total IgG responses to most (26/29) *P. vivax* proteins had an AUC value of >0.7 (range 0.589–0.833) ([Supplementary Table S5](#)). The top 5 antigens that were able to classify recent *P. vivax* infection using IgG3 were two Pv-fam-a proteins (PVX_125728, PVX_096995), MSP5, RBP2b₁₉₈₆₋₂₆₅₃, and MSP3b (AUC value = 0.714–0.764) ([Figure 4A](#), [Table 1](#)). The top 5 total IgG responses for classifying recent *P. vivax* infection were against the following: RBP2b₁₉₈₆₋₂₆₅₃, MSP3a, MSP7B, and two Pv-fam-a proteins (PVX_096995, PVX_090265) (AUC value = 0.818–0.833) ([Figure 4B](#), [Supplementary Table S5](#)). Individually, two Pv-fam-a proteins (PVX_125728, PVX_096995), RBP2b₁₉₈₆₋₂₆₅₃, MSP3b, and MSP3a generated both IgG3 (AUC > 0.7) and total IgG (AUC > 0.8) that were good markers of recent *P. vivax* infection within the prior 9 months ([Supplementary Table S5](#)).

Because IgG3 was short-lived, the classification performance of IgG3 was also assessed in a narrower time frame (from 1 to 8 months). However, the performance declined as the window of time to detect infection narrowed ([Table 1](#)). The same pattern was observed for total IgG (data not shown).

Characteristics that affected the acquisition of IgG3 in the Peruvian cohort

Because of the heterogeneity in the IgG3 response in the Peruvian individuals, we explored the factors that affected the acquisition of IgG3 in this cohort as has previously been reported for total IgG ([Rosado et al., 2021](#)). Linear regression models were fitted using age, gender, community, and the

number of blood-stage *P. vivax* infections in the past 13 months ([Table 2](#)). The IgG3 level increased with increasing age, being male, living in Lupuna, and having ≥3 blood-stage *P. vivax* infections. Age (in log₁₀) was the only factor that was associated with the response of IgG3 to all 29 *P. vivax* antigens in the panel (coefficient range: 0.182–0.849, $p < 0.01$). Age also had the highest coefficients compared to other variables to most antigens. Being male was associated with higher IgG3 levels to nine *P. vivax* antigens (coefficient range: 0.084–0.193, $p < 0.05$). Living in Lupuna was associated with higher IgG3 to 27 out of 29 antigens (coefficient range: 0.121–0.688, $p < 0.01$). Having ≥3 blood-stage infections within 13 months was positively correlated to higher IgG3 level to 15 *P. vivax* antigens (coefficient range: 0.125–0.347, $p < 0.05$).

The proportion of individuals with *P. vivax* infections was higher in Lupuna (84.05%) than in Cahuide (66.09%) as detected by qPCR in the last 13 months ([Rosado et al., 2021](#)). Hence, we assessed the classification performance of IgG3 and total IgG using the subset of individuals living in Lupuna ([Supplementary Table S5](#)). Classification performance using IgG3 on the individuals in Lupuna was higher than when using individuals from the whole cohort (AUC range 0.589–0.864 and 0.571–0.764, respectively). However, the classification performance of total IgG also improved (AUC range 0.83–0.912 Lupuna vs. 0.584–0.838 whole cohort), providing evidence that overall total IgG is a better marker of recent exposure than IgG3 in regions with moderate transmission intensity.

Comparison of total IgG data acquired using non-magnetic and magnetic beads

The strong performance of total IgG in this Peruvian cohort for classifying recent *P. vivax* infections in the prior 9 months was unexpected. A previous work had indicated total IgG was a poor performer in this cohort of moderate transmission intensity, using a number of the same *P. vivax* antigens and the same methods for testing the accuracy of classification ([Rosado et al., 2021](#)). A key difference between the two studies was the use of magnetic beads in the current work compared to non-magnetic beads in the prior work. The antibody levels generated in the Peruvian individuals, to the same *P. vivax* antigens, were therefore compared between the current data (magnetic beads) and the prior dataset (non-magnetic beads ([Rosado et al., 2021](#))). In the Peruvian individuals, there were moderate to strong correlations in total IgG antibody levels across the 19 *P. vivax* antigens in common (r values 0.38–0.91) ([Supplementary Figure S6](#)). However, within the negative controls, the correlations were weaker (0.16–0.62), with no correlation for one antigen (PVX_101530, $r = -0.015$, $p = 0.81$) ([Supplementary Figure S7](#)). There were lower antibody levels detected in the malaria-naïve controls for most of the *P. vivax* antigens assessed when using magnetic beads

TABLE 1 AUC value of each *Plasmodium vivax* antigen-specific IgG3 response for classifying recent *P. vivax* infections occurring within a different range of time (1–9 months).

Antigens	AUC value								
	1 month	2 months	3 months	4 months	5 months	6 months	7 months	8 months	9 months
Pv-fam-a (PVX_125728)	0.661	0.702	0.703	0.714	0.723	0.729	0.723	0.753	0.764
Pv-fam-a (PVX_096995)	0.673	0.707	0.716	0.728	0.728	0.733	0.728	0.738	0.740
MSP5	0.659	0.683	0.683	0.701	0.706	0.707	0.706	0.717	0.724
RBP2b ₁₉₈₆₋₂₆₅₃	0.614	0.656	0.677	0.695	0.714	0.716	0.714	0.720	0.722
MSP3b	0.630	0.669	0.666	0.677	0.699	0.705	0.699	0.709	0.714
MSP3a	0.622	0.645	0.657	0.675	0.693	0.698	0.693	0.702	0.703
PVX_101530	0.605	0.646	0.646	0.648	0.666	0.677	0.666	0.681	0.686
Pv-fam-a	0.609	0.646	0.647	0.657	0.670	0.671	0.670	0.683	0.685
MSP1-19	0.628	0.649	0.666	0.667	0.669	0.674	0.669	0.671	0.676
RBP2b ₁₆₁₋₁₀₀₉	0.620	0.659	0.657	0.667	0.677	0.678	0.677	0.677	0.675
MSP7L	0.603	0.645	0.641	0.650	0.657	0.664	0.657	0.667	0.673
MSP7B	0.614	0.623	0.626	0.637	0.656	0.664	0.656	0.664	0.672
CSP210	0.628	0.667	0.662	0.662	0.658	0.655	0.658	0.661	0.663
AMA1	0.598	0.634	0.644	0.642	0.650	0.653	0.650	0.651	0.655
Hypothetical protein	0.587	0.627	0.641	0.648	0.650	0.653	0.650	0.653	0.655
PVX_090970	0.587	0.619	0.625	0.629	0.643	0.651	0.643	0.652	0.654
RAMA	0.599	0.625	0.623	0.635	0.649	0.652	0.649	0.649	0.652
Pv-fam-a (PVX_092990)	0.594	0.634	0.635	0.645	0.645	0.648	0.645	0.650	0.648
MSP 8	0.583	0.611	0.619	0.636	0.637	0.645	0.637	0.644	0.647
PTX150	0.619	0.642	0.644	0.652	0.651	0.651	0.651	0.641	0.646
s16	0.610	0.631	0.632	0.640	0.645	0.645	0.645	0.640	0.639
RON2	0.589	0.616	0.610	0.631	0.633	0.641	0.633	0.634	0.637
Exported protein	0.600	0.625	0.617	0.628	0.632	0.635	0.632	0.638	0.634
Pv-fam-a (PVX_088820)	0.571	0.605	0.604	0.615	0.622	0.620	0.622	0.628	0.625
Pv-fam-a (PVX_112670)	0.556	0.593	0.607	0.618	0.623	0.628	0.623	0.623	0.623
MSP 7	0.564	0.588	0.594	0.614	0.615	0.626	0.615	0.622	0.621
PVX_091710	0.564	0.606	0.602	0.605	0.616	0.624	0.616	0.616	0.617
SIAP2	0.570	0.590	0.593	0.593	0.604	0.605	0.604	0.600	0.602
MSP7F	0.555	0.556	0.563	0.559	0.567	0.565	0.567	0.571	0.571

The two color scheme highlights the lowest AUC values in red and the highest AUC values in blue.

(Figure 5), which has resulted in a better signal-to-background ratio (when comparing antibody levels in those with recent infections to the negative controls), which in turn has likely contributed to the better classification performance of total IgG in the current study. This is further demonstrated through a focused analysis on the top performing antigen using total IgG, RBP2b₁₉₈₆₋₂₆₅₃. The ROC curves for RBP2b₁₉₈₆₋₂₆₅₃ generated using non-magnetic beads and magnetic beads are compared in Supplementary Figure S8, with the breakdown of the classification demonstrating that the improved overall AUC value when using magnetic beads (0.84 vs. 0.66) is due to improved performance in classifying the negative controls as not recently exposed [88.7% (243/274) correctly classified using non-magnetic bead data vs. 98.6% (270/274) with magnetic bead data]. There was no improvement evident in the classification of the Peruvian individuals with 66.8% (394/590) correctly

classified when using the non-magnetic bead data and 66.6% (393/590) when using magnetic bead data (Supplementary Figures S8B, C).

Discussion

In countries endemic to both *P. vivax* and *P. falciparum*, *P. vivax* is proving to be a significant challenge for control and elimination. New strategies for rapidly reducing the transmission of *P. vivax* need to be considered, such as serological testing and treatment (seroTAT) (Tayipto et al., 2022). The current development of seroTAT has focused on applying this strategy in low transmission settings. In settings with higher transmission, there is concern that serological

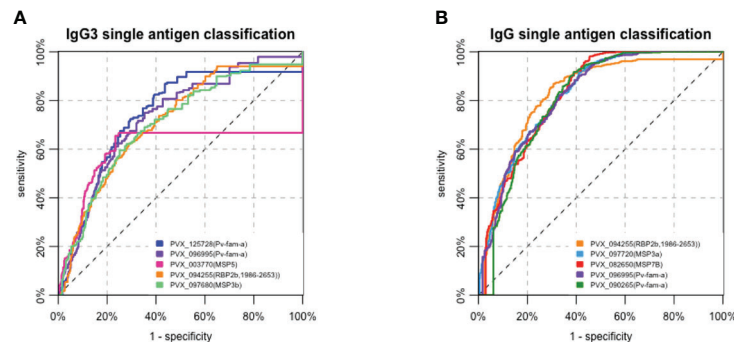


FIGURE 4

Receiver operating characteristic (ROC) curves of the top 5 (A) IgG3 and (B) total IgG responses to antigens in classifying recent *Plasmodium vivax* exposure (within 9 months) in a Peruvian cohort with moderate transmission intensity. The performance of each *P. vivax* antigen in the serological marker panel for classifying recent *P. vivax* infections in the prior 9 months was assessed individually using an ROC curve. (A) The top 5 antigen-specific IgG3 responses that can classify *P. vivax* infection were against the following: two Pf-vam-a proteins (PVX_125728, PVX_096995), MSP5, RBP2b1986-2653, and MSP3b (AUC value = 0.714–0.764). (B) The top 5 antigen-specific total IgG responses were against the following: RBP2b1986-2653, MSP3a, MSP7b, and two Pv-fam-a proteins (PVX_096995, PVX_090265) (AUC value = 0.818–0.833).

exposure markers will be less accurate (Rosado et al., 2021) given that individuals will likely have had higher levels of past exposure to *P. vivax* and therefore longer-lived IgG responses (Longley et al., 2017; Rosado et al., 2021). In the current study, the goal was to first characterize the longevity of total IgG, IgG1, IgG3, and IgM following asymptomatic *P. vivax* infections in a setting of moderate–high transmission intensity and then to assess the classification performance of the antibody with the most suitable longevity profile (i.e., short-lived). A limitation in the approach for our study was the need to characterize longevity and then assess classification performance using cohorts from two discrete populations (for both age and geography) (Rosado et al., 2021; Robinson et al., 2015). While both settings and cohorts had higher transmission than our prior work in Thailand, Brazil, and the Solomon Islands (Longley et al., 2020), there were also differences between them with the PNG community having even higher transmission at the time of the study than the Peruvian communities (based on *P. vivax* prevalence by PCR) (Rosado et al., 2021; Robinson et al., 2015).

As expected, total IgG responses in PNG children to most of the *P. vivax* antigens in the panel were maintained above baseline over 36 weeks. However, the response was only slightly above the seropositivity cutoff, except IgG to RBP2b₁₉₈₆₋₂₆₅₃, which was highly immunogenic. This observation is consistent with prior studies highlighting RBP2b as highly immunogenic (Liu et al., 2022) and indeed the top marker of recent exposure when using total IgG in low transmission settings (Longley et al., 2020). IgM responses in PNG children were of relatively low magnitude compared to the negative control panels, with seropositivity rates at the time of infection <50% for all but two antigens, but the levels were consistently maintained over the 36 weeks. We have previously observed long-lived IgM responses following clinical *P. vivax*

infections in a low transmission setting (Liu et al., 2022), and data on immune responses to *P. falciparum* indicate that IgM is a prominent feature of the antibody response to malaria, even in those with repeated infections over time (Boyle et al., 2019). IgG1 was more immunogenic and had higher seropositivity than IgG3 in the PNG children cohort, which could be explained by these children not yet undergoing the IgG subclass switch from IgG1 to IgG3 in relation to age (Fernandez-Becerra et al., 2010; França et al., 2016). IgG1 responses were maintained and slowly declined over time, mirroring total IgG, while the IgG3 responses that were elicited declined to background 6–8 weeks after enrolment. Among the tested antibodies, IgG3 had the most appropriate longevity profile for further testing as a marker of recent *P. vivax* exposure in areas with moderate/moderate–high transmission intensity.

To test the ability of antigen-specific IgG3 antibody responses to classify individuals as recently infected with *P. vivax* in the prior 9 months, samples from a Peruvian cohort were used. The ability of total IgG to classify recent infections in this cohort has previously been tested and shown to be suboptimal compared to classification in low transmission settings (Rosado et al., 2021). Overall, IgG3 was not strongly induced in the Peruvian cohort and, thus, not surprisingly, was a poor classifier of recent exposure. The performance of total IgG to most *P. vivax* antigens was more accurate than IgG3. The top 5 IgG3 markers were able to classify infection within 9 months with AUC values of >0.7, while the top 5 total IgG markers had AUC values of >0.8. Among the top 5 performers, IgG3 to MSP5 and one Pv-fam-a protein (PVX_125728) also had the highest IgG3 seropositivity rates of 41.2% and 62%, respectively, in the Peruvian cohort. Other top 5 performers, IgG3 to another Pv-fam-a protein (PVX_096995) and MSP3b, had the highest mean level of IgG3 detected across all Peruvian samples. On the

TABLE 2 Multivariable linear regression model of the effect of epidemiological factors on IgG3 antibody level in the Peruvian cohort.

Antigen	Age, Log ₁₀ Coefficient (95% CI)	Gender(Ref = female) Coefficient (95% CI)	Community(Ref = Cahuide) Coefficient (95% CI)	≥ 3 infection ^f (Ref = No) Coefficient (95% CI)
AMA 1	0.556*** (0.383, 0.730)		0.354*** (0.225, 0.482)	
CSP210	0.347*** (0.209, 0.486)		0.254*** (0.162, 0.346)	0.126* (0.005, 0.248)
exported	0.341*** (0.201, 0.481)		0.176*** (0.081, 0.271)	
hypothetical protein	0.462*** (0.297, 0.626)		0.229*** (0.107, 0.350)	0.147* (0.002, 0.292)
MSP 5	0.743*** (0.546, 0.940)		0.491*** (0.339, 0.643)	0.266** (0.073, 0.459)
MSP 7	0.368*** (0.197, 0.539)	0.153* (0.023, 0.283)	0.178* (0.042, 0.315)	0.265** (0.087, 0.443)
MSP1-19	0.366*** (0.176, 0.555)		0.249** (0.107, 0.390)	
MSP3a	0.497*** (0.313, 0.682)	0.160* (0.0306, 0.289)	0.409*** (0.270, 0.548)	0.272** (0.094, 0.449)
MSP3b	0.550*** (0.365, 0.734)		0.330*** (0.191, 0.469)	0.347*** (0.171, 0.523)
MSP7B	0.849*** (0.622, 1.076)	0.193* (0.028, 0.357)	0.688*** (0.516, 0.861)	0.293** (0.072, 0.514)
MSP7F	0.184*** (0.087, 0.281)		0.121*** (0.058, 0.184)	
MSP7L	0.182** (0.078, 0.286)			
MSP8	0.337*** (0.183, 0.490)	0.113* (0.002, 0.225)	0.323*** (0.216, 0.431)	0.256** (0.103, 0.410)
PTX150	0.385*** (0.242, 0.529)		0.207*** (0.102, 0.312)	0.154* (0.025, 0.283)
Pv-fam-a (PVX_088820)	0.311*** (0.198, 0.425)		0.160*** (0.079, 0.241)	0.125* (0.024, 0.226)
Pv-fam-a (PVX_090265)	0.295*** (0.134, 0.456)		0.203** (0.088, 0.3170)	0.206** (0.072, 0.340)
Pv-fam-a (PVX_092990)	0.202** (0.064, 0.341)	0.169*** (0.075, 0.264)	0.207*** (0.110, 0.304)	
Pv-fam-a (PVX_096995)	0.536*** (0.347, 0.725)		0.318*** (0.177, 0.459)	0.333*** (0.155, 0.510)
Pv-fam-a (PVX_112670)	0.193** (0.077, 0.309)			
Pv-fam-a (PVX_125728)	0.249*** (0.139, 0.360)	0.084* (0.006, 0.161)	0.183*** (0.104, 0.261)	
PVX_090970	0.368*** (0.234, 0.502)	0.113* (0.025, 0.201)	0.173*** (0.081, 0.265)	
PVX_091710	0.233*** (0.112, 0.354)	0.150** (0.065, 0.234)	0.126** (0.044, 0.207)	
PVX_101530	0.281*** (0.145, 0.417)		0.226*** (0.130, 0.321)	
RAMA	0.196*** (0.092, 0.301)		0.142*** (0.072, 0.213)	
RBP2b ₁₆₁₋₁₀₀₉	0.312*** (0.167, 0.458)	0.102* (0.000, 0.204)	0.190*** (0.085, 0.296)	0.185** (0.055, 0.314)
RBP2b ₁₉₈₆₋₂₆₅₃	0.285*** (0.142, 0.428)		0.301*** (0.199, 0.404)	0.173** (0.048, 0.298)
RON2	0.257*** (0.118, 0.396)		0.292*** (0.195, 0.388)	
s16	0.271** (0.111, 0.430)		0.286*** (0.171, 0.401)	
SIAP2	0.243** (0.100, 0.386)		0.213*** (0.110, 0.315)	0.146* (0.026, 0.265)

95% CI, 95% confidence interval.

*p < 0.05; **p < 0.01; ***p < 0.001.

^aPlasmodium vivax-positive qPCR result.

Only significant associations are shown.

contrary, despite being one of the best markers of recent *P. vivax* infection using IgG3, the seropositivity rates of IgG3 to RBP2b₁₉₈₆₋₂₆₅₃ were the lowest in the Peruvian cohort, either in those infected in the prior 9 months or among all participants in the cohort. IgG3 antibodies against RBP2b₁₉₈₆₋₂₆₅₃ were clearly induced; however, the seropositivity cutoff set was high given a large spread of IgG3 levels against this protein in the negative control panels. This is thus a factor that could be further optimized through construct design and/or purification. Overall, the top IgG3 performers for classifying recent *P. vivax* infections in the Peruvian cohort had characteristics of high seropositivity or high mean magnitude, except for RBP2b₁₉₈₆₋₂₆₅₃. Despite IgG3 levels being short-lived in PNG children, IgG3 classification of recent prior *P. vivax* infections in Peru was poorer for shorter intervals of classification (i.e., 1–8 vs.

9 months). The reason for this finding is currently unclear but could be influenced by different patterns of antibody kinetics in PNG children versus the Peruvians, despite similar levels of transmission (moderate/moderate-high). This is a challenge and is also highlighted by differences in the results for total IgG between the PNG and Peruvian cohorts and suggests that perhaps antibody kinetics need to be assessed in the same target population as where the serological exposure markers would be implemented; however, this is not always possible depending on the design of studies that have been conducted.

To further understand the acquisition of IgG3, epidemiologic variables that could influence the results were assessed. IgG1 switching to IgG3 has been associated with age as reported in other studies (Fernandez-Becerra et al., 2010; França et al., 2016). Age had the strongest association with IgG3 levels

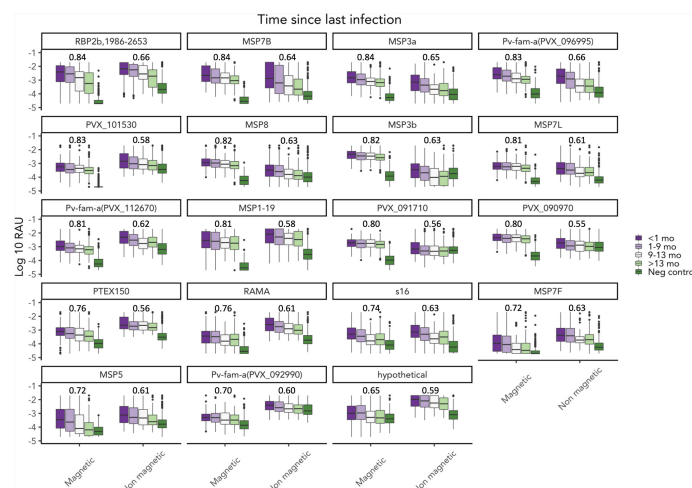


FIGURE 5

Comparison of total IgG measured using magnetic beads versus non-magnetic beads. Total IgG to 19 *P. vivax* antigens was measured using magnetic and non-magnetic beads in the multiplex assay. Total IgG was measured in the Peruvian cohort ($n = 590$) and negative controls ($n = 274$). AUC value was noted in the figure. Non-magnetic bead AUC value was obtained from a published paper by Rosado et al.

(coefficient range: 0.182–0.849, $p < 0.01$) compared to gender, location, and number of previous *P. vivax* infections in the Peruvian cohort. People living in Lupuna also had significantly higher IgG3 levels to 28 out of 29 *P. vivax* proteins. In the last 13 months, people in Lupuna had 18% more *P. vivax* infections than those in Cahuide (Rosado et al., 2021). Individuals living in Lupuna also had more past exposure at enrolment (Rosas-Aguirre et al., 2021). This correlates with the result in this study that showed that individuals who had at least three blood-stage *P. vivax* infections had high levels of IgG3. A prior study in the same Peruvian cohort also found that total IgG increased with increasing age and number of blood-stage *P. vivax* infections (Rosado et al., 2021). Gender, on the other hand, was associated weakly with the level of IgG3. Together, the data suggest that a high level of prior exposure to *P. vivax* is required to gain IgG3 antibodies, with too few individuals in the Peruvian cohort acquiring enough IgG3 to enable accurate classification of recent *P. vivax* exposure with this biomarker.

Total IgG to the *P. vivax* antigen panel in the Peruvian cohort resulted in better classification performance of recent *P. vivax* infections, with AUC >0.8 , than that obtained in the previous study of the same cohort (<0.7) (Rosado et al., 2021). There were 19 antigens in common between the two panels and similar top performers: total IgG to RBP2b₁₉₈₆₋₂₆₅₃, MSP3a, MSP7B, and one Pv-fam-a protein (PVX_096995). Importantly, the *P. vivax* antigens in common between the two studies were expressed using the same constructs and expression systems. The key difference was the use of a magnetic bead-based assay in the current study compared to a non-magnetic bead-based assay in the earlier study. Systematic comparisons of the use of non-magnetic versus magnetic beads for the multiplexed assays have

demonstrated that moderate–strong correlations in the data can be expected (Ondigo et al., 2019; Mazhari et al., 2020), dependent on the antigen. The current results are in support of this finding. However, the correlation was weaker in the malaria-naïve negative controls. The magnetic bead assay had a lower background, suggesting that a better signal-to-background ratio increases the classification accuracy [a trend we have observed previously (Longley et al., 2020)]. The non-magnetic bead assay was run on a BioPlex-200 instrument with the high RP1 (PMT) option selected, which is recommended when running plasma or sera samples. This option amplifies the signal resulting in improved sensitivity and, thus, is a likely contributing factor to the higher antibody levels detected in the negative controls using this system. Alternatively, the improved methods for plate washing that are enabled through the use of magnetic beads (such as an automatic plate washer) may also contribute to the lower background in the magnetic bead assay. Ultimately, the improved AUC was due to better classification of the negative control samples as not recently exposed to *P. vivax* and not due to improvements in classifying the Peruvian individuals as recently or not recently exposed. This highlights the importance of assessing classification algorithm performance specifically within defined groups (such as in Figure S8) and leads to the same finding as in our original study: the performance of *P. vivax* serological exposure markers (using total IgG) is poorer in moderate transmission settings than low transmission settings. The current study additionally shows that IgG3 is also inadequate for classifying recent exposure with high accuracy.

In exploring the use of IgG3 as a biomarker of recent *P. vivax* infection, further work is needed to assess the combinations of IgG3 responses to multiple *P. vivax* antigens. Prior evidence has

shown that using combined total IgG antibody responses to more than five *P. vivax* antigens was a better marker of recent infection than to one alone (Longley et al., 2020), so a combination of antigen-specific antibodies may increase the performance of IgG3. Rescreening a larger set of *P. vivax* proteins may also guide finding a better antigen that generates a stronger IgG3 response in individuals living in endemic areas with moderate transmission intensity. However, the heterogeneity seen for the IgG3 antibody profile, which was largely dependent on age and the level of previous exposure, demonstrates that IgG3 on its own is not well suited as a recent exposure marker in this epidemiological setting of Peru. Furthermore, IgG3 antibody kinetics in PNG children may differ to those in Peruvian individuals of all ages, which suggests that either i) other antibody biomarkers should be directly screened in the Peruvian cohort or ii) antibody kinetics need to be defined in Peruvian studies. Ultimately, the *P. vivax* serological exposure markers are designed for use in low transmission settings [where they perform very well (Longley et al., 2020)], and further consideration and optimization, and comparison to available alternatives, would be required before supporting their use in higher transmission settings.

Data availability statement

The original contributions presented in the study are included in the article/Supplementary Material. Further inquiries can be directed to the corresponding author.

Ethics statement

The studies involving human participants were reviewed and approved by Walter and Eliza Hall Institute Human Research Ethics Committee, PNG Institute of Medical Research Institutional Review Board, PNG Medical Advisory Committee, Ethics Committee of Basel, Ethics Review Board of Universidad Peruana Cayetano Heredia, University of California San Diego Human Subjects Protection Program. Written informed consent to participate in this study was provided by the participants' legal guardian/next of kin.

Author contributions

YT and RL wrote the first draft of the manuscript. YT generated data from the samples and conducted data analysis with the support of JR, RL, MW, and IM. JR, DG, BK, and LR collected the data and samples in the field. JH, DO, JB, ET, TT, and MH expressed proteins. All authors have contributed to the final version of the manuscript.

Funding

YT received an Australia Award from the Australian Department of Foreign Affairs and Trade to support her Master of Biomedical Science research. This work was supported by an Australian National Health and Medical Research Council (NHMRC) Investigator Grant (#1173210 to RL and #1173046 to JB). The PNG longitudinal cohort study was funded by NIH U19 AI089686. The Peruvian samples were collected under the ICEMR program (U19AI089681). LR was supported by NHMRC grants #1161627 and #1016443. IM was also supported by the NHRMC (grants #1092789, #1134989, #1132975, and #1043345). We acknowledge the support of the Victorian State Government Operational Infrastructure Support and Australian Government NHMRC IRISS.

Acknowledgments

The following people provided drafts of R scripts, PRISM file, or STATA do-file for data analysis: Dr. Connie Li Wai Suen (five-parameter logistic regression model) and Dr. Eamon Conway (antibody kinetics graphs). We thank Jessica Brewster for the assistance with coupling some beads for the multiplex assay. We thank all the teams in PNG and Peru involved in collecting samples or data from the cohort studies.

Conflict of interest

RL, MW, TT, and IM are inventors on patent PCT/US17/67926 on a system, method, apparatus, and diagnostic test for *P. vivax*. Author MH was employed by CellFree Sciences Co., Ltd., Yokohama, Japan.

The remaining authors declare that the research was conducted in the absence of any commercial or financial relationships that could be construed as a potential conflict of interest.

Publisher's note

All claims expressed in this article are solely those of the authors and do not necessarily represent those of their affiliated organizations, or those of the publisher, the editors and the reviewers. Any product that may be evaluated in this article, or claim that may be made by its manufacturer, is not guaranteed or endorsed by the publisher.

Supplementary material

The Supplementary Material for this article can be found online at: <https://www.frontiersin.org/articles/10.3389/fcimb.2022.950909/full#supplementary-material>

References

- Aggarwal, V., Nagpal, A., Agrawal, Y., Kumar, V., Kanwal, S. K., and Dhingra, B. (2014). *Plasmodium vivax* malaria complicated by splenic infarct. *Paediatr. Int. Child Health* 34 (1), 63–65. doi: 10.1179/2046905512Y.0000000029
- Ashley, E. A., Recht, J., and White, N. J. (2014). Primaquine: the risks and the benefits. *Malar J.* 13, 418. doi: 10.1186/1475-2875-13-418
- Aung, P. L., Soe, M. T., Soe, T. N., Oo, T. L., Aung, P. P., Khin, A., et al. (2021). The acceptability of targeted mass treatment with primaquine for local elimination of vivax malaria in a northern Myanmar township: A mixed-methods study. *Parasites Vectors*. 14 (1), 549. doi: 10.1186/s13071-021-05064-y
- Bourke, C., Takashima, E., Chan, L.-J., Dietrich, M. H., Mazhari, R., White, M., et al. (2022). Comparison of total immunoglobulin G antibody responses to different protein fragments of plasmodium vivax reticulocyte binding protein 2b. *Malaria J.* 21 (1), 71. doi: 10.1186/s12936-022-04085-x
- Boyle, M. J., Chan, J. A., Handayani, I., Reiling, L., Feng, G., Hilton, A., et al. (2019). IgM in human immunity to *Plasmodium falciparum* malaria. *Sci. Adv.* 5 (9), eaax4489. doi: 10.1126/sciadv.aax4489
- Drew, D. R., Sanders, P. R., Weiss, G., Gilson, P. R., Crabb, B. S., and Beeson, J. G. (2017). Functional conservation of the AMA1 host-cell invasion ligand between p. falciparum and p. vivax: A novel platform to accelerate vaccine and drug development. *J. Infect. Diseases*. 217 (3), 498–507. doi: 10.1093/infdis/jix583
- Fernandez-Becerra, C., Sanz, S., Brucet, M., Stanisic, D. I., Alves, F. P., Camargo, E. P., et al. (2010). Naturally-acquired humoral immune responses against the n- and c-termini of the *Plasmodium vivax* MSP1 protein in endemic regions of Brazil and Papua new Guinea using a multiplex assay. *Malaria J.* 9 (29), 1–8. doi: 10.1186/1475-2875-9-29
- Franca, C. T., He, W. Q., Gruszczyk, J., Lim, N. T., Lin, E., Kiniboro, B., et al. (2016). Plasmodium vivax reticulocyte binding proteins are key targets of naturally acquired immunity in young Papua new guinean children. *PLoS Negl. Trop. Dis.* 10 (9), e0005014. doi: 10.1371/journal.pntd.0005014
- França, C. T., He, W.-Q., Gruszczyk, J., Lim, N. T. Y., Lin, E., Kiniboro, B., et al. (2016). *Plasmodium vivax* reticulocyte binding proteins are key targets of naturally acquired immunity in young Papua new guinean children. *PLoS Negl. Trop. Diseases* 10 (9), e0005014. doi: 10.1371/journal.pntd.0005014
- Greenhouse, B., Daily, J., Guinovart, C., Goncalves, B., Beeson, J., Bell, D., et al. (2019). Priority use cases for antibody-detecting assays of recent malaria exposure as tools to achieve and sustain malaria elimination. *Gates Open Res.* 3, 131. doi: 10.12688/gatesopenres.12897.1
- Hsiang, M. S., Hwang, J., Tao, A. R., Liu, Y., Bennett, A., Shanks, G. D., et al. (2013). Mass drug administration for the control and elimination of plasmodium vivax malaria: an ecological study from jiangsu province, China. *Malar J.* 12, 383. doi: 10.1186/1475-2875-12-383
- Imirzalioglu, C., Soydan, N., Schaller, M., Bretzel, R. G., Chakraborty, T., and Domann, E. (2006). Diagnosis of mixed *Plasmodium malariae* and *P. vivax* infection in a development aid volunteer by examination of bone-marrow specimens by real-time PCR. *J. Clin. Microbiol.* 44 (6), 2307–2310. doi: 10.1128/JCM.02687-05
- Jiménez, B. C., Navarro, M., Huerga, H., and López-Vélez, R. (2007). Spontaneous splenic rupture due to *Plasmodium vivax* in a traveler: Case report and review. *J. Travel Med.* 14 (3), 188–191. doi: 10.1111/j.1708-8305.2007.00112.x
- Kurtovic, L., Agius, P. A., Feng, G., Drew, D. R., Ubbilos, I., Sacarlal, J., et al. (2019). Induction and decay of functional complement-fixing antibodies by the RTS,S malaria vaccine in children, and a negative impact of malaria exposure. *BMC Med.* 17 (1), 45–45. doi: 10.1186/s12916-019-1277-x
- Lacerda, M. V., Fragoso, S. C., Alecrim, M. G., Alexandre, M. A., Magalhães, B. M., Siqueira, A. M., et al. (2012). Postmortem characterization of patients with clinical diagnosis of *Plasmodium vivax* malaria: to what extent does this parasite kill? *Clin. Infect. Dis.* 55 (8), e67–e74. doi: 10.1093/cid/cis615
- Liu, Z. S., Sattabongkot, J., White, M., Chotirat, S., Kumpitak, C., Takashima, E., et al. (2022). Naturally acquired antibody kinetics against *Plasmodium vivax* antigens in people from a low malaria transmission region in western Thailand. *BMC Med.* 20 (1), 89. doi: 10.1186/s12916-022-02281-9
- Longley, R., White, M., Brewster, J., Liu, Z., Bourke, C., Takashima, E., et al. (2021). IgG antibody responses are preferential compared with IgM for use as serological markers for detecting recent exposure to *Plasmodium vivax* infection. *Open Forum Infect. Dis.* 8 (6), 1–5. doi: 10.1093/ofid/ofab228
- Longley, R. J., White, M. T., Takashima, E., Brewster, J., Morita, M., Harbers, M., et al. (2020) 8 (6), 1–5. Development and validation of serological markers for detecting recent *Plasmodium vivax* infection. *Nat. Med.* 26 (5), 741–749. doi: 10.1038/s41591-020-0841-4
- Longley, R. J., White, M. T., Takashima, E., Morita, M., Kanoi, B. N., Li Wai Suen, C. S. N., et al. (2017). Naturally acquired antibody responses to more than 300 *Plasmodium vivax* proteins in three geographic regions. *PLoS Negl. Trop. Dis.* 11 (9), e0005888. doi: 10.1371/journal.pntd.0005888
- Mazhari, R., Brewster, J., Fong, R., Bourke, C., Liu, Z. S. J., Takashima, E., et al. (2020). A comparison of non-magnetic and magnetic beads for measuring IgG antibodies against *Plasmodium vivax* antigens in a multiplexed bead-based assay using luminex technology (Bio-plex 200 or MAGPIX). *PLoS One* 15 (12), e0238010. doi: 10.1371/journal.pone.0238010
- O'Donnell, J., Goldman, J. M., Wagner, K., Ehinger, G., Martin, N., Leahy, M., et al. (1998). Donor-derived *Plasmodium vivax* infection following volunteer unrelated bone marrow transplantation. *Bone Marrow Transplant.* 21 (3), 313–314. doi: 10.1038/sj.bmt.1701073
- Ondigo, B. N., Park, G. S., Ayieko, C., Nyangahu, D. D., Wasswa, R., and John, C. C. (2019). Comparison of non-magnetic and magnetic beads multiplex assay for assessment of *Plasmodium falciparum* antibodies. *PeerJ*. 7, e6120. doi: 10.7717/peerj.6120
- Raghunandan, J., Rajeshwari, K., Dubey, A. P., and Singh, T. (2012). Peripheral gangrene in an 18-month-old boy with *Plasmodium vivax* malaria. *Paediatr. Int. Child Health* 32 (3), 164–166. doi: 10.1179/2046905512Y.0000000006
- Robinson, L. J., Wampfler, R., Betuela, I., Karl, S., White, M. T., Li Wai Suen, C. S., et al. (2015). Strategies for understanding and reducing the plasmodium vivax and plasmodium ovale hypnozoite reservoir in Papua new guinean children: a randomised placebo-controlled trial and mathematical model. *PLoS Med.* 12 (10), e1001891. doi: 10.1371/journal.pmed.1001891
- Rosado, J., White, M. T., Longley, R. J., Lacerda, M., Monteiro, W., Brewster, J., et al. (2021). Heterogeneity in response to serological exposure markers of recent *Plasmodium vivax* infections in contrasting epidemiological contexts. *PLoS Negl. Trop. Diseases*. 15 (2), e0009165. doi: 10.1371/journal.pntd.0009165
- Rosas-Aguirre, A., Guzman-Guzman, M., Chuquiyauri, R., Moreno, M., Manrique, P., Ramirez, R., et al. (2021). Temporal and microspatial heterogeneity in transmission dynamics of coendemic *Plasmodium vivax* and *Plasmodium falciparum* in two rural cohort populations in the Peruvian Amazon. *J. Infect. Dis.* 223 (8), 1466–1477. doi: 10.1093/infdis/jiaa526
- Rosas-Aguirre, A., Guzman-Guzman, M., Gamboa, D., Chuquiyauri, R., Ramirez, R., Manrique, P., et al. (2017). Micro-heterogeneity of malaria transmission in the Peruvian Amazon: a baseline assessment underlying a population-based cohort study. *Malaria J.* 16 (1), 312–312. doi: 10.1186/s12936-017-1957-y
- Ru, Y. X., Mao, B. Y., Zhang, F. K., Pang, T. X., Zhao, S. X., Liu, J. H., et al. (2009). Invasion of erythroblasts by *Plasmodium vivax*: A new mechanism contributing to malarial anemia. *Ultrastruct Pathol.* 33 (5), 236–242. doi: 10.3109/01913120903251643
- Ssewanyana, I., Rek, J., Rodriguez, I., Wu, L., Arinaitwe, E., Nankabirwa, J. I., et al. (2021). Impact of a rapid decline in malaria transmission on antimalarial IgG subclasses and avidity. *Front. Immunol.* 11, 576663–576663. doi: 10.3389/fimmu.2020.576663
- Sutanto, I., Kosasih, A., Elyazar, I. R. F., Simanjuntak, D. R., Larasati, T. A., Dahlan, M. S., et al. (2018). Negligible impact of mass screening and treatment on mesoendemic malaria transmission at West timor in Eastern Indonesia: A cluster-randomized trial. *Clin. Infect. Dis.* 67 (9), 1364–1372. doi: 10.1093/cid/ciy231
- Tayipto, Y., Liu, Z., Mueller, I., and Longley, R. J. (2022). Serology for plasmodium vivax surveillance: A novel approach to accelerate towards elimination. *Parasitol. Int.* 87, 102492. doi: 10.1016/j.parint.2021.102492



OPEN ACCESS

EDITED BY

Jeroen P. J. Saeij,
University of California, Davis,
United States

REVIEWED BY

Michael Fokuo Ofori,
University of Ghana, Ghana
Nathan A Tanner,
New England Biolabs, United States

*CORRESPONDENCE

Rentala Madhubala
rentala@outlook.com
Shailja Singh
shailjasingh@mail.jnu.ac.in

SPECIALTY SECTION

This article was submitted to
Parasite and Host,
a section of the journal
Frontiers in Cellular and
Infection Microbiology

RECEIVED 05 June 2022

ACCEPTED 02 August 2022

PUBLISHED 19 August 2022

CITATION

Puri M, Kaur Brar H, Madan E,
Srinivasan R, Rawat K, Gorthi SS,
Kumari G, Sah R, Ojha SB, Panigrahi S,
Dhangadamajhi G, Muthuswami R,
Singh S and Madhubala R (2022)
Rapid diagnosis of *Plasmodium*
falciparum malaria using a point-
of-care loop-mediated isothermal
amplification device.
Front. Cell. Infect. Microbiol. 12:961832.
doi: 10.3389/fcimb.2022.961832

COPYRIGHT

© 2022 Puri, Kaur Brar, Madan,
Srinivasan, Rawat, Gorthi, Kumari, Sah,
Ojha, Panigrahi, Dhangadamajhi,
Muthuswami, Singh and Madhubala.
This is an open-access article
distributed under the terms of the
Creative Commons Attribution License
(CC BY). The use, distribution or
reproduction in other forums is
permitted, provided the original
author(s) and the copyright owner(s)
are credited and that the original
publication in this journal is cited, in
accordance with accepted academic
practice. No use, distribution or
reproduction is permitted which does
not comply with these terms.

Rapid diagnosis of *Plasmodium falciparum* malaria using a point-of-care loop-mediated isothermal amplification device

Madhu Puri¹, Harsimran Kaur Brar¹, Evanka Madan¹,
Rajesh Srinivasan², Kapil Rawat², Sai Siva Gorthi²,
Geeta Kumari³, Raj Sah³, Sashi Bhusan Ojha⁴,
Subhendu Panigrahi⁵, Gunanidhi Dhangadamajhi⁴,
Rohini Muthuswami¹, Shailja Singh^{3*} and Rentala Madhubala^{1*}

¹School of Life Sciences, Jawaharlal Nehru University, New Delhi, India, ²Department of Instrumentation and Applied Physics, Indian Institute of Science, Bengaluru, India, ³Special Centre for Molecular Medicine, Jawaharlal Nehru University, New Delhi, India, ⁴Department of Biotechnology, Maharaja Sriram Chandra Bhanjdeo University, Baripada, India, ⁵Department of General Medicine, VSS Medical College and Hospital, Sambalpur, India

LAMP diagnosis of malaria is simple and cost-effective with acceptable sensitivity and specificity as compared to standard diagnostic modules such as microscopy, RDTs and nested PCR, and thus its deployment for onsite screening of malaria in resource-limited regions is under consideration. However, the requirement of an electricity-operated dry bath and bulky read-out unit is still a major concern. In an effort to simplify this limitation, we have developed a portable LAMP device and fluorescence readout unit which can be used in the rapid point-of-care diagnosis of malaria. We have developed a point-of-care diagnostic LAMP device that is easy to operate by a mobile application, and the results can be quantified with a fluorescent readout unit. The diagnostic performance of the device was evaluated in 90 *P. falciparum*-infected clinical isolates stored at 4°C for 6–7 years and 10 freshly collected isolates from healthy volunteers. The LOD and quantitative ability of LAMP in estimating parasitemia levels were revealed with laboratory-grown *P. falciparum* strain (3D7). The LAMP assay performed in our device was exclusive for *P. falciparum* detection with sensitivity and specificity determined to be 98.89% and 100%, respectively, in clinical isolates. The LOD was documented to be 1 parasite/μl at the cut-off ADC value of 20. Parasite density estimated from ADC values showed concordance with microscopically determined parasite density of the cultured *P. falciparum* 3D7 strain. The LAMP assay performed in our device provides a possible portable platform for its deployment in the point-of-care diagnosis of malaria. Further validation of the quantitative ability of the assay with freshly collected or properly stored clinical samples of known parasitemia is necessary for field applicability.

KEYWORDS

LAMP, *plasmodium falciparum*, diagnosis, LOD, parasite density, ADC value

Introduction

Malaria is a global health problem with an estimated 241 million cases and 627,000 deaths reported in 2020 (WHO, 2021). Human malaria is caused by six species of *Plasmodium* (*P. falciparum*, *P. vivax*, *P. malariae*, *P. ovale*, *P. knowlesi* and *P. simium*). Early diagnosis with prompt and species-specific effective treatment plays a crucial role in the improved care of patients and subsequent outcomes. Because clinical diagnosis is non-specific and unreliable, the World Health Organization (WHO) recommends treatment of only parasitologically confirmed cases of malaria with appropriate anti-malarial drugs. While microscopy serves as the gold standard for malaria diagnosis, detection of parasite-specific antigens/antibodies by rapid diagnostic tests (RDTs) has been a widely adopted point-of-care diagnosis method (Kotepui et al., 2020). However, malaria diagnosis by both these methods is challenging when the parasite density is low or the patient has been recently treated. While the limit of detection (LOD) by microscopy is about 88 parasites/ μ l of blood (Joanny et al., 2014), it is about 100–200 parasites/ μ l of blood by RDT (Mwesigwa et al., 2019). Interestingly, almost all the RDTs use histidine-rich protein-2 (HRP2) antigen for *P. falciparum* detection because of its exclusive expression in all stages of *P. falciparum* growth in the blood (Rock et al., 1987). However, recent studies have reported reduced sensitivity of HRP2 based RDTs in different malaria-endemic regions, especially in regions where the circulating populations of *P. falciparum* have *pfrp2* gene deletion or there is genetic variability in the target epitopes (leading to its presence or absence and copy number variation) within PfHRP2 (Poti et al., 2020).

Although a significant reduction in malaria incidence and deaths has been achieved over the last few decades, failure to detect asymptomatic patients and sub-microscopic infections in surveillance studies contributes to ongoing transmission and is a major threat to malaria control and elimination goals. In light of this, nucleic acid-based detection is promising because of its high sensitivity and specificity. The most reliable among these is diagnosis by nested PCR which has a LOD of 1 to 0.1 parasites/ μ l of blood (Wang et al., 2014). However, the requirement of expensive equipment and reagents and long turnaround time (due to sample processing to remove inhibitors of polymerase from the body fluid, reaction time and post-PCR events to visualize the amplified products) render PCR-based methods to be inadequate for point-of-care diagnosis and routine diagnosis in resource-limited settings.

Loop-mediated isothermal amplification (LAMP) method of malaria diagnosis is emerging as a recent alternative to PCR and can be employed directly on whole blood samples (with minimal processing) and purified DNA or RNA. Further, LAMP diagnosis of malaria has excellent sensitivity (as low as 0.5 to 0.05 parasites/ μ l) comparable to that of PCR and turnaround

time similar to RDTs depending upon the target DNA, improvement of read-out procedures and mitigation of DNA extraction process (Sattabongkot et al., 2014). However, commercial LAMP kits often require a bulky dry bath and a read-out unit such as a fluorescence spectrophotometer which restricts the applicability of LAMP in fieldwork or point-of-care analysis. Therefore, we have developed a portable, rapid, point-of-care LAMP assay system that comprises a LAMP device and a fluorescence readout unit for the diagnosis of *P. falciparum* malaria. Further, although LAMP is shown to be promising in diagnosing asymptomatic patients and sub-microscopic infections (Cook et al., 2015; Katrak et al., 2017), whether it is comparable to PCR in detecting malaria infection in stored and degraded blood samples is still unknown. Until now, LAMP has been used for the qualitative detection of malaria infection, however, its quantitative potential for estimating parasitemia level has been largely overlooked. Therefore, in the present study, we aimed to compare the diagnostic performance of the LAMP assay performed in our device with PCR using stored and degraded blood samples which were previously confirmed for *P. falciparum* infections by microscopy, RDT and PCR. Moreover, the ability of the LAMP assay in estimating sample parasitemia has also been demonstrated using the laboratory-grown *P. falciparum* strain (3D7).

Materials and methods

Chemicals

Bst DNA polymerase large fragment, magnesium sulphate and deoxynucleotide phosphates (dNTPs) were purchased from NEB (Ipswich, MA, USA). Thermo Pol Buffer was provided with the enzyme. Betaine, hypoxanthine and sodium bicarbonate were brought from Sigma-Aldrich (St. Louis, MO, USA). AlbuMax I was purchased from Gibco, Grand Island, NY, USA, and SYBR Gold nucleic acid stain (10,000x concentration) was purchased from Thermo Fischer Scientific (Waltham, MA, USA). RPMI 1640 media was obtained from Invitrogen, Carlsbad, CA, USA. All other materials used were of analytical grade and commercially available.

Parasite culture and isolation of dna

P. falciparum 3D7 strain was cultured in O+ve human erythrocytes (obtained from Rotary blood bank, New Delhi, India) at 2% hematocrit and incubated with mixed gas (5% O₂, 5% CO₂ and 90% N₂) condition in RPMI 1640 media supplemented with hypoxanthine (27.2 mg/L), sodium bicarbonate (2 gm/L) and AlbuMax I (0.5 gm/L) based on an established protocol (Trager and Jensen, 1976). Cultures of 3D7

maintained at 10% parasitemia were used for *P. falciparum* DNA isolation using the phenol-chloroform extraction method.

Study population and DNA isolation from clinical samples

Blood samples used for the detection of *P. falciparum* infections in LAMP assay were collected from Sambalpur, Odisha, India during 2012–2014, the details of which including inclusion and exclusion criteria are mentioned in our previous publication [Dhangadamajhi et al., 2019](#). About 90 of these randomly selected samples stored at 4°C for about 6–8 years, positive for *P. falciparum* infections in the peripheral blood smear and confirmed by the species-specific PCR diagnosis method of [Snounou et al. \(1993\)](#), were used for DNA isolation by the phenol-chloroform method as described previously ([Panigrahi et al., 2016](#)). RDT test (SD Bioline) of about 40 of these samples also confirmed *P. falciparum* infection. Freshly isolated DNA from 10 healthy volunteers was used as a negative control.

LAMP primer design

The sequences for 6 set of primers to amplify *P. falciparum* 18S rRNA were taken from ([Han et al., 2007](#)). Primer sequences are given in [Table 1](#).

LAMP assay

LAMP assay was performed in the device as previously described ([Puri et al., 2021](#)). Briefly, a working dilution of 10X was prepared from primer stocks (100 µM). This 10 X dilution comprised of 16 µM FIP, 16 µM BIP, 8 µM LPF, 8 µM LPB, 2 µM F3 and 2 µM B3C primers. The LAMP reaction contained 1X primer mix, 1X Thermo Pol buffer, 1.4 mM dNTPs, 6 mM MgSO₄, 8 units of Bst DNA polymerase, 0.8 M betaine and template DNA. Nuclease-free water was added to the reaction to make up the volume to 25 µl. To check the lowest concentration at which LAMP assay can detect infection, a reaction was set up with serial dilutions containing 0.000001%, 0.00001%, 0.00005%, 0.0001%, 0.0005%, 0.001%, 0.01%, 0.1%, 1% and 10% parasitemia of *P. falciparum* 3D7 genomic DNA. As a control, DNA from a sample with zero parasitemia, i.e., only blood, was also subjected to LAMP assay. Clinical samples were diluted to 100 pg to use as templates in the LAMP reaction. A non-template control was used as a negative control in every reaction. To ascertain that the LAMP primers were specific to *P. falciparum*, they were tested with genomic DNA from *P. vivax* and *L. donovani*. The reaction was performed at 60°C for 100 min in the LAMP device.

Detection of LAMP amplification

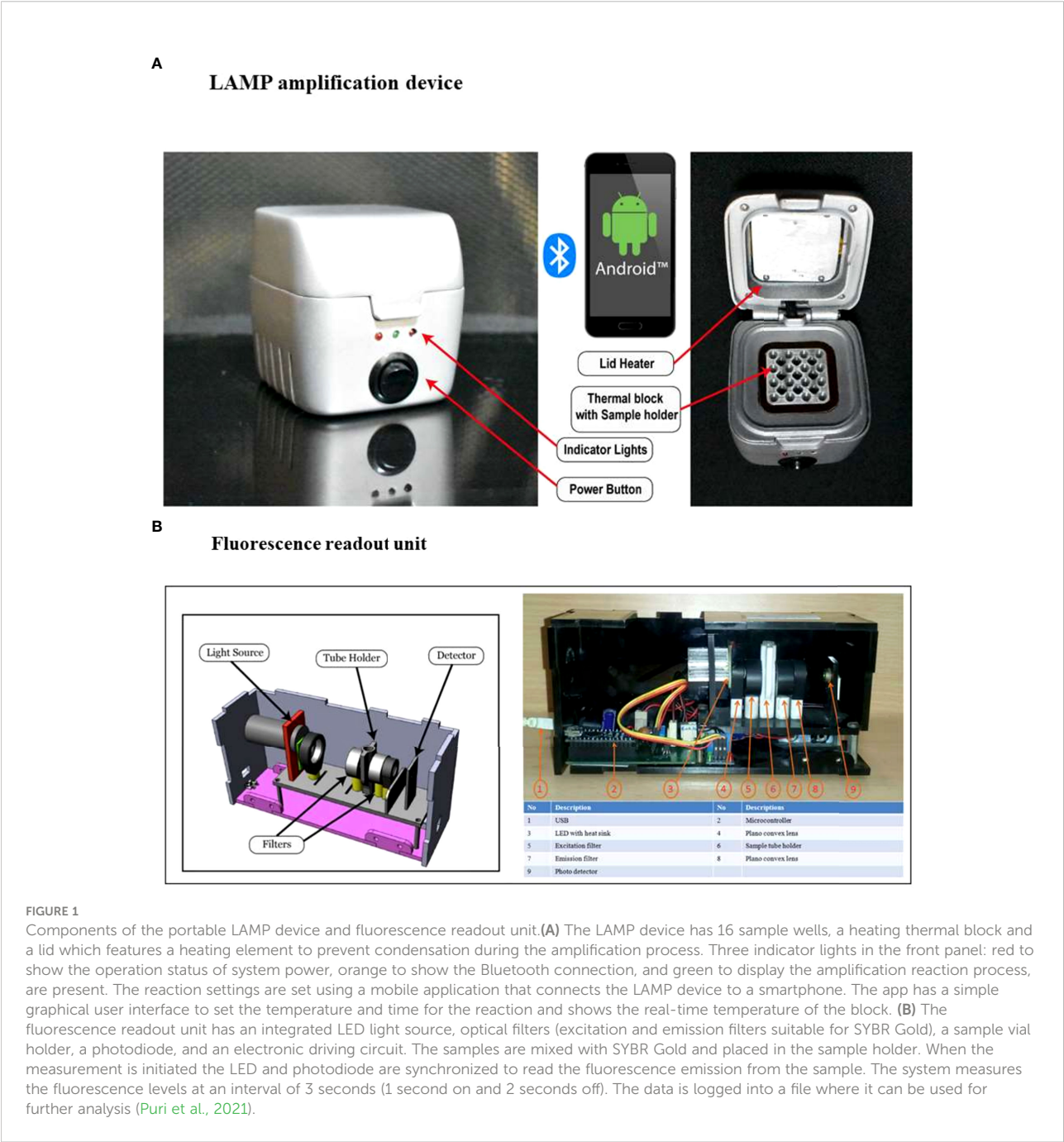
Two µl of SYBR gold dye was added to the reaction mixture to detect the amplification. Before use, the dye was diluted 10 times in nuclease-free water. SYBR gold is color sensitive and in the presence of amplification, it changes its color from orange to green. The change was visible with the naked eye and for quantification, LAMP products were placed inside the readout unit which measured the fluorescence intensity upon amplification (ADC values). The ADC values were directly proportional to the amount of amplified product. Amplification was also confirmed by electrophoresing 3 µl of the reaction mixture on a 2.5% agarose gel followed by staining it with ethidium bromide for visualization. LAMP positive samples displayed the characteristic ladder-like pattern.

LAMP amplification device and fluorescence readout unit

The LAMP amplification device which can be operated *via* a mobile application and fluorescent readout unit used in this study were the same as described by [Puri et al., 2021](#). Briefly, the core of the LAMP device consists of a resistive heating block and a system controller placed in a 3D printed casing shown in ([Figure 1A](#)). The heating block heats and holds samples at specific temperatures, ranging between 40–90°C, and the system controller maintains the specific temperature and time duration set by the user. The reaction temperature for amplification can be set between 50–72°C. For point-of-care applications, it is imperative to provide the test results immediately after completion of the test, therefore, a portable LAMP readout unit has been developed ([Figure 1B](#)). This unit is designed to analyze the test samples using nucleic acid intercalating dyes, such as the SYBR Gold nucleic acid stain. The components include a high-power LED with a wider spectrum (LXML-PE01-0070-High Power LEDs - Single Color Cyan 70lm, 350mA wavelength range of 490–515nm), an excitation filter between the LED and sample (CWL 490nm, Dia 12.5mm, BW: 15nm for excitation), a 15 mm focus lens, an emission filter (CWL 520 nm, Dia 12.5 mm, BW: 15 nm), a collector lens, and an LTC 1051 op-amp. The signal from the op-amp is read by the ADC pin of the microcontroller (Atmega328P) and can be recorded on a laptop using the software. The emitted fluorescence values are read at a 3-second interval wherein the LED is on for 1 second and off for the remaining 2 seconds. Our LAMP system has an edge over other LAMP systems in the market, as it can test a higher number of samples (16 samples) simultaneously than the Axxin Molecular T8 and Diagenetix Bioranger systems (8 samples) and the Dialunox ESEQuant TS2 (12 samples), and is more compact than the Agdia AmplifyRP system.

TABLE 1 List of LAMP primers used.

Primer	Sequence
Forward inner primer (FIP)	5' AGCTGGAATTACCGCGGCTG GGTTCCTAGAGAAACAATTGG 3'
Backward inner primer (BIP)	5' TGTTGCAGTTAAAACGTTTCGTAGCCCAAACCAAGTTTAAATGAAAC 3'
F3	5' TGTAAATTGGAATGATAGGAATTTA 3'
B3c	5' GAAAACCTTATTTGAACAAAGC 3'
LPF	5' GCACCAGACTTGCCCT 3'
LPB	5' TTGAATATTAAAGAA 3'



Statistical analysis

LAMP assay ADC value data were analyzed by GraphPad prism and represented as mean \pm standard error of the mean (S.E.M.). A standard curve was plotted using log-transformed parasitemia value on the x-axis and ADC value on the y-axis. For the prediction of parasitemia from the ADC value, the inverse logarithm value was calculated by raising the base10 to the logarithm of the log-transformed parasitemia value corresponding to a different ADC value. The percentage sensitivity, specificity and accuracy with 95% confidence intervals (CI) were calculated using Medcalc software as previously described by Puri et al., 2021.

Results

Exclusivity of the LAMP assay performed in the device

To determine if the LAMP assay performed in the device was exclusive to *P. falciparum*, 1 ng of genomic DNA from *Leishmania donovani* Bob strain and *P. vivax* was subjected to

LAMP assay in the device using primers specific to *P. falciparum* 18S rRNA. One ng of genomic DNA from *P. falciparum* was taken as a positive control in the same assay. To visualize amplification, one aliquot of LAMP products was incubated with SYBR Gold stain and another aliquot was electrophoresed on an agarose gel. There orange to green color change with SYBR Gold addition and the characteristic ladder-like band pattern was observed only in the *P. falciparum* sample and not in the *L. donovani* and *P. vivax* samples, thereby indicating that the 18S rRNA primers did not amplify *L. donovani* and *P. vivax* DNA and were specific to *P. falciparum* (Figures 2A–C). Therefore, these experiments demonstrate that the LAMP assay performed in the device was exclusive to *P. falciparum*.

Quantification ability and limit of detection of *P. falciparum* DNA amplified in the LAMP device

An essential parameter to evaluate the analytical performance of the LAMP device was to calculate the limit of detection of *P. falciparum* DNA that can be amplified. For this,

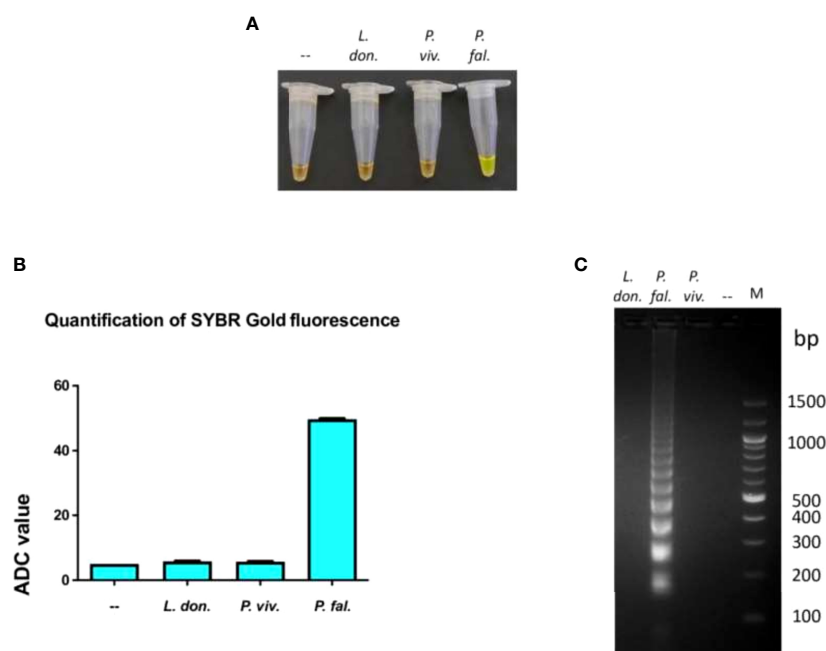


FIGURE 2

Exclusivity of the LAMP reaction performed in the device. The exclusivity of the LAMP reaction performed in the device was determined. One ng of genomic DNA from each of *L. donovani* Bob, *P. vivax* and *P. falciparum* strains was used in a LAMP reaction along with *P. falciparum* LAMP primers for 100 minutes, as described in Materials and Methods. (A) The confirmation of LAMP amplification was done by SYBR Gold detection. Diluted SYBR Gold nucleic acid stain was added to the LAMP products, and the color change was detected by visual examination. --: non-template control. (B) The quantification of SYBR Gold fluorescence was done by measuring the fluorescence intensity of the samples by a detection device, designated as ADC values. The mean + SEM of 10 ADC values are plotted for each sample. (C) Electrophoresis of LAMP products on a 2.5% agarose gel. M: 100 bp DNA ladder.

DNA isolated from *P. falciparum* cultures with 10% parasitemia serially diluted to 0.000001% parasitemia was tested for amplification. A negative control sample with zero parasitemia, i.e., only blood, was also included in the reaction. It was observed that DNA from cultures containing 0.00001 to 10% parasitemia could be amplified in the LAMP device, and the zero parasitemia control sample was not amplified (Figures 3A–C). Therefore, the limit of detection of the LAMP device was 1 parasite/μl of *P. falciparum* culture (as estimated by counting the number of trophozoites/100 RBCs). To ascertain if parasitemia can also be estimated from ADC value, 1 ng of genomic DNA isolated from different parasitemia of *P. falciparum* cultures (0.5, 1, 2 and 5%) were used in the LAMP assay. The ADC value obtained against these samples was used for parasite density estimation using the calibration equation ($y = 6.679x + 52.13$, $R^2 = 0.9751$) of serially diluted genomic DNA of *P. falciparum* (Figure 3B). The results showed an excellent agreement of parasitemia estimated from ADC value with parasitemia value determined by microscopy (Table 2).

Detection of *P. falciparum* DNA in patient samples

To test the ability of the LAMP device to detect and amplify *P. falciparum* DNA in clinical samples, DNA isolated from the stored blood of 90 malaria patient samples (which were previously confirmed for *P. falciparum* infections by standard diagnostic tests such as Quantitative Buffy Coat (QBC) and PCR were used in a LAMP assay in our device (Table S1). Additionally, 40 of these samples were also randomly tested positive by RDT (Table S1). In the LAMP assay, 89 samples were found to be positive and 1 was negative (Table S1). A representative image of LAMP assay data from 10 clinical samples is shown in (Figures 4A–C). In clinical samples, we did not find any correlation between ADC values and parasitemia. As a control, freshly isolated DNA from 10 healthy volunteers was also tested in the LAMP assay in our device and no amplification was observed (Supplementary Figures 1A–C).

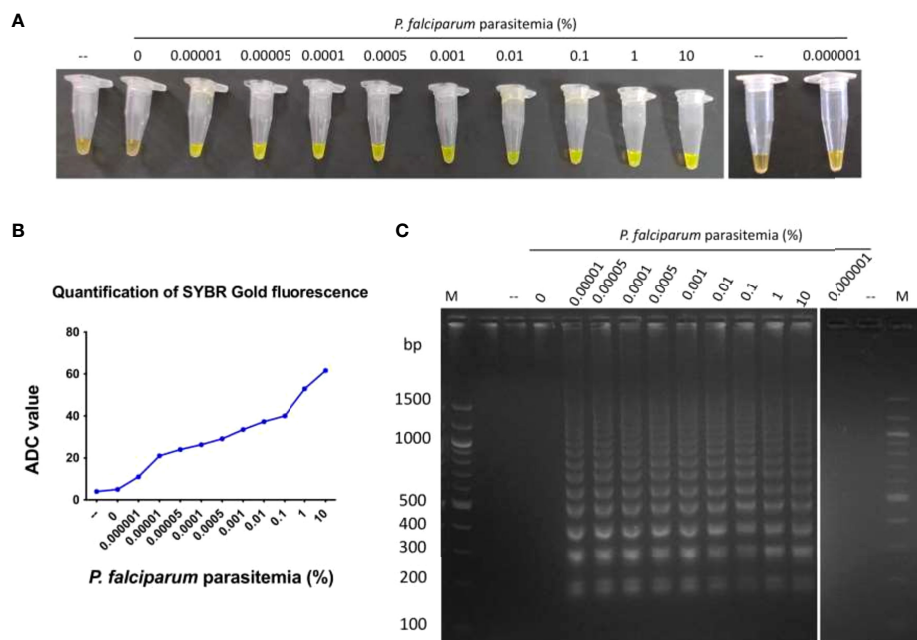


FIGURE 3

Limit of detection of *P. falciparum* genomic DNA amplified in the LAMP device. DNA isolated from *P. falciparum* cultures containing 0.000001 to 10% parasitemia was used in a LAMP reaction for 100 minutes, as described in Materials and Methods. As a control, DNA isolated from a sample containing zero parasitemia, i.e., only blood, was also tested in the LAMP reaction. (A) The confirmation of LAMP amplification was done by SYBR Gold detection. Diluted SYBR Gold nucleic acid stain was added to the LAMP products, and the color change was detected by visual examination. --: non-template control. (B) The quantification of SYBR Gold fluorescence was done by measuring the fluorescence intensity of the samples by a detection device, designated as ADC values. The mean + SEM of 10 ADC values are plotted for each sample. (C) Electrophoresis of LAMP products on a 2.5% agarose gel. M: 100 bp DNA ladder.

TABLE 2 Comparison of parasitemia estimated from ADC value with parasitemia determined by microscopy.

Parasitemia (%)	ADC value	Parasitemia estimated from ADC value
0.5	50	0.479
1	52	0.954
1.5	53	1.347
2	54	1.902
5	57	5.35

Comparison of diagnostic test evaluation parameters of QBC, ICT and *P. falciparum* PCR tests with the LAMP assay

An evaluation of the analytical performance of the LAMP assay, in comparison to that of QBC, ICT and *P. falciparum* PCR tests was performed (Table 3). Out of the total 100 (90 positive and 10 healthy volunteer) samples tested in the LAMP device, 1 false-negative and no false-positive results were obtained. The LAMP assay performed in the device demonstrated excellent sensitivity (98.89%; 95% CI= 93.96–99.97), specificity (100%; 95% CI= 69.15% to 100.00%) and accuracy (99.01%; 95% CI= 94.61% to 99.97%).

Discussion

The LAMP-based detection of human malaria exhibits acceptable sensitivity and specificity as compared to microscopy, RDTs and nested PCR, irrespective of *Plasmodium* species (Han et al., 2007; Paris et al., 2007; Yamamura et al., 2009). Further, LAMP being less expensive, simple and having the potential of amplifying both RNA and DNA at a constant temperature, its deployment for molecular testing of malaria in resource-limited regions is under consideration. However, the bulkiness of the dry bath and readout unit is still a major concern that may be likely to restrict the field applicability of LAMP in point-of-care diagnosis. In an effort to simplify this limitation, we have developed a compact LAMP device and fluorescence readout unit, both of which are portable, and have the potential to be used in the rapid point-of-care diagnosis of malaria.

Recently, considerable progress has been made in the development of LAMP diagnostic systems for malaria diagnosis. A LAMP-based lateral flow device method has been devised for the detection of malaria that uses biotin-labeled and fluorescein amidite-labeled loop primers in the LAMP reaction, and the end-product can be visualized on a dipstick (Malleshetti et al., 2018). This study tested 90 samples of *P. knowlesi* infection, 49 samples of *P. falciparum* infection, 56 samples of

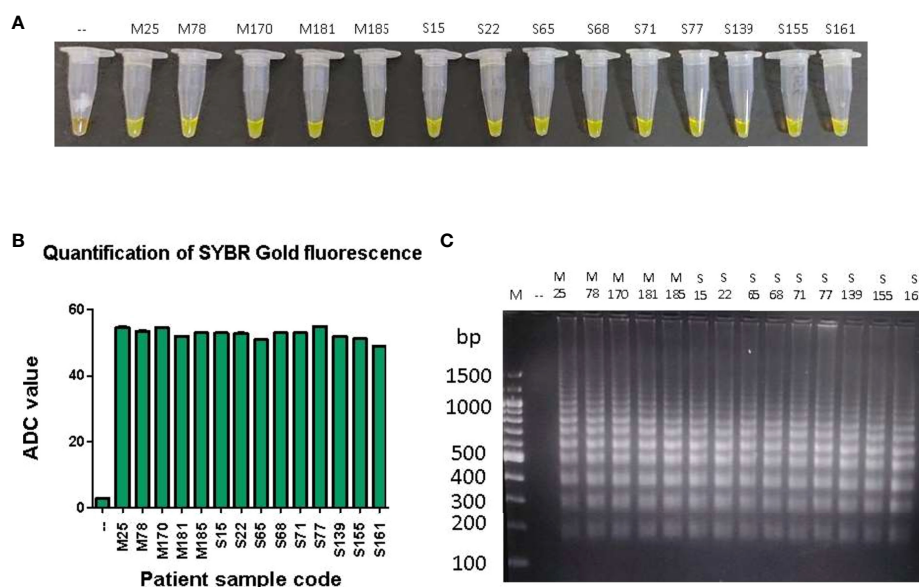


FIGURE 4

LAMP amplification of *P. falciparum* DNA from patient samples. One hundred pg of DNA from 90 patient samples were used in a LAMP reaction for 100 minutes, as described in Materials and Methods. (A) The confirmation of LAMP amplification was done by SYBR Gold detection. Diluted SYBR Gold nucleic acid stain was added to the LAMP products, and the color change was detected by visual examination. --: non-template control. (B) The quantification of SYBR Gold fluorescence was done by measuring the fluorescence intensity of the samples by a detection device, designated as ADC values. The mean + SEM of 10 ADC values are plotted for each sample. (C) Electrophoresis of LAMP products on a 2.5% agarose gel. M: 100 bp DNA ladder.

TABLE 3 Comparison of diagnostic test evaluation parameters of ITS-1 PCR and LAMP assay.

Parameters	QBC	RDT	PCR	LAMP assay
True positives	90	40	90	89
False negatives	0	0	0	1
True negatives	10	10	10	10
False positives	0	0	0	0
Sensitivity (%) (95% CI)	100.00 (95.98 - 100.00)	100.00 (91.19 - 100.00)	100.00 (95.98 - 100.00)	98.9 (94.03 - 99.97)
Specificity (%) (95% CI)	100 (69.15 - 100.00)	100 (69.15 - 100.00)	100 (69.15 - 100.00)	100 (69.15 - 100.00)
Accuracy (%) (95% CI)	100 (96.38 - 100.00)	100 (92.89 - 100.00)	100 (96.38 - 100.00)	99.01 (94.61 - 99.97)

Confidence intervals for sensitivity are exact Clopper-Pearson confidence intervals. Confidence intervals for predictive values are the standard logit confidence intervals given by (Mercaldo et al., 2007).

P. vivax infection, 15 samples of mixed infection with *P. falciparum* and *P. vivax*, 60 non-malaria infected human samples, one of *Toxoplasma gondii* infection, one of *Sarcocystis* spp. infection, and eight healthy donor samples. Their results indicated that all 90 *P. knowlesi* and *P. vivax* samples were positively amplified by the LAMP-LFD assay. However, one *P. falciparum* and one mixed-infection sample was not amplified, possibly because of low parasitemia or DNA degradation. Another study has reported the development of a paper-based microfluidic device that enables multiplex LAMP-based detection of malaria in the blood (Reboud et al., 2019). Although this offers a very cheap and simple alternative to the conventional LAMP assay, however, local climatic conditions like variations in temperature and humidity can affect test results by altering the rates of evaporation and speed of fluid movement during sample introduction into microfluidic matrices. A commercial Loopamp MALARIA Pan Detection Kit has also been developed by Eiken Chemical Co., Ltd., Tokyo, Japan, with a LOD of 20 parasites/μl for *P. falciparum* (Piera et al., 2017), which is considerably higher than that obtained in the LAMP assay performed in our device (1 parasite/μl).

Our LAMP system offers numerous advantages over contemporary LAMP diagnostic modules. The LAMP device is Bluetooth-enabled, compact, light-weight, and portable. It is also very user-friendly, as it is operated and controlled via a dedicated mobile application, thereby making remote operation possible. The fluorescent readout unit can be connected to a computer/laptop for recording ADC values and subsequent data analysis. More importantly, because assay cost is a limiting factor for diagnosis in under-developed and developing countries where malaria is endemic, we have developed a cost-effective diagnostic testing system in which one test costs less than 1.5 USD.

Using *P. falciparum*-specific LAMP primers (Han et al., 2007), we successfully diagnosed *P. falciparum* infections in previously confirmed stored blood samples with 98.89% sensitivity and 100% specificity by our LAMP device. The LAMP assay could not detect *P. falciparum* infection in one

sample. The same sample could also not be amplified with *P. falciparum*-specific primers in a nested PCR test, which indicates a possible degradation of parasite DNA. Interestingly, no color change was detected in the samples containing genomic DNA for *P. vivax*, *L. donovani* and healthy human volunteers, which depicts the exclusivity of the assay for *P. falciparum* DNA. In the present study, the LOD was determined to be as low as 0.00001% parasitemia (which is about 1 parasite/μl). Previous studies using similar LAMP primers have documented a LOD of 2 parasites/μl (Oriero et al., 2015). The LOD for parasite genomic DNA isolated by a simple heat-treated method is reported to be about 40 parasites/μl (Lucchi et al., 2016), whereas by chemical lysis with Illumigene lysis buffer is 0.5 parasites/μl (De Koninck et al., 2017). Further, LOD has been shown to vary with sample types (culture or clinical samples) and the base parasitemia level used for DNA isolation. Despite these variations, the excellent performance of our LAMP assay system could be due to the efficient extraction process for the high yield of parasite genomic DNA and the use of cultured parasites for DNA isolation. Since the present study aimed to validate the diagnostic performance of the LAMP assay system in diagnosing confirmed cases of *P. falciparum* infections, variations in LOD due to differences in DNA isolation processes, sample types, or base level parasite density were not examined. However, simple and rapid DNA isolation procedures like heat-treatment or rapid DNA extraction by chemical lysis seem to have field applicability in point-of-care LAMP diagnosis and require to be tested for determining the LOD.

Apart from the identification of *Plasmodium* species, the determination of parasite density is crucial for effective anti-malarial therapy and to understand the transmission dynamics and relative distribution of malaria species. However, LAMP-based diagnosis has been primarily used for qualitative screening. Microscopy and/or real-time PCR remain(s) essential for quantitative estimation of parasite density. Our approach to detecting *P. falciparum* infection through ADC value has an additional advantage of estimating parasite density.

A cut-off ADC value of ~ 20 (value for 0.00001% parasitemia) represented the presence of *P. falciparum* infection. More specifically, a significant positive correlation between serially diluted parasite genomic DNA isolated from fixed parasitemia (10%) and their corresponding ADC values uncovered its potential for parasite density estimation. Based on the calibration equation of ADC value, using *in vitro* cultures of *P. falciparum*, we successfully estimated parasite density which corroborated with the parasitemia obtained by microscopy. However, our attempt of estimating parasite density could not be replicated with DNA isolated from stored blood samples. The failure to quantify parasite density in clinical samples could be due to the degradation of parasite DNA during storage, as stored samples that were previously *P. falciparum* PCR-positive when re-analyzed by LAMP assay and PCR were observed to be negative. Furthermore, almost all the LAMP-positive clinical samples had ADC values between 40 and 57 despite their major differences in parasite density at the time of sample collection (data not shown). This narrow range of ADC values and PCR-negative results of *P. falciparum*-infected stored blood samples ascertained the degradation of parasite DNA during storage. Therefore, the parasite density estimation potential of our LAMP-based assay needs to be validated with freshly collected and properly stored clinical samples for its possible application in the field.

Although LAMP diagnosis has been proven to be highly sensitive and specific in diagnosing symptomatic malaria infections, its performance against thawed and degraded blood samples still remains unknown. In light of this, the results of the present study demonstrating the superior diagnostic performance of our LAMP assay system with improperly stored blood samples highlights the diagnostic ability of LAMP in degraded samples. To our knowledge, this is the first study that has tested *P. falciparum* malaria infection by LAMP assay in stored blood samples with possible degradation of parasite genomic DNA. Besides symptomatic infections, LAMP is also proven beneficial in diagnosing asymptomatic malaria with low or sub-microscopic parasitemia (Cook et al., 2015; Katrak et al., 2017). Based on its performance with degraded samples, we anticipate similar or better efficacy of our LAMP assay system for low-density infections, however, for this, field studies with a larger number of samples are warranted. Further, our preliminary study conducted with *P. falciparum*-specific LAMP primers needs to be extrapolated with other human malaria-causing *Plasmodium* species in future studies. Our study is limited by the fact that the 90 PCR-positive *P. falciparum* clinical samples stored for about 6–8 years could not be re-tested for PCR positivity before their use in LAMP assay due to the non-availability of DNA in adequate amounts. Since the current PCR-positive status of these samples might not be the same as it was before 6–8 years due to sample age and storage conditions, our inclusion of PCR data performed 6–8 years ago may influence the observed sensitivity and specificity of our LAMP assay. However, consistent reports of false-negative

results by both PCR and LAMP in one sample (due to possible degradation of DNA), and lack of false positivity by LAMP assay are the strengths of our LAMP test.

In conclusion, the reported LAMP assay system provides a possible portable platform for its deployment in the molecular testing of malaria in point-of-care diagnosis. Our validation of the quantitative potential of this system to estimate parasite density in laboratory-grown *P. falciparum* strain and its excellent diagnostic performance on stored and degraded clinical samples highlights its field applicability in the diagnosis of malaria. Future studies from our laboratory are directed towards testing freshly collected or properly stored symptomatic and asymptomatic clinical samples of known parasitemia using our LAMP device.

Data availability statement

The original contributions presented in the study are included in the article/Supplementary Material. Further inquiries can be directed to the corresponding authors.

Ethics statement

The studies involving human participants were reviewed and approved by IBSC, JNU, New Delhi (Ref Number: JNU/IBSC/2020/17). The patients/participants provided their written informed consent to participate in this study.

Author contributions

Conceptualization, ReM, SG, SS and RoM; Methodology, ReM, SS, SG, GD, MP, RS and KR; Investigation, MP, HB, EM, GK, RSr, SO, RSa and SP; Writing- original draft, MP, HB, ReM, SS and GD; Writing-review and editing, MP, SS, GD, RoM, and ReM. Funding acquisition, ReM, RoM, SS, SG and GD; Supervision, ReM, RoM, SS, SG and GD. All authors contributed to the article and approved the submitted version.

Funding

ReM was funded by EMR/2016/004948 from Science and Engineering Research Board, India (<https://www.serbonline.in/SERB/HomePage> do) and VI-D&P/569/2016-17/TDT/C from Department of Science and Technology, India (www.dst.gov.in). MP and EM were supported by the D. S. Kothari Post-Doctoral Fellowship from UGC. HB was supported by a fellowship from CSIR. The funders had no role in study design, data collection and analysis, decision to publish, or preparation of the manuscript.

Acknowledgments

We thank the Central Instrumentation Facility at the School of Life Sciences, Jawaharlal Nehru University, for providing the instrumentation facility. ReM is an A. S. Paintal Distinguished Scientist Chair of ICMR. This research was partly supported by the Gore Subraya Bhat chair in Digital Health, awarded to SG, and Meity-DST.

Conflict of interest

The authors declare that the research was conducted in the absence of any commercial or financial relationships that could be construed as a potential conflict of interest.

References

- Cook, J.Aydin-Schmidt, B.González, I. J.Bell, D.Edlund, E.Nassor, M. H., et al. (2015). Loop-mediated isothermal amplification (LAMP) for point-of-care detection of asymptomatic low-density malaria parasite carriers in Zanzibar. *Malar J.* 14, 43. doi: 10.1186/s12936-015-0573-y
- De Koninck, A. S.Cnops, L.Hofmans, M.Jacobs, J.Van den Bossche, D.Philippé, J. (2017). Diagnostic performance of the loop-mediated isothermal amplification (LAMP) based illumigene® malaria assay in a non-endemic region. *Malar J.* 16 (1), 418. doi: 10.1186/s12936-017-2065-8
- Dhangadamajhi, G.Panigrahi, S.Roy, S.Tripathy, S. (2019). Effect of plasmodium falciparum infection on blood parameters and their association with clinical severity in adults of odisha, India. *Acta Trop.* 190, 1–8. doi: 10.1016/j.actatropica.2018.10.007
- Han, E. T.Watanabe, R.Sattabongkot, J.Khuntirat, B.Sirichaisinthop, J.Irako, H., et al. (2007). Detection of four plasmodium species by genus- and species-specific loop-mediated isothermal amplification for clinical diagnosis. *J. Clin. Microbiol.* 45 (8), 2521–2528. doi: 10.1128/JCM.02117-06
- Joanny, F.Löhr, S. J.Engleitner, T.Lell, B.Mordmüller, B. (2014). Limit of blank and limit of detection of plasmodium falciparum thick blood smear microscopy in a routine setting in central Africa. *Malar J.* 13, 234. doi: 10.1186/1475-2875-13-234
- Katrak, S.Murphy, M.Nayebare, P.Rek, J.Smith, M.Arinitwe, E., et al. (2017). Performance of loop-mediated isothermal amplification for the identification of submicroscopic plasmodium falciparum infection in Uganda. *Am. J. Trop. Med. Hyg.* 97 (6), 1777–1781. doi: 10.4269/ajtmh.17-0225
- Kotepui, M.Kotepui, K. U.De Jesus Milanez, G.Masangkay, F. R. (2020). Summary of discordant results between rapid diagnosis tests, microscopy, and polymerase chain reaction for detecting plasmodium mixed infection: a systematic review and meta-analysis. *Sci. Rep.* 10 (1), 12765. doi: 10.1038/s41598-020-69647-y
- Lucchi, N. W.Gaye, M.Diallo, M. A.Goldman, I. F.Ljolie, D.Deme, A. B., et al. (2016). Evaluation of the illumigene malaria LAMP: A robust molecular diagnostic tool for malaria parasites. *Sci. Rep.* 6, 36808. doi: 10.1038/srep36808
- Malleppadi, P. C.Lai, M. Y.Podha, S.Ooi, C. H.Liew, J. W.Polavarapu, R., et al. (2018). Development of loop-mediated isothermal amplification-based lateral flow device method for the detection of malaria. *Am. J. Trop. Med. Hyg.* 99 (3), 704–708. doi: 10.4269/ajtmh.18-0177
- Mercaldo, N. D.Lau, K. F.Zhou, X. H. (2007). Confidence intervals for predictive values with an emphasis to case-control studies. *Stat. Med.* 26, 2170–2183. doi: 10.1002/sim.2677
- Mwesigwa, J.Slater, H.Bradley, J.Saidy, B.Ceasay, F.Whittaker, C., et al. (2019). Field performance of the malaria highly sensitive rapid diagnostic test in a setting of varying malaria transmission. *Malar J.* 18 (1), 288. doi: 10.1186/s12936-019-2929-1
- Oriero, C. E.van Geertruyden, J. P.Jacobs, J.D'Alessandro, U.Nwakanma, D. (2015). Validation of an apicoplast genome target for the detection of plasmodium species using polymerase chain reaction and loop mediated isothermal amplification. *Clin. Microbiol. Infect.* 21 (7), 686 e1–686.e7. doi: 10.1016/j.cmi.2015.02.025
- Panigrahi, S.Kar, A.Tripathy, S.Mohapatra, M. K.Dhangadamajhi, G. (2016). Genetic predisposition of variants in TLR2 and its co-receptors to severe malaria in odisha, India. *Immunol. Res.* 64 (1), 291–302. doi: 10.1007/s12026-015-8749-7
- Paris, D. H.Imwong, M.Faiz, A. M.Hasan, M.Yunus, E. B.Silamut, K., et al. (2007). (LAMP) for the diagnosis of falciparum malaria. *Am. J. Trop. Med. Hyg.* 77 (5), 972–976.
- Piera, K. A.Aziz, A.William, T.Bell, D.González, I. J.Barber, B. E., et al. (2017). Detection of plasmodium knowlesi, plasmodium falciparum and plasmodium vivax using loop-mediated isothermal amplification (LAMP) in a co-endemic area in Malaysia. *Malar J.* 16 (1), 29. doi: 10.1186/s12936-016-1676-9
- Poti, K. E.Sullivan, D. J.Dondorp, A. M.Woodrow, C. J. (2020). HRP2: Transforming malaria diagnosis, but with caveats. *Trends Parasitol.* 36 (2), 112–126. doi: 10.1016/j.pt.2019.12.004
- Puri, M.Brar, H. K.Mittal, N.Madan, E.Srinivasan, R.Rawat, K., et al. (2021). Rapid diagnosis of leishmania infection with a portable loop-mediated isothermal amplification device. *J. Biosci.* 46 (4), 92. doi: 10.1007/s12038-021-00211-0
- Reboud, J.Xu, G.Garrett, A.Adriko, M.Yang, Z.Tukaheba, E. M., et al. (2019). Paper-based microfluidics for DNA diagnostics of malaria in low resource underserved rural communities. *Proc. Natl. Acad. Sci. U S A.* 116 (11), 4834–4842. doi: 10.1073/pnas.1812296116
- Rock, E. P.Marsh, K.Saul, A. J.Wellems, T. E.Taylor, D. W.Maloy, W. L., et al. (1987). Comparative analysis of the plasmodium falciparum histidine-rich proteins HRP-I, HRP-II and HRP-III in malaria parasites of diverse origin. *Parasitology* 95 (Pt 2), 209–227. doi: 10.1017/s0031182000057681
- Sattabongkot, J.Tsuboi, T.Han, E. T.Bantuchai, S.Buates, S. (2014). Loop-mediated isothermal amplification assay for rapid diagnosis of malaria infections in an area of endemicity in Thailand. *J. Clin. Microbiol.* 52 (5), 1471–1477. doi: 10.1128/JCM.03313-13
- Snounou, G.Viriyakosol, S.Jarra, W.Thaitong, S.Brown, K. N. (1993). Identification of the four human malaria parasite species in field samples by the polymerase chain reaction and detection of a high prevalence of mixed infections. *Mol. Biochem. Parasitol.* 58 (2), 283–292. doi: 10.1016/0166-6851(93)90050-8
- Trager, W.Jensen, J. B. (1976). Human malaria parasites in continuous culture. *Science* 193 (4254), 673–675. doi: 10.1126/science/781840
- Wang, B.Han, S. S.Cho, C.Han, J. H.Cheng, Y.Lee, S. K., et al. (2014). Comparison of microscopy, nested-PCR, and real-Time-PCR assays using high-throughput screening of pooled samples for diagnosis of malaria in asymptomatic carriers from areas of endemicity in Myanmar. *J. Clin. Microbiol.* 52 (6), 1838–1845. doi: 10.1128/JCM.03615-13
- WHO (2021). World malaria report.
- Yamamura, M.Makimura, K.Ota, Y. (2009). Evaluation of a new rapid molecular diagnostic system for plasmodium falciparum combined with DNA filter paper, loop-mediated isothermal amplification, and melting curve analysis. *Jpn J. Infect. Dis.* 62 (1), 20–25.

Publisher's note

All claims expressed in this article are solely those of the authors and do not necessarily represent those of their affiliated organizations, or those of the publisher, the editors and the reviewers. Any product that may be evaluated in this article, or claim that may be made by its manufacturer, is not guaranteed or endorsed by the publisher.

Supplementary material

The Supplementary Material for this article can be found online at: <https://www.frontiersin.org/articles/10.3389/fcimb.2022.961832/full#supplementary-material>



OPEN ACCESS

EDITED BY

MARIA Carolina TOUZ,
Medical Research Institute Mercedes
and Martín Ferreyra (INIMEC),
Argentina

REVIEWED BY

Steven Singer,
Georgetown University, United States
Fernando Rivero,
National University of Santiago del
Estero, Argentina

*CORRESPONDENCE

M. Guadalupe Ortega-Pierres
gortega@cinvestav.mx

SPECIALTY SECTION

This article was submitted to
Parasite and Host,
a section of the journal
Frontiers in Cellular and
Infection Microbiology

RECEIVED 26 April 2022

ACCEPTED 09 August 2022

PUBLISHED 25 August 2022

CITATION

Barroeta-Echegaray E,
Fonseca-Liñán R, Argüello-García R,
Rodríguez-Muñoz R,
Bermúdez-Cruz RM, Nava P and
Ortega-Pierres MG (2022) *Giardia*
duodenalis enolase is secreted as
monomer during trophozoite-
epithelial cell interactions, activates
plasminogen and induces
necroptotic damage.
Front. Cell. Infect. Microbiol. 12:928687.
doi: 10.3389/fcimb.2022.928687

COPYRIGHT

© 2022 Barroeta-Echegaray,
Fonseca-Liñán, Argüello-García,
Rodríguez-Muñoz, Bermúdez-Cruz,
Nava and Ortega-Pierres. This is an
open-access article distributed under
the terms of the [Creative Commons
Attribution License \(CC BY\)](#). The use,
distribution or reproduction in other
forums is permitted, provided the
original author(s) and the copyright
owner(s) are credited and that the
original publication in this journal is
cited, in accordance with accepted
academic practice. No use,
distribution or reproduction is
permitted which does not comply with
these terms.

Giardia duodenalis enolase is secreted as monomer during trophozoite-epithelial cell interactions, activates plasminogen and induces necroptotic damage

Elisa Barroeta-Echegaray¹, Rocío Fonseca-Liñán¹,
Raúl Argüello-García¹, Rafael Rodríguez-Muñoz²,
Rosa María Bermúdez-Cruz¹, Porfirio Nava²
and M. Guadalupe Ortega-Pierres^{1*}

¹Department of Genetics and Molecular Biology, Centro de Investigación y de Estudios Avanzados del Instituto Politécnico Nacional, Mexico City, Mexico, ²Department of Physiology, Biophysics and Neurosciences, Centro de Investigación y de Estudios Avanzados del Instituto Politécnico Nacional, Mexico City, Mexico

Enolase, a multifunctional protein expressed by multiple pathogens activates plasminogen to promote proteolysis on components of the extracellular matrix, an important event in early host-pathogen interactions. A secreted form of enolase that is released upon the interaction of trophozoites with epithelial cells has been detected in the secretome of *G. duodenalis*. However, the role of enolase in the host-pathogen interactions remains largely unknown. In this work, the effects of *G. duodenalis* enolase (Gd-eno) on the epithelial cell model (IEC-6) were analyzed. Firstly, the coding sequence of *Giardia* enolase was cloned and the recombinant protein used to raise antibodies that were then used to define the localization and role of enolase in epithelial cell-trophozoite interactions. Gd-eno was detected in small cytoplasmic vesicles as well as at the surface and is enriched in the region of the ventral disk of *Giardia* trophozoites. Moreover, the blocking of the soluble monomeric form of the enzyme, which is secreted upon interaction with IEC-6 cells by the anti-rGd-eno antibodies, significantly inhibited trophozoite attachment to intestinal IEC-6 cell monolayers. Further, rGd-eno was able to bind human plasminogen (HsPlg) and enhanced plasmin activity *in vitro* when the trophozoites were incubated with the intrinsic plasminogen activators of epithelial cells. In IEC-6 cells, rGd-eno treatment induced a profuse cell damage characterized by copious vacuolization, intercellular separation and detachment from the substrate; this effect was inhibited by either anti-Gd-eno Abs or the plasmin inhibitor ϵ -aminocaproic acid. Lastly, we established that in epithelial cells rGd-eno treatment induced a necroptotic-like process mediated by tumor necrosis factor α (TNF- α) and the apoptosis inducing factor (AIF), but independent of caspase-3. All together, these results suggest that *Giardia* enolase is a secreted

moonlighting protein that stimulates a necroptotic-like process in IEC-6 epithelial cells via plasminogen activation along to TNF α and AIF activities and must be considered as a virulence factor.

KEYWORDS

Giardia duodenalis, enolase, plasminogen activation, necroptosis, epithelial cells

Introduction

Giardiasis is a parasitic diarrheal disease (Karanis et al., 2007) caused by the protozoan *Giardia duodenalis* (syn. *G. lamblia* or *G. intestinalis*) that is transmitted orally via contaminated drinking water or food. The persistent infection of the gastrointestinal tract by *Giardia* directly affects nutrient absorption and causes intestinal epithelial damage (Ankarklev et al., 2010; Cotton et al., 2011). The establishment, development and maintenance of *Giardia* infection are intimately related to the attachment of trophozoites to epithelial cells. Unravelling the molecular basis of this process is important for developing novel strategies aimed at controlling giardiasis.

The interaction of *G. duodenalis* trophozoites with epithelial cells affects the transcriptome and secretome of the parasite (Ringqvist et al., 2011; Ma'ayeh and Brook-Carter, 2012). For instance, the secretion of cysteine proteinases (Rodríguez-Fuentes et al., 2006), variant surface proteins (VSPs), high-cysteine membrane proteins (HCMPs), arginolytic enzymes, such as arginine deiminase (ADI) and ornithine carbamoyl transferase (OCT), and glycolytic enzymes, including enolase (Gd-eno), are increased in trophozoites which are in contact with epithelial cells (Ringqvist et al., 2008). Some of these molecules are involved in the pathogenesis of giardiasis. In that context, the VSP-type protease, VSP9B10A (Cabrera-Licona et al., 2017) and the cysteine proteinase giardipain-1 (Ortega-Pierres et al., 2018) markedly affect epithelial integrity, and the cysteine proteinases (CP) CP14019 (giardipain-1), CP16779 and CP16160 (Roxström-Lindquist et al., 2005) modulate inflammatory responses in the intestinal mucosa (Liu et al., 2018). In contrast, ADI and OCT, two enzymes of the arginine dihydrolase pathway, accelerate enterocyte turnover (Eckmann et al., 2000; Stadelmann et al., 2013). However, the role(s) of other proteins of the secretome, such as enolase, in the host-pathogen interactions remain(s) largely unknown.

Enolase (EC 4.2.1.11, syn. 2-phosphoglycerate hydrolase) is a conserved, ubiquitous metalloenzyme that catalyzes the reversible conversion of 2-phosphoglycerate (2PGA) into phosphoenolpyruvate (PEP) during glycolysis, but can also be a multifunctional protein (Day et al., 1993; Pancholi, 2001; Díaz-Ramos et al., 2012). Gd-eno is one of the most abundantly

expressed enzymes during the *Giardia* life cycle (Birkeland et al., 2010). Enolase has also been suggested to regulate host-pathogen interactions through activation of the plasminogen system (Ayón-Núñez et al., 2018). Plasminogen is a proenzyme of the fibrinolytic system, in which plasmin is produced (Vassalli et al., 1991; Castellino and Ploplis, 2005). Once activated, plasmin cleaves extracellular matrix components, such as fibrin, fibronectin, laminin, collagen, elastin and proteoglycans, among others (Smith and Marshall, 2010). Host-derived plasmin can increase the pathogenicity of several protozoan parasites other than *Giardia* (Ayón-Núñez et al., 2018).

Although current evidence shows that Gd-eno plays a role in the encystation of trophozoites (Castillo-Romero et al., 2012) this enzyme might be involved in the regulation of carbohydrate metabolism. As multiple isoforms of enolase are known to be expressed in other parasitic protozoa (Bolten et al., 2008), it is possible that Gd-eno might have moonlighting functions associated with its single copy gene not being developmentally restricted.

As Gd-eno is expressed by *Giardia* and is released into culture medium upon interaction of trophozoites with epithelial cells (Ringqvist et al., 2008) we hypothesize that, under particular conditions, this enzyme can act as an activator of plasminogen in host epithelial cells and induce the degradation of tissue extracellular matrix via the serine protease plasmin, as seen in bacteria and tissues (Peetermans et al., 2014). In the present study, we tested this hypothesis and explored whether enolase contributes to *Giardia*'s virulence.

Materials and methods

Parasite culture

For all experiments, *G. duodenalis* trophozoites (WB strain, assemblage A, ATCC # 30957) were grown at 37°C in 15 mL conical bottom tubes in TYI-S-33 modified medium (Keister, 1983) containing 10% v/v heat-inactivated bovine serum (HyClone) with 1% antibiotic/antimycotic mixture (HyClone). Trophozoites were harvested at logarithmic growth phase by cooling the tubes in an ice-water bath for 1h and detached

trophozoites were collected by centrifugation at 750 x g for 10 min at 4°C; the cell pellet was washed 3 times with phosphate-buffered saline (PBS; pH 7.4), and number of trophozoites determined using a Neubauer chamber (haemocytometer). The trophozoite concentration was adjusted according to the assays performed.

Gene cloning and protein expression of rGd-eno

The open reading frame of the *G. duodenalis* gene encoding enolase (Gd-eno) (gi|237688745) was amplified by PCR from genomic DNA from strain WB using specific primers: Eno_100_upper sense (5'-CAC CAT GGA GGC TCC GTC TAC G-3') and Eno_100_lower antisense (5'-TCA CTT CCA GGC CTC GAA ACC A-3'). The pET100-ENO was sequenced to verify that the linked gene was the correct one by using Big Dye Terminator v3.1 Cycle Sequencing Kit (Thermo Fisher Scientific) and PCR product cloned into the bacterial plasmid pET100/D-TOPO using the directional cloning system (Invitrogen). The resultant plasmid construct was used to transform *Escherichia coli* TOP10 and BL21. The BL21 bacteria were grown in Luria-Bertani (LB) medium at 37°C to an absorbance value (A_{600nm}) of 1; the expression of the recombinant protein (rGd-eno) was induced by addition of isopropyl-thio-D-galactosidase (IPTG) to a final concentration of 1 mM, and incubation was continued for 3 h, at which time the cells were harvested by centrifugation at 22,000 x g for 20 min. The recombinant protein carrying the His-tag was purified by metal-affinity chromatography using Ni-NTA agarose according to manufacturer's recommendations (Invitrogen). The recombinant protein was then passed through the high capacity endotoxin removal resin (PierceTM, Thermo Fisher) to eliminate any possible bacterial enterotoxins.

To assess whether there was residual endotoxin activity in the purified rGd-eno, pellets from bacteria transformed with the plasmid pET 100/TOPO with the enolase insert were resuspended in Lysis Buffer (50 mM Na₂HPO₄, 300 mM NaCl, 0.25 Triton X-100; Protease Inhibitors Complete EDTA Free (RocheTM) and 1 mM PMSF) and sonicated. The NiTA agarose column (QIAGEN) was prepared by washing with 10 ml of Lysis Buffer and the sample was passed through the column twice. The first washing of the column was carried out with lysis buffer and 0.25% Triton X 100. Two subsequent washings were performed with lysis buffer containing 30 mM and 50 mM of Imidazole, respectively. Finally, elution was performed using lysis buffer but with 200 mM imidazole in the presence of Protease Inhibitors Complete EDTA-free (RocheTM). SDS-PAGE (10% gel) was used to resolve protein fractions from bacterial extracts. The selected fractions were subjected to dialysis using a 12-14 kDa cut-off membrane (SpectraPor) and immersed in 2 L of PBS for 24 h and then again for the same

time. Finally, the collected fractions were passed through a column of the High-Capacity Endotoxin Removal Resin Kit (Pierce, from Thermo Fisher Scientific).

Enolase enzymatic activity assay

rGd-eno activity was determined by measuring the oxidation of NADH using a coupled assay with pyruvate kinase and lactate dehydrogenase as previously described (Saavedra et al., 2005). Briefly, the enzymatic assay was performed at 37 °C containing assay buffer (50 mM imidazole, 10 mM Tris, 10 mM acetate, 10 mM MES at pH 7.0), containing 5 mM MgCl₂, 1 mM ADP, 0.15 mM NADH, 1 mM 2PG, 10 Units pyruvate kinase, 10 Units lactate dehydrogenase and 1.64 µg of rGd-eno. The decrease in NADH absorbance was monitored at 340 nm using a diode-array Agilent 8451 spectrophotometer (Agilent Technologies). In all determinations of enzyme activity, a linear relationship between amount of protein and activity was measured. rGd-eno activity was recorded as µmole/min x mg of protein.

Anti-rGd-eno antibodies production

Polyclonal antibodies against rGd-eno were produced in mice. Female BALB/c mice (n = 10; females; 9 weeks old) were each inoculated intraperitoneally, four times at weekly intervals with 6 µg of purified recombinant protein extracted from polyacrylamide gels. The animals used in this study were fed ad libitum with rodent pellets (PurinaTM) and purified water and kept under constant standard temperature, humidity, and using filtered air. The handling of mice was performed according to Mexican regulations (NOM-062-ZOO-1999) for the production, care and use of laboratory animals (UPEAL-CINVESTAV). Pre-immune sera were obtained from individual mice and then pooled prior to immunization. One week after the fourth immunization, immune sera were collected from individual mice and pooled. The titers and specificity of the antibodies were determined by ELISA assays and immunoblotting analyses against the 6xHis-Tag.

Preparation of parasite total extracts

Trophozoites or encysting stages of *G. duodenalis* were cultured in 15 ml Falcon conical bottom tubes using TYI-S33 medium supplemented with 10% heat-inactivated bovine calf serum (HyClone) and 100 units/mL of penicillin, 100 µg/mL streptomycin sulfate and 25 µg/mL amphotericin B. Trophozoites (~50 million trophozoites/ml) were detached on ice for 30 min washed two times with PBS (at 10°C) and resuspended in 20 mM Tris pH 8.3 with protease inhibitors (Mini Complete, Roche) then sonicated on ice for 4 cycles of 15

sec at 30 sec intervals. After this, 40 µl/ml of Triton X-100 (Sigma) at 10% in Tris 20 mM, pH 8.3, were added and the lysate incubated on ice for 15 min, sonicated again and centrifuged at 10,000 xg for 30 min at 10°C. Finally, the supernatant was collected and protein concentration was determined using a kit (BCA Protein Assay, Pierce, Thermo Fisher Scientific); samples of 30 µg of protein were subjected to Western blot analysis.

Determination of the reactivity of the anti-rGd-eno antibodies by Western blot and localization of enolase in trophozoites by indirect immunofluorescence assays

The reactivity and specificity of anti-rGd-eno antibodies were determined by Western blot analysis. In this, 1 µg of the purified rGd-eno, or 30 µg of the following samples: whole protein extract from *G. duodenalis* trophozoites (T), whole protein extract from *G. duodenalis* encysting trophozoites (C), were used. As negative control, a recombinant protein Rad-52 from *G. duodenalis* (rGd-Rad-52) was used. The samples were mixed with 6X Laemmli buffer and then were subjected to electrophoresis in a 12% acrylamide gel (Laemmli, 1970). The separated proteins were transferred to a nitrocellulose membrane; the membrane was blocked with 0.1%TBS-T with 10% nonfat dried milk for 1h at RT. Membranes were incubated initially for 1h at RT with anti-rGd-eno antibody at a 1:5000 dilution and then for 1h with goat anti-mouse IgG antibody coupled to peroxidase (GAMP) at 1:10,000 dilution. Bands of reactivity were revealed using chemiluminescence ECL kit (AmershamTM Biosciences) following the manufacturer's instructions. Anti-histidine antibodies were used to detect rGd-eno.

Localization of enolase in trophozoites was determined by indirect immunofluorescence assays (IIF). In these, 4x10⁶ trophozoites in TYI-S-33 medium were incubated in a 24 microtiter plate containing coverslips for 40 min. Afterwards trophozoites were permeabilized by incubating for 15 min at -20 °C in a 1:1 methanol-acetone solution, followed by blockage of nonspecific sites with PBS containing 10% bovine serum for 30 min at 37°C. Then an overnight incubation with primary anti-rGd-eno antibody (dilution 1:400 in PBS-BSA 1%) was carried out at 4°C followed by another for 45 min at 37°C with FITC-conjugated goat anti-mouse IgG (dilution 1:400). Nuclei were stained with Hoechst (dilution 1:1000) for 15 min at 37°C. The anti-tubulin antibody (TAT-1, kindly provided by Dr. Keith Gull, University of Manchester, UK) was used to stain the ventral disk. Trophozoites were then fixed with 2% paraformaldehyde (PFA) and the samples were analyzed using a confocal laser microscope system (Leica Microsystems, Germany).

The amount of Gd-eno secreted by trophozoites was determined by Western blot of culture supernatants of IEC-6 cells exposed to *Giardia* trophozoites. For this, known quantities

of rGd-eno and supernatants from IEC-6 cultures were collected (volume 400 µl) and concentrated (10X) by centrifugation using columns for protein concentration (Amicon[®] 4ml Ultra, Merck). 32 µl of the final volume were Western blotted using the polyclonal anti-rGd-eno antibodies and a densitometric analysis was carried out. The secreted amount of enolase in supernatants was calculated considering the final volume of concentrated supernatants and the values obtained from the curve.

Native gel electrophoresis

The presence of secreted enolase monomer or the recombinant protein was determined in distinct samples by protein gel electrophoresis under non denaturing conditions. In these, samples containing ~1 µg of purified rGd-eno or concentrated culture supernatants (concentrated by centrifugation using 4 mL filters Amicon[®] Ultra, Merck) were mixed with a 5X solubilizing buffer (60% glycerol, 156 mM trizma-hydrochloride, 0.001% bromophenol blue). Proteins were analyzed by SDS-free electrophoresis in stacking 5% acrylamide gels and in separating 9% acrylamide gels for 4-5h at 80V and 4°C. The gels were stained with a solution containing 0.1% Coomassie blue- (40% methanol, 10% acetic acid) and destained with a similar solution lacking the dye.

Inhibition of trophozoite attachment to IEC-6 cell monolayers by anti-rGd-eno in interaction assays

For interaction assays, 5x10⁵ IEC-6 ATCC Cat. No. CRL-1592 cells were grown to confluence in 24 well plates (NuncTM well surface: 2 cm²) in DMEM medium supplemented with 10% heat-inactivated fetal calf serum (HyCloneTM) and with 1% of a solution containing 10,000 units/mL of Penicillin, 10,000 µg/mL Streptomycin Sulfate, and 25 µg/mL Amphotericin B in a 0.85% Saline (Caisson). For the interaction assays culture medium was removed from cultures of IEC-6 cells and DMEM medium with no serum was added before exposing the cells to 2x10⁶ trophozoites for 2h at 37°C. Interaction was carried out in the presence or absence of anti-rGd-eno antibody at 1:250 dilution and 1:500 dilution. No adhered trophozoites in the media were collected by washing the wells with PBS at 37° C and processed with lysis buffer (SDS and HEPES), then the lysate was incubated with SYTOX Green and fluorescence emission at 523 nm of SYTOX Green-DNA bound was determined. To infer the amount of non-attached parasites, the same lysis procedure was carried out in order to determine the total emission of 2x10⁶ trophozoites (100%) which was the number of parasites added per well.

Plasminogen binding assay

To test the ability of enolase to bind human plasminogen, 1 and 5 μg of human plasminogen (Athens) were spotted onto nitrocellulose membrane. In addition, 1 μg of *G. duodenalis* 6His-Rad50 and 1 μg BSA were also spotted and used as negative controls. After the dots were dried, the membrane was blocked with 5% nonfat dried milk in PBS for 40 min at room temperature, washed 5 times with PBS and incubated with 10 μg rGd-eno for an additional hour. Binding of proteins was assessed by incubation with anti-rGd-eno antibody at 1:5,000 dilution in PBS followed by incubation with goat anti-mouse IgG coupled to peroxidase (GAMP) at 1:10,000 dilution in PBS for 1 h at RT. The membrane was washed 5 times with PBS and then developed by chemiluminescence ECL kit (AmershamTM Biosciences) according to manufacturer's instructions.

Plasmin activity assay

Determination of plasmin activity was done using the specific chromogenic plasmin substrate D-Val-L-Leu-L-Lys-p-nitroanilide (S-2551, Chromogenix). Briefly, a reaction in PBS containing 450 μM S-2551 substrate, 1 μg human plasminogen (PI), 1 μg rGd-eno (reference glycolytic activity: 58 $\mu\text{mol}/\text{min} \times \text{mg}$ of protein) or 0.14 U streptokinase (Stk) were incubated for 15 min at 37°C in agitation (Thermomixer, Eppendorf). Each 5 min, samples of 50 μL were collected and the absorbance at 405 nm was determined; these values represent the activity of plasmin on the chromogenic substrate. To determine the direct effect of parasite's enolase on the plasmin activity, 1x10⁶ trophozoites were added to the reaction but in the absence of rGd-eno. In addition, enolase on the surface of trophozoites was blocked with anti-rGd-eno antibodies (1:150) prior to perform the interaction assays.

Inhibition of plasmin activity by ϵ -aminocaproic acid

To evaluate the specific activation of plasmin by Gd-eno lysine residues, competition experiments were performed using the lysine analogue ϵ -aminocaproic acid (ϵ -ACA) (Sigma). Briefly, in vitro reactions to determine plasmin activity were carried out as described above, but in the presence of different concentrations (25 mM to 100 mM) of ϵ -ACA diluted in water. Reactions were incubated 15 min at 37°C and then, plasmin activity was determined by absorbance at 405 nm.

Bioinformatics analyses

To identify domains and residues potentially involved in enolase catalysis (i.e. Mg^{2+} binding, substrate binding/protonation sites), interaction with plasminogen or variant residues amongst *G. duodenalis* assemblages, an alignment of the entire amino acid sequence of Gd-eno reported in GiardiaDB (<http://giardiadb.org/giardiadb/>; ORF GL50803_11118) was carried out with sequences from human, protozoan and yeast enolases using the CLUSTALW 2.1 software (<http://www.genome.jp/tools/clustalw/>) with default parameters. Further, the protein structure of Gd-eno was predicted by homology modeling using the Swiss Model server (<https://swissmodel.expasy.org/>) and three active conformations were obtained: "inactive" (without ion ligand, i-Gd-eno), "open" or "partially active" (with one Mg^{2+} atom, pa-Gd-eno) and "closed" or "fully active" (with two Mg^{2+} atoms, fa-Gd-eno) (Schreier and Höcker, 2010). This was based on the fact that recombinant or endogenous Gd-eno forms were experimentally used either purified or from trophozoite lysates, culture supernatants or interaction supernatants by monospecific antibodies forms, where the milieu varied in Mg^{2+} content. The stereochemical quality of all Gd-eno models were first evaluated by GMQE and QMEAN scores, then validated by the Ramachandran plot tool of the Discovery Studio 4.1 Client software to ensure its utility in further protein-protein docking analyses with crystal structures of human plasminogen type II (PDB ID: 4dur). These latter studies were carried out using the ClusPro platform (<https://cluspro.bu.edu/>) and the 15 most balanced complexes for each active conformation of Gd-eno were considered to select the optimal docking complex using as reference the most balanced complex of crystallized human enolase 1 (PDB ID: 3ucc) with the homologous plasminogen type II crystal structure indicated above. Visualization and editing of all protein structures and complexes were carried out using the UCSF ChimeraTM v.1.10.1 software.

Effect of rGd-eno on IEC-6 cell monolayers

IEC-6 cell monolayers were grown to confluence at 37° C in a 24 well plate using DMEM medium supplemented with 10% heat-inactivated fetal calf serum (HyCloneTM) and 1% of antibiotic-antimycotic solution containing 10,000 units/mL of Penicillin, 10,000 $\mu\text{g}/\text{mL}$ Streptomycin Sulfate, and 25 $\mu\text{g}/\text{mL}$ Amphotericin B in a 0.85% Saline (Caisson). Cell monolayers were incubated for 30, 60, 90 and 120 min with 100 $\mu\text{g}/\text{mL}$ of rGd-eno. Activity of the purified enzyme was 58 $\mu\text{mol}/\text{min} \times \text{mg}$ of protein. After this time, cultures were washed and fixed

according to the analysis to be performed. For Nomarski optics analysis, cells were fixed with PFA and observed using an Axioskop 40 Zeiss microscope and micrographs were analyzed with AxioVision Rel 4.8 software. For scanning electron microscopy, glutaraldehyde-fixed IEC-6 monolayers samples were dehydrated with increasing concentrations of ethanol, critical-point dried using a Samdri 780 apparatus (Tousimis, Rockville, Maryland, USA), coated with gold with a JEOL JFC-1100 ion-sputtering device, and examined with a JEOL JSM-7100F scanning electron microscope (Tokyo, Japan).

To further analyze the effect of rGd-eno in cell monolayers, cell confluence experiments were carried out as follows. Cells monolayers were grown in a 6 wells plate in 3 mL supplemented DMEM medium at 37°C 5% CO₂ to a final confluence of 50%, 70% and 100%. Then 100 µg of rGd-eno (reference glycolytic activity 58 µmol/min/mg of protein) were added to each well and after 180 min of interaction, cells were fixed and analyzed by microscopy. To analyze the inhibition of rGd-eno activity, different concentrations of anti-rGd-eno antibody (1:50, 1:100, 1:500 and 1:1000) diluted in DMEM media were added to the interaction assays of rGd-eno with IEC-6 epithelial cells. After 3h of incubation, cells were fixed with 2% PFA and then observed using an Axioskop 40 Zeiss microscope and micrographs were analyzed with AxioVision Release 4.8 software. The results were compared with the ones observed in control interactions assay in which no antibody was added.

Biochemical determination of Caspase 3 activity

Caspase 3 activity was determined using a Caspase 3 assay buffer that contained: 20 mM Hepes, 5 mM DTT, 2 mM EDTA and 0.1% Triton X-100 at pH 7.4. For each determination, the buffer assay was supplemented with 50 µL of the cell lysate and 1 µM Ac-DEVD-AMC (caspase-3 substrate) with or without 2 µM Ac-DEVD-CHO (caspase-3 inhibitor). The reactions mixtures were incubated at room temperature for 90 min. Caspase-3 activity was calculated by subtracting the fluorescence signal obtained when the substrate and inhibitor were mixed and compared with the reaction mixture that contained only the substrate. The corrected signal obtained from cells incubated with Staurosporine (STS) was considered as 100% response for caspase production (Benítez-Rangel et al., 2011; Benítez-Rangel et al., 2015).

Annexin V binding assays

IEC-6 cells were grown on coverslips in DMEM at 37°C and 5% CO₂ and when confluence was reached, the monolayers were exposed to purified rGd-eno at a final concentration of 100 µg/mL (reference glycolytic activity 58 µmol/min xmg of protein)

for 2 h. Negative controls were IEC-6 cells incubated with DMEM alone and positive controls were IEC-6 cell monolayers exposed to 50 µM H₂O₂, cells without enolase were then incubated for 2h under the same conditions. After this, coverslips were treated with Annexin V-FITC conjugate (BioVision, Milpitas, Ca, USA) for 5 min following the manufacturer's instructions, fixed with 2% PFA for 1 h, washed once with PBS and analyzed using an Axioscope Zeiss Zeiss epifluorescence microscope. For quantification by flow cytometry, cells were collected and exposed to the treatments mentioned above and analyzed with the Annexin V-FITC Apoptosis Kit (BioVision, Milpitas, Ca, USA) following the manufacturer's instructions.

Immunohistochemistry assays

Immunohistochemistry assays were performed for Caspase 3, Caspase 8, BID (BH3-interacting domain death agonist) and AIF (Apoptosis-inducing factor) proteins following standard procedures. Confluent IEC-6 monolayers were treated with rGd-eno at the concentration and times previously described. Cells were washed once with PBS and treated by 20 min with 4% PFA at room temperature to immobilize antigens while retaining cellular and subcellular structure. Cells were rehydrated following treatment with xylene, ethanol-xylene, ethanol 100%, ethanol 90%, ethanol 70% and water. Antigen retrieval was carried out at 90°C, in a bath, by treating the cells with sodium citrate (pH 6, 0.01M) for 20 min. Intrinsic peroxidase activity was eliminated by incubation of the cells with a 3% H₂O₂ -methanol solution at room temperature twice for 15 min. Blocking was performed using 2% normal porcine serum in PBS, for 1h in a wet camera at RT. The cells were then incubated with biotin for 15 min at room temperature and washed 3 times with PBS prior to the addition of the primary antibodies against the different proteins evaluated [anti-Caspase 3: (Cell signaling Technology, Rabbit mAb); anti-Caspase 8 (Cell signaling Technology, Rabbit mAb); anti-BID (Abcam, Rabbit mAb); anti-AIF (Cell signaling Technology, Rabbit polyclonal)], which were left overnight at room temperature. After 3 washes with PBS, universal biotinylated link (Dako, Carpinteria, CA) was added to the cells, and then incubated for 30 min with HRP-Conjugated Streptavidin and revealed with substrate diaminobenzidine (DAB). After analysis, cells were dehydrated and preserved.

Detection of AIF and TNFα in IEC-6 cells or supernatants after interaction of with rGd-eno

Detection of AIF and TNFα was carried out by Western blot assays using antibodies against AIF and TNFα as follows. For

AIF, Western blot analysis, after treatment with rGd-eno, IEC-6 epithelial cells were lysed with RIPA buffer and, equal amounts of proteins were separated by SDS-PAGE in a 10% polyacrylamide gel and transferred to a nitrocellulose membrane. Then, membranes were blocked and incubated overnight with anti-AIF at 1:1500 dilution (Cell Signaling) in 1.2% milk-PBS solution. Membranes were incubated with goat anti-mouse IgG coupled to peroxidase diluted 1:10,000 in PBS for 1 h at RT. Detection was carried out using a chemiluminescence kit. For detection of TNF α , 50 μ L of supernatants of interaction were diluted 1:5 in 5X Laemmli buffer with 1% β -mercaptoethanol and boiled for 5 min. Samples were then separated by SDS-PAGE on 10% polyacrylamide gel and blotted to PVDF membranes. Membranes were incubated with blocking buffer (3% v/v casein in 10 mM Tris-HCl pH 8.0, 150 mM NaCl, 0.05% v/v Tween-20), and then incubated overnight at 4°C with the primary antibody against TNF- α (1:1000, Santa Cruz Biotechnology) diluted in blocking buffer. Thereafter, membranes were incubated for 1 h with HRP conjugated donkey anti-goat IgG (Santa Cruz Biotechnology) antibody diluted at 1:10,000; after washing, reactivity was developed using the ECLTM prime Western blotting detection reagent (AmershamTM, GE Healthcare, Buckinghamshire, UK). Chemiluminescence was detected in an EC3 Imaging System (UVP Bio Imaging Systems, Cambridge, UK). Protein band density was quantified by transmittance densitometry (UVP Bio Imaging Systems software, Cambridge, UK).

In other sets of experiments, the specific TNF α inhibitor TAPI-0 (TAPI-0, CAS: 143457-40-3, Santa Cruz Biotechnology) was used. Briefly, interaction experiments of IEC-6 monolayers with 60 μ g/mL of rGd-eno (relative glycolytic activity 153 μ mol/min x mg of protein) in DMEM were developed as previously mentioned. Then TAPI-0 was added to the interaction assays to a final concentration of 100 mM and the epithelial cell damage was analyzed by Nomarski optics as described above. Additional studies were carried out using the I κ B α phosphorylation and NF- κ B inhibitor BAY 11-7082 (Cayman, Chemical). Briefly, IEC-6 cells were cultured in a 2 cm² coverslips in a 24 well plate and the interaction procedure with rGd-eno was carried in the absence or presence of the inhibitor at different concentrations (40 mM and 60 mM). After 3 h of incubation, the cells were fixed with 2% PFA and then observed using an Axioskop 40 Zeiss microscope and micrographs were analyzed with AxioVision Rel 4.8 software.

Statistical analyses

All statistical analyses were performed using the statistical package GraphPad Prism V.5. Data were analyzed by Student's T-test with a 95% confidence interval for significance. Results shown are the representation of at least of 3 independent experiments.

Results

Sequence-based comparison of Gd-eno with homologs from other organisms

Sequences representing enolase homologs from *H. sapiens*, *S. cerevisiae* and *T. brucei* (accession numbers Homo sapiens AAB59554.1; *S. cerevisiae*: AAA88713; *T. brucei*: AAF73201.1) were compared with Gd-eno (accession number G duodenalis: EES98422). These enolases shared 51% identity over 96–98% of the amino acid sequence, with some insertion/deletion events (Supplementary Figure S1). In the Gd-eno, several amino acid residues were inferred to be involved in PEP binding (H170, E222, K361, H389 and K412) as well as Mg²⁺ binding (S44, D257, E306 and E336) (Castillo-Romero et al., 2012). Four additional amino acids implicated in PEP binding (i.e. A43, E179, R390 and S391) were identified based on structural predictions of clashes/contacts of Gd-eno with its substrate (Supplementary Figure S1). In addition, the plasminogen interacting domain (PID) of Gd-eno dimer (S261–N274) (Aguayo-Ortiz et al., 2017) and three Lys residues involved in primary interaction with human plasminogen (K361, K412 and K342) were recognized (Supplementary Figure S1). The sequence of Gd-eno also contains two residues that allow the formation of the anti-parallel homodimer, E25 and R429 (E20 and R414 in human α -enolase), in accordance with the human homolog. Regarding intra-species polymorphism of Gd-eno, the amino acid sequences representing five *Giardia* strains and three assemblages (A, B and E) displayed up to 31 variable residues (cf. legend of Supplementary Figure S1), 16 of which were displayed in assemblage B (with reference to assemblage A).

Cloning and expression of rGd-eno

The nucleotide sequence (1338-bp) cloned into the pET100/D-TOPO was identical to a reference sequence from *G. duodenalis* Genbank accession no. EES98422 (Supplementary Figure S2). The purified recombinant protein (rGd-eno) was enzymatically functional, with a specific activity of 58 μ mol/min x mg of protein – similar to that reported for recombinant enolase of *Entamoeba histolytica* (Saavedra et al., 2005).

Specificity of anti-rGd-eno antibodies and localization of enolase in *Giardia* trophozoites and quantification of secreted enolase

The specificity of polyclonal antibodies generated against rGd-Eno was tested by Western blotting total extracts

obtained from trophozoites and encysting trophozoites, the recombinant protein rGd-eno and a non-related recombinant protein referred as rGd-rad52 from *G. duodenalis* that was used as negative control (Figure 1A). As observed in Figure 1A a single band with molecular weight of 48 kDa was recognized by anti-rGd-eno in total extracts obtained from trophozoites as well as with the purified rGd-eno while no reactivity was observed either with total trophozoite extracts or with rGd-eno using the pre-immune serum (Figure 1A). The 48 kDa protein was detected also in encysting cells (Figure 1B) but no reactivity was observed with the rG-rad52 protein. As expected, commercial anti-histidine antibodies reacted with the 48 kDa band corresponding to the rGd-eno that is fused to the his-tag (Figure 1B). Thus, our results show that the antibodies obtained against rGd-eno specifically recognized both the native and recombinant protein. Next these antibodies were used to localize Gd-eno in permeabilized *Giardia* by indirect immunofluorescence (Figure 1C). Gd-eno was localized enriched at the region of the ventral disk and within small,

rounded and well defined vesicles in the cytoplasm of trophozoites (Figure 1C-b). In non-permeabilized trophozoites, enolase was distributed on the whole parasite surface, including the flagella (Figure 1C-c). In conjunction, our results demonstrate that Gd-eno is localized to intracellular and epicellular components of trophozoites.

Specific experimental conditions can affect biological processes, including protein secretion. Therefore, our next goal was to evaluate the amount of Gd-eno secreted by trophozoites when interacting with IEC-6 cells. To such purpose, concentrated culture supernatants (concentrated by centrifugation using 4 mL filters Amicon® Ultra, Merck) were Western blotted using the anti-rGd-eno antibodies (Figures 1Df-h). A linear regression analysis of the densitometric values obtained from defined quantities of rGd-eno (Figures 1Da-e) were used to determine the concentration of the Gd-eno released. A calibration curve was obtained which displayed a hyperbolic trend and a good correlation coefficient ($R^2 > 0.99$), allowing to estimate by extrapolation the quantities of Gd-eno secreted in

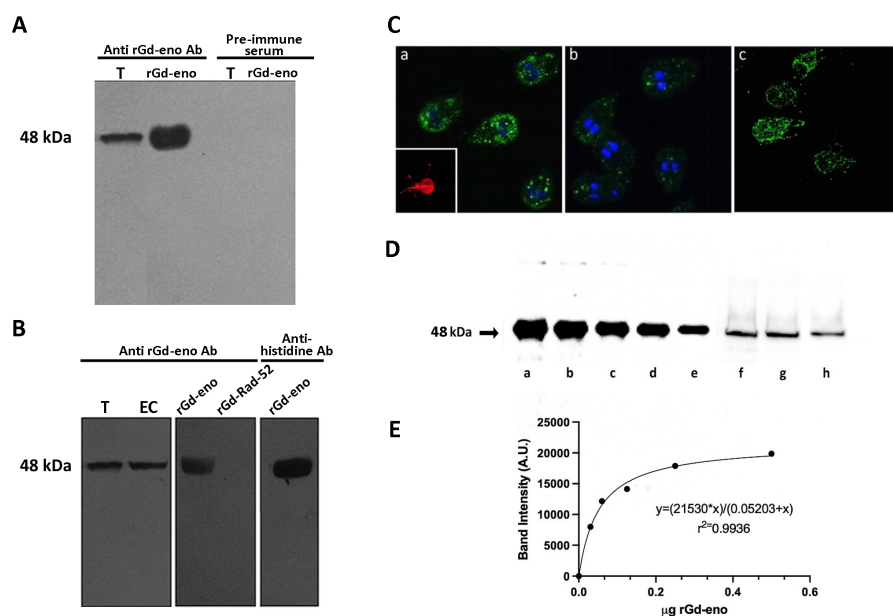


FIGURE 1

Specificity of anti-rGd-eno antibodies, subcellular localization of *Giardia* enolase and determination of secreted enolase in trophozoite interaction with IEC-6 cells. (A) Reactivity of anti-rGd-eno and pre-immune serum samples. Total extracts from *G. duodenalis* trophozoites (T) and purified rGd-eno (b) were separated by SDS-PAGE, and the membranes probed with anti-rGd-eno and pre-immune serum. (B) Total extracts from trophozoite (T) and encysting cells (EC), rGd-eno and a non-related recombinant protein from *Giardia* named rGd-Rad52 were probed with anti-rGd-eno antibodies. Western blotting the membranes with anti-histidine antibodies directed against the his-tag present in rGd-eno was used as positive control. (C) Indirect immunofluorescence for endogenous Gd-eno was performed in trophozoites. Gd-eno is enriched at the ventral disk region and in small vesicles in the cytoplasm (a and b); (insert: staining of the adhesion disk with anti-tubulin antibody). Cytosolic detection was performed in permeabilized parasites and surface detection was carried out in fixed non-permeabilized trophozoites. Gd-eno (c) is localized in the entire parasite surface and flagella in fixed trophozoites. (D) Quantification of secreted Gd-eno. Concentrated supernatants of IEC-6 cells interacted with trophozoites for 1h (f) 2h (g) and 3h (h) and different quantities of rGd-eno: 500 ng (a), 250 ng (b), 120 ng (c) 60 ng (d) and 30 ng (e) were Western blotted with anti-rGd-eno antibodies. (E) The regression standard curve shown in D was generated from the densitometric analysis carried out in the protein bands and used to determine the concentration of secreted enolase present in the supernatants. Results are representative of two independent experiments.

concentrated supernatants. As shown in Figure 1E, it was estimated that approximately 25 ng (Figure 1Df), 21 ng (Figure 1Dg) and 14 ng of Gd-eno (Figure 1Dh) were secreted during the trophozoite-IEC-6 interaction respectively. Thus, considering that 32 μ l of concentrated supernatant were Western blotted, the final values of secreted enolase were calculated for the final volume (40 μ l) of concentrated supernatants. Consequently, our approximate values were as follows: 1h-31 ng; 2h-26 ng and 3h-17ng. The values calculated in our experimental conditions corresponded to 2×10^6 trophozoites added to the IEC-6 cells and the specific activity of rGd-eno determined in our experiments was used as reference for further experiments where rGd-eno was incubated with epithelial cells.

Gd-eno is secreted as a monomer by *G. duodenalis* trophozoites

Enolase exhibits different homocomplex orders, such as monomers, dimers and octamers (tetramers of dimers) (Lu et al., 2012; Wu et al., 2015), and in our results we detected an endogenous Gd-eno of 48 kDa in trophozoites. Therefore, we determined the aggregation states of the enzyme present in culture supernatants. Under non-denaturing conditions,

antibodies recognized a band of ~48 kDa in supernatants collected from trophozoites cultured alone or co-cultured with IEC-6 cells that corresponded to the monomeric form of Gd-eno (Figure 2Aa–c). The secretion of the monomeric form of Gd-eno was higher in the presence of IEC6. No bands were observed in supernatants from IEC-6C cell monolayers (Figure 2Ad).

Since Gd-eno was secreted as a monomer, the active conformation of this molecule was evaluated by bioinformatic analyses. Models were predicted using distinct optimal templates: (a) α -enolase of *Toxoplasma gondii* (PDB ID: 3otr) for i-Gd-eno that showed scores QMEAN = -1.46 and GMQE = 0.77, (b) *Saccharomyces cerevisiae* enolase (PDB ID: 1ebh) for pa-Gd-eno with scores of QMEAN = -0.82 and GMQE = 0.76, and (c) *Homo sapiens* neural enolase (PDB ID: 3ucc) for fa-Gd-eno with scores QMEAN = -0.44 and GMQE = 0.77 (Figure 2B). In the latter model, similar results were obtained using *H. sapiens* enolase 1 (PDB ID: 2psn) as template. In all models, Ramachandran plots predicted that >99% of residues were within allowed zones in ψ - ϕ angle quadrants, indicating a high stereochemical quality of the models. As shown by structural alignment of all three models (Figure 2B), the expected closing of connecting loops L1, L2 and L3 were well defined. These conformations were considered as representative of extracellular/secreted Gd-eno and rGd-eno in further molecular docking studies.

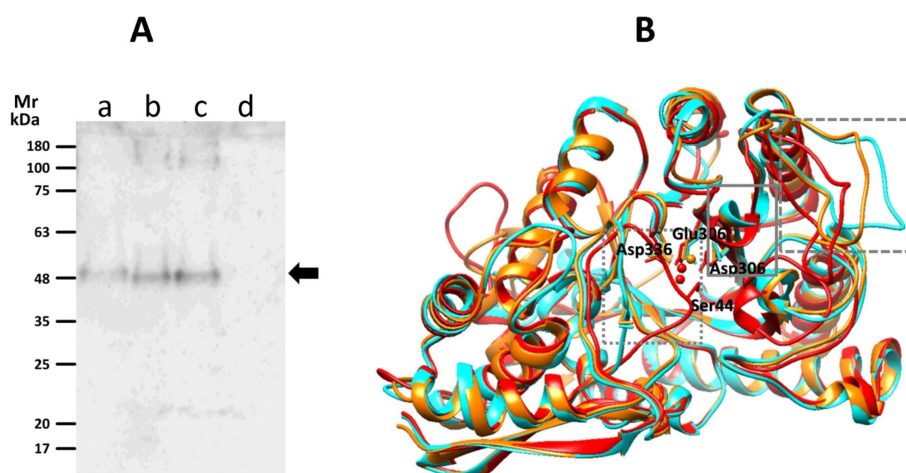


FIGURE 2

Detection of Gd-eno by native gel electrophoresis and active conformations of its monomer. (A) Western blot analysis using polyclonal anti-rGd-eno antibodies. Protein samples are as follows; (a) supernatants collected from a 2h trophozoite culture; (b) affinity chromatography purified rGdEno (1 μ g); (c) supernatants collected from a 2h trophozoite-IEC6 co-culture, 15X-concentrated; (d) supernatant collected from a 2h IEC6 culture 10X-concentrated. Molecular weight markers (m) are at the left of the figure. (B) Protein modeling of Gd-eno (GL50803_11118) in "inactive" (none Mg^{2+} -bound, displayed in cyan), "partially active" (one Mg^{2+} bound, displayed in orange) and "fully active" (two Mg^{2+} bound, displayed in red) conformations. The squares with dotted, continuous and dashed gray lines mark the closing of loop 1, loop 2 and loop 3 domains, respectively. Mg^{2+} ions are depicted in ball conformation and amino acid residues involved in Mg^{2+} binding are indicated and shown in ball-and-stick conformation.

Gd-eno participates in trophozoite attachment to epithelial cells

Based on the observations that Gd-eno was abundantly expressed in the parasite's surface and enriched in the region of the trophozoites' ventral disk the role of Gd-eno in the interaction with IEC-6 epithelial cells was analyzed. To this end, surface expressed Gd-eno on trophozoites was blocked by incubating the parasites with anti-rGd-eno antibody previous to the interaction with IEC-6 epithelial cells. Then the value of the fluorescence emission of SYTOX green-DNA complex from untreated, cultured trophozoites (2×10^6) which was 0.10873 ± 0.0071 (100%) was taken as reference (Figure 3A). In this manner, treatment of trophozoites with anti-rGd-eno antibody at 1:250 and 1:500 dilutions resulted in a significantly higher emission of SYTOX Green bound DNA values of 0.08003 ± 0.0032 and 0.07162 ± 0.0076 . [Figure 3B (74%) and 3c (66%) respectively], when compared with the control cultures in which no antibody was used [Figure 3D value of 0.04761 ± 0.0071 (44%)] representing a lower attachment ability of parasites to cell monolayers. These results suggest that Gd-eno participates in trophozoite attachment to epithelial cells.

rGd-eno specifically binds plasminogen and enhances plasmin activity

To evaluate whether Gd-eno acts as a plasminogen receptor, we exposed increasing amounts of purified human plasminogen in a nitrocellulose membrane to rGd-eno. The results showed a clear interaction between rGd-eno and plasminogen (Figures 4Aa, b). No binding of rGd-eno with 6xHis-Rad50 was observed or BSA (Figure 4Ad). (Figure 4 Ac). Given that 6xHis-Rad50 failed to interact with plasminogen, we concluded that the conditions used for the purification of rGd-eno, and the His-tag present in rGd-eno did not interfere with the association of both molecules (Figure 4Ad). Subsequently, we determined the transformation of plasminogen to its active form, the serine-protease plasmin. Thus, we evaluated the activity of plasmin on its chromogenic substrate S-2251 D-valyl-L-leucyl-lysine-p-nitroanilide (Chromogenix). The maximum time point of reaction was set at 15 min after incubation because at that time the reaction was saturated. As seen in Figure 4B, the activity of plasmin was enhanced in the presence of rGd-eno (Figure 4Ba) as compared with a samples lacking rGd-eno (Figure 4Bb). No plasmin activity was detected the control

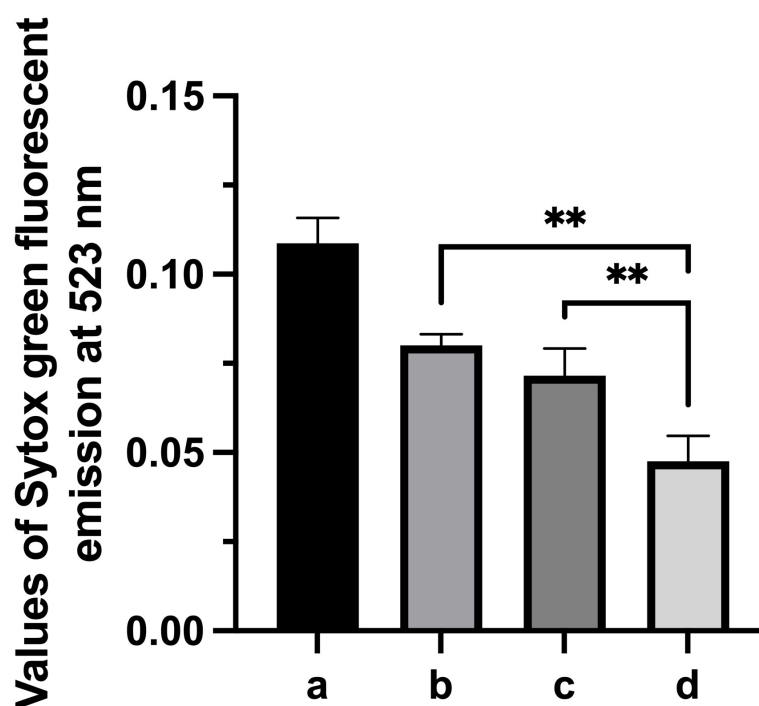


FIGURE 3

Effect of anti-Gd-eno antibodies in the attachment of *Giardia duodenalis* trophozoites to IEC-6 monolayers. IEC-6 epithelial cells monolayers were co-cultured with 2×10^6 trophozoites that were pre-incubated with anti-rGd-eno at (B) 1:250 dilution, (C) 1:500 dilution. (D) Control co-cultures lacking antibody. Attachment of trophozoites was determined by Sytox Green fluorescent emission at 523 nm considering as reference the values obtained of fluorescence emission generated by 2×10^6 cultured trophozoites (A). Data shown is the mean average of three independent experiments performed by quadruplicate. *** $P < 0.05$ in relation to control cultures lacking antibody and between antibody dilutions. ** $P < 0.05$.

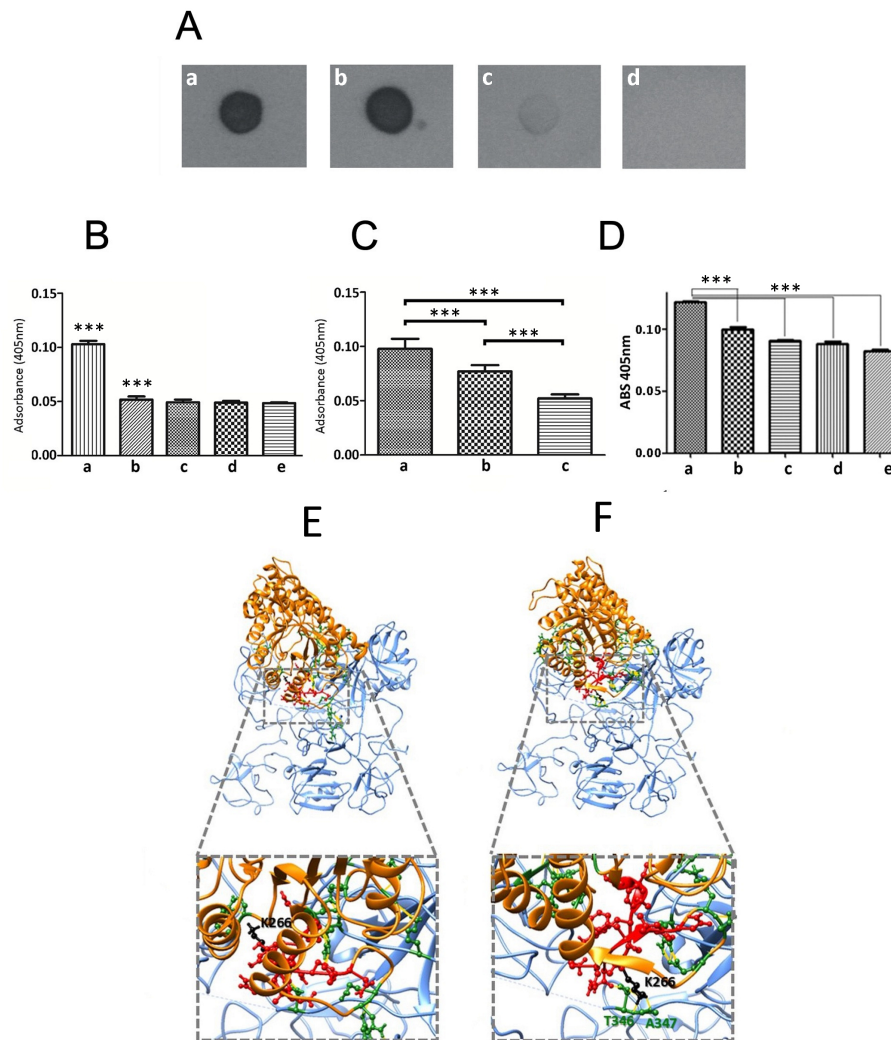


FIGURE 4

rGd-eno binding to plasminogen and activation of plasmin by rGd-eno and trophozoites. **(A)** Binding of rGd-eno to plasminogen was determined by dot blot assays. 1 μ g **(a)** or 5 μ g **(b)** of human plasminogen (PI) were added to the nitrocellulose membrane. 1 μ g of 6His-GdRad50 **(c)** and 1 μ g bovine serum albumin (BSA) **(d)** were used as controls. Membranes were incubated with 10 μ g of rGd-eno in PBS, washed 3 times with PBS/tween and then blotted with anti-rGd-eno (1:5000). **(B)** Quantification of the plasmin activity induced by rGd-eno. **(a)** *in vitro* reaction including Streptokinase (Stk), PI and S-2551 and rGd-eno, **(b)** *In vitro* reaction including Stk, PI and S-2551. Control samples included, **(c)** S-2551 in PBS, **(d)** Stk and S-2551 and, **(e)** rGd-eno, PI and S-2551. The data shown is the average of three independent experiments at 15 min reaction, each performed by triplicate. **(C)** Differential activity of plasmin induced by trophozoites. **(a)** 1×10^6 trophozoites incubated with the reaction mixture containing Stk, PI, S-2551; **(b)** trophozoites treated with anti-rGd-eno antibody previous to the interaction assays, each performed by triplicate. **(D)** Effect of ϵ -ACA on plasmin activity induced by rGd-eno. Protease activity was determined in the presence of rGd-eno, PI and increasing concentrations of the lysine analog ϵ -ACA. The use of the specific competitor ϵ -ACA significantly reduced the reactivity of S-2551 *in vitro* in a concentration dependent manner. No addition of ϵ -ACA **(a)**, 25mM **(b)**, 50mM **(c)**, 75mM **(d)** and **(e)** 100mM of ϵ -ACA were added in these assays. Asterisks (**) indicate the statistical significance of $P < 0.05$ in relation to control. **(E, F)** The putative binding of the Gd-eno monomer to human plasminogen was analyzed by protein-protein docking using the crystal structure of HsPlsII (PDB ID: 3ucc; displayed in blue) as ligand and the protein structures of Gd-eno monomer in "partially active" **(E)** and "fully active" **(F)** conformation (displayed in orange). The PBD of Gd-eno (S261-N274) is displayed in ball-and-stick conformation and colored red. The central residue K266 is colored in black. Residues displayed in ball-and-stick conformation and colored green are involved in clashes/contacts (displayed as yellow lines) between the two proteins. *** $P < 0.001$.

groups (Gd-rad50 and BSA; [Figures 4Bc, d](#)) These results demonstrated that Gd-eno is a human plasminogen receptor that enhances the protease activity of plasmin.

Subsequently, we carried out assays aimed to determine the presence of an extrinsic plasmin activator in trophozoites. For this purpose, trophozoites (2x10⁶) were included in reactions containing the plasmin specific chromogenic substrate S-2551, human plasminogen and streptokinase (Stk) as an external activator of plasmin ([Figure 4C](#)). The treatment of trophozoites with sub-agglutinating concentrations of anti-enolase antibody (1:250) prior to reaction, showed a reduced plasmin activation ([Figure 4Cb](#)) when compared with non-treated trophozoites ([Figure 4Ca](#)), or with the control reaction with no trophozoites or when trophozoites were treated with rGd-eno ([Figure 4Cc](#)). Controls, including trophozoites in the absence of Stk, did not show plasmin activity, suggesting that *G. duodenalis* trophozoites do not produce an extrinsic plasmin activator, as observed in other pathogens ([Lähteenmäki et al., 2001](#)). Further, the addition of 100 mM of the lysine analog ϵ -aminocaproic acid (ϵ -ACA) significantly inhibited the activation of plasmin, measured by the absorbance of the chromogenic substrate S-2551 in vitro ([Figure 4D](#)).

Inferring the molecular interaction of Gd-eno monomer and HsPIs

To obtain insights on the molecular interactions between Gd-eno and plasminogen, we undertook in silico structural docking analyses with crystal structure of dimeric human plasminogen II HSPIs (PDB ID: 4dur) z- the predominant type recruited to cell surfaces ([Law et al., 2012](#)). The most balanced Gd-eno-HsPIsII complexes from a set of 15 predictions ([Figures 4E, F](#)) revealed multiple clashes/contacts (<4 Å) with the target. In these models, Gd-eno monomer (ligand) in its “partially active” ([Figures 4E](#)) and “fully active” ([Figure 4F](#)) states display a similar ability to interact through its PBD (S261-N274) and K266 neighboring moieties with HsPIsII at the lysine-rich environment present at the serine protease (SP) and with Kringle (K3 and K4) domains of this protein. This interactive microenvironment is consistent with the inhibitory effect of the lysine analog, ϵ -ACA, on plasmin activity induced by rGd-eno ([Figure 4D](#)).

rGd-eno induces damage to IEC-6 monolayers

Because rGd-eno activates the cysteine protease plasmin, we evaluated whether rGd-eno affected the integrity of IEC-6 monolayers. In IEC-6 cell monolayers exposed to rGd-eno, rounded cells with blebs that lost their cell-cell contact were consistently detected. In some areas, shrunken cells with

vesiculated cytoplasm were observed ([Figures 5A–D](#)). This appearance was very similar to that described for epithelial cells undergoing apoptosis. Importantly, the treatment of the epithelial cells with an unrelated protein Rad-52 from *G. duodenalis*, which was purified using a similar method as that used for Gd-eno, did not show any effect on cell morphology (data not shown). IEC-6 monolayers cultured in DMEM alone ([Supplementary Figure 3A](#)) or exposed to protein fractions purified from extracts from *E. coli* BL21 Star alone remained undamaged ([Supplementary Figure 3B](#)), while IEC-6 monolayers exposed to rGd-eno showed cell damage, as previously described. Thus, our results indicated that rGd-eno caused the alterations seen in IEC-6 cells ([Supplementary Figure 3C](#)). Interestingly, sparse monolayers were less susceptible to the damage induced by rGd-eno than confluent monolayers (see [Supplementary Figure 4](#)). These results suggested that Gd-eno has the potential to activate plasminogen, as has been reported for enolases of bacteria and tissues ([Peetermans et al., 2014](#)) However, further studies of epithelial cells are still needed to fully characterize the relationship between cellular plasminogen and its activation by Gd-eno.

Anti rGd-eno antibody prevents the damage in IEC-6 cells that is mediated by rGd-Eno

To confirm the role of rGd-eno in the induction of cell death observed in IEC-6 cells, neutralizing experiments using anti-rGd-eno antibody were carried out. For this, increasing dilutions (1:50, 1:250, 1:500 and 1:1000) of anti-rGd-eno antibody were added to IEC-6 monolayers before the incubation with rGd-eno (100 µg/ml). As expected, no damage was detected in control monolayers ([Figure 6A](#)), while IEC-6 cells exposed to rGd-eno showed the cell-cell separation, blebbing and shrinkage ([Figure 6B](#)). In contrast, in epithelial cells previously incubated with anti-rGd-eno and then exposed to rGd-eno the cell damage was reduced in a concentration dependent manner ([Figures 6C–F](#)).

Evidence that AIF and TNF α mediate cell death in IEC-6 exposed to rGd-eno

Next, we evaluated the mechanism triggered by rGd-eno to induce IEC-6 cell death in vitro. Initially, we explored the Programed Cell Death Type 1 by assessing caspase 3 activation in the epithelial cells ([Figure 7](#)). Despite of inducing cell death, rGd-eno treatment failed to activate caspase 3 in IEC-6 cells ([Figure 7c](#)). Further analyses of the activation of caspase 3 using immunofluorescence and immunohistochemistry assays did not reveal changes in the expression of the molecule in rGd-eno-

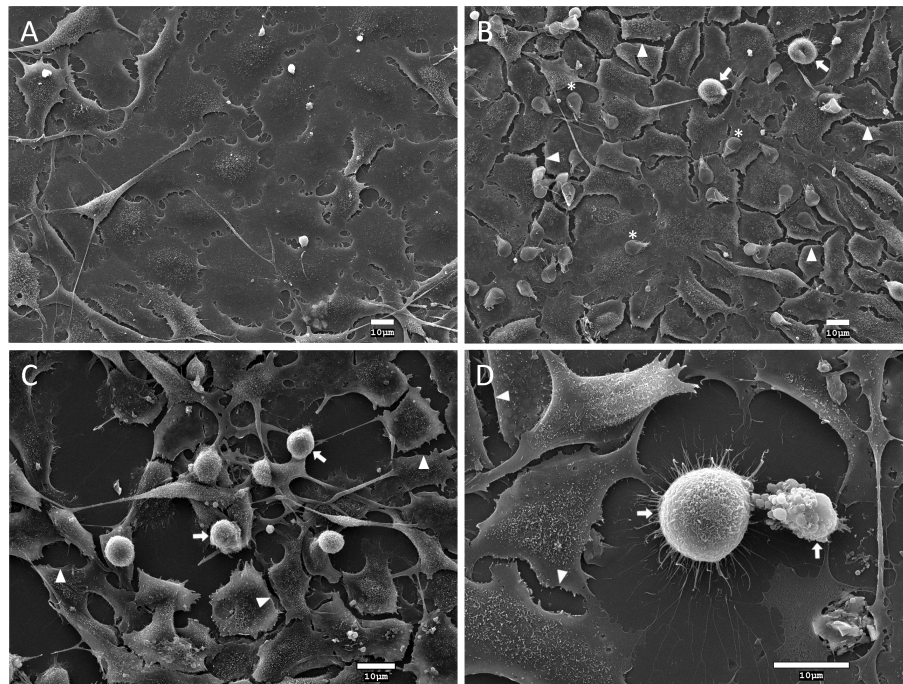


FIGURE 5

Analysis of the effect of *Giardia duodenalis* trophozoites and rGd-eno on IEC-6 epithelial cell monolayers. Intestinal epithelial cell monolayers of IEC-6 cells were incubated for 90 min with: (A) DMEM medium only; (B) *G. duodenalis* trophozoites expressing surface Gd-eno; or (C, D) rGd-eno (100 $\mu\text{g}/\text{ml}$; relative glycolytic activity 58 $\mu\text{mol}/\text{min}\times\text{mg}$ of protein). Samples were processed for scanning electron microscopy. Representative micrographs are shown. IEC-6 monolayers exposed to trophozoites that express surface Gd-eno (B) or rGd-eno (C, D) displayed cell damage characterized by cell-cell separation (arrowheads), cell blebbing and cell shrinkage (arrows). Asterisks denote trophozoites. (D) A magnified view of cell blebbing and a shrunk IEC-6 cell.

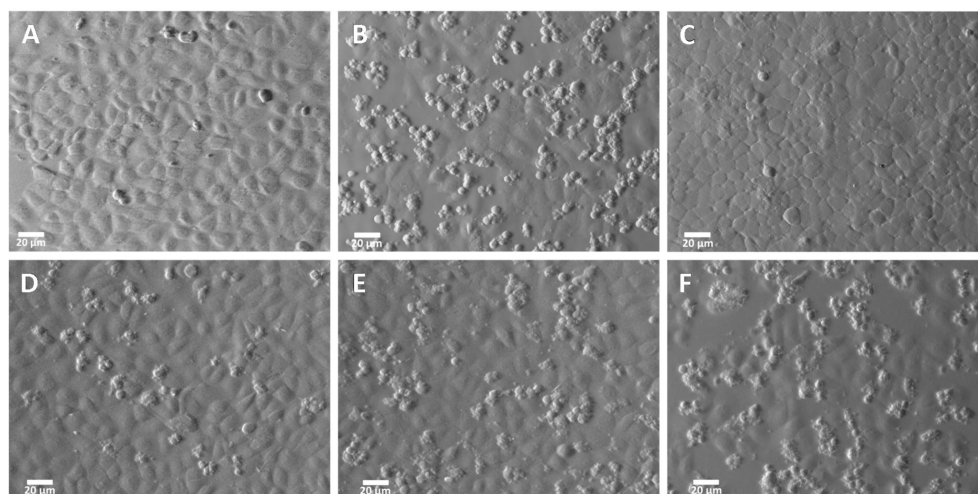


FIGURE 6

Inhibition of the damage induced by rGd-eno on IEC-6 epithelial cell monolayer by anti rGd-eno antibodies. IEC-6 cells were incubated with different antibody dilutions of anti-rGd-eno previous to the addition of rGd-eno (100 $\mu\text{g}/\text{ml}$ enolase relative glycolytic activity 58 $\mu\text{mol}/\text{min} \times \text{mg}$ of protein). (A) negative control no enolase or antibody added; (B) addition of rGd-eno only; anti-rGd-eno added at (C) 1:50; (D) 1:250; (E), 1:500 and (F) 1:1000 dilutions of anti rGd-eno antibodies. Images shown are representatives of three independent experiments.

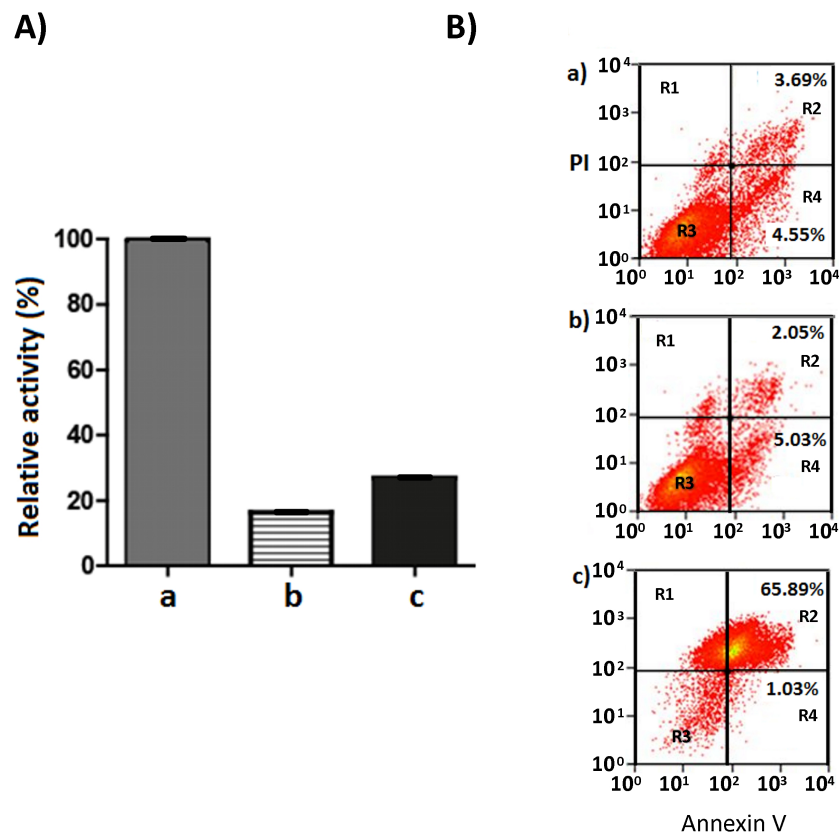


FIGURE 7

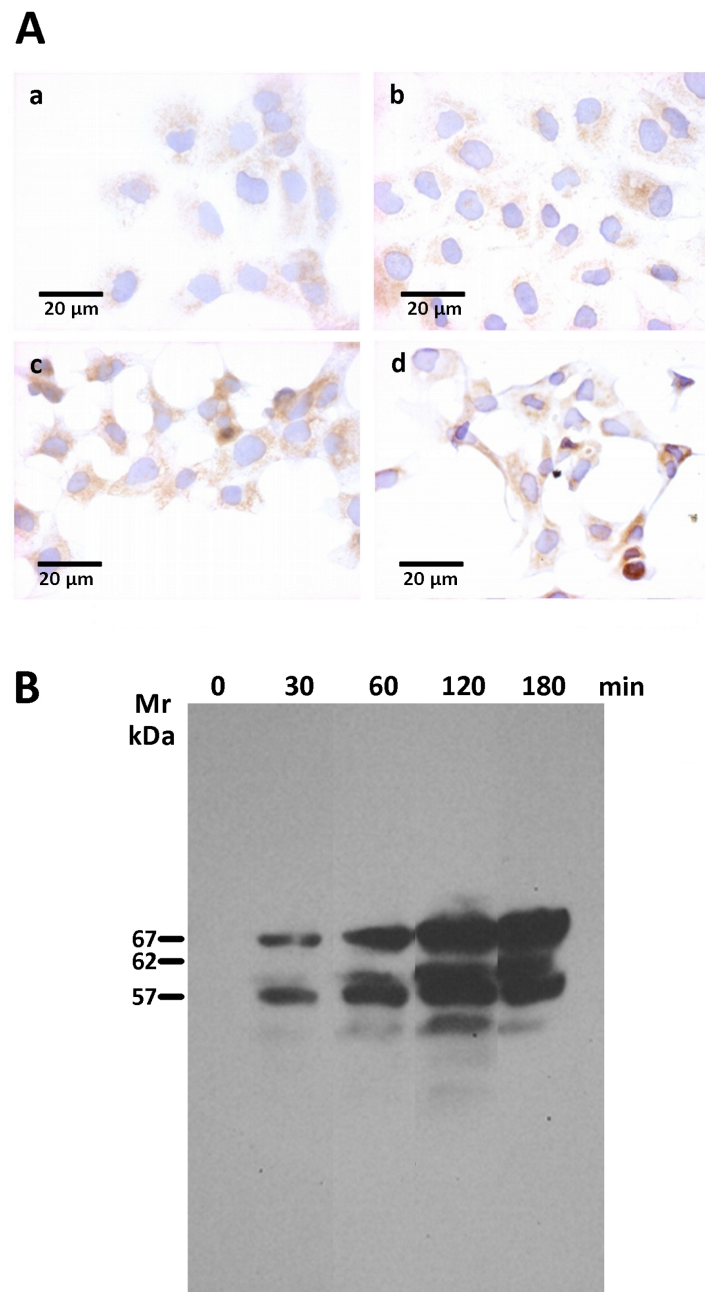
Caspase 3 activity in IEC-6 monolayers treated with rGd-eno and Annexin V-PI staining of IEC-6 cells exposed to rGd-eno. (A) Caspase 3 activity was determined in IEC-6 monolayers treated with rGd-eno (100 μ g/ml; relative glycolytic activity 58 μ mol/min \times mg of protein) for 3h. Staurosporine-treated cells = positive control (a). Control untreated cells (b). IEC-6 cells treated with rGd-eno (c). (B) Flow cytometry plots of Annexin V-PI staining of IEC-6 monolayers after 3h of exposure to (a) rGd-eno, (b) untreated control and c) H₂O₂-treated (control of apoptotic damage). R1: cells in necrotic damage (PI-positive), R2: cells in late apoptosis (Annexin V and PI-positive), R3: non stained cells, R4: cells in early apoptosis (Annexin V-positive). Percentages of cells in early and late apoptosis are indicated in each plot.

treated cells versus non-treated cell monolayers (Supplementary Figure 4). To corroborate these findings, we assessed the presence of phosphatidylserine on the outer cell surface of epithelial cells. Flow cytometry readings determined that cells interacting with rGd-eno (100 μ g/mL) displayed equal rates of annexin V positivity as non-rGd-eno treated cells (regions R2 and R4; Figure 7Ba, b). The propidium iodide staining (region R1) was also similar under both conditions (Figure 7Ba, b). However, annexin V was tightly bound to H₂O₂-treated IEC-6 cells (positive control for apoptosis), and these cells were also stained with propidium iodide (region R2) (Figure 7Bc). These results strongly suggest that apoptosis is not the principal mechanism of cell death triggered by rGd-eno.

Several other cell-death effectors, which included caspase 8, BID and LC3B were also assessed by immunofluorescence and immunohistochemistry assays. However, none of those cell death effectors displayed a differential expression between rGd-eno treated and non-treated cells (Supplementary

Figure 4). Nevertheless, as shown in Figure 8Ac, d we observed a clear increase in levels of the necroptosis marker AIF in IEC-6 monolayers rGd-eno-treated compared with non-treated IEC-6 monolayers (Figure 8Aa, b), suggesting that rGd-eno triggers necroptosis in IEC-6. The role of AIF-mediated necroptosis has been suggested previously (Delavallée et al., 2011). To analyze the role of AIF in this process, extracts from a temporal course of IEC6 cells exposed to purified Gd-eno were studied for AIF (Figure 8B); the results showed that rGd-eno treatment stimulates the release and activation of AIF in IEC-6.

Since AIF production is linked to TNF α signaling (Jurewicz et al., 2005; Xu et al., 2018), we evaluated the presence of this cytokine in supernatants from cultures of Giardia and IEC-6 interactions exposed to rGd-eno and in extracts of IEC-6 (only) (Figure 9A); rGd-eno treatment enhanced the presence of TNF α (17 kDa band) over time. Using a TNF- α processing inhibitor (TAPI-0) that blocks the

**FIGURE 8**

Determination of AIF activation upon the exposure of IEC-6 cells to rGd-eno. AIF activation was studied in IEC-6 cell monolayers exposed to rGd-eno (100 $\mu\text{g/mL}$; relative glycolytic activity 58 $\mu\text{mol/minxmg}$ of protein) for 3h. Then, immunohistochemistry and Western blot analysis of AIF expression in IEC-6 cell lysates were performed. **(A)** Immunohistochemistry images of no treated cells **(a, b)** and treated cells with rGd-eno at **(c)** 90 min and **(d)** 120 min. **(B)** Expression of AIF in its 3 forms (precursor, mature and apoptogenic) at different times of exposure to rGd-eno (0 min, 30 min, 60 min, 120 min, and 180 min).

generation of the active form of $\text{TNF}\alpha$ (17 kDa) by inhibiting TACE, we showed that TAPI-0 inhibited rGd-eno-induced damage to IEC-6 (Figure 9Bc,d). In addition, BAY 11-7082, a nuclear NF-kappa B inhibitor that reduces $\text{TNF}\alpha$ expression/secretion (Zhang and Feng, 2022) also decreased cell damage

in a dose-dependent manner (Figure 9b,e,f). The indirect effect of BAY 11-7082 on the $\text{TNF}\alpha$ production/signaling could partially explain the reduction in rGd-eno-mediated damage in IEC-6 cell monolayers. Taken together, these results showed that the activation of AIF and $\text{TNF}\alpha$ release

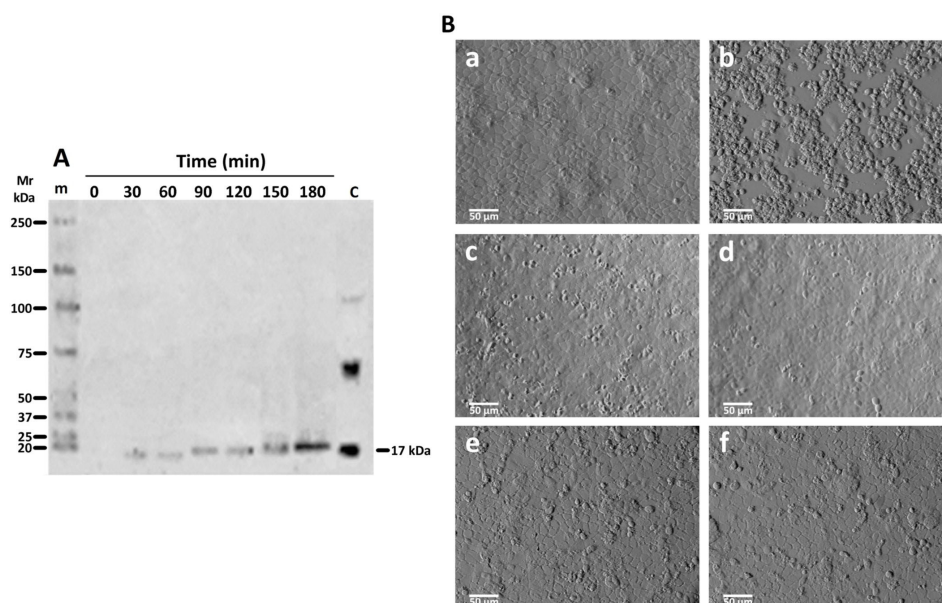


FIGURE 9

TNFα release in supernatants of IEC-6 cells exposed to rGd-eno and effect of the inhibition of TNFα activity with TAPI-0 and BAY 11-7082. Supernatants from IEC-6 cells incubated with rGd-eno at the indicated times were analyzed by Western Blot using anti-TNFα antibody. (A) Active TNFα, detected as a band of 17 kDa, Control (C) of non-active and active TNFα obtained from rat kidney extracts. (B) Inhibition of TNFα activation and IEC-6 cell damage by rGd-eno (100 μg/ml; relative glycolytic activity 58 μmol/min x mg of protein) was analyzed in the presence of different concentrations of TAPI-0 or BAY 11-7082. Untreated IEC-6 cells (a), IEC-6 cells after 3 h treatment with rGd-eno (b) then with TAPI-0 at 50 μM (c) and 100 μM (d) or with BAY 11-7082 at 40 mM (e), and 60 mM (f). Micrographs are representative of three independent experiments.

following the interaction of IEC-6 cell monolayers with rGd-eno is associated with necroptotic-like damage to epithelial cells.

Discussion

Enolase, an enzyme of the glycolytic/gluconeogenic metabolism, has been detected in the culture supernatant of different microorganisms (Lamonica et al., 2005; DelVecchio et al., 2006; Chitlaru et al., 2007) suggesting that this enzyme has functional roles other than in carbohydrate metabolism (Moore, 2004). In the case of *Giardia*, enolase (Gd-eno) is released into the medium by trophozoites during its interaction with epithelial cells (Ringqvist et al., 2011; Ma'ayeh and Brook-Carter, 2012) in a monomeric form, as shown here. However, the exact mechanism of enolase secretion in *Giardia*, how the enzyme arrives at the cell surface and how it is bound to the cell membrane are still unclear. Interestingly, the protein neither possesses a predicted transmembrane region or glycosylphosphatidylinositol (GPI) anchor site nor a detectable N-terminal transit peptide, suggesting that it is not transported via the classical secretory pathway. Nevertheless, immunofluorescence assays

using specific antibodies to rGd-eno revealed that this protein is present in the cytoplasm in small vesicles that could be part of the mechanism of secretion, as has been reported in *Trypanosoma* (Avilán et al., 2011), but this process needs further exploration.

Additionally, we demonstrated that Gd-eno is a protein with moonlighting functions, as observed for other parasites, and plays a role as an intracellular metabolic enzyme as well as an extracellular ligand for plasminogen. As a result of this interaction, plasmin activity is enhanced. Since enolase does not possess an intrinsic protease activity or protease domains, the generation of active plasmin with monomeric Gd-eno is possibly due to an induction of conformational changes that allow the exposure of zymogen domains in the plasminogen following ligand binding. Regarding Gd-eno-HsPIgII interactions, these were previously hypothesized and analyzed in silico, in terms of the “open” (with one Mg²⁺ bound, here named as partially active) and “closed” (with two Mg²⁺ ions bound, named here as “fully active”) conformations of the Gd-eno dimer (Aguayo-Ortiz et al., 2017). The importance of the PID and K266, along with the modeling data help to predict the putative conformational changes occurring in the Gd-eno dimer following Mg²⁺ binding (Aguayo-Ortiz et al., 2017). However, our findings suggest that the secreted Gd-eno monomer can

interact with host plasminogen at its SP, K3 and K4 domains and the lysine-rich interactive environment, as suggested by the inhibition of plasmin activity with the lysine analog ϵ -ACA. In addition, the docking of the closed or fully active conformation of Gd-eno monomer suggests that Gd-eno might interact with an open conformation of HsPlg and might be required to promote optimal plasmin activity. Once plasmin is generated and activated, it can cleave fibrin, fibronectin and laminin (Plow et al., 1995), and activates other proteolytic enzymes, resulting in the cleavage of collagen, elastin, proteoglycans (Murphy et al., 1999) and intercellular junctions (Attali et al., 2008), or induces the release of cytokines – as evidenced here. This process could, therefore, be responsible for inducing the damage in epithelial cells before undergoing cell death.

A key finding here was the release of the active form of TNF α (17 kDa) into the medium following the incubation of rGd-eno with IEC-6 epithelial cells. The damage induced by rGd-eno on the cells was inhibited using inhibitors of TNF α activators, such as TAPI-0, indicating that the TNF α released by epithelial cells after the interaction of enolase plays a role in the process. Therefore, is easy to speculate that the stimulation and enhancing of the plasminogen-plasmin system could mediate the activation of TACE (DasGupta et al., 2009). Furthermore, the reduction of epithelial cell damage in the monolayers incubated with rGd-eno after the inhibition of TNF α downstream signaling with BAY 11-7082, confirms that TNF α signaling participates in the epithelial cell damage, triggered by rGd-eno. Such findings correlate with previous reports linking necroptosis to the presence of TNF α (Günther et al., 2011). In addition, the increase activation of AIF in IEC-6 cells by rGd-eno supports the idea that rGd-eno induces a necroptosis-like damage in epithelial cells via TNF α . Currently, several studies have shown that secretion of TNF α was indeed stimulated during giardiasis (Saghaug et al., 2016), or induced by parasite components (Muñoz-Cruz et al., 2010). Indeed, direct activation of mast cells by live *G. duodenalis* trophozoites or trophozoite-derived antigens induced the release of TNF- α from mast cells through an Ig-independent pathway (Muñoz-Cruz et al., 2010). In a more recent study (Muñoz-Cruz et al., 2018), a parasite extract-fraction, named F2, which contains among other proteins, ADI and enolase, induced the release of IL-6 and TNF- α by mast cells, which have been shown previously to play an important role in controlling infection with both *G. muris* and *G. duodenalis* (Fink and Singer, 2017). Interestingly, the analysis of the mitochondrial flavoprotein AIF, a caspase-independent death effector (Candé et al., 2002), revealed its possible role in the epithelial damage triggered by the enolase/TNF α mechanism. Immunohistochemistry and Western blot analyses showed an increased activation of AIF into its three principal forms: precursor, mature and apoptogenic. In conjunction, these results also support the notion that rGd-eno induces a necroptosis-like

damage in IEC-6 monolayers in a way that occurs downstream of TNF α .

The pathway triggering the necroptotic-like damage caused by rGd-eno in epithelial cells is presently unknown and no microbial enolase has yet been reported to induce necroptosis of host cells. Based on the experimental findings here, it is plausible that rGd-eno interacts with HsPlg, to generate plasmin activity that degrade extracellular matrix components, and promotes enterocyte cell death. In this context, Gd-eno was detected as a monomer when secreted by trophozoites and, therefore, the presence of a monomeric Gd-eno may be necessary to trigger necroptotic-like damage in epithelial cell monolayers. In this context, the previously hypothesized monomer state of enolases could explain, at least in part, its multifunctionality (Pal-Bhowmick et al., 2007). Firstly, enolase has been reported previously to function as a plasminogen receptor for bacterial, fungal, protozoal and helminth pathogens that modulates the innate immunity and promotes the damage of host tissues as well as the disturbance of the fibrinolytic system, thereby facilitating pathogen invasion and establishment (Ayón-Núñez et al., 2018). Secondly, the secretion of Gd-eno monomer was enhanced upon interaction of trophozoites with epithelial cells, in agreement with previous reports, demonstrating the increase of both Gd-eno mRNA levels and Gd-eno protein amounts in supernatants due to these interactions (Ringqvist et al., 2008). Thirdly, the monomeric nature of secreted Gd-eno correlates not only with the experimental data obtained here and with the catalytic ability of the endogenous enzyme but also allowed to determine in a functional context its plasminogen-activating role and its driving contribution in the necroptosis-like damage of epithelial cells.

Lastly, to oversee the epithelial cell damage induced by the enolase we used high concentrations of the enzyme (100 μ g/mL) to exacerbate the outcome. However, ex vivo the trophozoites can locally induce cell damage in the enterocytes that are present in the surface of the villi and the injuries strongly mimic the observed in our in vitro model. Thus, based on the results we can envision two scenarios that contribute to the pathogenesis of the parasite: a) in a local microenvironment, the concentration of secreted enolase is higher than expected and, b) the parasite displays tropism for areas enriched with enolase receptor and that promotes the enolase-receptor interactions. However, with our results, the presence of additional mechanisms enolase-dependent that could be important in the pathogenesis induced by *Giardia* cannot be ruled out. We consider that all concepts are interesting and must be investigated in the future.

In conclusion, the present findings support the role of *G. duodenalis* enolase in the damage of epithelial cells; therefore,

this enzyme should be considered as an element of the virulence factors in this parasite (Argüello-García and Ortega-Pierres, 2021). Future studies of the participation of enolase during the interaction of *Giardia* trophozoites with host intestinal epithelial cells using experimental animal models will provide insights into its role on the pathogenesis of giardiasis.

Data availability statement

The original contributions presented in the study are included in the article/Supplementary Material, further inquiries can be directed to the corresponding author/s.

Author contributions

GO-P: conceptualization and supervision. EB-E RF-L, RA-G, RM-R and RB-C: experiments. GO-P, EB-E and RA-G: writing of the original draft. N-P writing, comments and revision. GO-P funding acquisition. All authors contributed to the article and approved the submitted version.

Funding

This work was supported in part by Fondo Sectorial Secretaría de Educación Pública-Consejo Nacional de Ciencia y Tecnología (SEP-CONACYT) México, Grant number A1-S-39422 and by the Miguel Aleman Foundation and Cinvestav. México.

Acknowledgments

The authors wish to express special thanks to Rusely Encalada (INCar, Mexico) for her help in determining enolase activity and to Emma Saavedra (INCar, Mexico) for her valuable comments and suggestions while performing this work. We thank Silvia Espinosa-Matías (UNAM Mexico) and Bibiana Chávez Munguía (Cinvestav Mexico) for their skillful assistance in obtaining scanning electron microscopy micrographs and Sara Huerta Yépez (HIMFG Mexico) for her advice and help in the detection of cell death markers. We also thank María Luisa Bazán Tejeda and Antonio Sandoval Cabrera (Cinvestav Mexico) for technical support in cloning *Giardia* enolase, to Adrián Chávez Cano and Arturo Pérez-Taylor (Cinvestav Mexico) for the artwork. We are most grateful to Prof. Robin B. Gasser for editorial comments on the manuscript. We thank Prof. Keith Gull, University of Oxford, Oxford, UK for the donation of the anti- α -tubulin antibody and to Héctor Romero (Cinvestav Mexico) for providing antibodies against TNF α .

Conflict of interest

The authors declare that the research was conducted in the absence of any commercial or financial relationships that could be construed as a potential conflict of interest.

Publisher's note

All claims expressed in this article are solely those of the authors and do not necessarily represent those of their affiliated organizations, or those of the publisher, the editors and the reviewers. Any product that may be evaluated in this article, or claim that may be made by its manufacturer, is not guaranteed or endorsed by the publisher.

Supplementary material

The Supplementary Material for this article can be found online at: <https://www.frontiersin.org/articles/10.3389/fcimb.2022.928687/full#supplementary-material>

SUPPLEMENTARY FIGURE 1

Alignment of the amino-acid sequences of *Giardia* enolase with similar proteins from different organisms. Amino-acid sequence alignment of enolases from *Homo sapiens* (α -enolase, accession number NP_001419), *Saccharomyces cerevisiae* (accession number AAA88713.1), *Trypanosoma brucei* (accession number XP_822542) and *G. duodenalis* assemblage A (GL50803_11118). Cyano-shaded letters indicate residues involved in ligand (phosphoenolpyruvate) binding and residues involved in Mg²⁺ binding are shown in brown-shaded letters. Green-shaded letters are unique reactive active-site residues found in enolases from some protozoa (Avilán et al., 2011) including *Giardia*. The three lysines considered as primary plasminogen binding sites are enclosed in green box whilst the red box indicates the proposed plasminogen binding motif. The underline in red identifies a conserved loop involved in the protonation of 2-phosphoglycerate by H159. The enolase signature is indicated in bold letters. Residues in red are that forming ionic bond in the enolase dimer. Yellow-shaded letters are variant residues between *Giardia* A, B and E assemblages and black-shaded letters are residues absent in assemblage E. Multiple sequence alignment was carried out using the CLUSTALW 2.1 software (<http://www.genome.jp/tools/clustalw/>) with default parameters

SUPPLEMENTARY FIGURE 2

Enolase gene amplification, cloning and production of recombinant enolase. (A) Plasmid map for PET-100_ENO with the enolase gene in the PET-100 D-TOPO® (Invitrogen) transition-expression vector and 6XHis Tag. (B) PCR amplification of a 1500 bp product resolved in a 1% agarose gel and stained with ethidium bromide which was, confirmed to be the enolase gene by automatic DNA sequencing. (C) SDS-PAGE of the fractions obtained during the purification process of rGd-eno; demonstrate an enriched band of \approx 48 kDa corresponding to enolase obtained in the fraction C.

SUPPLEMENTARY FIGURE 3

Absence of damage in IEC-6 cells by extracts from *E. coli* BL21 Star lacking Gd-eno. IEC-6 monolayers were incubated for 2h at 37°C in 2 cm² wells in serum free DMEM medium (A) Control IEC-6 cell monolayers incubated with DMEM only, showing the normal morphology of the cell monolayer. (B) IEC-6 monolayers incubated with *E. coli* BL21 Star extracts

dialyzed and passed through a High Capacity Endotoxin Removal (Pierce™) column. (C) IEC-6 cell monolayers exposed to rGd-eno.

SUPPLEMENTARY FIGURE 4

Determination of IEC-6 monolayer cell confluence on cell damage induced by rGd-eno. IEC-6 cell monolayers were incubated with rGd-eno as described in material and methods. IEC-6 cell monolayers were grown at three different confluences (D) 50%, (E) 70% and (F) 100% in the presence of 100 mg/ml; of rGd-eno. (relative glycolytic activity 58 mmol/minx mg of protein). Untreated IEC-6 cell monolayers grown at the same confluences of 50% (A), 70% (B) and 100% (C) were used

as negative controls. Micrographs are representative of three independent experiments.

SUPPLEMENTARY FIGURE 5

Determination of Caspase 3, Caspase 8, Caspase 9, BID and LC3B activity. Apoptosis and autophagy were analyzed by immunofluorescence (A). IEC-6 cell nuclei were stained with DAPI (A, B) while, caspase 3 (C) and LC3B (D) are shown in green. Immunohistochemistry assays with IEC-6 cells monolayers incubated in the absence (A–C) or in the presence of rGd-eno (D–F). Caspase 3 (A, D), Caspase 8 (B, E) or BID (C, F) was performed. Scale bar = 20mm.

References

- Aguiar-Ortiz, R., Meza-Cervantes, P., Castillo, R., Hernández-Campos, A., Domínguez, L., and Yépez-Mulia, L. (2017). Insights into the giardia intestinalis enolase and human plasminogen interaction. *Mol. Biosyst.* 13, 2015–2023. doi: 10.1039/C7MB00252A
- Ankarklev, J., Jerlström-Hultqvist, J., Ringqvist, E., Troell, K., and Svärd, S. G. (2010). Behind the smile: cell biology and disease mechanisms of giardia species. *Nat. Rev. Microbiol.* 8, 413–422. doi: 10.1038/nrmicro2317
- Argüello-García, R., and Ortega-Pierres, M. G. (2021). Giardia duodenalis virulence — “To be, or not to be.” *Curr. Trop. Med. Rep.* 8, 246–256. doi: 10.1007/S40475-021-00248-Z
- Attali, C., Durmort, C., Vernet, T., and Di Guilmi, A. M. (2008). The interaction of *Streptococcus pneumoniae* with plasmin mediates transmigration across endothelial and epithelial monolayers by intercellular junction cleavage. *Infect. Immun.* 76, 5350–5356. doi: 10.1128/IAI00184-08
- Avilán, L., Gualdrón-López, M., Quiñones, W., González-González, L., Hannaert, V., Michels, P. A. M., et al. (2011). Enolase: A key player in the metabolism and a probable virulence factor of trypanosomatid parasites—perspectives for its use as a therapeutic target. *Enzyme Res.* 2011, 1–14. doi: 10.4061/2011/932549
- Ayón-Núñez, D. A., Fragoso, G., Bobes, R. J., and Laclette, J. P. (2018). Plasminogen-binding proteins as an evasion mechanism of the host's innate immunity in infectious diseases. *Biosci. Rep.* 38:1–16. doi: 10.1042/BSR20180705
- Benítez-Rangel, E., García, L., Namorado, M. C., Reyes, J. L., and Guerrero-Hernández, A. (2011). Ion channel inhibitors block caspase activation by mechanisms other than restoring intracellular potassium concentration. *Cell Death Dis.* 2, e113–e113. doi: 10.1038/cddis.2010.93
- Benítez-Rangel, E., López-Méndez, M. C., García, L., and Guerrero-Hernández, A. (2015). DIDS (4,4'-Diisothiocyanatobenzene-2,2'-disulfonate) directly inhibits caspase activity in HeLa cell lysates. *Cell Death Disov.* 1:1–8. doi: 10.1038/cddiscovery.2015.37
- Birkeland, S. R., Preheim, S. P., Davids, B. J., Cipriano, M. J., Palm, D., Reiner, D. S., et al. (2010). Transcriptome analyses of the giardia lamblia life cycle. *Mol. Biochem. Parasitol.* 174, 62–65. doi: 10.1016/j.molbiopara.2010.05.010
- Bolten, K. E., Marsh, A. E., Reed, S. M., Dubey, J. P., Toribio, R. E., and Saville, W. J. A. (2008). Sarcocystis neurona: Molecular characterization of enolase domain I region and a comparison to other protozoa. *Exp. Parasitol.* 120, 108–112. doi: 10.1016/j.exppara.2008.05.004
- Cabrera-Licona, A., Solano-González, E., Fonseca-Liñán, R., Bazán-Tejeda, M. L., Argüello-García, Raúl, Bermúdez-Cruz, R. M., et al. (2017). Expression and secretion of the giardia duodenalis variant surface protein 9B10A by transfected trophozoites causes damage to epithelial cell monolayers mediated by protease activity. *Exp. Parasitol.* 179, 49–64. doi: 10.1016/j.exppara.2017.06.006
- Candé, C., Cohen, I., Daugas, E., Ravagnan, L., Larochette, N., Zamzami, N., et al. (2002). Apoptosis-inducing factor (AIF): a novel caspase-independent death effector released from mitochondria. *Biochimie* 84, 215–222. doi: 10.1016/S0300-9084(02)01374-3
- Castellino, F., and Ploplis, V. (2005). Structure and function of the plasminogen/plasmin system. *Thromb. Haemost.* 93, 647–654. doi: 10.1160/TH04-12-0842
- Castillo-Romero, A., Davids, B. J., Lauwaet, T., and Gillin, F. D. (2012). Importance of enolase in giardia lamblia differentiation. *Mol. Biochem. Parasitol.* 184, 122–125. doi: 10.1016/j.molbiopara.2012.04.011
- Chitlaru, T., Gat, O., Grosfeld, H., Inbar, I., Gozlan, Y., and Shafferman, A. (2007). Identification of *In vivo*-expressed immunogenic proteins by serological proteome analysis of the *Bacillus anthracis* secretome. *Infect. Immun.* 75, 2841–2852. doi: 10.1128/IAI02029-06
- Cotton, J. A., Beatty, J. K., and Buret, A. G. (2011). Host parasite interactions and pathophysiology in giardia infections. *Int. J. Parasitol.* 41, 925–933. doi: 10.1016/j.ijpara.2011.05.002
- DasGupta, S., Murumkar, P. R., Giridhar, R., and Yadav, M. R. (2009). Current perspective of TACE inhibitors: A review. *Bioorg. Med. Chem.* 17, 444–459. doi: 10.1016/j.bmc.2008.11.067
- Day, I. N. M., Peshavaria, M., and Quinn, G. B. (1993). A differential molecular clock in enolase isoprotein evolution. *J. Mol. Evol.* 36, 599–601. doi: 10.1007/BF00556365
- Delavallée, L., Cabon, L., Galán-Malo, P., Lorenzo, H. K., and Susin, S. A. (2011). AIF-mediated caspase-independent necroptosis: A new chance for targeted therapeutics. *IUBMB Life* 63, 221–232. doi: 10.1002/iub.432
- DelVecchio, V. G., Connolly, J. P., Alefantis, T. G., Walz, A., Quan, M. A., Patra, G., et al. (2006). Proteomic profiling and identification of immunodominant spore antigens of *Bacillus anthracis*, *Bacillus cereus*, and *Bacillus thuringiensis*. *Appl. Environ. Microbiol.* 72, 6355–6363. doi: 10.1128/AEM.00455-06
- Díaz-Ramos, A., Roig-Borrellas, A., García-Melero, A., Llorens, A., and López-Alemany, R. (2012). Requirement of plasminogen binding to its cell-surface receptor α -enolase for efficient regeneration of normal and dystrophic skeletal muscle. *PLoS One* 7, e50477. doi: 10.1371/journal.pone.0050477
- Eckmann, L., Laurent, F., Langford, T. D., Hetsko, M. L., Smith, J. R., Kagnoff, M. F., et al. (2000). Nitric oxide production by human intestinal epithelial cells and competition for arginine as potential determinants of host defense against the lumen-dwelling pathogen *Giardia lamblia*. *J. Immunol.* 164, 1478–1487. doi: 10.4049/jimmunol.164.3.1478
- Fink, M. Y., and Singer, S. M. (2017). The intersection of immune responses, microbiota, and pathogenesis in giardiasis. *Trends Parasitol.* 33, 901–913. doi: 10.1016/j.pt.2017.08.001
- Günther, C., Martini, E., Wittkopf, N., Amann, K., Weigmann, B., Neumann, H., et al. (2011). Caspase-8 regulates TNF- α -induced epithelial necroptosis and terminal ileitis. *Nature* 477, 335–339. doi: 10.1038/nature10400
- Jurewicz, A., Matysiak, M., Tybor, K., Kilianek, L., Raine, C. S., and Selmaj, K. (2005). Tumour necrosis factor-induced death of adult human oligodendrocytes is mediated by apoptosis inducing factor. *Brain* 128, 2675–2688. doi: 10.1093/brain/awh627
- Karanis, P., Kourenti, C., and Smith, H. (2007). Waterborne transmission of protozoan parasites: A worldwide review of outbreaks and lessons learnt. *J. Water Health* 5, 1–38. doi: 10.2166/wh.2006.002
- Keister, D. B. (1983). Axenic culture of giardia lamblia in TYI-S-33 medium supplemented with bile. *Trans. R. Soc. Trop. Med. Hyg.* 77, 487–488. doi: 10.1016/0035-9203(83)90120-7
- Laemmli, U. K. (1970). Cleavage of structural proteins during the assembly of the head of bacteriophage T4. *Nature* 227, 680–685. doi: 10.1038/227680a0
- Lähteenmäki, K., Kuusela, P., and Korhonen, T. K. (2001). Bacterial plasminogen activators and receptors. *FEMS Microbiol. Rev.* 25, 531–552. doi: 10.1111/j.1574-6976.2001.tb00590.x
- Lamonica, J. M., Wagner, M., Eschenbrenner, M., Williams, L. E., Miller, T. L., Patra, G., et al. (2005). Comparative secretome analyses of three *Bacillus anthracis* strains with variant plasmid contents. *Infect. Immun.* 73, 3646–3658. doi: 10.1128/IAI73.6.3646-3658.2005
- Law, R. H. P., Caradoc-Davies, T., Cowieson, N., Horvath, A. J., Quek, A. J., Encarnacao, J. A., et al. (2012). The X-ray crystal structure of full-length human plasminogen. *Cell Rep.* 1, 185–190. doi: 10.1016/j.celrep.2012.02.012
- Liu, J., Ma'ayeh, S., Peirasmaki, D., Lundström-Stadelmann, B., Hellman, L., and Svärd, S. G. (2018). Secreted giardia intestinalis cysteine proteases disrupt intestinal

epithelial cell junctional complexes and degrade chemokines. *Virulence* 9, 879–894. doi: 10.1080/21505594.2018.1451284

Lu, Q., Lu, H., Qi, J., Lu, G., and Gao, G. F. (2012). An octamer of enolase from streptococcus suis. *Protein Cell* 3, 769–780. doi: 10.1007/s13238-012-2040-7

Ma'ayeh, S. Y., and Brook-Carter, P. T. (2012). Representational difference analysis identifies specific genes in the interaction of giardia duodenalis with the murine intestinal epithelial cell line, IEC-6. *Int. J. Parasitol.* 42, 501–509. doi: 10.1016/j.ijpara.2012.04.004

Moore, B. d (2004). Bifunctional and moonlighting enzymes: lighting the way to regulatory control. *Trends Plant Sci.* 9, 221–228. doi: 10.1016/j.tplants.2004.03.005

Muñoz-Cruz, S., Gomez-García, A., Matadamas-Martínez, F., Alvarado-Torres, J. A., Meza-Cervantez, P., Arriaga-Pizano, L., et al. (2018). Giardia lamblia: identification of molecules that contribute to direct mast cell activation. *Parasitol. Res.* 117, 2555–2567. doi: 10.1007/s00436-018-5944-1

Muñoz-Cruz, S., Gómez-García, A., Millán-Ibarra, J., Giono-Cerezo, S., and Yépez-Mulia, L. (2010). Giardia lamblia: Interleukin 6 and tumor necrosis factor- α release from mast cells induced through an ig-independent pathway. *Exp. Parasitol.* 126, 298–303. doi: 10.1016/j.exppara.2010.06.013

Murphy, G., Stanton, H., Cowell, S., Butler, G., Knäuper, V., Atkinson, S., et al. (1999). Mechanisms for pro matrix metalloproteinase activation. *APMIS* 107, 38–44. doi: 10.1111/j.1699-0463.1999.tb01524.x

Ortega-Pierres, G., Argüello-García, R., Laredo-Cisneros, M. S., Fonseca-Linán, R., Gómez-Mondragón, M., Inzunza-Arroyo, R., et al. (2018). Giardipain-1, a protease secreted by giardia duodenalis trophozoites, causes junctional, barrier and apoptotic damage in epithelial cell monolayers. *Int. J. Parasitol.* 48, 621–639. doi: 10.1016/j.ijpara.2018.01.006

Pal-Bhowmick, I., Krishnan, S., and Jarori, G. K. (2007). Differential susceptibility of plasmodium falciparum versus yeast and mammalian enolases to dissociation into active monomers. *FEBS J.* 274, 1932–1945. doi: 10.1111/j.1742-4658.2007.05738.x

Pancholi, V. (2001). Multifunctional α -enolase: its role in diseases. *Cell. Mol. Life Sci.* 58, 902–920. doi: 10.1007/PL00000910

Peetermans, M., Vanassche, T., Liesenborghs, L., Claes, J., Vande Velde, G., Kwiecinski, J., et al. (2014). Plasminogen activation by staphylokinase enhances local spreading of s. aureus in skin infections. *BMC Microbiol.* 14, 310. doi: 10.1186/s12866-014-0310-7

Plow, E. F., Herren, T., Redlitz, A., Miles, L. A., and Hoover-Plow, J. L. (1995). The cell biology of the plasminogen system. *FASEB J.* 9, 939–945. doi: 10.1096/fasebj.9.10.7615163

Ringqvist, E., Avesson, L., Söderbom, F., and Svärd, S. G. (2011). Transcriptional changes in giardia during host–parasite interactions. *Int. J. Parasitol.* 41, 277–285. doi: 10.1016/j.ijpara.2010.09.011

Ringqvist, E., Palm, J. E. D., Skarin, H., Hehl, A. B., Weiland, M., Davids, B. J., et al. (2008). Release of metabolic enzymes by giardia in response to interaction with intestinal epithelial cells. *Mol. Biochem. Parasitol.* 159:277–85. doi: 10.1016/j.molbiopara.2008.02.005

Rodríguez-Fuentes, G. B., Cedillo-Rivera, R., Fonseca-Liñán, R., Argüello-García, R., Muñoz, O., Ortega-Pierres, G., et al. (2006). Giardia duodenalis: analysis of secreted proteases upon trophozoite-epithelial cell interaction *in vitro*. *Mem. Inst. Oswaldo Cruz* 101, 693–696. doi: 10.1590/S0074-02762006000600020

Roxström-Lindquist, K., Ringqvist, E., Palm, D., and Svärd, S. (2005). Giardia lamblia -induced changes in gene expression in differentiated caco-2 human intestinal epithelial cells. *Infect. Immun.* 73, 8204–8208. doi: 10.1128/IAI.73.12.8204-8208.2005

Saavedra, E., Encalada, R., Pineda, E., Jasso-Chávez, R., and Moreno-Sánchez, R. (2005). Glycolysis in entamoeba histolytica. *FEBS J.* 272, 1767–1783. doi: 10.1111/j.1742-4658.2005.04610.x

Saghaug, C. S., Sørnes, S., Peirasmaki, D., Svärd, S., Langeland, N., and Hanevik, K. (2016). Human memory CD4⁺ T cell immune responses against giardia lamblia. *Clin. Vaccine Immunol.* 23, 11–18. doi: 10.1128/CI.00419-15

Schreier, B., and Höcker, B. (2010). Engineering the enolase magnesium II binding site: Implications for its evolution. *Biochemistry* 49, 7582–7589. doi: 10.1021/bi100954f

Smith, H. W., and Marshall, C. J. (2010). Regulation of cell signalling by uPAR. *Nat. Rev. Mol. Cell Biol.* 11, 23–36. doi: 10.1038/nrm2821

Stadelmann, B., Hanevik, K., Andersson, M. K., Bruserud, O., and Svärd, S. G. (2013). The role of arginine and arginine-metabolizing enzymes during giardia – host cell interactions *in vitro*. *BMC Microbiol.* 13, 256. doi: 10.1186/1471-2180-13-256

Vassalli, J. D., Sappino, A. P., and Belin, D. (1991). The plasminogen activator/plasmin system. *J. Clin. Invest.* 88, 1067–1072. doi: 10.1172/JCI115405

Wu, Y., Wang, C., Lin, S., Wu, M., Han, L., Tian, C., et al. (2015). Octameric structure of Staphylococcus aureus enolase in complex with phosphoenolpyruvate. *Acta Crystallogr. Sect. D Biol. Crystallogr.* 71, 2457–2470. doi: 10.1107/S1399004715018830

Xu, B., Zhou, M., Wang, J., Zhang, D., Guo, F., Si, C., et al. (2018). Increased AIF-1-mediated TNF- α expression during implantation phase in IVF cycles with GnRH antagonist protocol. *Hum. Reprod.* 33, 1270–1280. doi: 10.1093/humrep/dey119

Zhang, Y., and Feng, L. (2022). Thyroid-stimulating hormone inhibits insulin receptor substrate-1 expression and tyrosyl phosphorylation in 3T3-L1 adipocytes by increasing NF- κ B DNA-binding activity. *Dis. Markers* 2022, 1–9. doi: 10.1155/2022/7553670



OPEN ACCESS

EDITED BY

Mario Alberto Rodriguez,
Instituto Politécnico Nacional de
México (CINVESTAV), Mexico

REVIEWED BY

Edwin Lasonder,
Northumbria University,
United Kingdom
Maria M. Corvi,
Consejo Nacional de Investigaciones
Científicas y Técnicas (CONICET),
Argentina
Karine Frénil,
UMR5234 Microbiologie
Fondamentale et Pathogénicité (MFP),
France

*CORRESPONDENCE

Shailja Singh
shailja.jnu@gmail.com
Anand Ranganathan
anand.icgeb@gmail.com
Soumya Pati
soumya.pati@snu.edu.in

[†]These authors share first authorship

SPECIALTY SECTION

This article was submitted to
Parasite and Host,
a section of the journal
Frontiers in Cellular and
Infection Microbiology

RECEIVED 20 April 2022

ACCEPTED 10 August 2022

PUBLISHED 29 September 2022

CITATION

Anam Z, Kumari G, Mukherjee S,
Rex DAB, Biswas S, Maurya P,
Ravikumar S, Gupta N, Kushawaha AK,
Sah RK, Chaurasiya A, Singhal J,
Singh N, Kaushik S, Prasad TSK, Pati S,
Ranganathan A and Singh S (2022)
Complementary crosstalk between
palmitoylation and phosphorylation
events in MTIP regulates its role during
Plasmodium falciparum invasion.
Front. Cell. Infect. Microbiol. 12:924424.
doi: 10.3389/fcimb.2022.924424

Complementary crosstalk between palmitoylation and phosphorylation events in MTIP regulates its role during *Plasmodium falciparum* invasion

Zille Anam^{1†}, Geeta Kumari^{1†}, Soumyadeep Mukherjee^{2†},
Devasahayam Arokia Balaya Rex^{3†}, Shreeja Biswas¹,
Preeti Maurya¹, Susendaran Ravikumar², Nutan Gupta¹,
Akhilesh Kumar Kushawaha¹, Raj Kumar Sah¹,
Ayushi Chaurasiya¹, Jhalak Singhal¹, Niharika Singh¹,
Shikha Kaushik¹, T. S. Keshava Prasad⁴, Soumya Pati^{2*},
Anand Ranganathan^{1*} and Shailja Singh^{1*}

¹Special Centre for Molecular Medicine, Jawaharlal Nehru University, New Delhi, India,

²Department of Life Sciences, School of Natural Sciences, Shiv Nadar University, Greater Noida, Uttar Pradesh, India, ³Center for Integrative Omics Data Science, Yenepoya (Deemed to be University), Mangalore, India, ⁴Center for Systems Biology and Molecular Medicine, Yenepoya (Deemed to be University), Mangalore, India

Post-translational modifications (PTMs) including phosphorylation and palmitoylation have emerged as crucial biomolecular events that govern many cellular processes including functioning of motility- and invasion-associated proteins during *Plasmodium falciparum* invasion. However, no study has ever focused on understanding the possibility of a crosstalk between these two molecular events and its direct impact on preinvasion- and invasion-associated protein–protein interaction (PPI) network-based molecular machinery. Here, we used an integrated *in silico* analysis to enrich two different catalogues of proteins: (i) the first group defines the cumulative pool of phosphorylated and palmitoylated proteins, and (ii) the second group represents a common set of proteins predicted to have both phosphorylation and palmitoylation. Subsequent PPI analysis identified an important protein cluster comprising myosin A tail interacting protein (MTIP) as one of the hub proteins of the glideosome motor complex in *P. falciparum*, predicted to have dual modification with the possibility of a crosstalk between the same. Our findings suggested that blocking palmitoylation led to reduced phosphorylation and blocking phosphorylation led to abrogated palmitoylation of MTIP. As a result of the crosstalk between these biomolecular events, MTIP's interaction with myosin A was found to be abrogated. Next, the crosstalk between phosphorylation and palmitoylation was confirmed at a global proteome level by click chemistry and the phenotypic effect of this crosstalk was observed *via* synergistic inhibition in *P. falciparum* invasion using checkerboard assay and isobologram method.

Overall, our findings revealed, for the first time, an interdependence between two PTM types, their possible crosstalk, and its direct impact on MTIP-mediated invasion via glideosome assembly protein myosin A in *P. falciparum*. These insights can be exploited for futuristic drug discovery platforms targeting parasite molecular machinery for developing novel antimalarial therapeutics.

KEYWORDS

malaria, *Plasmodium falciparum*, crosstalk, myosin A tail interacting protein (MTIP), post-translational modifications

Introduction

Plasmodium falciparum (*P. falciparum*) has remained a versatile and highly adaptable pathogen causing severe mortality in humans (Health Organization, 2019). The parasite successfully cycles through the non-vertebrate (female *Anopheles* mosquito) and vertebrate (human) hosts. The parasite enters its human hosts through the saliva upon a mosquito bite that injects sporozoites into blood. The sporozoites first reach the liver where the asexual reproduction happens; this increases the parasite numbers and leads to an eventual release of merozoites into the bloodstream leading to the infection of red blood cells (RBCs). The parasite is also conveniently able to undergo stage transformations, and reinfect, thereby causing drastic effects in humans. Notably, biomolecular events like post-translational modifications (PTMs), including phosphorylation, methylation, and ubiquitylation, are known to govern survival, life-cycle progression, biology, and pathogenesis in the Apicomplexan parasites by modulating the proteomic diversity (Jortzik et al., 2011; Douse et al., 2012; Doerig et al., 2015; Vembar et al., 2016; Yakubu et al., 2018).

Annotation of PTM modifications involved in critical biomolecular processes is a well-established tool to identify parasite-specific molecular targets (Park et al., 2015; Yakubu et al., 2018). Phosphorylation and palmitoylation are the two most critical PTM types known in *P. falciparum* and have been shown to play crucial roles during various stages of the parasite life-cycle progression (Jones et al., 2012; Yakubu et al., 2018; Perrin et al., 2020). Existing studies have shown that among all the modified proteins, phosphorylated and palmitoylated proteins, mostly expressed on the parasite surface and the inner leaflet, are responsible for host cell invasion processes (Jones et al., 2012). The force necessary for the *Plasmodium* spp. parasites to glide and invade the host RBCs is generated by the

glideosome complex. The differential states of the gliding and invasion machinery have been earlier associated with the phosphorylation and/or palmitoylation events in *Plasmodium* parasites (Douse et al., 2012; Jones et al., 2012; Ridzuan et al., 2012; Alam et al., 2015; Lasonder et al., 2015). However, there is a paucity in the understanding if these PTM types can crosstalk to regulate parasite processes during the asexual growth stages. Toward this, our study has shown for the first time 1) an experimental documentation of a cross-regulation of phosphorylation and palmitoylation at both global and individual protein levels and 2) interdependence of phosphorylation and palmitoylation over MTIP governing its essentialness, and interactions with myosin A during the asexual intraerythrocytic development of parasites. Additionally, a catalog of all PTM hotspots and specific proteins associated with parasite motility and invasion-related processes have been documented. The detailed strategy and findings of this study have been organized as a schematic representation (Figure 1).

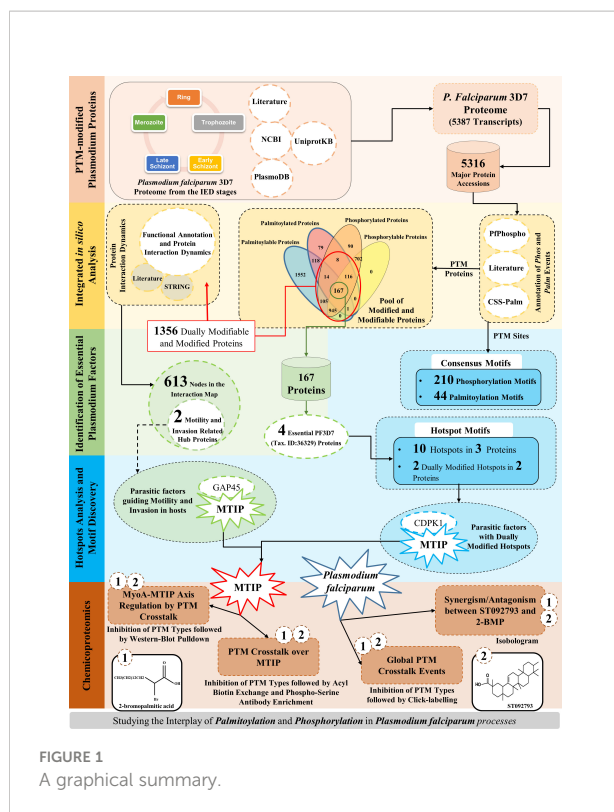
Materials and methods

In silico prediction of phosphorylation and palmitoylation in *Plasmodium falciparum*

The updated proteome of *P. falciparum* 3D7 was indexed from databases like PlasmoDB Release 58 (Amos et al., 2022), National Center for Biotechnology Information or NCBI (GCA_000002765), Pf-Phospho (Gupta et al., 2022), and UniProtKB Release 2022_02 (Bateman et al., 2021), and also from other curated resources (Solyakov et al., 2011; Jones et al., 2012; Lasonder et al., 2012; Govindasamy et al., 2016; Kumar et al., 2017a; Kumar et al., 2017b; Pease et al., 2018; Blomqvist et al., 2020; Gupta et al., 2022). Probable pseudogenes were removed from the library, and only the genes with a protein coding potential were selected for downstream processing.

Phosphorylation events specific to the proteome assembly were retrieved from curated mass spectrometry resources (Ganter et al., 2017), databases (PlasmoDB, UniProtKB,

Abbreviations: MTIP, Myosin A tail interacting protein; PTM, Post-translational modifications; CDPKs, Ca²⁺-dependent protein kinases; GAPs, Glideosome-associated proteins; 2-BMP, 2-Bromopalmitate.



PfPhospho, and NCBI), and Pf-Phospho (Gupta et al., 2022) prediction results. Proteome-specific palmitoylation events and sites were cataloged from CSS-Palm prediction results (Ren et al., 2008), publicly available mass spectrometry resources (Jones et al., 2012), and systematic database search results from PlasmoDB, NCBI, and UniProtKB. Consensus sequence windows around the central modification sites were then discovered for each of the modification types individually within all the modified proteins. The sequence windows were discovered and ranked based on their overall scores using the MoMo tool (Cheng et al., 2019) of the MEME Suite (Bailey et al., 2015).

All the proteins featuring in the union between parasite phosphoproteome and palmitome cataloged herein (curated or predicted) were termed as “Dually Modifiable” proteins. Interaction networks were generated between the dually modifiable proteins, with the highest confidence score (0.9 and above) and high FDR stringency (1% and below). The dually modifiable proteins mapped to the STRING-db were clustered into multiple functional groups using the k-mean clustering tool in the STRING database (Szklarczyk et al., 2021). The dually modifiable proteins which were predicted and referenced in the publicly available mass spectrometry datasets/curated databases (described in Section 3.1) were finally categorized as “Dually Modified” proteins. A high confidence list of essential parasitic factors with no paralogs in the human host proteome was prepared from the intersection subset ($A \cap B$) of curated

database searches and literature mining results. (Ali et al., 2021; Bateman et al., 2021; Amos et al., 2022). The dually modified proteins were subsequently mapped to the essential proteins. Only essential parasite factors exhibiting a strong probability of dual modifications were considered for the indexing of PTM sites and PTM hotspot discovery processes. For the hotspot analysis, all the modified residues were cataloged into motifs, each one featuring ± 5 amino acids. Every motif (of 11 amino acids) exhibiting a localization of ≥ 3 modified residues including the central PTM site was defined as PTM hotspots. The PTM hotspots were then categorized based on whether they featured amino acid residues corresponding to a single PTM type or both PTM types. All the overlapping hotspots were collated as actual hotspot stretches. All R-programming codes were drafted in accordance with the available literature (Aggarwal et al., 2020). Suitable filters were applied to classify the proteins with dually modified PTM hotspots.

The functional annotation tasks were executed for the proteins and clusters using DOSE (Yu et al., 2015) and “enrichKEGG” function of the clusterProfiler package (Yu et al., 2012; Wu et al., 2021) in R programming. Other annotations were retrieved from the PlasmoDB, UniProtKB, and KEGG databases (Kanehisa and Goto, 2000; Kanehisa, 2019; Kanehisa et al., 2021). All KEGG annotations and pathway components were visualized using the web-based KEGG mapper and the Bioconductor (v3.15) package Pathview (Luo and Brouwer, 2013). All chemical compound structures were generated using the PubChem Sketcher Tool (Ihlenfeldt et al., 2009). Important sites on the proteins of interest were marked interactively using the freely available visualization tool Protter (Omasits et al., 2014).

Anti-MTIP antibody generation

Purified recombinant MTIP protein residues 61–204 (XP_001350849) were resolved by SDS-PAGE and checked for purity. Approximately 100 μ g of this was mixed with complete Freund’s adjuvant for the first dose and incomplete Freund’s adjuvant for the booster dose after 7 days. The mixture was administered to female BALB/c mice (6–8 weeks old) subcutaneously, and the bleed was collected after 7 days of the first booster. Pre-immune sera were collected before immunizing the mice. Mice were administered three booster doses, and sera were collected every 7th day of the injection. The specificity of the anti-MTIP antibody was detected by probing *P. falciparum* lysates with anti-MTIP.

Acyl biotin exchange

The palmitoylated pool of proteins was purified using a modified version of the original acyl-biotin exchange (ABE)

protocol described in Wan et al. (2007). Purified segmented schizonts (~40–42 h post-invasion) were treated with 10 μ M ST092793 [originally identified from the virtual screening of MyriaScreen II Diversity Collection library that is composed of drug-like compounds in Jain et al. (2020)] and 50 μ M 2-bromopalmitate (2-BMP) for 4 h each. The treated parasite pellet was resuspended in a lysis buffer (150 mM NaCl, 50 mM Tris-HCl, 5 mM EDTA, pH 7.4) containing 10 mM N-ethylmaleimide (NEM). NEM causes the irreversible blockage of unmodified cysteine thiol groups. The mixture was incubated at 4°C for 16 h. Detergent-sensitive and detergent-resistant fractions were then separated by centrifugation at 13,000 rpm for 30 min at 4°C. The detergent-sensitive fraction was then processed for ABE. Briefly, after centrifugation, the protein from supernatant fractions was precipitated using the methanol/chloroform precipitation method (methanol:chloroform:water, in ratio 3:1:2). Precipitated proteins were then solubilized in four volumes of solubilization buffer containing 4% SDS, 50 mM Tris, and 5 mM EDTA (pH 7.4) in the presence of 10 mM NEM and incubated overnight at 4°C. Again, the precipitation step was repeated to remove NEM and the precipitated protein elutes were solubilized in four volumes of solubilization buffer in the presence of hydroxylamine (HA) buffer (0.7 M HA, 0.2 mM HPDP-biotin, 50 mM Tris pH 7.4, 0.25 Triton X-100; in Milli-Q water) for 2 h at 37°C. The final precipitation step-coupled resolubilization was performed in HPDP-biotin buffer (0.2 mM HPDP-biotin, 50 mM Tris pH 7.4, 150 mM NaCl, 5 mM EDTA, 0.2% Triton X-100; in Milli-Q water) for 2 h. At this step, a small amount of fraction from each of the treated samples was aliquoted. This served as the loading control. Further, each of the treated biotinylated samples was then pulled down using streptavidin beads and elution of proteins was performed in the presence of elution buffer (0.1% SDS, 0.2% Triton X-100, 1% β -mercaptoethanol; in Milli-Q water). The palmitoylated elutes were observed by Western blotting using the mouse anti-MTIP antibody (1:10,000). For the loading control, a lysate fraction aliquoted before streptavidin pull-down was observed by Western blot using mouse anti-MTIP. Band intensities were calculated using ImageJ software and plotted as fold change in MTIP expression before and after streptavidin pull-down.

Phospho-serine antibody-based pull-down assay

The pool of phosphorylated serine was pulled down from *P. falciparum* parasites treated with ST092793 and 2-BMP using Pierce Co-Immunoprecipitation Kit (Catalog Number 26149) as per manufacturer's protocol using a phosphoserine antibody (Catalog Number sc-81514). The elutes were analyzed by

Western blotting using mouse anti-MTIP antibody (1:10,000). An intensity graph was normalized with their respective inputs taken out before pull-down with phospho-serine antibody and plotted as bar graph.

MyoA/MTIP interaction pull-down assay

The biotin-tagged MyoA tail was bound to streptavidin beads (Catalog Number 20347) as per the manufacturer's instructions. Total cell lysates prepared in lysis buffer (150 mM NaCl, 50 mM Tris-HCl, 5 mM EDTA, pH 7.4) were allowed to interact with the streptavidin-bound MyoA tail overnight at 4°C (MyoA peptide residues 798–818 was synthesized from GenScript). The beads were washed with phosphate-buffered saline (PBS) followed by elution in 1 \times SDS loading dye. The elutes were analyzed by Western blotting using mouse anti-MTIP antibody (1:10,000). The intensity of each band was normalized with their respective input aliquoted before pull-down and plotted as a bar graph.

Click chemistry

ODYA-palmitic acid (Alk-C16) (Invitrogen, USA) was added to the untreated set of *P. falciparum* 3D7-infected RBCs at a final concentration of 100 μ M in PBS, for 4 h at 37°C with constant shaking. For 2-BMP, ST092793, and ST092793+2BMP treatment, cells were also simultaneously treated with 2-BMP (50 μ M), ST092793 (10 μ M), and 2-BMP+ST092793, respectively, for 4 h at 37°C. Following treatment, RBCs were pelleted down at 1,500 g. Thereafter, samples were washed thrice with ice-cold PBS, fixed with glutaraldehyde (0.25% in PBS) for 15 min at 4°C with shaking, and further permeabilized using 0.01% Triton X-100 (Sigma-Aldrich, USA) in PBS at room temperature for 5 min (shaking). After each step, a minimum of two washes with 1 \times PBS were done. These samples were then subjected to a click labeling reaction in 100 μ l of dye mix (in PBS) containing 0.1 mM azide dye (Oregon Green[®] 488, Thermo Fisher Scientific, USA), 1 mM tris-(2-carboxyethyl)-phosphine hydrochloride (TCEP, Sigma-Aldrich, USA), and 1 mM CuSO₄ (Sigma-Aldrich, USA) in water for 1 h. After incubation, cells were pelleted down and washed twice with 1 \times PBS. For microscopy, a drop (3–5 μ l) of the above sample was used to make a smear on a glass slide, mounted with Gold Antifade DAPI (Molecular Probes, USA), and analyzed using a Nikon A1 confocal microscope. NIS-Elements software was used for the processing of images. Mean fluorescent intensity (MFI) was determined for a single cell by measuring fluorescence intensity and plotted as a bar graph showing the MFI at a single-cell level. All imaging parameters were held constant during acquisitions.

Plasmodium falciparum growth inhibition assay

In order to analyze the effect of the crosstalk on *P. falciparum* growth, purified segmented schizonts [~44–48 h post-invasion (hpi)] were purified and diluted to a final parasitemia 2% (two schizonts per 100 RBCs) and 2% hematocrit followed by treatment with 2-BMP, ST092793, and 2-BMP+ST092793. Untreated parasites were taken as control. Following treatment, schizonts were incubated for 14 h. After 14 h, Giemsa-stained smears were made from treated and untreated parasites. The number of infected RBCs at the ring stage were counted in a total pool of 3,000 erythrocytes using a light microscope under $\times 100$ oil immersion to calculate percent invasion, and data were plotted graphically.

Checkerboard assay

Checkerboard assays were used to evaluate the effects of the combination of 2-BMP (palmitoylation inhibitor) and ST092793 (kinase inhibitor) against the malaria parasite (Mungthin et al., 1998; Semenov et al., 1998; Yapi et al., 2000). For this, schizont-stage parasites (42–44 h) were Percoll purified and dispensed in a 96-well plate at 2% hematocrit and 1% parasitemia. 2-BMP was added vertically at different concentration ranges while ST092793 was added horizontally at different drug concentration ranges in 8*8 format. As a result, the checkerboard consists of columns and rows in which each of the well along the x-axis contains drug 2-BMP at different concentrations (0.625, 1.25, 2.5, 5.0, 10.0, 20.0, and 40.0 μ M) and that along the y-axis contains ST092793 at different concentrations (0.625, 1.25, 2.5, 5.0, 10.0, 20.0, and 40.0 μ M) (King and Krogstad, 1983). The plate was incubated at 37°C in a humidified chamber for 14 h. The fractional inhibitory concentration (FIC index = FIC A + FIC B, where FIC A is the IC₅₀ of drug (A) in combination/IC₅₀ of drug A alone, and FIC B is the IC₅₀ of drug B in combination/IC₅₀ of drug B alone) of each drug was calculated and plotted as an isobologram. A straight diagonal line with an FIC index equal to 1 indicates an additive effect between drug A and drug B, a concave graph below the diagonal with an FIC index of less than 1 indicates a synergistic effect, and a convex curve above the diagonal with an FIC index of more than 0 indicates antagonism (Fivelman et al., 2004; Akoachere et al., 2005; Kelly et al., 2007).

Ethics statement

Animal studies were performed following CPCSEA guidelines and approved by the Institutional Animal Ethics Committee (IEAC) of JNU. Female BALB/c mice were obtained from the Central Laboratory Animal Resources, JNU,

New Delhi, and maintained under standard conditions. For experiments, donor blood was obtained from Rotary Blood Bank (RBB), New Delhi, India.

Results

Annotation of dually modified proteins in *Plasmodium falciparum*

A total of 5,316 proteins, encoded by 5,387 gene transcripts, could be identified as components of the *P. falciparum* 3D7 proteome (Supplementary Table 1). PTM types such as palmitoylation and phosphorylation modulate *P. falciparum* proteins to critically resolve molecular processes responsible for parasite propagation and survival during the intraerythrocytic developmental stages. To understand the interdependence between PTMs and its effect on the parasite life cycle, we began by annotating a pool of proteins within the *P. falciparum* 3D7 proteome, which are susceptible to either phosphorylation or palmitoylation. A cumulative of 2,148 “high confidence” phosphoproteins could be compounded from curated sources (Ganter et al., 2017; Gupta et al., 2022), systematic search results (search term = “phosphoprotein” in UniProtKB, NCBI, and PlasmoDB), and Pf-Phospho prediction results (Supplementary Table 2). Phosphoproteins predicted by Pf-Phospho were labeled “Phosphorylable,” and those retrieved from curated resources and databases, using systematic searches, were labeled as “Phosphorylated.” In addition, 3,105 proteins were either predicted (Ren et al., 2008) or found in curated datasets (Jones et al., 2012)/databases (NCBI, UniProtKB, and PlasmoDB) to be components of the parasite palmitome (Supplementary Table 3). Palmitoylated proteins predicted by the CSS-Palm were termed “Palmitoylable,” and those retrieved from curated resources and databases, using systematic searches, were categorized as “Palmitoylated” proteins (Figure 2A).

A cumulative pool of 176,872 (non-redundant) amino acid residues were found as plausible modification sites in (3,762 isoforms of) 3,721 proteins (Supplementary Table 4). For the rest of the modifiable proteins (176), no site-specific information could be gathered. Cysteines are known to be preferred amino acid residues/sites for palmitoylation. However, serines (55%) were concluded to be the most phosphorylated amino acid residues/sites in *Plasmodium falciparum* 3D7 (Supplementary Figure 1).

All the predicted or curated PTM sites aligned into 44 and 210 significant palmitoylation and phosphorylation sequence windows or motifs, respectively (FDR much less than 1%). The sequence windows were discovered and ranked based on their overall scores using the MoMo tool (Cheng et al., 2019) of the MEME Suite (Bailey et al., 2015) (Supplementary Table 5).

Among all the modifiable or modified proteins, 1,356 proteins were annotated to be dually modifiable by curated resources or prediction results (Supplementary Table 6). A list

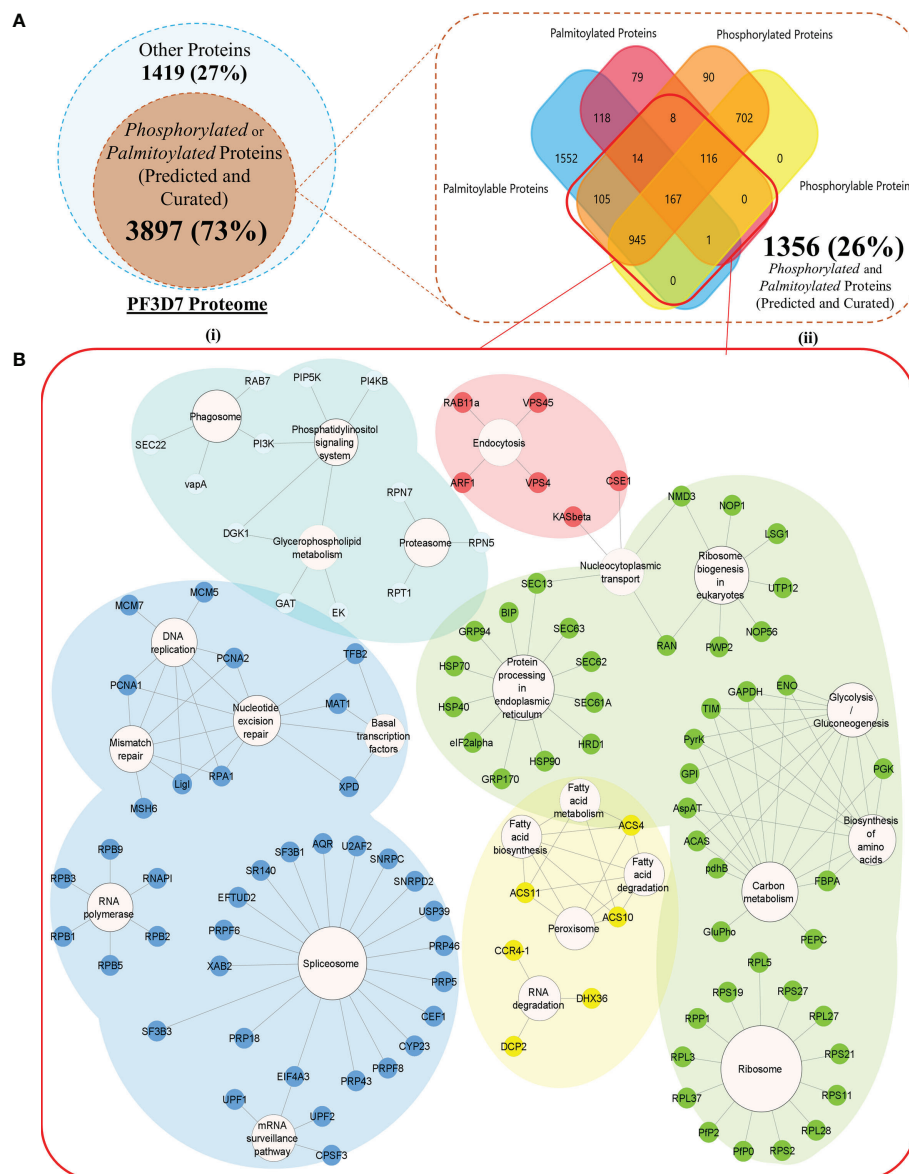


FIGURE 2

(A) (i) A Venn diagram representing all the *Modifiable* proteins (inner subset; dark orange) in the proteome of *Plasmodium falciparum* 3D7 (outer subset; light blue). (ii) A Venn diagram with a more detailed breakdown of the proteins processed or predicted to be processed by palmitoylation and phosphorylation (the red box encapsulates all the dually modifiable proteins) (B) Biological processes enriched by proteins grouped into each of the five k-mean clusters of the dually modifiable proteins. (Cluster 1 represented by Red, cluster 2 represented by Yellow, cluster 3 represented by Green, cluster 4 represented by Cyan, and cluster 5 represented by Blue nodes).

of 1,327 proteins (97.86% out of all dually modifiable) could be mapped to the STRING database for functional and PPI annotations. To find the functional relevance of dual modification in the *Plasmodium* parasite, all the nodes were grouped into five different STRING-generated k-mean clusters using default settings (Supplementary Table 7). Cluster 4 (cyan) had a significant enrichment (p value below 1%) of the *P. falciparum* 3D7 glideosome motor machinery and invasion complex-related proteins retrieved from the PlasmoDB searches

(filtered for only text-mined proteins and proteins studied in rodent malaria models). Cluster 4 was found to be significantly (q value below 5%) associated with critical parasite processes like phagocytosis, phosphatidylinositol signaling, glycerophospholipid metabolism, and proteasome abundance (Figure 2B). Each of the processes have time and again been reported to be guiding the intraerythrocytic development (IED) and plasticity of *Plasmodium* in dynamic hosts and microenvironmental conditions (Déchamps et al., 2010;

Tawk et al., 2010; Krishnan and Williamson, 2018). The cyan cluster can be regarded as one of the most critical functional units of parasite motility that are (plausibly) guided by both phosphorylation and/or palmitoylation (Supplementary Table 7).

Two hundred twenty-seven protein nodes, out of the 273 STRING-mapped and k-mean clustered protein nodes, were identified to have at least one edge connecting them to a certain other node in a PPI map created with the highest confidence

score (0.9) and a high FDR stringency (below 1%). The basic PPI map generated by the STRING database was visualized using the Cytoscape application. Nodes without a protein name (or N/A as node label) (found for 105 proteins) and other disconnected nodes (10 proteins) were hidden to boost the simplicity of the graph (Figure 3A). A subnetwork with 66 nodes was found to be highly enriched (p value below 1%) with the key components of the actomyosin, and glideosome motor machineries, including

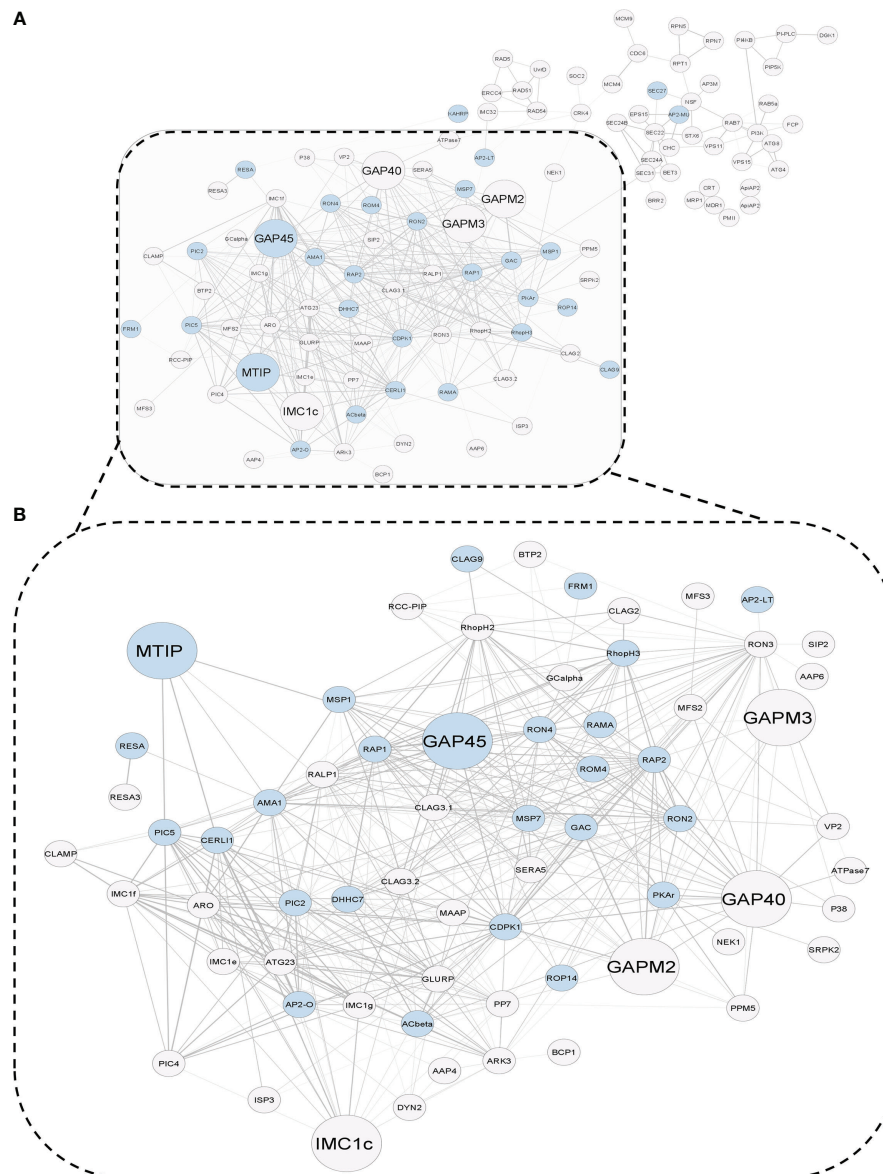


FIGURE 3

(A) STRING-generated Protein-Protein Interaction graph of dually modifiable proteins in k-means cluster 4. The PPI map draws a relationship between the molecular factors of parasitic invasion (blue nodes) and glideosome-mediated motility (larger nodes) in *P. falciparum* 3D7, which are processed by a crosstalk of Palmitoylation and Phosphorylation. (B) A functional subnetwork of major glideosome and invasion motor complex-related proteins, which has been termed as the infection-associated Motility and Invasion Complex (MIC) (dotted box).

GAP45, MTIP, CDPK1, and the essential light chains (ELCs), were renamed to “Motility and Invasion Complex” (MIC). These results indicated that the dual modification of MIC factors might be critical in the regulation of the parasitic motor complex or assembly responsible for the generation of a concerted force for the active invasion of the host cells. Within the MIC subnetwork, two core glideosome motor complex proteins, GAP45 and MTIP, were found to be the branching factors orchestrating both motility and general host-invasion processes in *P. falciparum* (Figure 3B).

***In-silico* motif analysis revealed PTM crosstalk hotspots possibly regulating parasite motility and invasion**

Within a set of 1,356 proteins qualifying as dually modifiable, a common set between the prediction results and curated datasets/databases unveiled 167 proteins exhibiting propensities for both palmitoylation and phosphorylation (Figure 1 and Supplementary Table 6). These 167 dually modified proteins were screened for essentiality using existing literature and systematic database searches (Aurrecochea et al., 2009; Ali et al., 2021; Bateman et al., 2021). Based on this, four dually modified proteins, namely, PMII (plasmepsin II), ADA (adenosine deaminase), CDPK1, and MTIP, were found to be essential for parasite IED and invasion having no paralogs in human hosts (Ali et al., 2021) (Figure 4A and Supplementary Table 6). These four proteins were surveyed for the modification sites and discovery of the hotspot motifs, yielding a list of 100 unique modification sites for palmitoylation and phosphorylation. Non-redundant modification sites upon the four proteins could be classified into 10 elaborate hotspots. Motifs featuring amino acid residues susceptible to both palmitoylation and phosphorylation can be considered as the best probable grounds of complementary crosstalk between the PTM types. Only two (out of 10 PTM hotspots) could be identified as amino acid motifs with high propensity for both palmitoylation and phosphorylation. These motifs in the corresponding proteins CDPK1 and MTIP were thus termed as “Dually Modified” hotspots for complementary crosstalk (Supplementary Table 8), and both of these proteins could be detected in the MIC subnetwork (Figure 3). MTIP, however, features a lower frequency of polymorphisms across all strains in comparison to CDPK1. Also, MTIP is more conserved than CDPK1 within the Apicomplexa phylum and shows a higher proteomic expression during the merozoite, ring, and schizont stages of parasite infection (Szkłarczyk et al., 2021; Amos et al., 2022). Interestingly, only MTIP serves as a core physical regulator of the actomyosin machinery, which is a critical functional unit that assists the glideosomes by inducing the potentiation of parasite movement and subsequent invasion processes in preferred hosts (Figure 4B). In addition, MTIP projects conserved amino acid motifs showcasing high propensity for PTMs and interactions with other proteins of

functional significance like MyoA. All the three hotspots predicted in MTIP, including the dually modified hotspot region, are located within the window of the first 100 amino acids. The second hotspot region in MTIP features as many as five known phosphorylation sites and completely spans the disordered region of the protein (UniProtKB annotations). This asserts evolutionary significance for the predicted hotspot motif (Figure 4C).

The adapter protein, MTIP, mediates the formation of the MyoA–MTIP complex that associates with co-expressing cytosolic GAP45 and relocates to the developing IMC, predominantly during early schizogony when the merozoites are released [Figure 4B (II)]. CytoHubba application-based Multiple Clique Centrality (MCC) scoring revealed the MyoA–MTIP–GAP45 (shared rank 1, MCC score = 4.0) complex as the core hub of the physical protein association networks underlying the glideosome motor complex (Supplementary Table 9). Since MTIP is a mediator of the MyoA : MTIP–GAP45 complex formation, it is critical to the integrity of the motility and erythrocytic invasion complex in the parasites (Bosch et al., 2006; Ridzuan et al., 2012). Although the expression patterns of MTIP are not specific to any particular growth stages, the protein or the corresponding mRNAs are highly expressed in the merozoites (both short and long lived) and the schizonts (Pease et al., 2013; Kumar et al., 2017a). Additionally, the functional implications of its protein orthologs in *P. berghei* establishes MTIP among those adapter protein-coding genes which are extremely essential for growth and propagation during the asexual stages of the Plasmodium life cycle (Bushell et al., 2017; Howick et al., 2019).

An extensive survey of proteins and PTMs depicts the presence of distinct and coinciding phosphorylation and palmitoylation motifs in crucial factors like PMII, CDPK1, and MTIP that govern *P. falciparum* infection. PTM events and their hotspots could be located in many proteins involved in discriminatory aspects of infection by Plasmodium spp. parasites. Thus, the cross-talking PTM events and hotspots, beyond proteins and mRNAs, can be explored as key molecular targets to expand the druggability of the critical Plasmodium spp. factors like the protein components of the MyoA : MTIP motor complex. Subsequently, MTIP was concluded as one of the most essential factors for asexual stage growth of parasites which featured multiple hotspot stretches with a concentrated chance of PTM crosstalk events between palmitoylation and phosphorylation.

The dynamic interplay between phosphorylation and palmitoylation status of MTIP

Individual studies have demonstrated that the *P. falciparum* protein machinery of invasion gets phosphorylated and palmitoylated (Rees-Channer et al., 2006; Alam et al., 2015;

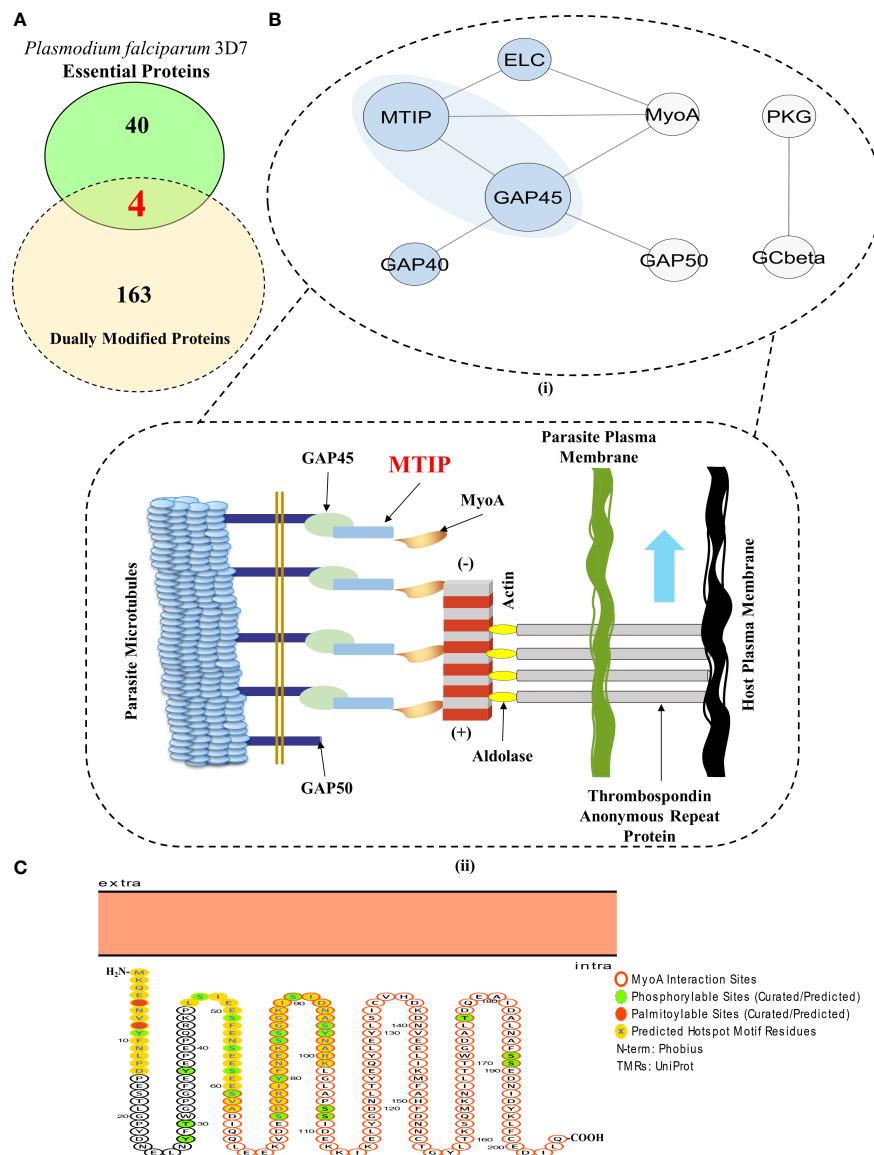


FIGURE 4

MTIP is an essential merozoite factor guiding parasite motility and erythrocytic invasion in hosts. (A) A Venn diagram showcasing the proteins which are dually modified by palmitoylation and phosphorylation and are essential for parasite survival. (Red fonts within the union of yellow and green ellipses; includes plasmepsin II, adenosine deaminase, calcium-dependent protein kinase 1 and myosin A-tail interacting protein). (B) (i) A STRING-generated PPI network of all the physical interactors constituting the glideosome motor complex. (Blue background) (ii) An illustration of the actomyosin motor complex with MTIP as one of the central physical interactors. Revisualized from the published concepts of the glideosome motor unit (Bosch et al., 2006; Saunders et al., 2020). (C) A Protter generated illustration of MTIP showing the colocalization of phosphorylation and palmitoylation sites in the hotspots and MyoA interaction motif (Omasits et al., 2014; Anam et al., 2020).

Edmonds et al., 2017; Schlott et al., 2018). Blocking these PTMs in glideosome-associated proteins leads to invasion inhibition (Yakubu et al., 2018). MTIP is known to be phosphorylated at serine residues 47, 51, 55, 58, 61, 107, and 108 (Green et al., 2008; Douse et al., 2012) and palmitoylated at cysteine 5 and 8 amino acid residues (Jones et al., 2012).

To answer whether silencing of one PTM type in MTIP would affect the other modification types, we used two PTM-specific inhibitors: (i) 2-bromopalmitate (2-BMP), a generic inhibitor of palmitoyl acyltransferases (Resh, 2006) that has been shown to block palmitoylation in *P. falciparum* (Jones et al., 2012), and (ii) ST092793 (Jain et al., 2020), a novel broad-

spectrum phosphorylation inhibitor shown to have strong inhibitory ability against pan-kinases during the intra-erythrocytic development of parasites, as shown by a previous study from our lab (Jain et al., 2020). A brief schematic of the ABE protocols is provided in Figure 5A (I). MTIP in parasite lysates was detected using an anti-MTIP antibody that gave a single band at 24 kDa after probing with *P. falciparum* lysates [Figure 5A (II)]. To ensure if the reduction in MTIP levels was due to crosstalk, but not because of the treatments, the levels of MTIP in input lysate after ST092793 and 2-BMP treatments in the presence and absence of hydroxylamine treatment were checked, which indicated no change in MTIP band intensities [Figure 5A (III)]. The palmitoylation status of MTIP was evaluated in the ABE-enriched purified palmitome (Wan et al., 2007; Edmonds et al., 2017) after ST092793 and 2-BMP treatments. The results demonstrated reduced band intensity of MTIP indicating attenuated palmitoylation of MTIP upon phosphorylation inhibition [Figure 5A (III, IV)], whereas a further reduced MTIP band was detected in 2-BMP (+HA wells) treatment in comparison to ST092793 confirming successful inhibition of palmitoylation that was used as a positive control [Figure 5A (III)]. The same was depicted in an intensity plot represented as bar graph [Figure 5A (IV)], which represents the fold change in intensity before and after ABE pull-down by streptavidin beads.

To understand whether the phosphorylation status of MTIP might also be regulated by palmitoylation, we first enriched the phosphorylated pool of *P. falciparum* using a phosphoserine-specific antibody from 2-BMP-treated lysate and identified the phosphorylation status of MTIP in the same. A brief description of the methodologies is provided in Figure 5B (I). To ensure the equal level of MTIP in all the samples, input lysates after ST092793 and 2-BMP were checked, which indicated no change in MTIP band intensities [Figure 5B (II)]. This was considered as a control/input. Probing with phospho-serine antibodies showed decreased intensity of phosphorylated MTIP suggesting palmitoylation-dependent phosphorylation [Figure 5B (III)]. Additionally, densitometry analysis was performed for the pull-down assays and represented as fold change in MTIP intensity after pull-down analysis [Figure 5B (IV)].

Effect of PTM crosstalk on MTIP's interaction with its primary motor complex partner Myosin A

The myosin A/myosin A tail interacting protein (MyoA-MTIP) complex is a notable molecular bridge of motor machinery that is modified post protein translation to drive the parasite entry into human RBCs (Bosch et al., 2006; Green et al., 2006). Precisely, the phospho motifs lying in the

C-terminal domain of MTIP interact with only the tail constituting 798–818 amino acids of myosin A (Bergman et al., 2003; Baum et al., 2006; Bosch et al., 2006; Green et al., 2006; Thomas et al., 2010; Khamrui et al., 2013). However, it is unknown whether blocking the palmitoylation-phosphorylation crosstalk has any impact on the myosin A/myosin A tail interacting protein (MyoA-MTIP) complex. To answer this, we used a synthetic biotinylated peptide mimicking the tail domain of myosin A that is sufficient for detecting its interaction to MTIP. This peptide was used as bait to pull down MTIP from the lysate treated with both phosphorylation and palmitoylation inhibitors sequentially [Figure 5C (I)]. The untreated lysate was used as a positive control. The data suggested that inhibiting palmitoylation by 2-BMP led to an abolished interaction of the MTIP C-terminal domain with the myosin A tail, while blocking phosphorylation by ST092793 demonstrated a diminished interaction [Figure 5C (II)] as shown by the reduced intensity of MTIP [Figure 5C (III)]. Findings from the study suggested that there might be a strong possibility of PTM crosstalk on amino acid domains of MTIP interacting with the myosin A tail.

Global crosstalk between phosphorylation and palmitoylation in *P. falciparum*

Click chemistry is a direct and well-defined tool to evaluate global palmitoylation (Jones et al., 2012; Ayana et al., 2018; Yadav et al., 2019) where all the probable palmitoyl motif-containing groups are labeled with Oregon Green 488 dye. By using click chemistry, the palmitome of parasites could be visualized [Figure 6A (I)]. The perturbations in the global palmitome of *P. falciparum* due to phosphorylation inhibition were assessed by using this assay, following treatment with ST092793. For this, *P. falciparum* parasites were treated with ST092793 (10 μ M), 2-BMP (50 μ M), and ST092793+2-BMP (10 μ M, 50 μ M respectively) in combination followed by visualization of palmitoylated proteins by measuring the fluorescence of incorporated palmitic acid analogue Oregon Green 488 dye as shown represented in the respective intensity plot [Figure 6A (II, III)]. A 50% reduction in fluorescence intensity of ST092793-treated parasites as compared to control showed the effect of phosphorylation inhibition on global *P. falciparum* palmitome [Figure 6A (III)], thereby confirming the crosstalk between phosphorylation and palmitoylation at a global level in *P. falciparum*. A decrease in fluorescence intensity in 2-BMP-treated parasites confirmed effective palmitoylation blockage. Additionally, the impact of palmitoylation inhibition was much more evident in the case of ST092793+2-BMP [Figure 6A (III)]. Overall, these results confirmed crosstalk between phosphorylation and palmitoylation in the *P. falciparum* proteome.

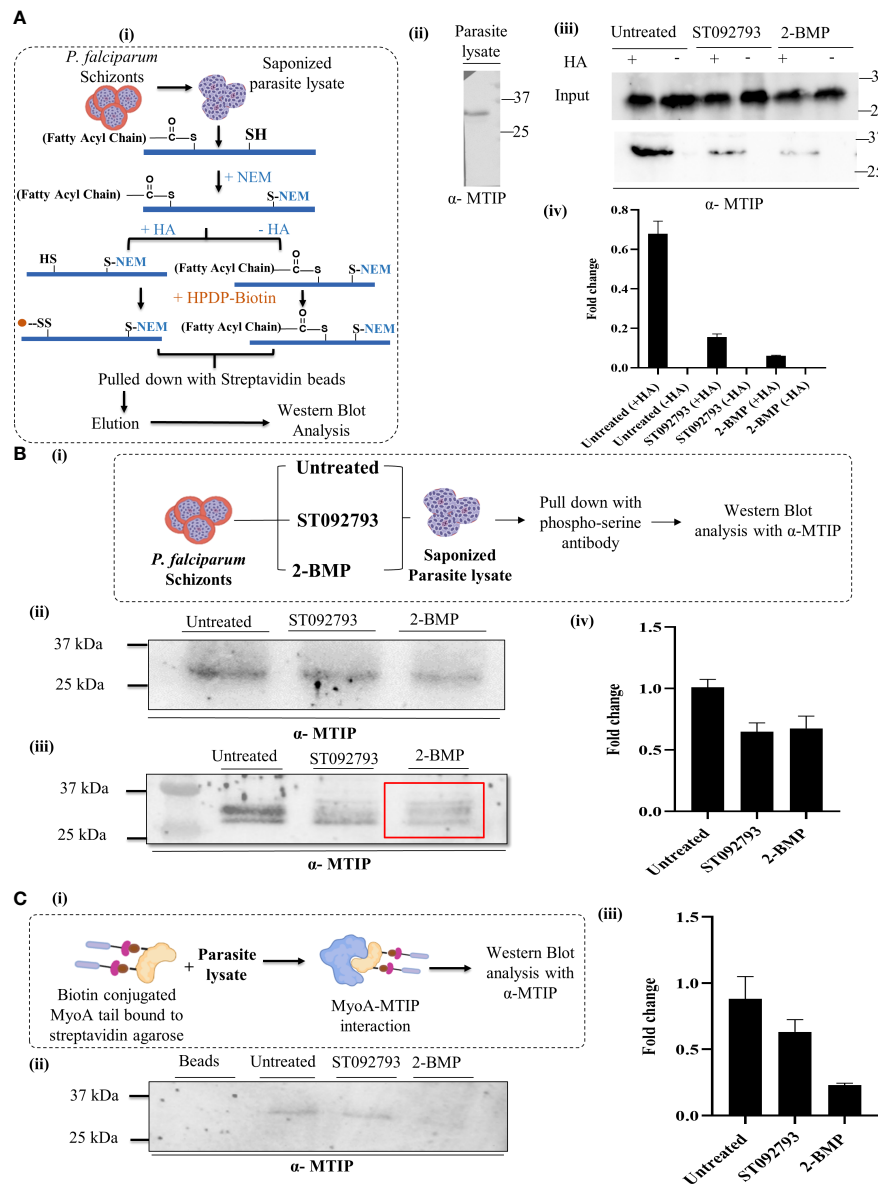


FIGURE 5

(A) (i) A schematic representation of acyl biotin exchange analysis to detect palmitoylation of parasite protein coupled with immunoblot analysis. (ii) *P. falciparum* 3D7 lysate blotted using mouse anti-MTIP antibody (1:20,000 dilution in phosphate-buffered saline 0.1% Tween 20). A single band at 24 kDa representing MTIP was observed. (iii) The representative immunoblot displayed inputs (upper panel) representing MTIP expression levels in untreated lysates and lysates treated with ST092793 and 2-BMP in presence and absence of HA. Immunoblots represent the MTIP expression in the ABE pulled fraction with and without HA treatment (lower panel). Low intensity of MTIP expression was detected in ST092793 and 2-BMP treated ABE pulled-down fraction in comparison to control. (iv) Bar graph represents the fold change in MTIP band intensity before and after ABE pull down. Two independent experiments have been performed, $n = 2$. (B) (i) Schematic representation to analyze the dynamic interplay between phosphorylation and palmitoylation status of MTIP. Schizont stage parasite were treated with ST092793, BMP alone. After treatment parasite lysates were subjected to pull-down analysis using phospho-serine antibody, eluate fractions were then probed with anti-MTIP antibodies. (ii) Immunoblot represents the input showing equal MTIP expression in untreated and ST092793- and 2-BMP treated samples. (iii) In the presence of 50 μM 2-BMP, the phosphorylation of MTIP (measured by pull-down using phospho-Ser antibody followed by probing with anti-MTIP) was predominantly reduced (red box) as compared to MTIP in untreated lane. (iv) Bar graph represents the change in fold intensity before and after pull-down using phospho-Ser antibody. (C) (i) Schematic representation of workflow to analyze the MTIP interaction with MyoA tail. (ii, iii) The immunoblot showed the synergistic impact of dual PTM on MTIP crosstalk with myosin A tail, in the presence of 50 μM 2-BMP. There was no MTIP band following pull-down using biotinylated myosin A tail as the bait. The graph denotes fold change in intensity of MTIP in comparison to inputs taken before pull-down with myosin A tail in individual lanes. Two independent experiments have been performed.

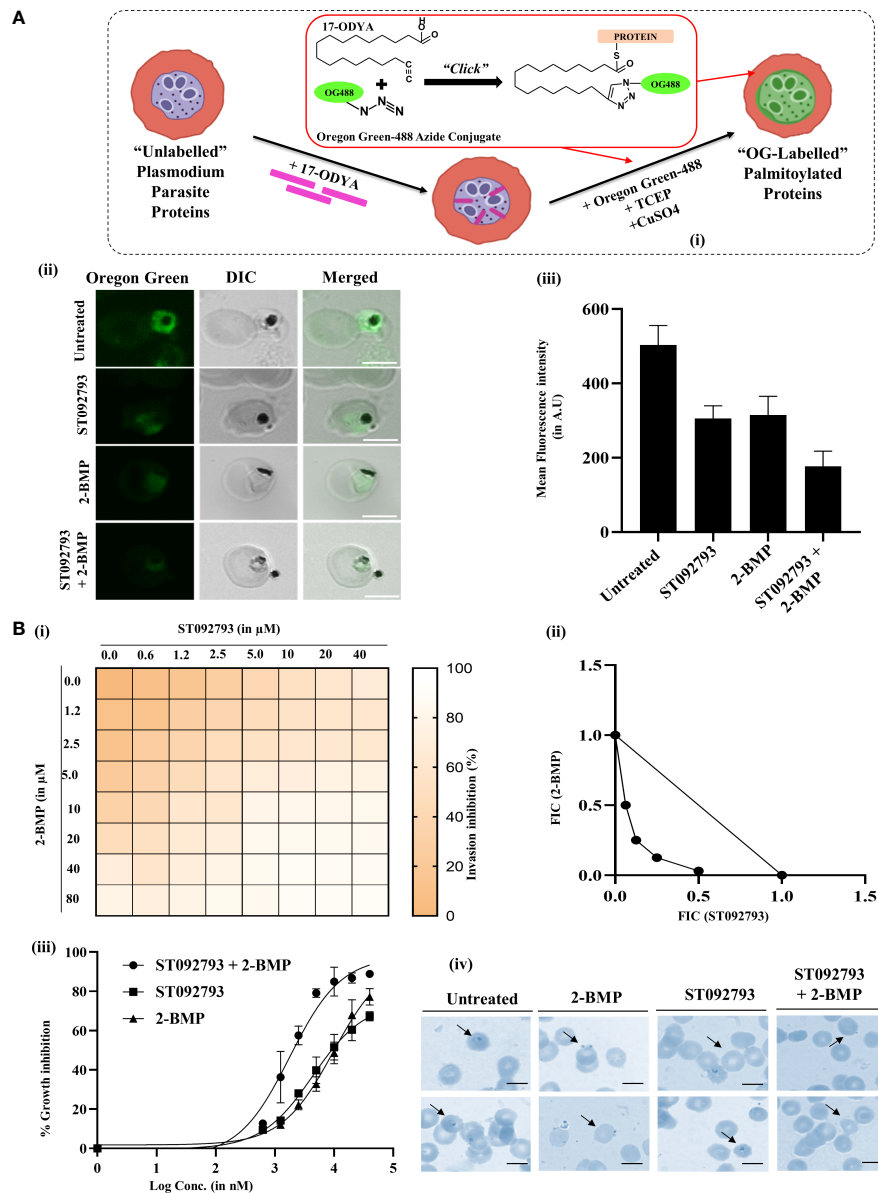


FIGURE 6

(A) (i) Schematic of the click chemistry approach for imaging *in situ* protein palmitoylation in malaria parasite during asexual development. Intraerythrocytic parasites were metabolically labeled with 17-ODYA (palmitic-acid analogue) followed by labeling with Oregon Green 488 in the presence of TCEP and copper sulfate. (ii) Clickable metabolic labeling of the *P. falciparum* parasites following ST092793, 2-BMP, and ST092793+2-BMP treatment. The weak palmitoylation profiles in comparison to untreated parasites, especially in the case of ST092793, were observed. Scale bar indicates 5 μ m. (iii) Bar graphs represent the mean fluorescence intensity (MFI) and denote the palmitoylation profile in treated and untreated erythrocytes, where 20 cells were used for calculation for two biological replicates. (B) (i) The heat plot of invasion inhibition in 3D7 in the presence of ST092793 and 2-BMP when used alone and in combination (ST092793 + 2-BMP). ST092793 was added horizontally in 96-well plates (0, 0.6, 1.2, 2.5, 5.0, 10, 20, 40 μ M) while 2-BMP was added vertically (0, 0.6, 1.2, 2.5, 5.0, 10, 20, 40, 80 μ M) in 8*8 format. Dose-response matrices from 0% to 100% indicate different percentages of invasion inhibition. (ii) The isobologram analysis of 2-BMP and ST092793 which shows a synergistic effect when used in combination against the 3D7 strain of *P. falciparum* with FIC index of <1. (iii) The dose-response curve for 2-BMP and ST092793 when used alone and in combination. (iv) Giemsa-stained smears from 2-BMP-, ST092793-, and 2BMP+ST092793-treated parasites. Arrowhead indicates the ring formation after successful invasion, while invasion defect was observed in the case of 2-BMP-, ST092793-, and 2BMP + ST092793-treated parasites.

Phosphorylation and palmitoylation show synergistic effects in *P. falciparum* invasion

Accumulating evidence has shown that global phosphorylation of *P. falciparum* proteome governs many cellular processes including invasion (Ekka et al., 2020; More et al., 2020; Perrin et al., 2020). In addition, there are scanty findings available that also suggest that global palmitoylation of glideosome-actinomycin motor assembly proteins in *P. falciparum* might impact the invasion phenotypes (Jones et al., 2012). However, there is a lacuna in the understanding of whether both these modifications might need to act synergistically during the invasion.

To explore this hypothesis, we have studied the global synergism of these dual PTMs on *P. falciparum* invasion using palmitoylation and phosphorylation inhibitors 2-BMP and ST092793, respectively. To check whether these two drugs, 2-BMP (palmitoylation inhibitor) and ST092793 (kinase inhibitor), when used in combination against malaria parasite show a synergistic effect, the *in vitro* isobologram method was used (Fivelman et al., 2004; Akoachere et al., 2005; Kelly et al., 2007). For this, schizont-stage parasites (42–44 h) were treated with each of the drugs alone and in combination at different concentrations. The Giemsa smears were made after 14 h of incubation, and parasitemia was calculated. The FIC index was calculated for each drug concentration and plotted as an isobologram. The result indicated that 2-BMP and ST092793 when used in combination show a synergistic effect *in vitro* with an FIC index of less than < 1 [Figure 6B (I, II)]. Also, a dose-response curve was plotted for each of the drug alone and in combination and the result showed that when the parasite was treated alone with each drug alone at different concentrations IC₅₀ came out to be 20 and 10 μ M, respectively, while when used in different drug doses in combination, IC₅₀ shifts to 2 μ M [Figure 6B (III)], indicating a synergistic effect of palmitoylation and phosphorylation when inhibited together *via* 2-BMP and ST092793, respectively.

Discussion

The integrated proteomic analysis provides new insights into PTMs, the biological building blocks underlying the functional diversity of proteins in eukaryotic organisms (Yakubu et al., 2018; Andrés et al., 2020). Emerging studies have shown the implications of the crosstalk of PTMs and their diverse roles across the spectrum of diseases (Hunter, 2007; Yakubu et al., 2018; Habibian and Ferguson, 2019). Accumulating evidence has shown that multiple PTMs like phosphorylation, palmitoylation, glycosylation, acetylation, ubiquitylation, and myristoylation are abundant in Apicomplexan parasites (Douse et al., 2012; Yakubu et al., 2018). These PTMs govern basic steps like motility, host-parasite interaction, cellular

homeostasis, and infectivity (Chuenkova et al., 2001; Soulat and Bogdan, 2017; Damianou et al., 2020; Ekka et al., 2020; Perrin et al., 2020).

Existing data also suggest that in the case of *P. falciparum*, PTMs regulate malaria disease progression (Hunter, 2007; Lonard and O'Malley, 2007; Yao et al., 2011; Swaney et al., 2013). Thus, the PTM sites and crosstalk among multiple biologically implicated PTM types can be targeted in Apicomplexan parasites which has a pronounced effect in overall parasite growth and host invasion. Phosphoproteome and palmitome analyses of *P. falciparum* have revealed multiple roles of these PTMs in invasion, survival, and progression (Treeck et al., 2011; Jones et al., 2012; Alam et al., 2015; Hodson et al., 2015; Lasonder et al., 2015). In other eukaryotic systems, the crosstalk between palmitoylation and phosphorylation is well-defined and has been correlated with various cellular functions (Hunter, 2007; Yao et al., 2011; Ahner et al., 2013; Vu et al., 2018) also linked to cardiovascular diseases (Habibian and Ferguson, 2019; Aggarwal et al., 2020). In *Plasmodium*, phosphorylation and palmitoylation are the abundant kinds of PTMs (Treeck et al., 2011; Jones et al., 2012; Lasonder et al., 2015; Park et al., 2015). Hence, it makes sense for the parasite to use these in order to fine-tune the cellular events for biological homeostasis. Thus, deciphering the crosstalk between phosphorylation and palmitoylation and the key regulatory hub proteins will aid in understanding the parasite's response mechanisms during parasite life-cycle progression and invasion.

To bridge this gap in understanding, we have tried to address a fundamental question, if phosphorylation and palmitoylation in *P. falciparum* act in dynamic interplay and are interdependent. In the direction, we introduced a new strategy involving de-convolution of (i) the cumulative catalog of PTM partners for phosphorylation and palmitoylation, (ii) common candidate proteins showcasing the dual PTMs, and (iii) dually modified regulatory hub proteins and their interacting partners that are committed to *Plasmodium* invasion. Moving ahead, first, we studied the global crosstalk between the phosphoproteome and palmitome of *P. falciparum* by *in silico* analysis that enriched the repertoire of proteins and underlying motifs and hotspots with dual PTM types. Although the predicted phosphorylation and palmitoylation hotspot motifs on these *Plasmodium* proteins may get exposed during different stages of the asexual life cycle of the parasite, our click chemistry analysis proved that crosstalk exists between phosphorylation and palmitoylation at the global proteome level during RBC infection stages of the parasite. The phenotypic effect of crosstalk was further studied by measuring *P. falciparum* growth inhibition against individual and combinatorial treatments with ST092793 and 2-BMP which are generic inhibitors of phosphorylation and palmitoylation, respectively. Although 2-BMP is known to have non-specific effects (DeJesus and Bizzozero, 2002; Zheng et al., 2015), it has been used extensively to target palmitoylation-based pathways in *L. donovani*, *T. cruzi*, and *Toxoplasma* (Foe et al., 2015;

Ayana et al., 2018; Batista et al., 2018b; Batista et al., 2018a) for reducing infectivity. Plausibly, one of our recent unpublished data has also shown that 2-BMP has no impact on overall morphology of host RBCs. Interestingly, some recent studies have identified certain erythrocytic kinase specific inhibitors targeting phosphorylation, with promising antimalarial activity (Kesely et al., 2016; Pantaleo et al., 2017). A recent published study from our laboratory has also detected ST092793 as the novel kinase inhibitor from the MyriaScreen II diversity collection library with promising antimalarial activity (Jain et al., 2020). Our data suggested that simultaneous treatment with ST092793 and 2-BMP, targeting phosphorylation and palmitoylation, respectively, in *P. falciparum* imposed strong synergistic effects on parasite growth inhibition, suggesting a significant impact of these modification types in shaping the intracellular growth dynamics of *P. falciparum*.

Next, we aimed to identify the crucial regulatory hub proteins and their interacting partners among the enriched repertoire of dually modified proteins responsible for parasite invasion processes. Merozoite invasion is a sequential process involving initial attachment of the merozoite to RBC, tight attachment, tight junction formation, and penetration involving multiple machinery proteins including myosin A, MTIP, GAP45, GAP50, ELC, and TRAP (Baum et al., 2006; Jones et al., 2006; Fréchal et al., 2010; Thomas et al., 2010). In our analysis, we found MTIP as the common emerging and hub protein which is also a key protein in the motility and invasion assembly controlling invasion. The role of the glideosome motor complex of which MTIP is a main member is well established by previous studies (Green et al., 2006; Turley et al., 2013). We asked if the dual PTM crosstalk might play any decisive role in underlying MTIP expression and its interaction with its target proteins during pre-invasion and invasion processes. Our *in vitro* data suggested that the regulation machineries of palmitoylation and phosphorylation of MTIP are strongly interdependent.

Next, we identified the interacting partners of the glideosome motor complex in *P. falciparum* that are modulated synergistically through phosphorylation and palmitoylation. Among these partners, we found the myosin A-MTIP complex to be strictly regulated by the dual PTM modifications of MTIP. It is also evident from our *in vitro* data that the molecular crosstalk between both phosphorylation and palmitoylation events in MTIP governs its possible interaction with myosin A (Figure 6). Based on these data, we suggest that dual PTM crosstalk in MTIP might have a role forming the myosin A–MTIP complex, critical for host invasion at the merozoite point of entry in the host erythrocytes.

Overall, our analysis has provided two important insights: (i) dual PTM crosstalk governs the MTIP-dependent molecular pathway involved in *P. falciparum* pre-invasion- and invasion-associated processes, and (ii) a combination of drugs targeting both palmitoylation and phosphorylation can provide a novel antimalarial therapeutic strategy that can offer the advantage of improved efficacy with reduced drug resistance.

Conclusion

The datasets presented herein provide the first evidence of the crosstalk between palmitoylation and phosphorylation in *P. falciparum* motility and parasite-mediated cell invasion. PTM crosstalk events and motifs discussed in the article may be beneficial for the development of novel chemotherapeutics. The strategies devised for the study may further be applied to research the crosstalk possibilities among multiple other PTM types, and underlying cell-regulatory networks in other apicomplexan parasites. Additionally, individual datasets, catalogs, and findings from the study have been made available and may be referred to as an up-to-date repository of palmitoylation and phosphorylation modification events and hotspots in *Plasmodium falciparum* (isolate 3D7) proteins.

Data availability statement

The original contributions presented in the study are included in the article/Supplementary Material. Further inquiries can be directed to the corresponding authors.

Author contributions

Conceptualization, SS, AR, ZA. Methodology, SS, SP, AR. Experimental design and execution ZA, GK, DR, SM, NG, AK, AC, NS, SK, JS, AR, SS. Software and bioinformatics TP, DR, SR, SM, SP. Validation, AR, SS and ZA. Investigation, GK, ZA. Resources, AR, SS. Data compilation, ZA, SM, GK, SP, AR, SS. Writing—original draft preparation, ZA, SP, AR, SS. Writing—review and editing, SP, AR, SS, ZA, SM. Visualization and malaria culture GK, RS, SB, PM. Supervision, AR, SS. Project administration, AR, SS. Funding acquisition, AR, SS. All authors contributed to the article and approved the submitted version.

Funding

This research was funded by the Department of Science and Technology, SERB grant number CRG/2019/00223 (AR, SS), and Drug and Pharmaceuticals Research Programme (DPRP, Project No. P/569/2016-1/TDT) (SS); the APC was funded by the Department of Science and Technology, SERB, IRHPA IPA/2020/000007 (AR, SS). SP is grateful for the funding support from the Cognitive Science Research Initiative (CSRI) program of the Department of Science and Technology (DST/CSRI/2018/247).

Conflict of interest

The authors declare that the research was conducted in the absence of any commercial or financial relationships that could be construed as a potential conflict of interest.

Publisher's note

All claims expressed in this article are solely those of the authors and do not necessarily represent those of their affiliated organizations, or those of the publisher, the editors and the reviewers. Any product that may be evaluated in this article, or claim that may be made by its manufacturer, is not guaranteed or endorsed by the publisher.

Supplementary material

The Supplementary Material for this article can be found online at: <https://www.frontiersin.org/articles/10.3389/fcimb.2022.924424/full#supplementary-material>

SUPPLEMENTARY FIGURE 1

(A) A bar graph comparison of amino acids preferred for phosphorylation and palmitoylation modification types (cataloged for the underlying study from all sources). (B) Amino acids of preference for phosphorylation cataloged from only curated datasets (Dotted Red Box) suggest Serines (83%) and Tyrosines (3%) as the most and least phosphorylated residues in *Plasmodium falciparum* 3D7. (C) Absolute frequencies and percentages of amino acid residues preferred as phosphorylation and palmitoylation sites (from the total pool of PTM sites cataloged for the underlying study from all sources).

SUPPLEMENTARY TABLE 1

Total proteome of *Plasmodium falciparum* 3D7 cataloged for the study.

SUPPLEMENTARY TABLE 2

Cumulative phosphoproteome of *Plasmodium falciparum* 3D7.

SUPPLEMENTARY TABLE 3

Cumulative palmitome of *Plasmodium falciparum* 3D7.

SUPPLEMENTARY TABLE 4

A list of all the PTM events and sites pertaining to *Plasmodium falciparum* 3D7 proteome.

SUPPLEMENTARY TABLE 5

Consensus palmitoylation and phosphorylation sequence windows discovered using the MoMo web interface along with the sequence logo graphs.

SUPPLEMENTARY TABLE 6

A catalog of all the "Dually Modifiable" and "Dually Modified" *Plasmodium falciparum* 3D7 proteins.

SUPPLEMENTARY TABLE 7

The results generated from the k-means clustering of the dually modifiable *Plasmodium falciparum* 3D7 proteins.

SUPPLEMENTARY TABLE 8

PTM hotspot regions in all the modifiable proteins acquired from curated datasets/databases and prediction results, including PTM events and hotspots distribution on dually modified *Plasmodium falciparum* 3D7 proteins essential for its survival.

SUPPLEMENTARY TABLE 9

A tabular representation of the physical PPI map constituting the Glideosome motor complex of *Plasmodium falciparum* 3D7 as nodes for the Cytohubba based identification of top interactors.

References

- Aggarwal, S., Banerjee, S. K., Talukdar, N. C., and Yadav, A. K. (2020). Post-translational modification cross-talk and hotspots in sirtuin interactors implicated in cardiovascular diseases. *Front. Genet.* 11. doi: 10.3389/FGENE.2020.00356/BIBTEX
- Ahner, A., Gong, X., and Frizzell, R. A. (2013). Cystic fibrosis transmembrane conductance regulator degradation: Cross-talk between the ubiquitylation and SUMOylation pathways. *FEBS J.* 280, 4430–4438. doi: 10.1111/FEBS.12415
- Akoachere, M., Buchholz, K., Fischer, E., Burhenne, J., Haefeli, W. E., Schirmer, R. H., et al. (2005). *In vitro* assessment of methylene blue on chloroquine-sensitive and -resistant plasmodium falciparum strains reveals synergistic action with artemisinins. *Antimicrob. Agents Chemother.* 49, 4592. doi: 10.1128/AAC.49.11.4592-4597.2005
- Alam, M. M., Solyakov, L., Bottrill, A. R., Flueck, C., Siddiqui, F. A., Singh, S., et al. (2015). Phosphoproteomics reveals malaria parasite protein kinase G as a signalling hub regulating egress and invasion. *Nat. Commun.* 6, 1–15. doi: 10.1038/ncomms8285
- Ali, F., Wali, H., Jan, S., Zia, A., Aslam, M., Ahmad, I., et al. (2021). Analysing the essential proteins set of plasmodium falciparum PF3D7 for novel drug targets identification against malaria. *Malar. J.* 20, 1–11. doi: 10.1186/S12936-021-03865-1/TABLES/3
- Amos, B., Aurrecochea, C., Barba, M., Barreto, A., Basenko, E. Y., Bažant, W., et al. (2022). VEuPathDB: The eukaryotic pathogen, vector and host bioinformatics resource center. *Nucleic Acids Res.* 50, D898–D911. doi: 10.1093/NAR/GKAB929
- Anam, Z. E., Joshi, N., Gupta, S., Yadav, P., Chaurasiya, A., Kahlon, A. K., et al. (2020). A *De novo* peptide from a high throughput peptide library blocks myosin A-MTIP complex formation in plasmodium falciparum. *Int. J. Mol. Sci.* 21, 1–17. doi: 10.3390/IJMS21176158
- Andrés, M., García-Gomis, D., Ponte, I., Suau, P., and Roque, A. (2020). Histone H1 post-translational modifications: Update and future perspectives. *Int. J. Mol. Sci.* 21, 1–22. doi: 10.3390/IJMS21165941
- Aurrecochea, C., Brestelli, J., Brunk, B. P., Dommer, J., Fischer, S., Gajria, B., et al. (2009). PlasmoDB: a functional genomic database for malaria parasites. *Nucleic Acids Res.* 37, D539–D543. doi: 10.1093/NAR/GKN814
- Ayana, R., Yadav, P., Kumari, R., Ramu, D., Garg, S., Pati, S., et al. (2018). Identification and characterization of a novel palmitoyl acyltransferase as a druggable rheostat of dynamic palmitoylation in *l. donovani*. *Front. Cell. Infect. Microbiol.* 8. doi: 10.3389/FCIMB.2018.00186
- Bailey, T. L., Johnson, J., Grant, C. E., and Noble, W. S. (2015). The MEME suite. *Nucleic Acids Res.* 43, W39–W49. doi: 10.1093/NAR/GKV416
- Bateman, A., Martin, M. J., Orchard, S., Magrane, M., Agivetova, R., Ahmad, S., et al. (2021). UniProt: The universal protein knowledgebase in 2021. *Nucleic Acids Res.* 49, D480–D489. doi: 10.1093/NAR/GKAA1100
- Batista, C. M., Kessler, R. L., Eger, I., and Soares, M. J. (2018a). Treatment of trypanosoma cruzi with 2-bromopalmitate alters morphology, endocytosis, differentiation and infectivity. *BMC Cell Biol.* 19, 1–16. doi: 10.1186/S12860-018-0170-3/FIGURES/10
- Batista, C. M., Saad, F., Ceccoti, S. P. C., Eger, I., and Soares, M. J. (2018b). Subcellular localisation of FLAG tagged enzymes of the dynamic protein s-palmitoylation cycle of *Trypanosoma cruzi* epimastigotes. *Mem. Inst. Oswaldo Cruz* 113(8). doi: 10.1590/0074-02760180086
- Baum, J., Richard, D., Healer, J., Rug, M., Krnajske, Z., Gilberger, T. W., et al. (2006). A conserved molecular motor drives cell invasion and gliding motility across malaria life cycle stages and other apicomplexan parasites. *J. Biol. Chem.* 281, 5197–5208. doi: 10.1074/JBC.M509807200
- Bergman, L. W., Kaiser, K., Fujioka, H., Coppens, I., Daly, T. M., Fox, S., et al. (2003). Myosin a tail domain interacting protein (MTIP) localizes to the inner membrane complex of plasmodium sporozoites. *J. Cell Sci.* 116, 39–49. doi: 10.1242/JCS.00194
- Blomqvist, K., Helm, M., Wang, C., Absalon, S., Labunska, T., Rudlaff, R. M., et al. (2020). Influence of plasmodium falciparum calcium-dependent protein kinase 5 (PfCDPK5) on the late schizont stage phosphoproteome. *mSphere*. 5(1), e00921–19. doi: 10.1128/MSPHERE.00921-19
- Bosch, J., Turley, S., Daly, T. M., Bogh, S. M., Villasmil, M. L., Roach, C., et al. (2006). Structure of the MTIP-MyoA complex, a key component of the malaria

- parasite invasion motor. *Proc. Natl. Acad. Sci. U. S. A.* 103, 4852–4857. doi: 10.1073/PNAS.0510907103/SUPPL_FILE/10907FIG9.JPG
- Bushell, E., Gomes, A. R., Sanderson, T., Anar, B., Girling, G., Herd, C., et al. (2017). Functional profiling of a plasmodium genome reveals an abundance of essential genes. *Cell* 170, 260–272.e8. doi: 10.1016/j.cell.2017.06.030
- Cheng, A., Grant, C. E., Noble, W. S., and Bailey, T. L. (2019). MoMo: Discovery of statistically significant post-translational modification motifs. *Bioinformatics* 35, 2774. doi: 10.1093/BIOINFORMATICS/BTY1058
- Chuenkova, M. V., Furnari, F. B., Cavenee, W. K., and Pereira, M. A. (2001). Trypanosoma cruzi trans-sialidase: A potent and specific survival factor for human schwann cells by means of phosphatidylinositol 3-kinase/Akt signaling. *Proc. Natl. Acad. Sci. U. S. A.* 98, 9936. doi: 10.1073/PNAS.161298398
- Damianou, A., Burge, R. J., Catta-Preta, C. M. C., Geoghegan, V., Romina Nievas, Y., Newling, K., et al. (2020). Essential roles for deubiquitination in leishmania life cycle progression. *PLoS Pathog.* 16, e1008455. doi: 10.1371/JOURNAL.PPAT.1008455
- Déchamps, S., Shastri, S., Wengelnik, K., and Vial, H. J. (2010). Glycerophospholipid acquisition in plasmodium - a puzzling assembly of biosynthetic pathways. *Int. J. Parasitol.* 40, 1347–1365. doi: 10.1016/j.ijpara.2010.05.008
- DeJesus, G., and Bizzozero, O. A. (2002). Effect of 2-fluoropalmitate, cerulenin and tunicamycin on the palmitoylation and intracellular translocation of myelin proteolipid protein. *Neurochem. Res.* 27 (12), 1669–1675. doi: 10.1023/A:1021643229028
- Doerig, C., Rayner, J. C., Scherf, A., and Tobin, A. B. (2015). Post-translational protein modifications in malaria parasites. *Nat. Rev. Microbiol.* 13 (3), 160–172. doi: 10.1038/nrmicro3402
- Douse, C. H., Green, J. L., Salgado, P. S., Simpson, P. J., Thomas, J. C., Langsley, G., et al. (2012). Regulation of the plasmodium motor complex: PHOSPHORYLATION OF MYOSIN A TAIL-INTERACTING PROTEIN (MTIP) LOOSENS ITS GRIP ON MyoA. *J. Biol. Chem.* 287, 36968. doi: 10.1074/jbc.M112.379842
- Edmonds, M. J., Geary, B., Doherty, M. K., and Morgan, A. (2017). Analysis of the brain palmitoyl-proteome using both acyl-biotin exchange and acyl-resin-assisted capture methods. *Sci. Rep.* 7 (1), 1–13. doi: 10.1038/s41598-017-03562-7
- Ekka, R., Gupta, A., Bhatnagar, S., Malhotra, P., and Sharma, P. (2020). Phosphorylation of rho-try protein RhopH3 is critical for host cell invasion by the malaria parasite. *MBio* 11, 1–12. doi: 10.1128/MBIO.00166-20
- Fivelman, Q. L., Adagu, I. S., and Warhurst, D. C. (2004). Modified fixed-ratio isobologram method for studying *in vitro* interactions between atovaquone and proguanil or dihydroartemisinin against drug-resistant strains of plasmodium falciparum. *Antimicrob. Agents Chemother.* 48, 4097–4102. doi: 10.1128/AAC.48.11.4097-4102.2004
- Foe, I. T., Child, M. A., Majumdar, J. D., Krishnamurthy, S., Van Der Linden, W. A., Ward, G. E., et al. (2015). Global analysis of palmitoylated proteins in toxoplasma gondii. *Cell Host Microbe* 18, 501–511. doi: 10.1016/j.chom.2015.09.006
- Frénal, K., Polonais, V., Marq, J. B., Stratmann, R., Limenitakis, J., and Soldati-Favre, D. (2010). Functional dissection of the apicomplexan glideosome molecular architecture. *Cell Host Microbe* 8, 343–357. doi: 10.1016/j.chom.2010.09.002
- Ganter, M., Goldberg, J. M., Dvorin, J. D., Paulo, J. A., King, J. G., Tripathi, A. K., et al. (2017). Plasmodium falciparum CRK4 directs continuous rounds of DNA replication during schizogony. *Nat. Microbiol.* 2(5), 1–9. doi: 10.1038/NMICROBIOL.2017.17
- Govindasamy, K., Jebiwott, S., Jaijyan, D. K., Davidow, A., Ojo, K. K., Van Voorhis, W. C., et al. (2016). Invasion of hepatocytes by plasmodium sporozoites requires cGMP-dependent protein kinase and calcium dependent protein kinase 4. *Mol. Microbiol.* 102, 349–363. doi: 10.1111/MMI.13466
- Green, J. L., Martin, S. R., Fielden, J., Ksagoni, A., Grainger, M., Yim Lim, B. Y. S., et al. (2006). The MTIP-myosin a complex in blood stage malaria parasites. *J. Mol. Biol.* 355, 933–941. doi: 10.1016/j.jmb.2005.11.027
- Green, J. L., Rees-Channer, R. R., Howell, S. A., Martin, S. R., Knuepfer, E., et al. (2008). The motor complex of plasmodium falciparum PHOSPHORYLATION BY A CALCIUM-DEPENDENT PROTEIN KINASE. *Journal of Biological Chemistry*, 283(45), 30980–9. doi: 10.1074/jbc.M803129200
- Gupta, P., Venkadesan, S., and Mohanty, D. (2022). Pf-phospho: A machine learning-based phosphorylation sites prediction tool for plasmodium proteins. *Brief. Bioinform.* 23(4), bbac249. doi: 10.1093/BIB/BBAC249
- Habibian, J., and Ferguson, B. S. (2019). The crosstalk between acetylation and phosphorylation: Emerging new roles for HDAC inhibitors in the heart. *Int. J. Mol. Sci.* 20(1), 102. doi: 10.3390/IJMS20010102
- Health Organization, W (2019) World malaria report 2019. Available at: www.who.int/malaria.
- Hodson, N., Invergo, B., Rayner, J. C., and Choudhary, J. S. (2015). Palmitoylation and palmitoyl-transferases in plasmodium parasites. *Biochem. Soc Trans.* 43, 240–245. doi: 10.1042/BST20140289
- Howick, V. M., Russell, A. J. C., Andrews, T., Heaton, H., Reid, A. J., Natarajan, K., et al. (2019). The malaria cell atlas: Single parasite transcriptomes across the complete plasmodium life cycle. *Science*, 365(6455), eaaw2619. doi: 10.1126/SCIENCE.AAW2619
- Hunter, T. (2007). The age of crosstalk: phosphorylation, ubiquitination, and beyond. *Mol. Cell* 28, 730–738. doi: 10.1016/j.molcel.2007.11.019
- Ihlenfeldt, W. D., Bolton, E. E., and Bryant, S. H. (2009). The PubChem chemical structure sketcher. *J. Cheminform.* 1, 20. doi: 10.1186/1758-2946-1-20
- Jain, R., Gupta, S., Munde, M., Pati, S., and Singh, S. (2020). Development of novel anti-malarial from structurally diverse library of molecules, targeting plant-like CDPK1, a multistage growth regulator of p. falciparum. *Biochem. J.* 477, 1951–1970. doi: 10.1042/BCJ20200045
- Jones, M. L., Collins, M. O., Goulding, D., Choudhary, J. S., and Rayner, J. C. (2012). Analysis of protein palmitoylation reveals a pervasive role in plasmodium development and pathogenesis. *Cell Host Microbe* 12, 246–258. doi: 10.1016/j.chom.2012.06.005
- Jones, M. L., Kitson, E. L., and Rayner, J. C. (2006). Plasmodium falciparum erythrocyte invasion: A conserved myosin associated complex. *Mol. Biochem. Parasitol.* 147, 74–84. doi: 10.1016/j.molbiopara.2006.01.009
- Jortzik, E., Kehr, S., and Becker, K. (2011). Post-translational modifications in apicomplexan parasites. *Prog. Parasitol.*, 93–120. Springer, Berlin, Heidelberg. doi: 10.1007/978-3-642-21396-0_6
- Kanehisa, M. (2019). Toward understanding the origin and evolution of cellular organisms. *Protein Sci.* 28, 1947–1951. doi: 10.1002/PRO.3715
- Kanehisa, M., Furumichi, M., Sato, Y., Ishiguro-Watanabe, M., and Tanabe, M. (2021). KEGG: Integrating viruses and cellular organisms. *Nucleic Acids Res.* 49, D545–D551. doi: 10.1093/NAR/GKAA970
- Kanehisa, M., and Goto, S. (2000). KEGG: kyoto encyclopedia of genes and genomes. *Nucleic Acids Res.* 28, 27–30. doi: 10.1093/NAR/28.1.27
- Kelly, J. X., Smilkstein, M. J., Cooper, R. A., Lane, K. D., Johnson, R. A., Janowsky, A., et al. (2007). Design, synthesis, and evaluation of 10-n-substituted acridones as novel chemosensitizers in plasmodium falciparum. *Antimicrob. Agents Chemother.* 51, 4133–4140. doi: 10.1128/AAC.00669-07
- Kesely, K. R., Pantaleo, A., Turrini, F. M., Olupot-Olupot, P., and Low, P. S. (2016). Inhibition of an erythrocyte tyrosine kinase with imatinib prevents plasmodium falciparum egress and terminates parasitemia. *PLoS One* 11, e0164895. doi: 10.1371/JOURNAL.PONE.0164895
- Khamrui, S., Turley, S., Pardon, E., Steyaert, J., Fan, E., Verlinde, C. L. M. J., et al. (2013). The structure of the D3 domain of plasmodium falciparum myosin tail interacting protein MTIP in complex with a nanobody. *Mol. Biochem. Parasitol.* 190, 87–91. doi: 10.1016/j.molbiopara.2013.06.003
- King, T. C., and Krogstad, D. J. (1983). Spectrophotometric assessment of dose-response curves for single antimicrobial agents and antimicrobial combinations. *J. Infect. Dis.* 147, 758–764. doi: 10.1093/INFDIS/147.4.758
- Krishnan, K. M., and Williamson, K. C. (2018). The proteasome as a target to combat malaria: Hits and misses. *Transl. Res.* 198, 40–47. doi: 10.1016/j.trsl.2018.04.007
- Kumar, S., Kumar, M., Ekka, R., Dvorin, J. D., Paul, A. S., Madugundu, A. K., et al. (2017b). PfCDPK1 mediated signaling in erythrocytic stages of plasmodium falciparum. *Nat. Commun.* 8 (1), 1–13. doi: 10.1038/s41467-017-00053-1
- Kumar, K., Srinivasan, P., Nold, M. J., Moch, J. K., Reiter, K., Sturdevant, D., et al. (2017a). Profiling invasive plasmodium falciparum merozoites using an integrated omics approach. *Sci. Rep.* 7(1), 1–17. doi: 10.1038/s41598-017-17505-9
- Lasonder, E., Green, J. L., Camarda, G., Talabani, H., Holder, A. A., Langsley, G., et al. (2012). The plasmodium falciparum schizont phosphoproteome reveals extensive phosphatidylinositol and cAMP-protein kinase a signaling. *J. Proteome Res.* 11, 5323–5337. doi: 10.1021/PR300557M
- Lasonder, E., Green, J. L., Grainger, M., Langsley, G., and Holder, A. A. (2015). Extensive differential protein phosphorylation in intraerythrocytic plasmodium falciparum schizonts develop into extracellular invasive merozoites. *Proteomics* 15, 2716–2729. doi: 10.1002/PMIC.201400508
- Lonard, D. M., and O'Malley, B. W. (2007). Nuclear receptor coregulators: Judges, juries, and executioners of cellular regulation. *Mol. Cell* 27, 691–700. doi: 10.1016/j.molcel.2007.08.012
- Luo, W., and Brouwer, C. (2013). Pathview: An R/Bioconductor package for pathway-based data integration and visualization. *Bioinformatics* 29, 1830–1831. doi: 10.1093/BIOINFORMATICS/BTT285
- More, K. R., Kaur, I., Gianetto, Q. G., Invergo, B. M., Chaze, T., Jain, R., et al. (2020). Phosphorylation-dependent assembly of a 14-3-3 mediated signaling complex during red blood cell invasion by plasmodium falciparum merozoites. *MBio* 11, 1–17. doi: 10.1128/MBIO.01287-20
- Munthinn, M., Bray, P. G., Ridley, R. G., and Ward, S. A. (1998). Central role of hemoglobin degradation in mechanisms of action of 4- aminoquinolines, quinoline methanols, and phenanthrene methanols. *Antimicrob. Agents Chemother.* 42, 2973–2977. doi: 10.1128/AAC.42.11.2973

- Omasits, U., Ahrens, C. H., Müller, S., and Wollscheid, B. (2014). Protter: Interactive protein feature visualization and integration with experimental proteomic data. *Bioinformatics* 30, 884–886. doi: 10.1093/BIOINFORMATICS/BTT607
- Pantaleo, A., Kesely, K. R., Pau, M. C., Tsamesidis, I., Schwarzer, E., Skorokhod, O. A., et al. (2017). Syk inhibitors interfere with erythrocyte membrane modification during *P. falciparum* growth and suppress parasite egress. *Blood* 130, 1031–1040. doi: 10.1182/BLOOD-2016-11-748053
- Park, J. M., Park, J. H., Mun, D. G., Bae, J., Jung, J. H., Back, S., et al. (2015). Integrated analysis of global proteome, phosphoproteome and glycoproteome enables complementary interpretation of disease-related protein networks. *Sci. Rep.* 5 (1), 1–12. doi: 10.1038/srep18189
- Pease, B. N., Huttlin, E. L., Jedrychowski, M. P., Dorin-Semblat, D., Sebastiani, D., Segarra, D. T., et al. (2018). Characterization of *Plasmodium falciparum* atypical kinase PfPK7 - dependent phosphoproteome. *J. Proteome Res.* 17, 2112–2123. doi: 10.1021/ACS.JPROTEOME.8B00062
- Pease, B. N., Huttlin, E. L., Jedrychowski, M. P., Talevich, E., Harmon, J., Dillman, T., et al. (2013). Global analysis of protein expression and phosphorylation of three stages of *Plasmodium falciparum* intraerythrocytic development. *J. Proteome Res.* 12, 4028–4045. doi: 10.1021/PR400394G
- Perrin, A. J., Patel, A., Flueck, C., Blackman, M. J., and Baker, D. A. (2020). cAMP signalling and its role in host cell invasion by malaria parasites. *Curr. Opin. Microbiol.* 58, 69–74. doi: 10.1016/j.mib.2020.09.003
- Rees-Channer, R. R., Martin, S. R., Green, J. L., Bowyer, P. W., Grainger, M., Molloy, J. E., et al. (2006). Dual acylation of the 45 kDa gliding-associated protein (GAP45) in *Plasmodium falciparum* merozoites. *Mol. Biochem. Parasitol.* 149, 113–116. doi: 10.1016/j.molbiopara.2006.04.008
- Ren, J., Wen, L., Gao, X., Jin, C., Xue, Y., and Yao, X. (2008). CSS-Palm 2.0: An updated software for palmitoylation sites prediction. *Protein Eng. Des. Sel.* 21, 639. doi: 10.1093/PROTEIN/GZN039
- Resh, M. D. (2006). Use of analogs and inhibitors to study the functional significance of protein palmitoylation. *Methods* 40, 191–197. doi: 10.1016/j.ymeth.2006.04.013
- Ridzuan, M. A. M., Moon, R. W., Knuepfer, E., Black, S., Holder, A. A., and Green, J. L. (2012). Subcellular location, phosphorylation and assembly into the motor complex of GAP45 during *Plasmodium falciparum* schizont development. *PLoS One* 7, e33845. doi: 10.1371/JOURNAL.PONE.0033845
- Saunders, C. N., Cota, E., Baum, J., and Tate, E. W. (2020). Peptide probes for *Plasmodium falciparum* MyoA tail interacting protein (MTIP): Exploring the druggability of the malaria parasite motor complex. *ACS Chem. Biol.* 15, 1313–1320. doi: 10.1021/ACSCHEMBO.0C00328
- Schlott, A. C., Holder, A. A., and Tate, E. W. (2018). N -myristoylation as a drug target in malaria: Exploring the role of n -myristoyltransferase substrates in the inhibitor mode of action. *ACS Infect. Dis.* 4, 449–457. doi: 10.1021/ACSINFECDIS.7B00203
- Semenov, A., Olson, J. E., and Rosenthal, P. J. (1998). Antimalarial synergy of cysteine and aspartic protease inhibitors. *Antimicrob. Agents Chemother.* 42, 2254–2258. doi: 10.1128/AAC.42.9.2254
- Solyakov, L., Halbert, J., Alam, M. M., Semblat, J. P., Dorin-Semblat, D., Reiningger, L., et al. (2011). Global kinomic and phospho-proteomic analyses of the human malaria parasite *Plasmodium falciparum*. *Nat. Commun.* 2(1), 1–12. doi: 10.1038/NCOMMS1558
- Soulat, D., and Bogdan, C. (2017). Function of macrophage and parasite phosphatases in leishmaniasis. *Front. Immunol.* 8. doi: 10.3389/fimmu.2017.01838/BIBTEX
- Swaney, D. L., Beltrao, P., Starita, L., Guo, A., Rush, J., Fields, S., et al. (2013). Global analysis of phosphorylation and ubiquitylation cross-talk in protein degradation. *Nat. Methods* 1 (07), 676–682. doi: 10.1038/nmeth.2519
- Szklarczyk, D., Gable, A. L., Nastou, K. C., Lyon, D., Kirsch, R., Pyysalo, S., et al. (2021). The STRING database in 2021: Customizable protein–protein networks, and functional characterization of user-uploaded gene/measurement sets. *Nucleic Acids Res.* 49, D605. doi: 10.1093/NAR/GKAA1074
- Taw, L., Chicanne, G., Dubremetz, J. F., Richard, V., Payrastre, B., Vial, H. J., et al. (2010). Phosphatidylinositol 3-phosphate, an essential lipid in *Plasmodium*, localizes to the food vacuole membrane and the apicoplast. *Eukaryot. Cell* 9, 1519. doi: 10.1128/EC.00124-10
- Thomas, J. C., Green, J. L., Howson, R. I., Simpson, P., Moss, D. K., Martin, S. R., et al. (2010). Interaction and dynamics of the *Plasmodium falciparum* MTIP–MyoA complex, a key component of the invasion motor in the malaria parasite. *Mol. Biosyst.* 6, 494–498. doi: 10.1039/B922093C
- Trecek, M., Sanders, J. L., Elias, J. E., and Boothroyd, J. C. (2011). The phosphoproteomes of *Plasmodium falciparum* and *Toxoplasma gondii* reveal unusual adaptations within and beyond the parasites' boundaries. *Cell Host Microbe* 10, 410–419. doi: 10.1016/j.chom.2011.09.004
- Turley, S., Khamrui, S., Bergman, L. W., and Hol, W. G. J. (2013). The compact conformation of the *Plasmodium knowlesi* myosin tail interacting protein MTIP in complex with the c-terminal helix of myosin a. *Mol. Biochem. Parasitol.* 190, 56–59. doi: 10.1016/j.molbiopara.2013.06.004
- Vembar, S. S., Droll, D., and Scherf, A. (2016). Translational regulation in blood stages of the malaria parasite *Plasmodium* spp.: Systems-wide studies pave the way. *Wiley Interdiscip. Rev. RNA* 7, 772–792. doi: 10.1002/WRNA.1365
- Vu, L. D., Gevaert, K., and De Smet, I. (2018). Protein language: Post-translational modifications talking to each other. *Trends Plant Sci.* 23, 1068–1080. doi: 10.1016/j.tplants.2018.09.004
- Wan, J., Roth, A. F., Bailey, A. O., and Davis, N. G. (2007). Palmitoylated proteins: Purification and identification. *Nat. Protoc.* 2 (7), 1573–1584. doi: 10.1038/nprot.2007.225
- Wu, T., Hu, E., Xu, S., Chen, M., Guo, P., Dai, Z., et al. (2021). ClusterProfiler 4.0: A universal enrichment tool for interpreting omics data. *Innov. (Cambridge)* 2 (3), 100141. doi: 10.1016/j.xinn.2021.100141
- Yadav, P., Ayana, R., Garg, S., Jain, R., Sah, R., Joshi, N., et al. (2019). *Plasmodium* palmitoylation machinery engineered in *E. coli* for high-throughput screening of palmitoyl acyl-transferase inhibitors. *FEBS Open Bio* 9, 248–264. doi: 10.1002/2211-5463.12564
- Yakubu, R. R., Weiss, L. M., and Silmon de Monerri, N. C. (2018). Post-translational modifications as key regulators of apicomplexan biology: Insights from proteome-wide studies. *Mol. Microbiol.* 107, 1–23. doi: 10.1111/MMI.13867
- Yao, Q., Li, H., Liu, B. Q., Huang, X. Y., and Guo, L. (2011). SUMOylation-regulated protein phosphorylation, evidence from quantitative phosphoproteomics analyses. *J. Biol. Chem.* 286, 27342. doi: 10.1074/JBC.M111.220848
- Yapi, A. D., Mustofa, M., Valentin, A., Chavignon, O., Teulade, J. C., Mallie, M., et al. (2000). New potential antimalarial Agents : Synthesis and biological activities of original diaza-analogs of phenanthrene. *Chem. Pharm. Bull.* 48, 1886–1889. doi: 10.1248/CPB.48.1886
- Yu, G., Wang, L. G., Han, Y., and He, Q. Y. (2012). clusterProfiler: An R package for comparing biological themes among gene clusters. *OMICS* 16, 284. doi: 10.1089/OMI.2011.0118
- Yu, G., Wang, L. G., Yan, G. R., and He, Q. Y. (2015). DOSE: An R/Bioconductor package for disease ontology semantic and enrichment analysis. *Bioinformatics* 31, 608–609. doi: 10.1093/BIOINFORMATICS/BTU684
- Zheng, B., Zhu, S., and Wu, X. (2015). Clickable analogue of cerulenin as chemical probe to explore protein palmitoylation. *ACS Chem. Biol.* 10, 115–121. doi: 10.1021/CB500758S

COPYRIGHT

© 2022 Anam, Kumari, Mukherjee, Rex, Biswas, Maurya, Ravikumar, Gupta, Kushawaha, Sah, Chaurasiya, Singhal, Singh, Kaushik, Prasad, Pati, Ranganathan and Singh. This is an open-access article distributed under the terms of the [Creative Commons Attribution License \(CC BY\)](https://creativecommons.org/licenses/by/4.0/). The use, distribution or reproduction in other forums is permitted, provided the original author(s) and the copyright owner(s) are credited and that the original publication in this journal is cited, in accordance with accepted academic practice. No use, distribution or reproduction is permitted which does not comply with these terms.



OPEN ACCESS

EDITED BY

Maria Carolina Touz,
Medical Research Institute Mercedes
and Martín Ferreyra (INIMEC),
Argentina

REVIEWED BY

Kevin Brown,
University of Oklahoma Health
Sciences Center, United States
Ricardo Correa,
Instituto de Investigaciones Científicas
y Servicios de Alta Tecnología, Panama

*CORRESPONDENCE

Cheryl A. Lobo
CLobo@Nybc.org

SPECIALTY SECTION

This article was submitted to
Parasite and Host,
a section of the journal
Frontiers in Cellular and
Infection Microbiology

RECEIVED 06 June 2022

ACCEPTED 05 September 2022

PUBLISHED 07 October 2022

CITATION

Beri D, Rodriguez M, Singh M, Liu Y,
Rasquinha G, An X, Yazdanbakhsh K
and Lobo CA (2022) Identification and
characterization of extracellular
vesicles from red cells infected with
Babesia divergens and *Babesia microti*.
Front. Cell. Infect. Microbiol. 12:962944.
doi: 10.3389/fcimb.2022.962944

COPYRIGHT

© 2022 Beri, Rodriguez, Singh, Liu,
Rasquinha, An, Yazdanbakhsh and Lobo.
This is an open-access article
distributed under the terms of the
Creative Commons Attribution License
(CC BY). The use, distribution or
reproduction in other forums is
permitted, provided the original
author(s) and the copyright owner(s)
are credited and that the original
publication in this journal is cited, in
accordance with accepted academic
practice. No use, distribution or
reproduction is permitted which does
not comply with these terms.

Identification and characterization of extracellular vesicles from red cells infected with *Babesia divergens* and *Babesia microti*

Divya Beri¹, Marilis Rodriguez¹, Manpreet Singh¹,
Yunfeng Liu², Giselle Rasquinha³, Xiuli An⁴,
Karina Yazdanbakhsh² and Cheryl A. Lobo^{1*}

¹Department of Blood-Borne Parasites, Lindsley F. Kimball Research Institute, New York Blood Center, New York, NY, United States, ²Department of Complement Biology, Lindsley F. Kimball Research Institute, New York Blood Center, New York, NY, United States, ³Department of Biology, Georgetown University, Washington, DC, United States, ⁴Department of Membrane Biology, Lindsley F. Kimball Research Institute, New York Blood Center, New York, NY, United States

Babesiosis is a zoonosis and an important blood-borne human parasitic infection that has gained attention because of its growing infection rate in humans by transfer from animal reservoirs. *Babesia* represents a potential threat to the blood supply because asymptomatic infections in man are common, and blood from such donors can cause severe disease in certain recipients. Extracellular vesicles (EVs) are vesicles released by cells that contain a complex mixture of proteins, lipids, glycans, and genetic information that have been shown to play important roles in disease pathogenesis and susceptibility, as well as cell–cell communication and immune responses. In this article, we report on the identification and characterization of EVs released from red blood cells (RBCs) infected by two major human *Babesia* species—*Babesia divergens* from *in vitro* culture and those from an *in vivo* *B. microti* mouse infection. Using nanoparticle tracking analysis, we show that there is a range of vesicle sizes from 30 to 1,000 nm, emanating from the *Babesia*-infected RBC. The study of these EVs in the context of hemoparasite infection is complicated by the fact that both the parasite and the host RBC make and release vesicles into the extracellular environment. However, the EV frequency is 2- to 10-fold higher in *Babesia*-infected RBCs than uninfected RBCs, depending on levels of parasitemia. Using parasite-specific markers, we were able to show that ~50%–60% of all EVs contained parasite-specific markers on their surface and thus may represent the specific proportion of EVs released by infected RBCs within the EV population. Western blot analysis on purified EVs from both *in vivo* and *in vitro* infections revealed several parasite proteins that were targets of the host immune response. In addition, microRNA analysis showed that infected RBC EVs have different microRNA signature from uninfected RBC EVs, indicating a potential role as disease biomarkers. Finally, EVs were internalized by other RBCs in culture, implicating a potential role for

these vesicles in cellular communication. Overall, our study points to the multiple functional implications of EVs in *Babesia*–host interactions and support the potential that EVs have as agents in disease pathogenesis.

KEYWORDS

Babesia, extracellular vesicles (EV), image flow cytometry, miRNA, microarray

Introduction

Membrane-bound vesicles containing proteins, nucleic acids, and lipids have been shown to be secreted by a diverse range of eukaryotic and prokaryotic cells. Although they were initially characterized as cell debris, they are now recognized to play an important role in transferring information among cells that are not in direct contact with each other (Wolf, 1967; Gill et al., 2019). Encased within a vesicle, their contents are protected from enzymatic cleavage and fluctuations in both pH and osmolarity encountered in the environment. Extracellular vesicles (EVs) are composed of a heterogeneous group of cell-derived vesicles including exosomes that range in size from 30 to 150 nm (exosomes) and microvesicles (MVs) that span 150–1,000 nm (Babatunde et al., 2020). The contents, size, and membrane composition of EVs are highly heterogeneous and dynamic and depend on the cellular source, state, and environmental conditions (Yanez-Mo et al., 2015).

Functional roles for EVs have been broadly categorized as regulation of gene expression, signal induction, distribution of catalytic activity, and disposal of cellular debris (Shifrin et al., 2013). Their main mechanism of action is serving as vehicles transporting their effector molecular cargo from one cell to another, resulting in functional consequences for the target recipient cells (Schorey et al., 2015). Sometimes, these signals are targeted to cells within a population, such as quorum sensing in bacteria; at other times, EVs from a donor cell modulate other cell types, with a prime example being immune cells as recipients of microbial signals during infection (Shifrin et al., 2013). The mechanisms of EV interaction with target cells are also diverse, ranging from examples of ligand/receptor-mediated binding, phagocytosis, or direct membrane fusion (Szempruch et al., 2016). The cargo content in EVs has been shown to vary with the cell of origin, suggesting a selective loading mechanism (Xie et al., 2022). In the context of infection, EVs have been shown to be secreted by the infectious agent itself or by the host cells (infected or uninfected), potentially influencing the course of the disease (Marti and Johnson, 2016; Martins and Alves, 2020).

In the last decade, there has been many reports on the release of EVs from major human parasitic pathogens including

Plasmodium, Leishmania, Giardia, Trypanosoma, Schistosoma, and Fasciola species (Marti and Johnson, 2016; Moyano et al., 2019). These pathogens have a dual-host life cycle that requires quick adaptation to changing environments, and EVs have been shown to form a key strategy that these parasites use to persist in the human host by regulating host immune responses and provide sensing mechanisms within the parasite population (Cipriano and Hajduk, 2018). In this study, we explored and characterized the EV repertoire of *Babesia*, a related apicomplexan parasite. Babesiosis is a zoonosis, a disease communicable from animals to man and an important blood-borne human parasitic infection (Ord and Lobo, 2015; Vannier et al., 2015; Lobo et al., 2020). Like the others, *Babesia* parasites present a complex life cycle spanning two hosts—a tick vector and a mammalian host. Of the five species that cause human disease, *B. divergens* and *B. microti* have received the most attention because of their growing infection rate in humans via transfer from animal reservoirs, and as asymptomatic infections in man are common, these can be life threatening in certain blood transfusion recipients like hemoglobinopathic individuals (Lobo et al., 2013; Schmidt et al., 2014; Beri et al., 2021).

The growing interest concerning exosomes in infectious diseases, their accessibility in various body fluids, and their capacity to carry a rich protein content highlights the potential use of EVs as new diagnostic and therapeutic tools (Properzi et al., 2013). Apart from protein, EVs have been shown to contain all types of biomolecules, including carbohydrates, lipids, and nucleic acid. Nucleic acid species found in these vesicles include DNA and both non-coding RNAs and messenger RNAs (Nolte-T Hoen et al., 2012; Kim et al., 2017). Of particular interest to our study is the presence of microRNAs (miRNAs), which could be transferred to and function in recipient cells.

In this article, we identify and characterize purified EVs secreted by *B. divergens* using an *in vitro* culture system and *B. microti* using an *in vivo* mouse model. Our data show that both *Babesia* species secrete vesicles that have a size and shape consistent with EVs from other parasites. Quantitative analysis of these vesicles revealed a correlation with parasite infection matrices. Importantly, we show that labeled EVs are taken up by

other red blood cells (RBCs) in culture. The presence of Babesia-derived components, including protein on the surface and within these EVs, makes them highly immunogenic, as demonstrated by reactivity with infected human and mouse sera. A detailed miRNA analysis also provides evidence of highly up-regulated miRNA species in EVs from infected cells, pointing to a potential role in influencing disease outcome. Our results provide a rationale for a detailed study of the role of these EVs in the pathogenesis of babesiosis, as well as to understand their mode of serving as a mechanism of parasite survival by mediating communication among infected cells, as has been implicated in other parasite systems (Marti and Johnson, 2016; Correa et al., 2020).

Materials and methods

B divergens in vitro culture

B. divergens (Bd Rouen 1986 strain) were maintained in human RBCs at 5% hematocrit in complete medium (RPMI-1640; supplemented with 50 µg/ml hypoxanthine, 0.24% (v/v) sodium bicarbonate, and 10% human serum) under low oxygen atmosphere (5% O₂, 5%CO₂, 90% N₂) at 37°C, as previously described (Cursino-Santos et al., 2019). A+ RBCs were collected in 10% CPD and washed 3× with RPMI-1640 medium for the complete plasma and white cells removal. Human A+ serum used to prepare culture media were centrifuged at 100,000 × g for 2 h at 4°C to remove exogenous EVs. Parasite proliferation analysis were carried out by flow cytometry. Characterization of parasite morphology and development was performed by Giemsa-stained slides using light microscopy using a 100× objective. Conditioned media or spent media is used to describe the media that is formed by cell growth and remains after culturing of cells, both iRBCs and uRBCs, for 24 h.

Propagation of *B. microti* in mice

C57BL/6J (000664) were purchased from The Jackson Laboratory (Bar Harbor, ME). Both male and female mice, 9–12 weeks old, were used for this study; animals were housed in microisolator cages in a special pathogen-free facility. The mice were injected with 1 × 10⁸ parasitized cells *via* intraperitoneal route. Once the desired parasitemia was reached, blood from infected BALB/C C57/6J mice (40%–50% parasitemia on day 7/ day 8 post invasion) was collected by cardiac puncture in anesthetized mice. For measuring parasitemia, 1 µl blood was withdrawn from the tail. For NanoSight, 20–30 µl of whole blood was drawn by retro-orbital bleeding in anesthetized mice; plasma was obtained and sent for analysis.

All animal studies were approved by the New York Blood Center's Animal Care and Use Committee.

Short-term ex vivo culture of *B. microti*

Infected blood was collected by retro-orbital bleeding when the parasitemia in the mice was ~10%. After removing buffy coat, RBC was washed 3× with serum-free RPMI and set into culture at 4% hematocrit for 24 h at 37°C in 1× RPMI supplemented with 367 mM hypoxanthine, 10% fetal bovine serum, and 10 mg/ml gentamycin. Fetal bovine serum used to prepare culture media was centrifuged at 100,000 × g for 2 h at 4°C to remove exogenous EVs. The cultures were grown for 36 h using a gas mixture of 5% O₂, 5% CO₂, and 90% N₂ (Lawres et al., 2016). In our hands, 1N ring parasites grew to 2N, 4N, and >4N, but the parasitemia of the culture did not increase. No new cycles of invasion occur, resulting in the same parasitemia as found *in vivo*, although culture medium had higher numbers of EVs than *in vivo* because of the higher parasite load within each RBC. Post-incubation, these culture supernatants were used to purify EVs as detailed below.

Isolation and staining of extracellular vesicles by differential ultracentrifugation from *B. divergens* and *B. microti* culture system

EVs were purified from culture supernatant of uRBCs or iRBCs from both *B. divergens* and *B. microti* by sequential centrifugations at 1600 × g, 3600 × g, and 12,000 × g each for 15 min each at 4°C. The supernatant was then filtered with 0.2-µm filter to remove any cellular debris and then spun at 100,000 × g for 2 hr at 4°C in Beckman Coulter SW28 tube to get a pellet enriched in EVs. This was resuspended in serum-free RPMI, layered on top of 8 ml 60% sucrose, and centrifuged for 16 h at 4°C in a Beckman SW41 tube at 100 000 × g. Purified EVs were collected from interface (500 ml) and washed with 10 ml phosphate-buffered saline (PBS) by spinning at 100,000 × g for 1.5 h at 4°C in a Beckman Coulter SW41 tube.

For carboxyfluorescein succinimidyl ester (CFSE) staining of EVs, 500 µl CFSE (V12883 Invitrogen) was added at a final concentration of 10 µM. The labeling was done for 15 min at 37°C, following which 30% bovine serum albumin (BSA) stock (Sigma-Aldrich, St. Louis, MO) was added at a final concentration of 1% BSA to stop the labeling. CFSE-labeled EV pellet was layered on 60% sucrose, spun for 16 h in a Beckman SW41 tube at 100 000 × g. EVs collected from interface were washed with 8 ml PBS by spinning 1.5 h in a Beckman SW41 tube at 100 000 × g.

Flow cytometry-based confirmation of identity of extracellular vesicles

As recommended by the International Society for Extracellular Vesicles, following differential centrifugation, we

verified the identity of EVs isolated from uRBCs and iRBCs using standard markers, as previously described (Andreu and Yanez-Mo, 2014). Toward this, we used Exosome-Human CD9 and Exosome-Human CD81 Flow Detection Reagents (Invitrogen), which contained magnetic beads attached to capture antibodies CD9 and CD81, respectively. The enriched fraction of EVs was incubated with the magnetic beads, with appropriate controls, as outlined by the manufacturer. Following this, two detection antibodies CD9 and CD81 conjugated to PE fluorophore (BD Pharmingen) were used at manufacturer-directed dilutions. The samples were read in the Cytoflex by Beckman Coulter using the violet side scatter and Phycoerythrin (PE) channels.

Flow cytometry–based calculation of parasitemia

Parasitemia measurements for *B. divergens* and *B. microti* were done using previously established protocols in our lab (Cursino-Santos et al., 2017). Briefly, mouse erythrocytes (1×10^7 cells/ml) were identified by allophycocyanin (APC) rat anti-mouse TER-119 at a final concentration 0.005 μ M (BD Pharmingen). iRBCs were identified by staining parasite DNA using Hoescht 33342 (0.1 μ M final concentration; Thermo Fisher Scientific). As all RBCs lack a nucleus, RBCs with a positive signal for DNA represent infected host cells bearing parasites. For *in vitro* cultures of *B. divergens* in human blood, samples were stained with the DNA-dye Vybrant[®] DyeCycle[™] Green (1:500) and BV421 mouse anti-human CD235a (BD-562938; 1:500), which labels human RBCs. Samples were analyzed on an LSR Fortessa SORP analyzer (BD Biosciences), equipped with a 355-nm UV laser for Hoechst detection (361/486 nm), a 640-nm red laser for APC-TER-119 detection [650/60 nm bandpass (BP)], a 488-nm blue laser for Vybrant[®] DyeCycle[™] Green detection (530/30 nm BP), and a 405-nm violet laser for anti-GPA detection (450/50 nm BP) in 10,000 target events (iRBCs). The forward scatter threshold was set on 300, and 10,000 total events were acquired at “low” flow rate. FACSDiva software (version 6.2; BD Biosciences) was used for data analysis. All parameters were processed using log scaling.

MicroRNA seq and microarray

Up to 12 T-75 culture flasks of uninfected RBCs (uRBCs) or *B. divergens*-infected RBCs (iRBCs) were used. EV pellet, obtained after from differential centrifugation and 60% sucrose cushion, was washed with PBS and stored at -70°C until ready to be shipped to Norgen Biotek (Thorold, ON, Canada), where miRNA isolation, concentration, and quality check were performed. The samples were treated with RNase prior to RNA isolation to remove extravesicular RNA. RNA from EVs

was isolated using the Norgen’s Plasma/Serum RNA Purification Mini Kit (Cat. 55000) according to the manufacturer’s instructions (Norgen Biotek, Thorold, ON, Canada). Quantification of isolated RNA using RiboGreen assay was determined along with reverse transcription quantitative real-time PCR amplification of the 5S rRNA and miR-21 to indicate the quality RNA. Norgen Biotek shipped the purified miRNA to LS Sciences (Houston, TX), where miRNA sequencing and miRNA microarray were performed and analyzed. LS Sciences human miRNA array used Part No. MRA-1001B2, version number miRHuman_21, and this was based on Sanger miRBase Release 21 (<http://www.mirbase.org/>). Detailed methods are provided in [Supplementary File 3](#).

Electron microscopy of extracellular vesicles and of extracellular vesicles with red blood cells

Sucrose-purified EVs or iRBCs were washed with $1\times$ PBS and resuspended in fixative with 1% paraformaldehyde and 0.1% glutaraldehyde in 0.1 M cacodylate buffer for 1 h at 4°C , washed in 0.1 M buffer (pH 7.4). They were then treated with 50 mM ammonium chloride to quench the remaining aldehydes and spun for 1.5 h in a Beckman SW41 tube at $100,000 \times g$ and resuspended in 50 ml PBS. Negative staining of purified vesicles from a sucrose gradient interface was performed by using uranyl acetate (1%) in water. After sections were stained with uranyl acetate, they were observed using a Philips 410 electron microscope (Holland).

Imaging flow cytometry antibody staining and acquiring

The 100,000 g EV-enriched pellet obtained after differential centrifugation was washed with PBS by spinning 1.5 h in a Beckman SW41 tube at $100,000 \times g$, resuspended in 500 μ l PBS. Staining for *B. divergens* iRBC-derived CFSE-labeled EVs was done as follows: 2 μ l rabbit anti-Bd37 antibody (used at 1:200) in 1% BSA/PBS at 4°C for 1 h, followed by a wash step and addition of 4 μ l Texas Red[®] (TR) goat anti-rabbit IgG antibody at 1:100 in 1% BSA/PBS (Vector Laboratories, Inc., Burlingame, CA). Antibodies prior to use were always spun down and filtered with a 0.22- μ m syringe filter to get rid of any aggregate. *B. microti*-derived CFSE labeled EVs were labeled similarly. Primary antibody anti-BM2 was used at 1:125, and secondary antibody Texas Red[®] horse anti-mouse IgG antibody (Vector Laboratories, Inc., Burlingame, CA) was used at 1:100.

For the internalization experiment involving RBCs, CFSE-labeled EVs were obtained as outlined above. BCA protein analysis was done, and 50 μ g of EVs was incubated with infected parasite culture at 5% hematocrit and 35%

parasitemia in 100 μ l of complete RPMI. At 1 and 3 h, cells were washed twice with RPMI to remove unbound EVs. This was followed by staining with primary antibody against red cell marker Band3 (1:250), which was conjugated to a secondary antibody linked to the APC fluorophore (Hu et al., 2013). In addition, DNA dye Hoechst was used at 0.1 μ M, and the samples were incubated at room temperature for 30 min. Cells were washed twice and were immediately run on the ImageStream.

For internalization experiment using monocytes, human monocytes were purified using anti-human CD14 microbeads (Miltenyi Biotec, Auburn, CA) (purity > 95%), as previously reported by our group (Liu et al., 2019). Purified EV were labeled with CFSE, as elaborated above. CFSE-labeled EVs were co-cultured with purified monocytes (2×10^5 /well) in 96-well plates containing RPMI-1640 medium supplemented with 100 U/ml penicillin, 100 μ g/ml streptomycin, and 10% heat-inactivated fetal bovine serum (Thermo Scientific) overnight. For analysis, Accutase (Sigma-Aldrich, St. Louis, MO) was added to the 96-well plates, following manufacturer's instruction to detach all cells in the wells. Following two washes, anti-human CD45-APC (HI30 from BD Biosciences) was used at manufacturer's standardized dilution.

Images were acquired using a 12-channel Amnis ImageStreamX Mark II (Luminex, Austin, Texas). Imaging flow cytometry (IFC) samples were acquired at 60 \times magnification on low speed and excitation lasers 488 (Channel 2 CFSE) and 562 (Channel 10 for Texas Red). Brightfield images were acquired in Channels 1 and 9, whereas side scatter was acquired in Channel 6. Speedbead Kit Amnis[®] Catalog #400041 were used. For RBC internalization experiments, CFSE-labeled EVs were incubated with red cells for the mentioned time points. RBCs were stained using an antibody against Band3 conjugated to secondary antibody linked to APC and acquired using a 640-nm laser (Channel 11 for APC). In addition, Hoechst was used to label parasite DNA and was acquired using a 405-nm excitation laser (Channel 7 for violet). For monocyte internalization experiment, 40 \times magnification was used. Compensation (.cif) files were applied to all the raw data files (.rif) to obtain data files (.daf) that were further analyzed in IDEAS[®] (data analysis software of Amnis Imagestream) 7.1 or FCS Express (Image) Version 7.1 to obtain flow plots and statistics. Internalization Wizard of the IDEAS[®] software was applied, as previously described (Phanse et al., 2012). Out of focus cells and doublets were removed from analysis by appropriate gating (shown in Supplementary Figure 2). Cell boundary was defined by Band3 staining, and internalization of CFSE-labeled EVs was probed. The analysis was applied on all single cells in the population, and a histogram was obtained. A population of cells of more than zero were labeled as "internalized," and those below 1 were "not internalized." Values of the internalization score were calculated for at least 10,000 cells.

Immunoblotting of extracellular vesicles

Sera of blood donors screened positive for *B. microti* were collected as per the guidelines of New York Blood Center Institutional Review Board ($n = 3$). Immunofluorescence was used to determine the dilution at which these sera recognized *B. microti*-infected cells. Mice were injected with *B. microti*, as explained above ($n = 5$), and reactivity of their sera was monitored over time. The above human sera and mouse sera were then used to detect immunoreactivity of purified EVs derived from *B. microti*. Purified EVs were incubated with 0.25% (w/v) trypsin solution at 37°C for 30 min, which results in digestion of non-associated membrane proteins, based on a previous protocol (Saari et al., 2015). Protease inhibitor was added and lysed in Laemmli sample buffer (Bio-Rad). Equal amounts of protein from uninfected and *B. divergens*- or *B. microti*-derived EVs were loaded onto 4%–20% Mini-PROTEAN TGX[™] gels (Bio-Rad). After electrophoresis, the proteins were transferred onto nitrocellulose membrane (Bio-Rad). The membranes were blocked with 5% (w/v) skim milk powder in PBS Tween 20 and then incubated for 1 h at room temperature with 5% milk in PBS Tween 20 with primary antibody *B. microti*-infected human or mice sera, as needed. This was followed by horseradish peroxidase (HRP)-labeled secondary antibody (Amersham ECL mouse IgG, HRP-linked whole antibody and Amersham ECL rabbit IgG, HRP-linked whole antibody, GE Healthcare; anti-human IgG (H+L) antibody, peroxidase-labeled, Kirkegaard & Perry Laboratories, Inc.; or donkey anti-goat IgG antibody, HRP conjugate, Sigma-Aldrich, St. Louis, MO) diluted in 5% non-fat milk.

Results

A heterogeneous population of extracellular vesicles are released by both *B. divergens*-infected red blood cells in culture and in circulation of *B. microti*-infected mice

To assess the presence of EVs in Babesia, we used two different infection model systems, using two distinct Babesia species, *B. divergens* and *B. microti*. The study of EVs in the context of hemoparasite infection is complicated by the fact that the host RBC makes and releases vesicles into the extracellular environment, necessitating a uRBC control in all experiments. As *B. divergens* is easily cultured in human RBCs *in vitro*, we used culture supernatants from uRBC and iRBCs as the source of EVs from this parasite. *B. microti*, on the other hand, requires an animal model to establish infection. C57/BL6 mice were infected with *B. microti*, and plasma from uninfected and infected mice were analyzed for EVs. To determine the size range heterogeneity

and the concentration of EVs in *B. divergens* culture supernatant, we used the nanoparticle tracking analysis technology offered by NanoSight™, which quantifies particles between 0.01 and 1 µm in small volumes (10–20 µl) of culture supernatant/plasma. For each set, a total of three samples were analyzed. First, we determined the total EVs in spent culture supernatant from increasing parasitemia percentage of parasitized host RBCs (cultures of *B. divergens* iRBCs). As shown in Figure 1A, we observed that as parasitemia increased, the total number of EVs in the conditioned medium of *B. divergens*-infected cells showed a proportionate increase. At 50% parasitemia, the EV concentration was almost four times that obtained from a 10% parasitemia culture, representing a 16-fold increase in EV output over uRBCs. This suggests that infection results in an amplification of EV yield in the spent media to further examine the sizes of the particles from uRBCs and iRBCs' spent media; culture supernatant originating from four distinct ~10% parasitemia asynchronous cultures were used as the source of EVs in these analyses. The light scattering data analysis revealed particles ranging from size 50 to 500 nm,

with the modal size of 66.5 ± 2.5 nm, with peaks seen at 100, 137, 188, 221, 277, and 329 nm. EV preparation from uRBCs that were kept under identical culture conditions for the same amount of time yielded a slightly different mode of size range (56.1 ± 0.9 nm). Figure 1B shows a representative graph of concentration (particles/ml culture supernatant) versus size of the EV in nm. As evident, the highest concentration of EVs was in the range of 70–120 nm. There was a longer distribution of size of EVs along the x-axis (Figure 2A) in iRBCs as compared with uRBCs. Furthermore, as shown in Figure 1C, concentration of EVs from iRBC conditioned media was ~2–3 times higher than EVs purified from uRBCs. This establishes that Babesia iRBCs secrete a much higher number of EVs as compared with uRBCs. To further study the Babesia EVs, they needed to be purified from culture supernatant. As described in detail under Methods, a method was developed based on previous literature (Mantel et al., 2013; Mantel and Marti, 2014). Briefly, the supernatant/plasma were spun at 100,000g for 2 h, following which it was laid on a continuous sucrose gradient and spun for 15 h at 100,000g. The

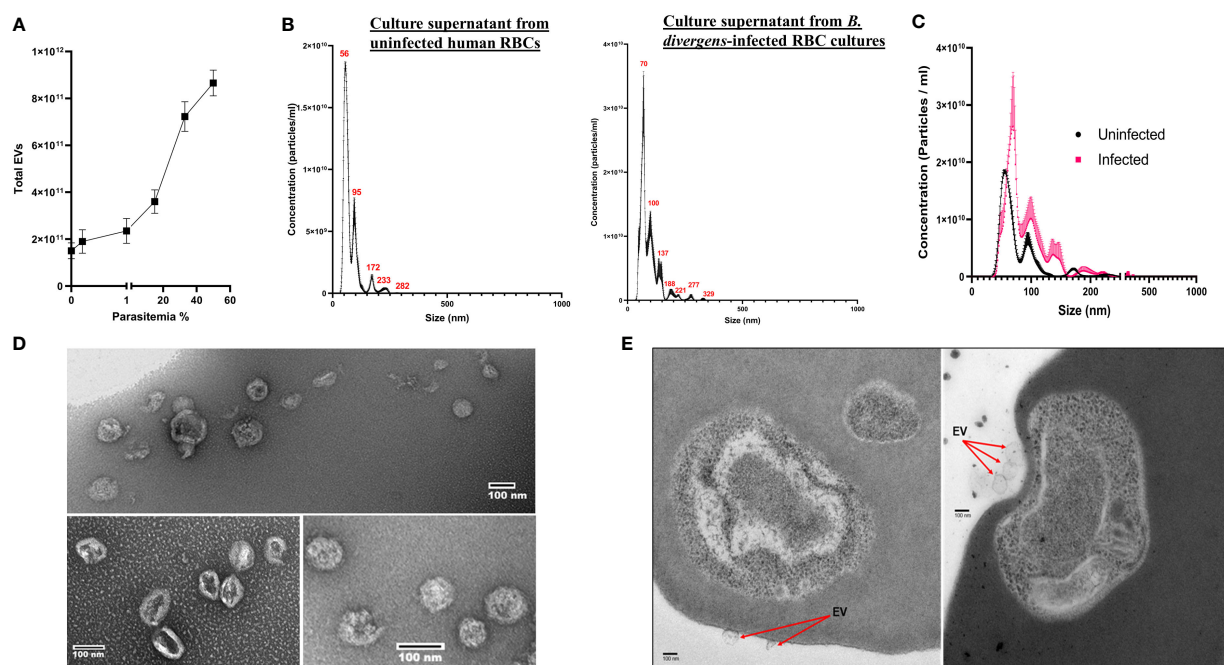


FIGURE 1

Characterization of extracellular vesicle (EV) derived from *B. divergens*-infected red blood cells (RBCs). EVs present in spent culture media of uninfected RBCs (uRBCs) and *B. divergens*-infected RBCs (iRBCs) were used for the analysis. (A) Total EVs in *B. divergens* spent culture supernatant increase with an increase in parasitemia. Approximately, a 4-fold increase in EV numbers was obtained as parasitemia increased from 10% to 60%. (B) Nanoparticle tracking analysis was performed on supernatant from uRBCs and *B. divergens* iRBCs. Profile of size (in nm) concentration is shown. As evident, the highest concentration peak of EVs in uRBCs was ~55 nm, whereas for iRBCs, it was ~70 nm. iRBCs also demonstrated a wider distribution of size of EVs as compared with uRBCs. (C) Direct comparison between uRBCs and iRBCs (~10% parasitemia) with respect to size (in nm) of EVs. At this parasitemia, iRBCs had 1.8- to 2-fold higher number of EVs as demonstrated by "concentration (particles/ml)" in the y-axis. (D) Density gradient-dependent purification of EVs was performed, followed by negative staining and visualization under transmission electron microscopy. A range of different sizes of EVs from *B. divergens*-derived culture supernatant were seen, concurrent with nanoparticle tracking analysis shown in (B). (E) When RBCs were visualized, particles in the size range of EVs were seen on the surface of red cells shown in (C).

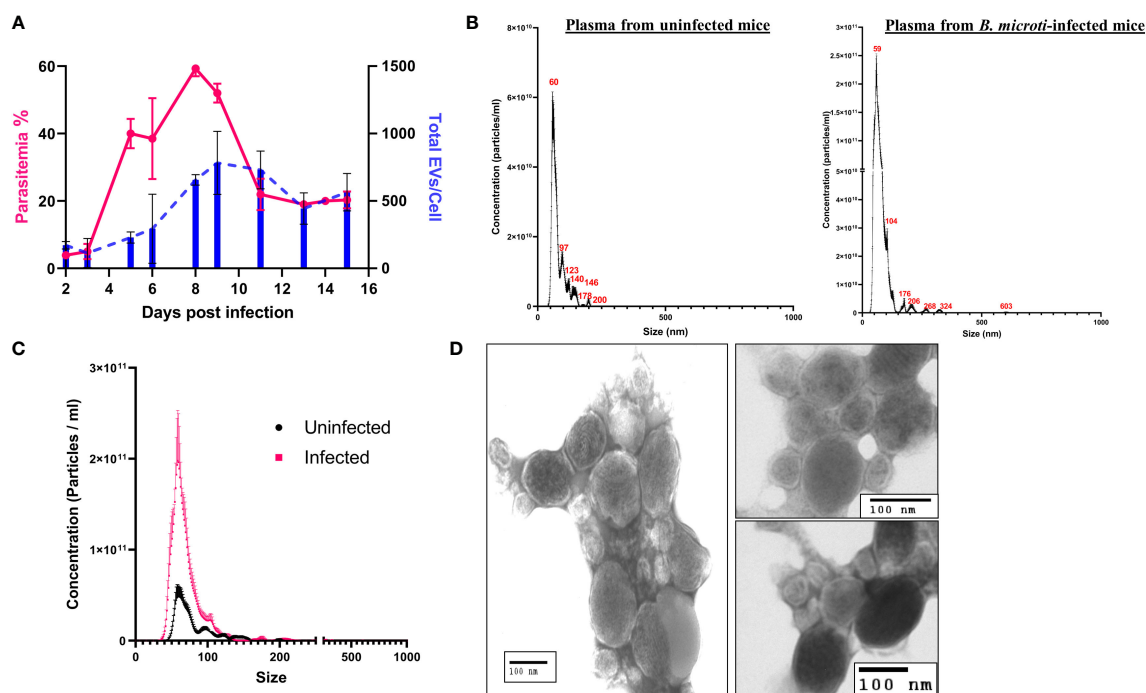


FIGURE 2

Characterization of extracellular vesicle (EV) derived from the plasma of control uninfected and *B. microti*-infected mice. EVs present in the plasma of uninfected and *B. microti*-infected mice were used for the analysis. (A) Comparison of total EVs/red cell (blue) with parasitemia (pink) and days post infection (x-axis) reveals that as parasitemia increases, there is an increase in the number of EVs, which peaks with a peak in parasitemia. As parasitemia begins to fall around day 12, the number of EVs/RBCs also decreases (n = 3 mice). (B) Nanoparticle tracking analysis in uninfected and *B. microti*-infected mouse plasma reveals the size distribution of EVs. As evident, most of the EVs in both sample sets were in the range of 60–120 nm. iRBCs showed a wider distribution of size of EVs. (C) A direct comparison between EVs from uRBCs and iRBCs (day 6 post invasion) in the mouse model. As evident, iRBCs showed a ~5-fold increase in EVs as compared with plasma from uninfected mouse. (D) EVs were enriched from mice infected with *B. microti* using the protocol detailed under Methods and visualized using transmission electron microscopy. A heterogeneous population of EVs with respect to size was shown, which is concurrent with the nanoparticle tracking analysis shown in (B).

interface was collected and used as the source of EVs for all described studies. Furthermore, the identity of EVs in this fraction was confirmed using standard markers (CD9 and CD81), as detailed under Methods and [Supplementary File 4](#). Furthermore, to assess the purity and size of the EVs obtained from the gradient, we stained the isolated EVs using negative stain methodology, followed by transmission electron microscopy (TEM). Our analysis ([Figure 1D](#)) revealed the approximate size and morphology of EVs, concurring with the nanoparticle tracking analysis data and those obtained in other parasite systems ([Marti and Johnson, 2016](#); [Moyano et al., 2019](#); [Sharma et al., 2020](#)). Examination of thin sections of *B. divergens* iRBCs using TEM revealed a population of small vesicles budding from the membrane of iRBCs ([Figure 1E](#)), indicating a possible interaction of EVs with iRBCs, as elaborated in the following section.

To test if *in vivo* Babesia infection also results in similar EV release dynamics, we infected mice with *B. microti* and monitored plasma from control and infected mice for the

presence and frequency of EVs using the service offered by NanoSight™ ([Figure 2](#)). A previous study in *B. microti* demonstrated the presence of vesicular-mediated antigen export ([Thekkiniath et al., 2019](#)), but to the best of our knowledge, no report of characterization of these EVs is available. First, we examined the total EVs in infected versus uninfected mice plasma (n = 3) up to 16 days post infection. As infection results in loss of hematocrit, the EV numbers were normalized to the total number of red cells. As shown in [Figure 2A](#), the total number of EVs in the plasma of infected mice increased with progression of parasitemia. As evident, parasitemia reaches a maximum of $59.33 \pm 1.33\%$ on day 8, whereas the total number of EVs/cell reaches a maximum of 783 ± 165.5 on day 9 post invasion. A size versus concentration analysis of EVs from uninfected and infected plasma (n = 3; day 6 post invasion) revealed key differences ([Figure 2B](#)); whereas uninfected plasma exhibited peaks 60, 97, 123, 140, 146, 179, and 200 nm (mode of 65.6 ± 3.0 nm), the peaks for EVs from the plasma of infected sample were at 59, 104, 176, 206, 268, 324,

and 603 nm (mode of 57.5 ± 3.2 nm). A direct comparison between plasma from uninfected and infected mice (Figure 2C) shows that plasma from infected mice have 3- to 4-folds higher EVs as compared with plasma from uninfected mice. Furthermore, purification of EVs was performed using plasma from infected mice, following a short *ex vivo* culture of *B. microti*, as detailed under Methods. TEM analysis (Figure 2D) shows that the RBCs from infected mice release EVs *in vivo*, and the size and shape of these vesicles are consistent with EV descriptions from other parasites (Marti and Johnson, 2016; Babatunde et al., 2018). It is important to emphasize that EVs from both host and parasite are enumerated in such analyses.

These results (Figures 1, 2) demonstrate the presence of EVs in both *in vitro* and *in vivo* Babesia infection of host RBCs. Although uRBCs in both models release EVs, we show that infection results in a significantly higher number of EVs. Furthermore, this EV frequency is proportional to the parasite load in both the *in vitro* and *in vivo* models of Babesia–host RBC infection.

Purified extracellular vesicles can be internalized by red blood cells and immune cells in culture

We next examined if the purified EVs could be internalized by uRBCs and iRBCs, as has been previously suggested in other systems (Mantel et al., 2013; Marti and Johnson, 2016). IFC can be used to detect multiple fluorescent markers and, together with data on cellular and vesicle morphology, allowed us to study the localization and other specific characteristics of EVs in the context of the parasite. The ability to numerically score large numbers of acquired images is ideally suited to the analysis of internalization, and therefore, this approach was used. Multiple fluorescence tags were used in this analysis: RBCs were labeled with Band3-APC (Red), parasites were labeled with DNA dye Hoechst (pink), and purified EVs (50 µg) were labeled with Vybrant-CFSE (Green) and incubated with a culture at 35% parasitemia for 1 and 3 h, as detailed under Methods. Toward quantitation of percent CFSE+ cells, which were internalized, we used the “Internalization” feature in the IDEAS® statistical analysis software of the ImageStream, as elaborated under Methods. The internalization histogram divides cells that are “internalized” and “not internalized” as shown by values of internalization erode above 0 and below 0, respectively, on the x-axis. The number in the box of Channel 1 represents the unique serial number of the cell in focus for that particular sample. As shown in Figures 3A–D, EVs were seen internalized into both uRBCs and iRBCs at 1 and 3 h post co-incubation. Representative images of internalized CFSE-stained EVs are shown in all cases, and EVs were seen to be often co-localizing with the parasite. Quantitation was performed using a minimum of 10,000 cells. As shown in Figure 3E, the number of cells with internalized EVs was higher in iRBCs as compared with uRBCs. In addition, with

an increase in time of co-incubation, an increasing percentage of cells (both uRBCs and iRBCs) were observed to uptake EVs. At 1 and 3 h, the percentages of uRBCs with internalized EVs \pm SEM were $12.6 \pm 1.1\%$ and $20.70 \pm 1.212\%$, respectively, whereas for iRBCs, they were $20.70 \pm 1.5\%$ and $27.50 \pm 1.8\%$, respectively ($n = 2$, one-way ANOVA, $p = 0.0417$). Therefore, these results suggest that EVs have the potential of transferring cargo containing effector molecules to RBCs and thus mediate communication between both host and parasite and within parasite populations.

Next, we wanted to examine if immune cells, like monocytes, can take up EVs released into Babesia-infected culture supernatants. Toward this, we purified human monocytes using anti-CD14 microbeads and overnight (~12 h) co-incubated 50 µg of CFSE-labeled EVs with 2×10^5 purified monocytes. Cells were stained with CD45, a common marker of leucocytes. Images were analyzed on IDEAS, and internalization was calculated. Interestingly, a significant majority of monocytes (>90%) were able to uptake *B. divergens* spent media-derived EVs. An earlier report has shown uptake of Plasmodium falciparum-derived EVs into peripheral blood mononuclear cell activation (Mantel et al., 2013) and implicated in the “cytokine storm” associated with malaria (Marti and Johnson, 2016). Our current data imply a possible role of *B. divergens* iRBCs-derived EVs in activation of immune cells and require further functional characterization.

Protein cargo from extracellular vesicles from *in vitro* and *in vivo* Babesia models are recognized by Babesia-infected human and mice sera

As EVs were released in the plasma of infected individuals, we hypothesized that their constituent proteins may be the target of the host immune response. To further investigate this, we used sera from both infected human and mouse hosts.

Sera were selected from human donors who were immunopositive against *B. microti* in an Indirect immunofluorescence assay (IFA) analysis (Figure 4A). Three positive donor sera were chosen with titers of 1:64 (AJ102), 1:512 (BB1015), and 1: 1024 (BB1030). These human sera were pooled and used to probe the EV blots (Figure 4D, right panel). Mice sera were obtained from *B. microti*-infected C57/BL6 mice. Mice were bled, and sera were analyzed for reactivity against *B. microti* lysates (Figure 4D). As shown, beginning from day 17, infected mice sera recognized multiple antigens on the lysate, and this peaked on day 45. Thus, day 45 sera from $n = 5$ mice were pooled and used to probe EV blots (Figure 4D, left panel). Equal amounts of purified EVs were loaded in all the lanes. Figure 4C shows the parasitemia profile of *B. microti* in mice. As evident, parasitemia increases initially and peaks at day 8 post invasion. Thereafter, the parasite is cleared by the immune system, and by day 20, parasitemia is almost zero with no further increase.

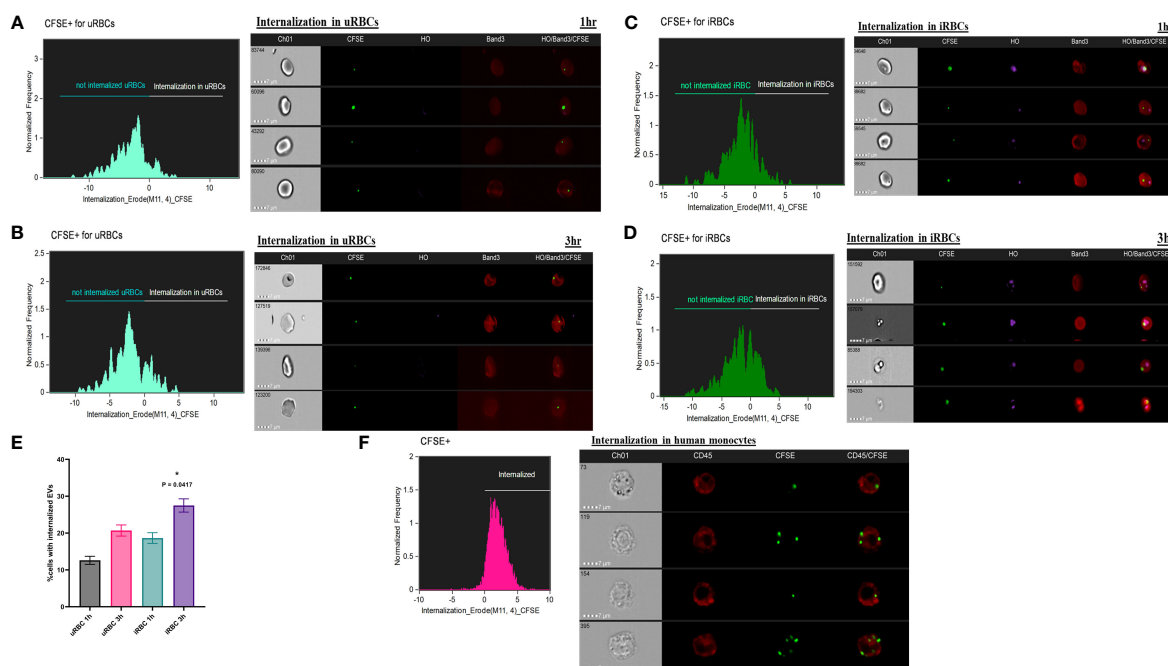


FIGURE 3

Internalization of carboxyfluorescein succinimidyl ester (CFSE)-labeled extracellular vesicles (EVs) by red blood cells (RBCs) and monocytes. (a–e) 50 μ g of purified EVs from spent culture supernatant of *B. divergens*-infected RBCs (iRBCs) were CFSE (green) labeled. These were incubated with iRBCs at 35% parasitemia for 1 and 3 h and stained with Band3-APC (red) and Hoechst (pink). ImageStream was performed followed by the application of Internalization Wizard of IDEASTM software. In the histogram obtained, cells above zero are “internalized,” whereas those below are “not internalized.” Gating strategy is elaborated in [Supplementary Figure 2](#) under [Supplementary File 4](#). (A, B) The histograms show internalization of CFSE-EVs in uninfected RBCs (uRBCs) (Band3+, HO–) at 1 and 3 h, respectively. Representative images of internalized EVs are shown. (C, D) The histograms show internalization of CFSE-EVs in iRBCs (Band3+, HO+) at 1 and 3 h, respectively. Representative images of internalized EVs are shown. (E) Quantification of percent cells with internalized EVs reveals that a marginally higher percentage of iRBCs internalize EVs than uRBCs (~1.5 folds). With time, internalization increases in both uRBCs and iRBCs [$p = 0.0417$ (*), $n = 2$]. (F) Monocytes were purified as elaborated under Methods and co-incubated with CFSE-labeled EVs. Internalization profile shows that >90% monocytes (labeled with CD45-APC in red) internalized CFSE (green)-labeled EVs purified from *B. divergens* spent culture supernatant.

EVs were purified from both uninfected and *B. microti*-infected mice short-term *ex vivo* cultures ([Lawres et al., 2016](#)) lysed, and proteins were run on SDS-PAGE and blotted and probed with the various mice and human sera defined above. We were specifically interested in defining the surface proteome of the EVs since these proteins would be most exposed to the host immune system. Thus, to establish if they were EV surface or internal proteins, fractions containing purified vesicles were digested with either trypsin to ensure that proteins that are associated with the EV surfaces are stripped. We carried out Western blot analysis on purified EVs from only *B. microti* *in vivo* infections, as shown in [Figure 4D](#). This is because *B. divergens* has no animal model system and there was no access to *B. divergens*-infected human sera. Immunoblotting analysis ([Figure 3C](#)) reveals presence of multiple *B. microti* proteins that are recognized by both infected mouse sera and immune-positive human sera (lanes I in each panel). When the EVs were treated with trypsin, multiple protein bands disappeared, suggesting that these were on the surface of the EV (lane I+ from each panel). We also examined reactivity of EVs from uninfected

mice as controls, using a similar number of EVs and normalized for the same protein content. Lane NI contains EVs from naive mouse and does not react with either infected mouse/human sera, demonstrating the specific presence of parasite proteins only on EVs from infected mice. Thus, our results suggest that parasite-specific proteins are present both on the surface of EVs and within EVs derived from *B. microti*-infected mice, and importantly, these are recognized by the immune sera derived from both *Babesia*-infected humans and mice.

Imaging flow cytometry-based confirmation and quantitation of parasite-specific extracellular vesicles derived from infected cells

For erythrocytic parasites, analysis of EVs was complicated because uRBCs also release vesicles. To obtain an idea of the proportion of EVs that are sourced from *Babesia* infection, we decided to use parasite markers to differentiate between EVs from

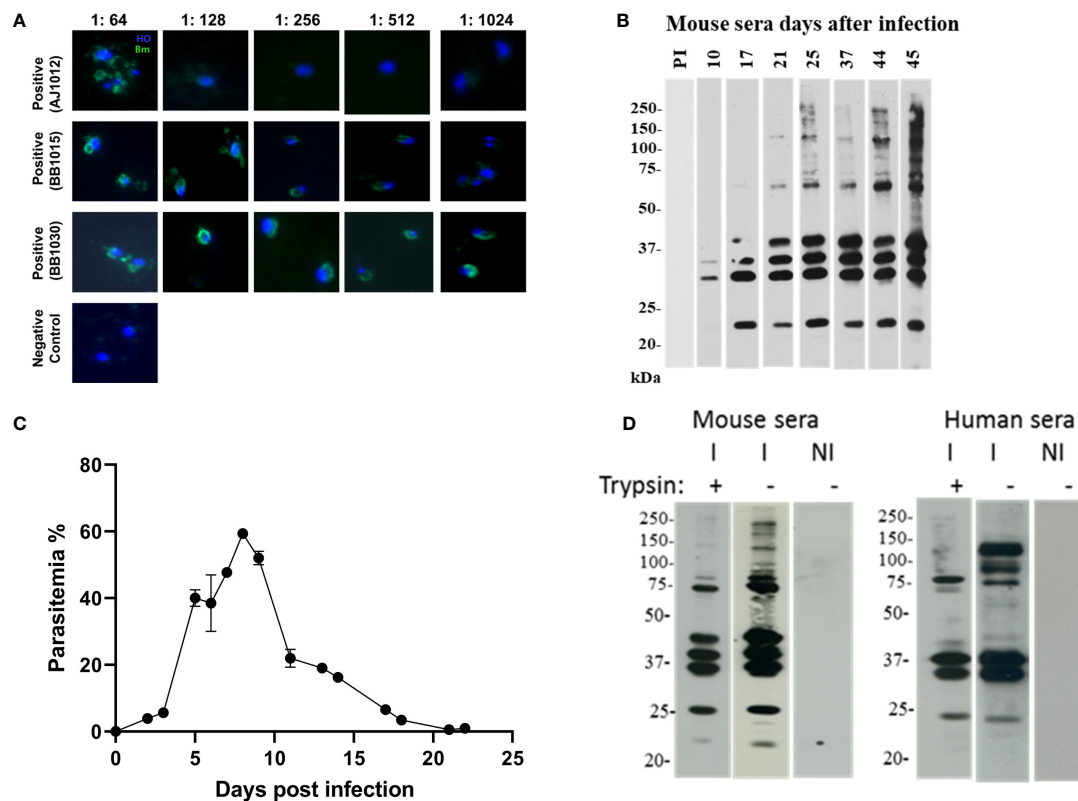


FIGURE 4

EV proteins are recognized by immune sera of *B. microti*-infected humans and mice. (a and b) Selection of sera and appropriate dilution to be used in extracellular vesicle (EV) immunoblots. (A) Sera were collected from human patient donors, and immunofluorescence was performed using *B. microti*-infected cells stained with Hoechst (blue). Anti-human secondary antibody (green) was used to detect immunopositive antigens. Three sera were used as labeled, and different sera titers were used. These sera were pooled and further used at 1:128 dilution. (B) Mice ($n = 5$) were infected with *B. microti*, and the reactivity of each mouse serum was monitored over days of infection. As shown, pre-immune (PI) sera did not react with *B. microti* lysate. At day 45, the maximum number of parasite antigens were recognized by the immune serum, and this was used for subsequent experiments. (C) Parasitemia profile of *B. microti*-infected mice is shown until day 22 post invasion. As evident, parasitemia increases and peaks around day 7, after which it progressively falls as the parasite is cleared by the immune system. By day 20, parasitemia reaches almost zero, and no further increase is seen. (D) EVs purified from control uninfected and *B. microti*-infected mice plasma (same number of EVs were used in all lanes) were run on SDS-PAGE and probed with immune human or immune mouse sera from (A) and (B), respectively. NI refers EVs purified from naïve mouse, and these did not react with either sera. As shown in the "I-" lanes, several antigens were recognized by the immune human and mouse sera. In lanes "I+," EVs were subjected to trypsin before running on the SDS-PAGE and then probed using the human and mouse sera. Several bands disappeared on this treatment, suggesting the presence of these proteins on the surface of the EVs.

uninfected versus iRBCs in both *B. divergens* and *B. microti* infection models. To identify *B. divergens*-specific EVs, we used antibodies against Bd37, which is an abundant 37-kDa protein from *B. divergens* (Delbecq, 2022). To identify *B. microti*-specific EVs, we used antibodies against BMN-2, which is an abundant protein from *B. microti* (Homer et al., 2000) (Elton et al., 2019). EVs were purified from ~30% to 40% parasitemia *B. divergens*-infected cultures and labeled with Vybrant-CFSE (Green) and Texas Red-Bd37. Figures 5A, B show the gating strategy used for EVs as a function of the intensity of side scatter signal and the intensity of CFSE signal and were labeled as EV+. Next, we plotted the intensity of CFSE signal versus the area of CFSE signal and gated cells that were labeled CFSE+/EV+.

Unstained samples were run to determine the positioning of the gate. More than 90% of our EVs were labeled with CFSE. Next, we used this population and plotted the intensity of Texas Red versus the intensity of CFSE and labeled the positive population as "double positive" (Figure 5B). We found that ~60% of EVs were positive for both CFSE and Texas Red (TR). Thus, ~60% of EVs derived from infected cells' conditioned medium contained the Bd37 marker, suggesting that they had been derived from parasite-infected host cells. Similarly, IFC analysis was performed for EVs purified from sera of *B. microti*-infected mice, where EVs were labeled with CFSE (Green) and the *B. microti*-specific marker Bm2 was used coupled with Texas Red (Red). Figure 5D shows the gating strategy used to separate *B. microti* EVs from beads and debris

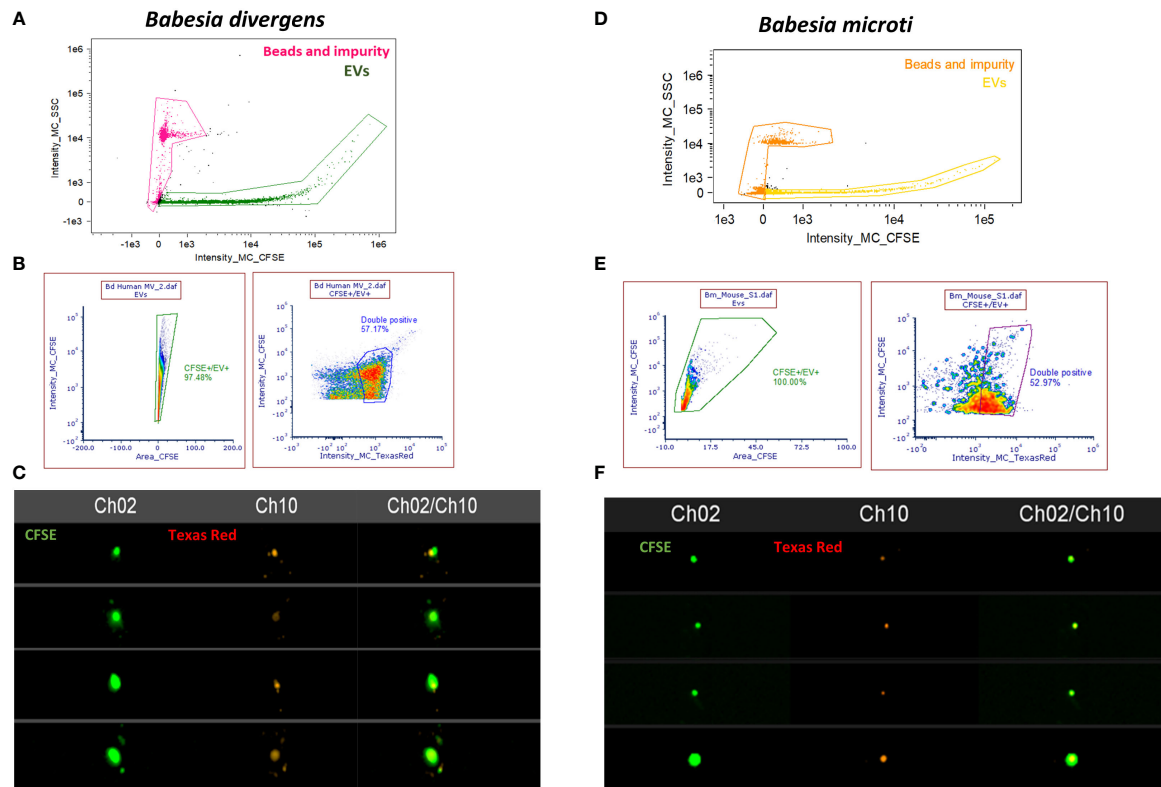


FIGURE 5

Imaging flow cytometry (IFC)-based quantitation of parasite-specific extracellular vesicles (EVs). (A) Gating strategy to select for EVs from *B. divergens*-infected cells. Debris and beads were excluded from further analysis. The EVs were stained with carboxyfluorescein succinimidyl ester (CFSE) (green) and Texas Red-Bd37, which is a *B. divergens*-specific marker (red). (B) CFSE-positive cells were gated based on the area-versus-intensity plot. Right panel shows events that were positive for both CFSE and Texas Red-Bd37 and represent ~60% of EVs. (C) Images showing EVs that were labeled with both CFSE (Channel 2) and TR (Channel 10) and the merged image for the two channels. (D) Similar gating strategy as (A) was used to exclude beads and debris from EVs derived from *B. microti*-infected plasma. (E) EVs were stained with CFSE (green) and TR-Bm2 (red), which is a specific marker of *B. microti*. CFSE+ cells were gated based on the area-versus-intensity plot. Right panel shows the events that were double positive for both (~50%). (F) IFC images showing EVs stained with CFSE (Channel 2) and TR (Channel 10) and their merged image.

(intensity of CFSE vs. intensity of side scatter) and was labeled as “EVs.” Next, the intensity of CFSE+ was plotted against the area of CFSE+ to obtain CFSE+ cells. More than 90% of EVs and this gate were labeled as “CFSE+/EV+.” Next, Texas Red-Bm2 was plotted with CFSE+/EV+ as parent gate, and we found that ~50% of EVs were positive for TR-Bm2. This gate was labeled as “double positive.” Thus, 50% of EVs derived from the plasma of *B. microti*-infected mice showed specificity for the parasite-specific marker Bm2. Figures 5C, F show representative IFC images of EVs derived from *B. divergens*-infected cells and *B. microti*-infected cells, respectively. As evident in the images, EVs were labeled with both CFSE and TR, evidencing their origin from parasitized host cells.

Thus, when coupled to fluorescence detection, IFC analysis is a powerful tool that can be used to analyze specific vesicles within heterogeneous populations. As evident, using Bd37 (Figures 5A–C) and BMN-2 (Figures 5D–F) as parasite EV-

specific markers, we were able to show that ~60% of EVs from *B. divergens* culture stained with Bd37 whereas ~50% of *in vivo* *B. microti*-infected mice EVs contained BMN-2 marker on their surface. Therefore, this represents the specific proportion of EVs released by iRBCs within the total EV population. EVs from uninfected cells did not show positive staining for either antigen.

MicroRNA sequencing analysis indicates multiple human miRNAs and novel miRNAs that are enriched in extracellular vesicles derived from *B. divergens*-infected red blood cells

To identify miRNAs in EVs from uRBCs and iRBCs (~35%–40% parasitemia), we purified EVs, as outlined under Methods. Two different platforms were used to analyze miRNA, next-

generation sequencing (NGS) and microarray analysis, to overcome the inherent drawbacks associated with each. Mature miRNAs are very short and thus require a rather error-prone identification method. miRNAs share high-sequence homology within families, with as low as one base difference, which can be difficult to differentiate, and miRNAs are known to have many isoforms due to RNA editing, resulting in single-nucleotide polymorphisms. These factors often present as challenges for primer or probe design and hybridization in microarrays. In NGS, sequence similarity of miRNAs can present a problem in discriminating between miRNAs prone to sequencing errors. The short and variable length of miRNA further reduces the ability to accurately identify the border between the miRNA and the adaptor (Willenbrock et al., 2009). Therefore, we used two different analytical platforms.

Figure 6A shows the analysis of miRNA population within the EVs using the NGS platform. The percentage of Rfam categories (Rfam refers to the collection of non-coding RNAs found in the sample) obtained from EVs of uRBCs and iRBCs are shown in Figure 6A. As evident, iRBCs (pink bars) had a higher content of tRNAs than uRBCs (black bars), and both had a miniscule percentage of snRNAs and snoRNAs. The small RNAs derived from the EVs were next analyzed to obtain the length distribution, and it was found that a majority of small RNAs were between 20 and 24 nucleotides, which is the size range for miRNAs (Figure 6B). The sequences obtained from the Illumina HiSeq were then mapped to miRbase 22.0. A total of 805 known miRNAs and 169 novel miRNAs, which have not previously been mapped in the database, were found in the analysis (Supplementary File 1). The criteria of secondary structures and annotations have been

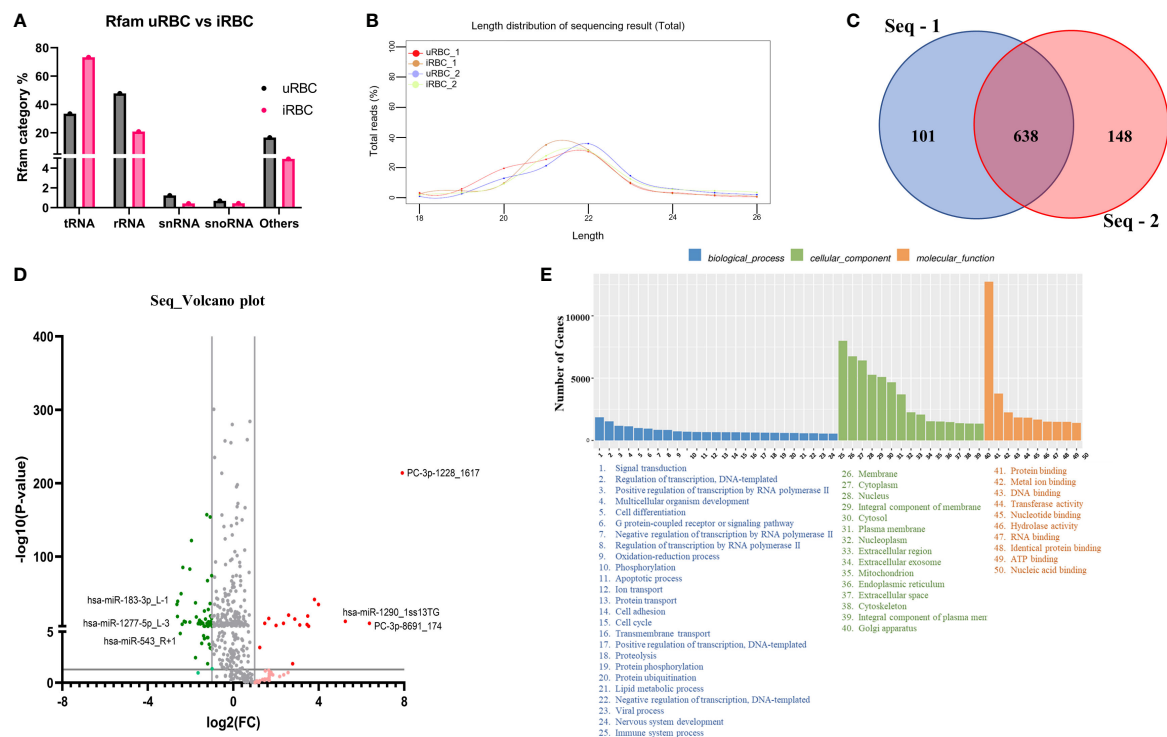


FIGURE 6

MicroRNA (miRNA) Illumina sequencing results in identification of differential miRNA expression in extracellular vesicles (EVs) from uninfected RBCs (uRBCs) and *B. divergens*-infected RBCs (iRBCs). (A) Percentage of different non-coding RNAs in EVs from uRBCs (black bars) and iRBCs (pink). "Others" refers to non-coding RNAs that did not match any known sequence in the Rfam 14.8 database. (B) Length distribution of small RNA used in the study was found to be between 20 and 24 nt. (C) Venn diagram depicting differences and similarities between the biological replicates used in the study shows significant overlap between the replicates. (D) Volcano plot showing differential expression of miRNAs. FC on x-axis refers to fold change in *B. divergens*-infected derived EVs compared with uRBCs and FC of more than/less than 2 were considered significant (shown by two vertical lines). Y-axis shows the statistical significance, and the cutoff chosen was $p < 0.005$, as shown by the black horizontal line. Gray dots were miRNAs that were non-significant in terms of p value and FC. Light red and light green dots represent miRNAs that were upregulated and downregulated, respectively, with an FC of more than/less than 2 but did not pass the p-value test. Dark red and dark green dots represent miRNAs with FC more than or less than 2, respectively, and significant p-values. The top three miRNAs in each set were identified. (E) Biological pathways (blue), cellular localization (green), and molecular function (orange) related to the miRNAs identified in the analysis and its related number of genes were plotted as bar graphs. As shown, several pathways are hypothesized to be altered by these miRNAs.

described in Supplementary File 1. The analysis was performed with two biological duplicates, and as shown in Figure 6C, they had 638 miRNAs in common among them. Next, we plotted the volcano plot in Figure 6D to visualize differentially expressed miRNAs in EVs derived from uRBCs and iRBCs. Gray dots represent the miRNAs that did not clear the statistical significance cutoff ($p < 0.05$) and/or had a fold change (FC) of expression in iRBCs/uRBCs < 2 . Light green and light red dots represent the miRNAs that have an FC of < 2 and > 2 , respectively, but do not pass the statistical significance test. Dark green and dark red dots are representative of miRNAs that have an iRBC/uRBC FC ≤ 2 or ≥ 2 and pass statistical significance test. The top 3 miRNA species from each set were marked. As shown in Figure 5D, the top three miRNAs identified in the analysis were novel miRNAs (labeled as PC) whose functions are yet unknown or have a 1-bp difference on the right (R) or left (L) from the annotated miRNA sequence. The gene ontology analysis of target genes identified several different pathways (Figure 6E) in which these miRNAs may be involved across different cellular locations. Thus, establishing miRNA signatures of both EVs from uRBCs and iRBCs and analyzing the differential expression between them can be used further to pin the functionality of these miRNAs

and their possible role in cell-to-cell communication and disease pathology.

We next turned to another classical miRNA detection and analysis platform to determine if it could be used to discriminate between the RNA cargo of EVs released from uRBCs and iRBCs. Toward this, RNA was isolated from uRBCs and *B. divergens*-infected culture-derived EVs using Norgen's Plasma/Serum RNA Purification Mini Kit (Cat. 55000) according to the manufacturer's instructions and sent for hybridization and identification of miRNAs in these samples.

A list of reporters used in the array is available in Supplementary File 2. As shown in Figure 7A, the miRNAs depicted in the heat map had statistically significant differences in expression levels in uRBC- versus iRBC-derived EVs using different p-value cutoffs. With a stringency of $p < 0.0001$, three miRNAs were observed to be differentially expressed between the two samples. In the heatmap, green depicts downregulation, whereas red depicts upregulation of miRNA expression. Of these, miR-4534 had been associated with cancer (Nip et al., 2016), whereas no data exist for the other two. To better visualize the different miRNA changes, we constructed the volcano plot

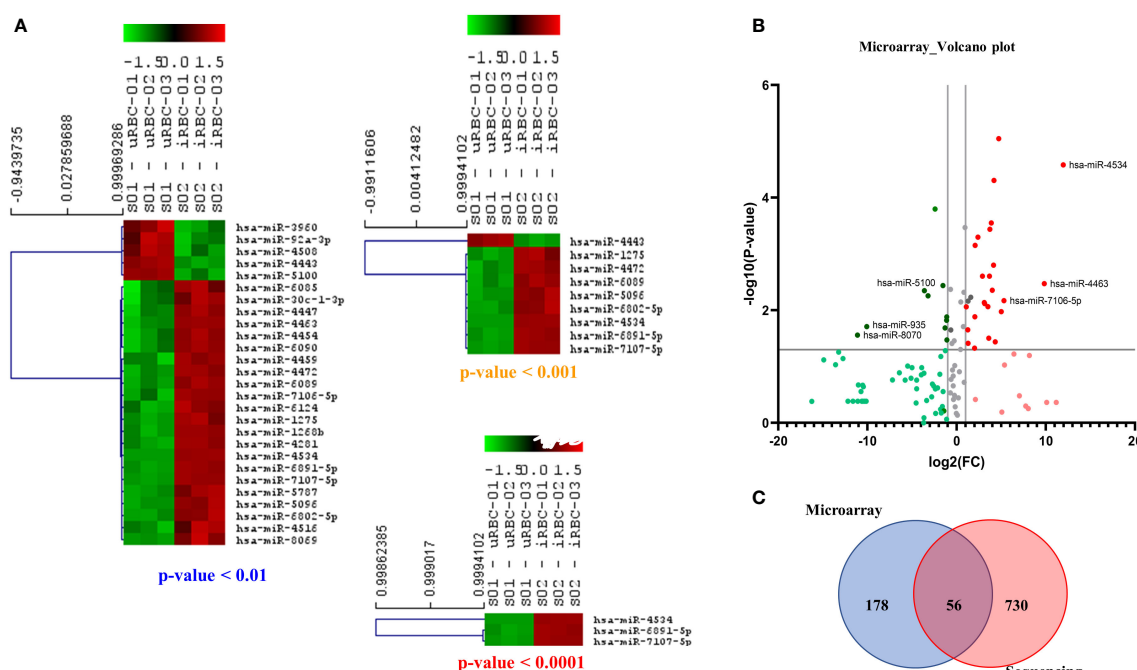


FIGURE 7

Microarray-based analysis of microRNAs (miRNAs) from extracellular vesicles (EVs) derived from uninfected RBCs (uRBCs) and *B. divergens*-infected RBCs (iRBCs). (A) Heat map shows the miRNAs that were changed at different p-value cutoffs (< 0.01 , < 0.001 , and < 0.0001) between EVs from uRBCs and iRBCs ($n = 3$). As shown, these miRNAs were differentially expressed between the two sample sets. (B) Volcano plot representing the fold change (FC) and p-value of miRNAs differentially expressed in EVs from iRBCs with respect to those from uRBCs. Interpretation of colors is identical to Figure 6D. The top three upregulated and downregulated miRNAs in the analysis have been identified. (C) Venn diagram showing the overlap between miRNAs detected by microarray versus sequencing using next-generation sequencing. Fifty-six miRNAs were detected in both the platforms, whereas 178 and 730 unique miRNAs were detected by the two platforms, respectively.

with FC of iRBC/uRBC derived in the x-axis and statistical significance of = in the y-axis ($p < 0.005$ as seen in Figure 7B). The colors used in the plot Figure 7B have identical interpretation as Figure 6D. As shown, miR-4534, miR-4463, and miR-7106-5p were the ones with maximal upregulation. Interestingly, miR-4463 is associated with apoptosis and oxidative stress in endothelial cells. Elevated oxidative stress in the host cells has been linked to intracellular parasite pathogens like *Mycobacterium tuberculosis* (Chawla et al., 2012) and *P. falciparum* (Beri et al., 2017; Beri et al., 2019), and our previous work had shown that *B. divergens*-infected red cells experience disturbed redox homeostasis (Beri et al., 2022). Thus, miRNAs may play a role in causing parasite-related oxidative stress and could be investigated in future transduction experiments. Both our platforms detected an upregulation of miR-4454, which has been associated with severe thrombocytopenia in *P. vivax*-infected human plasma. Data in our microarray platform showed a 3.5-fold increase in miR-4497 in iRBC-derived EVs. These have been associated with splenic sequestration in *P. falciparum*; however, their role in *Babesia* infection is yet unknown. Furthermore, miR-5787 was found to be 15-fold elevated in iRBC-derived EVs as compared with its uninfected counterpart. miR-5787 has been implicated in inhibition of eIF5 in fibroblasts, but their significance in *Babesia* infection is yet unknown. As seen in Figure 7C, our NGS and microarray analysis had a significant overlap with differential expression observed in 56 miRNAs across both platforms. The NGS platform clearly was able to detect more miRNAs than microarray, which is limited by the probes used in the analysis. Overall, significant differences in the levels of multiple miRNAs between EVs from uRBCs and iRBCs were detected, and a few of them have been implicated in pathogenesis of other diseases including malaria, tuberculosis, and cancer.

Discussion

EVs are generally categorized based on size and biogenesis, with exosomes ranging in size from 30 to 150 nm and MVs ranging from 150 nm to 1 μ m (Colombo et al., 2014). Although the majority of the vesicles identified in our study were smaller than 150 nm (Figures B, 2B), we have not purified the vesicle population based on size, and there is considerable overlay in both size and density between exosomes and MVs. Hence, because of the controversies and difficulties in defining and distinguishing between these two types of vesicles, we opted to use the more conservative term of EVs for the vesicles we have identified and characterized in this article.

In the last decade, EVs have been characterized in both unicellular and multicellular parasites, including apicomplexans, kinetoplastids, and parasitic worms, where they have been shown to mediate both host–parasite and parasite–parasite communication (Marti and Johnson, 2016). Our study is the first to document similar EV secretions from *Babesia* species,

using both *in vitro* cultures and *in vivo* infection models, although a previous report (Thekkiniath et al., 2019) has documented evidence for vesicular-mediated antigen export in *B. microti* (Thekkiniath et al., 2019). Use of both species is critical because the mammalian circulation offers a different and dynamic environment from culture conditions; thus, *in vivo* derived EVs may differ in composition and/or activity from the culture-derived EVs. Like other related parasites, *Babesia* exploits dual hosts, requiring the ability to sense environmental changes and rapidly respond to such changes in terms of both regulating parasite population numbers and modulating host response to the infection (Cursino-Santos et al., 2016). Therefore, like other pathogens, *Babesia* must develop effective strategies to survive in a variety of environments—both supportive and hostile. EV communication may represent one such strategy that *Babesia* exploits to ensure successful propagation (Lobo et al., 2019). We show that EVs are in fact taken up by both uninfected and infected cells in culture through labeling and uptake experiments. Thus, EVs may mediate communication among parasite-infected cell populations, as has been shown for malaria (Mantel et al., 2013). Such communication could help parasites to sense population density and allow shifts among the parasite populations to ensure persistence (Lobo et al., 2019). An interesting study from *P. falciparum* cultures provides similar evidence of the EV-associated PfLDH regulation of parasite population by inducing apoptosis in highly parasitized cultures (Correa et al., 2019).

The characteristics and composition of EV populations from hemoparasites are highly heterogeneous, differing in subcellular origin and their processing route, being either RBC membrane or parasite membrane derived. This is reflected in our data (Figures 1B, 2B) where we have identified such a heterogeneous population of EVs in both culture supernatants and infected mouse plasma in terms of both vesicular size and vesicular staining. NanoSight analysis demonstrated that the size of these vesicles for both *B. divergens* and *B. microti* iRBCs spanned from 30 to 300 nm, although most vesicles fell in the 60–100 nm range. Furthermore, this size range has also been reported for other parasites, including Plasmodium (Mantel et al., 2013). A further complication in studying *Babesia* EVs is that host RBCs also secrete EVs, and thus, it is important to discriminate between the contribution from host and parasite. Looking at uRBC and iRBC profiles, we show that *Babesia* infection heightens EV production both *in vitro* and *in vivo* (Figures 1A, 2A). The numbers of EVs have also been shown to increase during malaria infection both in patients and in experimental malaria models (Combes et al., 2004; Campos et al., 2010; Nantakomol et al., 2011; El-Assaad et al., 2014). Although a 10-fold increase has been reported for malaria infections, our data suggest a more modest elevation, approximating 4-fold in iRBCs over uRBCs (Figure 1C). However, both *Babesia* models argue for a direct correlation

between parasitemia and concentration of EVs, with increasing parasitemias yielding higher concentrations of EVs, which could then yield the 10-fold increase seen in malaria. In fact, the plasma of *B. microti*-infected mice exhibited back to baseline numbers of vesicles (Figure 2A) as infection is cleared, in agreement with data from patients treated with antimalarials to clear the parasite (Nantakomol et al., 2011). Thus, quantification of EV numbers can aid screening of infection. Qualitatively, we also show that EVs are heterogeneous, in that a third of them can be identified by surface parasite markers. We further purified the EVs by density gradient ultracentrifugation and verified their identity by flow cytometry using classical markers (CD9 and CD81). The observation that >75% of particles in our purification are EVs, as also reported by other researchers working on EVs (Mellisho et al., 2017), confirms that our methodology of purification is efficient in enriching for EVs (Supplementary Figure 1). TEM confirmed this size property of the purified EVs. For EVs originating from *B. divergens* iRBCs, we show that Bd37 is present on a population of EVs whereas BMN-2 is present on a proportion of EVs purified from *in vivo* *B. microti*-infected plasma (Figure 5). Overall, our results argue for an augmentation of EV secretion with infection, and besides host proteins, parasite proteins are also present in and on these vesicles.

Although we have not fully characterized the parasite EV proteome, our immunoblot analysis of the contents from EVs from *B. microti*-infected plasma with immune sera from mice and humans showed that several EV parasite proteins were targets of the host humoral response (Figure 4). Such proteins can serve as the basis of both diagnostic and vaccine platforms. Previous efforts to identify proteins secreted by *B. microti* iRBCs focused on the screening of a *B. microti* cDNA library using sera from infected mice. These efforts resulted in the identification of only a limited number of small molecular weight proteins, the main contenders being members of the BMN family (Homer et al., 2000). Peptides from this family were used as the basis of an ELISA for *B. microti* as a screening test applied to endemic and non-endemic blood donor populations (Levin et al., 2014; Levin et al., 2016), with mixed results for sensitivity and specificity. Recent effort has been devoted to identifying the parasites in glycosylphosphatidylinositol-anchored proteome, and 19 proteins have been characterized as potential molecules that can be used to detect antibody response (Cornillot et al., 2016). The advantage of using EV-associated biomarkers is that these are extremely stable within the circulation, in the order of days (vs. minutes for traditional soluble markers), and that EVs are found in all biological fluids, making diagnosis less intrusive (Properzi et al., 2013).

Small RNA cargo is specifically enriched for a subset of the cell's total small RNA pool (Nolte-T Hoen et al., 2012). miRNAs are often associated with life cycle regulation, susceptibility to infection of host cells, and modulation of host innate immune responses (Buck et al., 2014; Retana Moreira et al., 2019). Thus,

these non-coding RNA molecules are heavily involved in post-transcriptional gene regulation in most biological and pathological processes (Kim et al., 2015). We used a combination of microarray and NGS platforms to arrive at the different miRNA signatures obtained for EVs from uninfected and infected cultures (Figures 6 and 7). Both methods have their specific advantages and disadvantages (Willenbrock et al., 2009). Microarrays have been used extensively for the simultaneous profiling of thousands of genes in a single experiment. Along with quantitative real-time PCR, they are the most used platform to evaluate the expression of known miRNAs. They are relatively cost-effective, quick from RNA labeling to data generation, and simple to use. However, the short length of these molecules does not always allow for optimal probe design, as the miRNA sequences themselves must be used as the probe sequences. Based on these criteria, we also used the NGS platform in tandem to ensure a robust and more comprehensive expression profiling of miRNAs (Tam et al., 2014; Chatterjee et al., 2015). We first obtained miRNA profiles using microarrays because they can simultaneously profile thousands of sequences in a single experiment. However, only known miRNA species will be characterized. Sequencing allows the identification of novel miRNA species, and in fact, almost 200 novel miRNA species that had not been previously mapped to EVs were identified. More importantly, we found significant differences in both presence and concentration of specific miRNAs between EV contents from uRBCs and iRBCs. There were three highly upregulated miRNAs: miR-4534, miR-4463, and miR-7106-5p. Of these, the most significant difference was found to be with miR-4463, which was found to be present 20-fold times in uRBCs. Interestingly, miR-4463 is associated with apoptosis and oxidative stress in endothelial cells (Wang et al., 2017; He et al., 2018). Elevated oxidative stress in the host cells has been linked to intracellular parasite pathogens like *M. tuberculosis* and *P. falciparum* (Chawla et al., 2012; Beri et al., 2017; Beri et al., 2019), and our previous work had shown that *B. divergens*-infected red cells experience disturbed redox homeostasis. Thus, miRNAs may play a role in parasite-related oxidative stress, and future work will be directed toward understanding its role in potentially protecting the cell. Both our platforms detected an upregulation of miR-4454, which has been associated with severe thrombocytopenia in *P. vivax*-infected human plasma (Santos et al., 2021). Like malaria, babesiosis is also associated with a steep drop in platelets (Akel and Mobarakai, 2017; Ripoll et al., 2018). Furthermore, in our microarray platform, we also found an almost 3.5-fold increase in miR-4497 in iRBC-derived EVs. This miRNA has been associated with splenic sequestration in *P. falciparum* (Gupta et al., 2021; Gupta and Wassmer, 2021), but their role in Babesia infection is yet to be characterized. Overall, significant differences were found in the miRNA cargo of the EVs from uRBCs and iRBCs, and future experiments will help dissect out the role each of these play in the pathogenesis of disease.

Furthermore, such differentially expressed EV-resident RNAs can serve as biomarkers, as these RNAs can be detected at extremely low quantities (Kim et al., 2017).

EV secretion by parasites has been linked to multiple functions including intercellular communication between host and parasite and between parasites (Coakley et al., 2015; Wu et al., 2018; Babatunde et al., 2020; Olajide and Cai, 2020; Torrecilhas et al., 2020; Opadokun and Rohrbach, 2021) as well as modulation of the host immune response (Sisquella et al., 2017; Kuipers et al., 2018; Dantas-Pereira et al., 2021; Druerey and Maizels, 2021). For EVs to serve as vehicles of communication between various types of cells, EVs need to be taken up by other cells. Using CFSE-labeled EVs and ImageStream analysis, we showed that EVs are taken up by both uRBCs and iRBCs, albeit at a slightly higher percentage in the latter (Figures 3A–E). As the time of co-incubation increases, the percentage of cells that take up EVs also increases. Therefore, circulating EVs in a culture system can be internalized by uRBCs and iRBCs, possibly leading to the transfer of biomolecules, which are known to be contained within EVs. Furthermore, we also showed that 90% of the monocytes, when co-incubated with purified *B. divergens* EVs, internalize these EVs (Figure 3F). As elaborated above, in other parasite systems, EVs are known to aid in immune evasion and manipulation of the microenvironment by the parasite, and future work is needed to examine this cellular crosstalk in Babesia.

Overall, our work provides important data for understanding the biological components of Babesia EVs and lays the foundation to future studies directed toward analyzing the consequences of EV cargo in determining the outcome of parasite infection.

Data availability statement

The data presented in the study are deposited in NCBI repository with BioProject ID PRJNA874078 titled “miRNA analysis of EVs from Babesia divergens culture supernatant”.

Ethics statement

The studies involving human participants were reviewed and approved by NYBC IRB. The patients/participants provided their written informed consent to participate in this study. All animal studies were approved by the New York Blood Center’s Animal Care and Use Committee.

References

Akel, T., and Mobarakai, N. (2017). Hematologic manifestations of babesiosis. *Ann. Clin. Microbiol. Antimicrob.* 16, 6. doi: 10.1186/s12941-017-0179-z

Author contributions

DB, MR, YL, KY, and CL conceived the experiments. DB, MS, MR, and GR purified the EVs from culture and plasma and performed uptake experiments. DB, YL, and MR performed the IFC experiments. DB, MR, XA, KY, and CL analyzed the results. DB, KY, and CL wrote the manuscript. All authors contributed to the article and approved the submitted version.

Funding

This research was funded by National Institutes of Health Grants P01 HL149626 (KY and CL) and R01HL140625 (CL) and a grant from BNY Mellon (KY and CL).

Acknowledgments

The authors acknowledge help from the Flow Cytometry Lab (RRID: SCR_021779) at Lindsley F. Kimball Research Institute, New York Blood Center.

Conflict of interest

The authors declare that the research was conducted in the absence of any commercial or financial relationships that could be construed as a potential conflict of interest.

Publisher’s note

All claims expressed in this article are solely those of the authors and do not necessarily represent those of their affiliated organizations, or those of the publisher, the editors and the reviewers. Any product that may be evaluated in this article, or claim that may be made by its manufacturer, is not guaranteed or endorsed by the publisher.

Supplementary material

The Supplementary Material for this article can be found online at: <https://www.frontiersin.org/articles/10.3389/fcimb.2022.962944/full#supplementary-material>

Andreu, Z., and Yanez-Mo, M. (2014). Tetraspanins in extracellular vesicle formation and function. *Front. Immunol.* 5, 442. doi: 10.3389/fimmu.2014.00442

- Babatunde, K. A., Mbagwu, S., Hernandez-Castaneda, M. A., Adapa, S. R., Walch, M., Filgueira, L., et al. (2018). Malaria infected red blood cells release small regulatory RNAs through extracellular vesicles. *Sci. Rep.* 8, 884. doi: 10.1038/s41598-018-19149-9
- Babatunde, K. A., Yesodha Subramanian, B., Ahouidi, A. D., Martinez Murillo, P., Walch, M., and Mantel, P. Y. (2020). Role of extracellular vesicles in cellular cross talk in malaria. *Front. Immunol.* 11, 22. doi: 10.3389/fimmu.2020.00022
- Beri, D., Balan, B., Chaubey, S., Subramaniam, S., Surendra, B., and Tatu, U. (2017). A disrupted transsulphuration pathway results in accumulation of redox metabolites and induction of gametocytogenesis in malaria. *Sci. Rep.* 7, 40213. doi: 10.1038/srep40213
- Beri, D., Ramdani, G., Balan, B., Gadara, D., Poojary, M., Momeux, L., et al. (2019). Insights into physiological roles of unique metabolites released from plasmodium-infected RBCs and their potential as clinical biomarkers for malaria. *Sci. Rep.* 9, 2875. doi: 10.1038/s41598-018-37816-9
- Beri, D., Singh, M., Rodriguez, M. A., Barbu-Stevanovic, M., Rasquinha, G., Mendelson, A., et al. (2022). Elucidating parasite and host cell factors enabling babesia infection in sickle red cells under Hypoxic/Hyperoxic conditions. *Blood Adv.* doi: 10.1182/bloodadvances.2022008159
- Beri, D., Singh, M., Rodriguez, M., Yazdanbakhsh, K., and Lobo, C. A. (2021). Sickle cell anemia and babesia infection. *Pathogens* 10, 1435–1445. doi: 10.3390/pathogens10111435
- Buck, A. H., Coakley, G., Simbari, F., Mccorley, H. J., Quintana, J. F., Le Bihan, T., et al. (2014). Exosomes secreted by nematode parasites transfer small RNAs to mammalian cells and modulate innate immunity. *Nat. Commun.* 5, 5488. doi: 10.1038/ncomms6488
- Campos, F. M., Franklin, B. S., Teixeira-Carvalho, A., Filho, A. L., De Paula, S. C., Fontes, C. J., et al. (2010). Augmented plasma microparticles during acute plasmodium vivax infection. *Malar. J.* 9, 327. doi: 10.1186/1475-2875-9-327
- Chatterjee, A., Leichter, A. L., Fan, V., Tsai, P., Purcell, R. V., Sullivan, M. J., et al. (2015). A cross comparison of technologies for the detection of microRNAs in clinical FFPE samples of hepatoblastoma patients. *Sci. Rep.* 5, 10438. doi: 10.1038/srep10438
- Chawla, M., Parikh, P., Saxena, A., Munshi, M., Mehta, M., Mai, D., et al. (2012). Mycobacterium tuberculosis WhiB4 regulates oxidative stress response to modulate survival and dissemination in vivo. *Mol. Microbiol.* 85, 1148–1165. doi: 10.1111/j.1365-2958.2012.08165.x
- Cipriano, M. J., and Hajduk, S. L. (2018). Drivers of persistent infection: pathogen-induced extracellular vesicles. *Essays Biochem.* 62, 135–147. doi: 10.1042/EBC20170083
- Coakley, G., Maizels, R. M., and Buck, A. H. (2015). Exosomes and other extracellular vesicles: The new communicators in parasite infections. *Trends Parasitol.* 31, 477–489. doi: 10.1016/j.pt.2015.06.009
- Colombo, M., Raposo, G., and Thery, C. (2014). Biogenesis, secretion, and intercellular interactions of exosomes and other extracellular vesicles. *Annu. Rev. Cell Dev. Biol.* 30, 255–289. doi: 10.1146/annurev-cellbio-101512-122326
- Combes, V., Taylor, T. E., Juhan-Vague, I., Mege, J. L., Mwenechanya, J., Tembo, M., et al. (2004). Circulating endothelial microparticles in malawian children with severe falciparum malaria complicated with coma. *JAMA* 291, 2542–2544. doi: 10.1001/jama.291.21.2542-b
- Cornillot, E., Dassouli, A., Pachikara, N., Lawres, L., Renard, I., Francois, C., et al. (2016). A targeted immunomic approach identifies diagnostic antigens in the human pathogen babesia microti. *Transfusion* 56, 2085–2099. doi: 10.1111/trf.13640
- Correa, R., Coronado, L., Caballero, Z., Faral-Tello, P., Robello, C., and Spadafora, C. (2019). Extracellular vesicles carrying lactate dehydrogenase induce suicide in increased population density of plasmodium falciparum in vitro. *Sci. Rep.* 9, 5042. doi: 10.1038/s41598-019-41697-x
- Correa, R., Coronado, L., Caballero, Z., Faral-Tello, P., Robello, C., and Spadafora, C. (2020). Author correction: Extracellular vesicles carrying lactate dehydrogenase induce suicide in increased population density of plasmodium falciparum in vitro. *Sci. Rep.* 10, 12717. doi: 10.1038/s41598-020-69582-y
- Cursino-Santos, J. R., Singh, M., Pham, P., and Lobo, C. A. (2017). A novel flow cytometric application discriminates among the effects of chemical inhibitors on various phases of babesia divergens intraerythrocytic cycle. *Cytometry A* 91, 216–231. doi: 10.1002/cyto.a.23062
- Cursino-Santos, J. R., Singh, M., Pham, P., Rodriguez, M., and Lobo, C. A. (2016). Babesia divergens builds a complex population structure composed of specific ratios of infected cells to ensure a prompt response to changing environmental conditions. *Cell Microbiol.* 18, 859–874. doi: 10.1111/cmi.12555
- Cursino-Santos, J. R., Singh, M., Senaldi, E., Manwani, D., Yazdanbakhsh, K., and Lobo, C. A. (2019). Altered parasite life-cycle processes characterize babesia divergens infection in human sickle cell anemia. *Haematologica* 104, 2189–2199. doi: 10.3324/haematol.2018.214304
- Dantas-Pereira, L., Menna-Barreto, R., and Lannes-Vieira, J. (2021). Extracellular vesicles: Potential role in remote signaling and inflammation in trypanosoma cruzi-triggered disease. *Front. Cell Dev. Biol.* 9, 798054. doi: 10.3389/fcell.2021.798054
- Delbecq, S. (2022). Major surface antigens in zoonotic babesia. *Pathogens* 11, 99–113. doi: 10.3390/pathogens11010099
- Drurey, C., and Maizels, R. M. (2021). Helminth extracellular vesicles: Interactions with the host immune system. *Mol. Immunol.* 137, 124–133. doi: 10.1016/j.molimm.2021.06.017
- El-Asaad, F., Whewy, J., Hunt, N. H., Grau, G. E., and Combes, V. (2014). Production, fate and pathogenicity of plasma microparticles in murine cerebral malaria. *PLoS Pathog.* 10, e1003839. doi: 10.1371/journal.ppat.1003839
- Elton, C. M., Rodriguez, M., Ben Mamoun, C., Lobo, C. A., and Wright, G. J. (2019). A library of recombinant babesia microti cell surface and secreted proteins for diagnostics discovery and reverse vaccinology. *Int. J. Parasitol.* 49, 115–125. doi: 10.1016/j.ijpara.2018.10.003
- Gill, S., Catchpole, R., and Forterre, P. (2019). Extracellular membrane vesicles in the three domains of life and beyond. *FEMS Microbiol. Rev.* 43, 273–303. doi: 10.1093/femsre/fuy042
- Gupta, H., Rubio, M., Siteo, A., Varo, R., Cistero, P., Madrid, L., et al. (2021). Plasma MicroRNA profiling of plasmodium falciparum biomass and association with severity of malaria disease. *Emerg. Infect. Dis.* 27, 430–442. doi: 10.3201/eid2702.191795
- Gupta, H., and Wassmer, S. C. (2021). Harnessing the potential of miRNAs in malaria diagnostic and prevention. *Front. Cell Infect. Microbiol.* 11, 793954. doi: 10.3389/fcimb.2021.793954
- He, X., Du, C., Zou, Y., Long, Y., Huang, C., Chen, F., et al. (2018). Downregulation of MicroRNA-4463 attenuates high-glucose- and hypoxia-induced endothelial cell injury by targeting PNUMS. *Cell Physiol. Biochem.* 49, 2073–2087. doi: 10.1159/000493717
- Homer, M. J., Bruinsma, E. S., Lodes, M. J., Moro, M. H., Telford, S.3rd, Krause, P. J., et al. (2000). A polymorphic multigene family encoding an immunodominant protein from babesia microti. *J. Clin. Microbiol.* 38, 362–368. doi: 10.1128/JCM.38.1.362-368.2000
- Hu, J., Liu, J., Xue, F., Halverson, G., Reid, M., Guo, A., et al. (2013). Isolation and functional characterization of human erythroblasts at distinct stages: implications for understanding of normal and disordered erythropoiesis in vivo. *Blood* 121, 3246–3253. doi: 10.1182/blood-2013-01-476390
- Kim, K. M., Abdelmohsen, K., Mustapic, M., Kapogiannis, D., and Gorospe, M. (2017). RNA in extracellular vesicles. *Wiley Interdiscip. Rev. RNA* 8 (4). doi: 10.1002/wrna.1413
- Kim, D. K., Lee, J., Kim, S. R., Choi, D. S., Yoon, Y. J., Kim, J. H., et al. (2015). EVpedia: a community web portal for extracellular vesicles research. *Bioinformatics* 31, 933–939. doi: 10.1093/bioinformatics/btu741
- Kuipers, M. E., Hokke, C. H., Smits, H. H., and Nolte-T Hoen, E. N. M. (2018). Pathogen-derived extracellular vesicle-associated molecules that affect the host immune system: An overview. *Front. Microbiol.* 9, 2182. doi: 10.3389/fmicb.2018.02182
- Lawres, L. A., Garg, A., Kumar, V., Bruzual, I., Forquer, I. P., Renard, I., et al. (2016). Radical cure of experimental babesiosis in immunodeficient mice using a combination of an endochin-like quinolone and atovaquone. *J. Exp. Med.* 213, 1307–1318. doi: 10.1084/jem.20151519
- Levin, A. E., Williamson, P. C., Bloch, E. M., Clifford, J., Cyrus, S., Shaz, B. H., et al. (2016). Serologic screening of united states blood donors for babesia microti using an investigational enzyme immunoassay. *Transfusion* 56, 1866–1874. doi: 10.1111/trf.13618
- Levin, A. E., Williamson, P. C., Erwin, J. L., Cyrus, S., Bloch, E. M., Shaz, B. H., et al. (2014). Determination of babesia microti seroprevalence in blood donor populations using an investigational enzyme immunoassay. *Transfusion* 54, 2237–2244. doi: 10.1111/trf.12763
- Liu, Y., Zhong, H., Bao, W., Mendelson, A., An, X., Shi, P., et al. (2019). Patrolling monocytes scavenge endothelial-adherent sickle RBCs: a novel mechanism of inhibition of vaso-occlusion in SCD. *Blood* 134, 579–590. doi: 10.1182/blood.2019000172
- Lobo, C. A., Cursino-Santos, J. R., Alhassan, A., and Rodriguez, M. (2013). Babesia: an emerging infectious threat in transfusion medicine. *PLoS Pathog.* 9, e1003387. doi: 10.1371/journal.ppat.1003387
- Lobo, C. A., Cursino-Santos, J. R., Singh, M., and Rodriguez, M. (2019). Babesia divergens: A drive to survive. *Pathogens* 8, 95–102. doi: 10.3390/pathogens8030095
- Lobo, C. A., Singh, M., and Rodriguez, M. (2020). Human babesiosis: recent advances and future challenges. *Curr. Opin. Hematol.* 27, 399–405. doi: 10.1097/MOH.0000000000000606
- Mantel, P. Y., Hoang, A. N., Goldowitz, I., Potashnikova, D., Hamza, B., Vorobjev, I., et al. (2013). Malaria-infected erythrocyte-derived microvesicles

mediate cellular communication within the parasite population and with the host immune system. *Cell Host Microbe* 13, 521–534. doi: 10.1016/j.chom.2013.04.009

Mantel, P. Y., and Marti, M. (2014). The role of extracellular vesicles in plasmodium and other protozoan parasites. *Cell Microbiol.* 16, 344–354. doi: 10.1111/cmi.12259

Marti, M., and Johnson, P. J. (2016). Emerging roles for extracellular vesicles in parasitic infections. *Curr. Opin. Microbiol.* 32, 66–70. doi: 10.1016/j.mib.2016.04.008

Martins, S. T., and Alves, L. R. (2020). Extracellular vesicles in viral infections: Two sides of the same coin? *Front. Cell Infect. Microbiol.* 10, 593170. doi: 10.3389/fcimb.2020.593170

Mellisho, E. A., Velasquez, A. E., Nunez, M. J., Cabezas, J. G., Cueto, J. A., Fader, C., et al. (2017). Identification and characteristics of extracellular vesicles from bovine blastocysts produced *in vitro*. *PLoS One* 12, e0178306. doi: 10.1371/journal.pone.0178306

Moyano, S., Musso, J., Feliziani, C., Zamponi, N., Frontera, L. S., Ropolo, A. S., et al. (2019). Exosome biogenesis in the Protozoa parasite giardia lamblia: A model of reduced interorganellar crosstalk. *Cells* 8, 1600–1617. doi: 10.3390/cells8121600

Nantakomol, D., Dondorp, A. M., Krudsood, S., Udomsangpet, R., Pattanapanyasat, K., Combes, V., et al. (2011). Circulating red cell-derived microparticles in human malaria. *J. Infect. Dis.* 203, 700–706. doi: 10.1093/infdis/jiq104

Nip, H., Dar, A. A., Saini, S., Colden, M., Varahram, S., Chowdhary, H., et al. (2016). Oncogenic microRNA-4534 regulates PTEN pathway in prostate cancer. *Oncotarget* 7, 68371–68384. doi: 10.18632/oncotarget.12031

Nolte-T Hoen, E. N., Buermans, H. P., Waasdorp, M., Stoorvogel, W., Wauben, M. H., and T Hoen, P. A. (2012). Deep sequencing of RNA from immune cell-derived vesicles uncovers the selective incorporation of small non-coding RNA biotypes with potential regulatory functions. *Nucleic Acids Res.* 40, 9272–9285. doi: 10.1093/nar/gks658

Olajide, J. S., and Cai, J. (2020). Perils and promises of pathogenic protozoan extracellular vesicles. *Front. Cell Infect. Microbiol.* 10, 371. doi: 10.3389/fcimb.2020.00371

Opadokun, T., and Rohrbach, P. (2021). Extracellular vesicles in malaria: an agglomeration of two decades of research. *Malar J.* 20, 442. doi: 10.1186/s12936-021-03969-8

Ord, R. L., and Lobo, C. A. (2015). Human babesiosis: Pathogens, prevalence, diagnosis and treatment. *Curr. Clin. Microbiol. Rep.* 2, 173–181. doi: 10.1007/s40588-015-0025-z

Phanse, Y., Ramer-Tait, A. E., Friend, S. L., Carrillo-Conde, B., Lueth, P., Oster, C. J., et al. (2012). Analyzing cellular internalization of nanoparticles and bacteria by multi-spectral imaging flow cytometry. *J. Vis. Exp.* (64), e3884. doi: 10.3791/3884

Properzi, F., Logozzi, M., and Fais, S. (2013). Exosomes: the future of biomarkers in medicine. *Biomark. Med.* 7, 769–778. doi: 10.2217/bmm.13.63

Retana Moreira, L., Rodriguez Serrano, F., and Osuna, A. (2019). Extracellular vesicles of trypanosoma cruzi tissue-culture cell-derived trypomastigotes: Induction of physiological changes in non-parasitized culture cells. *PLoS Negl. Trop. Dis.* 13, e0007163. doi: 10.1371/journal.pntd.0007163

Ripoll, J. G., Rizvi, M. S., King, R. L., and Daniels, C. E. (2018). Severe babesia microti infection presenting as multiorgan failure in an immunocompetent host. *BMJ Case Rep.* 2018, 2018–2023. doi: 10.1136/bcr-2018-224647

Saari, H., Lazaro-Ibanez, E., Viitala, T., Vuorimaa-Laukkanen, E., Siljander, P., and Yliperttula, M. (2015). Microvesicle- and exosome-mediated drug delivery enhances the cytotoxicity of paclitaxel in autologous prostate cancer cells. *J. Control Release* 220, 727–737. doi: 10.1016/j.jconrel.2015.09.031

Santos, M. L. S., Coimbra, R. S., Sousa, T. N., Guimaraes, L. F. F., Gomes, M. S., Amaral, L. R., et al. (2021). The interface between inflammatory mediators and MicroRNAs in plasmodium vivax severe thrombocytopenia. *Front. Cell Infect. Microbiol.* 11, 631333. doi: 10.3389/fcimb.2021.631333

Schmidt, M., Geilenkeuser, W. J., Sireis, W., Seifried, E., and Hourfar, K. (2014). Emerging pathogens - how safe is blood? *Transfus. Med. Hemother.* 41, 10–17. doi: 10.1159/000358017

Schorey, J. S., Cheng, Y., Singh, P. P., and Smith, V. L. (2015). Exosomes and other extracellular vesicles in host-pathogen interactions. *EMBO Rep.* 16, 24–43. doi: 10.15252/embr.201439363

Sharma, M., Morgado, P., Zhang, H., Ehrenkauf, G., Manna, D., and Singh, U. (2020). Characterization of extracellular vesicles from entamoeba histolytica identifies roles in intercellular communication that regulates parasite growth and development. *Infect. Immun.* 88, 349–369. doi: 10.1128/IAI.00349-20

Shifrin, D. A., Demory Beckler, J. M., Coffey, R. J., and Tyska, M. J. (2013). Extracellular vesicles: communication, coercion, and conditioning. *Mol. Biol. Cell* 24, 1253–1259. doi: 10.1091/mbc.12-08-0572

Sisquella, X., Ofir-Birin, Y., Pimentel, M. A., Cheng, L., Abou Karam, P., Sampaio, N. G., et al. (2017). Malaria parasite DNA-harboring vesicles activate cytosolic immune sensors. *Nat. Commun.* 8, 1985. doi: 10.1038/s41467-017-02083-1

Szemprich, A. J., Sykes, S. E., Kieft, R., Dennison, L., Becker, A. C., Gartrell, A., et al. (2016). Extracellular vesicles from trypanosoma brucei mediate virulence factor transfer and cause host anemia. *Cell* 164, 246–257. doi: 10.1016/j.cell.2015.11.051

Tam, S., De Borja, R., Tsao, M. S., and McPherson, J. D. (2014). Robust global microRNA expression profiling using next-generation sequencing technologies. *Lab. Invest.* 94, 350–358. doi: 10.1038/labinvest.2013.157

Thekkiniath, J., Kilian, N., Lawres, L., Gewirtz, M. A., Graham, M. M., Liu, X., et al. (2019). Evidence for vesicle-mediated antigen export by the human pathogen babesia microti. *Life Sci. Alliance* 2, 382–392. doi: 10.26508/lsa.201900382

Torreilhas, A. C., Soares, R. P., Schenkman, S., Fernandez-Prada, C., and Olivier, M. (2020). Extracellular vesicles in trypanosomatids: Host cell communication. *Front. Cell Infect. Microbiol.* 10, 602502. doi: 10.3389/fcimb.2020.602502

Vannier, E. G., Diuk-Wasser, M. A., Ben Mamoun, C., and Krause, P. J. (2015). Babesiosis. *Infect. Dis. Clin. North Am.* 29, 357–370. doi: 10.1016/j.idc.2015.02.008

Wang, X., He, X., Deng, X., He, Y., and Zhou, X. (2017). Roles of miR4463 in H2O2-induced oxidative stress in human umbilical vein endothelial cells. *Mol. Med. Rep.* 16, 3242–3252. doi: 10.3892/mmr.2017.7001

Willenbrock, H., Salomon, J., Sokilde, R., Barken, K. B., Hansen, T. N., Nielsen, F. C., et al. (2009). Quantitative miRNA expression analysis: comparing microarrays with next-generation sequencing. *RNA* 15, 2028–2034. doi: 10.1261/rna.1699809

Wolf, P. (1967). The nature and significance of platelet products in human plasma. *Br. J. Haematol* 13, 269–288. doi: 10.1111/j.1365-2141.1967.tb08741.x

Wu, Z., Wang, L., Li, J., Wang, L., Wu, Z., and Sun, X. (2018). Extracellular vesicle-mediated communication within host-parasite interactions. *Front. Immunol.* 9, 3066. doi: 10.3389/fimmu.2018.03066

Xie, S., Zhang, Q., and Jiang, L. (2022). Current knowledge on exosome biogenesis, cargo-sorting mechanism and therapeutic implications. *Membranes (Basel)* 12, 498–526. doi: 10.3390/membranes12050498

Yanez-Mo, M., Siljander, P. R., Andreu, Z., Zavec, A. B., Borrás, F. E., Buzas, E. I., et al. (2015). Biological properties of extracellular vesicles and their physiological functions. *J. Extracell. Vesicles* 4, 27066. doi: 10.3402/jev.v4.27066



OPEN ACCESS

EDITED BY

Maria Carolina Touz,
Medical Research Institute Mercedes
and Martín Ferreyra (INIMEC),
Argentina

REVIEWED BY

Galia Andrea Ramirez-Tolosa,
University of Chile, Chile
Wanderley De Souza,
Federal University of Rio de Janeiro,
Brazil
Raquel Bello-Morales,
Autonomous University of Madrid,
Spain

*CORRESPONDENCE

Carolina Verónica Poncini
cvponcini@gmail.com

SPECIALTY SECTION

This article was submitted to
Parasite and Host,
a section of the journal
Frontiers in Cellular and
Infection Microbiology

RECEIVED 28 June 2022

ACCEPTED 20 October 2022

PUBLISHED 16 November 2022

CITATION

Gutierrez BC, Ancarola ME,
Volpato-Rossi I, Marcilla A,
Ramirez MI, Rosenzvit MC, Cucher M
and Poncini CV (2022) Extracellular
vesicles from *Trypanosoma cruzi*-
dendritic cell interaction show
modulatory properties and confer
resistance to lethal infection as a cell-
free based therapy strategy.
Front. Cell. Infect. Microbiol. 12:980817.
doi: 10.3389/fcimb.2022.980817

COPYRIGHT

© 2022 Gutierrez, Ancarola, Volpato-
Rossi, Marcilla, Ramirez, Rosenzvit,
Cucher and Poncini. This is an open-
access article distributed under the
terms of the [Creative Commons
Attribution License \(CC BY\)](#). The use,
distribution or reproduction in other
forums is permitted, provided the
original author(s) and the copyright
owner(s) are credited and that the
original publication in this journal is
cited, in accordance with accepted
academic practice. No use,
distribution or reproduction is
permitted which does not comply with
these terms.

Extracellular vesicles from *Trypanosoma cruzi*-dendritic cell interaction show modulatory properties and confer resistance to lethal infection as a cell-free based therapy strategy

Brenda Celeste Gutierrez¹, Maria Eugenia Ancarola¹,
Izadora Volpato-Rossi^{2,3}, Antonio Marcilla⁴,
Marcel Ivan Ramirez^{2,3}, Mara Cecilia Rosenzvit¹,
Marcela Cucher¹ and Carolina Verónica Poncini^{1,5*}

¹Instituto de Investigaciones en Microbiología y Parasitología Médicas (IMPAM), Consejo Nacional de Investigaciones Científicas y Técnicas (CONICET), Buenos Aires, Argentina, ²Programa de Pós-graduação em Biologia Celular e Molecular, Universidade Federal do Paraná, Curitiba, Paraná, Brazil, ³Instituto Carlos Chagas - Fiocruz Paraná, Curitiba, Paraná, Brazil, ⁴Departamento de Farmacia y Tecnología Farmacéutica y Parasitología, Universitat de Valencia, Valencia, Spain, ⁵Departamento de Microbiología, Facultad de Medicina, Universidad de Buenos Aires (UBA), Buenos Aires, Argentina

Extracellular vesicles (EVs) include a heterogeneous group of particles. Microvesicles, apoptotic bodies and exosomes are the most characterized vesicles. They can be distinguished by their size, morphology, origin and molecular composition. To date, increasing studies demonstrate that EVs mediate intercellular communication. EVs reach considerable interest in the scientific community due to their role in diverse processes including antigen-presentation, stimulation of anti-tumoral immune responses, tolerogenic or inflammatory effects. In pathogens, EV shedding is well described in fungi, bacteria, protozoan and helminths parasites. For *Trypanosoma cruzi* EV liberation and protein composition was previously described. Dendritic cells (DCs), among other cells, are key players promoting the immune response against pathogens and also maintaining self-tolerance. In previous reports we have demonstrate that *T. cruzi* downregulates DCs immunogenicity *in vitro* and *in vivo*. Here we analyze EVs from the *in vitro* interaction between blood circulating trypomastigotes (Tp) and bone-marrow-derived DCs. We found that Tp incremented the number and the size of EVs in cultures with DCs. EVs displayed some exosome markers and intracellular RNA. Protein analysis demonstrated that the parasite changes the DC protein-EV profile. We observed that EVs from the interaction of Tp-DCs were easily captured by unstimulated-DCs in comparison with EVs from DCs cultured without the parasite, and also modified the activation status of LPS-stimulated DCs.

Noteworthy, we found protection in animals treated with EVs-DCs+Tp and challenged with *T. cruzi* lethal infection. Our goal is to go deep into the molecular characterization of EVs from the DCs-Tp interaction, in order to identify mediators for therapeutic purposes.

KEYWORDS

T. cruzi, dendritic cells, extracellular vesicles (EVs), cell free therapy, immunotherapy, dendritic cells (DCs)

Introduction

Extracellular vesicles (EVs) are a heterogeneous group of particles that includes among others three major groups according to their subcellular origin and size: apoptotic bodies, exosomes and microvesicles (Gurunathan et al., 2019; Bazzan et al., 2021). To date, increasing studies confirm that EVs mediate intercellular communication (Colombo et al., 2014). They are detected in most body fluids such as nasal secretion, feces, urine, blood and breast milk (Keller et al., 2006; Yáñez-Mó et al., 2015). Circulating EVs are high in patients with acute or chronic inflammation, preeclampsia, atherosclerosis, diabetes mellitus or cancer among other pathogenic conditions (Yamamoto et al., 2016). An important breakthrough was the discovery of nucleic acids in EVs such as mRNA and miRNA. RNA molecules cargo in EVs can be a selective process and several studies have shown that EV-associated mRNAs and miRNAs can be functionally transferred to recipient cells (Valadi et al., 2007; Baj-Krzyworzeka et al., 2016).

In pathogens, EV shedding is well described in fungi, bacteria, protozoan and helminth parasites (Ramirez and Marcilla, 2021; Wang et al., 2022). Of note, they were described mediating host-parasite interactions (Silverman et al., 2010a; Buck et al., 2014). In models of infection with *Leishmania* spp., it was described the importance of EVs in cell communication, the modulation of the immune response (Silverman et al., 2010a) and the importance of parasite glycoproteins regulating these processes, including conditioning antigen presenting cells (APCs) (Silverman et al., 2010b).

EV liberation and also their protein composition were previously described for *Trypanosoma cruzi* (da Silveira et al., 1979; Alves and Colli, 2008; Bayer-Santos et al., 2013; Cortes-Serra et al., 2022). Noteworthy, some studies have demonstrated the presence of mediators inside the EVs from *T. cruzi* regulating cellular functions in the host, adhesion and cell invasion (Gazos-Lopes et al., 2014; Neves et al., 2014; Wang et al., 2022), and new evidence suggests the EVs role in remote signaling and inflammation (Dantas-Pereira et al., 2021). Although *T. cruzi* does not possess the miRNA synthesis

machinery, other small RNAs were found including transfer RNA-derived small RNA (stRNA), which make up the repertoire of small regulatory RNAs and are capable of modifying the genetic expression of host cells (Bayer Santos et al., 2013; Garcia Silva et al., 2014). The secretion of these EVs by *T. cruzi* would constitute a true information transfer mechanism between organisms from different kingdoms (Fernandez-Calero et al., 2015). In *T. cruzi* EVs there are glycoproteins from the trans-sialidase/gp85 superfamily (Ouaissi et al., 1990), and proteomic studies show the presence of α -Gal-glycoproteins, proteases and mucins normally membrane-associated by glycosylphosphatidylinositol or GPI anchors (Nakayasu et al., 2009; Torrecilhas et al., 2012; Bayer-Santos et al., 2013). Interestingly, animals injected with EVs from trypomastigotes (Tp) containing α -Gal residues increased amastigote nests in heart sections, triggered inflammation, and severe cardiac pathology (Trocoli-Torrecilhas et al., 2009). More recently, Lovo-Martins and colleagues have shown that the inoculation of EVs from Y *T. cruzi* strain prior to the infection reduces the inflammatory mediators and favors parasitism. *In vitro*, bone-marrow derived macrophages stimulated with these EVs before the interaction with the parasite increase its internalization and downregulate prostaglandin E2 and proinflammatory cytokines, suggesting a regulatory role for EVs supporting the parasite persistence (Lovo-Martins et al., 2018).

Immune cells are important targets for EVs and several reports demonstrate immune modulation by *T. cruzi* EVs (Torrecilhas et al., 2020; Dantas-Pereira et al., 2021). The parasite pathogen associated molecular patterns (PAMPs) are poorly detected at the initial steps of the infection (de Pablos Torró et al., 2018); however, *T. cruzi* EVs can trigger inflammatory responses and promote infection via TLR2 signalling in macrophages (Nogueira et al., 2015; Cronemberger-Andrade et al., 2020). EVs purified from peripheral blood of patients with Chagas induced proinflammatory cytokines in THP-1 cells (Groot-Kormelink et al., 2018), and both *T. cruzi* derived EVs from immune or non-immune cells are inflammatory for macrophages *in vitro*. The sensing of oxidized DNA inside EVs is involved in the

activation of the inflammatory response *via* TLR9 and cGAS-PARP1 signalling pathways (Choudhuri and Garg, 2020).

Dendritic cells (DCs) are professional APCs, key players in prompting the immune response against pathogens and in self-tolerance maintenance, with a pivotal role capturing, processing and presenting antigens to T cells (Merad et al., 2013). Exosomes are considered immune regulators in DC-based immunotherapy (Markov et al., 2019). It is well described that DC-derived EVs can carry functionally active molecules on the surface such as complexes of MHC class I and II with antigens or costimulatory molecules (Munich et al., 2012). During the last decades, the use of EVs was also described such as an alternative immunotherapy approach in cancer (Yang et al., 2021) and numerous infections. EVs can interact with target cells and modify cellular activity by delivering different mediators. EVs can be presented as conventional carriers for RNAs, lipids and proteins, and appear as an alternative cell-free vectors for antigen delivery. Tumor-derived EVs stimulate antitumor immunogenicity in DCs (André et al., 2002) and more interestingly, Ag-pulsed DC derived exosomes display prophylactic and therapeutic properties in tumour-bearing mice (Zitvogel et al., 1998). Immune protective response triggered by EVs from Ag-loaded DCs has also been described for different pathogens such as *Toxoplasma gondii* (Aline et al., 2004; Jung et al., 2020), *Eimeria* spp. (del Cacho et al., 2012) and *Leishmania major* (Schnitzer et al., 2010). However, no previous results in the field were described for *T. cruzi*.

Our group and others have previously demonstrated that *T. cruzi* downregulates DCs immunogenicity *in vitro* and *in vivo* (2015; Poncini et al., 2008; Gil-Jaramillo et al., 2016). Here we analyze EVs from the *in vitro* interaction between blood circulating Tp and bone-marrow derived DCs. We found that Tp increases the number and size of EVs in cultures with DCs. EVs displayed some exosome markers, and intracellular RNA. By proteomics we found that the presence of the parasite in DCs cultures has an impact in the protein composition of EVs. In addition, EVs from the interaction of Tp-DCs are easily uptaken by unstimulated DCs and modify the activation status of LPS-stimulated DCs. Finally, we found that the prophylactic treatment with EVs from DCs co-cultured with Tp (EVs-DCs +Tp) partially protects animals from the lethal infection, proposing EVs as promising mediators for therapeutic purposes against Chagas disease.

Materials and methods

Animals and parasites

Eight-to-ten week old C3H/HeN, C57BL/6 and CF1 male mice were obtained from the animal facilities of IMPaM UBA-

CONICET, School of Medicine, University of Buenos Aires. Animals were bred under sanitary barrier in specific-pathogen-free conditions.

Parasites from RA strain (González et al., 1981) were maintained by weekly intraperitoneal inoculation of three weeks-old male CF1 mice (1×10^5 parasites/mouse). RA bloodstream forms (Tp) were obtained from whole blood at the peak of parasitemia 7 days post-infection (dpi), thoroughly washed and purified by density gradient centrifugation as previously reported (Poncini et al., 2008). For the lethal infection challenge, ten-to-twelve week old C57BL/6 male mice received intradermic (hindfoot) injection with 1000 parasites as previously described (Poncini et al., 2015; Poncini et al., 2017; Gutierrez et al., 2021). Animal health condition, parasite load and mortality were periodically recorded.

All experiments were performed according to protocols CD N° 04/2015 approved by the University of Buenos Aires's Institutional Committee for the Care and Use of Laboratory Animals (CICUAL) in accordance with the Council for International Organizations of Medical Sciences (CIOMS) and International Council for Laboratory Animal Science (ICLAS) international ethical guidelines for biomedical research involving animals.

Cell culture and EV isolation

DCs were differentiated as previously described (Poncini et al., 2008). Briefly, femurs and tibias from C3H 8-12 week-old mice were flushed and bone marrow cells were incubated for 7 d in IMDM complete medium supplemented with: 10% (v/v) heat-inactivated FCS (Internegocios, Argentina), penicillin (100 U/mL) and streptomycin (100 mg/mL), 2-mercaptoethanol (50 μ M); with 20% conditioned medium from GM-CSF-producing J558 cells. After 7 days, cells were harvested, washed, plated (1×10^6 cells/mL) and cultured in serum free medium with or without Tp (1:2 cell: parasite) for 20 h. Control DCs were cultured with medium alone. Activated DCs were treated with a low dose of LPS (50ng/mL). Cell viability was assessed before and after culture by Trypan blue staining at 0.2% final concentration. Cell viability for experiments was 85% or more.

For EVs isolation, culture supernatants were collected and subjected to successive centrifugation steps according to Théry et al. (2006). At least 5 mL of culture medium was centrifuged at $300 \times g$ for 10 min in order to pellet cells, and then supernatants were harvested and centrifuged at $2,000 \times g$ for 20 min and at $10,000 \times g$ for 30 min. Finally, supernatants were ultracentrifuged at $100,000 \times g$ for 70 min at 4°C (Beckman Coulter Optima L-100 XP centrifuge using a fix angle rotor). Pellets were washed with PBS and ultracentrifuged at $100,000 \times g$

for 70 min at 4°C and then resuspended in PBS and used for transmission electron microscopy (TEM), RNA isolation, protein characterization and functional studies.

Transmission electron microscopy (TEM)

Cellular pellets and EVs resuspended in PBS were fixed in Karnovsky's fixative (0.5% glutaraldehyde, 2.5% paraformaldehyde), and processed according to [Marcilla et al. \(2012\)](#) at the Service of Microscopy, Servicios Centrales de Soporte a la Investigación Experimental (SCSIE), Universitat de València, Spain and analyzed by TEM.

Nanoparticle tracking analysis

For Nanoparticle Tracking Analysis (NTA), each pellet was suspended in filtered PBS (1:50) and analyzed with a Nanosight LM10 (MalvernTM, U.K.). Readings were performed in triplicate during 60 sec videos at 10 frames per sec at room temperature, with the following parameters: camera level 9, screen gain 9, detection threshold 6. The mode size and the concentration of particles resulting from 2 independent replicates from 2 pooled samples for each treatment.

Flow cytometry

For EVs characterization, samples were stained for 15 min at 4°C with anti-MHCII (FITC, M5/114.15.2) and anti-CD9 (biotin, MZ3) all from Miltenyi Biotec. The secondary reagent was Cy5-streptavidin (BD Biosciences). After washing in filtered PBS EV suspensions were diluted to a protein concentration of 5 µg/mL and analyzed in a CytoFLEX LX flow cytometer (Beckman Coulter). Particle detection was calibrated by using CytoFLEX fluorospheres from 160 to 900 nm (Beckman Coulter), as observed in [Figure 1D](#) (right panel). Acquisition was performed at continuous flow yielding the events per 30 µL in order to calculate EVs concentration per sample.

For T cell characterization, single cell suspensions were incubated with the following fluorophore-conjugated anti mouse monoclonal antibodies (Ab) for 30 min at 4°C: anti-CD3 (biotin, 145-2C11), anti-CD4 (FITC, GK1.5), anti-CD8 (PerCP, 53-6.7) all from Miltenyi Biotec. PE-Cy7-streptavidin was used as secondary reagent (BD Biosciences).

For intracellular staining, cells were incubated with *T. cruzi* Ag at 20 µg/mL and brefeldin A (10 µg/mL; Sigma) for 5 h as previously described ([Poncini et al., 2015](#)). After surface staining cells were washed, fixed and permeabilized with Cytotfix/Cytoperm solutions (BD Biosciences) and stained with anti-INF-γ (PE, W18272D; BioLegend). Cells were acquired in a

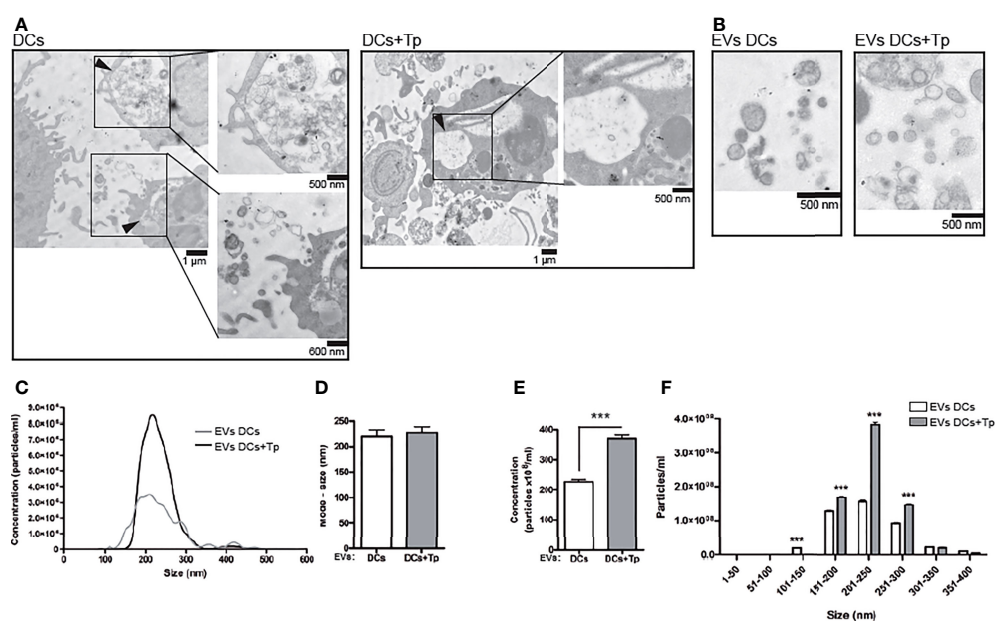


FIGURE 1

EVs from DCs+Tp presented higher diameters and abundance than EVs DCs. (A) Multivesicular compartments in DCs (upper panel) and DCs+Tp (lower panel) analyzed by TEM. Black arrows show amplified images. Bars, 500nm, 600 nm and 1µm. (B) EVs were isolated after sequential centrifugation from cultures of DCs at 1×10^6 cells/mL and 1:2 relation DC : Tp and processed for TEM. Bar, 500 nm. (C) Concentration distribution profile of EVs by size from 0 to 600 nm by Nanoparticle Tracking Analysis. (D) Mode size of EVs derived from DCs or DCs+Tp. (E) Concentration of EVs based in size ranges. Statistical analysis was performed with Wilcoxon test, *** $p < 0.001$. (F) EVs size distribution in 50 nm ranges. Statistical analysis was performed with two-way ANOVA and Bonferroni's post-test, *** $p < 0.001$.

FACSAria flow cytometer and analyzed using FlowJo 7.6. Gating strategy to study T cells is depicted in [Supplementary Figure 4](#).

RNA isolation, protein purification and characterization

RNA from EVs was isolated with Trizol LS (Life Technologies) according to [Ancarola et al. \(2017\)](#). RNA integrity was analyzed by gel electrophoresis and the concentration was determined using a Qubit Fluorometer (Invitrogen).

To confirm the intravesicular location of the isolated RNA, samples were differentially treated or not, prior to RNA isolation as follow: proteinase K (0.5 µg/µL) 10 min at 37°C, 10 min at 65°C followed by incubation with RNase A (0.04 µg/µL), depending on the sample and as it was described by [Ancarola et al. \(2017\)](#). The corresponding RNA profiles were analyzed by capillary electrophoresis in Fragment Analyser (Advanced Analytical Technologies, U.S.A.).

For protein analysis, immunoblot or liquid chromatography coupled with tandem mass spectrometry (LC-MS/MS) was performed on ultracentrifugation pellets according to [Marcilla et al. \(2012\)](#). For immunoblots, approximately 15 µg of cellular protein determined by Bradford (1×10^6 DCs) or the EVs-pellet obtained from 5×10^6 cells (cultured at 1×10^6 cells/mL) were resuspended in ice-cold lysis buffer (20 mM Tris-acetate, pH 7.0, 1 mM EGTA, 1% Triton X-100, 0.1 mM sodium fluoride, 5 µg/mL leupeptin, 1 mM sodium orthovanadate, 1 mM phenylmethylsulfonyl fluoride). Proteins were resolved by SDS-PAGE, transferred to nitrocellulose membranes (Amersham) and transfer verified by reversible membrane staining with Ponceau Red (5% w/v) in 1% (v/v) acetic acid. Then, membranes were probed with anti-CD63 polyclonal Ab (SC-31211, Santa Cruz), anti-MHCI monoclonal Ab (Sc-59309, Santa Cruz), anti-CD9 monoclonal Ab (MZ3, Miltenyi Biotec) and HRP-conjugated secondary Ab. Detection was assayed using ECL chemiluminescent system (Amersham) according to manufacturer's instructions. Three independent samples of EVs from DCs or DCs+Tp were analyzed.

Proteomics and bioinformatics analysis

Liquid chromatography coupled with tandem mass spectrometry (LC-MS/MS) was performed on EVs ultracentrifugation pellets according to [Marcilla et al. \(2012\)](#). The proteomic analysis was executed at the proteomics facility of SCSIE University of Valencia that belongs to ProteoRed, PRB2-ISCI, and is supported by grant PT13/0001, of the PE I+D+i 2013-2016, funded by ISCI and FEDER. The Paragon algorithm of ProteinPilot v 4.5 was used to search the NCBI complete database with the following parameters: trypsin

specificity, cys-alkylation, no taxonomy restriction, and the search effort set to thorough. Reported results correspond to those proteins showing unused score ≥ 1.3 (identified with confidence $\geq 96\%$), ≥ 2 distinct peptides having at least 95% confidence and *T. cruzi* or mouse protein sequence annotation. Proteins annotated under the terms “hypothetical protein”, “expressed protein” or “conserved protein” were searched for domains in the domains database CDART at the NCBI site, and re-annotated if necessary, as previously described ([Ancarola et al., 2017](#)).

For protein analysis, a Venn diagram was generated using the online tool Venny 2.1 ([Oliveros, 2007](#)). PANTHER database was used to retrieve the gene ontology (GO) terms for molecular function and cellular components of EV proteins from DCs and DCs+Tp. GO term descriptions were then downloaded from The European Bioinformatics Institute site (<https://www.ebi.ac.uk/QuickGO/>) as previously described ([Ancarola et al., 2017](#)).

Labelling of EVs and functional assay

DCs were labelled with the lipophilic dye PKH26 (Sigma-Aldrich) according to manufacturer's protocol, washed, and then cultured with or without Tp. DCs-derived EVs were enriched as described above. PKH26⁺ DC-derived EVs were then isolated and used for functional assays. EVs isolated from the culture of 2.5×10^6 cells DCs or DCs+Tp were added to DCs cultures (5×10^5 cells per well) for 24 h. Internalization by DCs was identified by confocal microscopy and flow cytometry. In addition, DC activation status was determined by flow cytometry as described below.

Determination of EVs internalization and DCs activation by confocal microscopy and flow cytometry

For confocal microscopy, cells were harvested, washed and fixed in cold methanol for 10 min and DAPI (Invitrogen™) staining was used for nuclear visualization on an Olympus FV1000 microscope (lasers exciting at 405 and 559 nm, $\times 60$ objective) using Olympus Fluoview (version 4.2b) at the confocal microscopy service of Instituto de Fisiología y Biofísica (IFIBIO-Houssay), School of Medicine, UBA. Images were analyzed using the ImageJ software (version 1.52p).

For flow cytometry and depending on the assay, the following Ab were used: anti-MHCII (FITC, M5/114.15.2), and anti-CD11c (Biotin, N418) all from Miltenyi Biotec. The secondary reagent was Cy5-streptavidin (BD Biosciences).

For DCs surface staining, cellular suspensions were incubated with fluorescent-labeled Ab, 30 min at 4°C. Sample

acquisition was achieved on FACS Aria flow cytometer (BD Biosciences) and analyzed by FlowJo 7.6 software.

ELISA

After 20 h of culture, cell supernatants were harvested and stored at -80°C until used. Mouse IL-10 or TNF- α was detected by ELISA (R&D Systems, Minneapolis, MN) according to manufacturer's protocol.

Experimental treatment with EVs and analysis of the effector response after the infection challenge

EVs from DCs or DCs+Tp were obtained as described above. PBS or EVs generated from 1×10^6 cells were intradermally injected per mice at day 0. At day 7 post EVs or PBS injection, animals were challenge with the lethal infection. To this end, ten-to-twelve week old C57BL/6 male mice received intradermic (id, hindfoot) injection with 1000 RA parasites (Gutierrez et al., 2021). Experimental procedure included four to five animals per group depending on the experiment and was defined as: i) PBS, negative for infection; ii) PBS+Tp, positive for infection; iii) EVs DCs treatment+Tp; iv) EVs DCs+Tp treatment+Tp. Animal health condition, parasite load and mortality were periodically recorded.

In a second round of experiments a second immunization dose with EVs was applied at day 7 after the first one, followed by the challenge with the parasite 10 days after the treatment. Immune response was studied at day 20 pi. To this end, T cell populations and intracellular INF- γ production were analyzed in cell suspensions from popliteal lymph nodes (pLN) by flow cytometry, as described above. Cell suspensions were obtained after mechanical disaggregation of pLNs in a 100 μm nylon mesh as previously described (Poncini and González-Cappa, 2017). Cell viability was assessed by Trypan blue dye exclusion. Experimental procedure included four to five animals per group depending on the experiment, and two to three repetitions.

Statistical analysis

Student's *t*-test or non-parametric Wilcoxon tests were performed in order to analyse statistical significance between two samples. For more samples ANOVA and Dunnett's or Bonferroni's post-test or the non-parametric Mann-Whitney U test were applied. Survival curves were analyzed by Kaplan-Meier. Analyses were carried out with GraphPad Prism 4 software for Windows. $P < 0.05$ value was defined as significant.

Results

Identification and quantification of EVs from the interaction of DCs with T. cruzi in vitro

Previous studies demonstrated the capacity of DCs to secrete EVs to the extracellular milieu (Zitvogel et al., 1998); especially four different populations of DC-EVs were described with variable size and protein content (Kowal et al., 2016). Particularly, the maturation state of these cells can influence the subcellular protein distribution and also the EVs-DCs composition and size (Théry et al., 2009; Ten Broeke et al., 2011). Ultracentrifugation and density gradients are still the most common methods for EV purification and EV structural characterization is currently carried out by transmission electron microscopy (TEM) (Royo et al., 2020).

We found by TEM that both control and Tp co-cultured DCs (DCs+Tp) presented structures compatible with internal multivesicular compartments next to the plasmatic membrane (Figure 1A, black arrows).

Here, small EVs were isolated from culture supernatants after differential ultracentrifugation (Figure 1B). Pellets obtained after 300, 2,000 and 10,000 $\times g$ centrifugation were discarded and only small EVs from 100,000 $\times g$ were analyzed. Size distribution determined by TEM showed a heterogeneous population of vesicles with diameters ranging from 30 to 200 nm in DCs cultures and from 60 to 400 nm in samples from DCs co-cultured with Tp (Supplementary Figure 1A). Particles derived from Tp-DC co-cultures (EVs DCs+Tp) were more abundant, as randomly quantified across 20 fields, and showed larger diameters than EVs DCs (Supplementary Figure 1B). The evaluation by Nanoparticle Tracking Analysis (NTA) effectively demonstrated that Tp induced a significant increase in EV release to milieu by DCs (Figures 1C, E). A similar mode for the size of EVs DCs and EVs DCs+Tp populations was observed (Figure 1D); however the EVs size profile distribution shows a higher proportion of EVs in the range from 150 to 300 nm for EVs DCs+Tp, consistent with microvesicles/ectosomes and confirming the TEM findings (Figure 1F).

Different RNA and protein content in EVs DCs+Tp compared with EVs DCs

The analysis of the RNA and the protein cargo showed that EVs DCs contain almost exclusively small RNA (< 200 nt) (Supplementary Figure 2A, panel a). On the contrary, EVs DCs +Tp showed a different RNA pattern including RNA species around 200 and 500 nt (Supplementary Figure 2A, panel b). This pattern also differed from the corresponding to ribosomal 18S and 28S RNAs found in cell samples (Supplementary Figure 2B, C). To

avoid possible contamination with 'free' RNA co-sedimented with EVs in the ultracentrifugation step and to confirm that the results obtained corresponded to intravesicular RNA, isolated EVs were treated with proteinase K and RNase A and then analyzed. RNA patterns from DCs and DCs+Tp EVs treated or not-treated were comparable, confirming the intravesicular location of the RNA found (Supplementary Figure 2A; a versus c, and b versus d).

Previous reports demonstrate that not only plasmatic membrane-derived vesicles from DCs, but also endosome-derived membrane vesicles can bear MHC class I and II molecules (Zitvogel et al., 1998; Kowal et al., 2016) and costimulatory molecules, features that enhance their immunotherapeutic potential as a cell-free strategy (Markov et al., 2019). In addition, the presence of tetraspanins such as CD9, CD63 and CD81 propose, to some extent, a protein signature for DCs exosomes (Kowal and Tkach, 2019). Apparently the composition of exosomes in DCs is related to cell maturation state (Segura et al., 2005). Interestingly, tetraspanins have been reported to be involved in antigen presentation by MHC interaction and by the immune synapse formation in DCs or other APCs (Unternaehrer et al., 2007; Petersen et al., 2011). Here, we observed by western blot that EVs DCs and EVs DCs+Tp contain CD9 and MHC class I molecules, also detected with different intensities in total cell lysates

(Figure 2A). No CD63 was detected in EVs, although CD63 signal was clearly observed in total cell lysates (Figure 2A). By flow cytometry, we also confirmed that EVs DCs+Tp displayed an enlarged population from 200-230 nm (P2) compared to EVs DCs (Figure 2B) as observed by TEM and NTA. Furthermore, we found a variable amount of MHCII in different subpopulations of EVs (P1, P2 and P3), both in EVs DCs and EVs DCs+Tp samples (Figure 2C). P2 and P3 subpopulation showed higher expression of MHCII. Interestingly, P3 in EVs DCs+Tp displayed increased median fluorescence intensity (MFI) of MHCII compared to EVs DCs (Figure 2C). To identify the protein content in EVs DCs and EVs DCs+Tp enriched fractions we performed an exploratory analysis by liquid chromatography coupled with tandem mass spectrometry (LC-MS/MS). We observed that both DCs and DCs+Tp EVs contained the presence of proteins typically found in exosomes derived from DCs such as CD9, MHCII, annexins, GAPDH and enolase (Supplementary Figure 3A), as previously reported (Kowal et al., 2016). However, some proteins were differentially detected in EVs from DCs versus DCs+Tp as expressed in the Venn diagram and GO terms for molecular function and cellular component (Supplementary Figures 3A, B, respectively). Interestingly, other proteins were detected with a lower unused score or number of peptides such as CD81, Alix, HSP70, Syntenin-1, TSG101, Galectin-1/3 and *T. cruzi* trans-

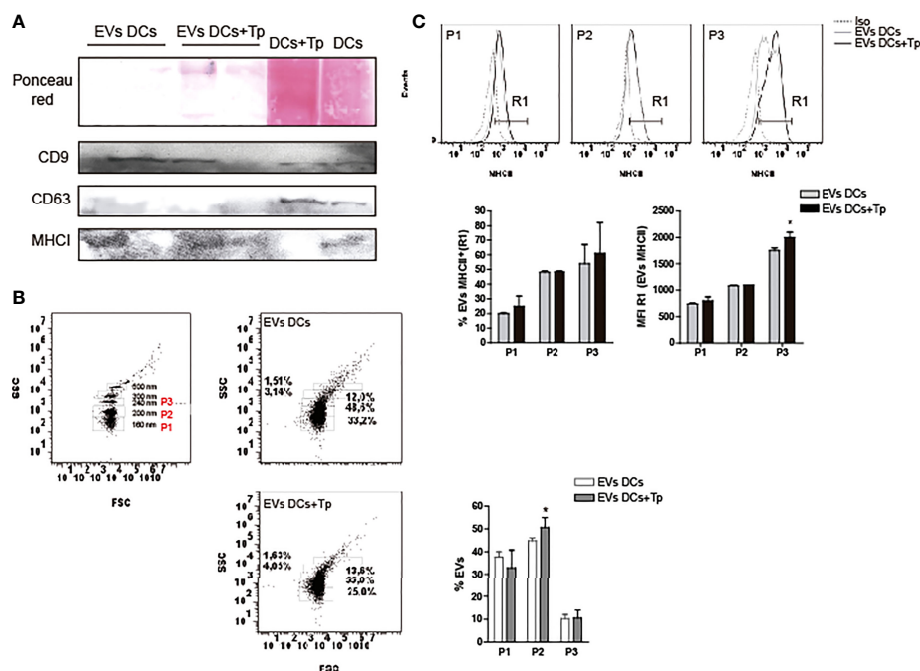


FIGURE 2

EVs protein characterization. (A) Detection of CD9, CD63 and MHC I in EVs DCs, EVs DCs+Tp and total cell lysates by immunoblot. Ponceau red staining confirmed the correct protein transfer to membranes prior to Ab incubation. B-C) EVs analysis by flow cytometry. (B) Gating strategy was performed based on the known sizes of commercial beads (left panel). Based in EVs concentration detected in samples, three major subpopulations were defined in EVs DCs and EVs DCs+Tp (P1, P2 and P3; right panels). (C) Percentage and median fluorescence intensity of the MHCII marker was analyzed in MHCII⁺ EVs (R1) in P1, P2 and P3. Data are representative of at least two biological replicates for each treatment. For comparisons between two groups student's t-test was used. * $p < 0.05$.

sialidase, the last one only in EVs DCs+Tp (The mass spectrometry proteomics data have been deposited to the ProteomeXchange Consortium via the PRIDE (Perez-Riverol et al., 2022) partner repository with the dataset identifier PXD037795.).

EVs from *T. cruzi*-DCs interaction modulate DC activation *in vitro*

Previously, we have reported that Tp interaction confers tolerogenic properties to DCs *in vitro*. However, this effect was observed with the whole parasite and not with medium enriched in Tp secretion products (Poncini et al., 2008). Here we studied the effect of DCs-derived EVs and EVs product of the parasite-DCs interaction over DCs in a steady and/or activated state. To this end, first we analyzed if EVs can be uptaken by DCs. EVs labeled with the lipid dye PKH26, were incubated with DCs in steady-state and uptake was determined by confocal microscopy and flow cytometry. By confocal microscopy we confirmed that both types of EVs were uptaken by DCs. While not quantified by microscopy, DCs incubated with EVs-DCs+Tp showed cells with high PKH26 incorporation, compatible with high EV uptake (Figure 3A, a versus b). By flow cytometry, we confirmed that DCs with MHCII^{int/low} expression incorporate more EVs DCs+Tp than EVs DCs (Figure 3B). In addition, DCs incubated with EVs DCs slightly increased MHCII expression,

while the EVs-DCs+Tp treated displayed the same expression observed in control DCs and expressed as mean fluorescence intensity (MFI) (Figure 3C). Next, we analyzed by ELISA the effect of EVs on TNF- α and IL-10 secretion in DCs activated with LPS. We found no differences in cytokine secretion between control DCs and DCs incubated with EVs DCs (Figure 3D). Interestingly, EVs DCs+Tp downregulated the IL-10 and TNF- α secretion, the former at undetectable levels (Figure 3D). Of note, no differences in cell viability were detected in cultures (data not shown). These results suggest that EVs from DCs+Tp modulate to some extent MHCII expression in DCs, also IL-10 and TNF- α secretion to the milieu.

EVs derived from the interaction between DCs and Tp partially protect mice from lethal infection

EVs derived from DCs have lately become an attractive tool since they can cargo specific antigen and display immunogenicity. A cell-free-based vaccine using EVs has been previously described (Keller et al., 2006). In addition, DCs derived EVs were reported to induce protective immunity in *Toxoplasma gondii* (Aline et al., 2004), *Leishmania major* (Schnitzer et al., 2010), among other infections. However, while there are extensive studies on EVs derived from *T. cruzi* (Dantas-Pereira et al., 2021), and their role in the host immune

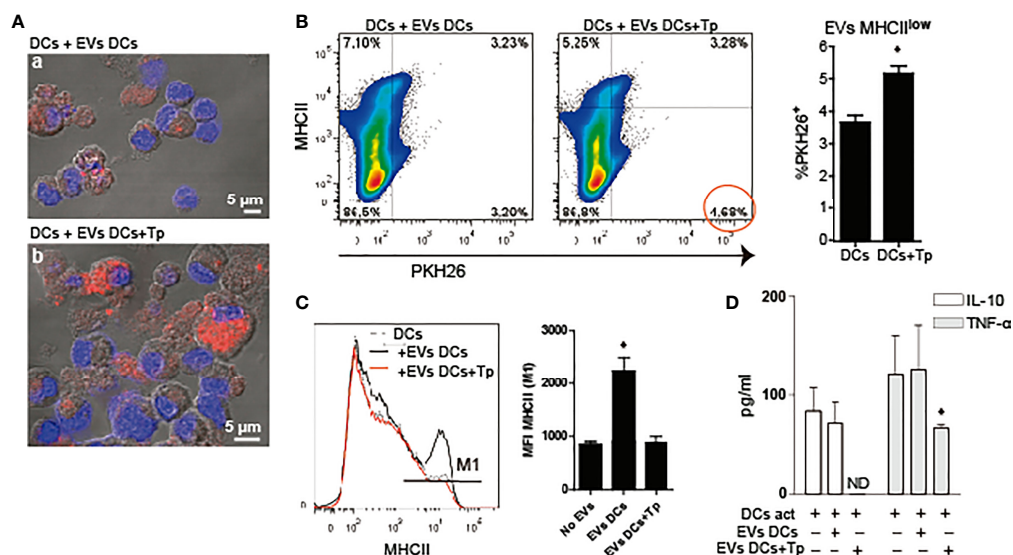


FIGURE 3

DCs-derived EVs are internalized by DCs in culture. (A) Confocal microscopy of DCs incubated with PKH26⁺ EVs (red) derived from DCs (a) or DCs+Tp (b) for 24 h at 37°C. Scale indicates 5 μ m. (B) Analysis of MHCII expression associated with PKH26⁺ EVs uptake by DCs in culture by flow cytometry. Statistical analysis was performed with Student's t-test, *p<0.05. (C) Analysis of MHCII median fluorescence intensity (MFI) in DCs stimulated or not with EVs-DCs or EVs-DCs+Tp. Statistical analysis was performed with ANOVA and Dunnett's test, *p<0.05. (D) TNF- α and IL-10 in culture supernatants detected by ELISA. Statistical analysis was performed with ANOVA and Dunnett's test, *p<0.05. Data are representative of at least three biological replicates for each treatment.

regulation (D'Avila et al., 2021), there is little information about therapy approaches with DCs in experimental Chagas disease.

Here we analyzed the effect of one dose of EVs-DCs+Tp and EVs DCs injected i.d. as described in material and methods, 7

days before the challenge with the infection with the lethal RA strain (Poncini et al., 2015). Parasitemia, body weight and mortality were registered, and animals losing more than 25% of their body weight were euthanized (represented in Figure 4A).

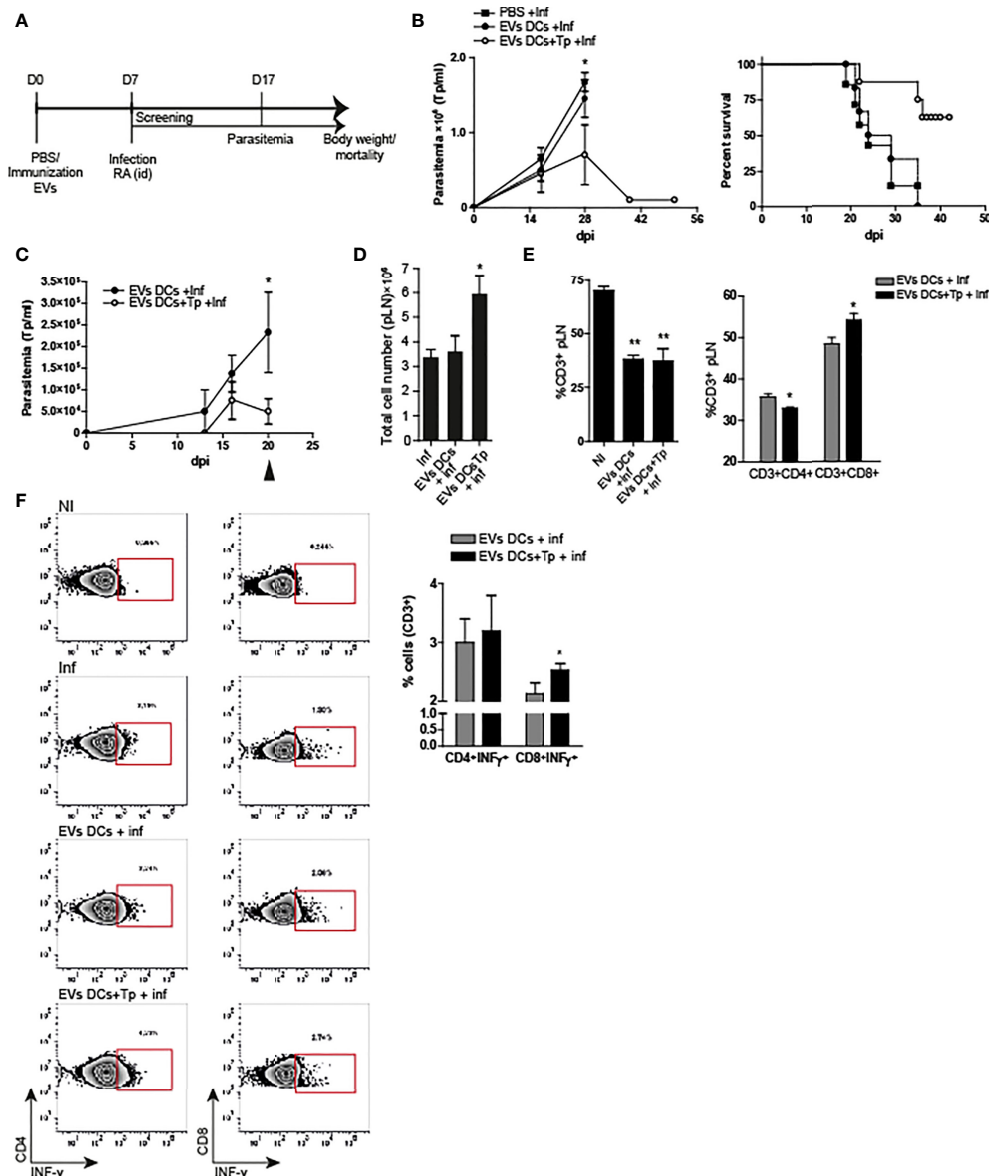


FIGURE 4

EVs DCs+Tp protect mice from lethal *T. cruzi* infection. (A) Schematic representation of the experimental design. (B) Peripheral blood parasitemia and mice survival. Animals were monitored during experimental infection. Control of infection (squares), EVs DCs treated and challenged (filled circle) and EVs DCs+Tp treated and challenged (fill circle) as described in materials and methods. (C) Peripheral blood parasitemia in animals treated with a second dose of EVs 7 days after the first application and challenged with RA 10 days after the treatment. (D) Absolute cell number in popliteal lymph nodes (pLN) 20 days post-infection. (E) Percentage of CD3⁺ T cells in pLN (left panel) and percentage of CD4⁺ and CD8⁺ T cells in pLN (right panel) by flow cytometry. No differences were detected between no-treated infected (Inf) and treated animals (data not shown). (F) Intracellular INF- γ detection from ag-specific CD4⁺ or CD8⁺ T cells by flow cytometry. One representative assay of the gating strategy for INF- γ detection in CD4⁺ and CD8⁺ T cells is shown (left panels). Bar graph representation summing up the values obtained from the biological replicates in independent experiments (right panel). One of three representative experiments designed with 4–5 mice per group is shown. For more than two treatments, statistical analysis was performed with ANOVA and Dunnett's test. For comparisons between two groups student's t-test was used. * $p < 0.05$, ** $p < 0.01$.

Treatment with EVs-DCs+Tp partially protected animals from the lethal infection; with approximately a 60% of survival (one representative experiment of three independent studies with similar results is shown; [Figure 4B](#) right panel). In addition, EVs-DCs+Tp treatment reduced the number of circulating parasites at the peak of parasitemia (28 dpi, [Figure 4B](#) left panel).

In order to analyze the immune response after the treatment in animals challenged with the lethal infection, we set a second round of experiments with a second immunization with EVs at day 7 after the first dose, followed by the challenge with the parasite 10 days after. Immune response was studied at 20 dpi. We found that animals treated with two EVs DCs+Tp doses controlled the parasitemia earlier in time in comparison with the ones that received one dose. In addition, treated animals, showed a marked decline in blood-Tp since 16 dpi ([Figure 4C](#)). No differences were observed between infected animals and EVs DCs treated and challenged (data not shown). We found a sharp adenomegaly in draining lymph node (pLNs), with high absolute cell-number in EVs DCs+Tp treated animals ([Figure 4D](#)). Although treatment with EVs DCs+Tp did not modify the proportion of total CD3⁺ T cells during the infection ([Figure 4E](#), left panel; EVs DCs versus EVs DCs+Tp treated), EVs DCs+Tp treatment enhanced the percentage of CD8⁺T cells ([Figure 4E](#), right panel). Of note, it was detected more INF- γ production by ag-specific CD8⁺ T cells ([Figure 4F](#)), compatible with a stronger effector T-cell response. These results provide the evidence that *T. cruzi*-DCs derived EVs are an attractive cell-free strategy for immunotherapy in Chagas disease.

Discussion

It is reasonable to assume that in protozoan infections the intracellular stages are the responsible for the EV exchange between the parasite and host cells, as described for amastigotes in *Leishmania major* ([Silverman and Reiner, 2012](#)). However, a paracrine/juxtacrine cross-talk between Tp (the extracellular forms of the parasite) and host cells through EVs secretion was described by [Ramirez et al. \(2017\)](#). In addition, it was also demonstrated a Ca²⁺ dependent up-regulation in the secretion of membrane derived vesicles in THP-1 monocytes induced by Tp ([Cestari et al., 2012](#)); nevertheless, the precise mechanism and the signaling cascades stimulated by the parasite are still unknown. Interestingly, previous reports show that low pH and other stress signals increment the release of EVs by the parasite which reach a peak at 120 min at 37°C *in vitro* ([Vasconcelos et al., 2021](#)), suggesting its possible participation in parasite invasion.

On the other hand, not only parasite products but also EVs released by human peripheral blood mononuclear cells infected with SylvioX10/4 strain of *T. cruzi* activate THP-1 in culture. Interestingly, it was shown that in infected mice and chronic patients with Chagas disease most of the vesicles are of leukocyte

or endothelial origin ([Chowdhury et al., 2017](#); [Choudhuri and Garg, 2020](#)).

In the present work we found that *T. cruzi* is capable of modulating the secretion of EVs derived from DCs *in vitro*. Due to *T. cruzi*-DC interaction time in cultures, the effects described here involve the Tp stage of the parasite. During the first 24 h of culture, and depending on the multiplicity of infection, the percentage of cells infected with amastigotes can be low ([Poncini et al., 2008](#)). Results obtained by proteomics showed low *T. cruzi* protein cargo in EVs (only trans-sialidase was detected), suggesting that most of the EVs released in supernatants are from DC origin. However, the presence of Tp modifies the abundance and the size of the EVs shedding to milieu by DCs.

While exosome-like particles display diameters up to 100 nm, ectosomes or microvesicles whose origin is the plasma membrane, display among 100-350 nm ([Cocucci and Meldolesi, 2015](#); [Witwer and Théry 2019](#)). In addition to modify the number and size of the EVs released, here we found that Tp apparently, change the RNA and protein content in EVs from DCs. These results suggest that the parasite could shape the nature and probably the origin of the EVs released by DCs; however more studies are needed in order to confirm this affirmation.

DCs in different maturation status delivered exosomes with different RNA cargo, especially miRNAs. Interestingly, immature DCs secrete high quantity of exosomes ([Montecalvo et al., 2012](#)). Here we observed that EVs DCs+Tp in addition to small RNA, present populations of longer RNA (>180nt and >400nt), different from large ribosomal RNA. No previous reports were found about these RNA populations in EVs and *T. cruzi*. This result needs further studies since these RNAs could represent long non-coding RNAs or mRNA transcripts. Long non-coding RNAs are heterogeneous group of regulators with a length of more than 200 nt and their description in EVs has not been thoroughly studied enough ([Wang et al., 2019](#)).

In the same line, we found different protein content between DCs and DCs+Tp EVs. It was previously described that tetraspanins are differentially expressed by human and murine subsets, and they display a key role in DC receptors regulation, including antigen presentation ([Zuidscherwoude et al., 2017](#)). As expected for murine DCs, we found more CD9 than CD63 expression in cell lysates and in EVs by immunoblot and LC-MS/MS. Interestingly, in DCs and DCs+Tp EVs we also detected MHCII. Previous studies reported the association of CD9 and MHCII for the formation of multimers in the membrane of DCs and by this interaction an enhanced efficiency for antigen presentation ([Unternaehrer et al., 2007](#)). On the contrary, tetraspanins content in EVs can be variable and in the case of small EVs isolated by ultracentrifugation MHCII might be abundant both in CD9⁺ or CD9⁻ particles ([Kowal et al., 2016](#)). CD63 is an accepted marker found in exosomes and predominantly an intracellularly expressed tetraspanin. In addition it was observed to be involved in the internalization of

complex ag (Mantegazza et al., 2004). Previous reports demonstrate that tetraspanins can be differentially expressed by different DCs subsets and CD9 is highly expressed in murine myeloid DCs (Zuidischerwoude et al., 2017). Here we found that EVs display CD9, while no CD63. Future studies would explain if this result is associated to the particles origin or if another mechanism is involved in the lack of CD63 in EVs.

By proteomics we observed that EVs DCs and EVs DCs+Tp share the presence of certain proteins; however, EVs DCs+Tp displayed an extended list of protein cargo. Of note, here we demonstrate that the larger population of EVs from DCs+Tp displays more MHCII. This result is extremely interesting since our group and others have previously described that Tp downregulate the surface expression of MHCII in DCs (Poncini et al., 2008). The release of MHCII molecules in EVs could be a possible evasion mechanism that the parasite exploits in order to modulate DCs immunogenicity. Studies in course may answer this question.

DC based vaccines have great potential for the treatment of different disorders, especially in cancer (Sprooten et al., 2019). Different approaches were described ranging from passive loading of *in vitro* differentiated DCs with tumor or pathogen peptides to transfection with nucleic acids or viral vector encoding diverse antigens. Although the FDA has approved monocyte-derived DC therapy for cancer, this presented some limitations (Palucka and Banchereau, 2013). One of the most important problems for DC-based vaccines, in addition to the high price, is the correct delivery of the antigen. In this context, EVs derived from DCs have lately become an attractive tool for cell-free-based vaccine since they display immunogenicity; can load specific antigens and the structure for antigen presentation (Markov et al., 2019). *In vitro* we found a greater uptake of EVs DCs+Tp than EVs DCs by control DCs. Surprisingly, EVs DCs+Tp modulated the activation status of DCs in culture. Not only MHCII surface expression, but also both IL-10 and TNF- α secretion were decreased. *In vivo* immunization with EVs as a cell-free immunotherapy shows that mice treated with only one dose of EVs-DCs+Tp have higher survival and low parasitemia after the challenge with the lethal infection with *T. cruzi*. Animals treated with two doses of EVs DCs +Tp showed fewer circulating parasites compared to those treated with one-dose and improved effector response of ag-specific T cell.

In conclusion, the results presented here, as well as go deep in the understanding of the parasite and the host interplay, suggest that *T. cruzi*-DCs derived EVs are a novel cell-free strategy as immunotherapy against Chagas disease. The results also propose EVs better molecular characterization for future development of new accessible synthetic tools.

Data availability statement

The mass spectrometry proteomics data have been deposited to the ProteomeXchange Consortium via the PRIDE (Perez-

Riverol et al., 2022) partner repository with the dataset identifier PXD037795.

Ethics statement

The animal study was reviewed and approved by CICUAL CD N° 04/2015.

Author contributions

BG, MA, MC, and CP contributed with the conception and the design of the study. BG and CP performed the experiments and analyzed data. MA and MC contributed with RNA purification and analysis of the results. AM contributed to TEM and LC/MS-MS. IR and MIR contributed with EVs quantification, the writing and the analysis of the results. CP wrote sections of the manuscript. All authors contributed to manuscript revision. All authors contributed to the article and approved the submitted version.

Funding

This work was supported by Fundación Bunge & Born, Universidad de Buenos Aires (UBACyT 2017 20020160100117BA and 2020 20020190100230BA), Grant for Research on Infectious Diseases and Agencia Nacional de Promoción Científica y Tecnológica (ANPCyT), Argentina, projects PICT2017 N°2062. AM is supported by the Agencia Estatal de Investigación, Ministerio de Ciencia e Innovación, Spain (Grant number PID2019-105713GB-I00/AEI/10.13039/501100011033), and Conselleria d'Educació, Cultura i Esports, Generalitat Valenciana, Valencia, Spain (Grant PROMETEO/2020/071).

Acknowledgments

We thank Eduardo Gimenez, Ricardo Chung and Marianela Lewicki for technical assistance. The Service of Proteomics, Servicios Centrales de Soporte a la Investigación Experimental (SCSIE), Universitat de València, for ProteomeXchangesubmission. Dr. Andrea Peralta for assisting with the use of the ultracentrifuge at Instituto de Biotecnología, Centro de Investigación en Ciencias Veterinarias y Agronómicas (CICVyA) Instituto Nacional de Tecnología Agropecuaria (INTA), Argentina and Dra. Paula Pérez at INBIRS, UBA-CONICET, Facultad de Medicina, Universidad de Buenos Aires.

Conflict of interest

The authors declare that the research was conducted in the absence of any commercial or financial relationships that could be construed as a potential conflict of interest.

Publisher's note

All claims expressed in this article are solely those of the authors and do not necessarily represent those of their affiliated

organizations, or those of the publisher, the editors and the reviewers. Any product that may be evaluated in this article, or claim that may be made by its manufacturer, is not guaranteed or endorsed by the publisher.

Supplementary material

The Supplementary Material for this article can be found online at: <https://www.frontiersin.org/articles/10.3389/fcimb.2022.980817/full#supplementary-material>

References

- Aline, F., Bout, D., Amigorena, S., Roingeard, P., and Dimier-Poisson, I. (2004). *Toxoplasma gondii* antigen-pulsed-dendritic cell-derived exosomes induce a protective immune response against *T. gondii* infection. *Infect. Immun.* 72, 4127–4137. doi: 10.1128/IAI.72.7.4127-4137
- Alves, M. J., and Colli, W. (2008). Role of the gp85/trans-sialidase superfamily of glycoproteins in the interaction of *Trypanosoma cruzi* with host structures. *Subcell. Biochem.* 47, 58–69. doi: 10.1007/978-0-387-78267-6_4
- Ancarola, M. E., Marcilla, A., Herz, M., Macchiaroli, N., Pérez, M., Asurmendi, S., et al. (2017). Cestode parasites release extracellular vesicles with microRNAs and immunodiagnostic protein cargo. *Int. J. Parasitol.* 47, 675–686. doi: 10.1016/j.ijpara.2017.05.003
- André, F., Scharzt, N. E., Chaput, N., Flament, C., Raposo, G., Amigorena, S., et al. (2002). Tumor-derived exosomes: a new source of tumor rejection antigens. *Vaccine* 4, A28–A31. doi: 10.1016/S0264-410X(02)00384-5
- Baj-Krzyworzeka, M., Mytar, B., Szatanek, R., Surmiak, M., Węglarczyk, K., Baran, J., et al. (2016). Colorectal cancer-derived microvesicles modulate differentiation of human monocytes to macrophages. *Transl. Med* 14, 36. doi: 10.1186/s12967-016-0789-9
- Bayer-Santos, E., Aguilar-Bonavides, C., Pessini Rodrigues, S., Cordero, E. M., Ferreira Marques, A., Varela-Ramirez, A., et al. (2013). Proteomic analysis of *Trypanosoma cruzi* secretome: characterization of two populations of extracellular vesicles and soluble proteins. *J. Proteome. Res.* 12, 883–897. doi: 10.1021/pr300947g
- Bazzan, E., Tinè, M., Casara, A., Biondini, D., Semenzato, U., Cocconcelli, E., et al. (2021). Critical review of the evolution of extracellular vesicles' knowledge: From 1946 to today. *Int. J. Mol. Sci.* 22, 6417. doi: 10.3390/ijms22126417
- Buck, A. H., Coakley, G., Simbari, F., McSorley, H. J., Quintana, J. F., Le Bihan, T., et al. (2014). Exosomes secreted by nematode parasites transfer small RNAs to mammalian cells and modulate innate immunity. *Nat. Commun.* 5, 5488. doi: 10.1038/ncomms6488
- Cestari, I., Ansa-Addo, E., Deolindo, P., Inal, J. M., and Ramirez, M. I. (2012). *Trypanosoma cruzi* immune evasion mediated by host cell-derived microvesicles. *J. Immunol.* 188, 1942–1952. doi: 10.4049/jimmunol.1102053
- Choudhuri, S., and Garg, N. J. (2020). *Trypanosoma cruzi* induces the PARP1/AP-1 pathway for upregulation of metalloproteinases and transforming growth factor β in macrophages: role in cardiac fibroblast differentiation and fibrosis in chagas disease. *mBio* 11, e01853-20. doi: 10.1128/mBio.01853-20
- Chowdhury, I. H., Koo, S., Gupta, S., Liang, L. Y., Bahar, B., Silla, L., et al. (2017). Gene expression profiling and functional characterization of macrophages in response to circulatory microparticles produced during *Trypanosoma cruzi* infection and chagas disease. *J. Innate. Immun.* 9, 203–216. doi: 10.1159/000451055
- Cocucci, E., and Meldolesi, J. (2015). Ectosomes and exosomes: shedding the confusion between extracellular vesicles. *Trends Cell Biol.* 25, 364–372. doi: 10.1016/j.tcb.2015.01.004
- Colombo, M., Raposo, G., and Théry, C. (2014). Biogenesis, secretion, and intercellular interactions of exosomes and other extracellular vesicles. *Annu. Rev. Cell. Dev. Biol.* 30, 255–289. doi: 10.1146/annurev-cellbio-101512-122326
- Cortes-Serra, N., Gualdron-Lopez, M., Pinazo, M. J., Torrecilhas, A. C., and Fernandez-Becerra, C. (2022). Extracellular vesicles in *Trypanosoma cruzi* infection: Immunomodulatory effects and future perspectives as potential control tools against chagas disease. *J. Immunol. Res.* 2022, 5230603. doi: 10.1155/2022/5230603
- Cronemberger-Andrade, A., Xander, P., Soares, R. P., Pessoa, N. L., Campos, M. A., Ellis, C. C., et al. (2020). *Trypanosoma cruzi*-infected human macrophages shed proinflammatory extracellular vesicles that enhance host-cell invasion via toll-like receptor 2. *Front. Cell. Infect. Microbiol.* 10. doi: 10.3389/fcimb.2020.00099
- Dantas-Pereira, L., Menna-Barreto, R., and Lannes-Vieira, J. (2021). Extracellular vesicles: Potential role in remote signaling and inflammation in *Trypanosoma cruzi*-triggered disease. *Front. Cell. Dev. Biol.* 9. doi: 10.3389/fcell.2021.798054
- daSilveira, J. F., Abrahamsohn, P. A., and Colli, W. (1979). Plasma membrane vesicles isolated from epimastigote forms of *Trypanosoma cruzi*. *Biochim. Biophys. Acta* 550, 222–232. doi: 10.1016/0005-2736(79)90209-8
- D'Avila, H., Souza, N. P., Albertoni, A. L. S., Campos, L. C., Rampinelli, P. G., Correa, J. R., et al. (2021). Impact of the extracellular vesicles derived from *Trypanosoma cruzi*: A paradox in host response and lipid metabolism modulation. *Front. Cell. Infect. Microbiol.* 11. doi: 10.3389/fcimb.2021.768124
- del Cacho, E., Gallego, M., Lee, S. H., Lillehoj, H. S., Quilez, J., Lillehoj, E. P., et al. (2012). Induction of protective immunity against *Eimeria tenella*, *Eimeria maxima*, and *Eimeria acervulina* infections using dendritic cell-derived exosomes. *Infect. Immun.* 80, 1909–1916. doi: 10.1128/IAI.06413-11
- de Pablos Torro, L. M., Retana, Moreira, L., and Osuna, A. (2018). Extracellular vesicles in chagas disease: A new passenger for an old disease. *Front. Microbiol.* 9. doi: 10.3389/fmicb.2018.01190
- Fernandez-Calero, T., Garcia-Silva, R., Pena, A., Robello, C., Persson, H., Rovira, C., et al. (2015). Profiling of small RNA cargo of extracellular vesicles shed by *Trypanosoma cruzi* reveals a specific extracellular signature. *Mol. Biochem. Parasitol.* 199, 19–28. doi: 10.1016/j.molbiopara.2015.03.003
- Garcia-Silva, M. R., Cabrera-Cabrera, F., das Neves, R. F., Souto-Padrón, T., de Souza, W., and Cayota, A. (2014). Gene expression changes induced by *Trypanosoma cruzi* shed microvesicles in mammalian host cells: relevance of tRNA-derived halves. *Biomed. Res. Int.* 2014, 305239. doi: 10.1155/2014/305239
- Gazos-Lopes, F., Oliveira, M. M., Hoelz, L. V., Vieira, D. P., Marques, A. F., Nakayasu, E. S., et al. (2014). Structural and functional analysis of a platelet-activating lysophosphatidylcholine of *Trypanosoma cruzi*. *PLoS Negl. Trop. Dis.* 8, e3077. doi: 10.1371/journal.pntd.0003077
- Gil-Jaramillo, N., Motta, F. N., Favali, C. B., Bastos, I. M., and Santana, J. M. (2016). Dendritic cells: A double-edged sword in immune responses during chagas disease. *Front. Microbiol.* 7. doi: 10.3389/fmicb.2016.01076
- Gonzalez Cappa, S. M., Bijovsky, A. T., Freilij, H., Muller, L. A., and Katzin, A. M. (1981). Aislamiento de una cepa de *Trypanosoma cruzi* a predominio de formas delgadas en la Argentina. *Medicina.* 41, 119–120.
- Groot-Kormelink, T., Mol, S., de Jong, E. C., and Wauben, M. H. M. (2018). The role of extracellular vesicles when innate meets adaptive. *Semin. Immunopathol.* 40, 439–452. doi: 10.1007/s00281-018-0681-1
- Gurunathan, S., Kang, M. H., Jeyaraj, M., Qasim, M., and Kim, J. H. (2019). Review of the isolation, characterization, biological function, and multifarious therapeutic approaches of exosomes. *Cells* 8, 307. doi: 10.3390/cells8040307
- Gutierrez, B. C., Lamm, E., González-Cappa, S. M., and Poncini, C. V. (2021). Early immune response elicited by different *Trypanosoma cruzi* infective stages. *Front. Cell. Infect. Microbiol.* 11. doi: 10.3389/fcimb.2021.768566

- Jung, B. K., Kim, E. D., Song, H., Chai, J. Y., and Seo, K. Y. (2020). Immunogenicity of exosomes from dendritic cells stimulated with *Toxoplasma gondii* lysates in ocularly immunized mice. *Korean J. Parasitol.* 58, 185–189. doi: 10.3347/kjp.2020.58.2.185
- Keller, S., Sanderson, M. P., Stoeck, A., and Altevogt, P. (2006). Exosomes: from biogenesis and secretion to biological function. *Immunol. Lett.* 107, 102–108. doi: 10.1016/j.imlet.2006.09.005
- Kowal, J., Arras, G., Colombo, M., Jouve, M., Morath, J. P., and Prindal-Bengtson, B. (2016). Proteomic comparison defines novel markers to characterize heterogeneous populations of extracellular vesicle subtypes. *Proc. Natl. Acad. Sci. U.S.A.* 113, E968–E977. doi: 10.1073/pnas.1521230113
- Kowal, J., and Tkach, M. (2019). Dendritic cell extracellular vesicles. *Int. Rev. Cell. Mol. Biol.* 349, 213–249. doi: 10.1016/b.sircmb.2019.08.005
- Lovo-Martins, M. I., Malvezi, A. D., Zanluqui, N. G., Lucchetti, B. F. C., Tatakibara, V. L. H., Mörking, P. A., et al. (2018). Extracellular vesicles shed by *Trypanosoma cruzi* potentiate infection and elicit lipid body formation and PGE2 production in murine macrophages. *Front. Immunol.* 9. doi: 10.3389/fimmu.2018.00896
- Mantegazza, A. R., Barrio, M. M., Moutel, S., Bover, L., Weck, M., Brossart, P., et al. (2004). CD63 tetraspanin slows down cell migration and translocates to the endosomal-lysosomal-MIICs route after extracellular stimuli in human immature dendritic cells. *Blood* 104, 1183–1190. doi: 10.1182/blood-2004-01-0104
- Marcilla, A., Treli, M., Cortés, A., Sotillo, J., Cantalapiedra, F., Minguez, M. T., et al. (2012). Extracellular vesicles from parasitic helminths contain specific excretory/secretory proteins and are internalized in intestinal host cells. *PLoS One* 7, e45974. doi: 10.1371/journal.pone.0045974
- Markov, O., Oshchepkova, A., and Mironova, N. (2019). Immunotherapy based on dendritic cell-targeted/- derived extracellular vesicles—a novel strategy for enhancement of the anti-tumor immune response. *Front. Pharmacol.* 10. doi: 10.3389/fphar.2019.01152
- Merad, M., Sathe, P., Helft, J., Miller, J., and Mortha, A. (2013). The dendritic cell lineage: Ontogeny and function of dendritic cells and their subsets in the steady state and the inflamed setting. *Annu. Rev. Immunol.* 31, 563–604. doi: 10.1146/annurev-immunol-020711-074950
- Montecalvo, A., Larregina, A. T., Shufesky, W. J., Stolz, D. B., Sullivan, M. L., Karlsson, J. M., et al. (2012). Mechanism of transfer of functional microRNAs between mouse dendritic cells via exosomes. *Blood* 119, 756–766. doi: 10.1182/blood-2011-02-338004
- Munich, S., Sobo-Vujanovic, A., Buchser, W. J., Beer-Stolz, D., and Vujanovic, N. L. (2012). Dendritic cell exosomes directly kill tumor cells and activate natural killer cells via TNF superfamily ligands. *Oncoimmunology* 1, 1074–1083. doi: 10.4161/onci.20897
- Nakayasu, E. S., Yashunsky, D. V., Nohara, L. L., Torrecilhas, A. C., Nikolaev, A. V., and Almeida, I. C. (2009). GPIomics: global analysis of glycosylphosphatidylinositol-anchored molecules of *Trypanosoma cruzi*. *Mol. Syst. Biol.* 5, 261. doi: 10.1038/msb.2009.13
- Neves, R. F., Fernandes, A. C., Meyer-Fernandes, J. R., and Souto-Pradon, T. (2014). *Trypanosoma cruzi*-secreted vesicles have acid and alkaline phosphatase activities capable of increasing parasite adhesion and infection. *Parasitol. Res.* 113, 2961–2972. doi: 10.1007/s00436-014-3958-x
- Nogueira, P. M., Ribeiro, K., Silveira, A. C. O., Campos, J. H., Martins-Filho, O. A., Bela, S. R., et al. (2015). Vesicles from different *Trypanosoma cruzi* strain trigger differential innate and chronic immune responses. *J. Extracell. Vesicles* 4, 28734. doi: 10.3402/jev.v4.28734
- Oliveros, J. C. (2007). VENN. An interactive tool for comparing lists with Venn diagrams. Available at: <https://bioinfo.cnb.csic.es/tools/venny/index.html>.
- Ouassii, M. A., Dubremetz, J. F., Kusnier, J. P., Cornette, J., Loyens, M., Taibi, A., et al. (1990). *Trypanosoma cruzi*: differential expression and distribution of an 85-kDa polypeptide epitope by *in vitro* developmental stages. *Exp. Parasitol.* 71, 207–217. doi: 10.1016/0014-4894(90)90023-6
- Palucka, K., and Banchereau, J. (2013). Dendritic-cell-based therapeutic cancer vaccines. *Immunity* 39, 38–48. doi: 10.1016/j.immuni.2013.07.004
- Perez-Riverol, Y., Bai, J., Bandla, C., Hewapathirana, S., García-Seisdedos, D., Kamatchinathan, S., et al. (2022). The PRIDE database resources in 2022: A Hub for mass spectrometry-based proteomics evidences. *Nucleic Acids Res.* 50, D543–D552. doi: 10.1093/nar/gkab1038
- Petersen, S. H., Odintsova, E., Haigh, T. A., Rickinson, A. B., Taylor, G. S., and Berditchevski, F. (2011). The role of tetraspanin CD63 in antigen presentation via MHC class II. *Eur. J. Immunol.* 41, 2556–2561. doi: 10.1002/eji.201141438
- Poncini, C. V., Alba-Soto, C. D., Batalla, E., Solana, M. E., and González-Cappa, S. M. (2008). *Trypanosoma cruzi* induces regulatory dendritic cells *in vitro*. *Infect. Immun.* 76, 2633–2641. doi: 10.1128/IAI.01298-07
- Poncini, C. V., and González-Cappa, S. M. (2017). Dual role of monocyte-derived dendritic cells in *Trypanosoma cruzi* infection. *Eur. J. Immunol.* 47, 1936–1948. doi: 10.1002/eji.201646830
- Poncini, C. V., Ilarregui, J. M., Batalla, E. I., Engels, S., Cerliani, J. P., Cucher, M. A., et al. (2015). *Trypanosoma cruzi* infection imparts a regulatory program in dendritic cells and T cells via galectin-1-Dependent mechanisms. *J. Immunol.* 7, 3311–3324. doi: 10.4049/jimmunol.1403019
- Ramirez, M. I., Deolindo, P., de Messias-Reason, I. J., Arigi, E. A., Choi, H., Almeida, I. C., et al. (2017). Dynamic flux of microvesicles modulate parasite host cell interaction of *Trypanosoma cruzi* in eukaryotic cells: dynamic flux of microvesicles modulate parasite-host cell interaction of *Trypanosoma cruzi* in eukaryotic cells. *Cell. Microbiol.* 19, e12672. doi: 10.1111/cmi.12672
- Ramirez, M. I., and Marcilla, A. (2021). Pathogens and extracellular vesicles: New paths and challenges to understanding and treating diseases. *Mol. Immunol.* 139, 155–156. doi: 10.1016/j.molimm.2021.09.006
- Royo, F., Théry, C., Falcón-Pérez, J. M., Nieuwland, R., and Witwer, K. W. (2020). Methods for separation and characterization of extracellular vesicles: Results of a worldwide survey performed by the ISEV rigor and standardization subcommittee. *Cells* 9, 1955. doi: 10.3390/cells9091955
- Schnitzer, J. K., Berzel, S., Fajardo-Moser, M., Remer, K. A., and Moll, H. (2010). Fragments of antigen-loaded dendritic cells (DC) and DC-derived exosomes induce protective immunity against *Leishmania major*. *Vaccine* 28, 5785–5793. doi: 10.1016/j.vaccine.2010.06.077
- Segura, E., Nicco, C., Lombard, B., Véron, P., Raposo, G., Batteux, F., et al. (2005). ICAM-1 on exosomes from mature dendritic cells is critical for efficient naive T-cell priming. *Blood* 106, 216–223. doi: 10.1182/blood-2005-01-0220
- Silverman, J. M., Clos, J., de Oliveira, C. C., Shirvani, O., Fang, Y., Wang, C., et al. (2010a). An exosome-based secretion pathway is responsible for protein export from *Leishmania* and communication with macrophages. *J. Cell. Sci.* 123, 842–852. doi: 10.1242/jcs.056465
- Silverman, J. M., Clos, J., Horakova, E., Wang, A. Y., Wiesgigl, M., Kelly, I., et al. (2010b). *Leishmania* exosomes modulate innate and adaptive immune responses through effects on monocytes and dendritic cells. *J. Immunol.* 185, 5011–5022. doi: 10.4049/jimmunol.1000541
- Silverman, J. M., and Reiner, N. E. (2012). *Leishmania* exosomes deliver preemptive strikes to create an environment permissive for early infection. *Front. Cell. Infect. Microbiol.* 1. doi: 10.3389/fcimb.2011.00026
- Sprooten, J., Ceusters, J., Coosemans, A., Agostinis, P., De Vleeschouwer, S., Zitvogel, L., et al. (2019). Trial watch: dendritic cell vaccination for cancer immunotherapy. *Oncoimmunology* 8, e1638212. doi: 10.1080/2162402X.2019.1638212
- Ten Broeke, T., van Niel, G., Wauben, M. H., Wubbolts, R., and Stoorvogel, W. (2011). Endosomally stored MHC class II does not contribute to antigen presentation by dendritic cells at inflammatory conditions. *Traffic* 12, 1025–1036. doi: 10.1111/j.1600-0854.2011.01212.x
- Théry, C., Amigorena, S., Raposo, G., and Clayton, A. (2006). Isolation and characterization of exosomes from cell culture supernatants and biological fluids. *Curr. Protoc. Cell Biol.* 3. doi: 10.1002/0471143030.cb0322s30
- Théry, C., Ostrowski, M., and Segura, E. (2009). Membrane vesicles as conveyors of immune responses. *Nat. Rev. Immunol.* 9, 581–593. doi: 10.1038/nri2567
- Torrecilhas, A. C., Schumacher, R. I., Alves, M. J., and Colli, W. (2012). Vesicles as carriers of virulence factors in parasitic protozoan diseases. *Microbes Infect.* 14, 1465–1474. doi: 10.1016/j.micinf.2012.07.008
- Torrecilhas, A. C., Soares, R. P., Schenkman, S., Fernández-Prada, C., and Olivier, M. (2020). Extracellular vesicles in trypanosomatids: Host cell communication. *Front. Cell. Infect. Microbiol.* 10. doi: 10.3389/fcimb.2020.602502
- Trocoli-Torrecilhas, A. C., Tonelli, R. R., Pavanelli, W. R., da Silva, J. S., Schumacher, R. I., de Souza, W., et al. (2009). *Trypanosoma cruzi*: parasite shed vesicles increase heart parasitism and generate an intense inflammatory response. *Microbes Infect.* 11, 29–39. doi: 10.1016/j.micinf.2008.10.003
- Untermaier, J. J., Chow, A., Pypaert, M., Inaba, K., and Mellman, I. (2007). The tetraspanin CD9 mediates lateral association of MHC class II molecules on the dendritic cell surface. *Proc. Natl. Acad. Sci. U.S.A.* 104, 234–239. doi: 10.1073/pnas.0609665104
- Valadi, H., Ekström, K., Bossios, A., Sjöstrand, M., Lee, J. J., and Lötvall, J. O. (2007). Exosome-mediated transfer of mRNAs and microRNAs is a novel mechanism of genetic exchange between cells. *Nat. Cell. Biol.* 9, 654–669. doi: 10.1038/ncb1596
- Vasconcelos, C. I., Cronemberger-Andrade, A., Souza-Melo, N., Maricato, J. T., Xander, P., Batista, W. L., et al. (2021). Stress induces release of extracellular vesicles by *Trypanosoma cruzi* trypomastigotes. *J. Immunol. Res.* 2021, 2939693. doi: 10.1155/2021/2939693
- Wang, X., Chen, J., and Zheng, J. (2022). The state of the art of extracellular vesicle research in protozoan infection. *Front. Genet.* 13. doi: 10.3389/fgene.2022.941561
- Wang, M., Zhou, L., Yu, F., Zhang, Y., Li, P., and Wang, K. (2019). The functional roles of exosomal long non-coding RNAs in cancer. *Cell. Mol. Life Sci.* 76, 2059–2076. doi: 10.1007/s00018-019-03018-3

Witwer, K. W., and Théry, C. (2019). Extracellular vesicles or exosomes? on primacy, precision, and popularity influencing a choice of nomenclature. *J. Extracell. Vesicles* 8, 1648167. doi: 10.1080/20013078.2019.1648167

Yamamoto, S., Azuma, E., Muramatsu, M., Hamashima, T., Ishii, Y., and Sasahara, M. (2016). Significance of extracellular vesicles: Pathobiological roles in disease. *Cell Struct. Funct.* 41, 137–143. doi: 10.1247/csf.16014

Yáñez-Mó, M., Siljander, P. R., Andreu, Z., Zavec, A. B., Borràs, F. E., Buzas, E. I., et al. (2015). Biological properties of extracellular vesicles and their physiological functions. *J. Extracell. Vesicles* 4, 27066. doi: 10.3402/jev.v4.27066

Yang, P., Peng, Y., Feng, Y., Xu, Z., Feng, P., Cao, J., et al. (2021). Immune cell-derived extracellular vesicles - new strategies in cancer immunotherapy. *Front. Immunol.* 12. doi: 10.3389/fimmu.2021.771551

Zitvogel, L., Regnault, A., Lozier, A., Wolfers, J., Flament, C., Tenza, D., et al. (1998). Eradication of established murine tumors using a novel cell-free vaccine: dendritic cell-derived exosomes. *Nat. Med.* 4, 594–600. doi: 10.1038/nm0598-594

Zuidscherwoude, M., Worah, K., van der Schaaf, A., Buschow, S. I., and van Spruiel, A. B. (2017). Differential expression of tetraspanin superfamily members in dendritic cell subsets. *PloS One* 12, e0184317. doi: 10.1371/journal.pone.0184317



OPEN ACCESS

EDITED BY

Tania F. De Koning-Ward,
Deakin University, Australia

REVIEWED BY

Sachie Kanatani,
Johns Hopkins University, United States
Tooba Mahboob,
University of Malaya, Malaysia
Lissinda Hester Du Plessis,
North-West University, South Africa
Selorme Aduko,
University of Ghana, Ghana
Carmen De Kock, University of Cape Town,
South Africa

*CORRESPONDENCE

Carmenza Spadafora
✉ cspadafora@indicat.org.pa

SPECIALTY SECTION

This article was submitted to
Parasite and Host,
a section of the journal
Frontiers in Cellular and
Infection Microbiology

RECEIVED 28 May 2022

ACCEPTED 17 January 2023

PUBLISHED 02 February 2023

CITATION

Coronado LM, Stoute JA, Nadovich CT,
Cheng J, Correa R, Chaw K, González G,
Zambrano M, Gittens RA, Agrawal DK,
Jemison WD, Donado Morcillo CA and
Spadafora C (2023) Microwaves can kill
malaria parasites non-thermally.
Front. Cell. Infect. Microbiol. 13:955134.
doi: 10.3389/fcimb.2023.955134

COPYRIGHT

© 2023 Coronado, Stoute, Nadovich, Cheng,
Correa, Chaw, González, Zambrano, Gittens,
Agrawal, Jemison, Donado Morcillo and
Spadafora. This is an open-access article
distributed under the terms of the [Creative
Commons Attribution License \(CC BY\)](#). The
use, distribution or reproduction in other
forums is permitted, provided the original
author(s) and the copyright owner(s) are
credited and that the original publication in
this journal is cited, in accordance with
accepted academic practice. No use,
distribution or reproduction is permitted
which does not comply with these terms.

Microwaves can kill malaria parasites non-thermally

Lorena M. Coronado^{1,2,3}, José A. Stoute⁴, Christopher
T. Nadovich^{5,6}, Jiping Cheng⁷, Ricardo Correa^{1,2,3},
Kevin Chaw^{1,3,8}, Guadalupe González^{3,9}, Maytee Zambrano^{3,9},
Rolando A. Gittens^{1,3}, Dinesh K. Agrawal⁷, William D. Jemison⁶,
Carlos A. Donado Morcillo^{1,3,8} and Carmenza Spadafora^{1,3*}

¹Biomedical Physics and Engineering Unit, Center of Cellular and Molecular Biology of Diseases (CBCMe), Instituto de Investigaciones Científicas y Servicios de Alta Tecnología (INDICASAT AIP), Panama City, Panama, ²Department of Biotechnology, Acharya Nagarjuna University, Guntur, India, ³Biomedical Physics and Engineering (BiomedPE) Group, Panama City, Panama, ⁴Department of Medicine, Division of Infectious Diseases and Epidemiology, Pennsylvania State University College of Medicine, Hershey, PA, United States, ⁵Electrical and Computer Engineering, Lafayette College, Easton, PA, United States, ⁶Wallace H. Coulter School of Engineering, Clarkson University, Potsdam, NY, United States, ⁷Department of Material Science and Engineering, Pennsylvania State University, University Park, PA, United States, ⁸School of Technology and Engineering, Universidad Católica Santa María La Antigua, Panama City, Panama, ⁹School of Electrical Engineering, Universidad Tecnológica de Panamá, Panama City, Panama

Malaria, which infected more than 240 million people and killed around six hundred thousand only in 2021, has reclaimed territory after the SARS-CoV-2 pandemic. Together with parasite resistance and a not-yet-optimal vaccine, the need for new approaches has become critical. While earlier, limited, studies have suggested that malaria parasites are affected by electromagnetic energy, the outcomes of this affectation vary and there has not been a study that looks into the mechanism of action behind these responses. In this study, through development and implementation of custom applicators for *in vitro* experimentation, conditions were generated in which microwave energy (MW) killed more than 90% of the parasites, not by a thermal effect but via a MW energy-induced programmed cell death that does not seem to affect mammalian cell lines. Transmission electron microscopy points to the involvement of the haemozoin-containing food vacuole, which becomes destroyed; while several other experimental approaches demonstrate the involvement of calcium signaling pathways in the resulting effects of exposure to MW. Furthermore, parasites were protected from the effects of MW by calcium channel blockers calmodulin and phosphoinositol. The findings presented here offer a molecular insight into the elusive interactions of oscillating electromagnetic fields with *P. falciparum*, prove that they are not related to temperature, and present an alternative technology to combat this devastating disease.

KEYWORDS

malaria, *Plasmodium falciparum*, therapeutic, electromagnetism, calcium signaling, microwaves (MW), Radio frequencies (RF), electromagnetic fields

1 Introduction

Despite important advances in the understanding of the biology of *Plasmodium falciparum* malaria, the mortality and morbidity caused by this parasite remain unacceptably high (WHO, 2021). The daunting issue of drug resistance haunts public health organizations worldwide and has created an urgency for the development of new therapeutic combinations (Shanks et al., 2015). The electromagnetic spectrum comprises waves of both magnetic and electrical origin traveling together through space. It can be divided into three major sections: first, direct current (DC) (0 frequency) to light spectrum, which includes radio and microwaves (MW) frequencies; second, the optical spectrum; and third, the highest, ionizing frequencies X and gamma rays. The work presented here deals with the first part of the spectrum, specifically MW, which exclude waves of high frequency, such as the ionizing ones. When moving in the form of waves, moving charges produce a magnetic field while the accompanying magnetism produces an electric field resulting in what are referred together as electromagnetic fields. These fields are able to interact with other objects, producing forces and reactions, depending on the electrical, magnetic and other physical properties of the object or material exposed to them. The hypothesis of this work was based on the fact that *P. falciparum* parasites, which cause malaria, when inside red blood cells synthesize an iron-containing crystal with paramagnetic properties (Inyushin et al., 2016) that could interact biophysically with the fields produced by electromagnetic waves.

At present, the heating properties of MW are used for certain medical treatments. MW are being used as thermotherapy to treat cancer and other diseases since the early 1980s, (Lubner et al., 2013; Burri et al., 2017). However, non-thermal effects due to the direct interaction of the electromagnetic field (EMF) with the biological specimen (Belyaev, 2005; Funk et al., 2009; Romanenko et al., 2017) have been viewed with greater reservation. Nonetheless, reports on the rate of calmodulin (CaM) activation, and subsequent CaM-dependent nitric oxide signaling, being involved in cell and tissue responses to weak EMF have been reviewed (Pilla, 2013). Some reports show that Direct Current Electric Fields (DC EF) can change intracellular Ca^{2+} concentration and induce directional movement in biological systems (Mycielska and Djamgoz, 2004). It was also reported that DC EF enhances the multiplication of *P. falciparum* by inducing changes in the Ca^{2+} transduction signals (Coronado et al., 2016). *P. falciparum* sensitivity to other types of energy, such as magnetic fields, has also been reported, (Wissing et al., 2002), (Smith and Kain, 2004; David Dele, 2015; Gilson et al., 2018). Be it affection to DNA molecules, breakage of protein bonds or disruption of crystal lattice growth, evidence mounts towards this parasite being as, or more, susceptible than other biological tissues to magnetism and electromagnetism. The study of a possible influence of MW on this parasite was compelling because of the capacity of these frequencies to penetrate living tissue, and the portability, low cost, and wearability of current MW devices which could be aimed towards the inhibition of growth of the parasite, selectively. Here, evidence that *P. falciparum* can be non-thermally susceptible to MW under conditions that spare mammalian cell lines is reported and evidence of part of the cellular mechanisms involved is provided.

These findings open the door for considering MW as a possible therapeutic application against malaria.

2 Results

2.1 MW energy kills malaria parasites non thermally but not healthy mammalian cells

Malaria parasites were exposed to MW with two in-house designed applicators: a closed waveguide (WG) system and an additional applicator device based on microstrip technology (M3) which allowed the sample to be placed in an open applicator system (Nadovich et al., 2014). The two systems are illustrated in Figure 1.

The optimal combination of exposure parameters that resulted in the death of the parasites was found at a frequency of 2.45 GHz; power levels of 12 W and 1 W delivered to the WG and M3 applicators, respectively; a total exposure time of 45 minutes; and a pulsed signal shape with a 20–30% duty cycle.

Electromagnetic models were used to estimate the electric and magnetic fields, and the average specific absorption rate (SAR) of the samples upon exposure. The SAR is a measure of the absorption of microwave energy per unit mass of biological matter. Samples were placed in a position of predominant electric field intensity within both applicator devices (Figures 2A, B). Simulation results showed that although only 1 W of microwave power was delivered to the M3 applicator, the sample presented a maximum local SAR of 12,479 W/Kg, whereas the sample in the WG applicator, which received 12 W of microwave power, presented a maximum local SAR of 3,038 W/kg (Table 1). The discrepancy is explained in the difference of sample volume and shape as the specific absorption rate is inversely proportional to these parameters. The M3 sample had a smaller volume, thinner shape than that of the sample used in the WG model hence, it showed a higher estimated peak local SAR.

When using the WG applicator to expose them, a considerable decrease in the proliferation of HB3 parasites was observed, with conditions that did not seem to affect mammalian cell lines J774 (macrophages) and Vero (epithelial), as monitored 24 h later for the parasite or 72 hours later for cells (Figure 3A and Supplementary Figure 1). When measuring viability of the samples by MTT assays, the same results were obtained (Figure 3B). The M3 applicator was also tested, with a similar outcome (Figure 3C). With changes in temperatures that, after rising above room temperature, stabilized and fluctuated approximately 6°C in the WG (not surpassing the fever limit of 42°C) and approximately only 0.4°C in the M3 applicator (Figure 3D), even if low, the role of temperature in the mortality of parasites had to be investigated. The temperature profile of one of the WG experiments with the highest peak temperature was reproduced in infected erythrocytes with a thermocycler. The use of temperature alone had no effect on parasite growth while exposure of other aliquot of the same batch to MW reduced their growth drastically 24 h later (Figure 3E) or even 72 h later (Figure 3F and Supplementary Figure 2).

Transmission electron microscopy (TEM) (Figure 4) also shows changes in the organelles and internal structures of the parasites as a result of MW treatment. In untreated parasites, the food vacuole (FV) membrane was clearly delineated forming a continuous boundary

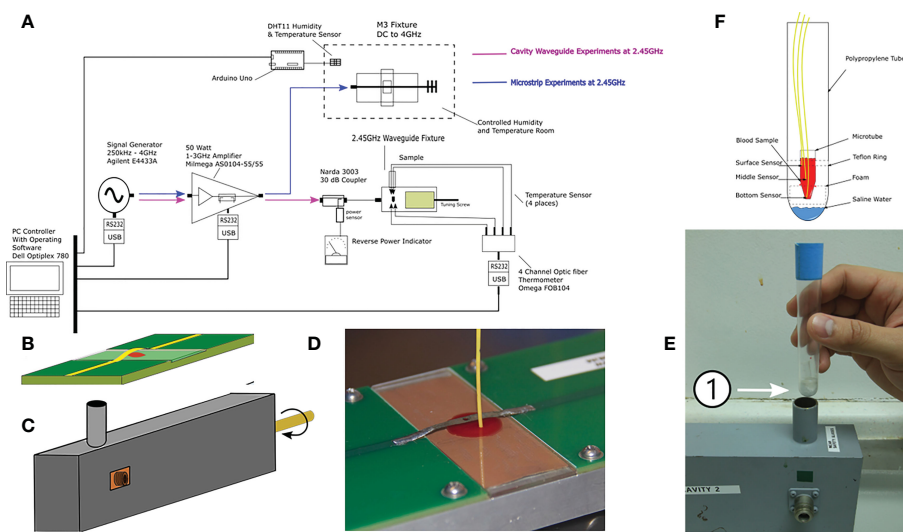


FIGURE 1

Microwave exposure system and their components. (A) Block diagram of all parts integrating the G and M3 microwave applicator systems (experiments were conducted separately); (B) M3 and (C) WG applicator device drawings. (D) Placement of the sample positioned under the metallic strip on a glass slide with a laser-milled cavity and the thermometer probe in the M3 (E) Test tube that holds inside the microtube that will carry the sample during microwave exposure inside the WG; the number 1 shows the microfuge (F) Drawing of the sample holders for the WG with the three thermometer probes placed at different depths of the sample. Dimensions are not to scale.

enveloping the haemozoin (HZ) crystals. The early trophozoite stage showed a preserved cytoplasm dotted with ribosomes, a food vacuole containing HZ, and a well-preserved nucleus with a homogeneous chromatin distribution. Late schizonts show merozoites with well-defined nuclei and typical apical organelles. In MW-treated parasites, however, 15 and 30 min after exposure, HZ crystals were scattered through the cytoplasm. One hour later, a disorganization of the organelles inside the infected red blood cell was evident. The FV was not defined and neither were the HZ crystals. The membrane of the FV in MW-exposed parasites showed abnormalities that resulted in its disappearance as well as condensation and vacuolization by 4 h

post-exposure, when the untreated parasites were entering the schizont stage. In some cases, multiple vesicles, reminiscent of apoptotic bodies, could be seen and nuclear chromatin condensation was observed in degenerated parasites, with formation of autophagosomes (double-membraned structures) 12 h after irradiation. A statistical analysis of these observations is found in [Supplementary Table 1](#). When examined by Giemsa-stained smears, parasites appeared more condensed and affected by the microwave treatment, in comparison with untreated controls (data not shown).

To investigate the mechanism of cell death of MW exposure in *P. falciparum*, the integrity of the food vacuole (FV) (the primary

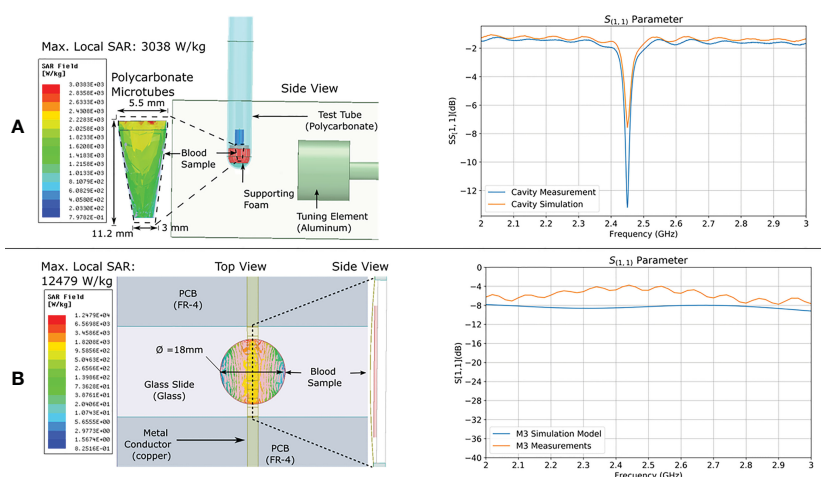


FIGURE 2

FEM SAR modeling and validation. Electromagnetic model of (A) WG and (B) M3; applicators showing calculated maximum local SAR intensity distribution in the sample. To the right of each model are the measured and simulated relative reflected power over frequency (scattering parameter S11).

TABLE 1 Measures obtained in simulations.

Applicator	Simulated Source Power (W)	Maximum Values Observed in Sample			Sample Volume (μL)	Sample Shape
		Local SAR (W/kg)	Electric field (V/m)	Magnetic field (A/m)		
WG	12	3,038	928	65	100	Microtube
M3	1	12,479	1387	25	50	Glass slide with recessed cavity

calcium store and haemozoin container) was analyzed using a fluorescent calcium dye (Cal 520). Immediately after treatment, the FV was still well delimited and clearly distinguishable in infected red blood cells (iRBCs) (Figure 5A). However, soon after exposure in 18% of parasites (20% one h after, 25% two h after and 38% four h after

treatment), FV was no longer as defined and there was a redistribution of fluorescence, from the food vacuole to the cytoplasm as compared to untreated controls. Using FURA 2AM, more pictures were taken and another count of observed events was obtained, with similar results (Supplementary Table 2). Confirming

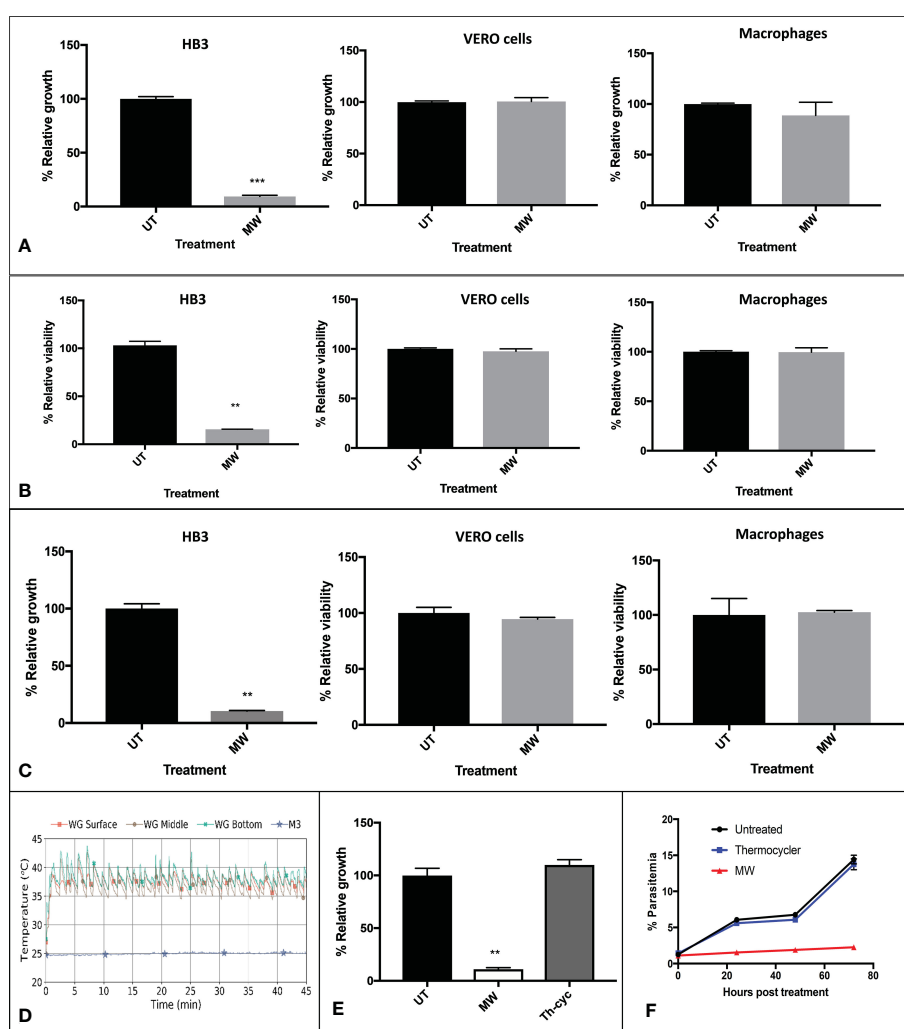


FIGURE 3

Non thermal effects of MW on *P. falciparum* parasites or mammalian cells. (A) Representative pattern of temperature changes caused by exposure of *P. falciparum*-infected cultures to MW. Infected cultures, epithelial (Vero) cells or J-774 macrophages were untreated or exposed to MW in the (A, B) WG or (C) M3 and the growth or viability of duplicates was assessed 24 h after treatment. Data was acquired through: A, flow cytometry for HB3 (n=3), and fluorometry with sulforhodamine for cells (n=2); B, MTT assays for all; (HB3, n=1; Vero cells and macrophages, n=3); C, flow cytometry for HB3 (n=3) and MTT assays for cells treated with M3 (n=3). (D) Fluctuations of temperature of the infected, exposed culture with both MW applicators. (E) Using a representative temperature profile generated in the WG, samples were either submitted to the same temperature fluctuations by using a thermocycler, or exposed to the MW treatment in the WG, and their growth was monitored 24 h later by flow cytometry. A representative experiment is shown. n=3. One-way ANOVA was used throughout. (F) Growth of thermo- or MW- treated parasites was monitored for 72 hours by flow cytometry. One representative experiment is shown. n=2. **p<0.01, ***p<0.005.

this, the first reading of a time course fluorometry with FURA 2AM, taken immediately after the microwave exposure had finished, showed a sharp increase in the amount of cytosolic calcium which decreased slightly as time passed, but never to the levels of the untreated controls (Figure 5B and Supplementary Figure 3), pointing to an irreversible process. Accordingly, after MW treatment, late-stage parasites showed an increase of acidity of 0.37 pH units when compared to the untreated control (Figure 5C). Chloroquine (CQ) (above IC₅₀ levels for the strain used) and NH₄Cl-treated parasites at 40 mM were used as positive controls. These results strongly support the notion that the food vacuole is being disrupted by MW treatment resulting in leakage of Ca²⁺ to the cytoplasm and acidification out of the vacuole.

2.2 MW trigger cytotoxic events and apoptosis

At the molecular level, the production of reactive oxygen species (ROS) was investigated, finding that it was augmented only in infected but not in uRBC exposed to the same treatment, confirming the parasite as the source of ROS (Figure 6A). Since these two events are usually related, lipid peroxidation was measured through a reaction with linoleamide alkyne coupled to a fluorophore which detects protein modifications caused by this harmful process. There was evidence of increased lipid peroxidation in MW-exposed samples (Figure 6B) in infected RBCs (iRBC); additionally, the peroxidation levels in uRBC subjected to MW treatment were not

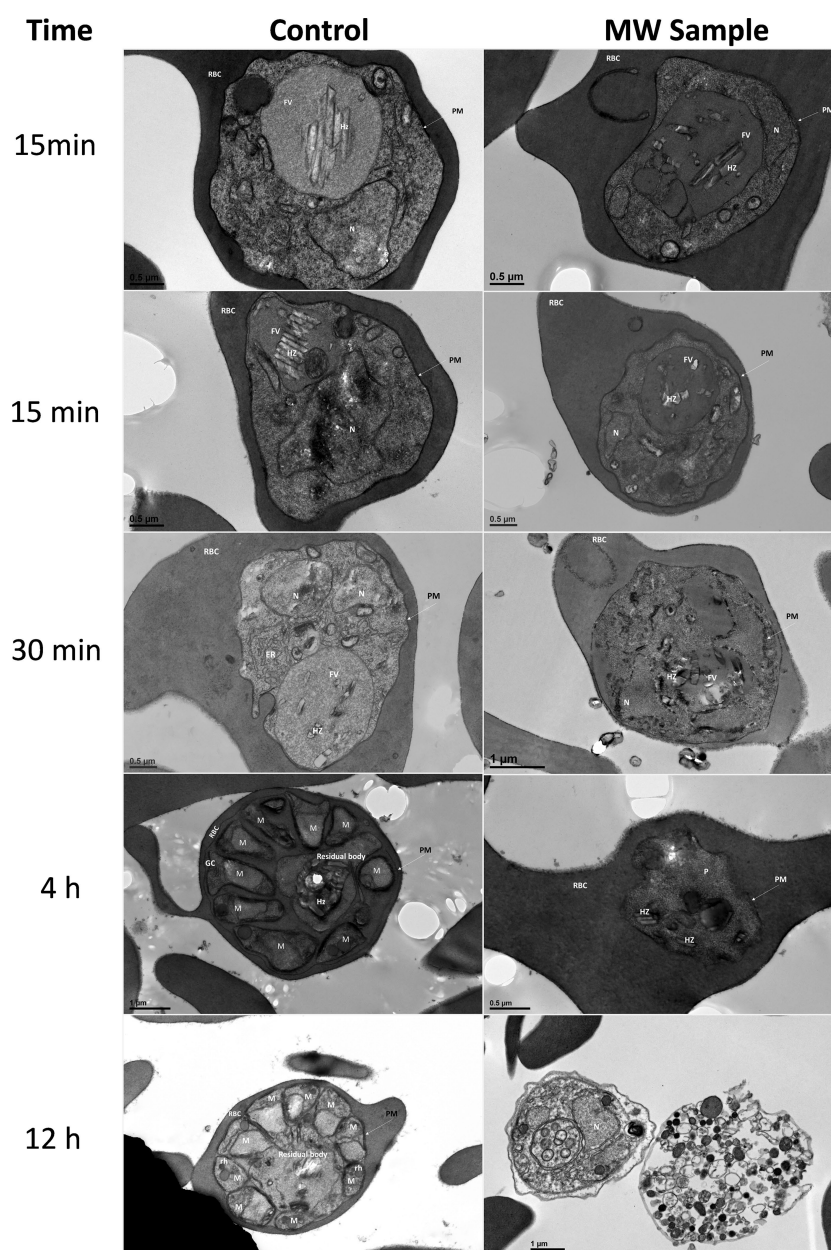


FIGURE 4

Ultrastructural changes in iRBCs after treatment with MW. MW-treated or untreated parasites were examined by transmission electron microscopy up to 12 h after MW treatment. The scale bar for Control 12 h is the same as MW sample 12 h. PM, Parasitophorous membrane; RBC, red blood cell; FV, food vacuole; HZ, haemozoin; N, nucleus; M, merozoite; Rh, rhoptry; GC, Golgi complex.

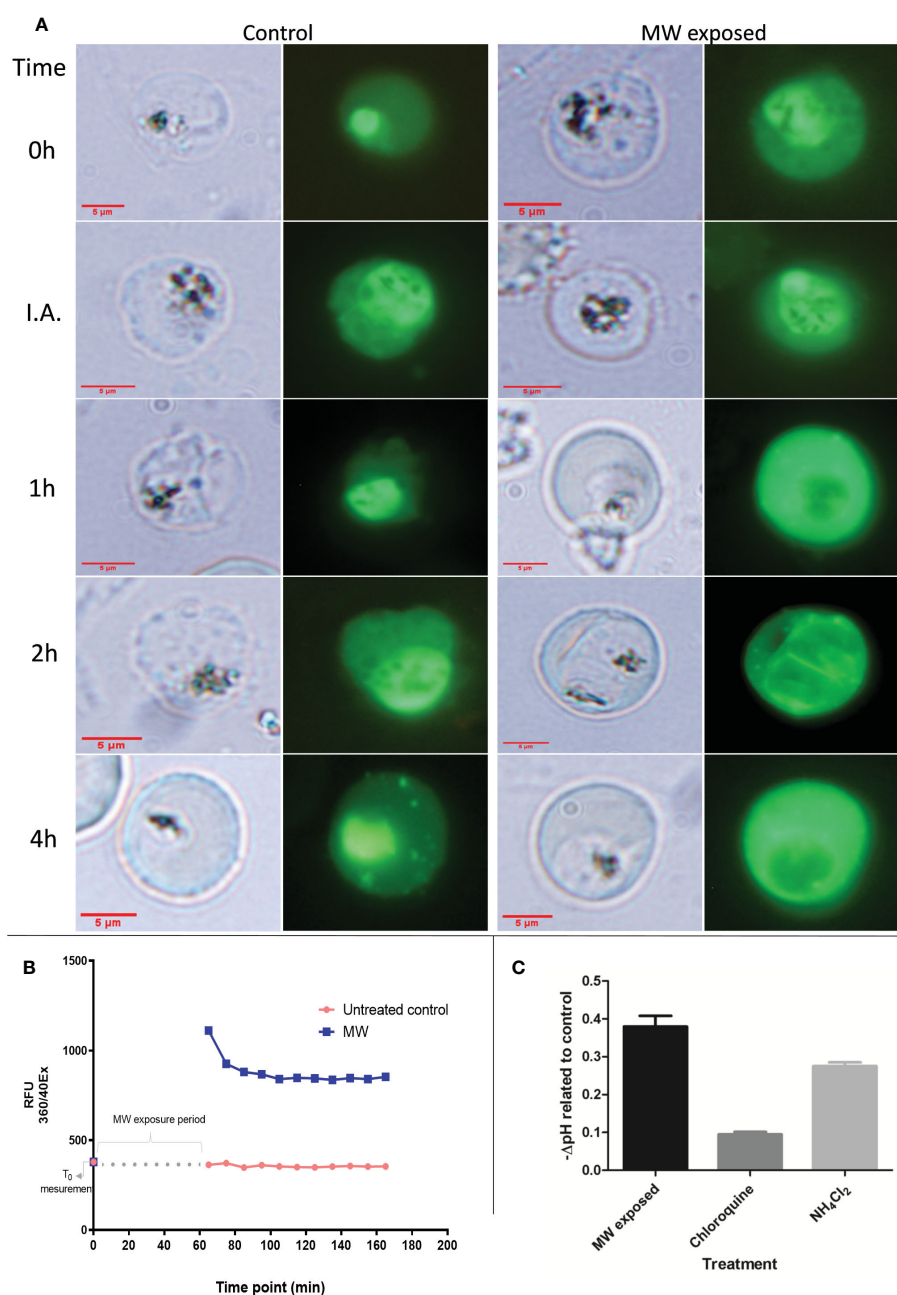


FIGURE 5

Calcium and pH changes in MW-exposed infected RBCs. **(A)** Localization of Ca²⁺ with time progression under microscopy of iRBCs stained with the calcium dye, seen under fluorescence (second and fourth exposure) or bright light (first and third images) corresponding to the same time points, with or without treatment or MW exposure (I.A., immediately after end of exposure). The pictures are representative images of one experiment out of two. **(B)** Measurement of cytosolic Ca²⁺ with the use of a fluorometer. The graph has been modified to show the time elapsed during treatment, in which no measurement was taken. A first reading was taken before exposure; the next ones, after the end of exposure, repeating the measurements every 10 min. A representative result, out of two, is shown. **(C)** The negative change in pH of samples after MW treatment was compared to untreated samples. Chloroquine and NH₄Cl₂ treatment were used as positive controls for acidification. n=3. Bars represent the mean ± SEM values; one-way ANOVA was used.

significantly different from those of untreated controls. Exposing epithelial cells or macrophages to the same treatment did not elicit an increase in either ROS formation or lipid peroxidation, confirming the selectivity of the treatment. Common apoptotic hallmarks found in most living cells were found in the malaria parasites after MW treatment, such as a large increase in the expression of caspase-like activity (>20 fold) (Figure 6C) and a significant DNA fragmentation (Figure 6D), although low levels of TUNEL-positive *P. falciparum* parasites during apoptosis have been reported before (Deponte and

Becker, 2004). Other signs of apoptosis, i.e. phosphatidyl serine externalization or mitochondrial membrane voltage variations were not detected (Figures 6E, F).

To further investigate which type of death was induced by MW exposure, necrosis was quantified by propidium iodide (PI) uptake since it crosses damaged membranes. As positive control of necrosis, infected and uninfected red blood cell samples were heated to 80°C degrees for 30 minutes. An apoptotic death-causing agent, staurosporine, was used as a positive control for programmed death.

There were no significant differences in the PI intake of MW- with respect to the staurosporine-treated samples in either healthy or infected RBCs, while heating at 80°C degrees distinctively showed necrosis (Figure 7A and Supplementary Figure 4). Autophagy was also measured through a 3-hour pre-incubation with an autophagosome inhibitor (3-MA) followed by MW treatment. As a positive control, RPMI medium without serum, -a starvation environment, was used to induce autophagy in parasites. Pre-incubation with 3-MA resulted in parasites growing to reach 70% of

the level of the untreated controls (100% growth), which represents a difference of 76% with respect to the MW-treated, autophagy-uninhibited parasites (Figure 7B), indicating that there is a contribution from autophagy in the death induced by MW exposure. This observation is consistent with TEM observations showing double membrane autophagosomes (Figure 7C). Finally, flow cytometry analysis of the infected erythrocytes exposes signs of cell shrinkage and chromatin condensation, typical morphology changes which accompany apoptosis (Darzynkiewicz et al., 1992) (Figure 7D).

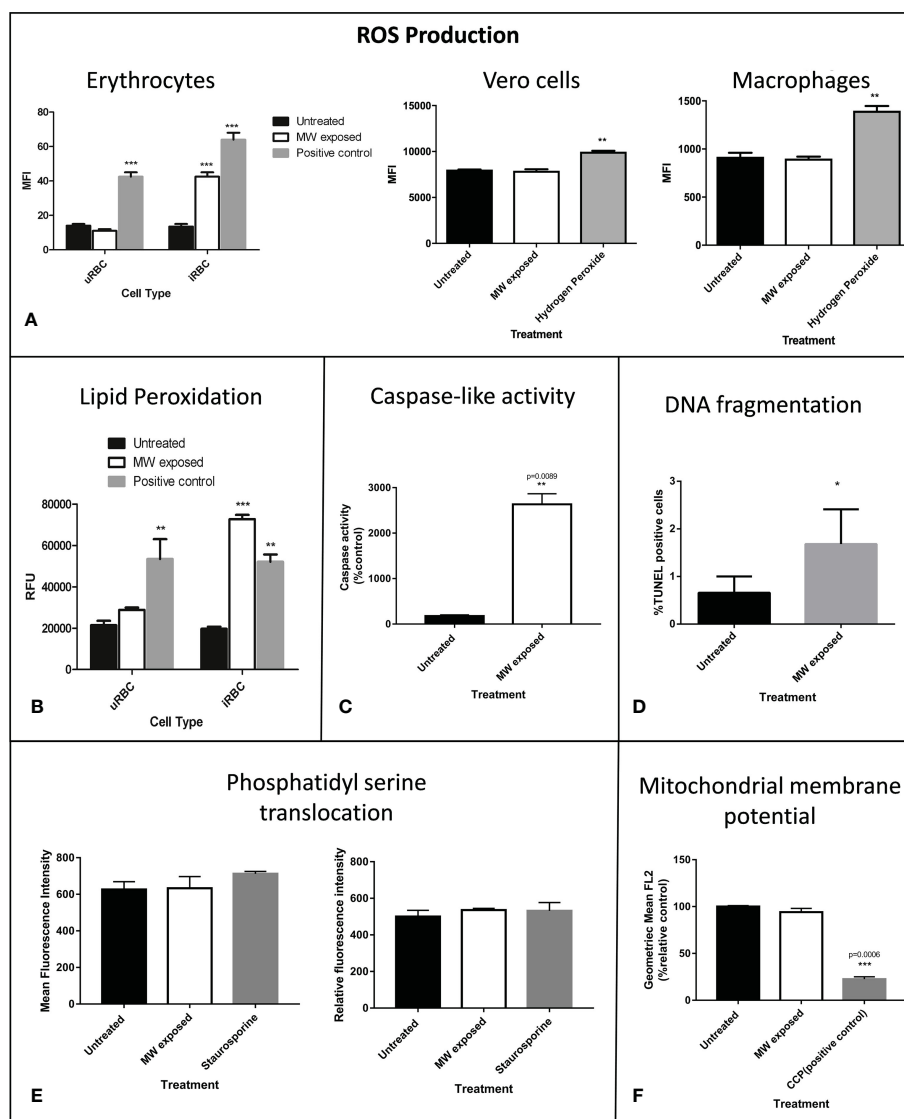


FIGURE 6

Molecular damage triggers apoptosis in MW exposed parasites. (A) ROS production of parasitized or uRBCs was assessed. Hydrogen peroxide was used as a positive control at a final concentration of 200 μ M. ROS production in Vero cells or in macrophages was analyzed after exposure to the same treatment as that of RBCs or iRBCs. Bars show the mean intensity fluorescence of triplicates, of three experiments read in a fluorometer. (B) Lipid peroxidation was detected through a Click-It LAA reaction. Cumene hydroperoxide at 100 μ M was used as a positive control. Bars show the relative fluorescence units of triplicates of one representative experiment out of three read in a fluorometer. (C) Caspase-like activity measured through flow cytometry. Data are expressed as % of control and are the means of duplicates, $n=3$. (D) DNA fragmentation was quantified by flow cytometry 24 hours after MW treatment. Experiments were run in triplicates, $n=3$. Data are the means \pm SEM. (E) Level of phosphatidylserine externalization after MW irradiation on uRBC (left) or iRBCs (right) using an Annexin V assay to measure its level. Staurosporine was used as positive controls for phosphatidylserine externalization. Data are the means of $n=3 \pm$ SEM. (F) The mitochondrial membrane potential was measured through flow cytometry measurement of red JC-1 fluorescence which correlates with the mitochondrial membrane potential $\Delta\Psi_m$. Bar graphs show the geometric mean of FL2 (red fluorescence) using 50 μ M CCCP as positive control for mitochondrial membrane depolarization. Data are the mean of $n=3 \pm$ SEM. Two-way ANOVA analysis was used in (A) and (B) and one-way ANOVA was used in (C-F). * $p<0.05$, ** $p<0.01$, *** $p<0.005$.

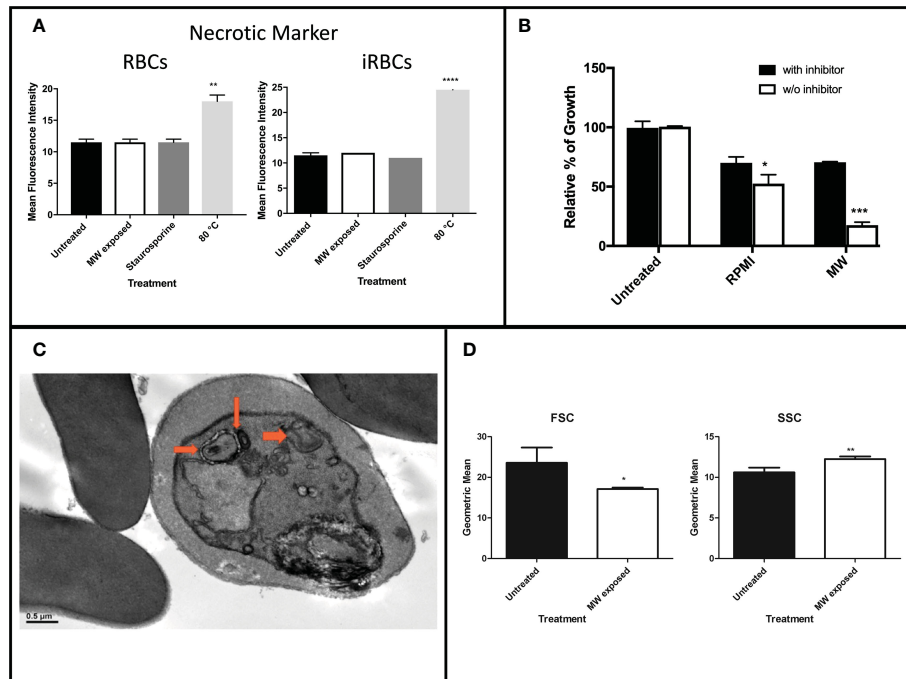


FIGURE 7

Assessment of necrosis or autophagy induced by MW exposure. (A) Levels of PI intake of uRBCs or iRBCs after MW treatment. Bars represent the mean relative fluorescence intensities of two independent experiments \pm SEM values read in a fluorometer. One-way ANOVA analysis was used. (B) iRBCs were incubated with or without an autophagy inhibitor (3-MA) before exposing them to MW, or placed in starvation media as a positive control; $n=3 \pm$ SEM values; two-way ANOVA was used. Readings were obtained through flow cytometry. (C) Transmission electron microscopy (TEM) image of *P. falciparum* infected red blood cells six hours post microwave treatment. Arrows point to doubled-membrane autophagosomes. (D) Flow cytometry analysis of infected erythrocytes exposed to MW shows changes in size (FSC) and complexity (SSC). Data are the means of $n=3 \pm$ SEM. T-test analysis was used. * $p<0.05$, ** $p<0.01$, *** $p<0.005$, **** $p<0.001$.

2.3 Ca^{2+} signaling molecules are key in MW effect

The signal transduction pathways involved in the movement of calcium were also investigated. There have been reports on MW and other low-frequency electromagnetic fields (LEMF) having a role in the activation of calmodulin and voltage gated calcium channels (VGCC) in human leukocytes and lymphocytes (Papatheofanis, 1990; Cadossi et al., 1992; Faas et al., 2011). Likewise, with MW treatment, the use of inhibitors targeting voltage-gated calcium channels on the cell membrane (verapamil) and prostaglandin synthesis (indomethacin) resulted in a complete reversal of the killing effect of MW treatment, causing exposed parasites to grow 99.8% and 127.8%, respectively. TMB8, an intracellular Ca^{2+} release inhibitor, and W7 -an inhibitor of calmodulin which is a secondary messenger that requires Ca^{2+} for its activation, reversed the killing effect of MW by 79.3% and 91.0% respectively (Figure 8 and Supplementary Figure 5). The addition of neomycin, which blocks the inositol trisphosphate (IP3) pathway, resulted in a partial reversal of the killing effect. The above molecular evidence of Ca^{2+} involvement is also consistent with the imaging data showing an early redistribution of calcium in the MW-affected parasites from the HZ-containing food vacuole (FV).

Taken together, all the findings suggest a sequence of events that lead to parasite death largely through a calcium signaling pathway that leads to apoptosis, with some autophagocytosis taking place, avoiding the damaging effects of necrosis. Moreover, through studies

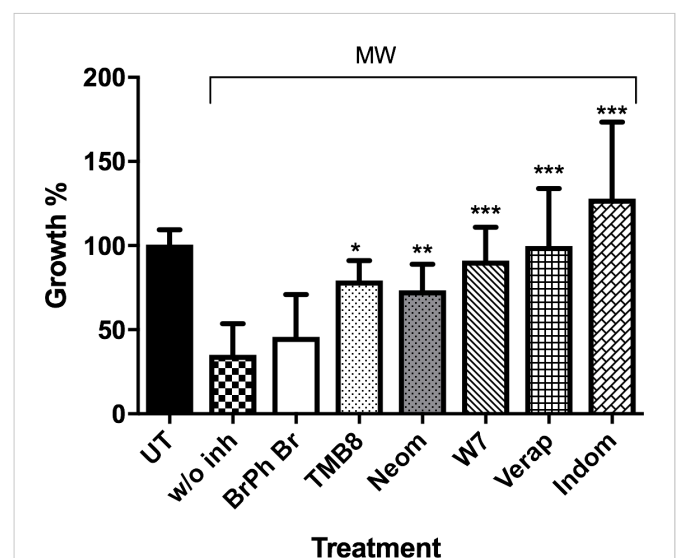


FIGURE 8

Ca^{2+} signaling proteins involved in MW-induced death. uRBCs or iRBCs were incubated 1 h before MW in WG with or without inhibitors of Ca^{2+} transduction pathways, and their growth assessed by flow cytometry (Bars from left to right: Untreated, bromophenyl bromide, TMB8, neomycin, W7, verapamil, and indomethacin). All bars represent means \pm SEM of duplicates. $n=2$, unpaired, one-way ANOVA (Bonferroni's multiple comparison). * $p<0.05$, ** $p<0.01$, *** $p<0.005$.

of HZ crystallization performed in *P. falciparum*-infected cultures treated with MW, it was clear that the treatment does not interfere with this process. A process of extraction of HZ, to measure its production by parasites exposed to them, included removal of all haem not processed, correctly identified by Fourier-transform infrared spectrometry (FT-IR) (Figure 9A). The identity of HZ isolated at the end of the experiment was also confirmed by FT-IR (Figure 9B) and measured through UV absorbance to calculate its concentration. This is important, as a significant reduction in their ability to crystallize haem into haemozoin was, as reported previously (Webster et al., 2008) (Combrinck et al., 2013) observed when parasites were treated with Chloroquine ($p < 0.05$) and Mefloquine ($p < 0.005$), clearly separating the MW mechanism of action from that of signature drugs against the disease (Figure 9C). A possible set of signaling events is shown in Figure 10.

3 Discussion

The data suggest that MW exposure, with the parameters described here, targets the FV, leading to release of intracellular calcium and acidification of the cytoplasm. The increase in cytoplasmic calcium seen in calcium ion kinetic assays and the protection afforded by verapamil support the hypothesis that an opening of calcium channels plays a critical role in this process.

The combined data supports an apoptotic manner of death following MW treatment. Even though it is still somewhat debated, typical markers of apoptosis have also been identified in the parasite, albeit the complete pathway remains unknown (Deponte and Becker,

2004; Totino et al., 2008; Mutai and Waitumbi, 2010; Mohapatra et al., 2022). This is the case of MW-treated parasites, in which induced morphological changes are visible under light microscopy and detectable by flow cytometry; and increases in ROS and lipid peroxidation, caspase activation and DNA fragmentation were detected. There is also a contribution of autophagy in the death of parasites treated with MW. The latter is corroborated with TEM images that show the formation of double membrane autophagic vacuoles. The activation of caspases results in the generation of a cascade of signaling events allowing the controlled demolition of cellular components. Morphology changes related to a programmed cell death (PCD) were corroborated by flow cytometry where side (SSC) and forward (FSC) scattering suggested a reduction in the size of the cell with an increase in density, usually due to chromatin condensation (Darzynkiewicz et al., 1992). Altogether, there is enough evidence to substantiate a PCD response of the parasites to MW stimulus.

A calcium signaling pathway has been reported to be involved in the effects of electric fields stimulation in *P. falciparum* (Coronado et al., 2016), and hence, the effects of MW on Ca^{2+} transport were explored. Several of the inhibitors tested in DC electric fields exposure assays in that study uncovered a role for calcium signaling in an increased proliferation of parasites. It is known that calmodulin acts as a multipurpose intracellular Ca^{2+} receptor, governing many Ca^{2+} regulated processes (Matsumoto et al., 1987; Brighton et al., 2001). There have been reports on MW and other low frequency electromagnetic fields (LEMF) having a role in the activation of calmodulin and voltage gated calcium channels (VGCC) in human leukocytes and lymphocytes (Papatheofanis, 1990; Cadossi et al.,

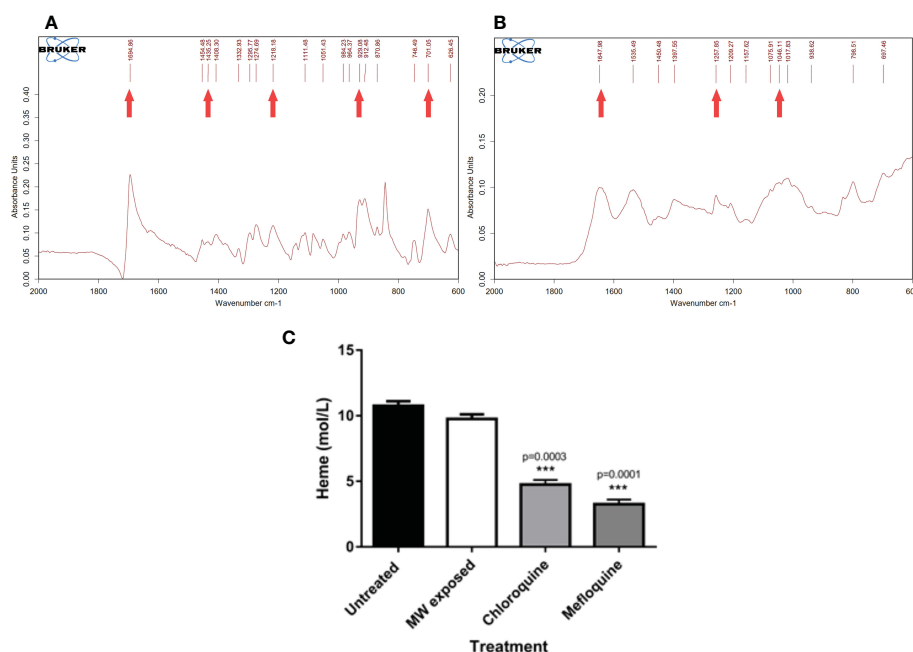


FIGURE 9
Effect of MW on the crystallization of haemozoin. A haemozoin formation assay based on the differential solubilities of haem and haemozoin was conducted in the presence of different agents by exposing infected erythrocytes to chloroquine, mefloquine or MW. (A) FT IR profile of haem from the samples and (B) FT IR profile of haemozoin. Arrows point to the characteristic peaks of both molecules. (C) Comparison of the effect of different treatments in the production of haemozoin. The values are the means of triplicates of one representative experiment (n=3). One-way ANOVA analysis was used. *** $p < 0.005$.

1992; Faas et al., 2011). The inhibition of growth of *P. falciparum* caused by MW irradiation was diminished by blocking the release of Ca^{2+} from intracellular storages and by blocking the activation of calmodulin. Also, blocking the inositol trisphosphate (IP₃) pathway partially rescued the killing effects of MW treatment. However, blockers targeting signaling molecules of the cell membrane, i.e., VGCC channels with verapamil, and prostaglandin synthesis with indomethacin, had major rescuing effects on the MW treatment consequences, suggesting these events take place early in the chain of signaling processes.

Through the experiments and extended data presented here the ability of *P. falciparum* to synthesize HZ after treatment with MW has been shown not to be affected. Thus, the MW effect differs in the mechanism of action of other known antimalarials such as CQ and MQ. This is important in two contexts: that of MW not discriminating against parasites resistant to other drugs and the possibility of synergism with antimalarials. It is worth mentioning that the strain used throughout this work is a *P. falciparum* parasite resistant to pyrimethamine, further supporting a novel mechanism of action behind MW treatment.

Based on all these results, it can be asserted that, using the conditions described here, microwaves do not affect the viability or integrity of mammalian epithelial cell lines, macrophages or erythrocytes. A macro thermal effect as a factor in the killing effect of MW over *P. falciparum* has been ruled out. These same conditions, however, almost completely inhibit the growth of *P. falciparum* parasites with a different mechanism of action than that of signature drugs against malaria. Obviously, more work needs to be done in order to truly assess how exposure to MWs achieves killing in the malaria parasites. Nanothermal effects cannot be completely ruled

out, but the series of apoptotic events observed in the parasites following MW exposure hardly agrees with thermal damage. The lightness, transportability, durability and present low cost of producing microwave devices opens wide the idea that MW could be used in the future in combination with other drugs or as a totally independent therapeutic alternative against malaria.

4 Materials and methods

4.1 Parasites and culture

The malaria parasite strain HB3 (pyrimethamine-resistant) of *P. falciparum* (a generous gift of the Experimental Therapeutics Division of the Walter Reed Army Institute of Research in Silver Spring, MD) was cultivated following the method described by Haynes et al. (Haynes et al., 1976), with some modifications. In brief, we used O + erythrocytes in complete medium that consisted of RPMI 1640 supplemented with 25 mM HEPES, 0.2% sodium bicarbonate, and 10% serum. Blood was obtained from donors who read and gave written consent to participate in the project. A pool of 11 persons with no specific ethnic background were called to donate not more frequently than every 6 months. All volunteers brought medical certificates before donation and were fasting until blood draw. They were free of medication schemes. Their ages ranged between 20 and 40 years, with 8 women and 3 men. The protocol of use of their blood was submitted and approved by the bioethical committee of the Gorgas Memorial Institute of Health Sciences (252/CBI/ICGES/21). Blood was drawn with citrate phosphate dextrose adenine (CPDA) as anticoagulant at 10% v/v. Cultures were maintained at 37°C in a gas

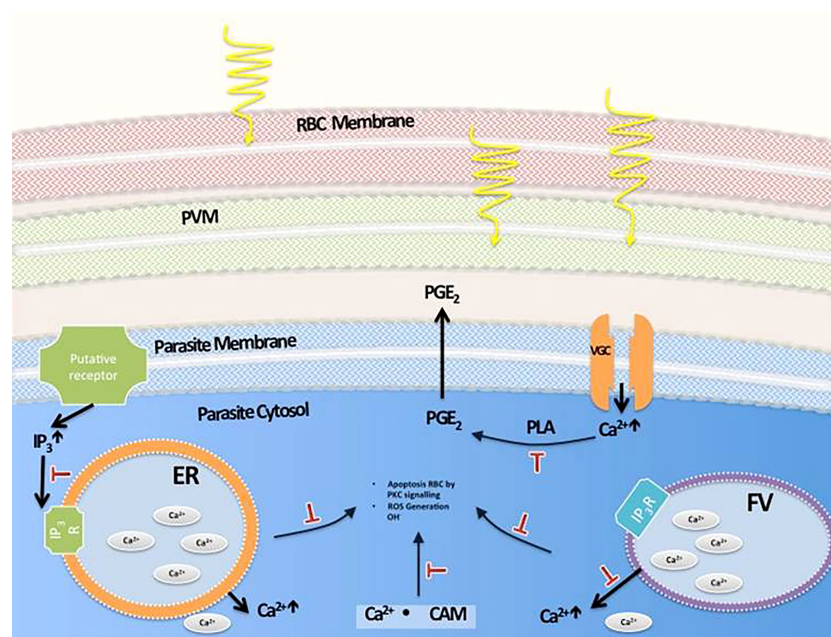


FIGURE 10

Proposed pathways involved in MW-induced death of malaria parasites. Movements of Ca^{2+} from this ion storages of the parasite take place after MW exposure. Their inhibition with target molecules can partially or totally prevent their death by irradiation. (PVM: Parasitophorous vacuole membrane, ER: Endoplasmic reticulum, FV: Food vacuole, PGE_2 : Prostaglandin E2, PLA: Phospholipase A, IP₃: Inositol Trisphosphate, CAM: Calmodulin).

mixture of 5% CO₂, 5% O₂ and 90% N₂ at 2% hematocrit and synchronized with alanine and thermal cycling as described in Almanza et al. (Almanza et al., 2011).

4.2 Microwave exposure system

The microwave exposure system was custom designed. Briefly, it consisted of a signal generator, a power amplifier, a power reflectometer, a microwave applicator device and optical fiber probes to measure temperature directly in the sample medium. All experiments were automatically controlled by a computer equipped with the custom software BioEMC (Bio Electro Magnetic Compatible), which allowed the operator to modify all the exposure parameters and to record temperature profiles, as well as incident and reflected power over time (Supplementary Figure 1). Four microwave applicators were used in separate experiment sets: a waveguide (WG) resonator, a microstrip (M3), parallel plates (PP) and a monopole antenna array (MAA). For the WG experiments, three optical fiber probes connected to a digital thermometer were used to measure temperature at different depths of the sample. The microfuge containing the blood sample rested on top of a small foam bedding that separated it from 150 µl of 0.9% saline water placed with the purpose of lowering the reflected power and achieving the proper tuning of the WG applicator. A Teflon ring was used to hold the microtube vertically placed inside a polypropylene test tube (see Supplementary Figure 3B). For the M3 experiments, a microscope slide with a concave cavity was used to hold 150 µl of sample in place. A single fiber optic probe was submerged in the sample medium to measure the temperature profile during the tests. In the PP experiment, a peristaltic pump was used to move 2.5 ml of *P. falciparum* erythrocyte culture back and forth through flexible tubing (NIPRO, Bridgewater, NJ, USA) that was deployed through the transmission line of the parallel plates with a constant speed of 0.4–8.5 ml/min.

4.3 Microwave exposure conditions

Each experiment had a duration of 45 min and was conducted at a frequency of 2.45 GHz using pulsed microwave power exposure with a duty cycle between 20 and 25%. A peak power of 12 W was delivered to the WG applicator, and reflected power was minimized using a tuning screw to maximize the absorption of energy by the sample. For the M3 experiments, a peak power of 1 W was delivered to the applicator, which reflected negligible microwave power levels without requiring additional tuning. With all applicators, the duty cycle was maintained.

4.4 Electromagnetic modeling

All electromagnetic models were developed using ANSYS Mechanical and Electronic Suite (under licenses from 2016–2020 to Universidad Tecnológica de Panamá). Properties of the materials used in the models were obtained from built in libraries, except for the dielectric properties of the blood samples, which were obtained from

experiments at 2.45 GHz using the coaxial probe dielectric characterization method and are as follows: dielectric permittivity of 75, loss tangent of 0.27. Standard values of conductivity (2.73 Siemens/m) and density (1100 kg/cm³) were used for the blood material as well.

The WG applicator was modeled using an air-filled resonant cavity with copper metallization (conductivity of 5.8e7 Siemens/m) and with the sample in a PCR microtube (thickness = 0.2 mm) that was placed inside a cylindrical container (thickness = 1 mm) both made of polycarbonate (Erel = 2.9 and Tanδ = 0.00066) as it is shown in Figure 1A. Upon loading the sample, the cavity is brought to resonance at 2.45 GHz by tuning the position of its short circuit termination. Microwave exposure occurs when the electromagnetic energy is fed into the cavity *via* an open-circuit coaxial probe and couples to the sample that is suspended in a region close to the midpoint of the cavity.

The M3 applicator model consisted of 50 Ω microstrip lines on the printed circuit board material FR4 (Erel = 4.4, Tanδ = 0.02, and thickness = 1.6 mm) with 1 oz copper metallization (Figure 1B). A length of 2.5 cm was cut off from the middle section of the PCB substrate to fit a glass slide (Erel = 5.5, Tanδ = 0.02 and thickness of 1.2 mm) with a recessed cavity that held 100 µl of sample material. A metallic copper strip bridge joins the microstrip sections on either side of the glass slide and the sample is placed underneath it. MW power is fed on one side of the microstrip line, and is terminated at the other end with a 50 load. Maximum interaction of electromagnetic fields with the sample occurs in the region right underneath the strip bridge edges where MW energy is delivered to the sample *via* inductive coupling.

MW power was injected into each simulated model using plane wave ports at power levels corresponding to those used in experiments, ranging from 1 W to 12 W at 2.45 GHz. Local SAR was computed by the software throughout the sample volumes and maximum values were registered, and are illustrated for all applicators in Figure 2 along with their corresponding granular mapping of microwave absorption throughout the 3D samples. Along with maximum local SAR values, excitation conditions, sample volume, and peak values of electric and magnetic fields are described in Table 1.

Finally, the validation of each applicator model was performed by comparing relative reflected power over frequency (scattering parameter S11) obtained in simulation to the measured S11 of constructed prototypes (Figure 2). Measurements were performed with a portable Vector Network analyzer (Keysight Field Fox Model N9913A).

4.5 Growth assays

Following exposure, duplicate samples of trophozoite or early schizont-synchronized cultures were seeded in 96-well plates at 2% parasitemia. Growth was monitored from 24 h to up to 48 h by microscopy or by flow cytometry. Any independent experiment where untreated controls did not reach 2% parasitemia or above, 24 h after infection, was discarded before analysis. For microscopy, Giemsa-stained thin smears were prepared and the number of infected erythrocytes out of at least 1,000 erythrocytes was counted.

The microscopist was always blinded to the experimental treatment of each sample. For flow cytometry, samples were stained with 2 µg/ml Hoechst 33342 (Invitrogen, Carlsbad, CA, USA) for 15 min prior to transferring a 125 µl aliquot to 125 µl of 4% paraformaldehyde in PBS. Additionally, background staining of an uninfected red blood sample was always performed (Spadafora et al., 2010) and used to define the population of red blood cells using FSC/SSC to gate all samples. Debris and other stained cellular populations were ungated. Samples were stored at 4 °C until acquisition. A CyFlow Space cytometer (Partec, Görlitz, Germany) was used for acquisition by exciting the samples with a UV laser. The data were analyzed with the FloMax version 2.7 (Quantum Analysis GmbH, Munster, Germany). The change in growth was calculated as (24 h Parasitemia - 0 h Parasitemia)/24 h Parasitemia.

4.6 Cytotoxicity

Vero cells (VERO C1008; ATCC CRL-1586) and J-744 macrophages were cultured in a 75 cm² flask in modified RPMI 1640 supplemented with 10% FBS, 0.2% NaHCO₃, HEPES (25Mm) and Penicillin/Streptomycin (100 U/ml and 100 µg/ml, respectively) in an atmosphere of 5% CO₂.

5000 cells/ml were used in all samples and treatments. Microwave irradiation was applied using the same conditions utilized for parasites. Viability was assessed using an assay for the incorporation of 3-(4,5 dimethylthiazol-2-yl)-2,5-diphenyl tetrazolium bromide (MTT). The absorbance of control and treated cells was recorded using a microplate fluorescence reader (BioTek Synergy HT, USA) at 570 nm using the Gen5 software v.1.11. As positive control, cells that were heated to 80°C were used. Six replicates were used for each treatment. To determine cellular growth, cell density was assessed with a hemocytometer after trypsinization every 24 h up to 72 h. Additionally, for proliferation assays, cells in duplicates were subjected to treatments or not. After incubating at 37 °C for 72 h, cells were ready for monitoring by fixing them with 50% trichloroacetic acid for one hour and air drying. Sulforhodamine B was added to 100 µl of fixed cultures placed in 96-well plates. Cells were washed with 1% acetic acid to remove excess of the fluorescent dye and then washed with distilled water to remove the acid. Bound sulforhodamine B was dissolved with 10 mM Tris. Plates were read in above fluorescence reader at 495 and 570 nm. A control of color containing only RPMI was subtracted from the readings. The level of proliferation was compared between treated and control samples.

4.7 Effect of temperature on parasite growth

To test the temperature effect on parasite growth, the temperature profile resulting from the microwave exposure of an infected erythrocyte showing one of the most extreme temperature patterns was simulated using a thermocycler (2720 Thermal Cycler, Applied Biosystems, USA). Following this treatment, parasite growth was assessed by flow cytometer as detailed above.

4.8 DNA fragmentation

DNA fragmentation was assessed on infected erythrocytes after the microwave irradiation treatment. Untreated erythrocytes were used as controls. Measurements were performed 0 and 24 hours post treatment. To this purpose, the DeadEndTM Fluorometric TUNEL System (TUNEL) (Promega, Madison, WI) was used. The protocol suggested by the manufacturer was used with small modifications.

4.9 Lipid peroxidation

A Click-iT LAA kit (Molecular Probes[®], Eugene, OR) was used according to the manufacturer's instructions. The fluorescence of the samples, i.e. uninfected erythrocytes, infected erythrocytes and infected untreated erythrocytes were analyzed with the use of a fluorometer reader at 485/20 excitation and 528/20 nm emission. As a positive control, cumene hydroperoxide at 100 µM, which induces lipid peroxidation, was used. The protocol suggested by the manufacturer was used.

4.10 Caspase-like activity

The CaspaTag *in situ* kit from Millipore (Burlington, MA) was used to perform the assays. Caspase-like activity was measured in the entire population of iRBCs. This signal can be used as a direct measurement of caspase activity by flow cytometry. The protocol suggested by the manufacturer was used.

4.11 Intracellular reactive oxygen species (ROS) production in *P. falciparum*

Intracellular ROS formation was measured by fluorometry with the CM-H₂DCFDA reactive dye from Molecular Probes[®] (Eugene OR, USA) at 10 mM. Samples were incubated for 30 min in the dark and washed with PBS before reading. Hydrogen peroxide was used as a positive control at a final concentration of 200 µM. The level of ROS present was inferred through the amount of oxidized DCF (Jakubowski and Bartosz, 2000).

4.12 Measurement of intracellular pH

The parasite cytosolic pH was measured by flow cytometry incubating the parasites after treatment with SNARF-4F pH sensitive dye (Invitrogen, ThermoFisher Scientific, UK) at 5 µM for 20 min at 37 °C. SNARF emission fluorescence signals were measured at 585 nm and 650 nm. To obtain the actual cytoplasmic pH values, autofluorescence values were subtracted and the ratio of 585/650 fluorescence was calculated (van Schalkwyk et al., 2013). The actual pH was calculated using a calibration curve created using nigericin and high K⁺ buffers.

4.13 Annexin V externalization

To measure phosphatidylserine externalization and possible propidium iodide uptake in *Plasmodium falciparum*-infected red blood cells, the BD Pharmingen FITC Annexin V kit was used and fluorescence was analyzed with a fluorometer microplate reader. Fluorescence was read in a plate-ready fluorometer at an excitation/emission of 485/20–528/20 nm for Annexin V, and at 485/20–645/40 nm for PI. The protocol suggested by the manufacturer was used.

4.14 Mitochondrial membrane potential ($\Delta\psi$)

Changes in membrane potential were measured using the Mitoprobe JC-1 from Molecular Probes® (Eugene OR, USA). The mitochondrial membrane disrupter CCP at 50 μ M was used as positive control. The fluorescence intensity of JC-1-stained infected red cells was calculated through flow cytometry using the FloMax software.

4.15 Inhibition of autophagy

Infected red blood cells were pre-incubated with the autophagy inhibitor 3-Methyladenine at a final concentration of 5 mM in RPMI for 3 hours before MW treatment. The survival of parasites was assessed through parasitemia levels read in a flow cytometer 24 hours after exposure.

4.16 *In vitro* β -haemozoin formation

The haemozoin crystallization assay was developed on the basis of the differential solubility of haemozoin and heme (Pandey et al., 1999). In short, schizonts and late trophozoites at a parasitemia of 2–4% were used for parasite lysate preparations as described by Tripathi et al. (Tripathi et al., 2004). After treatment or not, cultures were incubated overnight following their protocol. All haeme present in samples was removed and collected through the use of different solvents where haemozoin is insoluble. The pool of haem was precipitated with HCl (6 M) and air-dried for Fourier-Transformed Infrared spectroscopy (FT-IR) (Bruker, Germany) in attenuated total reflection (ATR) mode, at room temperature, to confirm its identity. The final haemozoin pellet left at the end of haeme removal was also examined through FT-IR and dissolved in NaOH which transforms haemozoin into free haeme. The absorbance of this solution at 405 nm corresponds with the haemozoin amount produced by the samples, as calculated with the Beer-Lambert equation: $A = \epsilon bc$, where ϵ is the molar absorptivity of the absorbing species, b is the path length, and c is the concentration of the absorbing species.

4.17 Calcium redistribution in cells and quantification

Cal-520 AM, a new fluorogenic calcium-sensitive dye, was used to visualize the distribution of calcium before and after treatment.

Infected RBCs were stained with 10 μ M Cal-520 in RPMI medium and 0.02% pluronic acid by letting them incubate with the dye for 2 hours at 37 °C, in the dark. After incubation, cells were washed with PBS and resuspended in 200 μ l of RPMI. The culture was subjected to microwave irradiation as previously described. 10 μ l of culture were placed on a slide and calcium-positive parasitic vacuoles were examined before MW irradiation, immediately after, and 2 and 4 hours after irradiation using a fluorescent Olympus IX70 microscope with a U MNIBA Ex 470/490 Em 515/550 nm filter and an Olympus 100X UPlanAPO. FURA 2AM, a membrane-permeable calcium indicator fluorescent probe, was used to study changes in parasite cytosolic calcium after treatment with microwaves. Parasites were stained with 10 μ M Fura 2 AM in ringer's solution and 0.01% pluronic acid for 2 h at 37°C in the dark. After incubation, cells were centrifuged at 2000× g for 1 min, washed with PBS once, and resuspended in culture media before treatment with microwaves for 45 min. Following exposure, fluorescence was measured in a fluorometer. Calcium levels, obtained by measuring cell fluorescence intensity at excitation and emission wavelengths of 360 and 510 nm, respectively, were determined every 10 min after treatment for almost 2 h.

4.18 Transmission electron microscopy

Microwave exposure was carried out as standardized and maintained in culture conditions until fixation. The process of fixation was done at different time points: 15 and 30 minutes, 1, 2, 4, and 12 hours post MW irradiation, also using unexposed controls. Following exposure, samples were fixed and stored with 2% paraformaldehyde/1% glutaraldehyde in sodium cacodylate buffer at pH 8.0. Before imaging, the samples were incubated overnight with 1% osmium tetroxide/1.5% potassium ferrocyanide in 0.1 M sodium cacodylate at 4°C overnight. They were dehydrated with graduated ethanol baths (35, 50, 70, 90, 95, 100%) for 10 min at room temperature. Propylene oxide was added and the sample was embedded in 100% 812 resin. Ultrathin sections were cut with an ultramicrotome and stained with uranyl acetate/lead citrate. Images were obtained with a JEM1400 Digital Capture Transmission Electron Microscope (JEOL Ltd., Japan).

4.19 Inhibition of signal transduction pathways

Six different inhibitors of transduction signals involved in proliferation or apoptosis pathways were used: W7 (0.2 μ M) (SIGMA); Neomycin 5 μ M (SIGMA); Indomethacin (4 μ g/ml) (Abcam); Verapamil 1 μ M (Abcam); TMB8 10 μ M (Abcam), which also inhibits the release of Ca^{2+} from intracellular stores; and bromophenacyl bromide 1 μ M (Abcam). Most of the inhibitors were diluted in culture media except for bromophenacyl bromide and indomethacin, which were diluted in DMSO to provide stock solutions which were then diluted 1:10,000 in the experimental wells, making the contribution of DMSO negligible. Parasites were preincubated for one hour with the inhibitors and then exposed to microwave treatment. After 24 h of subsequent incubation at 37°C,

the parasitemia was measured by flow cytometry and the morphology of the parasites was analyzed in Giemsa smears through a light microscope.

4.20 Statistical analysis

All *in vitro* experiments were independently repeated at least twice, with duplicates and triplicates and the mean results or a representative graph of all experiments is presented. “n” in figure captions refers to the number of biological, independent replicates that have been performed of an experiment. No data was excluded in any of the results. t-test was used for analysis when comparing one group to another, while for multiple comparisons, ANOVA was the choice. For most cases, such as when measuring growth, one-way ANOVA was used. Data were evaluated by analysis of variance, and significant differences between groups were determined using Bonferroni’s modification of one-tailed Student’s t-test. For multiple groups, statistical comparison of means was performed by one-way or two-way ANOVA, except where specified. No data was excluded. Independent experiments are shown as “n” in each graph legend. $p < 0.05$ was considered statistically significant. Significance was considered as follows: * $p < 0.05$; ** $p < 0.01$; *** $p < 0.005$, **** $p < 0.0001$.

Data availability statement

The raw data supporting the conclusions of this article will be made available by the authors, without undue reservation.

Ethics statement

The studies involving human participants were reviewed and approved by The Gorgas Memorial Institute of Health Sciences Number 252/CBI/ICGES/21. The patients/participants provided their written informed consent to participate in this study.

Author contributions

Conceptualization: CS, JS, DA, and CD. Methodology: LC, CN, JC, KC, GG, MZ, RG, DA, WJ, CD, and CS. Investigation: LC, RC, CN, and JC. Visualization: LC, KC, CD, and CS. Funding acquisition: LC, JS, GG, MZ, DA, and CS. Project administration: LC, JS, and CS. Supervision: JS, GG, MZ, DA, WJ, RAG, CD, and CS. Formal Analysis: LC, JS, CN, GG, MZ, DA, CD, and CS. Validation: KC, CD, and CS. Software: KC and CN. Writing (original draft): LC and CS. Writing (editing and revision): LC, JS, KC, CD, and CS. All authors contributed to the article and approved the submitted version. BiomedØEngine Group members participating as authors:

LC, RC, GG, MZ, RG, CD, and CS. Other members: Carlos Plazaola (Universidad Tecnológica de Panamá), Doriana Dorta (INDICASAT AIP), Erick Sarmiento Gómez (Universidad de Guanajuato).

Funding

The Bill and Melinda Gates Foundation GCE grants 51797 and OPP1018884 (CS and JS), Secretaría Nacional de Ciencia, Tecnología e Innovación (SENACYT) grant FID16-213 (CS), International Centre of Genetic Engineering and Biotechnology (ICGEB) grant CRP-PAN19-01 (LC), and other partial funds from Panama’s National Research System (SNI) (LC, RC, MZ, RG, and CS). Support also came from an IFARHU/SENACYT Ph.D. training grants (LC and RC).

Acknowledgments

The authors want to thank Laura Pineda, BSc, for help with culture; Doriana Dorta, BSc, for technical support; Michael Stariminov, EngD, for constructive ideas and discussions; John Smith, EngD, for advice; Mitzi Cubilla, PhD, for statistical advice; and Angie Magaña, DVM, for histopathology analysis.

Conflict of interest

A patent application has been submitted relating to the use of microwaves against malaria described in this work: Device for the treatment of malaria. Applicants: CS and The Penn State Research Foundation; Patent application number UK GB1902634.3, Filing date: Feb 27, 2019; PCT Application Number PCT/IB2020/051554, Filing date: Feb 24, 2020; USA Patent Application Number 17458101, Filing date: Aug 26, 2021.

Publisher’s note

All claims expressed in this article are solely those of the authors and do not necessarily represent those of their affiliated organizations, or those of the publisher, the editors and the reviewers. Any product that may be evaluated in this article, or claim that may be made by its manufacturer, is not guaranteed or endorsed by the publisher.

Supplementary material

The Supplementary Material for this article can be found online at: <https://www.frontiersin.org/articles/10.3389/fcimb.2023.955134/full#supplementary-material>

References

- Almanza, A., Coronado, L. M., Tayler, N. M., Herrera, L., and Spadafora, C. (2011). Automated synchronization of *P. falciparum* using a temperature cycling incubator. *Curr. Trends Biotechnol. Pharm.* 5 (2), 1130–1133.
- Belyaev, I. (2005) *Non-thermal biological effects of microwaves*. Available at: <http://citeseerx.ist.psu.edu/viewdoc/download?doi=10.1.1.521.6552&rep=rep1&type=pdf> (Accessed 26 Sep 2022).
- Brighton, C. T., Wang, W., Seldes, R., Zhang, G., and Pollack, S. R. (2001). Signal transduction in electrically stimulated bone cells. *J. Bone Joint surgery.* 83-A (10), 1514–1523. doi: 10.2106/00004623-200110000-00009
- Burri, S. H., Gondi, V., Brown, P. D., and Mehta, M. P. (2017). The evolving role of tumor treating fields in managing glioblastoma. *Am. J. Clin. Oncol.* 41 (2), 191–196. doi: 10.1097/COC.0000000000000395
- Cadossi, R., and Torelli, G. (1992). Lymphocytes and low-frequency electromagnetic fields. *FASEB J.* 6 (9), 2667–2674. doi: 10.1096/fasebj.6.9.1612290
- Combrinck, J. M., Mabotha, T. E., Ncokezi, K. K., Ambele, M. A., Taylor, D., Smith, P. J., et al. (2013). Insights into the role of heme in the mechanism of action of antimalarials. *ACS Chem. Biol.* 8 (1), 133–137. doi: 10.1021/cb300454t
- Coronado, L. M., Monteleagre, S., Chaverra, Z., Mojica, L., Espinosa, C., Almanza, A., et al. (2016). Blood stage plasmodium falciparum exhibits biological responses to direct current electric fields. *PLoS One* 11 (8), 1–21. doi: 10.1371/journal.pone.0161207
- Darzynkiewicz, Z., Bruno, S., Del Bino, G., Gorczyca, W., Hotz, M. A., Lassota, P., et al. (1992). Features of apoptotic cells measured by flow cytometry. *Cytometry* 13 (8), 795–808. doi: 10.1002/cyto.990130802
- David Dele, A. (2015). Oscillating magnetic field an anti malaria therapy. *International Journal of Physical Sciences* 10, 329–334. doi: 10.5897/IJPS2014.4205
- Deponte, M., and Becker, K. (2004). Plasmodium falciparum - do killers commit suicide? *Trends Parasitol.* 20 (4), 165–169. doi: 10.1016/j.pt.2004.01.012
- Faas, G. C., Raghavachari, S., Lisman, J. E., and Mody, I. (2011). Calmodulin as a direct detector of Ca²⁺ signals. *Nat. Neurosci.* 14 (3), 301–304. doi: 10.1038/nn.2746
- Funk, R. H. W., Monsees, T., and Özkucur, N. (2009) Electromagnetic effects - from cell biology to medicine. *Progress in histochemistry and cytochemistry*
- Gilson, R. C., Deissler, R. J., Bihary, R. F., Condit, W. C., Thompson, M. E., Blankenship, D., et al. (2018). Growth of plasmodium falciparum in response to a rotating magnetic field. *Malaria J.* 17 (1), 1–7. doi: 10.1186/s12936-018-2333-2
- Haynes, J. D., and Moch, K. J. (1976). Culture of human malaria parasites plasmodium falciparum. *Nature* 263 (5580), 767–769. doi: 10.1038/263767a0
- Inyushin, M., Kucheryavii, Y., Kucheryavii, L., Rojas, L., Khmelinskii, I., and Makarov, V. (2016). Superparamagnetic properties of haemozoin. *Sci. Rep.* 6 (1), 26212. doi: 10.1038/srep26212
- Jakubowski, W., and Bartosz, G. (2000). 2,7-dichlorofluorescein oxidation and reactive oxygen species: what does it measure? *Cell Biol. Int.* 24 (10), 757–760. doi: 10.1006/cbir.2000.0556
- Lubner, M. G., Brace, C. L., Ziemlewicz, T. J., Hinshaw, J. L., and Lee, F. T. Jr. (2013). Microwave ablation of hepatic malignancy. *Semin. intervent. Radiol.* 30 (1), 56–66. doi: 10.1055/s-0033-1333654
- Matsumoto, Y., Perry, G., Scheibel, L. W., and Aikawa, M. (1987). Role of calmodulin in plasmodium falciparum: implications for erythrocyte invasion by the merozoite. *Eur. J. Cell Biol.* 45 (1), 36–43.
- Mohapatra, A., Zuromski, J., and Kurtis, J. (2022). Assessing PfGARP-mediated apoptosis of blood-stage plasmodium falciparum parasites. *Methods Mol. Biol.* 2470, 659–672. doi: 10.1007/978-1-0716-2189-9_49
- Mutai, B. K., and Waitumbi, J. N. (2010). Apoptosis stalks plasmodium falciparum maintained in continuous culture condition. *Malaria J.* 9 Suppl 3 (Suppl 3), S6. doi: 10.1186/1475-2875-9-S3-S6
- Mycielska, M. E., and Djamgoz, M. B. A. (2004). Cellular mechanisms of direct-current electric field effects: galvanotaxis and metastatic disease. *J. Cell Sci.* 117 (Pt 9), 1631–1639. doi: 10.1242/jcs.01125
- Nadovich, C. T., Jemison, W. D., Stoute, J. A., and Spadafora, C. (2014). “Microwave exposure system for *In vitro* and *In vivo* studies,” Proceedings of the 2014 COMSOL Conference. Available at: <https://www.comsol.com/paper/microwave-exposure-system-for-in-vitro-and-in-vivo-studies-18605>
- Pandey, A., Singh, N., Tekwani, B. L., Puri, S. K., and Chauhan, V. S. (1999). Assay of β -hematin formation by malaria parasite. *J. Pharm. Biomed. Anal.* 20 (1–2), 203–207. doi: 10.1016/S0731-7085(99)00021-7
- Papatheofanis, F. J. (1990). Use of calcium channel antagonists as magnetoprotective agents. *Radiat. Res.* 122 (1), 24–28. doi: 10.2307/3577578
- Pilla, A. A. (2013). Nonthermal electromagnetic fields: From first messenger to therapeutic applications. *Electromagnet. Biol. Med.* 32 (2), 123–136. doi: 10.3109/15368378.2013.776335
- Romanenko, S., Begley, R., Harvey, A. R., Hool, L., and Wallace, V. P. (2017). The interaction between electromagnetic fields at megahertz, gigahertz and terahertz frequencies with cells, tissues and organisms: risks and potential. *J. R. Soc. Interface* 14 (137), 20170585. doi: 10.1098/rsif.2017.0585
- Shanks, G. D., Edstein, M. D., and Jacobus, D. (2015). Evolution from double to triple-antimalarial drug combinations. *Trans. R. Soc. Trop. Med. Hygiene.* 109 (3), 182–188. doi: 10.1093/trstmh/tru199
- Smith, T. G., and Kain, K. C. (2004). Inactivation of *Plasmodium falciparum* by photodynamic excitation of heme-cycle intermediates derived from δ -aminolevulinic acid. *J. Infect. Dis.* 190 (1), 184–191. doi: 10.1086/421503
- Spadafora, C., Awandare, G. A., Kopydlowski, K. M., Czege, J., Moch, J. K., Finberg, R. W., et al. (2010). Complement receptor 1 is a sialic acid-independent erythrocyte receptor of plasmodium falciparum. *PLoS Pathog.* 6 (6), e1000968. doi: 10.1371/journal.ppat.1000968
- Totino, P. R. R., Daniel-Ribeiro, C. T., Corte-Real, S., and de Fátima Ferreira-da-Cruz, M. (2008). Plasmodium falciparum: Erythrocytic stages die by autophagic-like cell death under drug pressure. *Exp. Parasitol.* 118 (4), 478–486. doi: 10.1016/j.exppara.2007.10.017
- Tripathi, A. K., Khan, S. I., Walker, L. A., and Tekwani, B. L. (2004). Spectrophotometric determination of *de novo* haemozoin/ β -hematin formation in an *in vitro* assay. *Analytical. Biochem.* 325 (1), 85–91. doi: 10.1016/j.ab.2003.10.016
- van Schalkwyk, D. A., Saliba, K. J., Biagini, G. A., Bray, P. G., and Kirk, K. (2013). Loss of pH control in plasmodium falciparum parasites subjected to oxidative stress. *PLoS One* 8, e58933. doi: 10.1371/journal.pone.0058933
- Webster, G. T., Tilley, L., Deed, S., McNaughton, D., and Wood, B. R. (2008). Resonance raman spectroscopy can detect structural changes in haemozoin (malaria pigment) following incubation with chloroquine in infected erythrocytes. *FEBS Lett.* 582 (7), 1087–1092. doi: 10.1016/j.febslet.2008.02.062
- WHO (2021). *World malaria report*. (Geneva: World Health Organization) 320 pp. doi: ISBN 978-92-722 4-001579-1
- Wissing, F., Sanchez, C. P., Rohrbach, P., Ricken, S., and Lanzer, M. (2002). Illumination of the malaria parasite plasmodium falciparum alters intracellular pH: implications for live cell imaging. *J. Biol. Chem.* 277 (40), 37747–37755. doi: 10.1074/jbc.M204845200

Frontiers in Cellular and Infection Microbiology

Investigates how microorganisms interact with their hosts

Explores bacteria, fungi, parasites, viruses, endosymbionts, prions and all microbial pathogens as well as the microbiota and its effect on health and disease in various hosts.

Discover the latest Research Topics

[See more →](#)

Frontiers

Avenue du Tribunal-Fédéral 34
1005 Lausanne, Switzerland
frontiersin.org

Contact us

+41 (0)21 510 17 00
frontiersin.org/about/contact

